Zoosystematics and Evolution

100 (**2**) 2024

PENSOFT

MUSEUM FÜR NATURKUNDE BERLIN

Zoosystematics and Evolution
A Bulletin of Zoology since 1898

Zoosystematics and Evolution

2024. Volume 100. 2 Issue

ISSN: 1435-1935 (print), 1860-0743 (online)
Abbreviated keys title: Zoosyst. Evol.

In Focus

The cover picture shows male holotype of *Pristimantis asimus* sp. nov. (MUSM 41241, FGZC 5342) from Panguana, Departamento Huánuco, Peru, in life.

See paper of **Köhler J, Glaw F, Aguilar-Puntriano C, Castroviejo-Fisher S, Chaparro JC, De la Riva I, Gagliardi-Urrutia G, Gutiérrez R, Vences M, Padial JM:** Similar looking sisters: A new sibling species in the *Pristimantis danae* group from the southwestern Amazon basin (Anura, Strabomantidae)

Cover design
Pensoft

Zoosystematics and Evolution
A Bulletin of Zoology since 1898

Content of volume **100** (**2**) 2024

Abstract & Indexing Information

Biological Abstracts® (Thompson ISI)
BIOSIS Previews® (Thompson ISI)
Cambridge Scientific Abstracts (CSA/CIG)
Web of Science® (Thompson ISI)
Zoological Record™ (Thompson ISI)

Zoosystematics and Evolution
A Bulletin of Zoology since 1898

Content of volume **100** (**2**) 2024

Zoosystematics and Evolution
A Bulletin of Zoology since 1898

Content of volume **100** (**2**) 2024

Zoosyst. Evol. 100 (2) 2024, 325–347 | DOI 10.3897/zse.100.120305

PENSOFT

MUSEUM FÜR NATURKUNDE BERLIN

Four new species and one newly-recorded species of the genus *Opopaea* Simon, 1892 (Araneae, Oonopidae) from southern China, with a key to Chinese species

Yang Zhou[1*], Dongju Bian[2*], Zizhong Yang[3], Zhisheng Zhang[4], Yanfeng Tong[1], Shuqiang Li[5]

1 *College of Life Science, Shenyang Normal University, Shenyang 110034, Liaoning, China*
2 *Key Laboratory of Forest Ecology and Management, Institute of Applied Ecology, Chinese Academy of Sciences, Shenyang 110016, China*
3 *National-Local Joint Engineering Research Center of Entomoceutics, Dali University, Yunnan Dali, 671000, China*
4 *Key Laboratory of Eco-environments in Three Gorges Reservoir Region (Ministry of Education), School of Life Sciences, Southwest University, Chongqing 400715, China*
5 *Institute of Zoology, Chinese Academy of Sciences, Beijing 100101, China*

https://zoobank.org/4B676BBB-C8DD-471C-A5BC-57ECDA275599

Corresponding author: Yanfeng Tong (tyf68@hotmail.com)

Academic editor: Danilo Harms ♦ **Received** 6 February 2024 ♦ **Accepted** 4 March 2024 ♦ **Published** 27 March 2024

Abstract

Five species of the genus *Opopaea* Simon, 1892 from southern China are recognised, including four new species: *Opopaea mangun* Tong & Li, **sp. nov.**, *Opopaea taibao* Tong & Yang, **sp. nov.**, *Opopaea wenshan* Tong & Zhang, **sp. nov.** and *Opopaea yuhuang* Tong & Li, **sp. nov.** from Yunnan and one newly-recorded species: *Opopaea foveolata* Roewer, 1963 from Hainan. Detailed diagnoses, descriptions and photomicroscopy images of new species are provided, based on specimens of both sexes. A key to species of the genus *Opopaea* from China is provided.

Key Words

biodiversity, goblin spiders, Hainan, Yunnan, taxonomy

Introduction

Goblin spiders (Araneae, Oonopidae) are small (usually < 3 mm), six-eyed, haplogyne, non-web building spiders distributed worldwide and are especially diverse in tropical regions. They occupy diverse habitats and mainly occur in leaf litter, under bark and in the tree canopy (Henrard and Jocqué 2012; Ranasinghe and Benjamin 2018). Oonopidae is amongst the nine most diverse spider families with 1940 extant described species in 115 genera (WSC 2024).

The goblin spider genus *Opopaea* Simon, 1892 is a widespread and highly diverse genus, with biodiversity hotspots in Africa, Asia and Australia (Baehr et al. 2013). A total of 187 valid extant species are currently known, in which 46 in Africa, 35 in Asia, 96 in Australia and New Caledonia and 10 in other areas (WSC 2024). *Opopaea* are small to medium-sized oonopids, ranging from 1.0 to 2.4 mm in body length, with the abdomen completely covered with ventral and dorsal scuta (Tong and Li 2015). Species of *Opopaea* have the male palpal patella greatly swollen, connected to the femur medially

* These authors contributed equally to this work.

and the cymbium and bulb are completely fused. The genus *Opopaea* can be easily distinguished from the other genera by the absence of legs spines, by the completely fused cymbium and bulb and by the presence of dorsolateral, triangular extensions on pedicel, as well as paired scutal ridges on the scuto-pedicel region (Andriamalala and Hormiga 2013; Baehr et al. 2013).

The *Opopaea* fauna of China is poorly known, with only 18 described species, of which one species (*O. media* Song & Xu, 1984) is from Anhui and Zhejiang; one species (*O. plumula* Yin & Wang, 1984) from Hunan; one species (*O. sauteri* Brignoli, 1974) from Taiwan; two pantropical species (*O. apicalis* (Simon, 1893), *O. deserticola* Simon, 1891) from Hainan and Taiwan; six species endemic to Hainan; six species endemic to Yunnan; and one species (*O. cornuta* Yin & Wang, 1984) widely distributed in southern China (Tong and Li 2010, 2014, 2015). Here, we recognise five species of the genus *Opopaea* from China, four of which are new to science.

Materials and methods

The specimens were examined using a Leica M205C stereomicroscope. Details of body parts and measurements were studied under an Olympus BX51 compound microscope. Photos were made with a Canon EOS 750D zoom digital camera (18 megapixels) mounted on an Olympus BX51 compound microscope. Endogynes were cleared in lactic acid. Scanning electron microscope images (SEM) were taken under high vacuum with a Hitachi S-4800 after critical-point drying and gold-palladium coating. All measurements in the text are expressed in millimetres. All materials studied are deposited in Shenyang Normal University (**SYNU**) in Shenyang, China.

Terminology mainly follows Andriamalala and Hormiga (2013) and Tong et al. (2020). The following abbreviations are used in the text: AL = abdomen length; ALE = anterior lateral eyes; ALE-ALE = distance between ALEs; ALE-PLE = distance between ALE and PLE; AW = abdomen width; CBL = cymbiobulbus length; CBW = cymbiobulbus width; CL = carapace length; CW = carapace width; EGW = eye group width; FI = femur insertion on patella; FML = femur length; PLE = posterior lateral eyes; PME = posterior median eyes; PME-PME = distance between PMEs; PLE-PME = distance between PLE and PME; PTL = patella length; TL = total length. Used in the figures: ap = apodeme; asr = anterior scutal ridge; ass = arch-shaped sclerite; boc = booklung covers; dte = dorsolateral, triangular extensions; ga = globular appendix; na = nail-like process; nle = needle-like extension; pd = postgynal depression; pls = paddle-like sclerite; prr = prolateral ridge; psr = posterior scutal ridge; rds = round dark spot; rer = retrolateral ridge; sr = scutal ridge; trp = triangular protrusion; usr = upper scutal ridge.

Taxonomy

Family Oonopidae Simon, 1890
Genus *Opopaea* Simon, 1892

Key to *Opopaea* species from China

Males of *O. flabellata*, *O. semilunata* and females of *O. chunglinchaoi*, *O. sanya* and *O. sauteri* are unknown; *O. plumula* Yin & Wang, 1984 is not included because of insufficient information found in the original description.

1 Male 2
– Female 21
2 With a pair of posterolateral spikes on the dorsum of carapace (e.g. Tong and Li (2010): fig. 1A–D) 3
– Without the aforementioned character 6
3 Clypeus height about 2.5 times ALE diameter (Tong and Li 2010: fig. 1B, K) ..... *O. cornuta* Yin & Wang, 1984
– Clypeus height less than 1.5 times ALE diameter 4
4 Booklung covers medium sized; distal part of palpal bulb with long medially bent outgrowth (Tong and Li 2010: figs 8A–C, E, 12A–F) ..... *O. vitrispina* Tong & Li, 2010
– Booklung covers very small; distal part of palpal bulb without the aforementioned character 5
5 Abdomen with strongly elevated and blackened area between posterior spiracles (Tong and Li 2010: fig. 1H, I) ..... *O. diaoluoshan* Tong & Li, 2010
– Abdomen without the aforementioned character ..... *O. gibbifera* Tong & Li, 2008
6 With dark spot at the posterior end of the abdominal dorsum (Platnick and Dupérré 2009: figs 105–110) 7
– Without the aforementioned character 8
7 With basal protrusion on the palpal bulb (Platnick and Dupérré 2009: fig. 151) ..... *O. apicalis* Simon, 1893
– Without the aforementioned character (Lin et al. 2023: fig. 7A, B) ..... *O. chunglinchaoi* Barrion, Barrion-Dupo & Heong, 2013
8 With nearly straight scutal ridge on scuto-pedicel region (e.g. Fig. 4H) 9
– With nearly arch-shaped scutal ridge on scuto-pedicel region (e.g. Figs 7H, 10G, 13H) 13

9 With a small apophysis in the retrolateral distal region of palpal bulb (Tong and Li 2010: fig. 5B; Tong and Li 2015: fig. 10B, E) 10
– Without the aforementioned character 11
10 Posterior eye row procurved from above (Tong and Li 2010: fig. 5C) ..... *O. sanya* Tong & Li, 2010
– Posterior eye row straight from above (Tong and Li 2015: fig. 8D) ..... *O. rigidula* Tong & Li, 2015
11 Cymbiobulbus as long as the palpal patella (Fig. 6I, K) ..... *O. mangun* sp. nov.
– Cymbiobulbus shorter than the palpal patella 12
12 Distal part of palp ear-shaped, with a small outgrowth (Tong and Li 2015: figs 1H, I, 3A–C) ..... *O. auriforma* Tong & Li, 2015
– Distal part of palp round, without small outgrowth (Tong and Li 2015: figs 5I, J, 7A–C) ..... *O. macula* Tong & Li, 2015
13 Clypeus height more than 2.0 times AME diameter 14
– Clypeus height less than 1.5 times AME diameter 15
14 With one triangle protrusion and two largely folded ridges on palpal bulb (Fig. 12C, E) ..... *O. wenshan* sp. nov.
– Without the aforementioned character (Tong and Li 2010: figs 4A–C, 10A–H) ..... *O. furcula* Tong & Li, 2010
15 Palpal femur very small, about 1/4 length of patella 16
– Palpal femur long, slightly shorter than half length of patella 17
16 Booklung covers large (Fig. 13C, H) ..... *O. yuhuang* sp. nov.
– Booklung covers very small ..... *O. media* Song & Xu, 1984
17 Cymbiobulbus shorter than palpal patella 18
– Cymbiobulbus longer than palpal patella 19
18 Bulb tip broad, with prolateral folded ridges (Fig. 9C) ..... *O. taibao* sp. nov.
– Bulb tip gradually narrower, without prolateral folded ridges (Tong and Li 2015: fig. 15A, B) ..... *O. zhengi* Tong & Li, 2015
19 With a long prolateral ridges at distal third (Fig. 3B) 20
– Without the aforementioned character ..... *O. deserticola* Simon, 1892
20 Distal part of prolateral ridges of palp enlarged (Fig. 3B) ..... *O. foveolata* Roewer, 1963
– Distal part of prolateral ridges of palp smoothly curved (Brignoli 1974: fig. 19) ..... *O. sauteri* Brignoli, 1974
21 With a pair of posterolateral spikes on the dorsum of carapace (e.g. Tong and Li (2010): fig. 1A–D) 22
– Without the aforementioned character 25
22 Epigastric region with a transparent, rather long, needle-like extension (Tong and Li 2010: fig. 8G) ..... *O. vitrispina* Tong & Li, 2010
– Without the aforementioned character 23
23 Epigastric region with a semicircular postgynal depression (Tong and Li 2010: fig. 2D) ..... *O. cornuta* Yin & Wang, 1984
– Without the aforementioned character 24
24 Middle part of anterior scutal ridge small triangular shape (Tong and Li 2010: fig. 2G) ..... *O. gibbifera* Tong & Li, 2008
– Middle part of anterior scutal ridge large triangular shape (Tong and Li 2010: fig. 3F) ... *O. diaoluoshan* Tong & Li, 2010
25 With dark spot at the posterior end of the abdominal dorsum; epigastric region with an inverted V-shaped sclerotisation (Platnick and Dupérré 2009: figs 149, 150) ..... *O. apicalis* Simon, 1893
– Without the aforementioned character 26
26 With nearly straight scutal ridge on scuto-pedicel region (e.g. Fig. 4H) 27
– With nearly arch-shaped scutal ridge on scuto-pedicel region (e.g. Figs 7H, 10G, 13H) 31
27 Epigastric region with a posterior scutal ridge (Tong and Li 2015: fig. 12E, K) ..... *O. rigidula* Tong & Li, 2015
– Without the aforementioned character 28
28 Epigastric region with a dark, chestnut-shaped spot and bean-shaped sclerotisation (Tong and Li 2015: figs 2G, H, 3D, E) ..... *O. auriforma* Tong & Li, 2015
– Without the aforementioned character 29
29 Postgynal depression narrow and long (Tong and Li 2015: fig. 6J, K) ..... *O. macula* Tong & Li, 2015
– Without the aforementioned character 30
30 ALE separated by less than their radius (Fig. 5G) ..... *O. mangun* sp. nov.
– ALE separated by more than their radius (Tong and Li 2015: fig. 11F) ..... *O. semilunata* Tong & Li, 2015
31 Epigastric region with a needle-like extension (Fig. 8H) ..... *O. taibao* sp. nov.
– Without the aforementioned character 32
32 Endogyne with arch-shaped sclerite (Fig. 16E, F) ..... *O. wenshan* sp. nov.
– Without the aforementioned character 33
33 Epigastric furrow with short fan-shaped extension (Tong and Li 2015: fig. 12C, D) ..... *O. flabellata* Tong & Li, 2015
– Without the aforementioned character 34
34 Booklung covers large 35
– Booklung covers very small 36

35 Epigastric region with posterior scutal ridge, interrupted medially (Fig. 14H) ..... *O. yuhuang* sp. nov.
– Without the aforementioned character ..... *O. furcula* Tong & Li, 2010
36 Clypeus height about 0.5 times AME diameter 37
– Clypeus height about 1.0 times AME diameter 38
37 Epigastric region with a very small postgynal depression (Platnick and Dupérré 2009: figs 67, 68) ..... *O. deserticola* Simon, 1892
– Without the aforementioned character ..... *O. foveolata* Roewer, 1963
38 Central part of the anterior scutal ridge with a small round projection (Tong and Li 2015: fig. 15C) *O. zhengi* Tong & Li, 2015
– Without the aforementioned character ..... *O. media* Song & Xu, 1984

Opopaea foveolata Roewer, 1963

Figs 1–3, 17

Opopaea foveolata Roewer, 1963: 121, fig. 6e–h. Holotype from Ajayan, Guam, Apr. 1945, Dybas; not examined.

Opopaea sauteri Tong & Li, 2010: 35, figs 1G, N, P, R, U, 6A–G (misidentified).

Opopaea sauteri Tong, 2013: 42, figs 25G, N, P, R, U, 61A–G (misidentified).

Opopaea foveolata Baehr et al., 2013: 114, figs 5A–I, 6A–G.

Material examined. 1♂1♀ (SYNU-623–624), **China, Hainan,** Lingshui Li Autonomous County, Diaoluoshan Mountain, roadside to the waterfall (18°40.440'N, 109°52.600'E, 494 m elev.), 10 August 2010, G. Zheng leg.; 2♂1♀ (SYNU-625–627), Jianfengling National Reserve, intersection of District 5, 13 August 2010, G. Zheng leg.; 1♂ (SYNU-628), Jianfengling, roadside near Tianchi; 1♂1♀ (SYNU-629–630), Jianfengling, Tiger Roar and Dragon Song Scenic Area (18°44.885'N, 108°52.268'E, 900 m elev.), 20 July 2007, C. Wang leg.; 1♀ (SYNU-629), Yinggeling National Reserve, Yinggezui protection station, 24 August 2010, G. Zheng leg.

Diagnosis and description. See Baehr et al. (2013).

Comment. *Opopaea foveolata* was originally described from numerous specimens collected throughout Micronesia, including the types from Guam (Roewer 1963). Tong and Li (2010) misidentified this species as *Opopaea sauteri* Brignoli, 1974, based on specimens collected from Hainan Island. Baehr et al. (2013) re-described this species from numerous specimens collected from Pacific Islands with detailed descriptions and figures. We re-checked the specimens from Hainan, which sufficiently match the description and illustrations of Baehr et al. (2013) to be confident of their identity.

Distribution. Newly recorded from Hainan Island. According to Baehr et al. (2013), this species is widespread in the Pacific Region and is known from many different islands.

Opopaea mangun Tong & Li, sp. nov.

https://zoobank.org/281F7530-0985-433B-9712-92489CDF428C

Figs 4–6, 16A, B, 17

Type material. ***Holotype*:** ♂ (SYNU-541), **China, Yunnan,** Menghai County, Mangun Stockaded Village (22°02'12"N, 100°23'28"E, 1179 m elev.), 20 March 2016, S. Li leg. ***Paratypes*:** 2♀ (SYNU-542–543), same data as holotype.

Etymology. The specific name refers to the type locality and is a noun in apposition.

Diagnosis. This new species is similar to *Opopaea macula* Tong & Li, 2015 in the large booklung covers and morphology of the scuto-pedical region, but can be distinguished by the acute tip of bulbus (Fig. 6I) vs. round tip (Tong and Li 2015: fig. 7A) and the semicircular-shaped postgynal depression (Figs 5H, 16A) vs. very narrow (Tong and Li 2015: fig. 7D).

Description. Male (holotype). Measurements: TL: 1.64; CL: 0.69; CW: 0.53; AL: 0.89; AW: 0.53; ALE: 0.07; PME: 0.06; PLE: 0.05; EGW: 0.18; ALE-ALE: 0.03; ALE-PLE: 0.01; PME-PME: 0; PLE-PME: 0.01; CBL: 0.25; CBW: 0.08; PTL: 0.26; FI: 0.09; FML: 0.10. Colouration: yellow, abdominal interscutal areas creamy-white, booklung covers brown, pedipalps reddish-brown. Habitus as in Fig. 4A, C, E. Carapace (Fig. 4B, F): oval in dorsal view; sides with longitudinal streaks; median area smooth with rows of setae at lateral edges. Eyes (Fig. 4B, G): ALE largest, PLE smallest; posterior eye row straight viewed from above, procurved from front; ALE separated by less than their radius, ALE–PLE separated by less than ALE radius, PME touching throughout most of their length, PLE–PME separated by less than PME radius. Clypeus height about 1.0 times ALE diameter (Fig. 4G). Sternum (Fig. 4D) longer than wide, fused to carapace; surface smooth; radial furrows present between coxae I-II, II-III and III-IV, with rows of small pits. Abdomen: booklung covers large, ovoid, without setae. Pedicel tube short, ribbed, with small, dorsolateral triangular extensions, scuto-pedicel region lower than pedicel diameter, with straight scutal ridges (Fig. 4H). Palp (Fig. 6A–K): femur slightly shorter than half length of patella and submedially attached to patella; patella strongly enlarged, elongate oval; tibia small, rounded; cymbiobulbus as long as the patella; bulb ventrally straight, tip acute, ventral with prolateral folded ridges (prr).

Female. As in male, except as noted. Measurements: TL: 1.84; CL: 0.72; CW: 0.55; AL: 1.10; AW: 0.72; ALE: 0.06; PME: 0.05; PLE: 0.05; EGW: 0.18; ALE-ALE: 0.03; ALE-PLE: 0.01; PME-PME: 0; PLE-PME: 0.01. Habitus as in Fig. 5A, C, E. Copulatory organ (Figs 5H, 16A, B): posterior margin of epigastric scutal ridge (asr) smooth, postgynal depression (pd) semicircular-shaped; dorsally with nail-like process (na) connected to paddle-like sclerite (pls) bearing thin, straight arms.

Distribution. Known only from the type locality.

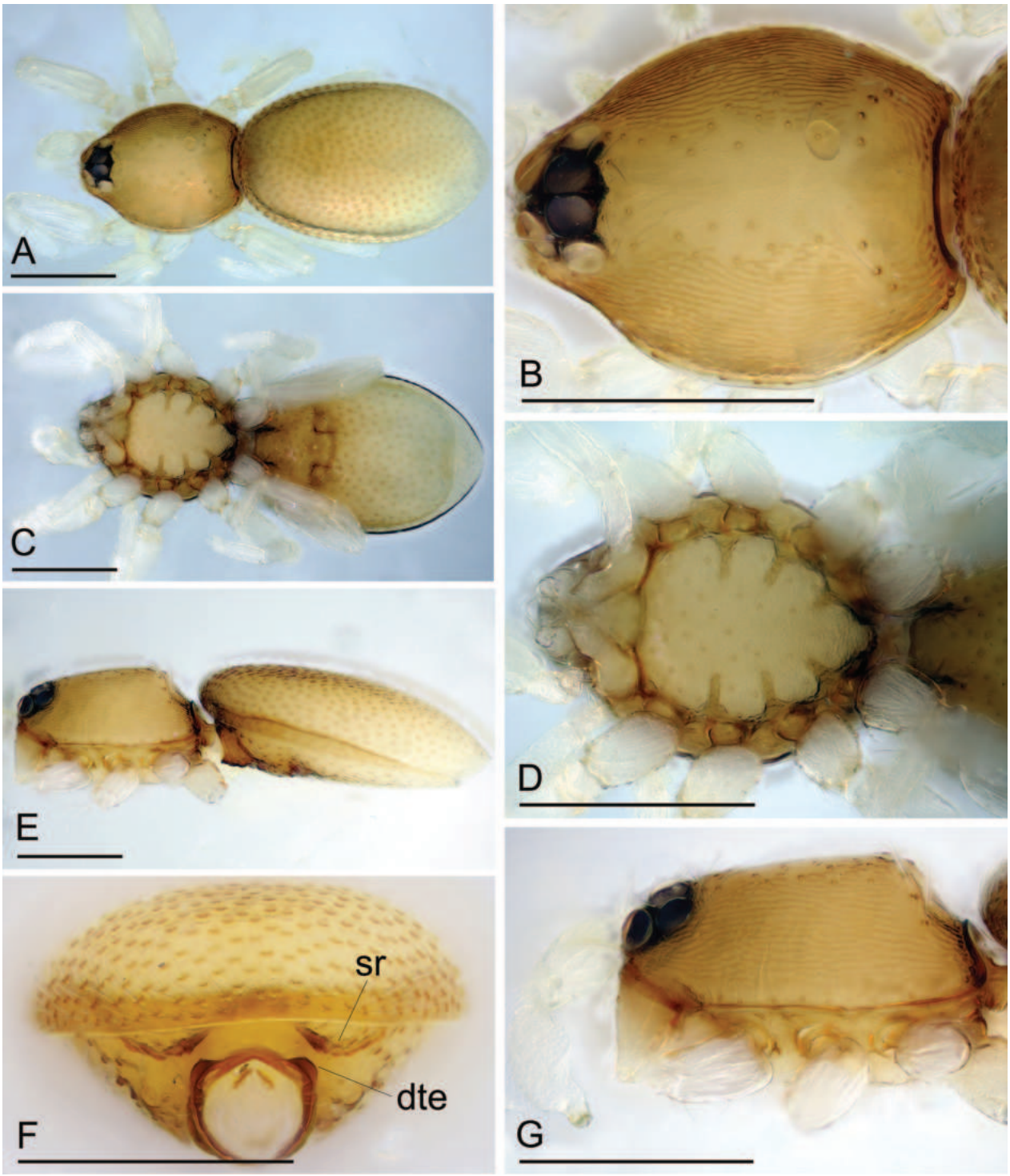

Figure 1. *Opopaea foveolata* Roewer, 1963, male. **A, C, E** Habitus, dorsal, ventral and lateral views; **B, D, G** Prosoma, dorsal, ventral and lateral views; **F** Abdomen, anterior view. Abbreviations: dte = dorsolateral, triangular extensions; sr = scutal ridge. Scale bars: 0.4 mm.

***Opopaea taibao* Tong & Yang, sp. nov.**

https://zoobank.org/AB3810A7-1924-4FA3-8AE0-7E3D943897ED

Figs 7–9, 16C, D, 17

Type material. ***Holotype*:** ♂ (SYNU-539), **China, Yunnan,** Baoshan City, Taibao Park (25°07'13.6"N, 99°09'15.0"E, 1752 m elev.), 3 November 2011, Z. Yang & H. Pu leg. ***Paratypes*:** 3♀ (SYNU-540–542), same data as holotype.

Etymology. The specific name refers to the type locality and is a noun in apposition.

Diagnosis. This new species is similar to *Opopaea deserticola* Simon, 1892 in the small booklung covers and morphology of the scuto-pedicel region, but can be distinguished by the large needle-like extension of the epigastric region (Fig. 8H) vs. lacking the needle-like extension (Platnick and Dupérré 2009: fig. 32) and the round tip

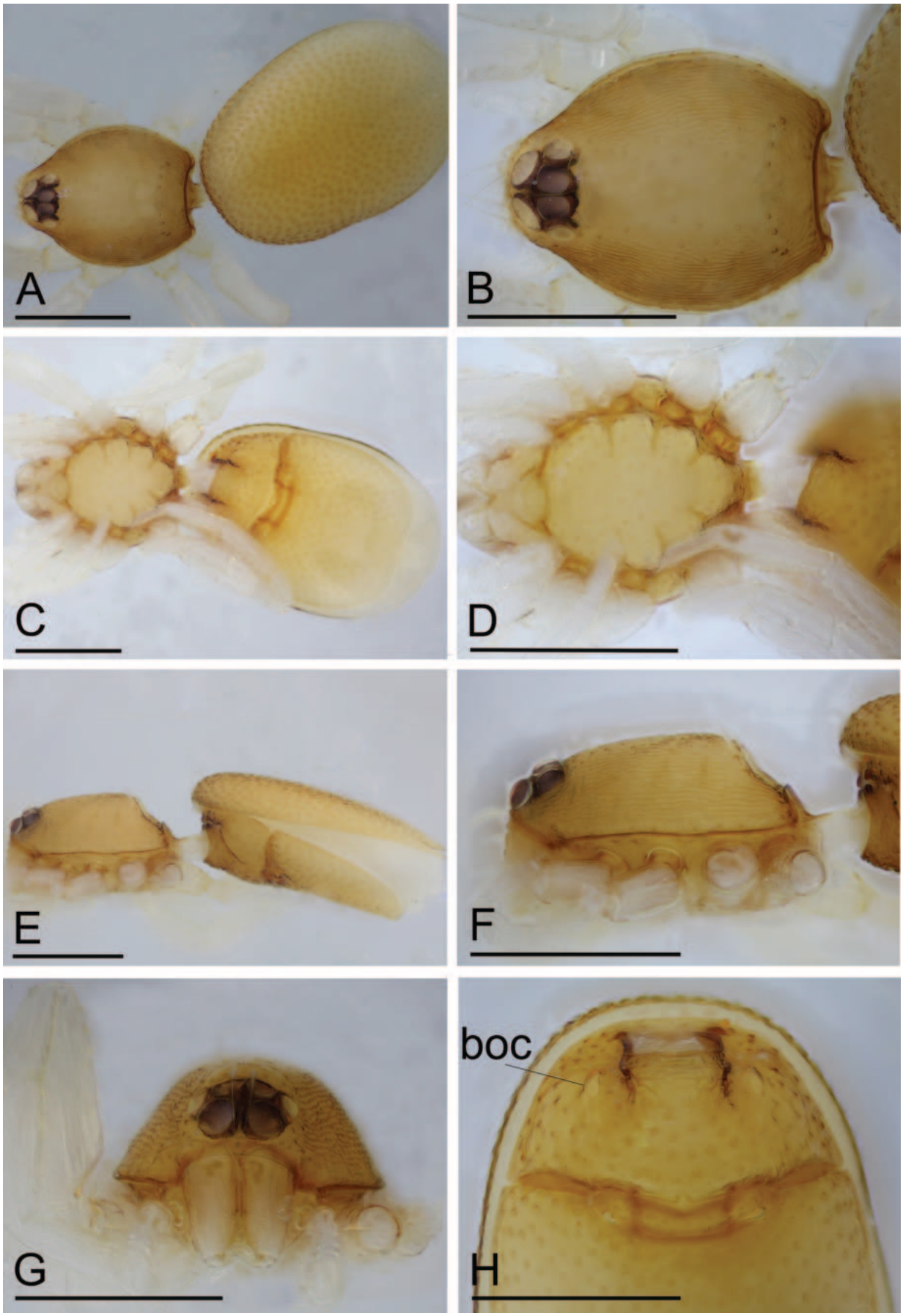

Figure 2. *Opopaea foveolata* Roewer, 1963, female. **A, C, E** Habitus, dorsal, ventral and lateral views; **B, D, F, G** Prosoma, dorsal, ventral, lateral and anterior views; **H** Abdomen, ventral view. Abbreviation: boc = booklung covers. Scale bars: 0.4 mm.

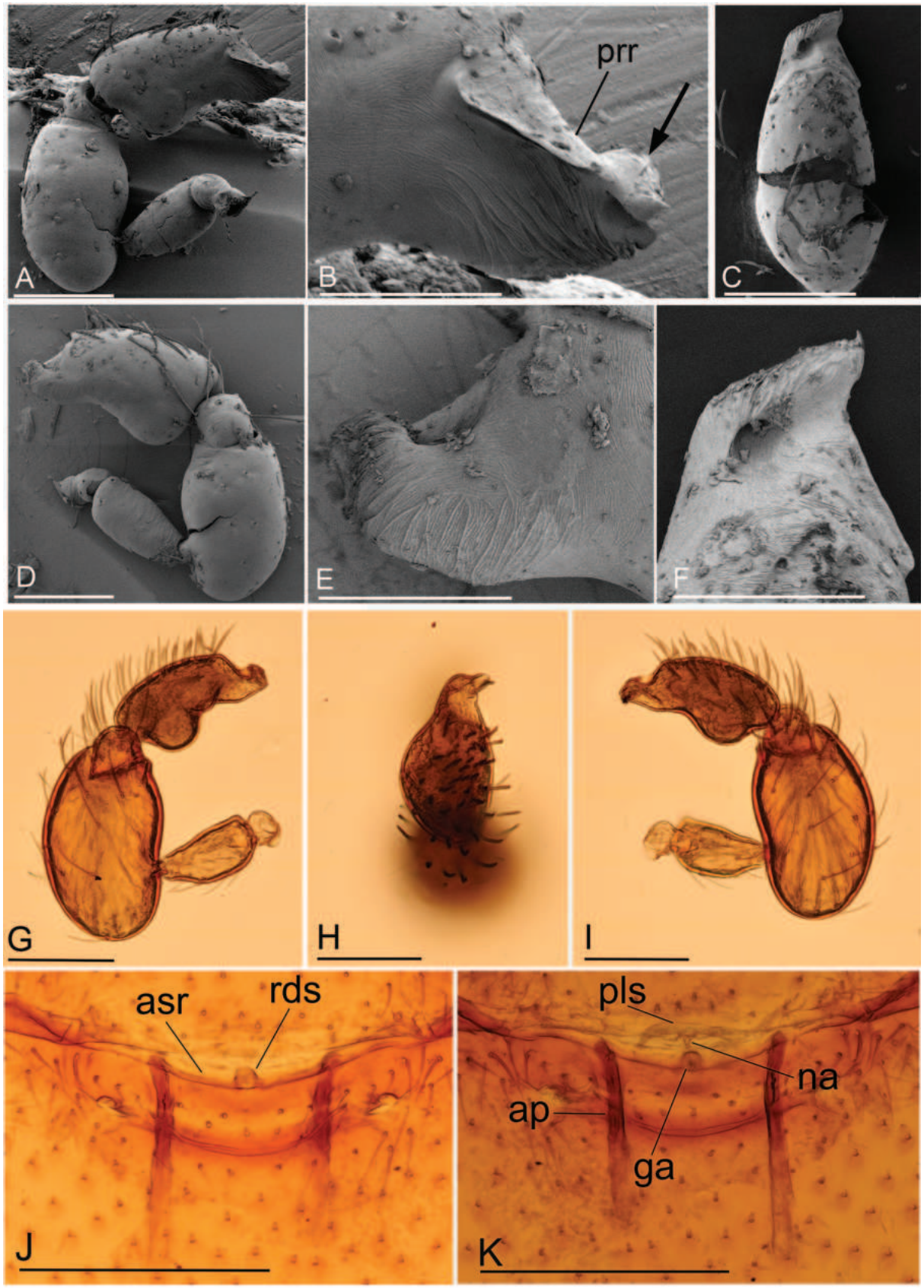

Figure 3. *Opopaea foveolata* Roewer, 1963, male left palp (**A–I)** and female copulatory organ (**J, K**). **A, G** Prolateral view; **B, E, F** Distal part of cymbiobulbus, prolateral, retrolateral and dorsal views, arrow shows the enlarged distal part; **C, H** Dorsal view; **D, I** Retrolateral view; **J** Ventral view; **K** Dorsal view. Abbreviation: ap = apodeme; asr = anterior scutal ridge; ga = globular appendix; na = nail-like process; pls = paddle-like sclerite; prr = prolateral ridge; rds = round dark spot. Scale bars: 0.1 mm (**A, C, D, G–I**); 0.05 mm (**B, E, F**); 0.2 mm (**J, K**).

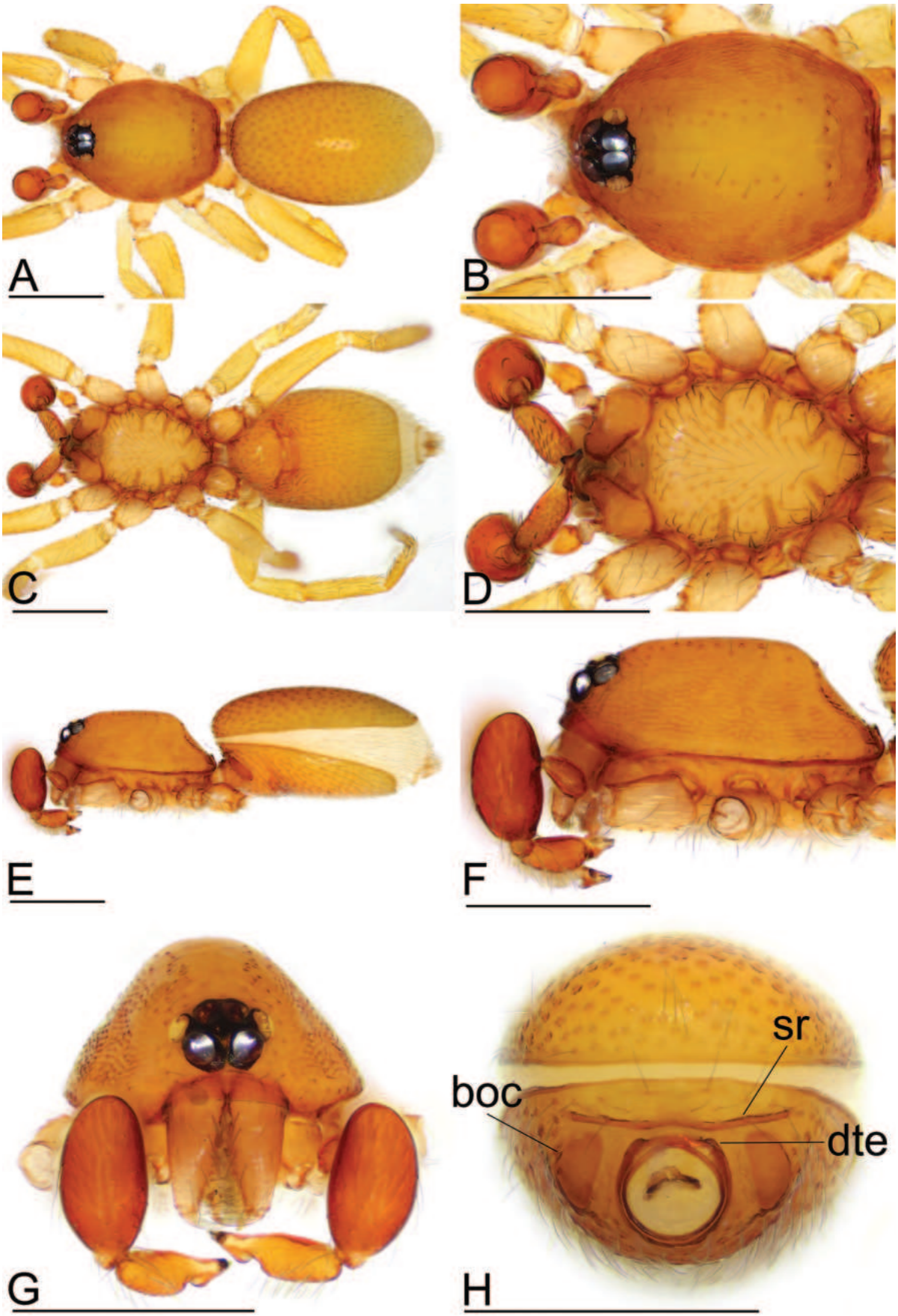

Figure 4. *Opopaea mangun* sp. nov., male. **A, C, E** Habitus, dorsal, ventral and lateral views; **B, D, F, G** Prosoma, dorsal, ventral, lateral and anterior views; **H** Abdomen, anterior view. Abbreviations: boc = booklung covers; dte = dorsolateral, triangular extensions; sr = scutal ridge. Scale bars: 0.4 mm.

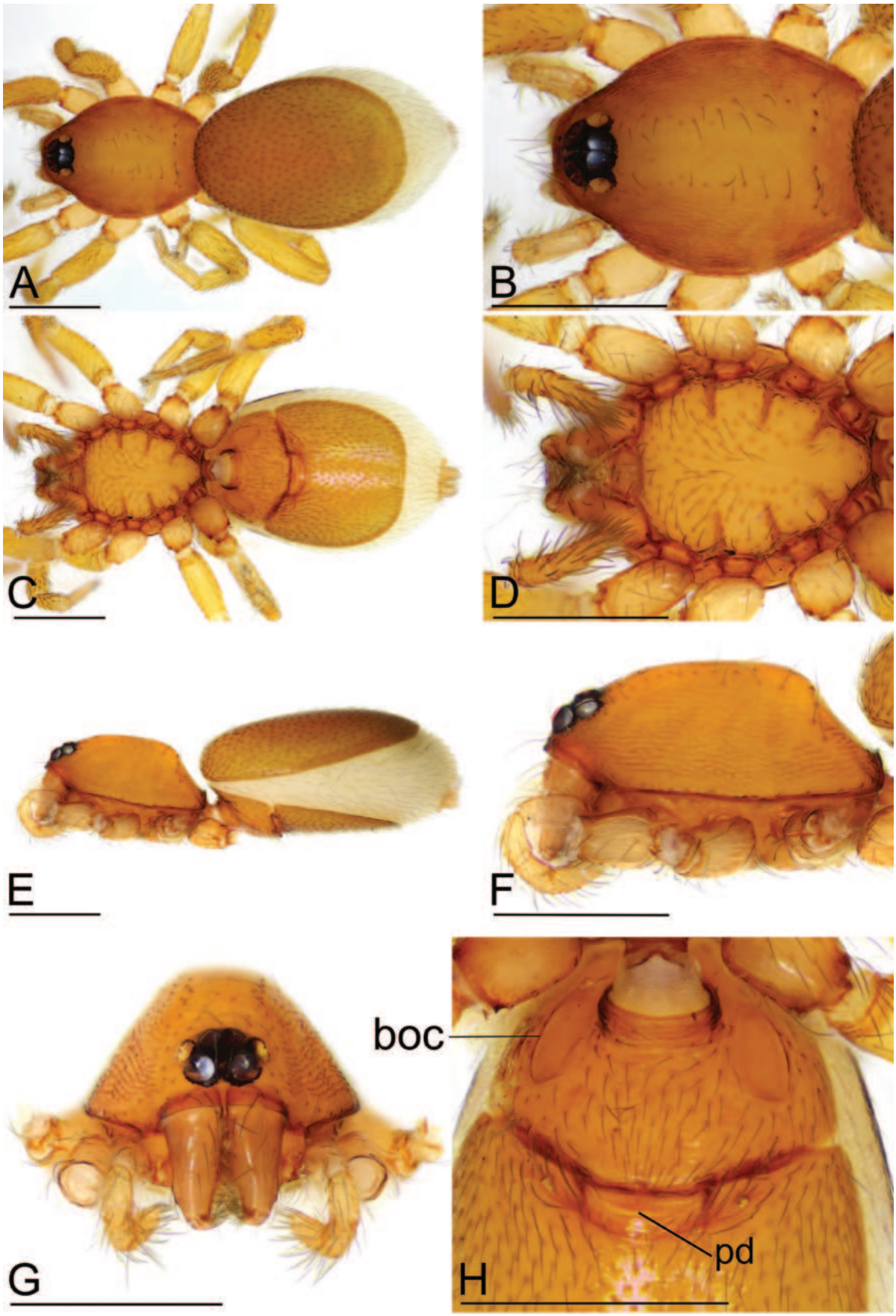

Figure 5. *Opopaea mangun* sp. nov., female. **A, C, E** Habitus, dorsal, ventral and lateral views; **B, D, F, G** Prosoma, dorsal, ventral, lateral and anterior views; **H** Abdomen, ventral view. Abbreviations: boc = booklung covers; pd = postgynal depression. Scale bars: 0.4 mm.

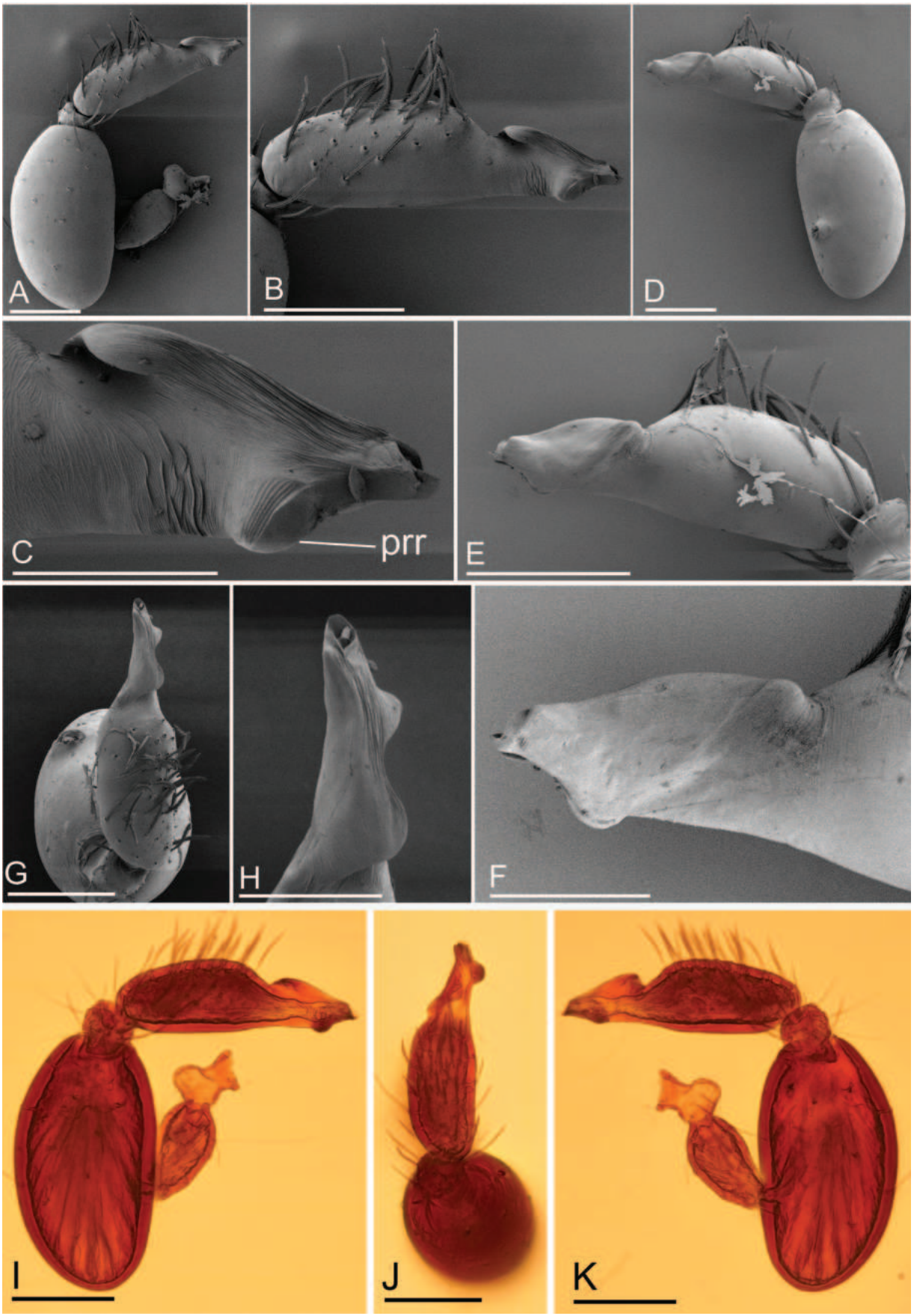

Figure 6. *Opopaea mangun* sp. nov., male left palp. **A, I** Prolateral view; **B, E** Cymbiobulbus, prolateral and retrolateral views; **C, F, H** Distal part of cymbiobulbus, prolateral, retrolateral and dorsal views; **D, K** Retrolateral view; **G, J** Dorsal view. Abbreviation: prr = prolateral ridge. Scale bars: 0.1 mm (**A, B, D, E, G, I–K**); 0.05 mm (**C, F, H**).

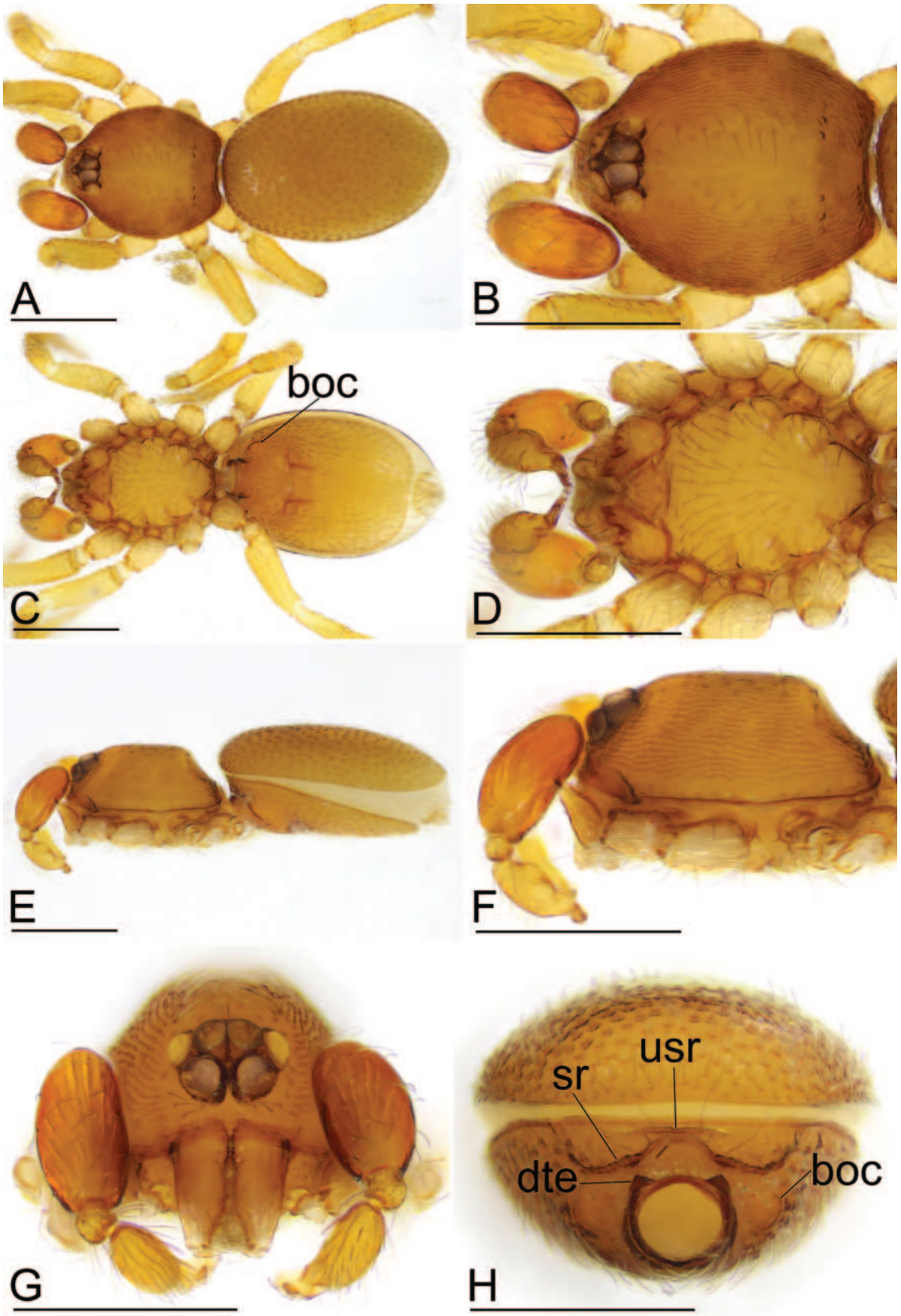

Figure 7. *Opopaea taibao* sp. nov., male. **A, C, E** Habitus, dorsal, ventral and lateral views; **B, D, F, G** Prosoma, dorsal, ventral, lateral and anterior views; **H** Abdomen, anterior view. Abbreviations: boc = booklung covers; dte = dorsolateral, triangular extensions; sr = scutal ridge; usr = upper scutal ridge. Scale bars: 0.4 mm.

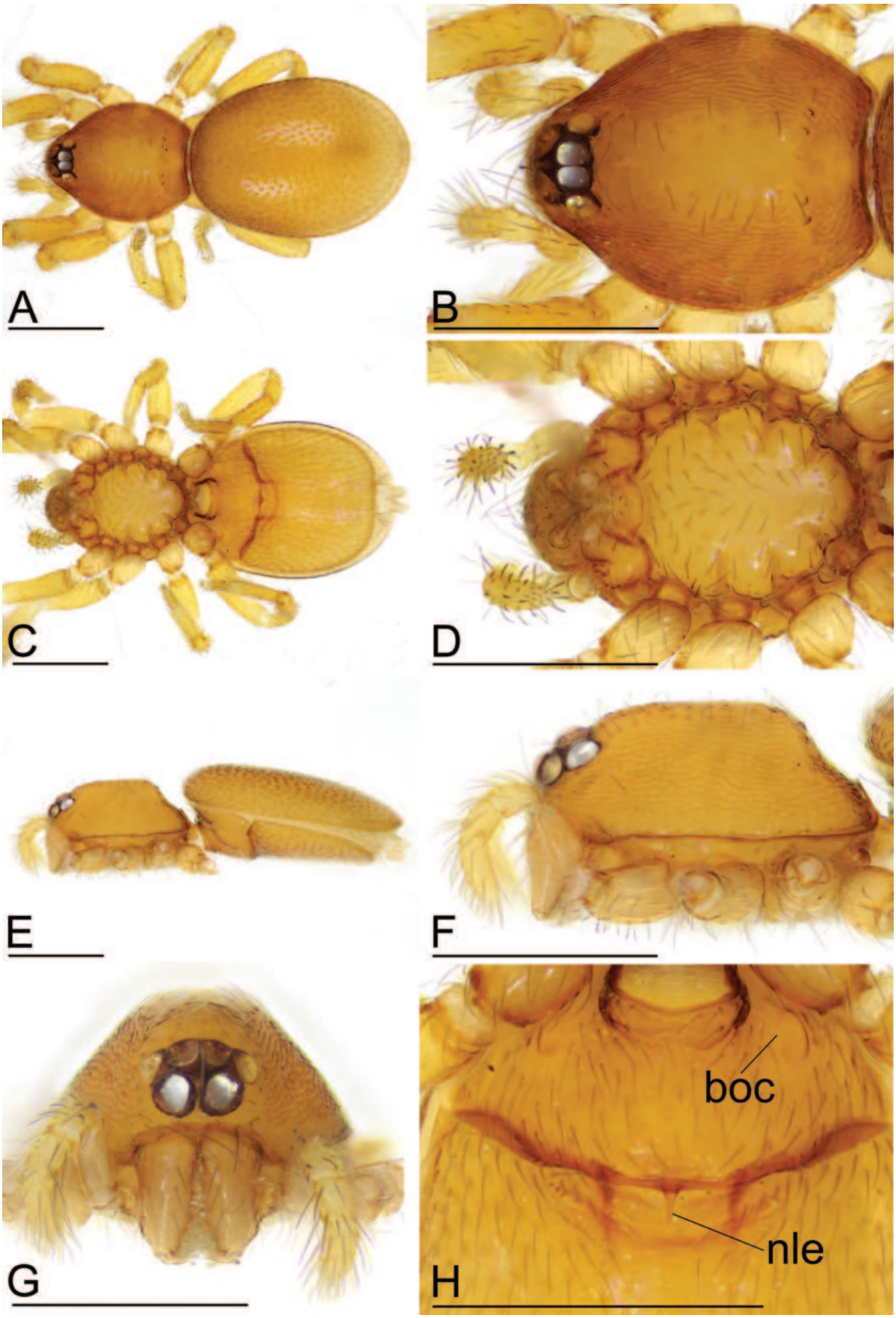

Figure 8. *Opopaea taibao* sp. nov., female. **A, C, E** Habitus, dorsal, ventral and lateral views; **B, D, F, G** Prosoma, dorsal, ventral, lateral and anterior views; **H** Abdomen, ventral view. Abbreviations: boc = booklung covers; nle = needle-like extension. Scale bars: 0.4 mm.

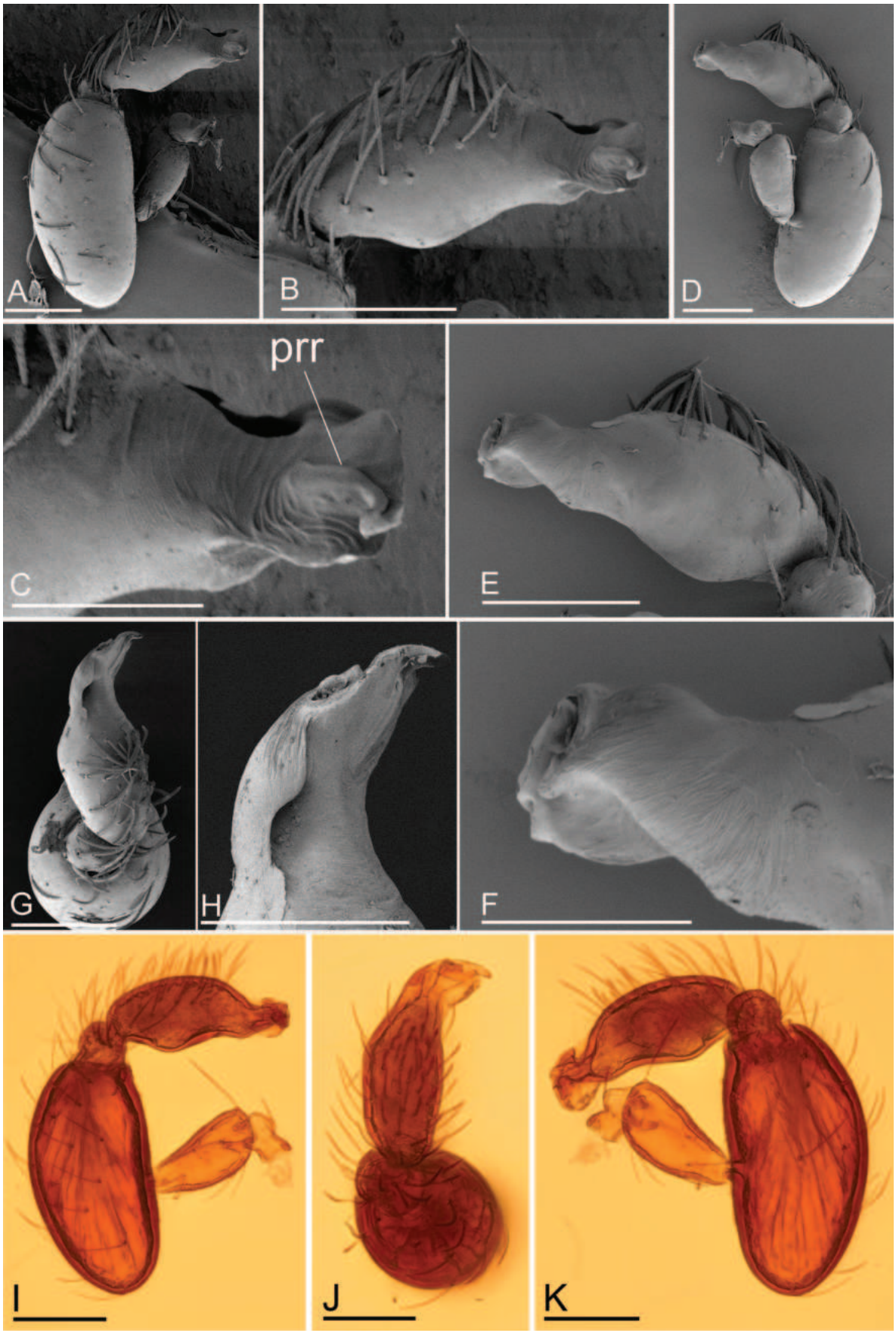

Figure 9. *Opopaea taibao* sp. nov., male left palp. **A, I** Prolateral view; **B, E** Cymbiobulbus, prolateral and retrolateral views; **C, F, H** Distal part of cymbiobulbus, prolateral, retrolateral and dorsal views; **D, K** Retrolateral view; **G, J** Dorsal view. Abbreviation: prr = prolateral ridge. Scale bars: 0.1 mm (**A, B, D, E, G, I–K**); 0.05 mm (**C, F, H**).

of distal part of palp (Fig. 9C, I) vs. narrow tip ventrally expanded (Platnick and Dupérré 2009: figs 55, 64).

Description. Male (holotype). Measurements: TL: 1.47; CL: 0.61; CW: 0.51; AL: 0.86; AW: 0.57; ALE: 0.07; PME: 0.06; PLE: 0.06; EGW: 0.21; ALE-ALE: 0.03; ALE-PLE: 0.01; PME-PME: 0; PLE-PME: 0; CBL: 0.20; CBW: 0.08; PTL: 0.27; FI: 0.11; FML: 0.11. Colouration: legs yellowish, carapace and abdomen yellow, abdominal interscutal areas creamy-white, booklung covers yellowish, pedipalps reddish-brown. Habitus as in Fig. 7A, C, E. Carapace (Fig. 7B, F): oval in dorsal view; sides with longitudinal streaks; median area smooth with rows of setae at lateral edges. Eyes (Fig. 7B, G): ALE largest, PLE and PME nearly equal size; posterior eye row recurved viewed from above, procurved from front; ALE separated by less than their radius, ALE–PLE separated by less than ALE radius, PME touching throughout most of their length, PLE–PME separated by less than PME radius. Clypeus height about 1.0 times ALE diameter (Fig. 7G). Sternum (Fig. 7D) longer than wide, fused to carapace; surface smooth; radial furrows present between coxae I-II, II-III and III-IV, with rows of small pits; endites anteriorly with a small, sharply-pointed projection. Abdomen: booklung covers very small, ovoid, without setae. Pedicel tube short, ribbed, with small, dorsolateral triangular extensions, scuto-pedicel region lower than pedicel diameter, with arched scutal ridges and straight upper scutal ridge (Fig. 7H). Palp (Fig. 9A–K): femur slightly shorter than half length of patella and submedially attached to patella; patella strongly enlarged, elongate oval; tibia small, rounded; cymbiobulbus shorter than the patella; bulb ventrally strongly bulging, tip broad, with prolateral folded ridges (prr).

Female. As in male, except as noted. Measurements: TL: 1.54; CL: 0.62; CW: 0.52; AL: 0.93; AW: 0.68; ALE: 0.07; PME: 0.06; PLE: 0.06; EGW: 0.20; ALE-ALE: 0.03; ALE-PLE: 0.01; PME-PME: 0; PLE-PME: 0. Habitus as in Fig. 8A, C, E. Copulatory organ (Figs 8H, 16C, D): in the middle of the epigastric scutal ridge, there is a needle-like extension (nle); dorsally with nail-like process (na) connected to paddle-like sclerite (pls) bearing long, fork-like arms.

Distribution. Known only from the type locality.

Opopaea wenshan Tong & Zhang, sp. nov.

https://zoobank.org/F0D61E77-D8F5-4161-A6B4-99145DC1A6E1

Figs 10–12, 16E, F, 17

Type material. ***Holotype*****:** ♂ (SYNU-568), **China, Yunnan,** Wenshan Zhuang and Miao Autonomous Prefecture, Funing County, Central National Level Ecological Forest, Z. Li & G. Zhou leg. ***Paratypes*****:** 4♀ (SYNU-565–567, 569), same data as holotype.

Etymology. The specific name refers to the type locality and is a noun in apposition.

Diagnosis. This new species is similar to *Opopaea rigidula* Tong & Li, 2015 in the ear-shaped tip of palpal bulb, but can be distinguished by the triangular protrusion of palpal bulb (Fig. 12C, I) vs. lacking the protrusion (Tong and Li 2015: figs 10A–D), the large prolateral ridge of male palp (Fig. 12A, I) vs. very small (Tong and Li 2015: fig. 10C) and the arch-shaped sclerite of endogyne (Figs 11H, 16E, F) vs. lacking the arch-shaped sclerite (Tong and Li 2015: fig. 12E, F).

Description. Male (holotype). Measurements: TL: 1.83; CL: 0.83; CW: 0.68; AL: 0.99; AW: 0.91; ALE: 0.10; PME: 0.08; PLE: 0.07; EGW: 0.24; ALE-ALE: 0.05; ALE-PLE: 0.01; PME-PME: 0; PLE-PME: 0; CBL: 0.29; CBW: 0.10; PTL: 0.44; FI: 0.21; FML: 0.11. Colouration: legs yellow, carapace and abdomen scuta yellow-brown, abdominal interscutal areas creamy-white, pedipalps reddish-brown. Habitus as in Fig. 10A, C, E. Carapace (Fig. 10A, E): oval in dorsal view; sides with longitudinal streaks; median area smooth with rows of setae at lateral edges. Eyes (Fig. 10A, F): ALE largest, PLE smallest; posterior eye row straight viewed from above, procurved from front; ALE separated by their radius, ALE–PLE separated by less than ALE radius, PME touching throughout most of their length, PLE–PME separated by less than PME radius. Clypeus height about 1.5 times ALE diameter (Fig. 10F). Sternum (Fig. 10C) longer than wide, fused to carapace; surface smooth; radial furrows present between coxae I-II, II-III and III-IV, with rows of small pits; endites anteriorly strongly sclerotised. Abdomen: booklung covers small, ovoid, without setae. Pedicel tube short, ribbed, with small, dorsolateral triangular extensions, scuto-pedicel region lower than pedicel diameter, with arched scutal ridges and curved upper scutal ridge (Fig. 10G). Palp (Fig. 12A–K): femur very small, about 1/4 length of patella and submedially attached to patella; patella strongly enlarged, elongate oval; tibia small, rounded; cymbiobulbus shorter than the patella; bulb ventrally slightly bulging, dorsally with one triangular protrusion, tip ear-shaped, with two largely-folded ridges.

Female. As in male, except as noted. Measurements: TL: 2.00; CL: 0.81; CW: 0.65; AL: 1.19; AW: 0.87; ALE: 0.07; PME: 0.06; PLE: 0.05; EGW: 0.22; ALE-ALE: 0.05; ALE-PLE: 0.01; PME-PME: 0; PLE-PME: 0. Habitus as in Fig. 11A, C, E. Copulatory organ (Figs 11H, 16E, F): posterior margin of epigastric scutal ridge smooth; dorsally with nail-like process (na) connected to paddle-like sclerite (pls); with an arch shaped sclerite (ass).

Distribution. Known only from the type locality.

Opopaea yuhuang Tong & Li, sp. nov.

https://zoobank.org/7BF565FE-8C35-428E-83D1-71C987896683

Figs 13–15, 16G, H, 17

Type material. ***Holotype*****:** ♂ (SYNU-596), **China, Yunnan,** Mile City, Yuhuang Park, 20 November 2021, W. Cheng leg. ***Paratypes*****:** 1♀ (SYNU-597), 2♂2♀ (SYNU-619–622), same data as holotype.

Etymology. The specific name refers to the type locality and is a noun in apposition.

Diagnosis. This new species is similar to *Opopaea syarakui* (Komatsu, 1967) in the morphology of the scu-

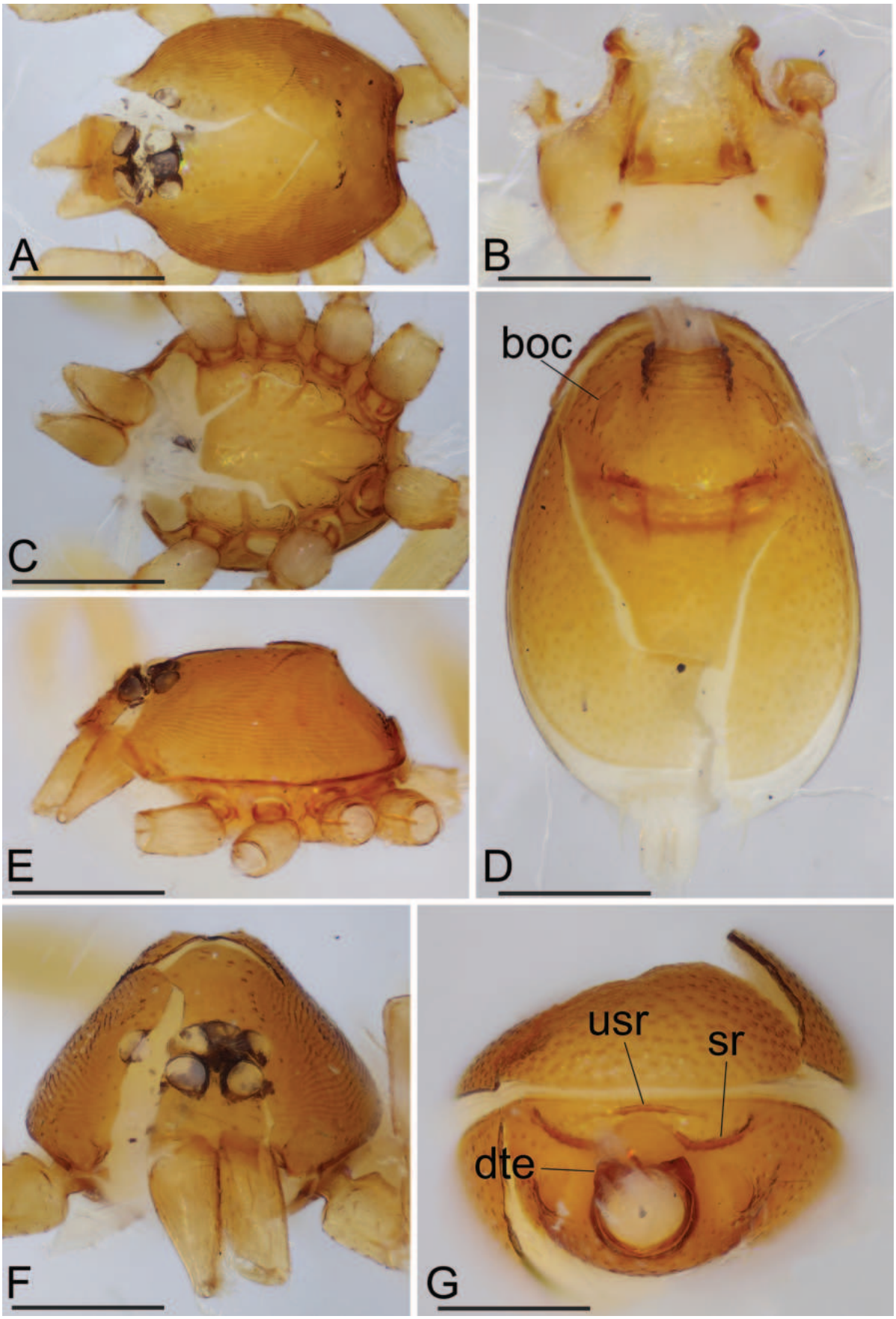

Figure 10. *Opopaea wenshan* sp. nov., male. **A, C, E, F** Prosoma, dorsal, ventral, lateral and anterior views; **B** Labium and endites, ventral view; **D, G** Abdomen, ventral and anterior views. Abbreviations: boc = booklung covers; dte = dorsolateral, triangular extensions; sr = scutal ridge; usr = upper scutal ridge. Scale bars: 0.4 mm.

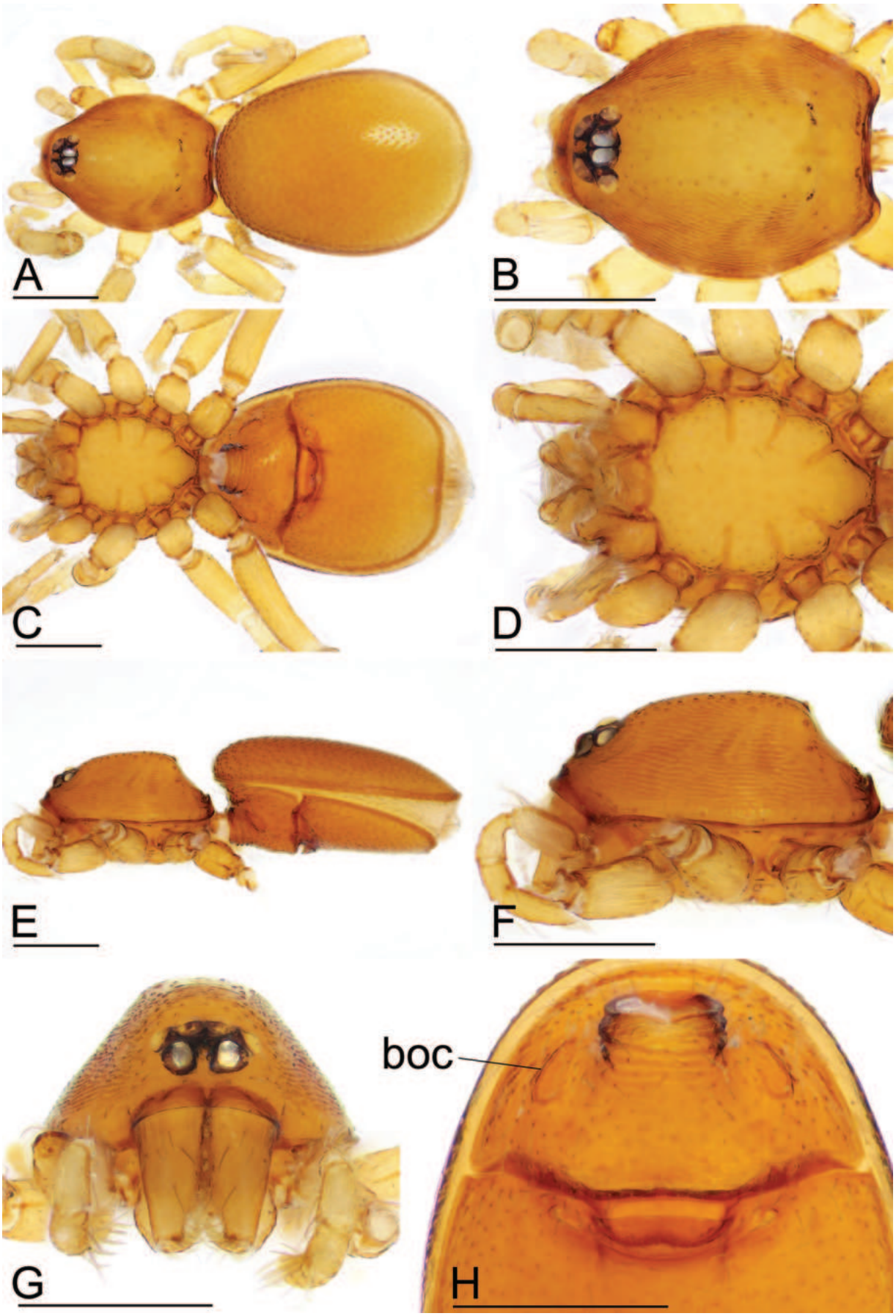

Figure 11. *Opopaea wenshan* sp. nov., female. **A, C, E** Habitus, dorsal, ventral and lateral views; **B, D, F, G** Prosoma, dorsal, ventral, lateral and anterior views; **H** Abdomen, ventral view. Abbreviation: boc = booklung covers. Scale bars: 0.4 mm.

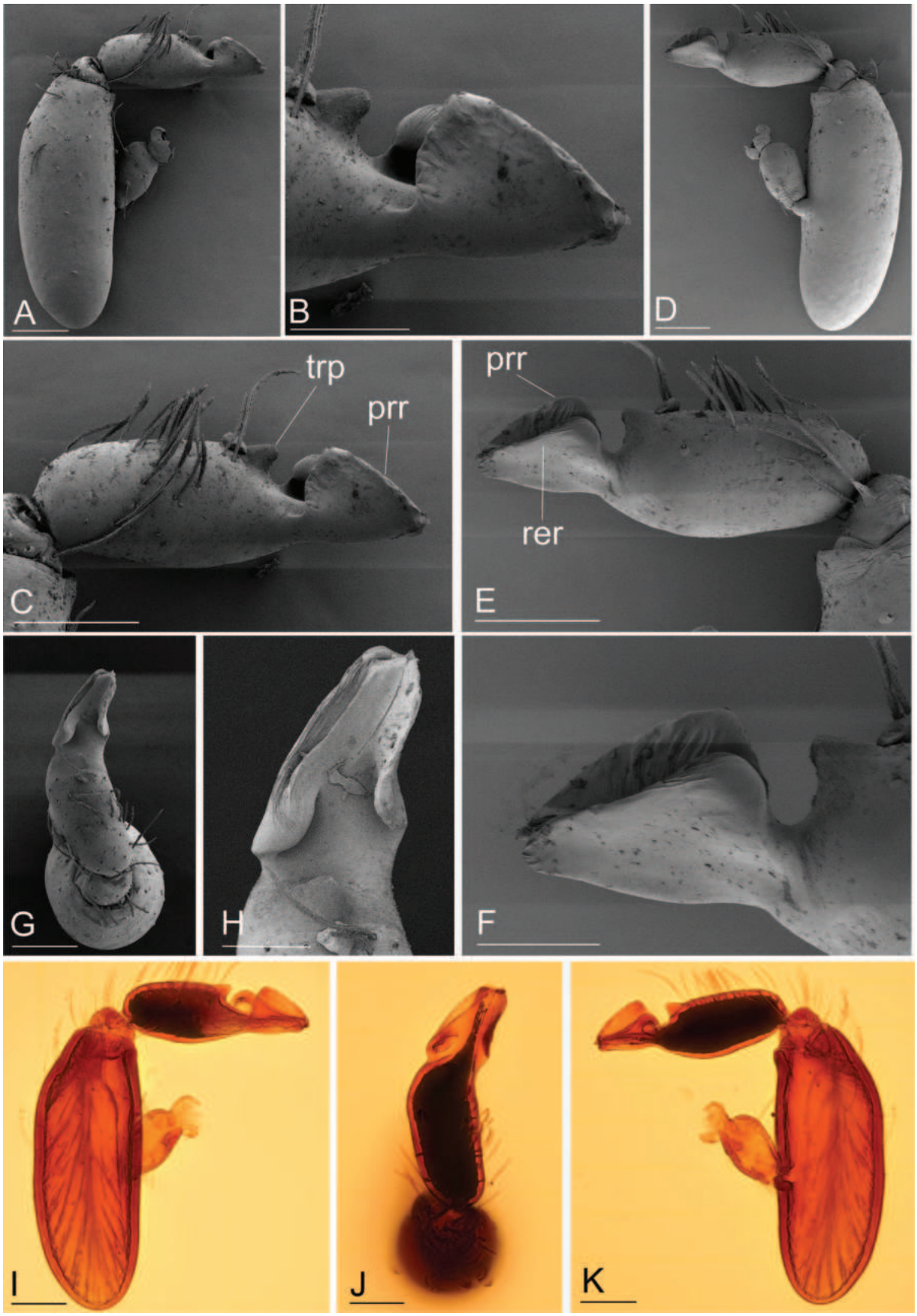

Figure 12. *Opopaea wenshan* sp. nov., male left palp. **A, I** Prolateral view; **B, F, H** Distal part of cymbiobulbus, prolateral, retrolateral and dorsal views; **C, E** Cymbiobulbus, prolateral and retrolateral views; **D, K** Retrolateral view; **G, J** Dorsal view. Abbreviations: prr = prolateral ridge; rer = retrolateral ridge; trp = triangular protrusion. Scale bars: 0.1 mm (**A, C–E, G, I–K**); 0.05 mm (**B, F, H**).

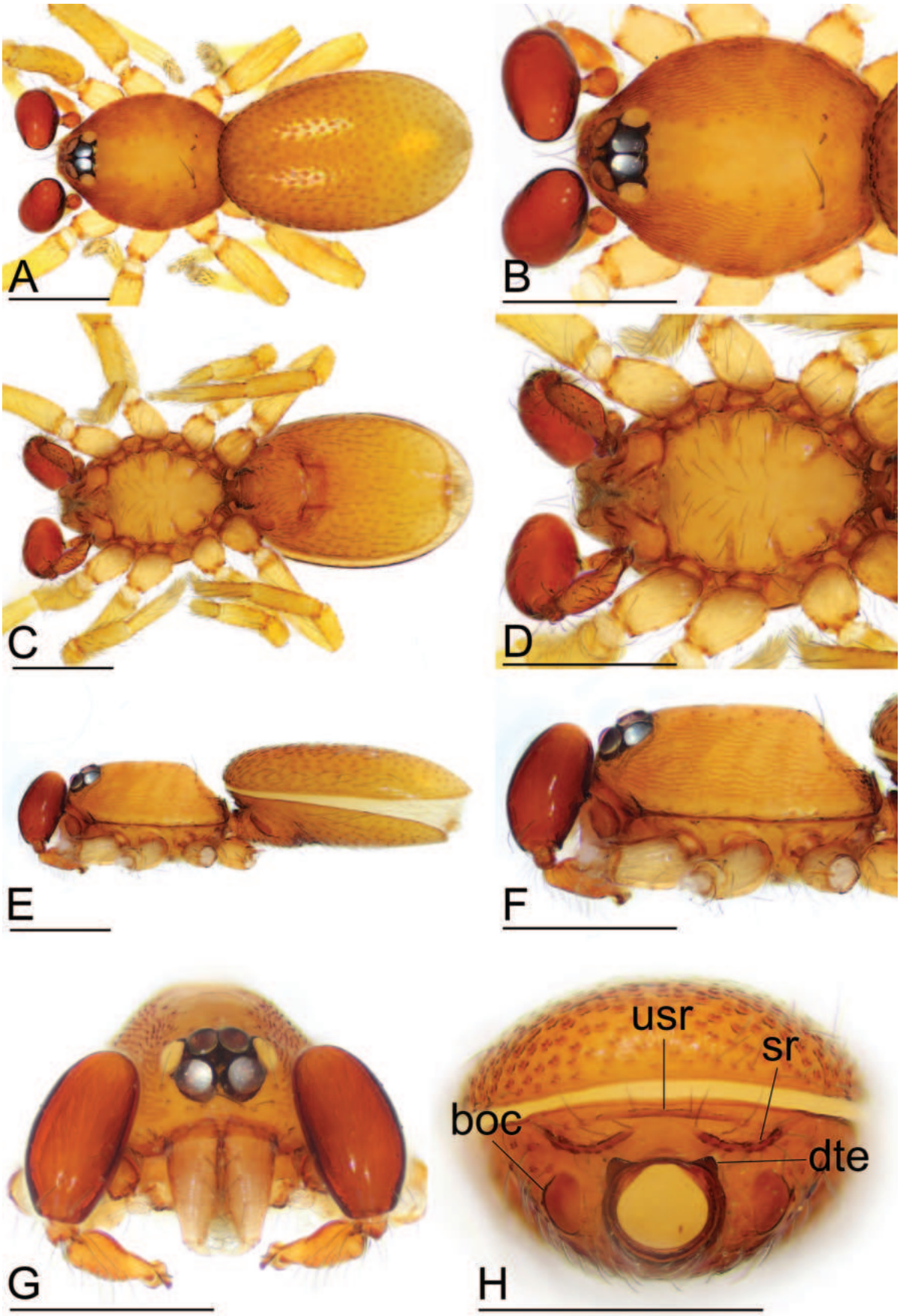

Figure 13. *Opopaea yuhuang* sp. nov., male. **A, C, E** Habitus, dorsal, ventral and lateral views; **B, D, F, G** Prosoma, dorsal, ventral, lateral and anterior views; **H** Abdomen, anterior view. Abbreviations: boc = booklung covers; dte = dorsolateral, triangular extensions; sr = scutal ridge; usr = upper scutal ridge. Scale bars: 0.4 mm.

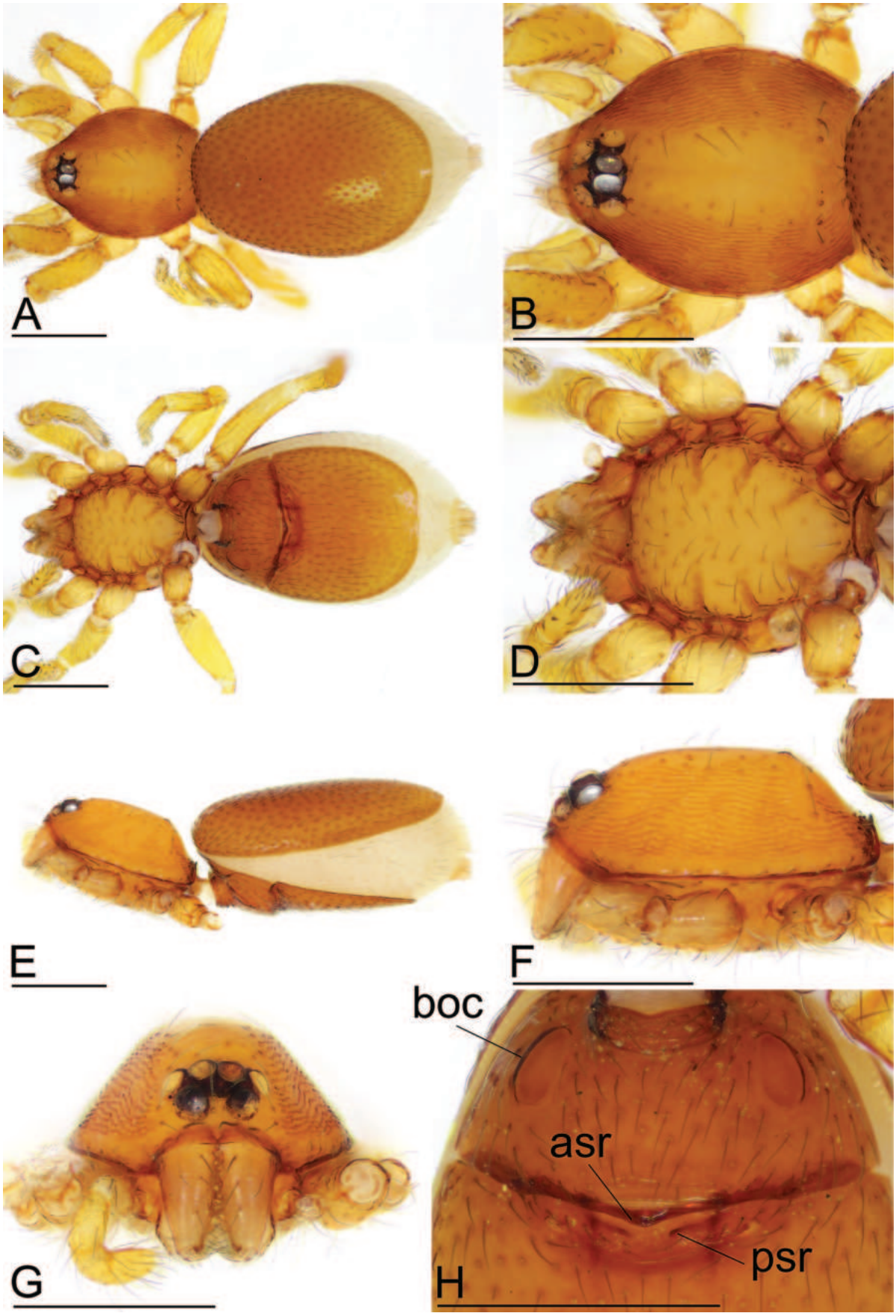

Figure 14. *Opopaea yuhuang* sp. nov., female. **A, C, E** Habitus, dorsal, ventral and lateral views; **B, D, F, G** Prosoma, dorsal, ventral, lateral and anterior views; **H** Abdomen, ventral view. Abbreviations: asr = anterior scutal ridge; boc = booklung covers; psr = posterior scutal ridge. Scale bars: 0.4 mm.

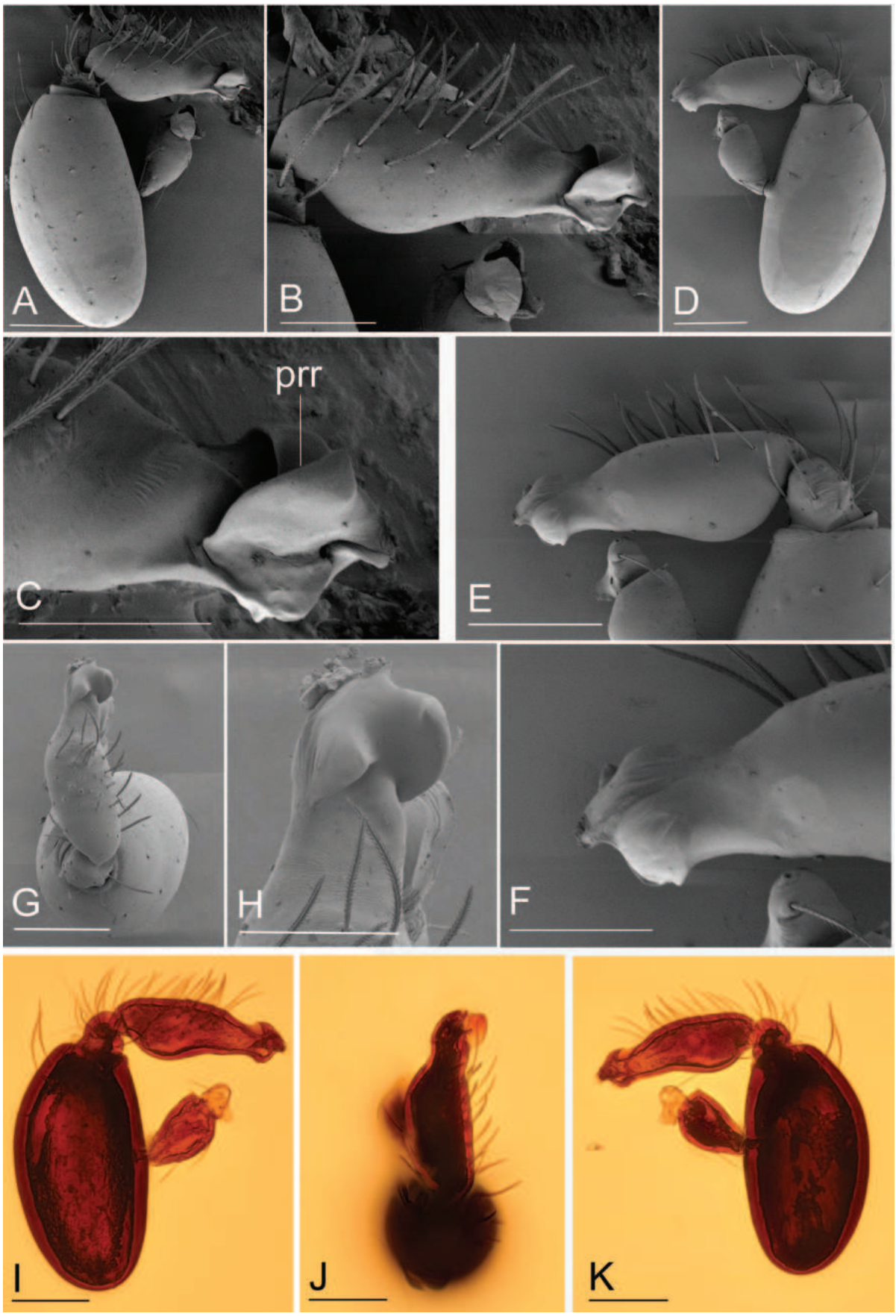

Figure 15. *Opopaea yuhuang* sp. nov., male left palp. **A, I** Prolateral view; **B, E** Cymbiobulbus, prolateral and retrolateral views; **C, F, H** Distal part of cymbiobulbus, prolateral, retrolateral and dorsal views; **D, K** Retrolateral view; **G, J** Dorsal view. Abbreviation: prr = prolateral ridge. Scale bars: 0.1 mm (**A, B, D, E, G, I–K**); 0.05 mm (**C, F, H**).

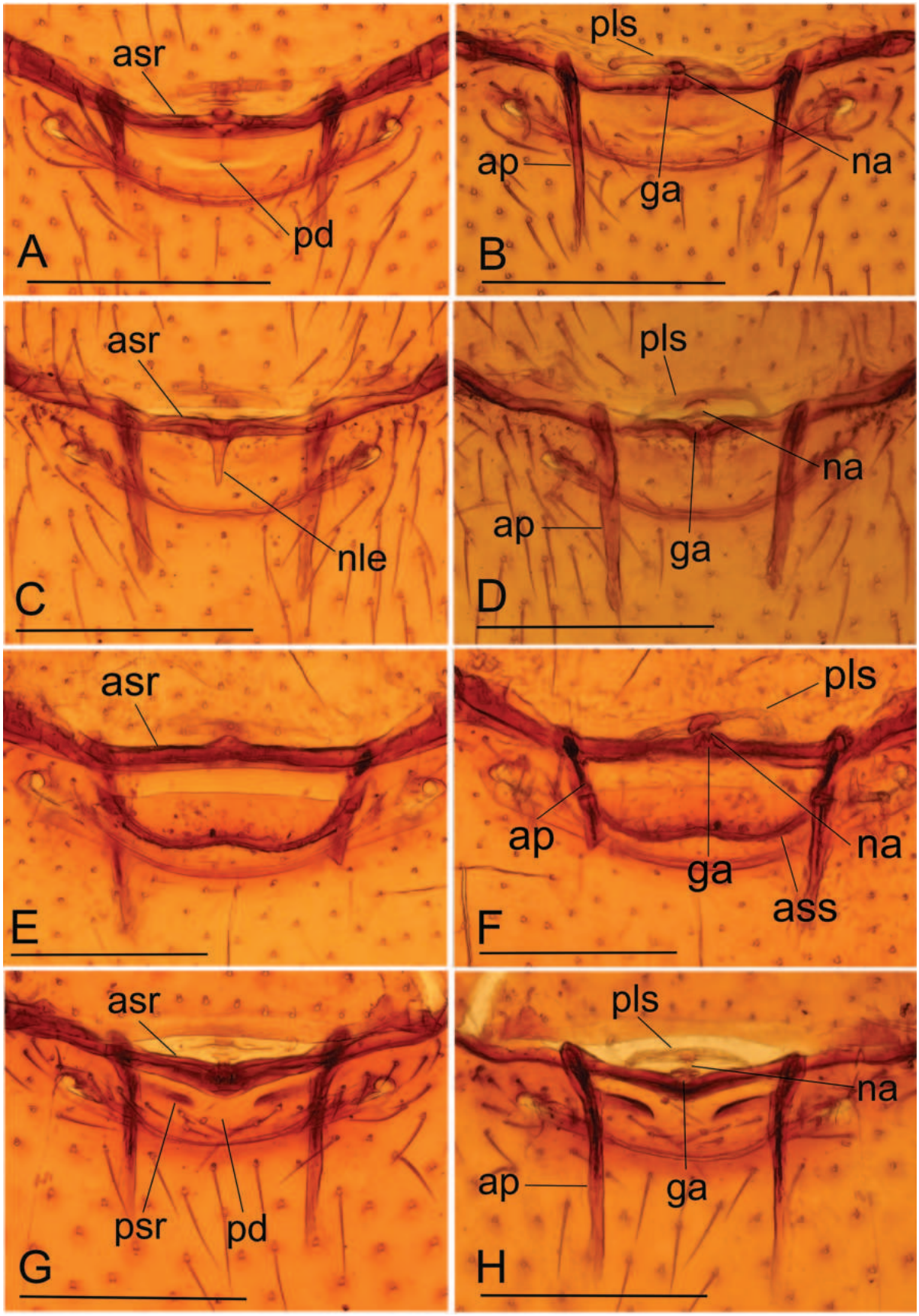

Figure 16. Female copulatory organ. **A, B** *Opopaea mangun* sp. nov.; **C, D** *Opopaea taibao* sp. nov.; **E, F** *Opopaea wenshan* sp. nov.; **G, H** *Opopaea yuhuang* sp. nov.; **A, C, E, G** Ventral view; **B, D, F, H** Dorsal view. Abbreviations: ap = apodeme; asr = anterior scutal ridge; ass = arch-shaped sclerite; ga = globular appendix; na = nail-like process; nle = needle-like extension; pd = postgynal depression; pls = paddle-like sclerite; psr = posterior scutal ridge. Scale bars: 0.2 mm.

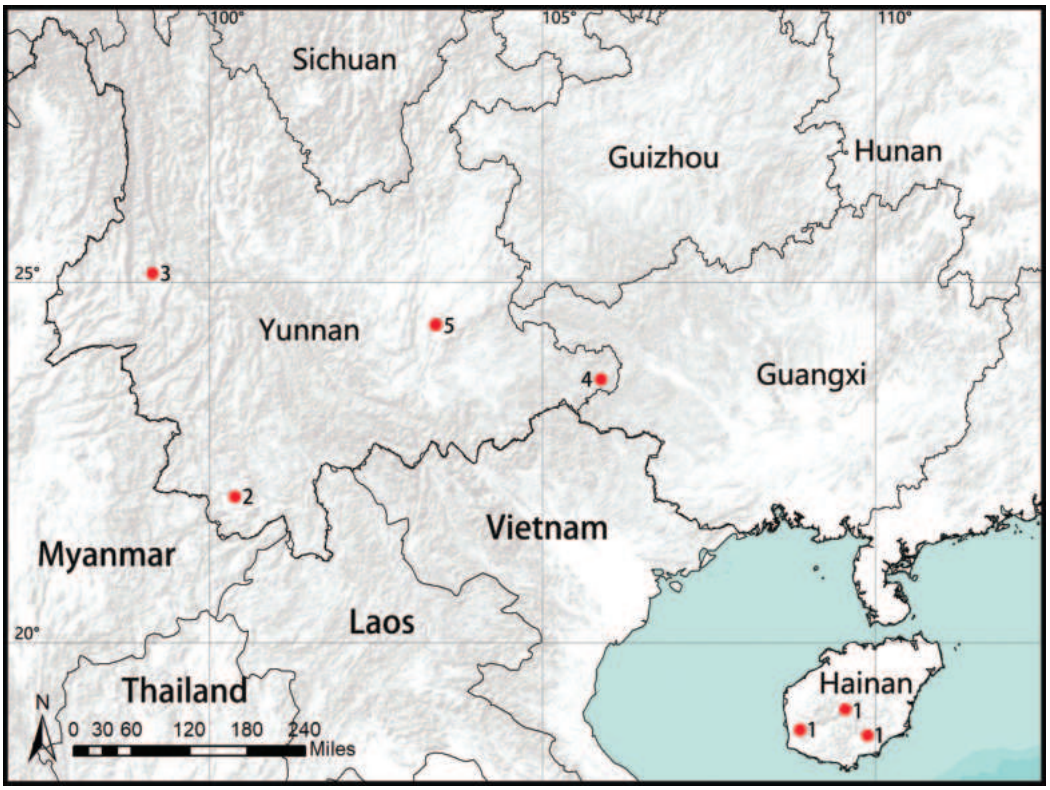

Figure 17. Distribution records of four new species and one newly-recorded species from southern China. **1.** *Opopaea foveolata* Roewer, 1963; **2.** *Opopaea mangun* sp. nov.; **3.** *Opopaea taibao* sp. nov.; **4.** *Opopaea wenshan* sp. nov.; **5.** *Opopaea yuhuang* sp. nov.

to-pedicel region and the triangular postgynal depression, but can be distinguished by the interrupted posterior scutal ridge (Fig. 14H) vs. not interrupted (Suzuki et al. 2023: fig. 5O) and the broad tip of palpal bulb (Fig. 15A, I) vs. gradually narrowed tip (Suzuki et al. 2023: fig. 5K).

Description. Male (holotype). Measurements: TL: 1.65; CL: 0.69; CW: 0.55; AL: 1.02; AW: 0.64; ALE: 0.08; PME: 0.07; PLE: 0.07; EGW: 0.22; ALE-ALE: 0.03; ALE-PLE: 0.01; PME-PME: 0; PLE-PME: 0; CBL: 0.21; CBW: 0.08: PTL: 0.31; FI: 0.18; FML: 0.09. Colouration: yellow, abdominal interscutal areas creamy-white, booklung covers brown, pedipalps reddish-brown. Habitus as in Fig. 13A, C, E. Carapace (Fig. 13B, F): oval in dorsal view; sides with longitudinal streaks; median area smooth with rows of setae at lateral edges. Eyes (Fig. 13B, G): ALE largest, PLE smallest; posterior eye row recurved viewed from above, procurved from front; ALE separated by less than their radius, ALE–PLE separated by less than ALE radius, PME touching throughout most of their length, PLE–PME separated by less than PME radius. Clypeus height about 1.0 times ALE diameter (Fig. 13G). Sternum (Fig. 13D) longer than wide, fused to carapace; surface smooth; radial furrows present between coxae I-II, II-III and III-IV, with rows of small pits; endites anteriorly with a small, sharply-pointed projection. Abdomen: booklung covers large, ovoid, without setae. Pedicel tube short, ribbed, with small, dorsolateral triangular extensions, scuto-pedicel region lower than pedicel diameter, with arched scutal ridges, interrupted medially, with straight upper scutal ridge (Fig. 13H). Palp (Fig. 15A–K): femur small, about 1/4 length of patella and medially attached to patella; patella strongly enlarged, elongate oval; tibia small, rounded; cymbiobulbus shorter than the patella; bulb ventrally strongly bulging, tip broad, with a large prolateral folded ridge (prr).

Female. As in male, except as noted. Measurements: TL: 1.84; CL: 0.68; CW: 0.56; AL: 1.21; AW: 0.74; ALE: 0.07; PME: 0.06; PLE: 0.06; EGW: 0.21; ALE-ALE: 0.04; ALE-PLE: 0.01; PME-PME: 0; PLE-PME: 0. Habitus as in Fig. 14A, C, E. Copulatory organ (Figs 14H, 16G, H): posterior margin of epigastric scutal ridge (asr) smoothly triangular, posterior scutal ridge (psr) adjacent to asr, interrupted medially, postgynal depression (pd) small; dorsally with nail-like process (na) connected to paddle-like sclerite (pls).

Distribution. Known only from the type locality.

Acknowledgements

The manuscript benefitted greatly from comments by Danilo Harms (Hamburg, Germany), Zhiyuan Yao (Shenyang, China) and one anonymous referee. This study was supported by the National Natural Science Foundation of China (NSFC-32370479, 31972867).

References

Andriamalala D, Hormiga G (2013) Systematics of the goblin spider genus *Opopaea* (Araneae, Oonopidae) in Magagascar. Bulletin of the American Museum of Natural History 380: 1–156. https://doi.org/10.1206/828.1

Baehr BC, Harvey MS, Smith HM, Ott R (2013) The goblin spider genus *Opopaea* in Australia and the Pacific islands (Araneae: Oonopidae). Memoirs of the Queensland Museum. Nature 58: 107–338. https://doi.org/10.17082/j.2204-1478.58.2013.2013-11

Brignoli PM (1974) On some Oonopidae from Japan and Formosa (Araneae). Acta Arachnologica 25(2): 73–85. https://doi.org/10.2476/asjaa.25.73

Henrard A, Jocqué R (2012) An overview of Afrotropical canopy-dwelling *Orchestina* (Araneae, Oonopidae), with a wealth of remarkable sexual dimorphic characters. Zootaxa 3284(1): 1–104. https://doi.org/10.11646/zootaxa.3284.1.1

Lin Y, Wu L, Cai D, Li S, Barrion AT, Heong KL (2023) Review of 43 spider species from Hainan Island, China (Arachnida, Araneae). Zootaxa 5351(5): 501–533. https://doi.org/10.11646/zootaxa.5351.5.1

Platnick NI, Dupérré N (2009) The goblin spider genera *Opopaea* and *Epectris* (Araneae, Oonopidae) in the New World. American Museum Novitates 3649: 1–43. https://doi.org/10.1206/664.1

Ranasinghe UGSL, Benjamin SP (2018) Three new species of *Aprusia* (Araneae: Oonopidae) from Sri Lanka with a phylogenetic analysis of the genus. Journal of Natural History 52(11–12): 713–738. https://doi.org/10.1080/00222933.2018.1444803

Roewer CF (1963) Araneina: Orthognatha. Labidognatha. Insects of Micronesia 3(4): 105–132.

Suzuki Y, Hidaka R, Tatsuta H (2023) Revision of goblin spiders (Araneae: Oonopidae) in the Nansei Islands, southwest Japan, with description of a new species. Zootaxa 5323(2): 216–242. https://doi.org/10.11646/zootaxa.5323.2.3

Tong Y (2013) Haplogynae spiders from Hainan, China. Science Press, Beijing, 96 pp. [81 pl.]

Tong Y, Li S (2010) The goblin spiders of the genus *Opopaea* (Araneae, Oonopidae) in Hainan Island, China. Zootaxa 2327(1): 23–43. https://doi.org/10.11646/zootaxa.2327.1.2

Tong Y, Li S (2014) A survey of oonopid spiders in Taiwan with descriptions of three new species. ZooKeys 396: 67–86. https://doi.org/10.3897/zookeys.396.7033

Tong Y, Li S (2015) Six new species of the genus *Opopaea* Simon, 1891 from Xishuangbanna Rainforest, southwestern China (Araneae: Oonopidae). Zootaxa 3931(1): 41–62. https://doi.org/10.11646/zootaxa.3931.1.3

Tong Y, Chen Z, Li S (2020) Two new species of the genus *Opopaea* (Araneae, Oonopidae) from Myanmar. ZooKeys 917: 51–61. https://doi.org/10.3897/zookeys.917.48924

WSC (2024) World Spider Catalog. Version 25.0. Natural History Museum Bern. http://wsc.nmbe.ch [Accessed on 17 January 2024]

Zoosyst. Evol. 100 (2) 2024, 349–356 | DOI 10.3897/zse.100.118766

PENSOFT

für Natur MUSEUM FÜR NATURKUNDE BERLIN

Is *Garra rezai* (Teleostei, Cyprinidae) a species known only from two widely disjunct areas in the Tigris drainage?

Cüneyt Kaya[1], Haydar Birol İmre[1], Irmak Kurtul[2,3]

1 *Recep Tayyip Erdogan University, Faculty of Fisheries, Rize, Turkiye*

2 *Marine and Inland Waters Sciences and Technology Department, Faculty of Fisheries, Ege University, İzmir, Turkiye*

3 *Department of Life and Environmental Sciences, Faculty of Science and Technology, Bournemouth University, Poole, Dorset, UK*

https://zoobank.org/BFB5D65B-79BA-4091-8C8D-E3EF568E4890

Corresponding author: Cüneyt Kaya (cnytkaya@yahoo.com)

Academic editor: Nicolas Hubert ♦ **Received** 14 January 2024 ♦ **Accepted** 13 March 2024 ♦ **Published** 27 March 2024

Abstract

Garra rezai was recently described from two geographically distant areas in the Tigris drainage: upper Yanarsu River (eastern Türkiye) and Bouein-Sofla Creek (Iran). In the scope of this study, we aimed to ascertain the distribution ranges of *G. rezai* and its morphologically most similar congener *G. rufa* in Türkiye by examining 1165 specimens from 73 lots, which were collected between 1957 and 2023 and currently curated in two broad fish collections. To achieve this, we focused on two important diagnostic morphological characters which distinguish these two species: scales on predorsal mid-line between dorsal-fin origin and nape, and branched dorsal-fin rays. The results revealed that *G. rufa* is a widely distributed species in the Tigris-Euphrates catchment, while *G. rezai* is regionally widespread, with populations identified in at least six different regions within the Tigris catchment. Additionally, *G. rezai* is documented for the first time in the upper Euphrates. Furthermore, we identified the drainage areas where *G. rezai* co-exists with *G. rufa*.

Key Words

Asia Minor, biodiversity, distribution, fish fauna, Mesopotamia

Introduction

Fish taxonomy, which provides a foundation for scientific research, involves the classification and naming of fish species. Taxonomy helps identify and document different species; it is also essential tasks for assessing biodiversity, tracking changes in populations and implementing effective conservation strategies (Mace 2004). Different species of *Garra* Hamilton, 1822 have gained popularity for their use in spa treatments. These species are also known as doctor fish or nibble fish. They are small freshwater fish belonging to the family Cyprinidae (Ruane et al. 2013; Aydın and Akhan 2020). Although they are not considered threatened or endangered on a global scale (Freyhof 2014), some threats such as habitat degradation and pollution might impact their populations.

Garra is one of the largest genera of the family Cyprinidae, containing approximately 150 species (Majeed et al. 2019). The species belonging to this genus are small to medium-sized fish which usually live in the bottom of fast-flowing rivers and mountain streams. However, some small-sized species of the genus *Garra* - which were previously considered under the genus *Hemigrammocapoeta* Pellegrin, 1927 - prefer vegetated and relatively more stagnant habitats. Approximately a decade ago, *Hemigrammocapoeta* was considered as a synonym of the genus *Garra* by Behrens-Chapuis et al. (2015). *Garra* is widely distributed from east, southeast, south and southwest Asia to tropical Africa (Zhang and Chen 2002; Kottelat 2020).

Garra rufa (Heckel, 1843) was traditionally considered to be distributed in Tigris, Euphrates, Orontes, Ceyhan and

Seyhan areas (Demirci et al. 2016; Ergüden 2016; Kaya et al. 2016; Bayçelebi 2020). However, after the revalidation of *Garra turcica* in Seyhan and Ceyhan (Bayçelebi et al. 2018) and the description of *Garra orontesi* Bayçelebi, Kaya, Turan & Freyhof, 2021 in Orontes (Bayçelebi et al. 2021), it was demonstrated that distribution of *G. rufa* is restricted to Persian Gulf Basin. Until 2022, only two species were known to occur in the upper Tigris-Euphrates River system. However, *Garra rezai* Mousavi-Sabet, Eagderi, Saemi-Komsari, Kaya & Freyhof, 2022 was recently described from the upper Yanarsu River (eastern Türkiye) and Bouein-Sofla Creek (Iran), drainage areas of the Tigris River (Mousavi-Sabet et al. 2022). Surprisingly, the two localities are over 450 km apart.

Another interesting point about *Garra rezai* is its similarity to its two congeneric species (*Garra variabilis* (Heckel, 1843) and *G. rufa*) distributed in the Euphrates-Tigris catchment. Although *G. rezai* is morphologically closer to *G. rufa*, it is genetically closer to *G. variabilis*, which has one pair of barbels, a small mental disc and a comparatively different body shape.

The description of *Garra rezai* raised some questions: Is this species a threatened species with a very limited range? Is *G. rezai* restricted to these two localities, or is it more widespread? Are *G. rezai* and *G. rufa* sympatric/syntopic?

Overall, the aims of this study are: i) to investigate the morphologically-based diagnostic characters of *G. rezai* and *G. rufa*, ii) to reveal the distribution of these species in Türkiye and iii) to answer the above-mentioned questions by analysing samples from two broad fish collections.

Materials and methods

In order to determine the distribution ranges of *Garra rufa* and *G. rezai* in Türkiye, 1165 specimens from 73 lots (Suppl. material 1) were examined from the Recep Tayyip Erdogan University Zoology Collection of the Faculty of Fisheries (FFR) and Collection of Ege University Faculty of Fisheries (ESFM). Material was examined in ESFM collected by electro-fishing and hand scoops between 1957 and 1997 and those in FFR collected with DC electro-fishing equipment between 2005 and 2023.

Since both collection samples were fixed in formaldehyde, it was not possible to perform a molecular study. However, considering the critical diagnostic characters (scales on predorsal mid-line between dorsal-fin origin and nape [PreDs]; branched dorsal fin rays [DFR]; total gill rakers on first branchial arch [GR]) determined by Mousavi-Sabet et al. (2022), many samples preserved in FFR and ESFM were examined.

In this sense, DFR and PreDs were counted for all specimens found in FFR and ESFM. In cases where the species could not be identified with these two critical diagnostic characters, individuals were identified by counting GR, the third critical diagnostic character. The reason why GR could not be counted in all specimens is that the gill covers are less open and the gill arches are smaller in *Garra* spp. compared to other species, so that the gill lamella has to be removed and dissection from the upper and lower parts of the operculum opening has to be performed in order to count the gill spines. However, the collection authorities did not consent to the partial dissection of over a thousand *Garra* specimens in the FFR and ESFM that were part of the study. The counting methods were followed as described by Armbruster (2012).

Results

As a result, we determined that *Garra rufa* is still a widespread species in the Tigris-Euphrates catchment and *G. rezai* is regionally widespread, with populations in at least six different regions in the Tigris. Furthermore, *G. rezai* is recorded for the first time in the upper Euphrates. Our study indicates that *G. rufa* is considerably more widespread compared to *G. rezai*. Based on the collections examined in this study, *G. rufa* was observed in almost the entire Euphrates, except in the trout zones and throughout the Tigris, except in the Great Zap, Hezil and the eastern part of the Botan. The presence of *G. rufa* in the Menfez Stream near Hezil, as well as in the drainage areas flowing into Botan from the north (Destumi and Bitlis streams), suggests the possibility of *G. rufa* inhabiting the eastern side of Botan and Hezil. However, none of the specimens examined in the Great Zap in this study was identified as *G. rufa*. These assumptions, of course, require confirmation, especially through molecular studies.

On the other hand, it was observed that *G. rezai* is more dominant in all regions of the Tigris where these two species have sympatric distribution. However, in Kaynarca Stream, the only sympatric area in the Euphrates, *G. rufa* was dominant (Fig. 1). This may be attributed to *G. rezai*'s preference for clean and shallow streams rather than large rivers. Kaynarca Stream, dominated by *G. rufa*, is larger and more turbid compared to streams dominated by *G. rezai* in the Tigris. In summary, based on the data obtained from this study, we can assume that, in areas where these two species co-exist, *G. rezai* is dominant in clear, shallow and small streams, whereas *G. rufa* is dominant in turbid, large and relatively deep streams. Sympatric comparison of *G. rufa* and *G. rezai* in Kaynarca, Menfez, Botan and Yanarsu drainage areas are presented in Fig. 2.

Family Cyprinidae

***Garra rufa* (Heckel, 1843)**

Fig. 3

Common names. Doctor fish.

Diagnosis. *Garra rufa* is distinguished from all the species of *Garra* in adjacent waters in having a combination of the following characters: Breast and belly covered by scales, scales embedded in skin, rarely ab-

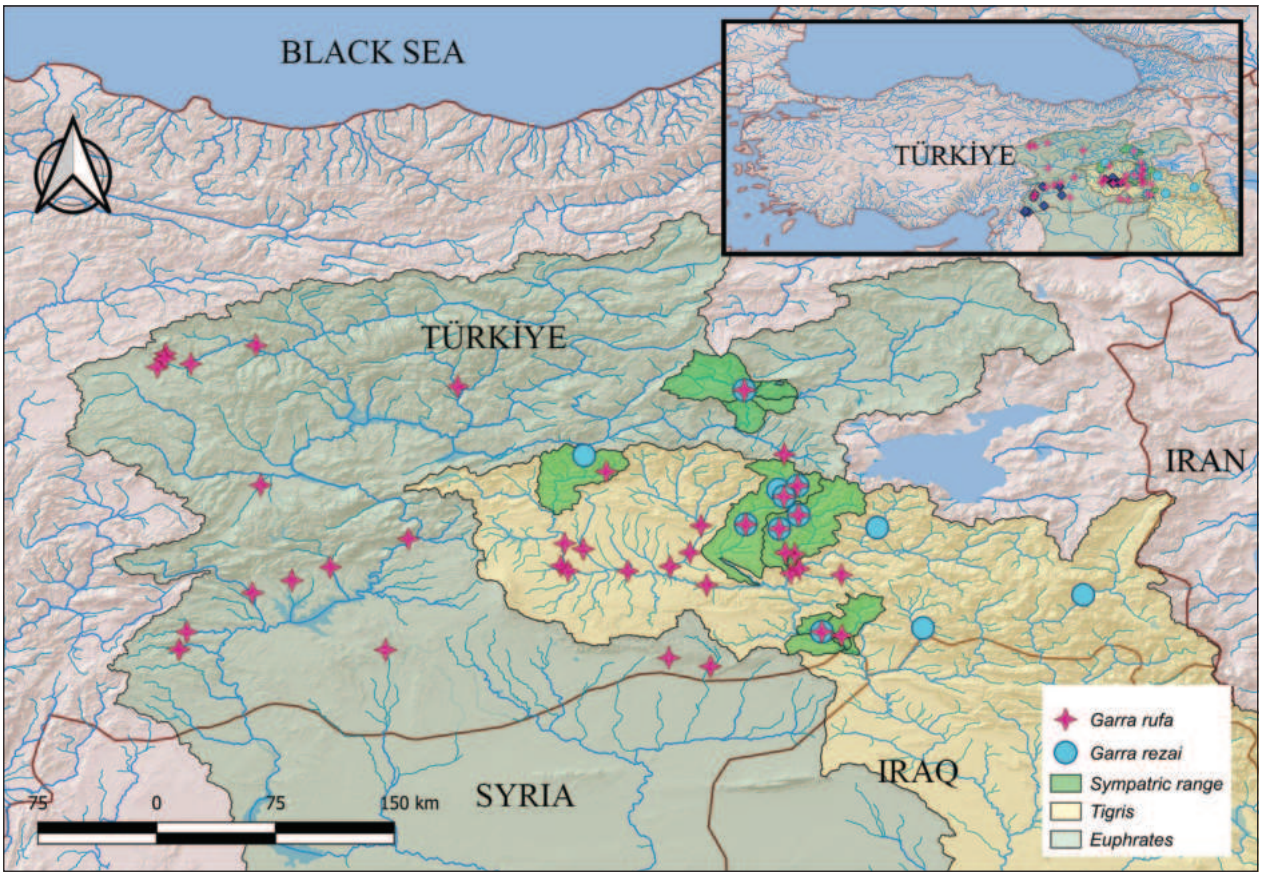

Figure 1. Distribution of the *Garra rufa* and *G. rezai* in Türkiye.

sent, mid-dorsal area in front of dorsal origin covered by (8)9–12(13–14) scales, 32–38 total lateral-line scales, usually 4½ transverse scale rows between lateral line and dorsal origin, 11–13 circumpeduncular scales, 20–29 total gill rakers, usually 8½ branched dorsal rays, eye fully developed.

Distribution in Türkiye. Extirpated in Qweik, does not occur in Lakes Van and Hazar. Very widespread in Euphrates. Widespread also in Tigris, but no specimens could be observed from the Great Zap, Hezil Stream and the eastern part of the Botan in FFR and EFSM.

IUCN Status. Least Concern (Freyhof 2014).

Garra rezai Mousavi-Sabet, Eagderi, Saemi-Komsari, Kaya & Freyhof, 2022

Fig. 3

Common names. Tigris garra.

Diagnosis. *Garra rezai* is distinguished from all the species of *Garra* in adjacent waters in having a combination of the following characters: Breast with embedded scales, predorsal mid-line covered by (12)13–18(19–21) scales, gular disc short and wide, 35–40 total lateral-line scales, 5½(rarely 4½ and 6½) transverse scale rows between lateral line and dorsal origin, 3½–4½ transverse scale rows between lateral line and pelvic origin, 15–18 circumpeduncular scales, axillary scale at pelvic origin large, 11–16 total gill rakers, usually 7½ branched dorsal rays, eye fully developed.

Distribution in Türkiye. Known only from Kaynarca Stream (Murat drainage) in Euphrates. In Tigris; Yanarsu, Botan, Menfez, Hezil and Batman drainages, as well as from Aktoprak Stream, an uppermost drainage of Tigris River.

IUCN Status. Not Evaluated. The results of this study revealed that *G. rezai* is distributed in at least seven different drainage areas in Türkiye. Although *G. rezai* is known from only one locality in Iran outside Türkiye, we expected it to inhabit also other localities in Iran, Iraq and possibly Syria. In summary, this species occurs in various drainage areas and, in general, its populations appear to be in good condition; its IUCN status is suggested to be Least Concern.

Intermediate specimens

Amongst all 73 lots, we had difficulty in identifying only five samples from the Aktoprak Stream station (FFR1821, n = 23). A total 18 of these samples were easily recognised as *G. rezai* with 12(3), 13(3), 14(2), 15(5), 17(4), 20(1) PreDs and 7½(16), 8½(2) DFR ranges. However, five individuals (later moved to another lot with a new collection code: FFR 4062) with 9(1), 11(3), 17(1) PreDs and 7½ (2), 8½ (3) DFR ranges did not match either *G. rufa* or *G. rezai* and

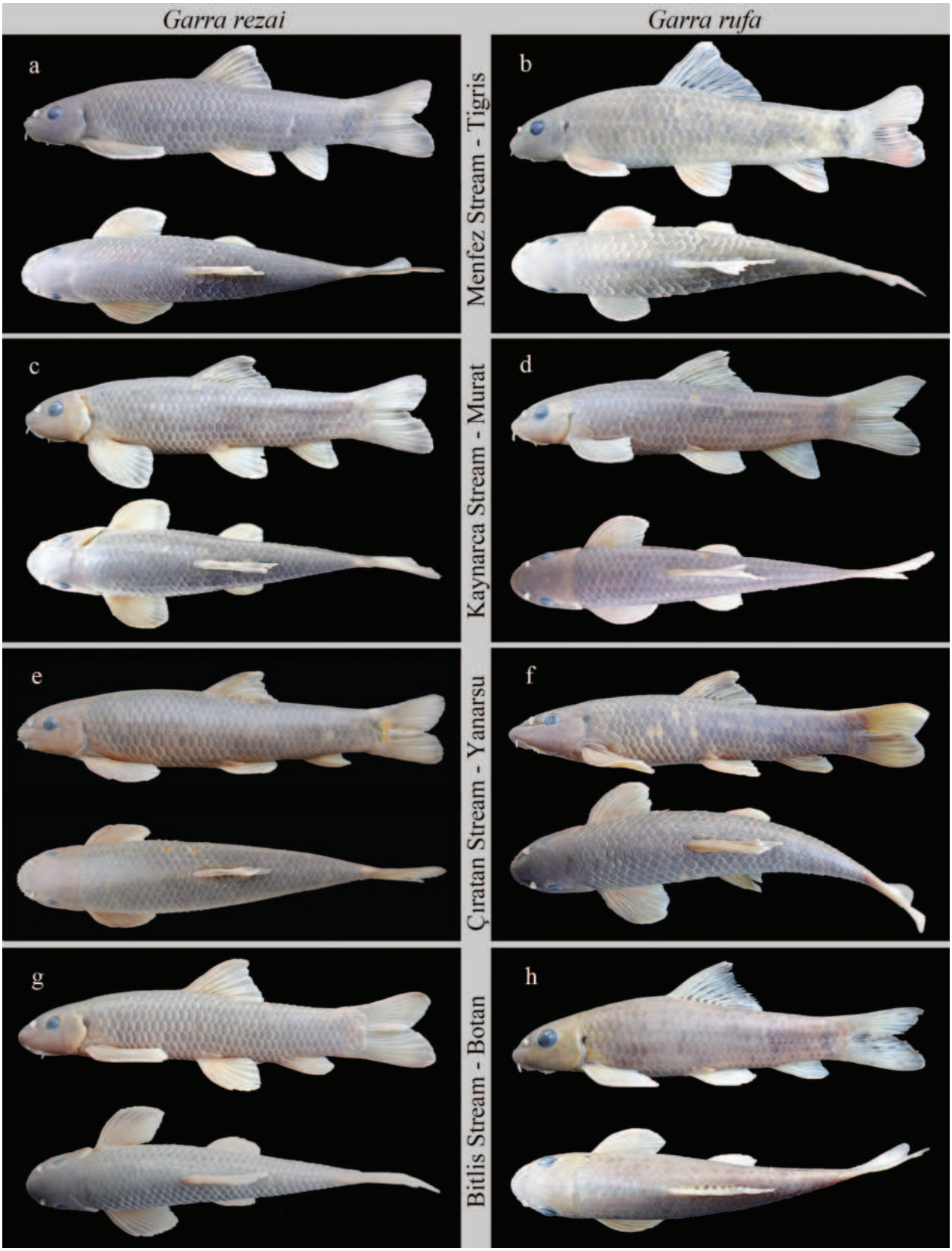

Figure 2. Sympatric comparison of *G. rufa* and *G. rezai*: Menfez Stream, Tigris drainage: (**a**) *G. rezai*, FFR 4044, 86 mm SL, (**b**) *G. rufa*, FFR 4044, 84 mm SL; Kaynarca Stream, Murat drainage, Euphrates, (**c**) *G. rezai*, FFR 4061, 70 mm SL, (**d**) *G. rufa*, FFR 1340, 69 mm SL; Çıratan Stream, Yanarsu drainage, Tigris, (**e**) *G. rezai*, FFR 1302, 113 mm SL, (**f**) *G. rufa*, FFR 4037, 125 mm SL; Bitlis Stream, Botan drainage, Tigris, (**g**) *G. rezai*, FFR 1274, 75 mm SL, (**h**) *G. rufa*, FFR 1348, 72 mm SL.

Figure 3. Upper one, *G. rufa*, not preserved, about 110 mm SL, from Merzimen Stream, Euphrates drainage: Lower one, *G. rezai*, FSJF 3824, 104 mm SL; Türkiye: Çıratan Stream, upper Yanarsu drainage, Tigris (Retrieved from Mousavi-Sabet et al. (2022)).

the values were grouped between the two species. Although GRs were analysed for control, these individuals did not match either species. The most notable example was an individual with 17 PreDs and 8½ DFR, which was expected to be *G. rezai*; however, it moved the individual closer to *G. rufa* with 20 GR (GR range of *G. rufa* is 20–29). Therefore, here we identified these five individuals as *Garra* sp. (Fig. 4). We encourage researchers to further study these populations, especially using molecular markers.

Discussion

Mousavi-Sabet et al. (2022) distinguished *Garra rezai* from *G. rufa* by a minimum K2P distance of 14.9% in the mtDNA COI barcode region, as well as the following morphologic characters: *G. rezai* is distinguished from *G. rufa* by having 11–16 total gill rakers [GR] (vs. 20–29), 15–19 scales on predorsal mid-line between dorsal-fin origin and nape [PreDs] (vs. 11–14), 7½ (rarely 8½) branched dorsal-fin rays [DFR] (vs. usually 8½, rarely 7½ or 9½), 15–18 circumpeduncular scales (vs. 11–13), 5½ (rarely 4½ and 6½) and transverse scale rows between the lateral line and the dorsal-fin origin (vs. 4½). Here, we selected the most diagnostic and easily distinguishable two characters: PreDs and DFR.

Based on the two critical diagnostic characters focused on in this study, Mousavi-Sabet et al. (2022) examined 25 *G. rezai* individuals for PreDs and counted as 15–19 [15(2), 16(3), 17(10), 18(8), 19(2)], while they examined 58 individuals for DFR [7½(54), 8½(4)]. In order to determine to what extent these characters are realistic and to reveal to which species the identified specimens belong, 1165 specimens preserved in FFR and ESFM were examined. Our morphological examination demonstrated that 1016 of these specimens belong to *G. rufa*, while 149 belong to *G. rezai* (Table 1 and Suppl. material 1). Our preliminary results are in agreement with Mousavi-Sabet et al. (2022) ranges for PreDs and DFR, even if they are partially expanded and the mode value of *G. rezai* changed. According to our comprehensive examination, PreDs range was (8)9–12(13–14) with mode 10 in 1016 *G. rufa* specimens and (12)13–18(19–21) with mode 15 in 149 *G. rezai* specimens (see Table 1 and Fig. 5 for details). Mousavi-Sabet et al. (2022) identified the PreDs range of *G. rezai* as 15–19 with a mode of 17. For DFR range of our results, we found (7½)8½(9½) in 1016 *G. rufa* specimens and 7½(8½) in 149 *G. rezai* specimens (see Table 1 and Fig. 5 for details).

Figure 4. Some intermediate specimens: FFR 4062, Aktoprak Stream, upper Tigris drainage, from the top, 65 mm SL, 67 mm SL, 69 mm SL, 71 mm SL.

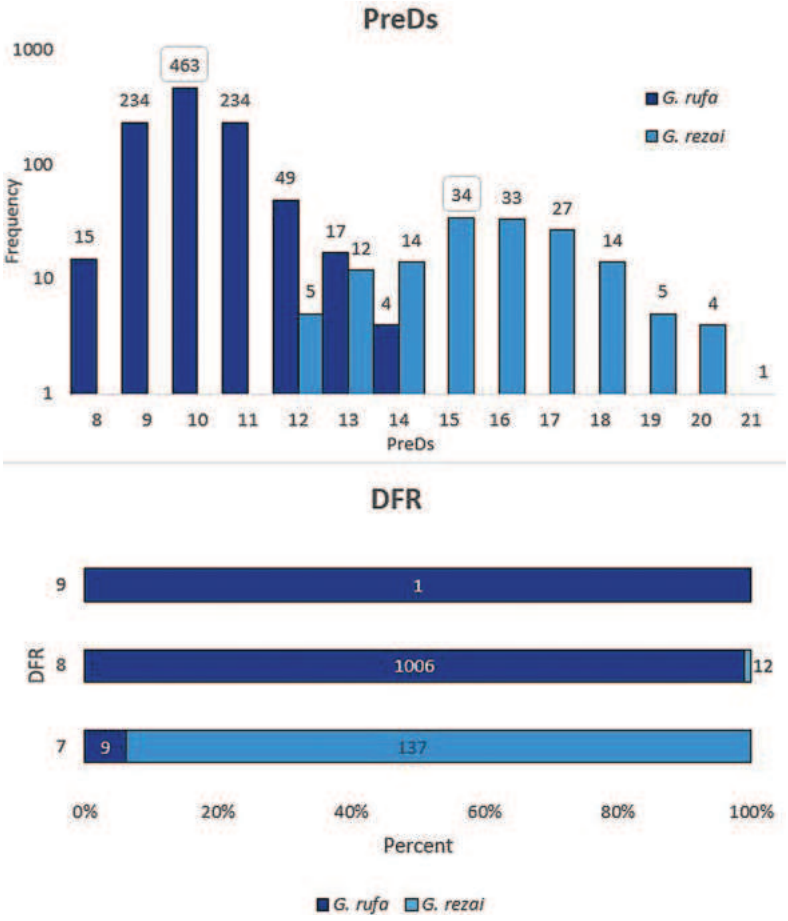

Figure 5. Frequency distributions of *G. rufa* and *G. rezai* for PreDs and DFR.

Table 1. Frequency distributions of *G. rufa* and *G. rezai* for PreDs and DFR.

	n	PreDs													
		8	9	10	11	12	13	14	15	16	17	18	19	20	21
G. rufa	1016	15	234	**463**	234	49	17	4	–	–	–	–	–	–	–
G. rezai	149	–	–	–	–	5	12	14	**34**	33	27	14	5	4	1
	n	DFR													
		7	8	9											
G. rufa	1016	9	**1006**	1											
G. rezai	149	**137**	12	–											

Our previous in-situ observations and examination of the collection specimens in FFR and ESFM revealed that there is an important relationship between *Garra rezai*, the main species of this study and the recently described *Turcinoemacheilus ekmekciae* Kaya, Yoğurtçuoğlu, Aksu, Bayçelebi & Turan, 2023, particularly concerning their distribution ranges. As mentioned in the Results section, *G. rezai* individuals were found from Kaynarca Stream (upper Murat River drainage, Euphrates), as well as from Yanarsu, Botan, Menfez, Hezil and Batman drainage areas (tributaries of the Tigris River). *T. ekmekciae* was described from Kaynarca Stream (upper Murat River drainage), as well as recorded from Yanarsu, Botan, Nerduş and Batman drainage areas (tributaries of the Tigris River) (Kaya et al. 2024). It is obvious that both species have a very similar distribution pattern. In fact, the most interesting point in the distribution of these two species is that they were not expected to be distributed in different rivers and inhabit limited areas. Despite this, the fact that these two species - in addition to their expected distribution outside the Tigris River - also occur in the Murat River, the most important tributary of the Euphrates River, shows that there may be a strong relationship between the Murat and Tigris Rivers. In particular, the distribution of *Turcinoemacheilus ekmekciae*, which is not known to inhabit more than one different river and belongs to a genus with a generally limited distribution range and *G. rezai*, which is thought to have a regional distribution in certain areas (Fig. 1), in both the Yanarsu and Murat Rivers indicates that the connection of these two rivers naturally points to the elevation of at least part of the Muş South Mountains not being very ancient.

This study has shown that the distribution of *G. rezai* is not restricted and that many previous records of *G. rufa* (e.g. Hashemzadeh et al. (2015); Kaya et al. (2016)) may actually belong to *G. rezai*. Therefore, this study will shed light on studies to determine the distribution of this species in Iran, Iraq and Syria. We strongly encourage morphological and molecular studies to reveal the distribution of *G. rezai* and *G. rufa* in Iran, Iraq and Syria.

Acknowledgements

We would like to express our appreciation to the Republic of Türkiye Ministry of Agriculture and Forestry for the legal permission for this research. As the senior author gave her contributions to this manuscript while she was at Bournemouth University, we would like to thank Bournemouth University for providing their facilities and TÜBİTAK BİDEB (2219 Program) which supported her with one-year scholarships during her post-doc research in the United Kingdom. We would like to thank Fadil Kaya (Bitlis), Jörg Freyhof (Berlin), Davut Turan and Esra Bayçelebi (Rize) who contributed to provide *Garra rufa* and *G. rezai* samples from the Tigris and Euphrates for FFR and ESFM. We also thank to Davut Turan (FFR) and Hasan Musa Sarı (ESFM) for letting us examine material deposited in their fish collections.

References

Armbruster JW (2012) Standardized measurements, landmarks, and meristic counts for cypriniform fishes. Zootaxa 3586(1): 8–16. https://doi.org/10.11646/zootaxa.3586.1.3

Aydın B, Akhan S (2020) Su ürünleri yetiştiriciliğinde alternatif bir tür: Doktor balığı (*Garra rufa*). Atatürk Üniversitesi Ziraat Fakültesi Dergisi 51(2): 199–206. https://doi.org/10.17097/ataunizfd.602530 [in Turkish]

Bayçelebi E (2020) Distribution and diversity of fish from Seyhan, Ceyhan and Orontes river systems. Zoosystematics and Evolution 96(2): 747–767. https://doi.org/10.3897/zse.96.55837

Bayçelebi E, Kaya C, Turan D, Ergüden SA, Freyhof J (2018) Redescription of *Garra turcica* from southern Anatolia (Teleostei: Cyprinidae). Zootaxa 4524(2): 227–236. https://doi.org/10.11646/zootaxa.4524.2.6

Bayçelebi E, Kaya C, Turan D, Freyhof J (2021) *Garra orontesi*, a new species from the Orontes River drainage (Teleostei: Cyprinidae). Zootaxa 4952(1): 169–180. https://doi.org/10.11646/zootaxa.4952.1.10

Behrens-Chapuis S, Herder F, Esmaeili HR, Freyhof J, Hamidan NA, Özuluğ M, Sanda R, Geiger MF (2015) Adding nuclear rhodopsin data where mitochondrial COI indicates discrepancies–can this marker help to explain conflicts in cyprinids. DNA Barcodes 3(1): 187–199. https://doi.org/10.1515/dna-2015-0020

Demirci S, Özdilek SY, Şimşek E (2016) Study on nutrition characteristics of *Garra rufa* on the River Asi. Fresenius Environmental Bulletin 25(12): 5999–6004.

Ergüden SA (2016) Length-weight relationships for six freshwater fish species from the Seyhan Reservoir (south-eastern Anatolia, Turkey). Journal of Applied Ichthyology 32(1): 141–143. https://doi.org/10.1111/jai.12905

Freyhof J (2014). *Garra rufa*. The IUCN Red List of Threatened Species 2014: e.T19086922A19223063. https://doi.org/10.2305/IUCN.

UK.2014-1.RLTS.T19086922A19223063.en [Accessed on 13 January 2024]

Hashemzadeh I, Tabatabaei SN, Mansouri A, Abdoli A, Ghalenoei M, Golzarianpour K (2015) Length-weight relationships of *Garra rufa*, in the Tigris and Persian Gulf basins of Iran. International Journal of Aquatic Biology 3(1): 25–27. https://doi.org/10.22034/ijab.v3i1.43

Kaya C, Turan D, Ünlü E (2016) The latest status and distribution of fishes in upper Tigris River and two new records for Turkish freshwaters. Turkish Journal of Fisheries and Aquatic Sciences 16(3): 545–562. https://doi.org/10.4194/1303-2712-v16_3_07

Kaya C, Yoğurtçuoğlu B, Aksu İ, Bayçelebi E, Turan D (2024) *Turcinoemacheilus ekmekciae*, a new dwarf loach from upper Tigris and Euphrates (Teleostei: Nemacheilidae). Journal of Fish Biology 104: 227–239. https://doi.org/10.1111/jfb.15578

Kottelat M (2020) *Ceratogarra*, a genus name for *Garra cambodgiensis* and *G. fasciacauda* and comments on the oral and gular soft anatomy in labeonine fishes (Teleostei: Cyprinidae). The Raffles Bulletin of Zoology 35: 156–178. https://lkcnhm.nus.edu.sg/wp-content/uploads/sites/10/app/uploads/2020/03/s35rbz156-178.pdf

Mace GM (2004) The role of taxonomy in species conservation. Philosophical Transactions of the Royal Society of London. Series B, Biological Sciences 359(1444): 711–719. https://doi.org/10.1098/rstb.2003.1454

Majeed SU, Feulner GR, Al Hmoudi AH (2019) *Garra barreimiae* Fowler & Steinitz, 1956 (Cyprinidae: Labeoninae): A video record of individuals scaling the main waterfall in Wadi Wurayah National Park, Fujairah. Tribulus 27: 43. https://doi.org/10.1007/s10641-018-0758-7

Mousavi-Sabet H, Eagderi S, Saemi-Komsari M, Kaya C, Freyhof J (2022) *Garra rezai*, a new species from two widely disjunct areas in the Tigris drainage (Teleostei: Cyprinidae). Zootaxa 5195(5): 419–436. https://doi.org/10.11646/zootaxa.5195.5.2

Ruane NM, Collins EM, Geary M, Swords D, Hickey C, Geoghegan F (2013) Isolation of *Streptococcus agalactiae* and an aquatic birnavirus from doctor fish *Garra rufa* L. Irish Veterinary Journal 66(1): 2–5. https://doi.org/10.1186/2046-0481-66-16

Zhang E, Chen YY (2002) *Garra tengchongensis*, a new cyprinid species from the upper Irrawaddy River basin in Yunnan, China (Pisces: Teleostei). The Raffles Bulletin of Zoology 50(2): 459–464. https://archive.org/embed/raffles-bulletin-zoology-50-459-464

Supplementary material 1

Material examined for this study with detailed collections data

Authors: Cüneyt Kaya, Haydar Birol İmre, Irmak Kurtul
Data type: docx

Link: https://doi.org/10.3897/zse.100.118766.suppl1

Zoosyst. Evol. 100 (2) 2024, 357–372 | DOI 10.3897/zse.100.117956

PENSOFT

MUSEUM FÜR NATURKUNDE BERLIN

New species of *Rockacestus* (Cestoda, Phyllobothriidea) from skates of the genus *Bathyraja* (Rajiformes, Arhynchobatidae) in the Southwestern Atlantic Ocean with comments on the distribution of the genus

Guillermina García Facal[1,2], Verónica A. Ivanov[1,2†], Adriana Menoret[1,2]

1 *Universidad de Buenos Aires, Facultad de Ciencias Exactas y Naturales, Departamento de Biodiversidad y Biología Experimental, Laboratorio de Sistemática y Biología de Parásitos de Organismos Acuáticos (SIBIPOA), Buenos Aires, Argentina*

2 *CONICET-Universidad de Buenos Aires, Instituto de Biodiversidad y Biología Experimental (IBBEA), Buenos Aires, Argentina*

https://zoobank.org/9ED1E923-03F7-4EA2-906B-76A828481099

Corresponding author: Guillermina García Facal (guillefacal@gmail.com); Adriana Menoret (menoret.a@gmail.com)

Academic editor: Pavel Stoev ♦ **Received** 29 December 2023 ♦ **Accepted** 14 March 2024 ♦ **Published** 3 April 2024

Abstract

Three new species of *Rockacestus* Caira, Bueno & Jensen, 2021 were recovered from arhynchobatid skates taken between 37°S–55°S in the Magellanic Province, Southwestern Atlantic Ocean. *Rockacestus blasi* **sp. nov.** was found in *Bathyraja macloviana* (Norman, 1937), whereas *Rockacestus magellanicus* **sp. nov.**, and *Rockacestus ottavianoi* **sp. nov.** were found in *Bathyraja magellanica* (Philippi, 1902). These species differ from their congeners in having a particular combination of anatomical features, including a moderate to highly folded bothridia, presence of a uteroduct, and a seminal receptacle. Cross-sections of mature proglottids were made for the first time in members of the genus. In addition, the microthrix pattern was described in detail, focusing on the distal bothridial surface, including the apical sucker and marginal loculi resulting in a common microthrix configuration with filitriches and small lanceolate, lingulate, and a particular kind of coniform spinitriches. The diagnosis of *Rockacestus* is revised to include several features exhibited by the new species. The distribution data of the species currently assigned to *Rockacestus* are compiled and updated. The finding of *R. blasi* **sp. nov.**, *R. magellanicus* **sp. nov.**, and *R. ottavianoi* **sp. nov.** not only increases the number of members of *Rockacestus* in the Magellanic Province in the Southwestern Atlantic from one to four but also expands our knowledge of phyllobothriideans and their association with the softnose skates of the genus *Bathyraja* Ishiyama, 1958 in the Southern Hemisphere.

Key Words

Bathyraja, genus distribution, MPA Namuncurá/Burdwood Bank, *Rockacestus blasi* sp. nov., *Rockacestus magellanicus* sp. nov., *Rockacestus ottavianoi* sp. nov., Southern Hemisphere

Introduction

The genus *Rockacestus* Caira, Bueno & Jensen, 2021 was recently erected to house phyllobothriidean species bearing folded bothridia, with apical sucker and marginal loculi, which parasitize rajiform skates (Caira et al. 2021).

The genus currently comprises ten species formally described from Arhynchobatidae and Rajidae skates, mostly inhabiting temperate and cold waters in the Northern and Southern Hemispheres (Kay 1942; Williams 1968a, 1968b; Schmidt 1986; Wojciechowska 1991; Caira et al. 2021). *Rockacestus brittanicus* (Williams, 1968) described from *Raja montagui* Fowler, 1910, *Rockacestus williamsi* (Schmidt, 1986) recovered from *Leucoraja fullonica* (Linnaeus, 1758), and *Rockacestus piriei* (Williams, 1968) found in *Leucoraja naevus* (Müller & Henle, 1841) were reported from the Northern European Seas Province sensu Spalding et al. (2007) (see Williams 1968a, 1968b). Caira et al. (2021) described *Rockacestus carvajali* Caira, Bueno & Jensen, 2021 from *Dipturus chilensis* (Guichenot, 1848) off Chiloé

† This paper was mostly discussed prior to the death of Verónica A. Ivanov in January 2020.

between the limits of the Magellanic and the Warm Temperate Southeastern Pacific Provinces, while *Rockacestus radioductus* (Kay, 1942) was found in *Beringraja binoculata* (Girard, 1855) in the Cold Temperate Northeast Pacific (Kay 1942; Caira et al. 2021). *Rockacestus conchai* Caira, Bueno & Jensen, 2021 was recovered from *Bathyraja albomaculata* (Norman, 1937) off Malvinas Islands in the Magellanic Province (Caira et al. 2021). The remaining four species of *Rockacestus* registered from the southernmost latitudes to date (i.e., *Rockacestus arctowskii* [Wojciechowska, 1991], *Rockacestus georgiensis* [Wojciechowska, 1991], *Rockacestus rakusai* [Wojciechowska, 1991], and *Rockacestus siedleckii* [Wojciechowska, 1991]) mostly parasitize skate species of the genus *Bathyraja* Ishiyama, 1958 with records in the Scotia Sea, and the Continental high Antarctic Province (Wojciechowska 1991).

During fieldworks conducted between 2011–2016 off Argentina in the Southwestern Atlantic Ocean (SWA), skates of the genus *Bathyraja* were found to be parasitized with cestodes of three new species of *Rockacestus*. The descriptions of the new species include detailed morphological features; cross-sections of mature proglottids are presented for the first time for the genus. Likewise, more information on microtriches of the genus is presented.

Materials and methods

Sampling

Tapeworms examined in this study were collected from a total of ten skates belonging to two species of the genus *Bathyraja*: five specimens of *Bathyraja macloviana* (Norman, 1937) and five specimens of *Bathyraja magellanica* (Philippi, 1902) (Rajiformes, Arhynchobatidae). The skates were caught from different localities along the SWA. Three specimens of *B. macloviana* were caught off Río Grande, Tierra del Fuego Province at 54°29.50'S, 65°3.16'W (assigned unique host number PD3-026), off Necochea, Buenos Aires Province at 39°53.99'S, 57°0.64'W (PD3-255) and 39°52.64'S, 56°38.72'W (PD3-257) all in March 2011. Two specimens of *B. macloviana* were caught off Villa Gesell, Buenos Aires Province at 37°33.10'S, 55°19.20'W (PD5-205) in August 2012 and off the Marine Protected Area Namuncurá/Burdwood Bank at 53°55.92'S, 61°31.93'W (PD12-430) in April 2016. Additionally, one specimen caught off Buenos Aires Province at 39°34.28'S, 56°16.16'W was examined in March 2011 and showed no signs of infection with phyllobothriideans. The specimens of *B. magellanica* were caught off Río Grande, Tierra del Fuego Province at 53°26.35'S, 64°58.56'W (assigned unique host number PD4-059) and 54°1.68'S, 67°6.81'W (PD4-097) in April 2012, 53°51.36'S, 67°03.84'W (PD10-039) in March 2014, 54°19.91'S, 64°14.26'W (PD12-479) in April 2016, and off the Marine Protected Area Namuncurá/Burdwood Bank at 54°32.60'S, 60°1.28'W (PD12-045) in March 2016. Also, five uninfected specimens were caught off Tierra del Fuego Province at 55°03.34'S, 66°07.82'W in March 2014. All hosts were obtained with bottom trawls on board the RV *Puerto Deseado* (CONICET). All tapeworms were removed from the spiral intestine of their respective host, relaxed in seawater, fixed in 10% formalin, and transferred to 70% ethanol for storage.

Preparation of specimens for light microscopy and scanning electron microscopy

Methods for preparing specimens as whole mounts for descriptive work using light microscopy and scanning electron microscopy (SEM) followed Menoret and Ivanov (2021). The terminal proglottid of one specimen of *Rockacestus* from *B. macloviana*, one tapeworm of *Rockacestus* from *B. magellanica*, and one detached mature proglottid of a specimen of *Rockacestus* from *B. magellanica* were embedded in paraffin, and serial cross-sections were cut at a thickness of 8 μm. Sections were stained with Harris' haematoxylin, counterstained with eosin, and mounted in Canada balsam. Whole mounts and histological sections were examined and measured using Olympus BX 51 and Zeiss Axioscope compound microscopes. Micrographs of whole mounts and histological sections were taken using Olympus LC30 camera; drawings were made with the aid of a drawing tube, both attached to the Olympus BX 51 compound microscope. Measurements are expressed as the range, followed in parentheses by the mean, standard deviation (when n ≥3), and the number of worms from which the measurements were taken. Measurements of genitalia and reproductive structures were taken from mature proglottids of mature and gravid worms. All measurements are in micrometres unless otherwise stated.

Mapping and geographic sites

Geographic coordinates in degrees and minutes of type locality and additional localities of the species ofthe species of *Rockacestus* were extracted from the original descriptions. Estimated coordinates were assigned to those records that lacked such information in the original publication. The geographic distribution of the *Rockacestus* species was charted using the PANMAP software v.0.9.6 (Diepenbroek et al. 2002).

Terminology

Terminology of microtriches follows Chervy (2009). Valid species of *Rockacestus* follow Caira et al. (2021). Valid host names follow Froese and Pauly (2023). Marine bioregions follow Spalding et al. (2007) for a global scale and Sabadin et al. (2020) for regionalization in the SWA.

Material examined and museum abbreviations

The museum material examined includes light micrographs of one paratype of *R. carvajali* (USNM No.

1638652), and two paratypes of *R. conchai* (USNM Nos. 1638654 and 1638655), provided by Anna Phillips from the Smithsonian National Museum of Natural History–Invertebrate Zoology Collection, Washington, D.C., USA. Museum abbreviations are as follows: MACN-Pa, Museo Argentino de Ciencias Naturales, Colección Parasitológica, Buenos Aires, Argentina; MLP-He, Museo La Plata, Colección Helmintológica, Buenos Aires, Argentina.

Results

Order Phyllobothriidea Caira, Jensen, Waeschenbach, Olson & Littlewood, 2014
Genus *Rockacestus* Caira, Bueno & Jensen, 2021

***Rockacestus blasi* sp. nov.**

https://zoobank.org/E014EFBD-32EB-489A-9449-B1E5B4D45A9D
Figs 1A, 2, 3, 7A–C, 8

Type material. ***Holotype*** whole mature worm, off Villa Gesell, Buenos Aires Province, Argentina (37°33.10'S, 55°19.20'W), 98.7 m, 06 Aug. 2012, A. Menoret leg., MACN-Pa No. 783.

Paratypes 1 whole mature worm, 1 whole gravid worm, 1 detached gravid proglottid, same data as holotype, MACN-Pa Nos. 784/1–3. One detached gravid proglottid, same data as for preceding, MLP-He No. 8097. One whole mature worm, 1 detached gravid proglottid, off Río Grande, Tierra del Fuego Province, Argentina (54°29.50'S, 65°3.16'W), 133 m, 16 Mar. 2011, V. A. Ivanov & A. Menoret leg., MACN-Pa Nos. 786/1–2. Nine whole gravid worms, cross-section of 2 attached mature proglottid, off Necochea, Buenos Aires Province, Argentina (39°52.64'S, 56°38.72'W), 91.3 m, 27 Mar. 2011, V. A. Ivanov & A. Menoret leg., MACN-Pa Nos. 785/1–9, 785/11–24. Three whole gravid worms, same data as for preceding, MLP-He No. 8096. One whole gravid worm, off Necochea, Buenos Aires Province, Argentina (39°53.99'S, 57°0.64'W), 94 m, same data as for preceding, MACN-Pa No. 785/10. One whole immature worm, off the Marine Protected Area Namuncurá/Burdwood Bank, Argentina (53°55.92'S, 61°31.93'W), 184 m, 19 Apr. 2016, A. Menoret leg., MACN-Pa No. 787.

Description. Based on 18 specimens (14 whole gravid worms, 3 whole mature worms, 1 immature worm), 3 detached gravid proglottids, cross-sections of 1 mature proglottid, and 3 scoleces examined with SEM. Worms apolytic, proglottids craspedote. Specimens possessing mature proglottids, 26.8–45.2 (35.7 ± 9.2, n = 3) mm long, 140–204 (163 ± 36, n = 3) proglottids per worm. Specimens possessing gravid proglottids, 22.3–50.9 (36.1 ± 7.6, n = 14) mm long, 106–162 (128 ± 18, n = 14) proglottids per worm (Fig. 1A). Maximum width at level of scolex or immature proglottid. Scolex composed of 4 bothridia, 400–830 (621 ± 127, n = 17) long, 580–1,220 (891 ± 193, n = 17) wide. Bothridia folded, 375–685 (506 ± 100, n = 8) long, 425–750 (571 ± 113, n = 8) wide when folded, sessile anteriorly, free posteriorly; with apical sucker and

Figure 1. Light micrographs of whole worms of *Rockacestus* from the Southwestern Atlantic Ocean. **A.** *Rockacestus blasi* sp. nov. (holotype MACN-Pa No. 783) from *Bathyraja macloviana*; **B.** *Rockacestus magellanicus* sp. nov. (holotype MACN-Pa No. 789) from *Bathyraja magellanica*; **C.** *Rockacestus ottavianoi* sp. nov. (holotype MACN-Pa 793) from *Bathyraja magellanica*.

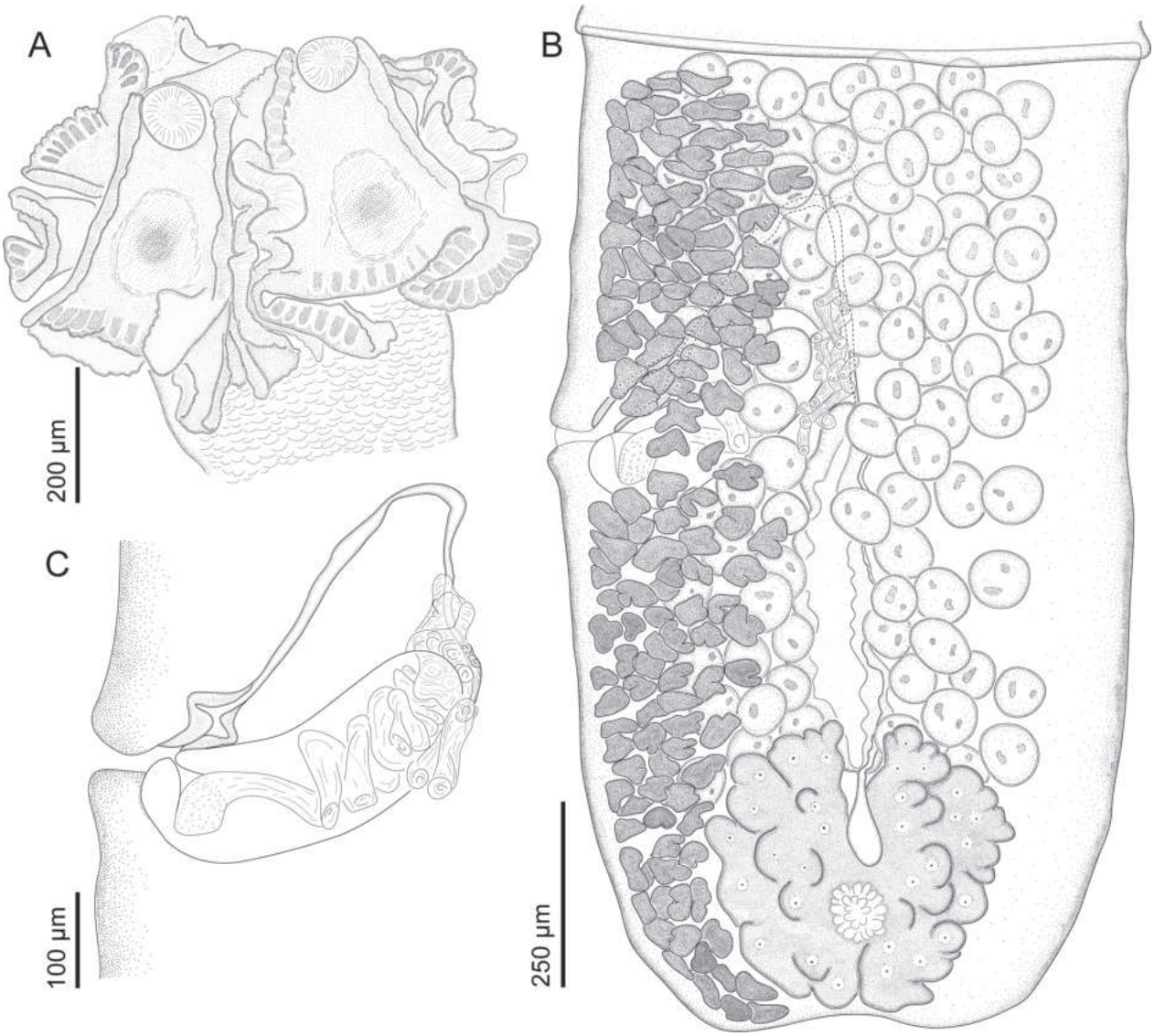

Figure 2. Line drawings of *Rockacestus blasi* sp. nov. from *Bathyraja macloviana*. **A.** Scolex (holotype MACN-Pa No. 783); **B.** Terminal mature proglottid (holotype MACN-Pa No. 783); **C.** Detail of terminal genitalia, terminal mature proglottid (holotype MACN-Pa No. 783).

marginal loculi (Figs 2A, 3A, 8B). Posterior part of each bothridium with weak depression surrounded by circular band of muscle (Fig. 2A). Apical sucker, 80–123 (107 ± 14, n = 13) long, 85–135 (113 ± 13, n = 13) wide (Figs 2A, 3A, B). Cephalic peduncle, absent. Neck 8.8–18.5 (14.0 ± 3.0, n = 17) mm long.

Apex of scolex proper covered with acicular filitriches. Proximal bothridial surface covered with acicular filitriches (Fig. 3I). Distal bothridial surface covered with acicular filitriches interspersed with lingulate spinitriches, lingulate spinitriches increasing in density posteriorly (Fig. 3F, J). Distal surface of apical sucker covered with acicular filitriches interspersed with lingulate spinitriches; posterior half of external rim of apical sucker with small lanceolate spinitriches (Fig. 3B–E). Distal surface of marginal loculi covered with papilliform to acicular filitriches interspersed with short coniform spinitriches (Fig. 3G, H). Capilliform filitriches on neck and strobila arranged in scutes (Fig. 3K). Cilia not observed.

Specimens possessing mature proglottids with 133–202 (158 ± 38, n = 3) immature proglottids and 2–7 (5 ± 3, n = 3) mature proglottid per worm. Mature proglottids becoming longer than wide posteriorly (Fig. 1A). Terminal mature proglottid, 940–1,360 (1,180 ± 216, n = 3) long, 600–800 (727 ± 110, n = 3) wide, length-to-width ratio, 1.6–1.7 (1.6 ± 0.1): 1. Specimens possessing gravid proglottids with 99–146 (120 ± 17, n = 14) immature proglottids, 4–8 (7 ± 1.5, n = 14) mature proglottids, and 1–2 (1 ± 0.4, n = 14) gravid proglottids per worm. Gravid proglottids longer than wide. Terminal gravid proglottid, 1,180–1,820 (1,591 ± 203, n = 14) long, 620–970 (783 ± 97, n = 14) wide, length-to-width ratio, 1.4–2.9 (2.1 ± 0.4): 1 (Fig. 2B).

Testes spherical to slightly oblong, 75–96 (86 ± 9, n = 4) in total number, 55–88 (78 ± 10, n = 17) long, 54–

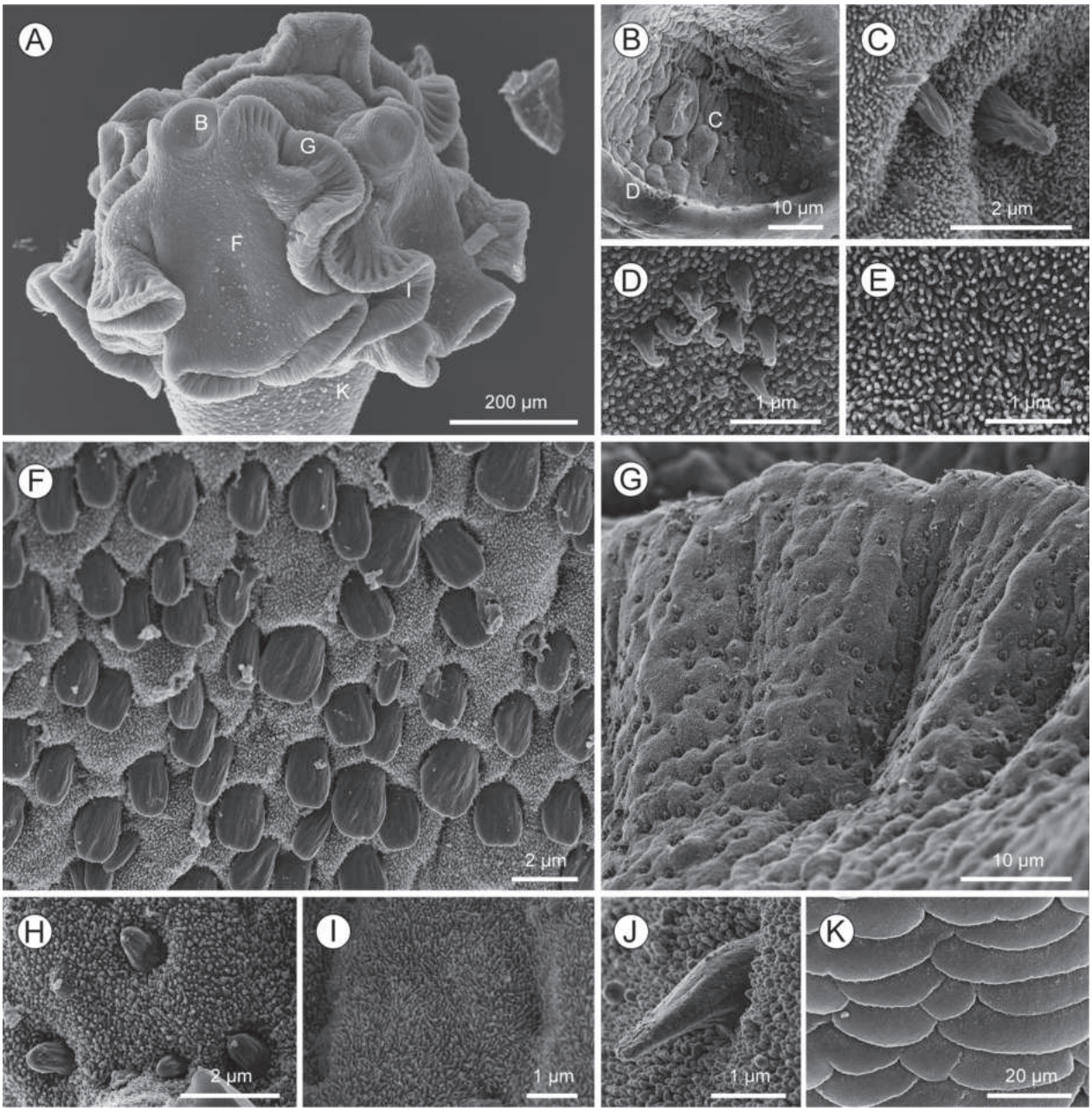

Figure 3. *Rockacestus blasi* sp. nov. from *Bathyraja macloviana*, scanning electron micrographs. **A.** Scolex, small letters indicate the location of details shown in Fig. 3B, 3F–G, 3I, 3K; **B.** Apical sucker, small letters indicate location of detail shown in Fig. 3C–D; **C.** Distal surface of apical sucker, acicular filitriches and lingulate spinitriches; **D.** Surface of the external apical sucker rim, lanceolate spinitriches; **E.** Detail of distal surface of the apical sucker, acicular filitriches; **F.** Distal bothridial surface, lingulate spinitriches; **G.** Distal surface of marginal loculi, acicular filitriches and short coniform spinitriches; **H.** Detail of distal surface of marginal loculi; **I.** Proximal bothridial surface, acicular filitriches; **J.** Distal bothridial surface, detail of lingulate spinitriches; **K.** Scutes on surface of neck.

93 (77 ± 10, n = 17) wide, extending from anterior margin of proglottid to anterior quarter of the ovary; arranged in 6–8 columns anteroposteriorly and 3–4 layers deep in cross-section observed in anterior portion of proglottid (Figs 2B, 7A). Postvaginal testes present. Cirrus sac oval, curved anteriorly, 276–450 (379 ± 42, n = 16) long, 115–175 (148 ± 19, n = 16) wide. Cirrus coiled, armed with minute spinitriches. Vas deferens highly coiled, anterior and adjacent to medial margin of cirrus sac, entering cirrus sac through anterior margin (Figs 2B, C, 7B).

Ovary lobulated, H-shaped in frontal view, X-shaped in cross-section at level of isthmus, 230–580 (350 ± 79, n = 17) long, 250–610 (456 ± 83, n = 17) wide (Figs 2B, 7C). Vagina thick-walled, extending anteriorly from ootype region forming a seminal receptacle, then running laterally along vas deferens bulk to anterior quarter of proglottid, recurving posteriorly to enter genital atrium anterior to cirrus sac (Figs 2B, C, 7C). Vagina and cirrus open into a small common genital atrium, 40–85 (66 ± 14, n = 16) deep. Genital pores al-

ternate irregularly, 54–73% (61 ± 5, n = 17) of proglottid length from posterior margin of proglottid. Vitellarium follicular, follicles irregular in shape, 31–52 (41 ± 9, n = 17) long, 50–80 (70 ± 10, n = 17) wide, arranged in 2 lateral bands almost reaching midline in anterior third of proglottid, each band consisting of multiple columns (5 columns of follicles anterior to cirrus sac), extending throughout the length of proglottid, uninterrupted by ovary, partially interrupted by genital atrium (Figs 2B, 7A–C). Uterus saccate, restricted to region between ovary and cirrus sac, running anteriorly up to genital pore level; uterine duct not observed (Fig. 2B). Mehlis´ gland, 80–115 (101 ± 8, n = 15) long, 60–110 (94 ± 13, n = 15) wide, posterior to the ovarian isthmus (Fig. 2B).

Detached gravid proglottids, 2,300–2,525 (2,392 ± 118, n = 3) long, 725–775 (758 ± 29, n = 3) wide, length-to-width ratio, 3.0–3.3 (3.2 ± 0.1): 1.

Host. *Bathyraja macloviana* (Norman, 1937), Patagonian skate (Rajiformes, Arhynchobatidae) (type host). Prevalence of infection, 83% in *B. macloviana* (5 hosts infected out of 6 examined).

Etymology. This species is named in memory of the first author's father, Blas García Mallarine for his invaluable love, support, and encouragement over the years.

Distribution. This species is widespread along the continental shelf of Argentina occurring from waters off Buenos Aires Province to southeast Patagonia including the Marine Protected Area Namuncurá/Burdwood Bank, Argentina (Fig. 9).

Remarks. Specimens of *R. blasi* sp. nov. can easily be distinguished from five valid species in the genus by the total length. *Rockacestus blasi* sp. nov. is longer than *R. carvajali* and *R. conchai* (22.3–50.9 mm vs. 13.1–14.5 mm and 9.9–16.9 mm, respectively), and is shorter than *R. brittanicus*, *R. georgiensis* and *R. williamsi* (22.3–50.9 mm vs. 170–250 mm, 60–170 mm, and 90 mm, respectively). *Rockacestus blasi* sp. nov. differs from *R. piriei*, *R. radioductus*, and *R. rakusai* in possessing fewer testes (75–96 vs. 137–165, ≥100, and 120–165, respectively). *Rockacestus blasi* sp. nov. can also be distinguished from *R. radioductus* in the distribution of testes (arranged in 6–8 columns in anteroposterior view vs. more than 15), the distribution of the vitelline follicles in the anterior third of the proglottid (reaching almost the midline of the proglottid vs. restricted to lateral bands), and in the position of the genital pore (54–73% from the posterior margin of the proglottid vs. equidistant from the anterior and posterior margin of the proglottid). *Rockacestus blasi* sp. nov. can be distinguished from *R. arctowskii* by the number of proglottids (140–204 vs. 24–98, respectively). *Rockacestus blasi* sp. nov. is different than *R. siedleckii* in the length of the scolex (400–830 vs. 840–960, respectively) and in the size of the apical sucker (80–135 vs. 185–220, respectively). Finally, *R. blasi* sp. nov. can be distinguished from 9 members in the genus by being apolytic instead of euapolytic.

***Rockacestus magellanicus* sp. nov.**

https://zoobank.org/E935F2CC-AFED-490F-98B7-C426CC919F07

Figs 1B, 4A–C, 5, 7D–F

Type material. ***Holotype*** whole mature worm; off Río Grande, Tierra del Fuego Province, Argentina (53°51.36'S, 67°03.84'W), 58 m, 31 Mar. 2014, A. Menoret leg., MACN-Pa No. 789.

Paratypes 1 whole mature worm, 1 mature strobila, 2 detached mature proglottid, cross-section of 1 detached mature proglottid, off Río Grande, Tierra del Fuego Province, Argentina (54°19.91'S, 64°14.26'W), 122 m, 22 Apr. 2016, A. Menoret leg., MACN-Pa Nos. 790/1–14. One strobila, 1 detached mature proglottid, same data as preceding, MLP-He No. 8098. One whole mature worm, off Río Grande, Tierra del Fuego Province, Argentina (53°26.35'S, 64°58.56'W), 130 m, 1 Apr. 2012, A. Menoret leg., MACN-Pa No. 792. One whole mature worm, off the Marine Protected Area Namuncurá/Burdwood Bank (54°32.60'S, 60°1.28'W), 98 m, 30 Mar. 2016, A. Menoret leg., MACN-Pa No. 791. One whole mature worm, same data as preceding, MLP-He No. 8099.

Description. Based on 7 specimens (5 whole mature worms and 2 strobilae without scoleces), 5 detached mature proglottids, 3 detached gravid proglottids, cross-sections of 1 detached mature proglottid, and 3 scoleces examined with SEM. Worms euapolytic, 9.9–19.5 (14.4 ± 4.0, n = 5) mm long, 61–115 (90.3 ± 23, n = 7) craspedote proglottids per worm (Fig. 1B). Maximum width at level of scolex or immature proglottids. Scolex composed of 4 bothridia, 520–810 (631 ± 113, n = 5) long, 779–1,050 (944 ± 116, n = 5) wide (Figs 4A, 5A). Bothridia folded, 450–471 (n = 2) long, 411–550 (n = 2) wide when folded, sessile anteriorly, free posteriorly, with apical sucker and marginal loculi. Posterior part of each bothridium with weak depression surrounded by circular band of muscle (Figs 4A, 5A). Apical sucker, 70–105 (84 ± 17, n = 4) long, 70–100 (85 ± 17, n = 4) wide (Figs 4A, 5A, B). Cephalic peduncle, absent. Neck, 3.6–8.3 (5.4 ± 2.0, n = 5) mm long.

Apex of scolex proper covered with acicular filitriches (Fig. 5H). Proximal bothridial surface covered with acicular filitriches (Fig. 5G). Distal bothridial surface covered with acicular filitriches interspersed with lingulate spinitriches, lingulate spinitriches increasing in density posteriorly (Fig. 5E, F). Distal surface of apical sucker covered with acicular filitriches interspersed with lingulate spinitriches; posterior half of external rim of apical sucker with lanceolate spinitriches (Fig. 5B–D). Distal marginal loculi surface covered with papilliform to acicular filitriches interspersed with short coniform spinitriches (Fig. 5I, L). Capilliform filitriches on neck and strobila arranged in scutes (Fig. 5J, K). Cilia observed in proximal and distal bothridial surfaces, including apical sucker and marginal loculi (Fig. 5G, L).

Immature proglottids wider than long, 59–109 (84 ± 23, n = 7) in number. Mature proglottids wider than long, becoming longer than wide with maturity, 2–7 (4 ± 2, n = 7)

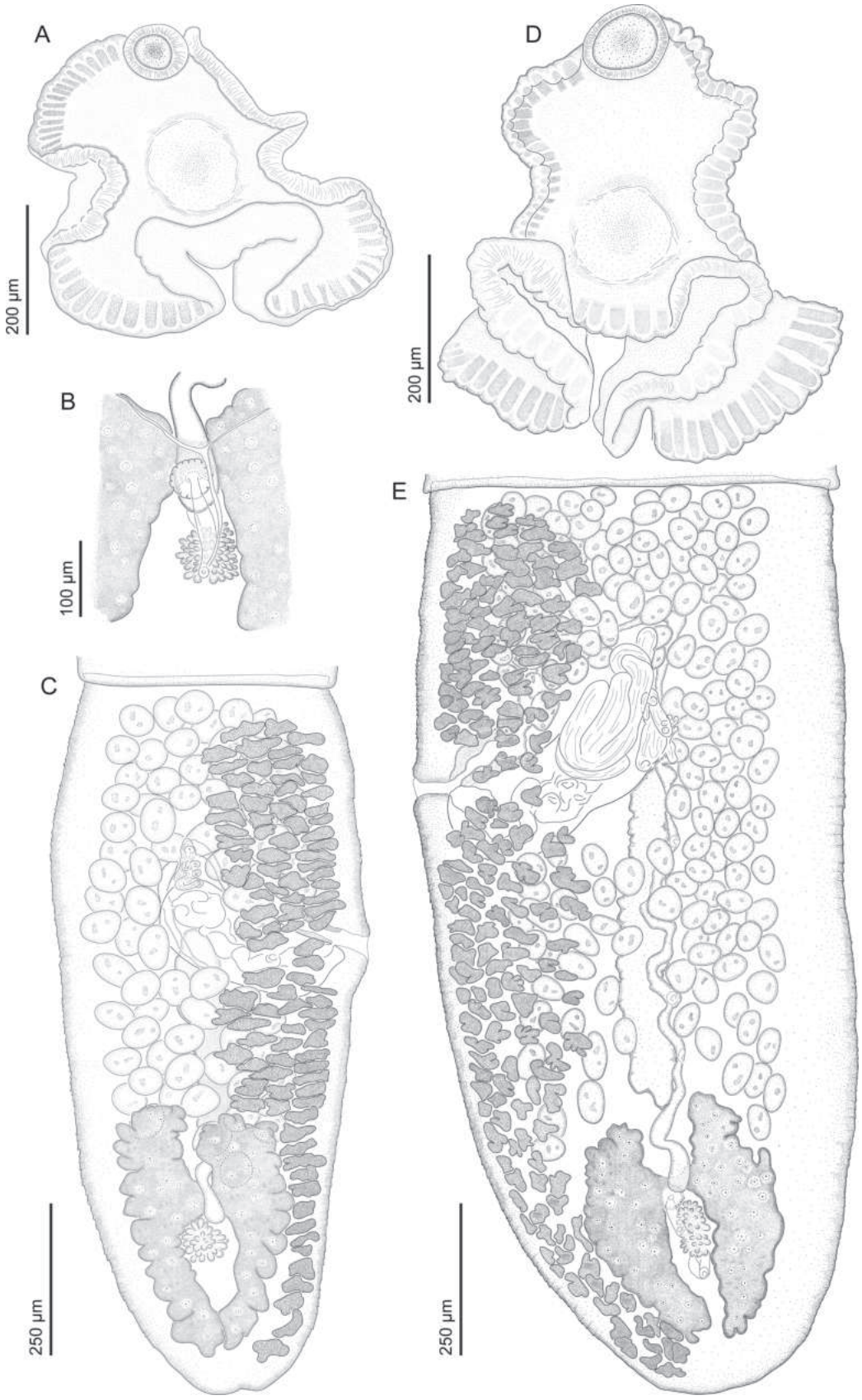

Figure 4. Line drawings of species of *Rockacestus* from the Southwestern Atlantic. **A–C.** *Rockacestus magellanicus* sp. nov. from *Bathyraja magellanica*; **A.** Bothridium (paratype MLP-He No. 8099); **B.** Detail of ootype region, mature proglottid (paratype MACN-Pa No. 790/4); **C.** Terminal mature proglottid (paratype MLP-He No. 8098); **D–E.** *Rockacestus ottavianoi* sp. nov. from *Bathyraja magellanica*; **D.** Bothridium (paratype MACN-Pa No. 794/1); **E.** Terminal mature proglottid (holotype MACN-Pa No. 793).

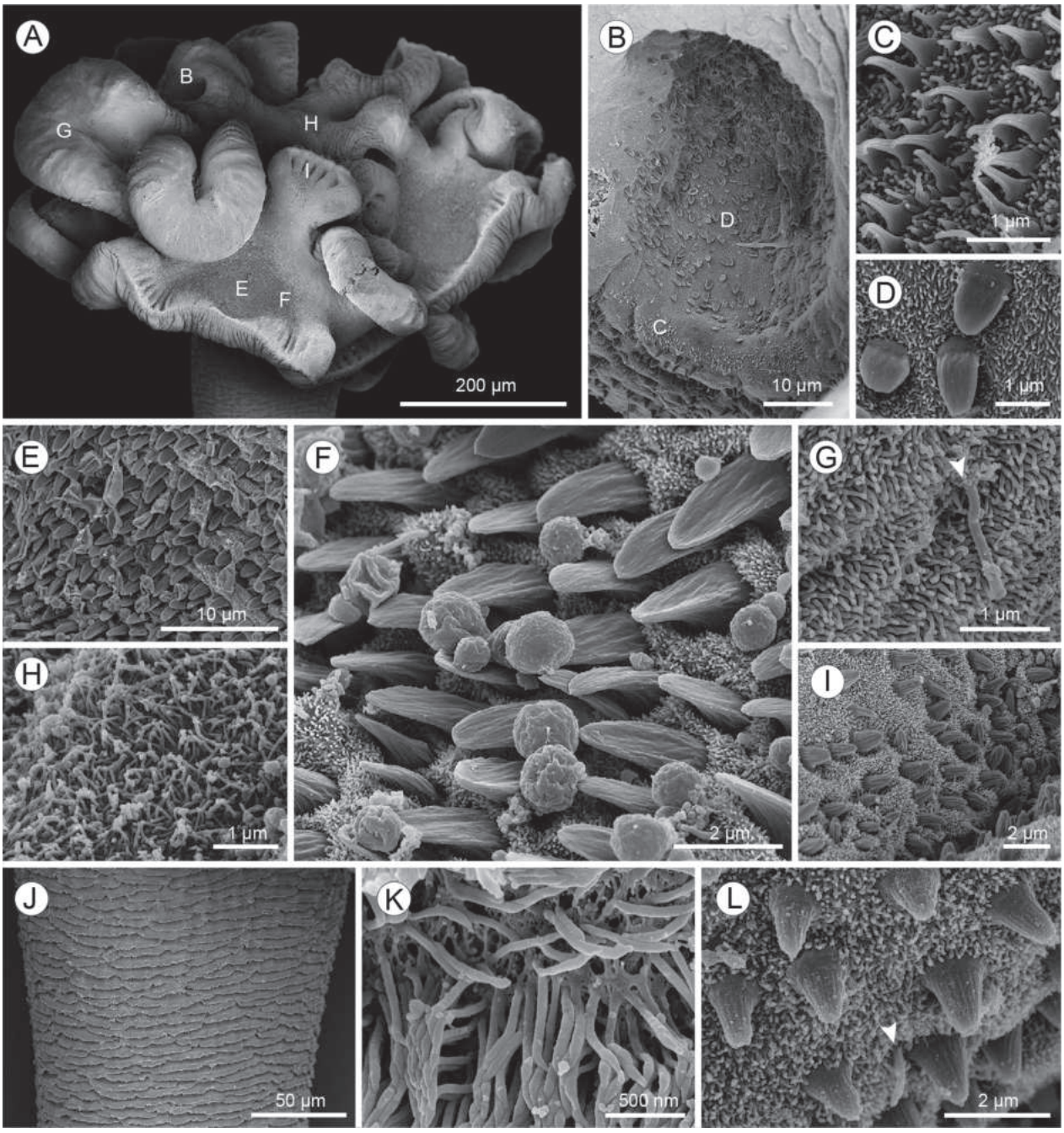

Figure 5. *Rockacestus magellanicus* sp. nov. from *Bathyraja magellanica*, scanning electron micrographs. **A.** Scolex, small letters indicate the location of details shown in Fig. 5B, 5E–I; **B.** Apical sucker, small letters indicate the location of details shown in Fig. 5C–D; **C.** Surface of the external apical sucker rim, acicular filitriches and lanceolate spinitriches; **D.** Distal apical sucker surface, acicular filitriches and lingulate spinitriches; **E–F.** Distal bothridial surface, acicular filitriches and lingulate spinitriches; **G.** Proximal bothridial surface, acicular filitriches, and cilium (white arrow); **H.** Apex of scolex, acicular filitriches; **I.** Distal surface of marginal loculi, acicular filitriches and coniform spinitriches; **J.** Scutes on surface of neck; **K.** Detail of scutes, capilliform filitriches; **L.** Detail of microtriches in marginal loculi and cilium (white arrow).

in number (Fig. 1B). Terminal mature proglottid longer than wide, 925–1,430 (1,115 ± 201) long, 376–680 (502 ± 111) wide, length-to-width ratio, 1.4–2.7 (2.3 ± 0.4, n = 6): 1 (Fig. 4C).

Testes oblong, 67–89 (76 ± 8, n = 6) in total number, 51–67 (62 ± 6, n = 6) long, 44–57 (49 ± 5, n = 6) wide, extending from anterior margin of proglottid to anterior quarter of ovary; arranged in 5–6 columns anteroposteriorly and 2 layers deep in cross-section observed in anterior portion of proglottid (Figs 4C, 7D). Cirrus sac oval, curved anteriorly, 200–340 (269 ± 58, n = 6) long, 95–140 (118 ± 18, n = 6) wide. Cirrus coiled, armed with minute spinitriches. Vas deferens highly coiled, extending anteriorly to vagina bend, overlapping medial margin of cirrus sac, entering cirrus sac through ventral margin (Figs 4C, 7E).

Ovary lobulated, H-shaped in frontal view, X-shaped in cross-section at level of isthmus, 255–615 (418 ± 135, n = 6) long, 163–375 (246 ± 75, n = 6) wide (Figs 4B, C,

7F). Vagina thick-walled, extending anteriorly from ootype region forming a seminal receptacle to bulk of vas deferens, then descending laterally along anterior margin of cirrus sac to enter genital atrium anterior to cirrus (Figs 4C, 7F). Vagina and cirrus sac join into genital atrium, 40–60 (53 ± 12, n = 3) deep. Genital pores alternate irregularly, 62–75% (68 ± 5, n = 6) of proglottid length from posterior margin of proglottid.

Vitellarium follicular, follicles irregular in shape, 15–34 (26 ± 7, n = 6) long, 38–55 (47 ± 6, n = 6) wide, arranged in 2 lateral bands almost reaching midline in anterior third of proglottid, each band consisting of multiple columns (4 columns of follicles anterior to cirrus sac), extending throughout proglottid length, uninterrupted by ovary, partially interrupted by genital atrium (Figs 4C, 7D–F). Uterus saccate, restricted to region between ovary and cirrus sac, running anteriorly up to genital pore level; uterine duct observed (Figs 4C, 7F). Mehlis´ gland, 55–110 (77 ± 20, n = 5) long, 55–75 (71 ± 9, n = 5) wide, posterior to ovarian isthmus (Fig. 4B, C).

Detached mature proglottids, 1,650–2,075 (1,875 ± 207, n = 5) long, 550–770 (654 ± 99, n = 5) wide, length-to-width ratio, 2.7–3.2 (2.9 ± 0.2, n = 5): 1. Detached gravid proglottids, 2,300–2,525 (2,392 ± 118, n = 3) long, 725–775 (758 ± 29, n = 3) wide, length-to-width ratio, 3.0–3.3 (3.2 ± 0.1): 1.

Host. *Bathyraja magellanica* (Philippi, 1902), Magellan skate (Rajiformes, Arhynchobatidae) (type host). Prevalence of infection, 40% in *B. magellanica* (4 hosts infected out of 10 examined).

Etymology. The specific name refers to the species distribution along the Magellanic Province in the Argentine Sea, SWA.

Distribution. This species is known from southern waters off Tierra del Fuego Province, Argentina including the Marine Protected Area Namuncurá/Burdwood Bank, Argentina (Fig. 9).

Remarks. *Rockacestus magellanicus* sp. nov. is shorter than *R. blasi* sp. nov., *R. brittanicus*, *R. georgiensis*, *R. piriei*, *R. radioductus*, *R. rakusai*, *R. siedleckii*, and *R. williamsi* (9.9–19.5 vs. 22.3–250 mm in total length, respectively). Specimens of *R. magellanicus* sp. nov. have fewer testes than those of *R. carvajali* (67–89 vs. 46–55, respectively). Moreover, *R. magellanicus* sp. nov. has lingulate spinitriches and acicular filitriches on the distal surface of the bothridia whereas *R. carvajali* has only papilliform filitriches. *Rockacestus magellanicus* sp. nov. differs from *R. conchai* in the scolex width (779–1,050 vs. 1,122–1,775, respectively), size of bothridia (450–471 long by 411–550 wide vs. 478–624 long by 600–830 wide, respectively). Additionally, *R. magellanicus* sp. nov. has acicular filitriches and small lingulate spinitriches on the distal surface of apical sucker whereas *R. conchai* only has acicular filitriches. *Rockacestus magellanicus* sp. nov. is different from *R. arctowskii* in the size of the cirrus sac (200–340 long by 95–140 wide vs. 370–480 long by 154–215 wide, respectively) and in the size of the apical sucker (70–105 long by 70–100 wide vs. 212–250 in diameter, respectively).

Rockacestus ottavianoi sp. nov.

https://zoobank.org/75E09CF2-DC8D-470D-97EA-1ACEA43C6644

Figs 1C, 4D, E, 6, 7G–I

Type material. ***Holotype*** whole mature worm, off Río Grande, Tierra del Fuego Province, Argentina (54°1.68'S, 67°6.81'W), 193 m, 2 Apr. 2012, A. Menoret leg., MACN-Pa No. 793.

Paratypes 1 whole mature worm, 1 whole mature strobila (SEM voucher), cross-section of 1 attached mature proglottid, same data as holotype, MACN-Pa Nos. 794/1–13. One whole mature worm, same data as for preceding, MLP-He No. 8100.

Description. Based on 4 specimens (3 whole mature worms, and 1 strobila without scolex), cross-sections of 1 mature proglottid, and 2 scoleces examined with SEM. Worms euapolytic, 23.1–53.1 (39.1 ± 13.8, n = 4) mm long, 124–195 (156 ± 36, n = 3) craspedote proglottids per worm (Fig. 1C). Maximum width at level of scolex. Scolex composed of 4 bothridia, 590–750 (648 ± 70, n = 4) long, 978–1,250 (1,133 ± 36, n = 4) wide (Figs 4D, 6A). Bothridia folded, 530–600 (570 ± 36, n = 3) long, 520–720 (613 ± 101, n = 3) wide when folded, sessile anteriorly, free posteriorly, consisting of apical sucker and marginal loculi. Posterior part of each bothridium with weak depression surrounded by circular band of muscle (Figs 4D, 6A). Apical sucker 100–130 (113 ± 15, n = 3) long, 110–140 (125 ± 13, n = 3) wide (Figs 4D, 6A, B). Cephalic peduncle, absent. Neck 11.6–25.3 (19.4 ± 6.0, n = 4) mm long.

Apex of scolex proper covered with acicular to capilliform filitriches (Fig. 6E). Proximal bothridial surface covered with acicular filitriches (Fig. 6H). Distal bothridial surface covered with acicular filitriches interspersed with lingulate spinitriches, lingulate spinitriches increasing in density posteriorly (Fig. 6F, G). Distal surface of apical sucker covered with acicular filitriches interspersed with small lingulate spinitriches; posterior half of external rim of apical sucker with lanceolate spinitriches (Fig. 6B–D); cilia found throughout distal surface of apical sucker. Distal surface of marginal loculi covered with acicular filitriches interspersed with short coniform spinitriches (Fig. 6I, L). Capilliform filitriches on neck and strobila arranged in scutes (Fig. 6J, K).

Immature proglottids wider than long, 123–179 (150 ± 28, n = 3) in number (Fig. 1C). Mature proglottids wider than long, becoming longer than wide with maturity, 2–16 (6 ± 7, n = 4) in number (Fig. 1C). Terminal mature proglottid longer than wide, 970–1,460 (1,220 ± 207) long, 570–760 (663 ± 81) wide, length-to-width ratio, 1.4–2.3 (1.9 ± 0.4, n = 4): 1 (Fig. 4E).

Testes oblong, 92–152 (108 ± 39, n = 3) in total number, 55–68 (60 ± 5, n = 4) long, 43–52 (46 ± 4, n = 4) wide, extending from anterior margin of proglottid to anterior quarter of ovary; arranged in 6–7 columns anteroposteriorly and 2 layers deep in cross-section observed in anterior portion of proglottid (Figs 4E, 7G). Cirrus sac oval, curved anteriorly, 350-395 (365 ± 26, n = 3) long, 125-165 (138 ± 23, n = 3) wide. Cirrus coiled, armed with

minute spinitriches. Vas deferens highly coiled, extending anteriorly to vagina bend, overlapping medial portion of cirrus sac, anterior to cirrus sac (Fig. 4E).

Ovary lobulated, H-shaped in frontal view, X-shaped in cross-section at level of isthmus, 345–500 (408 ± 81, n = 3) long, 235–355 (292 ± 60) wide (Figs 4E, 7I). Vagina thick-walled, extending anteriorly from the ootype region forming a seminal receptacle, to bulk of vas deferens descending laterally along anterior margin of cirrus sac to enter genital atrium anterior to cirrus (Figs 4E, 7I). Vagina and cirrus sac join into genital atrium, 50–60 (55 ± 7, n = 2) deep. Genital pores alternate irregularly, 68–74% (71 ± 2, n = 4) of proglottid length from posterior margin of proglottid. Vitellarium follicular, follicles irregular in shape, 28–55 (39 ± 12, n = 4) long, 43–50 (46 ± 3, n = 4) wide, arranged in 2 lateral bands almost reaching the mid-

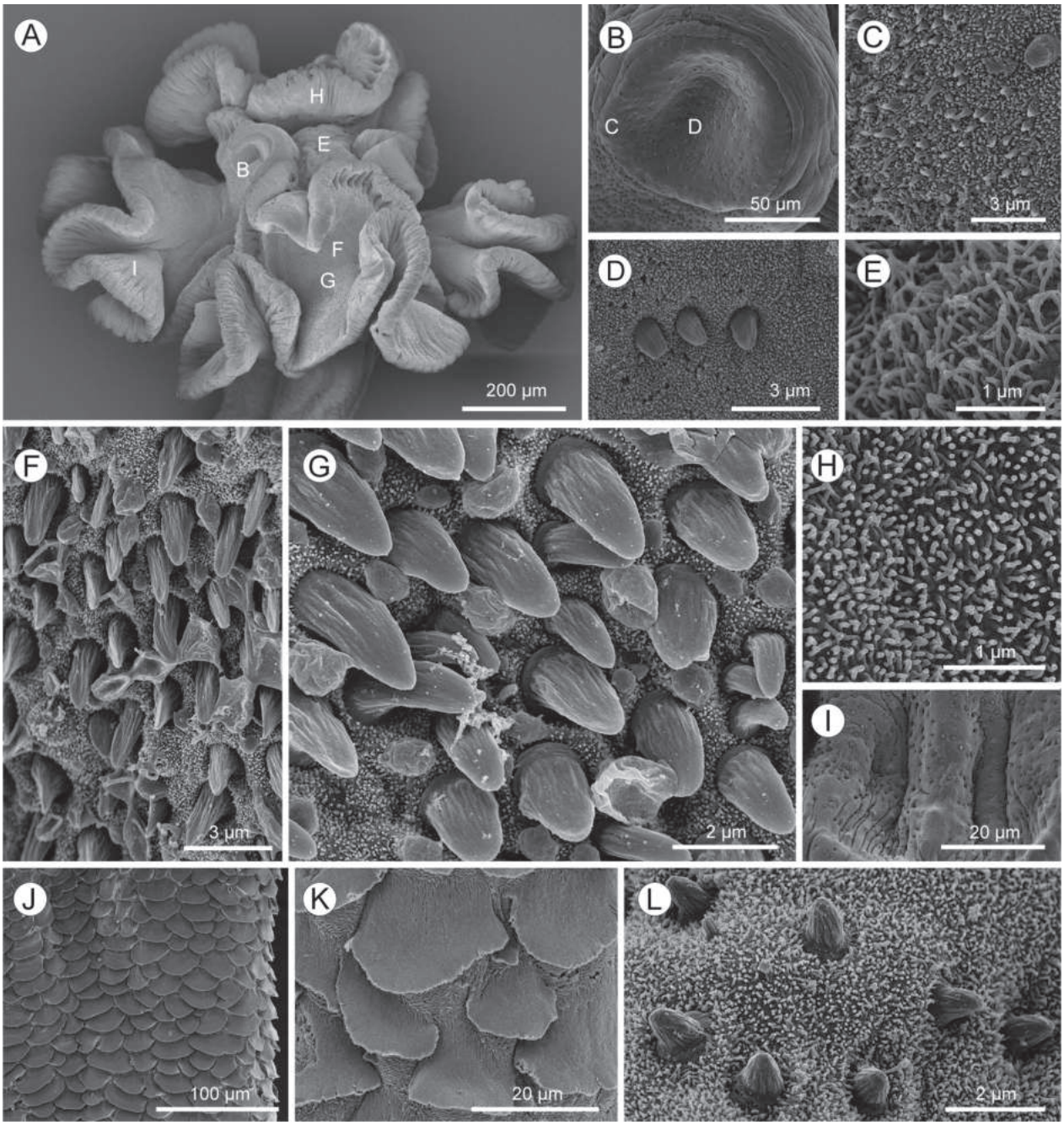

Figure 6. *Rockacestus ottavianoi* sp. nov. from *Bathyraja magellanica*, scanning electron micrographs. **A.** Scolex, small letters indicate the location of details shown in; **B.** Apical sucker, small letters indicate the location of details shown in Fig. 6C, D; **C.** Surface of the external apical sucker rim, acicular filitriches and small lingulate spinitriches; **D.** Detail of distal apical sucker surface, lingulate spinitriches; **E.** Apex of scolex, acicular to capilliform filitriches; **F, G.** Distal bothridial surface, acicular filitriches and lingulate spinitriches; **H.** Proximal bothridial surface, acicular filitriches; **I.** Distal surface of marginal loculi, acicular filitriches and short coniform spinitriches; **J, K.** Scutes on surface of neck; **L.** Detail of microtriches on marginal loculi.

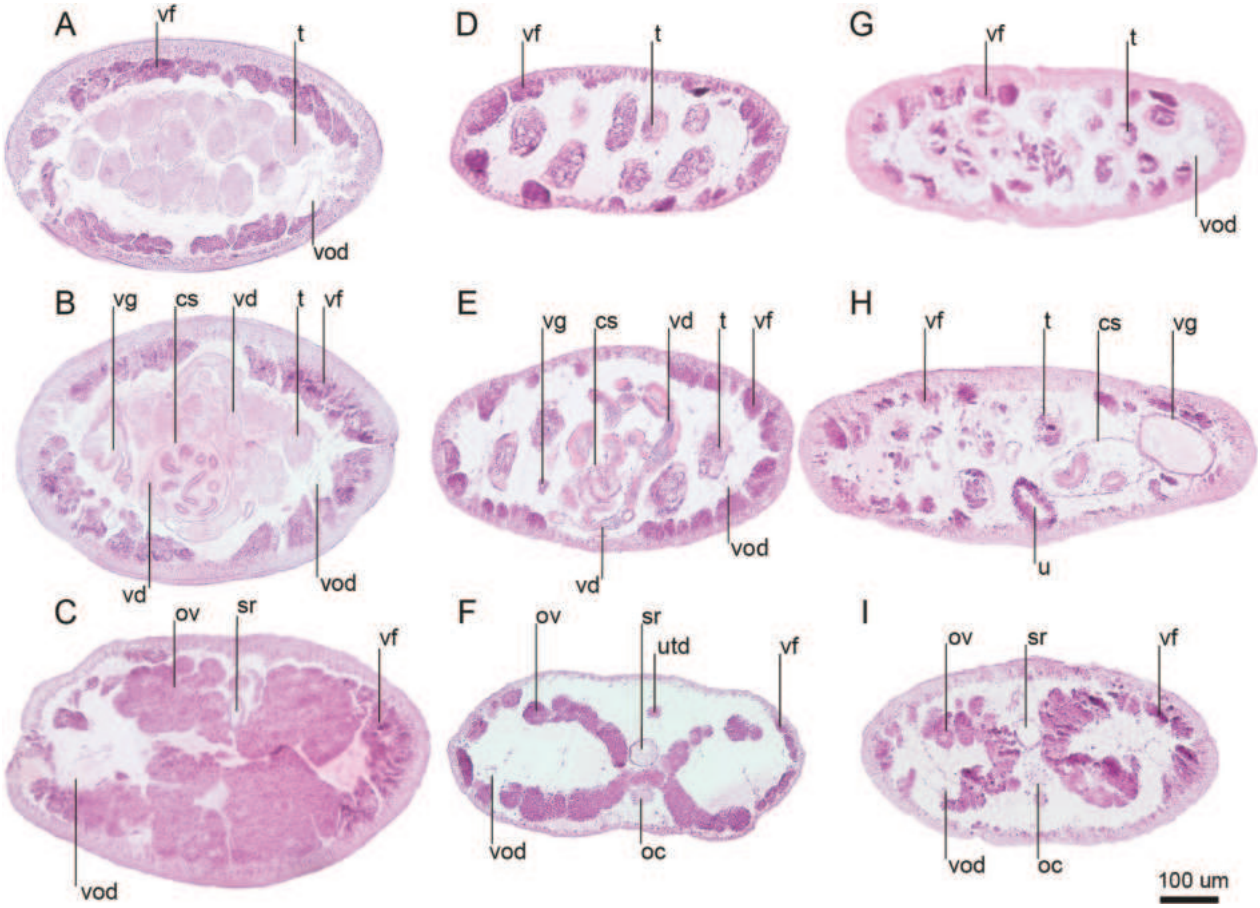

Figure 7. Light micrographs of cross-sections of mature proglottids of species of *Rockacestus* off Argentina. **A–C.** *Rockacestus blasi* sp. nov.; **A.** At the level of the testes, anterior to the cirrus sac; **B.** At the level of the cirrus sac; **C.** At the level of ovarian isthmus; **D–F.** *Rockacestus magellanicus* sp. nov.; **D.** At the level of the testes, anterior to the cirrus sac; **E.** At the level of the cirrus sac; **F.** At the level of ovarian isthmus; **G–I.** *Rockacestus ottavianoi* sp. nov; **G.** At the level of the testes, anterior to the cirrus sac; **H.** At the level of the cirrus sac; **I.** At the level of ovarian isthmus; **cs** — cirrus sac; **oc** — ovicapt; **ov** — ovary; **sr** — seminal receptacle; **t** — testes; **u** — uterus; **ut** — uteroduct; **vd** — vas deferens; **vf** — vitelline follicle; **vg** — vagina; **vod** — ventral osmoregulatory duct.

line in anterior third of proglottid, each band consisting of multiple columns (5–6 columns anterior to cirrus sac) of follicles, extending throughout the length of proglottid, uninterrupted by ovary, interrupted partially by genital atrium (Figs 4E, 7G–I). Uterus saccate, restricted to region between ovary and cirrus sac running anteriorly up to genital pore level, uterine duct observed (Figs 4E, 7H). Mehlis′ gland, 90–110 (99 ± 9, n = 4) long, 63–100 (76 ± 17, n = 4) wide, posterior to ovarian isthmus (Fig. 4E).

Host. *Bathyraja magellanica* (Philippi, 1902), Magellan skate (Rajiformes, Arhynchobatidae) (type host). Prevalence of infection, 10% in *B. magellanica* (1 host infected out of 10 examined).

Etymology. This species is named in honor of Juan Manuel Ottaviano for his genuine and loyal friendship over the years.

Distribution. This species is known from its type locality, off Río Grande, Tierra del Fuego Province, Argentina (54°1.68'S, 67°6.81'W).

Remarks. *Rockacestus ottavianoi* sp. nov. can be distinguished from *R. arctowskii*, *R. carvajali*, *R. conchai*, and *R. magellanicus* sp. nov. by having more testes (92–152 vs. 60–80, 46–55, 51–73, and 67–89, respectively) and a greater number of proglottids (124–195 vs. 24–98, 75–81, 64–105, and 61–115, respectively). *Rockacestus ottavianoi* sp. nov. is easily distinguished from three of its congeners by the worm length by being shorter than *R. brittanicus*, *R. georgiensis*, and *R. williamsi* (23.1–53.1 vs. 170–250, 60–170, and 90 mm, respectively). *Rockacestus ottavianoi* sp. nov. can be distinguished from three species in the genus by having different size of apical sucker. In *R. rakusai* and *R. siedleckii*, it is bigger than in *R. ottavianoi* sp. nov. (250–310 and 185–220 in diameter vs. 100–130 long by 110–140 wide, respectively), whereas in *R. piriei* it is smaller (90 in diameter vs. 100–130 long by 110–140 wide, respectively). *Rockacestus ottavianoi* sp. nov. has a narrower scolex (978–1,250 in scolex width) and bigger testes (43–52 long by 55–68 wide) than *R. radioductus* (1,800–2,000 in scolex width; 40 in testes diameter). Finally, *R. ottavianoi* sp. nov. is euapolytic and has testes distributed in 2 layers deep in cross-section, whereas *R. blasi* sp. nov.

is apolytic and has testes arranged in 3–4 layers deep in cross-section.

Update of generic diagnosis and distribution of valid species of *Rockacestus*

The diagnosis of *Rockacestus* sensu Caira et al. (2021) is revised to include the three species described below from the skates of the genus *Bathyraja* from continental shelf waters off Argentina. The generic diagnosis is updated as follows: worms euapolytic or apolytic; scolex spinitriches lingulate, lanceolate, coniform, filitriches papilliform or acicular; genital pores lateral, in midhalf or anterior half of proglottid, irregularly alternating; testes arranged in 2–4 rows in cross-section; vagina with seminal receptacle present or absent; uteroduct present or absent.

The valid species now include, *Rockacestus arctowskii* (Wojciechowska, 1991), *Rockacestus blasi* sp. nov., *Rockacestus brittanicus* (Williams, 1968), *Rockacestus carvajali* Caira, Bueno & Jensen, 2021, *Rockacestus conchai* Caira, Bueno & Jensen, 2021, *Rockacestus georgiensis* (Wojciechowska, 1991), *Rockacestus magellanicus* sp. nov., *Rockacestus ottavianoi* sp. nov., *Rockacestus piriei* (Williams, 1968), *Rockacestus radioductus* (Kay, 1942), *Rockacestus rakusai* (Wojciechowska, 1991), *Rockacestus siedleckii* (Wojciechowska, 1991), and *Rockacestus williamsi* (Schmidt, 1986).

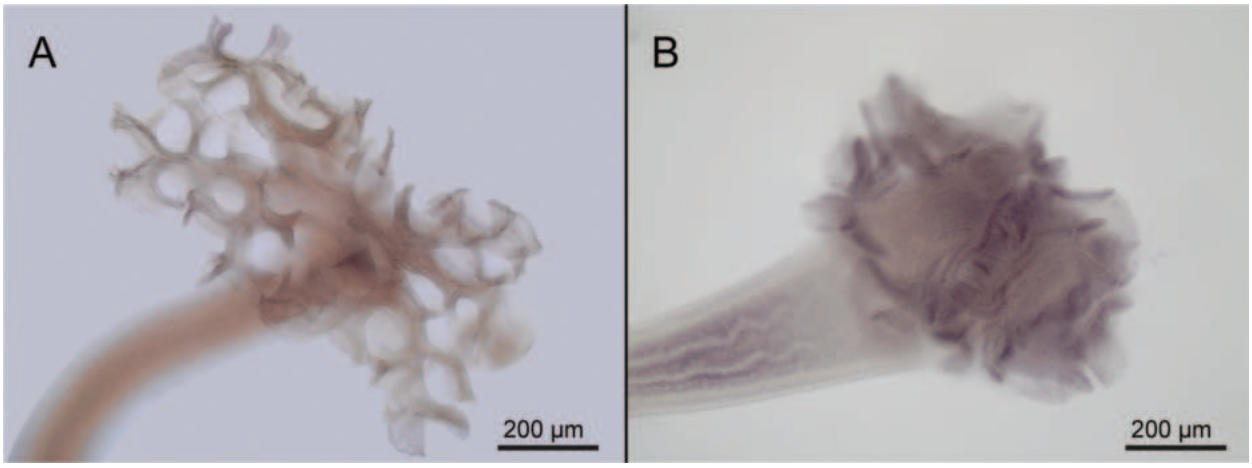

Figure 8. Light micrographs of scoleces of *Rockacestus blasi* sp. nov. **A.** Bothridia fixed while still attached to the host tissue (paratype MACN-Pa No. 787); **B.** Bothridia properly relaxed and fixed (paratype MACN-Pa No. 784/2).

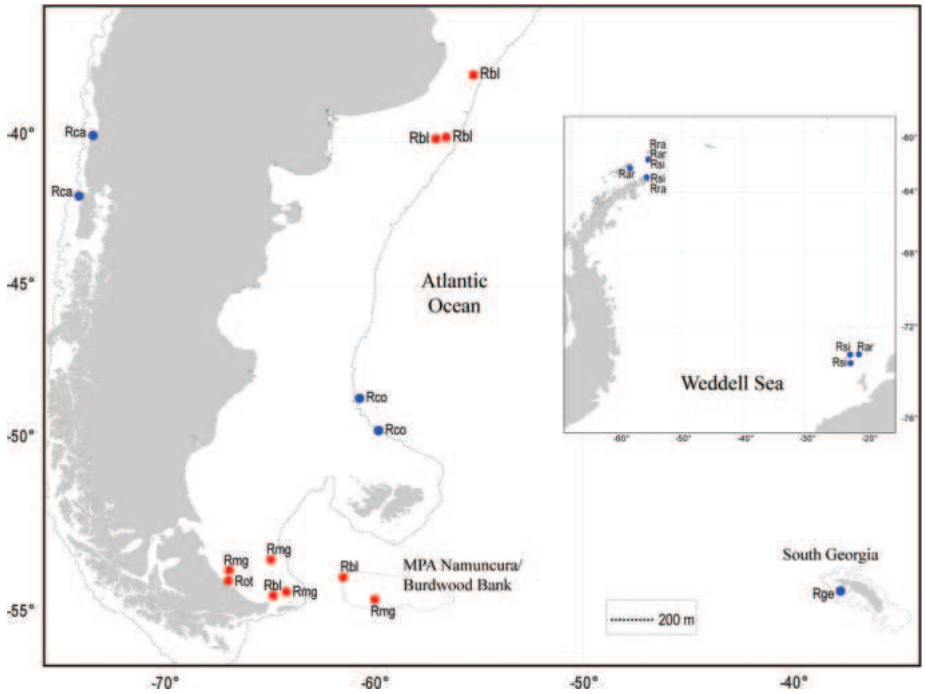

Figure 9. Geographic distribution of the valid species of *Rockacestus* from the Southern Hemisphere. Symbols: red dot: new records; blue dot: previous records; **Rar** – *Rockacestus arctowskii*; **Rbl** – *Rockacestus blasi* sp. nov.; **Rca** – *Rockacestus carvajali*; **Rco** – *Rockacestus conchai*; **Rge** – *Rockacestus georgiensis*; **Rma** – *Rockacestus magellanicus* sp. nov.; **Rot** – *Rockacestus ottavianoi* sp. nov.; **Rra** – *Rockacestus rakusai*; **Rsi** – *Rockacestus siedleckii*.

The genus is widespread among temperate waters of the East Pacific and Atlantic Oceans, with *R. brittanicus*, *R. piriei*, and *R. williamsi* inhabiting the Northeast Atlantic Ocean; *R. radioductus* in the Northeast Pacific Ocean, *R. carvajali* from off Chiloé Island in the Southeast Pacific Ocean, and *R. conchai* off Malvinas Islands in the SWA. A subset of *Rockacestus* species also inhabits sub-Antarctic and Antarctic waters, with *R. georgiensis* from off South Georgia Island, *R. rakusai* registered off the Antarctic Peninsula, and records of *R. arctowskii* and *R. siedleckii* off the Antarctic Peninsula and the Weddel Sea. *Rockacestus blasi* sp. nov., *R. magellanicus* sp. nov. and *R. ottavianoi* sp. nov. are restricted to the Magellanic Province *sensu* Sabadin et al. (2020) in the SWA. The finding of the new species increases the species richness from two to five in marine waters around South America. Thus, the known latitudinal range of the genus in the Northern Hemisphere covers from 48°N to 58°N whereas in the Southern Hemisphere *Rockacestus* now ranges between 37 to 74°S (Fig. 9).

Discussion

Scolex

A well-relaxed tapeworm scolex represents a challenge, as it often results in a contracted material, making difficult a proper characterization of the actual shape of the bothridia. For example, among members of the Phyllobothriidea, specimens of *Guidus* show a marked bothridial projection, and those of *R. piriei* exhibits highly folded bothridia when attached to the gut mucosa of their hosts (figs 13, 14 in Williams [1968b], fig. 4E in Menoret and Ivanov [2021]).

Among the scoleces herein described, *R. magellanicus* sp. nov. and *R. ottavianoi* sp. nov. exhibit bothridia with a higher degree of folding than *R. blasi* sp. nov. A few specimens of *R. blasi* sp. nov. were fixed while still attached to the host, appearing to have significantly folded bothridia (Fig. 8A). However, the typical scolex of these specimens is obtained once removed from the host and properly relaxed (Fig. 8B).

Rockacestus conchai was originally described as having a scolex with highly folded bothridia, however, it resembles the contracted scoleces of *R. piriei* and *R. blasi* sp. nov. (see Fig. 8A). Therefore, the degree of the bothridial folding would be a useful character to distinguish between species, as long as it is verified that this variability is not given by an artifact of the fixation technique.

Ultrastructure of the scolex (SEM)

The surface of the scolex has been analyzed with SEM in five of the now 13 valid species of *Rockacestus*. Among the five species, *R. carvajali* and *R. conchai* were partially studied, with *R. carvajali* mostly characterized by papilliform filitriches (see fig. 8B, D, E in Caira et al. [2021]). The new species of *Rockacestus* from off Argentina, in addition to *R. conchai*, exhibit a common microthrix pattern, with acicular filitriches distributed along the bothridial surfaces, capilliform filitriches arranged in scutes on the neck, and lingulate spinitriches in most of the distal bothridial surface. Both the apical sucker and the marginal loculi are novel results of the present study and characterize *R. blasi* sp. nov., *R. magellanicus* sp. nov., and *R. ottavianoi* sp. nov. by the presence of small lingulate and lanceolate spinitriches on the distal surface of the apical sucker and coniform spinitriches with rounded tips covering the distal surface of the marginal loculi (Figs 3C, D, G, 5B, D, I, L, 6B, D, I, L).

Given that most of these species studied with SEM exhibit a variety of spinitriches, it is likely that the scolex of *R. carvajali* has been based on micrographs with a low resolution or magnification. It would be important to complete the study all along the distal bothridial surface in *R. carvajali* and *R. conchai*, such as the apical sucker and the marginal loculi, to verify if they are similar in the type and distribution of microtriches and cilia to those observed in the new species of *Rockacestus* off Argentina. The majority of spinitriches found in *Rockacestus* belong to morphotypes rarely observed among the phyllobothrideans. For example, lingulate-like spinitriches were reported in the phyllobothriid *Crossobothrium laciniatum* Linton, 1889 (see Ruhnke 2011) but they actually are trullate spinitriches sensu Chervy (2009). In contrast, the lanceolate spinitriches exhibited by the new species and described in this study have not yet been reported among members of the order. Additionally, the particular kind of short coniform spinitriches with rounded tips observed in the marginal loculi of these three new species (Figs 3G, 5I, L, 6I, L) is reported for the first time among cestodes, showing an increasing variety of microtriches as new cestode taxa are discovered. Therefore, the diversity of spinitriches in the genus should be extended to include coniform and lanceolate morphotypes rather than only lingulate (not gladiate) as mentioned in the original diagnosis of *Rockacestus*.

Proglottid and terminal genitalia characters

Among the diagnostic features of the genus, Caira et al. (2021) characterized *Rockacestus* by being euapolytic and lacking a seminal receptacle.

Specimens of *R. brittanicus* were originally described by Williams (1968a) as euapolytic, however, this author showed a uterus filled with eggs in the terminal proglottids (see fig. 13 in Williams [1968a]). This discrepancy, also noticed by Ruhnke (2011), could be resolved once the type material of *R. brittanicus* is examined. To date, *R. blasi* sp. nov. remains the only apolytic species in the genus. Kay (1942) described *R. radioductus* having a seminal receptacle and provided ink drawings of its morphology (fig. 5 in Kay [1942]), being the first report of this structure in the

genus. Furthermore, Wojciechowska (1991) mentioned an enlarged vagina in the proximal portion between the ovary lobes in *R. arctowskii*, *R. georgiensis*, *R. rakusai*, and *R. siedleckii* (see fig. 1B in Wojciechowska [1991]). In addition, a vagina enlarged in a seminal receptacle near the ovary isthmus is observed in whole mounts and confirmed in cross-sections of mature proglottids of *R. blasi* sp. nov., *R. magellanicus* sp. nov. and *R. ottavianoi* sp. nov. (Fig. 7C, F, I). Therefore, the genus now consists of apolytic and euapolytic specimens and a seminal receptacle is present in some species. In addition, some information such as the size of the Mehlis´gland, the presence or absence of an uteroduct, and the entrance site of the vas deferens in the cirrus sac were described for the first time for the Argentinian species of *Rockacestus*.

Host associations and host-specificity

Previous records of *Rockacestus* include a total of nine oioxenous species found in marine skates belonging to the families Rajidae (i.e., *R. brittanicus*, *R. carvajali*, *R. georgiensis*, *R. piriei*, *R. radioductus*, and *R. williamsi*), and Arhynchobatidae (i.e., *R. arctowskii*, *R. conchai*, and *R. rakusai*) (Kay 1942; Williams 1968a, 1968b; Schmidt 1986; Wojciechowska 1991; Caira et al. 2021). The exception is *R. siedleckii*, which parasitizes two different species of *Bathyraja* (see Wojciechowska 1991; Rocka and Zditowiecki 1998). The finding of the three species described in this study, not only increases the number of oioxenous species of the genus, but also brings the total number of species of *Rockacestus* as parasites of arhynchobatid skates to seven. This study comprises the first report of *Rockacestus* species in *B. macloviana* and *B. magellanica*. Furthermore, it is the second record of a single softnose skate species harboring several species of *Rockacestus* (Wojciechowska 1991; Rocka and Zditowiecki 1998; this paper).

To date, a total of seven species of *Bathyraja* skates were registered as hosts of phyllobothriideans (Franzese et al. 2023; this work). Among them, *Rockacestus* most resembles *Guidus* Ivanov, 2006 since both exhibit a tight association with *Bathyraja* skates from the SWA and off Antarctica (Menoret and Ivanov 2021). Although *B. maccaini and B. magellanica* host several phyllobothriideans, more surprising is that a single individual of *B. magellanica* became a suitable host for a complex of phyllobothriidean species. Particularly, our individual PD4-097 was found to host simultaneously *R. ottavianoi* sp. nov., *Guidus francoi* Menoret & Ivanov, 2021, and *Guidus magellanicus* Menoret & Ivanov, 2021.

Beer et al. (2019), relying only on sequencing, identified several species of a new genus of phyllobothriids recovered from seven species of *Bathyraja* from the Malvinas Islands Shelf. Their specimens not deposited into any museum were later considered by Caira et al. (2021) as members of *Rockacestus*. It would be interesting to identify these specimens at specific level in order to estimate more precisely the richness of the genus in the SWA.

Geographic distribution

Species of *Rockacestus* are closely associated with temperate, sub-Antarctic, and Antarctic waters. The Northern Hemisphere is represented only by a few species, including *R. brittanicus*, *R. piriei*, *R. radioductus*, and *R. williamsi*, as parasites of rajid skates (Kay 1942; Williams 1968a, 1968b; Schmidt 1986). In contrast, the remaining nine species occur in the Southern Hemisphere, mostly parasitizing arhynchobatid skates of the genus *Bathyraja* (Wojciechowska 1991; Caira et al. 2021; this paper). Ten species (i.e., *R. brittanicus*, *R. carvajali*, *R. conchai*, *R. georgiensis*, *R. magellanicus* sp. nov., *R. ottavianoi* sp. nov., *R. piriei*, *R. radioductus*, *R. rakusai*, and *R. williamsi*) are restricted to their type locality and surrounding areas. In contrast, *R. arctowskii*, *R. blasi* sp. nov., and *R. siedleckii* do not show this pattern. *Rockacestus arctowskii* and *R. siedleckii* were recorded off the Antarctic Peninsula and in the eastern part of the Weddell Sea, whereas *R. blasi* sp. nov. is, to date, the species with the broadest latitudinal range (37°S–54°S) occurring from waters off Buenos Aires Province to southeast Patagonia (Fig. 9). The southern distribution of *R. magellanicus* sp. nov. and *R. ottavianoi* sp. nov. resembles members of *G. francoi* and *G. magellanicus* as they remain locally restricted to the Magellanic Province in the SWA despite the wider distribution of their host. Although reports in the SWA have increased in the recent years due to focused sampling efforts in the area (Menoret and Ivanov 2009, 2012a, 2012b, 2014, 2015, 2021, 2023; Mutti and Ivanov 2016; Menoret et al. 2017; Franzese and Ivanov 2018, 2020a, 2020b, 2021; Franzese et al. 2022, 2023), it would be interesting to see if the composition of the *Rockacestus* fauna which is currently restricted to the type locality changes as the sampling area of host continues to expand.

Recently, Sabadin et al. (2020) proposed a bioregionalization scheme of the SWA, based on chondrichthyan assemblages, and showed that eight species of *Bathyraja*, including *B. magellanica*, are dominant species of batoids in the Magellanic Province. Regarding the tight association of the genera *Rockacestus* and *Guidus* with the genus *Bathyraja* in the SWA and considering that the nine new geographic records of *Rockacestus* herein reported are in the Magellanic Province, we, therefore, expect that as the sampling spectrum increases among *Bathyraja* species in the region, the discovery of new species of *Rockacestus* and *Guidus* will also increase. Finally, *R. blasi* sp. nov. and *R. magellanicus* sp. nov. are new reports of phyllobothriideans after *Guidus argentinense* Ivanov, 2006, off a marine protected area (see Menoret and Ivanov 2021). The discovery of new species of *Rockacestus* from skates of the genus *Bathyraja* from off Argentina increases the number of species from one to four in the SWA and the number of valid species in the genus from ten to 13, expanding its geographical range and bringing the percentage of phyllobothriideans inhabiting the Southern Hemisphere to 39%.

Acknowledgements

Special thanks are due to Juan M. Díaz de Astarloa, Ezequiel Mabragaña, Gabriela Delpiani, and Diego M. Vázquez from Laboratorio de Biotaxonomía Morfológica y Molecular de Peces (Universidad Nacional de Mar del Plata-CONICET) for their help in the identification of hosts collected on board of the RV *Puerto Deseado*. The authors are indebted to Sebastián Franzese and Alejandro Martinez for sorting part of the material studied in the laboratory. Special thanks are due to Anna Phillips from the Smithsonian National Museum of Natural History for providing us with the digital micrographs of the type material of species of *Rockacestus*. We are also very grateful to Consejo Nacional de Investigaciones Científicas y Técnicas (CONICET) for allowing us to work on board the RV *Puerto Deseado*. Also special thanks to Pavel Stoev, Editor of Zoosystematics and Evolution, and to the reviewers for their helpful and insightful suggestions. This work was supported by the Universidad de Buenos Aires (UBACyT 20020130100617BA), CONICET (PIP 11220150100705), the Agencia Nacional de Promoción Científica y Tecnológica-ANPCyT (grant number PICT 2014-2358 to VAI and PICT 2016-3672 to AM), and the American Museum of Natural History (Lerner-Gray Memorial Fund for Marine Research 2018 to GGF). This study was conducted under collecting permits No. 39 and No. 260 from the Dirección Provincial de Pesca-Ministerio de Asuntos Agrarios de la Provincia de Buenos Aires, Argentina. This work is the contribution No. 75 to the MPA Namuncurá (Law 26.875).

References

Beer A, Ingram T, Randhawa HS (2019) Role of ecology and phylogeny in determining tapeworm assemblages in skates (Rajiformes). Journal of Helminthology 93(6): 738–751. https://doi.org/10.1017/S0022149X18000809

Caira JN, Jensen K, Waeschenbach A, Olson PD, Littlewood DTJ (2014) Orders out of chaos–molecular phylogenetics reveals the complexity of shark and stingray tapeworm relationships. International Journal for Parasitology 44(1): 55–73. https://doi.org/10.1016/j.ijpara.2013.10.004

Caira JN, Bueno V, Jensen K (2021) Emerging global novelty in phyllobothriidean tapeworms (Cestoda: Phyllobothriidea) from sharks and skates (Elasmobranchii). Zoological Journal of the Linnean Society 193(4): 1336–1363. https://doi.org/10.1093/zoolinnean/zlaa185

Chervy L (2009) Unified terminology for cestode microtriches: A proposal from the International Workshops on Cestode Systematics in 2002–2008. Folia Parasitologica 56(3): 199–230. https://doi.org/10.14411/fp.2009.025

Diepenbroek M, Grobe H, Reinke M, Schindler U, Schlitzer R, Sieger R, Wefer G (2002) PANGAEA–An information system for environmental sciences. Computers & Geosciences 28(10): 1201–1210. https://doi.org/10.1016/S0098-3004(02)00039-0

Fowler HW (1910) Notes on batoid fishes. Proceedings. Academy of Natural Sciences of Philadelphia 62: 468–475. https://www.jstor.org/stable/4063435

Franzese S, Ivanov VA (2018) Hyperapolytic species of *Acanthobothrium* (Cestoda: Onchoproteocephalidea) from batoids off Argentina. Parasitology International 67(4): 431–443. https://doi.org/10.1016/j.parint.2018.04.001

Franzese S, Ivanov VA (2020a): Two new species of *Acanthobothrium* Blanchard, 1848 (Cestoda: Onchoproteocephalidea) from rajiform batoids off Argentina. Folia Parasitologica 67: 016. https://doi.org/10.14411/fp.2020.016

Franzese S, Ivanov VA (2020b) A new genus of *Rhinebothriidea* from species of *Psammobatis* (Rajiformes: Arhynchobatidae) off Argentina. Zootaxa 4803(2): 355–372. https://doi.org/10.11646/zootaxa.4803.2.7

Franzese S, Ivanov VA (2021) Two new species of *Scalithrium* (Cestoda: Rhinebothriidea) from rajiform batoids of the Argentine Sea. Zootaxa 5005(1): 62–76. https://doi.org/10.11646/zootaxa.5005

Franzese S, Mutti LD, Tropea C, Ivanov VA (2022) Morphological study of members of the genus *Echeneibothrium* (Cestoda: Rhinebothriidea: Echeneibothriidae) from rajiform skates of the Argentine Sea and analysis of the phylogenetic relationships within the family Echeneibothriidae. Zoologischer Anzeiger 299: 1–20. https://doi.org/10.1016/j.jcz.2022.05.002

Franzese S, García Facal G, Menoret A (2023) Tapeworms (Platyhelminthes, Cestoda) from marine chondrichthyans of the Southwestern Atlantic Ocean, and the sub-Antarctic and Antarctic islands: A checklist. ZooKeys 1163: 78–119. https://doi.org/10.3897/zookeys.1163.100485

Froese R, Pauly D (2023) FishBase. World Wide Web electronic publication. http://www.fishbase.org [Accessed 1 September 2023]

Girard CF (1855) Characteristics of some cartilaginous fishes of the Pacific coast of North America. Proceedings. Academy of Natural Sciences of Philadelphia 7: 196–197. https://biostor.org/reference/67169

Guichenot A (1848) Notice sur l'établissement d'un nouveau genre de Chétodons. Revue Zoologique par la Société Cuvierienne 11: 12–14.

Ishiyama R (1958) Studies on the rajid fishes (Rajidae) found in the waters around Japan. Journal of the Shimonoseki College of Fisheries 7: 193–394.

Kay MW (1942) A new species of *Phyllobothrium* Van Beneden from *Raja binoculata* (Girard). Transactions of the American Microscopical Society 61: 261–266. https://doi.org/10.2307/3222596

Linnaeus C (1758) Systema Naturae. Laurentii Salvii: Stockholm. http://biodiversitylibrary.org/page/727068

Menoret A, Ivanov VA (2009) New name for *Progrillotia dollfusi* Carvajal et Rego, 1983 (Cestoda: Trypanorhyncha): description of adults from *Squatina guggenheim* (Chondrichthyes: Squatiniformes) off the coast of Argentina. Folia Parasitologica 56(4): 284–294. https://doi.org/10.14411/fp.2009.033

Menoret A, Ivanov VA (2012a) A new species of *Heteronybelinia* (Cestoda: Trypanorhyncha) from *Sympterygia bonapartii* (Rajidae), *Nemadactylus bergi* (Cheilodactylidae) and *Raneya brasiliensis* (Ophidiidae) in the south-western Atlantic, with comments on host specificity of the genus. Journal of Helminthology 87(4): 467–482. https://doi.org/10.1017/S0022149X12000545

Menoret A, Ivanov VA (2012b) Description of plerocerci and adults of a new species of *Grillotia* (Cestoda: Trypanorhyncha) in teleosts and elasmobranchs from the Patagonian shelf off Argentina. The Journal of Parasitology 98(6): 1185–1199. https://doi.org/10.1645/GE-3107.1

Menoret A, Ivanov VA (2014) Eutetrarhynchid trypanorhynchs (Cestoda) from elasmobranchs off Argentina, including the description of *Dollfusiella taminii* sp. n. and *Parachristianella damiani* sp. n., and amended description of *Dollfusiella vooremi* (São Celemente et Gomes, 1989). Folia Parasitologica 61(5): 411–431. https://doi.org/10.14411/fp.2014.056

Menoret A, Ivanov VA (2015) Trypanorhynch cestodes (Eutetrarhynchidae) from batoids along the coast of Argentina, including the description of new species in *Dollfusiella* Campbell et Beveridge, 1994 and *Mecistobothrium* Heinz et Dailey, 1974. Folia Parasitologica 62: 058. https://doi.org/10.14411/fp.2015.058

Menoret A, Ivanov VA (2021) New species of *Guidus* Ivanov, 2006 (Cestoda: Phyllobothriidea) from *Bathyraja magellanica* (Philippi) from the Patagonian Continental Shelf of Argentina. Folia Parasitologica 68: 011. https://doi.org/10.14411/fp.2021.011

Menoret A, Ivanov VA (2023) Cestodes of *Pseudobatos horkelii* (Müller and Henle) (Rhinopristiformes) including *Rhinebothrium quequense* n. sp. (Rhinebothriidea) and *Caulobothrium pieroi* n. sp. ("Tetraphyllidea") from the southwestern Atlantic. Zootaxa 5361(1): 87–102. https://doi.org/10.11646/zootaxa.5361.1.4

Menoret A, Mutti L, Ivanov VA (2017) New species of *Aberrapex* Jensen, 2001 (Cestoda: Lecanicephalidea) from eagle rays of the genus *Myliobatis* Cuvier (Myliobatiformes: Myliobatidae) from off Argentina. Folia Parasitologica 64: 009. https://doi.org/10.14411/fp.2017.009

Müller J, Henle FGJ (1841) Systematische Beschreibung der Plagiostomen. Veit, Berlin. https://doi.org/10.5962/bhl.title.6906

Mutti LD, Ivanov VA (2016) A new species of *Paraberrapex* Jensen, 2001 (Cestoda: Lecanicephalidea) from *Squatina guggenheim* Marini (Squatiniformes: Squatinidae) off Argentina. Folia Parasitologica 63: 007. https://doi.org/10.14411/fp.2016.007

Norman JR (1937) Coast fishes. Part 2. The Patagonian region. Discovery Reports 16: 1–150. https://doi.org/10.5962/bhl.part.29326

Philippi RA (1902) Descripción de cinco nuevas especies chilenas del orden de los Plagióstomos. Anales de la Universidad de Chile 109: 303–315.

Rocka A, Zditowiecki K (1998) Cestodes in fishes of the Weddell Sea. Acta Parasitologica 2: 43.

Ruhnke TR (2011) Tapeworms of elasmobranchs (Part III) A Monograph on the Phyllobothriidae (Platyhelminthes, Cestoda). Bulletin of the University of Nebraska State Museum 25 (i–xii), Nebraska, 205 pp. https://digitalcommons.unl.edu/museumbulletin/33/

Sabadin DE, Lucifora LO, Barbini SA, Figueroa DE, Kittlein M (2020) Towards regionalization of the chondrichthyan fauna of the Southwest Atlantic: A spatial framework for conservation planning. ICES Journal of Marine Science 77(5): 1893–1905. https://doi.org/10.1093/icesjms/fsaa064

Schmidt GD (1986): Handbook of tapeworm identification. CRC Press, Boca Raton, Florida. 24, 675 pp.

Spalding MD, Fox HE, Allen GR, Davidson N, Ferdaña ZA, Finlayson MAX, Halpner BS, Jorge MA, Lombana A, Lourie SA, Martin KD, McManus E, Molnar J, Recchia CA, Robertson J (2007) Marine ecoregions of the world: A bioregionalization of coastal and shelf areas. Bioscience 57(7): 573–583. https://doi.org/10.1641/B570707

Williams HH (1968a) The taxonomy, ecology and host-specificity of some Phyllobothriidae (Cestoda: Tetraphyllidea), a critical revision of *Phyllobothrium* Beneden, 1849 and comments on some allied genera. Philosophical Transactions of the Royal Society of London. Series B, Biological Sciences 253: 231–307. https://doi.org/10.1098/rstb.1968.0002

Williams HH (1968b) *Phyllobothrium piriei* sp. nov. (Cestoda: Tetraphyllidea) from *Raja naevus* with a comment on its habitat and mode of attachment. Parasitology 58(4): 929–937. https://doi.org/10.1017/S0031182000069699

Wojciechowska A (1991) New species of the genus *Phyllobothrium* (Cestoda, Tetraphyllidea) from Antarctic batoid fishes. Acta Parasitologica Polonica 36(2): 63–68.

Zoosyst. Evol. 100 (2) 2024, 373–383 | DOI 10.3897/zse.100.115813

PENSOFT

MUSEUM FÜR NATURKUNDE BERLIN

Five new species of *Exalloniscus* Stebbing, 1911 (Crustacea, Isopoda, Oniscidea) from China

Chao Jiang[1], Chonghui Yao[2], Luqi Huang[1], Weichun Li[2]

1 *State Key Laboratory for Quality Ensurance and Sustainable Use of Dao-di Herbs, National Resource Center for Chinese Materia Medica, China Academy of Chinese Medical Sciences, Beijing 100700, China*

2 *College of Agronomy, Jiangxi Agricultural University, Nanchang 330045, China*

https://zoobank.org/1B0AF998-E43A-4F82-9F97-F6F8C99133B4

Corresponding author: Weichun Li (weichunlee@126.com)

Academic editor: Luiz F. Andrade ♦ **Received** 15 November 2023 ♦ **Accepted** 12 March 2024 ♦ **Published** 3 April 2024

Abstract

Exalloniscus Stebbing, 1911 is investigated from China, and eleven species of the genus are now recorded from China. Five of them are described as new: *E. duospinatus* Li & Jiang, **sp. nov.**, *E. curvispinatus* Li & Jiang, **sp. nov.**, *E. triangulus* Li & Jiang, **sp. nov.**, *E. tridentatus* Li & Jiang, **sp. nov.** and *E. taitii* Li & Jiang, **sp. nov.** A map of China showing the recorded localities of *Exalloniscus* members is provided.

Key Words

China, distribution, morphology, new species, taxonomy

Introduction

The genus *Exalloniscus* was established by Stebbing (1911) to allocate *Alloniscus coecus* Dollfus, 1898 from Indonesia. To date, the genus includes twenty-eight species with Oriental and Palaearctic distribution, occurring in South Asia (India, Sri Lanka, Nepal), Southeast Asia (Cambodia, Laos, Indonesia, Malaysia, Myanmar, Philippines, Singapore, Thailand, Vietnam), and East Asia (China, Korea, Japan) (Manicastri and Argano 1986; Taiti and Ferrara 1988; Manicastri and Taiti 1991; Kwon 1993, 1995; Kwon and Taiti 1993; Nunomura 2000; Nunomura and Xie 2000; Taiti and Gruber 2008; Taiti and Cardoso 2020). The genus has been redefined (Taiti and Ferrara 1988), and its diagnosis has also been amended (Taiti and Cardoso 2020). Prior to this study, six *Exalloniscus* species were known from China (Taiti and Ferrara 1986; Kwon and Taiti 1993; Nunomura and Xie 2000; Chen 2003; Taiti and Gruber 2008; Taiti and Cardoso 2020). The present study aimed to describe five new species of the genus collected in China.

Materials and methods

Specimens were collected by hand using tweezers and preserved in 75% ethanol. The appendages were stained with acid fuchsin and mounted on micro-preparations in a neutral balsam mounting medium. Habitus were recorded with a Zeiss AxioCam Icc 5 digital camera attached to a Zeiss Stereo Discovery V12 microscope. Illustrations of the appendages were prepared using an Optec DV E3 630 digital camera attached to an Optec BK6000 microscope. GNU Image Manipulation Program (Montesanto 2015) was used for line drawings. The terminology for morphological structures followed Taiti and Cardoso (2020). The

specimens are deposited at the Insect Museum, Jiangxi Agricultural University, Nanchang, China (JXAUM) and National Resource Center for Chinese Materia Medica, China Academy of Chinese Medical Sciences, Beijing, China (CMMI).

Taxonomic account

***Exalloniscus duospinatus* Li & Jiang, sp. nov.**

https://zoobank.org/3F019AA6-3E86-4AD0-828F-20E115548925

Figs 1A, 2

Type material. *Holotype*. China: male, Sichuan Province, Qionglai, Datong Town (30°30'N, 103°18'E), alt. 770 m, 16 April 2021, Chao Jiang leg., habitus no. QL2301, prep. slide no. L23098 (JXAUM).

***Paratypes*. China, Sichuan Province**: One female, same data as holotype, no. 20210416044; two males, one female, Dayi County, near Xiling Snow Mountain Tunnel (30°37'N, 103°19'E), alt. 860 m, 16 April 2021, Chao Jiang leg., no. 20210416031−202104160033; one female, Dayi County, Heishuihe Nature Reserve, Dafeishui (30°38'N, 103°10'E), alt. 1290 m, 16 April 2021, Chao Jiang leg., no. 20210416026; one male, Chengdu, Jincheng Park (30°34'N, 104°02'E), alt. 450 m, 19 April 2021, Chao Jiang leg., no. 20210419001 (CMMI).

Diagnosis. Male pleopod 1 endopod has two spinelike lobes at apical part of outer margin.

Description. Maximum length: male 3.6 mm and female 4.2 mm.

Body oval, flattened and pale brown. Cephalon with lateral lobes slightly protruding laterally, apex rounded. Eyes with three ommatidia. Pereonites 1–2 with postero-lateral corners nearly right-angled, pereonites 3–7 with postero-lateral corners directed backwards. Pleonites 3–5 with epimera falciform, protruding backwards. Telson triangular, twice as wide as long, lateral margin slightly concave, ending with rounded apex. Uropod exopod as long as endopod (Fig. 1A).

Antenna with fifth article of peduncle slightly longer than flagellum; ratio of flagellum approximately 3:2:2 (Fig. 2A).

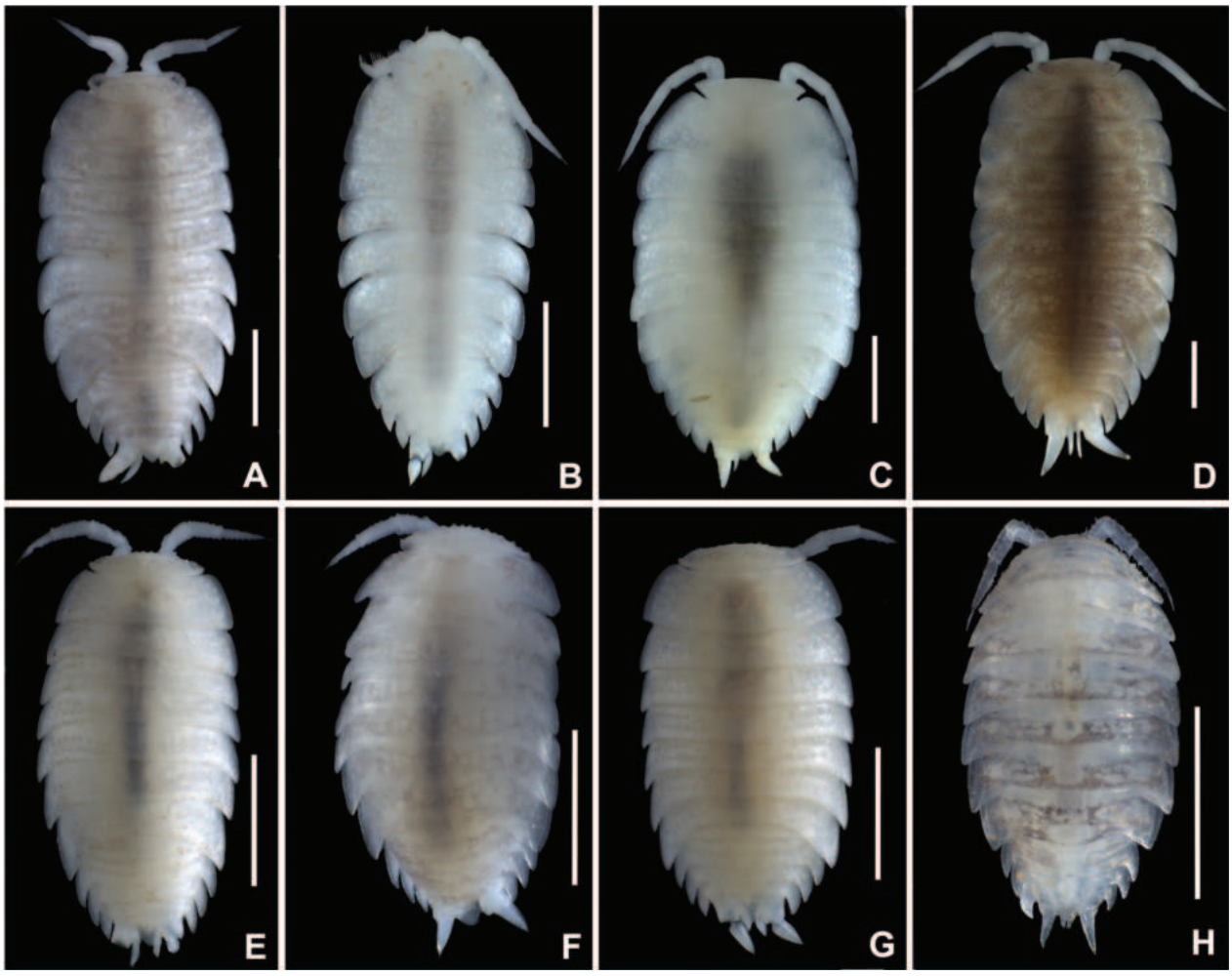

Figure 1. Habitus of *Exalloniscus* species. **A.** *E. duospinatus* sp. nov., holotype; **B** (holotype); **C** (paratype). *E. curvispinatus* sp. nov.; **D.** *E. thailandensis*, male; **E.** *E. triangulus* sp. nov., holotype; **F.** *E. tridentatus* sp. nov., holotype; **G.** *E. cortii*, male; **H.** *E. taitii* sp. nov., holotype. Scale bar: 1 mm.

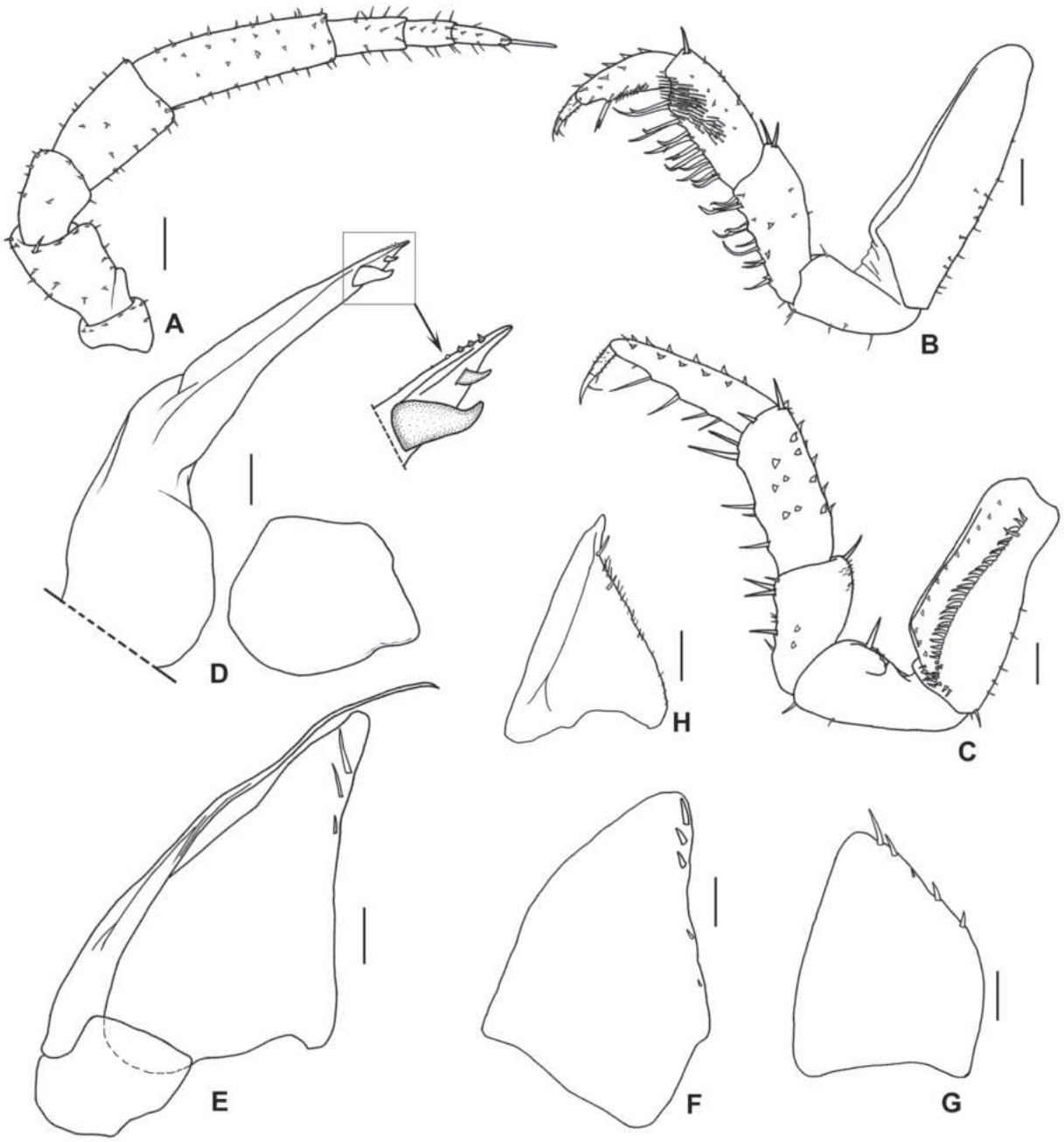

Figure 2. *Exalloniscus duospinatus* sp. nov., holotype. **A.** Antenna; **B.** Pereopod 1; **C.** Pereopod 7; **D.** Pleopod 1; **E.** Pleopod 2; **F.** Pleopod 3 exopod; **G.** Pleopod 4 exopod; **H.** Pleopod 5 exopod. Scale bar: 0.1 mm.

Pereopod 1 with long strong setae on sternal margin of merus and carpus, carpus with transversal antennal grooming brush (Fig. 2B). Pereopod 7 with several strong setae on sternal margin; basis with distinct water conducting system; ischium gently concave on rostral surface of base, and straight on sternal margin (Fig. 2C).

Male pleopod 1 exopod almost quadrangular, outer margin convex; endopod with apical part bearing two spinelike lobes on outer margin and four tiny spines on inner margin (Fig. 2D). Pleopod 2 exopod triangular with several setae on outer margin; endopod flagelliform, longer than exopod (Fig. 2E). Pleopods 3−5 exopods triangular with several setae on outer margin (Fig. 2F−H).

Etymology. Latin: prefix *duo-* = double plus *spinatus* = spinous. The new species name refers to the male pleopod 1 endopod with two spinelike lobes at the apical part of outer margin.

Remarks. This new species is similar to *E. silvestrii* Kwon & Taiti, 1993, but it can be distinguished by pereopod 7 ischium slightly concave at the base of the rostral surface, and pleopod 1 endopod bearing two spinelike lobes at the apical part of the outer margin (Fig. 2C, D). In *E. silvestrii*, the base of pereopod 7 ischium with a large flat rounded lobe on the rostral surface, and the apical part of pleopod 1 endopod with three triangular lobes on the outer margin (Kwon and Taiti 1993: figs 110, 112).

***Exalloniscus curvispinatus* Li & Jiang, sp. nov.**

https://zoobank.org/1CFF7EBE-9FBA-46A3-857C-25511D27B65E

Figs 1B, C, 3

Type material. ***Holotype*. China**: male, Yunnan Province, Mengla County, Xiaomo Road (21°14'N, 101°42'E), alt. 650 m, 18 August 2023, Chao Jiang leg., habitus no. ML23002, prep. slide no. L23104 (JXAUM).

***Paratypes*. China, Yunnan Province**: Two males, one female, same data as the holotype, no. 20230818301; one male, Menglian County, Nayunzhen (22°19'N, 99°35'E), 23 August 2023, Han Qiu leg., habitus no. NYZ23001, prep. slide no. L23105 (JXAUM); one male, Jinghong, Jinuo Village, Bakaxiaozhai (21°57'N, 101°12'E), 15 August 2023, Chao Jiang leg., no. 20230815301; three males, one female, Menglian County, Nayun Town, 23 August 2023, Han Qiu leg., nos. 20230302301 and 20230302202 (CMMI).

Diagnosis. Male pleopod 1 exopod almost pentagonal, and endopod recurved outwards at apical part.

Description. Maximum length: male 5.0 mm and female 4.2 mm.

Body oval, flattened and white. Cephalon with lateral lobes slightly protruding laterally, nearly triangular with blunted apex. Eyes absent. Pereonites with postero-lateral corner progressively more acute, directed backwards. Pleonites 3−5 with epimera falciform, protruding backwards. Telson triangular, twice as wide as long, lateral margin gently concave, ending with rounded apex. Uropod exopod as long as endopod (Fig. 1B).

Antenna with fifth article of peduncle slightly longer than flagellum; ratio of flagellum approximately 4:3:3 (Fig. 3A).

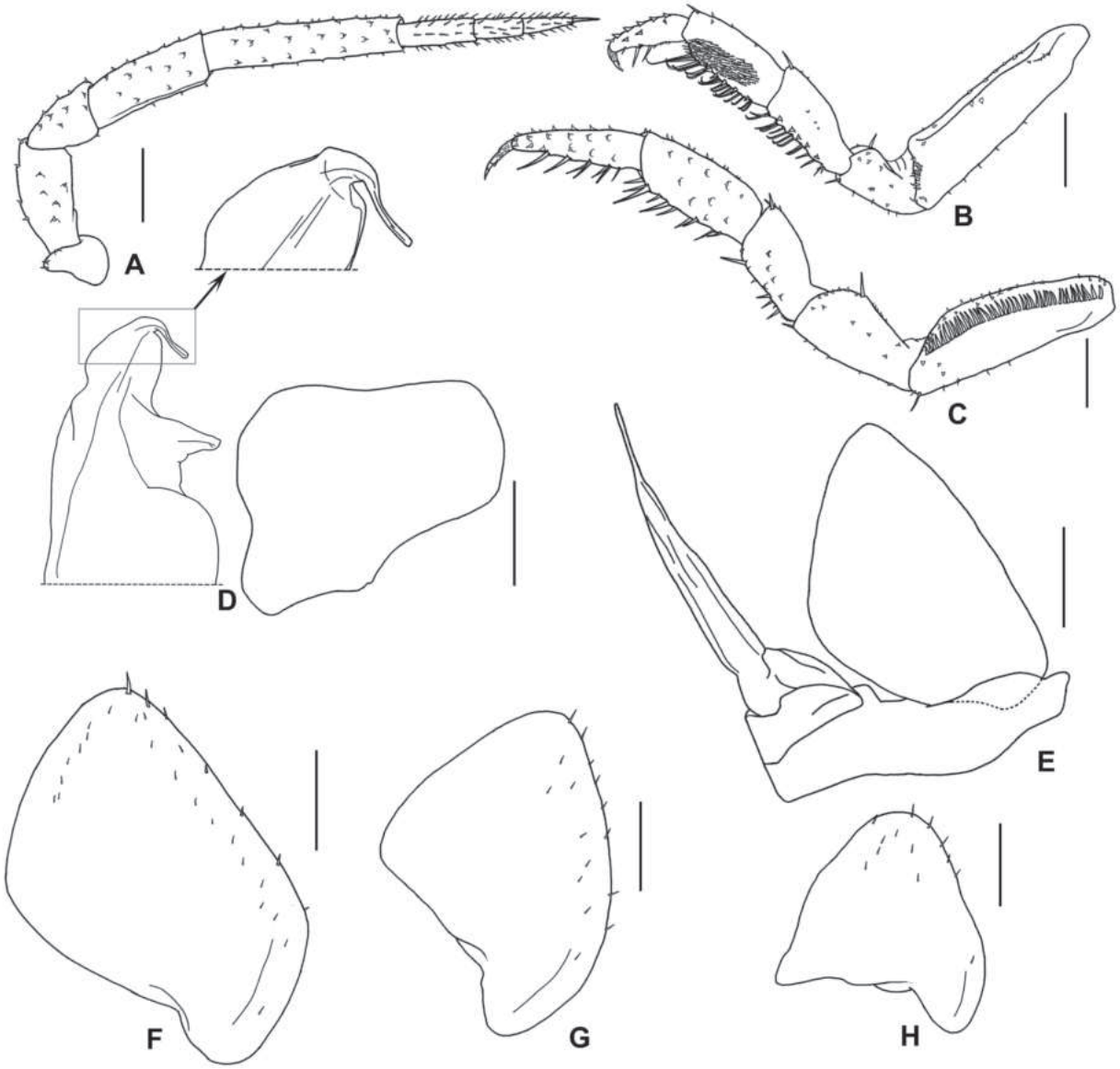

Figure 3. *Exalloniscus curvispinatus* sp. nov., holotype. **A.** Antenna; **B.** Pereopod 1; **C.** Pereopod 7; **D.** Pleopod 1; **E.** Pleopod 2; **F.** Pleopod 3 exopod; **G.** Pleopod 4 exopod; **H.** Pleopod 5 exopod. Scale bar: 0.2 mm.

Pereopod 1 with long strong setae on sternal margin of merus and carpus, carpus with basal part as wide as apical part, bearing transversal antennal grooming brush (Fig. 3B). Pereopod 7 with several strong setae on sternal margin; basis with distinct water conducting system; ischium straight on sternal margin (Fig. 3C).

Male pleopod 1 exopod almost pentagonal; endopod with triangular lobe on outer margin, apical part thin and long, recurved outwards (Fig. 3D). Pleopod 2 exopod oval, apical part narrowed toward round apex; endopod flagelliform, longer than exopod (Fig. 2E). Pleopods 3−5 exopods oval with several setae on outer margin (Fig. 3F−H).

Etymology. Latin: prefix *curv-* = curved plus *spinatus* = spinous. The new species name refers to the apical apex of male pleopod 1 endopod with a spinelike projection recurved outwards.

Remarks. This species varied in body shapes (Fig. 1B *versus* 1C). Specimens collected in Mengla (Fig. 1B) are distinctly thinner than the specimens found in Menglian (Fig. 1C).

The new species is similar to *E. thailandensis* in having a recurved pleopod 1 endopod (Fig. 3 *versus* Fig. 4). However, it can be distinguished by pereopod 1 with the basal part as wide as the apical part, pleopod 1 exopod almost pentagonal, and endopod without transversal sclerotized projections at the apical part (Fig. 3B, D). In *E. thailandensis*, the basal part of pereopod 1 is distinctly narrower than the apical part, pleopod 1 exopod is almost rounded, and endopod armed with transversal sclerotized projections at the apical part (Fig. 4B, D). Moreover, the body pigments of the new species (white, Fig. 1B, C) differ from *E. thailandensis* (brown, Fig. 1D) based on two

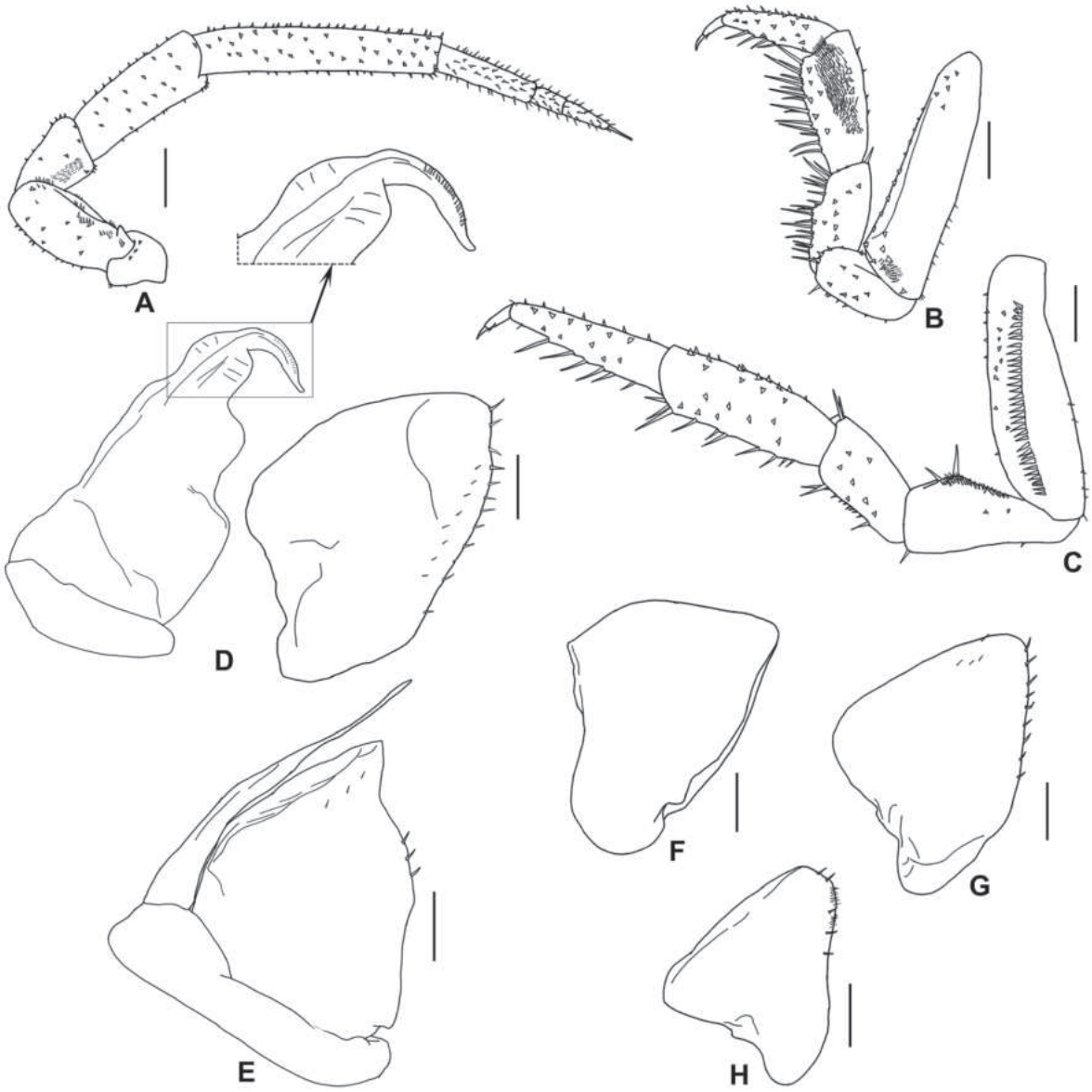

Figure 4. *Exalloniscus thailandensis* (two males, China, Yunnan Province, Mengla, County, Guanlei Town, Baojiaoniu Cave, 17 August 2023, Chao Jiang leg., prep. slide no. L23106). **A.** Antenna; **B.** Pereopod 1; **C.** Pereopod 7; **D.** Pleopod 1; **E.** Pleopod 2; **F.** Pleopod 3 exopod; **G.** Pleopod 4 exopod; **H.** Pleopod 5 exopod. Scale bar: 0.2 mm.

male specimens from China, Yunnan Province, Mengla County, Guanlei Town, Baojiaoniu Cave. However, the colourless individuals of *E. thailandensis* have been described previously (see Taiti and Ferrara 1988). Thus, the body shape and colour should not be considered as exact characters to identify species of the genus.

Exalloniscus triangulus Li & Jiang, sp. nov.

https://zoobank.org/1E234552-69F1-4128-BACA-9FC8609F649F
Figs 1E, 5

Type material. ***Holotype*.** **China**: male, Hubei Province, Jingshan County, Kongshandong Scenic Area (30°58'N, 113°02'E), alt. 100 m, 9 April 2021, Zhidong Wang and Tianyun Chen leg., habitus no. KSD2302, prep. slide no. L23097 (JXAUM).

Diagnosis. Male pleopod 1 exopod distinctly convex on outer margin, and endopod with a triangular lobe and a seta recurved inwards at apical part.

Description. Length 2.9 mm.

Body oval, flattened and white mixed with pale brown. Cephalon with lateral lobes slightly protruding laterally, apex rounded. Eyes with three ommatidia. Pereonites 1 with postero-lateral corner nearly right-angled, pereonites 2−7 with postero-lateral corners directed backwards. Pleonites 3−5 with epimera falciform, protruding backwards. Telson triangular, twice as wide as long, lateral margin gently concave, ending with rounded apex. Uropod exopod almost as long as endopod (Fig. 1E).

Antenna with fifth article of peduncle longer than flagellum; ratio of flagellum approximately 3:2:2 (Fig. 5A).

Pereopod 1 with long strong setae on sternal margin of merus and carpus, carpus with transversal anten-

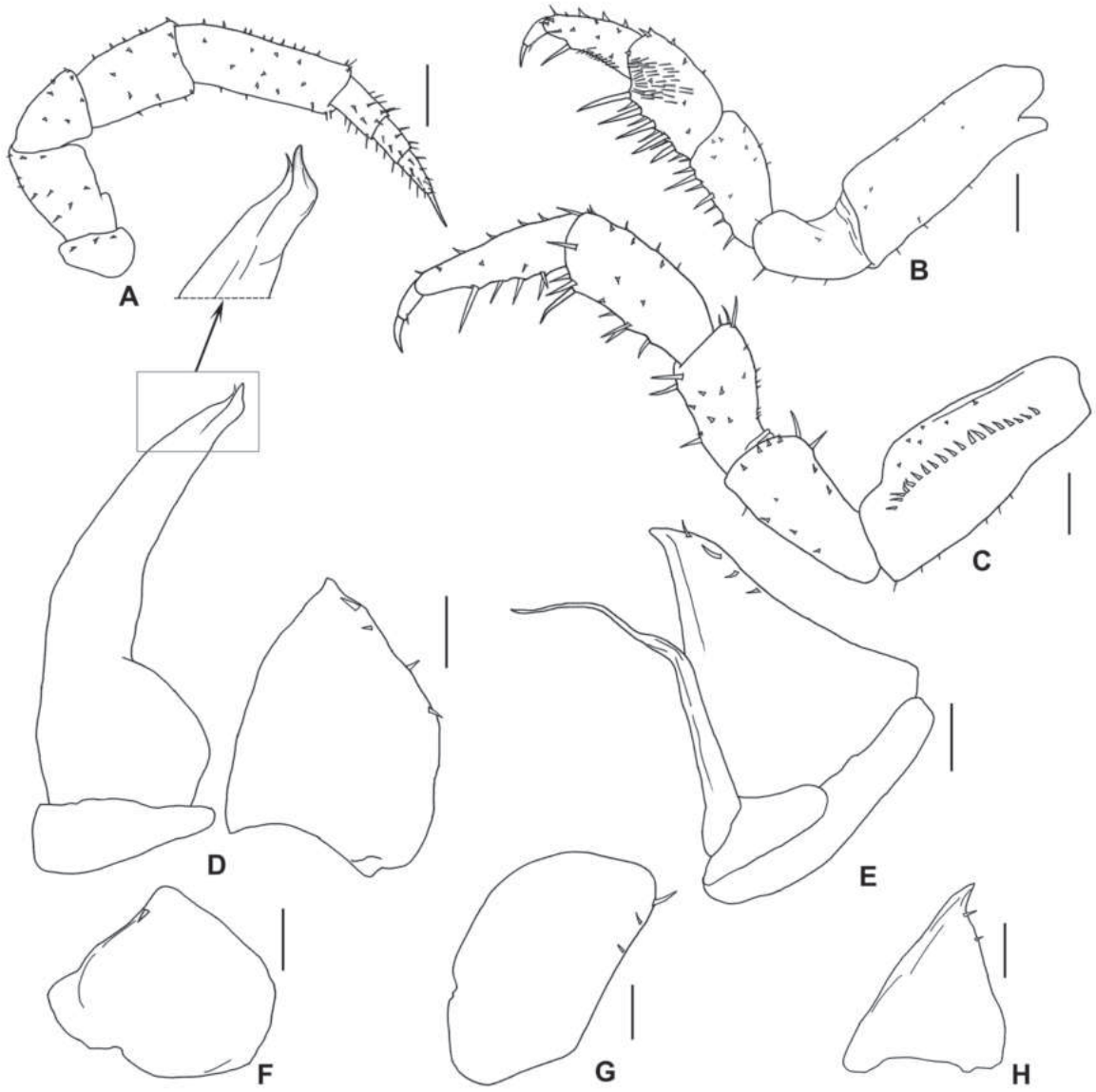

Figure 5. *Exalloniscus triangulus* sp. nov., holotype. **A.** Antenna; **B.** Pereopod 1; **C.** Pereopod 7; **D.** Pleopod 1; **E.** Pleopod 2; **F.** Pleopod 3 exopod; **G.** Pleopod 4 exopod; **H.** Pleopod 5 exopod. Scale bar: 0.1 mm.

nal grooming brush (Fig. 5B). Pereopod 7 with several strong setae on sternal margin; basis with distinct water conducting system; ischium slightly convex on sternal margin (Fig. 5C).

Male pleopod 1 exopod basal half broad, distal half narrowed towards blunted apex, distinctly convex on outer margin; endopod ending with triangular lobe and seta recurved inwards (Fig. 5D). Pleopod 2 exopod triangular with several setae on outer margin; endopod flagelliform, longer than exopod (Fig. 5E). Pleopods 3 and 4 exopods almost oval, pleopod 5 triangular with several setae on outer margin (Fig. 5F−H).

Etymology. Latin: *triangulus* = triangular. The new species name refers to the male pleopod 1 endopod ending with a triangular lobe.

Remarks. This new species is similar to *E. malaccensis* Taiti & Ferrara, 1988 in having a triangular lobe at the apical part of male pleopod 1 endopod. But it can be distinguished by pleopod 1 exopod distinctly convex on the outer margin, and the apical part of endopod with a triangular lobe and a seta recurved inwards (Fig. 5D). In *E. malaccensis*, pleopod 1 exopod is distinctly concave on the outer margin, and the apical lobe of endopod is thinner and recurved outwards (Taiti and Ferrara 1988: fig. 23D).

Exalloniscus tridentatus Li & Jiang, sp. nov.

https://zoobank.org/C7A742F7-5BCF-4A53-AA09-099FB4E8DDB3

Figs 1F, 6

Type material. ***Holotype.*** **China**: male, Shaanxi Province, Zhashui County, Dongshan Forestry Park (33°42'N, 109°01'E), alt. 1020 m, 12 May 2021, Chao Jiang leg., habitus no. ZS2301, prep. slide no. L23095 (JXAUM).

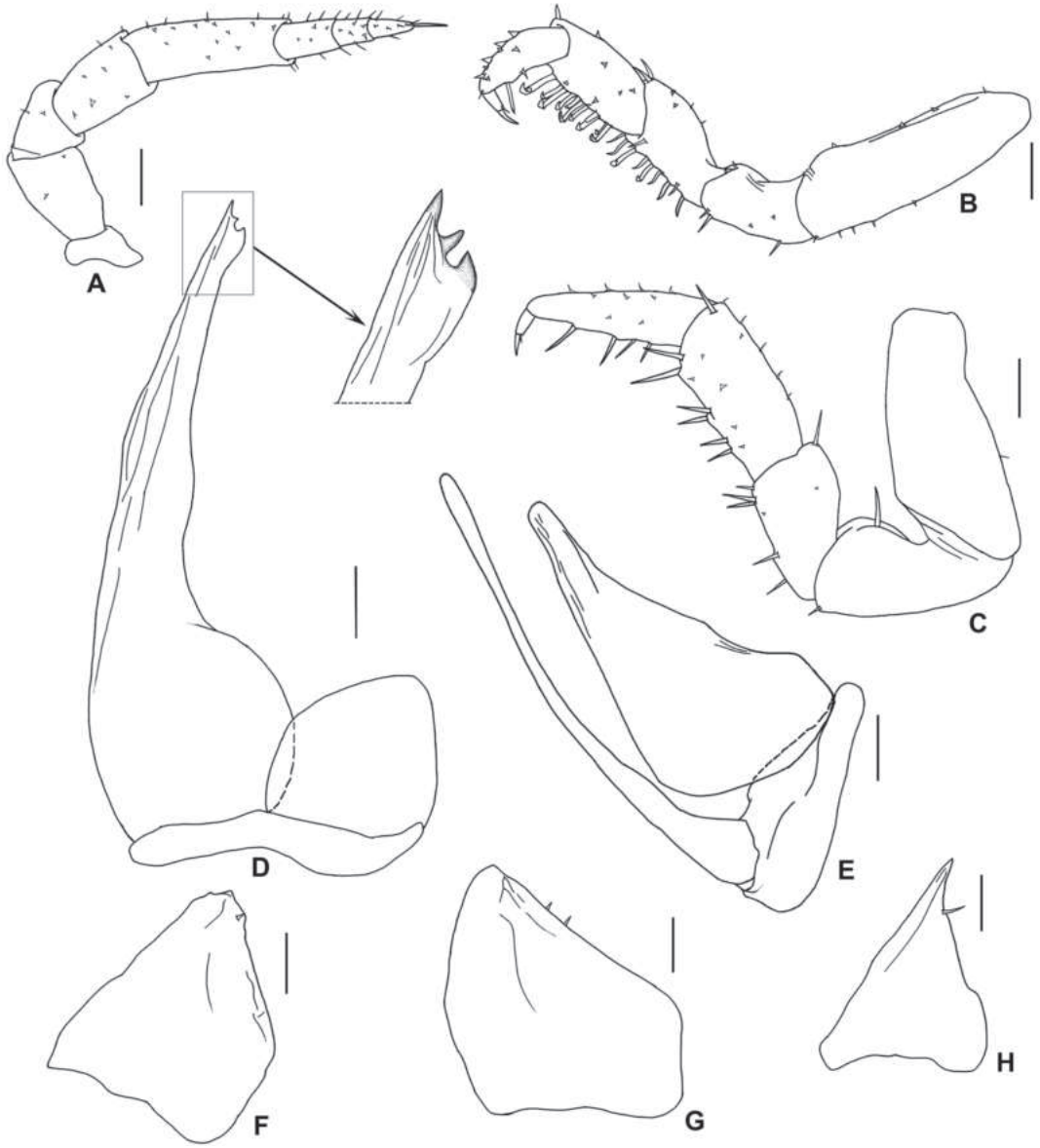

Figure 6. *Exalloniscus tridentatus* sp. nov., holotype. **A.** Antenna; **B.** Pereopod 1; **C.** Pereopod 7; **D.** Pleopod 1; **E.** Pleopod 2; **F.** Pleopod 3 exopod; **G.** Pleopod 4 exopod; **H.** Pleopod 5 exopod. Scale bar: 0.1 mm.

***Paratypes*. China**: two males, two females, same data as the holotype, nos. 20210512007−20210512009 (CMMI).

Diagnosis. Male pleopod 1 exopod straight on outer margin, and endopod bearing three well-developed dentations at apical part.

Description. Maximum length: male 2.5 mm and female 2.8 mm.

Body oval, slightly convex. Colour white mixed with pale brown. Cephalon with lateral lobes slightly protruding laterally, apex rounded. Eyes with three ommatidia. Pereonites with postero-lateral corners directed backwards. Pleonites 3−5 with epimera falciform, protruding backwards. Telson triangular, twice as wide as long, lateral margin slightly concave, apex rounded. Uropod exopod approximately twice as long as endopod (Fig. 1F).

Antenna with fifth article of peduncle slightly longer than flagellum; ratio of flagellum approximately 3:2:2 (Fig. 6A).

Pereopod 1 with long strong setae on sternal margin of merus and carpus (Fig. 6B). Pereopod 7 with several strong setae on sternal margin; basis without water conducting system; ischium almost straight on sternal margin (Fig. 6C).

Male pleopod 1 exopod oval, straight on outer margin; endopod with apical portion bearing rounded hyaline lobe and three well-developed dentations (Fig. 6D). Pleopod 2 exopod triangular; endopod flagelliform, longer than exopod (Fig. 6E). Pleopods 3−5 nearly triangular with several setae on outer margin (Fig. 6F−H).

Etymology. Latin: *tridentatus* = trident. The new species name refers to the male pleopod 1 endopod with three dentations at apical portion.

Remarks. This new species is similar to *E. cortii* Arcangeli, 1927 by body shape and male pleopod 1 endopod bearing a rounded hyaline lobe at the apical portion (Figs 1F, 6D *versus* Figs 1G, 7D). But it can be distinguished by pereopod 7 basis without water conducting

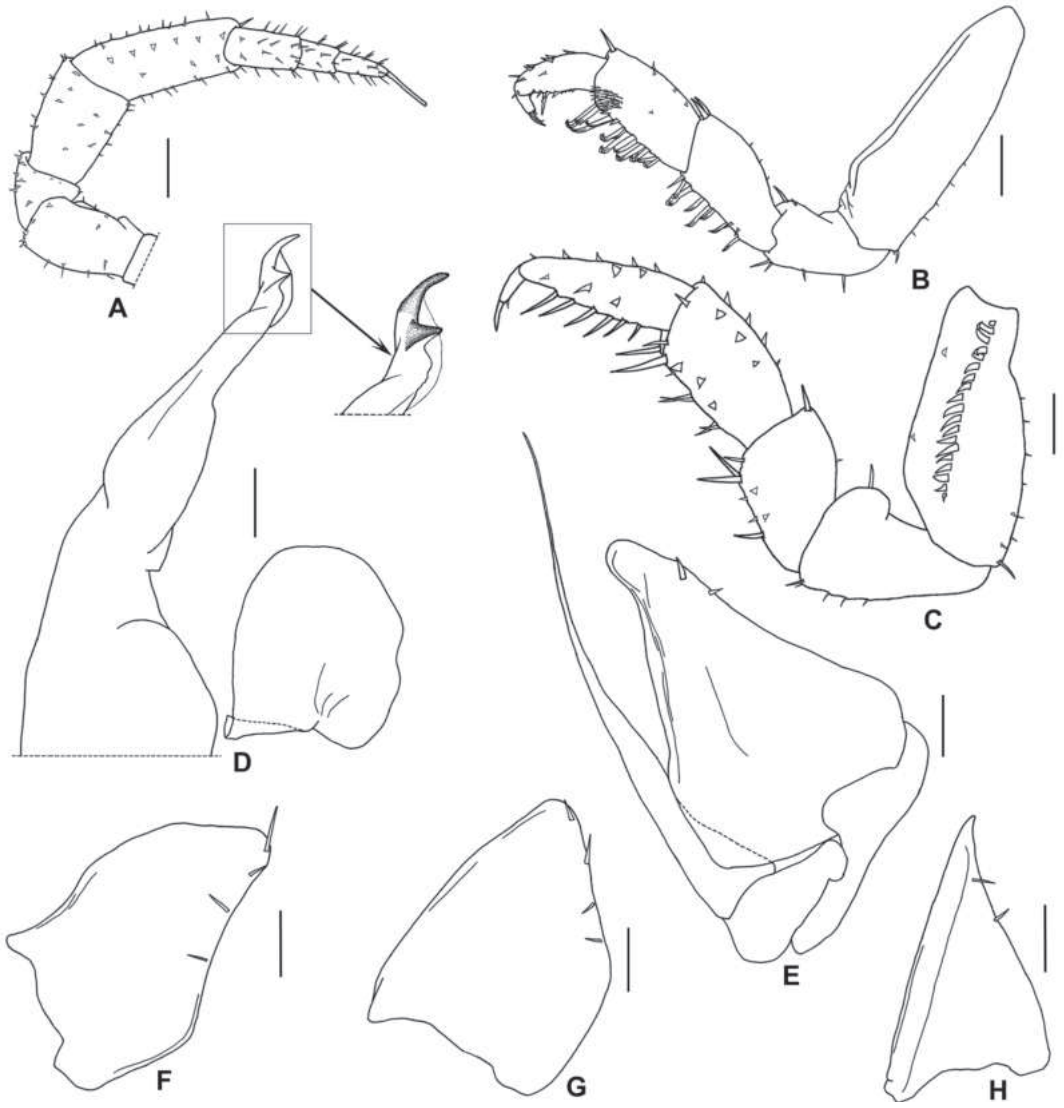

Figure 7. *Exalloniscus cortii* (one male, China, Hunan Province, Yongzhou, Puliqiao Town, 21 March 2019, Chao Jiang leg., prep. slide no. L23099). **A.** Antenna; **B.** Pereopod 1; **C.** Pereopod 7; **D.** Pleopod 1; **E.** Pleopod 2; **F.** Pleopod 3 exopod; **G.** Pleopod 4 exopod; **H.** Pleopod 5 exopod. Scale bar: 0.1 mm.

system, pleopod 1 exopod straight on the outer margin, and endopod bearing three well-developed dentations at the apical portion (Fig. 6C, D). In *E. cortii*, pereopod 7 basis has a well-developed water conducting system, pleopod 1 exopod is sinuous on the outer margin, and endopod with two spinelike projections at the apical apex (Fig. 7C, D).

Exalloniscus taitii Li & Jiang, sp. nov.

https://zoobank.org/D814EDC9-41DF-44F6-A6D6-FD5B4C9D9EF8

Figs 1H, 8

Type material. ***Holotype*.** **China**: male, Yunnan Province, Gengma County, Daxing Village (23°45'N, 99°46'E), alt. 2270 m, 29 May 2021, Chao Jiang leg., habitus no. DXX2302, prep. slide no. L23100 (JXAUM).

Diagnosis. Male pleopod 1 endopod conspicuously concave near middle of outer margin and bearing a tiny spine at apical part of inner margin, pleopods 3 concave on outer margin.

Description. Length 2.0 mm.

Body oval, slightly convex. Colour pale brown. Cephalon with lateral lobes slightly protruding laterally, apex rounded. Eyes with three ommatidia. Pereonites with postero-lateral corners directed backwards. Pleonites 3−5 with epimera falciform, protruding backwards. Telson triangular, twice as wide as long, lateral margin slightly concave, apex rounded. Uropod exopod approximately twice as long as endopod (Fig. 1H).

Antenna with fifth article of peduncle slightly shorter than flagellum; ratio of flagellum approximately 3:3:4 (Fig. 8A).

Pereopod 1 with long strong setae on sternal margin of merus and carpus, carpus without transversal antennal grooming brush (Fig. 8B). Pereopod 7 with several strong setae on sternal margin; basis without water conducting system; ischium almost straight on sternal margin (Fig. 8C).

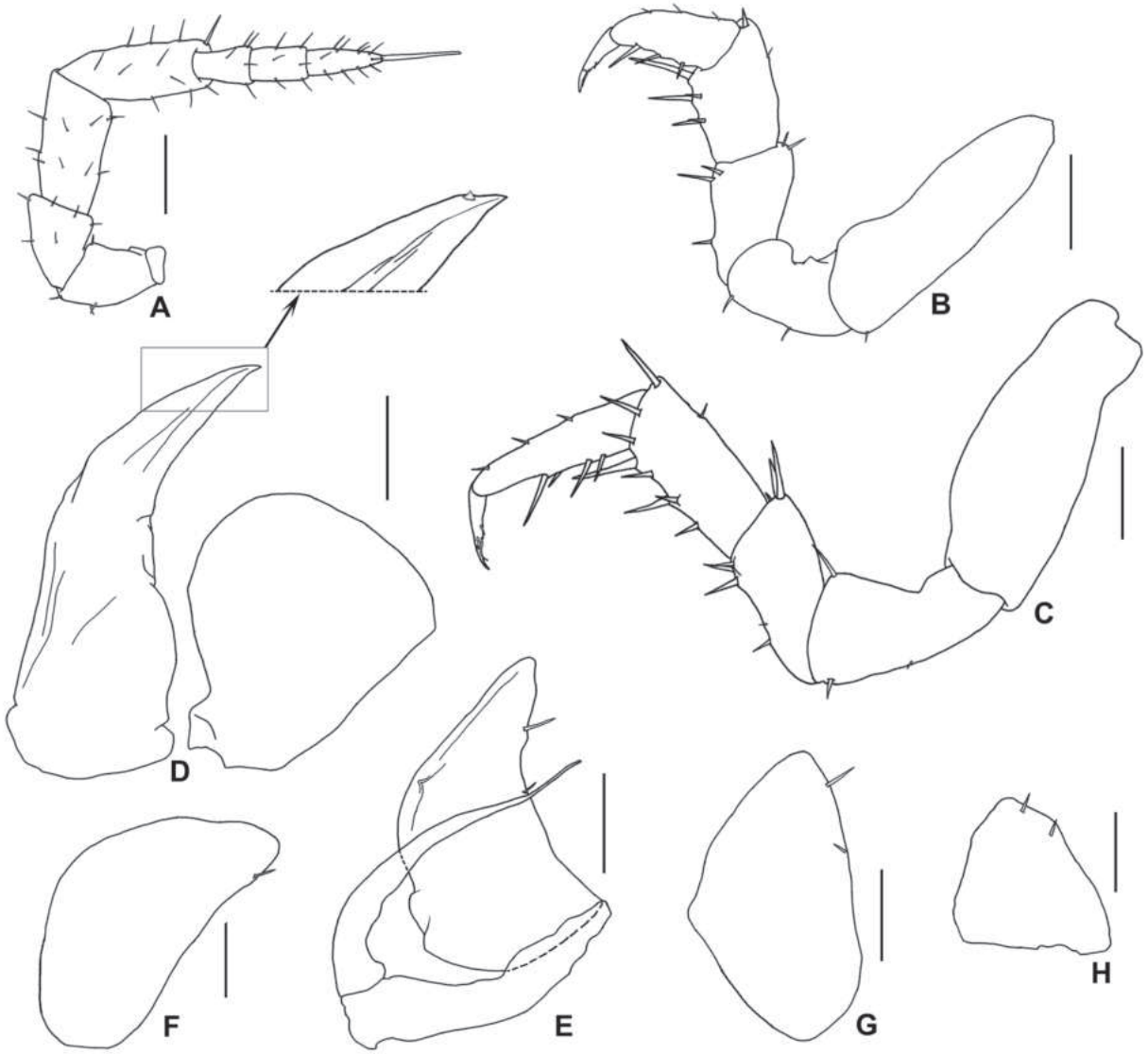

Figure 8. *Exalloniscus taitii* sp. nov., holotype. **A.** Antenna; **B.** Pereopod 1; **C.** Pereopod 7; **D.** Pleopod 1; **E.** Pleopod 2; **F.** Pleopod 3 exopod; **G.** Pleopod 4 exopod; **H.** Pleopod 5 exopod. Scale bar: 0.1 mm.

Male pleopod 1 exopod base narrow, distinctly broaden towards apical part, almost straight on outer margin; endopod base broad, narrowed towards point apex, outer margin conspicuously concave near middle, apical part with tiny spine on inner margin (Fig. 8D). Pleopod 2 exopod triangular, outer margin concave; endopod flagelliform, longer than exopod (Fig. 8E). Pleopods 3−5 nearly triangular, pleopods 3 concave on outer margin, pleopods 4−5 almost straight on outer margin (Fig. 8F−H).

Etymology. The new species name honors Dr. Stefano Taiti for his invaluable contribution to the taxonomy of terrestrial isopods.

Remarks. This new species is similar to *E. burmaensis* Taiti & Cardoso, 2020 by the traits of male pleopod 1. But it can be distinguished by the ratio of flagellum approximately 3:3:4; pereopod 1 carpus without transversal antennal grooming brush, and pereopod 7 basis without water conducting system; pleopod 1 endopod conspicuously concave near the middle of the outer margin, and bearing a tiny spine at the apical part of the inner margin, pleopods 3 concave on the outer margin (Fig. 8A−D, F). In *E. burmaensis*, flagellum is diminishing in length from the first segment to the third segment; pereopod 1 carpus with a transversal antennal grooming brush, and pereopod 7 basis has a well-developed water conducting system; pleopod 1 endopod is almost straight on the outer margin, and the apical part without spine on the inner margin, pleopods 3 is straight on the outer margin (Taiti and Cardoso 2020: Fig. 17H, 18B−D, F).

Biogeographical considerations

This taxonomic work describes five new species of the genus *Exalloniscus* from China. To date, a total of eleven species of the genus occur in China (Fig. 9). All the *Exalloniscus* species from China described here are distributed southward to the 0 °C isotherm of the coldest month (January) of the year, and their habitus almost locates in a humid area with annual precipitation above 800 mm. Among them, only *Exalloniscus cortii* Arcangeli, 1927 shows a wide distribution. In addition to South China, it is also recorded from sub-humid areas near 40°N of North China (Fig. 9). Based on our available specimens and historical records (Taiti and Ferrara 1988), *E. cortii* has the northernmost distribution in China reaching Shanhai Pass of Hebei Province, the border between Northeast China and North China (Fig. 8). Thus, all Chinese species of this genus are humidity and warmth dependent except for *E. cortii*, which has demonstrated to have some level of cold tolerance.

Furthermore, the worldwide records indicate the occurrence of *Exalloniscus* species from South Asia, Southeast Asia to East Asia (Manicastri and Argano 1986; Taiti and Ferrara 1988; Manicastri and Taiti 1991; Kwon 1993, 1995; Kwon and Taiti 1993; Nunomura 2000; Nunomura and Xie 2000; Taiti and Gruber 2008; Taiti and Cardoso 2020). This geographical region is strongly connected to climatic variables, in which the precipitation and minimum temperature are very close to the geographic

Figure 9. Map of China showing the localities where *Exalloniscus* species are recorded.

distribution in China. This suggests that the precipitation and minimum temperature may be the important factors affecting the geographical distribution of *Exalloniscus* members. In addition, most *Exalloniscus* species live in association with ants or termites, but the available data are still only fragmentary and insufficient for the biology of many species (Taiti and Ferrara 1988; Taiti and Cardoso 2020). Further research is necessary to precisely identify biotic and abiotic requirements for *Exalloniscus* species as well as to describe the largely unstudied diversity of the genus in China.

Acknowledgements

We are grateful to Dr. Stefano Taiti (Istituto per lo Studio degli Ecosistemi, Italy), Dr. Christian Schmidt (Senckenberg Naturhistorische Sammlungen Dresden, Germany), and Dr. Noboru Nunomura (Kanazawa University, Japan) for providing important references. We are greatly appreciative of the efforts of Christina Yuan (University of San Francisco, USA) for her help in improving the English. We are also indebted to Han Qiu, Zhidong Wang and Tianyun Chen for collecting specimens. Special thanks are given to Dr. Luiz F. Andrade and two anonymous reviewers for their insightful comments and suggestions on the manuscript. This research was supported by the National Natural Science Foundation of China (nos. 31960100, 82073972) and the Fundamental Research Funds for the Central Public Welfare Research Institutes (no. ZZ13-YQ-089-C1).

References

Chen GX (2003) Species Construction and Distribution of Terrestial Isopoda in Typical Zones of China. Journal of Jishou University 24(1): 14–19. [Natural Science Edition]

Kwon D (1993) Terrestrial Isopoda (Crustacea) from Korea. Tongmul Hakhoe Chi 36: 133–158.

Kwon D (1995) Terrestrial Isopoda (Crustacea) from Cheju Island, Korea. Korean Journal of Systematic Zoology 11: 509–538.

Kwon D, Taiti S (1993) Terrestrial Isopoda (Crustacea) from southern China, Macao and Hong Kong. Stuttgarter Beiträge zur Naturkunde, Serie A 490: 1–83.

Manicastri C, Argano R (1986) Terrestrial isopods from Sri Lanka. II. *Exalloniscus brincki* n. sp. (Crustacea, Malacostraca). Revue Suisse de Zoologie 93: 37–45. https://doi.org/10.5962/bhl.part.79678

Manicastri C, Taiti S (1991) A new species of *Exalloniscus* Stebbing, 1911 from Sumatra (Crustacea, Isopoda, Oniscidea). Treubia 30: 185–190.

Montesanto G (2015) A fast GNU method to draw accurate scientific illustrations for taxonomy. ZooKeys 515: 191–206. https://doi.org/10.3897/zookeys.515.9459

Nunomura N (2000) Terrestrial isopod and amphipod crustaceans from the Imperial Palace, Tokyo. Memoirs of the natural Science Museum Tokyo 35: 79–97.

Nunomura N, Xie RD (2000) Terrestrial isopod crustaceans of Yunnan, southwest China. In: Aoki J, Yin WY, Imadate G (Eds) Taxonomical Studies on the Soil Fauna of Yunnan Province in Southwest China. Tokai University Press, Tokyo, 43–89.

Stebbing TRR (1911) XII. Indian isopods. Records of the Indian Museum 4: 179–191. [pls. X–XII.] https://doi.org/10.5962/bhl.part.21332

Taiti S, Cardoso MC (2020) New species and records of *Exalloniscus* Stebbing, 1911 from southern Asia (Malacostraca, Isopoda, Oniscidea). Tropical Zoology 33(4): 125–158. https://doi.org/10.4081/tz.2020.83

Taiti S, Ferrara F (1986) Ricerche nell'Asia sudorientale. IX. Su due specie, una nuova, del genere *Exalloniscus* Stebbing, 1911 (Isopodi terrestri). Bollettino del Museo civico di Storia naturale di Verona 11: 237–246.

Taiti S, Ferrara F (1988) Revision of the genus *Exalloniscus* Stebbing, 1911 (Crustacea: Isopoda: Oniscidea). Zoological Journal of the Linnean Society 94(4): 339–377. https://doi.org/10.1111/j.1096-3642.1988.tb01200.x

Taiti S, Gruber GA (2008) Cave-dwelling terrestrial isopods from southern China (Crustacea, Isopoda, Oniscidea), with descriptions of four new species. In: Latella L, Zorzin R (Eds) Research in South China karsts. Memorie del Museo civico di Storia naturale di Verona, Monografie Naturalistiche 3: 101–123.

Zoosyst. Evol. 100 (2) 2024, 385–390 | DOI 10.3897/zse.100.120887

PENSOFT

für Natur MUSEUM FÜR NATURKUNDE BERLIN

A new parasitic barnacle (Crustacea, Cirripedia, Rhizocephala, *Mycetomorpha*) from the abyssal zone in the northwestern Pacific

Keiichi Kakui[1]

1 *Department of Biological Sciences, Faculty of Science, Hokkaido University, Sapporo 060-0810, Japan*

https://zoobank.org/C325C2A4-0279-43F5-B7C1-FB5B60D277F5

Corresponding author: Keiichi Kakui (kakui@eis.hokudai.ac.jp)

Academic editor: K. von Rintelen ♦ **Received** 14 February 2024 ♦ **Accepted** 19 March 2024 ♦ **Published** 3 April 2024

Abstract

I describe the parasitic barnacle *Mycetomorpha abyssalis* **sp. nov.** from the crangonid shrimp *Sclerocrangon zenkevitchi* collected from 3893–3890 m depth off the eastern coast of Iwate, Japan, northwestern Pacific. This is the first *Mycetomorpha* rhizocephalan from the abyssal zone and the third species in *Mycetomorpha*. *Mycetomorpha abyssalis* **sp. nov.** differs from its congeners *M. vancouverensis* and *M. albatrossi* in (1) triangular shield lacking, (2) stalk one-quarter of length from posterior end of externa, (3) mantle opening clearly anterior to stalk, (4) different host genus, and (5) depth range much deeper. I determined partial sequences for the mitochondrial cytochrome *c* oxidase subunit I (COI) and 16S rRNA genes and nuclear 18S rRNA and 28S rRNA genes from *M. abyssalis* **sp. nov.** for future DNA barcoding and phylogeny. Kimura 2-parameter distances between *M. abyssalis* **sp. nov.** and *M. vancouverensis* were 21.2% (16S), 0.6% (18S), and 1.5% (28S).

Key Words

Caridea, deep sea, integrative taxonomy, mesoparasite, parasite, turbo taxonomy

Introduction

Mycetomorpha Potts, 1912, the sole genus in the rhizocephalan barnacle family Mycetomorphidae, contains the two species *Mycetomorpha vancouverensis* Potts, 1912 and *Mycetomorpha albatrossi* Høeg & Rybakov, 1996 (Høeg and Rybakov 1996). These utilize crangonid shrimps as hosts and have been reported only from the northern Pacific, at depths shallower than 300 m (Potts 1912; Butler 1955, 1980; Høeg and Rybakov 1996; Sloan et al. 2001; Wheeler and McIntosh 2021; Eibye-Jacobsen et al. 2024; GBIF 2024; Orrell and Informatics Office 2024) (Fig. 1). The two species differ in external morphology (Høeg and Rybakov 1996) and utilize host shrimps in different genera: *Neocrangon communis* (Rathbun, 1899) for *M. vancouverensis*; *Metacrangon variabilis* (Rathbun, 1902) and *Metacrangon acclivis* (Rathbun, 1902) for *M. albatrossi*. Molecular phylogenetic analyses (Høeg et al. 2020; Korn et al. 2020) have suggested that Mycetomorphidae is closely related to the family Peltogastridae.

Here I describe a new *Mycetomorpha* species based on one individual parasitic on the crangonid *Sclerocrangon zenkevitchi* Birshtein & Vinogradov, 1953 from the abyssal zone in the Japan Trench, northwestern Pacific. This is the first abyssal record for *Mycetomorpha*. Additionally, I provide partial sequences for its cytochrome *c* oxidase subunit I (COI), 16S rRNA, 18S rRNA, and 28S rRNA genes for DNA barcoding and future phylogenetic analyses.

Methods

The host shrimp *Sclerocrangon zenkevitchi* (identified by Tomoyuki Komai; Natural History Museum and Institute, Chiba) was collected with a beam trawl on 29 September 2023 during cruise KH-23-5 of R/V *Hakuho-maru* (Japan Agency for Marine-Earth Science and Technology; JAMSTEC), at Station F2 (39°28.555'N, 143°47.347'E to 39°27.934'N, 143°47.240'E), depth 3893–3890 m. The fresh shrimp was photographed.

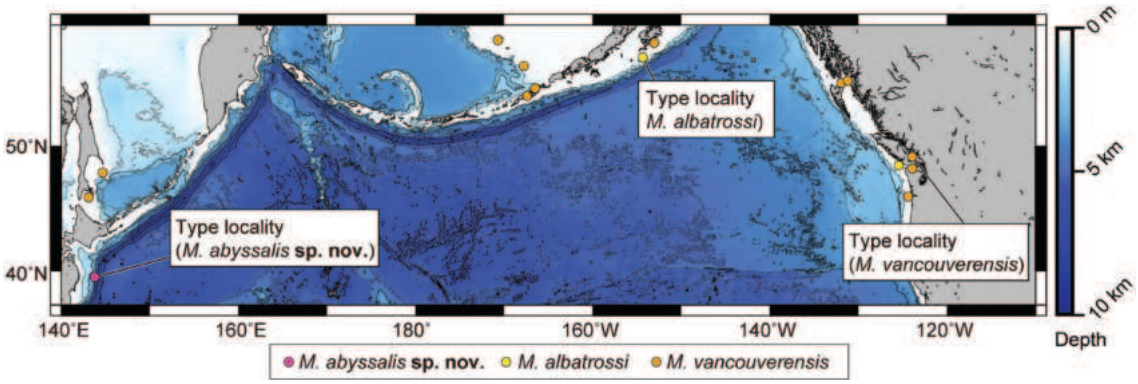

Figure 1. Map showing the global distribution of *Mycetomorpha*. Bathymetric contour intervals are 1000 m, with thicker contour lines every 2000 m. The map and plots were generated with GMT6 software (Wessel et al. 2019) based on data publicly available from ETOPO1 (Amante and Eakins 2009; NOAA National Geophysical Data Center 2009).

Pleonite 1 bearing the parasite was removed from the body with scissors and placed in a petri dish. Soft tissue from host pleonite 1 was recovered, and fixed and preserved in 99% ethanol. The pleonite-1 exoskeleton penetrated by the parasite stalk was photographed. The parasite and surrounding pleonite-1 exoskeleton were removed and photographed. Some lobes of the parasite were detached, and fixed and preserved in 99% ethanol. The remaining portions of the host and parasite were fixed and preserved in 80% ethanol. The fixed parasite was observed with a Nikon SMZ1500 stereomicroscope; it was not sectioned, in order to retain the option for future non-destructive observation. The material examined in this study is deposited in the Natural History Museum and Institute, Chiba, Japan, catalogued under the acronym CBM-ZC.

The terms for orientation (anterior, posterior, left, right, dorsal, ventral) used herein for the parasite's externa correspond to those for the host ("dorsal" herein corresponds to the "upper" or "stalk side" in Høeg and Rybakov 1996). Externa length was measured from the anterior to posterior ends, lobes excluded; externa width was measured at the widest portion, lobes excluded. The carapace length (cl) of the host was measured from the orbital margin to the midpoint of the posterodorsal margin of the carapace.

Total DNA was extracted from several lobes of the parasite and from pleonal muscle of the host shrimp by using a NucleoSpin Tissue XS Kit (Macherey–Nagel, Germany). For the COI gene, primers LCO1490 and HCO2198 (Folmer et al. 1994) were used for PCR amplification and cycle sequencing (CS). For the 16S gene, primers 16sar-L and 16sbr-H (Palumbi et al. 2002) were used for amplification and CS. For the 18S gene, primers SR1 and SR12 (Nakayama et al. 1996) were used for amplification, and primers SR3, 18S-b3F, 18S-b4F, 18S-b4R, 18S-a4R, 18S-b5F, 18S-b6F, 18S-a6R, and 18S-b8F (Nakayama et al. 1996; Kakui et al. 2011, 2021; Kakui and Shimada 2017, 2022; Kakui and Hiruta 2022) for CS. For the 28S gene, primers 300F and L1642 (Lockyer et al. 2003) were used for amplification, and primers 28S-Rd4.2b, 300F, 900F, and U1148 (Whiting 2002; Lockyer et al. 2003) for CS. Amplification conditions for COI and 16S with TaKaRa Ex Taq DNA polymerase (TaKaRa Bio, Japan) were 94 °C for 1 min; 35 cycles of 98 °C for 10 s, 50 °C (COI) or 42 °C (16S) for 30 s, and 72 °C for 50 s; and 72 °C for 2 min. Conditions for 18S and 28S with KOD FX Neo (Toyobo, Japan) were 94 °C for 2 min; 45 cycles of 98 °C for 10 s, 65 °C (18S) or 52 °C (28S) for 30 s, and 68 °C for 75 s; and 68 °C for 3 min. All nucleotide sequences were determined with a BigDye Terminator Kit ver. 3.1 and 3730 DNA Analyzer (Life Technologies, USA). Fragments were concatenated by using MEGA7 (Kumar et al. 2016). The sequences determined in this study were deposited in the International Nucleotide Sequence Database (INSD) through the DNA Data Bank of Japan (DDBJ).

The 16S, 18S, and 28S sequences from the new species were aligned individually with homologs from *M. vancouverensis* (16S, 534 bp, MH974513; 18S, 1757 bp, MH974514; 28S, 682 bp, MH974515; Høeg et al. 2019) by using MUSCLE (Edgar 2004) and trimmed to the shortest length between them (16S, 494 bp; 18S, 1757 bp; 28S, 683 bp) after alignment. Kimura's (1980) 2-parameter (K2P) distance between the two species was calculated with MEGA7 for each gene.

Taxonomy

Family Mycetomorphidae Høeg & Rybakov, 1992

New Japanese name: ミノフクロムシ科 (Mino-fukuromushi-ka)

Genus *Mycetomorpha* Potts, 1912

New Japanese name: ミノフクロムシ属 (Mino-fukuromushi-zoku)

Mycetomorpha abyssalis sp. nov.

https://zoobank.org/9C0FBC4F-5779-4100-BDC9-8D585C1A4160

Figs 2–4

New Japanese name: メイフノミノフクロムシ (Meifu-no-mino-fukuromushi)

Etymology. The specific name *abyssalis* (Latin: abyssal) is an adjective referring to the collection of this species from an abyssal depth.

Type host. *Sclerocrangon zenkevitchi* Birshtein & Vinogradov, 1953 (Decapoda: Caridea: Crangonidae).

Attachment site. Pleonite 1 sternite.

Type locality. Off the eastern coast of Iwate, Japan, northwestern Pacific (39°28.555'N, 143°47.347'E to 39°27.934'N, 143°47.240'E), depth 3893–3890 m.

Material examined. Holotype, female (CBM-ZC 17789), one vial, ex. *S. zenkevitchi* (cl 26.7 mm; CBM-ZC 17788), collected on 29 September 2023 at the type locality, R/V *Hakuho-maru* cruise KH-23-5, coll. by Keiichi Kakui.

Representative DNA sequences. One sequence each was determined from the holotype (CBM-ZC 17789) for COI (INSD accession number LC799150; 637 bp, encoding 212 amino acids), 16S (LC799151; 490 bp), 18S (LC799152; 1826 bp), and 28S (LC799153; 1169 bp).

Figure 2. *Mycetomorpha abyssalis* sp. nov., holotype, attached to the host, *Sclerocrangon zenkevitchi* Birshtein & Vinogradov, 1953, fresh specimen. Scale bar: 10 mm.

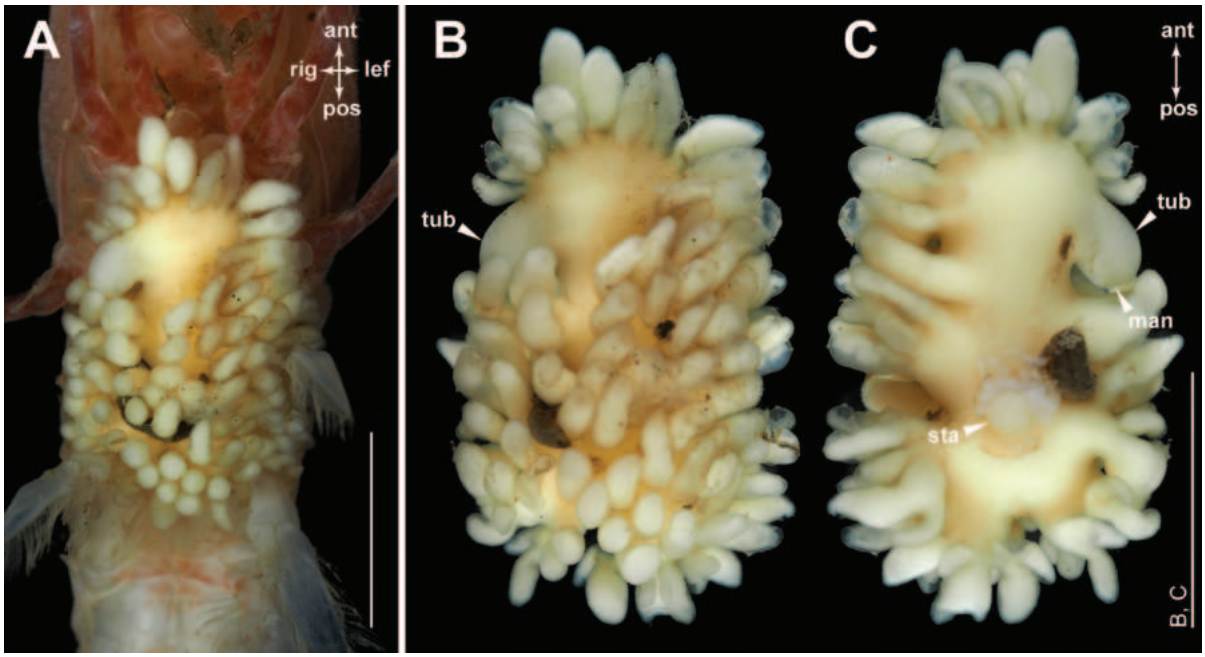

Figure 3. *Mycetomorpha abyssalis* sp. nov., holotype, fresh specimen. **A.** Habitus, parasitic on the host, ventral view; **B, C.** Habitus, ventral (**B**) and dorsal (**C**) views; **ant** – anterior; **lef** – left; **man** – mantle opening; **rig** – right; **pos** – posterior; **sta** – stalk; **tub** – tubular lobe. Scale bars: 10 mm.

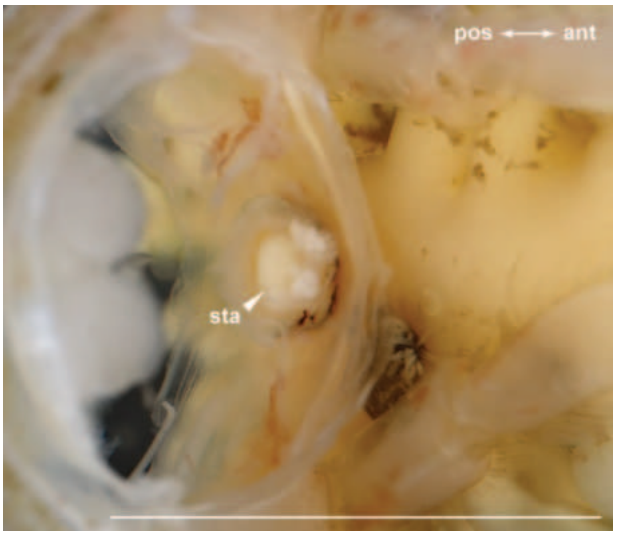

Figure 4. *Mycetomorpha abyssalis* sp. nov., holotype, showing stalk penetrating the host pleonite-1 sternite (soft tissue in pleonite 1 removed), anterodorsal view; no triangular shield observed. **ant** – anterior; **pos** – posterior; **sta** – stalk. Scale bar: 10 mm.

One sequence each was determined from the host (CBM-ZC 17788) for COI (LC799154; 658 bp, encoding 219 amino acids) and 18S (LC799155; 1846 bp).

Description of female holotype. Externa (Figs 2, 3) 16.6 mm in length, thinner than broad, a little over twice as long as maximum width (8.1 mm), rounded at ends, pale yellow (faded in ethanol, slightly yellowish); except dorsal and anteroventral regions, externa surface covered with short lobes; filled with developing embryos. Root system not observed. Stalk short, cylindrical, at one-quarter of length from posterior end of externa. Triangular shield lacking (Figs 3C, 4). Anterior, middle, and ventral lobes short, and ovoid or digitiform; posterior lobes short and branched. Tubular lobe anterior to stalk, at one-fifth of length from anterior end of externa, arising from right margin of externa, with mantle opening at tip; mantle opening anterior to stalk.

Distribution. Presently known only from the type locality.

Discussion

Mycetomorpha abyssalis sp. nov. is the third species described in this genus. The three congeners are morphologically similar to one another, but *M. abyssalis* sp. nov. differs from the others in (1) lacking a triangular shield (present in *M. vancouverensis*), (2) the location of the stalk at one-quarter the length from the posterior end of the externa (one-third in *M. albatrossi*), and (3) the mantle opening clearly anterior to the stalk (to the right of the stalk in *M. vancouverensis*; slightly anterior to the stalk in *M. albatrossi*) (Potts 1912; Høeg and Rybakov 1996). However, because the shape of the externa can vary ontogenetically (e.g., the size of externa, the distribution and size of lobes; cf. Høeg and Rybakov 1996: fig. 1), these morphological differences should be treated with caution.

The genus of host shrimps is different among three species: *M. vancouverensis*, *M. albatrossi*, and *M. abyssalis* sp. nov. utilize the crangonid genera *Neocrangon*, *Metacrangon*, and *Sclerocrangon*, respectively. The depth range of 3893–3890 m recorded for *M. abyssalis* sp. nov. is far deeper than for the others (240 m or shallower for *M. vancouverensis*; 291 m or shallower for *M. albatrossi*; Høeg and Rybakov 1996; Wheeler and McIntosh 2021). The known depth range for *S. zenkevitchi* (2995–4070 m; Komai and Komatsu 2009) does not overlap those for *N. communis* (16–1537 m; Komai and Komatsu 2009), *M. variabilis* (92–1271 m; Komai 2012), and *M. acclivis* (146.3–486.5 m; Rathbun 1902). These differences in host group and vertical distribution of parasites and hosts support the conclusion that the specimen from Japan is not conspecific with either *M. vancouverensis* or *M. albatrossi*.

I determined COI, 16S, 18S, and 28S sequences of *M. abyssalis* sp. nov., and sequences for the last three genes were available for *M. vancouverensis*. K2P distances between two species were 21.2% (16S), 0.6% (18S), and 1.5% (28S). Noever et al. (2016) found K2P distances for 16S between two *Briarosaccus* species (Rhizocephala, Peltogastridae) in the range of 4.3–4.6%, suggesting the above difference in 16S may correspond to interspecific variation. In a BLAST search (Altschul et al. 1990), the COI sequence most similar to my sequence was from the insect *Rhodopsalta cruentata* (Fabricius, 1775) (MZ470333; identity score 73.85%, query cover 100%; Bator et al. 2021), a misleading result likely due to the lack of any congeneric COI sequences in INSD (cf. Kakui and Hiruta 2022). A BLAST search with the "Organism" option set to "Rhizocephala" selected *Sacculina granifera* Boschma, 1973 (DQ059779; identity score 72.64%, query cover 98%; Gurney et al. 2006) as the most similar sequence, but again the identity score was low. If congeneric sequences become available, COI sequences, which seem to evolve faster than 16S sequences (cf. Noever et al. 2016; Jung et al. 2021), will likely be a useful tool for *Mycetomorpha* taxonomy.

Acknowledgments

I thank Shigeaki Kojima and Yasunori Kano for the opportunity to join R/V *Hakuho-maru* cruise KH-23-5, conducted as a part of the project "Comprehensive study of diversity and evolutionary mechanisms of deep-sea animals in trenches in the northwestern Pacific" supported by KAKENHI grant JP19H00999 from the Japan Society for the Promotion of Science (JSPS); Captain Naoto Sakai and the crew of R/V *Hakuho-maru*, technicians from Marine Work Japan and MOL Marine & Engineering, and researchers aboard for support in collecting; Tomoyuki Komai for identification of the host shrimp; Akito Ogawa for help in photography; Genki Ishiyama and Mako Nakao for help in map production; and Matthew H. Dick for

reviewing the manuscript and editing the English. This study was supported in part by the Atmosphere and Ocean Research Institute, The University of Tokyo, and KAKENHI grants JP19K06800 and JP22H02681 from JSPS.

References

Altschul SF, Gish W, Miller W, Myers EW, Lipman DJ (1990) Basic local alignment search tool. Journal of Molecular Biology 215(3): 403–410. https://doi.org/10.1016/S0022-2836(05)80360-2

Amante C, Eakins BW (2009) ETOPO1 1 arc-minute global relief model: procedures, data sources and analysis. NOAA Technical Memorandum NESDIS NGDC-24. National Geophysical Data Center, Boulder, 19 pp.

Bator J, Marshall DC, Hill KBR, Cooley JR, Leston A, Simon C (2021) Phylogeography of the endemic red-tailed cicadas of New Zealand (Hemiptera: Cicadidae: *Rhodopsalta*), and molecular, morphological and bioacoustical confirmation of the existence of Hudson's *Rhodopsalta microdora.* Zoological Journal of the Linnean Society 195(4): 1219–1244. https://doi.org/10.1093/zoolinnean/zlab065

Birshtein YA, Vinogradov LG (1953) New data on the decapod crustacean fauna in the Bering Sea. Zoologicheskii Zhurnal 32: 215–228. [in Russian]

Boschma H (1973) *Sacculina granifera* nov. spec., a rhizocephalan parasite of the crab *Portunus* (*Portunus*) *pelagicus* from the coast of Queensland. Proceedings of the Koninklijke Nederlandse Akademie van Wetenschappen, Series C 76: 313–318.

Butler TH (1955) Re-discovery of the parasitic cirripede, *Mycetomorpha vancouverensis* Potts, in British Columbia waters. The Journal of Parasitology 41: 321. https://doi.org/10.2307/3274218

Butler TH (1980) Shrimps of the Pacific coast of Canada. Canadian Bulletin of Fisheries and Aquatic Sciences 202: [i–x] 1–280.

Edgar RC (2004) MUSCLE: Multiple sequence alignment with high accuracy and high throughput. Nucleic Acids Research 32(5): 1792–1797. https://doi.org/10.1093/nar/gkh340

Eibye-Jacobsen D, Pavesi L, Schiøtte T, Sørensen MV, Olesen J (2024) NHMD Invertebrate Zoology Collection. Natural History Museum of Denmark. Occurrence dataset. https://doi.org/10.15468/wodhis [Accessed via GBIF.org on 2024-02-05]

Fabricius IC (1775) Systema Entomologiae, sistens insectorum classes, ordines, genera, species, adiectis synonymis, locis, descriptionibus, observationibus. Officina Libraria Kortii, Flensbvrgi and Lipsiae, 832 pp. https://doi.org/10.5962/bhl.title.36510

Folmer O, Black M, Hoeh W, Lutz R, Vrijenhoek R (1994) DNA primers for amplification of mitochondrial cytochrome *c* oxidase subunit I from diverse metazoan invertebrates. Molecular Marine Biology and Biotechnology 3: 294–299.

GBIF (2024) *Mycetomorpha* Potts, 1912. https://doi.org/10.15468/dl.zkx9z3 [Accessed on 2024-02-05]

Gurney RH, Grewe PM, Thresher RE (2006) Mitochondrial DNA haplotype variation in the parasitic cirripede *Sacculina carcini* observed in the cytochrome oxidase gene (COI). Journal of Crustacean Biology 26(3): 326–330. https://doi.org/10.1651/S-2655.1

Høeg JT, Rybakov AV (1992) Revision of the Rhizocephala Akentrogonida (Cirripedia), with a list of all the species and a key to the identification of families. Journal of Crustacean Biology 12(4): 600–609. https://doi.org/10.1163/193724092X00076

Høeg JT, Rybakov AV (1996) Development and taxonomy of the Mycetomorphidae and the significance of their reproductive system in rhizocephalan evolution (Crustacea: Cirripedia: Rhizocephala). Zoologischer Anzeiger 234: 253–269.

Høeg JT, Rees DJ, Jensen PC, Glenner H (2019) Unravelling the evolutions of the Rhizocephala: a case study for molecular-based phylogeny in the parasitic Crustacea. In: Smit NJ, Bruce NL, Hadfield KA (Eds) Parasitic Crustacea State of Knowledge and Future Trends. Springer Nature Switzerland, Cham, 387–419. https://doi.org/10.1007/978-3-030-17385-2_9

Høeg JT, Noever C, Rees DJ, Crandall KA, Glenner H (2020) A new molecular phylogeny-based taxonomy of parasitic barnacles (Crustacea: Cirripedia: Rhizocephala). Zoological Journal of the Linnean Society 190(2): 632–653. https://doi.org/10.1093/zoolinnean/zlz140

Jung J, Yoshida R, Lee D, Park J-K (2021) Morphological and molecular analyses of parasitic barnacles (Crustacea: Cirripedia: Rhizocephala) in Korea: preliminary data for the taxonomy and host ranges of Korean species. PeerJ 9: e12281. https://doi.org/10.7717/peerj.12281

Kakui K, Hiruta C (2022) Description of a new *Hamatipeda* species, with an 18S molecular phylogeny (Crustacea: Tanaidacea: Typhlotanaidae). Zoological Science 39(1): 140–146. https://doi.org/10.2108/zs210065

Kakui K, Shimada D (2017) A new species of *Tanaopsis* (Crustacea: Tanaidacea) from Japan, with remarks on the functions of serial ridges and grooves on the appendages. Zootaxa 4282(2): 324–336. https://doi.org/10.11646/zootaxa.4282.2.6

Kakui K, Shimada D (2022) Dive into the sea: first molecular phylogenetic evidence of host expansion from terrestrial/freshwater to marine organisms in Mermithidae (Nematoda: Mermithida). Journal of Helminthology 96: e33. https://doi.org/10.1017/S0022149X22000256

Kakui K, Katoh T, Hiruta SF, Kobayashi N, Kajihara H (2011) Molecular systematics of Tanaidacea (Crustacea: Peracarida) based on 18S sequence data, with an amendment of suborder/superfamily-level classification. Zoological Science 28(10): 749–757. https://doi.org/10.2108/zsj.28.749

Kakui K, Fukuchi J, Shimada D (2021) First report of marine horsehair worms (Nematomorpha: *Nectonema*) parasitic in isopod crustaceans. Parasitology Research 120(7): 2357–2362. https://doi.org/10.1007/s00436-021-07213-9

Kimura M (1980) A simple method for estimating evolutionary rates of base substitutions through comparative studies of nucleotide sequences. Journal of Molecular Evolution 16(2): 111–120. https://doi.org/10.1007/BF01731581

Komai T (2012) A review of the western Pacific species of the crangonid genus *Metacrangon* Zarenkov, 1965 (Decapoda: Caridea), with descriptions of seven new species. Zootaxa 3468: 1–77. https://doi.org/10.11646/zootaxa.3468.1.1

Komai T, Komatsu H (2009) Deep-sea shrimps and lobsters (Crustacea: Decapoda) from northern Japan, collected during the project "Research on deep-sea fauna and pollutants off Pacific coast of northern Japan". National Museum of Nature and Science Monograph 39: 495–580.

Korn OM, Golubinskaya DD, Rees DJ, Glenner H, Høeg JT (2020) Phylogenetic position, complete larval development and larval sexual dimorphism in a rhizocephalan barnacle, *Lernaeodiscus rybakovi* sp. nov. (Cirripedia: Rhizocephala: Peltogastridae), parasitizing the

crab *Pachycheles stevensii* Stimpson, 1858 (Decapoda: Anomura: Porcellanidae). Zoologischer Anzeiger 287: 178–197. https://doi.org/10.1016/j.jcz.2020.06.005

Kumar S, Stecher G, Tamura K (2016) MEGA7: Molecular evolutionary genetics analysis version 7.0 for bigger datasets. Molecular Biology and Evolution 33(7): 1870–1874. https://doi.org/10.1093/molbev/msw054

Lockyer AE, Olson PD, Littlewood DTJ (2003) Utility of complete large and small subunit rRNA genes in resolving the phylogeny of the Neodermata (Platyhelminthes): Implications and a review of the cercomer theory. Biological Journal of the Linnean Society. Linnean Society of London 78(2): 155–171. https://doi.org/10.1046/j.1095-8312.2003.00141.x

Nakayama T, Watanabe S, Mitsui K, Uchida H, Inouye I (1996) The phylogenetic relationship between the Chlamydomonadales and Chlorococcales inferred from 18SrDNA sequence data. Phycological Research 44(1): 47–55. https://doi.org/10.1111/j.1440-1835.1996.tb00037.x

NOAA National Geophysical Data Center (2009) ETOPO1 1 Arc-Minute Global Relief Model. NOAA National Centers for Environmental Information. https://www.ncei.noaa.gov/access/metadata/landing-page/bin/iso?id=gov.noaa.ngdc.mgg.dem:316 [Accessed on 2024-02-11]

Noever C, Olson A, Glenner H (2016) Two new cryptic and sympatric species of the king crab parasite *Briarosaccus* (Cirripedia: Rhizocephala) in the North Pacific. Zoological Journal of the Linnean Society 176(1): 3–14. https://doi.org/10.1111/zoj.12304

Orrell T, Informatics Office (2024) NMNH Extant Specimen Records (USNM, US). Version 1.77. National Museum of Natural History, Smithsonian Institution. Occurrence dataset. https://doi.org/10.15468/hnhrg3 [Accessed via GBIF.org on 2024-02-05]

Palumbi S, Martin A, Romano S, McMillan WO, Stice L, Grabowski G (2002) The simple fool's guide to PCR, version 2.0. https://searchworks.stanford.edu/view/9267895 [Accessed on 2024-02-08]

Potts FA (1912) *Mycetomorpha*, a new rhizocephalan (with a note on the sexual condition of *Sylon*). Zoologische Jahrbucher. Abteilung fur Systematik, Geographie und Biologie der Tiere 33: 575–594. https://doi.org/10.5962/bhl.part.17421

Rathbun MJ (1899) List of Crustacea known to occur on and near the Pribilof Islands. In: Jordan DS, Stejneger L, Lucas FA, Moser JF, Townsend CH, Clark GA, Murray J (Eds) The Fur Seals and Fur-Seal Islands of the North Pacific Ocean, Part 3. Government Printing Office, Washington, 555–557.

Rathbun MJ (1902) Descriptions of new decapod crustaceans from the west coast of North America. Proceedings of the United States National Museum 24(1272): 885–905. https://doi.org/10.5479/si.00963801.1272.885

Sloan NA, Bartier PM, Austin WC (2001) Living marine legacy of Gwaii Haanas. II: Marine invertebrate baseline to 2000 and invertebrate-related management issues. https://doi.org/10.15468/9o6jbj [Accessed via GBIF.org on 2024-02-05]

Wessel P, Luis JF, Uieda L, Scharroo R, Wobbe F, Smith WHF, Tian D (2019) The generic mapping tools version 6. Geochemistry, Geophysics, Geosystems 20(11): 5556–5564. https://doi.org/10.1029/2019GC008515

Wheeler E, McIntosh H (2021) Royal BC Museum—Invertebrates Collection. Version 1.2. Royal British Columbia Museum. Occurrence dataset. https://doi.org/10.5886/zh7n1e [Accessed via GBIF.org on 2024-02-05]

Whiting MF (2002) Mecoptera is paraphyletic: Multiple genes and phylogeny of Mecoptera and Siphonaptera. Zoologica Scripta 31(1): 93–104. https://doi.org/10.1046/j.0300-3256.2001.00095.x

Zoosyst. Evol. 100 (2) 2024, 391–403 | DOI 10.3897/zse.100.121174

PENSOFT

für Natur MUSEUM FÜR NATURKUNDE BERLIN

A new species of trout from the Köprüçay River, a drainage of Mediterranean Sea, Türkiye (Salmoniformes, Salmonidae)

Fahrettin Küçük[1], Gökhan Kalaycı[2], Salim Serkan Güçlü[1], Münevver Oral[2], Davut Turan[2]

1 *Department of Basic Sciences, Faculty of Eğirdir Fisheries, Isparta University of Applied Sciences, Isparta, Turkiye*

2 *Department of Basic Sciences, Faculty of Fisheries, Recep Tayyip Erdoğan University, Rize, Turkiye*

https://zoobank.org/54F22169-B8C9-4AE9-87E8-DD5E16A9BD0E

Corresponding author: Davut Turan (dvtturan@yahoo.com)

Academic editor: Nicolas Hubert ♦ **Received** 19 February 2024 ♦ **Accepted** 15 March 2024 ♦ **Published** 4 April 2024

Abstract

Salmo ekmekciae, new species, is described from the Köprüçay River, a drainage of Mediterranean Sea. It is distinguished from *Salmo* species in adjacent water by having 9–10 parr marks on flank; 11–13 scale rows between end of base of adipose-fin and lateral line; 22–24 gill rakers on first gill arch; a shorter distance between adipose-fin and caudal-fin base; a slenderer caudal peduncle; and a slenderer body at adipose-fin origin. According to the Bayesian, and maximum likelihood analyses, *Salmo ekmekciae* cyt *b* gene resulted in coherent trees supported by high bootstrap values.

Key Words

cytochrome b, freshwater fish, salmo, taxonomy

Introduction

The first known record of Anatolian inland fishes was provided by Abbolt K.E. in the first half of the 19th century, and later studies were particularly encountered in the Works of Heckel (1843), Boulenger (1896), and Steindachner (1897) (Geldiay and Balık 1999; Çiçek et al. 2023). In the subsequent century, Turkish researchers participated in studies aimed at determining the ichthyofauna. For example, F. Battalgil described 25 fish species from Turkish inland waters between 1940–1944. The studies of this researcher were followed by the works of Kuru (1975, 2004) and Geldiay and Balık (1999). Since the beginning of the 21st century, the number of described inland fish species in Türkiye has rapidly increased, supported by detailed morphology and molecular characteristics. Noteworthy contributions to the taxonomy of Anatolian freshwater fishes, in particular, can be attributed to the studies of Bogutskaya (1997), Bogutskaya et al. (2000), Turan et al. (2006, 2008, 2017, 2024), Özuluğ and Freyhof (2011), Küçük et al. (2016, 2017), Turan et al. (2010, 2012, 2020) and Yoğurtçuoğlu et al. (2022).

Salmo trutta has traditionally been acknowledged as a species widely distributed across Europe, extending southward to the Atlas Range (Morocco, Algeria) and eastward to the upper Amu-Darya drainage in Afghanistan. Despite numerous identified subspecies or distinct species over time, there has been a persistent inclination to dismiss this diversity, asserting a priori that they all fall under a highly variable "species" (Ferguson 1989, 2004; Guinand et al. 2021). This perspective contends that 'classical' taxonomy is inadequate for addressing this species. The state of *Salmo* taxonomy has been summarized in detail by Kottelat (1997), with some discussion of North African species by Delling and Doadrio (2005) and Balkan ones by Delling (2003), indicating some improvement in the taxonomic situation. Kottelat and Freyhof (2007) provide an overview of available data for European species, tentatively recognizing 29 species, though the status of several populations and nominal species remains unclear.

Recent molecular studies have revealed the existence of at least five molecular lineages (Bernatchez et al. 1992; Bernatchez and Osinov 1995; Bernatchez 2001),

yet modern biology has not effectively resolved the taxonomy of the species. Notably, no efforts have been made to correlate the molecular lineages with morphological data, resulting in a wealth of untapped, intriguing data. Although molecular data such as *COI*, *d Loop* and *Cyb* are not fully successful in distinguishing species, they have long been providing an important source of knowledge regarding *Salmo* lineages. Emerging next generation sequencing technologies seem to offer a much better resolution to better understand *Salmo* taxonomy. Segherloo et al. (2021) reviewed the taxonomic status of some species in Europe and Asia using the next generation DNA sequence method and successfully presented the taxonomic position of most species under investigation. More recently, Turan et al. (2024) put forward the distribution and taxonomic position of *S. duhani* (Marmara and Aegean basin) as well as described a new species, *S. brunoi*, from Susurluk (Marmara basin) for the first time using next generation sequencing technologies.

Extensive fieldwork and research carried out in Türkiye has demonstrated a significant diversity. A total of eighteen valid species were recorded or identified (Table 1). Of these, 9 species (*S. abanticus*, *S. araxensis*, *S. ardahanensis*, *S. brunoi*, *S. coruhensis*, *S. duhani*, *S. euphrataeus*, *S. fahrettini*, *S. murathani*, *S. rizeensis*) belong to the Danubian lineage, *Salmo tigridis* to the Tigris lineage. Other species of which (*S. baliki*, *S. kottelati*, *S. labecula*, *S. munzuricus*, *S. okumusi*, *S. opimus S. platycephalus*) belong to Adriatic lineage. (Tortonese 1955; Behnke 1968; Bernatchez and Osinov 1995; Sušnik et al. 2005; Bardakçı et al. 2006; Turan et al. 2010, 2011, 2012, 2014a, b, 2017, 2020, 2021, 2022; Ninua et al. 2018; Turan and Aksu 2021).

We reassessed Mediterranean *Salmo* populations in Türkiye. In our previous study (Turan et al. 2012), we examined only 4 samples from the Köprüçay River. In the study, we compared these samples and new materials from Köprüçay River in detail with the samples from the type locality of *S. labecula.* As a result of this comparison, it was concluded that the Köprüçay population belongs to a new species, thus was named as *S. ekmekciae*.

Table 1. Native *Salmo* species distributed in Türkiye.

Species	Type locality	Synonyms	Coordinates
Salmo abanticus Tortonese, 1954	FFR 3163, 13, 113–222 mm SL; Türkiye: Bolu prov.: Lake Abant Basin	None	40°36'47.32"N, 31°17'12.57"E
Salmo araxensis Turan, Kottelat & Kaya, 2022	FFR 3224, 259 mm SL; FFR 3122, 6, 140–250 mm SL; Türkiye: Kars prov.: Kırkpınar Stream, a tributary of Kars Stream, Aras River drainage	*Salmo trutta caspius*, Kessler, 1877 *Salmo caspius*, Kessler, 1877	40°51'0.00"N, 43°1'0.00"E
Salmo ardahanensis Turan, Kottelat & Kaya, 2022	FFR 3239, 222 mm SL; FFR 1130, 12, 135–253 mm SL; Türkiye: Ardahan prov.: Stream Toros, Kura River drainage	*Salmo trutta caspius*, Kessler, 1877 *Salmo caspius*, Kessler, 1877	41°6'0.00"N, 42°25'60.00"E
Salmo baliki Turan, Aksu, Oral, Kaya & Bayçelebi, 2021	FFR 3242, 212 mm SL; FFR 3234, 6, 132–276 mm SL; Türkiye: Ağrı prov.: Stream Sinek, a tributary of Murat River, Euphrates River drainage	None	39°45'31.50"N, 43°27'52.13"E
Salmo brunoi Turan, Baycelebi, Aksu & Oral, 2024	FFR 3243, 175 mm SL; FFR 3216, 188–153 mm SL; Türkiye, Bursa prov.: stream Aras, a tributary of Nilüfer River, Susurluk River drainage	None	40°03'13.07"N, 29°10'20.03"E
Salmo chilo Turan, Kottelat & Engin, 2012	FFR 3054, 190 mm SL; FFR 3055, 23, 65-235 mm SL; Türkiye: Sivas prov.: Akdere Stream, Ceyhan River drainage	*Salmo trutta macrostigma* (non Dumeril, 1858)	38°34'53.89"N, 36°57'17.62"E
Salmo coruhensis Turan, Kottelat & Engin, 2010	FFR 3036, 291 mm SL; FFR 3037, 10, 90-380 mm SL; Türkiye: Erzurum prov.: Pehlivanlı Stream, Çoruh River drainage	*Salmo trutta labrax*, Pallas, 1814	40°30'25.20"N, 41°29'10.20"E
Salmo duhani Turan & Aksu, 2021	FFR 3183, 228 mm SL; FFR 3184, 15, 95-287 mm SL; Türkiye: Çanakkale prov.: Stream Zeytinli, Gönen River drainage	*Salmo trutta macrostigma* (non Dumeril, 1858)	39°45'0.00"N, 27°1'1.20"E
Salmo euphrataeus Turan, Kottelat & Engin, 2014	FFR 1219, 195 mm SL; FFR 1220, 24, 80-260 mm SL; Türkiye: Erzurum prov.: Kuzgun Stream, a tributary of Karasu Stream, Euphrates River drainage	None	40°13'11.10"N, 41°6'18.30"E
Salmo fahrettini Turan, Kalaycı, Bektaş, Kaya & Bayçelebi, 2020	FFR03231, 232 mm SL; FFR03232, 20, 134–227 mm SL; Türkiye: Erzurum prov.: Stream Ömertepesuyu, a tributary of Karasu Stream, Euphrates River drainage	None	39°41'44.97"N, 34°56'4.07"E
Salmo kottelati Turan, Doğan, Kaya & Kanyılmaz, 2014	FFR 3180, 205 mm SL; FFR 03181, 21, 98–210 mm SL; Türkiye: Antalya prov.: Alakır Stream, a coastal stream in Mediterranean Sea Basin	None	36°32'34.85"N, 30°17'11.39"E
Salmo labecula Turan, Kottelat & Engin, 2012	FFR 3056, 208 mm SL; FFR 3057, 6, 103-237 mm SL; Türkiye: Nigde prov.: Ecemiş Stream, Seyhan River drainage	None	37°51'53.31"N, 35°4'46.37"E
Salmo munzuricus Turan, Kottelat & Kaya, 2017	FFR 3161, 205 mm SL; FFR 03162, 17, 127-270 mm SL; Türkiye: Tunceli prov.: Stream Munzur, Euphrates River drainage.	*Salmo trutta macrostigma* (not Dumeril, 1858)	39°20'50.00"N, 39°8'3.00"E
Salmo murathani Turan, Kottelat & Kaya, 2022	FFR 3240, 255 mm SL; FFR 3121, 18, 60–233 mm SL; Türkiye: Kars prov.: Keklik Stream, a tributary of Kars Stream, Aras River drainage	*Salmo trutta caspius*, Kessler, 1877 *Salmo caspius*, Kessler, 1877	40°16'60.00"N, 42°38'60.00"E
Salmo okumusi Turan, Kottelat & Engin, 2014	FFR 1251, 213 mm SL; FFR 1254, 10, 75-202 mm SL; Türkiye: Malatya prov.: Sürgü Stream, Euphrates River drainage	None	37°59'51.10"N, 37°57'29.90"E
Salmo opimus Turan, Kottelat & Engin, 2012	FFR 3047, 180 mm SL; FFR 3048, 12, 118-180 mm SL; Türkiye: Antalya prov.: Alara Stream, a coastal stream in Mediterranean Sea Basin	*Salmo trutta macrostigma* (non Dumeril, 1858)	36°45'45.04"N, 32°1'35.02"E
Salmo platycephalus Behnke, 1968	FFR 972, 7, 145-184 mm SL; Türkiye: Kayseri prov.: Pınarbaşı Stream, Seyhan River drainage	None	38°24'15.80"N, 37°27'39.44"E
Salmo rizeensis Turan, Kottelat & Engin, 2010	FFR 3000, 234 mm SL; FFR 3001, 16, 90-220; FFR 3038, 1, 250 mm SL; Türkiye: Erzurum prov.: Ovit (Kan) Stream, Çoruh River drainage	*Salmo trutta macrostigma* (non Dumeril, 1858)	40°35'19.20"N, 40°51'30.00"E
Salmo tigridis Turan, Kottelat & Bektaş, 2011	FFR 1250, 220 mm SL; FFR 1253, 9, 136–227 mm SL; Türkiye: Van prov.: Çatak Stream, Tigris River drainage	*Salmo trutta macrostigma* (non Duméril, 1858)	38°2'27.63"N, 43°2'57.29"E

Material and methods

Fish sampling

The care of experimental animals was in accordance with the animal welfare laws, guidelines declared by Republic of Türkiye and the policies approved by RTE University Local Ethics Committee for experimentations (Permit reference number 2014/72). First, 80mg/L MS222 was performed for anaesthesia. Secondly, fish were collected for faunal surveys and preserved in 5% formaldehyde or 96% ethanol, later stored in 70% ethanol. Surgical procedures were only performed for excision of fin clips. Thus, the experimental conditions did not cause severe stress on specimens under investigation.

Morphological analyses

All measurements were done point to point (never by projections) as specified in Turan et al., (2010) with a dial caliper calibrated to 1 mm. Number of lateral line scale count, standard length, and the length of the caudal peduncle were recorded according to Turan et al. (2010). The last two branched rays articulating on a single pterygiophore in the anal and dorsal fins are counted as "1½". Comparative materials used in this study are listed in Turan et al. (2010); Turan et al. (2011); Turan et al. (2014a, b); Turan et al. (2017); Turan et al. (2020); and Turan et al. (2022).

Comparison material

All materials are from Türkiye except *Salmo labrax*.

***Salmo abanticus*:** FFR 3163, 13, 77–272 mm SL; Bolu prov.: outlet of Abant Lake, 40.5737°N, 31.2957°E.

***Salmo ardahanensis*:** FFR 3164, 10, 154–217 mm SL; Ardahan prov.: stream Toros, Kura River drainage, 41.1000°N, 42.4333°E.—FFR 3107, 4, 156–192; FFR 3167, 2, 155–182 mm SL; Ardahan prov.: stream Alabalık, Kura River drainage, 41.0500°N, 42.3666°E.—FFR 3110, 4, 67–118 mm SL; Ardahan prov.: stream Karaman at Aşıkzülal, Kura River drainage, 41.4166°N, 42.6500°E.—FFR 3136, 16, 99–185 mm SL; Ardahan prov.: stream Kınavur at Çataldere, Kura River drainage, 41.1833°N, 42.6000°E.

***Salmo araxensis*:** FFR 3114, 12, 116–201 mm SL; Kars prov.: Susuz district Kayalık stream, a tributary of Kars Stream, Aras River drainage, 40.8166°N, 43.1166°E.—FFR 3115, 15, 93–237 mm SL; Kars prov.: Susuz district: Porsuklu (Akçalı) Stream, a tributary of Kars Stream, Aras River drainage, 40.8000°N, 43.1833°E.—FFR 3118, 6, 95–132 mm SL; Kars prov.: Sarıkamış district: Boyalı Stream, a tributary of Kars Stream, Aras River drainage, 40.4333°N, 42.5666°E.—FFR 3144, 16, 87–265 mm SL; Kars prov.: Susuz district: İncilipınar Stream, a tributary of Kars Stream, Aras River drainage, 40.8166°N, 43.0666°E.

Salmo brunoi: FFR 3213, 7, 142–195 mm SL;—FFR 3215, 7, 142–195 mm SL; Türkiye, Bursa prov.: stream Deliçay at Kestel, 40.1241°N, 29.2737°E.—FFR 3211, 18, 93– 180 mm SL; —FFR 3217, 12, 85–153 mm SL; Türkiye, Bursa prov.: stream Ericek at Osmangazi, 40.0426°N, 29.2098°E.

***Salmo baliki*:** FFR 3234, 6, 132–276 mm SL; Ağrı prov.: stream Sinek a tributary of Murat River at Taşlıçay, 39.7587°N, 43.4644°E.—FFR 3205, 3, 175–267 mm SL; Ağrı prov.: a tributary of Murat River, 39.7307°N, 43.4818°E.

***Salmo chilo*:** FFR 3055, 23, 65–235 mm SL; Sivas prov.: stream Akdere at Gürün, Ceyhan River drainage, 38.6088°N, 36.8962°E.

***Salmo coruhensis*:** FFR 3004, 16, 95–240 mm SL; Artvin prov.: stream Osmaniye at Karaosmaniye village, 41.4689°N, 41.5105°E.—FFR 3011, 11, 90–189 mm SL; Artvin prov.: stream Hopa at Çavuslu village, 41.4509°N, 41.7001°E.—FFR 3021, 25, 90–520 mm SL; Rize prov.: stream Fırtına at Çat village, 40.8653°N, 40.9311°E.—FFR 3022, 9,95–228 mm SL; Rize prov.: stream Kendirli at Kalkandere District on road to Kendirli village, İyidere drainage, 40.9373°N, 40.4320°E.—FFR 3023, 13, 120–450 mm SL; Rize prov.: stream Iyidere (Ikizdere) at Güneyce, 40.8219°N, 40.4765°E.—FFR 3024, 13, 115–330 mm SL; Artvin prov.: stream Dörtkilise at Tekkale village, Çoruh River, 40.7877°N, 41.4946°E.—FFR 3025, 13, 80–550 mm SL; Erzurum prov.: stream Çayırbası (Kırık) at Kırık village, Çoruh River, 40.2904°N, 40.8097°E.—FFR 3026, 6, 160–290 mm SL; Erzurum prov.: stream Büyük at Büyükköy village, Çoruh River, 40.4452°N, 40.8513°E.—FFR 3027, 6, 130–420 mm SL; Rize prov.: stream Veliköy at Veliköy village, 41.0332°N, 40.6145°E.—FFR 3029, 6, 130–220 mm SL; Rize prov.: stream Bozukkale at Bozukkale village, 41.0543°N, 40.6297°E.—FFR 3030, 6, 80–170 mm SL; Rize prov.: stream Çaglayan at Çaglayan district, 40.9230°N, 40.4452°E.—FFR 3031, 6, 190–265 mm SL; Bayburt prov.: stream Ölçer at Ölçer village, Çoruh River, 40.5147°N, 40.5609°E.—FFR 3032, 16, 70–310 mm SL; Rize prov.: stream Sögütlü at Sögutlü village, about 5 km west of Çayeli, 41.0659°N, 40.6526°E.—FFR 3033, 16, 110–210 mm SL; Bayburt prov.: stream Kurtbogazı at Kurtbogazı village, Çoruh River, 40.1883°N, 40.5033°E.—FFR 3034, 16, 70–210 mm SL; Gümüşhane prov.: stream Harşit at Yağmurdere, 40.5746°N, 39.8645°E.—FFR 3035, 9, 160–450 mm SL; Sivas prov.: stream Gemin at Camili, Yeşilırmak River drainage, 38.0536°N, 40.0619°E.—FFR 3037, 10, 90–380 mm SL; Erzurum prov.: stream Pehlivanlı at Pehlivanlı village, tributary of Tortum, Çoruh River, 40.5176°N, 41.4780°E.—FFR 3041, 10, 115–250 mm SL; Trabzon prov.: stream Solaklı at Taskıran village 40.6722°N, 40.2568°E.—FFR 3042, 6, 95–117 mm

SL; Rize prov.: stream Sarayköy at Sarayköy village, 41.0190°N, 40.3807°E.—FFR 3043, 5, 130–229 mm SL; Artvin prov.: stream Barhal at Sarıgöl village, Çoruh River, 40.9744°N, 41.4184°E.—FFR 3043, 9, 110–223 mm SL; Rize prov.: stream Derepazarı at Derepazarı 41.0237°N, 40.4293°E.—FFR 3044, 6, 100–250 mm SL; Rize prov.: stream İyidere at İyidere, 40.9676°N, 40.3778°E.—FFR 3045, 7, 150–450 mm SL; Rize prov.: stream Fırtına at Çamlıhemsin, 41.0517°N, 41.0032°E.—FFR3046, 5, 10–280 mm SL; Rize prov.: stream Limanköy at Limanköy village, 41.0714°N, 40.7121°E.

***Salmo duhani*:** FFR 3184, 15, 95–287 mm SL; Çanakkale prov.: stream Zeytinli about 9 km east of Kazdağı National Park, 39.750°N, 27.017°E. –FFR 3185, 14, 85–170 mm SL; Çanakkale prov.: stream Zeytinli, 39.749°N, 27.015°E.—FFR 3186, 12, 108–160 mm SL; Çanakkale prov.: stream Zeytinli 39.759°N, 27.021°E.—FFR 3194, 10, 62–122 mm SL; Çanakkale prov.: stream Kocaçayı, 12 km west of Kalkım, 39.804°N, 27.071°E.—FFR 3195, 15, 93–275 mm SL; Çanakkale prov.: stream Kocaçay at Yenice, 39.817°N, 27.099°E.

Salmo euphrataeus: FFR 1220, 24, 80–260 mm SL; Erzurum prov.: stream Kuzgun, a tributary of Karasu Stream, Euphrates River drainage, 40.2198°N, 41.1051°E.—FFR 1255, 25, 88–230 mm SL; Erzurum prov.: stream Şenyurt at Şenyurt, a tributary of Karasu Stream, Euphrates River, 40.1830°N, 41.5037°E.—FFR 1223, 5, 122–222 mm SL; Erzurum prov.: stream Sırlı, a tributary of Karasu Stream, Euphrates River, 40.2183°N, 41.1010°E.—FFR 1269, 8, 117–198 mm SL; Erzurum prov.: stream Kuzgun, Euphrates River, 40.2198°N, 41.1050°E.

***Salmo fahrettini*:** FFR 3232, 20, 134–227 mm SL; Erzurum prov.: stream Ömertepesuyu at Palandöken 39.7958°N, 40.9444°E.—FFR 3233, 5, 126–194 mm SL; Erzurum prov.: stream Tekke at Palandöken, 39.8197°N, 41.1516°E.

***Salmo kottelati*:** FFR 3181, 21, 98–210 mm SL; Antalya prov.: stream Alakır at Altınyaka, 36.5608°N, 30.3428°E.—FFR 3182, 16, 98–176 mm SL; Antalya prov.: stream Alakır at Altınyaka, 36.5608°N, 30.3428°E.

***Salmo labecula*:** FFR 3057, 4, 103–237 mm SL; Niğde prov.: stream Ecemiş at Çamardı, Seyhan River drainage, 37.8253°N, 34.9902°E.—FFR 3058, 5, 142–241 mm SL; Isparta prov.: stream Kartoz at Aşağıyaylabel, Köprüçay drainage, 37.5532°N, 31.3070°E.—FFR 3059, 5, 140–184 mm SL; Antalya prov.: stream Zindan at Aksu, Köprüçay drainage, 37.8064°N, 31.0734°E.

***Salmo munzuricus*:** FFR 3162, 17, 127–270 mm SL; Tunceli prov.: stream Munzur at Koyungölü, 39.3472°N, 39.1341°E.—FFR 3147, 8, 146–320 mm SL; stream Munzur at Koyungölü, 39.3461°N, 39.1316°E.

Salmo murathani: FFR 3121, 18, 60–233 mm SL; Kars prov.: Keklik stream [a tributary of Kars stream], Sarıkamış district, Aras River drainage, 40.2833°N, 42.6500°E.—FFR3117, 22, 95–192 mm SL; FFR 3113, 17, 91–206; Kars prov.: Keklik stream [a tributary of Kars stream] Sarıkamış district, Aras River drainage, 40.2500°N, 42.6666°E.—FFR 3120, 10, 69–163 mm SL, Kars prov.: Maksutçuk Stream [a tributary of Kars stream], Aras River drainage, 40.5333°N, 42.8666°E.—FFR 3108, 14, 90–186 mm SL; Ardahan prov.: Çıldır Lake, Aras River drainage, 41.0500°N, 43.3166°E.—FFR 3228, 23, 95–241 mm SL; Kars prov.: Arpaçay stream [a tributary of Kars stream] Arpaçay district, Aras River drainage, 40.9000°N, 43.1666°E.—FFR 3229, 8, 110–156 mm SL; Kars prov.: Keklik Stream [a tributary of Kars stream] Sarıkamış District, Aras River drainage, 40.2833°N, 42.6500°E.

***Salmo okumusi*:** FFR 1254, 10, 75–202 mm SL; Malatya prov.: stream Sürgü, Euphrates River drainage, 37.9975°N, 37.9583°E.—FFR 125, 10, 129–169 mm SL; Sivas prov.: stream Gökpınar, a tributary of Tohma Stream, Euphrates River, 38.6600°N, 37.3089°E.—FFR 1256, 10, 68–280 mm SL; Sivas prov.: stream Gökpınar, Euphrates River, 38.6600°N, 37.3089°E.—FFR 124, 2, 149–175 mm SL; Kahramanmaraş prov.: stream Göksu 4 km north of Düzbağ, Euphrates River, 37.8331°N, 37.4756°E.

***Salmo opimus*:** FFR 3048, 12, 118–180 mm SL; Antalya prov.: stream Alara at Gündoğmuş, 36.7921°N, 31.9749°E.—FFR 3049, 20, 115–186; Kahramanmaraş prov.: stream Göçüksu at Kömürköy, Ceyhan River drainage, 38.1447°N, 36.5630°E.—FFR 3050, 4, 175–210 mm SL; Kahramanmaras prov.: drainage of stream Tekir at Tekir, Ceyhan River drainage, 37.8767°N, 36.6058°E.—FFR 3051, 9, 90–300 mm SL; Kahramanmaras prov.: stream Fırnız at Fırnız, Ceyhan River drainage, 37.7591°N, 36.6983°E.

***Salmo platycephalus*:** FFR 972, 7, 145–184 mm SL; Kayseri prov.: Pınarbası Stream at Pınarbası district, Seyhan River drainage, 38.4043°N, 37.4609°E —FFR 1260, 10, 137–237 mm SL; Kayseri prov.: Pınarbası Stream at Pınarbası district, Seyhan River drainage, 38.4044°N, 37.4609°E.

***Salmo rizeensis*:** FFR 3001, 15, 90–220 mm SL; Erzurum prov.: stream Ovit (2) [Kan] at Ovit mountain, Çoruh River, 40.5887°N, 40.8583°E.—FFR 3002, 10, 114–245 mm SL; Trabzon prov.: stream Degirmen at Çosandere village, 40.7512°N, 39.5908°E.—FFR 3003, 12, 112–230 mm SL; Trabzon prov.: stream Solaklı at Demirkapı village, 40.7586°N, 40.5913°E.—FFR 3005, 13, 111–220 mm SL; Rize prov.: stream Çağlayan at Gürcüdüzü plateau, 41.1905°N, 41.3086°E.—FFR 3006, 18, 95–226 mm SL; Rize prov.: stream Sehitlik at Sehitlik village, 41.1407°N, 40.9828°E.—FFR 3007, 12, 90–118 mm SL; Rize prov.: stream Çayeli at Kaptanpasa village, 40.958°N, 40.7794°E.—FFR 3008, 18, 91–198 mm SL; Rize prov.: stream Fırtına at Tunca village, 41.1259°N, 41.1310°E.—FFR 3009, 10, 110–240 mm SL; Rize prov.: stream Taşlıdere at Pasaçur village, 40.8837°N, 40.5796°E.—FFR 3010, 9, 110–240 mm SL; Rize prov.: stream Taslıdere at Kangel village, 40.9453°N, 40.6642°E.—FFR 3011, 7, 100–180 mm SL; Rize prov.: stream Erenler at Erenler village, 41.0914°N, 40.8298°E.—FFR

3012, 7, 88–237 mm SL; Artvin prov.: stream Dörtkilise at Tekkale Village, Çoruh River, 40.7800°N, 41.5098°E.—FFR 3013, 12, 75–167 mm SL; Artvin prov.: Çifteköprü Stream at Cankurtaran mountain, Çoruh River, 41.3844°N, 41.5691°E.—FFR 3014, 7, 112–201 mm SL; Artvin prov.: stream Kapisre at Küçükköy village, 41.2753°N, 41.3755°E.—FFR 3015, 9, 113–228 mm SL; Bayburt prov.: stream Kop at Kop Mountain, Çoruh River, 40.0654°N, 40.4331°E.—FFR 3016, 9, 113–221 mm SL; Erzurum prov.: stream Yağlı at Yaglı village, Çoruh River, 40.3643°N, 41.0728°E.—FFR 3017, 12, 112–223 mm SL; Erzurum prov.: stream Büyük at Büyükdere plateau, Çoruh River drainage, 40.5698°N, 40.7140°E.—FFR 3018, 16, 145–224 mm SL; Gümüşhane prov.: stream Akbulak at Akbulak village, Yesilırmak River drainage, 40.281462°N, 39.0896°E.—FFR 3019, 10, 122–221 mm SL; Kütahya prov.: stream Sefaköy at Domaniç, Sakarya River drainage, 39.8426°N, 29.6706°E.—FFR 3020, 10, 111–119 mm SL; Kütahya prov.: Çatalalıç Stream at Domaniç, Sakarya River, 39.8600°N, 29.6291°E.—FFR 3036, 10, 130–170 mm SL; Rize prov.: stream Ikizdere at Anzer plateau, 40.5926°N, 40.5148°E.—FFR 3038b, 7, 130–170 mm SL; Rize prov.: stream Çiftekavak at Ortapazar village, 40.9959°N, 40.4851°E.—FFR 3039a, 14, 120–200 mm SL; Rize prov.: stream Fırtına at Elevit Plateau, 40.8471°N, 41.0151°E.—FFR 3038a, 1, 250 mm SL; Erzurum prov.: stream Ovit (2) [Kan] at Ovit mountain, Çoruh River, 40.5735°N, 40.8634°E.—FFR 3039b, 10, 90–238 mm SL; Rize prov.: stream Ovit at Ovit mountain, İyidere drainage, 40.6361°N, 40.8214°E.—FFR 3040, 14, 90–190 mm SL; Erzurum prov.: stream Merekum at Merekum, Çoruh River, 40.5527°N, 41.4592°E.

***Salmo tigridis*:** FFR 1253, 9, 136–227 mm SL; Van prov.: stream Çatak, Tigris River, 38.0077°N, 43.0652°E.

DNA extraction, PCR and Sequencing

Total DNA was extracted from fin clips via Hibrigen Genomic DNA isolation kit and DNA quality were checked on 0.8% agarose gel electrophoresis. Mitochondrial *cytochrome b* gene (Cyt *b*) (991 bp) was amplified using SsaL14437 (Warheit and Bowman 2008) and StrCBR (Turan et al. 2010) primer pair. PCRs were applied in a 50 µL reaction volume with a T100 thermal cycler (Bio-Rad, Hercules, CA, USA), including 100 ng of DNA, 10X PCR buffer, 3 mM $MgCl_2$, 5 µL of 0.5 mM dNTPs mix, 1 u Taq DNA polymerase (Thermo Scientific Inc.) and 0.5 mM of each primer. PCR amplifications were conducted under the following conditions: initial denaturation 2 min at 95 °C, denaturation 30 s at 95 °C, annealing 30 s at 56 °C, extension 70 s at 72 °C through 35 cycles and a final extension 7 min at 72 °C. The PCR products were run at 1% agarose gel electrophoresis and visualized under the UV Quantum–Capt ST4 system (Vilber Lourmat, France). Purification and sequencing of PCR products were performed by Macrogen Europa Inc. (Amsterdam, Netherlands).

Molecular data analysis

We have used the newly generated twelve Cyt *b* sequences from the present study and included an additional 51 specimens from earlier studies deposited to NCBI GenBank (Crête-Lafrenière et al. 2012; Tougard et al. 2018; Turan et al. 2020; Turan et al. 2022). Clustal W algorithm (Thompson et al. 1994) in Bioedit v7.2.5 (Hall, 1999) was used to align Cyt *b* sequences. Sequences were submitted to NCBI GenBank with accession numbers OR713904–OR713909. Nucleotide substitution model TrN+I+G model: -ln= 1781.6420 (Tamura and Nei 1993) was chosen as the best nucleotide substitution model according to the Bayesian information criterion (BIC) in jModeltest v. 0.0.1 (Posada, 2008). Phylogenetic relationships among species were carried out using maximum likelihood (ML) using MEGA X (Kumar et al. 2018) with 100 bootstrap and Bayesian inference (BI) analysis using MrBayes 3.2 software (Ronquist et al. 2012). BI analysis was run using a Metropolis-coupled Markov chain Monte Carlo (MCMC) algorithm for one million generations in the MrBayes 3.1.2 software (Ronquist and Huelsenbeck 2003), and the initial 25% of the saved trees sampled in each MCMC run were discarded as burn-in. *Salmo ohridanus* (JX960763) was selected as an outgroup taxa for all phylogenetic analyses. Pairwise genetic distance estimation among the species was calculated by MEGA X software using the *p-distance* substitution model (Kimura, 1980).

Collection codes

IFC-ESUF, Inland Fishes Collection, Faculty of Eğirdir Fisheries, Isparta University of Applied Sciences, Isparta; and FFR, Zoology Museum, Faculty of Fisheries, Recep Tayyip Erdoğan University, Rize.

Results

Phylogenetic placement of *Salmo ekmekciae*

The resulting phylogeny indicates that the studied *Salmo* species are divided into six main clades: Adriatic, Danubian, Tigris, Atlantic, Mediterranean and Marmoratus lineage. *Salmo ekmekciae* is involved Adriatic lineage with *S. kottelati*, *S. chilo*, *S. labecula*, *S. munzuricus*, *S. okumusi*, *S. baliki*, *S. platycephalus* and *S. opimus* with Marmoratus lineage. *Salmo ekmekciae* more closely related *Salmo chilo* and *Salmo kottelati* than to other species included in the analysis (Fig. 1). The Bayesian and Maximum Likelihood analyses of Cyt *b* gene resulted in coherent trees supported by high bootstrap values. *p* distance between species ranged from 0.00% (*S. kottelati* and *S.chilo*; *S. opimus* and *S. marmoratus*; *S. duhani* and *S. brunoi*; *S. euphrataeus* and *S. murathani*) to 1.6% (*S. tigridis* and *S. araxensis* (Suppl. material 1). *P* distance is 0.001% between *S. ekmekciae* sp nova and its closest relatives *S. kottelati* and *S.chilo*.

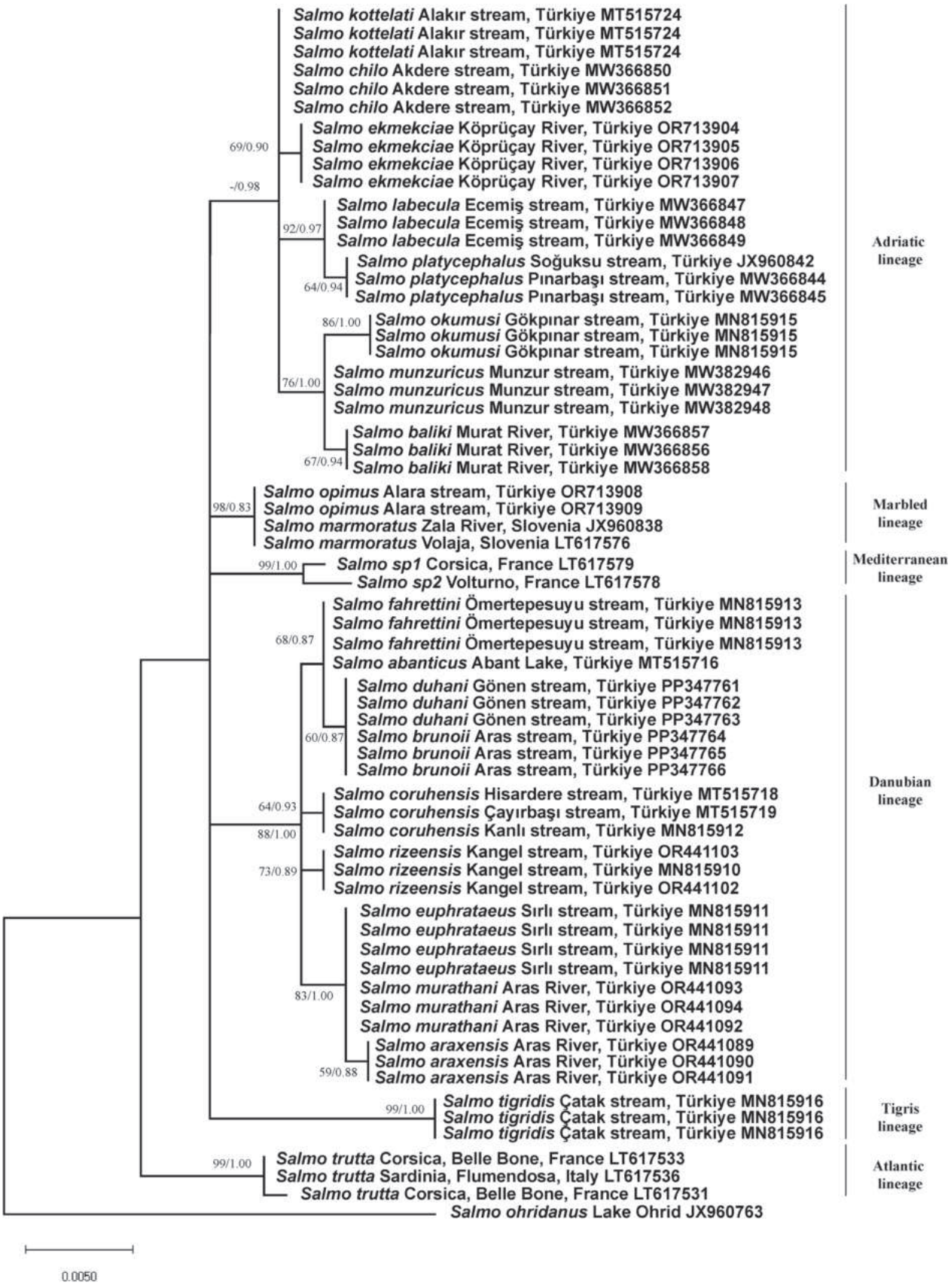

Figure 1. Maximum likelihood (ML) tree based on mitochondrial cytochrome b gene sequences of Salmo species. Bayesian inference and ML analyses resulted in congruent trees. Bootstrap and posterior probability values are shown above nodes on tree if 50% or higher.

Morphological differences and comparisons

Salmo populations from Köprüçay River are distinguished from the other species of trout recorded from the streams and rivers in Turkish Mediterranean coast (*S. labecula*, *S. kottelati*, *S. platycephalus*, *S. opimus* and *S. chilo*) by the following characters: *Salmo* populations from Köprüçay River differ from *S. labecula* by having fewer parr marks on flank (9–10, vs. 11–12), fewer scale rows between end of base of adipose fin and lateral line (11–13, vs. 14–15), a longer head (27–30% SL, vs. 25–27), a shorter distance between adipose fin and caudal-fin base (13–15% SL, vs. 16–18), a slenderer caudal peduncle (9–10% SL, vs. 10–11) and a slenderer body at adipose-fin origin (13–14% SL, vs. 14–15). *Salmo* populations from Köprüçay River differ from *S. kottelati* by the general body colour silvery in life (vs. brownish), and no black spots on top of head (vs. more or less presence). *Salmo* populations from Köprüçay River further differ from *S. kottelati* in having more gill rakers on first gill arch (22–24, vs. 18–20), a slenderer caudal peduncle (9–10% SL, vs. 10–13), a shorter maxilla in male (8–10% SL, vs. 10–13) and a smaller mouth gape in males (11–13% SL, vs. 13–19). *Salmo* populations from Köprüçay River differ from S. *platycephalus* by having fewer parr marks along lateral line (9–10, vs. 12–13), the presence of black spots in all size (vs. absent in specimens larger than about 200 mm SL), the head not flattened dorso-ventrally (vs. flattened dorso-ventrally), a shorter distance between adipose fin and caudal-fin base (13–15% SL, vs. 15–17), a slenderer caudal peduncle (9–10% SL, vs. 11–12) and a slenderer body at adipose-fin origin (13–14% SL, vs. 14–16. *Salmo* populations from Köprüçay River differ from *S. opimus* by no red spots on flank in specimens larger than about 160 mm SL, if the red spot present in specimens larger than about 160 mm SL, they almost covered with black dots (vs. presence in all size and not covered with black dots), a slenderer caudal peduncle (9–10% SL, vs. 11–12) and a slenderer body at adipose-fin origin (13–14% SL, vs. 15–17). It differs from *S. chilo* by the absence of red spots on flank in specimens larger than about 160 mm SL, if the red spot is present in specimens larger than about 160 mm SL, they are almost covered with black dots (vs. presence in all size, and red spots not covered with black dots), fewer parr marks along lateral line (9–10, vs. 11–13), more gill rakers on first gill arch (22–24, vs. 18–21) and a slenderer caudal peduncle (9–10% SL, vs. 11–12).

Salmo populations from Köprüçay River are distinguished from *S. baliki*, S. *okumusi* and *S. munzuricus* by having more gill rakers on first gill arch (22–24, vs. 16–21), fewer scale rows on lateral line and dorsal-fin origin (21–25, vs. 26–30), fewer scale rows on lateral line and anal-fin origin (16–18, vs. 18–28) and fewer scale rows between origin of the adipose fin and lateral line (11–13, vs. 13–17) and a longer head in males (28–30% SL, vs. 24–27). It further differs from *S. okumusi* and *S. munzuricus* by having fewer parr marks on flank (9–10, vs. 10–14).

Salmo populations from Köprüçay River are also distinguished from other species (*S. abanticus*, *S. araxensis S. ardahanensis*, *S. brunoi*, *S. coruhensis*, *S. duhani*, *S. euphrataeus*, *S. fahrettini*, *S. munzuricus*, *S. murathani*, *S. rizeensis*, *S. tigridis*) by having the presence of four broad dark bands on flank (vs. absent), black spots on body irregularly shaped (vs. roundish), height of parr marks on anterior of the flank 2.5–3.5 times its width (vs. 1.4–2.5), fewer parr marks on flank (9–10, vs. 10–14), more gill rakers on first gill arch (22–24, vs. 16–22, except *S. murathani*), fewer scale rows lateral line and dorsal-fin origin (21–25, vs. 26–35, except *S. araxensis*), fewer scale rows lateral line and anal-fin origin (16–18, vs. 18–26, except *S. ardahanensis*) and fewer scale rows between origin of the adipose fin and lateral line (11–13, vs. 13–20).

Thus, we describe *Salmo* populations from Köprüçay River, as a new species, *Salmo ekmekciae* sp. nov.

Salmo ekmekciae sp.nov

https://zoobank.org/32FCE1C6-ABD9-485A-9B37-D825C523447A

Type material. ***Holotype.*** IFC ESUF 02-0029, holotype, 216 mm SL, male; Türkiye: Isparta prov.: Yayla Stream, a drainage of Köprüçay River, 37.8115°N, 31.0925°E.

Paratypes. IFC-ESUF 02-0022, 6, 70–150 mm SL; same data as holotype; FFR 3058, 4, 141–185 mm SL; Türkiye: Isparta prov.: Kartoz Stream (Köprüçay River drainage), 37.7162°N, 31.1616°E.

Diagnosis. *Salmo ekmekciae* is distinguished from all the species of *Salmo* in Türkiye and adjacent areas by combination of follow characters: one small black spot in postorbital and suborbital areas, greater than pupil; seven to seventeen black spots on opercle; black spots on body few or numerous, scattered on the back (missing in the predorsal area), a middle portion of flank, sometimes upper and lower halves of the flank. Red spots few, ocellated, organized in two or three irregular longitudinal rows on median part of the body, and half of lower part of the flank; commonly no black spots on flank in specimens larger than 160 mm SL, if red spots present in specimens larger than about 160 mm SL, they are almost covered with black dots; maxilla short and narrow; lateral line with 108–118 scales; 21–25 scale rows between dorsal-fin origin and lateral line; 16–18 scale rows between anal-fin origin and lateral line; 11–13 scale rows between origin of the adipose fin and lateral line. 22–24 gill rakers on outer side of first gill arch.

Description. The general appearance is shown in Figs 2–4, morphometric data are in Table 2. Body moderately deep, compressed laterally, its maximum depth markedly smaller than head length. Dorsal profile slightly convex and ventral profile less convex than the dorsal profile. Head somewhat long, upper profile slightly convex in interorbital area, markedly convex in interorbital and on snout. Mouth small, slightly sub-terminal in males, sub-inferior in females. Tip of lower jaw slightly curved upwards, slightly pointed, with a slightly developed process at symphysis in males larger than 180 mm SL. Maxilla short, not reaching beyond posterior margin of the eye in males and females. Snout short, slightly rounded in males, rounded in females. Adipose fin somewhat large,

Figure 2. *Salmo ekmekciae*, IFC ESUF 02-0029, holotype, 216 mm SL, male; Türkiye: Köprüçay River.

Figure 3. *Salmo ekmekciae*, IFC-ESUF 02-0022, paratype, 150 mm SL, female; Türkiye: Köprüçay River.

Figure 4. *Salmo ekmekciae*, IFC-ESUF 02-0022, paratype, 84 mm SL, juvenile; Türkiye: Köprüçay River.

its height 7–9% SL in males and about 7% SL in females, slightly increasing with body size. Largest observed specimen 185 mm SL.

Lateral line with 108–118 scales; 21–25 scale rows between dorsal-fin origin and lateral line; 16–18 scale rows between anal-fin origin and lateral line; 11–13 scale rows between origin of the adipose fin and lateral line. Dorsal fin with 9–10 branched and 3–4 unbranched rays, its distal margin straight or slightly convex. Pectoral fin with 1 unbranched and 11–13 branched rays, its external margin convex. Pelvic fin with 1 unbranched and 8 branched rays, its external margin slightly convex. Anal fin with 3 unbranched and 8 branched rays, its distal margin straight or slightly convex anteriorly and slightly concave posteriorly. Caudal fin slightly forked, lobes slightly pointed. 22–24 gill rakers on the outer side of first gill arch.

Coloration. In formalin: General coloration of freshly preserved specimens silvery on back and flank, yellowish

Table 2. Morphometry of *Salmo ekmekciae* (holotype, IFC-ESUF 02-0029; paratypes FFR 3058, IFC-ESUF 02-0022, n=9. The calculations include the holotype.

	Holotype	Paratypes	
Sex	**male**	**male**	**female**
Number of specimens		**n = 5**	**n = 5**
Standard length (mm)	216	101–185	84–150
In percentage of standard length		Range (mean)	Range (mean)
Head length	25.9	27.5–30.4 (28.7)	27.1–28.0 (27.4)
Predorsal length	45.2	44.9–50.0 (47.2)	45.4–47.0 (46.3)
Prepelvic length	55.5	53.4–57.3 (55.4)	52.6–54.3 (53.4)
Preanal length	75.6	74.3–75.8 (75.2)	73.2–74.8 (73.4)
Body depth at dorsal-fin origin	20.9	24.1–27.5 (25.8)	22.3–23.5 (23.0)
Body depth at dipose-fin origin	14.1	13.1–14.4 (13.9)	12.7–13.0 (12.9)
Depth of caudal peduncle	10.2	9.2–10.2 (9.9)	9.6–10.1 (9.8)
Length of caudal peduncle	15.0	14.6–18.0 (16.1)	14.4–15.3 (15.0)
Distance between adipose- and caudal-fins	13.9	14.0–15.3 (14.6)	13.1–14.5 (14.0)
Body width at anal-fin origin	9.7	8.7–11.0 (10.2)	9.1–9.3 (9.2)
Length of dorsal-fin base	15.7	14.8–19.9 (17.3)	14.6–15.4 (15.0)
Depth of dorsal-fin	15.6	14.9–19.8 (18.4)	17.0–17.7 (17.3)
Length of pectoral-fin	18.3	17.3–22.3 (19.8)	18.3–20.9 (19.7)
Length of adipose-fin base	3.8	3.8–4.9 (4.4)	3.8–3.9 (3.9)
Depth of adipose-fin	7.1	7.0–8.7 (7.8)	6.6–7.5 (7.0)
Length of pelvic-fin	13.3	13.1–15.6 (14.8)	13.6–14.8 (14.2)
Depth of anal-fin	15.7	14.3–18.3 (15.7)	14.2–16.8 (15.3)
Length of anal-fin base	12.1	9.9–12.9 (11.5)	10.6–11.6 (11.2)
Length of upper caudal-fin lobe	13.4	15.8–20.0 (17.1)	14.3–15.9 (15.4)
Length of median caudal-fin rays	12.2	12.9–15.6 (14.1)	12.8–13.8 (13.3)
Length of lower caudal-fin lobe	14.6	15.9–20.3 (17.8)	16.3–17.5 (16.9)
Snout length	7.5	6.7–7.2 (7.0)	6.6–7.6 (7.0)
Distance between nasal openings	4.1	3.7–4.9 (4.4)	4.1–4.6 (4.3)
Eye diameter	4.8	5.6–7.3 (6.2)	5.4–6.3 (5.9)
Interorbital width	7.1	7.0–7.5 (7.3)	7.0–7.3 (7.2)
Head depth through eye	12.8	12.8–14.7 (13.9)	12.3–13.0 (12.7)
Head depth at nape	16.8	17.3–20.4 (18.9)	16.5–17.6 (17.0)
Length of maxilla	8.1	7.8–10.1 (8.8)	7.8–8.3 (8.1)
Maximum height of maxilla	2.5	3.0–3.8 (3.4)	3.1–3.5 (3.3)
Width of mouth gape	9.3	8.5–10.4 (9.6)	8.5–9.3 (8.9)
Length of mouth gape	11.2	11.8–13.1 (12.4)	11.3–12.2 (11.6)

on the belly. Four broad dark bands on flank, without or very faintly marked in specimens smaller than approximately 160 mm SL. One small black spot in postorbital and suborbital areas, greater than pupil; seven to seventeen black spots on opercle, smaller than pupil. Black spots on body few or numerous (more than 70 in most specimens larger than about 160 mm SL), smaller than pupil, ocellated, scattered on the back (missing in the predorsal area), a middle portion of flank, sometimes over upper and lower halves of the flank. No black spot on top of the head. Red spots few (less than about 20), ocellated, organized in two or three irregular longitudinal rows on median part of the body, and half of lower part of the flank. Commonly no red spots on flank in specimens larger than 160 mm SL, if red spots present in specimens larger than about 160 mm SL, they are almost covered with black dots; dorsal fin grey, with three or five rows of black spots (smaller than pupil), and one or two rows of red spots (smaller than pupil) in specimens smaller than about 120 mm SL. Caudal fin grey or dark grey; pectoral, anal and pelvic fins grayish. Adipose-fin plain greyish. Nine or ten mostly vertically elongated parr marks on the body, distinct in specimens up to at least about 160 mm SL.

In life: General body colour silvery. Back and halves of upper part of flank silver, belly and halves of lower part of flank yellowish. All fins yellowish. A conspicuously black spots behind eye, smaller than pupil. Red spots few and with almost covered black pigment in specimens larger than about 160 mm SL, scattered on median part of the body, and half of lower part of the flank. Adipose-fin plain greyish, with very inconspicuous reddish margin. Nine or ten vertically elongated dark grey parr marks along middle part of flank.

Distribution. *Salmo ekmekciae* inhabits clear and moderately swift-flowing water, with a substrate of stones and pebbles. It is only known from the Köprüçay River and its tributaries in Antalya-Isparta province (Fig. 5).

Sexual dimorphism. The snout of the male is more pointed than that of the female. The length of the head, and the length of the maxilla of the male are slightly greater than those of the female counterparts.

Etymology. The species is named for Dr. Fitnat Güler Ekmekçi (Türkiye), ichthyologist, in appreciation of her contribution to literature.

Conservation status. *Salmo ekmekciae* is only known from Köprüçay River, most probably endemic to that area. The species is threatened by overfishing similar to other Salmonids and there are rainbow trout (*Oncorhynchus mykiss*) farms in the region.

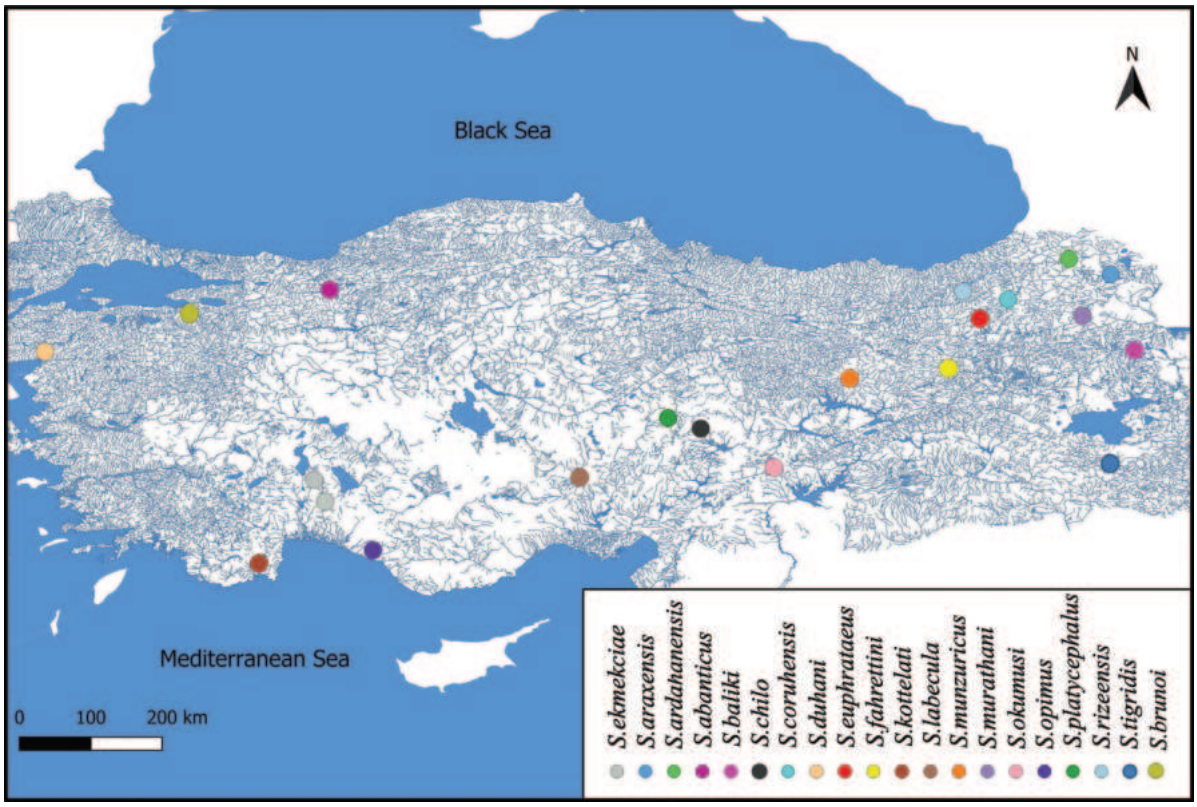

Figure 5. Type localties of *Salmo* species in the Türkiye.

Key to native *Salmo* species distributed in Türkiye

1 Red spots larger than eye pupil..... *S. baliki*
– Red spots smaller than eye pupil 2
2 There are four dark bands on flank; black spots on body irregularly shaped; in males, the lower jaw not curved upward; height of parr marks on anterior of the flank 2.5–3.5 times its width..... 3
– There are no dark bands on body; black spots on body roundish; in large males, the lower jaw curved upward; height of parr marks on anterior of the flank 1.4–2.5 times its width..... 11
3 There are no red spots in adult specimens..... 4
– There are red spots in both juvenile and adult specimens..... 5
4 The head flattened dorsoventrally; there are no black spots in specimens larger than 175 mm SL; there are numerous black dots on body..... *S. platycephalus*
– The head not flattened dorsoventrally; there are black spots in both juveniles and adults; there is no black dots on body ..... *S. labecula*
5 Length of maxilla more than 10% SL..... *S. kottelati*
– Length of maxilla less than 10% SL..... 6
6 There are 9–10 parr marks on flank..... *S. ekmekciae*
– There 10–13 parr marks on flank..... 7
7 22–23 gill rakers on first gill arch; a large (lager than eye pupil) white ring around red spots ..... *S. opimus*
– 18–21 gill rakers on first gill arch; a narrow (equal or smaller than eye pupil) white ring around red spots..... 8
8 There are 24–26 scales row between dorsal-fin origin and lateral line; 15–18 scale rows between anal-fin origin and lateral line..... *S. chilo*
– There are 26–35 scales row between dorsal-fin origin and lateral line; 18–26 scale rows between anal-fin origin and lateral line 9
9 There are 32–35 scales row dorsal-fin origin and lateral line..... *S. tigridis*
– There are 26–30 scales row dorsal-fin origin and lateral line..... 10
10 Lateral line with 103–112 scales ..... *S. okumusi*
– Lateral line with 116–123 scales ..... *S. munzuricus*
11 There are no black spots on the body in specimens larger than 200 mm SL; shape of black spots on body polygonal ... . *S. abanticus*
– There are red spots on body of both juvenile and adult specimens; shape of black spots on body circular 12

12 There are few black and red spots on body; number of black and red spots not increasing with size and age; black spots scattered on back and upper part of flank; one black spot behind eye 13
– There are numerous black and red spots on body; number of black and red spots increasing with size and age; black spots scattered on back, upper part and middle part of flank; more than one spots behind eye in specimens larger than 230 mm SL..... 16
13 General body colour silveri in life; length of maxilla 9–10% SL in males ..... *S. araxensis*
– General body colour brownish or greenish in life; length of maxilla 10–12% SL in males 14
14 Distance between adipose fin and caudal fin bases in females 12–14% SL..... *S. brunoi*
– Distance between adipose fin and caudal fin bases 14–17% SL..... 15
15 The head slightly compressed in adult male; anal-fin and adipose fins reaching to caudal-fin base ..... *S. euphrataeus*
– The head not compressed in adult male, anal-fin and adipose fins not reaching to caudal-fin base in adult males ..... *S. rizeensis*
16 There are 19–23 gill rakers on first gill arch; adipose-fin reaching to caudal-fin base; head slightly flattened..... 17
– There are 16–19 gill rakers on first gill arch; adipose-fin not reaching to caudal-fin base; head not flattened..... 18
17 Pores on top of head with small black spots (smaller than pupil) ..... *S. ardahanensis*
– There are no black spots on pores on top of head ..... *S. murathani*
18 Dorsal-fin with 8–9 unbranched rays; upper profile of head markedly convex in males..... *S. fahrettini*
– Dorsal-fin with 9–11 unbranched rays; upper profile of head straight or slightly convex 19
19 The number of spots conspicuously increasing with sizes in males ..... *S. coruhensis*
– The number of spots not increasing with sizes in males..... *S. duhani*

Discussion

In this study molecular data revealed that *Salmo ekmekciae* belongs to the Adriatic lineage. A total of 8 species of this lineage are distributed in Turkish inland waters. Among these species, *S. chilo*, *S. kottelati*, *S. labecula* and *S. platycephalus* are distributed in the streams and rivers in the Mediterranean region of Türkiye, while *S. baliki*, *S. munzuricus* and S. *okumusi* are found in the Euphrates River. On the other hand, the *S. opimus*, whose type locality is Alara Stream (a coastal stream in Mediterranean), belong to Marmoratus lineage together with *Salmo marmoratus* species. More detailed studies should be carried out to reveal the lineage status of this species. Molecular data from the present study show that *S. chilo* (upper drainage of Ceyhan River) is very closely related to other populations that were previously reported as *S. opimus* by Turan et al. (2012) in the lower part of Ceyhan River. Therefore, to the best of the authors' knowledge *S. opimus* is only restricted to Alara Stream. In the present study, we treated all Ceyhan trout as *S. chilo.* There is no genetic difference between *S. kottelati* and *S. chilo*, *S. opimus* and *S. marmoratus*, *S. duhani* and *S. brunoi*, and *S. euphrataeus* and *S. murathani*. They also share the same mt DNA *Cyt b* haplotypes. Segherloo et al. (2021) stated that the mostly absent or shallow mtDNA diversity leads to difficulties in defining salmonid taxonomy, despite the wide geographical distribution and high morphological and ecological diversity. However, they have published full genome data of some species in Europe and Asia. These results have begun to contribute significantly to new taxonomic studies based on the whole genome data. Following this, whole genome data were used for the first time to describe the *S. brunoi* species (Turan et al. 2024). Additionally, unpublished whole genome data confirms that mt DNA haplotypes only determine the level of lineage. Turan et al. (2012) examined a small number of samples from Köprüçay River in their study and reported this population as *S. labecula*. However, in this study, a thorough examination was carried out between these two populations and it was concluded that they are separate species. *Salmo ekmekciae* are similar to *S. labecula* in terms of color and pattern as well as number of gill rakers on the first gill arch, but there are significant morphological differences between these two species. Differences between *Salmo ekmekciae* and *S. labecula* are given in the diagnosis section. More detailed studies covering all natural trout in Türkiye are needed. However, this study focused on a new species distributed only in Köprüçay River.

Acknowledgements

This study was supported by a grant from the Isparta University of Applied Sciences, Scientific Research Projects Coordination Unit (ISUBÜ BAP) (Project No: 2021-ILK1-0154). We wish to thank Dr Ufuk Gürkan Yıldırım (Isparta) for great help in the field.

References

Bardakçı F, Değerli N, Özdemir O, Başıbüyük HH (2006) Phylogeography of the Turkish brown trout *Salmo trutta* L.: Mitochondrial DNA PCR-RFLP variation. Journal of Fish Biology 68(A, Suppl. A): 36–55. https://doi.org/10.1111/j.0022-1112.2006.00948.x

Behnke RJ (1968) A new subgenus and species of trout *Salmo* (*Platysalmo*) *platycephalus*, from south-central Turkey with comments on the classification of the subfamily salmoninae. Mitteilungen Aus Dem Hamburgischen Zoologischen Museum Und Institute 66: 1–15.

Bernatchez L (2001) The evolutionary history of brown trout (*Salmo trutta* L.) inferred from phylogeographic, nested clade, and mismatch analyses of mitochondrial DNA variation. Evolution; International Journal of Organic Evolution 55: 351–379. https://doi.org/10.1111/j.0014-3820.2001.tb01300.x

Bernatchez L, Osinov AG (1995) Genetic diversity of trout (genus *Salmo*) from its most eastern native range based on mitochondrial DNA and nuclear gene variation. Molecular Ecology 4(3): 285–297. https://doi.org/10.1111/j.1365-294X.1995.tb00222.x

Bernatchez L, Guyomard R, Bonhomme F (1992) DNA sequence variation of the mitochondrial control region among geographically and morphologically remote European brown trout *Salmo trutta* populations. Molecular Ecology 1(3): 161–173. https://doi.org/10.1111/j.1365-294X.1992.tb00172.x

Bogutskaya NG (1997) Contribution to the knowledge of Leuciscine fishes of Asia Minor: Part 2. An annotated checklist of Leuciscine fishes (Leuciscinae, Cyprinidae) of Turkey with descriptions of a new species and two new subspecies. Mitteilungen aus dem Hamburgischen Zoologischen Museum und Institut 94: 161–186.

Bogutskaya NG, Küçük F, Ünlü E (2000) *Alburnus baliki*, a new species of cyprinid fish from the Manavgat River system, Turkey. Ichthyological Exploration of Freshwaters 11(1): 55–64.

Boulenger GA (1896) On freshwater fishes from Smyrna. Annals and Magazine of Natural History (Series 6) 18(104): 153–154. https://doi.org/10.1080/00222939608680427

Çiçek E, Sungur S, Fricke R, Seçer B (2023) Freshwater lampreys and fishes of Türkiye; an annotated checklist, 2023. Turkish Journal of Zoology 47(6): 2. https://doi.org/10.55730/1300-0179.3147

Crête-Lafrenière A, Weir LK, Bernatchez L (2012) Framing the Salmonidae family phylogenetic portrait: A more complete picture from increased taxon sampling. PLOS ONE 7(10): e46662. https://doi.org/10.1371/journal.pone.0046662

Delling B (2003) Species diversity and phylogeny of *Salmo* with emphasis on southern trouts (Teleostei, Salmonidae). Thesis, Stockholm University, Stockholm.

Delling B, Doadrio I (2005) Systematics of the trouts endemic to Moroccan lakes, with description of a new species (Teleostei: Salmonidae). Ichthyological Exploration of Freshwaters 16: 49–64.

Ferguson A (1989) Genetic differences among brown trout, *Salmo trutta*, stocks and their Importance for the conservation and management of the species. Freshwater Biology 21(1): 35–46. https://doi.org/10.1111/j.1365-2427.1989.tb01346.x

Ferguson A (2004) The importance of identifying conservation units: Brown trout and pollan biodiversity in Ireland. Biology and Environment 104(3): 33–41. https://doi.org/10.3318/BIOE.2004.104.3.33

Geldiay R, Balık S (1999) Türkiye Tatlısu Balıkları. Ege Üniversitesi Su Ürünleri Fakültesi Yayınları, Izmir, No: 46, Ders Kitabı Dizini, No. 16, 519 pp. [in Turkish]

Guinand B, Oral M, Tougard C (2021) Brown trout phylogenetics: A persistent mirage towards (too) many species. Journal of Fish Biology 99(2): 298–307. https://doi.org/10.1111/jfb.14686

Hall TA (1999) BioEdit: A user–friendly biological sequence alignment editor and analysis program for Windows 95/98/NT. Nucleic Acids Symposium Series 41: 95–98.

Heckel JJ (1843) Ichthyologie [von Syrien]. In: Russegger J von (Ed.) Reisen in Europa, Asien und Africa, mit besonderer Rücksicht auf die naturwissenschaftlichen Verhältnisse der betreffenden Länder unternommen in den Jahren 1835 bis 1841, etc., Vol. 1, part 2, 990–1099.

Kimura M (1980) A simple method for estimating evolutionary rate of base substitutions through comparative studies of nucleotide sequences. Journal of Molecular Evolution 16(2): 111–120. https://doi.org/10.1007/BF01731581

Kottelat M (1997) European freshwater fishes. An heuristic checklist of the freshwater fishes of Europe (exlusive of former USSR), with an introduction for non-systematists and comments on nomenclature and conservation. Biologia 52(Suppl. 5): 1–271.

Kottelat M, Freyhof J (2007) Handbook of European freshwater fishes. Kottelat, Cornol & Freyhof, Berlin, 660 pp. https://www.nhbs.com/handbook-of-european-freshwater-fishes-book

Küçük F, Gülle İ, Güçlü SS (2016) *Pseudophoxinus iconii*, a new species of spring minnow from Central Anatolia (Teleostei: Cyprinidae). Ichthyological Exploration of Freshwaters 27(3): 283–288.

Küçük F, Turan D, Güçlü SS, Mutlu AG, Çiftçi Y (2017) Two new species of *Chondrostoma* Agassiz, 1832 (Teleostei: Cyprinidae) from the Ceyhan, Seyhan and Göksu Rivers in the East Mediterranean Region of Turkey. Turkish Journal of Fisheries and Aquatic Sciences 17(4): 795–803. https://doi.org/10.4194/1303-2712-v17_4_15

Kumar S, Stecher G, Li M, Knyaz C, Tamura K (2018) MEGA X: Molecular Evolutionary Genetics Analysis across computing platforms. Molecular Biology and Evolution 35(6): 1547–1549. https://doi.org/10.1093/molbev/msy096

Kuru M (1975) Dicle-Fırat, Kura-Aras, Van Gölü Karadeniz Havzası Tatlısularında Yasayan Balıkların (Pisces) Sistematik ve Zoocografik Yönden Incelenmesi [Systematic and zoogeographic investigation of the freshwater fishes living in Tigris-Euphrates, Kura-Arax rivers, and Lake Van Basins]. Doçentlik Tezi, Atatürk Üniv., Fen Fak., Erzurum, 180 pp.

Kuru M (2004) Recent systematic status of inland fishes of Turkey. GÜ. Gazi Egitim Fakültesi Dergisi 24(3): 1–21.

Ninua L, Tarkhnishvili D, Gvazava E (2018) Phylogeography and taxonomic status of trout and salmon from the Ponto-Caspian drainages, with inferences on European brown trout evolution and taxonomy. Ecology and Evolution 8(5): 2645–2658. https://doi.org/10.1002/ece3.3884

Özuluğ M, Freyhof J (2011) Review of the genus *Squalius* in Western and Central Anatolia, with description of four new species (Teleostei: Cyprinidae). Ichthyological Exploration of Freshwaters 22(2): 107–148.

Posada D (2008) jModelTest: Phylogenetic model averaging. Molecular Biology and Evolution 25(7): 1253–1256. https://doi.org/10.1093/molbev/msn083

Ronquist F, Huelsenbeck JP (2003) MrBayes 3: bayesian phylogenetic inference under mixed models. Bioinformatics 19: 1572–1574. https://doi.org/10.1093/bioinformatics/btg180

Ronquist F, Teslenko M, van der Mark P, Ayres DL, Darling A, Höhna S, Larget B, Liu L, Suchard MA, Huelsenbeck JP (2012) MRBAYES 3.2: Efficient Bayesian phylogenetic inference and model selection across a large model space. Systematic Biology 61(3): 539–542. https://doi.org/10.1093/sysbio/sys029

Segherloo IH, Freyhof J, Berrebi P, Ferchaud AL, Geiger M, Laroche J, Levin BA, Normandeau E, Bernatchez L (2021) A genomic perspective on an old question: *Salmo* trouts or *Salmo trutta* (Teleostei: Salmonidae)? Molecular Phylogenetics and Evolution 162: 107–204. https://doi.org/10.1016/j.ympev.2021.107204

Steindachner F (1897) Bericht über die von Dr. Escherich in der Umgebung von Angora gesammelten Fische und Reptilien. Denkschriften der Kaiserlichen Akademie der Wissenschaften in Wien. Mathematisch-Naturwissenschaftliche Classe 64: 685–699. [in German]

Sušnik S, Schöffmann J, Weiss S (2005) Genetic verification of brown trout from the Persian Gulf (Çatak Çay River, Tigris basin). Journal of Fish Biology 67(3): 879–884. https://doi.org/10.1111/j.0022-1112.2005.00780.x

Tamura K, Nei M (1993) Estimation of the number of nucleotide substitutions in the control region of mitochondrial DNA in humans and chimpanzees. Molecular Biology and Evolution 10(3): 512–526. https://doi.org/10.1093/oxfordjournals.molbev.a040023

Thompson JD, Higgins DG, Gibson TJ (1994) CLUSTAL W: Improving the sensitivity of progressive multiple sequence alignment through sequence weighting, position-specific gap penalties and weight matrix choice. Nucleic Acids Research 22(22): 4673–4680. https://doi.org/10.1093/nar/22.22.4673

Tortonese E (1955) The Trouts of Asiatic Turkey. Publications of the Hydrobiological Research Institute. University of Istanbul B 2(1): 1–25.

Tougard C, Justy F, Guinand B, Douzery EJP, Berrebi P (2018) *Salmo macrostigma* (Teleostei, Salmonidae): Nothing more than a brown trout (*S. trutta*) lineage? Journal of Fish Biology 93(2): 302–310. https://doi.org/10.1111/jfb.13751

Turan D, Aksu S (2021) A new trout species from southern Marmara sea drainages (Teleostei: Salmonidae). Journal of Anatolian Environmental and Animal Sciences 6(2): 232–239. https://doi.org/10.35229/jaes.903810

Turan D, Kottelat M, Ekmekçi FG, Imamoglu HO (2006) A review of *Capoeta tinca*, with descriptions of wo new species from Turkey (Teleostei: Cyprinidae). Revue Suisse de Zoologie 113(2): 421–436. https://doi.org/10.5962/bhl.part.80358

Turan D, Ekmekçi FG, Ilhan A, Engin S (2008) *Luciobarbus kottelati*, a new species of barbel (Teleostei: Cyprinidae) from the Büyük Menderes River, Turkey, with rediagnose of *L. lydianus*. Zootaxa 1824(1): 35–44. https://doi.org/10.11646/zootaxa.1824.1.4

Turan D, Kottelat M, Engin S (2010) Two new species of trouts, resident and migratory, sympatric in streams of northern Anatolia (Salmoniformes: Salmonidae). Ichthyological Exploration of Freshwaters 20(4) (2009 [2010]): 289–384.

Turan D, Kottelat M, Bektaş Y (2011) *Salmo tigridis*, a new species of trout from Tigris River, Turkey (Teleostei: Salmonidae). Zootaxa 2993(1): 23–33. https://doi.org/10.11646/zootaxa.2993.1.2

Turan D, Kottelat M, Engin S (2012) The trouts of the Mediterranean drainages of southern Anatolia, Turkey, with description of three new species (Teleostei: Salmonidae). Ichthyological Exploration of Freshwaters 23(3): 219–236.

Turan D, Kottelat M, Engin S (2014a) Two new species of trouts from the Euphrates drainage, Turkey (Teleostei: Salmonidae). Ichthyological Exploration of Freshwaters 24(3): 275–287.

Turan D, Doğan E, Kaya C, Kanyılmaz M (2014b) *Salmo kottelati*, a new species of trout from Alakır Stream, draining to the Mediterranean in southern Anatolia, Turkey (Teleostei, Salmonidae). ZooKeys 462: 135–151. https://doi.org/10.3897/zookeys.462.8177

Turan D, Kottelat M, Kaya C (2017) *Salmo munzuricus*, a new species of trout from the Euphrates River drainage, Turkey (Teleostei: Salmonidae). Ichthyological Exploration of Freshwaters 28: 55–63.

Turan D, Kalaycı G, Bektaş Y, Kaya C, Bayçelebi E (2020) A new species of trout from the northern drainages of Euphrates River, Turkey (Salmoniformes: Salmonidae). Journal of Fish Biology 96(6): 1454–1462. https://doi.org/10.1111/jfb.14321

Turan D, Aksu İ, Oral M, Kaya C, Bayçelebi E (2021) Contribution to the trout of Euphrates River, with description of a new species, and range extension of *Salmo munzuricus* (Salmoniformes, Salmonidae). Zoosystematics and Evolution 97(2): 471–482. https://doi.org/10.3897/zse.97.72181

Turan D, Kottelat M, Kaya C (2022) The trouts of the upper Kura and Aras rivers in Turkey, with description of three new species (Teleostei: Salmonidae). Zootaxa 5150(1): 43–64. https://doi.org/10.11646/zootaxa.5150.1.2

Turan D, Baycelebi E, Aksu S, Oral M (2024) The trouts of the Marmara and Aegean Sea drainages in Türkiye, with the description of a new species (Teleostei, Salmonidae). Zoosystematics and Evolution 100(1): 87–99. https://doi.org/10.3897/zse.100.112557

Warheit KI, Bowman C (2008) Genetic structure of kokanee (*Oncorhynchus nerka*) spawning in tributaries of Lake Sammamish, Washington. Report to King County Department of Natural Resources and Parks, Water and Land Resources Division, and Trout Unlimited – Bellevue/Issaquah, 50 pp. http://your.kingcounty.gov/dnrp/library/water-and-land/salmon/kokanee/warheit-genetics-report-062308.pdf

Yoğurtçuoğlu B, Kaya C, Freyhof J (2022) Revision of the *Oxynoemacheilus angorae* group with the description of two new species (Teleostei: Nemacheilidae). Zootaxa 5133(4): 451–485. https://doi.org/10.11646/zootaxa.5133.4.1

Supplementary material 1

Pairwise distance values (p distance model) based on cytochrome b sequences of *Salmo* species

Authors: Fahrettin Küçük, Gökhan Kalaycı, Salim Serkan Güçlü, Münevver Oral, Davut Turan

Data type: xlsx

Link: https://doi.org/10.3897/zse.100.121174.suppl1

Zoosyst. Evol. 100 (2) 2024, 405–423 | DOI 10.3897/zse.100.119297

PENSOFT

für Natur MUSEUM FÜR NATURKUNDE BERLIN

Taxonomic re-appraisal of *Scolopocryptops quadristriatus* (Verhoeff, 1934) and a description of a new species from Japan and Taiwan (Chilopoda, Scolopendromorpha, Scolopocryptopidae)

Taro Jonishi[1], Takafumi Nakano[1]

1 *Department of Zoology, Graduate School of Science, Kyoto University, Kyoto 606-8502, Japan*

https://zoobank.org/6B07BF7A-9ADA-4959-A654-59E747E200DE

Corresponding author: Taro Jonishi (ykn347635@gmail.com)

Academic editor: Martin Husemann ♦ **Received** 23 January 2024 ♦ **Accepted** 14 March 2024 ♦ **Published** 9 April 2024

Abstract

Centipedes of the genus *Scolopocryptops* Newport, 1844 are blind species mostly described from the New World and East Asia. In this study, a Japanese species, *S. quadristriatus* (Verhoeff, 1934), which is characterised by four longitudinal keels on the tergites, is re-described, based on the likely holotype preserved in the Zoologische Staatssammlung München and specimens newly collected from near the type locality. In addition, *S. longisetosus* **sp. nov.**, a new species that bears tergal keels like *S. quadristriatus*, is described from the Ryukyu Islands in Japan and Taiwan. Although the presence of four keels on tergites is unique to these two species, phylogenetic analyses using nuclear and mitochondrial markers showed that *S. longisetosus* **sp. nov.** is not sister to *S. quadristriatus*. The obtained phylogeny indicates that the tergal longitudinal keels evolved in parallel within *Scolopocryptops* or that the presence of keels represents a plesiomorphic character of the clade containing these species.

Key Words

molecular phylogeny, nomenclature, plesiomorphic character, Ryukyu Islands, tergal keels

Introduction

Scolopocryptops Newport, 1844 is a centipede genus that mostly inhabits epigean habitats in North and South America, West Africa, East Asia and Vietnam and species have been also recorded from India, the Philippines, Indonesia, New Guinea and Fiji (Chagas-Jr et al. 2023; Le et al. 2023). The genus currently comprises 33 species and subspecies, which are classified into two groups: the Asian/North American group and the Neotropical/Afrotropical group (Chagas-Jr 2008; Edgecombe et al. 2012; Vahtera et al. 2013; Chagas-Jr et al. 2023; Le et al. 2023; Jonishi and Nakano 2023). Recent studies showed that the Asian/North American group consists of two lineages: a lineage composed of *S. elegans* (Takakuwa, 1937) and its closest relatives (hereinafter the *elegans* lineage), which is known from Far East Asia and a lineage including the rest of the Asian and North American species (hereinafter, the ex-*elegans* lineage) (Jonishi and Nakano 2022, 2023).

Scolopocryptops centipedes are characterised by a distinctive kind of collared antennal setae, the absence of eyes, 23 leg-bearing segments (except for *S. sukuyan* Chagas-Jr, Edgecombe & Minelli, 2023, which has 25 segments) and an ultimate leg prefemur with one dorso-medial and/or one ventral spinous process (Koch et al. 2010; Chagas-Jr et al. 2023; Le et al. 2023). Several Asian/North American species, for example, *S. sexspinosus* (Say, 1821) and *S. spinicaudus* Wood, 1862, are distinguished from others by the absence of complete paramedian sutures on tergites (Le et al. 2023). Amongst them, the Japanese *S. quadristriatus* (Verhoeff, 1934) bears four longitudinal

keels on its tergites, which is a specific character that distinguishes this species from all other *Scolopocryptops* (Verhoeff 1934; Takakuwa 1940; Shinohara 1984; Le et al. 2023). After it was described as *Otocryptops sexspinosus quadristriatus*, based on a specimen from the vicinity of Tokyo, *S. quadristriatus* has been recorded from several localities in Honshu, the Izu Islands and Kyushu in the Japanese Archipelago (Shinohara 1949; Takashima and Shinohara 1952; Miyosi 1953; Takano 1973). Phylogenetic analyses indicated that this species belongs to the ex-*elegans* lineage (Jonishi and Nakano 2022). As summarised by Le et al. (2023), however, the taxonomic status of *S. quadristriatus* remains uncertain because only a low resolution of morphological features has been reported (Verhoeff 1934; Takakuwa 1939, 1940; Shinohara 1984).

In this study, a re-description of *S. quadristriatus*, based on the likely holotype is provided and newly-obtained specimens from near the type locality and adjacent areas were also investigated. In addition, several unidentified *Scolopocryptops* specimens obtained from the Ryukyu Islands in southern Japan and Taiwan have been studied. These individuals are morphologically similar to *S. quadristriatus*, but differ in several characters. Based on both morphological examination and phylogenetic analyses using nuclear and mitochondrial markers, these specimens are described as a new species herein.

Methods

Specimen collection and morphological observation

A specimen labelled as "*Otocryptops sexspinosus quadristriatus*" deposited at the Zoologische Staatssammlung München (ZSM A20051244), which is likely to represent the holotype of this taxon, was examined. Additional specimens of *S. quadristriatus* were collected from several localities in Tokyo and adjacent areas in eastern Honshu, Japan (Fig. 1). A total of 21 unidentified *Scolopocryptops* individuals were also collected from Okinawa, Ishigaki and Yonaguni Islands in the Ryukyu Islands and Hsinchu and Nantou Counties in Taiwan (Fig. 1). Specimens were placed in 30% ethanol for several minutes, fixed in 80% or 99% ethanol and then preserved in 75% ethanol. Ultimate leg-bearing segments of several specimens were dissected to examine genital segments.

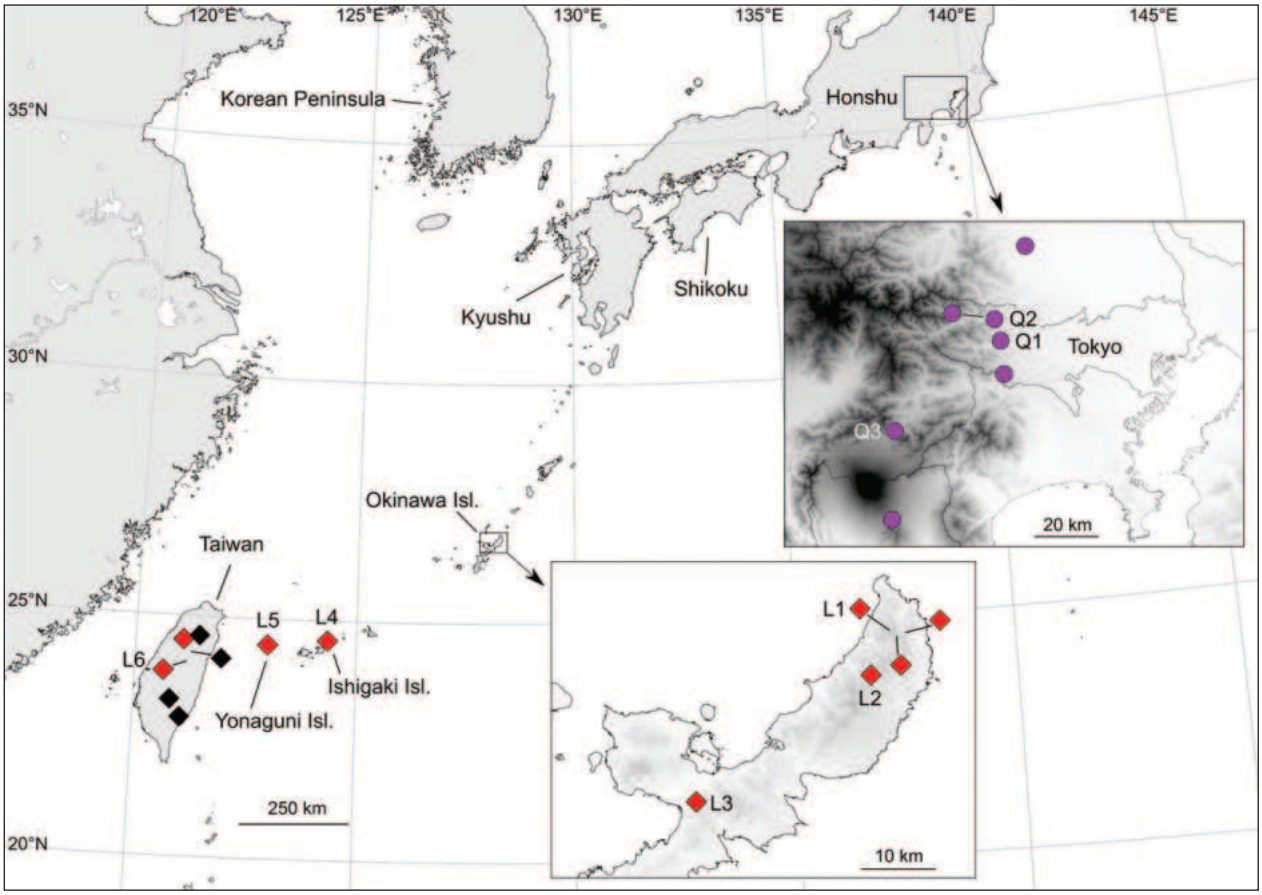

Figure 1. Collection localities of *Scolopocryptops quadristriatus* (Verhoeff, 1934) and *S. longisetosus* sp. nov. in the present study. Purple circles: *S. quadristriatus*; red diamonds: *S. longisetosus* sp. nov.; black diamonds: localities of the sequence data of Taiwanese "*S. capillipedatus*" (= *S. longisetosus* sp. nov.) obtained from INSD. Locality numbers (Q1–Q3 and L1–L6) are shown in Table 1 and Fig. 13.

All specimens were observed using a Leica M125C stereoscopic microscope with a drawing tube (Leica Microsystems, Wetzlar, Germany). The specimens were photographed using a Sony a6500 digital camera and a 65 mm macro lens and a Leica MC170 HD digital camera mounted on the Leica M125C. Images captured with the Leica MC170 were processed using Leica Application Suite v. 4.1.2. Specimens examined are deposited in the Zoological Collection of Kyoto University (KUZ).

The terminology for external features followed Bonato et al. (2010). For dissected adults and individuals with everted genital organs, genital morphology was examined following Takakuwa (1933a), Demange and Richard (1969), Iorio (2003), Siriwut et al. (2016) and Jonishi and Nakano (2022, 2023).

DNA extraction, PCR and DNA sequencing

Total DNA was extracted using a NucleoSpin Tissue kit (Macherey-Nagel, Duren, Germany). Following previous studies (e.g. Edgecombe et al. (2012, 2019)), nuclear internal transcribed spacer 2 (ITS2), 28S rRNA (28S), mitochondrial cytochrome *c* oxidase subunit 1 (COI) and 16S rRNA (16S) markers were selected for phylogenetic analyses. The primer sets used are as follows: the 5.8SF/28SRev (Murienne et al. 2011) for ITS2, 28Sa/28Sb (Whiting et al. 1997) for 28S, LCO1490/HCO2198 (Folmer et al. 1994) or the reverse primer HCOoutout (Schwendinger and Giribet 2005) for COI and 16Sar (Xiong and Kocher 1991)/16Sb (Edgecombe et al. 2002) for 16S. For ITS2 and 16S, reactions were performed using a LifeECO Thermal Cycler (Bioer Technology, Hangzhou, China); 28S and COI fragments were amplified using a GeneAmp PCR System 9700 (Thermo Fisher Scientific, Waltham, USA) and a T-100 Thermal Cycler (Bio-Rad, Hercules, USA), respectively. The PCR mixtures were heated to 94 °C for 5 min; followed by 35 cycles at 94 °C for 10 s, different annealing temperatures for each gene (50–60 °C for ITS2 and 16S, 60 °C for 28S and 50 °C for COI) for 20 s and 72 °C for 48 s for ITS2, 30 s for 28S and 16S and 42–48 s for COI; with a final extension at 72 °C for 6 min. The cycle sequencing reactions and sequencing process followed Jonishi and Nakano (2022, 2023). All sequences obtained in this study were deposited in the International Nucleotide Sequence Databases (INSD) through the DNA Data Bank of Japan (Table 1).

Molecular analyses

In addition to the 42 sequences obtained in this study, 39 sequences of Japanese and Taiwanese *Scolopocryptops* species (Jonishi and Nakano 2022, 2023) and 31 sequences of scolopocryptopid species retrieved from the INSD were included in the taxon set (Table 1).

The nuclear ITS2 sequences were aligned using MAFFT L-INS-i (Katoh and Standley 2013); the nuclear 28S and the mitochondrial 16S sequences were aligned using MAFFT Q-INS-i (Kuraku et al. 2013; Katoh et al. 2019) considering the RNA secondary structure; non-conserved regions of these genes were trimmed by Gblocks v. 0.91b (Castresana 2000). The mitochondrial COI sequences showed no indels; thus, alignment was straightforward. The first four COI positions were excluded from the analyses because this portion was missing in most of the sequences. The concatenated sequences yielded 2510 bp of aligned positions comprising 780 bp of ITS2, 536 bp of 28S, 654 bp of COI and 540 bp of 16S.

Table 1. Samples used for molecular analyses. The information on the voucher is accompanied by the collection locality and the INSD accession numbers of the DNA sequences. Locality numbers are shown in Fig. 1 and Fig.13. Acronyms: AMNH, American Museum of Natural History; KUZ; Zoological Collection of Kyoto University; MCZ, Museum of Comparative Zoology, Harvard University; and SYSU, National Sun Yat-sen University. References: 1, Jonishi and Nakano (2023); 2, Jonishi and Nakano (2022); 3, Chao et al. (unpublished); 4, Vahtera et al. (2013); 5, Vahtera et al. (2012); 6, Edgecombe et al. (2012); 7, Edgecombe and Giribet (2004); 8, Murienne et al. (2010). Sequences with an asterisk (*) were used only in the preliminary analyses.

Species	Voucher #	Locality	Locality #	INSD #				References
				ITS2	28S	COI	16S	
Asian/North American *Scolopocryptops*								
S. quadristriatus (Verhoeff, 1934)	KUZ Z4083	Hachioji, Tokyo, Japan	Q1	–	LC700508	LC700507	LC792589	This study for 16S; 2 for 28S and COI
S. quadristriatus (Verhoeff, 1934)	KUZ Z5098	Ome, Tokyo, Japan	Q2	LC792567	LC792573	LC792581	LC792590	This study
S. quadristriatus (Verhoeff, 1934)	KUZ Z5105	Minamitsuru, Yamanashi, Japan	Q3	–	LC792574	LC792582	LC792591	This study
S. longisetosus sp. nov.	KUZ Z5108	Kunigami, Okinawa Island, Japan	L1	LC792568	LC792575	LC792583	LC792592	This study
S. longisetosus sp. nov.	KUZ Z5122	Kunigami, Okinawa Island, Japan	L2	–	LC792576	LC792584	LC792593	This study
S. longisetosus sp. nov.	KUZ Z5111	Nago, Okinawa Island, Japan	L3	LC792569	LC792577	LC792585	LC792594	This study
S. longisetosus sp. nov.	KUZ Z5123	Ishigaki Island, Japan	L4	LC792570	LC792578	LC792586	LC792595	This study
S. longisetosus sp. nov.	KUZ Z5124	Yonaguni Island, Japan	L5	LC792571	LC792579	LC792587	LC792596	This study

Species	Voucher #	Locality	Locality #	INSD #				References
				ITS2	28S	COI	16S	
S. longisetosus sp. nov.	KUZ Z5127	Nantou, Ren'ai, Taiwan	L6	LC792572	LC792580	LC792588	LC792597	This study
"*S. capillipedatus* (Takakuwa, 1938)" (= *S. longisetosus* sp. nov.)	SYSU Chilo-044	Yanping, Taitung, Taiwan	–	–	–	AB617528*	–	3
"*S. capillipedatus* (Takakuwa, 1938)" (= *S. longisetosus* sp. nov.)	SYSU Chilo-056	Heping, Taichung, Taiwan	–	–	–	AB617529*	–	3
"*S. capillipedatus* (Takakuwa, 1938)" (= *S. longisetosus* sp. nov.)	SYSU Chilo-061	Datong, Yilan, Taiwan	–	–	–	AB617530*	–	3
"*S. capillipedatus* (Takakuwa, 1938)" (= *S. longisetosus* sp. nov.)	SYSU Chilo-143	Taoyuan, Kaohsiung, Taiwan	–	–	–	AB672646*	–	3
S. musashiensis Shinohara, 1984	KUZ Z4085	Ichikawa, Chiba, Japan	–	–	LC700512	LC700511	LC792598	This study for 16S; 2 for 28S and COI
S. nigridius McNeil, 1887	MCZ DNA100807	North Carolina, USA	–	–	HM453278	AY288744	AY288725	8 for 28S; 7 for COI and 16S
S. nigridius McNeil, 1887	MCZ IZ-130806	North Carolina, USA	–	–	JX422594	JX422680	JX422704	6
"*S. nipponicus*" Shinohara, 1990 sensu Edgecombe et al. (2012)	MCZ IZ-130804	Nagoya, Aichi, Japan	–	–	JX422595	JX422681	JX422705	6
S. ogawai Shinohara, 1984	KUZ Z4395	Fukuroi, Shizuoka, Japan	–	LC741599	LC741600	LC741601	–	1
S. rubiginosus L. Koch, 1878	KUZ Z4082	Enoshima, Kanagawa, Japan	–	LC741602	LC700506	LC700505	LC792599	This study for 16S; 1 for ITS2; 2 for 28S and COI
S. rubiginosus L. Koch, 1878	MCZ IZ-130823	Yuanshan, Yilan, Taiwan	–	–	–	JX422682	JX422706	6
S. sexspinosus (Say, 1821)	MCZ IZ-131450	North Carolina, USA	–	–	AY288710	AY288745	AY288726	7
S. spinicaudus Wood, 1862	AMNH IZC 00146514	California, USA	–	–	JX422596	JX422683	JX422707	6
S. elegans (Takakuwa, 1937)	KUZ Z4062	Katsurahama, Kochi, Japan	–	LC741566	LC700494	LC700493	LC792600	This study for 16S; 1 for ITS2; 2 for 28S and COI
S. elegans (Takakuwa, 1937)	KUZ Z4073	Higashimuro, Wakayama, Japan	–	LC741569	LC700500	LC700499	LC792601	This study for 16S; 1 for ITS2; 2 for 28S and COI
S. elegans (Takakuwa, 1937)	KUZ Z4373	Akiruno, Tokyo, Japan	–	LC741570	LC741571	LC741572	LC792602	This study for 16S; 1 for ITS2, 28S, and COI
S. miyosii Jonishi & Nakano, 2023	KUZ Z4375	Kirishima, Kagoshima, Japan	–	LC741573	LC741574	LC741575	LC792603	This study for 16S; 1 for ITS2, 28S, and COI
S. miyosii Jonishi & Nakano, 2023	KUZ Z4374	Saeki, Oita, Japan	–	LC741578	LC741579	LC741580	LC792604	This study for 16S; 1 for ITS2, 28S, and COI
S. miyosii Jonishi & Nakano, 2023	KUZ Z4380	Yamato-son, Amami Island, Japan	–	LC741581	LC741582	LC741583	LC792605	This study for 16S; 1 for ITS2, 28S, and COI
S. brevisulcatus Jonishi & Nakano, 2023	KUZ Z4389	Mt. Katsuu-dake, Okinawa Island, Japan	–	–	LC741587	LC741588	LC792606	This study for 16S; 1 for 28S and COI
S. brevisulcatus Jonishi & Nakano, 2023	KUZ Z4392	Mt. Fuenchiji, Okinawa Island, Japan	–	LC741589	LC741590	LC741591	LC792607	This study for 16S; 1 for ITS2, 28S, and COI
S. curtus (Takakuwa, 1939)	KUZ Z4079	Tai'an, Miaoli, Taiwan	–	LC741597	LC700502	LC700501	–	1 for ITS2; 2 for 28S and COI
S. curtus (Takakuwa, 1939)	KUZ Z4081	Iriomote Island, Okinawa, Japan	–	LC741598	LC700504	LC700503	LC792608	This study for 16S; 1 for ITS2; 2 for 28S and COI
Neotropical/Afrotropical *Scolopocryptops*								
"*S. macrodon*" (Kraepelin, 1903) sensu Chagas-Jr (2008) and Edgecombe et al. (2012)	MCZ IZ-130814	Guyana	–	–	–	JX422675	JX422699	6
S. miersii Newport, 1845	MCZ IZ-130729	Brazil	–	–	KF676364	JX422674	JX422697	6 for COI and 16S; 4 for 28S
S. miersii Newport, 1845	AMNH LP3868, IZ-130730	French Guiana	–	–	–	HQ402545	JX422698	5 for COI; 6 for 16S
Outgroup								
Newportia monticola Pocock, 1890	MCZ IZ-130777	Parque de Cahuita, Costa Rica	–	–	KF676360	KF676507	HQ402497	5 for 16S; 4 for 28S and COI

Maximum Likelihood (ML) and Bayesian Inference (BI) were applied to two separate datasets: a COI sequence dataset for preliminary analyses and a concatenated dataset of COI, 16S, ITS2 and 28S. The sequences of "*S. capillipedatus* (Takakuwa, 1938)" (see Results), of which only the COI region is available in the INSD (AB617528–AB617530, and AB672646), were used only in the preliminary analyses. The best-fit partition schemes and substitution models were identified, based on the Bayesian Information Criterion using ModelFinder (Kalyaanamoorthy et al. 2017) implemented in IQ-TREE v.1.6.12 (Nguyen et al. 2015) or PartitionFinder v.2.1.1 (Lanfear et al. 2016) with the "all" algorithm. The selected partition schemes and models are shown in Suppl. material 1. The ML phylogenetic trees were reconstructed using IQ-TREE v.1.6.12 with ultrafast bootstrapping (UFBoot; Hoang et al. (2017)) conducted with 1000 replicates. The BI trees and Bayesian posterior probabilities (BPP) were estimated using MrBayes v.3.2.7 (Ronquist et al. 2012). Two independent runs of four Markov chains were conducted for 10 million generations and the tree was sampled every 100 generations. Considering parameter estimates and assessments of convergence using Tracer v.1.7.2 (Rambaut et al. 2018), the first 2500 trees were discarded as burn-in.

Uncorrected pairwise distances for COI sequences (590–654 bp) were calculated with MEGA 11 (Tamura et al. 2021), with pairwise deletion of missing data (Suppl. material 2).

Results

Taxonomy

Order Scolopendromorpha Pocock, 1895
Family Scolopocryptopidae Pocock, 1896
Genus *Scolopocryptops* Newport, 1844

Scolopocryptops quadristriatus (Verhoeff, 1934)

Figs 2–7

Japanese name: Yosuji-akamukade

Otocryptops sexspinosus quadristriatus Verhoeff, 1934: 54; Takakuwa (1939: 699), fig. 3 (as *Octocryptops* [sic] *sexspinosus quadristriatus*); Takakuwa (1940: 73), fig. 77.

Scolopocryptops quadristriatus: Shinohara (1984: 41); Shinohara et al. (2015: 880, 906); Le et al. (2023: 437, 442).

Not *S. quadristriatus*. "*Otocryptops sexspinosus quadristriatus*": Takakuwa (1933b: 1457, 1459) (*nomen nudum*).

Type specimen. *Otocryptops s. quadristriatus* was described, based on a single specimen from the vicinity of Tokyo, without any information on the collector, collecting date or deposition of the specimen (Verhoeff 1934). Most of the Verhoeff's specimens are now kept at the Zoologische Staatssammlung München (ZSM), the Museum für Naturkunde (MfN) and the Naturhistorischen Museums Wien (NHMW) (Melzer et al. 2011). A specimen of *O. s. quadristriatus* is deposited at the ZSM, but neither MfN nor NHMW have specimens labelled as *O. s. quadristriatus* (Moritz and Fischer 1979; Schileyko and Stagl 2004). ZSM A20051244 (Fig. 2) is, thus, the only specimen of *O. s. quadristriatus* remaining within the Verhoeff's collection and is supposed to be the holotype of this nominal taxon, although the original label and collection data of this specimen are unavailable (Stefan Friedrich, personal communication). Its cephalic capsule, maxillae and left ultimate leg had been preserved in a separate vial (Fig. 2A); the body had been cut into two parts on leg-bearing segment 8 (Fig. 2B); its ultimate leg-bearing segment had been dissected. Additionally, its left legs 6, 8, 12, 14, 15, 17, 18, 20 and 22; right legs 3, 8, 12–18 and 20–22; and right ultimate leg had been lost or loosened; its left leg 16 was loosened during observation by the first author. Morphological features of the likely holotype are consistent with the original description and specimens newly obtained in this study. Thus, a description, based on both ZSM A20051244 and our specimens, is provided below.

Shinohara (1982) stated that a Japanese myriapodologist, the late Dr Yoshioki Takakuwa, sent a specimen of *O. s. quadristriatus* to Verhoeff. Given that Verhoeff also received other chilopod specimens from Takakuwa (e.g. Verhoeff (1934, 1935, 1937)), it is plausible that the likely holotype was also dispatched from Takakuwa to Verhoeff.

Material examined. *Holotype* (?): Japan • ♀ (approx. 33.5 mm); ZSM A20051244.

Additional material. Japan – **Tokyo** • 1, 33.9 mm (KUZ Z4083); Hachioji City, Uratakao-machi; 15 Apr 2017; Taiga Kato leg. • 1, 33.2 mm (KUZ Z5091); same data as for preceding • 1, 33.0 mm (KUZ Z5092); Hachioji City, Mt. Takao-san; 18 Nov 2017; T. Kato leg. • 1, 28.6 mm (KUZ Z5093); Hachioji City, Uratakao-machi; 35°38.69'N, 139°14.36'E; approx. 250 m alt.; 18 Oct 2021; T. Jonishi leg. • 1 ♂, 32.1 mm (KUZ Z5094) and 3, 33.1 mm (KUZ Z5095), 36.2 mm (KUZ Z5096), 27.7 mm (KUZ Z5097); same locality as for preceding; 35°38.72'N, 139°14.33'E; approx. 260 m alt.; 18 Oct 2021; T. Jonishi leg. • 1, 38.6 mm (KUZ Z5098); Ome City, Futamatao; 35°47.87'N, 139°13.56'E; approx. 230 m alt.; 19 Oct 2021; T. Jonishi leg. • 1 ♂, 38.2 mm (KUZ Z5099); Ome City, Sawai; 35°48.68'N, 139°10.91'E; approx. 350 m alt.; 19 Oct 2021; T. Jonishi leg. • 2, 33.6 mm (KUZ Z5100), 29.7 mm (KUZ Z5101) and 1 juvenile, 12.8 mm (KUZ Z5102); Akiruno City, Yokosawa; 35°44.28'N, 139°14.28'E; approx. 250 m alt.; 12 Apr 2022; Futaro Okuyama leg. • 1, 29.6 mm (KUZ Z5103); Hachioji City, Uratakao-machi; 35°38.75'N, 139°14.16'E; approx. 270 m alt.; 6 Nov 2022; T. Kato leg. – **Saitama Prefecture** • 1 ♀, 39.0 mm (KUZ Z5104); Hiki County, Hatoyama-machi; 36°0.01'N, 139°21.42'E; approx. 110 m alt.; 19 Oct 2021; T. Jonishi leg. – **Yamanashi Prefecture** • 1, 30.5 mm (KUZ Z5105); Minamitsuru County, Nishikatsura-cho; 35°30.82'N, 138°50.44'E; approx. 670 m alt.; 9 Apr 2022; Eitaro Matsushita leg. – **Shizuoka Prefecture** • 1, 30.4 mm (KUZ Z5106); Susono City, Suyama; 35°15.92'N, 138°47.95'E; approx. 910 m alt.; 2 June 2022; T. Nakano leg.

Figure 2. *Scolopocryptops quadristriatus* (Verhoeff, 1934), the likely holotype, ♀ (ZSM A20051244). **A.** Cephalic capsule, maxillae, legs and left ultimate leg; **B.** Forcipular segment, leg-bearing segments and legs. Scale bars: 5 mm.

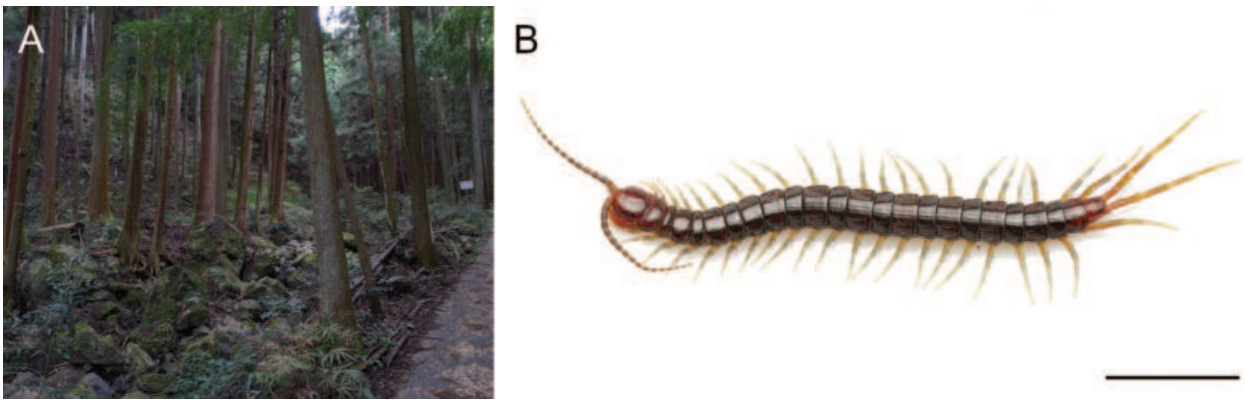

Figure 3. *Scolopocryptops quadristriatus* (Verhoeff, 1934), collected from near the type locality, ♀ (KUZ Z5104) and the habitat near the type locality. **A.** Habitat at Ome City, Tokyo; **B.** Live specimen, dorsal view. Scale bar: 10 mm.

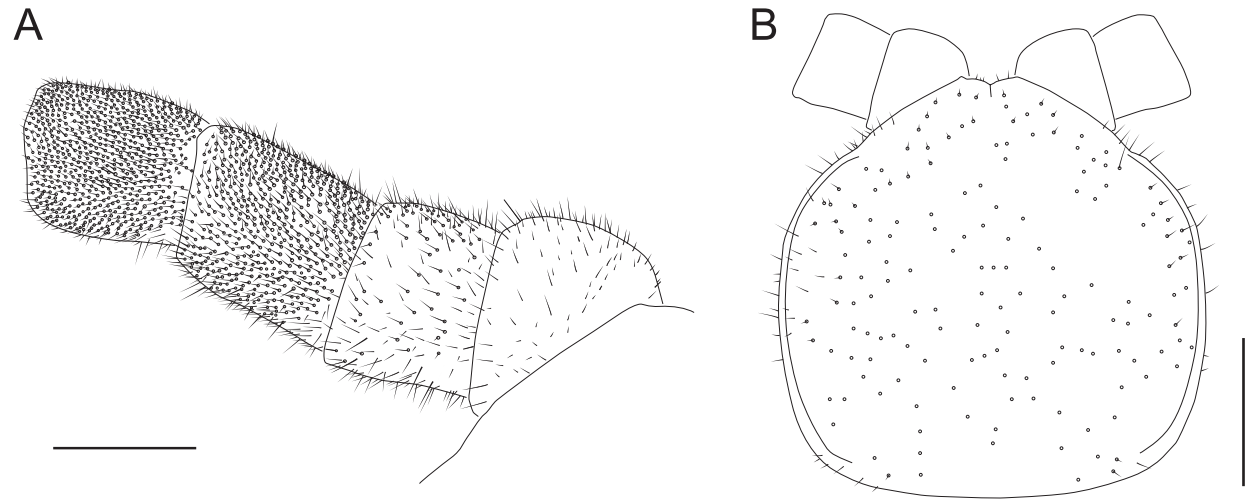

Figure 4. *Scolopocryptops quadristriatus* (Verhoeff, 1934) from near the type locality (KUZ Z5095). **A.** Basal articles of left antenna, dorsal view; **B.** Cephalic plate, dorsal view. Scale bars: 0.5 mm (**A**); 1 mm (**B**).

Diagnosis. Antenna with sparse short hairs and setae on dorsal surface of two basal articles, subsequent articles densely covered with short setae. Cephalic plate with complete lateral marginal sulci. Tergites lacking paramedian sutures, tergites 6–20 with four longitudinal keels and median depression bordered by paramedian keels.

Description [variations given in square brackets]. Body length approx. 27.7–39.0 mm in 75% ethanol.

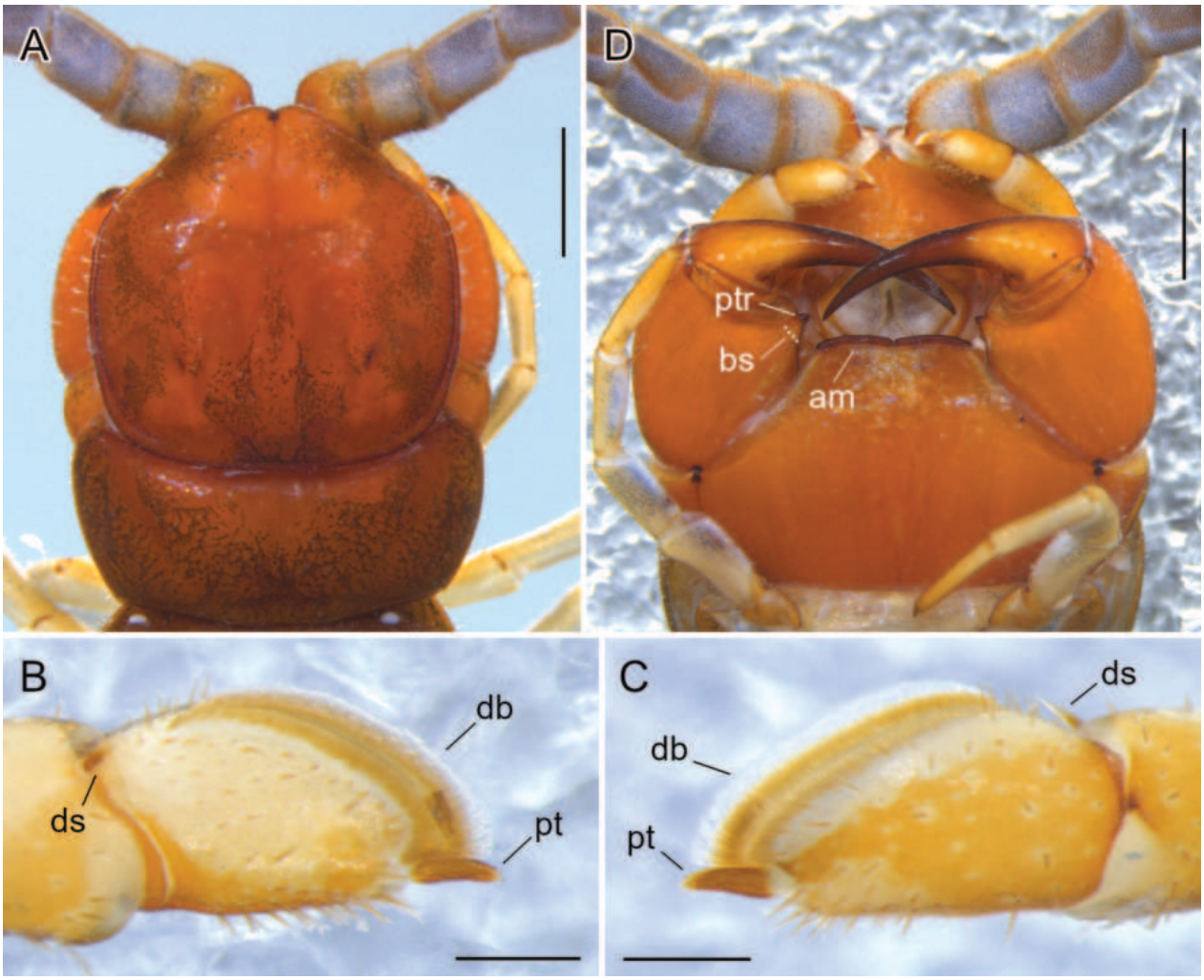

Figure 5. *Scolopocryptops quadristriatus* (Verhoeff, 1934) from near the type locality (KUZ Z5095). **A.** Cephalic plate and tergite 1, dorsal view; **B.** Distal part of article 2, article 3 and pretarsus of left second maxilla, medial view; **C.** Article 3 and pretarsus of left second maxilla, lateral view; **D.** Head, ventral view. Abbreviations: **am** — anterior margin of forcipular coxosternite; **bs** — basal suture on forcipular trochanteroprefemoral process; **db** — dorsal brush on article 3 of second maxilla; **ds** — dorsal spur on article 2 of second maxilla; **pt** — pretarsus of second maxilla; **ptr** — process of forcipular trochanteroprefemur. Scale bars: 1 mm (**A, D**); 0.2 mm (**B, C**).

Colour in life yellowish-brown with dark pigment on two basal antennal articles, purplish on subsequent articles; reddish-brown on forcipules; reddish-brown with dark pigment on anterior, lateral and posterior margins of cephalic plate, tergites 1, 22 and 23; purplish dark brown on tergites 2–21; legs and ultimate legs brownish-yellow or orange with bluish dark pigment (Fig. 3B). Colour in ethanol slightly greenish on tergites and legs (Fig. 6A).

Antennae 7.7–13.4 mm in length, approx. 0.2–0.35× as long as body, composed of 17 articles; two basal articles with sparse short hairs and setae (sensu Bonato et al. (2010)) dorsally, subsequent articles densely covered with short setae (Fig. 4A); each seta emerging from small collar. Cephalic plate as long as wide; its surface sparsely punctate with sparse minute hairs, with complete lateral margination (Figs 4B, 5A).

Second maxillae article 2 with elongated and semi-transparent [dark brown] dorsal spur distally; dorsal brush with transparent margination; pretarsus consisting of dark brown basal and semi-transparent short apical parts (Fig. 5B, C). Forcipular coxosternite and trochanteroprefemora sparsely punctate, coxosternite with median suture and transverse sutures cross median one on anterior third of coxosternite (Fig. 5D); trochanteroprefemur with small and blunt black process with basal suture (Fig. 5D); anterior margin of coxosternite strongly sclerotised and slightly convex, divided into two low lobes by median diastema (Fig. 5D).

Tergites sparsely punctate; tergite 1 with anterior transverse suture; anterior margin overlapped by cephalic plate (Figs 5A, 6A). All tergites lacking paramedian sutures; tergites 6 [5–7]–21 with longitudinal median depression bordered by paramedian keels, lateral keels present on tergites 6 [6–8]–20; median depression and keels unapparent on anterior and posterior tergites [depression and keels unapparent on all tergites in adult KUZ Z5099]

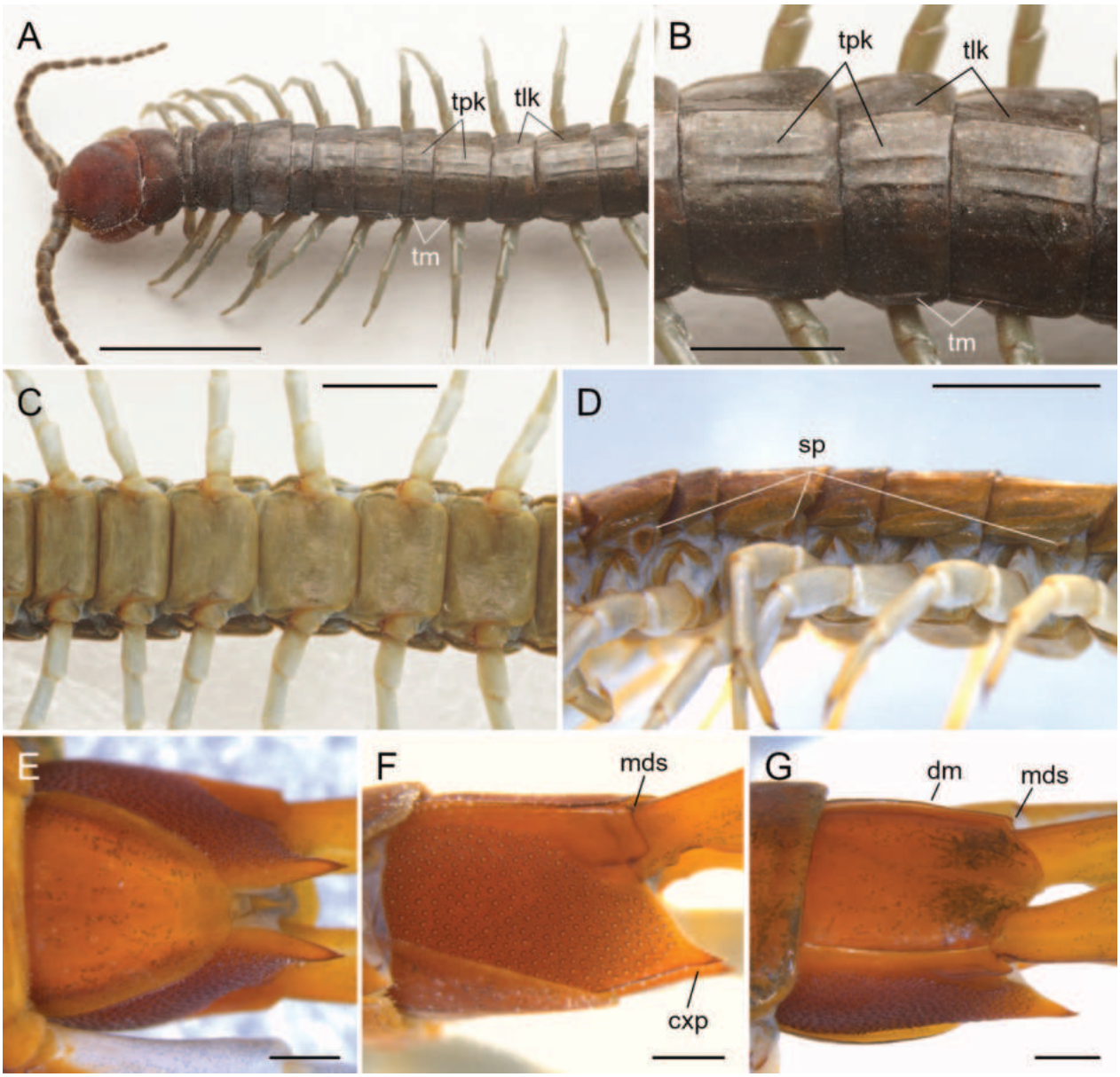

Figure 6. *Scolopocryptops quadristriatus* (Verhoeff, 1934) from near the type locality (KUZ Z5095). **A.** Cephalic plate and tergites 1–13, dorso-lateral view; **B.** Tergites 14–16, dorso-lateral view; **C.** Sternites 8–13, ventral view; **D.** Leg-bearing segments 3–8, lateral view; **E.** Sternite of ultimate leg-bearing segment and coxopleuron, ventral view; **F.** Left coxopleuron, lateral view; **G.** Tergite of ultimate leg-bearing segment, dorso-lateral view. Abbreviations: **cxp** — coxopleural process; **dm** — dorsal margin of ultimate pleuron; **mds** — minute dark spine on ultimate pleuron; **sp** — spiracle; **tlk** — tergal lateral keel; **tm** — tergal margination; **tpk** — tergal paramedian keel. Scale bars: 5 mm (**A**); 2 mm (**B–D**); 0.5 mm (**E–G**).

(Fig. 6A, B); tergites 6 [5–7]–21 [22] with complete or nearly complete lateral marginations (Fig. 6A, B); 2 or 3 short longitudinal sulci present on posterior margin of several tergites.

Sternites sparsely punctate, lacking paramedian sutures (Fig. 6C). Sides of sternite of ultimate leg-bearing segment converging posteriorly, posterior margin slightly concave [slightly convex in KUZ Z4083] (Fig. 6E).

Ovoid spiracles present on leg-bearing segments 3, 5, 8, 10, 12, 14, 16, 18, 20 and 22 (Fig. 6D).

Legs almost lacking setae [sparse minute setae present in several specimens]; tarsi of legs 1–21 undivided; legs 1–20 with lateral and ventral tibial spurs and tarsal spur, leg 21 with tibial spur and tarsal spur; leg 22 with tarsal spur only; all legs with two accessory spines.

Coxopleuron approx. 1.5–1.7× as long as sternite of ultimate leg-bearing segment (Fig. 6E, F). Dorsal margin of ultimate pleuron protruding from lateral side of tergite of ultimate leg-bearing segment, dorso-posterior margin with minute dark spine (Fig. 6F, G). Posterior and ventral margins of coxopleuron converging posteriorly, forming approx. 60–75° angle; coxopleural process short, tip of process pointed, slightly directed dorsally (Fig. 6F). Surface of coxopleuron without setae, covered with various-sized coxal pores (Fig. 6F). Pore-free area present on coxopleural process and dorso-posterior area of coxopleuron (Fig. 6F).

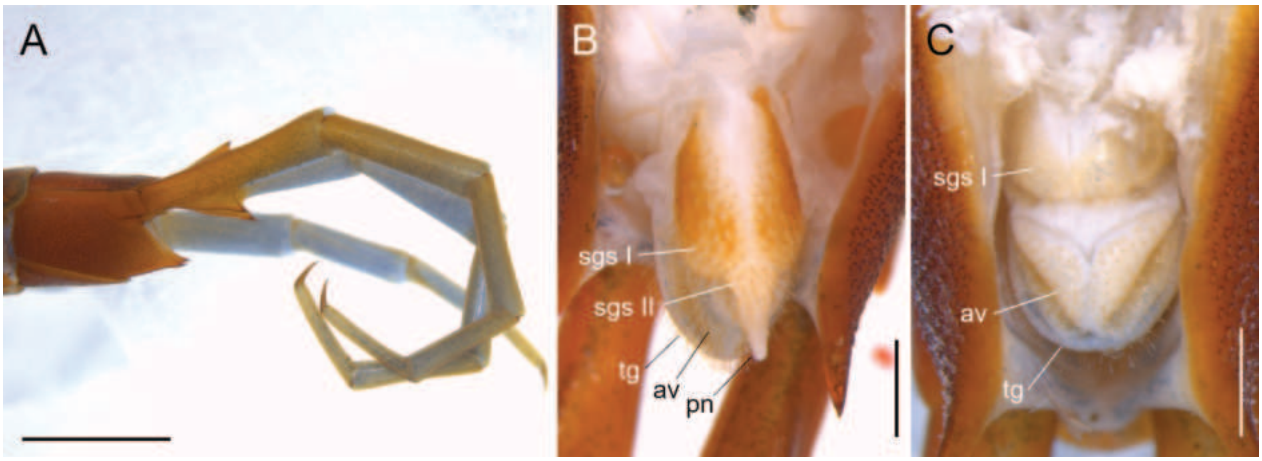

Figure 7. *Scolopocryptops quadristriatus* (Verhoeff, 1934) from near the type locality. **A.** KUZ Z5095; **B.** KUZ Z5094; **C.** KUZ Z5104. **A.** Left ultimate leg, lateral view; **B.** Male genital segments, penis and anal valves, ventral view; **C.** Female genital segment and anal valves, ventral view. Abbreviations: **av** — anal valve; **pn** — penis; **sgs I** — sternite of genital segment 1; **sgs II** — sternite of genital segment 2; **tg** — tergite of genital segment. Scale bars: 2 mm (**A**); 0.5 mm (**B, C**).

Ultimate leg 9.0–12.4 mm in length, approx. 0.3× as long as body; all articles almost lacking setae [tarsi with sparse minute setae]; prefemur with two conical and pointed spinous processes, ventral process larger than dorso-medial one; pretarsus with two accessory spines (Fig. 7A).

Genital segments occupying approx. 0.7–0.8× length of sternite of ultimate leg-bearing segment; tergite of genital segment covered with sparse minute setae (Fig. 7B, C). Sternite of genital segment 1 covered with sparse short setae, posterior margin weakly convex (Fig. 7B, C). Sternite of genital segment 2 well developed in male, covered with sparse short setae; posterior part of genital segment 2 overlapped by lamina subanalis, penis not visible in ventral view [penis visible in KUZ Z5094] (Fig. 7B); genital segment 2 not visible in female (Fig. 7C). Anal valves covered with sparse short setae (Fig. 7B, C).

Distribution. This species has been recorded from Honshu and the Izu Islands and is abundant in Tokyo and adjacent areas (Takakuwa 1939, 1940; Shinohara 1949; Takashima and Shinohara 1952; Takano 1973). Miyosi (1953) recorded *S. quadristriatus* from Nagasaki in Kyushu, but this species was not obtained during the survey conducted by the first author in Nagasaki and adjacent localities (25–27 July 2023).

Availability of "*quadristriatus*" based on Takakuwa's works. The name "*Otocryptops sexspinosus quadristriatus*", which was attributed to Verhoeff, was introduced by Takakuwa's two works (Takakuwa 1933a, b) before its formal description by Verhoeff in 1934. However, we herein decide that neither Takakuwa (1933a) nor Takakuwa (1933b) made the species-group name "*quadristriatus*" available. "*Otocryptops sexspinosus quadristriatus* Verh" first appeared in Takakuwa (1933a: 11), who intended to provide general anatomical features of *Scolopocryptops* (originally "*Otocryptops*"). Nonetheless, the detailed morphological features and figures provided in this work were unambiguously based on *S. rubiginosus* L. Koch, 1878 (referred as "*Otocryptops ruliginosus*" [sic]). Therefore, the name *quadristriatus* in the combination of *Otocryptops sexspinosus quadristriatus* in Takakuwa (1933a) did not satisfy the provision of Article 13.1 of the International Code of Zoological Nomenclature (hereinafter, Code; International Commission on Zoological Nomenclature 1999) and thus is unavailable.

In a synopsis of the Japanese centipedes, Takakuwa (1933b: 1459) provided a brief taxonomic account and morphological descriptions of the subspecies referred as "*Otocryptops sexspinosus quadristriatus* Verhoeff". However, Takakuwa considered that "*O. s. quadristriatus*" sensu Verhoeff was indistinguishable from the nominotypical subspecies "*O. s. sexspinosus*"; thus, he did not provide any description or definition that are purported to differentiate "*O. s. quadristriatus*" (see Article 13.1.1 of the Code). Therefore, we conclude that the species-group name *quadristriatus* in the combination of *Otocryptops sexspinosus quadristriatus* in Takakuwa (1933b) is also unavailable and the authorship of this nominal taxon is attributed to Verhoeff (1934), who established *O. s. quadristriatus* explicitly as a new subspecies. Moreover, according to Shinohara (1982, 1990), Takakuwa's (1933b) description of this taxon was based on specimen(s) misidentified as "*O. sexspinosus*"; *O. s. quadristriatus* sensu Takakuwa (1933b) was later described as *S. nipponicus* Shinohara, 1990 (placed in synonymy with *S. spinicaudus* by Shelley 2002).

Remarks. Verhoeff (1934) established this taxon as a subspecies of the North American *S. sexspinosus*, based on brief taxonomic accounts. He only described the absence of tergal paramedian sutures, the presence of four longitudinal keels on tergites and the colouration of head and leg-bearing segments.

Shinohara (1984) elevated *quadristriatus* to full species status, based on the following features: 1) cephalic marginal sulci reaching from postero-lateral margin of

cephalic plate to antennae; 2) tergites without paramedian sutures and with four longitudinal keels; 3) arrangement of tibial and tarsal spurs on legs 19–23; and 4) a slightly slender "general form" compared with other species of the genus. It is unclear whether Shinohara compared *quadristriatus* with the North American *O. sexspinosus sexspinosus* or the Japanese "*O. sexspinosus*" (see above) and the characters of 1), 3) and 4) cannot conclusively distinguish *quadristriatus* from other species. Nonetheless, the presence of four longitudinal keels on tergites distinguishes *S. quadristriatus* from all other *Scolopocryptops* (except *S. longisetosus* sp. nov.; see below). The distinctness of *S. quadristriatus* is also supported by the molecular phylogenetic analyses (Fig. 13).

This species is absent from, but should be added to Chilobase 2.0 (Bonato et al. 2016).

Scolopocryptops longisetosus sp. nov.

https://zoobank.org/3BCC9F07-141D-4D15-8613-3CE08877C0A6

Figs 8–12

Suggested Japanese name: Kuromadara-akamukade

Scolopocryptops capillipedatus: Chao and Chang (2003: 4), fig. 17; Chao (2008: 76–80), figs 82–87; Chao and Chang (2008: 14), fig. 9.

Material examined. ***Holotype*:** Japan – Okinawa Prefecture – **Okinawa Island** • ♂, 31.4 mm (KUZ Z5107); Kunigami-son, Uka; 26°48.45'N, 128°15.97'E; approx. 300 m alt.; 4 May 2021; F. Okuyama leg. ***Paratypes*:** Japan – Okinawa Prefecture – **Okinawa Island** • 1, 24.6 mm (KUZ Z5108); Kunigami-son, Oku; 26°48.3'N, 128°17.34'E; approx. 230 m alt.; 5 May 2021; F. Okuyama leg. • 1 ♂, 30.7 mm (KUZ Z5112); Nago City, Mt. Nago-dake; 26°35.45'N, 128°0.25'E; approx. 200 m alt.; 14 June 2022; T. Jonishi leg. • 1, 29.4 mm (KUZ Z5113); same locality as for preceding; 26°35.47'N, 128°0.27'E; approx. 210 m alt.; 14 June 2022; T. Jonishi leg. • 1 ♀, 28.9 mm (KUZ Z5115); same locality as for preceding; 26°35.73'N, 128°0.19'E; approx. 190 m alt.; 14 June 2022; T. Jonishi leg. • 1 ♂, 31.1 mm (KUZ Z5117); Kunigami-son, Uka; 26°48.43'N, 128°16.04'E; approx. 330 m alt.; 15 June 2022; T. Jonishi leg. • 1 ♂, 37.2 mm (KUZ Z5119); Kunigami-son, Benoki; 26°48.06'N, 128°16.65'E; approx. 350 m alt.; 15 June 2022; T. Jonishi leg. • 1, 30.4 mm (KUZ Z5121); Kunigami-son, Yona, Mt. Fuenchiji; 26°45.15'N, 128°14.58'E; approx. 380 m alt.; 16 June 2022; T. Kato leg. • 1, 28.6 mm (KUZ Z5122); same locality as for preceding; 26°45.17'N, 128°14.58'E; approx. 380 m alt.; 16 June 2022; T. Jonishi leg.

Additional material. Japan – Okinawa Prefecture – **Okinawa Island** • 1 ♂, 30.2 mm (KUZ Z5109); Kunigami-son, Uka; 26°48.30'N, 128°16.11'E; approx. 320 m alt.; 4 Jan 2022; F. Okuyama leg. • 2 juveniles, approx. 10 mm (KUZ Z5110), 1 ♀, 24.4 mm (KUZ Z5111); Nago City, Mt. Nago-dake; 26°35.45'N, 128°0.25'E; approx. 200 m alt.; 14 June 2022; T. Jonishi leg. • 1, 23.4 mm (KUZ Z5114); same locality as for preceding; 26°35.47'N, 128°0.27'E; approx. 210 m alt.; 14 June 2022; T. Kato leg. • 1 ♀, 29.4 mm (KUZ Z5116); same locality as for preceding; 26°35.73'N, 128°0.19'E; approx. 190 m alt.; 14 June 2022; T. Kato leg. • 1, 24.5 mm (KUZ Z5118); Kunigami-son, Uka; 26°48.43'N, 128°16.04'E; approx. 330 m alt.; 15 June 2022; T. Jonishi leg. • 1, 27.2 mm (KUZ Z5120); Kunigami-son, Benoki; 26°48.04'N, 128°16.62'E; approx. 360 m alt.; T. Jonishi leg. – **Ishigaki Island** • 1, 19.9 mm (KUZ Z5123); Hirakubo; 24°35.01'N, 124°20.15'E; approx. 20 m alt.; 17 Dec 2021; F. Okuyama leg. – **Yonaguni Island** • 2 ♂, 27.8 mm (KUZ Z5124), 20.8 mm (KUZ Z5125); Mantabaru Forest Park; 24°27.39'N, 122°58.56'E; approx. 100 m alt.; 16 Apr 2022; Naoto Sawada leg. **Taiwan** • 1, 21.5 mm (KUZ Z5126); Hsinchu County, Wufeng Township, Shei-Pa National Park; 24°30.01'N, 121°4.61'E; 19 Mar 2019; T. Nakano leg. • 1, 22.2 mm (KUZ Z5127); Nantou County, Ren'ai Township; 24°5.1'N, 121°10.73'E; 21 Mar 2019; T. Nakano leg.

Type locality. Japan, Okinawa Prefecture, Okinawa Island, Kunigami-son, Uka (26°48.45'N, 128°15.97'E, approx. 300 m alt.).

Diagnosis. Antenna with sparse hairs and setae of various lengths dorsally on two basal articles, subsequent articles densely covered with long setae and minute setae. Cephalic plate with complete lateral marginal sulci. Tergites lacking paramedian sutures, tergites 5–20 with four longitudinal keels and median depression bordered by paramedian keels.

Description of holotype [data from other specimens given in square brackets]. Body length approx. 31.4 mm [19.9–37.2 mm] in 75% ethanol. Colour in life and in ethanol yellowish-brown with dark pigment on two basal antennal articles, purplish on subsequent articles; reddish-brown on forcipules; reddish-brown with dark pigment on lateral and posterior margins of cephalic plate, tergites 1, 22 and 23; brown with dark pigment on tergites 2–21; legs and ultimate legs brownish-yellow or orange with purplish dark pigment (Figs 8B, 10A, 11A).

Antennae 10.1 mm in length, approx. 0.3× as long as body, composed of 17 articles; dorsal surface of two basal articles with sparse hairs and setae (sensu Bonato et al. (2010)) of various lengths, subsequent articles densely covered with long setae and minute short setae [in small specimens, most setae from article 3 shorter than those of two basal articles] (Fig. 9A); setae emerging from various-sized collars. Cephalic plate as long as wide; its surface sparsely punctate with minute hairs, with complete lateral margination (Figs 9B, 10A).

Second maxillae article 2 with elongated and semi-transparent dorsal spur distally; dorsal brush with transparent margin; pretarsus consisting of dark brown basal and semi-transparent short apical parts (Fig. 10C, D). Forcipular coxosternite and trochanteroprefemur sparsely punctate, coxosternite with transverse sutures on anterior third of coxosternite; trochanteroprefemur with small and blunt black process and basal suture; anterior margin of coxosternite strongly sclerotised and slightly convex, divided into two low lobes by median diastema (Fig. 10E).

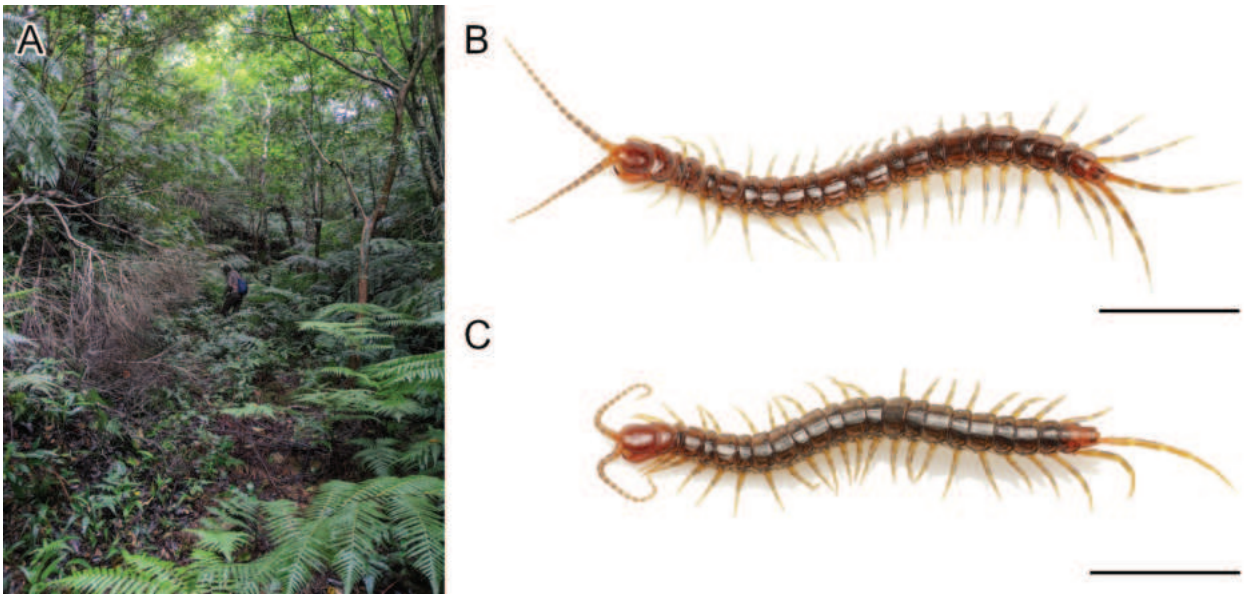

Figure 8. *Scolopocryptops longisetosus* sp. nov., paratype, ♂ (KUZ Z5119: **B**), non-type specimen from Yonaguni Island, ♂ (KUZ Z5124: **C**) and habitat near the type locality. **A.** Habitat (laurel tree forest) on Okinawa Island; **B, C.** Live specimen, dorsal view. Scale bars: 10 mm.

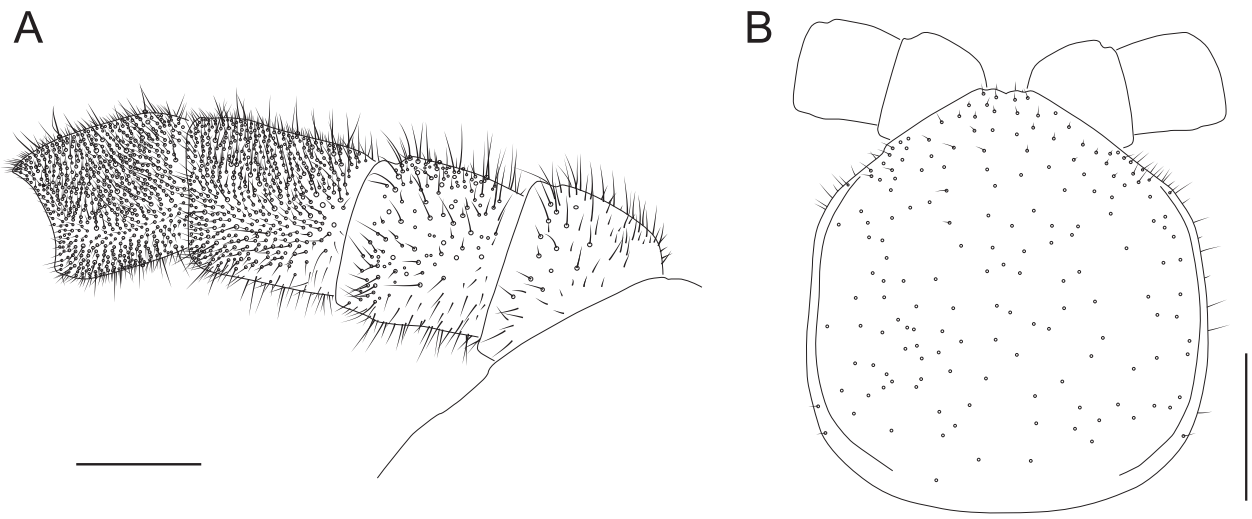

Figure 9. *Scolopocryptops longisetosus* sp. nov., holotype, ♂ (KUZ Z5107). **A.** Basal articles of left antenna, dorsal view; **B.** Cephalic plate, dorsal view. Scale bars: 0.5 mm (**A**); 1 mm (**B**).

Tergites sparsely punctate [sparse minute setae present in small individuals]; tergite 1 with anterior transverse suture, anterior margin overlapped by cephalic plate (Figs 10A, 11A). All tergites lacking paramedian sutures; tergites 5 [4]–21 [20] with longitudinal median depression bordered by paramedian keels, lateral keels present on tergites 5 [5–8]–20 [18–20]; median depression and keels unapparent on anterior and posterior tergites [depression and keels unapparent on all tergites in KUZ Z5119, Z5126 and Z5127] (Fig. 11A, B); lateral marginations complete or nearly complete on tergites 7 [5–7]–21 [22] (Fig. 11A, B); three short longitudinal sulci present on posterior margin of tergites 4, 6 [2 or 3 sulci present on tergites 3–21; absent in several specimens].

Sternites sparsely punctate, lacking paramedian sutures (Fig. 11C). Sides of sternite of ultimate leg-bearing segment converging posteriorly, posterior margin almost straight [slightly concave] (Fig. 11E).

Ovoid spiracles present on leg-bearing segments 3, 5, 8, 10, 12, 14, 16, 18, 20 and 22 (Fig. 11D).

Legs on anterior leg-bearing segments with sparse minute setae [setae denser in small individuals], posterior legs almost lacking setae [all legs setose in KUZ Z5123]; tarsi of legs 1–21 undivided; legs 1–19 with lateral and ventral tibial spurs and tarsal spur, legs 20 and 21, respectively, with tibial spur and tarsal spur; leg 22 without spurs. All legs with two accessory spines.

Coxopleuron approx. 1.8× [1.5–1.8×] as long as sternite of ultimate leg-bearing segment (Fig. 11F).

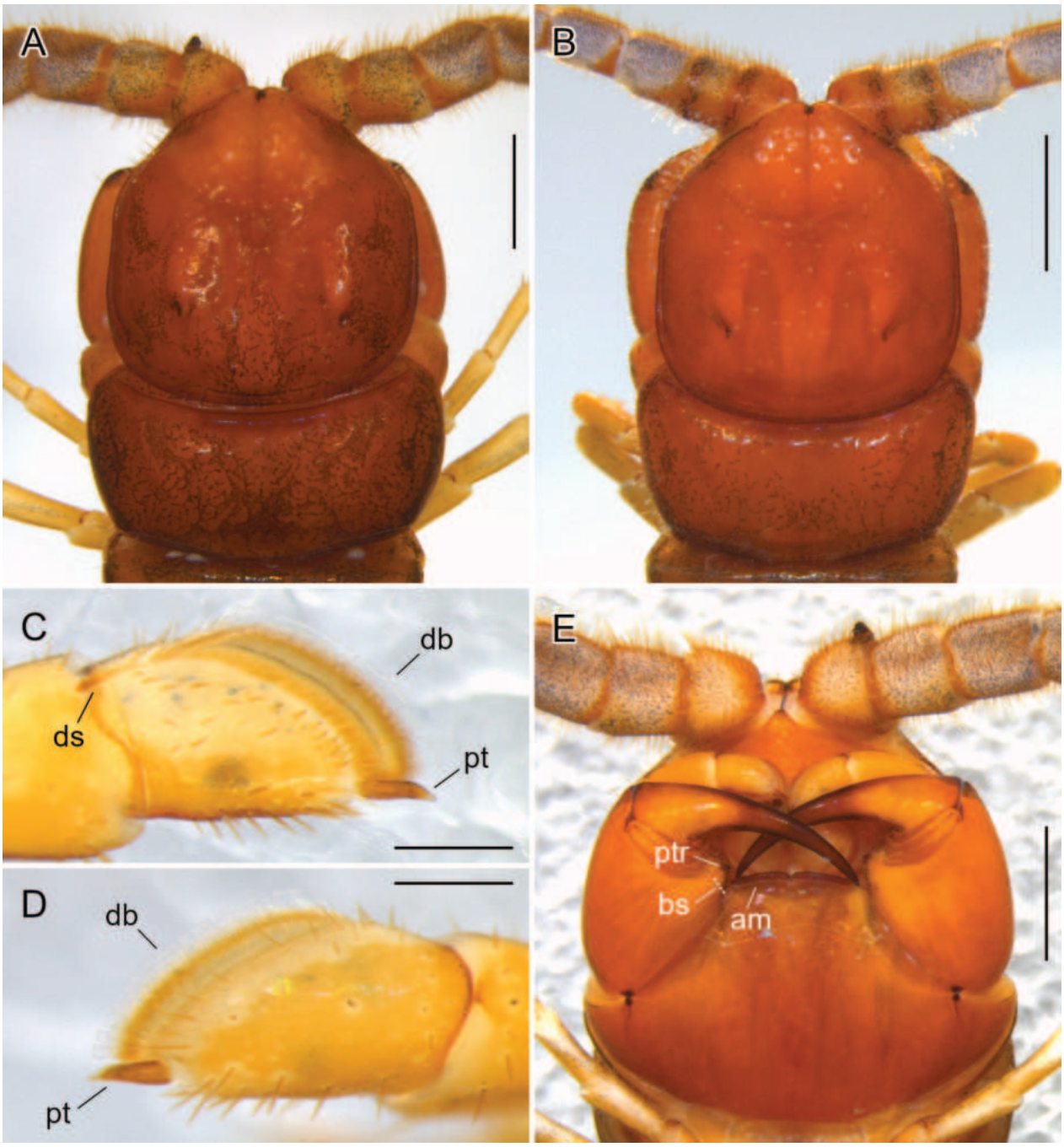

Figure 10. *Scolopocryptops longisetosus* sp. nov., holotype, ♂ (KUZ Z5107: **A, C–E**) and non-type specimen from Yonaguni Island, ♂ (KUZ Z5124: **B**). **A, B.** Cephalic plate and tergite 1, dorsal view; **C.** Distal part of article 2, article 3 and pretarsus of left second maxilla, medial view; **D.** Article 3 and pretarsus of left second maxilla, lateral view; **E.** Head, ventral view. Abbreviations: **am** — anterior margin of forcipular coxosternite; **bs** — basal suture on forcipular trochanteroprefemoral process; **db** — dorsal brush on article 3 of second maxilla; **ds** — dorsal spur on article 2 of second maxilla; **pt** — pretarsus of second maxilla; **ptr** — process of forcipular trochanteroprefemur. Scale bars: 1 mm (**A, B, E**); 0.2 mm (**C, D**).

Dorsal margin of ultimate pleuron protruding from lateral margin of tergite of ultimate leg-bearing segment, dorso-posterior margin with minute dark spine (Fig. 11F, G). Posterior and ventral margins of coxopleuron converging posteriorly, forming approx. 60° [60–65°] angle; coxopleural process short, tip of process pointed, slightly directed dorsally (Fig. 11F). Surface of coxopleuron without setae, covered with various-sized coxal pores (Fig. 11F). Pore-free area present on coxopleural process and dorso-posterior region of coxopleuron (Fig. 11F).

Ultimate leg 10.8 mm in length, approx. 0.3× [0.3–0.37×] as long as body; prefemur, femur and tibia almost lacking setae, tarsi with sparse minute setae [tarsi almost lacking setae]; prefemur with two conical and pointed spinous processes, ventral process larger than dorso-medial one; pretarsus with two accessory spines (Fig. 12A).

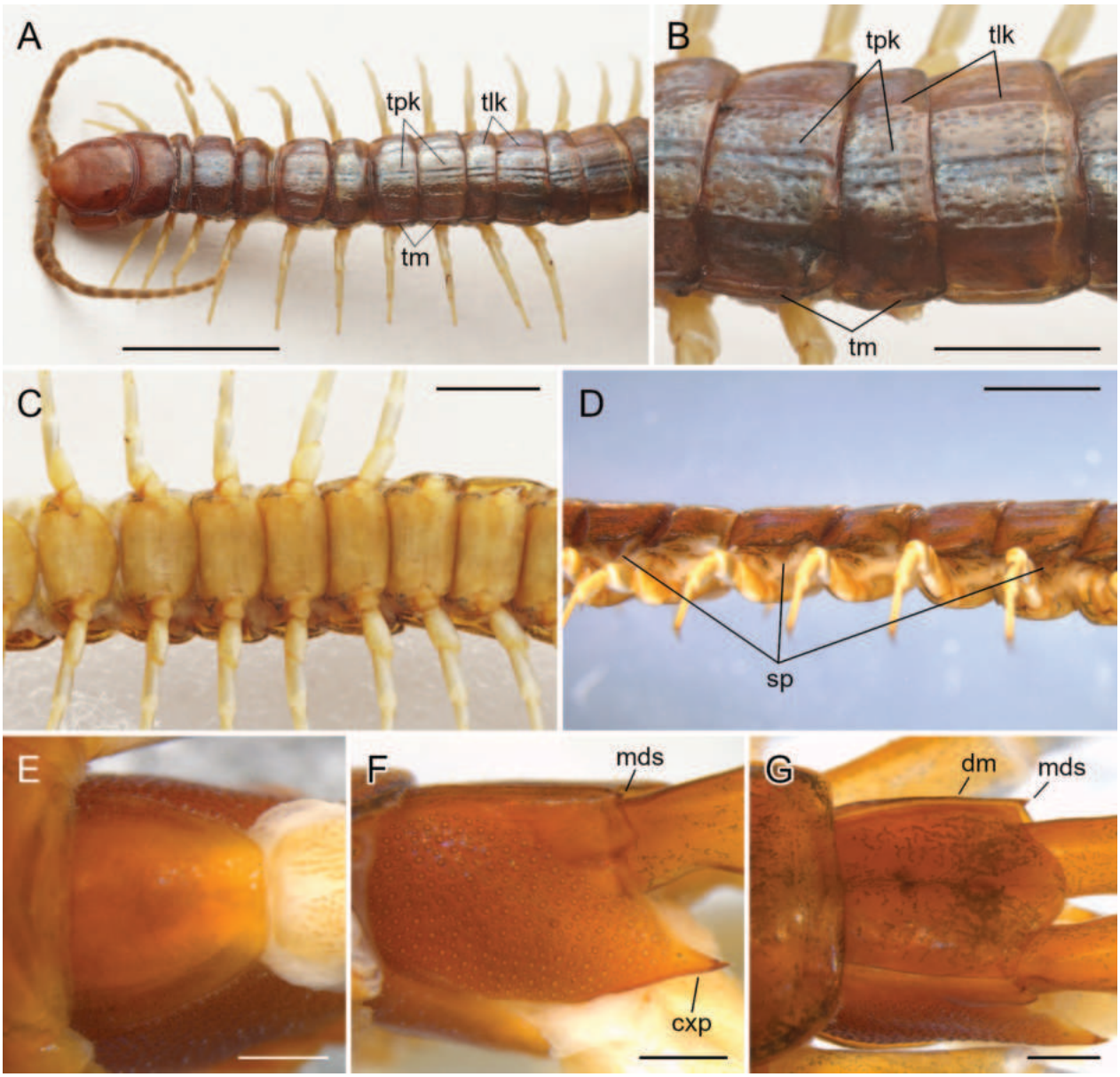

Figure 11. *Scolopocryptops longisetosus* sp. nov., holotype, ♂ (KUZ Z5107). **A.** Cephalic plate and tergites 1–12, dorso-lateral view; **B.** Tergites 10–12, dorso-lateral view; **C.** Sternites 6–12, ventral view; **D.** Leg-bearing segments 3–8, lateral view; **E.** Sternite of ultimate leg-bearing segment, ventral view; **F.** Left coxopleuron, lateral view; **G.** Tergite of ultimate leg-bearing segment, dorso-lateral view. Abbreviations: **cxp** — coxopleural process; **dm** — dorsal margin of ultimate pleuron; **mds** — minute dark spine on ultimate pleuron; **sp** — spiracle; **tlk** — tergal lateral keel; **tm** — tergal margination; **tpk** — tergal paramedian keel. Scale bars: 5 mm (**A**); 2 mm (**B–D**); 0.5 mm (**E–G**).

Genital segments occupying approx. 0.8× length of sternite of ultimate leg-bearing segment; tergite of genital segment sparsely setose (Fig. 12C, D). Sternite of genital segment 1 sparsely covered with setae, posterior margin slightly convex (Fig. 12C, D). Sternite of genital segment 2 well developed, covered with sparse setae; penis visible in ventral view; anal valves covered with sparse setae [in female, genital segment 1 as described for holotype; genital segment 2 not visible; anal valves as described for holotype] (Fig. 12C–E).

Variation. In specimens from the southern Ryukyus (Ishigaki and Yonaguni Islands; KUZ Z5123–Z5125) and Taiwan (KUZ Z5126, Z5127), dark pigment on cephalic plate absent or almost reduced (Figs 8C, 10B); ultimate leg with femur [tibia] and subsequent articles densely setose [setae relatively sparse in KUZ Z5127] (Fig. 12B).

Etymology. The specific name is derived from the Latin compound adjective, “longus” (long) and “setosus” (hairy), referring to the long antennal setae of this new species.

Distribution. This species is known from Okinawa, Ishigaki and Yonaguni Islands in the Ryukyu Islands, Japan and is also widespread in Taiwan.

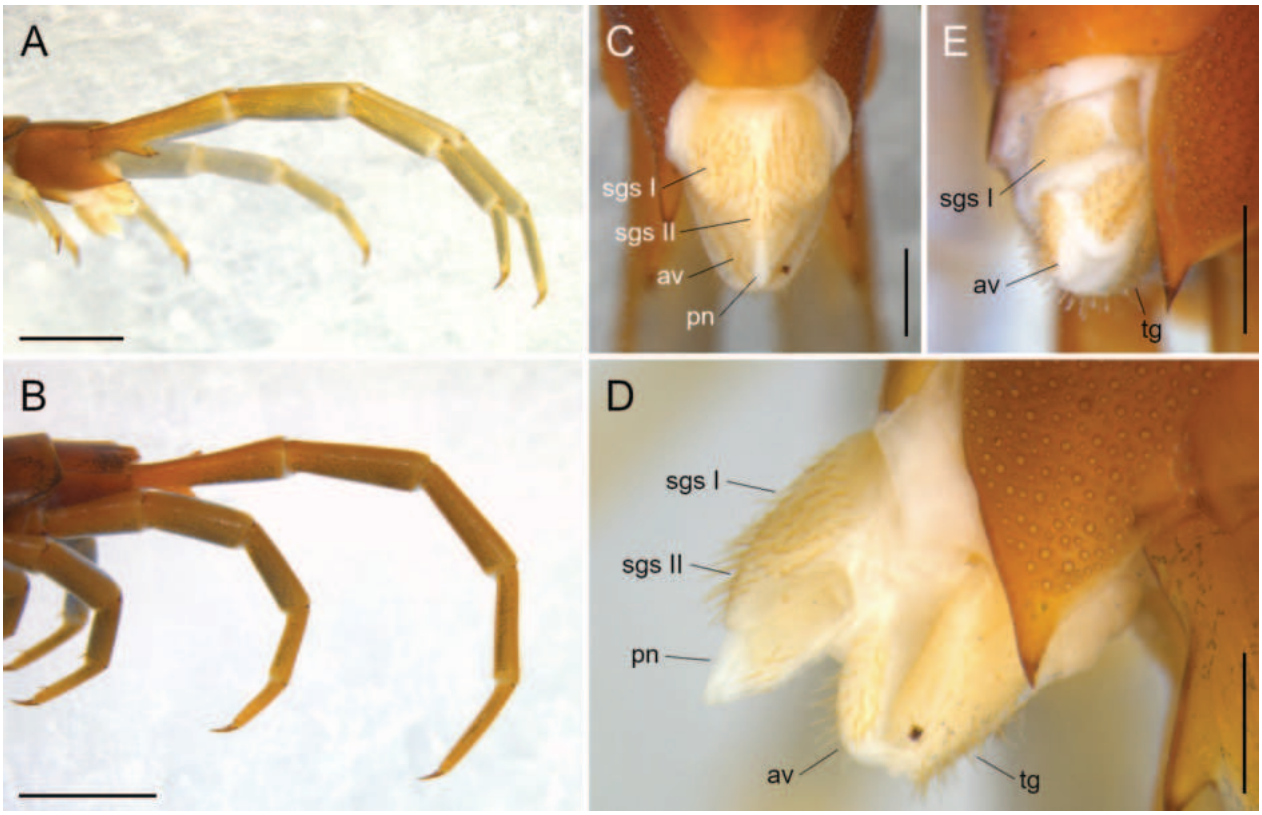

Figure 12. *Scolopocryptops longisetosus* sp. nov.**,** holotype, ♂ (KUZ Z5107: **A, C, D**); non-type specimen from Yonaguni Island, ♂ (KUZ Z5124: **B**); paratype, ♀ (KUZ Z5115: **E**). **A, B.** Left ultimate leg, lateral view; **C.** Male genital segments, penis and anal valves, ventral view; **D.** Male genital segments, penis and anal valves, lateral view; **E.** Female genital segment and anal valves, ventral view. Abbreviations: **av** — anal valve; **pn** — penis; **sgs I** — sternite of genital segment 1; **sgs II** — sternite of genital segment 2; **tg** — tergite of genital segment. Scale bars: 2 mm (**A, B**); 0.5 mm (**C–E**).

Remarks. This species resembles *S. quadristriatus*, but *S. longisetosus* sp. nov. can be distinguished by the presence of long antennal setae (vs. setae short in *S. quadristriatus*; also see the Identification key provided in the Discussion).

The phylogenetic analyses indicate that specimens of this species from Taiwan have been misidentified as *S. capillipedatus*, based on the dense setae on ultimate legs (Chao and Chang 2003, 2008; Chao 2008). However, *S. longisetosus* sp. nov. can be distinguished from *S. capillipedatus* by the presence of longitudinal keels and median depression on tergites.

Molecular phylogeny and genetic distances. The ML (ln *L* = –14816.13; not shown) and BI (mean ln *L* = –14846.27; Fig. 13) trees had almost identical topologies. In the Asian/North American group (UFBoot = 100%, BPP = 1.0), both the *elegans* lineage (UFBoot = 100%, BPP = 1.0) and the ex-*elegans* lineage (UFBoot = 98%, BPP = 1.0) were recovered as monophyletic groups. Within the latter lineage, the recovery of *S. quadristriatus* (UFBoot = 100%, BPP = 1.0) and *S. longisetosus* sp. nov. (UFBoot = 100%, BPP = 1.0) was strongly supported.

Although the interspecific relationships remained largely undetermined, the analyses showed that *S. longisetosus* sp. nov. is sister to a clade comprising three of the Japanese nominal species, *S. ogawai* Shinohara, 1984, *S. musashiensis* Shinohara, 1984 and "*S. nipponicus*" sensu Edgecombe et al. (2012) (UFBoot = 99%, BPP = 1.0) (Fig. 13).

In the preliminary analyses using the COI dataset, four sequences of "*S. capillipedatus*" from Taiwan (AB617528–AB617530, AB672646) were nested within *S. longisetosus* sp. nov. (UFBoot = 98%, BPP = 0.99; Suppl. material 3), but the relationships amongst populations were not resolved. In contrast, the concatenated analyses recovered two lineages within *S. longisetosus* sp. nov., which corresponded to the specimens from Okinawa Island (UFBoot = 100%, BPP = 1.0) and those from the southern Ryukyu Islands and Taiwan (UFBoot = 98%, BPP = 0.99). The COI pairwise distances within each lineage were 2.56–4.74% (Okinawa Island) and 4.89–9.17% (southern Ryukyus and Taiwan; including the sequences of Taiwanese "*S. capillipedatus*"). The divergence between the two lineages was 5.77–8.87% (Suppl. material 2).

Discussion

In the obtained phylogenetic trees, *S. quadristriatus* and *S. longisetosus* sp. nov. were strongly supported as monophyletic lineages. The analyses indicated that *S. longisetosus* sp. nov. comprises two lineages: Okinawa Island and the southern Ryukyus-Taiwan. These lineages differ in two external features, i.e. the presence/absence of dark pigment

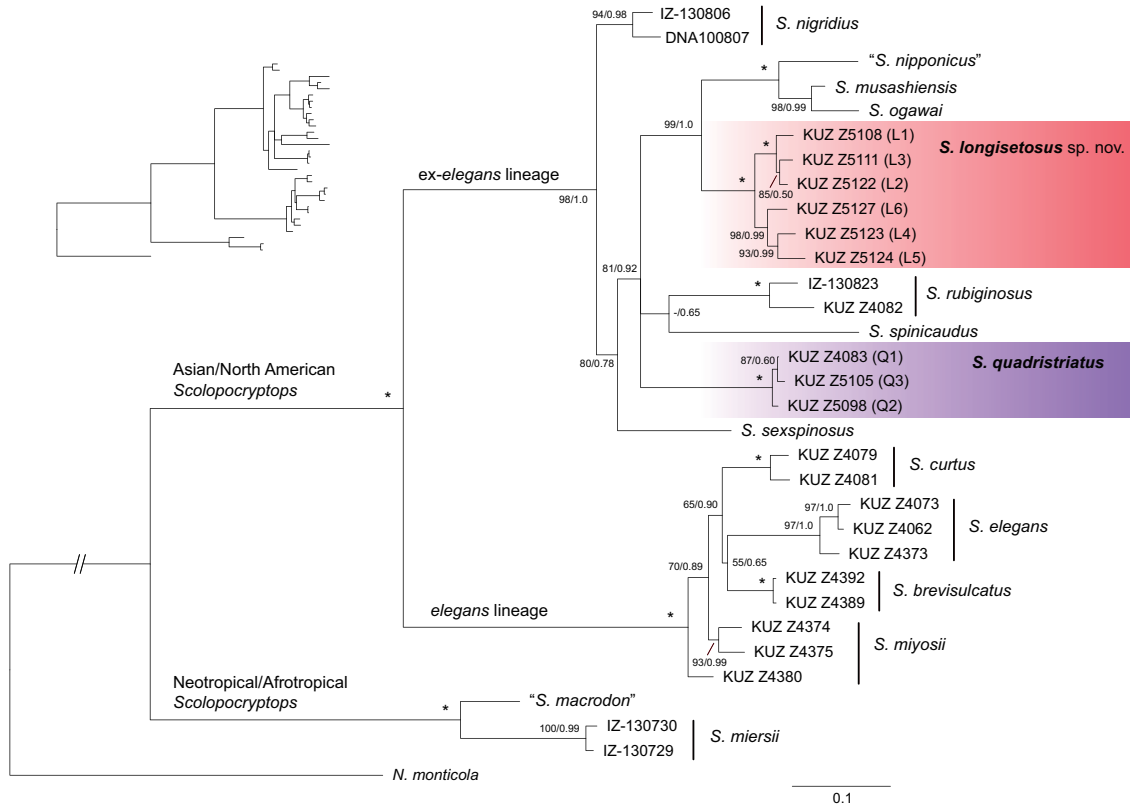

Figure 13. Bayesian Inference tree for 2510 bp-aligned positions of the ITS2, 28S, 16S and COI sequences. Real branch length is shown on the upper left. Numbers on nodes indicate ultrafast bootstrap values (UFBoot) and Bayesian posterior probabilities (BPP). An asterisk denotes the node with UFBoot = 100% and BPP = 1.0. Locality numbers (Q1–Q3 and L1–L6) are shown in Fig. 1 and Table 1.

on the cephalic plate and the density of setae on ultimate legs. However, the pigmentation is subject to intraspecific variation in this genus and other scolopendromorph taxa and the density of the ultimate leg setae is also variable within *Scolopocryptops* species (e.g. Lewis (2003); Le et al. (2023)). It should be noted that the body lengths of the specimens from the southern Ryukyus and Taiwan (19.9–27.8 mm) were generally smaller than those from Okinawa Island (23.4–37.2 mm; juveniles excluded). Nonetheless, body length difference is not considered a taxonomic character here because it may be the result of different growth rates under different habitats (as speculated on *Cryptops* species; Lewis (2007)) or simply due to sampling bias. Additionally, because the COI genetic distances between the two lineages (5.77–8.87%) fell within the intraspecific divergence of *Scolopocryptops* (Garrick et al. 2018) and is smaller than the divergence amongst the sequences from the southern Ryukyus and Taiwan (4.89–9.17%), all the specimens from the Ryukyu Islands and Taiwan are considered a single species, *S. longisetosus* sp. nov.

It is noteworthy that four COI sequences of "*S. capillipedatus*" from Taiwan belonged to *S. longisetosus* sp. nov. (Suppl. material 3). *Scolopocryptops capillipedatus*, which is characterised by the dense setae on femur and subsequent articles of ultimate legs, was originally described from South Korea and has been recorded from Japan, Taiwan and Vietnam (Takakuwa 1938; Miyosi 1971; Chao and Chang 2003, 2008; Chao 2008; Le et al. 2023). Chao (2008) provided a description of Taiwanese "*S. capillipedatus*" and noted that there were numerous long setae densely covering the femur, tibia and tarsi of the ultimate leg. However, this nominal species is clearly distinct from *S. longisetosus* sp. nov. because tergal keels are absent in *S. capillipedatus* (Takakuwa 1938, 1940). Although Chao (2008) did not mention the presence or absence of tergal keels, our specimens from Taiwan (KUZ Z5126 and Z5127) exhibited the characteristic longitudinal keels on tergites. The present result thus indicates that the records of "*S. capillipedatus*" from Taiwan were based on misidentified specimens of *S. longisetosus* sp. nov. Chao (2008) also described an unapparent median suture on tergites 1–3, which was not observed in our specimens, but described in Takakuwa's (1938) original description of *S. capillipedatus*. Morphological variability amongst Taiwanese populations needs to be examined, based on further taxon sampling.

Scolopocryptops longisetosus sp. nov. is quite similar to *S. quadristriatus* because they both have four longitudinal keels and median depression on tergites, as well as dark pigmentation on antennae and the dorsal surface of the body. Despite their phenotypic similarities, phylogenetic analyses did not support their sister relationship, but united *S. longisetosus* sp. nov. with three Japanese nominal species, *S. ogawai*, *S. musashiensis* and "*S. nipponicus*", which lack tergal keels (Fig. 13). The obtained phylogeny thus indicates that the longitudinal keels on tergites evolved in parallel within *Scolopocryptops* or that the presence of keels represents a

plesiomorphic character of the clade comprising these species. Within *Scolopocryptops*, the tergal keels and median depression are unique to these two species and *S. hoanglieni* Le, Schileyko & Nguyen, 2023, which bears "'drop-like' longitudinal median depression bordered by paramedian keels" (Le et al. 2023). However, the phylogenetic implication of the tergal keels remains uncertain because the phylogenetic position of *S. hoanglieni* is undetermined (Le et al. 2023).

It is also notable that all members of the ex-*elegans* lineage, except *S. rubiginosus*, lack complete paramedian sutures on tergites (Shinohara 1984, 1990; Shelley 2002; Le et al. 2023), whereas all species of the *elegans* lineage and most of the Neotropical/Afrotropical species bear complete paramedian sutures (e.g. Chagas-Jr (2008); Chagas-Jr et al. (2023); Jonishi and Nakano (2023); Le et al. (2023)). Nonetheless, the evolutionary history of their paramedian sutures and the tergal keels remains unclear because the analyses failed to reconstruct a robust phylogeny of the ex-*elegans* lineage. Further systematic studies, for example, phylogenetic analyses using a larger taxon set including data from additional loci, need to be conducted to reveal the morphological evolution of *Scolopocryptops* species.

An identification key to *Scolopocryptops* species of East Asia

Diagnostic characters and known localities mainly follow Le et al. (2023), but were updated, based on Jonishi and Nakano (2023) and the present study.

1 Leg-bearing segment 7 with well-developed spiracles 2
– Leg-bearing segment 7 lacking spiracles 3
2 Tergite of ultimate leg-bearing segment with median suture ..... *S. broelemanni broelemanni* Kraepelin, 1903 (eastern China)
– Tergite of ultimate leg-bearing segment lacking median suture ..... *S. broelemanni esulcatus* Attems, 1938 (southern Vietnam)
3 Cephalic plate with complete lateral margination 9
– Cephalic plate lacks lateral margination or margination is much shortened 4
4 Length of the ultimate leg up to 40% of body length ..... *S. zhijiensis* Qiao, Xiao & Di, 2021 (southern China)
– Length of the ultimate leg less than 30% of body length 5
5 Coxosternite with anterior margin concave, tergites without lateral margination ..... *S. melanostoma* Newport, 1845 ("Neotropical/Afrotropical" species recorded from Lanyu Island in Taiwan and southern Vietnam) (Chao and Chang 2003; Chao 2008)
– Coxosternite with anterior margin convex or almost straight, tergites 6–21 or 20 with lateral marginations 6
6 Only basalmost antennal article with sparse minute setae or all articles densely setose; coxopleural process moderately long ..... *S. elegans* (Takakuwa, 1937) (Honshu and Shikoku in Japan)
– Several basal antennal articles with sparse minute setae; coxopleural process short 7
7 Cephalic plate lacks lateral margination; dorsal margin of ultimate pleuron not protruding from tergite of ultimate leg-bearing segment ..... *S. curtus* (Takakuwa, 1939) (southern Ryukyu Islands in Japan and Taiwan)
– Cephalic plate with short lateral margination; dorsal margin of ultimate pleuron slightly protruding from tergite of ultimate leg-bearing segment 8
8 Three or two basal antennal articles with sparse minute setae; sclerotised bands on anterior margin of coxosternite almost reaching outer part ..... *S. miyosii* Jonishi & Nakano, 2023 (Kyushu and Amami Island in Japan)
– Four basal antennal articles with sparse minute setae, sclerotised bands on anterior margin of coxosternite not reaching outer part ..... *S. brevisulcatus* Jonishi & Nakano, 2023 (Okinawa Island and adjacent islet in Japan)
9 Length of the ultimate leg more than 40% of body length; tarsus 1 and 2 of leg 22 each with well-developed spur ..... *S. longipes* Xiao, Chen & Di, 2021 (southern China)
– Length of the ultimate leg approx. 30% of body length or less; leg 22 mostly with 1 tarsal spur or lacking spur 10
10 Tergites with complete paramedian sutures ..... *S. rubiginosus* L. Koch, 1878 (China, Korea, Japan, Taiwan and Vietnam)
– Tergites without complete paramedian sutures 11
11 Tergites with median depression bordered by paramedian keels 12
– Tergites without median depression 14
12 Tergites with drop-like median depression; lateral keels absent ..... *S. hoanglieni* Le, Schileyko & Nguyen, 2023 (northern Vietnam)
– Tergites with longitudinal median depression; lateral keels present 13
13 Antennal articles covered with short setae ..... *S. quadristriatus* (Verhoeff, 1934) (Honshu in Japan)
– Antennal articles covered with long setae and short setae . *S. longisetosus* sp. nov. (Ryukyu Islands in Japan and Taiwan)
14 Two basal antennal articles sparsely setose dorsally; tibia and tarsus of ultimate leg densely setose ..... *S. capillipedatus* (Takakuwa, 1938) (Korea, Japan, and Vietnam) + *S. ogawai* Shinohara, 1984 (Japan) + *S. musashiensis* Shinohara, 1984 (Japan) (see Le et al. (2023))
– Two basal antennal articles almost lacking setae dorsally; distal articles of ultimate legs mostly not setose ..... *S. spinicaudus* Wood, 1862 (China, Korea, Japan, Taiwan, Vietnam) + "*S. nipponicus*" Shinohara, 1990 (Japan) (see Le et al. (2023))

Acknowledgements

We give special gratitude to Stefan Friedrich (ZSM), Dr Roland Melzer (ZSM) and Dr Juliana Bahia (ZSM) for providing the opportunity to examine the specimen of "*O. s. quadristriatus*". The authors are grateful to Dr Gregory D. Edgecombe (Natural History Museum, London) and an anonymous reviewer for their valuable comments and suggestions on this manuscript. We also express our gratitude to Yasunori Hagino (Natural History Museum and Institute, Chiba) for providing literature; Dr Yi-Te Lai (National Taiwan University), Futaro Okuyama, Taiga Kato (Kyoto University; KU), Eitaro Matsushita (KU), Dr Naoto Sawada (The University of Tokyo), and Yusuke Sugawara for their help with collecting material; and Ryosuke Kuwahara and Ryosuke Uno (KU) for suggesting appropriate literature. We also thank Dr Mallory Eckstut, from Edanz (https://jp.edanz.com/ac) for editing a draft of this manuscript. This study was supported by JST SPRING (grant number JPMJSP2110) and the Sasakawa Scientific Research Grant from the Japan Science Society (grant number 2022-5017) to TJ, and JSPS KAKENHI (grant number JP22K06371) to TN.

References

Attems C (1938) Die von Dr. C. Dawydoff in Französisch Indochina gesammelten Myriopoden. Mémoires du Muséum national d'histoire naturelle, Nouvelle Série 6(2): 187–353. https://www.biodiversitylibrary.org/item/277837

Bonato L, Edgecombe GD, Lewis JGE, Minelli A, Pereira LA, Shelley RM, Zapparoli M (2010) A common terminology for the external anatomy of centipedes (Chilopoda). ZooKeys 69: 17–51. https://doi.org/10.3897/zookeys.69.737

Bonato L, Chagas-Jr A, Edgecombe GD, Lewis JGE, Minelli A, Pereira LA, Shelley RM, Stoev P, Zapparoli M (2016) ChiloBase 2.0–A World Catalogue of Centipedes (Chilopoda). *Scolopocryptops* Newport, 1844. https://chilobase.biologia.unipd.it/searches/result_genres/129 [Accessed 20 March 2024]

Castresana J (2000) Selection of conserved blocks from multiple alignments for their use in phylogenetic analysis. Molecular Biology and Evolution 17(4): 540–552. https://doi.org/10.1093/oxfordjournals.molbev.a026334

Chagas-Jr A (2008) Revisão Sistemática e Análise Filogenética dos Scolopocryptopinae (Chilopoda, Scolopendromorpha). PhD thesis, Universidade Federal do Rio de Janeiro, Rio de Janeiro, Brazil.

Chagas-Jr A, Edgecombe GD, Minelli A (2023) An unknown segment number in centipedes: a new species of *Scolopocryptops* (Chilopoda: Scolopendromorpha) from Trinidad with 25 leg-bearing segments. Organisms Diversity & Evolution 23(2): 369–380. https://doi.org/10.1007/s13127-022-00591-7

Chao JL (2008) Scolopendromorpha (Chilopoda) of Taiwan: Collection, Description, Illustration, Taxonomy, Distribution. VDM Verlag Dr. Müller Aktiengesellschaft & Co. KG, Saarbrücken, 94 pp.

Chao JL, Chang HW (2003) The scolopendromorph centipedes (Chilopoda) of Taiwan. African Invertebrates 44(1): 1–11. https://hdl.handle.net/10520/EJC84516

Chao JL, Chang HW (2008) Neotype designation for two centipedes, *Scolopocryptops curtus* (Takakuwa, 1939) and *Cryptops nigropictus* Takakuwa, 1936, and a review of species of Scolopendromorpha (Chilopoda) in Taiwan. Collection and Research 21: 1–15.

Demange JM, Richard J (1969) Morphologie de l'appareil génital mâle des Scolopendromorphes et son importance en systématique (Myriapodes Chilopodes). Bulletin du Muséum National d'Historie Naturelle 2e Série 40(5): 968–983. https://www.biodiversitylibrary.org/page/55344151

Edgecombe GD, Giribet G (2004) Adding mitochondrial sequence data (16S rRNA and cytochrome *c* oxidase subunit I) to the phylogeny of centipedes (Myriapoda: Chilopoda): an analysis of morphology and four molecular loci. Journal of Zoological Systematics and Evolutionary Research 42(2): 89–134. https://doi.org/10.1111/j.1439-0469.2004.00245.x

Edgecombe GD, Giribet G, Wheeler WC (2002) Phylogeny of Henicopidae (Chilopoda: Lithobiomorpha): a combined analysis of morphology and five molecular loci. Systematic Entomology 27(1): 31–64. https://doi.org/10.1046/j.0307-6970.2001.00163.x

Edgecombe GD, Vahtera V, Stock SR, Kallonen A, Xiao X, Rack A, Giribet G (2012) A scolopocryptopid centipede (Chilopoda: Scolopendromorpha) from Mexican amber: synchrotron microtomography and phylogenetic placement using a combined morphological and molecular data set. Zoological Journal of the Linnean Society 166(4): 768–786. https://doi.org/10.1111/j.1096-3642.2012.00860.x

Edgecombe GD, Huey JA, Humphreys WF, Hillyer M, Burger MA, Volschenk ES, Waldock JM (2019) Blind scolopendrid centipedes of the genus *Cormocephalus* from subterranean habitats in Western Australia (Myriapoda: Scolopendromorpha: Scolopendridae). Invertebrate Systematics 33(6): 807–824. https://doi.org/10.1071/IS19015

Folmer O, Black M, Hoeh W, Lutz R, Vrijenhoek R (1994) DNA primers for amplification of mitochondrial cytochrome *c* oxidase subunit I from diverse metazoan invertebrates. Molecular Marine Biology and Biotechnology 3(5): 294–299.

Garrick RC, Newton KE, Worthington RJ (2018) Cryptic diversity in the southern Appalachian Mountains: Genetic data reveal that the red centipede, *Scolopocryptops sexspinosus*, is a species complex. Journal of Insect Conservation 22(5–6): 799–805. https://doi.org/10.1007/s10841-018-0107-3

Hoang DT, Chernomor O, Haeseler A, Minh BQ, Vinh LS (2017) UFBoot2: Improving the Ultrafast Bootstrap Approximation. Molecular Biology and Evolution 35(2): 518–522. https://doi.org/10.1093/molbev/msx281

International Commission on Zoological Nomenclature (1999) International code of zoological nomenclature. Fourth Edition. The International Trust for Zoological Nomenclature, London.

Iorio E (2003) Morphologie externe des appareils génitaux mâle et femelle de la famille Scolopendridae (Chilopoda, Scolopendromorpha). Bulletin de Phyllie 16: 10–16.

Jonishi T, Nakano T (2022) Taxonomic accounts and phylogenetic positions of the Far East Asian centipedes *Scolopocryptops elegans* and *S. curtus* (Chilopoda: Scolopendromorpha). Zoological Science 39(6): 581–593. https://doi.org/10.2108/zs220029

Jonishi T, Nakano T (2023) Two new species of *Scolopocryptops* centipedes from southern Japan (Chilopoda: Scolopendromorpha: Scolopocryptopidae). European Journal of Taxonomy 908(1): 155–182. https://doi.org/10.5852/ejt.2023.908.2345

Kalyaanamoorthy S, Minh BQ, Wong TKF, von Haeseler A, Jermiin LS (2017) ModelFinder: Fast model selection for accurate phylogenetic estimates. Nature Methods 14(6): 587–589. https://doi.org/10.1038/nmeth.4285

Katoh K, Standley DM (2013) MAFFT multiple sequence alignment software version 7: Improvements in performance and usability. Molecular Biology and Evolution 30(4): 772–780. https://doi.org/10.1093/molbev/mst010

Katoh K, Rozewicki J, Yamada KD (2019) MAFFT online service: Multiple sequence alignment, interactive sequence choice and visualization. Briefings in Bioinformatics 20(4): 1160–1166. https://doi.org/10.1093/bib/bbx108

Koch L (1878) Japanesische Arachniden und Myriapoden. Verhandlungen der Kaiserlich-Königlichen Zoologisch-Botanischen Gesellschaft in Wien 27: 735–798. https://www.biodiversitylibrary.org/page/26709592

Koch M, Edgecombe GD, Shelley RM (2010) Anatomy of *Ectonocryptoides* (Scolopocryptopidae: Ectonocryptopinae) and the phylogeny of blind Scolopendromorpha (Chilopoda). International Journal of Myriapodology 3(1): 51–81. https://doi.org/10.1163/187525410X12578602960344

Kraepelin K (1903) Revision der Scolopendriden. Mitteilungen aus dem Naturhistorischen Museum in Hamburg 20: 5–276. https://www.biodiversitylibrary.org/page/29551135

Kuraku S, Zmasek CM, Nishimura O, Katoh K (2013) aLeaves facilitates on-demand exploration of metazoan gene family trees on MAFFT sequence alignment server with enhanced interactivity. Nucleic Acids Research 41(W1): W22–W28. https://doi.org/10.1093/nar/gkt389

Lanfear R, Frandsen PB, Wright AM, Senfeld T, Calcott B (2016) PartitionFinder 2: New methods for selecting partitioned models of evolution for molecular and morphological phylogenetic analyses. Molecular Biology and Evolution 34(3): 772–773. https://doi.org/10.1093/molbev/msw260

Le SX, Schileyko AA, Nguyen AD (2023) A review of Vietnamese *Scolopocryptops* Newport, 1844 (Chilopoda: Scolopendromorpha), with a description of *S. hoanglieni* n. sp. and the updated generic list of species. Zootaxa 5228(4): 411–447. https://doi.org/10.11646/zootaxa.5228.4.3

Lewis JGE (2003) The problems involved in the characterisation of scolopendromorph species (Chilopoda: Scolopendromorpha). African Invertebrates 44(1): 61–69. https://hdl.handle.net/10520/EJC84514

Lewis JGE (2007) On *Cryptops doriae* Pocock from the wet tropical biome of the Eden Project, Cornwall (Chilopoda, Scolopendromorpha, Cryptopidae). Bulletin of the British Myriapod and Isopod Group 22: 12–16. https://bmig.org.uk/view/resource/bmig-bulletin?page=1

McNeil J (1887) Description of twelve new species of Myriapoda, chiefly from Indiana. Proceedings of the United States National Museum 10(632): 328–334. https://doi.org/10.5479/si.00963801.10-632.328

Melzer RR, Friedrich S, Ritzerfeld M, Bohn J, Spelda J (2011) GLOMYRIS and TYMUNAC: Myriapoda and Acari databases of the GBIF-D node invertebrates II. Spixiana 34(1): 11–20. https://pfeil-verlag.de/publikationen/spixiana-zeitschrift-fuer-zoologie-inhalt-band-34/

Miyosi Y (1953) Myriapods of Siebold's residence (Narutaki, Nagasaki City). Supplement: myriapods from several localities in northern Kyushu. Collecting and Breeding 15(3): 73–75.

Miyosi Y (1971) *Otocryptops capillipedatus* Takakuwa. In: Okada K, Uchida S, Uchida T (Eds) New Illustrated Encyclopedia of the Fauna of Japan, 3rd edn. Hokuryukan, Tokyo, 734.

Moritz M, Fischer SC (1979) Die Typen der Myriapoden-Sammlung des Zoologischen Museums Berlin. II. Chilopoda. Mitteilungen aus dem Zoologischen Museum in Berlin 55: 297–352. https://doi.org/10.1002/mmnz.4830550215

Murienne J, Edgecombe GD, Giribet G (2010) Including secondary structure, fossils and molecular dating in the centipede tree of life. Molecular Phylogenetics and Evolution 57(1): 301–313. https://doi.org/10.1016/j.ympev.2010.06.022

Murienne J, Edgecombe GD, Giribet G (2011) Comparative phylogeography of the centipedes *Cryptops pictus* and *C. niuensis* (Chilopoda) in New Caledonia, Fiji and Vanuatu. Organisms Diversity & Evolution 11(1): 61–74. https://doi.org/10.1007/s13127-011-0041-7

Newport G (1844) Monograph of the class Myriapoda, order Chilopoda; with observations on the general arrangement of the Articulata. Part I. Transactions of the Linnean Society of London 19(3): 265–302. https://doi.org/10.1111/j.1096-3642.1842.tb00368.x

Newport G (1845) Monograph of the class Myriapoda, order Chilopoda; with observations on the general arrangement of the Articulata. Part II. Transactions of the Linnean Society of London 19(4): 349–439. https://doi.org/10.1111/j.1096-3642.1842.tb00370.x

Nguyen LT, Schmidt HA, von Haeseler A, Minh BQ (2015) IQ-TREE: A fast and effective stochastic algorithm for estimating maximum-likelihood phylogenies. Molecular Biology and Evolution 32(1): 268–274. https://doi.org/10.1093/molbev/msu300

Pocock RI (1890) A short account of a small collection of Myriopoda obtained by Mr. Edward Whymper in the Andes of Ecuador. Annals & Magazine of Natural History 6(32): 141–146. https://doi.org/10.1080/00222939008694014

Pocock RI (1895) Chilopoda. Part CXXVI. In: Godman FD, Salvin O (Eds) Biologia Centrali-Americana. Volume 14. Chilopoda and Diplopoda. Taylor & Francis, London, 1–24. https://doi.org/10.5962/bhl.title.730

Pocock RI (1896) Chilopoda. Part. CXXVII. In: Godman FD, Salvin O (Eds) Biologia Centrali-Americana. Volume 14. Chilopoda and Diplopoda. Taylor & Francis, London, 25–40. https://doi.org/10.5962/bhl.title.730

Qiao S, Xiao SQ, Di ZY (2021) *Scolopocryptops zhijinensis* sp.n. and a key to species of scolopocryptopine centipedes from China (Scolopendromorpha: Scolopocryptopidae). Arthropoda Selecta 30(1): 28–33. https://doi.org/10.15298/arthsel.30.1.02

Rambaut A, Drummond AJ, Xie D, Baele G, Suchard MA (2018) Posterior summarization in Bayesian phylogenetics using Tracer 1.7. Systematic Biology 67(5): 901–904. https://doi.org/10.1093/sysbio/syy032

Ronquist F, Teslenko M, van der Mark P, Ayres DL, Darling A, Höhna S, Larget B, Liu L, Suchard MA, Huelsenbeck JP (2012) MrBayes 3.2: Efficient Bayesian phylogenetic inference and model choice across a large model space. Systematic Biology 61(3): 539–542. https://doi.org/10.1093/sysbio/sys029

Say T (1821) Descriptions of the Myriapodæ of the United States. Journal of the Academy of Natural Sciences of Philadelphia 2(1): 102–114. https://www.biodiversitylibrary.org/page/36831290

Schileyko A, Stagl V (2004) The collection of the scolopendromorph centipedes (Chilopoda) in the Natural History Museum in Vienna: A critical re-evaluation of former taxonomic identifications. Annalen des Naturhistorischen Museums in Wien 105B: 67–137.

Schwendinger PJ, Giribet G (2005) The systematics of the south-east Asian genus *Fangensis* Rambla (Opiliones: Cyphophthalmi: Stylocellidae). Invertebrate Systematics 19(4): 297–323. https://doi.org/10.1071/IS05023

Shelley RM (2002) A Synopsis of the North American Centipedes of the Order Scolopendromorpha (Chilopoda). Virginia Museum of Natural History Memoir 5, Virginia Museum of Natural History, Virginia, 108 pp.

Shinohara K (1949) Notes on centipedes collected by Mr. Fujiyama in Hachijo Island. Acta Arachnologica 11(3–4): 80–85. https://doi.org/10.2476/asjaa.11.80

Shinohara K (1982) Organizing Japanese names of centipedes. Atypus 80: 25–28.

Shinohara K (1984) Two new species of the *Scolopocryptops* from Japan (Chilopoda: Cryptopidae). Edaphologia 31: 39–42. https://agriknowledge.affrc.go.jp/RN/2010842561

Shinohara K (1990) A new species of the genus *Scolopocryptops* (Chilopoda: Cryptopidae) from Japan. Proceedings of the Japanese Society of Systematic Zoology 41: 62–65. https://doi.org/10.19004/pjssz.41.0_62

Shinohara K, Takano M, Ishii K (2015) Chilopoda. In: Aoki J-I (Ed.) Pictorial Keys to Soil Animals of Japan, Second Edition. Tokai University Press, Hadano, 873–910.

Siriwut W, Edgecombe GD, Sutcharit C, Tongkerd P, Panha S (2016) A taxonomic review of the centipede genus *Scolopendra* Linnaeus, 1758 (Scolopendromorpha, Scolopendridae) in mainland Southeast Asia, with description of a new species from Laos. ZooKeys 590: 1–124. https://doi.org/10.3897/zookeys.590.7950

Takakuwa Y (1933a) External morphology of *Otocryptops* (Miscellaneous notes on centipedes. IX.). Hakubutsugaku Zasshi 31(49): 11–22.

Takakuwa Y (1933b) Scolopendromorpha of Japan. Shokubutsu oyobi Dobutsu 1(10): 1457–1464.

Takakuwa Y (1937) Eine neue Art von *Otocryptops* und ihre geographische Verbreitung in Japan. Dobutsugaku Zasshi 49(6): 203–205. https://www.doi.org/10.34435/zm002540

Takakuwa Y (1938) Eine neue *Otocryptops*-art aus Korea. Dobutsugaku Zasshi 50(6): 297–298. https://www.doi.org/10.34435/zm002622

Takakuwa Y (1939) Eine neue (dritte) art von *Otocryptops* aus Japan. Dobutsugaku Zasshi 51(10): 698–700.

Takakuwa Y (1940) Scolopendromorpha (Class Chilopoda: Epimorpha). Fauna Nipponica, Vol. IX, Fas. VIII, No. II. Sanseido, Tokyo, 88 pp.

Takano M (1973) Diplopoda and Chilopoda of Nii-jima island, Japan. Takakuwaia 6: 3–4.

Takashima H, Shinohara K (1952) The centipede-fauna of the Tokyo District. Acta Arachnologica 13(1): 3–17. https://doi.org/10.2476/asjaa.13.3

Tamura K, Stecher G, Kumar S (2021) MEGA 11: Molecular Evolutionary Genetics Analysis Version 11. Molecular Biology and Evolution 38(7): 3022–3027. https://doi.org/10.1093/molbev/msab120

Vahtera V, Edgecombe GD, Giribet G (2012) Evolution of blindness in scolopendromorph centipedes (Chilopoda, Scolopendromorpha): Insight from an expanded sampling of molecular data. Cladistics 28(1): 4–20. https://doi.org/10.1111/j.1096-0031.2011.00361.x

Vahtera V, Edgecombe GD, Giribet G (2013) Phylogenetics of scolopendromorph centipedes: Can denser taxon sampling improve an artificial classification? Invertebrate Systematics 27(5): 578–602. https://doi.org/10.1071/IS13035

Verhoeff KW (1934) Beiträge zur Systematik und Geographie der Chilopoden. Zoologische Jahrbücher Abteilung für Systematik 66(1–2): 1–112.

Verhoeff KW (1935) Über *Scolioplanes* (Chilopoda). Zoologischer Anzeiger 111: 10–23.

Verhoeff KW (1937) Chilopoden-studien. Zur Kenntnis der Lithobiiden. Archiv für Naturgeschichte N.F. 6: 171–257.

Whiting MF, Carpenter JM, Wheeler QD, Wheeler WC (1997) The Strepsiptera problem: Phylogeny of the holometabolous insect orders inferred from 18S and 28S ribosomal DNA sequences and morphology. Systematic Biology 46(1): 1–68. https://doi.org/10.1093/sysbio/46.1.1

Wood Jr HC (1862) On the Chilopoda of North America, with a catalogue of all the specimens in the collection of the Smithsonian Institution. Journal of the Academy of Natural Sciences of Philadelphia. Journal of the Academy of Natural Sciences of Philadelphia 5(1): 5–52. https://doi.org/10.5962/bhl.title.1585

Xiao S, Chen H, Di Z (2021) *Scolopocryptops longipes* sp. nov., a troglobitic scolopocryptopine centipede (Chilopoda: Scolopendromorpha: Scolopocryptopidae) from China. Zootaxa 5082(1): 87–94. https://doi.org/10.11646/zootaxa.5082.1.8

Xiong B, Kocher TD (1991) Comparison of mitochondrial DNA sequences of seven morphospecies of black flies (Diptera: Simuliidae). Genome 34(2): 306–311. https://doi.org/10.1139/g91-050

Supplementary material 1

Selected partitioning schemes and substitution models for the phylogenetic analyses

Authors: Taro Jonishi, Takafumi Nakano
Data type: xls

Link: https://doi.org/10.3897/zse.100.119297.suppl1

Supplementary material 2

Uncorrected pairwise distances for 654 bp of the COI sequences of *Scolopocryptops longisetosus* sp. nov.

Authors: Taro Jonishi, Takafumi Nakano
Data type: xls

Link: https://doi.org/10.3897/zse.100.119297.suppl2

Supplementary material 3

Bayesian Inference tree

Authors: Taro Jonishi, Takafumi Nakano
Data type: pdf
Explanation note: Bayesian Inference tree (mean ln $L = -5113.28$) for 654 bp of the COI sequences. Numbers on nodes indicate ultrafast bootstrap values and Bayesian posterior probabilities. Locality numbers (Q1–Q3 and L1–L6) are shown in Fig. 1 and Table 1.

Link: https://doi.org/10.3897/zse.100.119297.suppl3

Zoosyst. Evol. 100 (2) 2024, 425–436 | DOI 10.3897/zse.100.113972

PENSOFT

für Natur MUSEUM FÜR NATURKUNDE BERLIN

Description of a new species of the genus *Cultellus* Schumacher, 1817 (Bivalvia, Pharidae) from the South China Sea, based on integrative taxonomy

Yanan Yu[1], Yingyi Jiao[1], Junlong Zhang[1,2,3,4]

1 *Laboratory of Marine Organism Taxonomy and Phylogeny, Qingdao Key Laboratory of Marine Biodiversity and Conservation, Institute of Oceanology, Chinese Academy of Sciences, Qingdao 266071, China*

2 *Laoshan Laboratory, Qingdao, China*

3 *Marine Biological Museum, Chinese Academy of Sciences, Qingdao 266071, China*

4 *University of Chinese Academy of Sciences, Beijing 100049, China*

https://zoobank.org/A9F39F7B-24AD-44CC-A61C-73D9BF4066CE

Corresponding author: Junlong Zhang (zhangjl@qdio.ac.cn)

Academic editor: Thomas von Rintelen ♦ **Received** 11 October 2023 ♦ **Accepted** 19 March 2024 ♦ **Published** 9 April 2024

Abstract

The present study describes a new species within the genus *Cultellus* Schumacher, 1817 collected from the South China Sea. An integrative taxonomic approach incorporating morphological comparisons, geometric morphometrics and genetic analyses was used to identify and differentiate the new species. *Cultellus exilis* **sp. nov.** is distinguished from its congeners by its slender, fragile and translucent valves, curved posteroventral margins and relatively large protractor scars. The geometric morphometric analyses, based on outlines data, indicated that samples of *Cultellus exilis* **sp. nov.** clustered together and were distinctly separated from other species. Multiple species delimitation results, based on the mitochondrial COI gene, support the separation of *Cultellus exilis* **sp. nov.** from its related congeners. Phylogenetic analyses of a nuclear (28S rRNA) and two mitochondrial (COI, 16S rRNA) genes using Maximum Likelihood and Bayesian Inference methods revealed that the species belongs to the genus *Cultellus*. The superfamily Solenoidea Lamarck, 1809, which includes the families Solenidae Lamarck, 1809 and Pharidae H. Adams & A. Adams, 1856, exhibits closer affinity to the family Hiatellidae Gray, 1824 than to Solecurtidae d'Orbigny, 1846. Furthermore, we found that the genus *Siliqua* was clustered alongside the genera *Ensiculus* and *Phaxas* as a sister clade, which contradicts the current systematics of the subfamily within the family Pharidae. This work highlights the utility of integrative taxonomy for species identification, recognition and phylogenetic investigation.

Key Words

geometric morphometrics, integrative taxonomy, Pharidae, phylogeny, Solenoidea, species delimitation

Introduction

The superfamily Solenoidea Lamarck, 1809 including two families, namely Solenidae Lamarck, 1809 and Pharidae H. Adams & A. Adams, 1856, constitutes a collective of benthic bivalves that belong to the order Adapedonta Cossmann & Peyrot, 1909 (Cosel 1993; Bieler et al. 2010; Carter et al. 2011). These molluscs are commonly referred to as "razor clams" or "jackknife clams" due to their narrow-elongated shells and sharp edges (Saeedi et al. 2013; Giacomino and Signorelli 2021). Solenidae was regarded as a family by H. & A. Adams, containing two subfamilies Soleninae (including *Solen*, *Solena*, *Ensis*) and Pharinae (including *Pharus*, *Pharella*, *Cultellus*, *Siliqua*, *Macha* = *Solecurtus*, *Azor* = *Azorinus*, *Siliquaria* = *Tenagodus*, *Novaculina*) (Adams and Adams 1858). Cosel (1993) elevated the superfamily Solenoidea and allocated two families Solenidae and Pharidae within it, based on the number of central teeth. Solecurtidae d'Orbigny, 1846 and Psammobiidae J. Fleming, 1828 were currently taken as families within the superfamily Telli-

noidea Blainville, 1814 (Bieler et al. 2010). Huber (2010) documented that the family Solenidae encompasses the genera *Neosolen*, *Solen* and *Solena*, while the family Pharidae comprises 14 genera including *Afrophaxas*, *Cultellus*, *Ensiculus*, *Ensis*, *Phaxas*, *Sinucultellus*, *Orbicularia*, *Pharella*, *Sinonovacula*, *Novaculina*, *Nasopharus*, *Pharus*, *Sinupharus* and *Siliqua*. Furthermore, Novaculininae Ghosh, 1920 was considered a junior synonym of Pharellinae within the family Pharidae by Bolotov et al. (2018). At present, this systematics has been widely accepted.

The genus *Cultellus* was initially proposed by Schumacher (1817) to accommodate the jackknife clam *Cultellus magnus* Schumacher, 1817 = *C. maximus* (Gmelin 1791). The shells of this genus are of medium to large size, exquisitely elongated and slender, with the umbos located closer to the anterior end. Coen (1933) established the subgenus *Cultellus* (*Cultrensis*) Coen, 1933 to accommodate *Cultellus* (*Cultrensis*) *adriaticus* Coen, 1933. This species is characterised by its straight dorsal margin and two lines extending from the umbo to the posterior end (Thiele 1992), whereas this species was regarded as a junior synonym of *Phaxas pellucidus* (Pennant, 1777) (McKay and Smith 1979). Adams (1861) observed that *Cultellus cultellus* (Linnaeus, 1758) exhibits significant differences in characters compared to other species within the genus *Cultellus*. It has more curved margins and a shorter internal rib. Hence, he proposed a new genus *Ensiculus* H. Adams, 1861 within the family Pharidae for this species. Huber (2010) suggested that the genus *Cultellus* currently comprises five valid species, *C. attenuatus* Dunker, 1862, *C. hanleyi* Dunker, 1862, *C. maximus*, *C. subellipticus* Dunker, 1862 and *C. vitreus* Dunker, 1862. Three of these species are found along the coast of China: *C. maximus* (Gmelin 1791) reported from Taiwan island, *C. subellipticus* Dunker, 1862 distributed in the South China Sea and *C. attenuatus* Dunker, 1862 widespread in the Yellow Sea, the East and South China Seas (Liu 2008; Xu and Zhang 2008). Nonetheless, the generic allocations have yet to be validated by molecular analysis.

Razor clams are highly valued for their delectable taste and nutrition richness. In recent years, there has been an increasing interest amongst scholars in investigating the artificial breeding of these species (Zeng et al. 2010; Xu et al. 2013; Jiang et al. 2017; Li et al. 2022). However, the phylogeny of the genus *Cultellus* and even the superfamily Solenoidea has received limited attention. Previous studies that utilised single gene fragments or Random Amplified Polymorphic DNA (RAPD) methods consistently indicated that *Cultellus* belongs to Pharidae, a family closely related to Solenidae (Chen et al. 2005; Wu et al. 2008; Bolotov et al. 2018). Phylogenetic analysis, based on the mitochondrial genes, revealed a close relationship between the genera *Cultellus* and *Sinonovacula*, indicating their membership in the same family (Yuan et al. 2012; Yu et al. 2016). Analysis of two nuclear genes (18S and 28S) unveiled that the superfamilies Solenoidea and Hiatelloidea formed sister clades (Taylor et al. 2007). Bieler et al. (2014) demonstrated a well-supported clade between Hiatellidae and Solenoidea by utilising more genes (COI, 16S, 28S, 18S, H3) for constructing the phylogenetic tree. A recent mitochondrial phylogenomic study further indicated a closer relationship between Solenoidea and Hiatelloidea compared to Solecurtidae (Li et al. 2022). Given that the aforementioned studies were conducted on a limited number of taxonomic groups, the phylogenetic relationships of the taxa within the Solenoidea remain inadequately investigated.

In May 2021, a previously unknown jackknife clam was collected from the South China Sea using the Agassiz trawl and subsequently preserved at the Institute of Oceanology, Chinese Academy of Sciences (IOCAS). In this study, an integrative taxonomic approach incorporating molecular and geometric morphometrics was employed to identify and differentiate this species. Additionally, historical specimens collected in the last century and currently housed at the Marine Biological Museum, Chinese Academy of Sciences (MBMCAS) were also identified as this species. This methodology enables a more comprehensive understanding of the evolutionary relationships between species and a more reliable delimitation of species. Morphological examination and genetic analyses revealed that the specimen represented a hitherto undescribed species that belongs to the genus *Cultellus*. Herein, we formally describe and illustrate the new species, which adds to the known species diversity of the genus *Cultellus* from Chinese waters.

Materials and methods

Specimen collection and morphological analyses

The specimen was collected from the shallow water in the South China Sea using the Agassiz trawl (Fig. 1). Ocean Data View software version 5.4.0 (http://odv.awi.de) was used to plot the collection locations. The newly-sampled specimen was preserved in 75% ethanol solution and deposited in the Marine Biological Museum, Chinese Academy of Sciences (MBMCAS), Qingdao, China, alongside other historical shell specimens. The shells were observed under a Zeiss SteREO Discovery.V12 stereomicroscope (Zeiss, Wetzlar, Germany) and photographs were captured using a Canon EOS6D camera. Shell measurements were taken to the nearest 0.01 mm using a Vernier caliper. Abbreviations used in this study: L, shell length; H, shell height; W, width of right valve.

Geometric image acquisition

Each sample was assigned to a uniform numbering and the right inner surface of each shell was photographed using a Sony ILCE-7RM4. To minimise random errors caused by factors like angle and lighting, the camera was securely fixed on a camera stand during photography. The type specimen images of *C. attenuatus*, *C. hanleyi*, *C. subellipticus* and *C. vitreus* were provided by the Natural History Museum, London. The outline data used for morphometric analysis were captured by ImageJ v.2 (Schneider et al. 2012) software to ensure consistency in

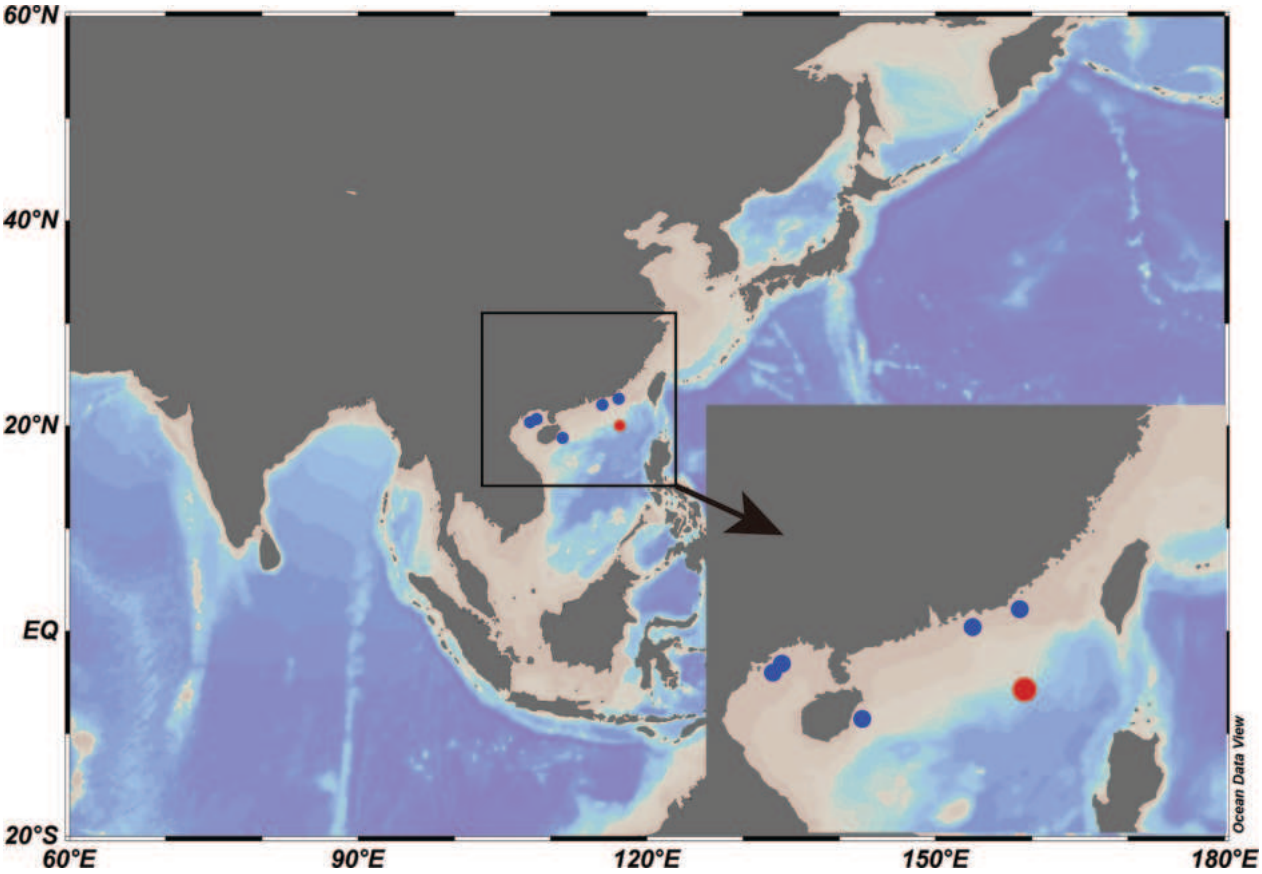

Figure 1. The location of *Cultellus exilis* sp. nov. in the South China Sea. The red dot represents holotype and the blue dots represent paratypes.

point selection direction. Subsequently, the above data were imported into Mathematica v.13.2 and uniformly sampled using the Polly.Morphometrics.12.4 package to obtain 150 semi-landmarks for each sample.

Geometric morphometric analyses

Initially, Generalised Procrustes Analysis (GPA) was conducted on the obtained data, in order to eliminate the influence of non-shape differences caused by sample size, photo size, position etc. Subsequently, Thin Plate Splines analysis (TPS) and Principal Component Analysis (PCA) were performed on the transformed data to convert the shape variation of all data points into a smaller number of uncorrelated principal component variation indicators. Then, the first three principal components were selected as representatives of morphological variation and analysed using Linear Discriminant Analysis (LDA). All the above data analyses were executed using Past v.4.12 software (Hammer et al. 2001).

DNA extraction and PCR amplification

Genomic DNA of specimens used in the present study was extracted from the foot of the animals using the Marine Animal Genomic DNA Extraction Kit (Tiangen Biotech, Beijing, China) following the manufacturer's instructions and frozen at -20 °C. The mitochondrial DNA cytochrome c oxidase subunit I (COI) region was amplified using universal primers LCO1490 and HCO2198 (Folmer et al. 1994). The mitochondrial 16S rRNA gene was amplified using 16Sa (Xiong and Kocher 1991) and 16Sb (Edgecombe et al. 2002) and the nuclear 28S rRNA gene was amplified using 28Sa and 28Sb (Whiting et al. 1997). Polymerase chain reaction (PCR) amplification was carried out in a total reaction volume of 25 µl, consisting of 12 µl of 2× Es TaqMasterMix (Dye) (CWBio Co., Ltd, Beijing, China), 1 µl of each primer, 2 µl of template DNA and 9 µl of DNase-free ddH_2O. The amplification conditions consisted of an initial denaturation at 95 °C for 5 min, followed by 35 cycles of denaturation at 95 °C for 30 s, annealing at 46 °C for 30 s (52 °C for 28S rRNA), extension at 72 °C for 1 min and a final extension at 72 °C for 10 min.

Sequencing and data analysis

Amplification products were detected using agarose gel electrophoresis and subsequently sequenced by Sangon Biotech (Shanghai, China). The obtained sequences were uploaded and compared to the existing sequences in GenBank (www.ncbi.nlm.nih.gov/Genbank) using the Basic Local Alignment Search Tool (BLAST) provided by the National Center for Biotechnology Information. To conduct phylogenetic analyses, available sequence

data for the superfamily Solenoidea were retrieved from GenBank (Suppl. material 1: table S1). *Hiatella arctica* (Linnaeus, 1767) and *Solecurtus divaricatus* (Lischke, 1869) were regarded as the outgroup taxa. The sequences of each gene fragment were independently aligned using MAFFT v.7 (Katoh and Standley 2013) with the G-INS-i and Q-INS-i algorithms for the protein-coding and ribosomal regions, separately. The sequences of three genes from the same individual were concatenated into a single sequence in SequenceMatrix v.1.8 (Vaidya et al. 2011). The best-fitting evolutionary model of the concatenated dataset was selected using the Akaike Information Criterion, as implemented in jModelTest 2.1.10 (Darriba et al. 2012). Phylogenetic trees were constructed based on the Maximum Likelihood (ML) using IQ-TREE v. 2.1.3 with bootstrap values for 2000 replicates (Minh et al. 2020). Bayesian Inference (BI) analysis was performed using MrBayes v.3.2.7, with three parallel runs of five million generations each, sampling every 1000 generations and burn-in set to 25% (Ronquist et al. 2012).

Multiple species delimitation methods were used to investigate the hypothesis that the specimen represents a distinct species. The COI data of 30 homologous sequences were analysed using Automated Barcode Gap Discovery (ABGD) carried out by the web-based interface (available at https://bioinfo.mnhn.fr/abi/public/abgd/abgdweb.html/) (Puillandre et al. 2012) using the Kimura 2 parameter substitution model (TS/TV = 2.0), prior for the maximum value of intraspecific divergence ranging between 0.001 and 0.1, 10 recursive steps and a relative gap width (X) of 1.0. Bayesian implementation of the Poisson Tree Processes (bPTP) species delimitation model was analysed (Zhang et al. 2013) at the web server of the Heidelberg Institute for Theoretical Studies, Germany (http://species.h-its.org/) using ML phylogenetic trees as input data. Markov Chain Monte Carlo (MCMC) runs were performed for 100,000 steps and sampled every 100 steps with burn-in set to 0.1. Removing the outgroup in initial runs did not affect delimitation results. The General Mixed Yule Coalescent (GMYC) model (Pons et al. 2006) was used in PyR8S of iTaxoTools v.0.1 (Vences et al. 2021) with default parameters to determine the species of analysed individuals, based on ultrametric time trees derived from single-locus data. Pairwise comparisons of the *p*-genetic distances, based on COI genes, were also calculated by MEGA X (Kumar et al. 2018).

Results

Systematics

Superfamily Solenoidea Lamarck, 1809
Family Pharidae H. Adams & A. Adams, 1856

Genus *Cultellus* Schumacher, 1817

Type species. *Solen maximus* Gmelin, 1971 (by monotypy).

***Cultellus exilis* sp. nov.**

https://zoobank.org/4F4ACFDD-3083-4EF7-900E-C259F51ECE95
Figs 2, 3, 4F

Type specimens. *Holotype*: MBM229032, one complete individual, collected on 28 May 2021 by Agassiz trawl on the research vessel "TAN KAH KEE" (muddy bottom, depth 55 m). ***Paratype*:** MBM264485, one complete specimen, collected from the Beibu Gulf, China, January 1962 (muddy bottom, depth 55 m); MBM264488, two complete specimens, collected from the Beibu Gulf, China, December 1959 (Habitat unknown); MBM264497, one complete specimen, collected from Haimen, Guangdong Province, China, March 1954 (Habitat unknown); MBM264500, one complete specimen, collected from Shanwei, Guangdong Province, China, January 1995 (Habitat unknown); MBM229040, one complete specimen, collected from Hainan Province, China, January 1959 (muddy bottom, depth 91.5 m).

Type locality. Neritic zone of the South China Sea (depth 55 m, 20°1'13.44"N, 117°10'45.84"E); Muddy bottom.

Etymology. The specific epithet "exilis" is derived from the Latin, referring to its slender shell, which is a remarkable difference from other species in this genus.

Description. Shell medium in size, flattened, elongate, fragile, glazed, translucent, equivalve, inequilateral. Some specimens are covered with various-sized bubbles on their surface (Figs 2A–D, 3A–D). Umbo depressed, weakly prosogyrous, situated at anterior 2/9 of shell. Anterior area short, elliptical, posterior area elongated, both ends gaping, anterior end slightly turned-up, posterior end slightly more pointed than anterior end; antero-dorsal margin downward sloping, postero-dorsal margin almost straight, ventral margin rather arcuate, postero-ventral margin more curved than antero-ventral, middle-ventral margin almost straight. Periostracum of valve surface yellowish; shell surface with fine, dense, regular and non-isometric co-marginal growth lines, without radial lines; lunule and escutcheon absent. Ligament short, but strong, dark brown and situated opisthodetic.

Interior shell off-white, with yellowish periostracum in margin. Each valve with one white, strong, thin, straight, internal radial rib extending from umbonal area to anterior end, forming ca. 21° angle with antero-dorsal margin (Fig. 2H–J). Anterior adductor muscle scar subtrigonal, obvious, near internal rib; posterior adductor scar falciform, almost straight near the dorsal margin; pedal retractor scars rhombic, situated at the corner between umbo and internal rib; pallial sinus shallow, pallial lines connected to adductor scars. Left valve with three strong and projecting cardinal teeth, central tooth bifid at the top and confluent at the base, without lateral tooth (Fig. 2H); right valve with two long and strong cardinal teeth, anterior protruding downwards, posterior pointing to the back end, without lateral tooth (Fig. 2I).

Siphons short and bifurcated, situated at posterior area; gills transversely folded; foot strong, depressed, truncated, situated at anterior area.

Measurement. Holotype: MBM229032: L = 34.66 mm, H = 10.35 mm, W = 2.27 mm. Paratype: MBM264485: L =

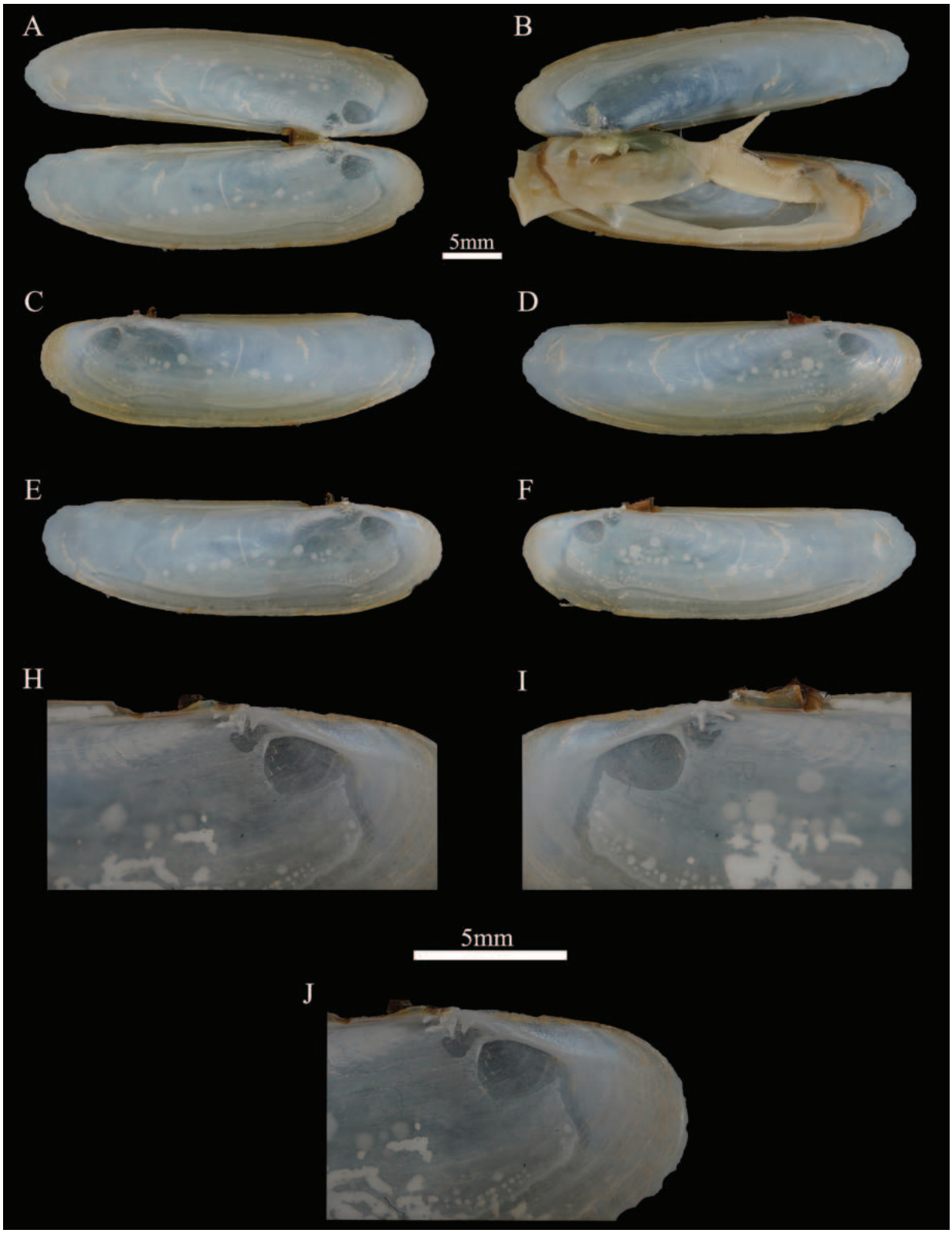

Figure 2. *Cultellus exilis* sp. nov. (holotype) **A, B.** MBM229032, L = 34.66 mm; **C, D.** Exterior views of left and right valve; **E, F.** Interior views of left and right valve; **H.** Hinge of left valve; **I.** Hinge of right valve; **J.** Internal radial rib of left valve.

45.42 mm, H = 12.65 mm, W = 2.37 mm; MBM264488: L = 61.51 mm, H = 16.26 mm, W = 3.73 mm; MBM264497: L = 77.05 mm, H = 21.14 mm, W = 4.72 mm; MBM264500: L = 73.30 mm, H = 19.74 mm, W = 4.52 mm; MBM264601: L = 44.32 mm, H = 12.42 mm, W = 2.33 mm.

Remarks. The shells of *Cultellus* are relatively less elongated compared to those of the other genera of Solenoidea. Typically, the shells of *Cultellus* have rounded anterior and posterior ends, an anteriorly located umbo, strong internal ribs and three cardinal teeth on the left

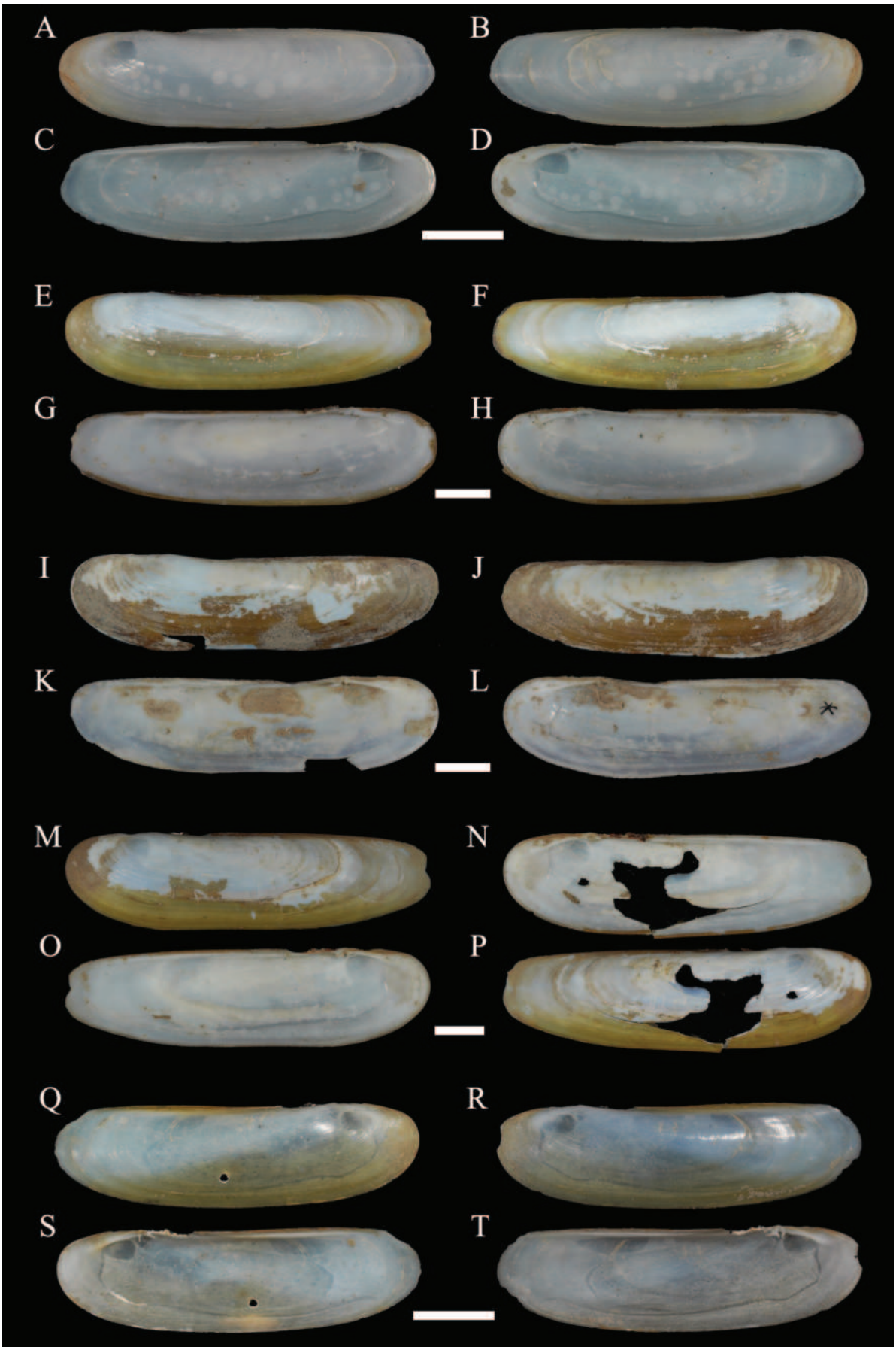

Figure 3. *Cultellus exilis* sp. nov. (paratypes) **A–D.** MBM264485; **E–H.** MBM264488; **I–L.** MBM264497; **M–P.** MBM264500; **Q–T.** MBM229040. Scale bars: 10 mm.

valve and two on the right (Thiele 1992). The remarkable morphologic similarity amongst *Cultellus* members makes species identification challenging. The distinguishing features that separate *Cultellus exilis* sp. nov. from other species in this genus are its particularly slender, fragile and translucent shells. Additionally, the new species differs from the *C. maximus* (Fig. 4E) in that its posterior end is notably narrower than its anterior end (Gmelin 1791). It closely resembles *C. attenuatus* (Fig. 4A) and *C. vitreus* (Fig. 4D). However, *C. attenuatus* (Fig. 4A) differs from the new species by the anterior area of the shell, which is obviously wider than the posterior part. Additionally, the posterior end of *C. vitreus* is slightly truncated (Fig. 4D), whereas *Cultellus exilis* is more curved. *C. subellipticus* (Fig. 4C) differs from the new species by the posterior area of the shell, which is much wider than the anterior part (Dunker 1862; Clessin 1888). Compared to this new species, the length-to-height ratio of *C. hanleyi* is 3.3–3.4:1 (Fig. 4B), whereas the ratio of *Cultellus exilis* is 3.5–3.8:1.

Geometric morphometrics of shell outlines. Principal Component Analysis (PCA) was conducted on the Progrustes alignment outline data of 32 samples representing six species. The results revealed that the first three principal components accounted for a cumulative contribution rate of 96.88% (PCA1 80.79%, PCA2 13.97% and PCA3 2.12%), indicating that they can represent the major morphological differences amongst the samples. According to the extreme distortion state of the thin plate spline plots, the main difference of all samples along the PCA1 axis occurs in the relative height of the shell (Fig. 5B, C). Differences in the PCA2 axis mainly involve the length-to-height ratio of the shells. Shells were increasingly elongated from the PCA2+ to PCA2- direction (Fig. 5A, D). Considering the distortion observed along both the PCA1 and PCA2 axes, the main variation in the outlines of the six species within the genus *Cultellus* is the relative length and height of the shell. Discriminant analysis of all data indicated that the first two variance values explain 96.98% of the overall variation. A Discriminant analysis plot clearly demonstrated that *Cultellus exilis* sp. nov. is distinctly separated from the other species, forming its own cluster (Fig. 6). Therefore, the geometric morphometric analysis results, based on outlines, support distinguishing the new species from other species within the genus *Cultellus*.

Species delimitation analyses. All species delimitation analyses, namely ABGD, bPTP and GMYC, conducted on the COI sequences, resulted in the delimitation of eleven species in the superfamily Solenoidea. The analysis confirmed that *Cultellus exilis* sp. nov. is a distinct species from other *Cultellus* species. Sequences of the genus *Cultellus* were delimited into four species, i.e. *C. attenuatus*, *C. subellipticus*, *C. maximus* and *Cultellus exilis* sp. nov. (Fig. 7). In addition, based on the available molecular data, the analysis of a 581-bp fragment of the COI gene yielded a 12.2%–13.9% pairwise distance between *Cultellus exilis* sp. nov. and other congeners, a divergence higher than the intraspecific variation (0–1.7%) of the genus *Cultellus* (Suppl. material 1: table S2).

Phylogenetic analyses. The best-fitting evolutionary model of the concatenated dataset (COI, 16S and 28S) was selected as GTR+G+I using the Akaike Information Criterion implemented in jModelTest 2.1.10. The evolutionary relationships amongst the razor clams were depicted on a phylogenetic tree constructed using the ML and BI methods. These trees exhibited highly similar topologies (Fig. 8). Phylogenetic trees obtained from the datasets were completely resolved and highly supported, as indicated by posterior probability (PP) or bootstrap scores (BS). *Cultellus exilis* sp. nov. and the two other *Cultellus* species formed a clade within the family Pharidae. The sequences of *Cultellus exilis* sp. nov. recovered a well-supported lineage distinct from the other congeners. Notably, *Ensiculus cultellus* and *Phaxas pellucidus* did not cluster together with the genus *Cultellus*. Instead, they occupied different branch positions in both ML and BI trees. On the ML tree, *Ensiculus cultellus* clustered with *Phaxas pellucidus* and formed a sister clade with the genus *Siliqua*. While on the BI tree, *Ensiculus cultellus* grouped with the genus *Siliqua*, constituting a sister lineage to *Phaxas pellucidus*. All phylogenetic results strongly supported the close relationship between pharids and solenids (PP = 0.99; BS = 92). Furthermore, the family Hiatellidae was found to be closely related as a sister to the superfamily Solenoidea (PP = 1; BS = 100). The best-fitting evolutionary model of the COI sequence was GTR+G. The phylogenetic tree inferred using ML criteria, based on single gene COI (Fig. 8), showed a similar overall topology.

Discussion

In this paper, we present a new species of razor clam that was confirmed using an integrative taxonomic approach involving shell morphological comparisons, geometric morphometrics and genetic analysis. This species can be morphologically distinguished from other congeners by its slender valve, more curved posteroventral margin and relatively larger protractor scar (Fig. 4). The geometric morphometric analyses, based on outline data, revealed that samples of *Cultellus exilis* sp. nov. were clustered together and clearly separated from other species of this genus (Fig. 6). The molecular analysis demonstrated that this species belongs to the genus *Cultellus*, but is genetically distinct from other known *Cultellus* species (Figs 7, 8).

The genus *Cultellus* currently encompasses five valid extant species that inhabit the waters of the Indo-West Pacific, with most ranging from tropical to temperate seas (Okutani 2000; Swennen et al. 2001; Min et al. 2004; Thach 2005; Thach 2007; Xu and Zhang 2008; Huber 2010; Coan and Petit 2011; Poppe 2011). The new species, *Cultellus exilis* sp. nov., was also found from this region (Fig. 1). The paratype specimens were previously misidentified as *C. attenuatus*, but our study corrected the misidentifications using integrative taxonomy. Geometric morphometrics has been used to quantify morphological changes in the process of biological evolution since

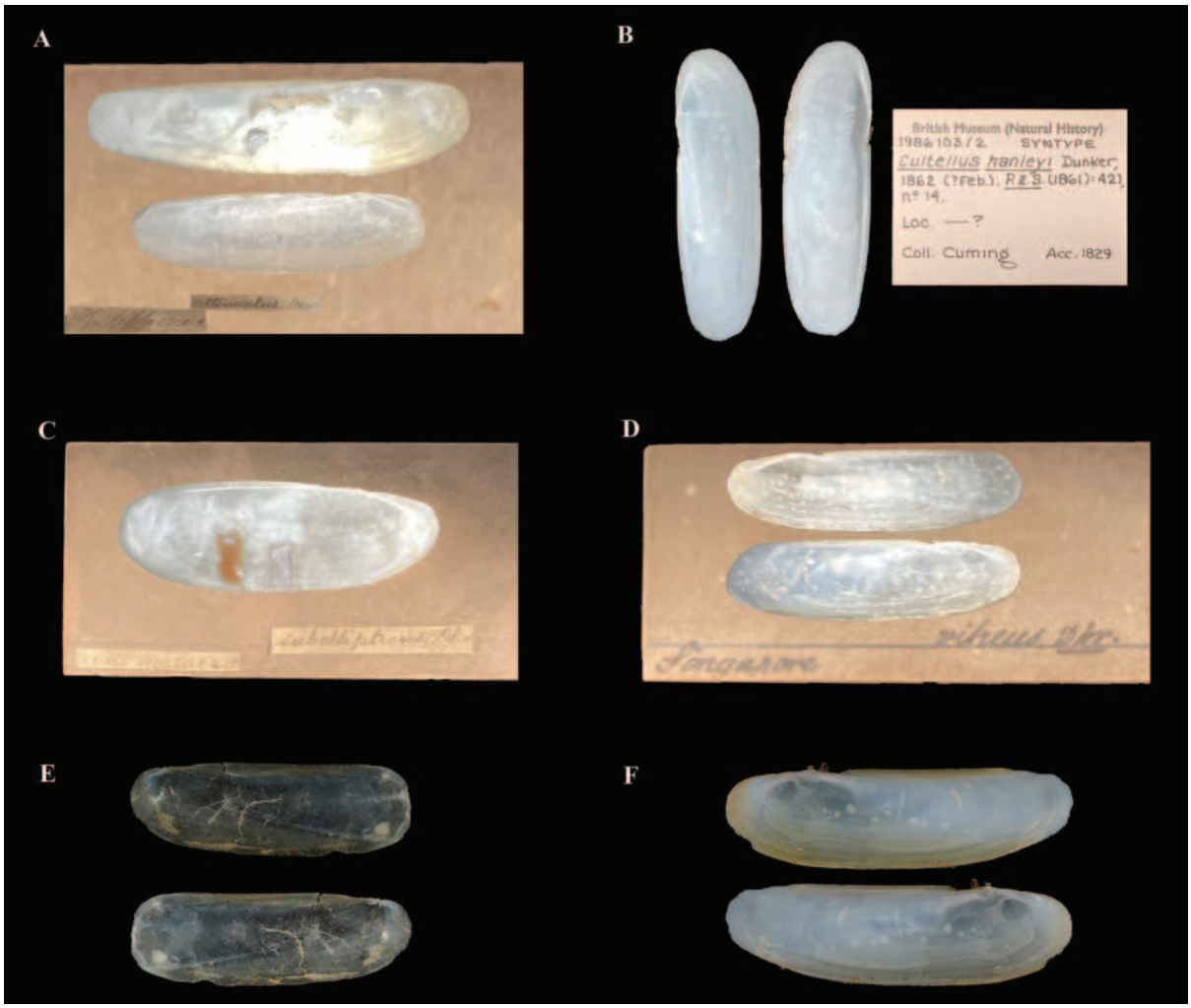

Figure 4. A. *Cultellus attenuatus* Dunker, 1862. Two syntypes, NHMUK 20240145: L = 54.7 mm, H = 13.9 mm; L = 45.2 mm, H = 12.2 mm; **B.** *Cultellus hanleyi* Dunker, 1862. One syntype, NHMUK 1986103: L = 54.1 mm, H = 16.1 mm; **C.** *Cultellus subellipticus* Dunker, 1862. One syntype, NHMUK 20240146: L = 46.3mm, H = 16.0 mm; **D.** *Cultellus vitreus* Dunker, 1862. One syntype, NHMUK 20240147: L = 39.5 mm, H = 10.9 mm; **E.** *Cultellus maximus* (Gmelin, 1791). MBM264615: L = 33.6 mm, H = 11.3 mm; **F.** *Cultellus exilis* sp. nov. MBM229032: L = 34.66 mm, H = 10.35 mm.

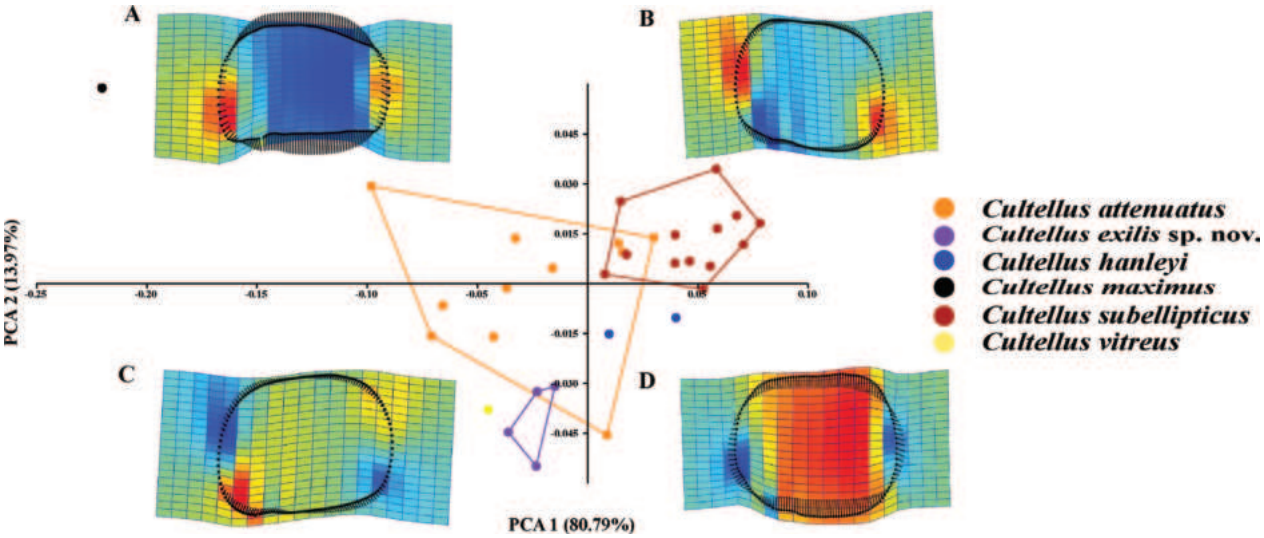

Figure 5. Principal component and thin plate spline analyses, based on outlines of the genus *Cultellus*. **A.** The extreme distortion of the outlines in the negative of PC2; **B.** The extreme distortion of the outlines in the positive of PC1; **C.** The extreme distortion of the outlines in the negative of PC1; **D.** The extreme distortion of the outlines in the positive of PC2. Each colour of the dot in the principal component analysis diagram represents a species.

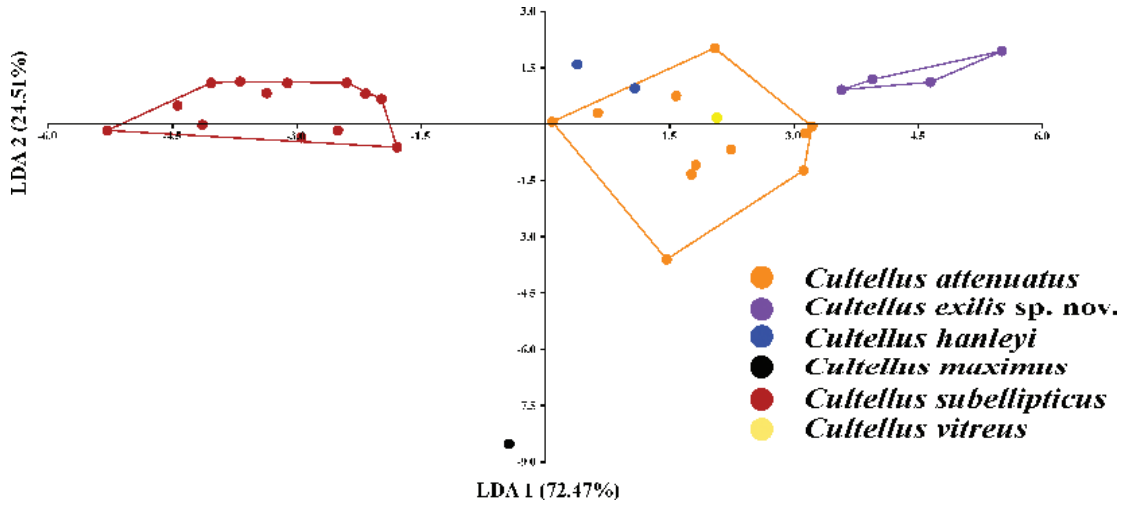

Figure 6. Scatter plot of discriminant analysis of the genus *Cultellus*. Each colour of the dot in the principal component analysis diagram represents a species.

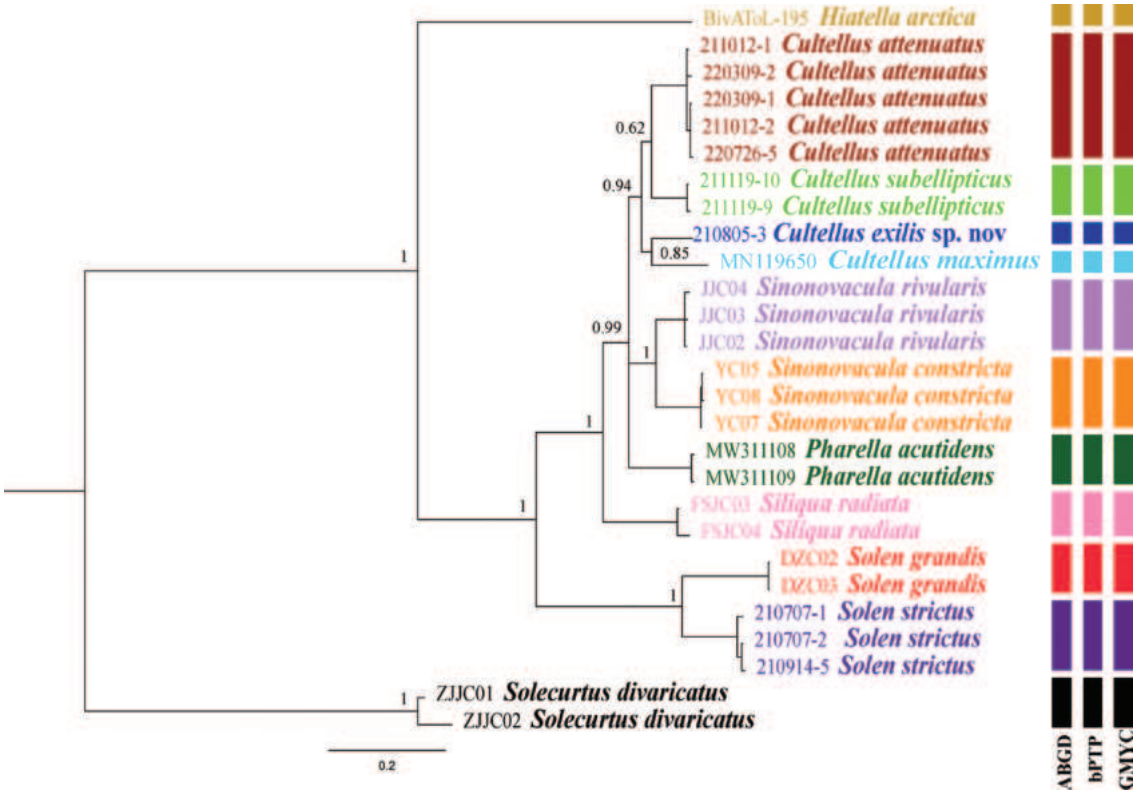

Figure 7. Phylogenetic tree obtained by the Maximum Likelihood (ML), based on COI gene sequences. Numbers adjacent to nodes refer to ML bootstrap scores (BS < 50 represented by "*"). The results of three species delimitation methods are shown on the right of the figure (Each species is represented by a single colour).

its proposal (Jacobson and Moyers 1993). Although it is not as widely used in molluscs as other methods, some studies have shown that geometric morphometrics analysis is suitable for explaining the convergent evolution of bivalves (Serb et al. 2011; Sherratt et al. 2016), discovering taxonomic information for species identification (Marinho and Arruda 2021) etc. This study highlights the importance of using integrative taxonomy for species identification and phylogenetic studies. In recent years, integrative taxonomy has been proven to be more reliable for biological taxonomy and species identification, especially for morphologically similar or indistinguishable species (Zhang et al. 2018a, 2018b; Sørensen et al. 2020; Zhang et al. 2020). Furthermore, integrative taxonomy facilitates phylogenetic analysis and exploration of evolutionary relationships amongst closely-related species (Sun et al. 2016; Liao et al. 2021). Integrative taxonomy will play a significant role in the taxonomy and phylogeny of marine organisms in the future.

The findings of this study are largely consistent with the previous molecular research on the phylogenetic relationships of the superfamily Solenoidea. Our phylogenetic trees, constructed using mitochondrial (COI, 16S) and nuclear (28S) genes, revealed that *Cultellus*,

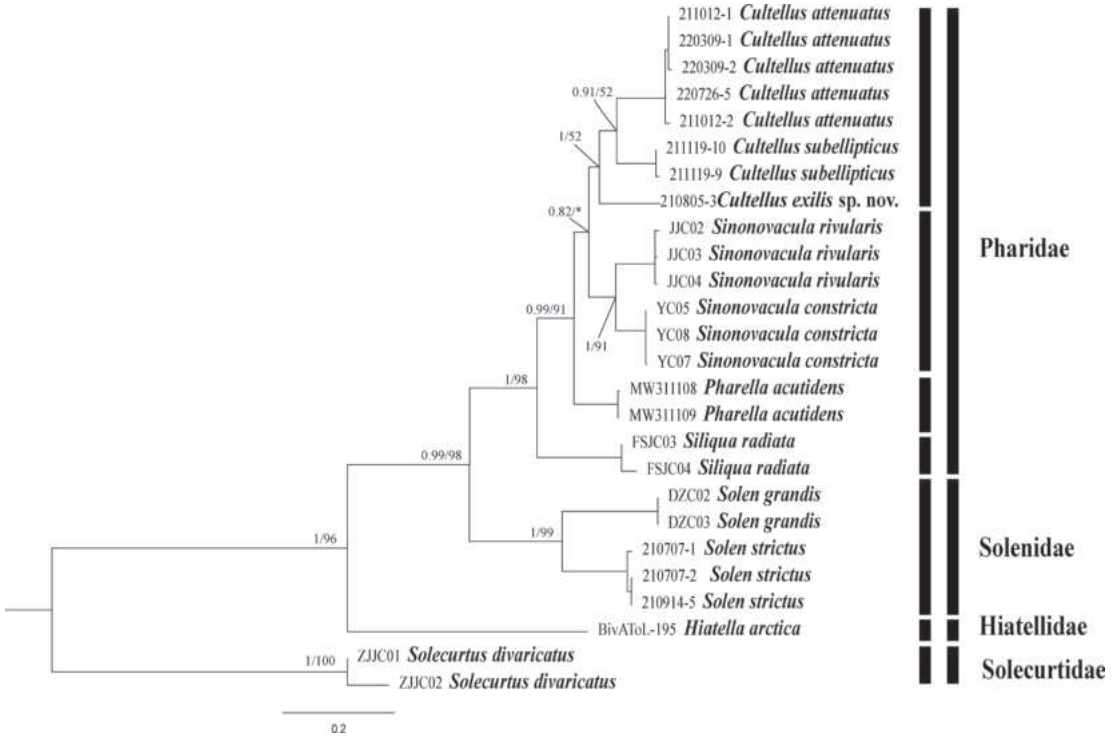

Figure 8. Phylogenetic tree inferred by Bayesian Inference analysis (BI) and Maximum Likelihood (ML), based on concatenated dataset of COI, 16S and 28S genes. Bayesian posterior probability and Maximum Likelihood bootstrap scores (left and right, respectively. "-" represents different branch position on ML and BI trees) are shown above the branch.

Sinonovacula, *Siliqua*, *Pharella*, *Ensiculus* and *Phaxas* belong to the family Pharidae. Interestingly, it appears that *Cultellus cultellus* (= *Ensiculus cultellus*) and *Cultellus* (*Cultrensis*) *adriaticus* (= *Phaxas pellucidus*) do not actually belong to the genus *Cultellus*, validating the morphological views proposed by Adams (1861) and McKay and Smith (1979). Both BI and ML results demonstrated that Pharidae and Solenidae formed a sister group. Furthermore, Pharidae, Solenidae and Hiatellidae clustered into a monophyletic group (Fig. 8), indicating that Solenoidea and Hiatellidae belong to the order Adapedonta. Bieler et al. (2014) pointed out the common characteristics amongst the species of Adapedonta, including the absence of the oesophageal lip, a simple transverse ridge pattern of the right wall sorting area and the presence of a ridge posteriorly bordering the right wall sorting area. Compared to previous studies, our study incorporated more molecular information and taxonomic groups, further verifying the reliability of the current systematics (Taylor et al. 2007; Bieler et al. 2014; Bolotov et al. 2018; Li et al. 2022).

Moreover, Bolotov et al. (2018) found that the genus *Cultellus* clustered together with *Sinonovacula* and *Pharella* in a phylogenetic tree of the family Pharidae, based on the concatenation of three genes (COI+16S+28S). They classified the genera *Novaculina*, *Sinonovacula*, *Pharella* and *Cultellus* as the subfamily Pharellinae. In our study, we observed that the genus *Siliqua* formed a sister clade with the genera *Ensiculus* and *Phaxas*. These findings collectively suggest that the current taxonomy of the family Pharidae is indeterminate and needs to be verified and reassessed by taking into account additional information.

Acknowledgements

We are grateful to Dr. Tom S. White and Dr. Andreia Salvador from the Natural History Museum, London for kindly providing photos of type materials of *Cultellus attenuatus*, *C. hanleyi*, *C. subellipticus* and *C. vitreus*. We also express our gratitude to Hao Wang, Huijie Liu and Yuyan Zhang from the Institute of Oceanology, Chinese Academy of Sciences, and the crews of RV TAN KAH KEE of Xiamen University, for their efforts and assistance in collecting samples for this study. This work was supported by the National Key Research and Development Program of China (2021YFE0193700), the Science and Technology Innovation Project of Laoshan Laboratory (LSKJ202203100), the Strategic Priority Research Program of the Chinese Academy of Sciences (XDB42000000; XDA22050203), the National Natural Science Foundation of China (31772422), the Taishan Scholars Program (tsqn202306280) and the Qingdao New Energy Shandong Laboratory Open Project (QNESL OP202306).

References

Adams H (1861) On two new genera of acephalous molluscs. Proceedings of the Zoological Society of London 1860(28): 369. https://www.biodiversitylibrary.org/page/12866937

Adams H, Adams A (1858) The genera of recent Mollusca: arranged according to their organization. Vol. 3, J. Van Voorst, London, 138 pp. https://doi.org/10.5962/bhl.title.4772

Barco A, Raupach MJ, Laakmann S, Neumann H, Knebelsberger T (2015) Identification of North Sea molluscs with DNA barcod-

ing. Molecular Ecology Resources 16(1): 288–297. https://doi.org/10.1111/1755-0998.12440

Bieler R, Carter JG, Coan EV (2010) Classification of Bivalve Families. Malacologia 52(2): 113–133. https://doi.org/10.4002/040.052.0201

Bieler R, Mikkelsen P, Collins T, Glover E, González V, Graf D, Harper E, Healy J, Kawauchi G, Sharma P, Staubach S, Strong E, Taylor J, Tëmkin I, Zardus J, Clark S, McIntyre E, Sharp P, Giribet G (2014) Investigating the Bivalve Tree of Life - An exemplar-based approach combining molecular and novel morphological characters. Invertebrate Systematics 28(1): 32–115. https://doi.org/10.1071/IS13010

Bolotov IN, Vikhrev IV, Lopes-Lima M, Lunn Z, Chan N, Win T, Aksenova OV, Gofarov MY, Kondakov AV, Konopleva ES, Tumpeesuwan S (2018) Discovery of *Novaculina myanmarensis* sp. nov. (Bivalvia: Pharidae: Pharellinae) closes the freshwater razor clams range disjunction in Southeast Asia. Scientific Reports 8(1): 16325. https://doi.org/10.1038/s41598-018-34491-8

Carter JG, Altaba CR, Campbell DC, Harries PJ, Skelton P (2011) A Synoptical Classification of the Bivalvia (Mollusca). Paleontological Contributions 2011(4): 1–47. https://doi.org/10.17161/PC.1808.8287

Chen L, Kong X, Yu Z, Yu S, Xu H (2005) Sequence comparison and phylogenetic analysis of mtDNA 16S rRNA and COI gene fragments in three species of razor shell. Marketing Science 29(8): 29–34.

Clessin S (1888) Die Familie der Solenaceen: In Abbildungen nach der Natur mit Beschreibungen. In: Systematisches Conchylien-Cabinet Von Martini Und Chemnitz. Forgotten Books, Lodon, 36–48.

Coan EV, Petit RE (2011) The publications and malacological taxa of William Wood (1774–1857). Malacologia 54(1–2): 1–76. https://doi.org/10.4002/040.054.0109

Coen GY (1933) Molluschi nuovi di Rovigno. Note dell'Istituto Italo-Germanico di Biologia marina di Rovigno d'Istria 6(8): 1–8.

Cosel RV (1993) The razor shells of the eastern Atlantic. Part 1: Solenidae and Pharidae I (Bivalvia: Solenacea). Archiv für Molluskenkunde der Senckenbergischen Naturforschenden Gesellschaft 122: 207–321. https://doi.org/10.1127/arch.moll/122/1993/207

Darriba D, Taboada GL, Doallo R, Posada D (2012) jModelTest 2: More models, new heuristics and parallel computing. Nature Methods 9(8): 772–772. https://doi.org/10.1038/nmeth.2109

Dunker W (1862) Solenacea nova collectionis Cumingianae. Proceedings of the Zoological Society of London 1861: 418–427. https://www.biodiversitylibrary.org/page/28672974

Edgecombe GD, Giribet G, Wheeler WC (2002) Phylogeny of Henicopidae (Chilopoda: Lithobiomorpha): A combined analysis of morphology and five molecular loci. Systematic Entomology 27(1): 31–64. https://doi.org/10.1046/j.0307-6970.2001.00163.x

Folmer O, Black M, Hoeh W, Lutz R, Vrijenhoek R (1994) DNA primers for amplification of mitochondrial cytochrome *c* oxidase subunit I from diverse metazoan invertebrates. Molecular Marine Biology and Biotechnology 3(5): 294–299. https://pubmed.ncbi.nlm.nih.gov/7881515/

Giacomino S, Signorelli JH (2021) Systematic redescription of *Solen* (*Ensisolen*) *tehuelchus* and *Ensis macha* (Bivalvia: Solenoidea) from Argentina, southwestern Atlantic Ocean. Zootaxa 4964(3): 541–558. https://doi.org/10.11646/zootaxa.4964.3.6

Gmelin JF (1791) Caroli a Linné. Systema naturae per regna tria naturae: secundum classes, ordines, genera, species, cum characteribus, differentiis, synonymis, locis. Vol. Tom. 1 Pars. 6, Impensis Georg, Emanuel Beer, Lipsiae, 3227 pp.

Hammer O, Harper D, Ryan P (2001) PAST: Paleontological Statistics Software Package for Education and Data Analysis. Palaeontologia Electronica 4(1): 1–9.

Huber M (2010) Compendium of bivalves. A full-color guide to 3,300 of the World's Marine Bivalves. A status on Bivalvia after 250 years of research. ConchBooks Hackenheim, 901 pp.

Jacobson A, Moyers RE (1993) Morphometric tools for landmark data. Cambridge University Press, England, 485 pp. https://doi.org/10.1016/S0889-5406(05)81803-7

Jiang X, Wei X, Feng Y, Han H, Waang S, Liu X, Tong T (2017) The Reproductive Biology of *Cultellus attenuatus* in the Laizhou Bay. Yuye Kexue Jinzhan 38(6): 107–111. https://doi.org/10.11758/yykxjz.20160920001

Katoh K, Standley DM (2013) MAFFT multiple sequence alignment software version 7: Improvements in performance and usability. Molecular Biology and Evolution 30(4): 772–780. https://doi.org/10.1093/molbev/mst010

Kumar S, Stecher G, Li M, Knyaz C, Tamura K (2018) MEGA X: Molecular Evolutionary Genetics Analysis across Computing Platforms. Molecular Biology and Evolution 35(6): 1547–1549. https://doi.org/10.1093/molbev/msy096

Li H, Yu R, Ma P, Li C (2022) Complete mitochondrial genome of *Cultellus attenuatus* and its phylogenetic implications. Molecular Biology Reports 49(8): 8163–8168. https://doi.org/10.1007/s11033-022-07276-6

Liao W, Campello-Nunes PH, Gammuto L, Abreu Viana T, de Oliveira Marchesini R, da Silva Paiva T, da Silva-Neto ID, Modeo L, Petroni G (2021) Incorporating mitogenome sequencing into integrative taxonomy: The multidisciplinary redescription of the ciliate Thuricola similis (Peritrichia, Vaginicolidae) provides new insights into the evolutionary relationships among Oligohymenophorea subclasses. Molecular Phylogenetics and Evolution 158: 107089. https://doi.org/10.1016/j.ympev.2021.107089

Liu RY (2008) Checklist of marine biota of China seas. China Science Press, Beijing, 1267 pp.

Marinho TA, Arruda EP (2021) Shell-specific differentiation: How geometric morphometrics can add to knowledge of Macominae species (Tellinidae, Bivalvia). Marine Biodiversity 51(2): 40. https://doi.org/10.1007/s12526-021-01176-x

McKay DW, Smith SM (1979) Marine Mollusca of East Saotland. Royal Scottish Museum, Edinburgh, 185 pp.

Min DK, Lee JS, Koh DB, Je JG (2004) Mollusks in Korea. Min Molluscan Research Institute, Korea, 566 pp.

Minh BQ, Schmidt HA, Chernomor O, Schrempf D, Woodhams MD, von Haeseler A, Lanfear R (2020) IQ-TREE 2: New Models and Efficient Methods for Phylogenetic Inference in the Genomic Era. Molecular Biology and Evolution 37(5): 1530–1534. https://doi.org/10.1093/molbev/msaa015

Okutani T (2000) Marine mollusks in Japan. Takai University Press, Tokyo, Japan, 1375 pp.

Pons J, Barraclough T, Gómez-Zurita J, Cardoso A, Duran D, Hazell S, Kamoun S, Sumlin W, Vogler A (2006) Sequence-Based Species Delimitation for the DNA Taxonomy of Undescribed Insects. Systematic Biology 55(4): 595–609. https://doi.org/10.1080/10635150600852011

Poppe G (2011) Philippine Marine Mollusks, Vol. IV: Bivalvia 2, Scaphopoda, Polyplacophora, Cephalopoda. Conchbooks, Czech Republic, 1375 pp.

Puillandre N, Lambert A, Brouillet S, Achaz G (2012) ABGD, Automatic Barcode Gap Discovery for primary species delimitation. Molecular Ecology 21(8): 1864–1877. https://doi.org/10.1111/j.1365-294X.2011.05239.x

Ronquist F, Teslenko M, van der Mark P, Ayres DL, Darling A, Höhna S, Larget B, Liu L, Suchard MA, Huelsenbeck JP (2012) MrBayes 3.2: Efficient Bayesian phylogenetic inference and model choice

across a large model space. Systematic Biology 61(3): 539–542. https://doi.org/10.1093/sysbio/sys029

Saeedi H, Costello MJ, von Cosel R (2013) First report of anterior pallial tentacles in *Solen dactylus* (Bivalvia: Solenidae) from the Northern Persian Gulf, Iran. PLoS ONE 8(5): e63487. https://doi.org/10.1371/journal.pone.0063487

Schneider CA, Rasband WS, Eliceiri KW (2012) NIH Image to ImageJ: 25 years of image analysis. Nature Methods 9(7): 671–675. https://doi.org/10.1038/nmeth.2089

Schumacher CF (1817) Essai d'un nouveau système des habitations des vers testacés. Schultz, Copenghagen, Denmark, 288 pp. https://doi.org/10.5962/bhl.title.35863

Serb JM, Alejandrino A, Otárola-Castillo E, Adams DC (2011) Morphological convergence of shell shape in distantly related scallop species (Mollusca: Pectinidae). Zoological Journal of the Linnean Society 163(2): 571–584. https://doi.org/10.1111/j.1096-3642.2011.00707.x

Sherratt E, Alejandrino A, Kraemer AC, Serb JM, Adams DC (2016) Trends in the sand: Directional evolution in the shell shape of recessing scallops (Bivalvia: Pectinidae). Evolution; International Journal of Organic Evolution 70(9): 2061–2073. https://doi.org/10.1111/evo.12995

Sørensen CG, Rauch C, Pola M, Malaquias MAE (2020) Integrative taxonomy reveals a cryptic species of the nudibranch genus *Polycera* (Polyceridae) in European waters. Journal of the Marine Biological Association of the United Kingdom 100(5): 733–752. https://doi.org/10.1017/S0025315420000612

Sun P, Clamp J, Xu D, Huang B, Shin MK (2016) An integrative approach to phylogeny reveals patterns of environmental distribution and novel evolutionary relationships in a major group of ciliates. Scientific Reports 6(1): 21695. https://doi.org/10.1038/srep21695

Swennen C, Moolenbeek R, Ruttanadakul N, Hobbelink H, Dekker H, Hajisamae S (2001) The Molluscs of the southern Gulf of Thailand. Vol. 4, The Biodiversity Research and Training Program, Bangkok, Thailand, 210 pp.

Taylor JD, Williams ST, Glover EA, Dyal P (2007) A molecular phylogeny of heterodont bivalves (Mollusca: Bivalvia: Heterodonta): new analyses of 18S and 28S rRNA genes. Zoologica Scripta 36(6): 587–606. https://doi.org/10.1111/j.1463-6409.2007.00299.x

Thach NN (2005) Shells of Vietnam. Conchbooks, Hackenheim, Germany, 338 pp.

Thach NN (2007) Recently collected shells of Vietnam. L'Informatore Piceno and N.N.T, Ancona, Italy, 384 pp.

Thiele J (1992) Handbook of systematic malacology pts 3–4. Smithsonian Institution Libraries: National Science Foundation, 1396 pp.

Vaidya G, Lohman DJ, Meier R (2011) SequenceMatrix: Concatenation software for the fast assembly of multi-gene datasets with character set and codon information. Cladistics 27(2): 171–180. https://doi.org/10.1111/j.1096-0031.2010.00329.x

Vences M, Aurélien M, Brouillet S, Ducasse J, Fedosov A, Kharchev V, Kostadinov I, Kumari S, Patmanidis S, Scherz M, Puillandre N, Renner S (2021) iTaxoTools 0.1: Kickstarting a specimen-based software toolkit for taxonomists. Megataxa 6(2): 77–92. https://doi.org/10.11646/megataxa.6.2.1

Whiting MF, Carpenter JC, Wheeler QD, Wheeler WC (1997) The Strepsiptera problem: Phylogeny of the holometabolous insect orders inferred from 18S and 28S ribosomal DNA sequences and morphology. Systematic Biology 46(1): 1–68. https://doi.org/10.1093/sysbio/46.1.1

Wu R, Wang J, Su Y, Zheng J, Chen X (2008) The polymorphism of genomic DNA in three species of razor shell. Journal of Xiamen University (Natural Science) 47(5): 739–742. https://jxmu.xmu.edu.cn/#/digest?ArticleID=793

Xiong B, Kocher TD (1991) Comparison of mitochondrial DNA sequences of seven morphospecies of black flies (Diptera: Simuliidae). Genome 34(2): 306–311. https://doi.org/10.1139/g91-050

Xu F, Zhang S (2008) An illustrated Bivalvia Mollusca fauna of China Seas. Science Press, Beijing, China, 336 pp.

Xu J, Xu G, Xu X, Yan B, Zhou H (2013) Analysis of Nutritional Composition of Edible Parts of *Cultellus attenuatus* Dunker. Shipin Kexue 34(17): 263–267. https://doi.org/10.7506/spkx1002-6630-201317056

Yu Z, Li Q, Kong L (2016) New insight into the phylogeny of *Sinonovacula* (Bivalvia: Solecurtidae) revealed by comprehensive DNA barcoding analyses of two mitochondrial genes. Mitochondrial DNA 27(2): 1554–1557. https://doi.org/10.3109/19401736.2014.953135

Yuan Y, Li Q, Yu H, Kong L (2012) The complete mitochondrial genomes of six heterodont bivalves (Tellinoidea and Solenoidea): Variable gene arrangements and phylogenetic implications. PLoS ONE 7(2): e32353. https://doi.org/10.1371/journal.pone.0032353

Zeng G, Fang J, Jia S, Zhang Y, Chen C, Zheng Y, Yu J (2010) Biochemical Genetic Analysis of Eight Isozymes in Intra-populations of Razor Clam *Cultellus attenuatus.* Fisheries Science 29(11): 669–673.

Zhang J, Kapli P, Pavlidis P, Stamatakis A (2013) A general species delimitation method with applications to phylogenetic placements. Bioinformatics (Oxford, England) 29(22): 2869–2876. https://doi.org/10.1093/bioinformatics/btt499

Zhang J, Wei P, Zhang S (2018a) A new species of *Calliostoma* (Gastropoda: Calliostomatidae) from Weizhou Island, South China Sea. The Nautilus 132(2): 58–64. https://doi.org/10.11646/zootaxa.4457.1.8

Zhang J, Yurchenko O, Lutaenko K, Kalachev A, Nekhaev I, Aguilar R, Zhan Z, Ogburn M (2018b) A tale of two soft-shell clams: An integrative taxonomic analysis confirms *Mya japonica* as a valid species distinct from *Mya arenaria* (Bivalvia: Myidae). Zoological Journal of the Linnean Society 184(3): 605–622. https://doi.org/10.1093/zoolinnean/zlx107

Zhang S, Liao M, Wang Y, Kong M, Li BIN (2020) Morphological and molecular evidence of a new species of *Melanochlamys* (Gastropoda: Heterobranchia) from the Bohai Sea, China. Zootaxa 4861(3): 399–410. https://doi.org/10.11646/zootaxa.4861.3.6

Supplementary material 1

Additional information

Authors: Yanan Yu, Yingyi Jiao, Junlong Zhang
Data type: docx
Explanation note: **table S1.** List of species and GenBank accession numbers of sequences used in the present study. **table S2.** Pairwise comparisons of the p-genetic distances based on COI sequences.

Link: https://doi.org/10.3897/zse.100.113972.suppl1

Zoosyst. Evol. 100 (2) 2024, 437–445 | DOI 10.3897/zse.100.114482

PENSOFT

MUSEUM FÜR NATURKUNDE BERLIN

Description of a new marine flatworm of *Prosthiostomum* (Platyhelminthes, Polycladida, Prosthiostomidae) from the South China Sea

Hai-Long Liu[1,2], Da-Hao Lin[1], An-Tai Wang[1], Zhang-Li Hu[1], Yu Zhang[1]

1 *Shenzhen Key Laboratory of Marine Bioresource and Eco-environmental Science, Guangdong Engineering Research Center for Marine Algal Biotechnology, College of Life Sciences and Oceanography, Shenzhen University, Shenzhen, China*

2 *Key Laboratory of Optoelectronic Devices and Systems of Ministry of Education and Guangdong Province, College of Physics and Optoelectronic Engineering, Shenzhen University, Shenzhen, China*

https://zoobank.org/47BB271B-27F7-48E6-A94B-C516DAEE2B53

Corresponding author: Yu Zhang (biozy@szu.edu.cn)

Academic editor: Pavel Stoev ♦ **Received** 22 October 2023 ♦ **Accepted** 14 March 2024 ♦ **Published** 12 April 2024

Abstract

A new species of the polyclad genus *Prosthiostomum* is described from the intertidal zone of the South China Sea, Huidong, China, based on morphological and molecular analyses. *Prosthiostomum huidongense* **sp. nov.** is characterized by i) few marginal eyes scattered between the marginal band and the cerebral eyes; ii) sucker located at two-thirds of the body length, being removed from the female gonopore by twice the distance between the male and female gonopores; iii) shallow male atrium with slightly ruffled inner wall, positioned approximately perpendicular to the body wall. Molecular phylogenetic analyses based on 28S rDNA sequence showed that the new species was nested in a clade composed of *Prosthiostomum* species. The uncorrected p-distance of COI between *P. huidongense* **sp. nov.** and other *Prosthiostomum* species ranged from 20.3 to 24.3%, and the high genetic divergence further supports *P. huidongense* as a new species.

Key Words

Cotylea, genetic distance, molecular phylogeny, morphology, taxonomy

Introduction

Polyclads are free-living, almost exclusively marine flatworms with an extremely ramified intestine. They inhabit a variety of environments ranging from the intertidal zone to the deep-sea, such as rocky shores, sand/mud flats, coral reefs, and deep-sea hydrothermal vents (Newman and Cannon 2003; Wolff 2005; Quiroga et al. 2006). Polyclads are important predators in hard bottom environments (Rawlinson et al. 2011), and prey on crustaceans, ascidians, cnidarians, gastropods, and bivalves (Jennings 1957; Newman and Cannon 2003; Lee 2006; Barton et al. 2020; Teng et al. 2022). Some species feed on scallops and oysters (Newman et al. 1993; Heasman et al. 1998; Gutiérrez et al. 2023), damaging commercial shellfish farming (Sluys et al. 2005).

About 1000 species of Polycladida have been described worldwide; they are classified into two suborders, namely Cotylea and Acotylea, on the basis of the presence or absence of a ventral sucker (Faubel 1983, 1984; Prudhoe 1985). The cotylean polyclad genus *Prosthiostomum* Quatrefages, 1845 includes the largest number of species in the family Prosthiostomidae Lang, 1884. It currently contains 54 species distributed worldwide (Tsuyuki et al. 2019, 2021), which are characterized by i) a pair of free prostatic vesicles without a muscular envelope, ii) a main intestine accompanied by a frontal branch, and iii) a penis armed with a pointed tubular stylet (Faubel 1984). To date, four species of *Prosthiostomum* have been reported from Hong Kong and Taiwan, China: *P. obscurum* Stimpson, 1855, *P. grande* Stimpson, 1857, *P. tenebrosum*

Stimpson, 1857 and *P. formosum* Kato, 1943. Stimpson's original descriptions were simple and incomplete, lacking illustrations. With the exception of *P. grande*, the above-mentioned three species have never been recorded again, and Stimpson's materials were destroyed during the Great Chicago Fire in 1871 (see Tsuyuki et al. 2021). Therefore, these species remain questionable and cannot be reidentified (cf. Lang 1884). In the last 80 years, since Kato's (1943) research, species of *Prosthiostomum* have not been reported from Chinese waters. In this paper, we describe a new species of *Prosthiostomum* from the coast of the South China Sea based on morphological and molecular data. We selected 28S rDNA for a phylogenetic analysis, considering the fact that this sequence is available for most species of prosthiostomids.

Materials and methods

Sample collection and morphological studies

Three specimens were collected under rocks at the intertidal zone in Huidong, Guangdong Province, China (Fig. 1). The worms were measured and then photographed alive with a digital camera. Two specimens were fixed for histological examination following the method modified from Newman and Cannon's (1995), in which i) worms are placed onto filter paper, which is then placed onto frozen 10% formalin seawater, ii) an additional fixative is added to just cover the worm, then worms are smoothened with a soft brush to ensure they are fixed flat. For histological examination, specimens were dehydrated in an ethanol series and cleared in xylene, thereafter, embedded in paraffin wax. Serial sections were cut at intervals of 7 µm and were stained with modified Cason's Mallory-Heidenhain stain solution (see Yang et al. 2020). One specimen was fixed in 95% ethanol for DNA extraction. Histological preparations are deposited at the Marine Biological Museum, Chinese Academy of Sciences (**MBMCAS**), Qingdao, China.

Molecular analyses

Total DNA was extracted using a DNeasy Blood & Tissue Kit (Qiagen, Germany). Three markers (partial nuclear 28S rDNA, mitochondrial 16S rRNA, and cytochrome c oxidase subunit I (COI) sequences) were amplified by polymerase chain reaction (PCR). The PCR was carried out using the primers: Acotylea_COI_F and Acotylea_COI_R (Oya and Kajihara 2017) for COI; 16sar-L and 16sbr-H (Palumbi et al. 2002) for 16S; LSU5 and LSU3 (Littlewood 1994) for 28S. Thermal cycling was initiated with 3 min at 94 °C, followed by 35 cycles of denaturation at 94 °C for 45 s, annealing at 50 °C (COI) or 49 °C (16S) or 52 °C (28S) for 45 s, and extension at 72 °C for 1 min. The cycling ended with a 7-min sequence extension at 72 °C. All amplified

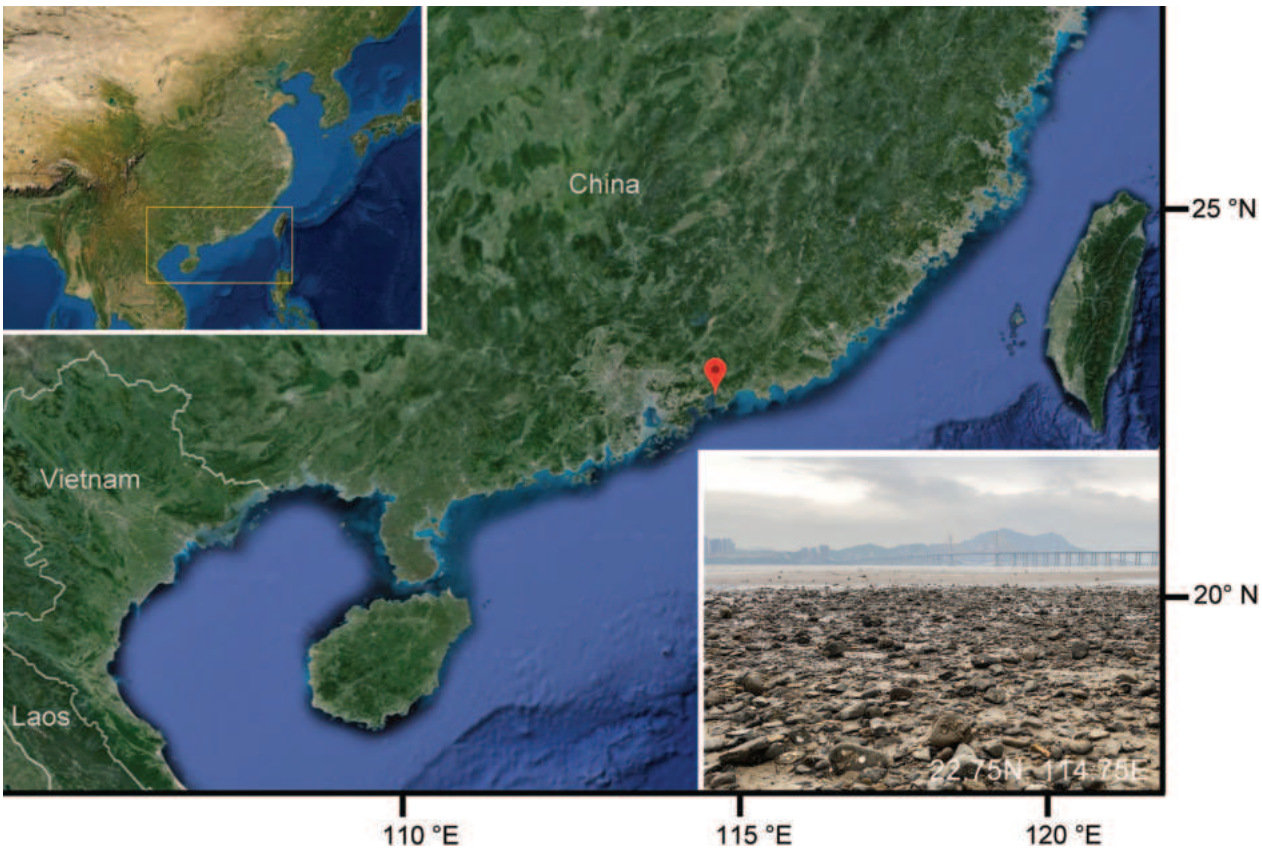

Figure 1. Map showing the sampling site of *Prosthiostomum huidongense* sp. nov. and photograph of the habitat.

products were purified using QIA-quick gel purification kit (Qiagen) and sequenced at BGI (Shenzhen, China), by means of double-stranded Sanger sequencing to verify accuracy. Sequences were checked and edited using SeqMan software (DNAStar Inc.). All the new sequences were submitted to GenBank.

A total of 27 sequences of 28S rDNA of prosthiostomid species were used for molecular analyses; *Pseudobiceros stellae* Newman & Cannon, 1994 was selected as outgroup (Suppl. material 1: table S1). Alignments were performed with MAFFT ver. 7 (Katoh and Standley 2013) using the Auto strategy. Ambiguous regions were removed with the web version of Gblocks ver 0.91b using default parameters (Castresana 2000). The Maximum likelihood (ML) analysis was performed at the CIPRES Science Gateway web with RAxML (Stamatakis 2014) on XSEDE, in which 1000 rapid bootstrap replicates and the GTRGAMMA model were used to evaluate and optimize the likelihood of the final tree. Bayesian inference (BI) was performed using MrBayes ver 3.2.2 (Ronquist et al. 2012), and the substitution model (GTR + G + I) was selected by MrModeltest ver 2.3 (Nylander 2004) according to the Akaike information criterion. MrBayes was run for 10 million generations with a tree being sampled every 1000 generations, with two parallel runs and four independent Markov chains per run and with the first 25% of trees discarded as burn-in. The standard deviation of the split frequencies (<0.01) was used as the criterion to validate the convergence of the analysis. In addition, we determined cytochrome c oxidase subunit I (COI) sequences for DNA barcoding. COI sequences of the *Prosthiostomum* species currently available from the GenBank were used for the genetic distances analysis (Suppl. material 1: table S1). Uncorrected p-distances of COI were calculated in MEGA ver 10 (Kumar et al. 2018). Voucher specimens of the material that was analyzed molecularly have been deposited at the Shenzhen Key Laboratory of Marine Bioresource and Eco-environmental Science.

Results

Family Prosthiostomidae Lang, 1884
Genus *Prosthiostomum* Quatrefages, 1845

Prosthiostomum huidongense Liu, sp. nov.

https://zoobank.org/9A6C8F9B-5664-4D50-806A-A50A4E4D119E

Material examined. ***Holotype*:** MBM287880, Huidong, 22°44.95'N, 114°45.05'E, Guangdong Province, China; under rocks at the intertidal zone, 21 April 2023, coll. Hai-Long Liu; sagittal sections on 10 slides, deposited at MBMCAS. ***Paratypes*:** MBM287881, sagittal sections on 11 slides, same data as for holotype. Molecular voucher specimens: 20230421A1, material of the following GenBank accession numbers have been deposited at the Shenzhen Key Laboratory of Marine Bioresource and Eco-environmental Science, GenBank: OR680085 (COI), OR680128 (16S), and OR680129 (28S). Collection data are the same as for the holotype and paratype.

Diagnosis. Body oval-elongated; dorsal surface cream-colored with numerous yellowish-brown maculae; a pair of cerebral eyes clusters forming an approximately inverted "V" shape; band of marginal eyes extending backwards to behind brain, few eyes scattered between the marginal band and the cerebral eyes; a pair of prostatic vesicles distinctly separated; male atrium shallow, inner wall slightly ruffled; sucker located at two-thirds of body length, removed from the female gonopore by twice the distance between the male and female gonopores.

Description. Body oval-elongated with rounded ends, 10.8–12.1 mm long and 5.6–7.0 mm wide at its widest in living state (n = 3) (Fig. 2A). Tentacles absent. Dorsal surface smooth, cream-colored, uniformly covered with numerous yellowish-brown maculae, pharynx slightly bulging (Fig. 2A). Ventral surface translucent, without color pattern. Cerebral region without pigmentation and provided with a pair of clusters of cerebral eyes, located at approximately 1 mm behind the anterior margin, each cluster comprising 15–20 eyes (Fig. 2B, C). About 140 marginal eyes irregularly scattered along the anterior body margin, extending backwards to a level just behind the brain; few eyes scattered between the marginal band and the cerebral eyes (Fig. 2B, C). Ventral eyes not observed. Frontal branch of the main intestine extending anteriorly to the brain (Fig. 3B). Tubular pharynx in a pharyngeal pocket, positioned in the anterior half of the body. Mouth opening ventrally, located shortly behind the brain (Fig. 3B). Male and female gonopores closely set at the body center, distance between male and female gonopores being 0.6–0.8 mm; sucker situated 1.4–1.8 mm posterior to the female gonopore, twice distance between the male and female gonopores (Fig. 3A, E). Male copulatory apparatus comprising a large seminal vesicle, a pair of prostatic vesicles, and an armed penis papilla, located immediately posterior to the pharyngeal pocket (Fig. 3A, C, E). A pair of spherical prostatic vesicles (0.05–0.07 mm in diameter) with a thin muscular wall (0.009–0.012 mm thick), located at both sides of the ejaculatory duct (Fig. 3A, D). Seminal vesicle oval, about 0.2 mm in diameter, with a muscular wall about 0.04 mm thick (Fig. 3A, E). Spermiducal vesicle separately open into the anterior portion of the seminal vesicle (Fig. 3A, D). Penis papilla armed with pointed tubular stylet (0.14–0.17 mm in length), enclosed in penis pouch, protruding into male atrium (Fig. 3C). Shallow male atrium with slightly ruffled inner wall, positioned approximately perpendicular to the body wall (Fig. 3A, E). Female reproductive system consisting of vagina, cement pouches, and uteri. Vagina short about 0.1 mm long, lined with a ciliated epithelium; the dorsal portion of the vagina enlarged and anteriorly curved, connecting to the uteri (Fig. 3A, E). Cement glands numerous, concentrated around the vagina (Fig. 3A, E). Pair of oviducts converging before joining proximal end of vagina. Ovaries not discerned.

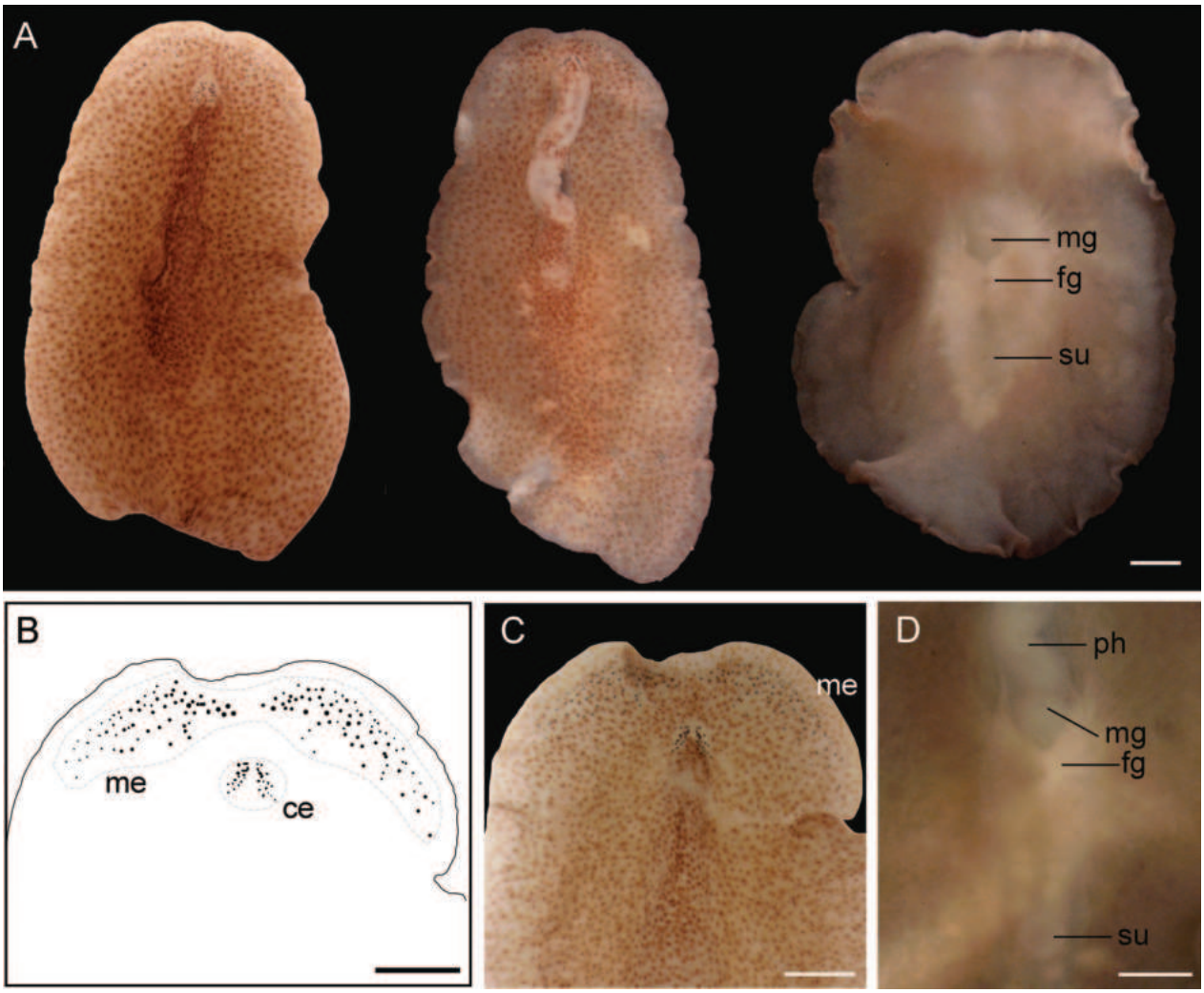

Figure 2. *Prosthiostomum huidongense* sp. nov. **A.** Photograph of entire body, 20230421A1 (left, living specimen in dorsal view), MBM287881 (middle, preserved specimen in dorsal view, paratype), MBM287880 (right, preserved specimen in ventral view, holotype); **B.** Schematic diagram of head, showing arrangement of the eyes; **C.** Magnification of head, dorsal view (holotype); **D.** Magnification of genital pore and sucker (paratype). Abbreviations: **fg** – female gonopore; **mg** – male gonopore; **ph** – pharynx; **su** – sucker. Scale bars: 1 mm.

Etymology. The name of the new species is originated from the name of Huidong City, Guangdong Province, China.

Distribution. So far only known from Huidong, Guangdong, China.

Habitat. Intertidal, under rocks.

Molecular phylogeny and genetic distances. The BI and ML trees based on the partial 28S sequences (904 bp) are almost identical in their general topology, and we show only the ML tree (Fig. 4). In the phylogenetic tree, all *Prosthiostomum* species form a clade with high support values (BP = 81%, PP = 1). *Prosthiostomum huidongense* sp. nov. is sister to the clade formed by all other species of the genus, excluding *P. lobatum*, with high support values (BP = 78%, PP = 1). The uncorrected p-distances of the partial COI sequences (658 bp) of the 11 *Prosthiostomum* species/molecular entities is 5.7–24.3% (Suppl. material 1: table S2).

Discussion

Our specimens are characterized by i) a median frontal branch of the main intestine, ii) a pair of prostatic vesicles that are distinctly separated, and iii) a penis armed with a pointed tubular stylet, features consistent with the generic diagnosis of the genus *Prosthiostomum* as proposed by Faubel (1984). The new species is easily distinguished from the four species reported from China (*P. obscurum*, *P. tenebrosum*, *P. grande*, and *P. formosum*) by the dorsal coloration and arrangement of the eyes. Among these species, *P. obscurum* is pale reddish-brown with red spots, a light-colored middle band and a pair of linear clusters of cerebral eyes, each composed of 8–10 eyes; *P. tenebrosum* is dark gray or sub-black; *P. grande* has reddish-brown maculae or spots, with a darker longitudinal band in the middle; *P. formosum* is uniformly chestnut brown without any color pattern.

Table 1. Comparison of characters between nine *Prosthiostomum* species that have similar arrangement of marginal eyes or color pattern.

Species	*P. awaensa*	*P. griseum*	*P. latocelis*	*P. milcum*	*P. huidongense* sp. nov.	*P. dohrni*	*P. grande*	*P. nozakensis*	*P. sonorum*
Body size	22 mm long; 5 mm wide	4 mm long	17 mm long; 4.5 mm wide	about 7 mm long	10.8–12.1 mm long; 5.6–7.0 mm wide	25 mm long; 6 mm in wide	22 mm long; 5 mm wide	15 mm long	20 mm long; 2 mm wide
Dorsal coloration	rather deep buffy, with a brownish longitudinal band in the median line	uniform dark gray	Yellow	whitish body with brown mottles	cream-colored surface uniformly covered with numerous yellowish-brown maculae	soft bright orange yellow, with darker orange yellow spots scattered over the body especially denser along midline	buffy ground color, with numerous small spots of ochraceous color distributed all over body	light brown, with numerous dark brown spots over the whole dorsal surface	translucent white covered with brown mottles, a number of which aggregate along the median line to form a brown stripe
Cerebral eyes	two oblong clusters, each composed of 28 eyes	each cluster composed of 6–8 eyes	two wedge-shaped clusters, each composed of about 50 eyes	oblong clusters, each composed of 22–23 eyes	each cluster consisting of 15–20 eyes	two oval clusters, composed of numerous eyes	two wedge clusters, each composed of about 25 eyes	two oblong clusters, each composed of about 10 eyes	two cluster, each composed of about 30 eyes
Marginal eyes	about 60, distributed anterior to brain; few eyes scattered between the marginal band and the cerebral eyes	about 30, distributed anterior to brain; few eyes scattered between the marginal band and the cerebral eyes	about 80, distributed anterior to brain; some eyes scattered between the marginal band and the cerebral eyes	95, elongated to the half position of the brain; 25 small scattered eyes between the marginal band and the cerebral eyes	about 140, elongated to the level behind brain; few eyes scattered between the marginal band and the cerebral eyes	numerous; elongated to the level behind brain	two irregular rows along the anterior margin	about 60, elongated to the half position of the brain	about 50, distributed anterior to brain
Male atrium	NA	NA	deep; anterior wall strongly folded	deep; inner wall slightly ruffled	shallow; inner wall slightly ruffled	NA	NA	NA	NA
Seminal vesicle	NA	NA	oval; lumen oval	elongated oval; lumen narrow	spherical or oval; lumen spherical or oval	NA	spherical; lumen shape unknown	oval; lumen oval	oval; lumen oval
Sucker	nearly central	located slightly behind body center	nearly central; distance between the female gonopore and the sucker similar to the distance between the female gonopore and the male gonopore	nearly central; distance between the female gonopore and the sucker similar to the distance between the female gonopore and the male gonopore	located at the two-thirds of body; distance between the female gonopore and the sucker twice the distance between the female gonopore and the male gonopore	present; details not described	located slightly behind body center	nearly central	nearly central; distance between the female gonopore and the sucker similar to the distance between the female gonopore and the male gonopore
Distribution	Shirahama, Amakusa, Japan	Parry Island, USA	California, USA	Bonaire, Netherlands; Florida, USA	Huidong, China	Naples, Italy	Noto, Misaki, Shimoda, Shirahama, Amakusa, Amami Oushima, Japan	Nozaki, Noto, Japan	Tomoe-zaki, Amakusa, Japan
Reference	Yeri and Kaburaki 1918	Hyman 1959	Hyman 1953	Marcus and Marcus 1968	this study	Lang (1884)	Stimpson (1857); Yeri and Kaburaki (1918); Tsuyuki et al. 2021	Kato 1944	Kato 1938

NA: not available from reference.

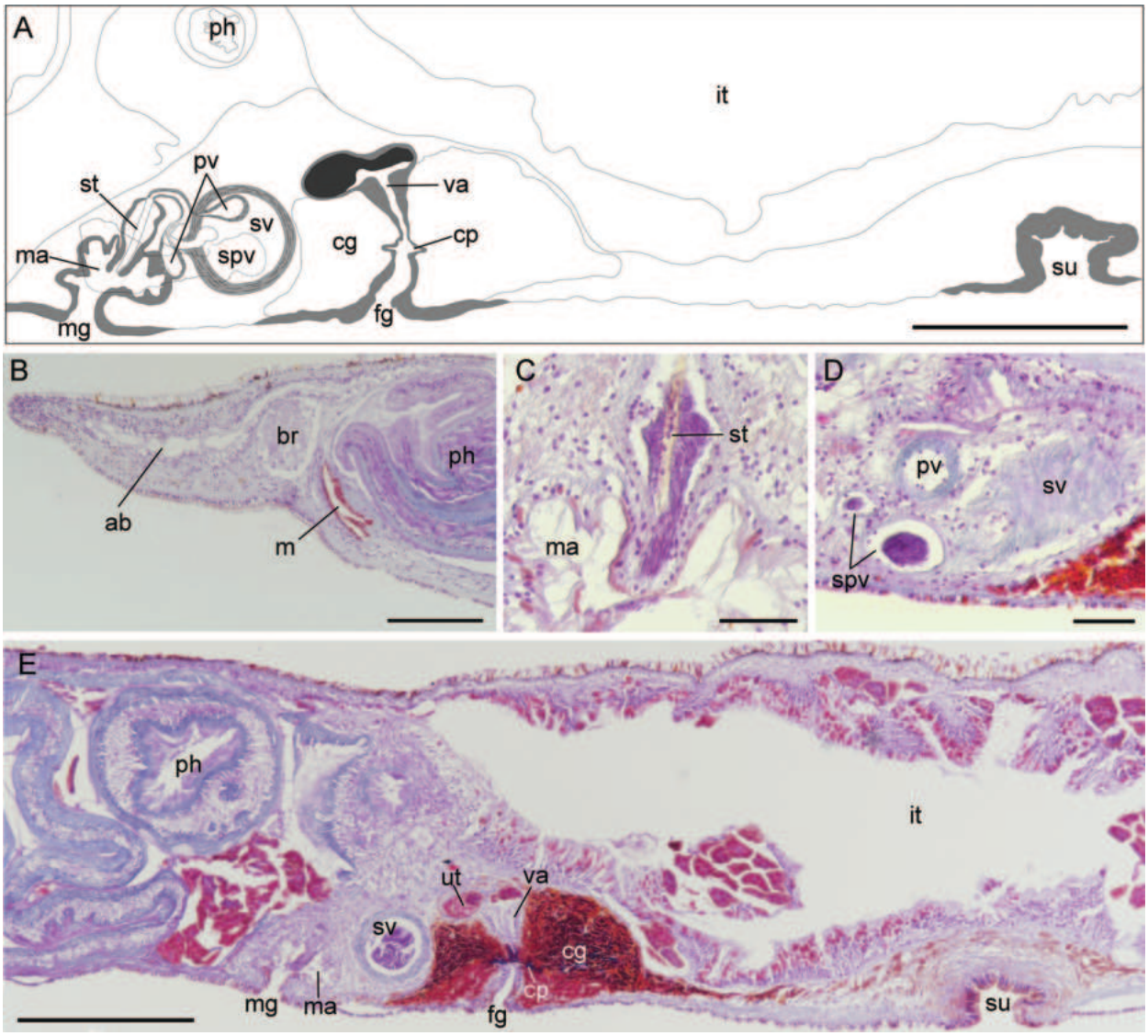

Figure 3. *Prosthiostomum huidongense* sp. nov., MBM287880 (holotype), schematic diagram (**A**) and photomicrographs of sagittal sections (**B–E**), anterior to the left. **A.** Copulatory complex and sucker; **B.** Anterior end of the body; **C.** Penis stylet; **D.** Male copulatory apparatus; **E.** Copulatory complex and sucker. Abbreviations: **ab** – anterior branch of main intestine; **br** – brain; **cg** – cement glands; **cp** – cement pouch; **fg** – female gonopore; **it** – intestine; **m** – mouths; **ma** – male atrium; **mg** – male gonopore; **ph** – pharynx; **pv** – prostatic vesicle; **spv** – spermiducal vesicle; **st** – stylet; **su** – sucker; **sv** – seminal vesicle; **va** – vagina; **ut** – uterus. Scale bars: 0.5 mm (**A, E**); 200 μm (**B**); 50 μm (**C, D**).

The new species has few eyes scattered between the marginal band and the cerebral eyes and thus can be easily distinguished from most congeners. Only five known species have been described with the above characteristics: *P. awaensa* Yeri & Kaburaki, 1918, *P. griseum* Hyman, 1959, *P. latocelis* Hyman, 1953, *P. milcum* Marcus & Marcus, 1968, and *P. notoensis* Kato, 1944. However, these species can be easily distinguished from the new species by the dorsal coloration or pigmentation pattern (except *P. milcum*) and the number of the marginal eyes (see Table 1). In addition, *P. awaensa*, *P. griseum*, and *P. latocelis* are also different from *P. huidongense* sp. nov. in the position of the band of marginal eyes (distributed anterior to the brain for these species; extending to the level of the posterior margin of the brain in *P. huidongense* sp. nov.). Although the dorsal coloration or pigmentation pattern of *P. milcum* is similar to that of the new species, it differs from *P. huidongense* sp. nov. by the deep male atrium and the distance between the female gonopore and sucker (Table 1). *Prosthiostomum sonorum* Kato, 1938, *P. dohrnii* Lang, 1884, *P. nozakensis* Kato, 1944, and *P. grande* also have yellow to brown mottles or spots on the dorsal surface, but they are different from *P. huidongense* sp. nov. in the arrangement of the eyes (Table 1). In general, identification of *Prosthiostomum* species is mainly achieved by features such as body size, dorsal color and pattern, eye arrangement and characteristics of the male and female reproductive system. Apart from that, the distance between the female gonopore and the sucker may be a noteworthy taxonomic feature within the genus, as in species *P. latocelis*, *P. milcum* and

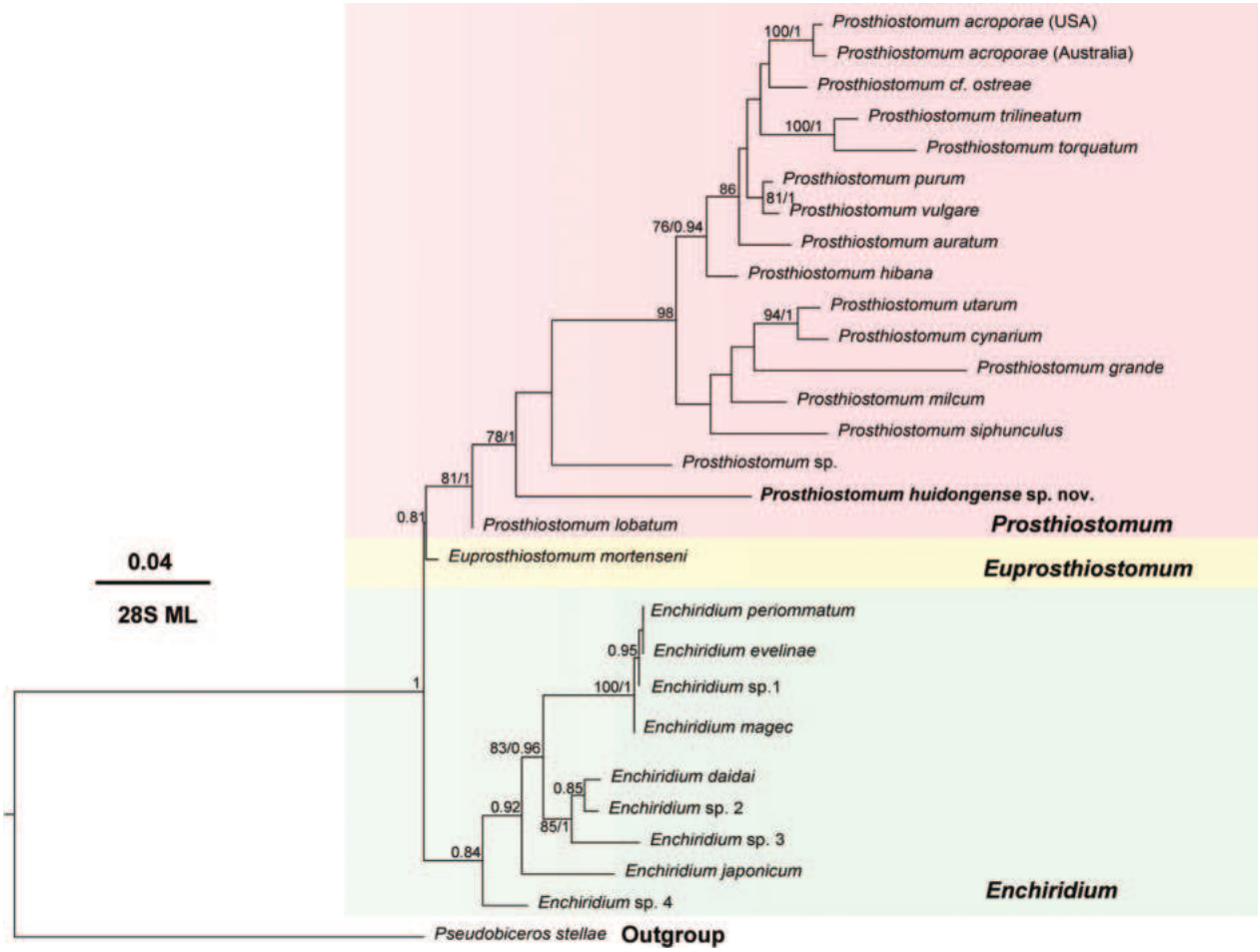

Figure 4. Maximum likelihood phylogenetic tree of species of the family Prosthiostomidae based on 28S rDNA. For clades that received either ≥70% ML bootstrap or ≥0.80 BI posterior probability, the support values are presented at the nodes.

P. sonorum this distance differs from that in the new species (see Table 1).

Our molecular phylogenetic analysis of Prosthiostomidae based on partial 28S rDNA is largely consistent with that of Tsuyuki et al. (2021), in which the genera *Prosthiostomum* and *Enchiridium* form well-supported taxa. Although some *Enchiridium* species (e.g., *E. evelinae*, *E. japonicum* and *E. punctatum*) have similar dorsal patterns to that of *P. huidongense* sp. nov., they can be easily distinguished from the new species by lacking a muscular sheath that completely encloses the prostatic vesicles. This feature distinguishing these two genera is further corroborated by the molecular phylogenetic tree. *Euprosthiostomum mortenseni* Marcus, 1948 is sister to the *Prosthiostomum* clade, with poor support (Fig. 4). According to Faubel (1984), absence of the frontal branch of the main intestine in *Euprosthiostomum* distinguishes this genus morphologically from *Prosthiostomum*, but whether that character can be reliably used to discriminate the genus has not been clarified in the present study due to the limited number of available sequences (only one sequence available for *Euprosthiostomum*).

Prosthiostomum huidongense sp. nov. is nested in the clade *Prosthiostomum*, thus corroborates our generic assignment based on the morphology. Uncorrected p-distance of COI among 11 species/molecular entities of *Prosthiostomum* are 5.7–24.3% (Suppl. material 1: table S2), while the average interspecific distance is 19% among these Prosthiostomum species that are morphologically distinguishable from each other. The uncorrected p-distance between *P. huidongense* sp. nov. and other tested species ranged from 20.3 to 24.3%, which is greater than the average interspecific distance among *Prosthiostomum* species, thus, provided further support for the notion that *P. huidongense* is a new species.

Acknowledgements

This study was supported by grants from the Scientific and Technical Innovation Council of Shenzhen Government (grant nos. jcyj20210324093412035 and kcxfz20201221173404012), Innovation Team Project of Universities in Guangdong Province (No. 2023KCXTD028) and China Undergraduate Training Program for Innovation and Entrepreneurship (S202310590068). We sincerely thank Prof. Ronald Sluys (Naturalis Biodiversity Center, P. O. Box 9517, 2300 RA Leiden, The Netherlands) for providing valuable comments on this work.

References

Barton JA, Bourne DG, Humphrey C, Hutson KS (2020) Parasites and coral-associated invertebrates that impact coral health. Reviews in Aquaculture 12(4): 2284–2303. https://doi.org/10.1111/raq.12434

Castresana J (2000) Selection of conserved blocks from multiple alignments for their use in phylogenetic analysis. Molecular Biology and Evolution 17(4): 540–552. https://doi.org/10.1093/oxfordjournals.molbev.a026334

Faubel A (1983) The Polycladida, Turbellaria. Proposal and establishment of a new system. Part I. The Acotylea. Mitteilungen aus dem Hamburgischen Zoologischen Museum und Institut 80: 17–121.

Faubel A (1984) The Polycladida, Turbellaria; Proposal and establishment of a new system. Part II. The Cotylea. Mitteilungen aus dem Hamburgischen Zoologischen Museum und Institut 81: 189–259.

Gutiérrez A, Auby I, Gouillieux B, Daffe G, Massé C, Antajan E, Noreña C (2023) A new polyclad flatworm, *Idiostylochus tortuosus* gen. nov., sp. nov. (Platyhelminthes, Polycladida) from France. Can this foreign flatworm be responsible for the deterioration of oyster and mussel farms? Zoological Studies (Taipei, Taiwan) 62: 15. https://doi.org/10.6620/ZS.2023.62-15

Heasman MP, O'Connor WA, O'Connor SJ, Walker WW (1998) Enhancement and farming of scallops in NSW using hatchery produced seedstock. NSW Fisheries Final Report Series Report No 8.

Hyman LH (1953) The polyclad flatworms of the Pacific coast of North America. Bulletin of the American Museum of Natural History 100: 269–391.

Hyman LH (1959) A further study of Micronesian polyclad flatworms. Proceedings of the United States National Museum 108(3410): 543–597. https://doi.org/10.5479/si.00963801.108-3410.543

Jennings JB (1957) Studies on feeding, digestion, and food storage in free-living flatworms (Platyhelminthes: Turbellaria). The Biological Bulletin 112(1): 63–80. https://doi.org/10.2307/1538879

Kato K (1943) Polyclads from Formosa. Nihon Seibutsu Chiri Gakkai Kaiho 13: 69–77.

Katoh K, Standley DM (2013) MAFFT multiple sequence alignment software version 7: Improvements in performance and usability. Molecular Biology and Evolution 30(4): 772–780. https://doi.org/10.1093/molbev/mst010

Kumar S, Stecher G, Li M, Knyaz C, Tamura K (2018) MEGA X: Molecular evolutionary genetics analysis across computing platforms. Molecular Biology and Evolution 35(6): 1547–1549. https://doi.org/10.1093/molbev/msy096

Lang A (1884) Die Polycladen (Seeplanarien) des Golfes von Neapel und der angrenzenden Meeresabschnitte. Eine Monographie. Engelmann W, Leipzig, 688 pp. https://doi.org/10.5962/bhl.title.10545

Lee KM (2006) Taxonomy and ecology of predatory marine flatworms (Platyhelminthes: Polycladida) in Botany Bay, New South Wales, Australia. PhD Thesis, University of New South Wales, Australia. https://doi.org/10.1080/00222930500485263

Littlewood DTJ (1994) Molecular phylogenetics of cupped oysters based on partial 28S rRNA gene sequences. Molecular Phylogenetics and Evolution 3(3): 221–229. https://doi.org/10.1006/mpev.1994.1024

Marcus E (1948) Turbellaria do Brasil. Boletins da Faculdade de Filosofia Cienciase Letras. Universidade de Sao Paulo Zoologia 13: 111–243. https://doi.org/10.11606/issn.2526-4877.bsffclzoologia.1948.125311

Marcus E, Marcus E (1968) Polycladida from Curaçao and faunistically related regions. Studies on the Fauna of Curaçao and other Caribbean Islands 101: 1–133.

Newman LJ, Cannon LRG (1995) Colour pattern variation in the tropical flatworm, Pseudoceros (Platyhelminthes: Polycladida), with descriptions of three new species. The Raffles Bulletin of Zoology 43(2): 435–446.

Newman LJ, Cannon LRG (2003) Marine flatworms: the world of polyclad flatworms. CSIRO Publishing, Collinwood. https://doi.org/10.1071/9780643101197

Newman LJ, Cannon LRG, Govan H (1993) *Stylochus* (*Imogene*) *matatasi* n. sp. (Platyhelminthes, Polycladida): Pest of cultured giant clams and pearl oysters from Solomon Islands. Hydrobiologia 257(3): 185–189. https://doi.org/10.1007/BF00765011

Nylander JAA (2004) MrModeltest 2.3 Uppsala University: Evolutionary Biology Centre.

Oya Y, Kajihara H (2017) Description of a new *Notocomplana* species (Platyhelminthes: Acotylea), new combination and new records of Polycladida from the northeastern Sea of Japan, with a comparison of two different barcoding markers. Zootaxa 4282(3): 526–542. https://doi.org/10.11646/zootaxa.4282.3.6

Palumbi S, Martin A, Romano S, McMillan WO, Stice L, Grabowski G (2002) The Simple Fools Guide to PCR, Ver. 2. Department of Zoology and Kewalo Marine Laboratory, University of Hawaii, Honolulu.

Prudhoe S (1985) A Monograph on Polyclad Turbellaria. Oxford University Press, Oxford, 253 pp.

Quatrefages A de (1845) Études sur les types inférieurs de l'embranchement des annelés: mé-moire sur quelques planairées marines appartenant aux genres *Tricelis* (Ehr.), *Polycelis* (Ehr.), *Prosthiostomum* (Nob.), *Proceros* (Nob.), *Eolidiceros* (Nob.), et *Stylochus* (Ehr.). Annales des Sciences Naturelles, Zoologie, 3ème Série 4: 129–184.

Quiroga SY, Bolaños DM, Litvaitis MK (2006) First description of deep-sea polyclad flatworms from the North Pacific: *Anocellidus* n. gen. *profundus* n. sp. (Anocelidae, n. fam.) and *Oligocladus voightae* n. sp. (Eurylepti dae). Zootaxa 1317(1): 1–19. https://doi.org/10.11646/zootaxa.1317.1.1

Rawlinson KA, Gillis JA, Billings Jr RE, Borneman EH (2011) Taxonomy and life history of the Acropora-eating flatworm *Amakusaplana acroporae* nov. sp. (Polycladida: Prosthiostomidae). Coral Reefs 30(3): 693–705. https://doi.org/10.1007/s00338-011-0745-3

Ronquist F, Teslenko M, van der Mark P, Ayres DL, Darling A, Höhna S, Larget B, Liu L, Suchard MA, Huelsenbeck JP (2012) MrBayes 3.2: Efficient Bayesian phylogenetic inference and model choice across a large model space. Systematic Biology 61(3): 539–542. https://doi.org/10.1093/sysbio/sys029

Sluys R, Faubel A, Rajagopal S, van der Velde G (2005) A new and alien species of 'oyster leech' (Platyhelminthes, Polycladida, Stylochidae) from the brackish North Sea Canal, The Netherlands. Helgoland Marine Research 59(4): 310–314. https://doi.org/10.1007/s10152-005-0006-3

Stamatakis A (2014) RAxML version 8: A tool for phylogenetic analysis and post-analysis of large phylogenies. Bioinformatics (Oxford, England) 30(9): 1312–1313. https://doi.org/10.1093/bioinformatics/btu033

Stimpson W (1857) Prodromus descriptionis animalium evertebratorum quae in Expeditione ad Oceanum Pacificum Septentrionalem,

Johanne Rodgers Duce a Republica Federata missa, observavit et descripsit. Pars. I. Tubellaria Dendrocoela. Proceedings. Academy of Natural Sciences of Philadelphia 9: 19–31. https://doi.org/10.5962/bhl.title.51447

Teng CJ, Su YJ, Yeh CY, Jie WB (2022) Predation of oysters using an autonomic pharynx in the oyster leech *Cryptostylochus* sp. (Polycladida: Stylochidae). Zoological Studies (Taipei, Taiwan) 61: 7. https://doi.org/10.52013/2658-7556-72-10-18

Tsuyuki A, Oya Y, Kajihara H (2019) A new species of *Prosthiostomum* (Platyhelminthes: Polycladida) from Shirahama, Japan. Species Diversity : An International Journal for Taxonomy, Systematics, Speciation, Biogeography, and Life History Research of Animals 24(2): 137–143. https://doi.org/10.12782/specdiv.24.137

Tsuyuki A, Kohtsuka H, Kajihara H (2021) Description of a new species of the marine flatworm *Prosthiostomum* (Platyhelminthes: Polycladida) and its three known congeners from Misaki, Japan, with inference of their phylogenetic positions within Prosthiostomidae. Zoological Studies (Taipei, Taiwan) 60: 29. https://doi.org/10.6620/ZS.2021.60-29

Wolff T (2005) Composition and endemism of the deep-sea hydrothermal vent fauna. Cahiers de Biologie Marine 46(2): 97–104.

Yang Y, Li JY, Sluys R, Li WX, Li SF, Wang AT (2020) Unique mating behavior, and reproductive biology of a simultaneous hermaphroditic marine flatworm (Platyhelminthes, Tricladida, Maricola). Invertebrate Biology 139(1): e12282. https://doi.org/10.1111/ivb.12282

Yeri M, Kaburaki T (1918) Description of some Japanese polyclad Turbellaria. Journal of the College of Science, Imperial University of Tokyo 39 Art. 9: 1–54.

Supplementary material 1

Supplementary information

Authors: Hai-Long Liu, Da-Hao Lin, An-Tai Wang, Zhang-Li Hu, Yu Zhang

Data type: docx

Explanation note: **table S1.** GenBank accession numbers of sequences for species taxa used in the phylogenetic analyses or genetic distance calculation; **table S2.** Interspecific uncorrected p-distances for the COI gene fragments; **figure S1.** The tree is reconstructed by Bayesian inference analyses based on the 28S rDNA.

Link: https://doi.org/10.3897/zse.100.114482.suppl1

Zoosyst. Evol. 100 (2) 2024, 447–455 | DOI 10.3897/zse.100.118686

PENSOFT

für Natur MUSEUM FÜR NATURKUNDE BERLIN

Taxonomic notes on the genus *Epeus* Peckham & Peckham, 1886 (Araneae, Salticidae) from India

Puthoor Pattammal Sudhin[1], Ramankutty Jwala[2,3], Souvik Sen[1], Vishwanath D. Hegde[2]

1 *Zoological Survey of India, Prani Vigyan Bhawan, M-Block, New Alipore, Kolkata 700053, West Bengal, India*
2 *Zoological Survey of India, Western Ghat Regional Centre, Jafferkhan Colony, Kozhikode, Kerala 673006, India*
3 *Department of Zoology, University of Calicut, Kerala 673635, India*

https://zoobank.org/EFDF9751-EB8B-4A03-8AC6-B3F3E0DE30B2

Corresponding author: Souvik Sen (sensouvik07@gmail.com)

Academic editor: Danilo Harms ♦ **Received** 12 January 2024 ♦ **Accepted** 19 March 2024 ♦ **Published** 17 April 2024

Abstract

This paper provides the re-description of *Epeus albus* Prószynski, 1992, with the first description of its male. Additionally, *Epeus chilapataensis* (Biswas & Biswas, 1992) is synonymised with *E. albus* and a new taxonomic combination is proposed: *Epeus khandalaensis* (Tikader, 1977) **comb. nov.** (ex *Phidippus*). Clarification on the record of *Epeus daiqini* Patoleta, Gardzińska & Żabka, 2020 from India is provided. The current distribution of the genus in India is also mapped.

Key Words

Jumping spiders, India, re-description, synonym, taxonomy, type material

Introduction

Members of the jumping spider genus *Epeus* Peckham & Peckham, 1886, are medium-to-large-sized spiders recorded from subtropical Himalayan valleys, through India, Indochina, southern China, Philippines and Sunda Archipelago (Patoleta et al. 2020; World Spider Catalog 2024). The living specimens of *Epeus* are usually light green or yellow in colour with palpi and legs of various colours (Sebastian and Peter 2009; Prószyński and Deeleman-Reinhold 2012; Mondal et al. 2020). Till now, the genus comprised 22 valid species, of which five have been reported from India: *Epeus albus* Prószynski, 1992; *Epeus chilapataensis* (Biswas & Biswas, 1992); *Epeus daiqini* Patoleta, Gardzińska & Żabka, 2020; *Epeus indicus* Prószyński, 1992; and *Epeus triangulopalpis* Malamel, Nafin, Sudhikumar & Sebastian, 2019 (Caleb and Sankaran 2024; World Spider Catalog 2024). The original description of *E. albus* Prószynski, 1992 was based on the female specimen collected from Orissa (now Odisha). During field surveys conducted in the Southern Western Ghats of India, we collected both male and female specimens of *Epeus albus* and this has led to the realisation that several taxa of this genus in India require re-evaluation. The paper thus aims to provide: (1) first description of the hitherto unknown male of *E. albus* and re-description of the female, based on the fresh materials; (2) update the current taxonomic status of *E. chilapataensis* and *Phidippus khandalaensis* Tikader, 1977; (3) clarify the record of *E. daiqini* Patoleta, Gardzińska & Żabka, 2020 from India; and (4) provide a distribution map of all known Indian *Epeus* spp.

Material and methods

The specimens were preserved in 70% ethanol and are deposited in the National Zoological Collections of the Zoological Survey of India (NZC-ZSI), Kolkata, India. The terminology used in the text and figures follows Patoleta et al. (2020) and leg spination follows the system used by Bosselaers and Jocqué (2000). Specimens were examined under a Leica M205A stereomicroscope and images were taken using a Flexacam C3 camera attached

to the stereomicroscope and processed using extended focus montage LAS X software. All measurements are given in millimetres (mm). Pedipalp and leg measurements are given as follows: total length [femur, patella, tibia, metatarsus (except for palp), tarsus]. The distribution map was prepared using the online mapping software SimpleMappr (Shorthouse 2010).

Abbreviations used in the text and figures are as follows: **ALE** — anterior lateral eye, **AME** — anterior median eye, **CA** — cymbial apophysis, **CD** — copulatory duct, **CO** — copulatory opening, **do** — dorsal, **E** — embolus, **EP** — epigynal pocket, **FD** — fertilisation duct, **MP** — mating plug, **pl** — prolateral, **PLE** — posterior lateral eye, **PME** — posterior median eye, **plv** — prolateral ventral, **rl** — retrolateral, **RTA** — retrolateral tibial apophysis, **rlv** — retrolateral ventral, **v** — ventral.

Taxonomy

Family Salticidae Blackwall, 1841

Genus *Epeus* Peckham & Peckham, 1886

Type species. *Epeus tener* (Simon, 1877)

Diagnosis. Species of this genus can be distinguished from other members of the tribe Plexippini by the high and elevated carapace, male palp with flattened and elongated cymbium, postero-ventrally pointing retrolateral basal apophysis, tegulum with a tongue-like basal process, filiform embolus surrounding the semicircle of tegulum and extending to the distal end of cymbium and the epigyne with a shallow anterior depression and long copulatory ducts forming several loops (Meng et al. 2015; Malamel et al. 2019).

Epeus albus Prószyński, 1992

Figs 1A–H, 2A–E, 3A–F, 4A–F, 5A–F, 7

Epeus albus Prószyński, 1992: 171, figs 20–21, 25.

Lyssomanes chilapataensis Biswas & Biswas, 1992: 386, figs 14–16. New synonymy.

Epeus chilapataensis: Logunov, 2004 (transfer from *Lyssomanes*).

Epeus daiqini Sibi, Gigi & Sudhikumar, 2023: 80, figs 1A–F, 2A–E. Misidentification.

Type material. ***Holotype*** female of *Epeus chilapataensis* from India, West Bengal: Koch Bihar District (now cooch Behar), Chilapata Forest, 09.i.1985, NZC-ZSI-5407/18-B. Biswas-coll. Examined.

Other material examined. **India: Karnataka:** 1♀ & 1♂ (NZC-ZSI-8372/18), Shimoga, Hulikal, 13°72'01.12"N, 75°02'54.13"E, 613 m alt., 05.xii.2022, P.P. Sudhin coll.; 13♀♀ & 1♂ (NZC-ZSI-8373/18), Shimoga, Mookambika Wildlife Sanctuary, 13°42'18.9"N, 75°03'47.7"E, 605 m alt., 07.xii.2022, P.P. Sudhin coll.; **Kerala**: 1♂ (NZC-ZSI-8533/18), Wayanad, Kalpetta, Elstone Tea Estate, 11°36'11.49"N, 76°5'11.96"E, 778 m alt., 20.ix.2021, R. Jwala coll.; **Meghalaya**: 5♀♀ (NZC-ZSI-8849/18), Ri Bhoi, Umsning, 25°45'18.2"N, 91°51'47.2"E, 777 m alt., 16.iii.2023, S. Sen & P.P. Sudhin coll.

Diagnosis. The male copulatory organ of *Epeus albus* Prószyński, 1992 is most similar to that of *Epeus glorius* Żabka, 1985 in having the similar shaped RTA and serrated cymbial apophysis, but it can be distinguished by the following combination of characters: RTA slender and anterodorsally directed (RTA relatively robust and apically directed in *E. glorius*); cymbial apophysis relatively short and posteroventrally directed (long and posteriorly directed in *E. glorius*) (cf. Figs 2A, B, 3A, B with figs 15–16 in Meng et al. (2015)). The female of *E. albus* is most similar to that of *Epeus indicus* Prószyński, 1992 and *Epeus szirakii* Patoleta, Gardzińska & Żabka, 2020 in having the similar epigynal morphology, but it can be distinguished by the following combination of characters: epigyne with large and wide atrium (narrower in *E. indicus*); copulatory openings more widely separated from each other, orientated more anteriorly with well-defined posterior margins (closely arranged, orientated face to face without well-defined posterior margins in *E. indicus*). (cf. Figs 2D, E, 3C–F, 4A–F, 5C, D, with fig. 22 in Prószyński (1992) and figs 6E–F in Patoleta et al. (2020)).

Justification of the synonymy of *E. chilapataensis*. Re-examination of the holotype of *E. chilapataensis* shows that the body colour pattern and epigyne structure are similar to those of *Epeus albus*: pale yellow to white-coloured body without any prominent markings and crescent shaped copulatory openings and the similar course of proximal spermathecal loop (cf. Figs 3E, 5A–C, E with figs 20–21, 25 in Prószyński (1992)). Based on these observations, we consider *E. chilapataensis* a junior synonym of *E. albus*. Prószyński (1992) described *E. albus* from Jajpur-Keonjahr District, Orissa and Biswas and Biswas (1992) described *E. chilapataensis* from Koch Bihar District (now Cooch Behar), West Bengal. Both the species were described from the eastern part of the country from neighbouring states in the same year, but in different months. Prószyński described *E. albus* in October 1992 and Biswas & Biswas described *E. chilapataensis* in November 1992. Here, we are giving preference to the name which was first described. Therefore, the second described species must be a junior synonym of the first.

Description. Male (Figs 1A–C, G, 2A–C, 3A–B): Measurements: Body length 4.87. Carapace length 1.96, width 1.76. Abdomen length 2.85, width 1.33. Ocular area length 1.30, width at AEs 1.55. Eye diameters and interdistances: AME 0.57, ALE 0.26, PME 0.07, PLE 0.26; AME-AME 0.03, ALE-ALE 1.21, AME-PME 0.59, PLE-PLE 1.13, PME-PME 1.21, PME-PLE 0.32. Clypeus height 0.08. Length of chelicera 0.80.

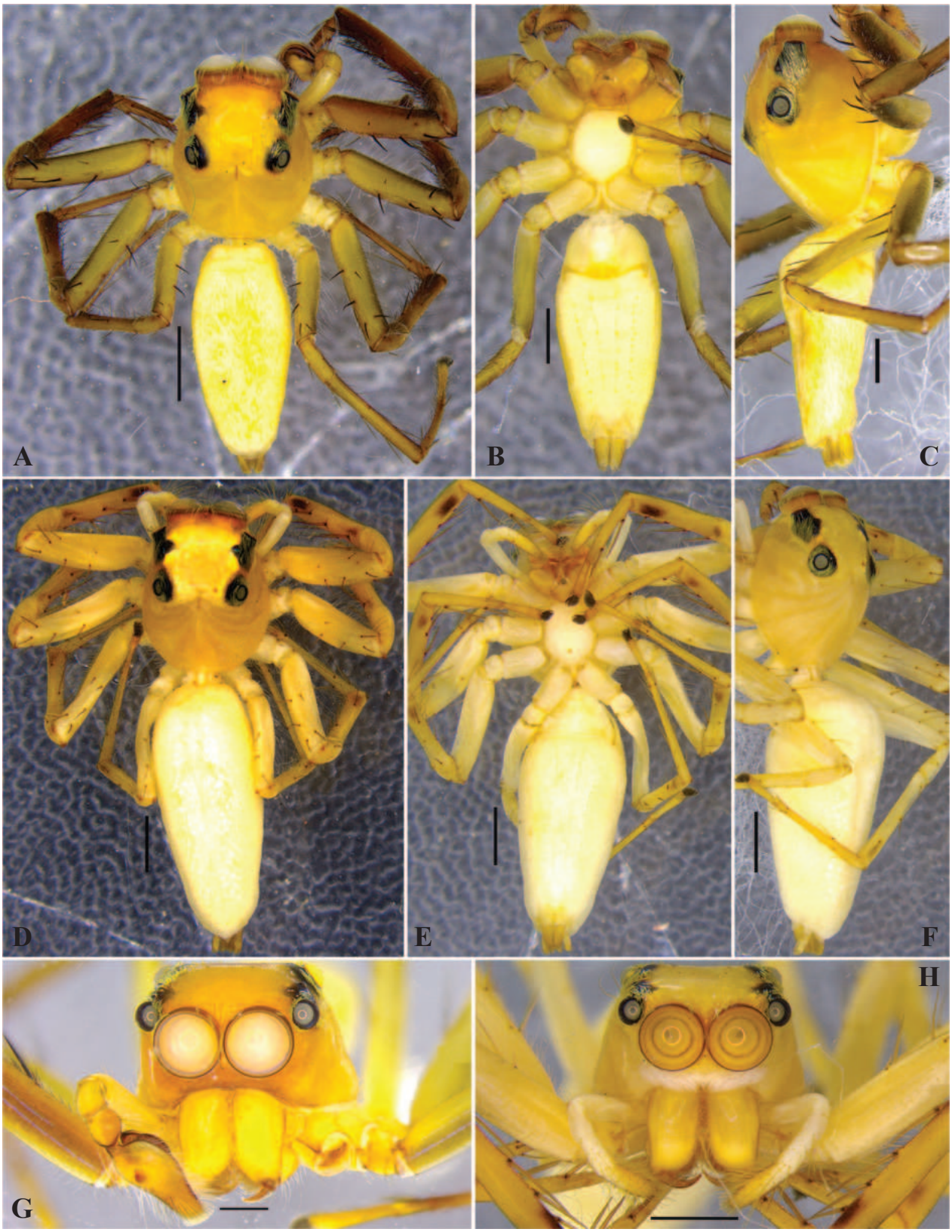

Figure 1. *Epeus albus* Prószyński, 1992. **A.** Male, dorsal view; **B.** Same, ventral view; **C.** Same, lateral view; **D.** Female, dorsal view; **E.** Same, ventral view, **F.** Same, lateral view; **G.** Male, frontal view; **H.** Female, frontal view. Scale bars: 1 mm.

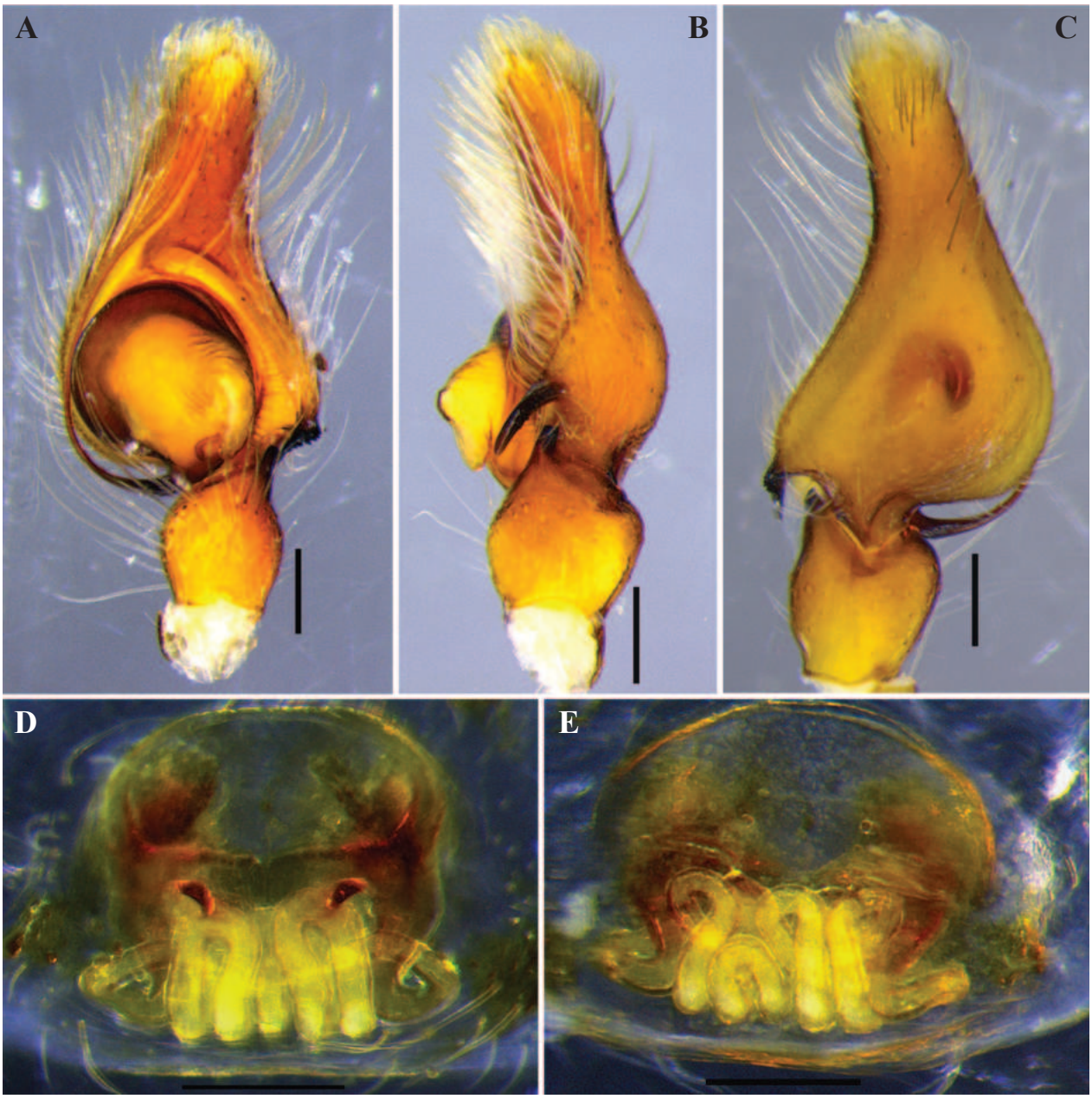

Figure 2. *Epeus albus* Prószyński, 1992. **A.** Left male palp, ventral view; **B.** Same, retrolateral view; **C.** Same dorsal view; **D.** Female epigyne, ventral view; **E.** Vulva, dorsal view. Scale bars: 0.2 mm.

Measurement of palp and legs: palp 2.19 [0.76, 0.31, 0.25, 0.87], leg I 7.90 [2.31, 0.86, 2.29, 1.51, 0.93], II 6.58 [2.12, 0.78, 1.71, 1.28, 0.69], III 7.18 [2.28, 0.59, 1.70, 1.82, 0.79], IV 6.42 [1.86, 0.58, 1.58, 1.78, 0.62]. Leg formula 1324. Leg spination: femur I pl 3 rl 3 do 3, II-III pl 2 rl 2 do 3, IV pl 1 do 3; patella I-IV pl 1 rl 1; tibia I pl 2 plv 4 rlv 4, II pl 1 rl 2 plv 3 rlv 3, III pl 1 rl 2 plv 2 rlv 2, IV pl 2 rl 3; metatarsus I-II pl 2 rl 2 plv 2 rlv 2, III pl 2 rl 2 plv 1 rlv 1 v 1, IV pl 2 rl 3 plv 2 rlv 2; tarsi I-IV spineless. Carapace high and elevated with posterior slope, pale yellow, covered with colourless setae (Fig. 1A); margin of carapace with light brown lines; eye field bright yellow, covered with bright yellow setae (Fig. 1A); AMEs rims light brown, encircled by bright yellow setae (Fig. 1A, G). Clypeus low, light yellow-brown (Fig. 1G). Chelicerae small, vertical, pale yellow, frontal side with long white setae (Fig. 1G); promargin with two teeth and retromargin with one tooth. Endites pale yellow, scopulate, with light brown margins and small anterolateral protuberance (Fig. 1B). Labium yellow, distally pale yellow, covered with setae (Fig. 1B). Sternum sub-pentagonal, whitish-yellow, with pale yellow margins (Fig. 1B). Abdomen nearly cylindrical, posteriorly narrowing, pale white, covered with golden yellow and colourless setae (Fig. 1A). Venter pale white, covered with colourless setae, medially and laterally with a pair of yellowish dotted lines (Fig. 1B). Spinnerets pale yellow, covered with light brown setae (Fig. 1A–C). Legs long and slender, covered with colourless and black setae (Fig. 1A). Legs I–III with pale yellow femora, patellae and tarsi; femora covered

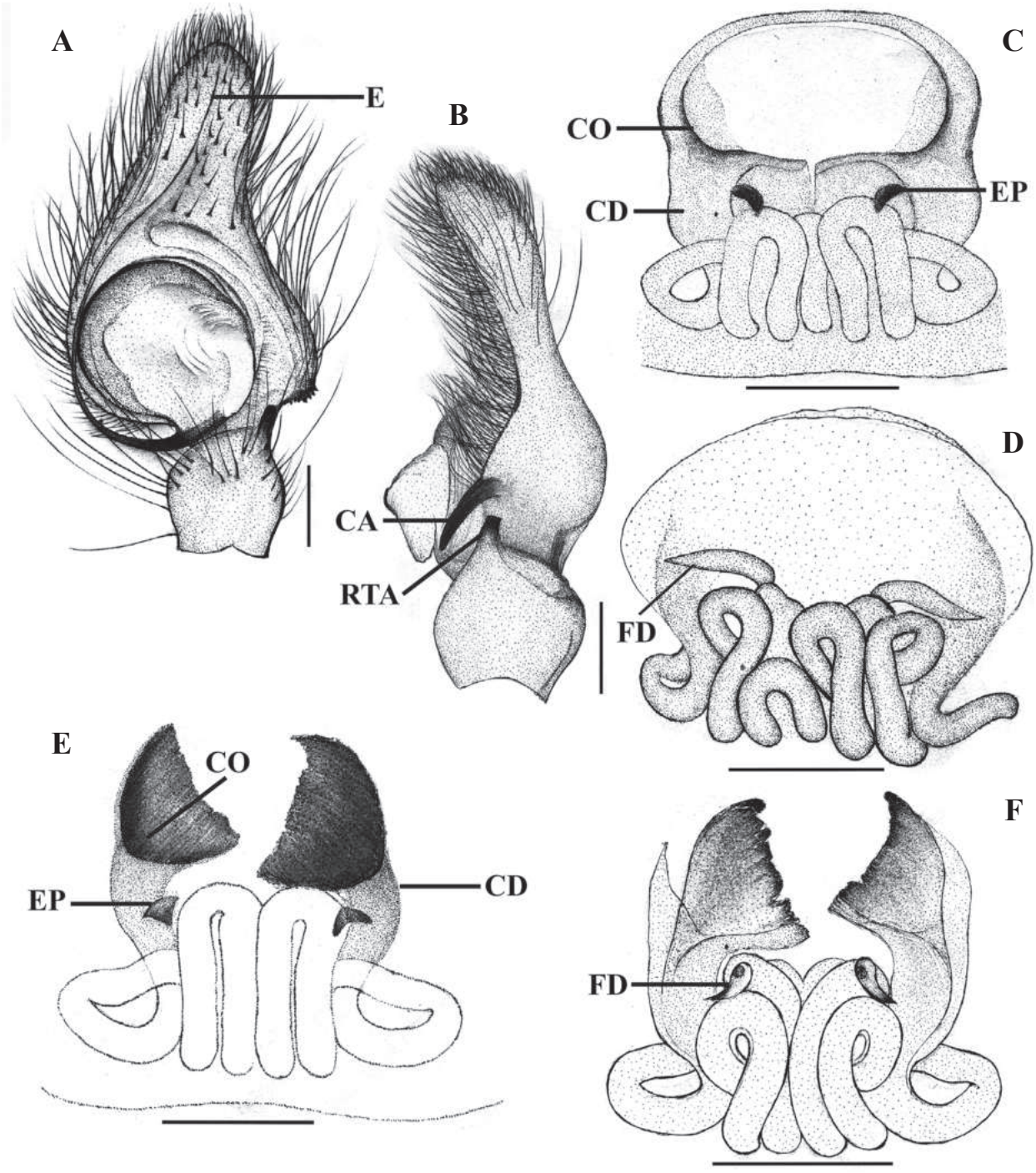

Figure 3. *Epeus albus* Prószyński, 1992. (**A–D**) and holotype female of *Epeus chilapataensis* (Biswas & Biswas, 1992) (**E–F**). **A.** Left male palp, ventral view; **B.** Same, retrolateral view; **C, E.** Female epigyne, ventral view; **D, F.** Vulva, dorsal view. Scale bars: 0.2 mm.

with light brown longitudinal bands on their prolateral and retrolateral sides; tibiae and metatarsi light yellowish-brown; tibia III and metatarsus III lighter in colour. Legs IV light yellowish-brown, with pale yellow femur and tarsus. Palp pale yellow to light yellowish-brown (Fig. 2A–C); RTA short, stout, anterodorsally directed with truncated tip (Figs 2B, 3B); cymbium nearly triangular, covered with white and black setae (Fig. 2A); cymbial apophysis long and slender, its outer margin serrated (Figs 2B, 3B); tegulum with much developed tongue-like flap (Figs 2A, 3A); embolus very thin and long, originating almost at eight o'clock position and extending to the distal end of cymbium (Figs 2A and 3A).

Female (Figs 1D–F, H, 2D, E, 3C–F, 4A–F, 5A–F) (Description based on newly-collected material): Measurements: Body length 7.57. Carapace length 3.06, width 2.22. Abdomen length 4.30, width 1.97. Ocular area length 1.57, width at AEs 1.88. Eye diameters and interdistances:

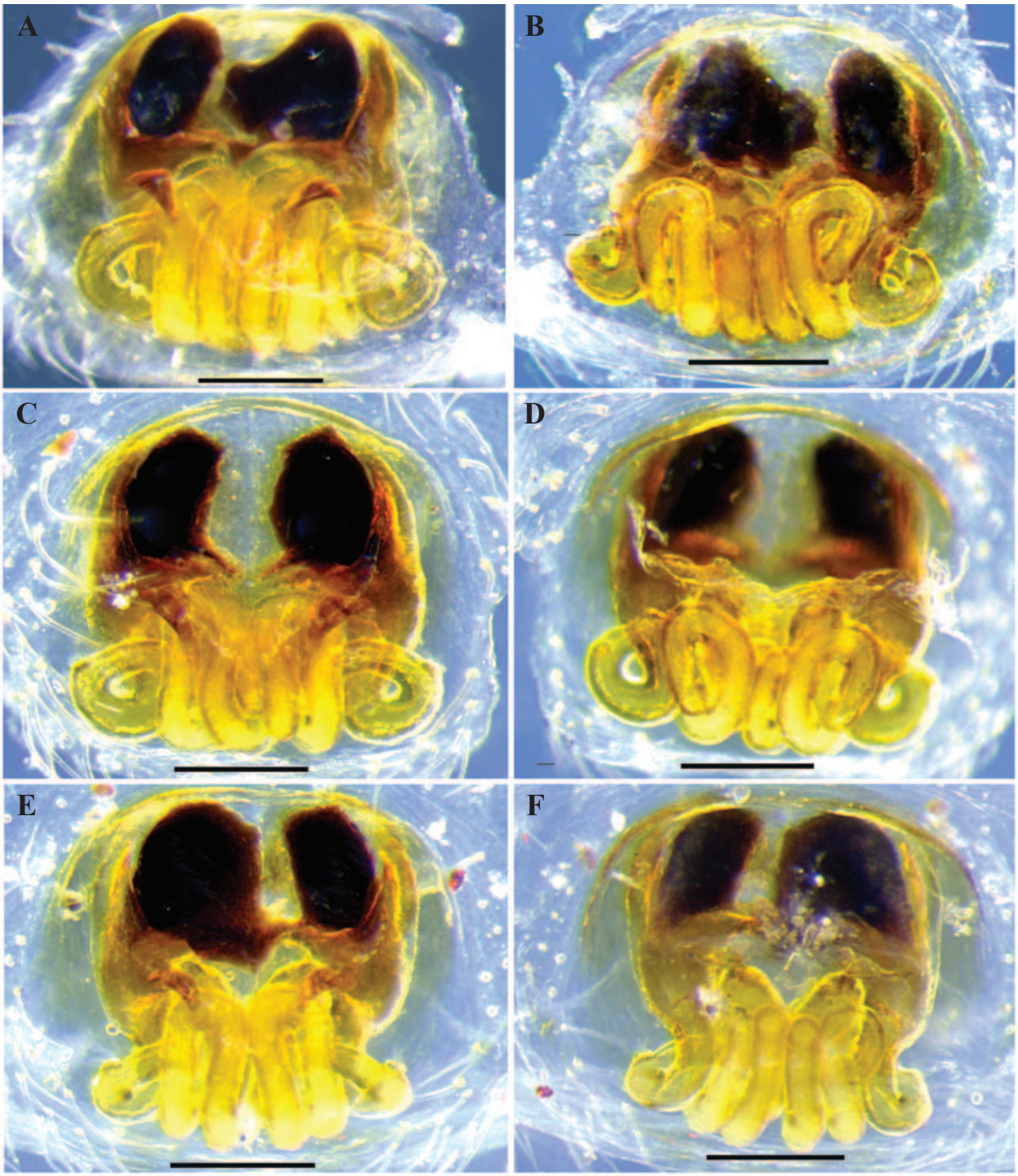

Figure 4. *Epeus albus* Prószyński, 1992, copulatory organs of the freshly-collected females showing variations. **A, C, E.** Female epigynum, ventral view; **B, D, F.** Vulvae, dorsal view. Scale bars: 0.2 mm.

AME 0.71, ALE 0.29, PME 0.07, PLE 0.29; AME-AME 0.03, ALE-ALE 1.34, AME-PME 0.63, PLE-PLE 1.34, PME-PME 1.44, PME-PLE 0.40. Clypeus height 0.16. Length of chelicera 0.93. Measurement of palp and legs: palp 2.46 [0.78, 0.34, 0.43, 0.91], leg I 7.67 [2.32, 0.92, 2.25, 1.43, 0.75], II 7.33 [2.29, 0.91, 1.95, 1.36, 0.82], III 8.17 [2.65, 0.68, 2.03, 1.97, 0.84], IV 7.52 [2.18, 0.62, 1.99, 2.02, 0.71]. Leg formula 3142. Leg spination: femur I pl 3 rl 3 do 3, II pl 2 rl 2 do 3, III pl 2 do 3, IV do 3; patella III-IV pl 1 rl 1; tibia I-II plv 4 rlv 4, III-IV pl 1 rl 3 plv 1 rlv 1; metatarsus I-II plv 2 rlv 2, III pl 2 rl 2 plv 2 rlv 2 v 1, IV pl 2 rl 2 plv 2 rlv 2; tarsi I-IV spineless. In all details mostly as male, except for the following: elongate and robust than male (Fig. 1D); clypeus pale yellow, densely covered with white setae (Fig. 1H); endites distal tip without anterolateral protuberance (Fig. 1E); abdomen covered with colourless and white setae, venter without any prominent markings (Fig. 1D, E). Epigyne wider than

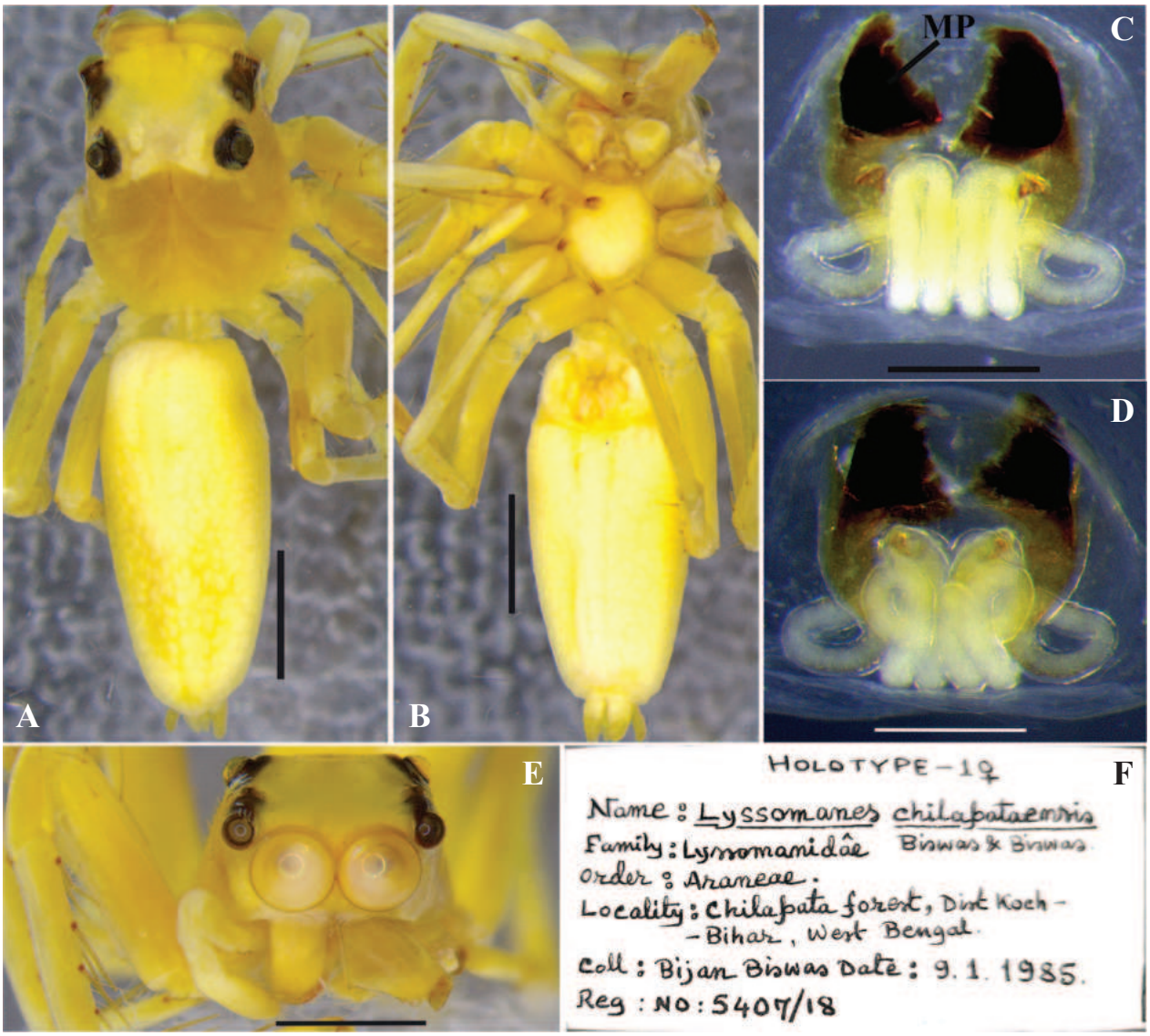

Figure 5. *Epeus albus* Prószyński, 1992 (the holotype of *Epeus chilapataensis* (Biswas & Biswas, 1992). **A.** Female, dorsal view; **B.** Same, ventral view; **C.** Female epigyne, ventral view; **D.** Vulva, dorsal view; **E.** Female, frontal view; **F.** Original label. Scale bars: 1 mm (**A, B, E**); 0.2 mm (**C, D**).

long, with a pair of small epigynal pockets, atrium ovoid (Figs 2D, 3C); copulatory openings widely separated, crescent-like, with closely-arranged posterior margins (Figs 2D, 3C); copulatory ducts very long with several loops, finally entering the spermathecal reservoir posteriorly (Figs 2E, 3D); fertilisation ducts long, orientated laterally, positioned at the anterior region of spermathecae (Figs 2E, 3D).

Distribution. India: Karnataka (new locality record), Kerala (new locality record), Meghalaya (new locality record), Odisha, West Bengal (Fig. 7).

Variations. Body length: Male: 4.87–7.83 (n = 3). Female: 4.89–9.58 (n = 19).

Remarks. Mating plugs were found covering the copulatory openings of the holotype female of *E. chilapataensis* (Biswas & Biswas, 1992) and of several other females examined from Karnataka and Meghalaya (Figs 3E, F, 4A–F, 5C, D).

The record of *Epeus daiqini* Patoleta, Gardzińska & Żabka, 2020 from India was based on the male and female specimens collected from Pathanamthitta, Kerala (Sibi et al. 2023). However, illustrations of the male and female copulatory organs provided by Sibi et al. (2023) do not match those of the type specimens of *E. daiqini*: the male palp with serrated cymbial apophysis (absent in the holotype male of *E. daiqini*); relatively short and less coiled copulatory ducts (long and strongly coiled in the paratype female of *E. daiqini*) (cf. figs 3E–G and 4G–H in Patoleta et al. (2020) with figs 1D–F and 2D–E in Sibi et al. (2023)). Their genital morphology is similar to those of freshly-collected male and female specimens of *E. albus* (cf. Figs 2A–E, 3A–D, 4A–F with figs 1D–F and 2D, E in Sibi et al. (2023)). Based on these observations, it is apparent that the species is misidentified by Sibi et al. (2023) and it belongs to *E. albus*.

***Epeus khandalaensis* (Tikader, 1977), comb. nov.**
Figs 6A–D, 7

Phidippus khandalaensis Tikader, 1977: 98, figs 6–8.

Type material. ***Holotype*** female of *Phidippus khandalaensis* from India, Maharashtra: Poona District, Khandala Rest House, Khandala Ghat, 04.xii.1963, NZC-ZSI-5391/18-B.K. Tikader-coll. Examined.

Justification of the transfer. Tikader (1977) described this species, based on a female specimen collected from Poona, Maharashtra. The ZSI collection has a single glass bottle for this species, containing a female specimen (labelled as 'holotype') in good conditions with detached abdomen and broken legs. The genitalia of the female was dissected, but was not found inside the bottle and is perhaps lost. The general morphology shows that this species shares the features of *Epeus* Peckham & Peckham, 1886: carapace high and elevated, AME much larger than ALE and the latter slightly behind AME (Patoleta et al. 2020) and the abdomen dorsally with indistinct black markings and white spots (Fig. 6A–C). Based on these observations, we are provisionally transferring it to *Epeus*.

Distribution. India: Maharashtra (Fig. 7).

Figure 6. *Epeus khandalaensis* (Tikader, 1977) comb. nov. **A.** Holotype female, dorsal view; **B.** Same, ventral view; **C.** Female, frontal view; **D.** Original label. Scale bars: 1 mm.

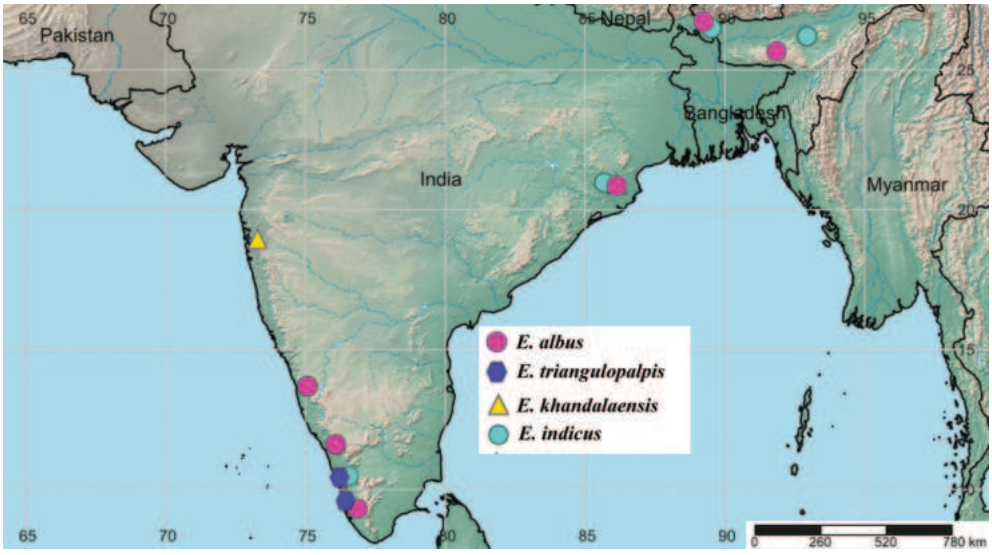

Figure 7. Map showing the distributional records of *Epeus* species in India.

Acknowledgements

The authors are grateful to Dr Dhriti Banerjee, Director of the Zoological Survey of India, Kolkata, for providing all the facilities for conducting this study. We are also thankful to the Chief Conservator of Forests and Chief Wildlife Warden, Karnataka State Forest Departments, for the collecting permit. We extend our heartfelt thanks to Dr John T. D. Caleb, Saveetha Institute of Medical and Technical Sciences, Chennai, for the insightful suggestions that greatly improved the manuscript. We are also grateful to Dr. P. M. Sureshan, Emeritus Scientist, Zoological Survey of India, Western Ghat Regional Centre, Kozhikode, Kerala for his encouragements and support. Many thanks to Mr Chandan Bera, ZSI, Kolkata, for his curatorial assistance. Jwala R is grateful to the UGC for financial assistance in the form of a Junior Research Fellowship and the authorities of the University of Calicut for providing facilities and encouragements. We extend our heartfelt thanks to the editor Dr Danilo Harms (Germany) and the reviewers, Dr Dmitri V. Logunov (U.K), Dr Wanda Wesolowska (Poland) and Dr Tamás Szűts (Hungary) for their constructive comments and suggestions on the manuscript.

References

Biswas B, Biswas K (1992) Araneae: Spiders. State Fauna Series 3. Fauna of West Bengal 3: 357–500.

Bosselaers J, Jocqué J (2000) Studies in Corinnidae: Transfer of four genera and description of the female of *Lessertina mutica* Lawrence, 1942. Tropical Zoology 13(2): 305–325. https://doi.org/10.1080/03946975.2000.10531138

Caleb JTD, Sankaran PM (2024) Araneae of India. Version 2024. http://www.indianspiders.in [Accessed 13 March 2024]

Logunov DV (2004) On the taxonomic position of "*Lyssomanes*" *karnatakaensis* and other Indian species formerly assigned to *Lyssomanes* (Araneae, Salticidae). Bulletin - British Arachnological Society 13: 73–75.

Malamel JJ, Nafin KS, Sudhikumar AV, Seastian PA (2019) Two new species of the jumping spiders (Araneae: Salticidae) from the genera *Epeus* Peckham et Peckham, 1886 and *Piranthus* Thorell, 1895 from India. Arthropoda Selecta 28(2): 267–276. https://doi.org/10.15298/arthsel.28.2.10

Meng XW, Zhang ZS, Shi AM (2015) Description of two unknown females of *Epeus* Peckham and Peckham from China (Araneae: Salticidae). Zootaxa 3955(1): 147–150. https://doi.org/10.11646/zootaxa.3955.1.11

Mondal A, Chanda D, Vartak A, Kulkarni S (2020) A Filed Guide to the Spider Genera of India, CDC Printers, West Bengal, India, 405 pp.

Patoleta BM, Gardzińska J, Żabka M (2020) Salticidae (Arachnida, Araneae) of Thailand: New species and records of *Epeus* Peckham and Peckham, 1886 and *Ptocasius* Simon, 1885. PeerJ 8(e9352): 1–23. https://doi.org/10.7717/peerj.9352

Prószyński J (1992) Salticidae (Araneae) of India in the collection of the Hungarian National Natural History Museum in Budapest. Annales Zoologici, Warszawa 44: 165–277.

Prószyński J, Deeleman-Reinhold CL (2012) Description of some Salticidae (Aranei) from the Malay Archipelago. II. Salticidae of Java and Sumatra, with comments on related species. Arthropoda Selecta 21(1): 29–60. https://doi.org/10.15298/arthsel.21.1.04

Sebastian PA, Peter KV (2009) Spiders of India, Universities Press, Hyderabad, India, 615 pp.

Shorthouse DP (2010) SimpleMappr, an online tool to produce publication-quality point maps. http://www.simplemappr.net [Accessed 26 October 2023]

Sibi KK, Gigi P, Sudhikumar AV (2023) First report of the jumping spider *Epeus daiqini* (Patoleta, Gardzińska & Żabka, 2020) (Araneae: Salticidae) from India. Natura Somogyiensis 41(41): 79–84. https://doi.org/10.24394/NatSom.2023.41.79

Tikader BK (1977) Description of two new species of jumping-spiders of the genus *Phidippus* (family: Salticidae) from India. Entomon 2(1): 97–99.

World Spider Catalog (2024) World Spider Catalog. Version 24. Natural History Museum Bern. https://wsc.nmbe.ch [Accessed 13 March 2024] https://doi.org/10.24436/2

Zoosyst. Evol. 100 (2) 2024, 457–468 | DOI 10.3897/zse.100.118612

PENSOFT

für Natur MUSEUM FÜR NATURKUNDE BERLIN

Oxynoemacheilus chaboras, a new loach species from the Euphrates drainage in Türkiye (Teleostei, Nemacheilidae)

Cüneyt Kaya[1], Irmak Kurtul[2,3], İsmail Aksu[1], Münevver Oral[1], Jörg Freyhof[4]

1 *Recep Tayyip Erdogan University, Faculty of Fisheries, 53100 Rize, Turkiye*
2 *Marine and Inland Waters Sciences and Technology Department, Faculty of Fisheries, Ege University, İzmir, Turkiye*
3 *Department of Life and Environmental Sciences, Faculty of Science and Technology, Bournemouth University, Poole, Dorset, UK*
4 *Museum für Naturkunde, Leibniz Institute for Evolution and Biodiversity Science, 10115 Berlin, Germany*

https://zoobank.org/31342190-DE9E-42A9-AF83-AD5AE4F0C7D1

Corresponding author: Cüneyt Kaya (cnytkaya@yahoo.com)

Academic editor: Nicolas Hubert ♦ **Received** 13 January 2024 ♦ **Accepted** 28 March 2024 ♦ **Published** 26 April 2024

Abstract

Oxynoemacheilus chaboras, new species, from the stream Beyazsu in the Euphrates drainage, belongs to the *O. persa* species group, being closely related to *O. shehabi* from the Orontes, *O. sarus* from the Seyhan and Ceyhan, *O. euphraticus* from the Euphrates and Tigris, *O. karunensis* from the Karkheh, and *O. persa* from Central Iran. The new species is distinguished from others in the *O. persa* group by having 8–9 pores in the supraorbital canal, two distinct black blotches at the caudal-fin base, a rudimentary and shallow pelvic axillary lobe, 6–10 irregularly shaped bars on the flank, and a deep head, body, and caudal peduncle. *Oxynoemacheilus chaboras* **sp. nov.** is most closely related to *O. euphraticus*, from which it is differentiated by a mean uncorrected *p*-distance of 3.24% (min. 3.09%) in its COI barcode gene.

Key Words

Cypriniformes, Cytochrome c oxidase subunit I, freshwater fish, taxonomy, Western Asia

Introduction

The genus *Oxynoemacheilus* Bănărescu & Nalbant, 1966, with 63 recognised species, is the most speciose genus of freshwater fishes in the western Palaearctic (Yoğurtçuoğlu et al. 2022). The hotspot of species richness of *Oxynoemacheilus* is Mesopotamia and the adjacent Levant, where there are 21 species of the genus only in the Tigris-Euphrates drainage. This high species richness can be attributed to several factors such as the unique hydrological conditions, diverse habitat types, and historical biogeographical processes of the region. Seven species are endemic to the Euphrates drainage, and 11 are endemic to the Tigris drainage (Freyhof et al. 2021, 2022). But additional species of *Oxynoemacheilus* are still being discovered in this region, as vast areas especially in Iraq and Syria remain unexplored.

There are many tributaries to the upper and middle Euphrates. One of these rivers is the Khabur that has few springs in Türkiye, but mostly flows in Syria. The stream Beyazsu, located in the Turkish Mardin province, is one of the headwater streams in the Khabour drainage. It flows into Syria after crossing the border at the city of Nusaybin, only 17.5 km below its source, the spring Beyazsu (Canpolat and Bozdoğan 2019). This karstic spring has much water throughout the year and its average annual flow rate is approximately 3.8 m^3/sec. (Canpolat and Bozdoğan 2019).

Until now, only Turan et al. (2014) seems to have studied the fishes of the Beyazsu and reported the presence of *Alburnus caeruleus* Heckel, 1843, *Alburnus sellal* Heckel, 1843 (as *Alburnus mossulensis* Heckel, 1843), *Barbus lacerta* Heckel, 1843, *Capoeta damascina* (Valenciennes, 1842) (as *Capoeta umbla* (Heckel, 1843)), *Garra rufa* (Heckel, 1843), and an unidentified species of genus

Oxynoemacheilus. These authors described *Alburnoides emineae* Turan, Kaya, Ekmekçi & Doğan, 2014 as a new species from the stream Beyazsu, indicating its unique fauna. Here we examine the *Oxynoemacheilus* population from the Beyazsu in detail to test if they might represent an undescribed species.

Materials and methods

The care of experimental animals was consistent with the Republic of Türkiye's animal welfare laws, guidelines, and policies. After anaesthesia, fishes were fixed in 5% formalin and stored in 70% ethanol, fin clips directly fixed in 99% ethanol. Measurements were made with a dial calliper, recorded to 0.1 mm, from a precise point-to-point approach, never by projections. Methods for counts and measurements followed Kottelat and Freyhof (2007), structures of the suborbital groove and the adipose crest followed Freyhof et al. (2019), and nomenclature of head pores followed Kottelat (1990). Standard length is measured from the tip of the snout to the posterior extremity of the hypural complex. The length of the caudal peduncle is measured from behind the base of the last anal-fin ray to the posterior extremity of the hypural complex, at mid-height of the caudal-fin base. The last two branched rays articulating on a single pterygiophore in the dorsal and anal fins are counted as "1½". Simple rays of dorsal- and anal-fins are not counted as they are deeply embedded.

Morphological data for *Oxynoemacheilus zagrosensis* Kamangar, Prokofiev, Ghaderi & Nalbant, 2014 are taken from Kamangar et al. (2014) and its position in the *Oxynoemacheilus persa* (Heckel, 1847) group follow Freyhof and Geiger (2021).

Abbreviations used

SL, standard length; **HL**, head length; Collection codes: **FFR**, Recep Tayyip Erdogan University Zoology Collection of the Faculty of Fisheries, Rize; **FSJF**, Fischsammlung J. Freyhof, Berlin, Germany. **IUSHM**, Istanbul University, Faculty of Science, Hydrobiology Museum, Istanbul; **NMW**, Natural History Museum Vienna; **ZFMK-ICH**, Zoological Research Museum Alexander Koenig, Ichthyology Collection, Bonn; **ZMH**, Zoologisches Museum Hamburg, Hamburg.

DNA extraction, PCR and sequencing

Genomic DNA extraction of *Oxynoemacheilus* specimens was performed according to the application protocol recommended by the manufacturer using the DNeasy Blood & Tissue Kit (Qiagen, Hilden, Germany). Amplification of the barcode region of the cytochrome c oxidase subunit 1 (COI) gene of vertebrate mitochondrial DNA was performed according to Bektaş et al. (2022)'s thermocycler conditions of which PCR protocol (4 min. first denaturation at 94 °C, followed by 30 cycles of denaturing for 30 1 min. at 94 °C, annealing for 30 sec. at 61 °C, extending for 1 min. at 72 °C and final extension for 7 min. at 72 °C) using forward FishF1 (5'-TCAACCAACCACAAAGACATTGGCAC-3'; Ward et al. 2005) and reverse FishR1 (5'-TAGACTTCTGGGTGGCCAAAGAATCA-3'; Ward et al. 2005) primers were used for amplification. PCR products were purified using the QIAquick PCR Purification Kit (Qiagen, Hilden, Germany) and bidirectional sequencing of PCR products was performed with an ABI PRISM 3730×1 Genetic Analyser using a Big-Dye Terminator 3.1 cycle sequencing ready reaction kit (Applied Biosystem) at Macrogen Europe. The obtained sequences were deposited in NCBI's GenBank with the accession numbes between OR689585–OR689588.

Molecular analysis

Oxynoemacheilus species distributed in the Euphrates and all other species, except *O. zagrosensis*, of the *O. persa* species group, as well as all other species known from the Euphrates drainage, were included in our dataset (Fig. 1). References to the sequences downloaded from Genbank are as follows: Geiger et al. (2014); Esmaeili et al. (2014); Freyhof et al. (2016); Sayyadzadeh and Esmaeili (2020); Kaya et al. (2020); Freyhof and Geiger (2021); Bektaş et al. (2022); Freyhof et al. (2022). The chromatograms of raw COI sequences obtained after sequencing were examined with the Bioedit 7.2.5 (Hall, 1999) program and the detected errors were manually edited. Base composition, and distinctive and diagnostic nucleotide positions were determined with the MEGA version X (Kumar et al. 2018) programme. The mean inter-species genetic distance values of *Oxynoemacheilus* were calculated in MEGA X according to the uncorrected *p*-distance model (Srivathsan and Meier 2012).

Phylogenetic relationships among *Oxynoemacheilus* species were estimated using Maximum Likelihood (ML; Felsenstein 1981) algorithm in MEGA X programme, and Bayesian analysis (BI) in MrBayes v3.2.1 programme (Ronquist et al. 2012). For ML and BI analyses, the best-fit evolution models were determined according to Akaike Information Criteria (AIC) and Bayesian Information Criteria (BIC) in the jModeltest 0.1.1 (Posada 2008). The ML tree was generated with 1000 bootstrap replicates using the GTR+G model that was selected by the lowest AIC score. The BI tree was generated implementing the GTR+G model that was selected by the lowest BIC score. The BI analyses were run for 5 million generations, sampling every 1000 generations. A conservative 25% of the trees were discarded as burn-in based on Bayesian analysis. No further software was used for checking the runs' convergence. Visualization of the BI tree was performed by iTOL (Interactive Tree of Life; https://itol.embl.de/), a web-based software.

Figure 1. Maximum Likelihood (ML) phylogenetic tree was reconstructed based on the COI-Barcode gene. ML and BI methods resulted in generally similar topologies with minor differences, and therefore only the ML tree is shown. The bootstrap values of ML and posterior probability values of BI are indicated on nodes (ML/BI). The bootstrap percentage values (BP) ≥ 50% from ML analysis and Bayesian posterior probabilities (PP) ≥ 0.50 are shown on the nodes.

Results

Sequence characteristic and phylogenetic reconstruction

Molecular analysis was conducted with four newly-generated DNA barcodes (see Genetic material section) and in addition already published data from NCBI GenBank. The average nucleotide frequency of four sequences of *O. chaboras* were A = 22.0%, T = 30.2%, C = 28.2% and G = 19.7%, and the nucleotide composition was A-T (52.2%) rich. Although the phylogenetic tree topologies reconstructed by both ML and BI methods indicated some minor differences from each other, they were generally compatible. In both topologies, some of the internal branches corresponding to the phylogenetic relationships between species, were weakly supported (Fig. 1).

The members of the *O. persa* species group (as defined by Freyhof and Geiger 2021) are distributed in two sub-clades with strong support according to the BI (PP: 0.96; Fig. 1) and ML (BP: 77%; Fig. 1) results. The first sub-clade includes *O. chaboras*, *Oxynoemacheilus shehabi* Freyhof & Geiger, 2021, *Oxynoemacheilus euphraticus* (Bănărescu & Nalbant, 1964), *O. persa*, *Oxynoemacheilus sarus* Freyhof, Yoğurtçuoğlu & Kaya, 2021 and *Oxynoemacheilus karunensis* Freyhof, 2016, while the second sub-clade includes *Oxynoemacheilus argyrogramma* (Heckel, 1847), *Oxynoemacheilus kentritensis* Freyhof, Kaya & Turan, 2017, *Oxynoemacheilus zarzianus* Freyhof & Geiger, 2017, *Oxynoemacheilus hanae* Freyhof & Abdullah, 2017, *Oxynoemacheilus kurdistanicus* Kamangar, Prokofiev, Ghaderi & Nalbant, 2014, *Oxynoemacheilus marunensis* Sayyadzadeh & Esmaeili, 2020, *O. zagrosensis* and *O. chomanicus*. *Oxynoemacheilus chaboras* clusters as the sister species of the first sub-clade with weak support (BP: less than 50%; PP: 0.54; Fig. 1). *Oxynoemacheilus chaboras* is distinguished from *O. euphraticus*, *O. shehabi*, *O. persa*, *O. sarus* and *O. karunensis* by 19, 23, 23, 27 and 29 diagnostic base positions, respectively. It is genetically most similar to *O. euphraticus* with a mean uncorrected *p*-distance value of 3.24% (minimum 3.09% – maximum 3.58%). It is distinguished from *O. shehabi*, *O. persa*, *O. sarus* and *O. karunensis* by mean 3.82% (min. 3.74%), 3.82% (min. 3.74%), 4.88% (min. 4.39%) and 5.20% (min. 4.88%), respectively. Table 1 displays the mean pairwise genetic distance results for each species.

Oxynoemacheilus chaboras sp. nov.

https://zoobank.org/A8C6E729-44C3-4B5C-9FCE-4A1906C9CDBE

Figs 2–4

Type material. ***Holotype.*** FFR 15646, 53 mm SL; Türkiye: Mardin prov.: stream Beyazsu 14 km north of Nusaybin, 37.1989, 41.3076.

Paratypes. FFR 1428, 11, 46–60 mm SL: same data as holotype. — FFR 15633, 2, 40–51 mm SL; FSJF 4116, 4, 46–55; Türkiye: Mardin prov.: stream Beyazsu 12 km north of Nusaybin, 37.1730, 41.2690.

Genetic material. FFR DNA-Oxy378, 379, 380, 381; same data as holotype (GenBank accession numbers: OR689585, OR689586, OR689587, OR689588).

Diagnosis. *Oxynoemacheilus araxensis*, *O. argyrogramma*, *Oxynoemacheilus arsaniasus* Freyhof, Kaya, Turan & Geiger, 2019, *Oxynoemacheilus bergianus* (Derjavin, 1934), *O. euphraticus*, *Oxynoemacheilus kaynaki* Erk'akan, Özeren & Nalbant, 2008, *Oxynoemacheilus muefiti* Freyhof, Kaya, Turan & Geiger, 2019, *Oxynoemacheilus paucilepis* (Erk'akan, Nalbant & Özeren, 2007), and *Oxynoemacheilus tigris* (Heckel, 1843) are other species of *Oxynoemacheilus* known from the Euphrates drainage (Fig. 5). *Oxynoemacheilus chaboras*, is distinguished from these by a combination of characters, none of them unique to the species.

Oxynoemacheilus chaboras belongs to a group of species (*O. argyrogramma*, *O. chaboras*, *O. euphraticus*) having two bold, black, round or comma-shaped blotches on the caudal-fin base (vs. absent in *Oxynoemacheilus araxensis*, *O. arsaniasus*, *O. bergianus*, *O. kaynaki*, *O. muefiti*, *O. paucilepis*, and *O. tigris*). Furthermore, male *O. chaboras* have a suborbital groove (as in *O. araxensis* and *O. bergianus* vs. absent in *O. arsaniasus*, *O. kaynaki*, *O. muefiti*, *O. paucilepis*, and *O. tigris*).

Oxynoemacheilus chaboras is further distinguished from *O. araxensis* by having a forked caudal fin (vs. slightly emarginate), and it is further distinguished from *O. bergianus* by having a forked caudal fin (shortest middle caudal-fin ray is 57–70% of longest ray of the upper caudal-fin lobe, vs. deeply emarginated, 70–84), and a deeper caudal peduncle (depth 1.4–1.7 times in its length vs. 1.7–3.5).

Oxynoemacheilus chaboras is distinguished from *O. argyrogramma* and *O. euphraticus* by possessing a mid-lateral series of blotches (vs. marbled or mottled pattern in *O. argyrogramma*), without a mottling pattern above or below the blotches in front of dorsal-fin base (vs. irregularly mottled or marbled in *O. euphraticus*), and having no, or a very short, incision in the upper lip (vs. a deep median incision in *O. euphraticus*). It is further distinguished from *O. euphraticus* by having a deeper caudal peduncle (caudal-peduncle depth 1.4–1.7 times in its length vs. 2.0–2.8).

Description. See Figs 2–4 for general appearance and Table 2 for morphometric data. Small-sized and slender species. Body deepest at dorsal fin origin or slightly anterior of it. Body width greatest at pectoral-fin base. Section of head roundish, flattened on ventral surface, straight or slightly convex in interorbital space, convex on snout. Snout blunt. Caudal peduncle compressed laterally, 1.4–1.7 times longer than deep. Pelvic axillary lobe shallow and fully attached to flank. Pelvic-fin origin below second or third branched dorsal-fin ray. Anal-fin origin located in front of vertical of midline between dorsal and caudal-fin origins. Pectoral fin reaching to approximately 72–99% of distance from pectoral-fin origin to pelvic-fin origin. Pelvic

Table 1. The interspecies genetic distances calculated by the uncorrected *p*-distance model for the *Oxynoemacheilus* species of Euphrates-Tigris and other *O. persa* species group.

	Species	1	2	3	4	5	6	7	8	9	10
1	*O. chaboras*										
2	*O. euphraticus*	0.0324									
3	*O. shehabi*	0.0382	0.0300								
4	*O. persa*	0.0382	0.0265	0.0423							
5	*O. marunensis*	0.0455	0.0340	0.0431	0.0431						
6	*O. hanae*	0.0455	0.0349	0.0374	0.0439	0.0285					
7	*O. kurdistanicus*	0.0463	0.0366	0.0455	0.0512	0.0268	0.0301				
8	*O. kentritensis*	0.0472	0.0356	0.0415	0.0480	0.0390	0.0366	0.0415			
9	*O. zagrosensis*	0.0488	0.0323	0.0480	0.0480	0.0260	0.0268	0.0220	0.0374		
10	*O. sarus*	0.0488	0.0358	0.0415	0.0431	0.0520	0.0480	0.0545	0.0504	0.0537	
11	*O. argyrogramma*	0.0507	0.0406	0.0509	0.0472	0.0388	0.0390	0.0388	0.0480	0.0363	0.0604
12	*O. zarzianus*	0.0512	0.0395	0.0488	0.0423	0.0325	0.0341	0.0390	0.0415	0.0350	0.0545
13	*O. chomanicus*	0.0512	0.0332	0.0455	0.0488	0.0268	0.0309	0.0260	0.0415	0.0187	0.0545
14	*O. karunensis*	0.0520	0.0414	0.0488	0.0374	0.0593	0.0537	0.0577	0.0577	0.0569	0.0472
15	*O. araxensis*	0.0772	0.0706	0.0764	0.0732	0.0854	0.0829	0.0837	0.0724	0.0854	0.0732
16	*O. kaynaki*	0.0789	0.0683	0.0715	0.0764	0.0772	0.0780	0.0780	0.0756	0.0732	0.0894
17	*O. arsaniasus*	0.0821	0.0716	0.0715	0.0780	0.0756	0.0764	0.0748	0.0740	0.0691	0.0854
18	*O. tigris*	0.0821	0.0688	0.0699	0.0748	0.0789	0.0780	0.0846	0.0724	0.0780	0.0813
19	*O. muefiti*	0.0894	0.0796	0.0821	0.0846	0.0862	0.0854	0.0878	0.0813	0.0756	0.0967
20	*O. paucilepis*	0.1024	0.0948	0.0878	0.0976	0.0951	0.0959	0.0935	0.0870	0.0927	0.0967
21	*O. bergianus*	0.1122	0.1156	0.1220	0.1122	0.1228	0.1171	0.1146	0.1098	0.1146	0.1179
		11	**12**	**13**	**14**	**15**	**16**	**17**	**18**	**19**	**20**
1	*O. chaboras*										
2	*O. euphraticus*										
3	*O. shehabi*										
4	*O. persa*										
5	*O. marunensis*										
6	*O. hanae*										
7	*O. kurdistanicus*										
8	*O. kentritensis*										
9	*O. zagrosensis*										
10	*O. sarus*										
11	*O. argyrogramma*										
12	*O. zarzianus*	0.0455									
13	*O. chomanicus*	0.0390	0.0358								
14	*O. karunensis*	0.0515	0.0650	0.0537							
15	*O. araxensis*	0.0808	0.0748	0.0862	0.0862						
16	*O. kaynaki*	0.0705	0.0748	0.0683	0.0902	0.0878					
17	*O. arsaniasus*	0.0721	0.0732	0.0683	0.0902	0.0846	0.0228				
18	*O. tigris*	0.0770	0.0732	0.0715	0.0894	0.0862	0.0423	0.0488			
19	*O. muefiti*	0.0851	0.0813	0.0829	0.1024	0.0967	0.0220	0.0358	0.0512		
20	*O. paucilepis*	0.0981	0.0992	0.0943	0.1008	0.0878	0.0992	0.0959	0.0943	0.1033	
21	*O. bergianus*	0.1187	0.1203	0.1106	0.1163	0.1057	0.1098	0.1114	0.1203	0.1154	0.1008

fin reaching to genital papillae, rarely to anus; not reaching vertical of tip of last dorsal-fin ray. Anus about 40–70% of an eye diameter anterior to anal-fin origin. Anal fin not reaching caudal-fin base. No dorsal or ventral adipose crest on caudal peduncle. Largest known individual 60 mm SL.

Dorsal fin with 9½–10½ branched rays, outer margin straight or slightly concave. Anal fin with 5½ branched rays, outer margin straight. Pectoral fin with 9–11 branched rays, outer margin straight or slightly convex, tip pointed in male. Pelvic fin with 6 branched rays, outer margin straight or slightly convex. Caudal fin forked with (8+8)9+8 branched rays, lobes pointed. Flank and back covered by cycloid scales. Chest and belly without scales. Lateral line complete, terminating between origin of hypural complex and caudal fin base. Anterior nostril opening at end of a low, ovoid, flap-like tube. Posterior tip of anterior nostril overlapping posterior nostril when folded backwards. One central pore and one lateral pore on each side of supratemporal head canal, 3(4) + 9–10 pores in infraorbital canal, 8–9 pores in supraorbital canal, and 9–10 pores in mandibular canal. A suborbital groove in male. Mouth small, arched. Lips thick without furrows, lower lip thicker than upper lip. A median interruption in lower lip. Upper lip without median incision, rarely with a very small and short median incision. *Processus dentiformis* narrow and rounded. Lower jaw rounded, without median notch. Barbels long; inner rostral barbel reaching base of maxillary barbel, outer reaching to vertical of posterior of anterior eye margin. Maxillary barbel reaching or almost reaching to vertical of posterior eye-margin.

Coloration. Body with yellowish or cream background and dark-brown pattern in live and preserved individuals. Preserved individuals with a dark-grey, narrow inner-axial stripe, absent in life. Dorsal head and upper

Figure 2. *Oxynoemacheilus chaboras*, FFR 15646, holotype, 53 mm SL; Türkiye: stream Beyazsu.

part of cheek brown, with marbled pattern. Ventral surface of head yellowish without pattern. Flank with 6–10 dark-brown bars or blotches, as much as, or thicker than, interspaces. Bars and blotches irregularly shaped and set, generally vertically elongated, sometimes oval, or horizontally elongated, usually extending to mid-dorsal saddles and meeting contra laterals. Back with 1–3 predorsal saddles, one saddle at dorsal-fin origin and one at posterior dorsal-fin base, and 3 saddles behind dorsal fin, as much as or thicker than interspaces. One dark-brown or black blotch at lower caudal-fin base, a second, much smaller blotch at uppermost caudal-fin base, both distinct in both live and preserved individuals. Dorsal, caudal and pectoral fins with many, small brown blotches on rays. These blotches forming 2–3 narrow bands on dorsal, and 3–5 on caudal. Pectoral, anal and pelvic fins hyaline, sometimes with a few dark-brown blotches on rays.

Distribution. The species known from the stream Beyazsu in the Euphrates drainage (Figs 6, 7).

Etymology. The species is named *Chaboras*, an ancient Greek name of the Khabur (Χαβώρας), as it was first documented by Ptolemy and Pliny the Elder ichthyofauna. A noun in genitive, indeclinable.

Discussion

Following our molecular analysis, *Oxynoemacheilus chaboras* belongs to the *O. persa* species group as defined by Freyhof and Geiger (2021). Within the *O. persa* species group, *O. chaboras* belongs to a group of species (*O. argyrogramma*, *O. euphraticus*, *O. hanae*, *O. karunensis*, *O. kurdistanicus*, *O. marunensis*, *O. persa*, *O. sarus*, and *O. shehabi*) that have a deeply emarginate or forked caudal fin (vs. slightly emarginate or truncate in *O. chomanicus*, *O. kentritensis*, *O. zagrosensis*, and *O. zarzianus*) and in which the male has a suborbital groove (vs. absent in *O. chomanicus*, *O. kentritensis*, *O. zagrosensis*, and *O. zarzianus*).

Oxynoemacheilus chaboras is most closely related to *O. shehabi* from the upper Orontes, *O. sarus* from the Seyhan and Ceyhan, *O. euphraticus* from the Euphrates and

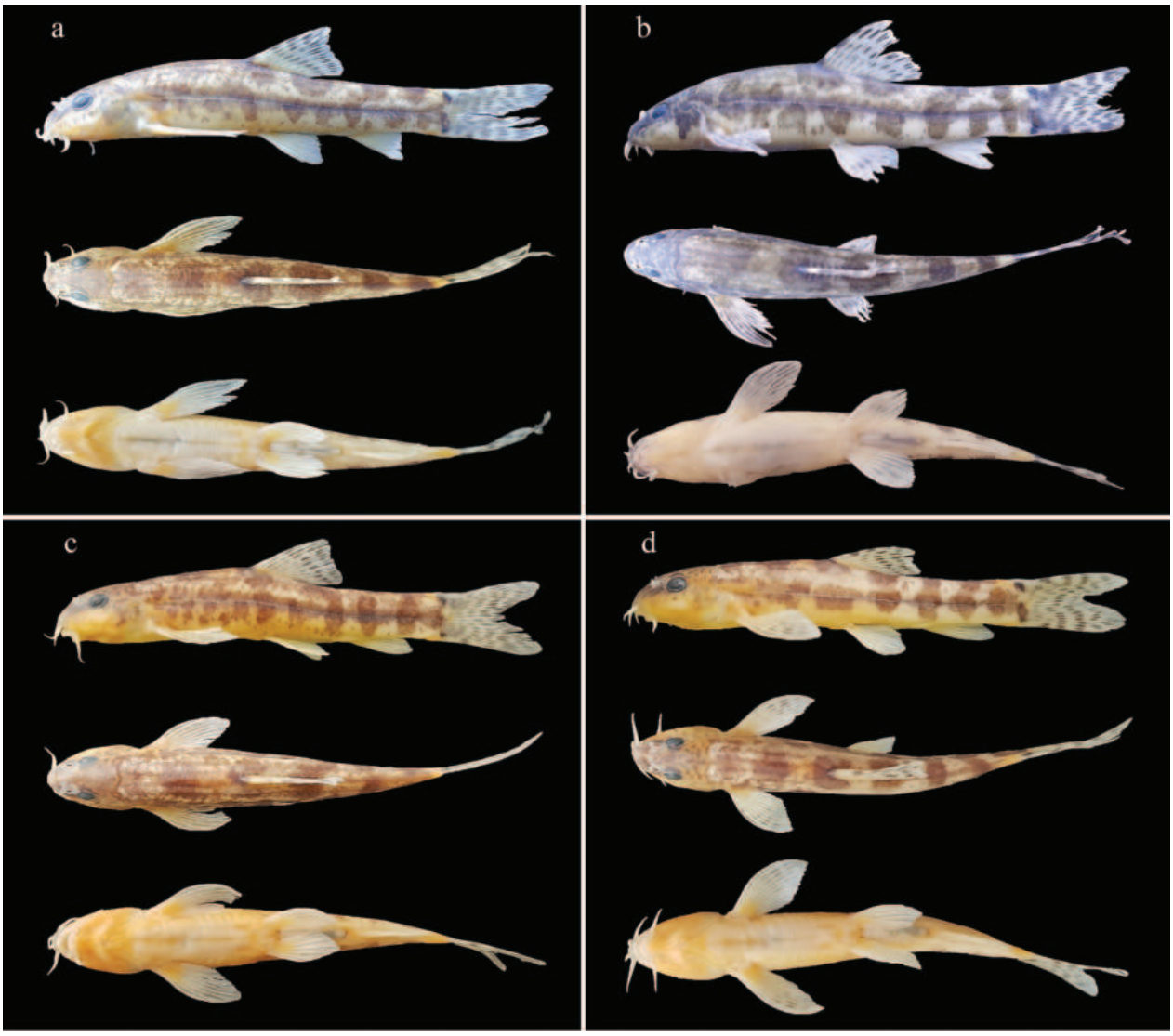

Figure 3. *Oxynoemacheilus chaboras*, paratypes, stream Beyazsu. **a.** FFR 1428, 50 mm SL; **b.** FFR 15633, 51 mm SL; **c.** FFR 1428, 50 mm SL; **d.** FFR 1428, 49 mm SL.

Figure 4. *Oxynoemacheilus chaboras*, FFR 15633, paratype, 51 mm SL; Türkiye: stream Beyazsu.

Tigris, *O. karunensis* from the Karkheh, and *O. persa* from Central Iran. *Oxynoemacheilus argyrogramma*, *O. hanae*, *O. kurdistanicus*, *O. marunensis* are placed in a second cluster of species within the *O. persa* species group and are not closely related. While all these species are well-supported in our molecular analysis (Table 1), their phylogenetic relationships are poorly supported in our phylogenetic tree (Fig. 1).

Oxynoemacheilus chaboras is distinguished from *O. shehabi* and *O. sarus* by possessing 8–9 pores in the supraorbital canal (vs. 5–7), a rudimentary and shallow

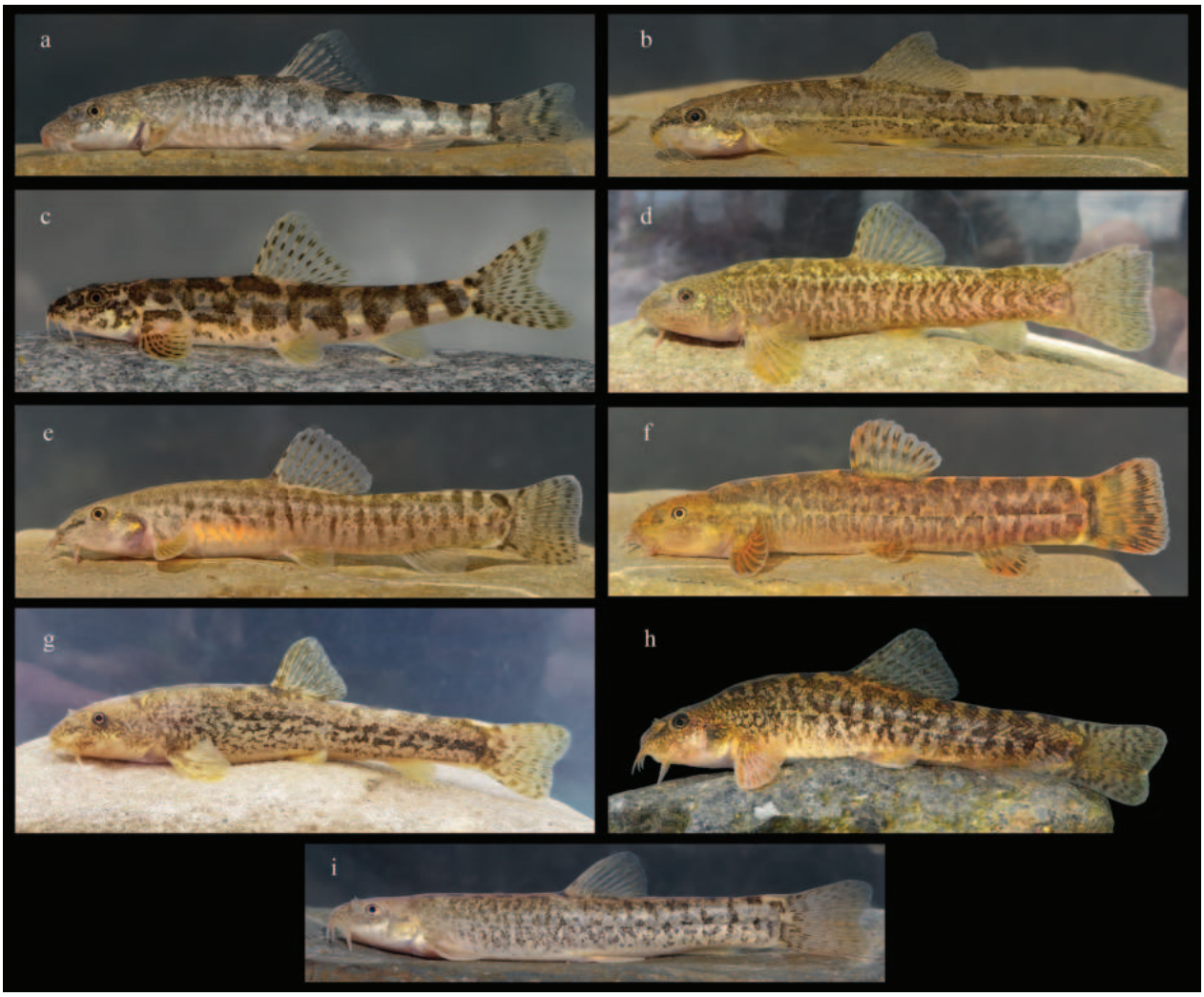

Figure 5. *Oxynoemacheilus* species in the Euphrates drainages: **a.** *O. bergianus*, stream Sason, 61 mm SL; **b.** *O. argyrogramma*, stream Sünnep, 50 mm SL; **c.** *O. euphraticus*, Great Zap River, 55 mm SL; **d.** *O. muefiti*, Murat River, 69 mm SL; **e.** *O. tigris*, stream Sünnep, 55 mm SL; **f.** *O. kaynaki*, Göksu River, 68 mm SL; **g.** *O. paucilepis*, stream Balıklıtohma, 70 mm SL; **h.** *O. arsaniasus*, stream Kaleli, 90 mm SL; **i.** *O. araxensis*, stream Arkaçayırlar, 71 mm SL.

pelvic axillary lobe fully attached to the body (vs. well-developed with a free tip), a deeper body (body depth at dorsal fin origin 17–22% SL vs. 14–17 in *O. shehabi*), deeper caudal peduncle (10–12% SL vs. 8–9 in *O. shehabi*), deeper head (head depth at eye 51–60% HL vs. 44–51 in *O. sarus*) and a longer anal fin (anal-fin height 18–22% SL vs. 16–19 in *O. sarus*). It is distinguished from *O. hanae* by lacking isolated patches of dark-brown spots or blotches on the lower part of the flank (vs. present) and possessing two distinct black blotches at the caudal-fin base (vs. usually absent or very small, overlaid by a chevron shaped bar).

The new species is distinguished from *O. karunensis* and *O. persa* by lacking the dense mottling in the interspaces between the blotches on the flank in almost all individuals (vs. very dense mottling in all individuals), possessing a deeper caudal peduncle (caudal peduncle depth 1.4–1.7 times in its length vs. 1.7–3.1 in *O. karunensis*), and two distinct black blotches at the caudal-fin base (vs. two very large blotches, usually fused to an irregularly shaped bar in *O. persa*).

We were not able to compare *O. chaboras* to *O. marunensis* as we had no materials available. We noted that the description of this species by Sayyadzadeh and Esmaeili (2020) is solely based on juvenile individuals. This limitation made it impossible to make definitive statements about the adult colour pattern and some other character states of *O. marunensis*. *Oxynoemacheilus chaboras* is distinguished from *O. marunensis*, based on Sayyadzadeh and Esmaeili (2020), by possessing a deeper body (body depth at dorsal-fin origin 17–22% mm SL vs. 14–18), a narrower interorbital width (18–24% mm HL vs. 23–31), and 9+8 branched caudal-fin rays (vs. 8+7 or 8+8). It should be noted that *O. marunensis* is only distantly related to *O. chaboras*. The mean genetic distance between these species is 4.55%.

Oxynoemacheilus chaboras is distinguished from *O. kurdistanicus* by possessing no, or rarely, a very short incision in the upper lip (vs. usually a deep, rarely a shallow median incision), and a series of mid-lateral blotches disconnected from the saddles on the back below the

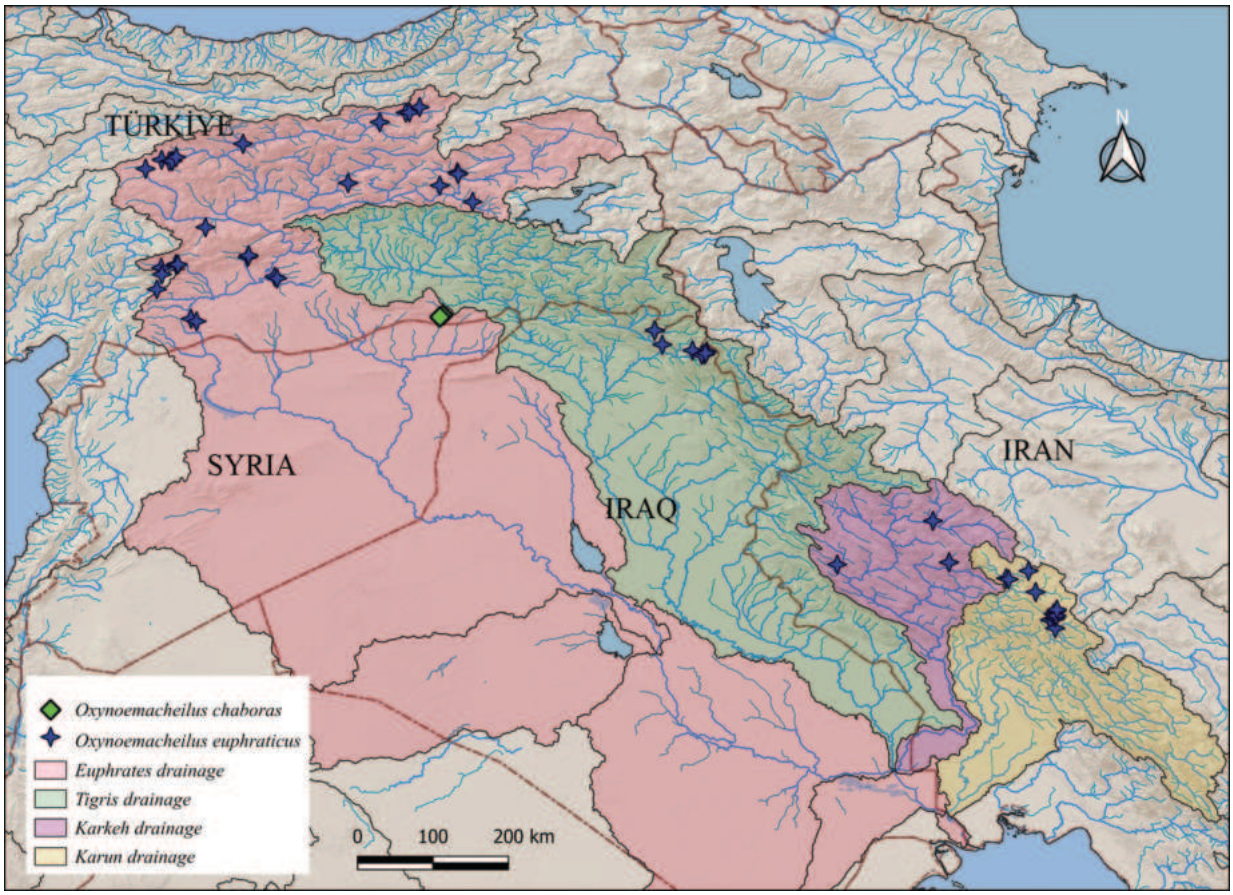

Figure 6. Distribution map of *Oxynoemacheilus chaboras* and *O. euphraticus*.

Table 2. Morphometric data of *Oxynoemacheilus chaboras* (holotype FFR 15646 and paratypes FFR 1428, n = 11).

	Holotype	min	max	mean	SD
Standard length (mm)	53	46	60	51.9	4.0
In percent of standard length					
Head length	24.2	23.0	25.0	24.1	0.6
Body depth at dorsal-fin origin	18.4	17.4	21.8	18.8	1.2
Predorsal length	50.9	47.4	51.1	49.7	1.2
Postdorsal length	35.8	33.8	37.4	35.5	1.2
Prepelvic length	51.2	49.6	55.5	52.1	1.2
Preanal length	72.7	72.7	78.7	75.7	1.8
Distance between pectoral and pelvic-fin origins	30.1	26.2	30.6	28.4	1.6
Distance between pelvic and anal-fin origins	21.4	21.4	25.2	22.8	1.0
Distance between vent and anal-fin origin	3.0	2.1	3.7	2.9	0.5
Dorsal-fin height	22.7	19.9	24.3	22.4	1.2
Anal-fin height	18.9	15.8	19.2	17.9	1.0
Pectoral-fin length	24.1	21.8	26.7	24.2	1.7
Pelvic-fin length	18.7	16.5	19.3	18.1	0.8
Length of caudal peduncle	19.8	16.9	19.8	18.2	0.9
Depth of caudal peduncle	11.9	10.2	12.2	11.6	0.5
In percent of head length					
Head depth at eye	51	51	60	53.9	3.3
Maximum head width	59	59	66	63.2	2.6
Snout length	40	39	44	41.4	1.8
Eye diameter	19	19	23	20.6	1.4
Postorbital distance	45	40	50	45.2	2.7
Interorbital width	21	18	24	21.6	2.3
Length of inner rostral barbel	30	20	30	24.7	2.5
Length of outer rostral barbel	41	34	44	38.5	3.2
Length of maxillary barbel	40	33	44	39.6	3.3

dorsal-fin origin (vs. bars connected to saddles in most, but not all individuals). All *O. kurdistanicus* examined have a pattern of bars on flank, while most *O. chaboras* have a series of mid-lateral blotches usually narrowly connected to saddles. In *O. chaboras*, this pattern is usually formed by two wide and dark elements (blotch and saddle) connected by a narrower and paler field of pigments while in *O. kurdistanicus* (and *O. euphraticus* and *O. marunensis*), bars are usually (not always) regularly shaped and not wider along the lateral midline.

Comparative materials

Oxynoemacheilus araxensis ZMH 4827, holotype, 61 mm SL; ZMH 4826, paratypes, 5, 36–50 mm SL; ZMH 5951, paratypes, 4, 44–64 mm SL; Türkiye: Erzurum prov.: Kandili Karasu, Euphrates drainage.—FFR 1354, 11, 66–90 mm SL Türkiye: Erzurum prov.: stream Sırlı at Ilıca 40.2130°N, 41.0699°E.—FFR 1451, 2, 68–75 mm SL; Türkiye: Erzurum prov.: stream Ağarcık at Ilıca, 40.2460°N, 41.0710°E.—FFR 1468, 12, 53–70 mm SL; Türkiye: Erzurum prov.: stream Baş about 1 km west of Çayköy, 39.9470°N, 40.8040°E.—FSJF 3440, 6, 42–71 mm SL; Türkiye: Erzurum prov.: stream Arkaçayırlar at Paşayurdu, 39.9833°N, 40.9920°E.

Oxynoemacheilus argyrogramma FFR 15516, 26, 37–49 mm SL; Türkiye: Kilis prov.: stream Sünnep at

Figure 7. Type locality of *Oxynoemacheilus chaboras*.

northeastern Küplüce, 36.7640°N, 37.2540°E.—FFR 1574, 14, 41–62 mm; FFR 1448, 11, 37–48 mm SL; Türkiye: Gaziantep prov.: stream Merziman about 3 km south of Yavuzeli, 37.2910°N, 37.5730°E.

Oxynoemacheilus arsaniasus FFR 15531, paratypes, 5, 36–54 mm SL; Türkiye: Muş prov.: stream Kaynarca at Tepe, 39.1070°N, 41.4920°E.—FFR 1449, 1, 49 mm SL; Türkiye: Muş prov.: stream Kaynarca about 3 km southeast Tepe, 39.0680N, 41.5290°E.—FSJF 4019, 12, 46–97 mm SL; Türkiye: Bitlis prov.: Reservoir of stream Karasu in Kaleli, 38.5537°N, 42.0257°E.

Oxynoemacheilus bergianus FFR 1577, 19, 54–62 mm SL; Türkiye: Samsun prov.: stream Soruk 20 km east of Vezirköprü, 41.1189°N, 35.2269°E.—FFR 15561, 9, 35–69 mm SL; Türkiye: Kayseri prov.: stream Sarnaz a drainage of stream Zamantı at Taşçı, 38.1953°N, 35.7805°E.—FSJF 2983, 15, 38–77 mm SL; Türkiye: Kayseri prov.: stream Zamantı at Pınarbaşı, 38.7366°N, 36.4131°E. —FFR 1457, 11, 64 –72 mm SL; Türkiye: Malatya prov.: stream Sultansuyu 8 km east of Akçadağ, 38.3388°N, 38.0620°E.—FFR 1467, 28, 54–64 mm SL; Türkiye: Erzurum prov.: stream Baş 10 km east of Aşkale, 39.9478°N, 40.8040°E.—FFR 15506, 25, 33–59 mm SL; Türkiye: Ağrı prov.: Murat River 17 km west of Taşlıçay, 39.6785°N, 43.1887°E.

Oxynoemacheilus chomanicus FSJF 3644, 5, 33–61 mm SL; Iraq: Choman River at Alut, 35.9563°N, 45.6155°E.

Oxynoemacheilus euphraticus FFR 1434, 1, 56 mm SL; Türkiye: Sivas prov.: Euphrates at İliç, 39.4850°N, 38.5850°E.—FFR 1471, 25, 27–63 mm SL; Türkiye: Sivas prov.: stream Kangal about 1 km west of Çetinkaya, 39.2560°N, 37.6250°E.—FFR15520, 14, 41–57 mm SL; Malatya prov.: stream Sultan Suyu about 7 km east of Akçadağ, 38.3390°N, 38.0620°E.—FFR 15508, 13, 53–70 mm SL; Türkiye: Adıyaman prov.: stream Göksu at Düzbağ, 37.7950°N, 37.4710°E.

Additional distribution records

Own data: 39.9124°N, 40.8540°E. 39.9094°N, 40.8028°E. 36.943333°N, 44.19533°E. 39.2516°N, 37.6189°E. 38.9500°N, 40.0166°E. 38.9166°N, 41.2666°E. 39.2515°N, 37.6189°E. 39.2515°N, 37.6189°E. 39.2515°N, 37.61894°E. 39.2515°N, 37.6189°E. 38.9167°N, 41.2667°E. 39.3013°N, 37.6743°E. 37.8370°N, 37.6848°E. 39.1439°N, 37.2571°E. 39.2516°N, 37.6189°E. 36.9433°N, 44.1953°E. 37.7950°N, 37.4705°E. 37.8444°N, 37.6702°E. 37.6500°N, 39.0500°E. 37.0666°N, 37.9500°E. 39.9833°N, 40.9920°E. 36.7484°N, 44.2997°E. 36.9433°N, 44.1953°E. 36.6164°N, 44.8781°E. 36.6106°N, 44.8381°E. Saygun et al. (2021): 37.8369°N, 37.6848°E. 39.0956°N, 41.5054°E. 39.4850°N, 38.5850°E. 39.2561°N, 37.6251°E. 39.2463°N, 37.5807°E. 37.9409°N, 38.6470°E. 37.8391°N, 37.6977E. 37.7052°N, 37.4790°E. 37.5021°N, 37.4108°E. Çiçek et al. (2022): 39.7800°N, 40.4486°E. Rakıcı et al. (2020): 39.0741°N, 41.5195°E. 38.6928°N, 41.7142°E. 39.2672°N, 37.4748°E. 38.3471°N, 38.0737°E. 37.8392°N, 37.6766°E. 37.9635°N, 38.6624°E. Krupp (1985): 37.1006°N, 37.8758°E. 37.6742°N, 39.0158°E. Jouladeh Roudbar et al. (2016): 33.1382°N, 49.6788°E. 33.1182°N, 49.6676°E. 33.7846°N, 48.2068°E. 33.7820°N, 48.2080°E. 33.5507°N, 49.0207°E. 33.0108°N, 49.6478°E. 33.0674°N, 49.6500°E. 33.0559°N, 49.6701°E. 32.9988°N, 49.5823°E. 33.7543°N, 46.6847°E. 34.3478°N, 47.9885°E. Zare-Shahraki et al. (2022): 33.5647°N, 48.9855°E. 33.3783°N, 49.3888°E. 33.0819°N, 49.6319°E. 33.0570°N, 49.6668°E. 32.8860°N, 49.6560°E. 32.9997°N, 49.5888°E. 33.0322°N, 49.6564°E. Musa and Abdulrahman (2023): 36.6705°N, 44.71154°E. 36.6553°N, 44.9055°E. 36.6325°N, 44.8884°E.

Oxynoemacheilus hanae ZFMK 103020, holotype, 57 mm SL; FSJF 3359, paratypes, 22, 46–61 mm SL; Iraq: stream Zalm south of Taparezina, 35.3064°N, 45.9705°E.—FSJF 3641, 63, 34–61 mm SL; Iraq: stream Zalm south of Taparezina, 35.3064°N, 45.9705°E.

Oxynoemacheilus karunensis FSJF 3525, 8, 33–55 mm SL; Iran: Hamadan prov.: Gamasiab River at Do Ab, 47.9167°N, 34.3724°E.—FSJF 3523, 6, 34–51 mm SL; Iran: Hamadan prov.: Haram Abad River at Ashmizan, 34.1105°N, 48.8704°E.—FSJF 3524, 7, 37–53 mm SL; Hamadan prov.: Dehno stream about 2 km south-west of Nahavand, 48.3532°N, 34.1691°E.—FSJF 3526, 2, 30–40 mm SL; Iran: Hamadan prov.: Gamasiab River at Chesme Mahi, 34.3382°N, 48.0324°E.—SMF IR7, 3, 36–44 mm SL; Iran: Khozestan prov.: Marun River near Behbehan, 30.6567°N, 50.1883°E.

Oxynoemacheilus kentritensis FFR 1566, holotype, 67 mm SL; Türkiye: FFR 01403, paratypes, 3, 57–68 mm SL; Bitlis prov.: stream Kesan about 1 km south of Güntepe, 38.3566°N, 42.6275°E.—FSJF

3645, paratypes, 3, 65–79 mm SL; Türkiye: Bitlis prov.: stream Horozdere east of Hizan, 38.2447°N, 42.4791°E.—FSJF 3646, paratypes, 2, 68–70 mm SL; Türkiye: Bitlis prov.: stream Oraniz about 1 km east of Dönertaş, 38.3141°N, 42.5655°E.

Oxynoemacheilus kurdistanicus FSJF 3369, 28, 40–61 mm SL; Iraq: Nalparez River, 35.5707°N, 45.8630°E.—FSJF 3347, 25, 50–62 mm SL; Iraq: stream north-west of Saburawa, a tributary of Tabin River, 35.8336°N, 45.1044°E.—FSJF 3353, 9, 40–61 mm SL; Iraq: stream KunaMassi in Sevanja, 35.7892°N, 45.4030°E.—FSJF 3373, 54, 35–62 mm SL; Iraq: stream Suraw near Suraw village, 35.7626°N, 45.9848°E.—FSJF 3643, 15, 36–62 mm SL; Iraq: Choman River at Alut, 35.9564°N, 45.6155°E.

Oxynoemacheilus muefiti FFR 15507, paratypes, 2, 29–45 mm SL; Ağrı prov.: Türkiye: Murat River at Ballıbostan; 39.6780°N, 43.1890°E.—FFR 1432, 7, 42–63 mm SL, Ağrı prov.: Türkiye: Murat River at Taşlıçay; 39.6460°N, 43.3670°E.—FSJF 3444, 4, 33–46 mm SL; Türkiye: Ağrı prov.: Murat River at Ballıbostan, 12 km east of Ağrı, 39.6789°N, 43.1896°E.—FSJF 2556, 3, 45–47 mm SL; Türkiye: Adıyaman prov.: stream Eğri south of Adıyaman, tributary to Atatürk Reservoir, 37.7417°N, 38.3351°E.—IUSHM 2019-1410, 3, 37–68 mm SL; Türkiye: Ağrı prov.: stream near Sarıköy, 16 km west of Eleşkirt, 39.8016°N, 42.4816°E.—IUSHM 2019-1411, 3, 43–52 mm SL; Türkiye: Ağrı prov.: Murat River at Balıbostan, 12 km east of Ağrı, 39.6789°N, 43.1896°E.

Oxynoemacheilus paucilepis FFR15510, 10, 34–73 mm SL; Türkiye: Sivas prov.: stream Balıklıtohma about 3 km south of Kocakurt, 39.1440°N, 37.2570°E.—FFR15521, 15, 41–76 mm SL; Türkiye: Sivas prov.: stream Balıklıtohma at Kuruayşe, 39.2070°N, 37.2010°E.—FSJF 2852, 50, 24–39 mm SL; Türkiye: Sivas prov.: stream Tersakan about 15 km southwest of Kangal, 39.1439°N, 37.2571°E.

Oxynoemacheilus persa NMW 48567, holotype, 50 mm SL; Iran: spring at Persepolis.—FSJF 3214 (earlier IZA 7826), 25 paratypes of O. farsicus, 34–56 mm SL; Iran: Fars prov.: Shur River at Dasht-e-Arzhan, a tributary of Mond River.— FSJF 2245, 44, 31–65 mm SL; Iran: Fars prov.: Kor River about 73 km north of Shiraz, 30.1936°N, 52.4657°E.

Oxynoemacheilus sarus FFR 15585, holotype, 52.5 mm SL; FFR 15522, paratypes, 4, 39–54 mm SL;Türkiye: Adana prov.: lower stream Çakıt, south of Salbaş, 37.1031°N, 35.1094°E.—FSJF 2327, paratypes, 10, 32–49 mm SL; Türkiye: Adana prov.: lower stream Çakıt, south of Salbaş, 37.0961°N, 35.1170°E.—FSJF 2377, paratypes, 2, 48–49 mm SL; Türkiye: Adana prov.: stream Körkün at Karakuyu, 37.1529°N, 35.1606°E.—FFR 15586, 3, 47–51 mm SL; Türkiye: Kahramanmaraş Prov.; stream Aksu at 8 km northeast of Pazarcık, 37.5390°N, 37.3480°E.—FSJF 2567, 1, 48 mm SL; Türkiye: Adıyaman prov.: stream Çelik at road south of Gölbaşı, 37.6239°N, 37.5034°E.

Oxynoemacheilus shehabi ZFMK ICH 124181, holotype, 46.3 mm SL; ZFMK ICH-125126-28, paratypes, 3, 41.5–47.6 mm SL; Syria: Orontes at Al Qusayr, 34.5086°N, 36.5389°E.

Oxynoemacheilus zarzianus FSJF 3352, 28, 39–69 mm SL; Iraq: stream Kunamasi in Sevanja, 35.7892°N, 45.4030°E.—FSJF 3348, 16, 46–68 mm SL; Iraq: stream in Merga village, 36.0515°N, 45.0945°E.—FSJF 3651, 18, 54–75 mm SL: Iraq: stream Kunamasi in Kunamasi, 35.7967°N, 45.4136°E.—FSJF 3372, 30, 43–71 mm SL; Iraq: stream Suraw near Suraw village, 35.7626°N, 45.9848°E.

Acknowledgments

Authors would like to thank Fadil Kaya (Bitlis) for his help during the fieldwork. We also thank Müfit Özuluğ (IUSHM), Anja Palandacic (NMW), Serkan Wesel (ZFMK-ICH), and Ralf Thiel (ZMH) for allowing JF to examine materials under their care. Because the second author contributed to this manuscript at Bournemouth University, we would like to thank Bournemouth University for providing their facilities, and TÜBİTAK BİDEB (2219 Program) which supported her with one-year scholarships during her post-doc research at United Kingdom.

References

Bektaş Y, Aksu İ, Kaya C, Bayçelebi E, Turan D (2022) DNA barcoding and species delimitation of the genus *Oxynoemacheilus* (Teleostei: Nemacheilidae) in Anatolia. Journal of Fish Biology 101(3): 505–514. https://doi.org/10.1111/jfb.15114

Canpolat E, Bozdoğan M (2019) Beyazsu Havzası'nın (Mardin) flüvyal jeomorfolojisi ve hidrografik özellikleri. Türk Coğrafya Dergisi 73: 96–105. [In Turkish] https://doi.org/10.17211/tcd.658375

Çiçek E, Seçer B, Eagderi S, Sungur S (2022) Length-weight relations and condition factors of 34 *Oxynoemacheilus* species (Actinopterygii: Cypriniformes: Nemacheilidae) from Turkish inland waters. Acta Ichthyologica et Piscatoria 52(1): 29–34. https://doi.org/10.3897/aiep.52.81211

Esmaeili HR, Sayyadzadeh G, Özuluğ M, Geiger M, Freyhof J (2014) Three new species of *Turcinoemacheilus* from Iran and Turkey (teleostei: Nemacheilidae). Ichthyological Exploration of Freshwaters 24(3): 257–273. https://www.pfeil-verlag.de/wp-content/uploads/2017/04/ief24_3_07.pdf

Felsenstein J (1981) Evolutionary trees from DNA sequences: A maximum likelihood approach. Journal of Molecular Evolution 17(6): 368–376. https://doi.org/10.1007/BF01734359

Freyhof J, Geiger MF (2021) *Oxynoemacheilus shehabi*, a new nemacheilid loach from the upper Orontes in southern Syria (Teleostei: Nemacheilidae). Zootaxa 4908(4): 571–583. https://doi.org/10.11646/zootaxa.4908.4.9

Freyhof J, Geiger MF, Golzarianpour K, Patimar R (2016) *Sasanidus*, a new generic name for *Noemacheilus kermanshahensis* Bănărescu & Nalbant, with discussion of *Ilamnemacheilus* and *Schistura*

(Teleostei; Nemacheilidae). Zootaxa 4107(1): 65–80. https://doi.org/10.11646/zootaxa.4107.1.3

Freyhof J, Kaya C, Turan D, Geiger MF (2019) Review of the *Oxynoemacheilus tigris* group with the description of two new species from the Euphrates drainage (Teleostei: Nemacheilidae). Zootaxa 4612(1): 29–57. https://doi.org/10.11646/zootaxa.4612.1.2

Freyhof J, Kaya C, Ali A (2021) A Critical Checklist of the Inland Fishes Native to the Euphrates and Tigris Drainages. In: Jawad LA (Ed.) Tigris and Euphrates Rivers: Their Environment from Headwaters to Mouth. Aquatic Ecology Series Vol. 11. Springer, Cham. https://doi.org/10.1007/978-3-030-57570-0_35

Freyhof J, Kaya C, Geiger MF (2022) A practical approach to revise the *Oxynoemacheilus bergianus* species group (Teleostei: Nemacheilidae). Zootaxa 5128(2): 151–194. https://doi.org/10.11646/zootaxa.5128.2.1

Geiger MF, Herder F, Monaghan MT, Almada V, Barbieri R, Bariche M, Berrebi P, Bohlen J, Casal-Lopez M, Delmastro GB, Denys GP, Dettai A, Doadrio I, Kalogianni E, Karst H, Kottelat M, Kovacic M, Laporte M, Lorenzoni M, Marcic Z, Özuluğ M, Perdices A, Perea S, Persat H, Porcelotti S, Puzzi C, Robalo J, Sanda R, Schneider M, Slechtova V, Stoumboudi M, Walter S, Freyhof J (2014) Spatial heterogeneity in the Mediterranean biodiversity hotspot affects barcoding accuracy of its freshwater fishes. Molecular Ecology Resources 14(6): 1210–1221. https://doi.org/10.1111/1755-0998.12257

Hall TA (1999) BioEdit: A user-friendly biological sequence alignment editor and analysis program for windows 95/98/NT. Nucleic Acids Symposium Series 41: 95–98. https://www.scirp.org/reference/ReferencesPapers?ReferenceID=1383440

Jouladeh-Roudbar A, Eagderi S, Hosseinpour T (2016) *Oxynoemacheilus freyhofi*, a new nemacheilid species (Teleostei, Nemacheilidae) from the Tigris basin, Iran. FishTaxa 1(2): 94–107. https://doi.org/10.7508/fishtaxa.2016.02.005

Kamangar BB, Prokofiev AM, Ghaderi E, Nalbant TT (2014) Stone loaches of Choman River system, Kurdistan, Iran (Teleostei: Cypriniformes: Nemacheilidae). Zootaxa 3755(1): 33–61. https://doi.org/10.11646/4364

Kaya C, Turan D, Kalaycı G, Bayçelebi E, Freyhof J (2020) The westernmost known population of *Paracobitis* (Teleostei, Nemacheilidae), with the description of a new species from the Euphrates River in southern Anatolia. Zootaxa 4838(4): 525–534. https://doi.org/10.11646/zootaxa.4838.4.6

Kottelat M (1990) Indochinese nemacheilines. A revision of nemacheiline loaches (Pisces: Cypriniformes) of Thailand, Burma, Laos, Cambodia and southern Viet Nam. Verlag Dr. Friedrich Pfeil, München, 262 pp.

Kottelat M, Freyhof J (2007) Handbook of European freshwater fishes. Kottelat, Cornol and Freyhof, Berlin, [xiv +] 646 pp.

Krupp F (1985) Systematik und Zoogeographie der Süsswasserfische des levantinischen Grabenbruchsystems und der Ostküste des Mittelmeers. Dissertation, Johannes Gutenberg Universität, Mainz, 215 pp.

Kumar S, Stecher G, Li M, Knyaz C, Tamura K (2018) MEGA X: Molecular Evolutionary Genetics Analysis across computing platforms. Molecular Biology and Evolution 35(6): 1547–1549. https://doi.org/10.1093/molbev/msy096

Musa N, Abdulrahman R (2023) Watershed Assessment for Threatened Fish in Halgurd-Sakran Park in Iraqi-Kurdistan. https://doi.org/10.2023

Posada D (2008) jModelTest: Phylogenetic model averaging. Molecular Biology and Evolution 25(7): 1253–1256. https://doi.org/10.1093/molbev/msn083

Rakıcı H, Aksu İ, Bektaş Y (2020) Genetic identification and phylogenetic relations of *Oxynoemacheilus* species (Teleostei: Nemacheilidae) from drainage of Euphrates in Turkey based on COI-barcode region. Journal of Anatolian Environmental and Animal Sciences 5(3): 408–418. https://doi.org/10.35229/jaes.776381

Ronquist F, Teslenko M, van der Mark P, Ayres DL, Darling A, Höhna S, Larget B, Liu L, Suchard MA, Huelsenbeck JP (2012) MrBayes 3.2: Efficient Bayesian phylogenetic inference and model choice across a large model space. Systematic Biology 61(3): 539–542. https://doi.org/10.1093/sysbio/sys029

Saygun S, Ağdamar S, Özuluğ M (2021) *Oxynoemacheilus fatsaensis*, a new nemacheilid loach from the Elekçi Stream in Northern Anatolia (Teleostei: Nemacheilidae). Zoologischer Anzeiger 294: 39–49. https://doi.org/10.1016/j.jcz.2021.07.011

Sayyadzadeh G, Esmaeili HR (2020) *Oxynoemacheilus marunensis*, a new loach species from the Persian Gulf basin with remarks on *O. frenatus* (Teleostei: Nemacheilidae). Zootaxa 4885(2): 189–206. https://doi.org/10.11646/zootaxa.4885.2.2

Srivathsan A, Meier R (2012) On the inappropriate use of Kimura-2-parameter (K2P) divergences in the DNA-barcoding literature. Cladistics 28(2): 190–194. https://doi.org/10.1111/j.1096-0031.2011.00370.x

Turan D, Kaya C, Ekmekçi FG, Bayçelebi E (2014) Three new species of *Alburnoides* (Teleostei: Cyprinidae) from Euphrates River, Eastern Anatolia, Turkey. Zootaxa 3754(2): 101–116. https://doi.org/10.11646/4295

Ward RD, Zemlak TS, Innes BH, Last PR, Hebert PDN (2005) DNA barcoding Australia's fish species. Philosophical Transactions of the Royal Society of London. Series B, Biological Sciences 360(1462): 1847–1857. https://doi.org/10.1098/rstb.2005.1716

Yoğurtçuoğlu B, Kaya C, Freyhof J (2022) Revision of the *Oxynoemacheilus angorae* group with the description of two new species (Teleostei: Nemacheilidae). Zootaxa 5133(4): 451–485. https://doi.org/10.11646/zootaxa.5133.4.1

Zare-Shahraki M, Ebrahimi-Dorche E, Brude A, Flotemersch J, Blocksom K, Bănăduc D (2022) Fish species composition, distribution and community structure in relation to environmental variation in a semi-arid mountainous river basin. Water (Basel) 14(14): 2226. https://doi.org/10.3390/w14142226

Zoosyst. Evol. 100 (2) 2024, 469–482 | DOI 10.3897/zse.100.119153

PENSOFT

für Natur MUSEUM FÜR NATURKUNDE BERLIN

A new species of genus *Urophonius* Pocock, 1893 (Scorpiones, Bothriuridae), from Andean Mauline Chilean forests, with a phylogenetic re-analysis of the genus

Andrés A. Ojanguren-Affilastro[1], Fermín M. Alfaro[2,3,4], Martín J. Ramírez[1], Bernardino Camousseigt-Montolivo[5], Jaime Pizarro-Araya[2,4,6,7]

1 *División Aracnología, Museo Argentino de Ciencias Naturales "Bernardino Rivadavia" (CONICET), Avenida Ángel Gallardo 470, 1405 DJR, Buenos Aires, Argentina*
2 *Laboratorio de Entomología Ecológica (LEULS), Departamento de Biología, Facultad de Ciencias, Universidad de La Serena, Casilla 554, La Serena, Chile*
3 *Programa de Doctorado en Biología y Ecología Aplicada, Universidad Católica del Norte, Universidad de La Serena, La Serena, Chile*
4 *Grupo de Artrópodos, Sistema Integrado de Monitoreo y Evaluación de Ecosistemas Forestales Nativos (SIMEF), La Serena, Chile*
5 *Environment & Permitting - HSEQ, Enel Green Power & Thermal Generation, Roger de Flor 2725, Torre 1, Piso 1, Las Condes, Santiago, Chile*
6 *Instituto de Ecología y Biodiversidad (IEB), Santiago, Chile*
7 *Programa de Doctorado en Conservación y Gestión de la Biodiversidad, Facultad de Ciencias, Universidad Santo Tomás, Santiago, Chile*

https://zoobank.org/1A6B3F2D-ADB7-412B-A2AD-BB7A9BC35757

Corresponding author: Jaime Pizarro-Araya (japizarro@userena.cl)

Academic editor: Danilo Harms ♦ **Received** 19 January 2024 ♦ **Accepted** 28 March 2024 ♦ **Published** 7 May 2024

Abstract

Urophonius trewanke **sp. nov.** is described from the Mauline Andean woods of northern Chilean Patagonia. This species belongs to the *granulatus* species group, which includes the most basal species within the genus. This species is only active in summer as in all species of its group. We performed a phylogenetic analysis of the genus *Urophonius* based on morphological characters to establish the position and relationships of the new species in the genus.

Key Words

Bothriuridae, Chile, Mauline woods, new species, phylogeny

Introduction

The scorpion genus *Urophonius* Pocock, 1893 comprises small burrowing species from southern South America. In the last two decades, there has been a remarkable increase in the knowledge of this genus; in this period, the number of described species has almost doubled (Acosta 2003; Ojanguren-Affilastro and Cheli 2009; Ojanguren-Affilastro et al. 2010, 2011, 2020), the first phylogenetic analysis of the genus has been performed (Ojanguren-Affilastro et al. 2020) and, more recently, the historical time frame of its evolution and diversification has been unveiled using transcriptomes and UCEs (Ojanguren-Affilastro et al. 2023).

Urophonius is remarkable amongst all known scorpion genera from temperate and cold areas because of its adaptations to low temperatures (Maury 1969, 1973; Ojanguren-Affilastro et al. 2020; Garcia et al. 2021). This genus reaches the southernmost and colder part of South America (Maury 1979; Ojanguren-Affilastro et al. 2020) and most *Urophonius* species exhibit surface activity in winter, contrary to other species from the region (and temperate areas of the world), which are active during the warmer period of the year (Pizarro-Araya et al. 2011; Ojanguren-Affilastro and Kovarik 2013).

The first morphological phylogeny of the genus (Ojanguren-Affilastro et al. 2020) suggested a single and relatively

early origin of winter activity in *Urophonius*. A posterior dated phylogeny, based on diverse phylogenomic datasets (Ojanguren-Affilastro et al. 2023), supported this early origin of the winter activity period and dated it between 68 and 42 million years ago (MYA), before the most important uplift of the Andes (Ghosh et al. 2006; Garzione et al. 2008).

On the other hand, some species of the genus still retain the summer activity period, which is common to most species of the family and the order (Ojanguren-Affilastro and Kovarik 2013). These summer *Urophonius* species are grouped in the *granulatus* species group and occur exclusively in cold areas of southern South America, both in steppes and temperate woods.

In a recent comprehensive study of arthropods conducted at the "Fundo La Escuadra" (Figs 1a, 2), a small well-preserved area located within the Cipreses River Basin, a tributary of the Maule River Basin in the Maule Region of Chile, our research team made notable discoveries. The upper Maule River Basin is partially isolated by the Andes and has proven to harbour several endemic species of arthropods and even vertebrates (Corbalán et al. 2010; Correa et al. 2018, 2020; Ojanguren-Affilastro et al. 2020). This study allowed us to identify and collect numerous species of arachnids and insects not previously documented. In particular, amongst these newly-discovered taxa, we found a hitherto unknown species of scorpion that belongs to the genus *Urophonius* Pocock, 1893. This research, rooted in the rich and highly endemic biodiversity of the area, contributes significantly to our understanding of the local arthropod fauna. The identification and documentation of a new scorpion species underlines the ecological importance of the ecosystem preserved at "Fundo La Escuadra". The findings of this study not only expand our knowledge of regional arthropod diversity, but also emphasise the need for further research and conservation efforts in this ecologically important area.

In this contribution, we describe *Urophonius trewanke* sp. nov. (Fig. 1b) from the Maule Valley in the upper Maule River Basin (Fig. 2b). *Urophonius trewanke* sp. nov. is the second known endemic *Urophonius* from this area, the other species being *Urophonius pehuenche* Ojanguren-Affilastro & Pizarro-Araya, 2020, which, contrary to the new species, is only active in winter (Ojanguren-Affilastro et al. 2020). We also perform a phylogenetic analysis, based in morphological characters to clearly stablish the phylogenetic position of the new species in the genus.

Methods

Cladistic analysis

Taxa. The matrix in the cladistics analysis comprises a total of 21 species, 17 species of *Urophonius* and four outgroups. We used the same species as Ojanguren-Affilastro et al. (2020), including all known species of *Urophonius*, together with the new species herein described: *U. trewanke* sp. nov. Outgroups belonging to four other genera in the family Bothriuridae include: one species of the Australian bothriurid *Cercophonius*, which, according to all previous phylogenetic analyses, is the sister genus of *Urophonius* (Prendini 2000, 2003; Ceccarelli et al. 2016; Ojanguren-Affilastro et al. 2020, 2023; Santibañez-López et al. 2023); one species of *Phoniocercus* Pocock, 1893, which has also been suggested as closely related to *Urophonius* (Acosta 1988); one species of *Thestylus* Simon, 1880, which, according to previous phylogenetic analysis, is the most basal split in the American bothriurids (Prendini 2000, 2003; Ceccarelli et al. 2016); and one species of *Centromachetes* Lonnberg, 1897, which also shares several morphological characters with *Urophonius* (Ojanguren-Affilastro and Kovarik 2013). The tree was rooted on *Thestylus aurantiurus* Yamaguti & Pinto-da-Rocha, 2003, based on previous evidence for the relationships amongst bothriurid genera (Prendini 2000, 2003).

Materials

Specimens examined are deposited in the following collections: Museo Argentino de Ciencias Naturales "Bernardino Rivadavia," Buenos Aires, Argentina (**MACN-Ar**, Martín J. Ramírez); Museo Nacional de Historia Natural, Santiago, Chile (**MNHN**, Mario Elgueta Donoso); Museo de Zoología de la Universidad de Concepción (**MZUC**, Laura Tavera Martínez); Laboratorio de Entomología Ecológica, Universidad de La Serena, Chile (**LEULS**, Jaime Pizarro-Araya). A table with exemplars and locality data used for the analyses are presented as Suppl. material 1.

Characters

We used a matrix, based in 114 morphological characters. The complete list of characters and the matrix are available as supplementary material online, as Suppl. materials 2, 3, respectively. We used the same matrix as in Ojanguren-Affilastro et al. (2020) with the sole addition of the new species herein described.

Analyses

Analyses were made with TNT 1.5 (Goloboff et al. 2008), using parsimony under equal weights and implied weights, exploring the sensitivity of the results to a range of values of the concavity constant *k* from 1 to 99. Branch support was estimated with 1000 pseudoreplicates of symmetric resampling. Tree searches were made with 100 random addition sequences (RAS) followed by tree

bisection-reconnection (TBR) branch swapping; since all the RAS+TBR replicates reached the same result, it is likely that optimal trees were found.

Systematics

All new material reported here was collected by the authors; most specimens were collected at night by UV detection. Some specimens were also collected in daytime under logs or stones. Measurements, taken using an ocular micrometer, are recorded in mm. Descriptive terminology follows Mattoni and Acosta (2005) for hemispermatophores; Vachon (1973) for trichobothria; Francke (1977) for metasomal carinae abbreviated as follows: DL: dorsolateral; LIM: lateral inframedian; LSM: lateral supramedian; LM: lateral median; VSM: ventral submedian; VL: ventrolateral; VM: ventromedian; and Prendini (2000) for pedipalp carinae, abbreviated as follows: DI: dorsal internal; DE: dorsal external; VI: ventral internal; VE: ventral external; D: digital; E: external; IM: internomedian; EM: externomedian; V: ventral; VM: ventral median; DM: dorsal marginal; DS: dorsal secondary. Illustrations were produced with a Leica M165C stereomicroscope and a camera lucida. Digital images of pigmentation pattern and habitus were taken under visible light, images of external morphology under UV light, using a digital camera (Leica DFC290 or Nikon DS-Fi1) attached to a stereomicroscope (Leica M165C or Nikon SMZ1500) and the focal planes combined with Helicon Focus 3.10.3 (http://helicon.com.usa/heliconfocus/). Point locality records were georeferenced in the field with portable Global Positioning System devices (Garmin® Etrex Vista and Etrex Vista C). The distribution map was generated using https://www.simplemappr.net/.

Results

Cladistic analyses

The analysis under equal and implied weights resulted in highly concordant trees. All the analyses under implied weights with concavity constant below 20 produced the resolution of Fig. 3. The support values were calculated under implied weights with $k = 15$.

In our phylogenetic tree (Fig. 3), the genus *Urophonius* appears as monophyletic and *Cercophonius* appears as the sister genus of *Urophonius*, as in previous phylogenetic analyses (Prendini 2000; Ojanguren-Affilastro et al. 2020).

We recovered two major clades confirming the results of Acosta (1988) and Ojanguren-Affilastro et al. (2020). One of these corresponds to the concept of *granulatus* species group (Fig. 3) and includes all species with summer activity period and the new species herein described. In our analyses, *Urophonius trewanke* sp. nov. groups with *Urophonius tregualemuensis* Cekalovic, 1981, as expected by their external similarities and environmental proximity, both inhabiting southern Chilean woods. Species from the Patagonian steppe of the *granulatus* group, *Urophonius granulatus* Pocock, 1898, *Urophonius somuncura* Acosta, 2003 and *Urophonius araucano* Ojanguren-Affilastro & Pizarro-Araya, 2020 form a separate clade. *Urophonius pizarroi* Ojanguren-Affilastro, Ochoa, Mattoni & Prendini, 2010, fits in the *granulatus* group, but it is not part of either clade.

On the other hand, we recovered all species with winter activity as another monophyletic group (Fig. 3), with two internal clades corresponding to *exochus* and *brachycentrus* groups (Acosta 1988; Ojanguren-Affilastro et al. 2020). *Urophonius mondacai* Ojanguren-Affilastro, Pizarro-Araya & Prendini, 2011 appears as basal to the species with winter activity; however, its actual activity period is in debate. The original records of this species are from spring, but it has recently been collected also in winter by the authors, raising more doubts about the position of this enigmatic species.

Systematics

***Urophonius trewanke* sp. nov.**

https://zoobank.org/50D20A04-1E7A-47E1-9EF3-3C60F4BA8922

Figs 1–8; Table 1

Type material. ***Chile***, *Maule Region (VII)*, Maule Valley, Fundo La Escuadra: Holotype ♂ (MNHN 8411), Bocatoma-Ojos de Agua (35°46'06.1"S, 70°47'44.4"W), 1009 m a.s.l.; 14–17/X/2022, Pizarro-Araya, Alfaro & Calderón coll. Paratipes: 2 ♂, same data as holotype (MACN); Laguna Invernada (35°43'16.1"S, 70°47'04.9"W), 1260 m a.s.l.; 14–17/X/2022, Pizarro-Araya, Alfaro & Calderón coll. 2 ♀, 10 ♂ (LEULS); 2 ♀, 2 ♂ (MACN). Woods of *Quillaja saponaria* and *Cryptocarya alba* (35°46'04.1"S, 70°47'45.6"W), 1020 m a.s.l.; 10/XII/2023, Pizarro-Araya, Alfaro & Calderón coll. 3 ♀ (LEULS); 3 ♀, 6 ♂ (MACN). Bocatoma-Ojos de Agua (35°46'06.1"S, 70°47'44.4"W), 1009 m a.s.l.; 9/XII/2023, Pizarro-Araya, Alfaro & Calderón coll. 4 ♀, 2 ♂, 1 juvenile (LEULS); 2 ♀, 3 ♂ (MACN).

Etymology. The specific epithet "*trewanke*" is a noun in apposition meaning scorpion in *Mapungudun*, the language of the Mapuche people, the original inhabitants from most parts of southern and central Chile.

Diagnosis. *Urophonius trewanke* sp. nov. is most closely related to *U. tregualemuensis* from south-central Chile (Fig. 2a). Both species can be easily separated by their pigment pattern; in *U. trewanke* sp. nov. the dorso-submedian spots of tergites are poorly developed, being reduced to small triangles in the posterior half of the segment (Figs 4a, 5a), whereas in *U. tregualemuensis*, these spots are much more developed, occupying almost the whole median part of the segment (Fig. 5b).

Both species can also be separated by the shape of pedipalp chela, which is stouter in *U. trewanke* sp. nov.

Figure 1. a. Habitat of *Urophonius trewanke* sp. nov., woods at Fundo La Escuadra, Maule Valley, Maule Region, Chile; **b.** Couple of *Urophonius trewanke* sp. nov. during courtship in its natural environment; **c.** *Urophonius trewanke* sp. nov. male, living specimen.

(Fig. 6b, f). Pedipalp chela length/height ratio varies from 3.15–3.38 (n = 11, mean = 3.29) in *U. trewanke* sp. nov. males and between 3.96 and 4.24 (n = 12, mean = 4.09) in *U. tregualemuensis* males; it varies between 3.31 and 3.61 (n = 3, mean = 3.45) in *U. trewanke* sp. nov. females and between 4.06 and 4.33 (n = 10, mean = 4.19) in *U. tregualemuensis* females; length/width ratio varies between 3.35 and 3.70 (n = 11, mean = 3.54) in *U. trewanke* sp. nov. males and between 4.13 and 4.24 (n = 12, mean = 4.09) in *U. tregualemuensis* males; and varies between 3.70 and 3.93 (n = 3, mean = 3.80) in *U. trewanke* sp. nov. females and between 4.48 and 4.82 (n = 10, mean = 4.63) in *U. tregualemuensis* females.

They can also be separated by some details of the hemispermatophore; in *U. tregualemuensis*, the bifid lobe of the internal lobe is connected to the superior concavity of the basal portion by a thick carina (Fig. 8b), that is very subtle in *U. trewanke* sp. nov. (Fig. 8a). Additionally, the distal margin of capsular concavity of the basal lobe is arranged more distally in *U. trewanke* sp. nov. (Fig. 8c, d) than in *U. tregualemuensis* (Fig. 8e, f).

There are also some differences in the development of the ventral carinae of metasomal segments I and II, which are clearly more developed in *U. tregualemuensis* (Fig. 7d, e) than in *U. trewanke* sp. nov. (Fig. 7a, b), particularly in males, in which these carinae are barely visible in *U. trewanke* sp. nov. (Fig. 7a) and well developed in *U. tregualemuensis* (Fig. 7d).

Description. Based on the holotype ♂ (MNHN) and the paratypes ♀ (LEULS, MACN-Ar).

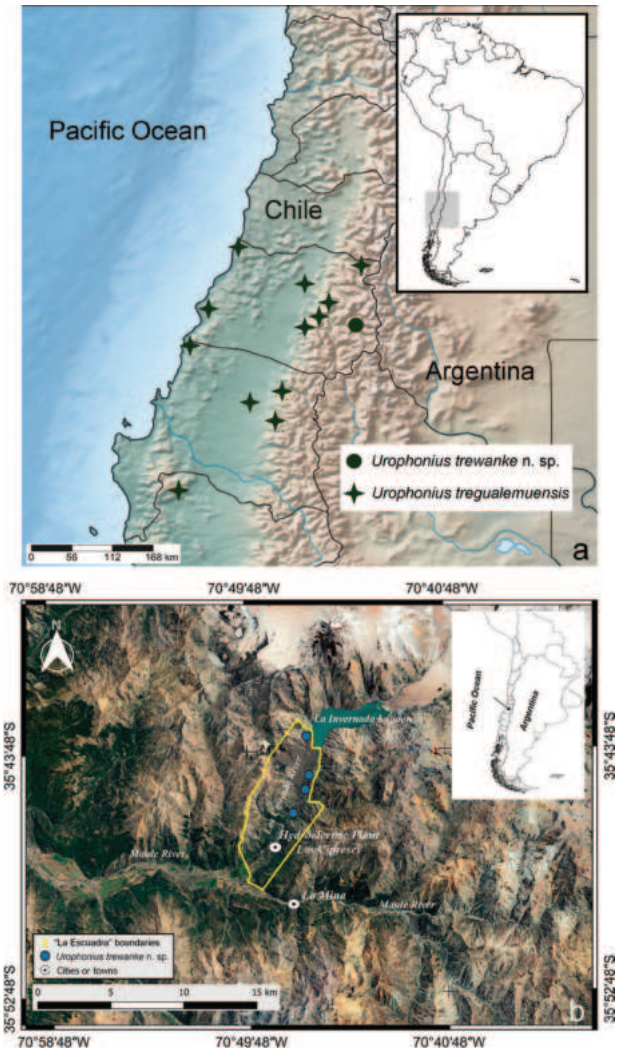

Figure 2. a. Map of central Chile with the distribution of *Urophonius trewanke* sp. nov. and its closest species, *Urophonius tregualemuensis*; **b.** Map of the study area, marking the collection sites, the Cipreses River and the Maule River.

***Total length*:** 30–41 mm in ♂ (n = 12; mean = 34.7); 34.5–41 mm in ♀ (n = 4; mean = 38.88).

***Colour*:** Base colour yellowish, with dark brown spots (Figs 1b, c, 4). Chelicerae with reticulate pigmentation on dorsal and retrolateral surface of manus, densely pigmented on the retrolateral margins of the fingers. Carapace, densely pigmented (Fig. 5a); anterior margin pigmented, with two broad, dark lateral stripes, extending from lateral sides of the anterior margin to the ocular tubercle and the anterior part of posterior longitudinal sulcus, with two other lateral dark stripes placed more posteriorly and reaching the lateral margins; median ocular tubercle and area around lateral ocelli dark brown; with two posterolateral triangular dark spots covering most of latero-posterior margin, leaving a median unpigmented area in the postocular furrow. Tergites I–VI each with four dark spots (Fig. 5a), two external-lateral forming a stripe along the segment and two submedian-subtriangular in the posterior half of the segment; lateral and median spots can be connected by pigment in the posterior margin, median area of the segment always unpigmented; tergite VII with two postero-lateral spots on each side, posterior to dorso-median and dorso-lateral carina, respectively. Sternum, genital opercula, pectines and pleura unpigmented. Sternites: sternites III, IV and V unpigmented medially (Fig. 5c), pigmented in the lateral margins; sternites VI and VII, lateral margins pigmented, posterior margin with faint posterior VL spots and a VM posterior spot that can continue in a thin median stripe, particularly in segment VII. Metasomal segments I–III: dorsal surface with two triangular posterior spots and two anterior small spots, with a thin stripe over the DL carina, with faint paired median spots that can be absent in some specimens; lateral surfaces densely pigmented between LM and LIM carinae; ventral surface: with VL stripes well marked, extending the entire length of the segment, slightly thicker posteriorly, without VSM stripes, VM stripe thin and extending the entire length of the segment, not connecting with VL stripes; segment IV similar to III, but the dorsal spots are elongated; segment V clearly darker than the rest of the segments, with a dark reddish base colour, with faint dorsal submedian stripes; with a lateral stripe along the LM carina, connecting with the VL stripe in the second half of the segment, postero-lateral margins densely pigmented, ventrally similar to remaining segments, but with VL stripes connected to lateral stripes. Telson, general colour dark reddish-brown, as metasomal segment V, dorsal gland of males barely paler than the rest of the vesicle; aculeus dark brown. Pedipalps, trochanter dorsally pigmented; femur with DI, DE and VE wide stripes across the whole segment, fusing in the articulation with patella. Patella, with a DI reticular stripe extending the entire length of the segment, but with an unpigmented median area, with a DE thin stripe in the proximal third of the segment and a retrolateral median stripe extending the entire length of the segment. Chela with seven dark stripes which seem to correspond to DI, DM, DS, D, E, V and VM carinae; area near articulation of fingers and fingers, pigmented. Legs: coxae unpigmented; trochanter with a median retrolateral spot; femur, retrolateral margin with anterior and posterior elongated spots; patella with retrolateral and dorsal stripes; tibia with dorsal and ventral spots; basitarsi with ventral and dorsal spots near articulation with tibia; telotarsi with a dorsal faint spot near articulation with basitarsi.

***Carapace*:** lateral surfaces granular (♂♀), medially smooth (♀) or slightly granular (♂). Anterior margin straight. Anterior longitudinal sulcus shallow; interocular sulcus weakly developed; posterior longitudinal and lateral sulci well developed. Median ocular tubercle not very pronounced, median ocelli large, ca. one diameter apart; with one macroseta behind each eye and one microseta in front of each eye. Three pairs of small lateral ocelli on each side of carapace, posterior ocellus slightly smaller than the rest of the ocelli; anterior and median ocelli almost in the same horizontal axis, posterior ocellus situated clearly dorsal to others; lateral ocelli pattern type 3A (Loria and Prendini 2014).

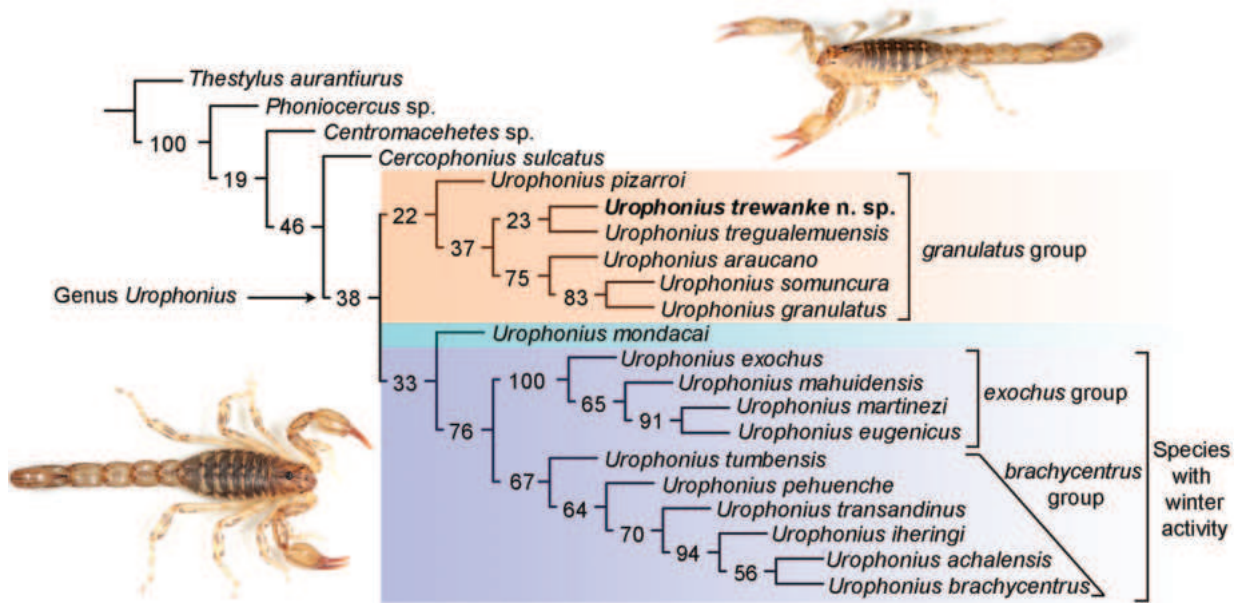

Figure 3. Phylogeny of the genus *Urophonius* Pocock, 1893 estimated with morphological characters under implied weights (k = 15), with Jackknifing frequencies indicated inside branches.

***Pedipalps*:** Femur with DI, DE and VI carinae granular, extending the entire length of segment (Fig. 6h); with some sparse coarse granules in the anterior margin of the segment; with one macroseta related to trichobothria *d* and *i*; trichobothrium *e* situated distal to dorsal macroseta M1 (Fig. 6h). Patella with smooth tegument and without distinct carinae (Fig. 6i). Chela manus robust, more so in ♂, length/width ratio varying from 3.15–3.38 in ♂ (n = 11, mean = 3.29) and from 3.31–3.61 in ♀ (n = 3, mean = 3.45); length/height ratio varies from 3.35–3.70 in ♂ (n = 11, mean = 3.54) and from 3.70–3.93 in ♀ (n = 3, mean = 3.80); acarinate (Fig. 6a–e, g), prolateral surface with a pronounced, subtriangular projection and a shallow depression near articulation of movable finger (Fig. 6b), with a group of granules near the base of the movable finger (♂); all of them absent in ♀ (Fig. 6c, g); fingers elongated, median denticle row medially uneven in the basal quarter of its length, with five pairs of accessory granules.

***Pectines*:** Tooth count: 15–17 in ♂ (n = 12, median = 16) and 14–15 in ♀ (n = 4, mean = 15).

***Legs*:** Surfaces smooth in ♀, granular in ♂. Basitarsi each with two well developed, equal length, pedal spurs. Telotarsi elongated, shallow, each with well-developed ventromedian row of hyaline setae and paired rows of ventrosubmedian spiniform setae with the following counts on each telotarsus: I: 1/1, II: 2/2, III: 5–6, IV: 6–6/6–7. The only pair of spines of telotarsus I and the first pair of spines of telotarsus II are less sclerotised than the remaining spines, the rest are well sclerotised. Ungues slightly curved, equal in length.

***Tergites*:** Surfaces, I–VI: anterior area smooth, posterior and lateral margins finely granular; more so in ♂; VII with sparse, coarse granules in posterolateral margins, with paired dorso-submedian carinae in posterior third and paired dorso-lateral carinae in posterior two-thirds of the segment.

Sternites Surfaces, III–VI smooth, with small elliptical spiracles; VII, surface sparsely granular, more so in ♂; in ♀ with two VM and two VL barely visible carinae in posterior third of the segment, not conspicuous in ♂ (Fig. 7a, b).

Table 1. measurements in mm of the holotype male (MNHN) and a female paratype (MACN) of *Urophonius trewanke* sp. nov.

	***Urophonius trewanke* sp. nov.**	
	Holotype ♂	**Paratype ♀**
Total length	32.53	38.72
Carapace, length	3.71	5.01
Carapace, anterior width	2.58	3.39
Carapace, posterior width	4.12	5.17
Mesosoma, total length	8.88	9.69
Metasoma, total length	19.94	21.02
Metasomal segment I, length	1.94	2.58
Metasomal segment I, width	2.42	3.23
Metasomal segment I, height	2.02	2.58
Metasomal segment II, length	2.34	2.82
Metasomal segment II, width	2.18	2.91
Metasomal segment II, height	1.85	2.50
Metasomal segment III, length	2.58	3.47
Metasomal segment III, width	2.15	2.74
Metasomal segment III, height	1.85	2.42
Metasomal segment IV, length	3.07	4.04
Metasomal segment IV, width	2.02	2.58
Metasomal segment IV, height	1.85	2.42
Metasomal segment V, length	4.68	5.41
Metasomal segment V, width	2.10	2.83
Metasomal segment V, height	1.77	2.42
Telson, length	5.33	5.70
Vesicle, width	1.77	2.26
Vesicle, height	1.53	1.82
Chela, length	6.06	7.62
Chela, width	1.85	1.94
Chela, height	1.64	2.10

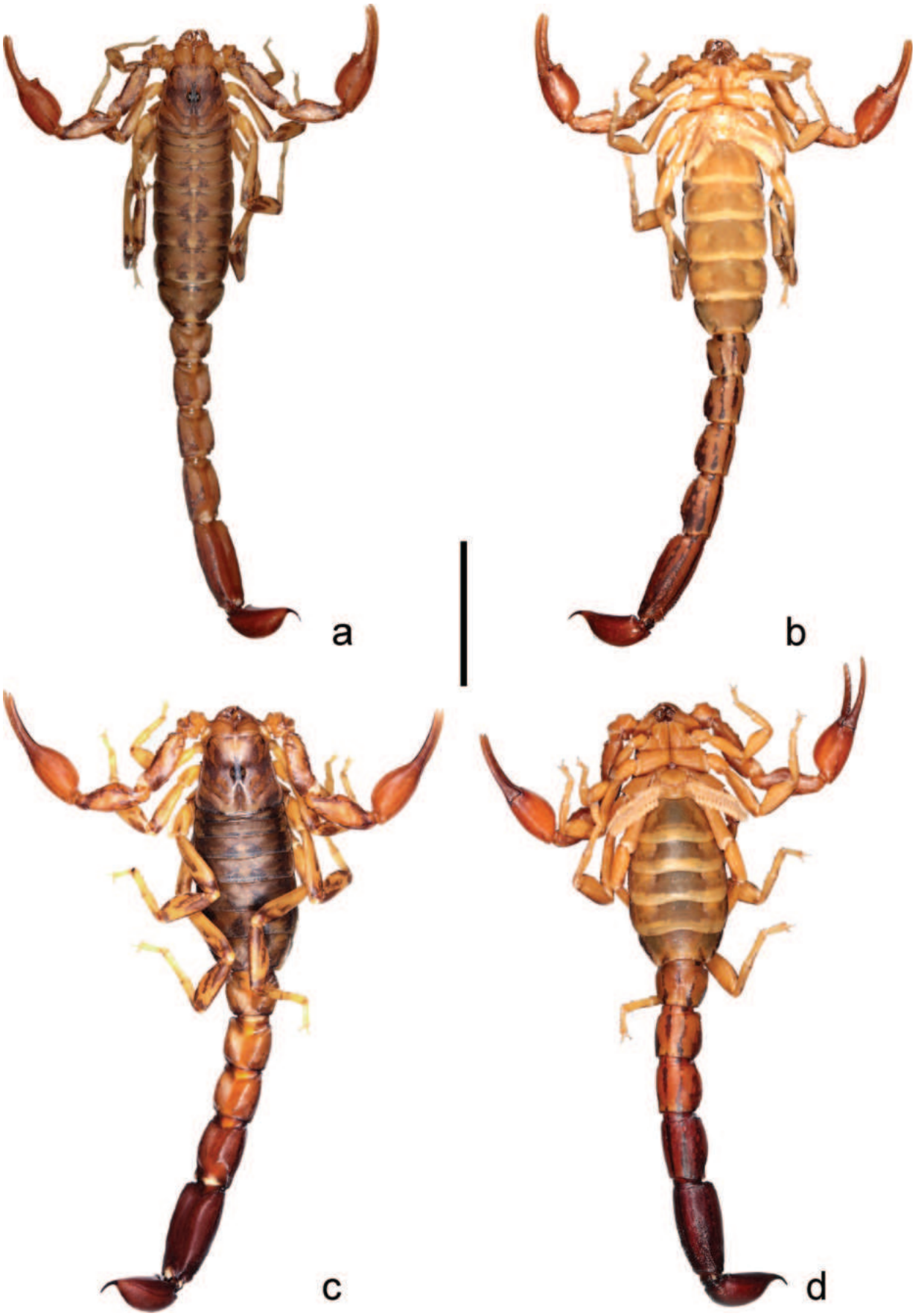

Figure 4. *Urophonius trewanke* sp. nov., **a, b.** Holotype ♂; **c, d.** Paratype ♀; **a, c.** Dorsal aspect; **b, d.** Ventral aspect. Scale bar: 10 mm.

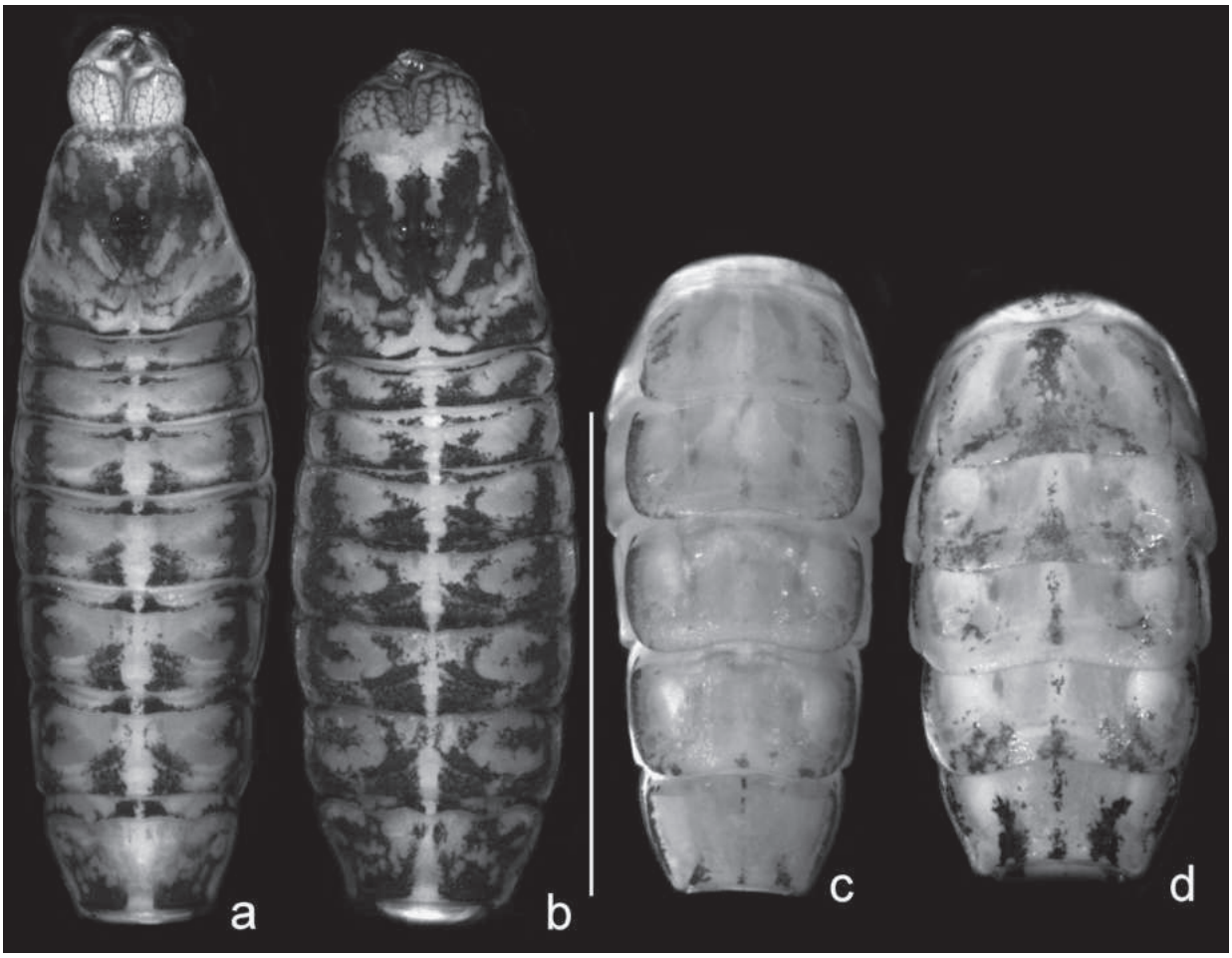

Figure 5. Pigment pattern. **a, c.** *Urophonius trewanke* sp. nov. **a.** Carapace and tergites; **c.** Sternites; **b, d.** *Urophonius tregualemuensis* Cekalovic, 1981; **b.** Carapace and tergites; **d.** Sternites.

***Metasoma*:** Metasomal segment I, dorsal surface finely granular; DL carinae granular, extending the entire length of segment with anterior and posterior granules more developed than the rest; dorso-lateral margins granular, LSM carinae represented by some tiny granules in the posterior part of the segment, LM carina with an anterior blunt small keel and a granular part extending the posterior two-thirds of the segment; LIM carinae granular, restricted to the posterior half of the segment, with one macroseta; ventral surface smooth, VL carinae extending the entire length of the segment, granular in ♀, as an elevation of the tegument in ♂, VSM carinae well developed and granular in ♀, barely visible in ♂, with two pairs of VSM macrosetae and three pairs of VL macrosetae (Fig. 7a, b). Metasomal segment II, similar to I, but with less developed carinae, being the ventral carinae barely visible in ♂; with a DL, a LM and a LIM macroseata and with three pairs of VSM and VL macrosetae. Metasomal segment III similar to segment II, but with less developed carinae, without ventral carinae, LIM carina restricted to posterior third of the segment; metasomal segment IV elongated, LIM carina absent, the rest similar to segment III. Segment V elongated (Fig. 7d, e); dorsal and lateral margins smooth; DL carinae restricted to some well-developed granules in the anterior third of the segment, with two dorsal macrosetae and four lateral macrosetae; VL carinae granular, extending the posterior two-thirds of the segment, with five pairs of VL macrosetae, being the posterior pair in the posterior margin; ventral surface densely granular in the posterior two-thirds of the segment, so that VSM and VM carinae are not conspicuous between the granulation (Fig. 7c, f), with four pairs of VSM macrosetae, being the posterior pair in the posterior margin.

***Telson*:** Vesicle, shallow, more lobular in ♀; ventral surface with medium sized granules in ♀, less granular in ♂; dorsal surface smooth, with (♂) or without (♀) an elliptical median well-developed depression corresponding to the telson gland. Aculeus short, shallowly curved (Fig. 7g, h).

***Hemispermatophore*:** Basal portion well developed. Distal lamina well developed, ca. 30% shorter than basal portion; distal crest almost straight, orientated almost in same direction to the posterior margin of the DL; frontal crest (distal posterior flexure) present; internal lobe with two well-developed denticles, not connected with the distal lamina (Fig. 8a), external denticle ca. twice larger than internal denticle. Lobe region poorly developed (Fig. 8c, d); basal lobe well developed, barely protruding, with a flat internal laminar extension, with an internal concavity; genital plug poorly developed, barely exceeding the capsular concavity.

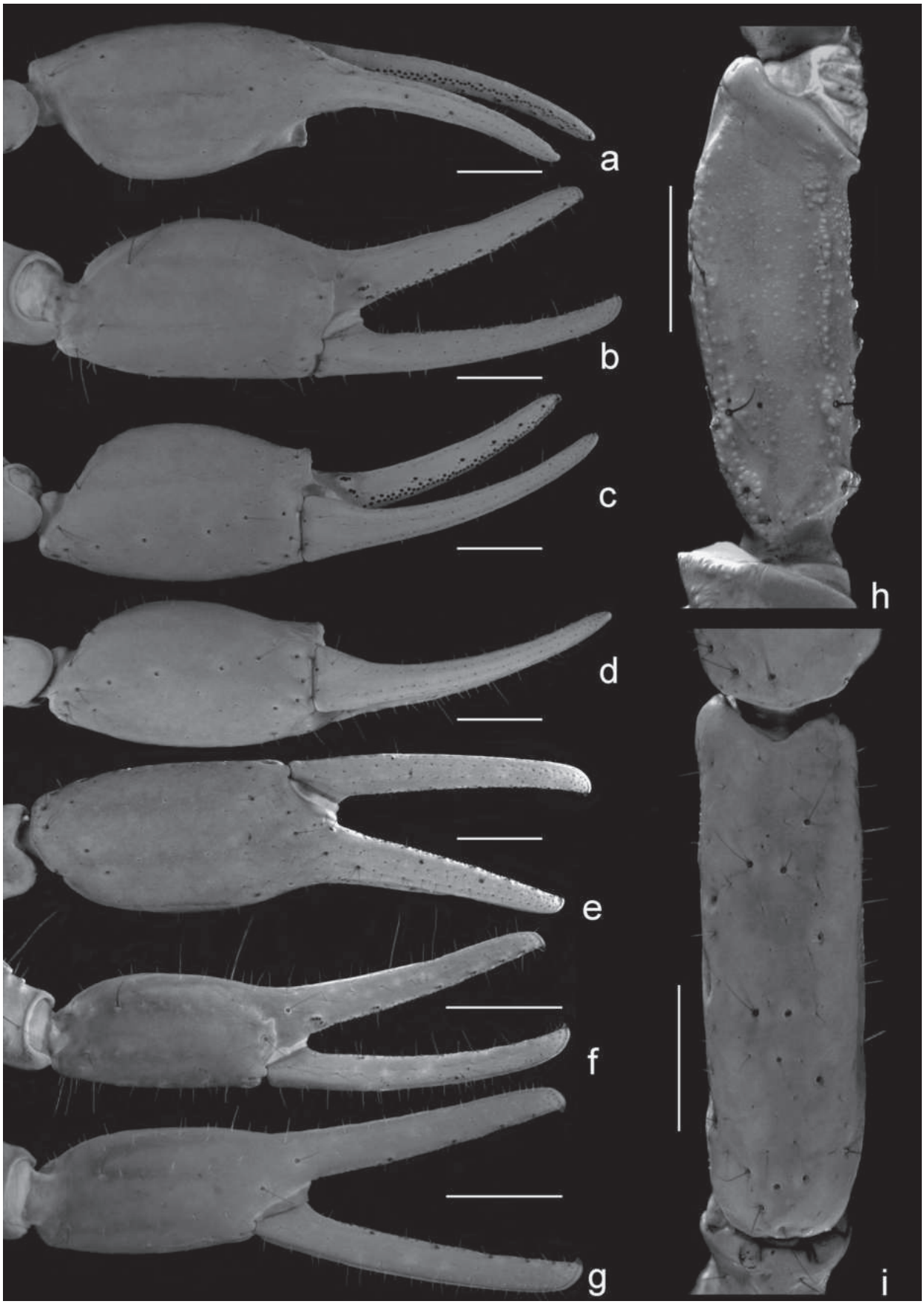

Figure 6. Left pedipalp. **a–e, g–i.** *Urophonius trewanke* sp. nov. **a–e.** Chela, ♂; **a.** Dorsal aspect; **b.** Prolateral aspect; **c.** Ventro-prolateral aspect; **d.** Ventral aspect; **e.** Retrolateral aspect; **g.** Chela ♀, prolateral aspect; **h.** Femur, ♂, dorsal aspect; **i.** Patella, ♂, retrolateral aspect; **f.** *Urophonius tregualemuensis* Cekalovic, 1981. Left pedipalp chela, ♂, prolateral aspect. Scale bars: 1 mm.

Figure 7. a–c, f–h. *Urophonius trewanke* sp. nov., **a, b.** Sternite V and metasomal segments I and II, ventral aspect **a.** ♂ and **b.** ♀; **c.** metasomal segment V, ♂, ventral aspect; **f.** Metasomal segment V, ♀, ventral aspect; **g.** Telson, ♂, lateral aspect; **h.** Telson, ♀, lateral aspect; **d, e.** *Urophonius tregualemuensis* Cekalovic, 1981, sternite V and metasomal segments I and II, ventral aspect; **d.** ♂; **e.** ♀. Scale bars: 1 mm.

Figure 8. a, c, d, *Urophonius trewanke* sp. nov., **a.** Left hemispermatophore, external aspect; **c.** Left hemispermatophore, lobe region, internal aspect; **d.** Right hemispermatophore, lobe region, internal aspect; **b**, **e**, **f**, *Urophonius tregualemuensis* Cekalovic, 1981; **b.** Left hemispermatophore, external aspect; **e.** left hemispermatophore, lobe region, internal aspect; **f.** Right hemispermatophore, lobe region, internal aspect. Scale bars: 1 mm.

Distribution. This species has only been collected in its type locality, in the small preserved area of "Fundo La Escuadra", 35°46'06.1"S, 70°47'44.4"W (Fig. 1). This area is placed in the Maule Valley, in the Maule Region, Chile, close to the Pehuenche international pass which connects Chile with Argentina (Fig. 2).

Ecology. The area where *Urophonius trewanke* sp. nov. has been collected is located within the landscape of the "Estepa de los Andes Maulinos" (Mauline Andean Steppe) Botanical Formation. This distinctive formation represents the southernmost extension of the high Andean steppes. From this point, towards the south, a change in ecological conditions is perceived, characterised by an increase in precipitation and snowfall. This transition marks a natural limit for the distribution of numerous southern and boreal species (Gajardo 1993).

The ecological matrix of this region is made up of various types of vegetation, which has defined its heterogeneity. Dry forests intersect with shrub steppes, creating a plant mosaic. Notable vegetation components include species such as *Chuquiraga oppositifolia* D.Don, *Gochnatia foliorosa* D.Don and *Proustia cuneifolia* D.Don (Asteraceae), each of which plays a role in shaping the unique habitat of *Urophonius trewanke* sp. nov. (Fig. 1a).

In addition, the landscape presents different herbaceous steppes, where species such as *Acaena alpina* Poepp ex. Walp. (Rosaceae) and *Festuca acanthophylla* Desv. (Poaceae) contribute to the overall floral composition. In the midst of this botanical diversity, the presence of the Cordillera cypress (*Austrocedrus chilensis* (D.Don) Pic-Serm. & Bizzarri.) stands out, which adds to the ecological tapestry with its characteristic shape and contributes to the general microhabitat where *Urophonius trewanke* sp. nov. occurs. This environment, with its varied types of vegetation and the inclusion of notable species, such as the Cypress of the mountain range, highlights the ecological importance of the "Estepa de los Andes Maulinos" Botanical Formation as a unique and valuable habitat for the diversity of arachnids, providing crucial information on the ecology and habitat preferences of *Urophonius trewanke* sp. nov.

The Maule Valley and its associated area along the Maule River in the Pehuenche Andean Pass, seems to constitute an area of endemism for the epigean fauna, separated from surrounding valleys by transverse mountain chains. This area is already known to harbour an endemic and highly restricted species of Anuran, *Alsodes pehuenche* Cei, 1976 (Corbalán et al. 2010; Correa et al. 2018, 2020).

In nearby localities outside the Maule Valley, but with similar habitats, *U. trewanke* sp. nov. is replaced by *U. tregualemuensis*, another species of the *granulatus* group, which occupies similar environments and niches as *U. trewanke* sp. nov., but has a wider distribution in south central Chile (Fig. 2a) (Ojanguren-Affilastro et al. 2011). *Urophonius trewanke* sp. nov. has a spring/summer activity period, as in all species within the *granulatus* species group, therefore retaining what we consider the ancestral condition of the genus. In winter, in nearby areas of the Pehuenche Valley, the only active species of *Urophonius* (and of the whole order) is *U. pehuenche*, also endemic from the Pehuenche Valley (Ojanguren-Affilastro et al. 2020).

Urophonius trewanke sp. nov. has been collected in sympatry with an undescribed species of *Brachistosternus*, which also seems to be endemic of the Pehuenche Pass (Ojanguren-Affilastro et al. in prep.).

Discussion

The description of *U. trewanke* sp. nov., a rare species belonging to the *granulatus* group from southern Chile, supports our previous hypothesis that the few species of *Urophonius* with a summer activity period, are restricted to central and southern Chile and to the colder areas of southern South America, whereas the species with a winter activity period are more widely distributed (Ojanguren-Affilastro et al. 2020, 2023). Our analyses included all known species of the genus and most of the characters used in all recent morphological phylogenies in the family; the lack of major changes in the general topology respect to our previous phylogeny in the genus (Ojanguren-Affilastro et al. 2020) despite the inclusion of a new species to our analysis, provides more support to our previous hypothesis about the relationships inside the genus.

Urophonius trewanke sp. nov. has been collected in "Fundo La Escuadra", meaning La Escuadra farm or ranch, a small preserved area currently under management by ENEL ("Empresa Nacional de Energía Eléctrica" or National Electric Energy Company). This area has been part of the "Cipreses" operational system of the Chilean Electric National System since 1955 and has, therefore, had highly restricted access for the last seventy years. This inaccessibility has resulted in an unintended, but yet remarkable, degree of preservation. This area is placed in the partially isolated Maule Valley which has proved to harbour an exceptional number of endemics, but lacks any kind of formal protection. We hope that the description of the actual diversity of this area could shed light on the need to preserve this important biological resource and lead to future preservation of the endemic species of the Maule Valley.

Acknowledgements

Our special thanks to the staff of the Los Cipreses hydroelectric power plant, especially to Christian Cartes for his help in logistics (La Escuadra, ENEL). Project funded by Environment & Permitting - HSEQ, Enel Green Power & Thermal Generation (ENEL). J.P-A thanks the Academic Excellence Scholarship (B134) from the Academic Vice-Rector's Office, Research and Postgraduate Studies of the Universidad Santo Tomás, Santiago, Chile and ANID doctoral fellowship 2024. F.M.A. thanks the ANID doctoral fellowship 2023-21230592. We are indebted to the four reviewers of the manuscript Stepahnie Loria, Oscar Francke, Edmundo Gonzalez-Santillán and an anonymous reviewer, as well as to the editor Danilo Harms, for their helpful comments on the first version of the manuscript.

References

Acosta LE (1988) Contribución al conocimiento taxonómico del género *Urophonius* Pocock, 1893 (Scorpions, Bothriuridae). The Journal of Arachnology 16: 23–33.

Acosta LE (2003) Description of a new Patagonian species of *Urophonius* Pocock (Scorpiones, Bothriuridae), from Meseta de Somuncurá, Argentina. Zootaxa 187(1): 1–12. https://doi.org/10.11646/zootaxa.187.1.1

Ceccarelli FS, Ojanguren-Affilastro AA, Ramírez MJ, Ochoa JA, Mattoni CI, Prendini L (2016) Andean uplift drives diversification of the bothriurid scorpion genus *Brachistosternus*. Journal of Biogeography 43(10): 1942–1954. https://doi.org/10.1111/jbi.12760

Corbalán V, Debandi G, Martínez F (2010) *Alsodes pehuenche* (Anura: Cycloramphidae): Past, Present and Future. Cuadernos de Herpetología 24(1): 17–23.

Correa C, Zepeda P, Lagos N, Salinas H, Palma RE, Vásquez D (2018) New populations of two threatened species of *Alsodes* (Anura, Alsodidae) reveal the scarce biogeographic knowledge of the genus in the Andes of central Chile. Zoosystematics and Evolution 94(2): 349–358. https://doi.org/10.3897/zse.94.25189

Correa C, Morales J, Schussler C, Ortiz JC (2020) An enigmatic population of *Alsodes* (Anura, Alsodidae) from the Andes of central Chile with three species-level mitochondrial lineages. Mitochondrial DNA, Part A, DNA Mapping, Sequencing, and Analysis 31(1): 25–34. https://doi.org/10.1080/24701394.2019.1704744

Francke OF (1977) Scorpions of the genus *Diplocentrus* from Oaxaca, México (Scorpionida, Diplocentridae). The Journal of Arachnology 4: 145–200.

Gajardo R (1993) La vegetación natural de Chile, clasificación y distribución geográfica. Editorial Universitaria, Santiago, Chile, 165 pp.

Garcia F, Oviedo-Diego M, Laino A, Peterson G, Mattoni CI, Peretti AV, Ojanguren-Affilastro AA (2021) Low temperatures induce physiological changes in lipids, fatty acids and hydrocarbons, in two rare winter scorpions of genus *Urophonius* (Scorpiones, Bothriuridae). Journal of Thermal Biology 96: 102841. https://doi.org/10.1016/j.jtherbio.2021.102841

Garzione CN, Hoke GD, Libarkin JC, Withers S, MacFadden B, Eiler J, Ghosh P, Mulch A (2008) Rise of the Andes. Science 320: 304e1307. https://doi.org/10.1126/science.1148615

Ghosh P, Garzione CN, Eiler JM (2006) Rapid uplift of the Altiplano revealed through 13C-18O bonds in paleosol carbonates. Science 311: 511e515. https://doi.org/10.1126/science.1119365

Goloboff PA, Farris JS, Nixon KC (2008) TNT, a free program for phylogenetic analysis. Cladistics 24(5): 774–786. https://doi.org/10.1111/j.1096-0031.2008.00217.x

Loria SF, Prendini L (2014) Homology of the lateral eyes of Scorpiones: A six-ocellus model. PLoS ONE 9(12): e112913. https://doi.org/10.1371/journal.pone.0112913

Mattoni CI, Acosta LE (2005) A new species of *Bothriurus* from Brazil (Scorpiones, Bothriuridae). The Journal of Arachnology 33(3): 735–744. https://doi.org/10.1636/H04-31.1

Maury EA (1969) Observaciones sobre el ciclo reproductivo de *Urophonius brachycentrus* (Thorell 1877) (Scorpiones, Bothriuridae). Physics Section C 29(78): 131–139.

Maury EA (1973) Los escorpiones de los sistemas serranos de la Provincia de Buenos Aires. Physics Section C 32(85): 351–371.

Maury EA (1979) Escorpiofauna patagónica. II. *Urophonius granulatus* Pocock 1898 (Bothriuridae). Physics Section C 38(94): 57–68.

Ojanguren-Affilastro AA, Cheli G (2009) New data on genus *Urophonius* Pocock 1893 in Patagonia, with a description of a new species of the *exochus* group (Scorpiones; Bothriuridae). The Journal of Arachnology 37(3): 346–356. https://doi.org/10.1636/H08-76.1

Ojanguren-Affilastro AA, Kovarík F (2013) Bothriuridae. 6-130. in Kovarík F, Ojanguren-Affilastro AA 2013. Illustrated catalog of scorpions. Part II. Bothriuridae; Chaerilidae; Buthidae I., genera *Compsobuthus*, *Hottentotta*, *Isometrus*, *Lychas*, and *Sassanidotus*. Jakub Rolčík Publisher, Czech Republic, 400 pp.

Ojanguren-Affilastro AA, Ochoa JA, Mattoni CI, Prendini L (2010) Systematic revision of the *granulatus* group of *Urophonius* Pocock, 1893 (Scorpiones, Bothriuridae), with description of a new species from central Chile. American Museum Novitates 3695: 1–40. https://doi.org/10.1206/3695.2

Ojanguren-Affilastro AA, Pizarro-Araya J, Prendini L (2011) New data on Chilean *Urophonius* Pocock 1893, with description of a new species. American Museum Novitates 3725: 1–44. https://doi.org/10.1206/3725.2

Ojanguren-Affilastro AA, Ramírez M, Pizarro-Araya J (2020) Phylogenetic analysis of the winter and southernmost scorpion genus *Urophonius* Pocock, 1893 (Bothriuridae), with the description of two new Patagonian species. Zoologischer Anzeiger 289: 50–66. https://doi.org/10.1016/j.jcz.2020.09.003

Ojanguren-Affilastro AA, Pizarro-Araya J, Santibañez-López CE (2023) Old and cold: Diverse phylogenomic datasets support an ancient transantarctic dispersive route on the scorpion family Bothriuridae in temperate Gondwana. Molecular Phylogenetics and Evolution 187: 107886. https://doi.org/10.1016/j.ympev.2023.107886

Pizarro-Araya J, Ojanguren-Affilastro AA, Prendini L (2011) First report of an arboreal bothriurid (Scorpiones: Bothriuridae) from the temperate forests of southern Chile. Gayana 62(2): 166–170. https://doi.org/10.4067/S0717-65382011000200008

Prendini L (2000) Phylogeny and classification of the superfamily Scorpionoidea Latreille 1802 (Chelicerata, Scorpiones): An exemplar approach. Cladistics 16(1): 1–78. https://doi.org/10.1111/j.1096-0031.2000.tb00348.x

Prendini L (2003) A new genus and species of bothriurid scorpion from the Brandberg Massif, Namibia, with a reanalysis of bothriurid phylogeny and a discussion of the phylogenetic position of *Lisposoma* Lawrence. Systematic Entomology 28(2): 1–24. https://doi.org/10.1046/j.1365-3113.2003.00207.x

Santibañez-López CE, Ojanguren-Affilastro AA, Graham MR, Sharma PP (2023) Congruence between ultraconserved element-based matrices and phylotranscriptomic datasets in the scorpion Tree of Life. Cladistics 39(6): 533–547. https://doi.org/10.1111/cla.12551

Vachon M (1973) [1974] Étude des caractères utilisès pour classer les familles et les genres de scorpions (Arachnides). 1. La trichobothriotaxie en arachnologie. Sigles trichobothriaux et types de trichobothriotaxie chez les scorpions. Bulletin du Muséum National d´Histoire Naturelle 3e sér 140: 857–958.

Supplementary material 1

Studied material *Urophonius* phylogeny

Authors: Andrés A. Ojanguren-Affilastro, Fermín M. Alfaro, Martín J. Ramírez, Bernardino Camousseigt-Montolivo, Jaime Pizarro-Araya

Data type: docx

Link: https://doi.org/10.3897/zse.100.119153.suppl1

Supplementary material 2

Characters *Urophonius* phylogeny

Authors: Andrés A. Ojanguren-Affilastro, Fermín M. Alfaro, Martín J. Ramírez, Bernardino Camousseigt-Montolivo, Jaime Pizarro-Araya

Data type: doc

Link: https://doi.org/10.3897/zse.100.119153.suppl2

Supplementary material 3

Matrix *Urophonius* phylogeny

Authors: Andrés A. Ojanguren-Affilastro, Fermín M. Alfaro, Martín J. Ramírez, Bernardino Camousseigt-Montolivo, Jaime Pizarro-Araya

Data type: txt

Link: https://doi.org/10.3897/zse.100.119153.suppl3

Zoosyst. Evol. 100 (2) 2024, 483–492 | DOI 10.3897/zse.100.119915

PENSOFT

für Natur MUSEUM FÜR NATURKUNDE BERLIN

Oxynoemacheilus kottelati, a new species from the Havran and Karınca streams in Northern Aegean Basin, Türkiye (Teleostei, Nemacheilidae)

Davut Turan[1], Sadi Aksu[2], Salim Serkan Güçlü[3], Gökhan Kalaycı[1]

1 *Recep Tayyip Erdoğan University, Faculty of Fisheries, Rize, Turkiye*

2 *Eskişehir Osmangazi University, Vocational School of Health Services, Eskişehir, Turkiye*

3 *Isparta University of Applied Sciences, Faculty of Eğirdir Fisheries, Isparta, Turkiye*

https://zoobank.org/3B0940F0-970F-4CDE-9323-6BBD4413DABC

Corresponding author: Gökhan Kalaycı (gokhan.kalayci@erdogan.edu.tr)

Academic editor: Nicolas Hubert ♦ **Received** 31 January 2024 ♦ **Accepted** 2 April 2024 ♦ **Published** 9 May 2024

Abstract

The taxonomic status of the *Oxynoemacheilus* from the Karınca and Havran streams in the north Aegean Basin was evaluated, and it was concluded that these populations contain a new species. The new species, *Oxynoemacheilus kottelati* **sp. nov.**, is distinguished by a body with a marbled pattern, a deeper caudal peduncle, a shorter caudal peduncle, a wider interorbital distance, and a shorter middle caudal-fin lope. *Oxynoemacheilus kottelati* **sp. nov.** is differentiated from the closest species, *O. marmaraensis*, in possessing 51 nucleotide substitution sites, a genetic distance of 8.40%, the presence of an axillary lobe at the base of the pelvic fin (vs. absent), and a narrower median incision in the upper lip (vs. absent). Three species delimitation tests (ASAP, ABGD, and PTP) and phylogenetic analyses reinforce the validity of *O. kottelati* **sp. nov.** as a distinct species.

Key Words

Anatolia, COI, freshwater fish, loach, taxonomy

Introduction

The species-rich genus *Oxynoemacheilus*, established by Banarescu and Nalbant in 1966 within the family Nemacheilidae, exhibits a wide distribution across the Eastern Mediterranean, the southern Caucasus, Anatolia, Mesopotamia, and Central Iran (Freyhof et al. 2011; Kottelat 2012). Despite its extensive range, our understanding of its diversity remains limited, particularly in the Asian portion of its distribution, where several new species have been described in recent years, notably from the Anatolian and Tigris River drainages. A total of 67 species within this genus have been described or reported in the literature (Erk'akan et al. 2007; Freyhof et al. 2011; Erk'akan 2012; Kamangar et al. 2014; Freyhof 2016; Sayyadzadeh et al. 2016; Freyhof and Abdullah 2017; Freyhof et al. 2017; Freyhof and Özuluğ 2017; Turan et al. 2019; Bektaş et al. 2022; Yoğurtçuoğlu et al. 2022; Çiçek et al. 2023; Turan et al. 2023a, b). Forty-eight of these species are distributed in inland waters throughout Türkiye, with 36 of them being endemic to the region. The Tigris and Euphrates basins harbor the highest number of *Oxynoemacheilus* species in Türkiye (n = 16), followed by the Mediterranean (n = 14), the Black Sea (n = 6), the Caspian (n = 4), the Aegean (n = 4), Konya (n = 2), Marmara (n = 2), and the Van basins (n = 1). Notably, the *Oxynoemacheilus* species distributed in the Aegean basin of Türkiye have not been adequately investigated.

In the Aegean region, Erk'akan et al. (2007) and Erk'akan (2012) described three species from the Büyük Menderes River: *Barbatula germencicus* from around Aydın-Germencik, *Barbatula cinica* from Cindere Stream between Kütahya and Denizli, and *Barbatula mesudae* from Büyük Menderes around Çivril. Yoğurtçuoğlu et al.

(2022) and Bektaş et al. (2022) later reported these species as synonyms of *O. germencicus*. Stoumboudi et al. (2006) described *O. theophilii* from Lesbos Island in Greece, based on three individuals. Subsequently, Yoğurtçuoğlu et al. (2022) recognized three species in the Aegean basin: *O. theophilii* (Bakır Stream), *O. germencicus* (Büyük Menderes and Gediz rivers), and *O. eliasi* (Tahtalı reservoir, Küçük Menderes, and Gediz rivers). Additionally, Turan et al. (2024) described *O. fatmae* from the Güzelhisar Stream. Considering the reported species, *Oxynoemacheilus* appears to be in a poor region in terms of species composition. However, in the detailed field studies we have carried out recently, it has been seen that there are still undescribed species in the Aegean region.

In this study, specimens from Havran and Karınca streams were examined and compared with other species from the Aegean and adjacent basins. The comparison results revealed that the materials from Havran and Karınca streams belong to a new species named *O. kottelati*.

Materials and methods

The fish samplings and experiments conducted in this study were approved by the Recep Tayyip Erdoğan University Local Ethics Committee for Animal Experiments in the Republic of Türkiye, under permit reference number 2020/4. Following anesthesia, sample fixation was initially carried out in 5% formaldehyde, with subsequent immersion in 70% ethanol whenever feasible. Alternatively, some samples were directly fixed in absolute ethanol for tissue collection for genetic analysis. Measurements were performed using a dial caliper set precisely to 0.1 mm, adhering to the stringent point-to-point measurement procedures outlined in the guidelines provided by Kottelat and Freyhof (2007). Morphometric data for *O. angorae*, *O. simavicus*, and *O. marmaraensis* were sourced from Turan et al. (2019) and Turan et al. (2023b), respectively.

DNA extraction, PCR, sequencing, and molecular analysis

DNA was isolated from fin clips via Hibrigen genomic DNA extraction kits. DNA quality was checked by agarose gel electrophoresis. The vertebrata *COI* barcode region (624 bp) was amplified with the FishF1 and FishR1 (Ward et al. 2005) primer pairs. The PCR reactions' conditions and components' volumes were detailed in Turan et al. (2023a). The PCR products were visualized with a gel documentation system, and eligible PCR products were sent to Macrogen Europa Inc. (Amsterdam, Netherlands) for purification and Sanger sequencing with the ABI PRISM 3730XL Genetic Analyzer (Applied Biosystems; appliedbiosystems.com). We have used the six newly produced COI barcodes and 41 sequences from previously published studies (Geiger et al. 2014; Turan et al. 2019; Bektas et al. 2022; Yoğurtçuoğlu et al. 2022) for the molecular data analysis. *Oxynoemacheilus bureschi* (Genbank number: KJ553692) and *Seminemacheilus lendlii* (Genbank number: MT077008) were added to the analysis as outgroup taxa. Multiple sequence alignment was done with Clustal W options (Thompson et al. 1994) in Bioedit v7.2.5 software (Hall 1999). Sequences were submitted to NCBI GenBank with accession numbers PP085162–PP085167. Phylogenetic correlations were determined with maximum likelihood (ML) and Bayesian inference (BI) analysis using MEGA X (Kumar et al. 2018) and MrBayes 3.1.2 (Ronquist and Huelsenbeck 2003) software. The nucleotide substitution model was estimated as the TrN+G model (Tamura and Nei 1993) concerning the Bayesian information criterion (BIC) in jModeltest v. 0.0.1 (Posada 2008). To estimate pairwise genetic distances, a *p*-distance model was used in MEGA X software. In total, three single-locus species delimitation methods were used as follows: ASAP (Puillandre et al. 2021), ABGD (Puillandre et al. 2012), and GMYC (Fujisawa and Barraclough 2013). Analysis parameters and settings were given in the study by Turan et al. (2023a, b).

Collection codes

IFC-ESUF, Inland Fishes Collection, Faculty of Eğirdir Fisheries, Isparta University of Applied Sciences, Isparta; and **FFR**, Zoology Museum, Faculty of Fisheries, Recep Tayyip Erdoğan University, Rize.

Results

Phylogenetic placement of *Oxynoemacheilus kottelati*

COI barcode region sequences were analyzed in eleven *Oxynoemacheilus* species distributed in the Aegean and Marmara basins. The species were divided into two main clades in all the phylogenetic analyses, supported by high bootstrap values. The first clade consists of *O. kottelati* sp. nov. and *O. marmaraensis*. The second clade consists of *O. anatolicus*, *O. angorae*, *O. eliasi*, *O. fatmae*, *O. germencicus*, *O. mediterraneus*, *O. nasreddini*, *O. simavicus*, and *O. theophilii*. *Oxynoemacheilus kottelati* sp. nov. constituted a highly supported clade sister to *O. marmaraensis* (Fig. 5). The uncorrected *p* distance between species ranged from 1.00% (*O. mediterraneus* and *O. nasreddini*) to 11.2% (*O. kottelati* sp. nov. and *O. simavicus*). The p-distance was determined to be 8.4% between *O. kottelati* sp. nov. and its closest relative, *O. marmaraensis* (Table 3). *Oxynoemacheilus kottelati* sp. nov. differed from its most closely related congener, *O. marmaraensis*, by 51 nucleotide substitution sites.

In the ASAP analysis, we found 10 OTUs. ASAP's best partition (score = 3.50) results from a *p*-distance threshold of 0.012428. However, the PTP determined 13 clusters, and ABGD resulted in 12 groups. Some barcoding analyses tended to over-split; however, *O. kottelati* sp. nov. was predicted as a candidate species in all three barcoding analyses.

Morphological differences and comparisons

The genetically closest species to *Oxynoemacheilus kottelati* sp. nov. is *O. marmaraensis*, distributed in the Susurluk River (Marmara basin). It is distinguished from *O. marmaraensis* by body color and pattern (marbled vs. vermiculated), presence of an axillary lobe at the base of the pelvic fin (vs. absent), a narrower median incision in the upper lip (vs. absent), and 4–6 small irregularly shaped narrow greyish or brownish saddles on the dorsal part of the caudal peduncle (vs. 3–4). *Oxynoemacheilus kottelati* sp. nov. differs from *O. theophilii* by having a greater interorbital distance (28–36% SL, vs. 20–28), the absence of the dorsal and ventral adipose crest on the caudal peduncle (vs. slightly developed), and no black bars or blocks on the flank (vs. 10–13 small irregularly shaped black bars or blocks on the flank in most individuals). *Oxynoemacheilus kottelati* sp. nov. differs from *O. eliasi* in having a shorter caudal peduncle (13–16, vs. 17–21), a greater interorbital distance (28–36% SL, vs. 20–27), the depth of the caudal peduncle 1.0–1.3, vs. 1.5–1.7 times in its length, and the body marbled pattern (vs. more or less black or brown blocks on the flank in most individuals). *Oxynoemacheilus kottelati* sp. nov. differs from *O. germencicus* by having a shorter caudal peduncle (13–16, vs. 16–22), the depth of the caudal peduncle 1.0–1.3, vs. 1.3–2.2 times in its length, and the body marbled pattern (vs. more or less black or brown blocks on the flank in most individuals). *Oxynoemacheilus kottelati* sp. nov. differs from *O. angorae* by having a shorter postdorsal distance (31–36% SL, vs. 38–42), a deeper caudal peduncle (12–14% SL, vs. 10–12), a shorter caudal peduncle (13–16, vs. 16–19), the depth of caudal peduncle 1.0–1.3, vs. 1.4–1.8 times in its length, and the body marbled pattern (vs. showing a dark-brown mid lateral stripe or a series of fused, dark-brown blotches interrupted by a whitish or pale brown lateral line). *Oxynoemacheilus kottelati* sp. nov. differs from *O. simavicus* by having a longer head (24–27% SL, 19–22), a deeper caudal peduncle (12–14% SL, vs. 6–10), a deeper body (body depth at dorsal-fin origin 18–22% SL, vs. 12–17), the depth of the caudal peduncle 1.0–1.3, vs. 2.2–3.1 times in its length, and the body marbled pattern (vs. 2–8 dark brown blocks on flank). It differs from *O. fatmae* by the body color and pattern (marbled vs. having 4–8 irregularly shaped narrow black bars commonly on the posterior part of the flank and anterior part of the flank with a marbled pattern), having a deeper caudal peduncle (12–14% SL, vs. 10–12), a shorter caudal peduncle (14–16% SL, vs. 17–20), a longer middle caudal-fin lobe (21–24% SL, vs. 16–19), and a greater interorbital distance (28–36% HL, vs. 21–26).

Thus, we describe *Oxynoemacheilus* populations from Karınca and Havran streams as a new species, *Oxynoemacheilus kottelati* sp. nov.

Oxynoemacheilus kottelati sp. nov.

https://zoobank.org/FDB3F47E-E4B4-411F-8D82-F4AB05BC2F3A

Figs 1, 2

Type material. *Holotype*: FFR 15655, 47 mm SL, male; Türkiye, Balıkesir prov., Havran Stream, F. Aksu, S. Aksu, 26 October 2023, 39°30'33.3"N, 27°09'39.0"E.

Figure 1. *Oxynoemacheilus kottelati* sp. nov., FFR 15655, **a, b.** Holotype, male, 47 mm SL; FFR 15656; **c.** Paratype, female, 49 mm SL; Türkiye, Balıkesir prov., Havran Stream.

Figure 2. *Oxynoemacheilus kottelati* sp. nov., FFR 15657, paratypes: **a.** Male, 47 mm SL; **b.** Female, 46 mm SL; **c.** Male, 45 mm SL; Havran Stream; FFR 15656; **d.** Female, 48 mm SL; Karınca Stream; Türkiye, Balıkesir prov.

***Paratypes*:** FFR 15657, 21, 39–50 mm SL; same data as holotype. FFR 15656, 34, 35–54 mm SL; Türkiye, Balıkesir prov., Karınca Stream, F. Aksu, S. Aksu, 26 October 2023, 39°27'12.2"N, 27°00'30.9"E.

Material used in molecular genetic analysis. FFRDNA 15657, 6; Türkiye, Balıkesir prov., Karınca Stream, 39°27'12.2"N, 27°00'30.9"E. (GenBank accession numbers: PP085162–PP085167).

Diagnosis. *Oxynoemacheilus kottelati* sp. nov. is distinguished from other species in the Aegean and adjacent basins due to a distinctive combination of characteristics: a body with a marbled pattern (vs. more or less irregularly shaped dark brown or pale brown blocks or bars on the flank in *O. germencicus*, *O. theophilii*, *O. eliasi*, *O. simavicus*, *O. fatmae*, and *O. angorae*), a deeper caudal peduncle (caudal peduncle depth 1.0–1.3 in its length, vs. 1.3–2.2, except *O. theophilii*), and a wider interorbital distance (28–36% HL, vs. 20–28, except *O. germencicus* and *O. angorae*). It is distinguished from *O. marmaraensis* by the presence of an axillary lobe at the base of the pelvic fin (vs. absent) and a narrower median incision in the upper lip (Fig. 3a, b; vs. absent; Fig. 3c, d).

Description. The general appearance of the species is depicted in Figs 1, 2, with accompanying morphometric data provided in Table 1. The body is deep and compressed at the caudal peduncle, with the greatest depth occurring slightly in front of the dorsal-fin origin and gradually decreasing towards the base of the caudal fin. There is no noticeable hump at the nape, and the greatest body width is observed at the pectoral-fin base. The head is pointed, featuring a straight upper profile at the interorbital area and a convex profile on the snout. The snout is somewhat long and slightly pointed at the tip. Mouths are narrow and arched, with slightly developed lips, and there is a narrow median interruption in the lower lip and a narrow median incision in the upper lip. Males typically exhibit a suborbital groove. Barbels are somewhat long, with the inner rostral barbel typically reaching to the base of the maxillary barbel in most individuals and the outer rostral barbel reaching vertically through the anterior eye margin. The maxillary barbel usually extends to the posterior eye margin in most individuals. The caudal peduncle is deep and laterally compressed, with a length 1.0–1.3 times longer than its depth. An axillary lobe is present at the pelvic-fin base, albeit very slightly devel-

Table 1. Morphometric data of *Oxynoemacheilus kottelati* sp. nov. (holotype FFR 115655 and paratypes FFR 15657, n = 21).

	O. kottelati (n = 21)		SD
	H	Range (mean)	
Standard length (mm)	47	39–50	
In percent of standard length			
Head length	25.5	23.6–27.1 (25.3)	0.8
Body depth at dorsal–fin origin	19.3	17.8–21.6 (19.2)	0.9
Body width at dorsal–fin origin	14.0	11.9–15.4 (13.5)	0.8
Predorsal length	53.0	49.5–54.1 (51.4)	1.3
Postdorsal length	34.9	31.3–35.9 (34.2)	1.3
Preanal length	74.7	72.1–80.0 (75.3)	1.6
Prepelvic length	50.9	48.7–54.2 (51.1)	1.3
Dist. betw. pectoral and pelvic-fin origins	28.4	26.0–31.2 (28.6)	1.2
Dist. between pelvic and anal-fin origins	23.2	21.2–26.2 (23.5)	1.2
Depth of caudal peduncle	13.1	11.6–14.2 (12.8)	0.6
Length of caudal peduncle	15.2	13.0–16.2 (15.0)	0.9
Dorsal-fin depth	23.3	20.1–26.2 (22.5)	1.2
Anal-fin depth	18.4	16.6–22.1 (18.4)	1.3
Pectoral-fin length	22.7	20.0–25.0 (22.2)	1.7
Pelvic-fin length	17.7	14.8–19.6 (17.2)	1.1
Caudal-fin length	27.1	24.2–30.2 (27.5)	1.4
Middle lop of caudal-fin length	24.3	20.7–24.3 (22.6)	1.1
In percent of head length			
Head depth at eye	43.5	37.8–47.1 (41.7)	2.5
Snout length	38.3	32.4–42.6 (37.5)	2.9
Eye diameter	16.5	16.5–25.6 (20.1)	2.3
Postorbital distance	48.5	45.2–59.8 (50.6)	3.7
Maximum head width	57.2	49.9–63.8 (57.3)	3.7
Interorbital width	30.8	27.7–35.6 (30.9)	2.4
Length of inner rostral barbel	30.9	24.8–40.7 (29.2)	3.4
Length of outer rostral barbel	37.7	32.0–42.8 (36.0)	2.3
Length of maxillary barbel	25.6	25.6–36.8 (32.1)	3.0
In percent of caudal peduncle length			
Depth of caudal peduncle	1.2	1.0–1.3 (1.2)	0.7
In percent of body depth at dorsal-fin origin			
Caudal peduncle depth	69.4	69–86 (79)	5.1
In percent of length of caudal-fin length			
Length of middle caudal-fin lope	89.6	76–90 (82)	4.1

oped and fully attached to the body. The pelvic-fin origin typically lies below the first or second branched dorsal-fin ray, and the anal-fin origin is positioned vertically behind the dorsal-fin tip. In males, the pectoral fin almost reaches vertically through the tip of the dorsal-fin origin, whereas in females, it falls short of this mark. There are no dorsal or ventral adipose crests present on the caudal peduncle. The lateral line is complete, extending to the base of the caudal fin. The body is covered by embedded scales on the flank, back, and belly. The dorsal fin typically possesses 7½–8½ branched rays, with its outer margin being straight. The anal fin typically has 5½ branched rays along with a straight outer margin. The pectoral fin usually comprises 10–12 rays, with its outer margin either straight or slightly convex. The pelvic fin typically consists of 7–8 rays, with its outer margin straight or slightly convex. The caudal fins are deeply emarginated, with lobes that are slightly rounded.

Coloration. The body has a marbled pattern; the general body color is brownish in live specimens and grayish in preserved individuals. In the population of the Karınca Stream, the head and cheeks are plain without any discernible color pattern ventrally, whereas in the Havran population, the head and cheeks display a modeled pattern. There is no pigmentation below a line extending from the pectoral-fin base to the anus. A small, irregularly shaped, dark-brown blotch is present at the origin of the dorsal fin. The flank appears plain grayish with a marbled pattern, while the back may exhibit zero to six small, slightly distinct brownish blotches anterior to the dorsal fin origin. The dorsal part of the caudal peduncle bears 4–6 small, irregularly shaped, small, and narrow greyish or brownish saddles. Additionally, one vertically elongated black spot is observed on the base of the caudal peduncle fin. The dorsal fin typically displays 2–3 fine, irregularly shaped black bands on its rays, while the caudal fin may feature 2–4 similar bands. The anal, pectoral, and pelvic fins present a yellowish hue, with the pectoral fins occasionally exhibiting a few small black spots on the rays.

Distribution. *Oxynoemacheilus kottelati* sp. nov. was found in the Havran and Karınca streams, which are drainages in the Northern Aegean Sea basin (Fig. 4).

Etymology. This species is named in honor of Maurice Kottelat, whose contributions significantly advanced the understanding of the world's fish fauna.

Discussion

The newly identified species, *Oxynoemacheilus kottelati* sp. nov., exhibits a close genetic relationship to *O. marmaraensis*, as indicated by the genetic dataset, showing a genetic distance of 8.4% between the two species. Both genetic divergences sufficiently support their distinctiveness, as the two species are clearly distinguished from each other morphologically (see comparison section above).

We obtained some morphometric data from the Şaşal Stream (a drainage of Tahtalı reservoir), Büyük Menderes, and Gediz rivers (Table 2). The morphometric data for *O. germencicus* (FFR 1523, n = 7, 52–58 mm SL; FFR 1528, n = 12, 39–56 mm SL; IFC-ESUF 19-0015, n = 11, 44–65 mm SL; IFC-ESUF 19-0016, n = 7, 47–59 mm SL) are as follows: body depth at dorsal-fin origin 15–23% SL; caudal peduncle depth 9–13% SL; caudal peduncle depth 1.3–2.2 times in length; interorbital distance 19–32% HL; and caudal-fin length 21–32% SL. The morphometric data for *O. eliasi* (FFR 1558, n = 7, 38–41 mm SL and IFC-ESUF 19-0015, n = 11, 44–65 mm SL; IFC-ESUF 19-0016, n = 7, 47–59 mm SL) are: body depth at dorsal-fin origin 19–22% SL in Şaşal and 17–22% SL in Gediz; caudal peduncle depth 12–13% SL in two populations; caudal peduncle length 1.5–1.7 times its depth in two populations; interorbital distance 21–26 in Şaşal and 20–27% SL in Gediz; and caudal-fin length 21–29% SL in two populations. The morphometric data obtained from *O. theophilii* from the Bakır Stream (FFR 15538, n = 14, 38–55 mm SL) are: body depth at dorsal-fin origin 17–19% SL; caudal peduncle depth 12–14% SL; caudal peduncle length 1.2–1.5 times its depth; interorbital dis-

Table 2. Morphometric data of *Oxynoemacheilus germencicus* (FFR 1523, n = 7, 52–58 mm SL; FFR 1528, n = 12, 39–56 mm SL; IFC-ESUF 19-0015, n = 11, 44–65 mm SL; IFC-ESUF 19-0016, n = 7, 47–59 mm SL), *O. theophilii* (FFR 15538, n = 14, 38–55 mm SL) and *O. eliasi* (FFR 1558, n = 7, 38–41 mm SL; IFC-ESUF 19-0015, n = 11, 44–65 mm SL; IFC-ESUF 19-0016, n = 7, 47–59 mm SL)).

	***O. germencicus* n = 37**		***O. theophilii* n = 14**		***O. eliasi* n = 25**	
	Range (mean)	**SD**	**Range (mean)**	**SD**	**Range (mean)**	**SD**
Standard length (mm)	39–65		38–55		38–65	
In percent of standard length						
Head length	22.7–27.8 (25.2)	1.2	23.6–25.7 (24.6)	0.7	23.0–27.6 (24.9)	1.1
Body depth at dorsal–fin origin	14.8–22.8 (18.8)	1.7	16.9–19.0 (18.1)	0.7	17.2–22.3 (19.2)	1.3
Body width at dorsal–fin origin	10.1–16.8 (13.5)	1.6	11.6–14.3 (12.7)	0.9	10.2–16.6 (13.3)	1.5
Predorsal length	48.3–55.3 (51.8)	1.5	46.7–53.8 (51.2)	1.8	39.0–54.5 (51.1)	3.0
Postdorsal length	32.5–39.5 (36.0)	1.7	32.6–37.1 (35.4)	1.5	33.2–41.1 (37.6)	2.1
Preanal length	70.9–77.3 (74.1)	2.9	74.6–79.5 (76.5)	1.4	70.1–78.6 (74.7)	2.2
Prepelvic length	48.1–56.3 (52.2)	1.7	51.6–54.6 (52.6)	1.0	48.6–59.9 (51.6)	2.5
Dist. betw. pectoral and pelvic-fin origins	24.1–32.2 (28.2)	2.8	26.7–32.2 (29.2)	1.7	25.6–33.7 (29.2)	2.2
Dist. between pelvic and anal-fin origins	20.8–27.4 (24.1)	1.4	20.6–27.3 (23.4)	1.7	18.4–25.0 (22.3)	1.8
Depth of caudal peduncle	9.4–13.4 (11.4)	0.1	11.9–14.4 (12.8)	1.2	11.6–13.1 (12.2)	0.4
Length of caudal peduncle	15.9–22.0 (19.0)	1.5	15.2–18.8 (17.0)	0.7	17.1–21.1 (18.9)	1.0
Dorsal-fin depth	19.4–25.4 (22.5)	1.0	17.6–24.5 (20.9)	1.6	16.0–23.6 (18.9)	1.8
Anal-fin depth	16.0–23.8 (19.9)	2.3	15.8–20.1 (18.0)	1.2	14.8–21.0 (17.6)	1.6
Pectoral-fin length	19.6–28.6 (24.1)	2.0	20.1–23.7 (21.9)	1.1	16.1–28.6 (23.9)	2.7
Pelvic-fin length	15.5–23.9 (9.7)	1.8	15.7–19.9 (17.7)	1.5	15.7–19.5 (17.9)	1.2
Caudal-fin length	20.8–31.8 (26.3)	2.6	22.8–29.2 (25.8)	2.0	20.8–29.0 (26.6)	1.9
Middle lop of caudal-fin length	16.4–23.6 (20.0)	1.8	18.7–22.8 (20.3)	1.2	18.3–24.4 (20.9)	1.7
In percent of head length						
Head depth at eye	34.6–55.8 (47.4)	3.5	33.6–48.6 (42.8)	3.9	34.0–49.3 (42.2)	4.2
Snout length	32.8–49.2 (41.0)	3.8	34.5–44.9 (39.3)	2.6	30.5–46.9 (39.4)	3.6
Eye diameter	12.2–27.9 (20.0)	3.8	16.2–25.5 (19.6)	2.6	14.9–29.9 (19.1)	5.8
Postorbital distance	42.6–54.6 (48.6)	2.6	47.5–63.0 (53.2)	5.2	41.0–58.9 (50.8)	3.7
Maximum head width	52.8–66.2 (59.5)	3.6	52.9–64.5 (58.4)	3.7	50.4–64.5 (57.1)	3.8
Interorbital width	19.2–31.5 (25.3)	2.9	19.7–28.2 (24.1)	2.6	19.7–27.2 (24.0)	3.8
Length of inner rostral barbel	19.4–41.8 (30.1)	5.2	16.3–32.3 (24.7)	4.9	17.8–35.6 (25.1)	4.6
Length of outer rostral barbel	25.7–48.1 (36.9)	5.7	26.1–40.2 (31.2)	4.8	23.0–47.2 (33.4)	5.8
Length of maxillary barbel	23.9–59.0 (41.5)	7.1	20.8–37.5 (29.6)	4.0	21.9–42.2 (30.9)	5.6
In percent of caudal peduncle length						
Depth of caudal peduncle	1.3–2.1 (1.7)	1.9	1.2–1.5	1.2	1.5–1.7 (1.6)	0.7
In percent of body depth at dorsal-fin origin						
Caudal peduncle depth	52.6–70.0 (61.2)	4.8	65.1–83.0 (70.2)	4.8	53.4–72.7 (63.5)	4.5
In percent of length of caudal-fin length						
Length of middle caudal-fin lope	63.4–67.9 (75.6)	6.8	73.3–83.1 (78.4)	3.4	69.8–94.4 (79.4)	6.6

Table 3. Pairwise distance values based on cytochrome oxidase sequences of *Oxynoemacheilus* species. (Intraspecific genetic diversity is shown in gray).

	O. kottelati	***O. marmaraensis***	***O. eliasi***	***O. theophilii***	***O. angorae***	***O. fatmae***	***O. mediterraneus***	***O. nasreddini***	***O. germencicus***	***O. anatolicus***	***O. simavicus***
O. kottelati	0.001										
O. marmaraensis	0.084	0.002									
O. eliasi	0.100	0.108	0.003								
O. theophilii	0.106	0.110	0.037	0.001							
O. angorae	0.106	0.104	0.040	0.042	0.001						
O. fatmae	0.107	0.109	0.035	0.022	0.033	0.000					
O. mediterraneus	0.100	0.106	0.034	0.036	0.033	0.034	0.000				
O. nasreddini	0.101	0.102	0.030	0.029	0.030	0.027	0.010	0.001			
O. germencicus	0.103	0.105	0.041	0.036	0.041	0.038	0.033	0.030	0.005		
O. anatolicus	0.112	0.109	0.038	0.040	0.043	0.041	0.033	0.029	0.019	0.001	
O. simavicus	0.112	0.111	0.073	0.084	0.082	0.080	0.082	0.081	0.081	0.078	0.005

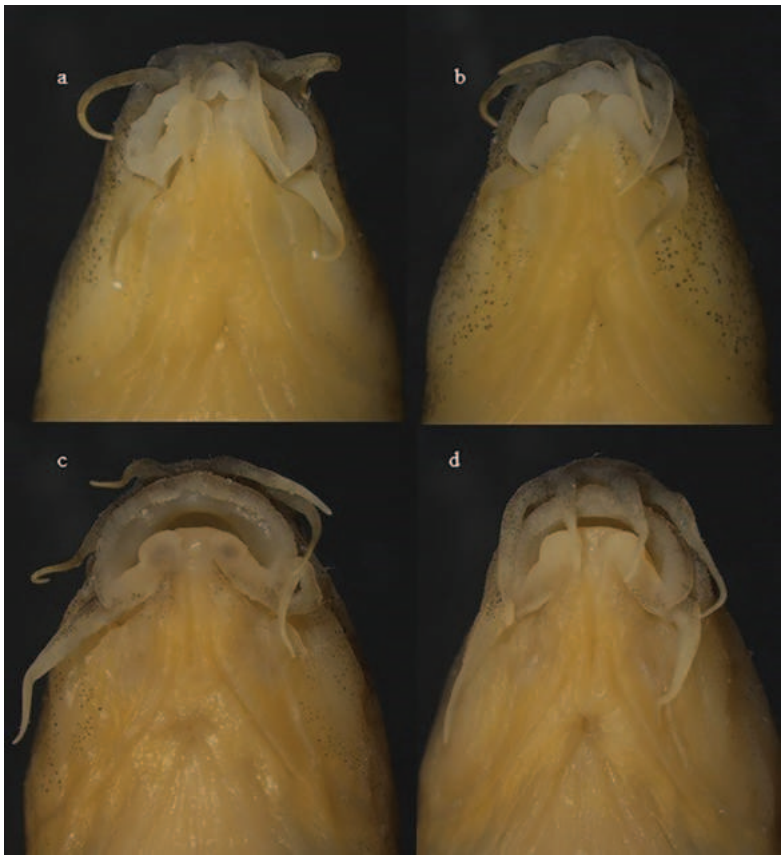

Figure 3. Mouth shape and structure: *Oxynoemacheilus kottelati*, 15655, **a.** Holotype, 49 mm SL, male; **b.** FFR 15657, paratype, 45 mm SL, female; Türkiye, Balıkesir prov., Havran Stream. *Oxynoemacheilus marmaraensis*, FFR 1511; **c.** 52 mm SL, males; **d.** 46 mm SL, female; Türkiye, Balıkesir prov., Susurluk River.

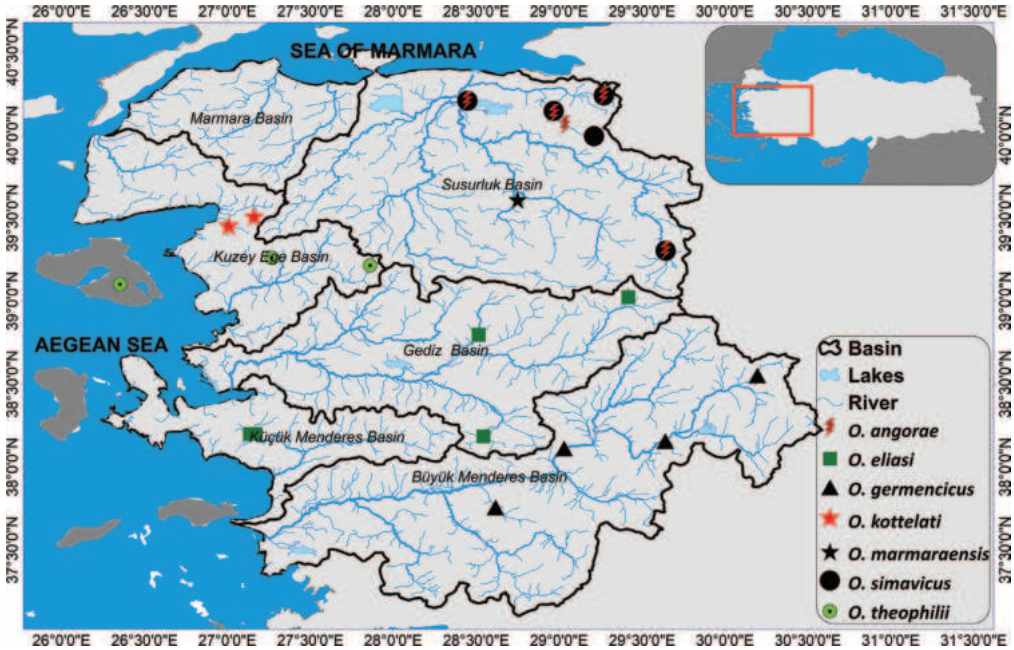

Figure 4. Distribution of *Oxynoemacheilus* species in Aegean and Marmara Sea basins of Anatolia.

tance 20–28% SL; and caudal-fin length 23–29% SL. Based on morphometric data, it is difficult to distinguish these three species (*O. germencicus*, *O. eliasi*, and *O. theophilii*) from each other. This might be due to the high morphological variation within *O. germencicus*, or it may include the possibility of one or more species in the Büyük Menderes River.

Comparative materials

Oxynoemacheilus marmaraensis, FFR 1511, 12, 46–59 mm SL; Türkiye, Balıkesir Province, stream Dursunbey 10 km east of Dursunbey, D. Turan, G. Kalaycı, and S. Aksu, 22.11.2022, 39°36'32.4"N, 28°45'01.9"E.

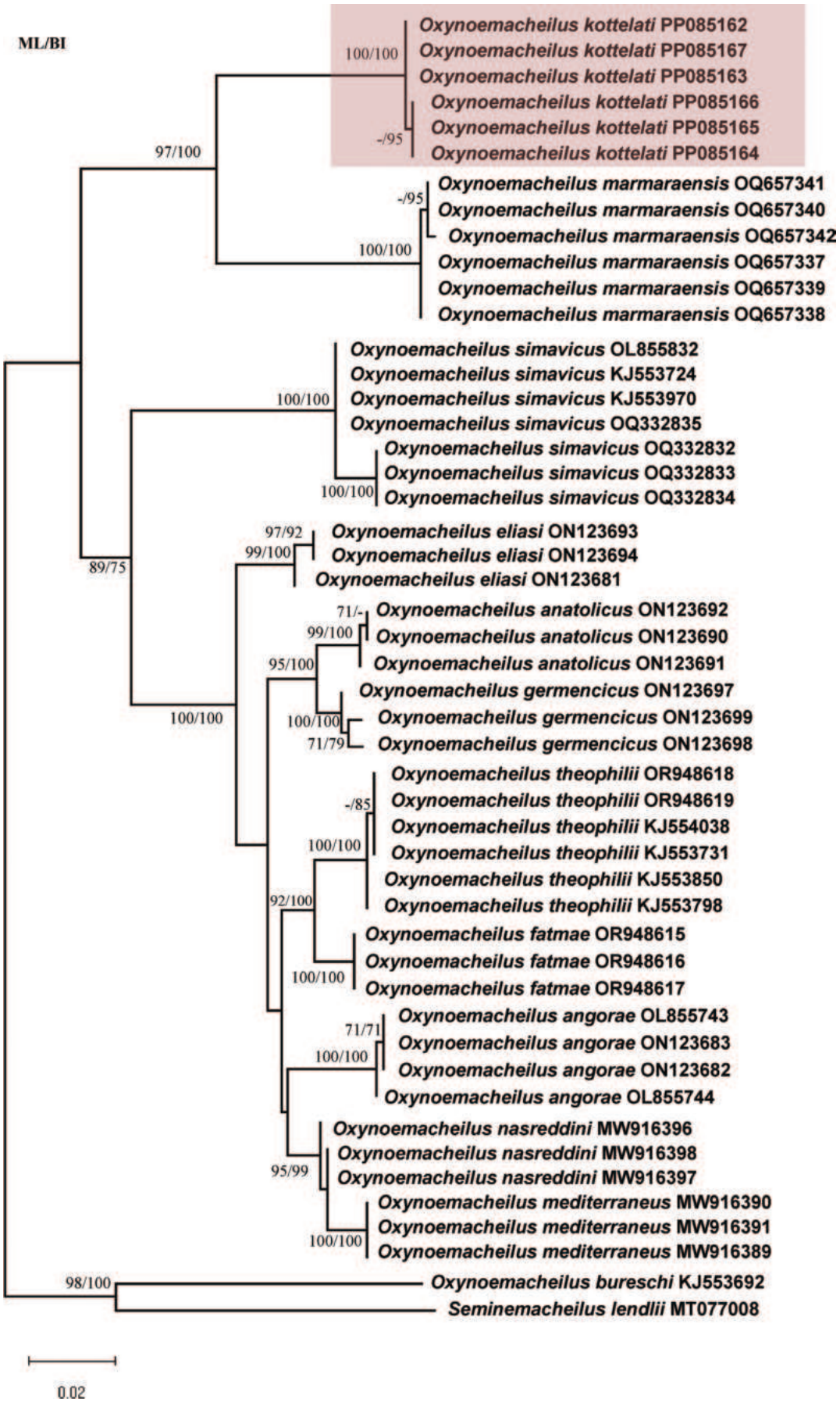

Figure 5. Maximum likelihood tree based on mitochondrial cytochrome oxidase subunit I (*COI*; 624 bp) gene sequences of *Oxynoemacheilus* spp. Bootstrap values (ML/BI) are shown above or below nodes on the tree if they are 70% or higher.

Oxynoemacheilus angorae, FFR01549, 50, 20–59 mm SL; Türkiye, Ankara prov., stream Peçenek, 7 km east of Şereflikoçhisar, D. Turan, C. Kaya, and E. Bayçelebi, 01.10.2015, 40°28'15.6"N, 32°39'18.0"E.

Oxynoemacheilus simavicus, FFR01505, 28, 32–56 mm SL; Türkiye, Balıkesir prov, stream Sakar at Manyas, 29.08.2014, D. Turan, C. Kaya, and E. Bayçelebi, 40°03'00.0"N, 27°57'43.2"E.

Oxynoemacheilus theophilii, FFR 15538, 5, 27–36 mm SL; Türkiye, İzmir prov., Çağlayan Stream, a tributary of Bakırçay River 15 km east of Bergama, D. Turan, C. Kaya, and E. Bayçelebi, 16.07.2018, 39°27'12.2"N, 27°00'30.9"E.

Oxynoemacheilus eliasi, FFR 15658, 7, 38–41 mm SL; Türkiye, İzmir prov., inlet of Tahtalı reservoir, under Şaşal bridge, D. Turan, C. Kaya, and E. Bayçelebi, 16.07.2018, 38°11'57.56"N, 27°08'09.79"E.—IFC-ESUF 19-0015, 14, 43-66 mm SL; Türkiye, Manisa prov., Derbent Stream, Gediz River, Uluderbent village bridge, Alaşehir, S.S. Güçlü, and G.K. Akyıldız, 28.04.2017, 38°11'3.43"N, 28°32'37.65"E.—IFC-ESUF 19-0016, 91, 38–62 mm SL; Türkiye, Manisa prov., Derbent Stream, Gediz River, Uluderbent village bridge, Alaşehir, S.S. Güçlü, and G.K. Akyıldız, 28.04.2017, 38°11'3.43"N, 28°32'37.65"E.—IFC-ESUF 19-0021, 7, 42–53 mm SL; Türkiye; Manisa prov., Demirci Stream, Gediz River, Saraycık village Demirci, F. Küçük, S.S. Güçlü, and G.K. Akyıldız, 01.11.2016, 38°47'48.36"N, 28°30'52.48"E.—IFC-ESUF 19-0022, 15, 37–74 mm SL; Türkiye, Manisa prov., Gediz River, Derbent bridge, Hacıbaba village, F. Küçük, and S.S. Güçlü, 22.06.2012, 39°01'23.50"N, 29°25'02.23"E.—IFC-ESUF 19-0011, 5, 41–58 mm SL; Türkiye, Kütahya prov., Gediz River, Bahçeler Creek, Dörtdeğirmen village bridge, Gediz, F. Küçük, S.S. Güçlü, and G.K. Akyıldız, 31.10.2016, 38°58'36.14"N, 29°23'43.66"E.—IFC-ESUF 19-0012, 3, 44–48 mm SL; Türkiye, Manisa prov., Gediz River, Hacıhalliler village, F. Küçük, S.S. Güçlü, and G.K. Akyıldız, 03.11.2016, 38°38'23.92"N, 27°32'37.74"E. —IFC-ESUF 19-0014, 5, 37–55 mm SL; Türkiye, Manisa prov., Gördük Stream, Gediz River, Zeytinbağı village, Akhisar, F. Küçük, S.S. Güçlü, and G.K. Akyıldız, 02.11.2016, 39°2'55.19"N, 27°55'39.27"E.—IFC-ESUF 19-0017, 2, 46–61 mm SL; Türkiye, Kütahya prov., Gediz River, Bahceler Creek, Dörtdeğirmen village bridge, Gediz, S.S. Güçlü, and G.K. Akyıldız, 27.04.2017, 38°58'36.14"N, 29°23'43.66"E.—IFC-ESUF 19-0018, 3, 35–37 mm SL; Türkiye, Manisa prov., Gördük Stream, Gediz River, Zeytinbağı village, Akhisar, S.S. Güçlü, and G.K. Akyıldız, 27.04.2017, 39°2'55.19"N, 27°55'39.27"E.—IFC-ESUF 19-0023, 1, 54 mm SL; Türkiye; Manisa prov., Akpınar Spring, Gölmarmara Lake, Gölmarmara, F. Küçük, and S.S. Güçlü, 21.06.2012, 38°42'04.40"N, 27°58'07.97"E.—IFC-ESUF 19-0024, 1, 43 mm SL; Türkiye, Kütahya prov., Gediz River, Gümüşlü DSI Regl., Gediz, F. Küçük, and S.S. Güçlü, 21.06.2012, 38°58'18.76"N, 29°28'01.56"E.—IFC-ESUF 19-0025, 9, 40–50 mm SL; Türkiye, Manisa prov., Gediz River, Yurtbaşı bridge, Kula, S.S. Güçlü, and H. Güçlü, 12.07.2010, 38°36'16.19"N, 28°48'54.68"E.—IFC-ESUF 19-0028, 1, 48 mm SL; Türkiye, Manisa prov., Demirci Stream, Gediz River, Saraycık village, Demirci, S.S. Güçlü, and G.K. Akyıldız, 25.04.2017, 38°47'48.36"N, 28°30'52.48"E.

Oxynoemacheilus germencicus, FFR 1523, 7, 52–58 mm SL; Türkiye, Denizli prov., Aksu Stream, Büyük Menderes River, 4 km north of Honaz, D. Turan, C. Kaya, and E. Bayçelebi, 19.08.2014, 37°47'21.55"N, 29°15'41.16"E.—FFR 1508, 22, 35–65 mm SL; Türkiye, Muğla prov., Çine Stream, Büyük Menderes River, a tributary of Adnan Menderes reservoir 8 km south of Çine, D. Turan, C. Kaya, and E. Bayçelebi, 25.08.2014, 37°32'34.15"N, 28°03'44.85"E.—FFR 1528, 12, 39–56 mm SL; Türkiye, Denizli prov., Suçıkan Stream, Büyük Menderes River, tributary of Lake Işıklı 1 km north of Çıtak, D. Turan, C. Kaya, and E. Bayçelebi, 18.08.2014, 38°09'20.15"N, 29°38'16.68"E.—FFR 1530, 61, 28–68 mm SL; Türkiye, Uşak prov., Banaz River, Büyük Menderes River, 8 km north of Sivaslı, D. Turan, C. Kaya, and E. Bayçelebi, 18.08.2014, 38°32'58.72"N, 29°37'12.98"E.—FFR 1597, 10, 47–63 mm SL; Türkiye, Aydın prov., Karacasu Stream, Büyük Menderes River, D. Turan, C. Kaya, and E. Bayçelebi, 18.08.2014, 37°48'22.96"N, 28°34'49.47"E—IFC-ESUF 19-0006, 10, 27–60 mm SL; Türkiye, Denizli prov., Cindere reservoir, Büyük Menderes River, Güney, F. Küçük, and S.S. Güçlü, 15.05.2017, 38°06'45.47"N, 29°01'47.65"E.—IFC-ESUF 19-0007, 14, 33–56 mm SL; Türkiye, Denizli prov., Büyük Menderes River, Çıtak Bridge, Çivril, O. Çetinkaya, 30.10.2017, 38°09'23.69"N, 29°38'24.29"E.—IFC-ESUF 19-0009, 9, 54–64 mm SL; Türkiye, Afyonkarahisar prov., Karadirek Stream, Büyük Menderes River, Karadirek, F. Küçük, and S.S.Güçlü, 29.10.2017, 38°33'08.29"N, 30°11'45.52"E.—IFC-ESUF 19-0026, 11, 52–61 mm SL; Türkiye, Aydın prov., Dandalas Stream, Büyük Menderes River, Karacasu, S.S. Güçlü, and H. Güçlü 14.07.2010, 37°45'26.00"N, 28°36'58.53"E.—IFC-ESUF 19-0010, 7, 36–67 mm SL; Türkiye, Denizli prov., Işıklı Lake canal, Büyük Menderes River, Çivril, O. Çetinkaya, 31.08.2017, 38°16'22.89"N, 29°54'23.64"E.—IFC-ESUF 19-0019, 6, 51–65 mm SL; Türkiye, Aydın prov., Şirindere Stream, Büyük Menderes River, İncirliova, F. Küçük, and S.S. Güçlü, 22.07.2019, 37°55'41.87"N, 27°46'39.37"E.—IFC-ESUF 19-0020, 7, 46–61 mm SL; Türkiye, Uşak prov., Banaz Stream, Büyük Menderes River, Ulubey, F. Küçük, and S.S. Güçlü, 27.07.2019, 38°31'48.46"N, 29°36'43.56"E.—IFC-ESUF 19-0027, 4, 38–40 mm SL; Türkiye, Denizli prov., Büyük Menderes River, Yenicekent DSI Regl., Sarayköy, F. Küçük, 04.06.1998, 38°02'15.45"N, 28°57'47.50"E.

Acknowledgements

This study was supported by the Scientific Research Project Coordination Unit of Recep Tayyip Erdoğan University (Project No. FBA-2022-1419). We thank Yasemen ŞENTÜRK (Rize) for taking photographs of the mouth shapes of the specimens. We also thank the subject and copy editors of the article.

References

Bektaş Y, Aksu I, Kaya C, Bayçelebi E, Turan D (2022) DNA barcoding and species delimitation of the genus *Oxynoemacheilus* (Teleostei, Nemacheilidae) in Anatolia. Journal of Fish Biology 101(3): 505–514. https://doi.org/10.1111/jfb.15114

Çiçek E, Sungur S, Fricke R, Seçer B (2023) Freshwater lampreys and fishes of Türkiye; an annotated checklist. Turkish Journal of Zoology 47(6): 324–468. https://doi.org/10.55730/1300-0179.3147

Erk'akan F (2012) Two new *Oxynoemacheilus* (Teleostei, Nemacheilidae) species from western Turkey. Research Journal of Biological Sciences 7(2): 97–101. https://doi.org/10.3923/rjbsci.2012.97.101

Erk'akan F, Nalbant TT, Özeren SC (2007) Seven new species of *Barbatula*, three new species of *Schistura* and a new species of *Seminemacheilus* (Ostariophysi, Balitoridae, Nemacheilinae) from Turkey. Journal of Fisheries International 2: 69–85.

Freyhof J (2016) *Oxynoemacheilus karunensis*, a new species from the Persian Gulf basin Teleostei. Nemacheilidae. Zootaxa 4175(1): 94–100. https://doi.org/10.11646/zootaxa.4175.1.9

Freyhof J, Abdullah YS (2017) Two new species of *Oxynoemacheilus* from the Tigris drainage in Iraqi Kurdistan (Teleostei, Nemacheilidae). Zootaxa 4238(1): 73–87. https://doi.org/10.11646/zootaxa.4238.1.5

Freyhof J, Özuluğ M (2017) *Oxynoemacheilus hazarensis*, a new species of from Lake Hazar in Turkey with remarks on *O. euphraticus* (Teleostei, Nemacheilidae). Zootaxa 4247(4): 378–390. https://doi.org/10.11646/zootaxa.4247.4.2

Freyhof J, Erk'akan F, Özeren C, Perdices AJ (2011) An overview of the western Palaearctic loach genus *Oxynoemacheilus* (Teleostei, Nemacheilidae). Ichthyological Exploration of Freshwaters 22: 301–312.

Freyhof J, Kaya C, Turan D (2017) *Oxynoemacheilus kentritesensis*, a new species from the upper Tigris drainage in Turkey with remarks on the distribution of *O. frenatus* (Teleostei, Nemacheilidae). Zootaxa 4258(6): 551–560. https://doi.org/10.11646/zootaxa.4258.6.4

Fujisawa T, Barraclough TG (2013) Delimiting species using single-locus data and the generalized mixed yule coalescent approach: A revised method and evaluation on simulated data sets. Systematic Biology 62: 707–724. https://doi.org/10.1093/sysbio/syt033

Geiger MF, Herder F, Monaghan MT, Almada V, Barbieri R, Bariche M, Berrebi P, Bohlen J, Casal-Lopez M, Delmastro GB, Denys GPJJ, Dettai A, Doadrio I, Kalogianni E, Kärst H, Kottelat M, Kovačić M, Laporte M, Lorenzoni M, Marčić Z, Özuluğ M, Perdices A, Perea S, Persat H, Porcelotti S, Puzzi C, Robalo J, Šanda R, Schneider M, Šlechtová V, Stoumboudi M, Walter S, Freyhof J (2014) Spatial heterogeneity in the mediterranean biodiversity hotspot affects barcoding accuracy of its freshwater fishes. Molecular Ecology Resources 14: 1210–1221. https://doi.org/10.1111/1755-0998.12257

Hall TA (1999) BioEdit a user-friendly biological sequence alignment editor and analysis program for Windows 95/98/NT. Nucleic Acids Symposium Series 41: 95–98.

Kamangar BB, Prokofiev AM, Ghaderi E, Nalbant TT (2014) Stone loaches of Choman River system, Kurdistan, Iran (Teleostei, Cypriniformes, Nemacheilidae). Zootaxa 3755(1): 33–61. https://doi.org/10.11646/4364

Kottelat M (2012) Conspectus cobitidum: An inventory of the loaches of the world (Teleostei, Cypriniformes, Cobitoidei). The Raffles Bulletin of Zoology 26(Supplement): 1–199.

Kottelat M, Freyhof J (2007) Handbook of European Freshwater Fishes: Kottelat, Cornol and Freyhof, Berlin, [xiv +] 646 pp.

Kumar S, Stecher G, Li M, Knyaz C, Tamura K (2018) MEGA X: Molecular evolutionary genetics analysis across computing platforms. Molecular Biology and Evolution 35(6): 1547–1549. https://doi.org/10.1093/molbev/msy096

Posada D (2008) jModelTest: Phylogenetic model averaging. Molecular Biology and Evolution 25(7): 1253–1256. https://doi.org/10.1093/molbev/msn083

Puillandre N, Lambert A, Brouillet S, Achaz G (2012) ABGD, Automatic Barcode Gap Discovery for primary species delimitation. Molecular Ecology 21(8): 1864–1877. https://doi.org/10.1111/j.1365-294X.2011.05239.x

Puillandre N, Brouillet S, Achaz G (2021) ASAP: Assemble species by automatic partitioning. Molecular Ecology Resources 21(2): 609–620. https://doi.org/10.1111/1755-0998.13281

Ronquist F, Huelsenbeck JP (2003) MrBayes 3: Bayesian phylogenetic inference under mixed models. Bioinformatics 19(12): 1572–1574. https://doi.org/10.1093/bioinformatics/btg180

Sayyadzadeh G, Eagderi S, Esmaeili HR (2016) A new loach of the genus *Oxynoemacheilus* from the Tigris River drainage and its phylogenetic relationships among the nemacheilid fishes (Teleostei, Nemacheilidae) in the Middle East based on mtDNA COI sequences. Iranian Journal of Ichthyology 3: 236–250.

Stoumboudi MT, Kottelat M, Barbieri R (2006) The fishes of the inland waters of Lesbos Island, Greece. Ichthyological Exploration of Freshwaters 17(2): 129–146.

Tamura K, Nei M (1993) Estimation of the number of nucleotide substitutions in the control region of mitochondrial DNA in humans and chimpanzees. Molecular Biology and Evolution 10(3): 512–526. https://doi.org/10.1093/oxfordjournals.molbev.a040023

Thompson JD, Higgins DG, Gibson TJ (1994) CLUSTAL W: Improving the sensitivity of progressive multiple sequence alignment through sequence weighting, position-specific gap penalties and weight matrix choice. Nucleic Acids Research 22(22): 4673–4680. https://doi.org/10.1093/nar/22.22.4673

Turan D, Kaya C, Kalaycı G, Baycelebi E, Aksu İ (2019) *Oxynoemacheilus cemali*, a new species of stone loach (Teleostei, Nemacheilidae) from the Çoruh River drainage. Journal of Fish Biology 94(3): 458–468. https://doi.org/10.1111/jfb.13909

Turan D, Aksu S, Kalaycı G (2023a) Two new *Oxynoemacheilus* species in western Anatolia (Teleostei, Nemacheilidae). Zoosystematics and Evolution 99(2): 439–455. https://doi.org/10.3897/zse.99.102575

Turan D, Bayçelebi E, Kalaycı G (2023b) *Oxynoemacheilus marmaraensis*, a new species from the Susurluk River, Türkiye (Teleostei, Nemacheilidae). Journal of Fish Biology 103(5): 1106–1112. https://doi.org/10.1111/jfb.15506

Turan D, Aksu S, Güçlü SS, Kalaycı G (2024) [in press] *Oxynoemacheilus fatmae*, a new species from the Güzelhisar Stream in Aegean Sea basin, Türkiye (Telostei: Nemacheilidae). Journal of Fish Biology. https://doi.org/10.1111/jfb.15779

Ward RD, Zemlak TS, Innes BH, Last PR, Hebert PDN (2005) DNA barcoding Australia's fish species. Philosophical Transactions of the Royal Society of London, Series B, Biological Sciences 360(1462): 1847–1857. https://doi.org/10.1098/rstb.2005.1716

Yoğurtçuoğlu B, Kaya C, Freyhof J (2022) Revision of the *Oxynoemacheilus angorae* group with the description of two new species (Teleostei, Nemacheilidae). Zootaxa 5133(4): 451–485. https://doi.org/10.11646/zootaxa.5133.4.1

Zoosyst. Evol. 100 (2) 2024, 493–513 | DOI 10.3897/zse.100.122288

PENSOFT

für Natur MUSEUM FÜR NATURKUNDE BERLIN

Natural history collections help resurrecting *Glomeris herzogowinensis* Verhoeff, 1898 and further clarify the nomenclature of two *Onychoglomeris* subspecies of Attems (Diplopoda, Glomerida, Glomeridae)

Dragan Antić[1], Thomas Wesener[2], Nesrine Akkari[3]

1 *University of Belgrade – Faculty of Biology, Institute of Zoology, Center for Biospeleology, Studentski Trg 16, 11000 Belgrade, Serbia*
2 *Leibniz Institute for the Study of Biodiversity Change, Zoogisches Forschungsmuseum Alexander Koenig, Adenauerallee 127, 53113 Bonn, Germany*
3 *3rd Zoological Department, Natural History Museum Vienna, Burgring 7, 1010 Vienna, Austria*

https://zoobank.org/CF9FDD8F-1432-4A0D-BA41-5D11B642110A

Corresponding author: Dragan Antić (dragan.antic@bio.bg.ac.rs)

Academic editor: Luiz Felipe Iniesta ♦ **Received** 4 March 2024 ♦ **Accepted** 1 April 2024 ♦ **Published** 9 May 2024

Abstract

Based on the study of freshly-collected material and old museum specimens, we have solved a decades-old riddle surrounding the name *Onychoglomeris herzogowinensis* (Verhoeff, 1898). The southern Dinaric coastal species *Glomeris herzogowinensis* Verhoeff, 1898 is revived, while *Onychoglomeris herzogowinensis australis* Attems, 1935 and *O. h. media* Attems, 1935, are treated here as full species after returning the specific name to *Glomeris* Latreille, 1902, *O. australis* Attems, 1935, **stat. nov.** and *O. media* Attems, 1935, **stat. nov.** Besides the designation of lectotypes, we provide comprehensive illustrations, diagnoses, detailed remarks and a distribution map for all three species. In addition, DNA barcoding provided COI sequences for *Glomeris herzogowinensis* and *Onychoglomeris australis* **stat. nov.**, along with the first barcoding data of one additional species of *Onychoglomeris* Verhoeff, 1906, *O. ferraniensis* Verhoeff, 1909 and two *Glomeris* species, the Balkan *G. balcanica* Verhoeff, 1906 and the trans-Adriatic *G. pulchra* Koch, 1847. The significance of historical specimens from natural history museums is briefly discussed.

Key Words

Balkan Peninsula, COI, Europe, Glomerinae, lectotype, syntypes, taxonomy

Introduction

The Western Palaearctic genus *Glomeris* Latreille, 1802 comprises about 75 species with a smaller number of taxa in the Canary Islands, North Africa and Anatolia and the majority of species on the European continent (Enghoff et al. 2015). Apart from the fact that this genus includes some of the most attractive and colourful millipedes in Europe, it is certainly a nightmare for taxonomists. Around 60 species of the genus live on the continent today, with an unfathomably large number of subspecies, varieties, forms or morphs having been described in the past, counted in hundreds (Golovatch et al. 2009). It is interesting to note that more than 80 forms have been described within the common central and southeast European species *Glomeris hexasticha* Brandt, 1833 alone (Kime and Enghoff 2011). Due to insufficient taxonomic information on the structure of the telopods and their uniformity in this group, the species, subspecies or "lower categories" are mostly described on the basis of colour patterns. While in some species this pattern may be stable, in many others, there is variability, even within the same population, where the colouration of one species may be similar or identical to the colour pattern of an-

other species. Fortunately, the chaotic situation within the genus and the order Glomerida, in general, has improved somewhat in recent decades, largely due to an integrative approach to the problem (Hoess et al. 1997; Hoess and Scholl 1999a, 1999b, 2001; Hoess 2000; Oeyen and Wesener 2015; Wesener 2015a, 2015b, 2018; Wilbrandt et al. 2015; Wesener and Conrad 2016; Reip and Wesener 2018; Antić et al. 2021).

One of the taxa that have been forgotten and completely excluded from the European fauna is *Glomeris herzogowinensis* Verhoeff, 1898. Verhoeff (1898) described this taxon under the name "*Glomeris europaea*, *herzogowinensis*" on the basis of specimens from near Trebinje, Herzegovina, collected by Victor Apfelbeck, the then curator of the National Museum of Bosnia and Herzegovina in Sarajevo. Although the description of this taxon is relatively short, Verhoeff (1898) already points out in the first sentence: "...der marginata in der Färbung äusserst ähnlich...", indicating a great similarity in colouration between *G. herzogowinensis* and one of the most common western-central-northern European species, *Glomeris marginata* (Villers, 1789). Albeit geographically completely separate, both species are characterised by mostly black, shiny tergites with yellowish or white posterior margins. Verhoeff (1898) noted several differences between the two taxa, including details of the telopods, although he never illustrated them. This deficiency led to *G. herzogowinensis* falling into oblivion. Two years later, Verhoeff (1901: 248, 249) cited *G. herzogowinensis* from several localities in Albania and Greece, apparently only on the basis of a large, dark body with lighter posterior margins, evidently without examining the telopods of males from Greece. Later, it will turn out that, in these parts of Albania and Greece, there is or are one or even two species similar in appearance to *G. herzogowinensis*, but belonging to a different genus, *Onychoglomeris* Verhoeff, 1906. The fact that Verhoeff did not actually examine the telopods of the Greek male specimens is supported by the fact that, when establishing the then subgenus, *Onychoglomeris*, he included in it what we know today as *Onychoglomeris tyrolensis* (Latzel, 1884) and *Simplomeris montivaga* (Faës, 1902) (Verhoeff 1906). The telopods of these species differ markedly from those of the genus *Glomeris* and *G. herzogowinensis*. In his contribution to the knowledge of the genus *Glomeris*, Verhoeff (1911: 118, 119) included *Glomeris herzogowinensis* in the *marginata* species-group, stating some of the characteristics of the species. It is clear from the above that the species he described from the Trebinje area really belongs to the genus *Glomeris*.

However, the problem emerged in the papers of Attems (1929, 1935), after which the species name *Glomeris herzogowinensis* was no longer mentioned. Strangely and without any explanation, Attems (1929: 289, 312) listed Verhoeff's species under the name "*Onychoglomeris herzegovinensis* Verh.". The crux of the problem with this taxon happened six years later. Probably confused by Verhoeff's (1901: 248, 249) earlier (obviously incorrect) record of *G. herzogowinensis* from Albania and Greece and the confusing similarity in the habitus between the latter species of which he received some syntypes and the specimens of the genus *Onychoglomeris* from Albania and Greece he was studying, Attems (1935) just treated the species *G. herzogowinensis* as *Onychoglomeris herzogowinensis*. Attems (1935) was not sure of his act, especially because the structure of the telopods of *G. herzogowinensis* was unknown to him. He stated that only Verhoeff could clarify this by examining the telopods, although Attems himself could have done so (see below in Remarks under *G. herzogowinensis*). Despite this error, Attems was, however, right in the fact that his new specimens belonged to the genus *Onychoglomeris*. He described two taxa: *Onychoglomeris herzegovinensis media* Attems, 1935 from Albania and *O. h. australis* Attems, 1935 from Greece (Attems 1935). He treated the taxon from Croatia, Bosnia and Heregovina and Montenegro as the nominotypical subspecies *O. h. herzegovinensis* (*herzogowinensis* is the correct spelling in all cases). Attems (1935) provided illustrations of the telopods of the two subspecies, which undoubtedly speak in favour of the genus *Onychoglomeris*, but at the same time, he pointed out some differences in habitus between his subspecies on the one hand and the nominotypical subspecies distributed further north on the other.

Six decades later, Mauriès et al. (1997), based on relatively abundant material of *Onychoglomeris* from Albania, but without studying the specimens from the type locality of *G. herzogowinensis* nor the Greek specimens of *Onychoglomeris*, questioned the existence of three subspecies, considered all under the name *Onychoglomeris herzogowinensis*. The name appeared as such in Thaler (1999) and Kime and Enghoff (2011).

Based on newly-collected material from near the type localities and on the study of the syntypes and historical specimens of Verhoeff's *G. herzogowinensis* and Attems' subspecies *O. h. australis* and *O. h. media*, we revive Verhoeff's species *Glomeris herzogowinensis* after almost nine decades and we consider both of Attems' subspecies as species, viz. *Onychoglomeris australis* Attems, 1935 stat. nov. and *Onychoglomeris media* Attems, 1935 stat. nov.

Materials and methods

Live specimens were collected by hand and preserved in 70% ethanol for mophological and 96% ethanol for DNA analyses. Several live individuals of *Glomeris herzogowinensis* were first placed in glass vials containing 500 µl methylene chloride (DCM) for 5 minutes to extract their defensive secretions for future semiochemical studies. Later, the specimens were transferred to 70% ethanol.

Depository

IZB Institute of Zoology, University of Belgrade – Faculty of Biology, Belgrade, Serbia
NHMW Naturhistorisches Museum Wien, Vienna, Austria
ZFMK Zoological Research Museum A. Koenig, Leibniz Institute for Biodiversity Change, Bonn, Germany
ZMB Museum für Naturkunde Berlin, Germany
ZSM Zoologische Staatssammlung München, Germany

Morphology, photography and map

Specimens were examined with a Nikon SMZ 25 (NHMW), Nikon SMZ 745T, Nikon SMZ 1270 (IZB) or Olympus SZX12 (ZFMK) binocular stereomicroscopes. Old microscopic preparations were examined with a Nikon SMZ 25 (NHMW) binocular stereomicroscope or with a Carl Zeiss Axioscope 40 microscope (IZB). Photographs of habitus, leg pairs 17 and 18 and telopods were taken using a Nikon DS-Ri-2 camera mounted on a Nikon SMZ25 binocular stereomicroscope using NIS-Elements Microscope Imaging Software with an Extended Depth of Focus (EDF) patch (NHMW, Figs 2–6, 8–11A–D, G) or with a Nikon DS-Fi2 camera with a Nikon DS-L3 camera controller attached to a Nikon SMZ 1270 binocular stereomicroscope (IZB, Fig. 11E, F). The photos of the living animals were taken with a Canon PowerShot SX530 HS (Fig. 7A, B), Olympus Stylus Tough TG-6 (Fig. 7C, D), Nikon D750 (Fig. 12A, B) and Panasonic DMC-G81 (Fig. 12E, F) digital cameras as well as with a cellphone (Fig. 12C, D). The distribution map was created using Google Earth Pro (version 7.3.6.9750) and Adobe Photoshop CS6. The final images were processed and assembled in Adobe Photoshop CS6.

DNA extraction, amplification and sequencing

In order to find close relatives to *Glomeris herzogowinensis*, as well as *Onychoglomeris australis* stat. nov., a DNA barcoding analysis (Hebert et al. 2003) was conducted. COI sequences of both taxa, as well as those of potential related *Glomeris* species, such as *G. balcanica* Verhoeff, 1906 and *G. pulchra* Koch, 1847 and additionally *Onychoglomeris ferraniensis* Verhoeff, 1909 were analysed (see Table 1). In addition, sequences of similarily coloured (= black) *Glomeris* species were downloaded from GenBank: *Glomeris marginata* (Villers, 1789) from Central Europe, *G. apuana* Verhoeff, 1911 from the Apuan Alps and *G. maerens* Attems, 1927 from Spain. Additionally, sequences of widespread species occurring in the Balkans and surrounding areas were added from GenBank: *G. pustulata* Latreille, 1804, *G. hexasticha* Brandt, 1833, *G. tetrasticha* Brandt, 1833 and *G. klugii* Brandt, 1833. As outgroup taxa, sequences of *Glomeridella minima* (Latzel, 1884) and *Tonkinomeris huzhengkuni* Liu & Golovatch, 2020 from the family Glomeridellidae Cook, 1896 were added. Our dataset included 25 COI sequences from 15 species, of which eight sequences from five species were newly sequenced.

The DNA extraction, amplification and sequencing protocol was similar to earlier studies (Wesener 2015a; Sagorny and Wesener 2017), using the degenerate (Astrin and Stüben 2008) primer pair HCO-JJ/LCO-JJ (HCOJJ AWACTTCVGGRTGVCCAAARAATCA/ LCOJJ CHACWAAYCATAAAGATATYGG). Sequences were concatenated by hand or by utilising the software Seqman (DNASTAR Inc.). BLAST searches (Altschul et al. 1997) were performed to confirm sequence identities. The whole dataset was translated into amino acids to rule out the accidental amplification of pseudogenes. The eight new sequences have been uploaded to GenBank under the accession codes PP475126–PP475133 (Table 1). All sequences were aligned in Bioedit (Hall 1999).

The number of base differences per site (p-distances) between sequences was calculated (See Suppl. material 1). The analysis involved 25 nucleotide sequences. Codon positions included were $1^{st}+2^{nd}+3^{rd}$. All ambiguous positions were removed for each sequence pair. There were a total of 657 positions in the final dataset. Evolutionary analyses were conducted in Mega11 (Tamura et al. 2021).

The best fitting substitution model for a Maximum Likelihood analysis was calculated with ModelTest (Tamura and Nei 1993) as implemented in MEGA11. The best fitting model was the general time reversible (GTR)-Model (Tavaré 1986) with gamma distribution and invariant sites (GTR+G+I) (lnL = -4292.222, Invariant = 0.609, Gamma = 0.624, Freq A: 25.7, T: 38.89, C: 14.17, G: 21.24).

The evolutionary history was inferred by using the Maximum Likelihood method and the General Time Reversible model (GTR+G+I) (Nei and Kumar 2000). The tree with the highest log likelihood (-4292.19) is shown in Fig. 1. Initial trees for heuristic search were automatically obtained by applying Neighbour-Joining and BioNJ algorithms to a matrix of pairwise distances estimated using the Maximum Composite Likelihood (MCL) approach. Codon positions included were 1^{st}-2^{nd}-3^{rd}. All positions with less than 95% site coverage were eliminated, i.e. fewer than 5% alignment gaps, missing data and ambiguous bases were allowed at any position (partial deletion option). There were a total of 657 positions in the final dataset. The bootstrap consensus tree was calculated from 1000 replicates (Felsenstein 1985) in MEGA11 (Tamura et al. 2021). The obtained tree was edited in Adobe Illustrator 2023 with all bootstrap values > 50% illustrated (Fig. 1).

Table 1. Newly-analysed specimens, vouchers and GenBank numbers. More detailed localities are only given for newly-sequenced specimens. Abbreviations: **SCAU** = South China Agricultural University, Guangzhou, China; **ZSM** = Bavarian State Collection, Munich, Germany; **ZFMK** = Zoological Research Museum Koenig, Leibniz Institute for the Analysis of Biodiversity Change (LIB), Bonn, Germany.

Species	Locality	Voucher #	GenBank #
Glomeridella minima (Latzel, 1884)	Austria	ZSM MYR 00371	JN271878
Tonkinomeris huzhengkuni Liu & Golovatch, 2020	China	SCAU TY01	MT522013
Glomeris pustulata Latreille, 1804	Germany	ZSM MYR 00024	HM888093
Glomeris pustulata Latreille, 1804	Germany	ZSM MYR 00376	JN271880
Glomeris hexasticha Brandt, 1833	Germany	ZFMK MYR1460	MG931023
Glomeris hexasticha Brandt, 1833	Germany	ZFMK MYR3898	MG931024
Glomeris tetrasticha Brandt, 1833	Germany	ZSM MYR 00036	HM888105
Glomeris tetrasticha Brandt, 1833	Germany	ZSM MYR 00035	HM888104
Glomeris marginata Villers, 1789	France	ZFMK MYR6084	MG931022
Glomeris marginata Villers, 1789	Luxembourg	ZFMK MYR1363	MG931021
Glomeris maerens Attems, 1927	Spain	ZFMK MYR6097	MG892108
Glomeris maerens Attems, 1927	Spain	ZFMK MYR6092	MG892110
Glomeris klugii Brandt, 1833	Italy	ZFMK MYR637	KX714076
Glomeris klugii Brandt, 1833	Italy	ZFMK MYR4734	KX714072
Glomeris apuana Verhoeff, 1911	Italy	ZFMK MYR753	KT188944
Glomeris apuana Verhoeff, 1911	Italy	ZFMK MYR752	KT188943
Onychoglomeris tyrolensis Latzel, 1884	Italy	ZFMK MYR1276	KP205571
Glomeris pulchra Koch, 1847	Croatia, Dalmatia, Cetina River	ZFMK MYR8217	PP475126
Glomeris pulchra Koch, 1847	Croatia, Dalmatia, Cetina River	ZFMK MYR8217b	PP475127
Glomeris balcanica Verhoeff, 1906	Greece, Dion-Olympos	ZFMK MYR11331	PP475128
Onychoglomeris ferraniensis Verhoeff, 1909	Italy, Piemonte, Cuneo, Ceva	ZFMK MYR623	PP475129
Onychoglomeris ferraniensis Verhoeff, 1909	Italy, Piemonte, Cuneo, Ormea	ZFMK MYR2287	PP475130
Onychoglomeris australis Attems, 1935 stat. nov.	Greece, Kalambaka	ZFMK MYR11332	PP475131
Glomeris herzogowinensis Verhoeff, 1898	Bosnia & Herzegovina, Trebinje, Taleža	ZFMK MYR8970	PP475132
Glomeris herzogowinensis Verhoeff, 1898	Bosnia & Herzegovina, Trebinje, Taleža	ZFMK MYR8969	PP475133

Results

Analysis of the COI barcoding gene

All species were recovered with high statistical support (94–100%, Fig. 1), while deeper nodes and interspecific relationships were statistically not supported. Neither the families Glomeridae and Glomeridellidae, nor the genus *Glomeris* are recovered as monophyletic (Fig. 1). *Glomeris herzogowinensis* does not group with *Onychoglomeris* species, but is in an unsupported sister-group with the similarily coloured *G. maerens* from the Mediterranean coast of Spain (Fig. 1). *G. herzogowinensis* and *G. maerens* show also the lowest genetic distance to one another (11.9–12.6%), while *G. herzogowinensis* also shows lower genetic distances to the similarily coloured (black) *G. apuana* (12.2–12.9%) and the Balkan *G. balcanica* (12.6–13.4%), while it shows genetic distances of 13.4–16.4% to all other analysed species. The genus *Onychoglomeris* is recovered as monophyletic with moderate statistical support (74), with *O. australis* stat. nov. and the Italian *O. tyrolensis* in a weakly-supported sister-group (54, Fig. 1). *O. australis* stat. nov. shows the lowest genetic distance to *O. tyrolensis* (10.5%) and *O. ferraniensis* (11.1–11.4%), while it differs from species of the other genera by 12.8–15.7%.

Taxonomy

Class Diplopoda de Blainville in Gervais, 1844
Order Glomerida Brandt, 1833
Family Glomeridae Leach, 1816
Subfamily Glomerinae Leach, 1816
Genus *Glomeris* Latreille, 1802

***Glomeris herzogowinensis* Verhoeff, 1898**

Figs 1–7

Glomeris europaea, *herzogowinensis* Verhoeff, 1898: 163, fig. 18.
not *Glomeris herzegowinensis* (sic!).– Verhoeff (1901: 248).
not *Glomeris herzogowinensis*.– Verhoeff (1901: 249).
Gl. herzegowinensis (sic!).– Verhoeff (1906: 211).
herzegowinensis (sic!).– Verhoeff (1911: 119). [in the genus *Glomeris*].
Onychoglomeris hercegovinensis (sic!) in part.– Attems (1929: 289, 312).
Onychoglomeris hercegovinensis hercegovinensis (sic!).– Attems (1935: 149).
Onychoglomeris hercegovinensis hercegovinensis (sic!).– Attems (1959: 323).
Onychoglomeris herzegowinensis (sic!).– Strasser (1971: 12).
not *Onychoglomeris herzegowinensis* (sic!).– Thaler (1999: 198, 199, figs 16, 17).
Glomeris marginata.– Ceuca (1990: 10).
Onychoglomeris herzogowinensis in part.– Kime and Enghoff (2011: 34, 118).

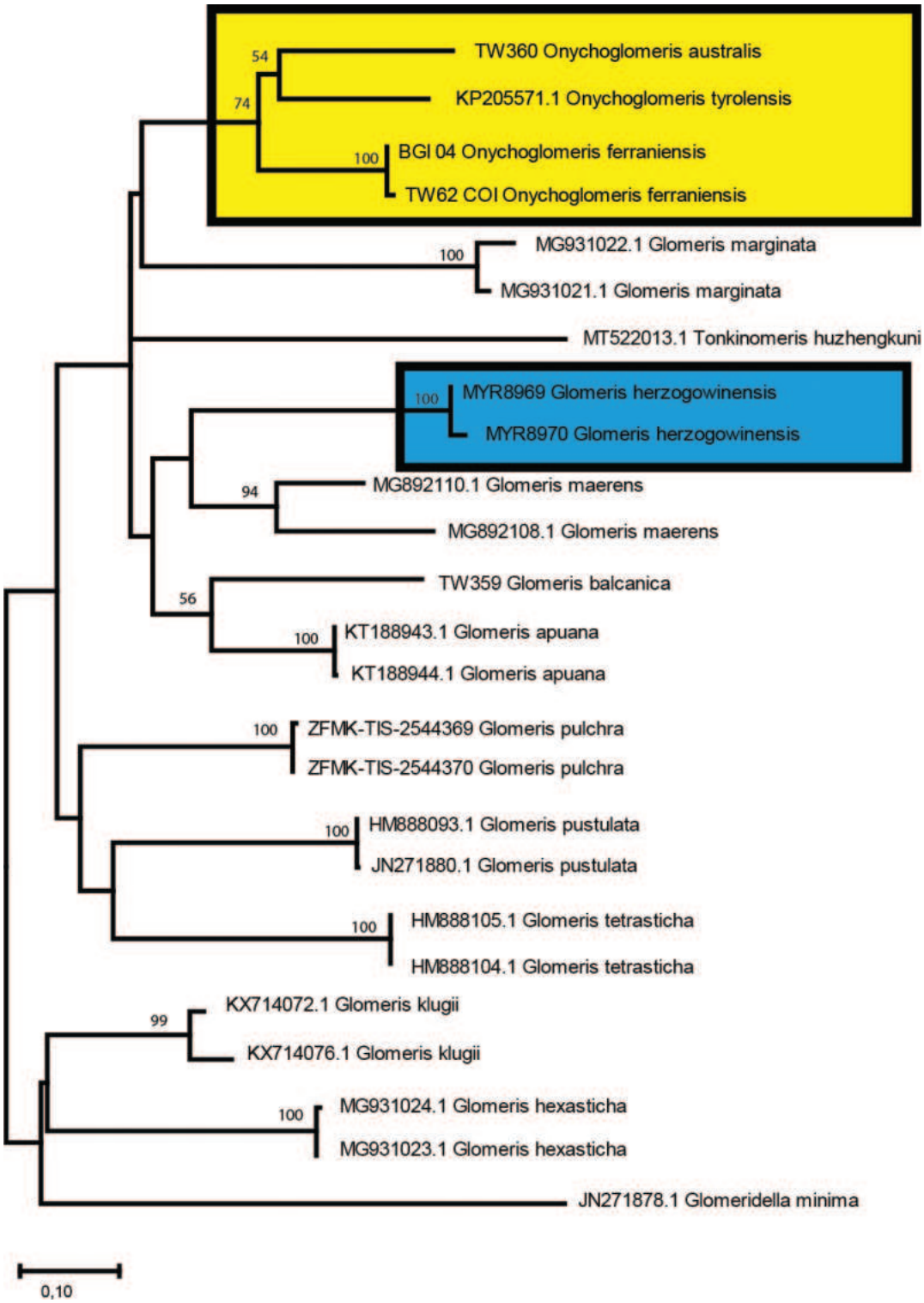

Figure 1. Maximum Likelihood tree (ML) of millipedes of the order Glomerida, based on 657 bp of the COI gene. Yellow box = *Onychoglomeris* Verhoeff, 1906; blue box = *Glomeris herzogowinensis* Verhoeff, 1898. Numbers on nodes are bootstrap values from the ML analysis and are shown when > 50%.

Diagnosis. Large species (up to 20 mm) with mostly black, shiny tergites with contrasting yellowish or white posterior margins. Similar to *G. marginata* in general appearance, but differs by strongly-pronounced light-coloured anterolateral margins of the thoracic shield which is in the form of a narrow band in *G. marginata*. Additionally, *G. herzogowinensis* has two complete or almost complete striae on the thoracic shield (tergite 2), while *G. marginata* has one complete stria.

Material studied. ***Lectotype.*** 1 male (NHMW 3903); Bosnia and Herzegovina, Trebinje; V. Apfelbeck leg.; K. Verhoeff don. 1897. Lectotype here designated.

Paralectotypes. ● 1 male, slide preparation (ZMB-MYR12772) (Verhoeff slide 953): leg pair 18 and telopods; Trebinje. ● 1 male, 1 female (ZMB-MYR2261); Trebinje.

?Types. ● 1 female (NHMW MY10415); Herzegovina: K. Verhoeff don. 1899. (Although this female arrived later in the NHMW collection than the lectotype, it may well represent another type specimen collected by Apfelbeck near Trebinje). ● 2 tubes (ZSM-A 20070848), 1 whole male, 1 male dissected (missing telopods and posterior leg pairs), 1 female, 1 juvenile; "ehemals Trockenmaterial" [material previously dry], Etk Nb. 28; Herzegowina. ● 1 tube (ZSM-A20070848), (Etk Nb. 28): 1 entire female specimen, a detached collum and thoracic shield, "ehemals Trockenmaterial; Tier m Original determinat. Etikett C Typüs-verdächtig" [material previously dry, animal with original determination, probable type], Trebinje. ● 1 male, slide preparation (ZSM-A20031802): telopods, leg pairs ?16, 17 and 18; Schuma (= Šuma, karst region around Trebinje).

Other material examined. Bosnia and Herzegovina: ● 1 female (NHMW MY10414); Trebinje ● 2 males, 1 female (IZB); in front of Taleža Cave, Taleža Village, near Trebinje, under stones; 15 November 2019; D. Antić leg. ● 3 males, 7 females (IZB); same locality as previous; 8 April 2022; D. Antić and D. Stojanović leg. ● 1 female (IZB); in front of Pavlova Cave, Bihovo Village, near Trebinje, under a stone; 16 November 2019; D. Antić leg. ● 1 female (IZB); same as previous but inside Pavlova Cave. Croatia: ● 1 female (NHMW MY10427); Pridvorje ● 2 females (ZFMK MYR89); Dubrovnik-Neretva, Konavle Region, Gruda, Konavoski dvori, under stones close to river, 50 m elev.; 3 April 2010; R. Ozimec & A. Schönhofer leg. ● 1 male (ZFMK MYR95); Dubrovnik-Neretva, Konavle Region, Vignje, near Sklenica Cave, under stones in dense, humid, mossy forest, 89 m elev.; 3 April 2010; R. Ozimec & A. Schönhofer leg. ● 3 males (ZFMK MYR153); Dubrovnik-Neretva, Konavle region, Vignje, Špilja at Vignje Cave; under stones; 3 April 2010; R. Ozimec & A. Schönhofer leg. ● 1 female (ZFMK MYR173); Dubrovnik-Neretva, Konavle Region, Vignje, surroundings of entrance of Tunnel of Konavle Polje, under stones, 50 m elev.; 3 April 2010; R. Ozimec & A. Schönhofer leg. Montenegro: ● 1 male, 4 females (NHMW MY10413); Savina ● 1 male (IZB) ethanol and slide with leg pairs 17 and 18 and telopods; Orjen Mountain, Balješina Lokva, 1400 m elev.; 4 July 1997; I. Karaman leg. ● 1 female (ZFMK MYR220); Rumija Mountain, near Sutorman, sieving in oak forest near rocks and under stones along open path, 42°9'22.8"N, 19°6'32.1"E, 805 m elev.; 9 May 2006; A. Schönhofer leg. ● 1 ex.; Borovik, near Cetinje; 11 May 2011; D. Antić observed.

Remarks. After examining type and old museum specimens, as well as freshly-collected animals, we confidently conclude that Verhoeff's *herzogowinensis* has typical *Glomeris* telopods. Attems (1935) examined

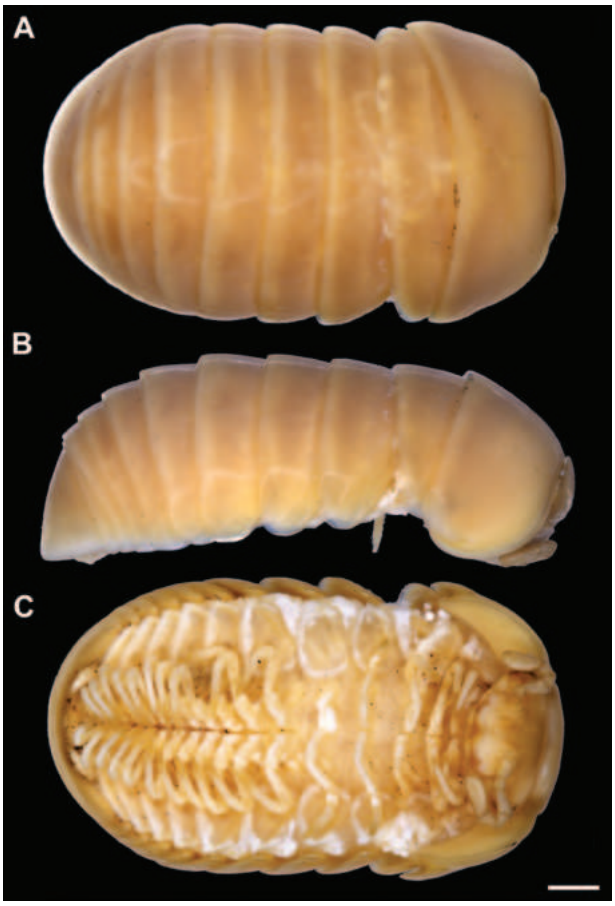

Figure 2. *Glomeris herzogowinensis* Verhoeff, 1898, lectotype male (NHMW MY3903), habitus. **A.** Dorsal view; **B.** Lateral view; **C.** Ventral view. Scale bar: 1 mm.

Verhoeff's material sent to the NHMW and listed that they were both females, so there was no possibility of examining the telopods. Interestingly, we found and examined these two specimens, among which one revealed to actually be a male (now lectotype, see Figs 2, 3). In addition, Attems (1929) indicated the locality Savina in Montenegro as one of the collecting cites of *Onychoglomeris hercegovinensis* (sic!). We found one male (Fig. 4) among five specimens from this locality, again with typical *Glomeris* telopods (Fig. 4D). Thus, Attems missed the opportunity to see the telopods in two males, including Verhoeff's syntype and to conclude that it was, indeed, a species of the genus *Glomeris* and not of *Onychoglomeris*.

Glomeris herzogowinensis shows a striking resemblance with *G. marginata*, both in habitus (Figs 5–7) and in the structure of the telopods (Figs 3C, 4D), which are almost identical in both species. Verhoeff (1898) pointed out that *G. herzogowinensis* has more prominent light-coloured posterolateral margins compared to *G. marginata*. However, this is not entirely correct, as one individual analysed by us (Fig. 6A) has identical margins to most *G. marginata*. Indeed, most of the studied specimens of *G. herzogowinensis* have more pronounced margins than the classic *G. marginata*, but

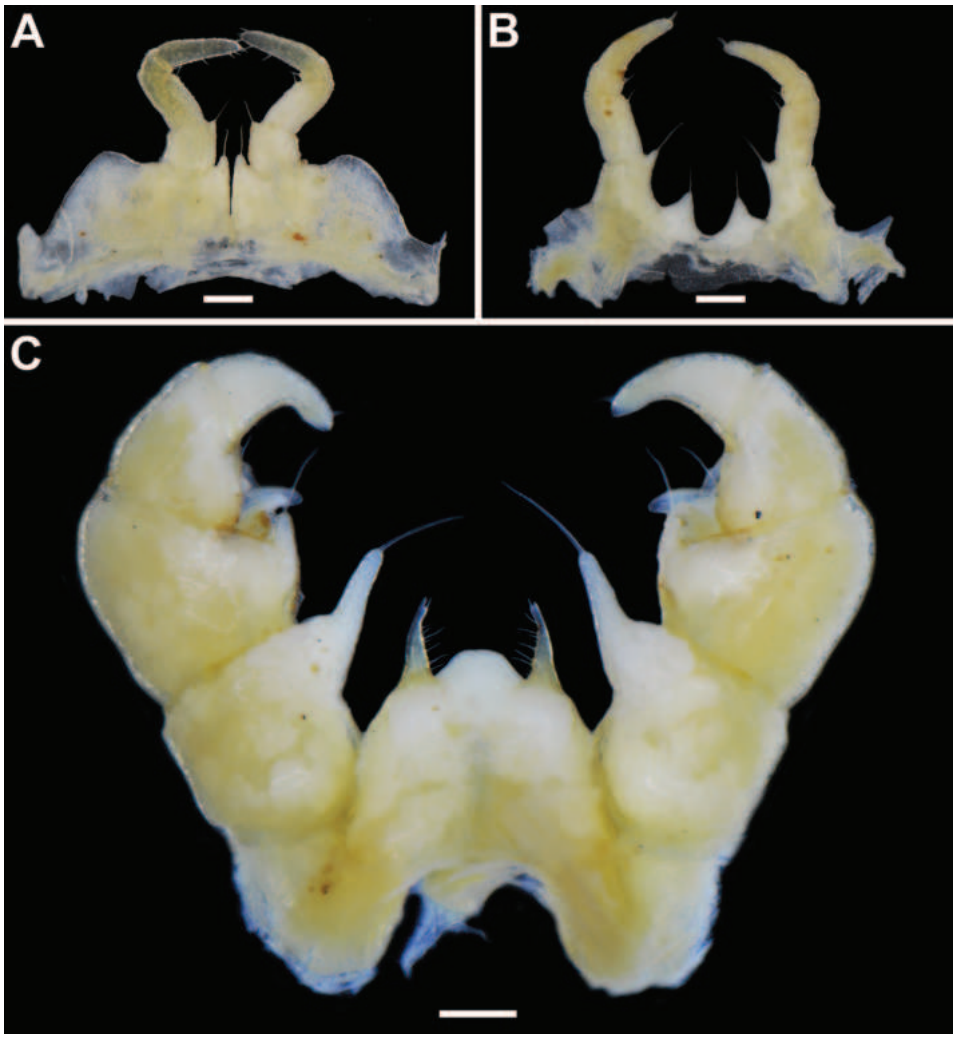

Figure 3. *Glomeris herzogowinensis* Verhoeff, 1898, lectotype male (NHMW MY3903). **A.** Leg pair 17, anterior view; **B.** Leg pair 18, anterior view; **C.** Telopods, anterior view. Scale bars: 0.2 mm.

some French populations of the latter present posterolateral margins that are more developed than in *G. herzogowinensis* (see Reip and Wesener (2018: 96, fig. 1D, E)). Verhoeff (1898, 1911) mentioned the presence of strongly-pronounced light-coloured anterolateral margins of the thoracic shield as one of the most important features distinguishing these two species. Indeed, the thoracic shield of all examined individuals of *G. herzogowinensis* has very distinct anterolateral margins (Figs 5A, C, 6B, D, E), in contrast to *G. marginata*, where it is only present in the form of a narrow band. The colouration of the fresh specimens that we have analysed corresponds completely to the description of Verhoeff (1898). They are mostly black with clearly demarcated lighter, whitish or yellowish posterolateral margins of the tergites. The collum also has a lighter posterior margin, as does the anal shield. As already mentioned, the thoracic shield also has a pronounced anterolateral margin. Some specimens are characterised by the presence of a pair of pale marbled patches on the tergites, including the thoracic shield, as well as an unpaired patch on the anal shield (Figs 5A, B, D, 6B). The presence of demarcated posterolateral light-coloured margins is clearly visible in old museum specimens too (Figs 2A, B, 4A).

Verhoeff (1898) listed some differences in the structure of the telopods, but they were apparently so insignificant that he never drew these structures. Nevertheless, in this paper, we present for the first time illustrations of the telopods of *G. herzogowinensis*, as well as of the 17th pair of legs and the entire 18th pair of legs (Figs 3, 4B–D), which are of typical *Glomeris* appearance.

We would also like to mention that all examined specimens show two transverse ridges on the collum (Figs 5C, 6B, E). Verhoeff (1911) found that, in addition to the two characteristic ridges, a third ridge starts on both sides of the collum. In the fresh material, the beginning of the third ridge was only observed in one specimen and only on the left side. Concerning the thoracic shield (tergite 2), Verhoeff (1898) distinguished *G. herzogowinensis* from *G. marginata* by the presence of two complete striae and an incomplete one (2+1 vs. 1+2, 1+1 or 1+0 sensu Schubart (1934: 33, fig. 28)). Indeed, all but

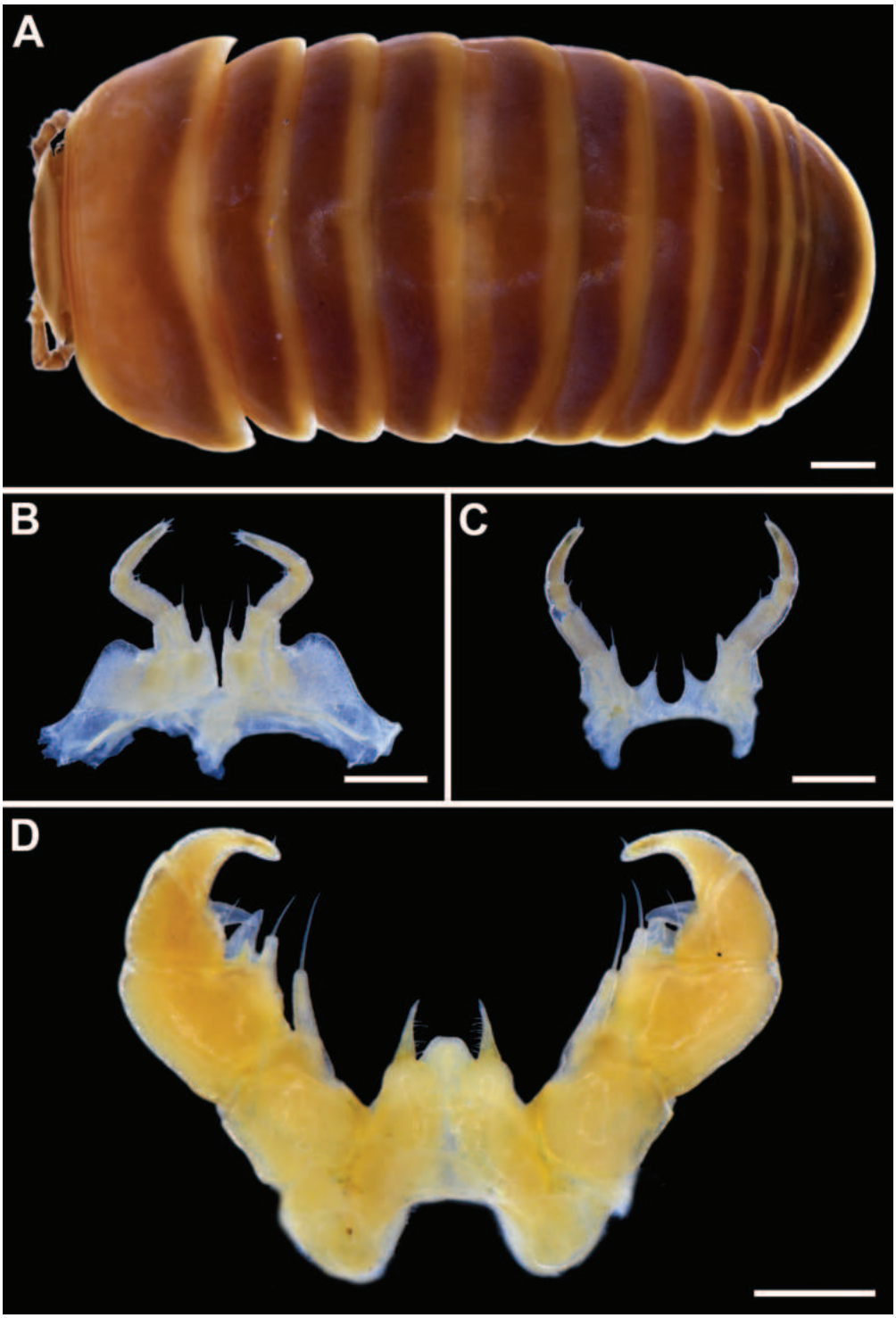

Figure 4. *Glomeris herzogowinensis* Verhoeff, 1898, male from Savina, Montenegro (NHMW MY10413). **A.** Habitus, dorsal view; **B.** Leg pair 17, anterior view; **C.** Leg pair 18, anterior view; **D.** Telopods, anterior view. Scale bars: 1 mm (**A**); 0.5 mm (**B–D**).

two of the specimens examined show two complete striae and an incomplete one. In two specimens, the second stria is almost complete, with only a small interruption dorsally. Some specimens are characterised by the presence of additional, 4th incomplete striae in front of the first complete one.

Habitat. Known from almost near sea level up to 1400 m elev. in the Orjen Mountain. Scrubs of *Carpinus*, *Quercus*, *Juniperus*, under stones in limestone areas. Inside caves.

Distribution. The extreme south of Croatia and Bosnia and Herzegovina, as well as the coastal part of

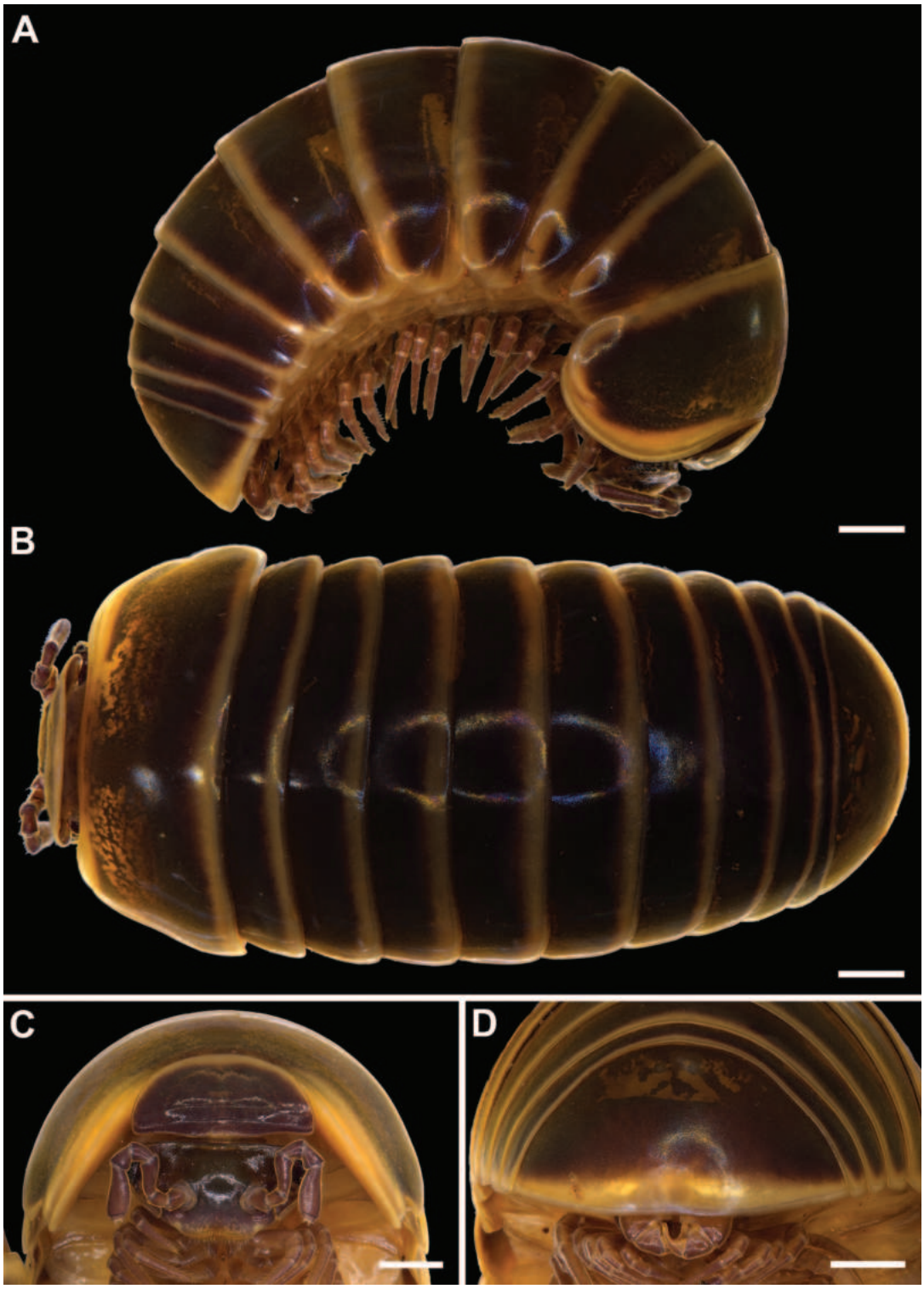

Figure 5. *Glomeris herzogowinensis* Verhoeff, 1898, male from Taleža, Bosnia and Herzegovina (IZB). **A.** Habitus, lateral view; **B.** Habitus, dorsal view; **C.** Head, collum and thoracic shield, anterior view; **D.** Anal shield, posterior view. Scale bars: 1 mm.

Montenegro (Fig. 13). Endemic south Dinaric coastal species. Croatia: Pridvorje (Attems 1929), Konavoski Dvori (Ceuca 1990, as *G. marginata*; present study), Gruda near Konavle (T. Dražina pers. comm.; present study), Vignje (present study); Bosnia and Herzegovina: Surroundings of Trebinje (Verhoeff 1898; Attems 1929, 1935), Taleža near Trebinje (present study), Bihovo near Trebinje (present study). Montenegro: Savina (Attems 1929, 1935), Orjen (present study), Rumija, near Sutorman (present study), Cetinje, Borovik (present study).

Type locality. Near Trebinje, Bosnia and Herzegovina.

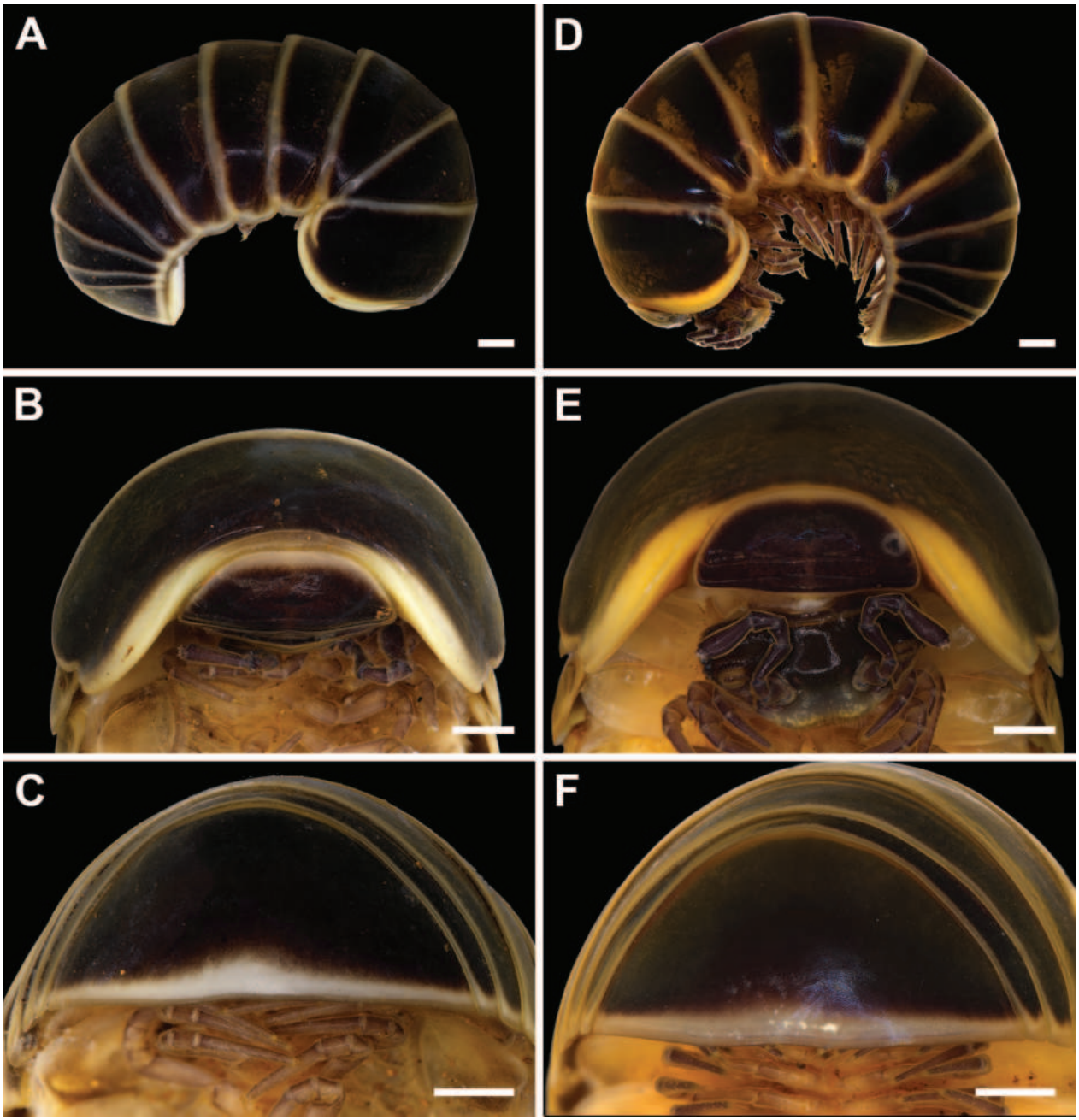

Figure 6. *Glomeris herzogowinensis* Verhoeff, 1898, male (**A–C**) and female (**D–F**) from Taleža, Bosnia and Herzegovina (IZB). **A.** Habitus, lateral view; **B.** Collum and thoracic shield, anterior view; **C.** Anal shield, posterior view; **D.** Habitus, lateral view; **E.** Head, collum and thoracic shield, anterior view; **F.** Anal shield, posterior view. Scale bars: 1 mm.

Genus *Onychoglomeris* Verhoeff, 1906

Onychoglomeris australis Attems, 1935, stat. nov.

Figs 8, 9, 12A–D

Onychoglomeris hercegovinensis australis (sic!).– Attems (1935: 150, figs 6–8).

Glomeris herzogowinensis in part.– Verhoeff (1901: 249).

Onychoglomeris herzegowinensis australis (sic!).– Strasser (1976: 580).

Onychoglomeris herzegowinensis (sic!).– Thaler (1999: 198, 199, figs 16, 17).

Onychoglomeris herzogowinensis in part.– Kime and Enghoff (2011: 34, 118).

Diagnosis. Similar in colouration (Fig. 12A–D) and morphology to the geographically very close *O. media* stat. nov., but differs in the appearance of the anal shield, leg pair 18 and telopods. Anal shield straight in lateral view (vs. distinctly concave in *O. media* stat. nov.). Leg pair 18 with short podomere 2, which is 1.5 times longer than wide, with straight mesal margin (vs. podomere 2 longer, twice as long as wide with distinctly convex mesal margin in *O. media* stat. nov.). Telopods apparently less robust, with a less developed posteriomesal process of telopoditomere 2 (= femur) and a shorter telopoditomere 4 (= tarsus), brownish stripes at the base of posteromesal process of telopoditomere 2 absent (vs. present in *O. media*

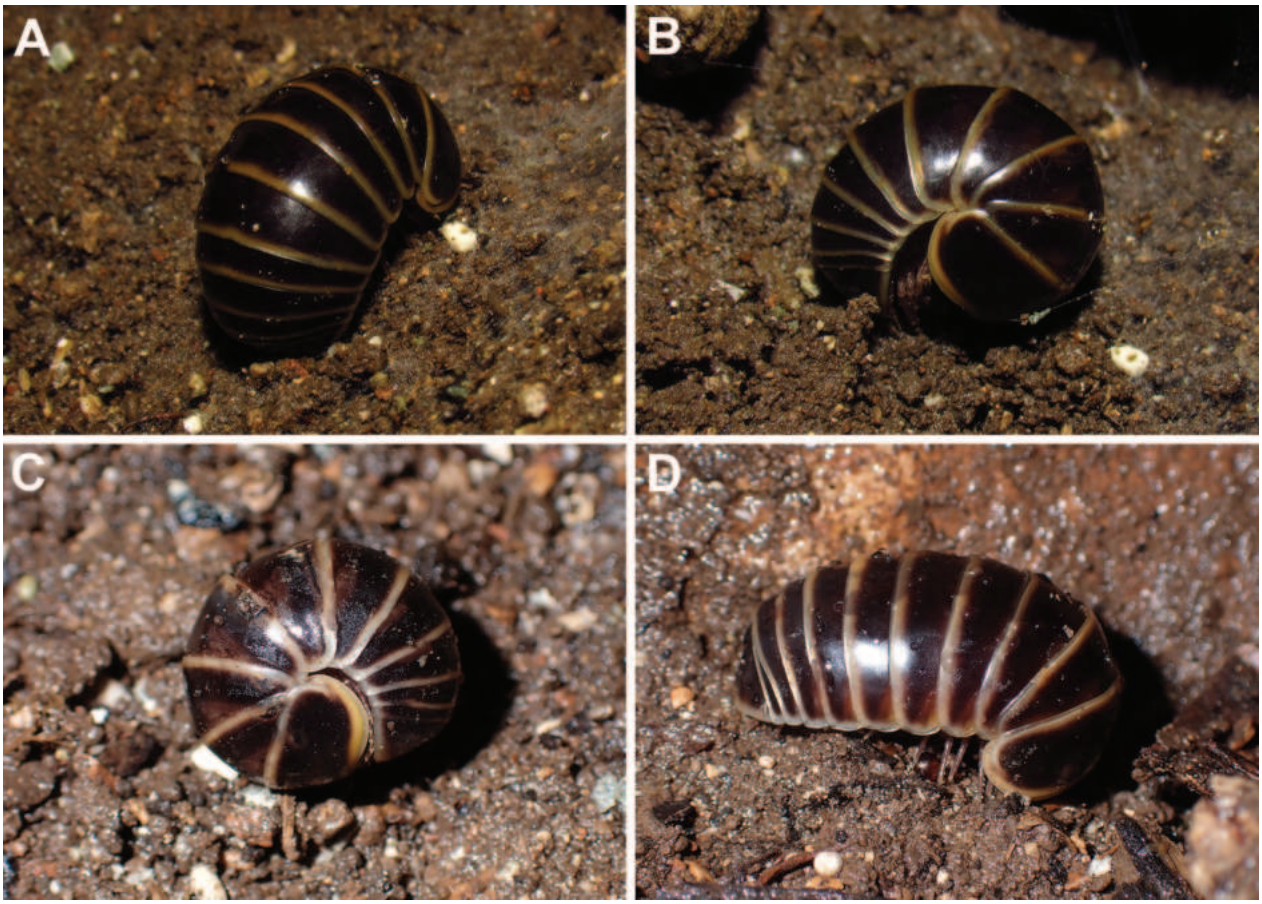

Figure 7. *Glomeris herzogowinensis* Verhoeff, 1898, living specimens. **A, B.** Female from Pavlova Cave, Bosnia and Herzegovina (IZB); **C, D.** Specimen from Taleža, Bosnia and Herzegovina (IZB). Photos by Dragan Antić.

stat. nov.), telopoditomere 3 (= tibia) with a well-developed posterior tooth that is more or less conical (vs. tooth poorly developed, subtriangular, sometimes almost absent in *O. media* stat. nov.), the syncoxite is usually high, rounded (vs. syncoxite mostly lower, bilobed in *O. media* stat. nov.). For more details see remarks below.

Material studied. ***Lectotype.*** 1 male (NHMW MY10424); Greece, Epirus, Athamanika (= Tzoumerka) Mountain, Paraskevi, *Abies*, 1400 m elev.; 16 June 1933; M. Beier leg. Lectotype here designated.

Paralectotypes. 13 males, 11 females (NHMW MY3900); same data as for lectotype. Including one slide (NHMW MY3900) with two pairs of leg pair 18, two pairs of leg pair 17 and additional leg ?17.

Other material examined. All in Greece: ● 1 male (NHMW MY10418); Epirus, Buka Chalasmata near Platanoussa; 14 May 1932; M. Beier leg. ● 2 males, 2 females (NHMW MY10419); Epirus, Katarraktis; 1932/1933; M. Beier leg. ● 1 female (NHMW MY10416); Prosgoli; V. Apfelbeck leg. ● 5 males (NHMW MY10420); Epirus, Aoos Gorge near Konitsa, 550 m elev., *Carpinus*; 9 September 1996; K. Thaler and B. Knoflach leg. ● 8 males, 5 females (NHMW MY10421); Epirus, Timfi Mountain near Micropapingo, 800 m elev., bush; 10 September 1996; K. Thaler and B. Knoflach leg. ● 1 female (ZFMK MYR122); Epirus, Pindus Mountain, Zagori, Monodendri - Ano Pedina junction, under stone on the road, 835 m elev., 39.868002, 20.722076; 3 April 2006; A. Schönhofer leg. ● 5 males, 5 females, 2 juveniles (ZFMK MYR4517); Epirus, Vikos Gorge, near Monodendri, *Quercus* forest with lichens, 1000 m elev., 39.881527, 20.755473; 4 April 2006; A. Schönhofer leg. ● 7 males, 2 females, (ZFMK MYR4518); Epirus, SW Ioannina, Zoodochos Pigi, open bushland with partly evergreen *Quercus* close to stream under stones, old tree trunks and sieving from leaf litter, 460 m elev., 39.56492, 20.72300; 13 August 2009; S. Huber & A. Schönhofer leg. ● 1 female (ZFMK MYR162); Thessaly, road to Kastanea, Elafi, *Carpinus*, *Quercus*, N-exposition, sieving from depressions in trees, 454 m elev., 39.723250, 21.475917; 1 April 2006; A. Schönhofer leg. ● 2 males, 4 females (ZFMK MYR124); Thessaly, road E92a between Panagia and Metsovo; sieving in a damp, shady stream valley, moss and between stones, pine forest and alpine meadows, 1084 m elev., 39.80344, 21.306998; 2 April 2006; A. Schönhofer leg. ● 1 male (ZFMK MYR11332); Thessaly, Kalambaka, Meteora; September 2019; P. Knautt leg. ● 2 males, 1 juvenile (ZFMK MYR11334); same data ● 2 females (NHMW MY10417); Central Greece, Karpenisi; V. Apfelbeck leg. ● 1 female "?type", (ZSM-A20070858), Epirus.

Remarks. Attems (1935), although he examined only a few males, already pointed out differences in the telopods between his *australis* and *media*, which we found to be constant after examining more males. The median lobe

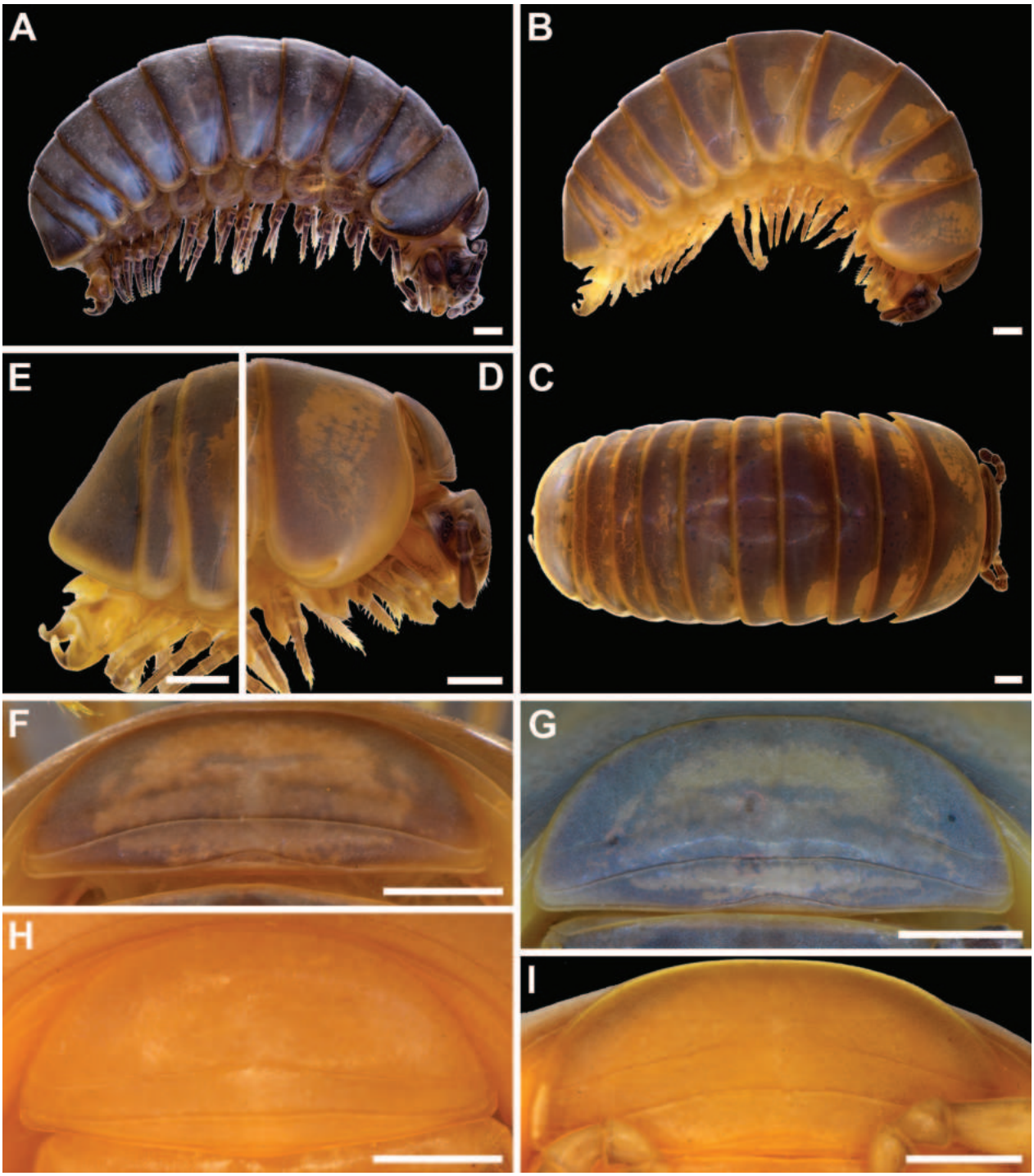

Figure 8. *Onychoglomeris australis* Attems, 1935, stat. nov. **A.** Lectotype male (NHMW MY10424), habitus, lateral view; **B–G.** Males from Konitsa, Greece (NHMW MY10420). **B.** Male 1, habitus, lateral view; **C.** Male 1, habitus, dorsal view; **D.** Male 1, anterior part of body, lateral view; **E.** Male 3, anal shield, lateral view; **F.** Male 1, collum, anterior view; **G.** Male 3, collum, anterior view; **H.** Female from Katarraktis, Greece (NHMW MY10419), collum, anterior view; **I.** Male from Katarraktis, Greece (NHMW MY10419), collum, anterior view. Scale bars: 1 mm.

of the syncoxite is high and rounded distally (Fig. 9A, B, D, H) in all but one of the males examined. In one, it is lower and flattened distally (Fig. 9C), which looks more like an anomaly. Attems (1935: 150, fig. 7) also noted a strongly developed conical tooth on the telopoditomere 3 (= tibia). The same was clearly illustrated by Thaler (1999: 199, figs 16, 17). In the males examined by us, this structure is always the same, conical and well developed (Fig. 9A, B, E, white arrows). Such a structure is mentioned for *O. media* stat. nov. by Attems (1935) as much smaller compared to *O. australis* stat. nov. Our observation was the same (see remarks under *O. media* stat. nov.).

As one of the differences, Attems (1935: 150, fig. 6) mentioned the absence of the medial syncoxital lobe of

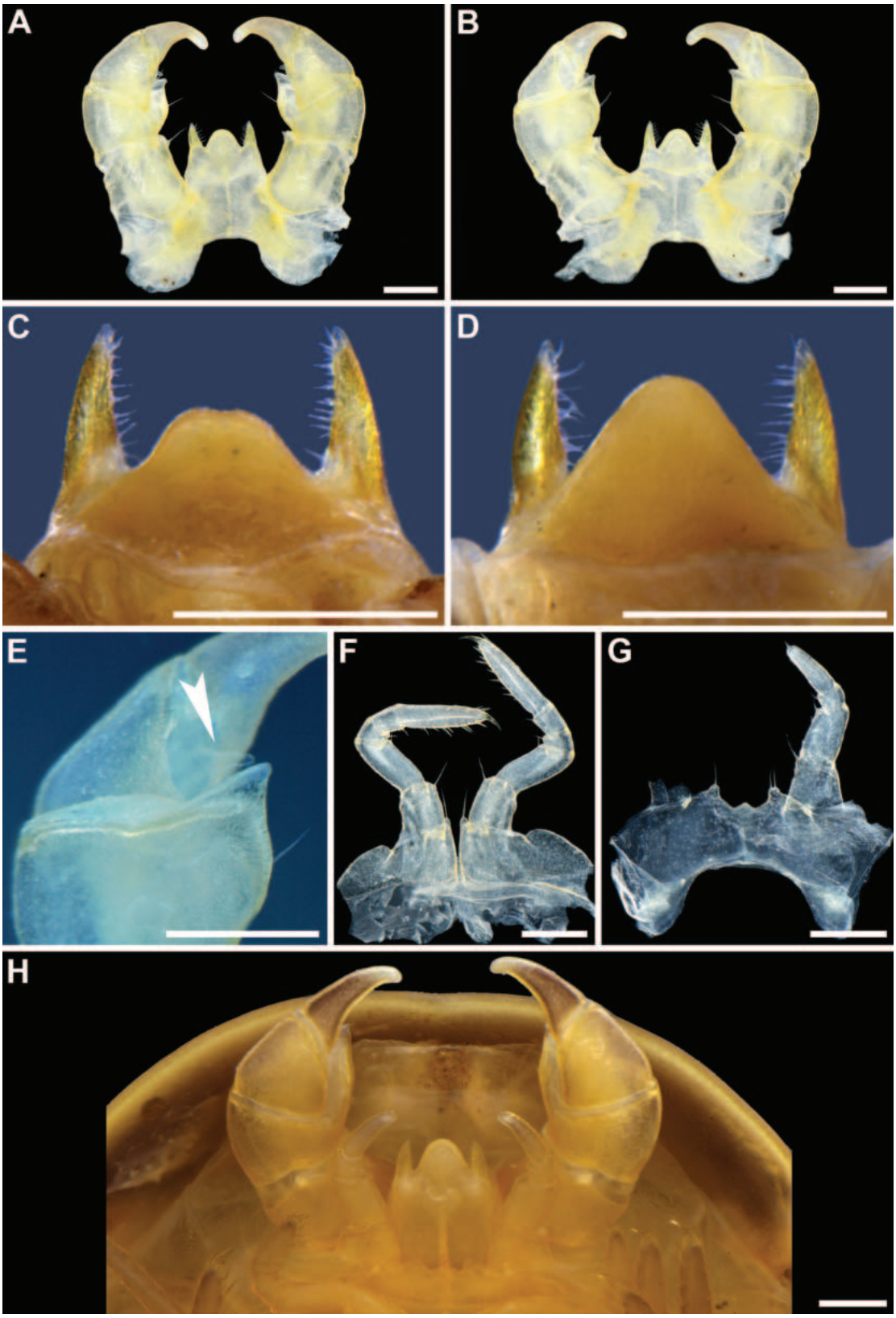

Figure 9. *Onychoglomeris australis* Attems, 1935, stat. nov. **A.** Male 4 from Konitsa, Greece (NHMW MY10420), telopods, anterior view; **B.** Male 4 from Konitsa, Greece (NHMW MY10420), telopods, posterior view; **C.** Paralectotype male 1 (NHMW MY3900), telopod syncoxite, posterior view; **D.** Paralectotype male 2 (NHMW MY3900), telopod syncoxite, posterior view; **E.** Male 4 from Konitsa, Greece (NHMW MY10420), part of right telopod, posterior view; **F.** Male 4 from Konitsa, Greece (NHMW MY10420), leg pair 17, anterior view; **G.** Male 4 from Konitsa, Greece (NHMW MY10420), leg pair 18, anterior view; **H.** Male 1 from Konitsa, Greece (NHMW MY10420), leg pair 18 and telopods *in situ*, anterior view. White arrow indicates posterior tooth of telopoditomere 3. Scale bars: 0.5 mm.

leg pair 18 in *O. australis* stat. nov. However, after having checked all males available to us, we conclude that this feature is variable, as some males present this lobe (Fig. 9G). On the other hand, we found that podomere 2 is short and has a straight mesal margin (Fig. 9G, H), as also drawn by Attems (1935: 150, fig. 6), quite different from *O. media* stat. nov. (see Remarks under *O. media* stat. nov.).

In all examined males, the anal shield is predominantly straight in lateral view (Fig. 8A, B), in some only slightly concave (Fig. 8E), but never as distinct as in *O. media* stat. nov. (see below, Fig. 10A). Attems (1935) reported two transverse ridges on the collum. After examining all males and females, we found that this feature is variable and that, in addition to specimens with one (Fig. 8F) or two (Fig. 8H) ridges, there are also those with lateral beginnings of the second ridge (Fig. 8G) or that the second ridge is interrupted only in the centre (Fig. 8I).

We would like to emphasise that juveniles of this species are lighter in colour and are characterised by colour patterns that are not seen or not that obvious in adults and should not be confused with other glomerids from the region (Fig. 12C, D).

The two southernmost finds of this species in Central Greece were apparently misidentified as *G. herzogowinensis* by Verhoeff (1901: 249). Although Verhoeff stated that he had three males from Karpenisi, it is very likely that he did not check the telopods, but made his identification on the basis of the very similar habitus with *G. herzogowinensis*. Unfortunately, we were unable to track down this Verhoeff material. We only found two females in the NHMW collection. As we were unable to look at the males, these two southernmost localities are marked with a question mark on the map.

Habitat. From 170 m to 1400 m elev. *Abies*, *Carpinus*, *Quercus*, *Juniperus*, *Pinus*, under stones, under tree trunks, under mossy limestone debris, leaf litter in limestone areas, open areas, bushland.

Distribution. Known from Epirus, Thessaly and central Greece (Fig. 13). *Epirus:* Paraskevi on Athamanika (Attems 1935), Buka Chalasmata near Platanoussa (Attems 1935), Katarraktis (Attems 1935), Prosgoli (Verhoeff 1901 [missidentification]; Attems 1935), Graveniti (Strasser 1976), Elati (Strasser 1976), Ligiades (Strasser 1976), Metsovon (Strasser 1976), Filiate (Strasser 1976), Aoos near Konitsa (Thaler 1999), Timfi near Mikropapingo (Thaler 1999), Monodendri - Ano Pedina (present study), Zoodochos Pigi (present study). *Thessaly:* Kastanea, Elafi (present study), Panagia (present study), Kalambaka (present study). *Central Greece:* Karpenisi (Verhoeff 1901 [missidentification]; Attems 1935), Velouchi on Tymfristos (Verhoeff 1901 [missidentification]).

Type locality. Paraskevi, Epirus, Greece. Attems (1935: 143) stated: "Paraskevi ist ein Gipfel des Cumerka-Gebirges" which translates that Paraskevi is a summit on the Tzoumerka (= Athamanika) Mountain. We could not find out where exactly Paraskevi is located.

Onychoglomeris media Attems, 1935, stat. nov.

Figs 10, 11, 12E, F

Onychoglomeris hercegovinensis media (sic!).– Attems (1935: 149, figs 4, 5).

Onychoglomeris hercegovinensis (sic!) in part.– Attems (1929: 289, 312).

Onychoglomeris herzogowinensis.– Mauriès et al. (1997: 258–260, fig. 2).

Onychoglomeris herzegowinensis (sic!).– Ćurčić et al. (1999: 11P).

Onychoglomeris herzogowinensis in part.– Kime and Enghoff (2011: 34, 118).

Glomeris herzogowinensis.– Verhoeff (1901: 248).

Glomeris herzogowinensis in part.– Verhoeff (1901: 249).

?*Glomeris marginata*.– Sekulić and Živić (2017: 193). [Missidentification, but see Remarks below].

Diagnosis. Similar in colouration (Fig. 12E, F) and morphology to the geographically very close *O. australis* stat. nov., but differs in the appearance of the anal shield, leg pair 18 and telopods. Anal shield distinctly concave in lateral view (vs. straight in *O. australis* stat. nov.). Leg pair 18 with podomere 2 longer, twice as long as wide with distinctly convex mesal margin (vs. podomere 2 shorter, ca. 1.5 times longer than wide, with straight mesal margin in *O. australis* stat. nov.). Telopods apparently more robust, with a well-developed posteriomesal process of telopoditomere 2 (= femur) and longer telopoditomere 4 (= tarsus), brownish stripes at the base of posteromesal process of telopoditomere 2 present (vs. absent in *O. australis* stat. nov.), telopoditomere 3 (= tibia) with a poorly developed, sometimes almost absent, posterior tooth that is subtriangular (vs. tooth well developed, conical in *O. australis* stat. nov.), the syncoxite is mostly low, somewhat bilobed (vs. syncoxite usually higher and rounded in *O. australis* stat. nov.). For some more details, see Remarks below.

Material studied. ***Lectotype.*** 1 male (NHMW MY3901) in ethanol; Albania, Dukati [= Dukat]; 5 August 1911; A. Winneguth leg. Including two slides: one with telopods, second one with leg pairs 16–18 and right leg 13 or 14. Lectotype here designated.

Paralectotypes. ● 2 females (NHMW MY10425); same data as for lectotype; ● 1 female (NHMW MY3902); Albania, Kanina [= Kaninë]; November 1908; A. Winneguth leg.

Other material examined. Albania: ● 1 male, 1 female (NHMW MY10412); Valona [= Vlorë]; Dr. K. Patsch leg.; ● 5 males, 2 females (IZB); Gjirocastro [= Gjirokastër]; 10 May, 1973; M. Karaman leg. ● 1 male, 2 females (ZFMK MYR13662); Gjirokastër District, Vjosa Valley, Përmet, Strëmbec, hiking trail Ri Soptit Waterfall; forest of low *Carpinus*, *Quercus*, *Platanus* and *Crataegus*, in leaf litter, 40.1488, 20.4543; 6 October 2023; H. Reip leg. Serbia: ● 1 male (IZB), slide with a male telopods and leg pairs 17 and 18; Visoki Dečani, Kosovo and Metohija; 1973; M. Karaman leg.

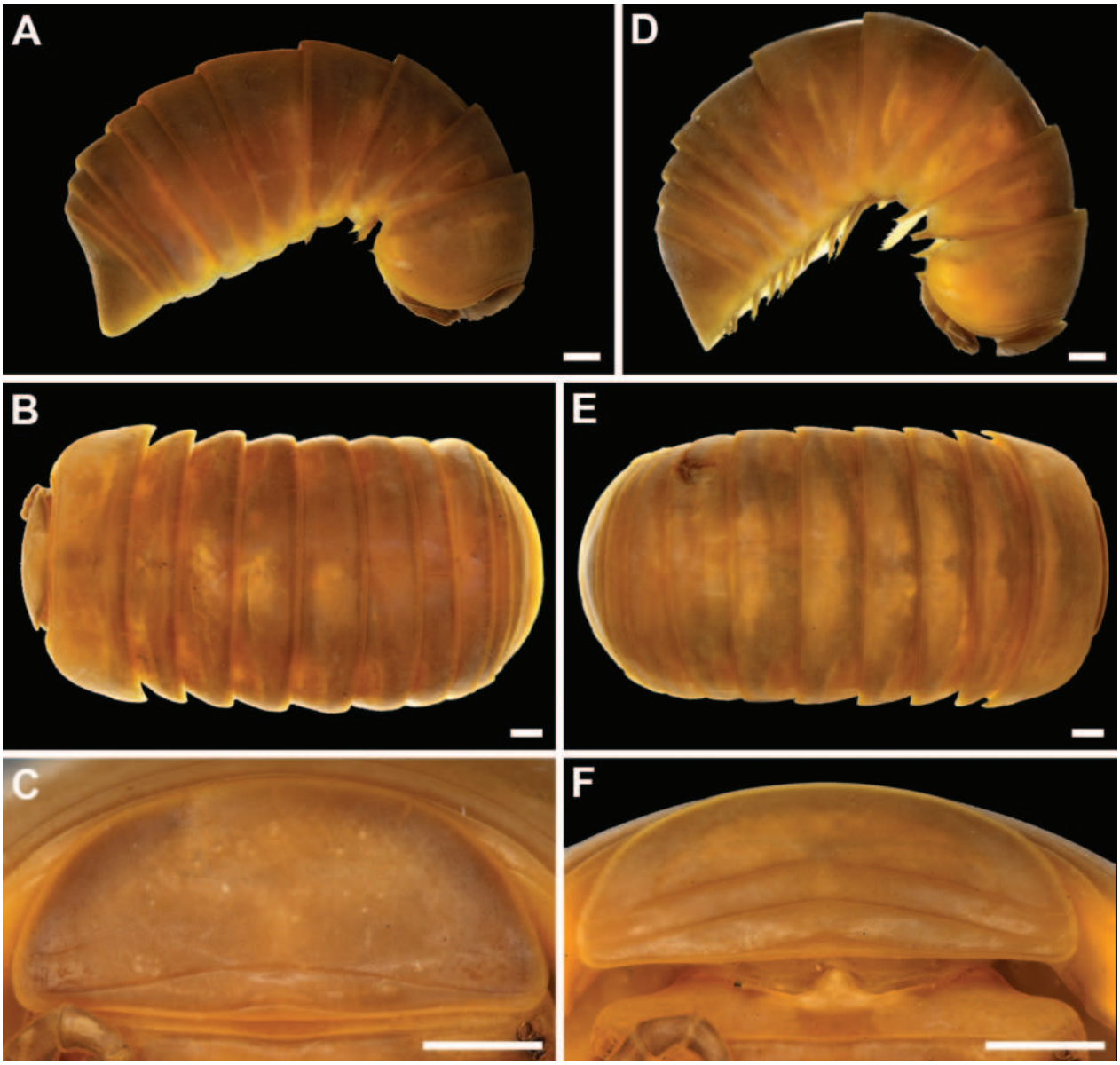

Figure 10. *Onychoglomeris media* Attems, 1935, stat. nov., lectotype male (**A–C**, NHMW MY3901) and paralectotype female (**D–F**, NHMW MY10425). **A, D.** Habitus, lateral views; **B, E.** Habitus, dorsal views; **C, F.** Collum, anterior and anterodorsal views respectively. Scale bars: 1 mm.

Remarks. As written above, one of the differences between *O. media* stat. nov. and *O. australis* stat. nov. is a much smaller tooth of telopoditomere 3 (= tibia) of the telopods in *O. media* stat. nov. In all males we had, this tooth is poorly developed and sometimes almost absent (Fig. 11D–F, white arrows). This structure was probably overlooked by Mauriès et al. (1997). It is interesting to note that, at the base of the strongly-developed posteromesal process of telopoditomere 2 (= femur), one or more brownish darker stripes were observed in all males available to us (Fig. 11A, C, E, black arrows). Such stripes are absent from all males of *O. australis* stat. nov. at hand. In comparison with *O. australis* stat. nov., podomere 2 of leg pair 18 is longer and has a convex mesal margin that looks somewhat like a blade (Fig. 11B, G). The medial syncoxital lobe of leg pair 18 may be present or absent as in *O. australis* stat. nov. (Fig. 11B, G; see also Mauriès et al. (1997: 259, fig. 2B, F)). All males at our disposal have a distinctly concave anal shield (Fig. 10A). In contrast to Mauriès et al. (1997), who found consistency in Albanian specimens with regard to the presence of only one transverse ridge on the collum, we found it variable as in *O. australis* stat. nov. with one or two complete ridges, sometimes a second only as lateral remains (Fig. 10C, F).

It is of interest to mention a very isolated find in southern Serbia, near Visoki Dečani. This site is almost 250 km by air from the nearest site in the core area of southern Albanian sites (Fig. 13). In the IZB collection, only the microslide with the telopods and the leg pairs 17 and 18 have been found so far and both the telopods and the leg pair 18 fit into the concept of *O. media* stat. nov. Whether it was a mistake

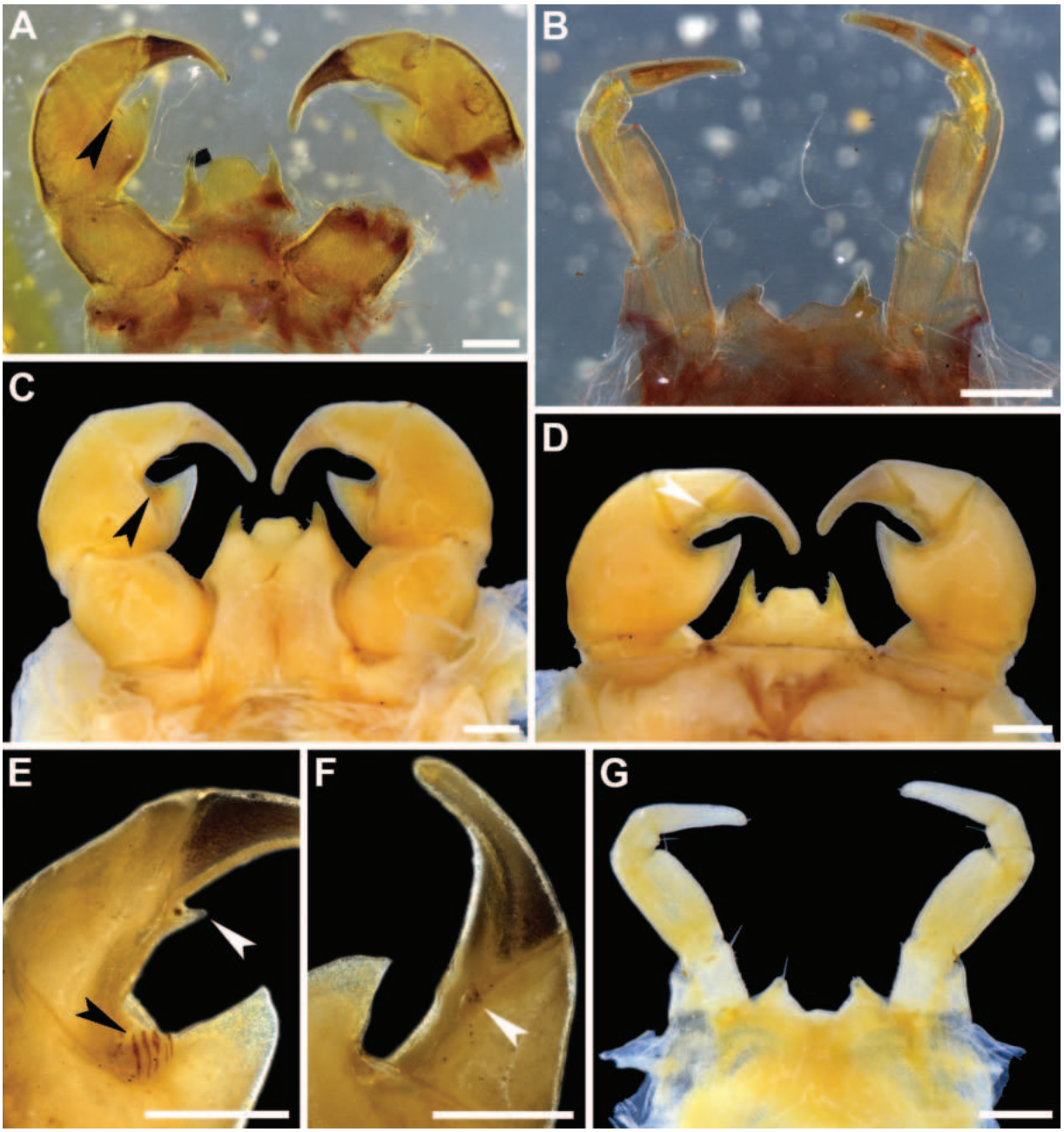

Figure 11. *Onychoglomeris media* Attems, 1935, stat. nov. **A.** Lectotype male **(**NHMW MY3901), telopods, anterior view; **B.** Lectotype male **(**NHMW MY3901), leg pair 18, anterior view; **C.** Male from Vlorë, Albania (NHMW MY10412), telopods, anterior view; **D.** Male from Vlorë, Albania (NHMW MY10412), telopods, posterior view; **E.** Male from Gjirokastër, Albania (IZB), part of the left telopod, anterior view; **F.** Male from Gjirokastër, Albania (IZB), part of the left telopod, posterior view; **G.** Male from Vlorë, Albania (NHMW MY10412), leg pair 18, anterior view. White arrows indicate posterior tooth on telopoditomere 3, black arrows indicate characteristic brownish stripes of telopoditomere 2. Scale bars: 0.5 mm.

in labelling or the species is really so widespread must be clarified in the future. The latter is supported by the fact that Sekulić and Živić (2017) recorded the occurrence of *Glomeris marginata* in southern Serbia (Znosek, Leposavić), about 80 km north-east of Visoki Dečani. It is obvious that this is not *G. marginata*, but it remains questionable which species Sekulić and Živić (2017) actually found. For the purposes of this paper, we will refer to these two Serbian records as *O. media* stat. nov. with a question mark.

Habitat. There is no information about the habitat of this species in the literature, except that Mauriès et al. (1997) mentioned that specimens were found under stones and in leaf litter. Considering the distribution of the species, the habitat should be considered the same as for *G. herzogowinensis* and *O. australis* stat. nov. According to new data, it can be found in *Carpinus*, *Quercus*, *Platanus* and *Crataegus* forest, in leaf litter.

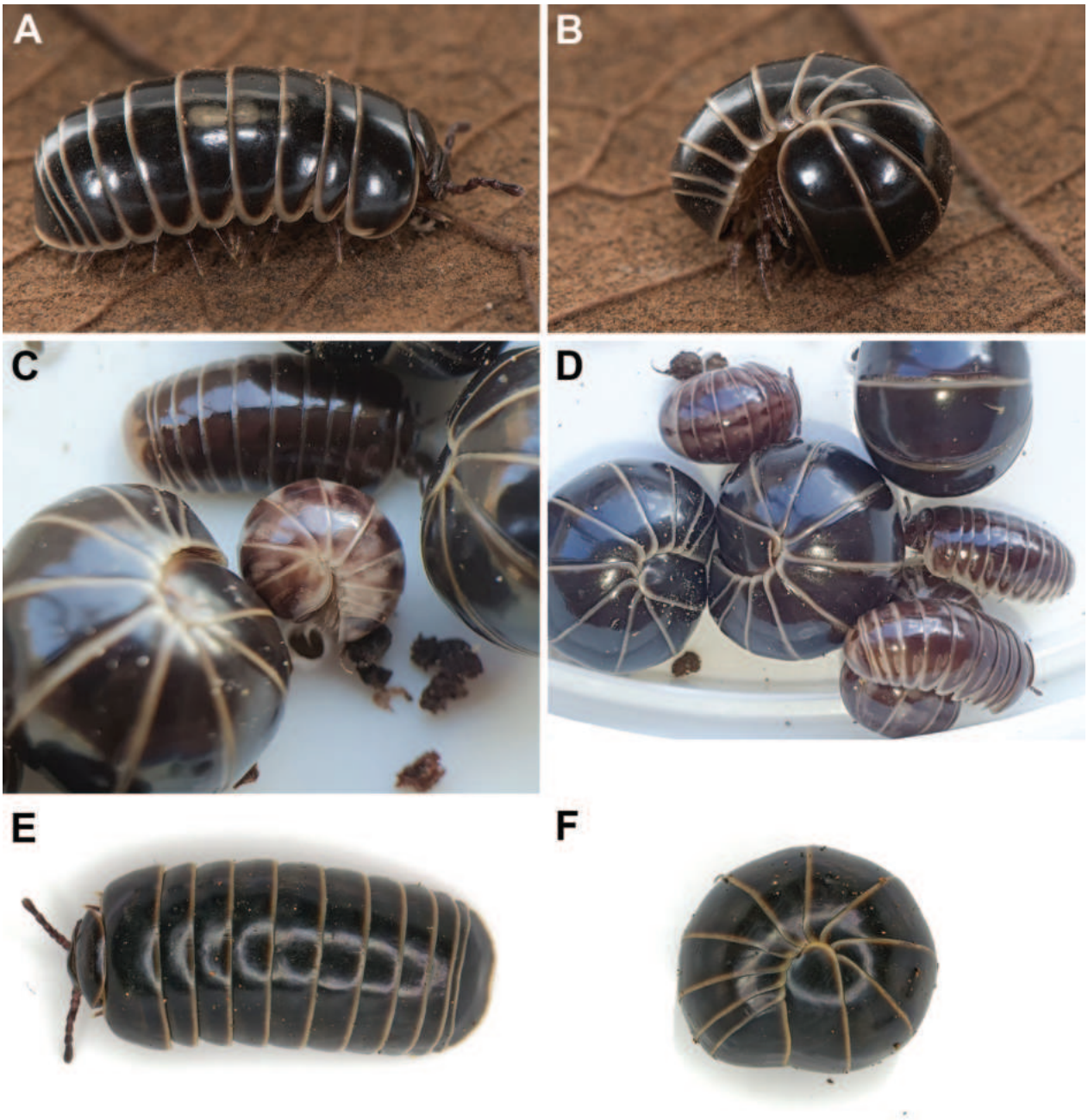

Figure 12. Living specimens. **A–D.** *Onychoglomeris australis* Attems, 1935, stat. nov., specimens from Kalambaka, Greece. **E–F.** *Onychoglomeris media* Attems, 1935, stat. nov., specimens from Përmet, Albania. Photos by Morris Fleck (**A, B**), Peter Kautt (**C, D**) and Hans Reip (**E, F**).

Distribution. Southern Albanian species with a single, isolated locality in southern Serbia (Fig. 13). Albania: Dukat (Attems 1935; Mauriès et al. 1997), Kaninë (Attems 1935); Vlorë (Verhoeff 1901 [missidentification]; Attems 1929 [missidentification], 1935); Dhërmi (Mauriès et al. 1997), Himarë (Mauriès et al. 1997), Llogara Pass (Mauriès et al. 1997), Gjirokastër (Mauriès et al. 1997; present study), Përmet (present study). Serbia: Visoki Dečani (Ćurčić et al. 1999), ?Leposavić (Sekulić and Živić 2017 [missidentification]).

Type locality. Dukat, Vlorë County, southern Albania.

Discussion

Our DNA barcoding analysis clearly confirms the results of the morphological analysis of the telopods: *Glomeris herzogowinensis* groups with other *Glomeris* species and not with *Onychoglomeris*, while *O. australis* stat. nov. clearly groups with *Onychoglomeris*. Interestingly, the sister species to *G. herzogowinensis* seems to be *G. maerens* from Spain, a similarly-coloured species living in a similar Mediterranean habitat. However, there are indications that more than one species is currently hiding

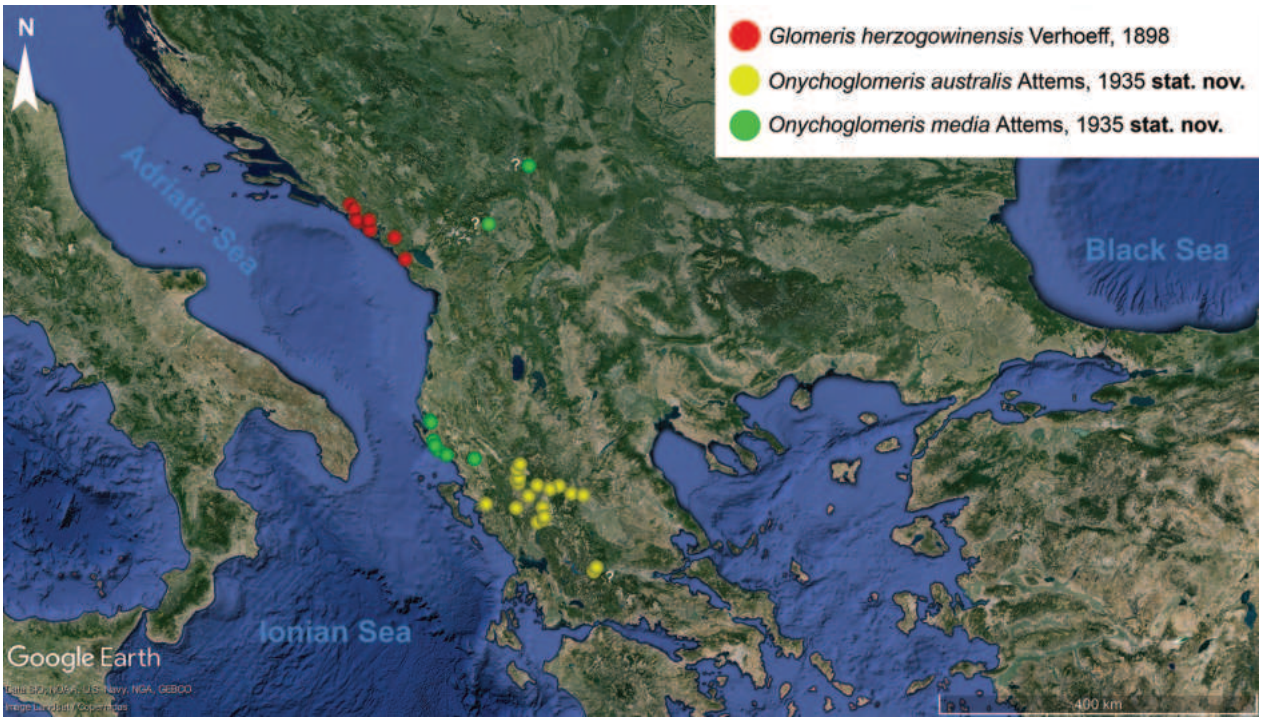

Figure 13. Distribution map of *Glomeris herzogowinensis* Verhoeff, 1898, *Onychoglomeris australis* Attems, 1935, stat. nov. and *Onychoglomeris media* Attems, 1935, stat. nov.

under the name *G. maerens* (Reip and Wesener 2018). The observed genetic distances of the COI barcoding gene between *G. herzogowinensis* and other *Glomeris* species, as well as those between *O. australis* stat. nov. and other *Onychoglomeris*, are with 11–16% similarity to interspecific distances found in other barcoding studies of species of the family Glomeridae (Wesener and Conrad 2016; Kuroda et al. 2022; Recuero and Caterino 2023), but lower than those observed in the diverse genus *Trachysphaera* Heller, 1858 (Wilbrandt et al. 2015). The interspecific distances observed here fit well within the range observed in millipedes from other taxonomic groups and other geographic areas, such as the related (Oeyen and Wesener 2018) giant pill-millipedes (order Sphaerotheriida) from Madagascar (Wesener et al. 2014; Wesener and Sagorny 2021) and southeast Asia (Wesener 2019; Bhansali and Wesener 2022) or in Spirobolida from Madagascar (Wesener et al. 2011; Wesener 2020) and Thailand (Pimvichai et al. 2020, 2022).

This work represents another example demonstrating the importance of natural history collections as a timeless resource allowing us to study organisms and their systematics, sometimes even discover and describe completely unknown taxa, awaiting on shelves of museums to be determined, described and documented. The average shelf-life of all kinds of species of living organisms was estimated to be around 20.7 years (see Fontaine et al. (2012)) with extreme cases exceeding 100 years like *Pleonopurus tanzanicus* Enghoff & Akkari, 2022 and reaching as high as 149 years such as *Ommatoiulus schubarti* Akkari & Enghoff, 2012 (Akkari and Enghoff 2012; Enghoff and Akkari 2022). In other cases, taxa have inadevertedly been mixed with other hitherto described species, therefore remaining hidden for decades. One of the latest examples is perhaps that of *Lophostreptus neglectus* Enghoff & Akkari, 2024 discovered amongst the syntypes of its congener *Lophostreptus regularis* Attems, 1909 in two different collections in Sweden and Vienna and described more than a century after it was originally collected (Enghoff and Akkari 2024). The scientific collections, especially type series and historical specimens, are most defintely an invaluable source of information for taxonomists to update information, unravel the identity of obscure historical names (e.g. Akkari et al. (2010); Akkari (2013); Antić and Akkari (2020); Antić et al. (2021)), clarify the taxonomic status of taxa and solve complicated riddles like the one presented in this work. Morphology-based taxonomy remains a subjective exercise, especially when the studied groups did not traditionally have well-defined characters for species characterisation, which is the case for the order Glomerida. Taxonomy is also very prone to human error and this has been illustrated in numerous cases, especially in times when a tremendeous amount of taxa had to be described by a generation of taxonomists who did not enjoy the same advantages of communication means and technological facilities, not the least microscopy. Amending these mistakes and updating the nomenclature of taxa, adding pieces of knowledge on their genetic information remains an ongoing process that make us acknowledge the colossal work accomplished by myriapod experts like Attems and Verhoeff, but also humble us once we also think towards the future and what could be achieved in perhaps less time given the same resources and further technological progress.

In this article, we tried to solve the case of three species that have been hidden under the same name. *Glomeris herzogowinensis* was confirmed as an unquestionably good taxon. We have raised the other two taxa of the genus *Onychoglomeris*, former subspecies, to species level. Considering the fact that we have no genetic data for *O. media* stat. nov. and that both *O. media* stat. nov. and *O. australis* stat. nov. very likely occur sympatrically at least in the Vjosa (in Albanian) or Aoos (in Greek) river valley in southern Albania and north-western Greece, respectively, some might disagree with such an act. In this context, and due to some morphological differences that obviously exist, we believe that the Albanian and Greek populations should be treated as separate species for the time being.

Acknowledgements

We are gratefull to Stefan Friedrich (ZSM) and Jason Dunlop (ZMB) for making the material under their care available to us for study. Oliver Macek (NHMW) kindly provided technical support handling the specimens and useful comments on the molecular part. Many thanks to the collectors Axel Schönhofer, Siegfried Huber, Hans Reip, Peter Kautt (all from Germany), R. Ozimec (Croatia) and I. Karaman (Serbia) for kindly providing specimens. In addition, Hans Reip, Peter Kautt and Morris Fleck (ZFMK) contributed beautiful photos (Fig. 12) of living *Onychoglomeris australis* Attems, 1935 stat. nov. and *O. media* Attems, 1935 stat. nov. Claudia Etzbauer and Jana Thormann extracted and sequenced the barcoding data at the ZFMK, for which we are very grateful. Last but not least, we would like to thank the reviewers Sergei Golovatch (Russia), Henrik Enghoff (Denmark) and Nikolaus Szucsich (Austria) for their comments and corrections, which have improved this manuscript. Luiz Felipe Iniesta (Brazil) helped with the editing of this manuscript. DA would like to thank his friends Dalibor Stojanović (Serbia), Ivo Karaman (Serbia) and Marjan Komnenov (North Macedonia) for the wonderful time during the field trips in Bosnia and Herzegovina. DA's field research was partly financed by the Serbian Ministry of Science, Technological Development and Innovation (grant no. 451-03-65/2024-03/ 200178). DA's visit to the NHMW in December 2023 was funded by the Synthesys + project AT-TAF.

References

Akkari N (2013) On the identity of *Julus rimosus* Karsch, 1881 (Diplopoda, Julida, Julidae), the only schizophylline known from Libya (North Africa) and notes on Libyan millipedes. Zootaxa 3652(3): 392–396. https://doi.org/10.11646/zootaxa.3652.3.7

Akkari N, Enghoff H (2012) Review of the genus *Ommatoiulus* in Andalusia, Spain (Diplopoda: Julida) with description of ten new species and notes on a remarkable gonopod structure, the fovea. Zootaxa 3538(1): 1–53. https://doi.org/10.11646/zootaxa.3538.1.1

Akkari N, Enghoff H, Stoev P, Mauriès J-P (2010) On the identity of *Basigona lucasii* Silvestri, 1896, a poorly known millipede from Tunisia, with notes on the North African Chordeumatida (Diplopoda: Chordeumatida: Chamaesomatidae). Zootaxa 2427(1): 64–68. https://doi.org/10.11646/zootaxa.2427.1.7

Altschul SF, Madden TL, Schäffer AA, Zhang J, Miller W, Lipman DJ (1997) Gapped BLAST and PSI-BLAST: A new generation of protein database search programs. Nucleic Acids Research 25(17): 3389–3402. https://doi.org/10.1093/nar/25.17.3389

Antić D, Akkari N (2020) *Haasea* Verhoeff, 1895—a genus of tumultuous history and chaotic records—redefinition, revision of taxonomy and geographic distributions, with descriptions of two new species from Austria and Serbia (Diplopoda, Chordeumatida, Haaseidae). Zootaxa 4798(1): 001–077. https://doi.org/10.11646/zootaxa.4798.1.1

Antić D, Šević M, Macek O, Akkari N (2021) Review of *Trachysphaera* Heller, 1858 (Diplopoda: Glomerida: Glomeridae) in Serbia, with taxonomic notes on the genus. Zootaxa 5047(3): 273–299. https://doi.org/10.11646/zootaxa.5047.3.3

Astrin JJ, Stüben PE (2008) Phylogeny in cryptic weevils: molecules morphology and new genera of western Palaearctic Cryptorhynchinae (Coleoptera: Curculionidae). Invertebrate Systematics 22(5): 503–522. https://doi.org/10.1071/IS07057

Attems C (1929) Die Myriopodenfauna von Albanien und Jugoslavien. Zoologische Jahrbucher. Abteilung fur Systematik, Ökologie und Geographie der Tiere 56: 269–356.

Attems C (1935) Myriopoden vom Epirus. Zoologischer Anzeiger 110(5–6): 141–153.

Attems C (1959) Die Myriopoden der Höhlen der Balkanhalbinsel. Nach dem Material der "Biospeologica balcanica". Annalen des Naturhistorischen Museums in Wien 63: 281–406.

Bhansali S, Wesener T (2022) New Thai giant pill-millipede species, with new genetic barcoding data (Diplopoda, Sphaerotheriida, Zephroniidae). Zootaxa 5105(3): 357–380. https://doi.org/10.11646/zootaxa.5105.3.2

Ceuca T (1990) Diplopoden aus Jugoslavien (Kroatien) gesammelt von Dr. Dragutin Rucner. Studia Universitatis Babes-Bolyai 35(1): 10–14.

Ćurčić BPM, Makarov SE, Karaman IM, Dimitrijević RN, Ćurčić SB (1999) Some comments on the diplopods (Diplopoda, Myriapoda) from Yugoslavia. Part 1 - Glomerida. Archives of Biological Sciences 51(1): 11–12.

Enghoff H, Akkari N (2022) A new species of the hitherto monospecific genus *Pleonoporus* Attems, 1938 (Diplopoda, Spirostreptida, Odontopygidae). ZooKeys 1117(1–2): 189–202. https://doi.org/10.3897/zookeys.1117.87765

Enghoff H, Akkari N (2024) A new species of *Lophostreptus* Cook, 1895 discovered among syntypes of *L. regularis* Attems, 1909 (Diplopoda, Spirostreptida, Spirostreptidae). ZooKeys 1188: 265–274. https://doi.org/10.3897/zookeys.1188.115802

Enghoff H, Golovatch S, Short M, Stoev P, Wesener T (2015) Diplopoda – Taxonomic overview. In 'The Myriapoda 2. Treatise on Zoology – Anatomy, Taxonomy, Biology'. (Ed. A. Minelli.), 363–453. [Brill: Leiden.] https://doi.org/10.1163/9789004188273_017

Felsenstein J (1985) Confidence Limits on Phylogenies: An Approach Using the Bootstrap. Evolution; International Journal of Organic Evolution 39(4): 783–791. https://doi.org/10.2307/2408678

Fontaine B, Perrard A, Bouchet P (2012) 21 years of shelf life between discovery and description of new species. Current Biology 22(22): R943–R944. https://doi.org/10.1016/j.cub.2012.10.029

Golovatch SI, Mauriès J-P, Akkari N, Stoev PE, Geoffroy J-J (2009) The millipede genus *Glomeris* Latreille, 1802 (Diplopoda, Glomerida, Glomeridae) in North Africa. ZooKeys 12: 47–86. https://doi.org/10.3897/zookeys.12.179

Hall T (1999) BioEdit: A user-friendly biological sequence alignment editor and analysis program for Windows 95/98/NT. Nucleic Acids Symposium Series 41: 95–98.

Hebert PDN, Cywinska A, Ball S, deWaard JR (2003) Biological identifications through DNA barcodes. Proceedings. Biological Sciences 270(1512): 313–321. https://doi.org/10.1098/rspb.2002.2218

Hoess R (2000) Bestimmungsschlüssel für die *Glomeris*-Arten Mitteleuropas und angrenzender Gebiete (Diplopoda: Glomeridae). Jahrbuch des Naturhistorischen Museums Bern 13: 3–20.

Hoess R, Scholl A (1999a) *Glomeris undulata* Koch and *Glomeris conspersa* Koch are conspecific. Enzyme electrophoretic evidence and taxonomical consequences (Diplopoda: Glomeridae). Revue Suisse de Zoologie 106(3): 643–661. https://doi.org/10.5962/bhl.part.80100

Hoess R, Scholl A (1999b) The identity of *Glomeris quadrifasciata* C. L. Koch (Diplopoda: Glomeridae). Revue Suisse de Zoologie 106(4): 1013–1024. https://doi.org/10.5962/bhl.part.80113

Hoess R, Scholl A (2001) Allozyme and literature study of *Glomeris guttata* Risso, 1826, and *G. connexa* Koch, 1847, a case of taxonomic confusion (Diplopoda: Glomeridae). Zoologischer Anzeiger 240(1): 15–33. https://doi.org/10.1078/0044-5231-00003

Hoess R, Scholl A, Lörtscher M (1997) The *Glomeris*-taxa *hexasticha* and *intermedia*: species or subspecies? Allozyme data (Diplopoda, Glomerida: Glomeridae). Entomologica Scandinavica (Supplementum 51): 133–138.

Kime RD, Enghoff H (2011) Atlas of European millipedes (Class Diplopoda), Vol. 1, orders Polyxenida, Glomerida, Platydesmida, Siphonocryptidae, Polyzoniida, Callipodida, Polydesmida. Fauna Europaea Evertebrata 3, Pensoft, Sofia-Moscow, 282 pp.

Kuroda M, Eguchi K, Oguri E, Nguyen AD (2022) Two new cave *Hyleoglomeris* species (Glomerida, Glomeridae) from northern Vietnam. ZooKeys 1108: 161–174. https://doi.org/10.3897/zookeys.1108.85423

Mauriès J-P, Golovatch SI, Stoev PE (1997) The millipedes of Albania: Recent data, new taxa; systematical, nomenclatural and faunistical review (Myriapoda, Diplopoda). Zoosystema 19(2–3): 255–292.

Nei M, Kumar S (2000) Molecular Evolution and Phylogenetics. Oxford University Press, New York, 352 pp. https://doi.org/10.1093/oso/9780195135848.001.0001

Oeyen JP, Wesener T (2015) Steps towards a phylogeny of the pill millipedes: Non-monophyly of the family Protoglomeridae, with an integrative redescription of *Eupeyerimhoffia archimedis* (Diplopoda, Glomerida). ZooKeys 510: 49–64. https://doi.org/10.3897/zookeys.510.8675

Oeyen JP, Wesener T (2018) A first phylogenetic analysis of the pill millipedes of the order Glomerida, with a special assessment of mandible characters (Myriapoda, Diplopoda, Pentazonia). Arthropod Structure & Development 47(2): 214–228. https://doi.org/10.1016/j.asd.2018.02.005

Pimvichai P, Enghoff H, Panha S, Backeljau T (2020) Integrative taxonomy of the new millipede genus *Coxobolellus*, gen. nov. (Diplopoda: Spirobolida: Pseudospirobolellidae), with descriptions of ten new species. Invertebrate Systematics 34(6): 591–617. https://doi.org/10.1071/IS20031

Pimvichai P, Panha S, Backeljau T (2022) Combining mitochondrial DNA and morphological data to delineate four new millipede species and provisional assignment to the genus *Apeuthes* Hoffman & Keeton (Diplopoda: Spirobolida: Pachybolidae: Trigoniulinae). Invertebrate Systematics 36(2): 91–112. https://doi.org/10.1071/IS21038

Recuero E, Caterino MS (2023) A second species of the pill millipede genus *Nearctomeris* Wesener, 2012 (Diplopoda, Glomerida) from the Great Smoky Mountains, USA. ZooKeys 1166: 33–349. https://doi.org/10.3897/zookeys.1166.103516

Reip HS, Wesener T (2018) Intraspecific variation and phylogeography of the millipede model organism, the Black Pill Millipede *Glomeris marginata* (Villers, 1789) (Diplopoda, Glomerida, Glomeridae). In: Stoev, P. and Edgecombe, G.D. (Eds.), Proceedings of the 17th International Congress of Myriapodology, Krabi, Thailand. ZooKeys 741: 93–131. https://doi.org/10.3897/zookeys.741.21917

Sagorny C, Wesener T (2017) Two new giant pill-millipede species of the genus *Zoosphaerium* endemic to the Bemanevika area in northern Madagascar (Diplopoda, Sphaerotheriida, Arthrosphaeridae). Zootaxa 4263(2): 273–294. https://doi.org/10.11646/zootaxa.4263.2.4

Schubart O (1934) Tausendfüßler oder Myriapoda. In: Die Tierwelt Deutschlands und der angrenzenden Meeresteile nach ihren Merkmalen und nach ihrer Lebensweise „28“. Gustav Fischer Verlag, Jena, 318 pp.

Sekulić SLj, Živić NV (2017) Fauna stonoga (Myriapoda) okoline Leposavića (Srbija). Zbornik radova učiteljskog fakulteta 11: 191–199. https://doi.org/10.5937/zrufpl1711191S

Strasser K (1971) Catalogus Faunae jugoslaviae. III/5. Diplopoda. Academia Scientarum et Artium Slovenica, Ljubljana, 48 pp.

Strasser K (1976) Über Diplopoda-Chilognatha Griechenlands, II. Revue Suisse de Zoologie 83(3): 579–645. https://doi.org/10.5962/bhl.part.91453

Tamura K, Nei M (1993) Estimation of the number of nucleotide substitutions in the control region of mitochondrial DNA in humans and chimpanzees. Molecular Biology and Evolution 10: 512–526.

Tamura K, Stecher G, Kumar S (2021) MEGA 11: Molecular Genetics Analysis Version 11. Molecular Biology and Evolution 28(7): 3022–3027. https://doi.org/10.1093/molbev/msab120

Tavaré S (1986) Some probabilistic and statistical problems in the analysis of DNA sequences. Lectures on Mathematics in the Life Sciences 17: 57–86.

Thaler K (1999) Über Kugeltausendfüsser aus Griechenland und Zypern (Diplopoda, Glomerida). Entomologische Nachrichten und Berichte 43(3–4): 195–201.

Verhoeff KW (1898) Über Diplopoden aus Bosnien, Herzegowina und Dalmatien. V. Theil: Glomeridae und Polyzoniidae (Schluss). Archiv für Naturgeschichte 64(1): 161–176. https://doi.org/10.5962/bhl.part.6891

Verhoeff KW (1901) Beiträge zur Kenntniss paläarktischer Myriopoden. XX. Aufsatz: Diplopoden des östlichen Mittelmeergebietes. Archiv für Naturgeschichte 67(1): 241–270. https://doi.org/10.5962/bhl.part.7278

Verhoeff KW (1906) Über Diplopoden. 4. (24.) Aufsatz: Zur Kenntnis der Glomeriden (zugleich Vorläufer einer Glomeris-Monographie) (Beiträge zur Systematik, Geographie, Entwickelung, vergleichenden Morphologie und Biologie). Archiv für Naturgeschichte 72(1): 107–226.

Verhoeff KW (1911) Ueber Diplopoden. 20. (40.) Aufsatz: Neuer Beitrag zur Kenntnis der Gattung Glomeris. Jahreshefte des Vereins für Vaterländische Naturkunde in Württemberg 67: 78–147.

Wesener T (2015a) No millipede endemics north of the Alps? DNA-Barcoding reveals *Glomeris malmivaga* Verhoeff, 1912 as a synonym of *G. ornata* Koch, 1847 (Diplopoda, Glomerida, Glomeridae). Zootaxa 3999(4): 571–580. https://doi.org/10.11646/zootaxa.3999.4.7

Wesener T (2015b) Integrative redescription of a forgotten Italian pill millipede endemic to the Apuan Alps—*Glomeris apuana* Verhoeff, 1911 (Diplopoda, Glomerida, Glomeridae). Zootaxa 4039(2): 391–400. https://doi.org/10.11646/zootaxa.4039.2.11

Wesener T (2018) An Integrative and Citizen Science based Approach to the Rediscovery and Redescription of the only known High-Altitude Endemic Pill Millipede, *Glomeris aurita* Koch (Diplopoda, Glomerida). PeerJ 6: e5569. https://doi.org/10.7717/peerj.5569

Wesener T (2019) First records of giant pill-millipedes from Laos (Diplopoda, Sphaerotheriida, Zephroniidae). Zootaxa 4563(2): 201–248. https://doi.org/10.11646/zootaxa.4563.2.1

Wesener T (2020) Ecotone shifts in southern Madagascar: First barcoding data and six new species of the endemic millipede genus *Riotintobolus* (Spirobolida, Pachybolidae). ZooKeys 953: 1–29. https://doi.org/10.3897/zookeys.953.53977

Wesener T, Conrad C (2016) Local Hotspots of Endemism or Artifacts of Incorrect Taxonomy? The Status of Microendemic Pill Millipede Species of the Genus *Glomeris* in Northern Italy (Diplopoda, Glomerida). PLoS ONE 11(9): e0162284. https://doi.org/10.1371/journal.pone.0162284

Wesener T, Sagorny CL (2021) Seven new giant pill-millipede species and numerous new records of the genus *Zoosphaerium* from Madagascar (Diplopoda, Sphaerotheriida, Arthrosphaeridae). European Journal of Taxonomy 758: 1–48. https://doi.org/10.5852/ejt.2021.758.1423

Wesener T, Raupach MJ, Decker P (2011) Mountain Refugia Play A Role In Soil Arthropod Speciation On Madagascar. A Case Study Of The Endemic Giant Fire-Millipede Genus *Aphistogoniulus* (Diplopoda, Spirobolida, Pachybolidae). PLoS ONE 6(12): 1–15. https://doi.org/10.1371/journal.pone.0028035

Wesener T, Le DM-T, Loria SF (2014) Integrative revision of the giant pill-millipede genus *Sphaeromimus* from Madagascar, with the description of seven new species (Diplopoda, Sphaerotheriida, Arthrosphaeridae). ZooKeys 414: 67–107. https://doi.org/10.3897/zookeys.414.7730

Wilbrandt J, Lee P, Read H, Wesener T (2015) A first integrative study of the identity and origins of the British Dwarf Pill Millipede populations, *Trachysphaera* cf. *lobata* (Diplopoda, Glomerida, Glomeridae). Biodiversity Data Journal 3: e5176. https://doi.org/10.3897/BDJ.3.e5176

Supplementary material 1

Number of base differences per site (*p*-distances) between sequences

Authors: Dragan Antić, Thomas Wesener, Nesrine Akkari

Data type: xls

Link: https://doi.org/10.3897/zse.100.122288.suppl1

Zoosyst. Evol. 100 (2) 2024, 515–529 | DOI 10.3897/zse.100.119520

PENSOFT

MUSEUM FÜR NATURKUNDE BERLIN

Description of a new troglobitic *Sinocyclocheilus* (Pisces, Cyprinidae) species from the upper Yangtze River Basin in Guizhou, South China

Wei-Han Shao[1], Guang-Yuan Cheng[2], Xiao-Long Lu[3], Jia-Jun Zhou[4,5], Zhi-Xuan Zeng[6]

1 *Institute of Hydrobiology, Chinese Academy of Sciences, Wuhan, China*
2 *Guiyang Bureau of Ecology and Environment, Guiyang, China*
3 *Guiyang Qianren Ecological Conservation Center, Guiyang, China*
4 *Zhejiang Forest Resource Monitoring Center, Hangzhou, China*
5 *Zhejiang Forestry Survey Planning and Design Company Limited, Hangzhou, China*
6 *The Department of Endocrinology, Branch of National Clinical Research Center for Metabolic Diseases, Tongji Hospital, Huazhong University of Science and Technology, Wuhan, China*

https://zoobank.org/5B410772-DA79-437F-8ABB-A047B4FDC604

Corresponding authors: Zhi-Xuan Zeng (985801524@qq.com); Jia-Jun Zhou (cnwaters@foxmail.com)

Academic editor: Nicolas Hubert ♦ **Received** 29 January 2024 ♦ **Accepted** 28 March 2024 ♦ **Published** 14 May 2024

Abstract

Sinocyclocheilus guiyang, a new troglobitic species from a subterranean tributary of the upper Yangtze Basin in Guiyang City, Guizhou Province, China is described in the present study. The new species is distinguishable from its congeneric species by a combination of the following characters: tip of maxillary barbel reaching to posterior edge of orbit; forehead horn absent; eye absent (or highly reduced) and tip of pectoral fins not significantly extending beyond the base of the pelvic fin. Molecular evidence, based on the mitochondrial cytochrome *b* (cyt*b*) gene, further supports the validity of the species and also reveals its close relationship with *S. cyphotergous*, *S. multipunctatus*, *S. punctatus* and *S. sanxiaensis*. In addition, the new species faces a high risk of extinction, underscoring the urgency for habitat protection measures within its limited range.

Key Words

cavefish, conservation, morphology, phylogenetic analysis, Yangtze River

Introduction

Sinocyclocheilus Fang, 1936 (golden-line barbel), endemic to south China, is one of the most diversified genera in the family Cyprinidae, consisting of more than seventy species (Jiang et al. 2019; Mao et al. 2022; Xu et al. 2023; Luo et al. 2024). Highly-developed subterranean river systems in this region are a major contributor to its remarkable diversity because *Sinocyclocheilus* is restricted to subterranean river systems and adjacent regions (Ma et al. 2019). To date, sixty-six *Sinocyclocheilus* species are endemic to the Pearl River Basin, with only six species (*S. grahami* Regan, 1904, *S. wumengshanensis* Li, Mao & Lu, 2003, *S. huizeensis* Cheng, Pan, Chen, Li, Ma & Yang, 2015, *S. wui* Li & Li, 2013, *S. sanxiaensis* Jiang, Li, Yang & Chang, 2019 and *S. multipunctatus* Pellegrin, 1931) occurring in the Yangtze River Basin (Eschmeyer et al. 2024). In addition, three of them (*S. grahami*, *S. wumengshanensis* and *S. huizeensis*) are restricted to Yunnan Province which belongs to the Jinshajiang River (a section of the mainstream of upper Yangtze River) System. Only one species, *S. multipunctatus*, is found in the Wujiang River System, a major southern tributary of the upper Yangtze River in Guizhou Province.

However, similar to the Pearl River Basin, the Wujiang River System also exhibits extensive and well-developed

karst landforms (Che and Yu 1985), which has provided good conditions for the formation of subterranean river systems and the subsequent evolution of troglobitic fishes. This can be seen in the high diversity of the hypogean *Triplophysa* which has five described species within this river system (Liu et al. 2022). Moreover, a recent breakthrough study reported *S. sanxiaensis* from the Three Gorges Reservoir which belongs to the mainstream of the upper Yangtze River Basin in west Hubei Province. Molecular phylogenetic analysis has grouped *S. sanxiaensis* with *S. cyphotergous* Dai, 1988, *S. multipunctatus* and *S. punctatus* Lan & Yang, 2017 (Jiang et al. 2019). The *S. cyphotergous – S. multipunctatus* group, herein defined for the abovementioned four species, is characterised by a typically convex dorsal profile, short barbels and high head depth. For a long time, members of this species group were only mainly known from Hongshui River (a section of the mainstream of the Pearl River) System and Liujiang River (north tributary of the Pearl River) System, with only *S. multipunctatus* spanning from Hongshui River to Wujiang River (Wu 1989; Zhao and Zhang 2009). The description of *S. sanxiaensis* greatly expanded the distribution boundary of this species group, providing insights into the potentially underestimated diversity of *Sinocyclocheilus* in the Wujiang River System, situated between the Three Gorges Reservoir and the Hongshui River.

Various morphological features that are adapted to subterranean environments have been found in troglobitic species of *Sinocyclocheilus* including degenerated eyes, reduced (or lost) pigmentation, degenerated scales, elongated fins and horn-like structures (e.g. humpback and horn) (Zhao and Zhang 2009; Ma et al. 2019). In addition, possession of extended barbels in *Sinocyclocheilus* species is common as the long barbels better detect water flow and aid foraging in subterranean water systems which are marked by permanent darkness and food scarcity (Ma et al. 2019). Fewer than one third (twenty-one) of *Sinocyclocheilus* species have short maxillary barbels that do not extend to the posterior edge of the preoperculum (Zhao and Zhang 2009; Lan et al. 2013; Xu et al. 2023) and more than half possess horn-like structures (e.g. *S. anatirostris* Lin & Luo, 1986, *S. aquihornes* Li & Yang, 2007, *S. cyphotergous*, *S. rhinocerous* Li & Tao, 1994 and *S. longicornus* Luo, Xu, Wu, Zhou & Zhou, 2023). Amongst the currently recognised species of *Sinocyclocheilus*, only two, *S. jinxiensis* Zheng, Xiu & Yang, 2013 and *S. sanxiaensis*, possess a combination of short maxillary barbels, degenerated eyes, reduced pigmentation and lack of horn-like structures. These combined characters are unique within *Sinocyclocheilus* and represent exceptional cases for evolutionary studies.

The authors conducted a fish field survey in a subterranean stream within the Wujiang River System in central Guizhou Province, south China. This survey yielded seven specimens characterised by short maxillary barbels, no horn-like structures and absent or highly reduced eyes, traits shared with *S. jinxiensis* and *S. sanxiaensis*. Careful morphological examination revealed that they are, in fact, not conspecific with any other known species of *Sinocyclocheilus* and, thus, represent an unnamed species. Genetic analyses further revealed that these specimens formed a distinct cluster within the *S. cyphotergous – S. multipunctatus* group. The purpose of the present paper is to provide a formal description of this unnamed species, based on multiple lines of evidence including morphological and molecular datasets.

Material and methods

Specimen sampling and preservation

The treatment of experimental animals in this study was consistent with the Chinese animal welfare laws (GB/T 35892–2018). Specimens were collected from central-south Guizhou and north Guangxi from 2019 to 2023. After anaesthesia, specimens were fixed in 10% formaldehyde and then preserved in 75% ethanol for morphological comparison. The right pelvic fin of some specimens was dissected and fixed in 95% ethanol for DNA extraction. Specimens newly collected for this study have been deposited in the Institute of Hydrobiology, Chinese Academy of Sciences (**IHB**), Guangxi University (**GXU**) and Zhejiang Forest Resource Monitoring Center (**ZJFR**). Other comparative materials have been stored in Kunming Institute of Zoology, Chinese Academy of Sciences (**KIZ**).

Morphological analyses

Measurements were taken point-to-point on the left side of the specimens with a Vernier caliper to a precision of 0.1 mm. All measurements, counts and terminologies follow Zhao et al. (2006), with the following exceptions: maxillary barbel in the present study refers to the barbel rooted at the corner of the mouth and rostral barbel refers to the barbel rooted at the rostrum. The major morphometrics are shown in Fig. 1. All morphometric measurements have been transferred to percentage of standard length (SL) and recorded to the closest 0.1%. The caudal peduncle depth (CPD) to caudal peduncle length (CPL) ratios are calculated and recorded to the closest 0.01. For osteological observation, specimens were scanned by micro-computed tomography (micro-CT) (Siemens Somatom Definition X-ray machine). The 3D renderings of the osteological structure of the whole specimen and pharyngeal dentition were created and visualised in VG Studio Max 2.1 (He et al. 2013). Total vertebrae were counted from the first free vertebra to the last half-centrum.

Morphometric measurements were subject to principal component analysis (PCA) to explore the relative contributions of specific variables to morphological variations. PCA was conducted on the Statistical Package for the Social Sciences (SPSS) 19.0 (IBM, Armonk, NY, USA). Prior to PCA, all included measurements were normalised by log transformation. Linear regression analysis for origin data of each character was also computed on SPSS 19.0.

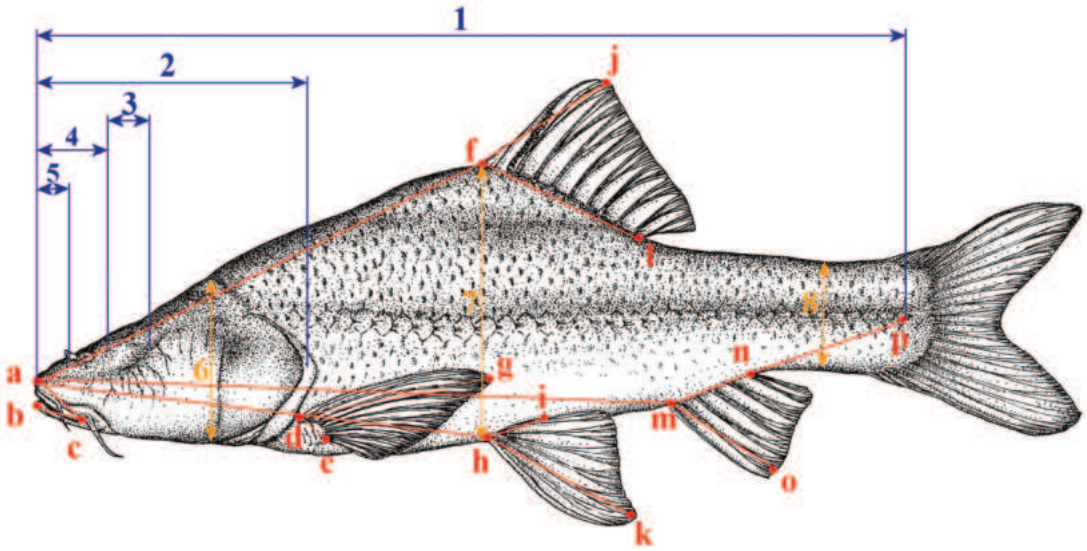

Figure 1. Major morphometrics demonstrated on original drawing of *Sinocyclocheilus guiyang*. standard length (**1**), head length (**2**), eye diameter (**3**), snout length (**4**), pre-nostril length (**5**), head depth (**6**), body depth (**7**), caudal peduncle depth (**8**), upper jaw length (**a–c**), lower jaw length (**b–c**), pre-pectoral length (**a–d**), pre-dorsal length (**a–f**), pre-pelvic length (**a–h**), pre-anal length (**a–m**), pectoral-fin base length (**d–e**), pectoral-fin length (**d–g**), dorsal-fin length (**f–j**), dorsal-fin base length (**f–l**), pelvic-fin base length (**h–i**), pelvic-fin length (**h–k**), anal-fin base length (**m–n**), anal-fin length (**m–o**), caudal peduncle length (**n–p**).

DNA extraction, PCR and sequencing

Genomic DNA was extracted from 95% ethanol-fixed fin tissue using the modified salt-extraction method described by Tang et al. (2008). Fragments containing the mitochondrial cytochrome *b* (cyt*b*) gene were amplified by polymerase chain reaction (PCR) with the primer pairs (L14724 and H15915) (Zhao et al. 2006) in a 30 µl reaction system: 3 µl 10 × PCR buffer, 30–50 ng DNA template, 1 µl primers (each 10 µM), 1.5 µl dNTPs (each 2.5 mM), 2.5 U Taq DNA polymerase and ddH_2O added to reach the final volume. PCR procedures also follow Tang et al. (2008). The PCR products were purified and sequenced in both directions with the corresponding primers by a commercial sequencing company. All newly-generated sequences have been submitted to GenBank.

Molecular data analyses

Phylogenetic analysis was performed, based on nine newly-obtained cyt*b* sequences and an additional 47 sequences downloaded from NCBI GenBank, including 49 *Sinocyclocheilus* species and a single species *Cyprinus carpio* Linnaeus, 1758 as outgroup (Table 1). The sequences were revised manually and then aligned using ClustalW in MEGA7.0 (Kumar et al. 2016). Both Maximum Likelihood (ML) and Bayesian Inference (BI) methods were utilised to reconstruct the phylogenetic relationship. The optimal nucleotide substitution model was selected in ModelFinder (Kalyaanamoorthy et al. 2017) according to Akaike Information Criterion. Maximum Likelihood analysis was run in IQ-TREE 1.6.8 (Nguyen et al. 2015), with the selected TIM3+F+I+G4 model and 1,000 non-parametric bootstrap replicates. Bayesian Inference was performed in MrBayes 3.2.6 (Ronquist et al. 2012) under the selected GTR+F+I+G4 model, using the MCMC method (four chains simultaneously run for 20,000,000 generations) to calculate posterior probability, with tree sampling frequency set to 1 per 1000 cycles and the initial 25% of the sampled data discarded as burn-in. The convergence of BI analysis was reached when the average standard deviation of split frequencies was less than 0.01. Uncorrected pairwise genetic distances (p-distance), based on cyt*b*, were computed in MEGA 7.0.

Results

***Sinocyclocheilus guiyang* sp. nov.**

https://zoobank.org/67337E27-2D91-4C21-B557-AA36ECABDAA1

Fig. 2, Table 2

Type materal. *Holotype*. IHB 202012250001, 124.0 mm SL; China: Guizhou Province: Guiyang City: Qingzhen County: a subterranean stream tributary of the Wujiang System in the upper Yangtze River Basin, 26°50'26"N, 106°16'37"E, 1250 m elevation; Jia-Jun Zhou, Dec 2020.

***Paratypes*.** IHB 201911140001, 1 specimen, 57.5 mm SL; Zhi-Xuan Zeng, Nov 2019; other data same as holotype. IHB 202012250002, 1 specimen, 86.4 mm SL; collected with holotype. IHB 202207260001, GXU 202207260002–04, 4 specimens, 124.3–174.1 mm SL; Jia-Jun Zhou, Jul 2022; other data same as holotype.

Diagnosis. *Sinocyclocheilus guiyang* is distinguishable from all other congeners by a combination of the

Table 1. GenBank accession numbers for molecular phylogenetic analysis. n/a, not available.

Taxon	Voucher specimen	Locality	Accession No.	Source
Sinocyclocheilus sanxiaensis	KIZ 2019000001	Hubei, Yangtze River	MN106258	NCBI
Sinocyclocheilus grahami	XH0701	Yunnan, Yangtze River	AY854694	NCBI
Sinocyclocheilus wumengshanensis	YNUSM20160817008	Yunnan, Yangtze River	MG021442	NCBI
Sinocyclocheilus guiyang 01	IHB 202012250001	Guizhou, Yangtze River	OR141734	This study
Sinocyclocheilus guiyang 02	IHB 202012250002	Guizhou, Yangtze River	OR141735	This study
Sinocyclocheilus guiyang 03	IHB 202207260001	Guizhou, Yangtze River	OR141736	This study
Sinocyclocheilus multipunctatus 01	IHB 202302080001	Guizhou, Yangtze River	OR141737	This study
Sinocyclocheilus multipunctatus 02	n/a	Guizhou, Pearl River	MG026730	NCBI
Sinocyclocheilus cyphotergous 01	IHB 202302080002	Guizhou, Pearl River	OR141738	This study
Sinocyclocheilus cyphotergous 02	IHB 202207280010	Guizhou, Pearl River	OR141739	This study
Sinocyclocheilus punctatus 01	ZJFR 2311001	Guangxi, Pearl River	PP112594	This study
Sinocyclocheilus punctatus 02	ZJFR 2311004	Guizhou, Pearl River	PP112595	This study
Sinocyclocheilus punctatus 03	ZJFR 2312002	Guangxi, Pearl River	PP112596	This study
Sinocyclocheilus punctatus 04	GZNU 20150811002	Guizhou, Pearl River	MK610341	NCBI
Sinocyclocheilus longibarbus	XH2901	Guizhou, Pearl River	AY854714	NCBI
Sinocyclocheilus longicornus	GZNU 20210503016	Guizhou, Pearl River	MZ634123	NCBI
Sinocyclocheilus zhenfengensis	GZNU 20150112021	Guizhou, Pearl River	MK610342	NCBI
Sinocyclocheilus bicornutus	XH8301	Guizhou, Pearl River	AY854730	NCBI
Sinocyclocheilus angularis	GZNU 202001332	Guizhou, Pearl River	MW362289	NCBI
Sinocyclocheilus xingyiensis	GZNU SLS202008180	Guizhou, Pearl River	ON573221	NCBI
Sinocyclocheilus guanyangensis	n/a	Guangxi, Pearl River	OQ718399	NCBI
Sinocyclocheilus lateristriatus	XH1601	Yunnan, Pearl River	AY854707	NCBI
Sinocyclocheilus malacopterus	XH0901	Yunnan, Pearl River	AY854697	NCBI
Sinocyclocheilus angustiporus	XH1203	Yunnan, Pearl River	AY854702	NCBI
Sinocyclocheilus hyalinus	XH4701	Yunnan, Pearl River	AY854721	NCBI
Sinocyclocheilus rhinocerous	XH3901	Yunnan, Pearl River	AY854720	NCBI
Sinocyclocheilus tingi	YNUST 201406180002	Yunnan, Pearl River	MG323567	NCBI
Sinocyclocheilus guishanensis	XH5401	Yunnan, Pearl River	AY854722	NCBI
Sinocyclocheilus maculatus	n/a	Yunnan, Pearl River	MF325010	NCBI
Sinocyclocheilus maitianheensis	XH2301	Yunnan, Pearl River	AY854710	NCBI
Sinocyclocheilus anophthalmus	XH3002	Yunnan, Pearl River	AY854716	NCBI
Sinocyclocheilus qiubeiensis	n/a	Yunnan, Pearl River	MF324998	NCBI
Sinocyclocheilus qujingensis	XH3801	Yunnan, Pearl River	AY854719	NCBI
Sinocyclocheilus purpureus	IHB 2006637	Yunnan, Pearl River	EU366194	NCBI
Sinocyclocheilus lunanensis	XH0302	Yunnan, Pearl River	AY854686	NCBI
Sinocyclocheilus huaningensis	XH3701	Yunnan, Pearl River	AY854718	NCBI
Sinocyclocheilus oxycephalus	XH0201	Yunnan, Pearl River	AY854685	NCBI
Sinocyclocheilus yangzongensis	XH6102	Yunnan, Pearl River	AY854726	NCBI
Sinocyclocheilus macrocephalus	XH0110	Yunnan, Pearl River	AY854684	NCBI
Sinocyclocheilus yishanensis	n/a	Guangxi, Pearl River	MK387704	NCBI
Sinocyclocheilus macrophthalmus	XH8401	Guangxi, Pearl River	AY854733	NCBI
Sinocyclocheilus xunlensis	IHB 04050268	Guangxi, Pearl River	EU366187	NCBI
Sinocyclocheilus lingyunensis	XH0502	Guangxi, Pearl River	AY854691	NCBI
Sinocyclocheilus donglanensis	ASIZB 94746	Guangxi, Pearl River	AB196440	NCBI
Sinocyclocheilus ronganensis	n/a	Guangxi, Pearl River	KX778473	NCBI
Sinocyclocheilus macrolepis	XH8201	Guangxi, Pearl River	AY854729	NCBI
Sinocyclocheilus anatirostris	XH1901	Guangxi, Pearl River	AY854708	NCBI
Sinocyclocheilus anshuiensis	n/a	Guangxi, Pearl River	KR069120	NCBI
Sinocyclocheilus microphthalmus	XH0402	Guangxi, Pearl River	AY854687	NCBI
Sinocyclocheilus tianeensis	XH3403	Guangxi, Pearl River	AY854717	NCBI
Sinocyclocheilus furcodorsalis	XH2202	Guangxi, Pearl River	AY854709	NCBI
Sinocyclocheilus altishoulderus	XH5801	Guangxi, Pearl River	AY854724	NCBI
Sinocyclocheilus jiuxuensis	XH8501	Guangxi, Pearl River	AY854736	NCBI
Sinocyclocheilus jii	XH8101	Guangxi, Pearl River	AY854727	NCBI
Sinocyclocheilus yimenensis	IHB 2006645	Yunnan, Red River	EU366192	NCBI
Cyprinus carpio (outgroup)	n/a	n/a	MK088487	NCBI

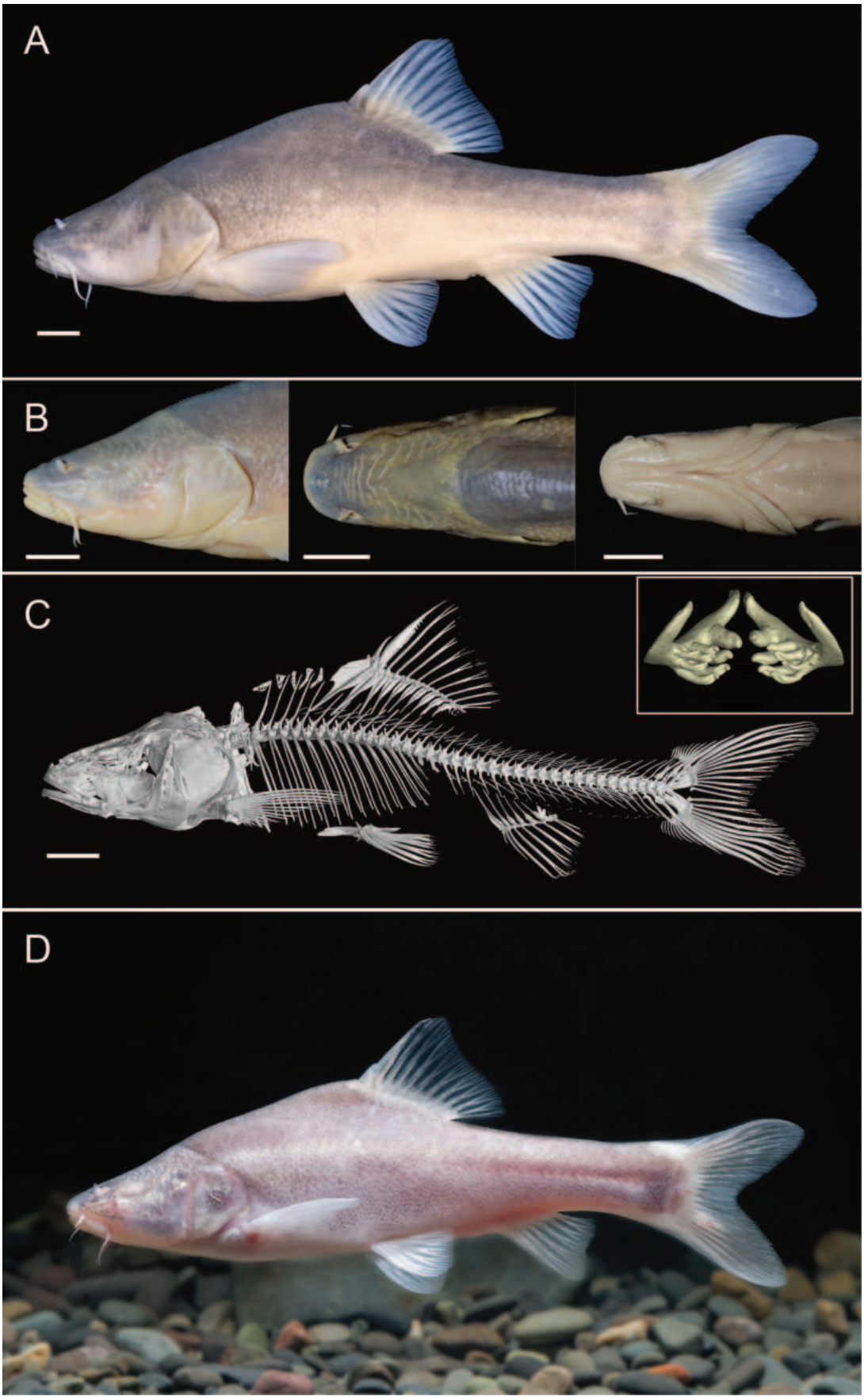

Figure 2. *Sinocyclocheilus guiyang*, IHB 202012250001, holotype, 124.0 mm SL; China: Guizhou Province: Guiyang City: Qingzhen County: Yangtze River Basin. **A.** Lateral view; **B.** Lateral, dorsal and ventral view of head; **C.** Micro-CT graph and reconstructed pharyngeal dentition; **D.** Live photo. Scale bar: 1 cm.

following characters: tip of maxillary barbel not reaching to posterior edge of preoperculum, horn-like structure in forehead absent, eye absent or highly reduced, pectoral fin not significantly extending beyond base of pelvic fin. The major diagnostic characters for *S. guiyang* and related species are summarised in Table 3.

Description. Morphometric measurements of type specimens have been transferred to percentage of standard length (SL), as summarised in Table 2. Body laterally compressed; maximum body depth positioned at insertion of dorsal-fin. Dorsal profile convex from snout tip to dorsal-fin base end and slightly concave after dorsal-fin base. Ventral profile of pre-anal part slightly convex and slightly concave after anal-fin origin.

Head slightly compressed, conical in lateral view. Eyes absent (5) or highly reduced and partially covered with skin (2). Eye orbits located in dorsal anterior part of head, filled with soft tissue. Nostrils located at midway between snout tip and anterior margin of orbit; anterior nostril with rim forming an oblique tube, posteriorly thickening and elongating; posterior nostril open and elliptical. Snout blunt in dorsal view and slightly pointed in lateral view. Mouth subterminal and arched; with two pairs of barbels; rostral pair positioned anterior to anterior nostril, extending to the insertion of anterior margin of orbit, being 6.2% (4.9–7.1%) of SL; maxillary pair positioned at corners of mouth, extending to the posterior margin of orbit, being 7.1% (5.8–8.3%) of SL. Gill opening large; opercular membranes not connected at isthmus. Joints of dentary-angulars not close at isthmus. Ten outer rakers (1) on first gill arch. Pharyngeal teeth pattern 1,3,4–4,3,0 (1); tooth tip pointed and compressed. Vertebrae 36 (2) (Fig. 2C).

Dorsal fin with 3 unbranched and 8 (5) or 9 (2) branched rays, with last one divided at base; dorsal-fin length being 20.2% (17.6–24.5%) SL; origin closer to snout tip than to caudal-fin base; distal margin slightly concave, last unbranched ray strong, with serration on posterior edge; last unbranched ray split to base. Pectoral fin with 1 unbranched and 14 (6) or 15 (1) branched rays; tip extending to pelvic-fin insertion; pectoral-fin length being 21.5% (20.8–22.2%) of SL. Pelvic fin with 1 unbranched and 7 branched rays; inserted slightly posterior to dorsal-fin origin; tip not reaching to anus. Anal fin with 3 unbranched and 5 branched rays, last one divided at base; distal margin slightly concave; origin closer to pelvic-fin insertion than to caudal-fin base. Caudal fin deeply forked, with 17 (6) or 18 (1) branched rays; upper and lower lobes pointed.

Table 2. Morphometric characters of *Sinocyclocheilus guiyang*.

Character	Holotype	Holotype + Paratypes (n = 7)		
		Range	Mean	SD
Standard length (mm)	124.0	57.5–144.1		
In Percentage of SL (%)				
Body depth	29.8	26.7–33.1	29.4	2.1
Predorsal length	55.4	53.6–59.6	55.9	2.1
Dorsal-fin base length	16.8	15.3–16.8	15.8	0.8
Dorsal-fin length	18.8	17.6–24.5	20.2	2.2
Pre-anal length	71.4	70.8–75.7	73.2	1.8
Anal-fin base length	9.8	7.5–10.2	9.2	1.0
Anal-fin length	16.6	16.0–18.3	17.1	0.9
Prepectoral length	31.3	30.7–35.7	32.5	1.6
Pectoral-fin base length	4.4	4.0–4.6	4.3	0.2
Pectoral-fin length	21.3	20.8–22.2	21.5	0.5
Prepelvic length	50.6	50.6–55.3	52.9	1.6
Pelvic-fin base length	5.7	4.5–5.7	5.2	0.4
Pelvic-fin length	16.5	15.4–19.8	17.3	1.4
Caudal peduncle length (CPL)	19.5	16.5–20.7	18.5	1.5
Caudal peduncle depth (CPD)	11.8	10.0–13.2	11.2	1.2
Head length	31.5	30.2–34.1	32.2	1.4
Head depth	19.0	16.8–21.0	19.14	1.3
Head width	16.0	10.4–17.6	15.3	2.4
Snout length	10.9	9.9–11.0	10.5	0.5
Eye diameter	3.5	3.5–5.9	4.6	1.2
Interorbital width	10.4	8.3–10.5	9.7	0.8
Prenostril length	5.7	4.5–6.0	5.6	0.5
Width between posterior nostrils	7.2	5.8–7.4	6.6	0.6
Upper jaw length	10.2	10.1–10.3	10.2	0.1
Lower jaw length	9.4	8.9–9.5	9.2	0.2
Mouth width	8.3	6.8–8.3	7.5	0.6
Rostral barbel length	5.2	4.9–7.1	6.2	0.9
Maxillary barbel length	5.9	5.8–8.3	7.1	0.9
CPD to CPL ratio	0.60	0.55–0.67	0.61	0.04

Table 3. Major diagnostic characters for *Sinocyclocheilus guiyang* and its close congeners. n/a, not available.

Characters	*S. guiyang*	*S. multipunctatus*	*S. punctatus*	*S. sanxiaensis*	*S. jinxiensis*	*S. jiuxuensis*	*S. mashanensis*	*S. brevibarbatus*	*S. yangzongensis*
Eye	Absent or highly reduced	Normal	Normal	Absent	Absent	Normal	Normal	Normal	Normal
Tip of maxillary barbel	Reaching to posterior edge of orbit	Reaching to posterior edge of preoperculum	Reaching to anterior edge of orbit	Not reaching to anterior edge of orbit	Reaching to posterior edge of orbit	Reaching or extending to posterior edge of orbit	Extending to anterior edge of orbit	Not reaching to anterior edge of orbit	Extending to anterior edge of orbit
Pectoral-fin extending to pelvic-fin insertion	Yes	No	Yes	Yes	Yes	Yes	Yes	Yes	No
Gill rakers	10	n/a	7–8	7	13–14	8–10	7–9	8–9	8–11
Lateral-line scales	45–47	53–60	48–60	41	38–41	42–51	47–50	49–51	71–81
Degenerated body scales above and below lateral line	Yes	Yes	Yes	Yes	No	Yes	Yes	Yes	Yes
Black blotches on body	Absent	Present	Present	Absent	Absent	Absent	Absent	Absent	Present

Body covered with small scales, partially embedded subcutaneously; scales on lateral line slighter larger than other. Lateral line complete and horizontal, with 45 (4), 46 (2) or 47 (1) perforated scales. Scale rows above lateral line 20 (1), 21 (3), 22 (2) or 24 (1); below 13 (2) or 14 (5). Circumpeduncular scales 32 (1), 33 (1), 34 (2), 35 (2) or 36 (1).

All original morphometric measurements and meristic counts are available in Suppl. material 1.

Colouration. In freshly collected individuals (Figs 2D, 3), head and body generally pinkish, with or without pigments dorsally. A pair of dark stripes present on dorsal-posterior part of head, extending to dorsal mid-point of nape; a gold stripe extending along dorsal mid-line from nape to dorsal-fin origin. All fins transparent.

In preserved specimens (Fig. 2A, B), body and head slightly yellowish, with or without pigments dorsally. Abovementioned dark stripes and gold stripe faded. All fins transparent.

Distribution and habitat. This species is presently only known from a subterranean stream flowing into the Wujiang River in the upper Yangtze River Basin in Qingzhen County, Guiyang City, Guizhou Province, China (Fig. 4). The species inhabits pools of subterranean stream with gravel substrate (Fig. 5). Video record of *Sinocyclocheilus guiyang* in situ is available in Suppl. material 2.

Etymology. The location of the subterranean stream where this new species was first collected: Guiyang City, the capital of Guizhou Province, is directly utilised as a specific epithet. The common name proposed for the new species is '贵阳金线鲃' (Guiyang Golden-line Barbel).

Morphometric comparisons. Principal component analysis for *Sinocyclocheilus guiyang*, *S. punctatus*, *S. multipunctatus* and *S. sanxiaensis*, based on 29 log-transformed characters, showed that 95.23% of total variance was explained by the first three components, including 87.24% by PC1, 4.79% by PC2 and 3.20% by PC3, respectively. In the PC1 vs. PC3 scatter plot, *S. guiyang* and *S. punctatus* form a distinct cluster from the other two congeners on the PC3 axis (Fig. 6A). The characters with major loading on PC3 included maxillary barbel length, rostral barbel length, eye diameter, width between posterior nostrils and pectoral-fin base length (Table 4). Further PCA in *S. guiyang* and *S. punctatus* demonstrated that the first three components explained 97.26% of total variance, in which PC1, PC2 and PC3 explained 93.31%, 2.29% and 1.66%, respectively. *Sinocyclocheilus guiyang* is separated from *S. punctatus* on the PC2 axis in the PC1 vs. PC2 scatter plot (Fig. 6B). Eye diameter, maxillary barbel length, width between posterior nostrils, rostral barbel length and snout width are major loading characters on PC2 (Table 4). Linear regression analysis also support *S. multipunctatus* as distinct from *S. guiyang* and *S. punctatus* by shorter maxillary (7.2–13.3% SL vs. 5.8–8.3% in *S. guiyang*, 4.9–9.4% in *S. punctatus*) and rostral barbel lengths (6.0–10.7% SL vs. 4.9–7.1% in *S. guiyang*, 4.9–

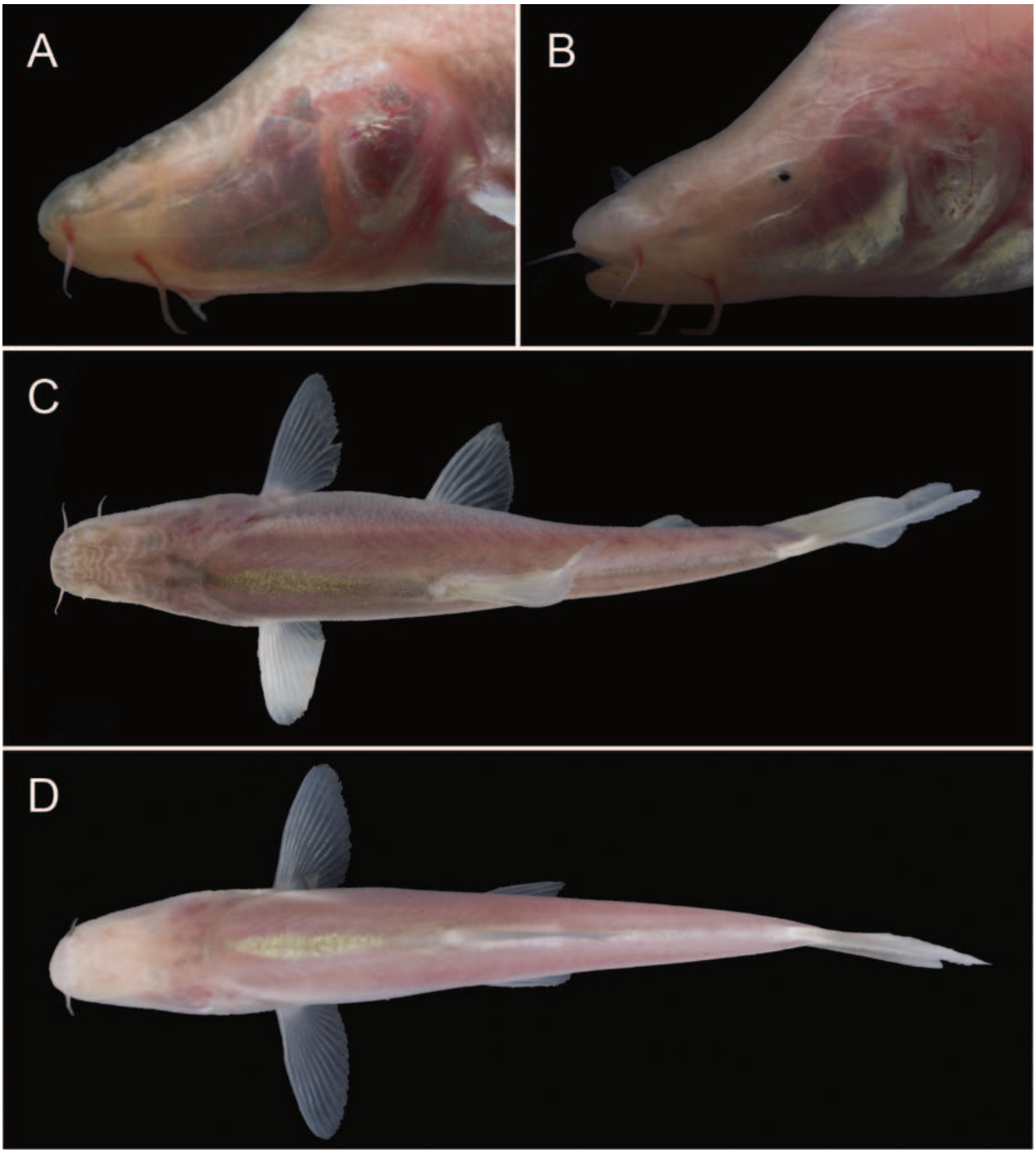

Figure 3. Intraspecific morphological variations of *Sinocyclocheilus guiyang*. **A.** Individual with no eyes; **B.** Individual with highly reduced eyes, partially covered with skin; **C.** Individual with dorsal pigment; **D.** Individual without pigment. Note that individuals of both colouration types share the presence of dark stripes on the dorsal-posterior part of the head and a gold stripe along the midline from the nape to the dorsal-fin origin.

6.7% in *S. punctatus*) (Fig. 6C, D), whereas *S. guiyang* further differed from *S. punctatus* by shorter prenostril length (4.5–6.0% of SL vs. 5.8–7.6%) and higher caudal peduncle depth to caudal peduncle length ratio (0.55–0.67 vs. 0.45–0.56) (Fig. 6E, F).

Molecular data analyses. A total of 1134 bps were included in the aligned dataset of cyt*b* gene, with 661 conservative sites, 473 variable sites, 390 parsimony informative sites and 83 singleton sites. The mean frequency of four nucleotides in the sequences of *Sinocyclocheilus guiyang* is A = 29.7%, G = 14.2%, C = 26.2% and T = 29.9%. The phylogenetic trees, reconstructed by ML and BI methods, are identical in topology (Fig. 7). The monophyletic lineage of *Sinocyclocheilus guiyang* is robustly supported by 100% posterior probabilities and 99% bootstrap supports and is sister to *S. punctatus*. The lineage of the two spe-

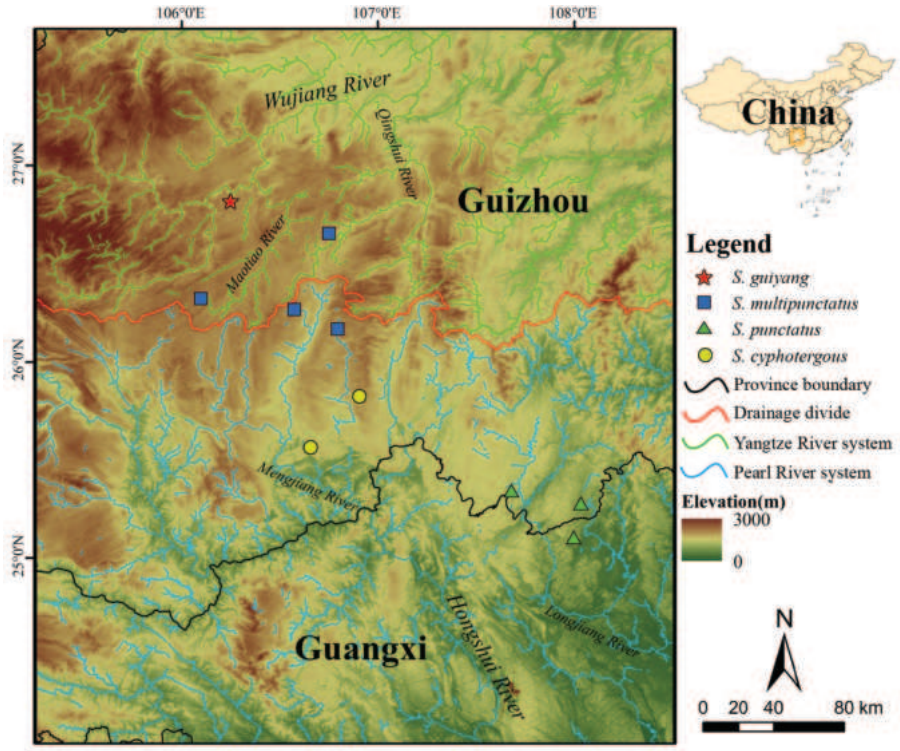

Figure 4. Sampling sites of *Sinocyclocheilus guiyang* and related species in this study.

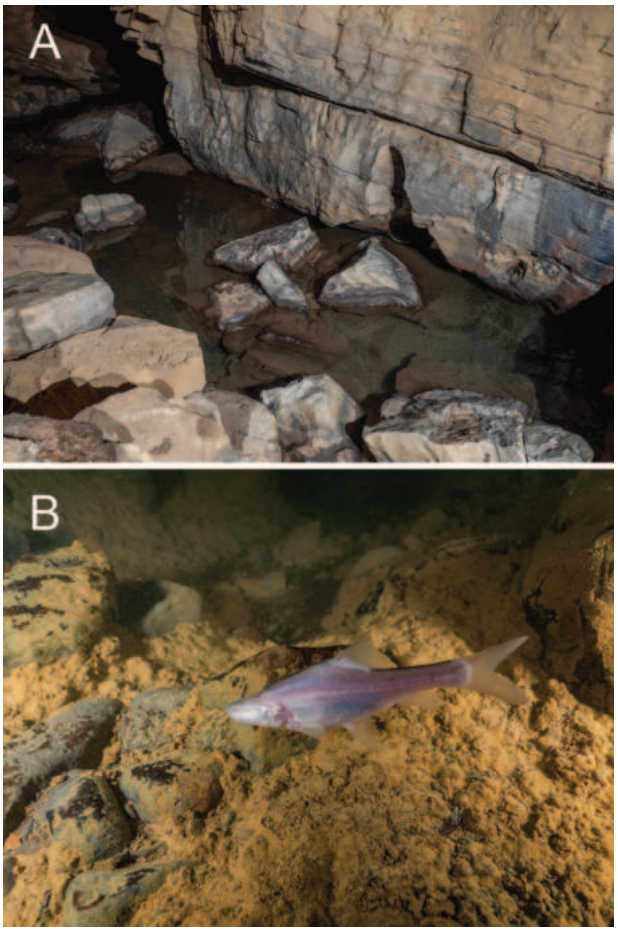

Figure 5. Habitat of *Sinocyclocheilus guiyang*. **A.** The pool of a subterranean stream where *S. guiyang* was collected; **B.** *S. guiyang* in situ.

cies clustered with the lineage comprising sequences of *S. multipunctatus*, *S. cyphotergous* and *S. sanxiaensis*. Additionally, the topology of phylogenetic reconstruction in the present study supports the monophyly of the *S. cyphotergous* – *S. multipunctatus* species group. Average genetic distances derived from cyt*b* sequences of *Sinocyclocheilus* species distributed in Guizhou Province or the Yangtze River Basin are given in Table 5. The intraspecific distance of *S. guiyang* is 0.1% and the mean distances between the new species and other congeners range from 2.3% (vs. *S. punctatus*) to 13.8% (vs. *S. wumengshanensis*).

Discussion

The new species is the first described troglobiotic species of genus *Sinocyclocheilus* in the Wujiang River of upper Yangtze River Basin in Guizhou Province. Three characters are useful for distinguishing *Sinocyclocheilus guiyang* from all other *Sinocyclocheilus* species, except *S. jinxiensis* and *S. sanxiaensis* (Fig. 8): short maxillary barbel not reaching posterior edge of preoperculum, absence of horn-like structure and degenerated (lost or highly reduced) eye. It is distinct from *S. jinxiensis* and *S. sanxiaensis* in having shorter (vs. longer) pectoral fins, just reaching (vs. significantly extending beyond) the base of pelvic fin. It further differs from *S. jinxiensis* in possessing degenerated body scales (20–24 scale rows above lateral line vs. 8–9), and from *S. sanxiaensis* in having shorter (vs. longer) snout (length 9.9–11.0% of SL vs. 16.4%) and longer (vs. shorter) maxillary barbel, reaching to posterior edge of orbit, length 5.8–8.3% of SL (vs. not reaching to anterior edge of orbit, 4.2%).

Table 4. PCA loadings of the first three principal components extracted from 29 morphometric data for *Sinocyclocheilus guiyang* and related species.

	S. guiyang*, *S. punctatus*, *S. multipunctatus*, *S. sanxiaensis			***S. guiyang*, *S. punctatus***		
	PC1	**PC2**	**PC3**	**PC1**	**PC2**	**PC3**
Standard length	0.991	-0.062	0.028	0.995	0.026	-0.045
Body depth	0.948	-0.034	-0.165	0.966	-0.049	-0.204
Predorsal length	0.991	-0.035	-0.022	0.996	0.008	0.050
Dorsal-fin base length	0.978	-0.090	0.030	0.989	-0.011	-0.027
Dorsal-fin length	0.928	0.027	0.019	0.895	-0.115	0.376
Pre-anal length	0.986	-0.058	0.037	0.995	0.020	-0.015
Anal-fin base length	0.967	-0.107	-0.041	0.974	0.020	-0.104
Anal-fin length	0.962	-0.032	-0.075	0.985	0.073	0.101
Prepectoral length	0.990	-0.029	-0.071	0.992	-0.024	0.074
Pectoral-fin base length	0.712	0.655	0.193	0.963	0.161	-0.080
Pectoral-fin length	0.978	-0.011	-0.043	0.970	-0.092	0.132
Prepelvic length	0.991	-0.040	0.020	0.996	-0.005	-0.008
Pelvic-fin base length	0.732	0.636	0.097	0.954	-0.019	-0.228
Pelvic-fin length	0.976	0.002	-0.134	0.987	0.097	0.056
Caudal peduncle length	0.954	-0.074	0.049	0.958	0.092	-0.170
Caudal peduncle depth	0.957	-0.019	-0.065	0.956	-0.107	-0.230
Head length	0.990	-0.035	-0.072	0.997	0.008	0.034
Head depth	0.991	-0.053	-0.046	0.996	-0.014	0.000
Head width	0.972	-0.080	0.048	0.970	-0.104	0.006
Snout length	0.966	0.183	-0.094	0.983	-0.056	0.029
Eye diameter	0.716	0.389	0.408	0.758	0.632	0.056
Interorbital width	0.982	0.010	-0.086	0.979	-0.147	-0.107
Prenostril length	0.961	0.052	-0.036	0.954	0.150	0.045
Width between posterior nostrils	0.956	0.009	-0.199	0.959	-0.183	-0.170
Upper jaw length	0.962	-0.116	-0.179	0.983	-0.040	0.108
Lower jaw length	0.964	-0.118	-0.156	0.986	-0.008	0.103
Mouth width	0.958	0.031	-0.052	0.954	0.155	-0.003
Rostral barbel length	0.731	-0.440	0.492	0.956	-0.161	0.081
Maxillary barbel length	0.764	-0.300	0.524	0.938	-0.185	0.169

Table 5. Average uncorrected pairwise genetic distance (p-distance, %) derived from cyt*b* in 15 species of *Sinocyclocheilus* distributed in Guizhou Province or the Yangtze River Basin. Bold numbers, intraspecific distances; regular numbers, interspecific distances; n/a, not available.

	1	**2**	**3**	**4**	**5**	**6**	**7**	**8**	**9**	**10**	**11**	**12**	**13**	**14**	**15**
1. *S. guiyang*	**0.1**														
2. *S. multipunctatus*	2.5	**0.4**													
3. *S. punctatus*	2.3	2.6	**0.7**												
4. *S. cyphotergous*	2.8	1.1	3.1	**0.8**											
5. *S. sanxiaensis*	3.2	1.0	2.9	1.6	**n/a**										
6. *S. longibarbus*	10.9	11.0	11.2	11.2	11.6	**n/a**									
7. *S. grahami*	11.7	11.6	11.8	11.9	12.2	11.5	**n/a**								
8. *S. wumengshanensis*	12.3	11.8	12.1	12.1	12.3	11.7	4.2	**n/a**							
9. *S. angustiporus*	11.4	11.1	11.5	11.3	11.6	10.4	7.7	7.1	**n/a**						
10. *S. macrolepis*	11.5	11.4	11.9	11.7	12.0	11.1	12.7	12.6	11.5	**n/a**					
11. *S. bicornutus*	10.8	10.9	11.4	11.1	11.4	10.3	12.2	12.4	11.1	11.3	**n/a**				
12. *S. zhenfengensis*	10.9	10.8	11.2	10.9	11.3	10.0	12.0	12.4	11.3	11.2	2.9	**n/a**			
13. *S. angularis*	11.2	11.2	11.1	11.5	11.6	9.6	11.8	12.3	11.2	11.6	2.8	2.4	**n/a**		
14. *S. longicornus*	11.9	11.9	11.8	11.9	12.4	10.8	12.3	12.5	11.3	11.8	5.8	6.5	5.9	**n/a**	
15. *S. xingyiensis*	11.1	11.1	11.5	11.3	11.5	10.1	12.6	12.8	11.3	12.0	2.3	2.9	1.9	6.3	**n/a**

Although *Sinocyclocheilus guiyang* displays a high degree of eye degeneration, there is intraspecific variations in the eyes, ranging from absence of eye to highly reduced eyes partially covered by skin (Fig. 3A, B). Similar variations have been recorded in observations of its congeners. The eyes of *S. cyphotergous* have been described as 'very small' in its re-description (Huang et al. 2017) and it is the same case with some of our newly-collected specimens (Fig. 8E); however, some specimens are presented as eyeless (See Suppl. material 3). *Sinocyclocheilus bicornutus*

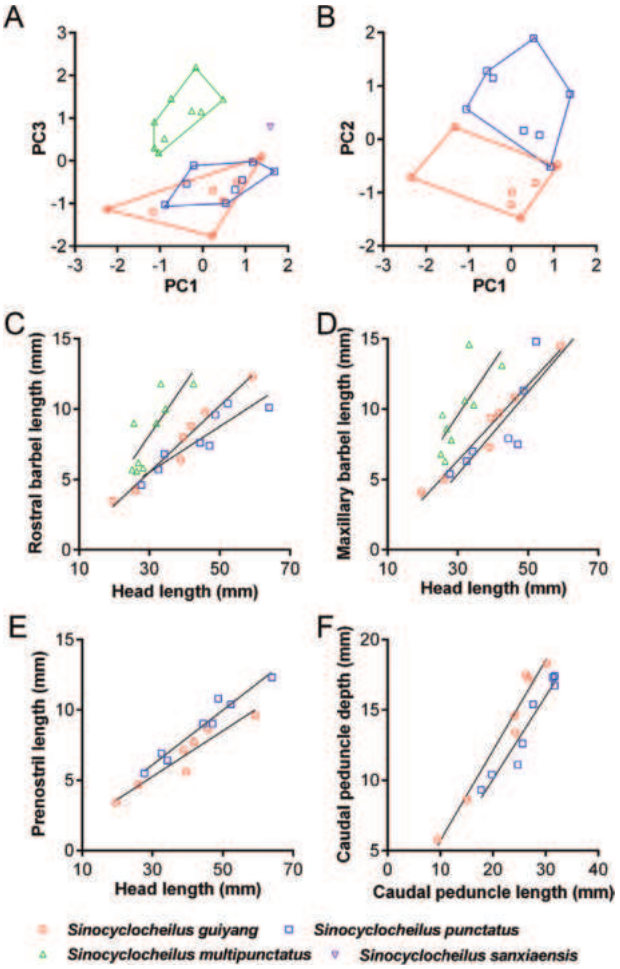

Figure 6. A. Scatter plot of 1st and 3rd principal components for *Sinocyclocheilus guiyang*, *S. punctatus*, *S. multipunctatus* and *S. sanxiaensis*; **B.** Scatter plot of 1st and 2nd principal components for *S. guiyang* and *S. punctatus*; relationships between **C.** Rostral barbel length and head length, **D.** Maxillary barbel length and head length for *S. guiyang*, *S. punctatus* and *S. multipunctatus*; relationships between **E.** Prenostril length and head length, **F.** Caudal peduncle depth and caudal peduncle length for *S. guiyang* and *S. punctatus*.

Wang & Liao, 1997, a cave-dwelling species, also demonstrated polymorphism in eye mode (Wen et al. 2023). Variations in such regressive characters in troglobitic fishes are common, indicating that eye degeneration might not be a totally reliable character in morphology species delineation of *Sinocyclocheilus*. Accordingly, it is of vital importance to also compare the morphology of this new species with other congeneric species possessing a short maxillary barbel, no horn-like structure and normal eyes, including *S. jiuxuensis* Li & Lan, 2003, *S. brevibarbatus* Zhao, Lan & Zhang, 2009, *S. mashanensis* Wu, Liao & Li, 2010, *S. yangzongensis* Chu & Chen, 1977, *S. multipunctatus* and *S. punctatus*. Amongst these species, *S. multipunctatus* and *S. punctatus* showed close phylogenetic relationships with *S. guiyang*, which all belong to the *S. cyphotergous* – *S. multipunctatus* group. *Sinocyclocheilus guiyang* can be further differentiated from *S. jiuxuensis*, *S. brevibarbatus* and *S. mashanensis* by the following characters: pectoral fin just reaching pelvic fin insertion (vs. pectoral fin highly developed, significantly reaching beyond pelvic fin insertion), pelvic-fin origin posterior to dorsal-fin origin (vs. anterior to dorsal-fin origin) (Zhao and Zhang 2009). In addition, *S. guiyang* further differs from *S. yangzongensis* in having a deeper body (depth 26.7–33.1% SL vs. 21.3–28.5%), longer dorsal fin base (length 15.3–16.8% SL vs. 8.0–12.6%) and less lateral line scales (45–47 vs. 71–79) (Zhao and Zhang 2009).

Sinocyclocheilus guiyang is undoubtedly a member of the *S. cyphotergous* – *S. multipunctatus* species group, as evidenced by both morphology and phylogenetic results in this study. The monophyly of the *S. cyphotergous* – *S. multipunctatus* group has also been confirmed in previous works (Wen et al. 2022; Jiang et al. 2023; Xu et al. 2023). Excluding *S. sanxiaensis*, which has been mentioned above, *S. guiyang* differs from *S. cyphotergous* by the absence of a humpback, from *S. multipunctatus* in having developed pectoral fins extending (vs. not extending) to pelvic-fin insertion and fewer lateral line scales (45–47 vs. 53–60), from *S. punctatus* in having longer maxillary barbels reaching to posterior edge of orbit (vs. reaching to anterior edge of orbit). The principal component analysis of measurement characters also confirms the morphological distinctness of *S. guiyang* from other members of the *S. cyphotergous* – *S. multipunctatus* group lacking horn-like structures (Fig. 6A).

As sister to one another, the pairwise distance between *Sinocyclocheilus guiyang* and *S. punctatus* is 2.3%, exceeding the 2% mitochondrial DNA threshold which is often indicative of valid species in most groups (Avies and Walker 1999) and coincides with distances used for currently described species in *Sinocyclocheilus*. The genetic distances between sibling species being comparatively low might be a trait common across the genus *Sinocyclocheilus*, which has undergone recent divergence in extreme subterranean environments (Mao et al. 2022). In addition, *S. guiyang* and *S. punctatus* display allopatric distribution patterns as *S. punctatus* is confined in the Longjiang River (a tributary of Liujiang River in the Pearl River Basin), while *S. guiyang* only occurs in Wujiang River that belongs to the upper Yangtze River Basin. The species validity of *S. guiyang* can be confirmed under an integrative framework combining numerous lines of evidence, comprised of morphological distinctness, molecular phylogeny and geographical range. Moreover, samples of *S. multipunctatus* formed a paraphyletic entity in the phylogenetic tree. It is evident that geographic divergence has occurred as the Yangtze River population showed close affinities to *S. sanxiaensis*, while the Pearl River population is located at the base of the paraphyly (Fig. 7), implying the existence of cryptic species diversity within *S. multipunctatus* that warrants taxonomic revision in the future.

The fish diversity in the Yangtze River Basin of Guiyang City, the most urbanised area of Guizhou, has long been underestimated (Zeng and Liu 2020). The increasing discoveries of narrowly distributed species in this area have raised concerns for the conservation of these species

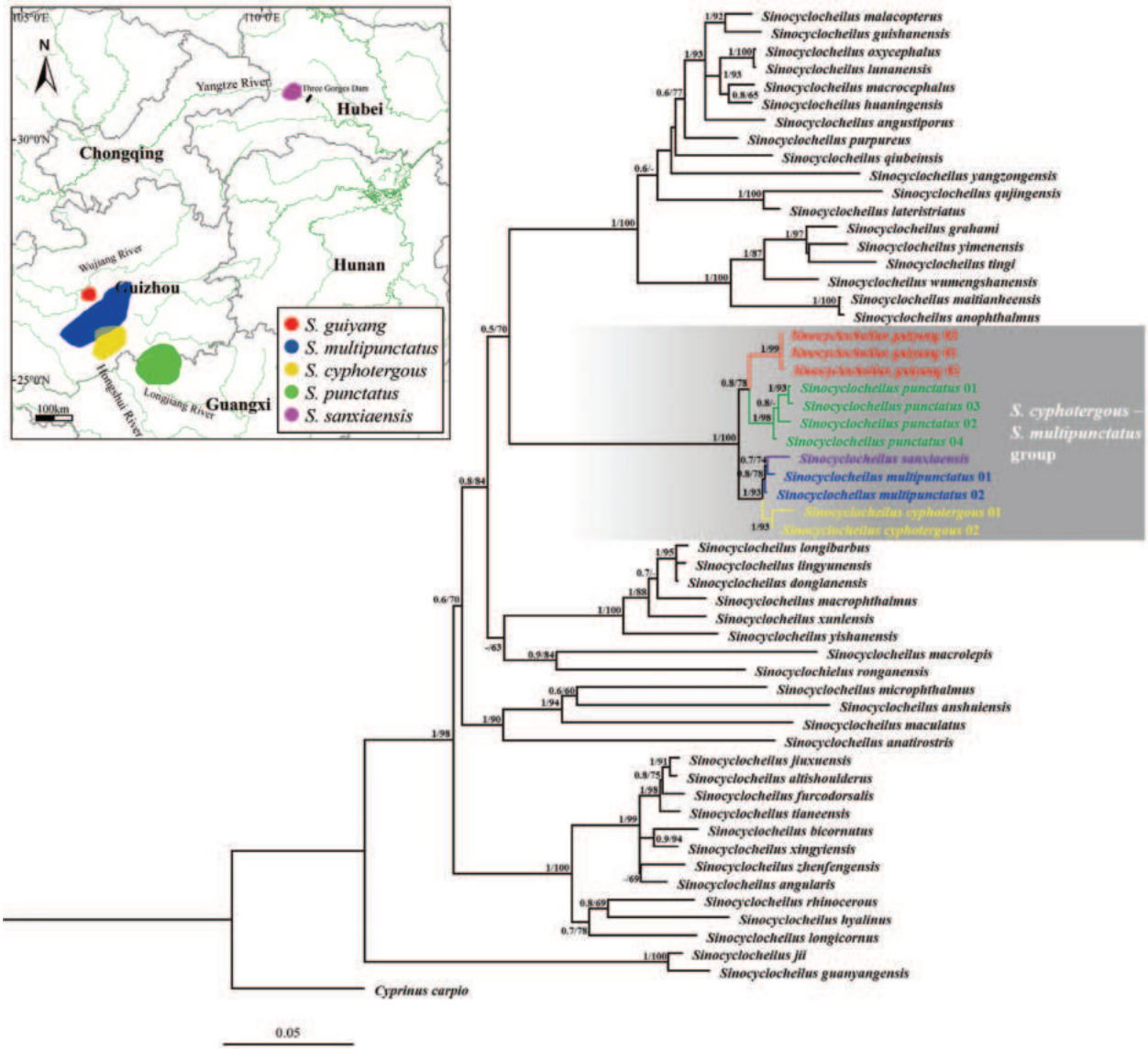

Figure 7. Phylogenetic tree of *Sinocyclocheilus* species inferred from cyt*b* using Bayesian Inference and Maximum Likelihood methods. Node values show posterior probabilities/bootstrap supports if greater than 50%. Currently known distribution of species of the *S. cyphotergous* – *S. multipunctatus* group are shown on map.

(Liu et al. 2022; Zeng et al. 2022). Human disturbance to the habitat and climate change have exacerbated the risk of extinction of cave species (Shu et al. 2013; Mouser et al. 2022). Recent years have witnessed a dramatic increase in land use, fishing pressure, cave tourism and invasion of a large amount of *Procambarus clarkii* Girard, 1852 in the type locality of *Sinocyclocheilus guiyang* (See Suppl. material 4), as well as frequent onset of droughts. Moreover, the estimated population size of the new species is extremely small, as only 25 individuals in total were recorded during our surveys and has suffered a population decline in the recent 2 years (Table 6). *S. guiyang* will be automatically assigned to the list of 2nd Class of the national protected animals after its description as the whole *Sinocyclocheilus* species are within this list since 2021. Construction of a small conservation area with limited human disturbance in the existing habitats of this new species under extreme threat should be considered in priority.

Table 6. Number of individuals of *Sinocyclocheilus guiyang* in type locality recorded each year during the survey.

Year	2019	2020	2021	2022	2023	2024
Number	5	7	5	6	1	1

Material examined

Sinocyclocheilus cyphotergous: IHB 202207280006–12, 7 specimens, 54.2–82.0 mm SL; a tiankeng of the Mengjiang River System in the Pearl River Basin at Pingtang County, Qiannan Prefecture, Guizhou Province, China. IHB 202302080002–03, 2 specimens, 71.5–84.6 mm SL; a subterranean tributary of the Mengjiang River System in the Pearl River Basin at Luodian County, Qiannan Prefecture, Guizhou Province, China.

Sinocyclocheilus multipunctatus: IHB 2014040001, 1 specimen, 96.4 mm SL; a vauclusian spring of the Mengjiang River System in the Pearl River Basin at

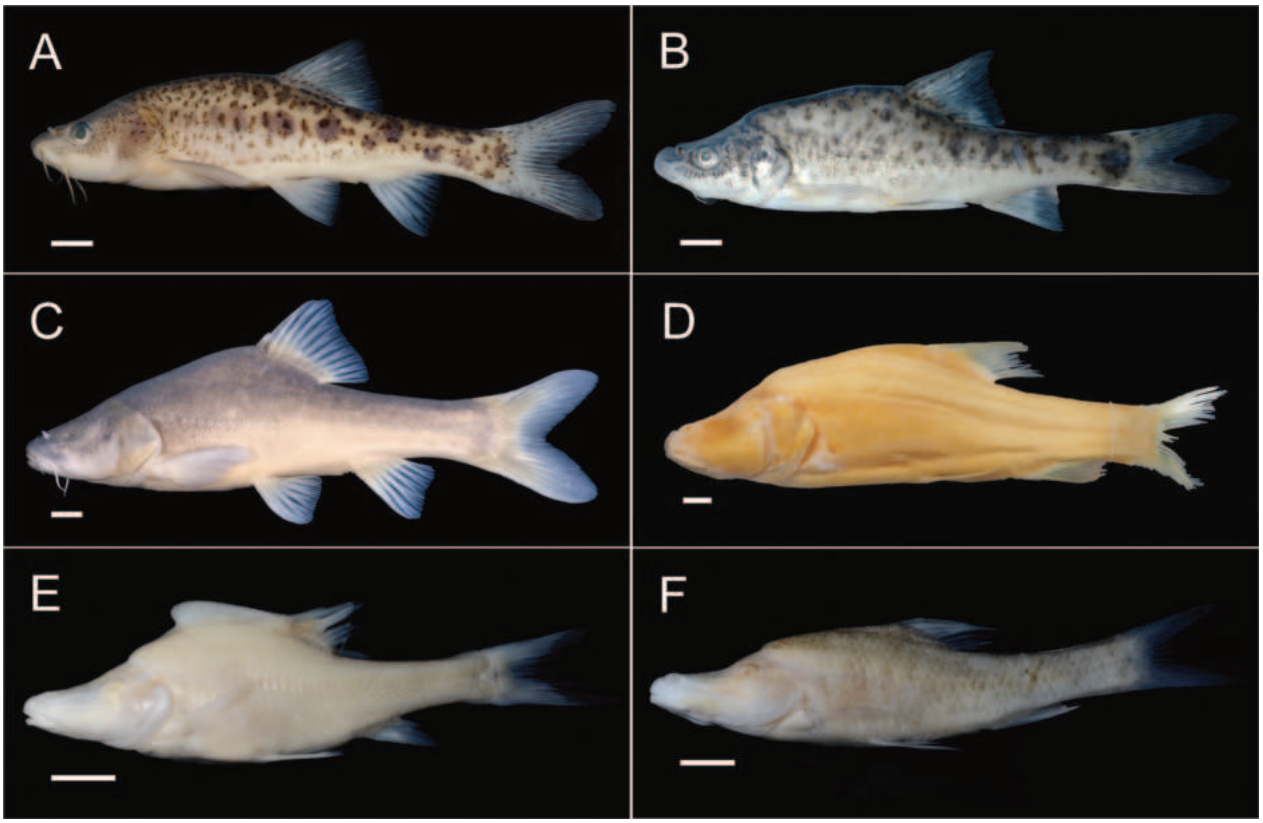

Figure 8. Lateral view of **A.** *Sinocyclocheilus multipunctatus*, IHB 202302080001, 110.3 mm SL; China: Yangtze River Basin; **B.** *S. punctatus*, ZJFR 2311004, 110.1 mm SL; China: Pearl River Basin; **C.** *S. guiyang*, IHB 202012250001, holotype, 124.0 mm SL; China: Yangtze River Basin; **D.** *S. sanxiaensis*, KIZ 2019000001, holotype, 164.1 mm SL; China: Yangtze River Basin; **E.** *S. cyphotergous*, IHB 202207280011, 71.3 mm SL; China: Pearl River Basin; **F.** *S. jinxiensis*, GXU 23070020, 85.8mm SL; China: Pearl River Basin. Scale bar: 1 cm.

Huaxi District, Guiyang City, Guizhou Province, China. IHB 2019070001, IHB 202302080001, 2 specimens, 87.6–110.3 mm SL; a vauclusian spring of the Wujiang River System in the Yangtze River Basin at Wudang District, Guiyang City, Guizhou Province, China. IHB 202307067001–02, 2 specimens, 83.6–88.0 mm SL; Bawang River of the Mengjiang River System in the Pearl River Basin at Huishui County, Qiannan Prefecture, Guizhou Province, China. ZJFR 2306003–05, ZJFR 2312003, 4 specimens, 110.3–137.7 mm SL; a vauclusian spring of the Wujiang River System in the Yangtze River Basin at Xixiu District, Anshun City, Guizhou Province, China.

Sinocyclocheilus punctatus: IHB 20210697587, IHB 202311064952, ZJFR 2311004, 3 specimens, 109.4–152.3 mm SL; a subterranean tributary of the Liujiang River System in the Pearl River Basin at Libo County, Qiannan Prefecture, Guizhou Province, China. IHB 20222936A–38A, ZJFR 202311001, ZJFR 202312002, 5, 129.4–226.0 mm SL; a subterranean tributary of the Liujiang River System in the Pearl River Basin at Huanjiang County, Hechi City, Guangxi Province, China.

Sinocyclocheilus sanxiaensis: KIZ 2019000001, holotype, 164.1 mm SL; near the north bank of the Three Gorges Reservoir in the mainstream of Yangtze River at Zigui County, Yichang City, Hubei Province, China.

Sinocyclocheilus jinxiensis: GXU 23070020, 1 specimen, 85.8mm SL; a vauclusian spring of the Yujiang River System in the Pearl River Basin at Jingxi County, Baise City, Guangxi Province, China.

Conflict of interest

The authors declare that they have no conflict of interest.

Funding

This work was partially funded by a grant from the Ecological Monitoring and Restoration in Dongfeng Lake and Liuchong River Basin (No: 2023-1).

Authors' contributions

Zhi-Xuan Zeng and Jia-Jun Zhou designed the study and revised the manuscript. Guang-Yuan Cheng launched the surveys. Xiao-Long Lu extracted the genomic DNA and performed the molecular analysis. Wei-Han Shao examined the specimens and prepared the manuscript. All authors read and approved the final version of the manuscript.

Acknowledgements

We are grateful to Rui Min (Kunming Natural History Museum of Zoology, KIZ) and Ye-Wei Liu, Cheng-Hai Fu (College of Forestry, Guangxi University) for providing comparative specimens; to Ji-Yong Wang (Guiyang Qianren Ecological Conservation Center) for assistance in the field survey; and to Zheng-Meng Yang for drawing of the new species.

References

Avies JC, Walker D (1999) Species realities and numbers in sexual vertebrates: Perspectives from an asexually transmitted genome. Proceedings of the National Academy of Sciences of the United States of America 96(3): 992–995. https://doi.org/10.1073/pnas.96.3.992

Che Y, Yu J (1985) Chinese Karst. Science Press, Beijing, 230 pp.

Eschmeyer WN, Fricke R, Laan R (2024) Catalog of fishes: genera, species, references. http://researcharchive.calacademy.org/research/ichthyology/catalog/fishcatmain.asp [Electronic version accessed 18 Mar 2024]

He Y, Chen C, Xiao T, Yang J (2013) Three-dimensional morphology of the *Sinocyclocheilus hyalinus* (Cypriniformes: Cyprinidae) horn based on synchrotron X-ray microtomography. Zoological Research 34(E4–5): E128–134.

Huang J, Gluesenkamp A, Fenolio D, Wu Q, Zhao Y (2017) Neotype designation and redescription of *Sinocyclocheilus cyphotergous* (Dai) 1988, a rare and bizarre cavefish species distributed in China (Cypriniformes: Cyprinidae). Environmental Biology of Fishes 100(11): 1483–1488. https://doi.org/10.1007/s10641-017-0658-2

Jiang W, Li J, Lei X, Wen Z, Han Y, Yang J, Chang J (2019) *Sinocyclocheilus sanxiaensis*, a new blind fish from the Three Gorges of Yangtze River provides insights into speciation of Chinese cavefish. Zoological Research 40(6): 552–557. https://doi.org/10.24272/j.issn.2095-8137.2019.065

Jiang W, Li J, Xiang H, Sun C, Chang J, Yang J (2023) Comparative analysis and phylogenetic and evolutionary implications of mitogenomes of Chinese Sinocyclocheilus cavefish (Cypriniformes: Cyprinidae). Zoological Research 44(4): 779–781. https://doi.org/10.24272/j.issn.2095-8137.2022.439

Kalyaanamoorthy S, Minh BQ, Wong TKF, von Haeseler A, Jermiin LS (2017) ModelFinder: Fast model selection for accurate phylogenetic estimates. Nature Methods 14(6): 587–589. https://doi.org/10.1038/nmeth.4285

Kumar S, Stecher G, Tamura K (2016) MEGA7: Molecular evolutionary genetics analysis version 7.0 for bigger datasets. Molecular Biology and Evolution 33(7): 1870–1874. https://doi.org/10.1093/molbev/msw054

Lan J, Gan X, Wu T, Yang J (2013) Cave fishes of Guangxi, China. Science Press, Beijing, 266 pp.

Liu F, Zeng Z, Gong Z (2022) Two new hypogean species of *Triplophysa* (Cypriniformes: Nemacheilidae) from the River Yangtze drainage in Guizhou, China. Journal of Vertebrate Biology 71(22062): 22062. https://doi.org/10.25225/jvb.22062

Luo Q, Tang Q, Deng L, Duan Q, Zhang R (2024) A new cavefish of *Sinocyclocheilus* (Teleostei: Cypriniformes: Cyprinidae) from the Nanpanjiang River in Guizhou, China. Journal of Fish Biology 104(2): 484–496. https://doi.org/10.1111/jfb.15490

Ma L, Zhao Y, Yang J (2019) Cavefish of China. Encyclopedia of Caves (Third edition). ELSEVIER, Academic Press, London, Chapter 28: 237–254. https://doi.org/10.1016/B978-0-12-814124-3.00027-3

Mao T, Liu Y, Vasconcellos MM, Pie MR, Ellepola G, Fu C, Yang J, Meegaskumbura M (2022) Evolving in the darkness: Phylogenomics of *Sinocyclocheilus* cavefishes highlights recent diversification and cryptic diversity. Molecular Phylogenetics and Evolution 168: 107400. https://doi.org/10.1016/j.ympev.2022.107400

Mouser JB, Brewer SK, Niemiller ML, Mollenhauer R, Van Den Bussche RA (2022) Lithology and disturbance drive cavefish and cave crayfish occurrence in the Ozark Highlands ecoregion. Scientific Reports 12(1): 19559. https://doi.org/10.1038/s41598-022-21791-3

Nguyen LT, Schmidt HA, von Haeseler A, Minh BQ (2015) IQ-TREE: A fast and effective stochastic algorithm for estimating maximum-likelihood phylogenies. Molecular Biology and Evolution 32(1): 268–274. https://doi.org/10.1093/molbev/msu300

Ronquist F, Teslenko M, van der Mark P, Ayres DL, Darling A, Höhna S, Larget B, Liu L, Suchard MA, Huelsenbeck JP (2012) MrBayes 3.2: Efficient Bayesian phylogenetic inference and model choice across a large model space. Systematic Biology 61(3): 539–542. https://doi.org/10.1093/sysbio/sys029

Shu S, Jiang W, Whitten T, Yang J, Chen X (2013) Drought and China's cave species. Science 340(6130): 272. https://doi.org/10.1126/science.340.6130.272-a

Tang Q, Freyhof J, Xiong B, Liu HZ (2008) Multiple invasions of Europe by East Asian cobitid loaches (Teleostei: Cobitidae). Hydrobiologia 605(1): 17–28. https://doi.org/10.1007/s10750-008-9296-1

Wen H, Luo T, Wang Y, Wang S, Liu T, Xiao N, Zhou J (2022) Molecular phylogeny and historical biogeography of the cave fish genus *Sinocyclocheilus* (Cypriniformes: Cyprinidae) in Southwest China. Integrative Zoology 17(2): 311–325. https://doi.org/10.1111/1749-4877.12624

Wen H, Wang Y, Yang X, Yan S, Luo T, He Y, Zhou J (2023) Variable eyes degeneration of the cave carp *Sinocyclocheilus bicornutus* (Cyprinidae) from Guizhou Province, Southwest China. Journal of Ichthyology 63(1): 41–47. https://doi.org/10.1134/S0032945223010162

Wu L (1989) The fishes of Guizhou. Guizhou People's Publishing House, Guiyang, 314 pp.

Xu C, Luo T, Zhou J, Wu L, Zhao X, Yang H, Xiao N, Zhou J (2023) *Sinocyclocheilus longicornus* (Cypriniformes, Cyprinidae), a new species of microphthalmic hypogean fish from Guizhou, Southwest China. ZooKeys 1141: 1–28. https://doi.org/10.3897/zookeys.1141.91501

Zeng Z, Liu F (2020) Current status of fish diversity in the Qingshui River of Guizhou Province. Journal of Guizhou Normal University 38(6): 11–18. https://doi.org/10.16614/j.gznuj.zrb.2020.06.002 [Natural Sciences]

Zeng Z, Shao W, Jin Z, Zhang E (2022) *Hongshuia brevibarba*, a new species of labeonin fishes (Pisces: Cyprinidae) from the upper ChangJiang basin in Guizhou Province, South China. Ichthyological Exploration of Freshwaters 32(3): 217–227. https://doi.org/10.23788/IEF-1184

Zhao Y, Zhang C (2009) Endemic fishes of *Sinocyclocheilus* (Cypriniformes: Cyprinidae) in China – species diversity, cave adaptation, systematics and zoogeography. Science Press, Beijing, 271 pp.

Zhao Y, Watanabe K, Zhang C (2006) *Sinocyclocheilus donglanensis*, a new cavefish (Teleostei: Cypriniformes) from Guangxi, China. Ichthyological Research 53(2): 121–128. https://doi.org/10.1007/s10228-005-0317-z

Supplementary material 1

Measurements of the type specimens of *Sinocyclocheilus guiyang*

Authors: Wei-Han Shao, Guang-Yuan Cheng, Xiao-Long Lu, Jia-Jun Zhou, Zhi-Xuan Zeng
Data type: xlsx

Link: https://doi.org/10.3897/zse.100.119520.suppl1

Supplementary material 2

Video of *Sinocyclocheilus guiyang* in situ

Authors: Wei-Han Shao, Guang-Yuan Cheng, Xiao-Long Lu, Jia-Jun Zhou, Zhi-Xuan Zeng
Data type: mp4

Link: https://doi.org/10.3897/zse.100.119520.suppl2

Supplementary material 3

Eyeless specimen of *Sinocyclocheilus cyphotergous*

Authors: Wei-Han Shao, Guang-Yuan Cheng, Xiao-Long Lu, Jia-Jun Zhou, Zhi-Xuan Zeng
Data type: tif
Explanation note: IHB 202207280010, 82.0 mm SL; China: Qiannan Prefecture: Pingtang County: Pearl River Basin.

Link: https://doi.org/10.3897/zse.100.119520.suppl3

Supplementary material 4

Human disturbance and alien species invasion to the type locality of *Sinocyclocheilus guiyang*

Authors: Wei-Han Shao, Guang-Yuan Cheng, Xiao-Long Lu, Jia-Jun Zhou, Zhi-Xuan Zeng
Data type: tif

Link: https://doi.org/10.3897/zse.100.119520.suppl4

Zoosyst. Evol. 100 (2) 2024, 531–542 | DOI 10.3897/zse.100.122034

PENSOFT

für Natur MUSEUM FÜR NATURKUNDE BERLIN

Phylogenomic placement and revision of *Iranattus* Prószyński, 1992 jumping spiders (Salticidae, Plexippini, Plexippina)

Kiran Marathe[1,2*], Rishikesh Tripathi[3*], Ambalaparambil V. Sudhikumar[3], Wayne P. Maddison[4*]

1 *Department of Zoology, University of British Columbia, 6270 University Boulevard, Vancouver, British Columbia, V6T 1Z4, Canada*
2 *National Centre for Biological Sciences, Tata Institute of Fundamental Research, GKVK Campus, Bengaluru, 560065, India*
3 *Centre for Animal Taxonomy and Ecology, Department of Zoology, Christ College, Irinjalakuda, Kerala, 680 125, India*
4 *Departments of Zoology and Botany and Beaty Biodiversity Museum, University of British Columbia, 6270 University Boulevard, Vancouver, British Columbia, V6T 1Z4, Canada*

https://zoobank.org/4488FFD3-5621-439E-9253-058E974EB0B3

Corresponding author: Kiran Marathe (marathe12@gmail.com)

Academic editor: Danilo Harms ♦ **Received** 1 March 2024 ♦ **Accepted** 18 April 2024 ♦ **Published** 14 May 2024

Abstract

The jumping spider genus *Iranattus* Prószyński, 1992, distributed from Africa to southwestern Asia, has been placed within the Harmochirina because of their male palp structures and elongated third legs. Here, we present phylogenomic evidence that it belongs instead to the subtribe Plexippina, further supported by the presence of two coupling pockets in the female epigyne. In this study, we redescribe *I. principalis* (Wesołowska, 2000) and *I. rectangularis* Prószyński, 1992. Additionally, the female of *I. rectangularis*, the type species of the genus, is described for the first time, and we report its range extension east to India.

Key Words

Afrotropics, Araneae, biodiversity research, classification, deserts, Harmochirina, Indomalaya, phylogenomics, systematics, taxonomy, xeric scrublands

Introduction

When Prószyński (1992) originally described the jumping spider genus *Iranattus* Prószyński, 1992, based on a single male specimen from Iran, he characterized it by features such as a simple tegulum (bulbus) and embolus, unusual cymbial apophysis, and an extraordinarily long pair of legs (which his text erroneously states are the fourth pair, but which in fact are the third, as in his figures 35–36). These traits led Maddison (2015) to place it within the Harmochirina, some of which have very long third legs (e.g., *Neaetha* Simon, 1885), and some of which (e.g., *Pellenes limbatus* Kulczyński, 1895) have an apophysis on the male cymbium very similar to that of *Iranattus*. A relationship with Harmochirines was suggested by Wesołowska (2000), who, when describing *Monomotapa* Wesołowska, 2000 (later synonymized with *Iranattus*; Prószyński 2017), commented on its similarity in body and leg lengths with the harmochirines *Neaetha* Simon, 1885, and *Pellolessertia* Strand, 1929.

Subsequent studies and new material now give the opportunity to reconsider the phylogenetic placement of *Iranattus*, currently composed of two species (World Spider Catalog 2024). Females were unknown until Wesołowska and Russell-Smith's (2022) recent redescription of the African *I. principalis* (Wesołowska, 2000), known from Côte d'Ivoire, Nigeria, and Zimbabwe (Wesołowska 2000; Wesołowska and Russell-Smith 2011, 2022). We have recently collected *I. rectangularis* Prószyński, 1992,

* These authors are with equal authorship.

in India, allowing us to not only characterize it through living photographs and natural history information but also to describe its female for the first time and to gather genetic data. We set out to clarify its placement phylogenomically using ultraconserved element (UCE) data and with information on female genitalic morphology. Additionally, we provide a comprehensive generic diagnosis and redescribe both species.

Materials and methods

Materials examined

The specimens of *I. rectangularis* were recently collected from the Desert National Park, Rajasthan, India. They are currently housed in the collection of the Centre for Animal Taxonomy and Ecology (CATE), Christ College, Kerala, with plans for eventual transfer to the Research Collections at the National Centre for Biological Sciences (NCBS), Bengaluru, Karnataka, India (http://collections.ncbs.res.in), for permanent deposition. NRC-AA-#### represent NCBS voucher codes of *I. rectangularis* used for taxonomic work, where #### represents a four-digit number.

The *I. principalis* specimens used in this study were in vials in a large jar of poorly labeled salticid specimens in the Natural History Museum, London (NHMUK). All the vials in the jar contained, typically, African salticids. Their labels bore only codes of the form "PNB ###", where ### is a two- or three-digit number. We interpret these to likely be Lamotte's collection from Parc Nacional Banco (hence, "PNB"), Côte d'Ivoire, from which Wanless (1985) cites similar code labels under *Sonoita lightfooti* Peckham & Peckham, 1903, e.g., PNB 179, PNB 146. Some specimens are identified by voucher codes of the form DDKM21.###, where ### is a three-digit number.

Morphology

We examined and photographed ethanol-preserved specimens using an Olympus OM-D E-M10 II camera mounted on an Olympus SZX12 or a Leica DMC4500 camera attached to a Leica M205 C stereoscope. We used a drawing tube attached to a Nikon ME600L compound microscope to prepare illustrations of *I. principalis*. We used clove oil for clear viewing of epigyne after digesting the internal epigynal soft tissues with pancreatin. We stacked photographs using Helicon Focus 7.6.6 Pro. We prepared the drawings of *I. rectangularis* specimens by digitally tracing the photographs.

Descriptions of color patterns are based on ethanol-preserved specimens. Carapace length is measured from the base of the anterior median eyes to the posterior margin of the carapace medially, while abdomen length is measured from the anterior to the end of the anal tubercle. All measurements are in millimeters. Leg measurements are represented as follows: total length (femur, patella, tibia, metatarsus, and tarsus). Abbreviations used here are as follows: **CO**, copulatory opening; **ECP**, epigynal coupling pocket; **PME**, posterior median eye; **PLE**, posterior lateral eye; **RTA**, retrolateral tibial apophysis.

Taxon sampling for phylogenomic analysis

To test the phylogenetic placement of *Iranattus*, molecular data was gathered for *I. rectangularis* and added to Marathe et al.'s (2024) UCE phylogenomic dataset, which included 15 plexippines, two harmochirines, and one salticine. Because *Iranattus*'s former placement in the Harmochirina was based in part on some *Pellenes* having a similar cymbial apophysis, one such *Pellenes* (*Pellenes limbatus*) was added to the dataset to give the harmochirines the best chance to capture *Iranattus* in the phylogenetic analysis. An extra outgroup taxon, *Chrysilla volupe* (Karsch, 1879), was also added. The total set of 21 species used in the phylogenomic analysis, with their taxonomic authority indicated, is listed in Table 1.

Ultraconserved element (UCE) data

Molecular data was gathered for UCE loci using target enrichment sequencing methods (Faircloth 2017), using the RTA_v2 probeset (Zhang et al. 2023), and following the protocols of Marathe et al. (2024).

Raw demultiplexed reads were processed with PHYLUCE v. 1.6 (Faircloth 2016), quality control and adapter removal were performed with Illumiprocessor wrapper (Faircloth 2013), and assemblies were created with SPAdes v. 3.14.1 (Nurk et al. 2013) using options at default settings. The UCE loci were recovered using RTA_v2 probeset (Zhang et al. 2023). The recovered loci were aligned with MAFFT using L-INS-i option (Katoh and Standley 2013). The aligned UCE loci were then trimmed with Gblocks (Castresana 2000; Talavera and Castresana 2007) using –b1 0.5, –b2 0.7, –b3 8, –b4 8, –b5 0.4 settings and re-aligned with MAFFT using L-INS-i option within Mesquite v. 3.81 (Maddison and Maddison 2023b). As in the analysis of Maddison et al. (2020), suspected paralogous loci were deleted based on branch lengths in RAxML (Stamatakis 2014) inferred gene trees. Loci represented in fewer than 10 taxa total were deleted.

Phylogenetic analysis

Maximum-likelihood phylogenetic and bootstrap analyses were performed with IQ-TREE v. 2.2.0 (Nguyen et al. 2015) using the Zephyr v. 3.31 package (Maddison and Maddison 2023a) in Mesquite v. 3.81 (Maddison and Maddison 2023b) on the concatenated, unpartitioned UCE dataset with 20 taxa. For the phylogenetic tree inference, the option -m TEST (standard model selection followed by tree inference, edge-linked partition model,

Table 1. Specimens used in phylogenomic analysis.

Species	Voucher	Sex	Locality	Lat, long
Anarrhotus fossulatus Simon, 1902	AS19.1319	♂	Singapore	1.379, 103.816
Artabrus erythrocephalus (C.L. Koch, 1846)	AS19.2205	♂	Singapore	1.355–7, 103.774–5
Baryphas ahenus Simon, 1902	d536	♂	South Africa	-25.95, 30.56
Bianor maculatus (Keyserling, 1883)	NZ19.9864	♂	New Zealand	-42.1691, 172.8090
Carrhotus sp.	AS19.4650	♂	India	12.2145, 75.653–4
Chrysilla volupe (Karsch, 1879)	AS19.6089	♂	India	12.223, 76.627
Epeus sp.	DDKM21.055	♂	Singapore	1.355, 103.78
Evacin bulbosa (Żabka, 1985)	AS19.2123	♂	Singapore	1.406, 103.971
Evarcha falcata (Clerck, 1757)	RU18-5264	♂	Russia	53.721, 77.726
Ghatippus paschima Marathe & Maddison, 2024	IBC-BP833	♂	India	12.220–1, 75.657–8
Habronattus hirsutus (Peckham & Peckham, 1888)	IDWM.21018	♂	Canada	48.827, -123.265
Hyllus keratodes (van Hasselt, 1882)	DDKM21.028	♂	Malaysia	3.325, 101.753
Hyllus semicupreus (Simon, 1885)	AS19.4415	♂	India	12.2156, 75.6606
Iranattus rectangularis Prószyński, 1992	DDKM21.091	juv.	India	26.28, 70.40
Pancorius dentichelis (Simon, 1899)	SWK12-0042	♂	Malaysia	1.605–6, 110.185–7
Pancorius petoti Prószyński & Deeleman-Reinhold, 2013	SWK12-0195	♂	Malaysia	1.603–4, 110.185
Pellenes limbatus Kulczyński, 1895	RU18-5679	♂	Russia	50.0501, 89.3878
Plexippus paykulli (Audouin, 1826)	AS19.7337	♂	India	12.825–6, 78.252–3
Ptocasius weyersi Simon, 1885	DDKM21.069	♂	Singapore	1.36, 103.78
Telamonia festiva Thorell, 1887	DDKM21.048	♂	China	21.8105, 107.2925
Thyene imperialis (Rossi, 1846)	AS19.6443	♂	India	12.216, 76.625

no partition-specific rates) was used with 10 search replicates. For the bootstrap analysis, a single IQ-TREE search was used for each of the 1000 search replicates.

Data availability

The raw sequence reads obtained from UCE capture are stored within the Sequence Read Archive (BioProject: https://www.ncbi.nlm.nih.gov/bioproject/1101580), and their accession numbers are listed in Table 1. The UCE loci matrices from SPAdes assemblies, pre-Gblocks, and the concatenated matrices used for phylogenetic and bootstrap analysis, along with trees, are available on the Dryad data repository (https://doi.org/10.5061/dryad.ht76hdrpz).

Results

Phylogenetic results

Table 2 lists the sequence data recovered from the 21 taxa. 3398 UCE loci were initially recovered. Of these, 3140 remained after removing those represented in fewer than 10 taxa, and 3104 remained after removing those suspected to include paralogies on branch lengths. These were concatenated into the final matrix, whose aligned length is 2779616 base pairs, in which each taxon had on average ~2.2 million base pairs of sequence data (min. 985191, max. 2462121).

The phylogenetic results are shown in Fig. 1. The reciprocal monophyly of the subtribes Plexippina and Harmochirina

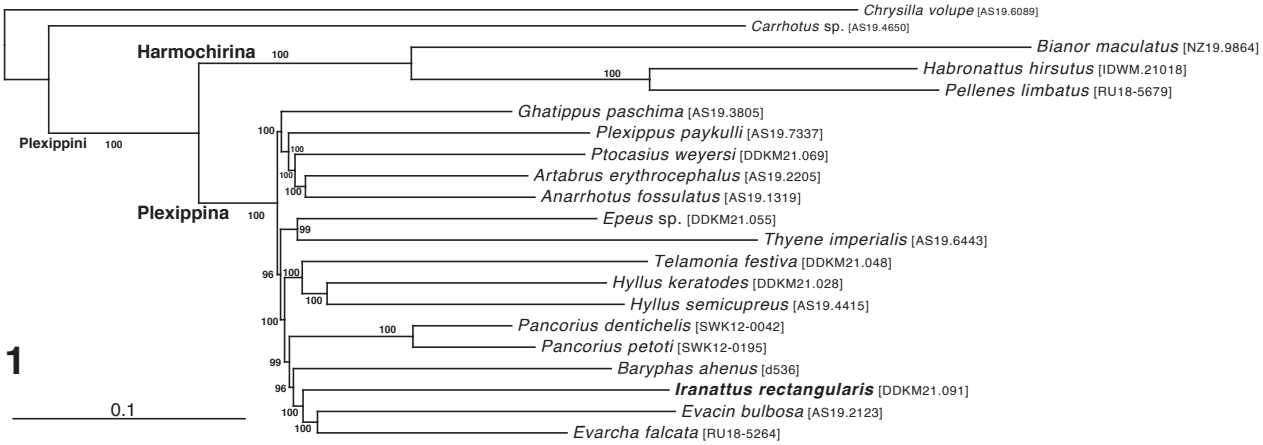

Figure 1. The IQ-TREE-based maximum-likelihood tree, represented here, is the best of 10 replicates, inferred from a concatenated dataset of 3104 UCE loci. The numbers at the nodes are the percentage recovery of the clade based on 500 bootstrap replicates. *Iranattus rectangularis* is recovered distantly from the subtribe Harmochirina and placed as the sister lineage to *Evarcha sensu lato* within the subtribe Plexippina.

Table 2. Specifics of molecular data used for this phylogenomic analysis. Molecular data was generated based on the RTA_v2 probeset. "SRA" is the Sequence Read Archive accession number available through NCBI; "Reads pass QC" is the number of reads after the removal of adapter contamination and low-quality bases using Illumiprocessor; "Total UCE loci" is the total number of UCE loci recovered with RTA_v2 probeset; "After paralogy filter" is the number of UCE loci after deletion of suspected paralogous loci based on branch length ratios; "In at least 10 taxa" is the number of UCE loci in at least 10 or more taxa after branch length criteria; "Filtered UCE sequence length" is the concatenated sequence length of filtered UCE loci; "Total loci" is the number of UCE loci represented among all taxa.

Species	Voucher	SRA	Reads pass QC	Total UCE loci	In at least 10 taxa	After paralogy filter	Filtered UCE sequence length
Anarrhotus fossulatus	AS19.1319	SRR27728361	15542927	2525	2444	2414	2100562
Artabrus erythrocephalus	AS19.2205	SRR27728359	14903498	2837	2792	2759	2333639
Baryphas ahenus	d536	SRR27728358	2653688	2256	2243	2217	985191
Bianor maculatus	NZ19.9864	SRR27728369	7914005	2962	2853	2820	2422490
Carrhotus sp.	AS19.4650	SRR27728370	5272657	2920	2838	2806	2324883
Chrysilla volupe	AS19.6089	SRR28802507	4968344	2877	2782	2752	2313910
Epeus sp.	DDKM21.055	SRR27728357	13896435	2897	2834	2802	2452270
Evacin bulbosa	AS19.2123	SRR27728356	10851810	2766	2684	2653	2157554
Evarcha falcata	RU18-5264	SRR27728355	11538276	2762	2714	2683	2215341
Ghatippus paschima	IBC-BP833	SRR27728354	7881860	2893	2836	2804	2430054
Habronattus hirsutus	IDWM.21018	SRR27728360	6581974	2821	2732	2702	2218729
Hyllus keratodes	DDKM21.028	SRR27728353	11349372	2926	2843	2811	2415960
Hyllus semicupreus	AS19.4415	SRR27728368	9874003	2942	2874	2839	2422661
Iranattus rectangularis	DDKM21.091	SRR28802508	14825117	2926	2849	2818	2008593
Pancorius dentichelis	SWK12-0042	SRR27728367	6025337	3092	3022	2988	2316987
Pancorius petoti	SWK12-0195	SRR27728366	5116119	2980	2908	2875	2304191
Pellenes limbatus	RU18-5679	SRR28802506	4288156	2661	2603	2576	1977916
Plexippus paykulli	AS19.7337	SRR27728365	7445183	2931	2852	2817	2186676
Ptocasius weyersi	DDKM21.069	SRR27728364	9926900	2880	2821	2790	2326688
Telamonia festiva	DDKM21.048	SRR27728363	7908436	2950	2889	2855	2462121
Thyene imperialis	AS19.6443	SRR27728362	7797854	2893	2818	2789	2421843
			Average:	2843	2773	2741	2228488
			Minimum:	2256	2243	2217	985191
			Maximum:	3092	3022	2988	2462121
			Total loci:	3398	3140	3104	2779616

is consistent with previous molecular phylogenetic studies with both Sanger sequencing and UCEs (Maddison and Hedin 2003; Maddison et al. 2008; Bodner and Maddison 2012; Marathe et al. 2024). The phylogenetic structure within Plexippina is largely consistent with Marathe et al. (2024) and has generally high bootstrap values.

Iranattus is nestled well within Plexippina, placed as a sister lineage to *Evarcha* Simon, 1902 *sensu lato* (see Fig. 1). The harmochirine included in the analysis with a similar cymbial apophysis, *Pellenes limbatus*, is placed as expected within the harmochirines. Thus, the similarities between *Iranattus* and harmochirines noted by Wesołowska (2000) and Maddison (2015) are convergences.

The placement of *Iranattus* in the Plexippina is also supported by the form of the epigyne. Wesołowska and Russell-Smith (2022) report a pair of coupling pockets in *I. principalis*, one on either side of a central atrium housing the copulatory openings, the same as we have found in *I. rectangularis* (Figs 22, 28). This arrangement is discordant with that of harmochirines, which have a single epigynal coupling pocket placed centrally, anterior to the margin, flanked by copulatory openings on either side. Two pockets are typical, however, for members of the Plexippina (e.g., *Evarcha*, *Baryphas* Simon, 1902; *Pancorius* Simon, 1902; *Telamonia* Thorell, 1887; *Vicirionessa* Wesołowska & Russell-Smith, 2022).

We therefore recognize *Iranattus* as a member of the subtribe Plexippina.

Taxonomic results

Family Salticidae Blackwall, 1841
Tribe Plexippini Simon, 1901
Subtribe Plexippina Simon, 1901

Iranattus Prószyński, 1992

Figs 2–41

Iranattus Prószyński, 1992: 97–98, f. 35–40.

Monomotapa Wesołowska, 2000: 159, f. 42–46 (synonymized by Prószyński, 2017: 36.).

Type species. *Iranattus rectangularis* Prószyński, 1992.

Species included. *Iranattus principalis* (Wesołowska, 2000); *Iranattus rectangularis* Prószyński, 1992.

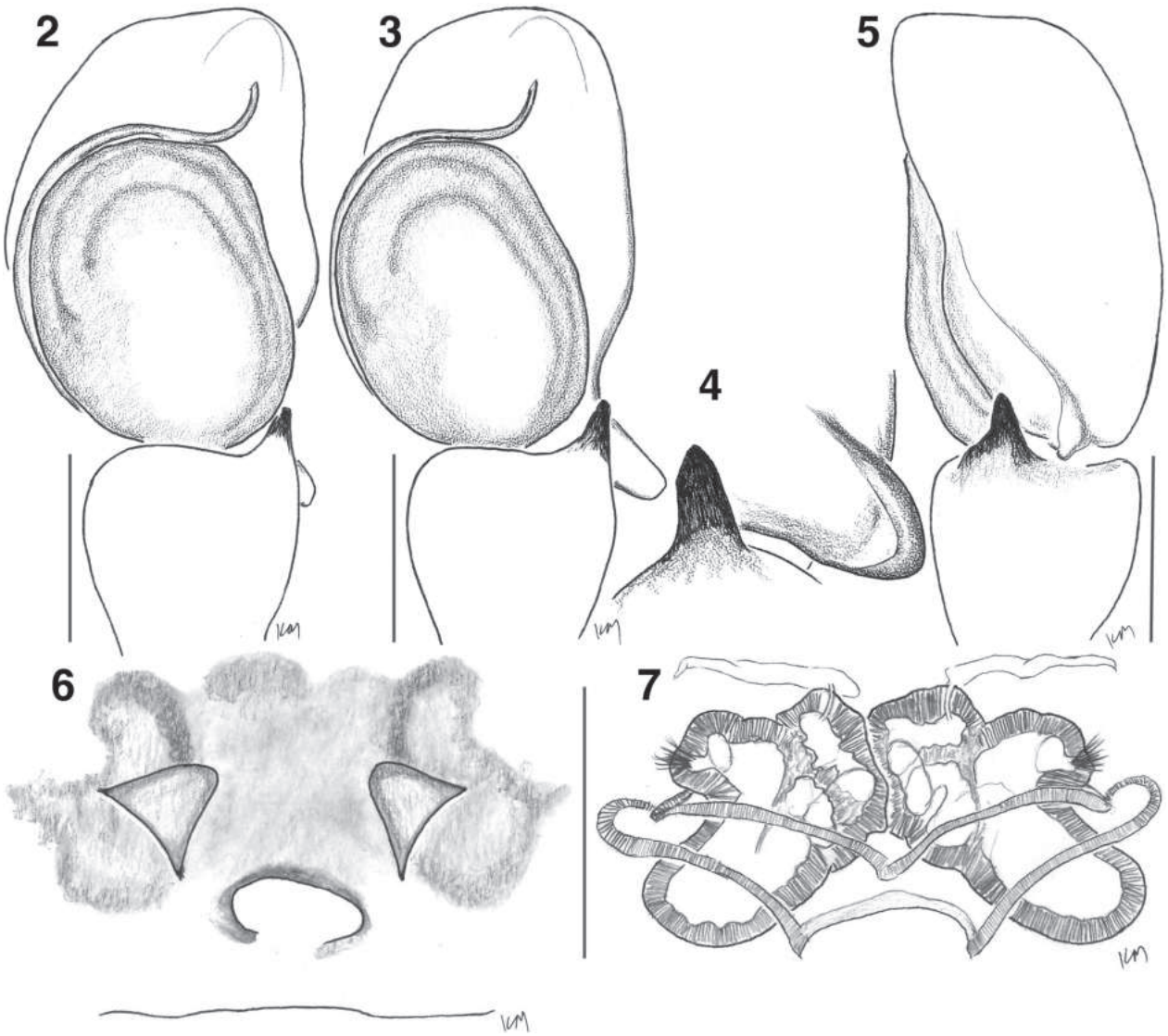

Figures 2–7. *Iranattus principalis* genitalia drawings. **2.** Male left palp, ventral view (DDKM21.089); **3.** Ditto, oblique view (DDKM21.089); **4.** Ditto, oblique view, closeup of the cymbial apophysis (DDKM21.089); **5.** Ditto, retrolateral view (DDKM21.089); **6.** Epigyne, ventral view (DDKM21.090); **7.** Vulva, dorsal view (DDKM21.089). Scale bars: 0.2 mm.

Diagnosis. The remarkably long third legs of *Iranattus* (Figs 15, 18, 30, 32) and scoop-shaped cymbial apophysis (Fig. 4) differentiate it from all other plexippines. The very robust carapace, bulging outward at the PLE and bearing the PLEs on tubercles, is unusual but shared also with *Afrobeata* Caporiacco, 1941, and *Vailimia* Kammerer, 2006. *Vailimia* especially might be confused with *Iranattus*, as they share erect hairs on the carapace (see Figs 34, 38, 41) and a compact crouch stance, but, besides the cymbial apophysis and long third legs, *Iranattus* also has a shorter embolus lacking membrane (membrane-accompanied long embolus in *Vailimia*), a short RTA (long and curved in *Vailimia*), and two distinct deep conical ECPs (absent in *Vailimia*). From *Afrobeata*, *Iranattus* differs in having longer third legs, a cymbial apophysis (lacking in *Afrobeata*), a shorter embolus (longer in *Afrobeata*), a simple short RTA (bifurcated in *Afrobeata*), shorter copulatory ducts (long in *Afrobeata*), and deep conical ECPs (shallow in *Afrobeata*). Some other plexippines have cymbial apophyses (*Plexippoides* Prószyński, 1984; *Epeus* Peckham & Peckham, 1886; and *Erasinus* Simon, 1899), but their apophyses are different in shape—in *Iranattus*, a long, broad blade with a rounded tip, concave in front so as to form a scoop; in *Plexippoides*, sharply pointed, for example.

Iranattus principalis (Wesołowska, 2000)

Figs 2–19

Monomotapa principalis Wesołowska, 2000: 160, 42–46.

Monomotapa principalis Wesołowska & Russell-Smith, 2011: 581, 96–98, 229–230.

Iranattus principalis Prószyński, 2017: 36, 14K, 17F (transferred from *Monomotapa*).

Iranattus principalis Wesołowska & Russell-Smith, 2022: 47, 29A–D, 30A–D.

Materials examined. In NHMUK, lacking complete labels. These are likely from Parc Nacional Banco, Côte d'Ivoire (see "Materials examined" for explanation).

2♀♀ (PNB21) • 1♂ 1♀ (PNB146) • 3♀♀ (PNB156) • 2♀♀ (PNB159) • 2♂♂ (PNB167) • 2♀♀ (PNB181) • 1♂ 1♀ (PNB192) • 2♂♂ 2♀♀ (PNB203).

Diagnosis. Larger than *I. rectangularis*, with an almost ovoid tegulum with a less prominent shoulder, RTA slightly bent near the tip (Figs 10, 11), and a multi-chambered spermatheca sandwiched between copulatory ducts dorsally and the epigynal plate ventrally.

Description. ♂ (DDKM21.089). Measurements: Carapace 2.2 long, 2.1 wide. Abdomen length 1.7; width 1.4. Leg measurements: I–11.2 (3.4, 2.2, 2.4, 1.8, 1.3); II–10 (2.8, 2, 2.4, 1.5, 1.2); III–16.6 (6.3, 2.9, 3.2, 2.5, 1.7); IV–10.1 (3.7, 1.6, 1.7, 1.8, 1.3). Leg formula III-IV-II-I. ***Carapace*** wider than abdomen. Ocular area shaped like an isosceles trapezoid, narrow at the anterior eye row and wide at the PLEs. PLEs on tubercles. Thoracic area slopes acutely downward behind ocular area. Ocular area anteriorly golden yellow, and remaining carapace dark brown. Lateral sides posteriorly and back sparsely covered with pale hairs. ***Clypeus*** narrow, yellowish-brown sparsely covered with hairs. ***Chelicerae*** vertical, narrow, yellowish brown. ***Palp*** (Figs 2–5, 8–11): Embolus medium-long, starting at 7 o'clock. RTA stout, short with blunt tip. Cymbium extends retrolaterally to form scoop-shaped apophysis. Tegulum prolaterally rounder; retrolaterally slightly angular at distal and proximal edges. ***Legs*****:** III femur distinctly long. Femur golden yellow, distal segments yellowish-brown. ***Abdomen*** narrow, ovoid. Golden yellow with less prominent transverse pale bands. Spinnerets yellowish.

♀ (DDKM21.090). Measurements: Carapace 5.1 long, 5.1 wide. Abdomen length 6.4; width 4.8. Leg measurements: I–11.7 (3.8, 1.8, 2.7, 2.1, 1.3); II–11.6 (3.3, 2.8, 2.4, 1.8, 1.3); III–19.7 (6.9, 3.3, 4.7, 3.1, 1.8); IV–11.4 (2.9, 2.1, 2.3, 2.6, 1.5). Leg formula III-I-II-IV. ***Carapace*** shape similar to male, width about same as abdomen. Brown, sparsely covered with pale hairs. ***Clypeus*** similar to male. ***Chelicerae*** similar to male. ***Legs*** similar to male. ***Abdomen*** ovoid, bulky, yellowish, covered with brown hairs, and more posteriorly.

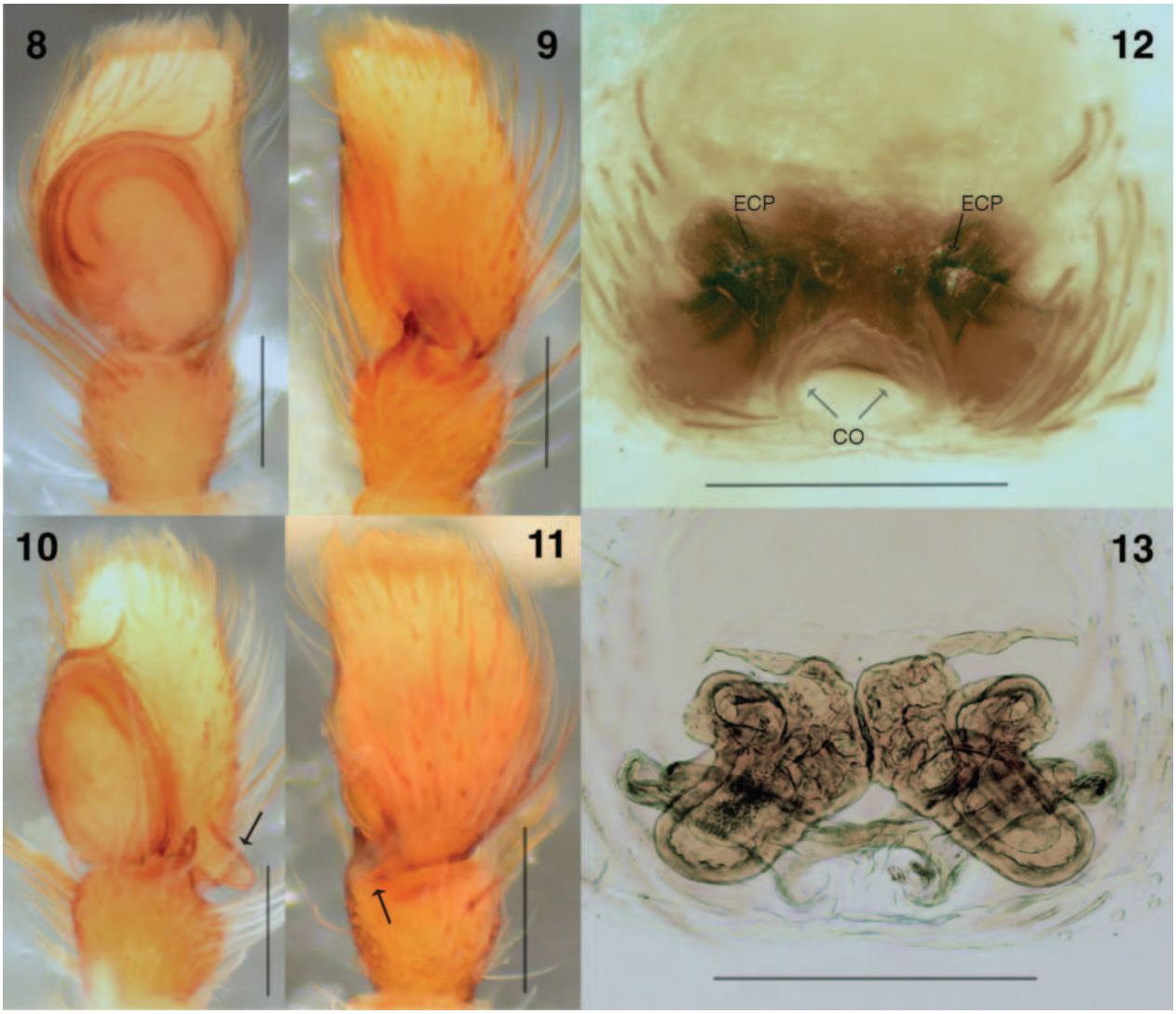

Figures 8–13. *Iranattus principalis* genitalia photographs. **8.** Male left palp, ventral view (DDKM21.089); **9** Ditto, retrolateral view (DDKM21.089); **10.** Ditto, oblique view (DDKM21.089); **11.** Ditto, retrolateral view (DDKM21.089); **12.** Epigyne, ventral view (DDKM21.090); **13.** Vulva, dorsal view (DDKM21.089). **ECP**, epigynal coupling pocket. **CO**, copulatory opening. Scale bars: 0.2 mm. Arrows in Figs **10** and **11** point to the scoop-shaped retrolateral cymbial apophysis.

Spinnerets yellowish. ***Epigyne*** (Figs 6, 7, 12, 13): Medially located copulatory opening flanked by conical-shaped ECP.

Natural history. Wesołowska and Russell-Smith (2022) report *Iranattus principalis* as collected from the branches of savannah shrubs. G. Azarkina (pers. comm.) has seen material of this species from canopy fogging in tropical savannas in Cameroon (2♀ 8.40°N, 12.80°E) and Côte d'Ivoire (1♀ 8.40°N, 12.80°E; 2♂ 2♀ 8°44'N, 3°49'W) in the Musée royal de l'Afrique centrale, collected from the trees *Cola laurifolia*, *Combretum fragrans*, *Anogeissus leiocarpus*, and *Crossopteryx febrifuga*.

Distribution. Côte d'Ivoire, Nigeria, Zimbabwe, and Cameroon.

Iranattus rectangularis Prószyński, 1992

Figs 20–41

Iranattus rectangularis Prószyński, 1992a: 97, f. 35–40.

Materials examined. 1 ♂, 1♀, & 4 juveniles. From INDIA: RAJASTHAN: Jaisalmer: Thar Desert: Desert National Park, Myajlar area, 26.28°N, 70.40°E, 275 m elev., 20 Aug 2022, leg. R. Tripathi.

Diagnosis. Smaller than *I. principalis*, with a bright orange face and erect hairs on the carapace, an angular tegulum with a prominent shoulder, a simple RTA, and a simple spermatheca with copulatory ducts ventrally.

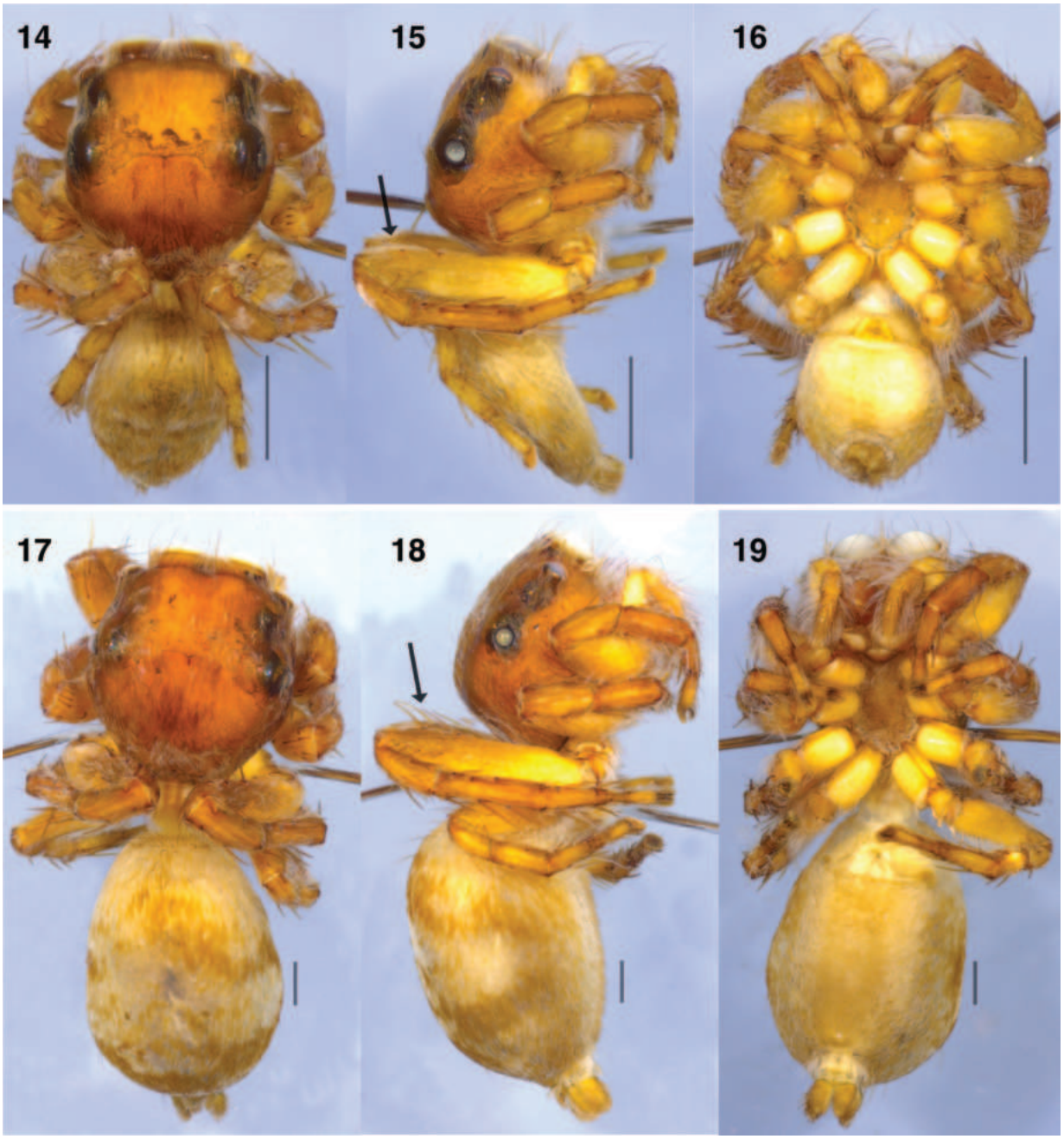

Figures 14–19. *Iranattus principalis* habitus. **14.** Male, dorsal view (DDKM21.089); **15.** Ditto, lateral view (DDKM21.089); **16.** Ditto, ventral view (DDKM21.089); **17.** Female, dorsal view (DDKM21.090); **18.** Ditto, lateral view (DDKM21.090); **19.** Ditto, ventral view (DDKM21.090). Scale bars: 1 mm. Arrows in Figs **15** and **18** point to the long third legs.

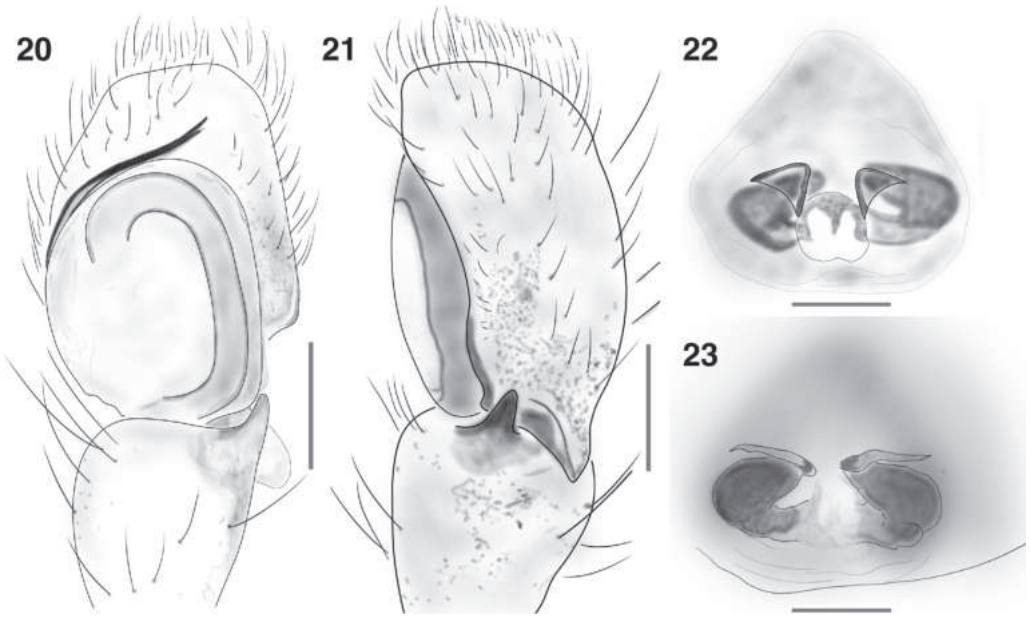

Figures 20–23. *Iranattus rectangularis* genitalia drawings. **20.** Male left palp, oblique view (NRC-AA-7708); **21.** Ditto, retrolateral view (NRC-AA-7708); **22.** Epigyne, ventral view (NRC-AA-7709); **23.** Vulva, dorsal view (NRC-AA-7709). Scale bars: 0.1 mm.

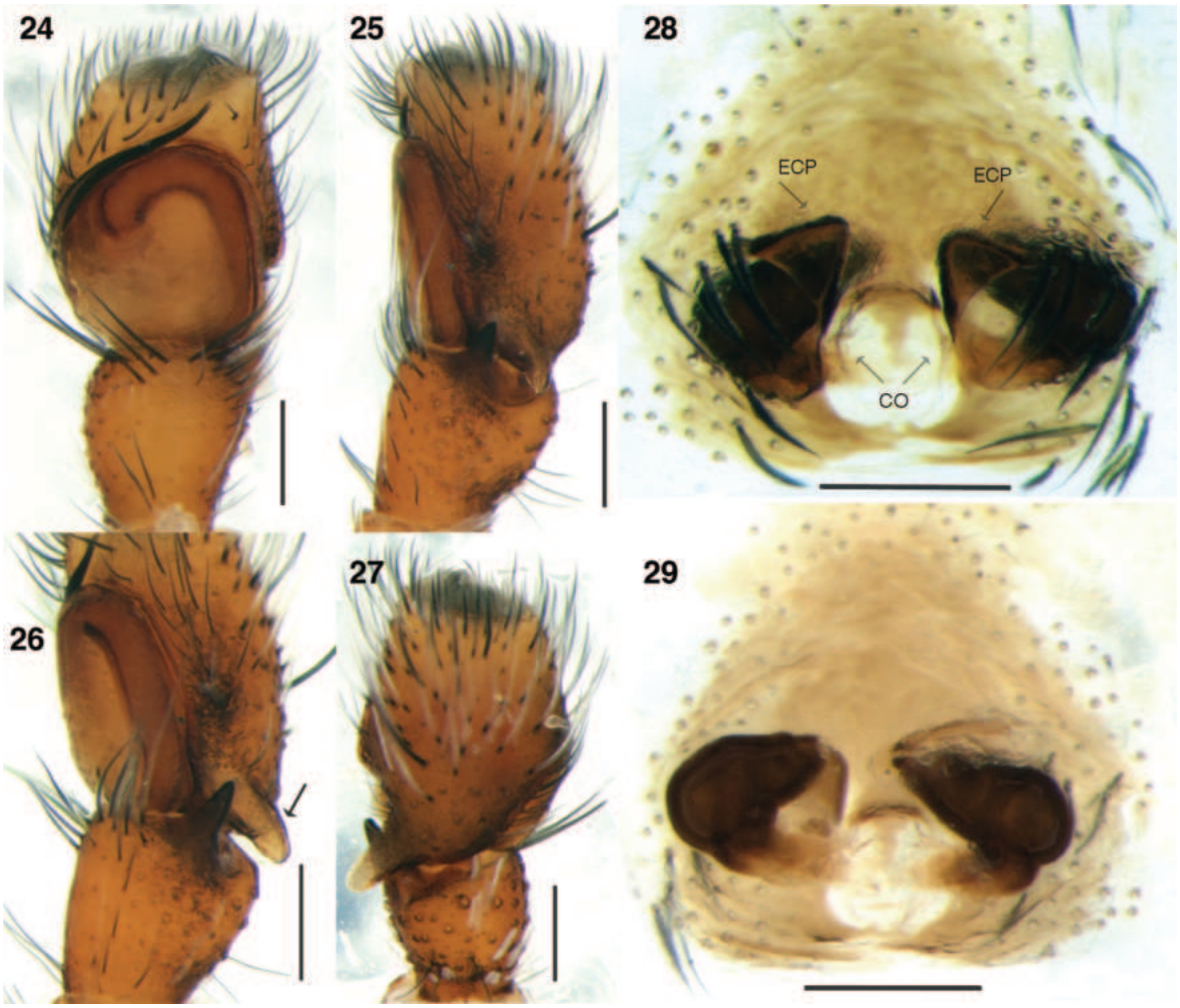

Figures 24–29. *Iranattus rectangularis* genitalia photographs. **24.** Male left palp, ventral view (NRC-AA-7708); **25.** Ditto, retrolateral view (NRC-AA-7708); **26.** Ditto, oblique view (arrow points to the scoop-shaped retrolateral cymbial apophysis); **27.** Ditto, dorsal view (NRC-AA-7708); **28.** Epigyne, ventral view (NRC-AA-7709); **29.** Vulva, dorsal view (NRC-AA-7709). **ECP**, epigynal coupling pocket. **CO**, copulatory opening. Scale bars: 0.1 mm.

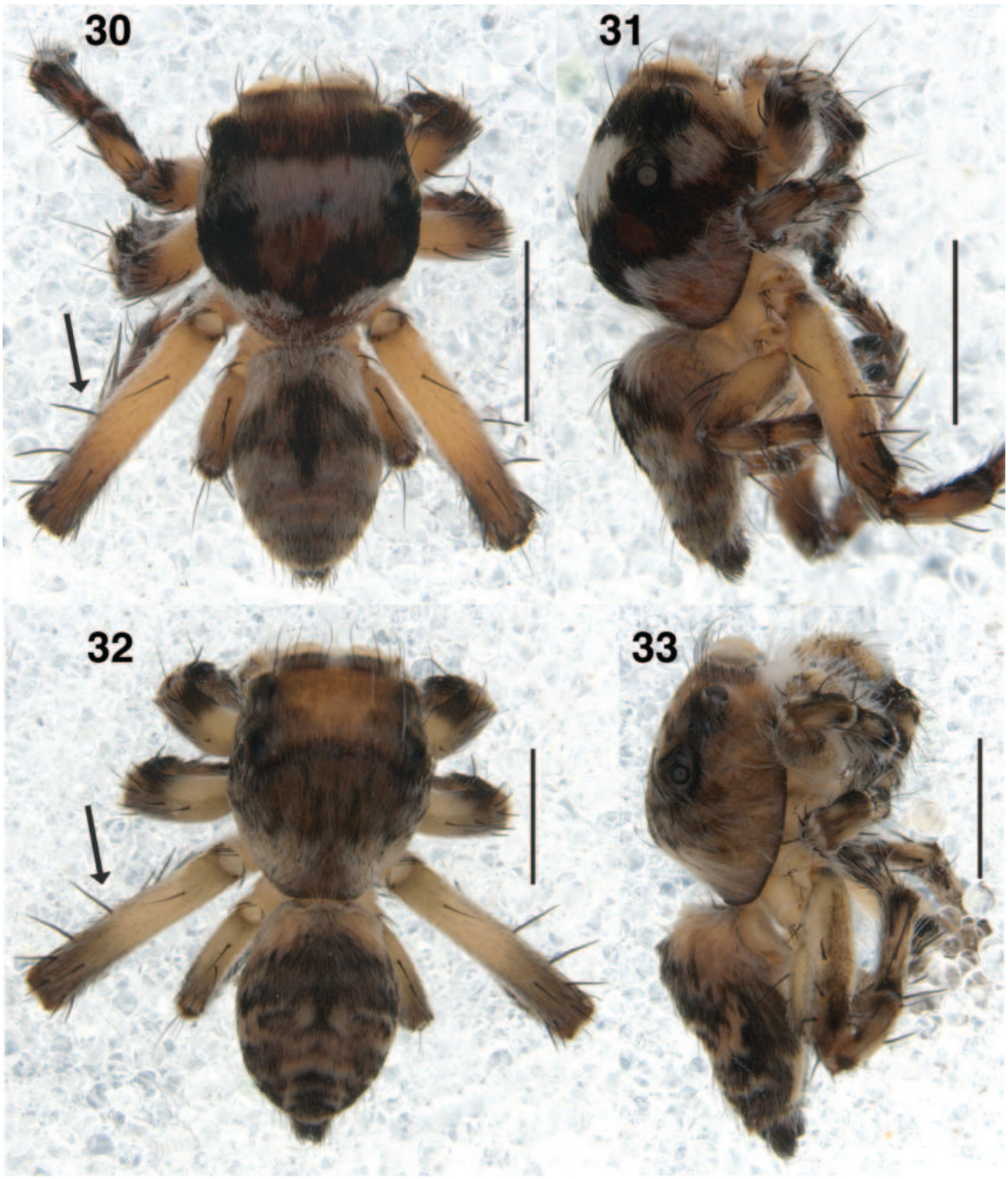

Figures 30–33. *Iranattus rectangularis* habitus. **30.** Male, dorsal view (NRC-AA-7708); **31.** Ditto, lateral view (NRC-AA-7708); **32.** Female, dorsal view (NRC-AA-7709); **33.** Ditto, lateral (NRC-AA-7709). Scale bars: 1 mm. Arrows in Figs **30** and **32** point to the elongated third legs.

Description. ♂ (NRC-AA-7708). Measurements: Carapace 1.46 long, 1.26 wide. Abdomen length 1.32, width 0.86. Leg measurements: Leg I 2.04 [0.69, 0.33, 0.48, 0.32, 0.22], leg II 1.88 [0.67, 0.33, 0.44, 0.28, 0.16], leg III 3.56 [1.52, 0.55, 0.72, 0.43, 0.34], leg IV 1.94 [0.70, 0.31, 0.34, 0.38, 0.24. Leg formula: III–I–IV–II. ***Carapace*** wider than abdomen. Ocular area shaped like an isosceles trapezoid, narrow at the anterior eye row and wide at the PLEs. PLEs on tubercles. Thoracic area slopes acutely downward behind ocular area. Ocular area from base of front eyes to PMEs orange, covered with black hairs, posterior with pale hairs. Pale erect hairs on ocular area. Pale hair patch beneath PMEs. Black hair band starts anteriorly, encircles carapace at ocular area edge. White band along lateral edge, narrow front, broadens posteriorly and behind. ***Clypeus*** narrow. Orange, covered with pale hairs, more densely near integument edge. ***Chelicerae*** vertical, narrow, yellowish brown. ***Palp*** (Figs 20, 21, 24–27): Embolus medium-long, starting at 9 o'clock, somewhat thick. RTA stout, short with blunt tip. Cymbium extends retrolaterally to form scoop-shaped apophysis. Tegulum prolaterally rounder; retrolaterally angular at distal and proximal edges. ***Legs*****:** III femur distinctly long relative to others. Femur yellowish, distal segments yellowish

Figures 34–41. *Iranattus rectangularis* habitus. **34–38.** Male; **39–41.** Female.

covered with black hair. ***Abdomen*** narrow, ovoid. Brown with gray hair overlay. Spinnerets brown.

♀ (NRC-AA-7709). Measurements: Carapace 1.91 long, 1.56 wide. Abdomen length 1.83, width 1.27. Leg measurements: Leg I 2.67 [0.95, 0.53, 0.56, 0.36, 0.27], leg II 2.41 [0.85, 0.47, 0.50, 0.32, 0.27], leg III 4.30 [1.78, 0.70, 0.92, 0.50, 0.40], leg IV 2.44 [0.87, 0.40, 0.42, 0.44, 0.31]. Leg formula III–I–IV–II. ***Carapace*** shape similar to male. Ocular area orange anteriorly, white hairs sparsely posteriorly. Pale erect hairs on ocular area. Thoracic slope covered with black hairs. Lateral sides covered with pale hairs, almost merging behind. ***Clypeus*** similar as in male. ***Chelicerae*** similar to male. ***Legs*** similar to male. ***Abdomen*** shape comparable to male, but with a 'kite'-shaped black color pattern between posterior edge and median. ***Epigyne*** (Figs 22, 23, 28–29): Medially located copulatory opening flanked by conical-shaped ECP.

Natural history. *Iranattus rectangularis* was collected from the branches of non-native *Vachellia tortilis* alongside artificial water canals in the Desert National Park, a xeric and desert ecosystem located in Rajasthan, India (Figs 42, 43). The mosaic of orange, black, and grey body coloration helps them blend in with the branches, making them inconspicuous, except that in the field, the orangish faces of males (Fig. 34) sometimes stood out.

Distribution. Iran, India (Rajasthan).

Figures 42, 43. *Iranattus rectangularis* habitat. **42.** *Vachellia tortilis* woodland; **43.** Aerial views of the landscape of the Desert National Park, Rajasthan, India.

Discussion. *Iranattus rectangularis* is reported for the first time east of Iran, in western India. This seemingly 'disjunct' distributional pattern is quite possibly due to a lack of collecting between the sites and mirrors that of *Stenaelurillus marusiki* Logunov, 2001 (Salticidae: Aelurillina), where the type locality of *S. marusiki* is Iran. However, it has been reported much farther southeast in Maharashtra, India (Marathe et al. 2022). With the transfer of *Iranattus* to Plexippina, the subtribe now contains 35 genera, and the number of plexippines in India stands at 47 species and 18 genera.

Acknowledgements

Collection of *I. rectangularis* was facilitated by the Bustard Recovery Programme of the Wildlife Institute of India (WII), funded by the National Compensatory Afforestation Fund Management and Planning Authority, Government of India, and supplemented by an additional grant from the Rajasthan State Pollution Control Board. RT and AVS thank Rev. Fr. Jolly Andrews, CMI of Christ College (Irinjalakuda), for facilities and NCBS research collections. RT acknowledges the support of Dr. Sutirtha Dutta, Dr. Manju Siliwal, and Mr. Ashish Kumar Jangid from WII, as well as the Rajasthan State Forest Department, for the collecting permit. Special thanks to Sohan Lal Genwa and Amrat Genwa for their assistance during field activities. RT thanks Anshuman Pati and Jason D. Gerard for habitat photographs. RT acknowledges CSIR-UGC for fellowship. KM thanks Dr. Krushnamegh Kunte, NCBS, for providing the lab space and supplies. KM and WPM thank Carol Ritland and Allyson Miscampbell of the Genetic Data Centre at the University of British Columbia for assistance with lab facilities. We thank J. Beccaloni (NHMUK) for the loan of *I. principalis* specimens. We thank Galina Azarkina for providing information on additional material of *I. principalis* she examined. We thank Dmitry Logunov, Galina Azarkina, and Tamás Szűts for their time reviewing the manuscript and providing valuable comments. Funding to WPM was provided by an NSERC Canada Discovery Grant.

References

Bodner MR, Maddison WP (2012) The biogeography and age of salticid spider radiations (Araneae: Salticidae). Molecular Phylogenetics and Evolution 65(1): 213–240. https://doi.org/10.1016/j.ympev.2012.06.005

Castresana J (2000) Selection of conserved blocks from multiple alignments for their use in phylogenetic analysis. Molecular Biology and Evolution 17(4): 540–552. https://doi.org/10.1093/oxfordjournals.molbev.a026334

Faircloth BC (2013) illumiprocessor: a trimmomatic wrapper for parallel adapter and quality trimming. https://doi.org/10.6079/J9ILL

Faircloth BC (2016) PHYLUCE is a software package for the analysis of conserved genomic loci. Bioinformatics (Oxford, England) 32(5): 786–788. https://doi.org/10.1093/bioinformatics/btv646

Faircloth BC (2017) Identifying conserved genomic elements and designing universal bait sets to enrich them. Methods in Ecology and Evolution 8(9): 1103–1112. https://doi.org/10.1111/2041-210X.12754

Katoh K, Standley DM (2013) MAFFT Multiple Sequence Alignment Software Version 7: Improvements in Performance and Usability. Molecular Biology and Evolution 30(4): 772–780. https://doi.org/10.1093/molbev/mst010

Maddison WP (2015) A phylogenetic classification of jumping spiders (Araneae: Salticidae). The Journal of Arachnology 43(3): 231. https://doi.org/10.1636/arac-43-03-231-292

Maddison WP, Hedin MC (2003) Jumping spider phylogeny (Araneae : Salticidae). Invertebrate Systematics 17(4): 529. https://doi.org/10.1071/IS02044

Maddison DR, Maddison WP (2023a) Zephyr: a Mesquite package for interacting with external phylogeny inference programs. http://zephyr.mesquiteproject.org

Maddison WP, Maddison DR (2023b) Mesquite: a modular system for evolutionary analysis. http://www.mesquiteproject.org/ [August 18, 2023]

Maddison WP, Bodner MR, Needham KM (2008) Salticid spider phylogeny revisited, with the discovery of a large Australasian clade (Araneae: Salticidae). Zootaxa 1893(1): 49. https://doi.org/10.11646/zootaxa.1893.1.3

Maddison WP, Beattie I, Marathe K, Ng PYC, Kanesharatnam N, Benjamin SP, Kunte K (2020) A phylogenetic and taxonomic review of baviine jumping spiders (Araneae, Salticidae, Baviini). ZooKeys 1004: 27–97. https://doi.org/10.3897/zookeys.1004.57526

Marathe K, Sanap R, Joglekar A, Caleb JTD, Maddison WP (2022) Three new and notes on two other jumping spider species of the genus *Stenaelurillus* Simon, 1886 (Salticidae: Aelurillina) from the Deccan Plateau, India. Zootaxa 5125(1): 1–19. https://doi.org/10.11646/zootaxa.5125.1.1

Marathe K, Maddison WP, Kunte K (2024) *Ghatippus paschima*, a new species and genus of plexippine jumping spider from the Western Ghats of India (Salticidae, Plexippini, Plexippina). ZooKeys 1191: 89–103. https://doi.org/10.3897/zookeys.1191.114117

Nguyen L-T, Schmidt HA, Von Haeseler A, Minh BQ (2015) IQ-TREE: A fast and effective stochastic algorithm for estimating maximum-likelihood phylogenies. Molecular Biology and Evolution 32(1): 268–274. https://doi.org/10.1093/molbev/msu300

Nurk S, Bankevich A, Antipov D, Gurevich A, Korobeynikov A, Lapidus A, Prjibelsky A, Pyshkin A, Sirotkin A, Sirotkin Y, Stepanauskas R, McLean J, Lasken R, Clingenpeel SR, Woyke T, Tesler G, Alekseyev MA, Pevzner PA (2013) Assembling Genomes and Mini-metagenomes from Highly Chimeric Reads. In: Deng M, Jiang R, Sun F, Zhang X (Eds) Research in Computational Molecular Biology. Lecture Notes in Computer Science. Springer Berlin Heidelberg, Berlin, Heidelberg, 158–170. https://doi.org/10.1007/978-3-642-37195-0_13

Prószyński J (1992) Salticidae (Araneae) of the Old World and Pacific Islands in several US collections. Annales Zoologici, Warszawa 44: 87–163.

Prószyński J (2017) Pragmatic classification of the world's Salticidae (Araneae). Ecologica Montenegrina 12: 1–133. https://doi.org/10.37828/em.2017.12.1

Stamatakis A (2014) RAxML version 8: A tool for phylogenetic analysis and post-analysis of large phylogenies. Bioinformatics (Oxford, England) 30(9): 1312–1313. https://doi.org/10.1093/bioinformatics/btu033

Talavera G, Castresana J (2007) Improvement of Phylogenies after Removing Divergent and Ambiguously Aligned Blocks from Protein Sequence Alignments. Kjer K, Page R, Sullivan J (Eds) Systematic Biology 56: 564–577. https://doi.org/10.1080/10635150701472164

Wanless FR (1985) A revision of the spider genera *Holcolaetis* and *Sonoita* (Araneae: Salticidae). Bulletin of the British Museum (Natural History). Bulletin of the British Museum, Natural History. Zoology 48: 249–278. https://doi.org/10.5962/bhl.part.23463

Wesołowska W (2000) New and little known species of jumping spiders from Zimbabwe (Araneae: Salticidae). Arnoldia Zimbabwe 10: 145–174.

Wesołowska W, Russell-Smith A (2011) Jumping Spiders (Araneae: Salticidae) from Southern Nigeria. Annales Zoologici 61(3): 553–619. https://doi.org/10.3161/000345411X603409

Wesołowska W, Russell-Smith A (2022) Jumping spiders from Ivory Coast collected by J.-C. Ledoux (Araneae, Salticidae). European Journal of Taxonomy 841(1): 1–143. https://doi.org/10.5852/ejt.2022.841.1943

World Spider Catalog (2024) World Spider Catalog. https://wsc.nmbe.ch/ [August 18, 2023]

Zhang J, Li Z, Lai J, Zhang Z, Zhang F (2023) A novel probe set for the phylogenomics and evolution of RTA spiders. Cladistics 39(2): 116–128. https://doi.org/10.1111/cla.12523

Zoosyst. Evol. 100 (2) 2024, 543–553 | DOI 10.3897/zse.100.121238

PENSOFT

MUSEUM FÜR NATURKUNDE BERLIN

A new species of *Cyrenoida* (Bivalvia, Cyrenoididae) from the Western Atlantic, with remarks on Cyrenoididae anatomy

Bárbara L. Valentas-Romera[1], Luiz Ricardo L. Simone[1], Rodrigo Cesar Marques[2]

1 *Museu de Zoologia da Universidade de São Paulo, Laboratório de Malacologia, Avenida Nazaré, 481, CEP:04263–000, São Paulo, Brazil*

2 *Universidade Federal dos Vales do Jequitinhonha e Mucuri - Campus JK, Departamento de Ciências Biológicas (DCBio-FCBS), Rodovia MGT, 367, CEP 39100–000, Diamantina, Brazil*

https://zoobank.org/552EBECE-2FAB-4C54-8171-047763535D67

Corresponding author: Bárbara L. V. Valentas-Romera (barbarella.lou@gmail.com)

Academic editor: Thomas von Rintelen ♦ **Received** 20 February 2024 ♦ **Accepted** 3 April 2024 ♦ **Published** 14 May 2024

Abstract

Cyrenoida implexa **sp. nov.** is the first species of Cyrenoididae in the Southern West Atlantic. This new species exhibits external similarities to *C. floridana* but is distinguished by distinct right hinge dentition, larger siphons and a more extensive siphonal area at the mantle border, an incurrent siphon with three rows of papillae, a lack of papillae at the middle mantle fold, and smaller adductor muscle volume. In the environment, it possesses a higher saline tolerance than *C. floridana*.

Key Words

Anatomy, Bivalvia, *Cyrenoida*, Cyrenoididae, estuary, mangrove, taxonomy, Western Atlantic

Introduction

Mangroves and estuaries globally face numerous challenges (Lugo et al. 2014; Romañach et al. 2018). These environments have increasingly garnered attention, prompting extensive study and protection efforts. Consequently, public and political awareness of their economic, cultural, and social significance has heightened (Romañach et al. 2018; Moore et al. 2022). This increased attention has facilitated advancements in understanding the inhabitants of these unique environments.

In Brazil, studies on mangroves and estuaries have shed light on various topics, including litter (e.g. Duarte et al. 2023; Cavalcante et al. 2024), carbon storage (e.g. Mariano Neto et al. 2024), impacts of urbanization (e.g. Saad et al. 2019), and faunal distribution (e.g. Barroso and Matthews-Cascon 2009; Rodrigues et al. 2016). As anticipated, the advancement of these studies has resulted in the discovery of new species.

Cyrenoida Joannis, 1835, is a poorly known genus comprising six living species with infaunal filter-feeding habits that inhabit nutrient-rich sediments in the brackish waters of estuaries and mangroves across Western Africa, the Western Atlantic, the Eastern Pacific of North and Central America, and the Caribbean islands (Coan and Valentich-Scott 2012; Huber 2015; Valentas-Romera et al. 2019; Wu et al. 2023). Historically, this genus has been associated with lucinids, but recent phylogenetic studies have placed it within the Cyrenoididae, primarily consisting of species found in brackish, estuarine, or freshwater environments (Taylor et al. 2009; Lemer et al. 2019; Wu et al. 2023). Presently, the bulk of data on this taxon stems from a single species, *Cyrenoida floridana* Dall, 1896. However, *C. floridana* is restricted in distribution to North and Central America, the Caribbean, and Suriname, and is rare in scientific collections (Valentas-Romera et al. 2019).

With the goal of enhancing mollusk records along the Brazilian coast and advancing the understanding of taxonomy, morphology, and anatomy within *Cyrenoida*, a new species, *Cyrenoida implexa* sp. nov., is described based on shell and soft tissue data. Additionally, a brief comparison between the new species and *C. floridana* is conducted, expanding the morphological, anatomical, and physiological characterization of the genus and shedding light on new avenues for future research concerning this genus.

Methods

The specimens were initially identified as *Cyrenoida* sp. in Barroso and Matthews-Cascon (2009), Rodrigues et al. (2016), and Saad et al. (2019). Morphology of dry shells and anatomy of soft parts were studied using standard techniques (Valentas-Romera et al. 2019). All depictions of soft parts in this study are based on specimens from lots MZSP 99988 and MZSP 109105. Scanning electron microscopy (SEM) was provided by the Laboratório de Microscopia Eletrônica from the Museu de Zoologia of the Universidade de São Paulo.

The following abbreviations are used in the anatomical descriptions and figures: **aa:** anterior adductor muscle; **an:** anus; **ar:** anterior pedal retractor muscle; **au:** auricle; **cc:** cerebral connective; **cg:** cerebral ganglia; **cg:** cerebral ganglia; **dd:** digestive diverticula; **dg:** digestive gland; **dh:** dorsal hood; **dm:** dorsal siphonal retractor muscles; **eo:** excurrent opening; **er:** esophageal rim; **es:** esophagus; **ex:** excurrent siphon; **fg:** food groove; **fo:** esophageal folds; **fs:** F-shaped tooth **ft:** foot; **gf:** gill fusion; **gi:** gill; **go:** gonad; **gp**: genital pore; **gs:** gastric shield; **id:** inner demibranch; **if:** mantle border inner fold; **in:** intestine; **io:** incurrent opening; **ip:** inner palp; **ir:** inner row of siphonal papillae; **is:** incurrent siphon; **ki:** kidney; **lc:** left caecum; **li:** ligament; **lp**: left pouch; **lv:** inverted-V-shaped tooth; **mf:** mantle border middle fold; **mo:** mouth; **mr:** middle row of siphonal papillae; **mt:** major typhlosole; **np:** nephropore; **nt:** minor typhlosole; **od:** outer demibranch; **of:** mantle border outer fold; **op:** outer palp; **or:** outer row of siphonal papillae; **pa:** posterior adductor muscle; **pg:** pedal ganglia; **pl:** pallial line; **pm:** pallial muscle; **pp:** papillae; **pr:** posterior pedal retractor muscle; **rc:** right caecum; **sa1:** sorting area 1; **sa2:** sorting area 2; **sa3:** sorting area 3; **ss:** style sac; **st:** stomach; **t1:** large lateral tooth of right valve; **t2:** cardinal tooth of right valve; **t3:** small lateral tooth of right valve; **t4:** lateral tooth of left valve; **t5:** posterior cardinal tooth of left valve; **t6:** anterior cardinal tooth of left valve; **ub:** umbones; **ve:** ventricle; **vg:** visceral ganglia; **vm:** ventral siphonal retractor muscles.

Institutional abbreviations: **MZSP:** Museu de Zoologia da Universidade de São Paulo.

Results

Superfamily Cyrenoidea J. E. Gray, 1840
Family Cyrenoididae H. Adams & A. Adams, 1857 (1853)
Genus *Cyrenoida* Joannis, 1835

***Cyrenoida implexa* sp. nov.**

https://zoobank.org/B12440D9-ABCB-4A6B-8E8A-528C8C697ED3
Figs 1–23

Diplodonta punctata: Barroso and Matthews-Cascon 2009: 82–83 (non Say, 1822).

Cyrenoida sp.: Rodrigues et al. 2006: 395, 397; Huber 2015: 812; Saad et al. 2019: 5–6.

Types. ***Holotype*:** BRAZIL • specimen; MZSP 54637. Paratypes: 40 specimens; same locality as holotype; Barroso C.X. leg.;17 Oct.2005; MZSP 99988.

Type locality. BRAZIL. **Ceará**; Fortaleza, Ceará River estuary, Parque Soledade, 3°42'07.94"S, 38°36'36.22"W, IX Martins leg., 17.x.2005.

Extra material examined. BRAZIL • 1 specimen; **Maranhão**, São Luís, São Marcos Bay, Carangueijos Island, Igarapé mangrove; 2011; MZPS 100525. 2 specimens: **São Paulo**, São Vicente, Branco River mangrove; 23°56'17"S, 46°25'12"W; 2 Jul. 2011; Saad, L.O. leg.; MZSP 109103. 06 specimens; 08 Feb. 2012; Saad, L.O. leg; MZSP 109105. 2 specimens: Peruíbe, Una River mangrove, Ecological Station Juréia Itatins; 24°25'33"S, 47°05'05"W; 03 Apr.2012; Saad, L.O. leg; MZSP 109104.

Measurements (length, height, and maximum width in mm). MZUSP 54637: 7.2 by 7.3 by 4.3; MZSP 99988 #1: 7.1 by 6.9 by 4; #2: 8.2 by 8.3 by 4.5; #3: 6.7 by 6.6 by 3.6; #4: 6.7 by 6.2 by 3.4; #5: 4.9 by 4.6 by 2.9; #6: 5.4 by 5 by 3.1; #7: 6.8 by 6.3 by 3.4; #8: 6.1 by 5.5 by 3.3; #9: 5.5 by 5.3 by 3.3; MZSP 100525: 7.7 by 7.2 by 4.1.

Diagnosis. Shell rounded to subquadrate, posteriorly pointed; umbones high, thin; valves fragile; periostracum thin, light brown. Internal surface opaque; no nacreous aspect; no distinguishable muscular impression or pallial line. Hinge with laminar cardinal and lateral teeth; right hinge with inverse V-shaped tooth, formed by fusion between cardinal and lateral tooth; laminar, lateral tooth; left valve with recumbent F-shaped teeth, formed by fusion of two cardinal teeth and lateral tooth. Nymph is long and thin.

Description. Shell (Figs 1–7): Outline rounded to subquadrate, with ventral margin slightly posteriorly pointed. Width ~55% of shell length. External surface covered with well-marked growth lines. Equivalve, almost equilateral, ~5% longer than high, reaching maximum length of ~8 mm. Laterally inflated, width ~55% of total shell length. Externally white, adorned only by growth lines. Periostracum thin, light brown; slightly wrinkled at ventral shell margin (Figs 1, 2). Walls thin, fragile. Umbones central, prosogyre, low, ~6% of total shell height and ~27% of shell length, located almost at midpoint of shell length (Fig. 5). Internal surface opaque (Figs 3, 4). Muscle scars and pallial line almost imperceptible. Anterior adductor muscle scar reniform, occupying ~1.32% of total internal surface; twice higher than wide, located at mid third of shell height; Posterior adductor muscle scar oval, occupying ~1.49% of total internal surface; located at mid-third of shell height. Pallial line entire, away from shell margins ~8% of shell height. Hinge heterodont (Figs 6, 7): right valve with inverse V-shaped tooth (Fig. 7: lv), looking fusion between short cardinal tooth and long lateral tooth, with ~1% of total shell length and single laminar lateral tooth (Fig. 7: t3) located under inversed V-shaped tooth, ~38% longer than superior lateral tooth, forming groove between superior and inferior lateral teeth. Left valve with recumbent F-shaped tooth (Fig. 6: fs), forming ~90° angle, with bifid appearance, looking fusion of two cardinal tooth (t5, t6) at one lateral

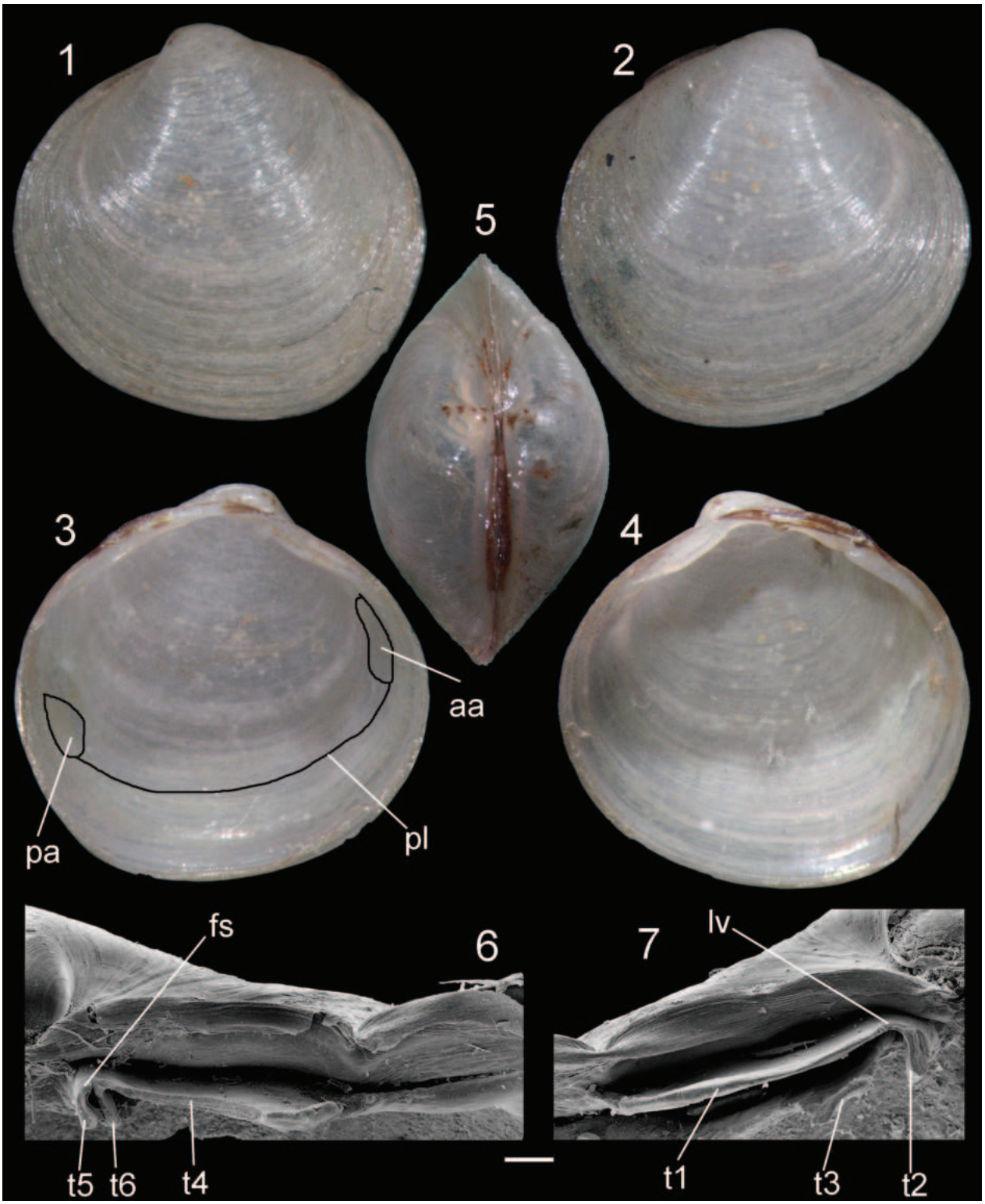

Figures 1–7. Holotype of *Cyrenoida implexa* sp. nov. (MZSP 54637, 7.2 mm, H 7.3 mm, W 4.3 mm). **1.** Left valve, outer view; **2.** Right valve, outer view; **3.** Left valve, inner view; **4.** Right valve, inner view; **5.** Whole dorsal view; **6.** Right hinge under SEM; **7.** Left hinge under SEM. Scale bar: 200 μm (**6, 7**).

tooth (t4). Dorsal margin concave. Ligament parvincular, opisthodetic, length ~40% of total shell length. Nymph ~9 times longer than wide, shape rhomboid. Lunule and escutcheon absent.

Main muscle system (Figs 8, 9, 13): Anterior adductor (aa) muscle reniform in transverse section, twice heigh than wide; ventral portion ~2.5 times wider than dorsal portion; occupying ~5% of total internal shell volume; located at median third of valve, clearly divided into quick and slow components, quick component occupying ~30% of anterior portion of muscle, dark grey in color, slow component occupying ~70% of posterior portion of muscle, light cream in color. Posterior adductor muscle (**pa**) elliptical in cross section, ~1.5 times wider than tall,

~30% shorter and ~1.3 times wider than anterior adductor muscle, located at opposite extremity of anterior adductor muscle, clearly divided into quick and slow components, the former occupying ~45% of posterior portion of muscle, dark gray in color, the latter occupying ~55% of anterior portion of muscle, light cream in color. Pair of foot anterior retractor muscles (ar) oval in section, thin, elongated; originated dorsally at anterior adductor muscle; running posteriorly and ventrally at ~20% of total shell length; both branches fusing at anterior edge of foot base. Pair of foot posterior retractor muscled (pr) oval in section, thin; originated dorsally at posterior adductor muscle; ~50% longer than pair of anterior retractors; both fusing posterior edge of foot base (Fig. 11). Two pairs of siphonal retractor muscles; dorsal siphonal retractors (dm) ~6 times longer than wide; insertion almost at central portion of mantle lobe, 2 times as long as excurrent opening, originating laterally at half of siphonal base height; ventral siphonal retractors (vm) thin, ~5 times longer than wide, length ~65% of total length of dorsal siphonal muscle, originating at ventral end of inhalant opening.

Foot and byssus (Figs 8, 11): Foot (ft) short; relaxed length ~50% of total shell height. Laterally flattened; end blunt, swollen. Foot base at median portion visceral sac. Byssus or byssal groove.

Mantle (Figs 8, 9, 11): Mantle lobes symmetrical, thin, translucent, colorless. Pallial muscles (pm) reunited in long muscles, distributed sparsely along ventral side of mantle lobe; height ~12% of total shell length, separated from each other by ~15 times pallial muscle basal width. Mantle edge trifolded (Fig. 9), unpigmented; outer fold (of) thick, ~7 times taller than wide; middle fold (mf) short, half of total outer fold height, same width; inner fold (if) short, length ~20% of outer fold height, ~30% of its width. Periostracum produced between external and middle fold. Mantle lobes totally free except for siphonal area. Anterior mantle fusion occurring at ~45% of anterior adductor muscle height; posterior mantle fusion occurring at ~68% of posterior adductor muscle height (Fig. 11). Siphonal area corresponding to ~42% of total mantle lobe length. Mantle lobes mostly free from each other, except for siphonal area, relative to 42% of mantle lobe total length (more details below).

Pallial cavity (Figs 8, 10–14, 16): Occupying about half of inner shell volume. Palps small, occupying ~30% of total shell volume. Pair of hemipalps triangular (Figs 11, 16), ~20% shorter but same width of insertion area of anterior adductor muscle; pair of external hemipalps (op) connected at mantle lobe by hemipalp dorsal border, in half of hemipalp length; pair of internal hemipalps (ip) connected at visceral mass by dorsal border, in ~30% of total hemipalp length. Internal surface of both palps covered by ~24 transverse folds; internal hemipalp folds high and rounded, covering ~90% of hemipalp internal surface, forming thin smooth area at hemipalp borders corresponding ~1% of total hemipalp internal area, folds decreasing towards mouth, forming shallow channels towards mouth (mo). Gills area ~30% of total valve area; outer demibranch (od) fusiform, twice longer than wide, folded on ~30% of total demibranch extension, covering pericardium and kidney areas, connected to mantle lobe by ~15% of total length of dorso posterior border of demibranch. Inner demibranch (id) triangular, ~twice longer than wide, folded on half of demibranch total extension, ~40% of internal demibranch area covered by external demibranch (Fig. 8); presenting food groove (fg); demibranchs connected to each other by tissue at posterior end, in ~20% of total gill length (Fig. 12). Suprabranchial chamber volume ~60% of infrabranchial chamber volume. Incurrent (is) and excurrent (ex) siphons originated by inner mantle fold; length ~30% of total shell length; each one ~3 times longer than wide in retracted condition; externally fused with each other; internally separated by thick, smooth muscular wall. Inner siphonal openings directly to pallial cavity (Figs 11, 14). Incurrent siphon length ~20% of total shell length, height ~1% of total shell height. Excurrent siphon length ~80% of inhalant siphon length; same width. Distal opening of incurrent siphon flanked by three rows of papillae (Fig. 14: ir, mr, or); papillae length equivalent ~5% of total inhalant siphon length. Distal opening of excurrent siphon with single row of flattened papillae (Fig. 14: 9p). Siphon attached to mantle by 2 pairs of muscle described above.

Visceral mass (Fig. 11): Visceral sac occupying half of inner shell volume; shape triangular. Slightly flattened; twice wider than muscular base; located dorsally at foot retractor muscles; ~20% of anterior portion filled with digestive diverticula of brown color; remaining areas with gonad of cream color. Stomach and style sac located vertically at central region.

Circulatory and excretory systems (Figs 11, 15, 23): Pericardium located dorsally in posterior half of visceral sac, between posterior portion of umbonal cavity and dorsal surface of kidney; twice longer than wide; occupying ~25% of total visceral sac volume. Pair of auricles (au) antero posteriorly long; connected to central axis of gill in ~30% of total auricle length; walls thin, translucent walls thin; located at central portion of pericardium; surrounding ~50% of intestinal portion crossing pericardium; connected to auricles in median portion of lateral walls. Kidney (ki) located postero ventrally at visceral mass (Figs 11, 15), below posterior end of pericardium and dorsal surface of posterior foot retractor muscles, color light brown; shape triangular, occupying ~25% of visceral mass volume. Gonopore (gp) rounded, located at posterior portion of visceral mass, at ~25% of visceral mass height, opening in suprabranchial chamber, next to nephropore (np).

Digestive system (Figs 16, 20–22): Palps and digestive diverticula described above. Mouth small, located in central portion at intersection of palps (Fig. 16), lips small. Esophagus (es) elongate, narrow, cylindric; length and height respectively ~16% and 1% of total visceral sac; no contact with anterior adductor muscle; passing through anterior portion of foot anterior retractors; internal surface with low longitudinal folds (fo); low esophageal rim (er) at stomach entrance; stomach (Figs 20–21: st) occupying

~25% of total visceral sac volume; shape elliptical, funnel-like; located slightly posteriorly to umbones; length ~80% of total visceral sac length, ~30% of visceral sac heigh; posterior portion ~60% wider than anterior portion. Paired apertures to digestive caeca located ventro-laterally of gastric anterior portion, in transition with esophagus; turned to ventral side of visceral sac. Dorsal hood (dh) narrow, thin, length ~25% of total stomach length, distally

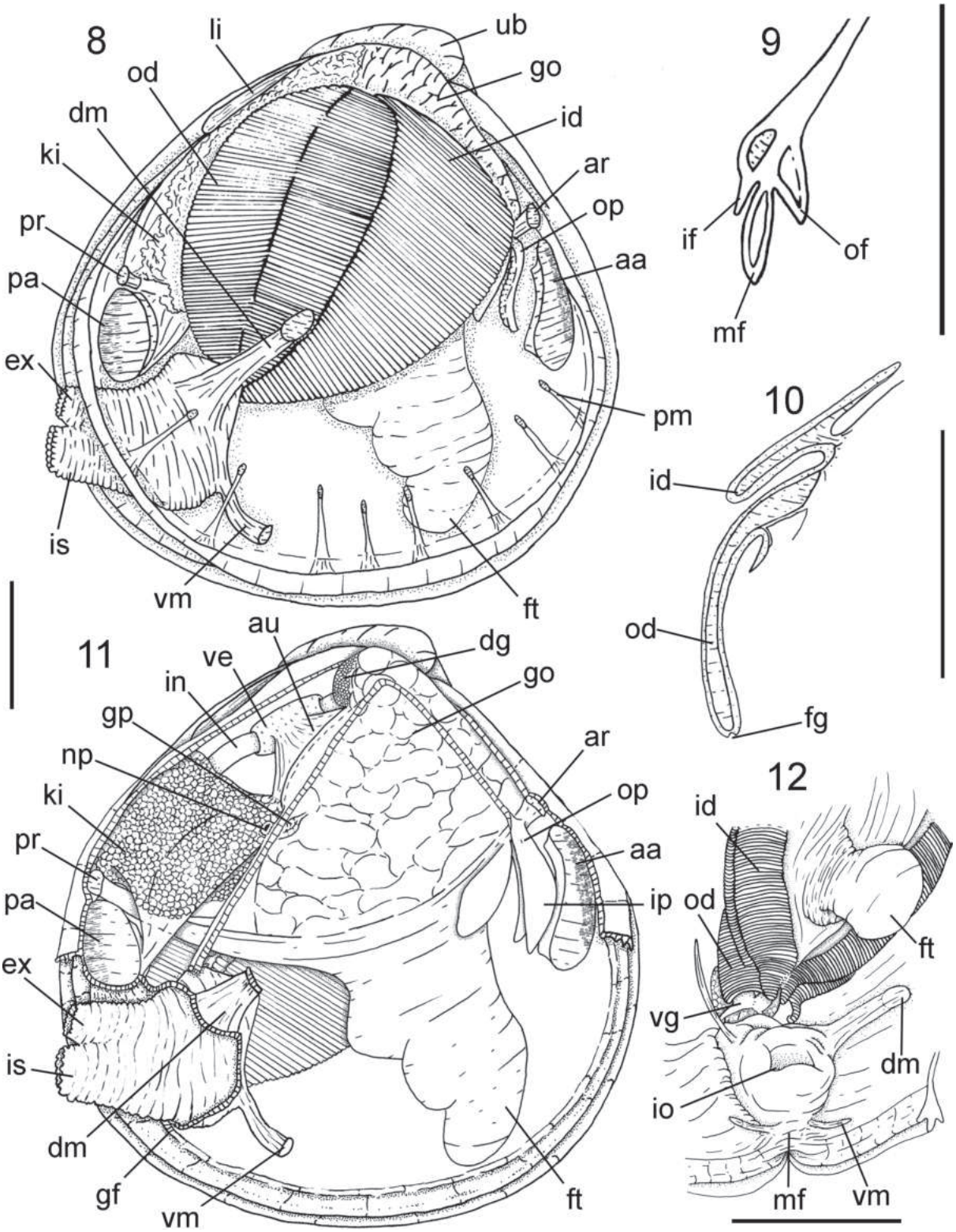

Figures 8–12. *Cyrenoida implexa*, anatomical drawings. **8.** Right view, valve removed, structures seen by transparency of mantle lobe; **9.** Mantle border, transverse section in its ventromedial portion; **10.** Gill, transverse section in its central portion; **11.** Right view, right mantle, and gill removed; **12.** Postero-ventral visceral region, ventral view, showing fusion of inner demibranchs in siphonal base and mantle fusion at siphonal area. Scale bars: 2 mm.

pointed. Left pouch (lp) located below anterior portion of dorsal hood, anteriorly to connection of digestive diverticula; shallow and wide; occupying ~20% of total area of left external wall of stomach. Internal surface of stomach (Fig. 22) mostly smooth, covered by three sorting areas well defined. First sorting area starting at left side of esophageal rim, running along dorsal wall of anterior stomach chamber, penetrating dorsal hood, narrow, comprised of small transverse folds (sa1). Second sorting area originating ventral to first sorting area, at left side of esophageal rim, running along left wall of anterior stomach chamber, entering left pouch and dorsal hood, both on their ventral surfaces, broad, formed by thickening of stomach wall (sa2). Third sorting area starting inside dorsal wall of dorsal hood, running along dorsal and right walls of posterior stomach chamber, until diffusing on ventral portion of right wall (sa3). Gastric shield (gs) located at central dorsal wall, occupying ~30% of total gastric area, with two anterior projections, one dorsal at left border, penetrating dorsal hood, and one left ventral, penetrating left pouch. Two narrow, tall gastric ridges running along ventral stomach chamber, forming major and minor typhlosoles at style sac opening. Longer ridge originating at ventral surface of stomach, surrounding left digestive diverticula, penetrating style sac at its right side, forming major typhlosole (mt). Shorter fold originating at style sac entrance, at region of major typhlosole penetration into style sac, forming rim bordering style sac entrance and

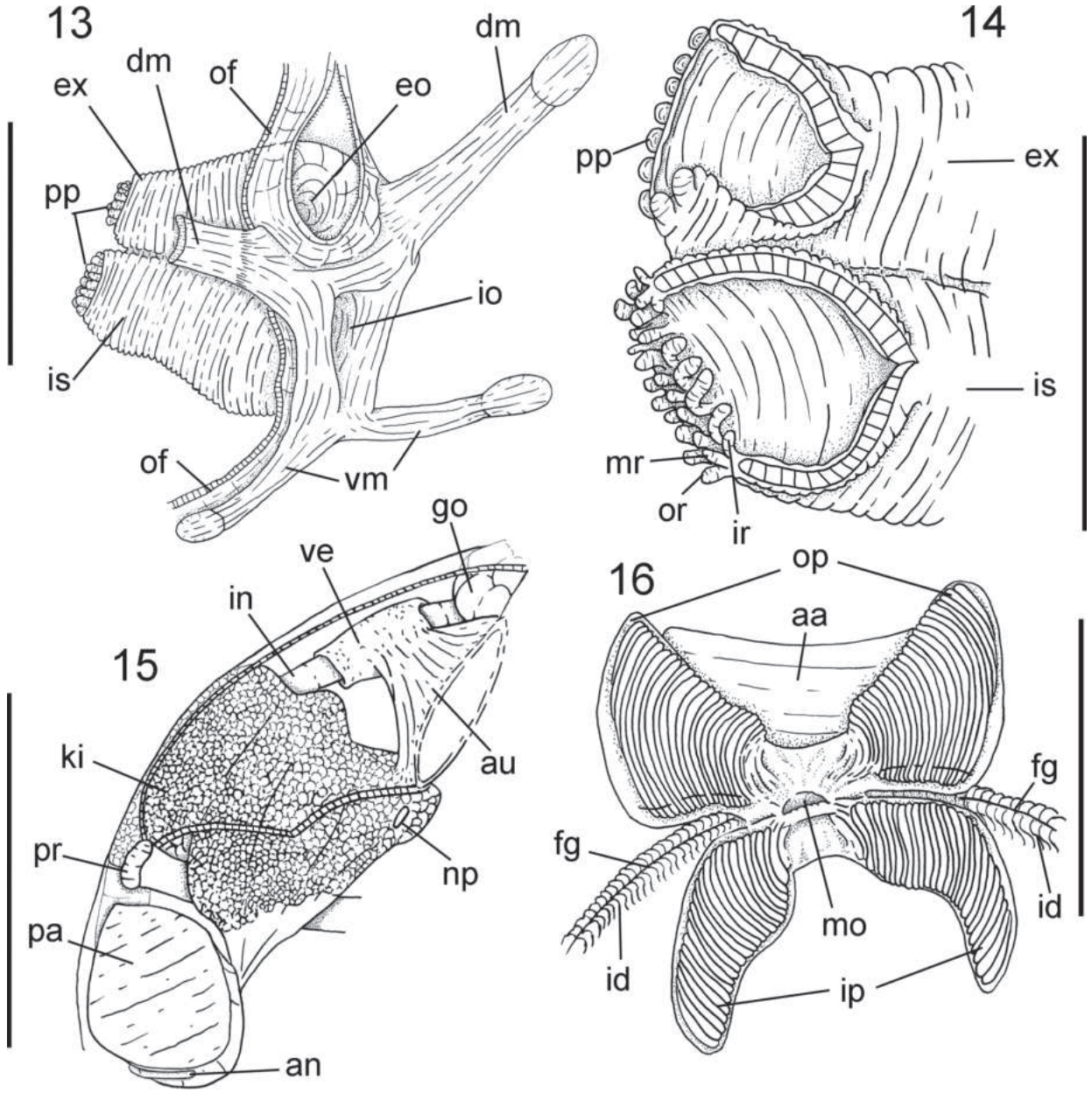

Figures 13–16. *Cyrenoida implexa* anatomical drawings. **13.** Incurrent and excurrent siphons, anterolateral view, right mantle lobe partially removed, some adjacent structures shown; **14.** Siphon tips; right view, both partially sectioned longitudinally; **15.** Pericardial region and kidney, right view, right mantle wall partially removed; **16.** Labial palps, ventral view, outer hemipalps deflected dorsally. Scale bars: 2 mm.

ultimately minor typhlosole (nt). Style sac (ss) connecting ventrally to dorsal portion of stomach; conical; tapering in ventral surface of visceral sac; ~3.5 times longer than wide; occupying ~16% of total visceral sac volume; height equivalent to half of visceral sac total length, length ~1% of visceral sac length. Intestine (in) narrow, long; starting in style sac; performing an inverted U-shaped loop under the anterior portion of the stomach, reaching the style sac high (Fig. 20), running towards dorso-posterior region of visceral sac parallel to style sac; leaving posterior portion of visceral sac, crossing pericardium and kidney; passing between posterior ends of foot posterior retractor muscles. Flanking entire posterior surface of posterior adductor muscle. Anus (an) on ventral surface of posterior adductor muscle; intestine total length ~9 times longer than style sac. Anus simple, sessile.

Genital system (Figs 11, 15): Gonads described above. Pair of gonoducts receiving sort of gonad acini along length along anterior portion of visceral sac. Genital pore simple, located at posterior region of visceral sac (Fig. 11: gp), opening next to nephropore (Figs 11, 15: np).

Central nervous system (Figs 17–19): Pair of cerebral ganglia (Fig. 17: cg) surrounding anterior dorsal half of esophagus, dorsally to labial palps; shape slightly triangular; longer than wide; size ~50% of esophagus width; cerebral commissure (cc) length ~60% of each ganglion length; from anterior portion connecting anterior adductor muscle nerve, bifurcating in two branches, internal branch

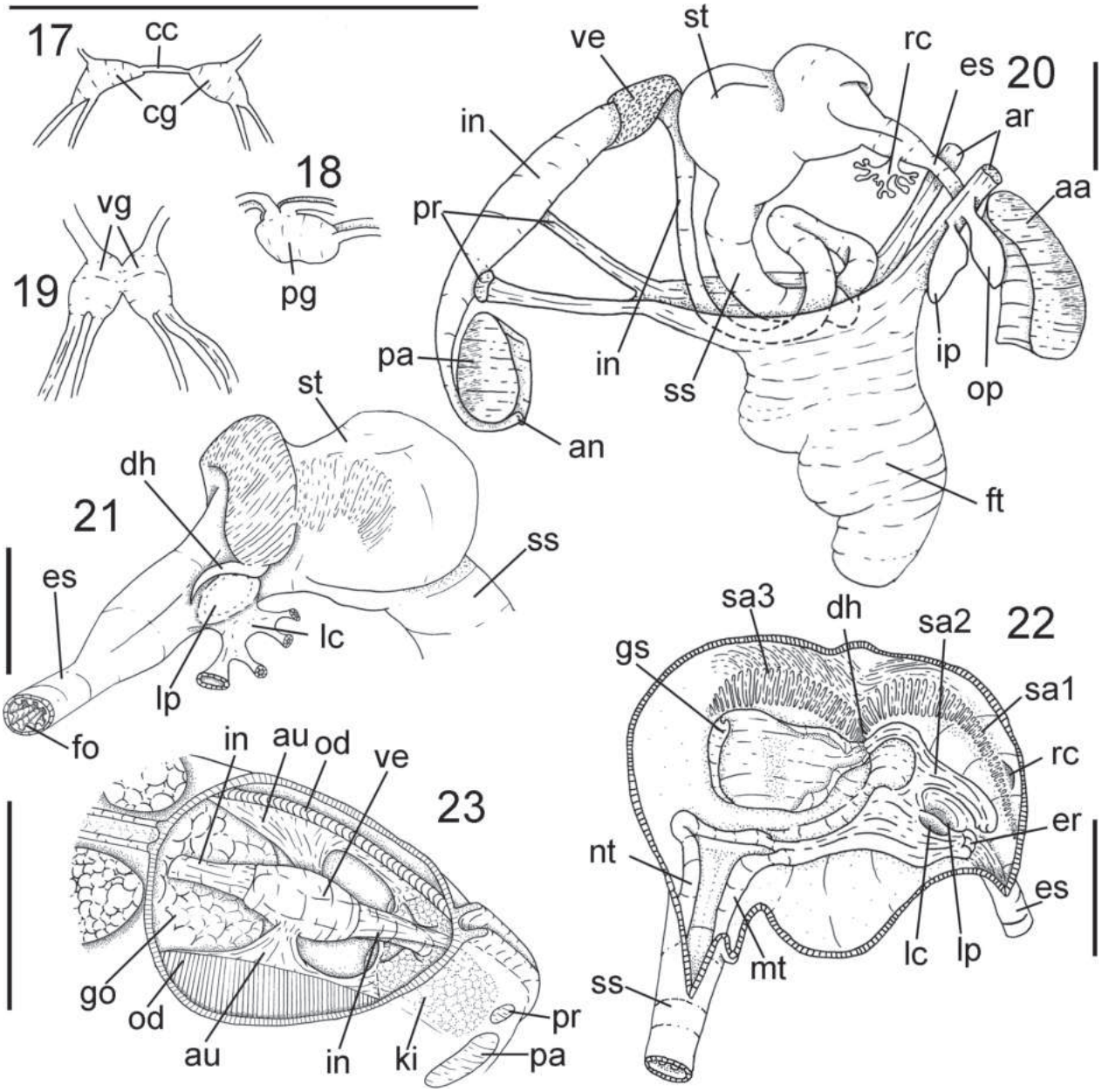

Figures 17–23. *Cyrenoida implexa* anatomical drawings. **17.** Cerebral ganglia, ventral view; **18.** Pedal ganglia, right view; **19.** Visceral ganglia, ventral view; **20.** digestive tubes and main musculature as in situ, right lateral view; **21.** stomach, left lateral view; **22.** Pericardial region, posterodorsal view, dorsal mantle wall partially removed; **23.** stomach, right lateral view, right wall opened and deflected to show inner gastric surface. Scale bars: 2 mm.

penetrating dorso posterior third of muscle and leaving at ventral surface of muscle; other branch bordering posterior surface of anterior muscle, both branches fusing at ventral region of anterior muscle; two connectives originating dorsally in ganglia, anteriorly to cerebro-visceral connective crossing visceral mass, touching gonopore dorsally, bordering anterior portion of kidney and connecting dorsally at visceral ganglia, connecting posteriorly cerebro-pedal connective running immersed at pedal muscles, connecting to anterior region of pedal ganglia. Pair of visceral ganglia (Fig. 19: vg) fusiform; each ganglion slightly longer than wide; ~80% of cerebral ganglia size; partially fused at median portion, with presence of shallow central groove; located ventrally at kidney, parallel to posterior adductor muscle; in dorsal tip connecting cerebra-visceral connective and renal nerve, penetrating into kidney area; laterally originating ctenidial nerves running thought central axis of posterior portion of gills; dorsally originating posterior adductor muscle nerve, penetrating median region of anterior surface of posterior muscle; at ventral tip originating pallial nerve, touching anterior surface of ventral portion of posterior adductor muscle, running parallel to inhalant and exhalant apertures and mantle border, diffusing at mantle lobe board. Pair of pedal ganglia (Fig. 18: pg) 40% larger than pair of cerebral ganglia; shape elliptic; longer than wide; totally fused with each other, without vestigial commissure; located immerse on foot retractor muscles, above foot insertion; in anterior tip connects cerebro-pedal connectives from cerebral ganglia; in posterior tip connecting two pairs of nerves, dorsal pair running towards posterior region inside posterior foot retractor muscles; postero-ventral nerves curved to ventral region, running internally.

Etymology. The specific epithet *implexa* is a Latin word for "tangled," referring to species commonly found between the roots of estuarine and mangrove plants.

Distribution. Brazil, Maranhão to São Vicente, São Paulo (Fig. 24).

Habitat. Mangroves in brackish water, buried until 15 cm in muddy sand.

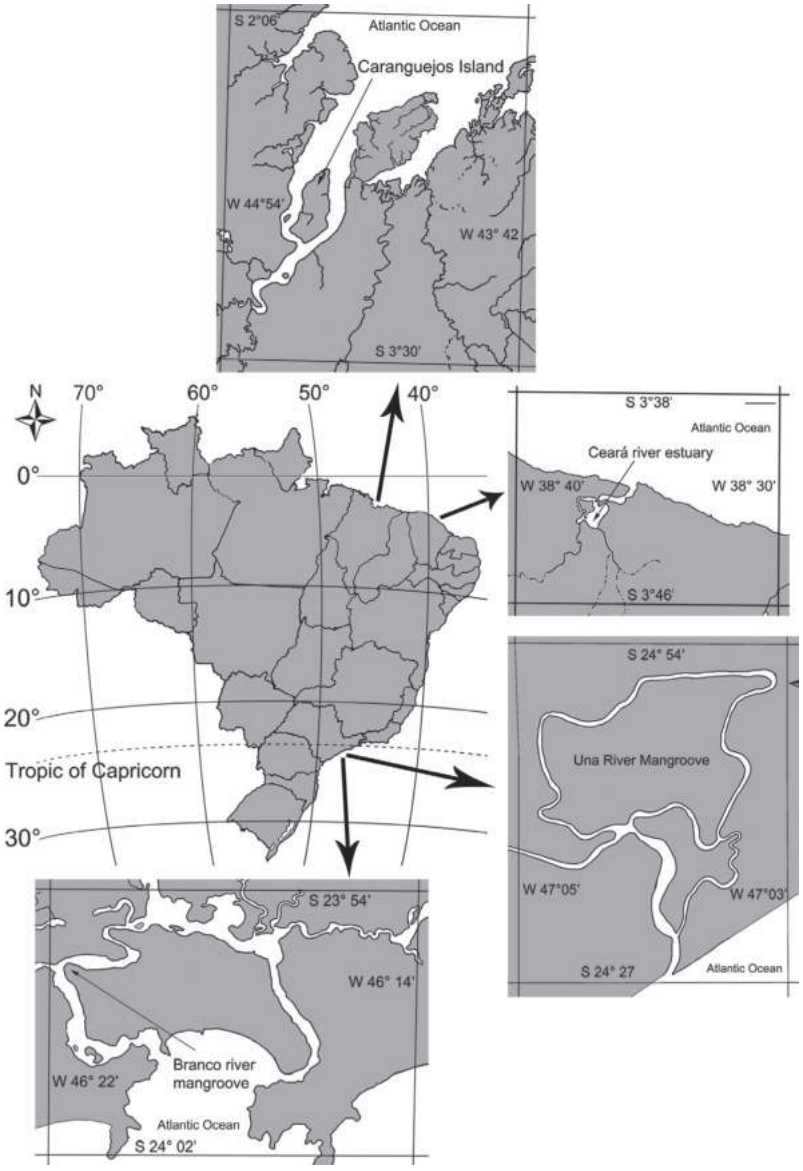

Figure 24. *Cyrenoida implexa* distribution along the Brazilian coast.

Discussion

At first glance, the external shell features of *C. implexa* closely resemble those of *Diplodonta punctata* (Say, 1822), which may strongly indicate misidentifications along the Brazilian coast (e.g., Barroso and Matthews-Cascon 2009). Both species exhibit rounded shells covered by a thin periostracum, displaying a light color, a posteriorly pointed shape, and living infaunally. Despite these initial similarities, differentiation differences between the two species are evident. *C. implexa* is found in estuaries and mangroves, featuring a slightly wrinkled and light brown periostracum (noticeable on dried specimens that retain it) and a fragile shell, while *D. punctata* inhabits a predominantly marine environment, burrowing into muddy or sandy bottoms, and possesses a hinge dentition composed exclusively of cardinal teeth (Mikkelsen and Bieler 2007; Rios 2009).

The classification of *C. implexa* within the genus *Cyrenoida* is primarily based on limited studies comparing it to *C. dupontia*, the type species of *Cyrenoida* (Joannis 1835; Deshayes 1836), as well as comments made on C. d'Ailly, 1869 (Taylor et al. 2009). These three species share several distinguishing features, including a hinge dentition characterized by fused laminar and cardinal teeth, the absence or faint presence of muscle scar impressions on the internal shell surface, valves covered with a brownish periostracum, a larger inner demibranch in the gills, paired triangular labial palps located at the anterior part of the ctenidia, and a pair of incurrent and excurrent siphons (Joannis 1835; Deshayes 1836; Taylor et al. 2009; Valentas-Romera et al. 2019). Furthermore, it is important to note the habitat of *C. implexa*, as these organisms are typically found thriving in freshwater to brackish environments, often intertwined among plant roots. Similar cyrenoidids with these characteristics are prevalent in both African and American ecosystems.

Most of the knowledge about the six *Cyrenoida* species stems from studies focusing on *C. floridana* in the Western Atlantic. Taylor et al. (2009), through molecular analysis of *C. floridana*, identified similarities among the families Cyrenoididae, Corbiculidae, and Glauconomidae. This finding led to the proposal of removing Cyrenoidindae from the superfamily Lucinoidea and assigning it to the superfamily Cyrenoidoidea, now known as Cyrenoidea. Subsequently, Wu et al. (2023) conducted another molecular analysis involving various *Cyrenoida* species, including *C. floridana*, and concluded that the family Cyrenoididae also encompasses *Geloina* J. E. Gray, 1842, *Cyanocyclas* Blainville, 1818, and *Polymesoda* Rafinesque, 1820.

Regarding *C. floridana* specifically, Valentas-Romera et al. (2019) undertook an extensive anatomical study comparing this species with others within Cyrenoidea, unveiling new morphological and anatomical insights, such as microtubules within shell walls, pairs of siphonal retractor muscles, the first description of the species' stomach, and evidence of shell parasitism in this species.

Given that additional studies involving the sequencing of *C. implexa* material are planned, the species is currently described based on its shell morphology and soft parts anatomy. These features are deemed comparable to those of *C. floridana*, as the available data is sufficiently convincing. Regarding the shell characters, both species are similar in outline and the characteristics of the left hinge teeth, especially the shape of the lateral tooth complex (t4) and cardinal teeth (t4 and t5). The studied specimens of *C. implexa* are also similar to *C. floridana* in size, as they fall within the species size range. The largest specimen documented in this study measures 8 mm, while *C. floridana* exhibits a length range of 10 to 14 mm (Valentas-Romera et al. 2019). Notably, reproductive populations of *C. floridana* described by Leathem et al. (1976), Kat (1982), and Wingard et al. (2022) include smaller individuals with average shell sizes of 9 mm, 3.5 to 4.5 mm, and less than 5 mm, respectively.

However, *C. implexa* and *C. floridana* can be differentiated by two sets of characteristics: a) right hinge teeth; b) internal anatomy; and c) ecological requirements.

a) The hinge in *C. implexa* is composed of three teeth: two lateral teeth, forming a single inverted V-shaped tooth, along with a solitary cardinal tooth (Fig. 1F, H). In contrast, *C. floridana* displays a different pattern with four teeth: two cardinal and two lateral teeth, creating two inverted V-shaped structures, where the smaller one is positioned beneath the larger one (Valentas-Romera et al. 2019). Notably, in *C. implexa*, only the larger or superior inverted V-shaped tooth (sv) is present, while the smaller one consists solely of the lateral tooth (t3) (Valentas-Romera et al. 2019).
b) Anatomically, *C. implexa* differs from *C. floridana* in the following features: the anterior and posterior adductor muscles in *C. implexa* are respectively ~12% and ~7% smaller than those in *C. floridana* (Valentas-Romera et al. 2019). However, this discrepancy in adductor muscle size could represent a specific trait or may be influenced by ontogenetic stages. *C. implexa* is also characterized by a sizable pair of siphons and a well-defined siphonal area at the mantle border. It also possesses a single pair of dorsal siphonal retractors muscles, whereas *C. floridana* has a smaller pair of dorsal siphonal retractors muscles, separated into two bundles (Valentas-Romera et al. 2019). Notably, *C. implexa* is further differentiated by the presence of three rows of papillae at the tip of the incurrent siphon and one row of papillae at the tip of the excurrent siphon. Additionally, the mantle borders of *C. implexa* lack papillae.
c) The salinity range of *C. floridana* varies from 0.25 to 20.7 practical salinity units (psu), while *C. implexa* tolerates salinities between 20.3 and 30 psu (Brewster-Wingard and Ishman 1999; Gaiser et al. 2006; Barroso and Matthews-Cascon 2009; Rodrigues et al. 2016; Saad et al. 2019; Wingard et al. 2022).

According to Wingard et al. (2022), *C. floridana* is a stenohaline species that inhabits oligohaline zones and can be used as an indicator of low-salinity environments. However, this feature apparently is not found in *C. implexa*, as samples were absent in Ceará´s river estuary, where the salinity was below 5 psu. This might indicate that *C. implexa* tolerates higher salinities than *C. floridana*.

The differentiation between both species is further substantiated by the consistent presence of these traits in all samples of *C. implexa* collected from the Brazilian coast, whereas the attributes of *C. floridana* remain uniform across Caribbean and North American samples. Given that the southernmost occurrence of *C. floridana* is observed on the coast of Guyanas (Valentas-Romera et al. 2019), it is plausible to suppose that the Amazon River Plume may have functioned as a reproductive barrier, as seen in mollusk groups (Giachini-Tosseto et al. 2022).

Conclusions

Based on the present findings, it is evident that the newly identified species, *Cyrenoida implexa* sp. n., is a member of the Cyrenoididae family. This species exhibits distinct morphological and anatomical characteristics in both shell morphology and soft parts anatomy, setting it apart from *C. floridana*. Furthermore, *Cyrenoida implexa* sp. n. represents the first documented record of the genus in the South region of the Western Atlantic, specifically in Brazilian mangroves and estuaries.

Acknowledgements

We thank Lara Guimarães (MZSP) for assistance with scanning electron microscopy; Luiza Saad (Instituto de Biociências da USP); Inês Xavier Martins (Universidade Federal Rural do Semi Árido); and Cristiane Xerez Barroso (Universidade Federal do Ceará) for granting material. This project was partly supported by Fapesp (Fundação de Amparo à Pesquisa) proc. #2010/11401–8 and CNPq (Conselho Nacional de Desenvolvimento Científico e Tecnológico) proc. #134425/2010–3, #159490/2012–0, and #203533/2014–3.

References

Adams H, Adams A (1853–1858) The Genera of Recent Mollusca: Arranged According to their Organization (Vol. 2). John van Voorst, London, 661 pp. https://doi.org/10.5962/bhl.title.4772

Barroso CX, Matthews-Cascon H (2009) Distribuição espacial e temporal da malacofauna no estuário do rio Ceará, Ceará, Brasil. Pan-American Journal of Aquatic Sciences 4: 79–86. https://panamjas.org/pdf_artigos/PANAMJAS_4(1)_79-86.pdf

Brewster-Wingard GL, Ishman SE (1999) Historical trends in salinity and substrate in central Florida Bay: A paleoecological reconstruction using modern analogue data. Estuaries 22(2): 369–383. https://doi.org/10.2307/1353205

Cavalcante ER, Ribeiro VV, Taddei RR, Castro IB, Alves MJ (2024) High levels of anthropogenic litter trapped in a mangrove area under the influence of different uses. Marine Pollution Bulletin 200: 116045. [ISSN 0025–326X] https://doi.org/10.1016/j.marpolbul.2024.116045

Coan EV, Valentich-Scott P (2012) Bivalve Seashells of Tropical West America – Marine Bivalve Mollusks from Baja California to Northern Peru (2 vols). Santa Barbara Museum of Natural History, Santa Barbara, 1258 pp.

Deshayes M (1836) Sur la cyrénoide de M. de Joannis. Suivie d'une lettre de M. Joannis. (Cl. V, n°64). Magasin de Zoologie 6, Classe V: 1–3. https://biodiversitylibrary.org/page/2633064

Duarte LFA, Ribeiro RB, Medeiros TV, Scheppis WR, Gimiliani GT (2023) Are mangroves hotspots of marine litter for surrounding beaches? Hydrodynamic modeling and quali-quantitative analyses of waste in southeastern Brazil. Regional Studies in Marine Science 67: 103177. [ISSN 2352–4855] https://doi.org/10.1016/j.rsma.2023.103177

Gaiser EE, Zafiris A, Ruiz PL, Tobias FAC, Ross MS (2006) Tracking rates of ecotone migration due to salt-water encroachment using fossil mollusks in coastal south Florida. Hydrobiologia 569(1): 237–257. https://doi.org/10.1007/s10750-006-0135-y

Giachini-Tosseto E, Bertrand A, Neumann-Leitão S, Nogueira-Júnior M (2022) The Amazon River plume, a barrier to animal dispersal in the Western Tropical Atlantic. Scientific Reports 12(1): 537. https://doi.org/10.1038/s41598-021-04165-z

Gray JE (1840) Shells of molluscous animals. In: British Museum (Ed.) Synopsis of the contents of the British Museum. ed 42. G Woodfall, London, 105–152. https://www.biodiversitylibrary.org/page/55287672

Huber M (2015) Compendium of Bivalves 2. A Full-Color Guide to the Remaining Seven Families. A Systematic Listing of 8'500 Bivalve Species and 10'500 Synonyms. ConchBooks, 907 pp.

Joannis [L.] De (1835) Cyrénoide. *Cyrenoida*. Joannis. Magasin de Zoologie 5. Classe V, 2 pp. [pl. 64] https://www.biodiversitylibrary.org/page/37121825

Kat PW (1982) Reproduction in a peripheral population of *Cyrenoida floridana* (Bivalvia, Cyrenoididae). Malacologia 23(1): 47–54. https://biodiversitylibrary.org/page/13112410

Leathem W, Kinner P, Mauer D (1976) Northern range extension of the Florida marsh clam *Cyrenoida floridana* (superfamily Cyrenoidacea). The Nautilus 90(3): 93–94. https://biodiversitylibrary.org/page/8276463

Lemer S, Bieler R, Giribet G (2019) Resolving the relationships of clams and cockles: dense transcriptome sampling drastically improves the bivalve tree of life. Proceedings of the Royal Society B: Biological Sciences 286(1896): 1–9. https://doi.org/10.1098/rspb.2018.2684

Lugo AE, Medina E, McGinley K (2014) Issues and challenges of mangroves conservation in the Anthropocene. Madera y Bosques 20: 11–38. https://doi.org/10.21829/myb.2014.200146

Mariano Neto M, da Silva JB, de Brito HC (2024) Carbon stock estimation in a Brazilian mangrove using optical satellite data. Environmental Monitoring and Assessment 196(9): 9. https://doi.org/10.1007/s10661-023-12151-3

Mikkelsen PM, Bieler R (2007) Seashells of Southern Florida: Living Marine Mollusks of the Florida Keys and Adjacent Regions. Bivalves. Princetion University Press, Princeton, New Jersey, 503 pp. https://doi.org/10.1515/9780691239453

Moore AC, Hierro L, Mir N, Stewart T (2022) Mangrove cultural services and values: Current status and knowledge gaps. People and culture 4: 1083–1097. https://doi.org/10.1002/pan3.10375

Rios EC (2009) Compendium of Brazilian Sea Shells. Rio Grande, RS,668 pp.

Rodrigues CA, Ribeiro RP, Santos NB, Almeida ZS (2016) Patterns of mollusc distribution in mangroves from the São Marcos Bay, coast of Maranhão State, Brazil. Acta Amazonica 46(4): 391–400. https://doi.org/10.1590/1809-4392201600493

Romañach SS, DeAngelis DL, Koh HL, Li Y, Teh SY, Raja Barizan RS, Zhai L (2018) Conservation and restoration of mangroves: Global status, perspectives, and prognosis. Ocean and Coastal Management 154(15): 72–82. https://doi.org/10.1016/j.ocecoaman.2018.01.009

Saad LO, Cunha CM, Colpo KD (2019) How mollusk assemblages respond to different urbanization levels: Characterization of the malacofauna in subtropical Brazilian mangroves. Marine Biodiversity 49(2): 989–999. https://doi.org/10.1007/s12526-018-0883-8

Say T (1822) An account of some of the marine shells of the United States. Journal of the Academy of Natural Sciences of Philadelphia 2: 302–325. https://www.biodiversitylibrary.org/item/113421#page/318/mode/1up

Taylor JD, Glover EA, Williams ST (2009) Phylogenetic position of the bivalve family Cyrenoididae – removal from (and further dismantling of) the superfamily Lucinoidea. The Nautilus 123(1): 9–13. https://biodiversitylibrary.org/page/50438173

Valentas-Romera BL, Simone LRL, Mikkelsen PM, Bieler R (2019) Anatomical redescription of *Cyrenoida floridana* (Bivalvia, Cyrenoididae) from the Western Atlantic and its position in the Cyrenoidea. Zoosystematics and Evolution 95(2): 517–534. https://doi.org/10.3897/zse.95.38456

Wingard GL, Stackhouse BL, Daniels AM (2022) Using mollusks as indicators of restoration in nearshore zones of south Florida's estuaries. Bulletin of Marine Science 98(3): 351–380. https://doi.org/10.5343/bms.2022.0004

Wu R, Liu L, Liu X, Ye Y, Wu X, Xie Z, Liu Z, Li Z (2023) Towards a systematic revision of the superfamily Cyrenoidea (Bivalvia, Imparidentia): Species delimitation, multi-locus phylogeny and mitochondrial phylogenomics. Invertebrate Systematics 37(9): 607–622. https://doi.org/10.1071/IS23015

Zoosyst. Evol. 100 (2) 2024, 555–563 | DOI 10.3897/zse.100.122472

PENSOFT

für Natur MUSEUM FÜR NATURKUNDE BERLIN

A new species of *Liobagrus* Hilgendorf, 1878 (Teleostei, Siluriformes, Amblycipitidae) from the lower Changjiang River basin in southeast China

Zhong-Guang Chen[1], Yan-Shu Guo[2], Yu-Ting Dai[1], Xiao-Chen Huang[1], Jun-Hao Huang[3], Jiao Jiang[4], Shan Ouyang[1], An-Xiang Wen[5], Xiao-Ping Wu[1]

1 *School of Life Sciences, Nanchang University, Nanchang, Jiangxi 330031, China*
2 *Ecological Restoration and Conservation on Forest and Wetland Key Laboratory of Sichuan Province, Sichuan Academy of Forestry Sciences, Chengdu, Sichuan 610081, China*
3 *Museum of Aquatic Organisms, Institute of Hydrobiology, Chinese Academy of Sciences, Wuhan, Hubei 430072, China*
4 *Zhejiang Museum of Natural History, Hangzhou, Zhejiang 310012, China*
5 *College of Life Sciences, Sichuan Agricultural University, Yaan, Sichuan 625014, China*

https://zoobank.org/88AE11F0-FC3E-44E2-920B-273CA4370F0F

Corresponding authors: An-Xiang Wen (2960657740@qq.com); Xiao-Ping Wu (xpwu@ncu.edu.cn)

Academic editor: Nicolas Hubert ♦ **Received** 7 March 2024 ♦ **Accepted** 2 April 2024 ♦ **Published** 16 May 2024

Abstract

A new catfish species, *Liobagrus chenhaojuni* Chen, Guo & Wu, **sp. nov.**, is described from the Tiaoxi River, a tributary of Taihu Lake, located in Zhejiang Province, China. This description is based on morphological characteristics and phylogenetic analysis. This species belongs to a group defined by the presence of a smooth posterior edge of the pectoral-fin spine and can be distinguished from other species in the group by a unique combination of characteristics, including: an upper jaw longer than the lower jaw; maxillary barbels reaching the middle of the pectoral fin; irregular blotches present on the lateral body; a rounded caudal-fin with a length ranging from 16.5% to 19.9% of the standard length; 39 to 41 post-Weberian vertebrae; and 15 to 17 anal-fin rays. The validity of this new species is further supported by the molecular phylogenetic analysis based on *Cytb* sequences.

Key Words

catfish, phylogeny, taxonomy, Zhejiang Province

Introduction

The genus *Liobagrus* comprises a group of small freshwater catfish endemic to East Asia. To date, 20 species have been described, with 12 of them found in mainland China: *Liobagrus marginatus* (Günther, 1892), *Liobagrus nigricauda* Regan, 1904, *Liobagrus styani* Regan, 1908, *Liobagrus anguillicauda* Nichols, 1926, *Liobagrus marginatoides* (Wu, 1930), *Liobagrus kingi* Tchang, 1935, *Liobagrus aequilabris* Wright & Ng, 2008, *Liobagrus chenghaiensis* Sun, Ren & Zhang, 2013; *Liobagrus huaiheensis* Chen, Wu & Wen, 2021; *Liobagrus pseudostyani* Chen & Guo, 2021; *Liobagrus brevispina* Xie, Cao & Zhang, 2022; and *Liobagrus chengduensis* Chen, Guo, Wu & Wen, 2022 (He 1999; Wright and Ng 2008; Sun et al. 2013; Chen and Guo 2021; Chen et al. 2021; Chen et al. 2022; Xie et al. 2022). Research on the taxonomy of Chinese *Liobagrus* has mainly focused on the upper and middle reaches of the Changjiang River (Yangtze) and the Huaihe River basin. However, the *Liobagrus* species in the lower Changjiang River have not been thoroughly surveyed or studied, potentially leaving other undescribed species undiscovered.

The Tiaoxi River is a small river situated in the western part of the Hangjiahu Plain in Zhejiang Province and is one of the main tributaries of Taihu Lake. Despite its small

watershed area, the Tiaoxi River boasts a diverse fish population, with a total of 84 recorded fish species (Li and Shimatani 2016; Zhang et al. 2022). Among these species, the presence of *L. styani* is highly questionable, as it is believed to be narrowly distributed in the Juanshui River basin in the middle Changjiang River (Wu et al. 2013). Moreover, the *L. styani* recorded in the basin is not only far from its type locality but also from the distribution regions of all other *Liobagrus* species in China. Based on collections made between 2022 and 2024, it has been discovered that *Liobagrus* specimens with a smooth posterior edge of the pectoral-fin spine, distributed in the Tiaoxi River, represent an undescribed species. Here, we introduce this species as new to science. The discovery of this new taxon contributes to our understanding of the high level of fish endemism in the lower Changjiang River basin.

Materials and methods

Specimens were manually collected from the Tiaoxi River between 2022 and 2024. Thirty-six type specimens were initially preserved in 10% formalin and subsequently transferred to 70% ethanol for long-term storage. Additionally, seven type specimens were preserved in 99% ethanol for molecular phylogenetic analyses. Vertebrae and fin rays were detected and counted using X-ray imaging. Measurements were obtained using digital calipers, with values recorded to the nearest 0.1mm.

Genomic DNA was extracted from the ventral fin of specimens preserved in 99% ethanol using the Baypure Magnetic Bead Method Animal Genomic DNA Extraction Kit (BayBio, Guangzhou, China). The quality and concentration of the DNA were checked using 1% agarose gel electrophoresis and NanoDrop 2000 (Thermo Scientific, USA). *Cytb* sequences were amplified using primers L14724 (GACTTGAAAAACCACCGTTG) and H15915 (CTCCGATCTCCGGATTACAAGAC). Polymerase chain reaction (PCR) amplifications of *Cytb* were performed in a final 25-μL volume mixture containing 1 μL of template DNA, 1 μL of each pair of primers, 12.5 μL of Green Taq Mix (Vazyme, China), and 9.5 μL ddH2O. Thermal cycling began with one cycle at 95 °C for 10 s, followed by 35 cycles of denaturation at 94 °C for 1 min, 55 °C for 1 min, and 72 °C for 1 min, with a final extension step at 72 °C for 10 min. PCR products were purified and sequenced using an ABI 3730XL analyzer by Sangon Biotech (China). Accession numbers of all newly obtained sequences are provided in Table 1. Sequences were aligned using MEGA v. 6.0 (Tamura et al. 2013) and manually checked. Genetic distance, based on the uncorrected p-distance model, was calculated using MEGA v. 6.0. Phylogenetic relationships were reconstructed using Bayesian inference (BI) and maximum likelihood (ML). *Xiurenbagrus xiurenensis* (Yue, 1981), *X. gigas* Zhao, Lan & Zhang, 2004, *Akysis brachybarbatus* Chen, 1981, *Ictalurus furcatus* (Valenciennes, 1840), and *Noturus taylori* Douglas, 1972, were used as the outgroup for rooting the tree. ML analyses were performed in IQ-TREE v. 1.6.12 (Minh et al. 2013) using the Ultrafast Fast Bootstrap approach (Minh et al. 2013) with 10,000 reiterations. The most appropriate model of sequence evolution (GTR+I+G) was selected using PartitonFinder2 v. 1.1 (Robert et al. 2017). Bayesian inference (BI) was conducted in MrBayes v. 3.2.6 (Ronquist et al. 2012). The most appropriate model of sequence evolution (GTR+I+G) was selected under ModelFinder (Subha et al. 2017). Four simultaneous runs with four independent Markov Chain Monte Carlo (MCMC) algorithms were executed for 10 million generations, and trees were sampled every 1000 generations with a burn-in of 25%. The convergence was verified with the average standard deviation of split frequencies of <0.01 and the potential scale reduction factor (PSRF) of ~1. Trees were visualized using FigTree v.1.4.3 (http://tree.bio.ed.ac.uk/software/figtree/). Institutional abbreviations used: NCU_XPWU Laboratory of Xiao-Ping Wu, Nanchang University (Nanchang, Jiangxi, China); IHB Museum of Aquatic Organisms, Institute of Hydrobiology, Chinese Academy of Sciences (Wuhan, Hubei, China).

Results

***Liobagrus chenhaojuni* Chen, Guo & Wu, sp. nov.**

https://zoobank.org/9966A844-20BC-4DCD-9E09-A5FFA9F14659

Figs 1, 2A–C, Table 2

Liobagrus styani Li & Shimatani, 2016: 165–167 (Tiaoxi River, Zhejiang, China).

Type material. ***Holotype.*** 24_NCU_XPWU_Y01, Siling Reservoir [四岭水库], Tiaoxi River [苕溪], Yuhang district [余杭区], Hangzhou City [杭州市], Zhejiang Province [浙江省], China, 30°25'42"N, 119°45'18"E, leg. Hao-Jun Chen, February 2024.

September 2022. ***Paratypes.*** 24_NCU_XPWU_Y02–16, n=15, other information same as holotype; 22_NCU_XPWU_Y01–17, n=17, leg. Zhong-Guang Chen & Hao-Jun Chen, September 2022, other information same as holotype; 22_NCU_XPWU_Y18–25, n=8, IHB-T-A0000007–8, n=2, Tiaoxi River [苕溪], Deqing County [德清县], Huzhou City [湖州市], Zhejiang Province [浙江省], China, leg. local people, September 2022.

Diagnosis. *Liobagrus chenhaojuni* sp. nov. is a member of the group defined by the presence of a smooth posterior edge of the pectoral-fin spine (i.e., *L. reinii*, *L. formosanus*, *L. styani*, *L. nantoensis*, *L. anguillicauda*, *L. marginatoides*, and *L. aequilabris*). It can be distinguished from all other species in this group by the following characteristics: the upper jaw is longer than the lower jaw (vs. equal in *L. aequilabris* and *L. formosanus*; shorter in *L. marginatoides*); the maxillary barbels reach the middle of the pectoral fin (vs. reach the pectoral-fin

Table 1. GenBank accession numbers of the sequences for this study.

Species	Access number	Locality	Reference
Liobagrus chenhaojuni sp. nov. 1	PP446311	Huzhou, Zhejiang, China	This study
Liobagrus chenhaojuni sp. nov. 2	PP446312	Huzhou, Zhejiang, China	This study
Liobagrus chenhaojuni sp. nov. 3	PP446313	Huzhou, Zhejiang, China	This study
Liobagrus chenhaojuni sp. nov. 4	PP446314	Hangzhou, Zhejiang, China	This study
Liobagrus chenhaojuni sp. nov. 5	PP446315	Hangzhou, Zhejiang, China	This study
Liobagrus chenhaojuni sp. nov. 6	PP446316	Hangzhou, Zhejiang, China	This study
L. styani 1	KY653576	Xianning, Hubei, China	NCBI
L. styani 2	KY653577	Xianning, Hubei, China	NCBI
L. aequilabris 1	KY653673	Unknown	NCBI
L. aequilabris 2	KY653674	Unknown	NCBI
L. anguillicauda 1	KY653651	Wuyishan, Fujian, China	NCBI
L. anguillicauda 2	KY653652	Wuyishan, Fujian, China	NCBI
L. marginatus 1	KY653578	Chongqing, China	NCBI
L. marginatus 2	KY653579	Chongqing, China	NCBI
L. kingi	KC193779	Unknown	NCBI
L. huaiheensis 1	ON638213	Xinyang, Henan, China	NCBI
L. huaiheensis 2	ON638214	Xinyang, Henan, China	NCBI
L. obesus	DQ321752	Korea	NCBI
L. andersoni	DQ321753	Korea	NCBI
L. pseudostyani 1	ON638209	Chengdu, Sichuan, China	NCBI
L. pseudostyani 2	ON638210	Chengdu, Sichuan, China	NCBI
L. brevispina 1	ON638211	Chengdu, Sichuan, China	NCBI
L. brevispina 2	ON638212	Chengdu, Sichuan, China	NCBI
L. chengduensis 1	ON638203	Chengdu, Sichuan, China	NCBI
L. chengduensis 2	ON638204	Chengdu, Sichuan, China	NCBI
L. mediadiposalis 1	KX265422	Korea	NCBI
L. mediadiposalis 2	KX265423	Korea	NCBI
L. hyeongsanensis	MZ066608	Korea	NCBI
L. geumgangensis 1	KX265431	Korea	NCBI
L. geumgangensis 2	KX265433	Korea	NCBI
L. somjinensis	MN756661	Korea	NCBI
L. reinii 1	LC333217	Japan	NCBI
L. reinii 2	LC333224	Japan	NCBI
Xiurenbagrus xiurenensis	DQ192464	Guangxi, China	NCBI
Xiurenbagrus gigas	EU490936	Guangxi, China	NCBI
Akysis brachybarbatus	AF499603	Yunnan, China	NCBI
Ictalurus furcatus	KM576102	Unknown	NCBI
Noturus taylori	KP013089	Unknown	NCBI

insertion in *L. styani*, *L. reinii*, and *L. nantoensis*); presence of irregular blotches on the lateral body (vs. absence in *L. formosanus*, *L. nantoensis*, *L. anguillicauda*, *L. marginatoides*, and *L. aequilabris*); the caudal fin is rounded (vs. sub-truncate in *L. marginatoides*); the caudal fin length ranges from 16.5% to 19.9% standard length (vs. 13.1–16.2 in *L. styani*, 20.3–27.0 in *L. anguillicauda* and 20.1–26.9 in *L. aequilabris*); it possesses 39–41 post-Weberian vertebrae (vs. 35–37 in *L. aequilabris*), the anal-fin rays range from 15 to 17 (vs. 12 in *L. nantoensis*) (Table 3).

Description. Morphometric data for type specimens are shown in Table 2. Body elongated, anteriorly depressed (wider than deep), and posteriorly evenly compressed to the tail. Lateral line short, with 6–9 pores. Head depressed and broad when viewed dorsally, with a broadly rounded snout in dorsal view. Anterior nostril tubular, with a rim bearing a fleshy flap forming a short tube; posterior nostril pore-like, with the rim posteriorly confluent with the base of the nasal barbel. Eyes small, dorsolateral, and subcutaneous. Mouth terminal, with the upper jaw noticeably longer than the lower jaw, lips thickened. Premaxillary and mandibular tooth pads curved, bearing small and setiform teeth; palatine teeth absent. Four pairs of barbels: the maxillary barbel long, extending to the pectoral-fin insertion; nasal barbel short, not reaching the gill-membrane margin; inner mandibular barbel approximately half the length of the outer mandibular barbel and does not extend to the pectoral-fin insertion; outer mental barbel longest, reaching the middle of the pectoral fin.

Dorsal fin II, 5–6 rays, with a convex distal margin; tip of adpressed fins does not reach the pelvic-fin insertion. Dorsal-fin spine covered by thick, straight skin with smooth anterior and posterior margins, slightly shorter than the pectoral-fin spine. Adipose fin high,

Figure 1. *Liobagrus chenhaojuni* sp. nov. **A–C.** Dorsal, lateral, and ventral view of holotype (24_NCU_XPWU_Y01); **D.** Dorsal view of pectoral-fin spine of paratype (22_NCU_XPWU_Y31). Arrows show the anus.

with its base longer than the anal-fin base, confluent with the caudal fin without a marked incision at the confluence. Pectoral fin I, 7–8 rays, with its origin at the vertical through the edge of the operculum, partially covered by the opercular membrane. Pectoral-fin spine long and sharp, with smooth anterior and posterior margins (Fig. 1D), reaching the dorsal-fin insertion. Pelvic fin i, 5–6 rays, short, with the adpressed tip not reaching the anal-fin origin. Anal fin 15–17 rays with a rounded distal margin, and its tip approaches the origin of the ventral procurrent caudal-fin rays, longer than the dorsal-fin base but shorter than the adipose-fin base, with a convex distal edge. Anus closer to the pelvic-fin insertion than to the anal-fin origin. Caudal fin rounded, with 43–50 rays. Vertebral column consists of 39–41 post-Weberian elements.

Body generally dark brown to brownish red, adorned with irregular yellowish blotches that fade to light yellow ventrally. All barbels grayish white to light yellow, while dorsal fins dark brown, and adipose and caudal fins grayish white to light brown. All fins exhibit narrow, grayish white to light yellowish distal margins (Fig. 2A, B).

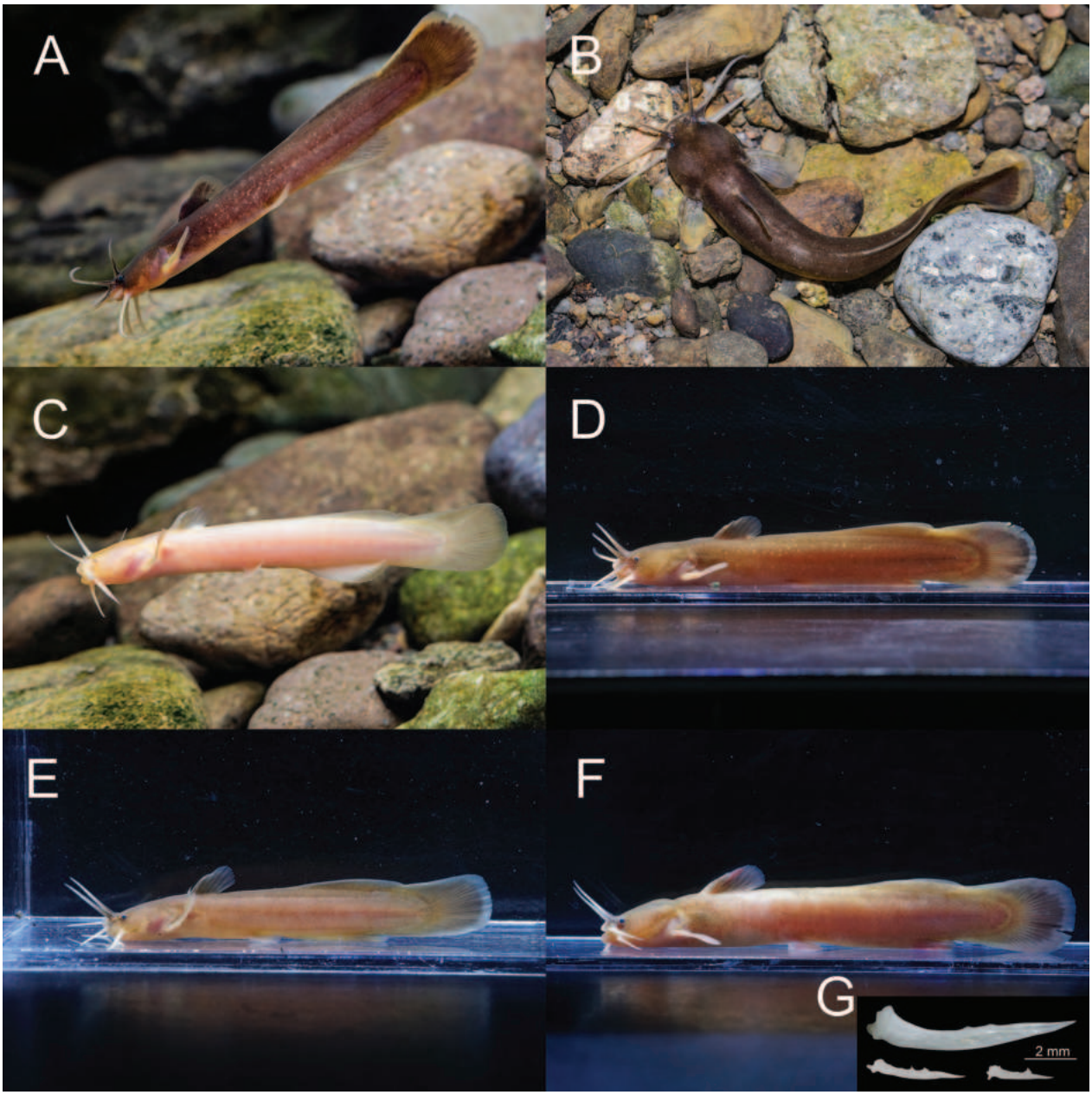

Figure 2. Living specimens of *Liobagrus chenhaojuni* sp. nov. and its similar congeneric species. **A, B.** *Liobagrus chenhaojuni* sp. nov.; **C.** *Liobagrus chenhaojuni* sp. nov. albino individual; **D.** *L. styani*; **E.** *L. anguillicauda*; **F.** *L. brevispina*; **G.** dorsal view of pectoral-fin spine of *L. brevispina*.

An albino individual was found, exhibiting a generally pink body without irregular yellowish blotches (Fig. 2C).

Etymology. This species is named after Mr. Hao-Jun Chen, who assisted in the field survey.

Vernacular name. 浙江鮡 (Pinyin: zhe jiang yang).

Distribution and ecology. *Liobagrus chenhaojuni* sp. nov. is exclusively found within the Tiaoxi River basin (Fig. 3). Within this habitat, it typically resides at the bottom of the stream with medium pebbly substrates, together with *Rhinogobius leavelli* (Herre, 1935), *Microphysogobio bicolor* (Nichols, 1930), *Vanmanenia stenosoma* (Boulenger, 1901), *Acrossocheilus fasciatus* (Steindachner, 1892), *Opsariichthys bidens* Günther, 1873, and *Zacco tiaoxiensis* Zhang, Zhou & Yang, 2022 (Fig. 4).

Molecular analyses. A dataset consisting of 33 *Cytb* sequences and five outgroup taxa was employed for phylogenetic analyses (Table 1). The alignment of *Cytb* exhibited a length of 1116 characters, with 343 variable sites and 313 sufficiently informative sites. Phylogenetic analyses generated ML and BI trees with largely congruent topologies (Fig. 5). Notably, species from China with a smooth posterior edge of the pectoral-fin spine formed a monophyletic group, while those with a serrated posterior edge of the pectoral-fin spine constituted a paraphyletic group. The validity of *Liobagrus chenhaojuni* sp. nov. is supported by the molecular-phylogenetic result. It belongs to the group with a smooth posterior edge of the pectoral-fin spine, and the phylogenetic relationship with-

Table 2. Morphometric data for type specimens of *Liobagrus chenhaojuni* sp. nov.

Morphometrics	Holotype	Paratypes
Standard length (mm)	70.2	38.8–79.3
% of standard length		
Head length	22.4	20.6–23.0
Body depth	18.8	13.6–18.4
Dorsa-fin base length	10.0	9.1–10.0
Anal-fin base length	16.5	12.3–19.7
Adipose-fin base length	28.8	27.7–37.2
Caudal peduncle length	20.4	19.3–23.1
Caudal peduncle depth	17.2	14.0–17.7
Dorsal-fin spine length	7.5	6.3–7.4
Pectoral-fin spine length	9.3	7.2–9.6
Caudal-fin length	18.4	16.5–19.9
Anus to pelvic-fin insertion	3.6	3.4–6.4
Anus to anal-fin origin	4.3	4.9–7.5
Predorsal length	28.8	27.0–30.5
Prepectoral length	18.4	17.7–21.4
Prepelvic length	46.0	42.9–45.5
Preanal length	58.4	57.3–60.1
Dorsal to adipose-fin origin	29.3	25.3–31.8
% of head length		
Head width	89.2	83.0–93.3
Head depth	61.8	50.0–59.4
Snout length	31.8	26.3–32.0
Mouth width	69.4	68.0–76.1
Interorbital width	35.7	33.1–40.0
Nasal barbel length	73.2	67.6–73.9
Maxillary barbel length	94.9	81.4–95.4
Inner mandibular barbel length	61.8	50.0–62.1
Outer mandibular barbel length	99.4	93.0–98.7
Width between anterior nares	12.7	12.5–16.1
Width between postoral nares	28.7	28.0–36.6

in the group is represented as *Liobagrus chenhaojuni* sp. nov. + (*L. anguillicauda* + (*L. aequilabris* + *L. styani*)). The genetic distances between *Liobagrus chenhaojuni* sp. nov. and other congeneric species ranged from 5.8% to 14.2% (Suppl. material 1).

Discussion

The placement of the new species within *Liobagrus* is supported by both its morphology and phylogeny. Species of *Liobagrus* can be divided into two groups based on the possession of a smooth or serrated posterior edge of the pectoral-fin spine. Xie et al. (2022) described *L. brevispina* as having a smooth posterior edge of the pectoral-fin spine. However, based on the examination of specimens, *L. brevispina* was found to have a serrated posterior edge of the pectoral-fin spine (Fig. 2G). The serrations on its pectoral-fin spine weaken but do not disappear as it grows. Currently, the group defined by the presence of a smooth posterior edge of the pectoral-fin spine comprises only seven species: *L. reinii*, *L. formosanus*, *L. styani*, *L. nantoensis*, *L. anguillicauda*, *L. marginatoides*, and *L. aequilabris*. In this group, *Liobagrus chenhaojuni* sp. nov. can be easily distinguished from *L. aequilabris*, *L. formosanus*, and *L. marginatoides* by having the upper jaw longer than the lower (vs. shorter or equal). *Liobagrus chenhaojuni* sp. nov. is similar to *L. reinii*, *L. styani*, *L. nantoensis*, *and L. anguillicauda* by the similar upper and lower jaw positions, but differs based on the maxillary barbels reaching the middle of the pectoral fin (vs. reaching the

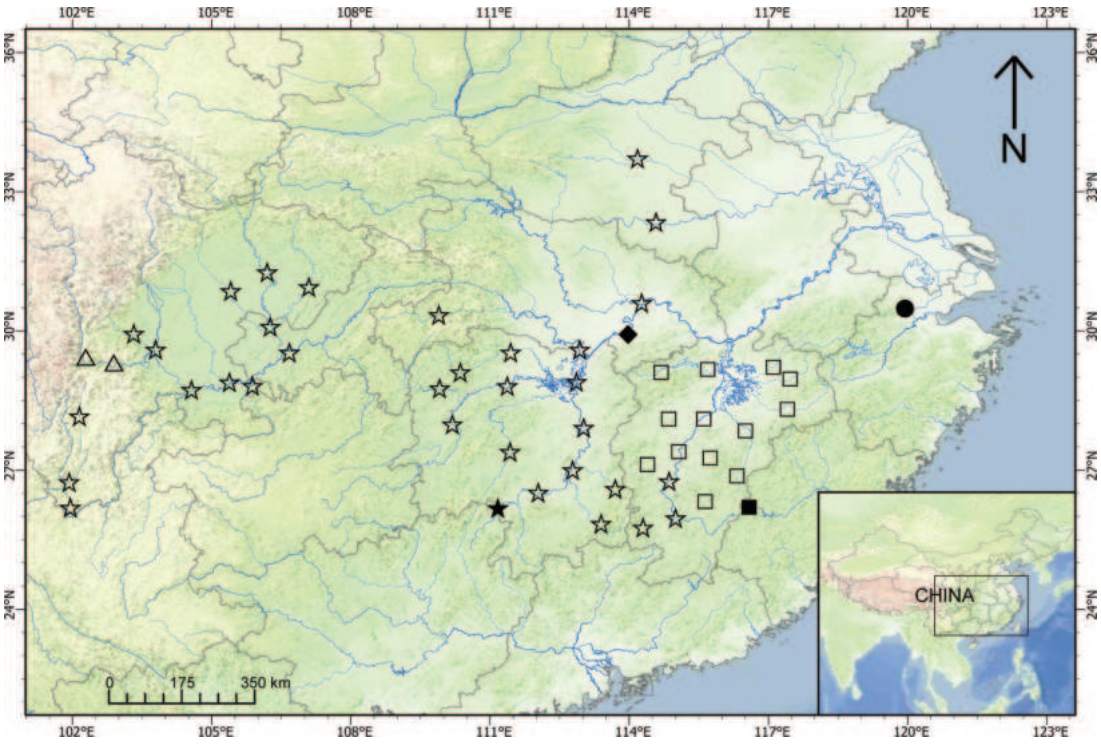

Figure 3. Distribution of *Liobagrus* with a smooth posterior edge of the pectoral-fin spine in Mainland China. **Dot.** *Liobagrus chenhaojuni* sp. nov.; **square.** *L. anguillicauda*; **rhombus.** *L. styani*; **star.** *L. aequilabris*; **triangle.** *L. marginatoides*. Solid show the type localities.

Figure 4. Sampling locality of *Liobagrus chenhaojuni* sp. nov. Siling Reservoir, Tiaoxi River, Yuhang district, Hangzhou City, Zhejiang Province, China.

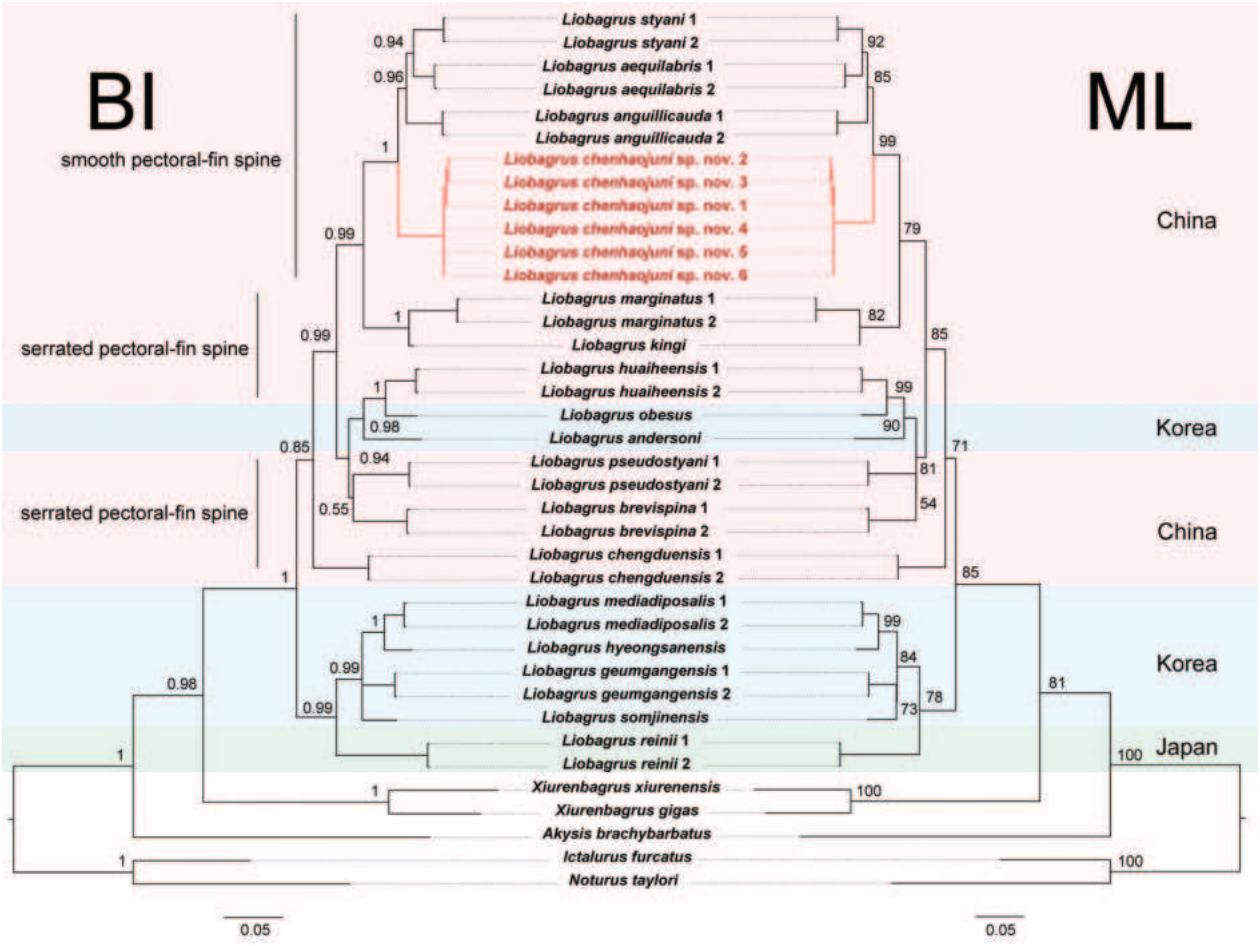

Figure 5. Bayesian inference tree and maximum likelihood tree inferred from *Cytb* gene sequences. Posterior probabilities/bootstrap supports are shown on the left/right of nodes.

pectoral-fin insertion in *L. reinii*, *L. styani*, and *L. nantoensis*), presence of irregular blotches on the body lateral (vs. absence in *L. nantoensis* and *L. anguillicauda*), caudal-fin length is 16.5–19.9% of standard length (vs. 13.1–16.2% in *L. styani* and 20.3–27.0% in *L. anguillicauda*), 15–17 anal-fin rays (vs. 12 in *L. nantoensis*). Furthermore, *Liobagrus chenhaojuni* sp. nov. has a distinctive distribution, being exclusively found in the Tiaoxi River within the lower Changjiang River basin, far from any other congeners.

The discovery of *Liobagrus chenhaojuni* sp. nov., as well as *Zacco tiaoxiensis* in the Tiaoxi River, shows

Table 3. Comparisons of major diagnostic characters of *Liobagrus* with a smooth posterior edge of the pectoral-fin spine.

Characters	*Liobagrus chenhaojuni* sp. nov.	*L. nantoensis*[a]	*L. reinii*[a]	*L. styani*[b]
Upper/lower jaw in length	>1	>1	>1	>1
post-Weberian vertebrae	39–41	Unknown	Unknown	39–41
Anal-fin rays	15–17	12	17	17–19
Caudal-fin length as % of standard length	16.5–19.9	Unknown	Unknown	13.11–16.2
Caudal-fin shape	Rounded	Rounded	Rounded	Rounded
Maxillary barbels	Reaching middle of pectoral fin	Reaching pectoral-fin insertion	Reaching pectoral-fin insertion	Reaching pectoral-fin insertion
Irregular blotches on body lateral	Present	Absent	Present	Present
Characters	*L. anguillicauda*[b]	*L. aequilabris*[a]	*L. formosanus*[b]	*L. marginatoides*[c]
Upper/lower jaw in length	>1	=1	=1	<1
Post-Weberian vertebrae	38–40	35–37	38–39	Unknown
Anal-fin rays	15–17	15–17	15	13–15
Caudal-fin length as % of standard length	20.3–27.0	20.1–26.9	17.7–20.0	18.1–20.1
Caudal-fin shape	Rounded	Rounded	Rounded	Sub-truncate
Maxillary barbels	Reaching middle of pectoral fin	Reaching pectoral-fin insertion	Reaching pectoral-fin insertion	Reaching middle of pectoral fin
Irregular blotches on body lateral	Absent	Absent	Absent	Absent

Notes: data from a, Xie et al. 2022; b, Wu et al. 2016; c, Chen and Guo 2021.

that fish diversity in this area has been underestimated. There is a need for systematic fish surveys in the basin to uncover cryptic species diversity and generate data essential for conservation efforts. Unlike most congeners distributed in streams within sparsely populated regions, the new species was found in the Yangtze River Delta region, which is the economic hub of China. Given its distribution, the new species is exposed to greater risks from human activities compared to other congeners. Therefore, it is imperative to closely monitor and protect it to ensure its survival.

Acknowledgments

We thank De-Kui He (Institute of Hydrobiology, Chinese Academy of Sciences) for his assistance in preserving type specimens and conducting x-ray imaging; Hao-Jun Chen (Linhai); Yi-Jun Li (The University of Sydney, Sichuan Agricultural University); Xin Liu (Sichuan Agricultural University); Yi Feng (Chengdu); and Wei Lei (Chengdu) for their assistance in collecting specimens. This study was supported by the National Natural Science Foundation of China under Grant Nos. 31772412 and 32360132.

References

Chen ZG, Guo YS (2021) *Liobagrus pseudostyani*. In: Guo YS, Sun ZY, He XH, Jin W, Chen YL (Eds) Colored Atlas of Fishes in Sichuan (II). Science Press, Beijing, 795–799. [in Chinese]

Chen ZG, Wu JY, Wen AX (2021) *Liobagrus huaiheensis*, a new species of torrent catfish (Teleostei: Siluriformes: Amblycipitidae) from the Huaihe River basin in Central China. Zootaxa 4952(2): 391–400. https://doi.org/10.11646/zootaxa.4952.2.11

Chen ZG, Guo YS, Wu JY, Wen AX (2022) *Liobagrus chengduensis*, a new species of torrent catfish (Teleostei: Siluriformes: Amblycipitidae) from the upper Changjiang River basin in southwest China. Zoological Research 43(4): 679–682. https://doi.org/10.24272/j.issn.2095-8137.2022.114

He MJ (1999) Amblycipitidae. In: Chu XL (Eds) Fauna Sinica (Osteichthyes: Siluriformes). Science Press, Beijing, 103–111. [in Chinese]

Li JH, Shimatani Y (2016) *Liobagrus styani*. In: Li JH, Shimatani Y (Eds) Illustrated fish handbook in the east Tiaoxi River. Science Press, Beijing, 165–167. [in Chinese]

Minh BQ, Nguyen MAT, von Haeseler A (2013) Ultrafast approximation for phylogenetic bootstrap. Molecular Biology and Evolution 30(5): 1188–1195. https://doi.org/10.1093/molbev/mst024

Robert L, Paul BF, April MW, Tereza S, Brett C (2017) Partitionfinder 2: New methods for selecting partitioned models of evolution for molecular and morphological phylogenetic analyses. Molecular Biology and Evolution 34: 772–773. https://doi.org/10.1093/molbev/msw260

Ronquist F, Teslenko M, van der Mark P, Ayres DL, Darling A, Höhna S, Larget B, Liu L, Suchard MA, Huelsenbeck J (2012) Mrbayes 3.2: Efficient bayesian phylogenetic inference and model choice across a large model space. Systematic Biology 61(3): 539–542. https://doi.org/10.1093/sysbio/sys029

Subha K, Bui Quang M, Wong TKF (2017) Modelfinder: Fast model selection for accurate phylogenetic estimates. Nature Methods 14(6): 587–589. https://doi.org/10.1038/nmeth.4285

Sun ZW, Ren SJ, Zhang E (2013) *Liobagrus chenghaiensis*, a new species of catfish (Siluriformes: Amblycipitidae) from Yunnan, South China. Ichthyological Exploration of Freshwaters 23(4): 275–384.

Tamura K, Stecher G, Peterson D, Filipski A, Kumar S (2013) MEGA6: Molecular evolutionary genetics analysis version 6.0. Molecular Biology and Evolution 30(12): 2725–2729. https://doi.org/10.1093/molbev/mst197

Wright JJ, Ng HH (2008) A new species of *Liobagrus* (Siluriformes: Amblycipitidae) from South China. Proceedings of the Academy of Natural Sciences of Philadelphia, Philadelphia 157: 37–43. https://doi.org/10.1635/0097-3157(2008)157[37:ANSOLS]2.0.CO;2

Wu YA, Zhang E, Sun ZW, Ren SJ (2013) Identity of the catfish *Liobagrus styani* (Teleostei: Amblycipitidae) from Hubei Province, China. Ichthyological Exploration of Freshwaters 24: 73–84.

Xie RX, Cao L, Zhang E (2022) *Liobagrus brevispina*, a new species of torrent catfish (Siluriformes: Amblycipitidae) from the upper Chang-Jiang basin, South China. Journal of Fish Biology 101(3): 478–490. https://doi.org/10.1111/jfb.15109

Zhang Y, Zhou JJ, Yang JQ (2022) A new species of Genus *Zacco* from Southern China (Cypriniformes: Cyprinidae). Journal of Shanghai Ocean University 32(03): 544–552. [in Chinese] https://doi.org/10.12024/jsou.20220703918

Supplementary material 1

Genetic distances of Cytb sequences computed by MEGA 6 of *Liobagrus*

Authors: Zhong-Guang Chen, Yan-Shu Guo, Yu-Ting Dai, Xiao-Chen Huang, Jun-Hao Huang, Jiao Jiang, Shan Ouyang, An-Xiang Wen, Xiao-Ping Wu

Data type: xlsx

Link: https://doi.org/10.3897/zse.100.122472.suppl1

Zoosyst. Evol. 100 (2) 2024, 565–582 | DOI 10.3897/zse.100.119143

PENSOFT

MUSEUM FÜR NATURKUNDE BERLIN

Similar looking sisters: A new sibling species in the *Pristimantis danae* group from the southwestern Amazon basin (Anura, Strabomantidae)

Jörn Köhler[1], Frank Glaw[2], César Aguilar-Puntriano[3], Santiago Castroviejo-Fisher[4], Juan C. Chaparro[5,6], Ignacio De la Riva[7], Giussepe Gagliardi-Urrutia[8], Roberto Gutiérrez[9,10], Miguel Vences[11], José M. Padial[12,13]

1 *Hessisches Landesmuseum Darmstadt, Friedensplatz 1, 64283 Darmstadt, Germany*
2 *Zoologische Staatssammlung München (ZSM-SNSB), Münchhausenstr. 21, 81247 München, Germany*
3 *Universidad Nacional Mayor de San Marcos, Museo de Historia Natural (MUSM), Departamento de Herpetología, Av. Arenales 1256, Lima 11, Peru*
4 *Departamento de Zoología, Facultad de Biología, Universidad de Sevilla, Av. Reina Mercedes, 41012 Sevilla, Spain*
5 *Museo de Biodiversidad del Perú, Urbanización Mariscal Gamarra A-61, Zona 2, Cusco, Peru*
6 *Museo de Historia Natural de la Universidad Nacional de San Antonio Abad del Cusco, Paraninfo Universitario (Plaza de Armas s/n), Cusco, Peru*
7 *Museo Nacional de Ciencias Naturales-CSIC, C/ José Gutiérrez Abascal 2, 28006 Madrid, Spain*
8 *Dirección de Investigación en Diversidad Biológica Terrestre Amazónica, Instituto de Investigaciones de la Amazonía Peruana (IIAP), Av. Abelardo Quiñones km 2.5, Iquitos, Peru*
9 *Museo de Historia Natural de la Universidad Nacional de San Agustín de Arequipa (MUSA), Av. La Pampilla s/n, Cercado, Arequipa, Peru*
10 *Servicio Nacional de Áreas Naturales Protegidas por el Estado (Sernanp), Calle 17 N° 355, San Isidro, Lima, Peru*
11 *Zoological Institute, Technische Universität Braunschweig, Mendelssohnstr. 4, 38106 Braunschweig, Germany*
12 *Departamento de Zoología, Facultad de Ciencias, Universidad de Granada, Avenida de Fuente Nueva s/n, 18071 Granada, Spain*
13 *Department of Herpetology, American Museum of Natural History, Central Park West at 79th St, 10024 New York, NY, USA*

https://zoobank.org/3D0B1824-9405-4F44-ADB9-6890B0C5C0D3

Corresponding author: Jörn Köhler (joern.koehler@hlmd.de)

Academic editor: Pedro Taucce ♦ **Received** 19 January 2024 ♦ **Accepted** 22 April 2024 ♦ **Published** 16 May 2024

Abstract

We describe a new frog species that is the sibling of *Pristimantis reichlei*. These two sister species inhabit the Amazonian lowlands and adjacent foothills of the Andes, from central Bolivia to central Peru. *Pristimantis reichlei* occurs from central Bolivia to southern Peru (Alto Purús National Park), while the new species occurs from northern Bolivia (Departamento Pando) to Panguana in central Peru (Departamento Huánuco), at elevations between 220 and 470 m a.s.l. In spite of their morphological crypsis, these siblings occur in syntopy without evidence of interbreeding (in the Alto Purús area) and are recovered as reciprocally monophyletic. Their uncorrected pairwise genetic distances in the 16S rRNA gene range from 9.5–13.5%, and their advertisement calls differ in both qualitative and quantitative traits. Moreover, our study found uncorrected pairwise distances within the new species of up to 5.0% and up to 9.3% within *P. reichlei*. We therefore cannot rule out the possible existence of hybrids or additional species-level lineages hidden in this complex. Furthermore, we found another potential pair of sibling species composed of *P. danae* and an unnamed lineage, with divergences of 9.4% in the 16S gene, whose in-depth analysis and taxonomic treatment are pending future revision. With the new nominal species, the *Pristimantis danae* species group now includes 20 species, distributed across the upper Amazon basin and in the eastern Andes, from western Brazil to Bolivia and Peru. Our study, together with an increasing number of other studies, indicates that sibling species are far from being rare among Amazonian amphibians and that species resolution remains low even for groups that have received considerable attention in recent years.

Key Words

Amphibia, bioacoustics, integrative taxonomy, morphology, molecular genetics, systematics, Bolivia, Brazil, Peru

Introduction

The genus *Pristimantis* Jiménez de la Espada, 1870 represents an extremely species-rich and ecologically diverse clade of Neotropical frogs. It is considered challenging for researchers with respect to their systematics because of the many genealogically distant species co-occurring in sympatry yet showing highly similar phenotypes, and due to the numerous geographically and phylogenetically distant yet also similar-looking species (e.g., Elmer et al. 2007; Padial and De la Riva 2009; García et al. 2012; Pinto-Sánchez et al. 2012). These patterns of variation and distribution led to the erection of many non-monophyletic species groups (see Padial et al. 2014). Although our knowledge of species diversity and relationships remains rudimentary, the application of molecular phylogenetics has improved the systematics of the genus considerably over the last two decades (e.g., Heinicke et al. 2007; Hedges et al. 2008; Canedo and Haddad 2012; Pinto-Sánchez et al. 2012; Padial et al. 2014; Páez and Ron 2019; Ron et al. 2020; Sánchez-Nivicela et al. 2021; Arroyo et al. 2022). Among other results, many non-monophyletic species groups and genera have been redefined so as to represent monophyletic groups (Padial et al. 2014; Gonzáles-Durán et al. 2017; Páez and Ron 2019; Chávez et al. 2021; Zumel et al. 2021). Still, most nominal *Pristimantis* species remain unassigned to any species group, and the affinities of many assigned ones remain uncorroborated, both because of our limited understanding of phenotypic variation and a lack of genetic data (e.g., Padial et al. 2014).

Hedges et al. (2008) erected the *Pristimantis peruvianus* species group for some species formerly in the *P. conspicillatus* and *P. unistrigatus* groups. However, these authors did not study topotypic material of *P. peruvianus*. Instead, they relied on samples from populations in the Amazon lowlands of SW Peru, which at the time were considered *P. peruvianus* (Padial and De la Riva 2005) and which later were identified as belonging to a new species, *P. reichlei* (Padial and De la Riva 2009). Thus, the nominal species group could not be maintained as the species for which it was named belonged to a different clade. Padial et al. (2014) re-allocated *P. peruvianus* to the *P. conspicillatus* group and erected the *P. danae* species group for some species formerly considered part of the *P. peruvianus* group (sensu Hedges et al. 2008), which included *P. danae* and *P. reichlei* as well as others (*P. albertus*, *P. aniptopalmatus*, *P. cuneirostris*, *P. ornatus*, *P. pharangobates*, *P. rhabdolaemus*, *P. sagittulus*, *P. stictogaster*, *P. toftae*). They found this group to be monophyletic and sister to the *P. conspicillatus* group. Further research resulted in new species that were part of this species group (Lehr and von May 2017; Herrera-Alva et al. 2023; Lehr et al. 2017; Venegas et al. 2023), adding six species to it, all but two (*P. clarae*, *P. similaris*), from high elevations of the Pui Pui Protected Forest in central Peru (*P. attenboroughi*, *P. bounides*, *P. humboldti*, *P. puipui*). In addition, Herrera-Alva et al. (2023) revealed *P. scitulus* as part of the *P. danae* species group.

The systematics among several populations in southwestern Amazonia and along the eastern Andean slopes of Bolivia and Peru, today considered part of the *P. conspicillatus* and *P. danae* species groups, has been historically complex and partly chaotic, with certain populations misidentified at the species level and repeatedly allocated to the wrong groups (see Padial and De la Riva 2005, 2009). The reason for these long-lasting uncertainties was caused by superficial morphological similarities among species as well as by traits shared among species in both species groups. Padial and De la Riva (2009), with the descriptions of *P. koehleri* (*P. conspicillatus* group) and *P. reichlei* (*P. danae* group), cleared part of the existing chaos, as both species were previously confused with other taxa of both groups, respectively. They also demonstrated that among Amazonian frogs, there could be many sister and similar-looking unnamed species (i.e., sibling species; see Bickford et al. 2007) hidden under names that are applied to populations of more than one species.

In a recent study on the taxonomy and systematics of species in the *P. conspicillatus* group, Köhler et al. (2022) included species of the related *P. danae* group and provided a first indication of the presence of two divergent lineages among populations currently considered part of *P. reichlei*, as later also demonstrated by Herrera-Alva et al. (2023). In this new study, we follow clues provided by Köhler et al. (2022) and Herrera-Alva et al. (2023), and, based on genetic and bioacoustic evidence, we describe and name a new species of *Pristimantis* that is morphologically most similar and phylogenetically sister to *P. reichlei*, and with which it occurs in sympatry in some areas of the southwestern Amazon basin.

Material and methods

Fieldwork and voucher specimens

Fieldwork was conducted in different areas of the southwestern Amazon basin. Specimens were observed and collected during opportunistic searches during the day and night using torchlights and headlamps. Geographic position was recorded using handheld GPS receivers set to WGS84 datum. Collected specimens were euthanized with an overdose of 5% lidocaine or benzocaine gel applied to the ventral surfaces of individuals (McDiarmid 1994). Tissue samples were taken prior to fixation and stored in pure ethanol, while specimens were fixed using 96% ethanol or 4% formalin and subsequently stored in 70% ethanol. Newly collected specimens were deposited in the herpetological collections of the Museo de Historia Natural, Universidad Nacional Mayor de San Marcos (**MUSM**), Lima, Peru; Zoologische Staatssammlung München (**ZSM**), Germany; Museo de Biodiversidad del Perú (**MUBI**), Cusco, Peru; and Carnegie Museum of Natural History (**CM**), Pittsburgh, USA. **KU** refers to the University of Kansas, Museum of Natural History, Lawrence, USA; **MNCN** refers to the Museo Nacional

de Ciencias Naturales, Madrid, Spain; **MCZ** refers to the Museum of Comparative Zoology, Harvard University, Cambridge, USA; **MNK-A** refers to the amphibian collection of the Museo Noel Kempff Mercado, Santa Cruz, Bolivia; **NMP6V** refers to the Department of Zoology, National Museum, Prague, Czech Republic; **SMNS** refers to Staatliches Museum für Naturkunde Stuttgart, Germany; **ZFMK** refers to Zoologisches Forschungsmuseum A. Koenig, Bonn, Germany; **FGZC** refers to Frank Glaw field numbers.

External morphology

Morphometric measurements (in millimeters) were taken by CAP, JCC, JK, and JMP with calipers to the nearest 0.1 mm. Measurements taken and used throughout the text are those used by Köhler et al. (2022): **SVL**, snout–vent length (distance from tip of snout to posterior end of the body); **TL**, tibia length (distance from knee to distal end of tibia); **HW**, head width (at level of angle of jaws); **HL**, head length (from posterior margin of lower jaw to tip of snout); **IOD**, interorbital distance (distance between upper eyelids); **ED**, horizontal eye diameter (length of the visible eye); **E–N**, eye–nostril distance (straight line distance between anterior corner of orbit and posterior margin of external nares); **TD**, tympanum diameter (horizontal distance between the peripheral borders of the tympanic annulus); **HandL**, hand length (from proximal border of outer metacarpal tubercle to tip of third finger); **FootL**, foot length (from proximal border of inner metatarsal tubercle to tip of fourth toe). Fingers and toes are numbered preaxially to postaxially from I–IV and I–V, respectively. The lengths of fingers I and II were determined by adpressing the fingers against each other. For character state definitions, we followed Duellman and Lehr (2009). Descriptions and diagnostic schemes follow Padial et al. (2016). Coloration in life was described based on digital photographs.

Bioacoustics

Vocalizations in the field were recorded using an Edirol R-09 digital recorder with built-in microphones (at 44.1 KHz and 16-bit resolution, saved as uncompressed wave format) or a Sony WM-D6C tape recorder with an attached directional microphone Sennheiser Me-80 (for calls of *P. reichlei*). Recordings were sampled or re-sampled at 22.05 kHz and 32-bit resolution and analyzed using the software Cool Edit Pro 2.0. Frequency information was obtained through Fast Fourier Transformation (FFT; width 1024 points) at the Hanning window function. Spectrograms were obtained with the Blackman window function with 256 bands resolution. Sensitive filtering was applied to remove background sounds, but only to frequencies outside the prevalent bandwidths of calls. Temporal measurements are summarized as a range, with the mean ± standard deviation in parentheses. Description, terminology, and methods follow those recommended by Köhler et al. (2017), using the call-centered terminological scheme. Representative sections of the call recordings analyzed were archived in the Zenodo repository under DOI https://doi.org/10.5281/zenodo.10852627.

Molecular data

Monophyly and sister relationships between the focal lineage and putative new species were tested through phylogenetic analyses of a fragment of the mitochondrial 16S rRNA gene. As revealed by preliminary data presented by Köhler et al. (2022), the focal lineage (*P.* cf. *reichlei* sensu Köhler et al. 2022; hereafter referred to as *P.* aff. *reichlei*) is part of the *P. danae* species group. For taxon sampling, we therefore selected representative samples of this group as well as of its sister clade, the *P. conspicillatus* group (Padial et al. 2014). As the focal lineage is morphologically most similar to *P. reichlei* and *P. danae*, which are sister species (Padial and De la Riva 2009; Padial et al. 2014), we included all homologous DNA sequences of these species available from GenBank. We rooted our tree with *Yunganastes*, which is sister to *Pristimantis* (Padial et al. 2009). We extracted DNA using a standard salt extraction protocol and performed polymerase chain reactions (PCR) with primers 16SAr-L (5'-CGCCTGTTTATCAAAAACAT-3') and 16SBr-H (5'-CCGGTCTGAACTCAGATCACGT-3') (Palumbi et al. 1991). PCR products were then directly sequenced on automated DNA sequencers by LGC Genomics (Berlin, Germany). All new DNA sequences were submitted to GenBank (accession numbers PP621188–PP621210). We used MAFFT (Katoh and Standley 2013) with the G-INS-i algorithm as implemented in Concatenator (Vences et al. 2022) to align sequences to reference sequences of other *Pristimantis* downloaded from GenBank. After removing differences in length resulting from variations in priming regions, we obtained an alignment of 496 base pairs and 75 terminals. We used these data to infer the best model (TIM2+F+I+R3) under Model Finder (Kalyaanamoorthy et al. 2017), as well as the maximum likelihood tree (log-likelihood: -4805.1412) (Nguyen et al. 2015), using IQ-TREE 2.2.0 (Minh et al. 2020). Branch support was assessed through 500 replicates of standard non-parametric bootstrapping as well as 1000 iterations of the Shimodaira-Hasegawa approximate likelihood ratio test (SH-aLRT) (Shimodaira and Hasegawa 1999), both implemented in IQ-TREE. Genetic divergences were quantified as uncorrected pairwise distances (p-distances) on pairwise alignments, not considering gaps using TaxI2 (Vences et al. 2021). A table with all used sequences, GenBank accession numbers, voucher numbers, and locality information is archived in the Zenodo repository under DOI https://doi.org/10.5281/zenodo.10958854.

Results

Molecular data

The inferred maximum likelihood tree (log-likelihood: -4805.1412; Fig. 1), based on an alignment of 496 nucleotides of the 16S rRNA gene, recovered the *Pristimantis conspicillatus* and *P. danae* species groups as monophyletic, with higher support for the latter. Our samples of *P. reichlei* are grouped into two well-supported and highly divergent clades, although the support for their sister relationship is low (bootstrap/SH-aLRT = 45/78). One clade includes all topotypical samples, and we considered it *P. reichlei* sensu stricto. Within this clade of nominal *P. reichlei*, considerable differentiation is evident among samples. The other clade includes samples from Panguana, central Peru, south-eastern Peru, and northernmost Bolivia. We labeled this clade *P.* aff. *reichlei*. The clade containing *P.* aff. *reichlei* and *P. reichlei* is sister to *P.* aff. *danae* samples from Bolivia, and the clade containing *P.* aff. *reichlei*, *P. reichlei*, and *P.* aff. *danae* is sister to nominal *P. danae* samples from Peru. These four mentioned subclades together are sister to all samples in the *P. danae* group from high elevations, and these all together are sister to samples of *P. cosnipatae* + *P. toftae* and *Pristimantis* sp. (GenBank accession number KY652655; a sample formerly identified as *P. pharangobates*; see Herrera-Alva et al. 2023), although some of the basal nodes received no significant bootstrap support.

Genetic divergences between the target lineages were rather high compared to other known sister lineage divergences in *Pristimantis* (e.g., Köhler et al. 2022; Herrera-Alva et al. 2023). *Pristimantis* aff. *reichlei* differed from *P. reichlei* in uncorrected pairwise distances by 9.5–13.5% (mean 11.4%), and *P.* aff. *danae* from Bolivia differed from *P. danae* from Peru invariably by 9.4% for all available sequences. *Pristimantis* aff. *danae* differed from *P. reichlei* by 11.9–15.2% (mean 12.7%) and from *P.* aff. *reichlei* by 7.4–9.1% (mean 8.3%). The respective values for nominal *P. danae* were 12.3–14.8% (mean 13.2%) and 7.4–9.1% (mean 8.3%).

Genetic distances were also high within two of these four main lineages. While no sequence divergence was found among the *P. danae* samples from Peru (all from the same or nearby localities) and only up to 0.2% among sequences from Bolivian *P.* aff. *danae*, uncorrected pairwise distances within *P.* aff. *reichlei* amounted up to 5.0% and within *P. reichlei* up to 9.3% (between samples from the Bolivian type locality Los Guácharos and Santo Domingo de Carabaya, Peru, but <6% between numerous other populations). See the Zenodo archive (DOI https://doi.org/10.5281/zenodo.10958854) for a table with all pairwise distances.

Morphology

Our external morphological examination of specimens of the focal lineage *P.* aff. *reichlei* and comparisons with paratype specimens of *P. reichlei* from close to its type locality (Provincia Chapare, Departamento Cochabamba, Bolivia; ZFMK 66975, 72564–72565, 72587–72589) revealed no diagnostic differences in measurements (Table 1), proportions, or color pattern. The only qualitative morphological differences observed are comparatively faint and were: (1) specimens of *P.* aff. *reichlei* exhibit a barely recognizable small, flat, round outer metatarsal tubercle in life, which is virtually absent in preservative, whereas in *P. reichlei* it is distinct, prominent, ovate, and subconical, both in life and preservative (Fig. 4); (2) a difference in the outline of the canthus rostralis when viewed in straight angle from above. In *P.* aff. *reichlei*, the canthus rostralis runs almost straight from the anterior corner of the eye to the tip of snout, whereas in *P. reichlei*, the canthus rostralis is concavely curved around the nostrils, resulting in an indentation that allows to see a larger portion of the nostrils in straight dorsal view (Fig. 5). However, given the limited number of individuals available for direct examination (Table 1), we are not completely confident that the latter is a constant diagnostic character to distinguish among both major lineages across their entire ranges.

Bioacoustics

The advertisement call of *P.* aff. *reichlei* from Panguana is characterized by being a single pulsatile note, simple in structure, and repeated at irregular intervals (see species account below for a detailed call description). Compared to Bolivian calls of *P. reichlei* from close to its type locality (Köhler 2000; Márquez et al. 2002 [as *Eleutherodactylus danae*]), the sister taxon of the focal lineage, the following differences are evident: Advertisement calls of *P. reichlei* are always composed of two pulsed calls (= notes) emitted in conjunction (a two-note call when following the note-centered terminology of Köhler et al. 2017) that differ from each other in duration and dominant frequency, with the second call being slightly longer in duration and higher in dominant frequency compared to the first call. Call duration (= note duration) in calls of *P. reichlei* is longer (49–68 ms) compared to calls of *P.* aff. *reichlei* at Panguana (23–47 ms), without overlap, and calls are emitted at a different temporal pattern (see Köhler 2000). Moreover, calls of *P. reichlei* are distinctly pulsed, with pulses being clearly separated and countable (pulse rate 155–194 pulses/second), versus pulses being largely fused and barely separated from each other but emitted at a distinctly higher rate in *P.* aff. *reichlei* (pulse rate ca. 300–375 pulses/second). Despite similar male body sizes (Table 1), the dominant frequency in calls of *P. reichlei* is significantly lower (1685–2384 Hz) when compared to those of *P.* aff. *reichlei* (3289–3628 Hz). Calls of both species are immediately distinguishable in the field, as they sound quite different to the human ear.

Although only very few call recordings are available for analysis and respective comparisons among the focal lineages in consideration (calls of two individuals of *P.* aff *reichlei* and three individuals of *P. reichlei*), the qualitative and quantitative differences in advertisement call structure revealed are far beyond those that could

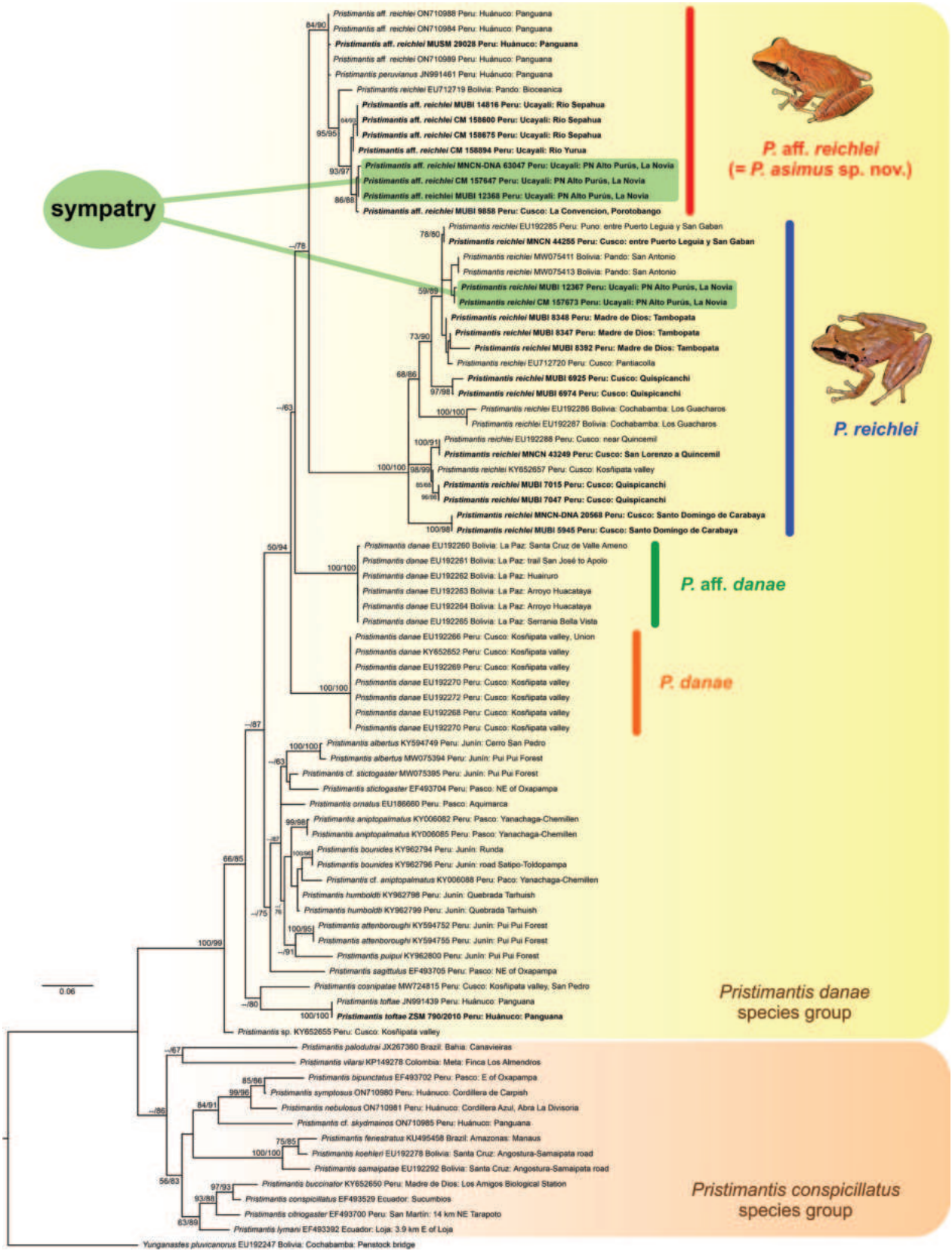

Figure 1. Maximum likelihood phylogenetic tree of selected samples of *Pristimantis*, representing the *P. conspicillatus* and *P. danae* species groups, inferred from an alignment of 496 nucleotides of the mitochondrial 16S rRNA gene. *Yunganastes pluvicanorus* was used to root the tree. Numbers at nodes are bootstrap values in percent (500 replicates; not shown if <50%) followed by SH-aLRT values (1000 iterations; not shown if <50) as calculated with IQ-Tree. The taxon name is followed by the GenBank accession number, or voucher number for newly produced sequences (bold terminals), and sample locality. Samples highlighted in green indicate the sympatric locality of *P. asimus* and *P. reichlei*. Inset photos depict paratopotypes of *P. asimus* sp. nov. (MUSM 29074) and *P. reichlei* (ZFMK 66975) in life, respectively.

Table 1. Morphometric measurements (in mm) of specimens of *Pristimantis asimus* sp. nov., *P. reichlei*, and *P. danae*, including holotypes and paratypes. BO = Bolivia; PE = Peru; m = male; f = female; subad. = subadult (all other adult specimens); * = paratype; ** = holotype; — = not available. For other abbreviations used, see Material and methods.

	sex	SVL	TL	HL	HW	IOD	ED	TD	E-N	HandL	FootL
P. asimus											
MUSM 41241** PE: Panguana	m	30.6	17.9	12.1	11.2	3.1	4.3	1.9	4.1	7.8	14.3
MUSM 29028* PE: Panguana	m	27.7	17.1	10.6	9.8	3.1	4.3	1.7	3.3	7.6	13.6
MUSM 29073* PE: Panguana	m	27.7	17.1	11.2	9.9	3.6	4.0	2.0	3.3	7.7	13.3
MUSM 29074* PE: Panguana	m	28.3	17.0	11.3	10.1	3.5	4.0	2.1	3.6	8.1	14.2
ZSM 1986/2008* PE: Panguana	m	28.4	17.3	12.7	10.4	3.2	4.1	1.9	3.5	7.8	14.2
ZSM 1985/2008* PE: Panguana	m	30.6	17.2	12.8	10.9	3.4	3.9	2.0	4.2	7.6	13.9
SMNS 8856* PE: Panguana	m	29.8	17.7	11.9	10.6	3.7	3.9	2.1	3.9	10.0	14.1
MUBI 12368* PE: La Novia	m	30.6	18.5	11.9	11.1	3.0	4.0	1.9	4.0	8.6	16.9
MUBI 14816* PE: Rio Sepahua	f subad.	26.0	15.4	9.6	9.5	2.7	3.0	1.5	3.3	7.2	11.4
SMNS 6386* PE: Panguana	f	37.9	22.4	14.7	13.7	4.7	4.8	2.5	5.1	10.8	17.7
P. reichlei											
ZFMK 66975* BO: Chapare	m	30.5	19.8	12.7	11.1	3.2	4.0	2.0	3.9	9.0	16.3
ZFMK 72588* BO: Chapare	m	27.7	15.6	10.7	9.8	3.1	4.0	1.7	3.8	8.3	14.0
ZFMK 72589* BO: Chapare	m	28.2	18.3	11.3	10.8	3.5	4.6	2.2	3.6	9.3	15.4
ZFMK 72564* BO: Chapare	m	28.8	16.9	13.1	10.5	3.6	3.9	2.0	4.0	8.6	14.4
ZFMK 72565* BO: Chapare	m	27.9	16.9	11.4	9.6	2.8	3.9	2.3	3.2	8.5	14.5
MNCN 43028* BO: Chapare	m	25.3	15.4	9.6	9.1	—	3.6	1.6	3.2	—	12.6
MNK-A 6620** BO: Chapare	f	32.3	20.5	12.6	11.8	—	3.8	1.7	4.0	—	17.0
MNCN 43024* BO: Chapare	f	35.0	21.4	12.7	12.1	—	4.6	2.0	4.4	—	17.4
ZFMK 72587* BO: Chapare	f	39.1	24.4	15.2	15.0	4.3	5.4	2.6	4.8	11.8	21.5
MUBI 8347 PE: Tambopata	f	33.4	19.8	12.1	11.4	4.0	4.2	1.8	4.2	8.7	14.8
MUBI 8347 PE: Tambopata	f	31.5	17.3	12.0	11.3	3.8	3.4	1.8	3.7	8.5	13.5
MUBI 12367 PE: La Novia	f	30.9	19.2	12.3	11.4	3.4	4.0	1.9	4.0	8.5	14.8
P. danae											
KU 162307** PE: Kosñipata	m	34.3	16.8	13.6	12.9	—	5.6	2.1	4.3	—	16.6
MCZ 93305* PE: Kosñipata	m	30.7	17.6	12.0	11.4	—	4.9	1.9	4.1	—	15.1
MCZ 93306* PE: Kosñipata	m	26.0	15.9	10.6	9.6	—	4.4	1.7	3.7	—	13.4
MUSM 13957* PE: Santa Isabel	m	24.3	15.7	10.9	9.9	3.5	4.2	1.8	3.6	7.9	12.5

be attributed to intra-specific call variation (see Köhler et al. 2017). Even if more recordings become available in the future, it is more than unlikely that an increased sample size would alter the conclusions derived from our bioacoustic analyses by interpreting observed differences in calls as intra-specific variation. On the contrary, call parameters and spectrograms available in the published literature (e.g., Schlüter 1980; Rodríguez 1994; Duellman 2005) indicate a misidentification of respective populations and corroboration of the call characteristics described for both lineages compared herein (see below).

Calls of *P. danae* from Manu National Park in Peru (https://soundcloud.com/user-416416746/pristimantis-danae?in=user-416416746/sets/cantos-de-nfibios-del-pn-manu) are trill-like calls of approximately 80–120 ms duration, composed of 3–4 widely spaced pulses (pulse rate approximately 30 pulses/second). Calls of *P.* aff. *danae* from Bolivia are characterized by being composed of two notes, each note containing two distinctly separated pulses only (Padial and De la Riva 2009).

In summary, the bioacoustic differences observed among the clades here allocated to *P. reichlei*, *P. danae*, *P.* aff. *danae*, and the focal lineage *P.* aff. *reichlei* provide further evidence for the specific distinctness of respective lineages, particularly in view of the partly sympatric occurrence of *P. reichlei* and *P.* aff. *reichlei* (see below). Consequently, we describe the lineage hitherto referred to as *P.* aff. *reichlei* as a new species.

Taxonomy

Pristimantis asimus **sp. nov.**

https://zoobank.org/298F59D4-1918-4833-8C64-B935FA7E826E

Remarks. This species has been previously referred to as *Eleutherodactylus peruvianus* by Schlüter (1980) and Lehr (2002 [partim]); *Eleutherodactylus fenestratus* by Rodríguez (1994); *Eleutherodactylus* aff. *conspicillatus* by Schlüter (2005); *Pristimantis* cf. *danae* by Moravec and Aparicio (2005); *Pristimantis reichlei* by Padial and De la Riva (2009 [partim]), Moravec et al. (2020 [partim]), and Herrera-Alva et al. (2023 [partim]); *Pristimantis peruvianus* by Pinto-Sánchez et al. (2012), de Oliveira et al. (2020), and Fouquet et al. (2022); and *Pristimantis* cf. *reichlei* by Köhler et al. (2022).

Type material. ***Holotype*.** MUSM 41241 (FGZC 5342, formerly ZSM 177/2017), adult male (Figs 2, 3), from the Área de Conservación Privada Panguana (9.6166°S, 74.9333°W, 260 m above sea level), lower Río Yuyapichis, Provincia Puerto Inca, Departamento Huánuco, Peru, collected on 29 September 2017 by F. Glaw. GenBank accession number for 16S: ON710989.

***Paratypes*.** A total of 16 specimens: ZSM 1985–1986/2008 (FGZC 3388–3389), two adult males, same locality as holotype, collected on 10 December 2008 by F. Glaw; MUSM 29073–29074 (FGZC 3300, 3273), two adult males, MUSM 29028 (FGZC 3274), an adult male (call voucher), same locality as holotype, collected between 26 November and 2 December 2008 by F. Glaw; FGZC 6334 (to be deposited in ZSM), an adult male, same locality as holotype, collected on 17 November 2019 by E. Castillo-Urbina, F. Glaw and J. Köhler; SMNS 6386, an adult female, same locality as holotype, collected on 11 November 1985 by A. Schlüter; SMNS 8856, an adult male, same locality as holotype, collected in 1972 by R. Aussem; MUBI 14816, a subadult female, CM 158675, an adult male, from Campamento 4, between Quebrada Sungaro and Quebrada Esther, Río Sepahua (11.0801°S, 72.1258°W, 395 m a.s.l.), Distrito

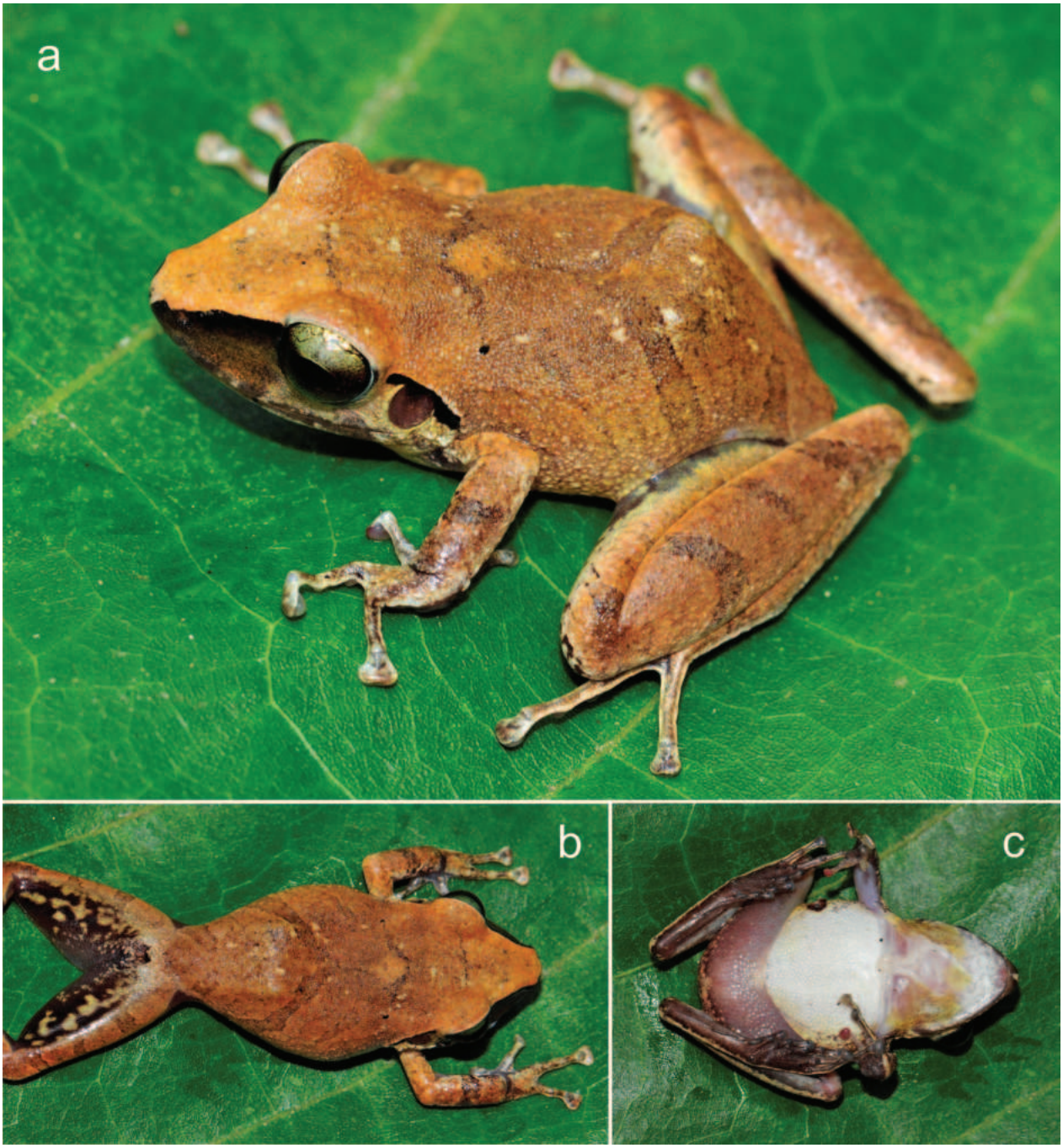

Figure 2. Male holotype of *Pristimantis asimus* sp. nov. (MUSM 41241, FGZC 5342) from Panguana, Departamento Huánuco, Peru, in life (SVL 30.6 mm): **a.** Dorsolateral view; **b.** Dorsal view (showing posterior thighs coloration); **c.** Ventral view.

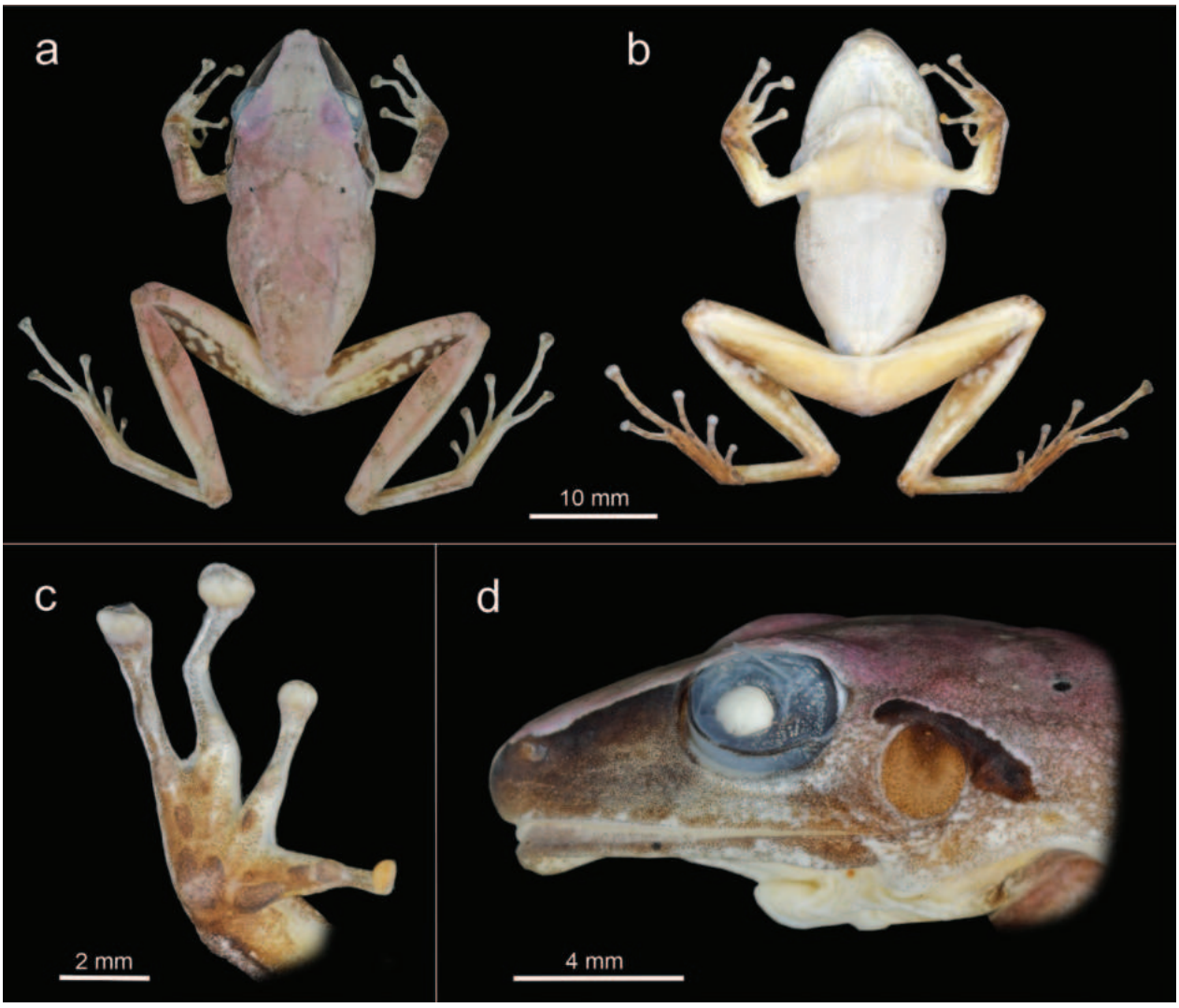

Figure 3. Preserved male holotype of *Pristimantis asimus* sp. nov. (MUSM 41241, FGZC 5342) from Panguana, Departamento Huánuco, Peru: **a.** Dorsal view; **b.** Ventral view; **c.** Palmar surface of the right hand; **d.** Lateral view of the head.

Sepahua, Provincia Atayala, Departamento Ucayali, Peru, collected on 3 and 6 March 2014, respectively, by J. M. Padial, L. A. G. Gagliardi, J. C. Chaparro and R. Gutiérrez; CM 158600, an unsexed adult, from a track across the river from Campamento 2, Río Sepahua (11.0491°S, 72.4489°W, 408 m a.s.l.), Distrito Sepahua, Provincia Atayala, Departamento Ucayali, Peru, collected on 24 February 2014 by J. M. Padial, L. A. G. Gagliardi, J. C. Chaparro and R. Gutiérrez; CM 158894, an adult male from a track ca. 4 km west of Breu, on the road to Victoria (9.5451°S, 72.7933°W, 223 m a.s.l.), Distrito Yurúa, Departamento Ucayali, Peru, collected on 12 February 2015, by J. M. Padial, L. A. G. Gagliardi, R. Gutiérrez, O. Rojas and S. Castroviejo-Fisher; MUBI 12368, an adult male, from Puesto de Control y Vigilancia La Novia, Río La Novia (9.9883°S, 70.7084°W, 262 m a.s.l.), Distrito Purús, Departamento Ucayali, Peru, collected on 25 January 2013 by J. M. Padial, L. A. G. Gagliardi, R. Gutiérrez and S. Castroviejo-Fisher; MUBI 9858, an unsexed adult from Porotobango (11.4311°S, 73.3471°W, 469 m a.s.l.) Provincia La Convención, Departamento Cusco, Peru, collected on 25 January 2010 by L. Tejada; NMP6V 72578/1–2, two adult males (also paratypes of *P. reichlei*), from Bioceanica (11.1333°S, 69.3666°W, 290 m a.s.l.), Departamento Pando, Bolivia, collected on 25 January 2005 by J. Moravec.

Definition. A medium-sized species of the *Pristimantis danae* species group (based on molecular relationships and morphological similarity), with 27.7–30.6 mm SVL in adult males (n = 7), and 37.9 mm SVL in adult females (n = 1), characterized by: (1) skin on dorsum finely shagreened, lacking enlarged tubercles or warts; throat smooth, venter areolate; discoidal fold inconspicuous; dorsolateral folds absent; upper eyelid lacking tubercles and granules; posterior surfaces of thighs smooth; (2) tympanic membrane and annulus distinct, slightly higher than long, their length less than half of eye diameter; supratympanic fold prominent, curved, slightly covering upper edge of tympanic annulus; (3) head slightly longer than wide; snout subacuminate in dorsal view, bluntly rounded in lateral profile; canthus rostralis straight in dorsal view, slightly rounded in profile; (4) cranial crests

absent; (5) dentigerous process of vomers elongate, oblique, situated posteromedial to choanae; (6) males with vocal slits, single subgular vocal sac; indistinct nuptial asperities on dorsal surface of thenar tubercle; (7) hands with slender fingers, first finger slightly shorter or about equal in length to second; subarticular tubercles subconical, prominent; supernumerary tubercles absent; palmar tubercle cordiform; thenar tubercle prominent, elongated; terminal discs of inner two fingers enlarged and round, those of external fingers enlarged, truncate, about twice the width of digit proximal to disc; circumferential grooves conspicuous, ungual flap not indented; narrow lateral fringes on fingers weakly developed; basal webbing between fingers absent; (8) ulnar tubercles absent; (9) tubercles on heel and tarsus absent, tarsal fold present; (10) inner metatarsal tubercle prominent, ovate; outer metatarsal tubercle small, round, flat, barely recognizable in life, virtually absent in preservative; supernumerary tubercles absent; (11) toes long and slender; lateral fringes narrow, weak; basal toe webbing present; toe V reaching beyond distal level of penultimate subarticular tubercle of toe IV; tips of toes rounded to slightly ovate, enlarged; circumferential grooves conspicuous; (12) in life, dorsal coloration light brown, reddish-brown, or tan, usually with dark brown chevrons and flecks on dorsum; dark brown bars on dorsal surfaces of arms and legs; a pair of black spots dorsolaterally in scapular region; black supratympanic stripe; black canthal stripe; belly creamy white; throat with fine dark mottling in males; posterior surfaces of thighs blackish with yellowish-cream spots and flecking; iris bronze, with black reticulation in life; posterior iris periphery cream to turquoise; bones white; (13) advertisement call consisting of a single pulsatile note of 23–47 ms duration and with a dominant frequency of 3289–3628 Hz, repeated at irregular intervals, containing groups of 2–4 calls repeated in faster succession.

Diagnosis. *Pristimantis asimus* differs from other species in the *Pristimantis danae* species group as follows: The new species differs from *P. albertus*, *P. attenboroughi*, *P. bounides*, *P. clarae*, *P. cosnipatae*, *P. humboldti*, *P. ornatus*, *P. pharangobates*, *P. puipui*, *P. rhabdolaemus*, *P. sagittulus*, *P. similaris*, *P. stictogaster*, and *P. toftae*, at least by the lack of dorsolateral folds (versus presence). Furthermore, *P. attenboroughi*, *P. bounides*, *P. humboldti*, and *P. puipui* have stout bodies with relatively shorter legs when compared to *P. asimus*. *Pristimantis attenboroughi* and *P. puipui* lack a tympanum (prominent in the new species), and *P. attenboroughi* lacks vocal slits in males (present in the new species). *Pristimantis clarae* additionally differs from the new species by dorsal and ventral color pattern, advertisement call, and smaller adult male size (12.9–15.6 versus 27.7–30.6 mm). As the new species, *P. aniptopalmatus* lacks dorsolateral folds (Duellman and Hedges 2005) but differs by its smaller adult male size (16.5–23.2 versus 27.7–30.6 mm), presence of a tubercle on the upper eyelid, and color pattern (Duellman and Lehr 2009). *Pristimantis cuneirostris* lacks dorsolateral folds but differs from the new species by a long wedge-shaped snout (unique in the *P. danae* species group; Duellman and Pramuk 1999; Duellman and Lehr 2009), lack of toe webbing (versus basal webbing present), and posterior surfaces of thighs uniformly brown (versus blackish with yellowish-cream blotches and flecks). *Pristimantis scitulus* mainly differs from the new species by the presence of a single conical tubercle on upper eyelid (absent), dentigerous processes of vomers absent (present), presence of a conical tubercle on heel (absent), and webbing on toes absent (basal webbing present) (Duellman 1978).

Morphologically, *P. asimus* is most similar or even cryptic to *P. danae* and *P. reichlei*. However, as a tendency, nominal *P. danae* (from Kosñipata valley, Peru) exhibit a more contrasting dorsal color pattern in life (see, e.g., Duellman and Lehr 2009: fig. 150) when compared to *P. asimus*. Moreover, in dorsal view, the snout in *P. danae* is rounded (versus subacuminate in *P. asimus*). From *P. reichlei*, the new species seems to differ by a very small, round, flat outer metatarsal tubercle, barely recognizable in life and virtually indistinguishable in preservative (versus distinct, ovate, subconical, recognizable in life and in preservative; Fig. 4). Moreover, there are slight differences in the dorsal outline of the canthus rostralis, with a relatively smaller portion of the nostrils being visible when viewed from straight above in *P. asimus* compared to *P. reichlei*, where nostrils are almost completely visible from above as the canthus rostralis shows a curved indentation around the nostrils (Fig. 5). The new species differs from both *P. danae* and *P. reichlei* by substantial differentiation in the 16S gene and differences in the advertisement call (see above).

The new species occurs in sympatry with some species of the *P. conspicillatus* group, which superficially may have a similar appearance. However, these are distinguishable from *P. asimus* by molecular phylogenetic relationships, differences in advertisement calls, and most of them by different relative finger lengths, i.e., the first finger being longer than the second. However, the sympatric *P. iiap* has the first and second fingers equal in length but differs from the new species at least by exhibiting distinct dorsolateral folds (Padial et al. 2016).

Description of the holotype. An adult male, in good state of preservation (Fig. 3), with subgular vocal sac and vocal slits. Head slightly longer than wide (HL/HW = 1.08); snout subacuminate in dorsal view, bluntly rounded in profile; nostrils oriented posterolaterally; canthus rostralis straight in dorsal view, slightly rounded in profile; loreal region slightly concave; lips not flared; upper eyelid without tubercles; cranial crests absent. Supratympanic fold prominent, long, slightly curved, covering uppermost tympanic annulus; tympanic membrane and annulus distinct; tympanic membrane slightly higher than long, its length slightly less than half the eye diameter; one flat round postrictal tubercle. Choanae not concealed by palatal shelf of the maxillary arch when roof of mouth is viewed from below; choanae large, oval, separated by distance equal to five times diameter of a choana; dentigerous process of vomers present, but barely evident, flat,

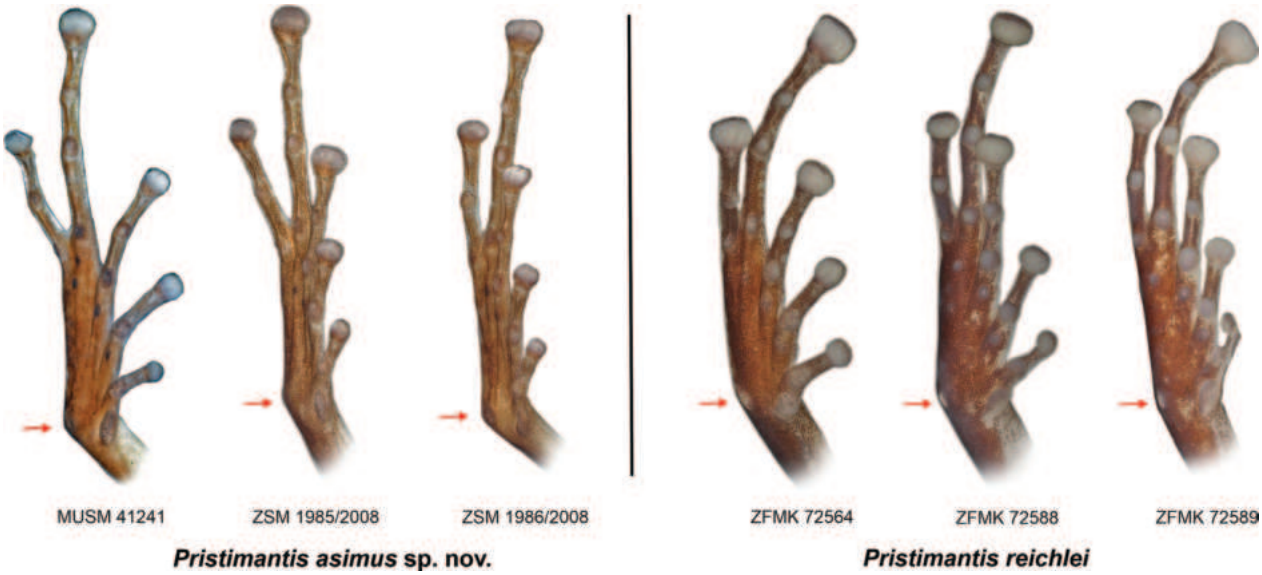

Figure 4. Comparative plate showing plantar surfaces of the right feet of preserved type specimens of *Pristimantis asimus* sp. nov. (all from Panguana, Huánuco, Peru) and *P. reichlei* (all from Chapare, Cochabamba, Bolivia). Red arrows point to the outer metatarsus, showing the virtual absence versus the presence of an outer metatarsal tubercle. Not to scale.

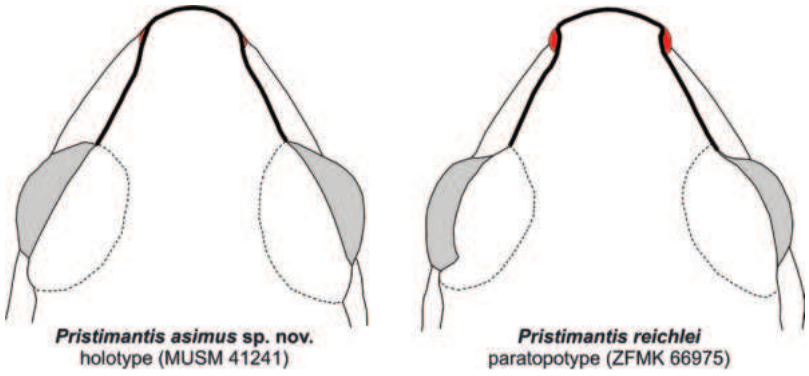

Figure 5. Schematic line drawings of dorsal views of the heads of male *Pristimantis asimus* sp. nov. and *P. reichlei*, exemplifying the differing outlines of the canthus rostralis (bold line), resulting in the visibility of different portions of the nostrils (red) in straight dorsal view. Not to scale.

elongate, not in contact, oblique, situated posteromedial to choanae, bearing vomerine teeth; tongue removed for tissue sample; vocal sac subgular, vocal slits placed posterolaterally. Skin on dorsum finely shagreened, lacking enlarged tubercles or warts; dorsal surfaces of hind limbs finely shagreened, dorsal surfaces of forearms and flanks finely shagreened; skin on throat and chest smooth, that on belly areolate; occipital folds absent; dorsolateral folds absent; discoidal fold indistinct. Arm without ulnar tubercles; palmar tubercle cordiform, about double in size to elongate thenar tubercle; supernumerary tubercles absent; subarticular tubercles prominent, subconical; fingers long and slender; finger tips enlarged, rounded on inner two fingers, on two outer fingers truncate, their width about twice the width of digit proximal to disc; circumferential grooves conspicuous, ungual flap not indented on outer fingers; lateral fringes and keels on fingers weak, barely recognizable; basal webbing between fingers absent; relative length of fingers III>IV>II≥I; nuptial asperities on dorsal surface of thenar tubercle indistinct. Toes long and slender (FootL 47% of SVL); heel and tarsus lacking tubercles; tarsal fold present; inner metatarsal tubercle ovate, prominent; outer metatarsal tubercle not recognizable; supernumerary tubercles absent; subarticular tubercles prominent, subconical; narrow lateral fringes on toes present, weakly developed; basal toe webbing present; toe tips enlarged, rounded, their width about 1.5 times the width of toe proximal to disc; circumferential grooves conspicuous; relative length of toes IV>V>III>II>I; toe V reaching slightly beyond distal level of penultimate subarticular tubercle of toe IV. Tibiotarsal articulation reaching distinctly beyond tip of snout when hindlimb flexed parallel to axis of body; heels broadly overlapping when hind limbs flexed perpendicular to axis of body. For morphological measurements, see Table 1.

In life (Fig. 2), dorsal ground color light brown, with darker brown chevron-shaped marking slightly anterior to sacral region; irregular dark brown U-shaped line in scapular region, bordered posteriorly by orange-brown blotch; irregular indistinct dark brown markings and lines

Figure 6. Paratypes of *Pristimantis asimus* sp. nov. in life (dorsolateral and ventral views): **a.** ZSM 1985/2008 (FGZC 3388; SVL 30.6 mm); **b.** ZSM 1986/2008 (FGZC 3389; SVL 28.4 mm); **c.** MUSM 29074 (FGZC 3273; SVL 28.3 mm), all from the type locality Panguana, Huánuco, Peru; **d.** CM 158600, from Río Sepahua, Ucayali, Peru.

on dorsum; minute cream flecks, irregular in outline, scattered on dorsum; triangular cream fleck on snout tip; dark brown bars on dorsal surfaces of arms and legs; dark brown interorbital line, partly interrupted, not extending to upper eyelids; a pair of small black spots dorsolaterally in scapular region; black supratympanic stripe; broad blackish canthal stripe; lips dark brown to black, irregularly barred with cream; flanks light brown with irregular dark brown markings; belly creamy-white; anterior throat grayish-white with scattered fine gray mottling, posterior throat yellowish with irregular fine brown mottling; chest pinkish-white; ventral surfaces of thighs and shanks pinkish-gray; posterior surface of thighs blackish with irregular yellow-cream blotches and flecks; tarsus, plantar, and palmar surfaces dark brown; iris bronze, with black reticulation, with a dark reddish-brown median streak; posterior iris periphery cream with a turquoise tint; bones white. After six years in preservative (Fig. 3), the general color pattern remains the same as in life. Brown ground coloration turned to grayish-tan, with some pinkish tint, particularly on upper eyelids; brown flecks, bars, and markings on dorsum slightly faded; chest and ventral surfaces of thighs yellowish-cream; belly creamy-white; throat creamy-white with gray mottling.

Variation. For variation in morphological measurements among type specimens, see Table 1. Females are significantly larger than males, approximately reaching 25% greater SVL. We observed some limited variation in color and color pattern among the specimens studied. In some individuals, the dorsal ground coloration is yellowish-tan to yellowish-brown in life (e.g., ZSM 1985/2008; Fig. 6a), whereas in most specimens, the dorsal ground color was reddish-brown in life (e.g., ZSM 1986/2008, MUSM 29074, CM 158600; Fig. 6b, c, d), as it was in the holotype. Darker dorsal markings might be more or less distinctly outlined with fine cream lines, with some individuals seemingly lacking these fine cream lines (Fig. 6a, b). A dark interorbital stripe is present in all specimens but narrow, less conspicuous, and barely extending on upper eyelids in the holotype and some paratypes (Figs 2, 6a, b), whereas a broader, distinct stripe outlined with fine cream lines extends to the upper eyelids in other specimens (Figs 6c, d, 7). Scattered dorsal cream spots and flecking might be present to different extent or completely absent. The contrasting color pattern on the posterior surfaces of thighs (dark brown with yellow-orange flecking) is present in all studied specimens, with CM 158600 having some orange color extending to the groin (Fig. 6d). Some males exhibit shades of

Figure 7. Male paratopotype (FGZC 6334) of *Pristimantis asimus* sp. nov. in life at: **a.** Night coloration in situ; **b.** Day coloration the day after collection, demonstrating a limited ability of color change. Note the dark brown, almost black, loreal region and upper lip in the day coloration, resulting in a dark facemask.

yellow on the throat in life (Fig. 6). Remarkably, the male paratype MUBI 14816 exhibits a well-marked, W-shaped occipital fold that is lacking in other specimens.

Natural history. At Panguana, individuals of this species have been observed being active at night, perching on small trees and bushes within disturbed primary forest. Schlüter (1980) reported males calling from vegetation mainly at 1–2 m height, with calling activity being most intense at dusk and at dawn, which is confirmed by our own observations. Schlüter (1980) described a vertical calling position with the head down as typical, but we observed calling males in a horizontal position on the upper side of leaves. Individuals of this species have some limited ability to change color, with nocturnal color being characterized by a light brown loreal region, whereas diurnal color is characterized by a dark loreal region and upper lip, turning dark brown to almost black (see Fig. 7). The habitat close to the type locality has recently been impacted by illegal gold mining activities, which constitute a potential threat to the anuran fauna of Panguana.

Vocalization. Advertisement calls of *Pristimantis asimus*, emitted by the male MUSM 29028, were recorded on 29 November 2008, at dusk (18:15 h) at the type locality (ambient temperature not recorded). The calling male was sitting on top of a horizontally oriented leaf at approximately 2.1 m height within the forest. The call consists of a single short pulsatile note, repeated at somewhat irregular intervals (see below). In our recording, 4 to 14 calls were emitted in succession and then interrupted by few seconds of silence. Each call (= note) has a clearly pulsatile structure, although 'pulses' are largely fused and, in most cases, barely countable. However, in some cases, distinct and thus countable energy peaks (4–10/call) are recognizable in the oscillograms of calls. In these calls, the pulse rate varies between 300 and 375 pulses/second. There is further amplitude modulation recognizable within each call, with maximum call energy being present around the center of each call, rapidly decreasing to a lower level, and further fading towards the call's end. Calls were usually emitted in slow succession but regularly contained sections of more rapidly repeated calls, usually 2–4 calls emitted at shorter intervals, altering the relatively regular pattern of call repetition (see Fig. 8a). In other words, call repetition rate may change temporarily from ca. 140 calls/min to ca. 900 calls/min. The character of calls in these rapidly repeated sections did not differ from other calls. It remains unknown whether this increased speed in call succession has a different function (e.g., territorial) or is just part of the ordinary advertisement call. Numerical parameters for 65 analyzed calls of the mentioned male are as follows: call duration (= note duration) 23–47 ms (36.0 ± 7.1 ms); inter-call interval in slow calling sections 305–597 ms (394.6 ± 73.6 ms); inter-call interval in rapid calling sections 26–37 ms (31.8 ± 4.6 ms); dominant frequency 3289–3628 Hz (3518 ± 97 Hz); second frequency peak at around 2000 Hz; prevalent bandwidth 1600–5400 Hz.

Schlüter (1980) described the call from the same locality (under the name *Eleutherodactylus peruvianus*). The spectrogram and numerical parameters (call duration ca. 40 ms) provided by him agree with our analysis. The call described by Rodríguez (1994) as that of *Eleutherodactylus fenestratus* from Cocha Cashu, Manu National Park, Madre de Dios, Peru, is also clearly referable to *P. asimus*. The parameters described by Duellman (2005) for calls of *P. fenestratus* from Cusco Amazónico clearly differ from those of *P. asimus*, but the corresponding audiospectrogram and oscillogram are in disagreement with the numerical parameters provided and may possibly correspond to *P. asimus*. Although difficult to compare according to another terminology used, the call described for *E. fenestratus* from Manaus, Brazil, by Zimmerman and Bogart (1984) seems to agree with that of *P. asimus*.

Distribution. As far as known and confirmed by bioacoustic and/or genetic data, *P. asimus* occurs in lowland rainforests from the southern Departamento Huánuco (Panguana, type locality) and eastern Departamento Ucayali (Breu, Río Yurua) southward across most of the lowlands of southeastern Peru, reaching the border of Machiguenga Communal Reserve (Departamento Cusco) and Manu National Park (Departamento Madre de Dios) in the south as well as northernmost Bolivia (Bioceanica, Departamento Pando) to the east (Fig. 9). All known localities are at elevations between 220 and 470 m a.s.l. The new species occurs

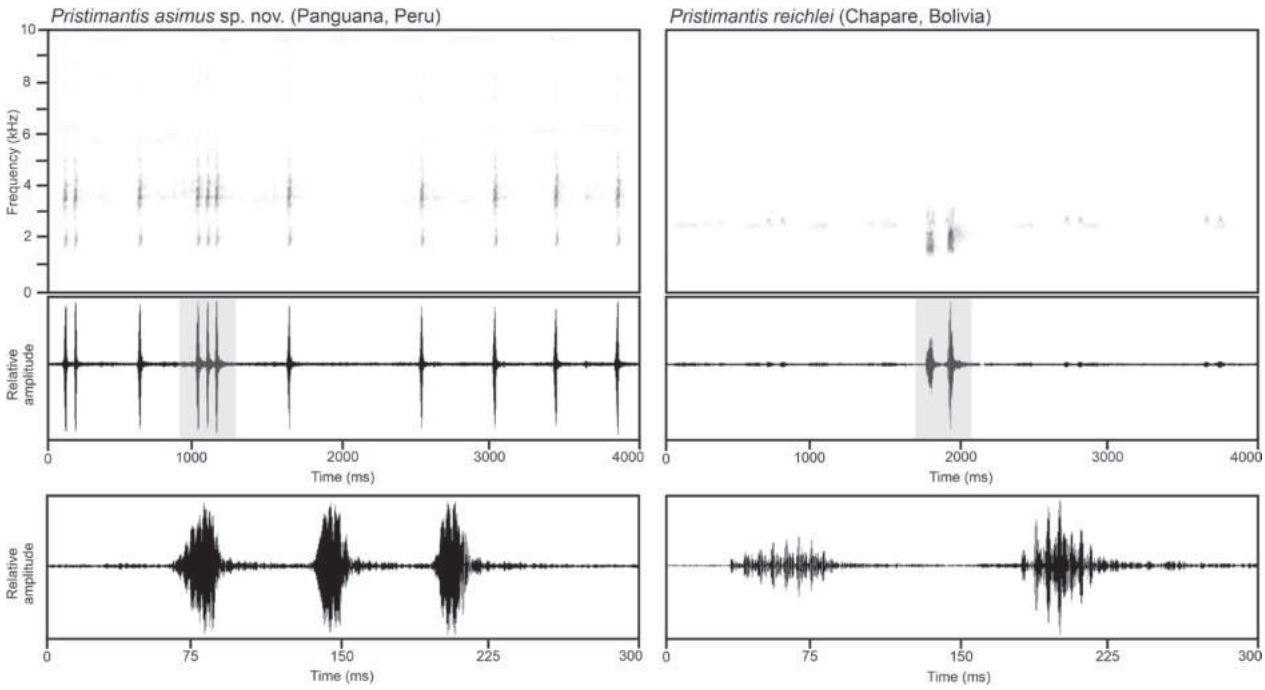

Figure 8. Audiospectrograms and corresponding oscillograms of the advertisement calls of *Pristimantis asimus* sp. nov. from the type locality Panguana, Peru (emitted by paratype MUSM 29028) and *Pristimantis reichlei* from close to its type locality in the Chapare region, Bolivia, at the same temporal and spectral scale (4000 ms and 10 kHz, respectively). Oscillograms at the bottom show respective calls (those highlighted in gray in the oscillograms above) at an expanded time scale of 300 ms. Recording of *P. asimus* high-pass filtered at 700 Hz and that of *P. reichlei* band-pass filtered at 900–3600 Hz.

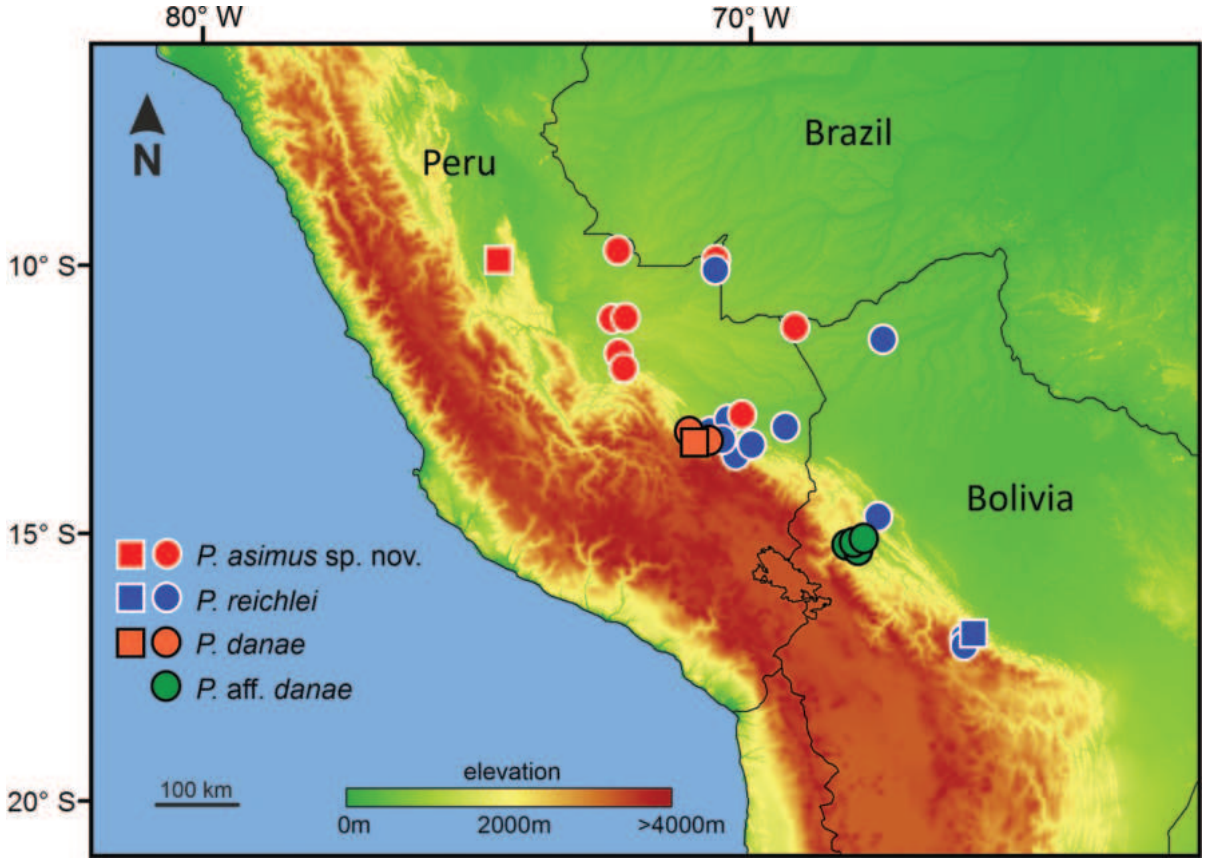

Figure 9. Schematic map of central-western South America showing the known distribution of species of the *Pristimantis danae* group referred to in the text, as inferred by molecular genetics and/or bioacoustic data. Broadly overlapping symbols may refer to the same locality. Square symbols refer to the type localities of the respective species.

in syntopy with *P. reichlei* at least in Alto Purús National Park (La Novia, Departamento Ucayali, Peru) and probably in other places in southeastern Peru and northern Bolivia. The new species most likely also occurs further east in the Brazilian Amazon, as indicated by the call description of Zimmerman and Bogart (1984) from Manaus, but respective records are in need of clarification (see Discussion).

Etymology. The specific epithet is a Latinized adjective derived from the Greek άσημος (ásimos), meaning 'inconspicuous, nameless'. It refers to the morphologically cryptic nature of the new species and the fact that it has been associated with different species names in the past, missing its status as a separate species to be named.

Discussion

Morphological crypsis among genetically distant (i.e., non-sister) species seems to be uncommon among anuran species (e.g., Castroviejo-Fisher et al. 2017). Striking similarity between sister or closely related species (i.e., siblings; Mayr 1942) is nonetheless common and has been recognized for a long time (see Winker 2005). Similarity caused by recent shared descent poses difficulties distinguishing among species in complexes with little morphological variation, yet difficulties tend to fade once additional evidence becomes available to clarify the sophisticated issues of the complex (e.g., Scherz et al. 2022). Thus, for example, it is not uncommon that after a study reveals multiple closely related species hidden under a single name, the new species discovered are more readily distinguishable once the external morphology is examined anew with the results of genetics in mind, or when different dimensions of the phenotype and the geographic ranges of the species are known better (Saéz and Lozano 2005; Korshunova et al. 2019).

Like in the case of the species pair *Pristimantis asimus* and *P. reichlei*, it is increasingly common that studies of Neotropical amphibians reveal sister and similar-looking species showing large genetic divergences (Padial and De la Riva 2009; Padial et al. 2009; Hutter and Guayasamin 2015; Ortega-Andrade et al. 2015; Páez and Ron 2019; Trevisan et al. 2020). In many cases, these are allopatric species that, upon closer examination, are readily diagnosable morphologically, but cases of sympatry/parapatry are not rare either, as in the example reported herein. The challenge with such cases is to ascertain whether such morphologically similar but genetically divergent frogs are, in fact, different species. Vicariance with secondary contact after reproductive isolation is the usual evolutionary scenario invoked to explain the pattern (Mayr 1942; Wiley and Lieberman 2011). Thus, when mitochondrial DNA (mtDNA) analyses of populations of one putative species reveal the existence of two distinct genetic lineages in sympatry, and the mtDNA-divergent individuals are found to also differ at least faintly in other, unlinked characters, the results are interpreted as strong evidence for the existence of similar-looking sibling/cryptic species isolated reproductively. However, as shown by Chan et al. (2020) and others (e.g., Ruane et al. 2014), gene flow and past introgression with another species can lead traditional tree analysis of gene sequences and genetic distance analyses to results identical to those produced by speciation through vicariance. Therefore, populations of the same species, some of which may carry part of the mitochondrial genome of a closely related species, will be inferred as two divergent lineages, even in sympatry. As discussed by Chan et al. (2020), this has serious implications. Many barcoding and integrative analyses relying on 16S or COI and traditional ML or Bayesian inference tree analyses are reporting cases of divergent mtDNA gene lineages in sympatric populations. These are often considered full species that are readily described and named. In order to detect such cases, it is key to rely on additional sources of evidence that may allow us to critically evaluate whether the distinct genetic lineages are part of two distinct species ('integrative taxonomy'; see Padial et al. 2010), and in cases where they are undescribed, they can be classified as a confirmed candidate species (Vieites et al. 2009). On the other hand, mitochondrial divergences in situations of sympatry can be among the strongest possible lines of evidence for the species status of the lineages involved, as soon as they are fully concordant with differentiation in unlinked nuclear-encoded markers, bioacoustics, or morphology, and this concordance is confirmed with substantial sample sizes (Miralles et al. 2024). In our case, support for the existence of two species is provided by differences in the respective advertisement calls, which are most likely explained as mechanisms of reproductive isolation (Köhler et al. 2017), and possibly by a few morphological traits. However, it remains desirable to assess both the genealogies and differences in calls with increasing sampling to refine and corroborate the limits of these two species.

Within the *Pristimantis danae* species group, Padial and De la Riva (2009) were unable to identify any qualitative morphological character distinguishing *P. danae* from *P. reichlei*, and the statistical differences in morphometric measurements were at least ambiguous, thus emphasizing the cryptic nature of both species. With the description of *P. asimus*, we add another morphologically cryptic sibling species to this complex of frogs. Although we detected two minor morphological differences between topotypes of *P. asimus* and *P. reichlei* (virtual absence versus presence of the outer metatarsal tubercle in preservative; different outlines of the canthus rostralis in straight dorsal view of the head), variation in these character states has yet to be studied in additional specimens and across the entire species' ranges. However, *P. asimus*, *P. danae*, and *P. reichlei* clearly differ by pronounced molecular divergence (but see above) and advertisement call differences.

Given that morphological differences between *P. asimus* and *P. reichlei* are yet to be corroborated, identification of the two species can be considered reliable only with the aid of bioacoustic and/or molecular genetic analyses. Consequently, several published records referring to *P. reichlei* should be reviewed. These include lowland records from the Bolivian departments of Beni and La Paz (Padial et al.

2004; Padial and De la Riva 2009), records from Manu National Park in southeastern Peru (Villacampa-Ortega et al. 2017), from Serrania de Sira, central Peru (Whitworth et al. 2016), and Brazilian records from the state of Acre (Melo-Sampaio and de Souza 2010; Bernarde et al. 2011; Melo-Sampaio 2015). These and other populations (e.g., Manaus, Brazil; Zimmerman and Bogart 1984) should be studied genetically and/or bioacoustically for their correct allocation to one of the two species, and researchers should check for the respective morphological character states.

With the description of *P. asimus*, we accounted for a more adequate taxonomic resolution of frogs formerly subsumed under the name *P. reichlei* (sensu Padial and De la Riva 2009). However, the high genetic diversification within *P. reichlei* sensu this work, with several deeply differentiated mtDNA lineages (Fig. 1) and uncorrected 16S p-distances of up to 9.3%, argue for further investigation of these populations, particularly of their calls, as possibly the name *P. reichlei* as used herein still represents a complex of species.

As evidenced by our molecular phylogenetic analysis and the mentioned differences in advertisement calls, the situation of *P. asimus* and *P. reichlei* is somehow paralleled by a second species pair, namely *P. danae* from Peru and *P.* aff. *danae* from Bolivia (see Fig. 1). Currently, the respective populations from the montane rainforests of southern Peru and western Bolivia are all treated as *P. danae* (Padial and De la Riva 2009). However, the genetic differentiation, with uncorrected p-distances in 16S of 9.4% between both major lineages and apparently significant differences in advertisement calls (see above), makes it highly improbable that nominal *P. danae* from the Kosñipata valley in Peru are conspecific with *P.* aff. *danae* from the Yungas de La Paz, Bolivia, although data from the area in between these two regions are lacking (Fig. 9). Solving the taxonomic status of Bolivian *P.* aff. *danae* was beyond the scope of this study, and a detailed investigation of *P. danae* remains necessary.

Despite the still substantial limitations in geographic and character sampling outlined above, our understanding of species limits in *Pristimantis* is rapidly growing. It is now customary in phylogenetic studies of *Pristimantis* to discover the existence of unnamed species overlooked and confounded across the range with their similar-looking nominal sister species or closely related ones (e.g., Hutter and Guayasamin 2015; Ortega-Andrade et al. 2015; Páez and Ron 2019; Trevisan et al. 2020; Castillo-Urbina et al. 2023; Herrera-Alva et al. 2023). This increasing level of species resolution is a fundamental step toward more rigorous inferences of evolutionary scenarios as well as to attain taxonomic stability (Padial and De la Riva 2021).

In contrast to the growing taxonomic knowledge in the *P. danae* group, there is a disproportional lack of knowledge about the ecology and natural history of its species, which remains almost completely unknown. Martínez and Rodríguez (2007) reported on egg clutch size and egg numbers in *P. danae* from Peru. Quintero-Muñoz and Aguayo (2022) described observations on parental care (clutch guarding) and reproduction in *P. reichlei* from Bolivia, where a collected gravid female laid an egg clutch in captivity (without male individuals being present during capture or in the tank), from which half the eggs developed into froglets. This remarkable observation indicates either the presence of internal fertilization or parthenogenesis in this group of frogs. These two potential explanations deserve further study, as it either constitutes a rarely documented case in oviparous anurans (e.g., Townsend et al. 1981) or is so far undocumented in frogs (natural parthenogenesis). Such observations and potential phenomena argue for a more careful scientific consideration of these inconspicuous, brown-colored frogs.

Acknowledgements

Collecting permits for specimens in MUBI and CM were kindly granted by SERFOR (#192-2015-SERFOR-DGGSPFFS), those for specimens in MUSM and ZSM by INRENA (#124-2008-INRENA-IFFS-DCB), and SERFOR (#007-2014-SERFOR-DGGSPFFS, #0406-2017-SERFOR-DGGSPFFS). Additional specimens held at MUBI were collected with permits #024-2017-SERFOR-DGGSPFFS (SERFOR) and #001-2013-SERNANP-PNAP (Resolución Jefatural del Área Natural Protegida Parque Nacional Alto Purús). We would like to express our highest gratitude to staff members of the Alto Purús National Park (SERNANP), especially to its director, Arsenio Calle, for encouraging and facilitating our work in the area, as well as to those who participated in the expedition to the Sepahua River: Viviana Ramos, Carlos Ruelas, Cerilo López, Diego Saavedra, Michel Díaz, Abraham Ramírez (all SERNANP), Jamil Ponce (PRONATURALEZA), and Julio Flores (SERFOR). Special thanks to Maira Duarte Quiroga for assisting during fieldwork and for filming activities at PN Alto Purús and to Ernesto Castillo-Urbina for joint fieldwork at Panguana. We thank Juliane Diller, Carlos 'Moro' Vásquez Módena, and Hibraín Vásquez Panduro for their generous support of our work at ACP Panguana. Wolfgang Böhme, Ursula Bott, Morris Flecks, Claudia Koch (ZFMK), Alexander Kupfer (SMNS), and Jiří Moravec (NMP6V) provided access to specimens under their care and/or miscellaneous information. This article greatly benefited from comments and suggestions provided by Valia Herrera-Alva, Santiago Ron, and Pedro Taucce.

References

Arroyo SB, Targino M, Rueda-Solano LA, Daza JM, Grant T (2022) A new genus of terraranas (Anura: Brachycephaloidea) from northern South America, with a systematic review of *Tachiramantis*. Systematics and Biodiversity 20(1): 1–25. https://doi.org/10.1080/14772000.2022.2123865

Bernarde PS, Machado RA, Turci LCB (2011) Herpetofauna da área do Igarapé Esperança na Reserva Extrativista Riozinho da Liberdade, Acre – Brasil. Biota Neotropica 11(3): 117–144. https://doi.org/10.1590/S1676-06032011000300010

Bickford D, Lohman DJ, Sodhi NS, Ng PK, Meier R, Winker K, Ingram K, Das I (2007) Cryptic species as a window on diversity and conservation. Trends in Ecology & Evolution 22(3): 148–155. https://doi.org/10.1016/j.tree.2006.11.004

Canedo C, Haddad CFB (2012) Phylogenetic relationships within anuran clade Terrarana, with emphasis on the placement of Brazilian Atlantic rainforest frogs genus *Ischnocnema* (Anura: Brachycephalidae). Molecular Phylogenetics and Evolution 65(2): 610–620. https://doi.org/10.1016/j.ympev.2012.07.016

Castillo-Urbina E, Vences M, Aguilar-Puntriano C, Glaw F, Köhler J (2023) Contributing to the taxonomic inventory of green-colored rain frogs: A new species of the *Pristimantis lacrimosus* group (Anura: Strabomantidae) from the southern Cordillera Azul, central Peru. Vertebrate Zoology 73: 1047–1061. https://doi.org/10.3897/vz.73.e109309

Castroviejo-Fisher S, Köhler J, De la Riva I, Padial JM (2017) A new morphologically cryptic species of *Phyllomedusa* (Anura: Phyllomedusidae) from Amazonian forests of northern Peru revealed by DNA sequences. Zootaxa 4269(2): 245–264. https://doi.org/10.11646/zootaxa.4269.2.4

Chan KO, Hutter CR, Wood Jr PL, Grismer LL, Das I, Brown RM (2020) Gene flow creates a mirage of cryptic species in a Southeast Asian spotted stream frog complex. Molecular Ecology 29(20): 3970–3987. https://doi.org/10.1111/mec.15603

Chávez G, García-Ayachi LA, Catenazzi A (2021) Beauty in the eye of the beholder: Cruciform eye reveals new species of direct-developing frog (Strabomantidae, *Pristimantis*) in the Amazonian Andes. Evolutionary Systematics 5(1): 81–92. https://doi.org/10.3897/evolsyst.5.63674

de Oliveira EA, da Silva LA, Silva EAP, Guimarães KLA, Penhacek M, Martínez JG, Rodrigues LRR, Santana DJ, Hernández-Ruz EJ (2020) Four new species of *Pristimantis* Jiménez de la Espada, 1870 (Anura: Craugastoridae) in the eastern Amazon. PLOS ONE 15(3): e0229971. https://doi.org/10.1371/journal.pone.0229971

Duellman WE (1978) Two new species of *Eleutherodactylus* (Anura: Leptodactylidae) from the Peruvian Andes. Transactions of the Kansas Academy of Science 81(1): 65–71. https://doi.org/10.2307/3627358

Duellman WE (2005) Cusco Amazónico. The lives of amphibians and reptiles in an Amazonian rainforest. Comstock Books in Herpetology, Cornell University, 433 pp.

Duellman WE, Hedges SB (2005) Eleutherodactyline frogs (Anura: Leptodactylidae) from the Cordillera Yanachaga in central Peru. Copeia 2005(3): 526–538. https://doi.org/10.1643/CH-05-019R

Duellman WE, Lehr E (2009) Terrestrial-breeding frogs (Strabomantidae) in Peru. Natur und Tier Verlag, Münster, 382 pp.

Duellman WE, Pramuk JB (1999) Frogs of the genus *Eleutherodactylus* (Anura: Leptodactylidae) in the Andes of northern Peru. Scientific Papers of the Natural History Museum, the University of Kansas 13: 1–78. https://doi.org/10.5962/bhl.title.16169

Elmer KR, Dávila JA, Lougheed SC (2007) Cryptic diversity and deep divergence in an upper Amazonian leaflitter frog, *Eleutherodactylus ockendeni*. BMC Evolutionary Biology 7(1): 247. https://doi.org/10.1186/1471-2148-7-247

Fouquet A, Réjaud A, Rodrigues MT, Ron SR, Chaparro JC, Osorno-Muñoz M, Werneck FP, Hrbek T, Lima AP, Camacho-Badani T, Jaramillo-Martinez AF, Chave J (2022) Diversification of the *Pristimantis conspicillatus* group (Anura: Craugastoridae) within distinct Neotropical areas throughout the Neogene. Systematics and Biodiversity 20(1): 1–16. https://doi.org/10.1080/14772000.2022.2130464

García JC, Crawford AJ, Mendoza ÁM, Ospina O, Cardenas H, Castro F (2012) Comparative phylogeography of direct-developing frogs (Anura: Craugastoridae: *Pristimantis*) in the southern Andes of Colombia. PLOS ONE 7(9): e46077. https://doi.org/10.1371/journal.pone.0046077

Gonzáles-Durán GA, Targino M, Rada M, Grant T (2017) Phylogenetic relationships and morphology of the *Pristimantis leptolophus* species group (Amphibia: Anura: Brachycephaloidea), with the recognition of a new species group in *Pristimantis* Jiménez de la Espada, 1870. Zootaxa 4243(1): 42–74. https://doi.org/10.11646/zootaxa.4243.1.2

Hedges SB, Duellman WE, Heinicke MP (2008) New World direct-developing frogs (Anura: Terrarana): molecular phylogeny, classification, biogeography, and conservation. Zootaxa 1737(1): 1–182. https://doi.org/10.11646/zootaxa.1737.1.1

Heinicke MP, Duellman WE, Hedges SB (2007) Major Caribbean and Central American frog faunas originated by ancient oceanic dispersal. Proceedings of the National Academy of Sciences of the United States of America 104(24): 10092–10097. https://doi.org/10.1073/pnas.0611051104

Herrera-Alva V, Catenazzi A, Aguilar-Puntriano C (2023) A new cryptic species of terrestrial breeding frog of the *Pristimantis danae* Group (Anura, Strabomantidae) from montane forests in Ayacucho, Peru. ZooKeys 1187: 1–29. https://doi.org/10.3897/zookeys.1187.104536

Hutter CR, Guayasamin JM (2015) Cryptic diversity concealed in the Andean cloud forests: Two new species of rainfrogs (*Pristimantis*) uncovered by molecular and bioacoustic data. Neotropical Biodiversity 1(1): 36–59. https://doi.org/10.1080/23766808.2015.1100376

Kalyaanamoorthy S, Minh BQ, Wong TK, Von Haeseler A, Jermiin LS (2017) ModelFinder: Fast model selection for accurate phylogenetic estimates. Nature Methods 14(6): 587–589. https://doi.org/10.1038/nmeth.4285

Katoh K, Standley DM (2013) MAFFT multiple sequence alignment software version 7: Improvements in performance and usability. Molecular Biology and Evolution 30(4): 772–780. https://doi.org/10.1093/molbev/mst010

Köhler J (2000) Amphibian diversity in Bolivia: A study with special reference to montane forest regions. Bonner Zoologische Monographien 48: 1–243.

Köhler J, Jansen M, Rodríguez A, Kok PJR, Toledo LF, Emmrich M, Glaw F, Haddad CFB, Rödel MO, Vences M (2017) The use of bioacoustics in anuran taxonomy: Theory, terminology, methods and recommendations for best practice. Zootaxa 4251(1): 1–124. https://doi.org/10.11646/zootaxa.4251.1.1

Köhler J, Castillo-Urbina E, Aguilar-Puntriano C, Vences M, Glaw F (2022) Rediscovery, redescription and identity of *Pristimantis nebulosus* (Henle, 1992), and description of a new terrestrial-breeding frog from montane rainforests of central Peru (Anura, Strabomantidae). Zoosystematics and Evolution 98(2): 213–232. https://doi.org/10.3897/zse.98.84963

Korshunova T, Picton B, Furfaro G, Mariottini P, Pontes M, Prkić J, Fletcher K, Malmberg K, Lundin K, Martynov A (2019) Multilevel fine-scale diversity challenges the 'cryptic species' concept. Scientific Reports 9(1): 6732. https://doi.org/10.1038/s41598-019-42297-5

Lehr E (2002) Amphibien und Reptilien in Peru. Natur und Tier Verlag, Münster, 208 pp.

Lehr E, von May R (2017) A new species of terrestrial-breeding frog (Amphibia, Craugastoridae, *Pristimantis*) from high elevations of the Pui Pui Protected Forest in central Peru. ZooKeys 660: 17–42. https://doi.org/10.3897/zookeys.660.11394

Lehr E, von May R, Moravec J, Cusi JC (2017) Three new species of *Pristimantis* (Amphibia, Anura, Craugastoridae) from upper montane forests and high Andean grasslands of the Pui Pui Protected Forest in central Peru. Zootaxa 4299(3): 301–336. https://doi.org/10.11646/zootaxa.4299.3.1

Márquez R, De la Riva I, Bosch J, Matheu E (2002) Sounds of frogs and toads of Bolivia. Fonoteca Zoologica, Alosa, AHE, MNCN, Madrid [CD + booklet].

Martínez JL, Rodríguez LO (2007) *Eleutherodactylus danae*. Reproduction. Herpetological Review 38: 184.

Mayr E (1942) Systematics and the origin of species, from the viewpoint of a zoologist. Harvard University Press, 1999.

McDiarmid RW (1994) Preparing amphibians as scientific specimens. In: Heyer WR, Donnelly MA, McDiarmid RW, Hayek LC, Foster MS (Eds) Measuring and monitoring biological diversity. Standard methods for amphibians. Smithsonian Institution, Washington DC, 289–297.

Melo-Sampaio PR (2015) *Pristimantis reichlei*. Eye coloration. Herpetological Review 46: 614.

Melo-Sampaio PR, de Souza MB (2010) Amphibia, Anura, Strabomantidae, *Pristimantis reichlei* Padial and De la Riva, 2009: First record from Brazil, southwestern Amazonia. Check List 6(3): 385–386. https://doi.org/10.15560/6.3.385

Minh BQ, Schmidt HA, Chernomor O, Schrempf D, Woodhams MD, Von Haeseler A, Lanfear R (2020) IQ-TREE 2: New models and efficient methods for phylogenetic inference in the genomic era. Molecular Biology and Evolution 37(5): 1530–1534. https://doi.org/10.1093/molbev/msaa015

Miralles A, Puillandre N, Vences M (2024) DNA barcoding in species delimitation: from genetic distances to integrative taxonomy. In: De Salle R (Ed.) DNA Barcoding: Methods and Protocols. Methods in Molecular Biology 2744: 77–104. https://doi.org/10.1007/978-1-0716-3581-0_4

Moravec J, Aparicio J (2005) Notes on the herpetofauna of Bioceanica and Bolpebra (Provincia Nicolas Suaréz, Departamento Pando, Bolivia). Journal by the National Museum. Natural History Series 174: 95–113.

Moravec J, Lehr E, Kodejš K (2020) A new species of *Pristimantis* (Amphibia, Anura, Strabomantidae) from the Pui Pui Protected Forest (central Peru), with comments on *Pristimantis albertus* Duellman & Hedges, 2007. ZooKeys 994: 125–148. https://doi.org/10.3897/zookeys.994.56277

Nguyen LT, Schmidt HA, Von Haeseler A, Minh BQ (2015) IQ-TREE: A fast and effective stochastic algorithm for estimating maximum-likelihood phylogenies. Molecular Biology and Evolution 32(1): 268–274. https://doi.org/10.1093/molbev/msu300

Ortega-Andrade HM, Rojas-Soto OR, Valencia JH, Espinosa de los Monteros A, Morrone JJ, Ron SR, Cannatella DC (2015) Insights from integrative systematics reveal cryptic diversity in *Pristimantis* frogs (Anura: Craugastoridae) from the Upper Amazon Basin. PLOS ONE 10(11): e0143392. https://doi.org/10.1371/journal.pone.0143392

Padial JM, De la Riva I (2005) Rediscovery, redescription and advertisement call of *Eleutherodactylus heterodactylus* (Miranda Ribeiro, 1937) (Anura: Leptodactylidae), and notes on other *Eleutherodactylus*. Journal of Herpetology 39(3): 372–379. https://doi.org/10.1670/191-04A.1

Padial JM, De la Riva I (2009) Integrative taxonomy reveals cryptic Amazonian species of *Pristimantis* (Anura: Strabomantidae). Zoological Journal of the Linnean Society 155(1): 97–122. https://doi.org/10.1111/j.1096-3642.2008.00424.x

Padial JM, De la Riva I (2021) A paradigm shift in our view of species drives current trends in biological classification. Biological Reviews of the Cambridge Philosophical Society 96(2): 731–751. https://doi.org/10.1111/brv.12676

Padial JM, Gonzales-Álvarez L, Reichle S, Aguayo-Vedia CR, De la Riva I (2004) First records of five species of the genus *Eleutherodactylus* Dumeril and Bibron, 1841 (Anura, Leptodactylidae) for Bolivia. Graellsia 60(2): 167–174. https://doi.org/10.3989/graellsia.2004.v60.i2.212

Padial JM, Castroviejo-Fisher S, De la Riva I (2009) The phylogenetic relationships of *Yunganastes* revisited (Anura: Terrarana). Molecular Phylogenetics and Evolution 52(3): 911–915. https://doi.org/10.1016/j.ympev.2009.05.006

Padial JM, Miralles A, De la Riva I, Vences M (2010) The integrative future of taxonomy. Frontiers in Zoology 7(1): 16. https://doi.org/10.1186/1742-9994-7-16

Padial JM, Grant T, Frost DR (2014) Molecular systematics of terraranas (Anura: Brachycephaloidea) with an assessment of the effects of alignment and optimality criteria. Zootaxa 3825(1): 1–132. https://doi.org/10.11646/zootaxa.3825.1.1

Padial JM, Gagliardi-Urrutia G, Chaparro JC, Gutiérrez RC (2016) A new species of the *Pristimantis conspicillatus* group from the Peruvian Amazon (Anura: Craugastoridae). Annals of Carnegie Museum 83(3): 207–218. https://doi.org/10.2992/007.083.0302

Páez NB, Ron SR (2019) Systematics of *Huicundomantis*, a new subgenus of *Pristimantis* (Anura, Strabomantidae) with extraordinary cryptic diversity and eleven new species. ZooKeys 868: 1–112. https://doi.org/10.3897/zookeys.868.26766

Palumbi S, Martin A, Ramano S, McMillan WO, Stice L, Grabowski G (1991) The Simple Fool's Guide to PCR, Version 2. University of Hawaii Zoology Department, Honolulu, Hawaii.

Pinto-Sánchez NR, Ibáñez R, Madriñán S, Sanjur OI, Bermingham E, Crawford AJ (2012) The Great American Biotic Interchange in frogs: multiple and early colonization of Central America by the South American genus *Pristimantis* (Anura: Craugastoridae). Molecular Phylogenetics and Evolution 62(3): 954–972. https://doi.org/10.1016/j.ympev.2011.11.022

Quintero-Muñoz O, Aguayo R (2022) Parental care and clutch size of *Pristimantis reichlei* (Anura: Strabomantidae) from Bolivia. Revista Latinoamericana de Herpetología 5: 123–126. https://doi.org/10.22201/fc.25942158e.2022.2.306

Rodríguez LO (1994) A new species of the *Eleutherodactylus conspicillatus* group (Leptodactylidae) from Peru, with comments on its call. Alytes 12: 49–63.

Ron SR, Carrión JC, Caminer MA, Sagredo Y, Navarrete MJ, Ortega JA, Varela-Jaramillo A, Maldonado-Castro GA, Terán C (2020) Three new species of frogs of the genus *Pristimantis* (Anura, Strabomantidae) with a redefinition of the *P. lacrimosus* species group. ZooKeys 993: 121–155. https://doi.org/10.3897/zookeys.993.53559

Ruane S, Bryson Jr RW, Pyron RA, Burbrink FT (2014) Coalescent species delimitation in milksnakes (genus *Lampropeltis*) and impacts on phylogenetic comparative analyses. Systematic Biology 63(2): 231–250. https://doi.org/10.1093/sysbio/syt099

Saéz AG, Lozano E (2005) Body doubles. Nature 433(7022): 111. https://doi.org/10.1038/433111a

Sánchez-Nivicela JC, Urgilés VL, Cedeño-Palacios J, Abad-Peñafiel H, Guayasamin JM (2021) Una fantástica nueva especie del grupo *Pristimantis orcesi* de los Andes sur de Ecuador. Neotropical Biodiversity 6(1): 224–237. https://doi.org/10.1080/23766808.2020.1869449

Scherz MD, Crottini A, Hutter CR, Hildenbrand A, Andreone F, Fulgence TR, Köhler G, Ndriantsoa SH, Ohler A, Preick M, Rakotoarison A, Rancilhac L, Raselimanana AP, Riemann JC, Rödel M-O, Rosa GM, Streicher JW, Vieites DR, Köhler J, Hofreiter M, Glaw F, Vences M (2022) An inordinate fondness for inconspicuous brown frogs: Integration of phylogenomics, archival DNA analysis, morphology, and bioacoustics yields 24 new taxa in the subgenus *Brygoomantis* (genus *Mantidactylus*) from Madagascar. Megataxa 7(2): 113–311. https://doi.org/10.11646/megataxa.7.2.1

Schlüter A (1980) Bio-akustische Untersuchungen an Leptodactyliden in einem begrenzten Gebiet des tropischen Regenwaldes von Peru (Amphibia: Salentia: Leptodactylidae). Salamandra (Frankfurt) 16: 227–247.

Schlüter A (2005) Amphibien an einem Stillgewässer in Peru mit einer illustrierten Cecklist der Amphibien und Reptilien des unteren Río Llullapichis. Edition Chimaira, Frankfurt am Main, 347 pp.

Shimodaira H, Hasegawa M (1999) Multiple comparisons of log-likelihoods with applications to phylogenetic inference. Molecular Biology and Evolution 16(8): 1114–1116. https://doi.org/10.1093/oxfordjournals.molbev.a026201

Townsend DS, Steward MM, Pough FH, Brussard PF (1981) Internal fertilization in an oviparous frog. Science 212(4493): 469–471. https://doi.org/10.1126/science.6894203

Trevisan CC, Batalha-Filho H, Garda AA, Menezes L, Dias IR, Solé M, Cando C, Acuna F, Napoli MF (2020) Cryptic diversity and ancient diversification in the northern Atlantic Forest *Pristimantis* (Amphibia, Anura, Craugastoridae). Molecular Phylogenetics and Evolution 148: 106811. https://doi.org/10.1016/j.ympev.2020.106811

Vences M, Miralles A, Brouillet S, Ducasse J, Fedosov A, Kharchev V, Kostadinov I, Kumari S, Patmanidis S, Scherz MD, Puillandre N, Renner SS (2021) iTaxoTools 0.1: Kickstarting a specimen-based software toolkit for taxonomists. Megataxa 6(2): 77–92. https://doi.org/10.11646/megataxa.6.2.1

Vences M, Patmanidis S, Kharchev V, Renner SS (2022) Concatenator, a user-friendly program to concatenate DNA sequences, implementing graphical user interfaces for MAFFT and FastTree. Bioinformatics Advances 2(1): 1–4. https://doi.org/10.1093/bioadv/vbac050

Venegas PJ, García-Ayachi LA, Marchelie A, Ormeño JR, Catenazzi A (2023) A new species of terrestrial-breeding frog, genus *Pristimantis* (Anura, Strabomantidae), from the Peruvian Yungas of central Peru. Taxonomy 3(2): 331–345. https://doi.org/10.3390/taxonomy3020019

Vieites DR, Wollenberg KC, Andreone F, Köhler J, Glaw F, Vences M (2009) Vast underestimation of Madagascar's biodiversity evidenced by an integrative amphibian inventory. Proceedings of the National Academy of Sciences of the United States of America 106(20): 8267–8272. https://doi.org/10.1073/pnas.0810821106

Villacampa-Ortega J, Serrano-Rojas SJ, Whitworth A (2017) Amphibians of the Manu Learning Centre and other areas of the Manu region. The Crees Foundation, Cuzco, Peru, 282 pp.

Whitworth A, Beirne C, Pillco Huarcaya R, Serrano Rojas SJ, Chávez G (2016) Amphibians of the Sira Communal Reserve. Fieldmuseum Fiedguide 809: 1–7.

Wiley EO, Lieberman BS (2011) Phylogenetics: theory and practice of phylogenetic systematics. John Wiley & Sons, New Jersey, USA, 406 pp. https://doi.org/10.1002/9781118017883

Winker K (2005) Sibling species were first recognized by William Derham (1718). The Auk 122(2): 706–707. https://doi.org/10.1093/auk/122.2.706

Zimmerman BL, Bogart JP (1984) Vocalizations of primary forest frog species in the central Amazon. Acta Amazonica 14(3–4): 473–519. https://doi.org/10.1590/1809-43921984143519

Zumel D, Buckley D, Ron SR (2021) The *Pristimantis tachyblepharis* species group, a clade of miniaturized frogs: Description of four new species and insight into the evolution of body size in the genus. Zoological Journal of the Linnean Society 195(1): 315–354. https://doi.org/10.1093/zoolinnean/zlab044

Zoosyst. Evol. 100 (2) 2024, 583–595 | DOI 10.3897/zse.100.120676

PENSOFT

MUSEUM FÜR NATURKUNDE BERLIN

Tachysurus wuyueensis (Teleostei, Bagridae), a new species of catfish from the Qiantang-Jiang basin, southeast China

Jia-Jun Zhou[1], Le-Yang Yuan[2], Wei-Han Shao[3]

1 *Zhejiang Forest Resource Monitoring Center, Hangzhou, China*
2 *Zhejiang Museum of National History, Hangzhou, China*
3 *Institute of Hydrobiology, Chinese Academy of Sciences, Wuhan, China*

https://zoobank.org/3D10FE75-FC05-4A93-A03A-17C77BD60999

Corresponding author: Wei-Han Shao (shaoweihan1008@163.com)

Academic editor: Nicolas Hubert ♦ **Received** 10 February 2024 ♦ **Accepted** 28 March 2024 ♦ **Published** 17 May 2024

Abstract

Tachysurus wuyueensis, new species, is described from the Qiantang-Jiang Basin, situated in Suichang County, Zhejiang Province and Xiuning County, Anhui Province, southeast China. The coastal basin drains into the East China Sea. The new species belongs to the *T. pratti-T. truncatus* group within the genus *Tachysurus* defined by having a smooth anterior margin of the pectoral-fin spine, short maxillary barbels not extending beyond the base of the pectoral-fin spine, short dorsal spine not exceeding two thirds of head length and an emarginated caudal fin. This new species is distinct from all other species of this group, *Tachysurus pratti* (Gunther, 1892), *T. truncatus* (Regan 1913), *T. gracilis* (Li, Chen & Chan, 2005) and *T. brachyrhabdion* (Cheng, Ishihara & Zhang, 2008), in having a shorter prepelvic body (length 40.0–46.4% of SL vs. 45.8–54.8%). It further differs from *T. pratti*, *T. truncatus* and *T. gracilis* in having more vertebrae (45–47 vs. 37–44) and more anal fin rays (21–25 vs. 14–20), from *T. brachyrhabdion* in having a more slender body (depth 10.1–13.5% of HL vs. 13.1–17.6%). Molecular phylogeny, based on the mitochondrial cytochrome *b* (cyt. *b*) gene confirms the validity of *T. wuyueensis* and the *T. pratti-T. truncatus* group. Furthermore, this study addresses the diagnostic traits distinguishing the *T. pratti-T. truncatus* group from the *T. tenuis-T. crassilabris* group which have historically been treated as a single species group due to morphological similarities.

Key Words

Caudal fin shape, new taxon, stream-dewelling species, taxonomy

Introduction

The genus *Tachysurus* Lacépède 1803 is a group of East Asian endemic catfish that is widely distributed throughout most of the East Asian continent (Ku et al. 2007; Watanabe 2010; Shao and Zhang 2023). It is also one of the most diversified catfish genus in China containing more than thirty species with strong differentiation in ecological niches (Shao et al. 2021; Shao and Zhang 2023). South China, which is characterised by high mountains, deep valleys and abundant precipitation (López-Pujol et al. 2011; Wang et al. 2018; Sun et al. 2021), harbours numerous *Tachysurus* species restricted to montane streams with fast-flowing high-oxygen waters and predominance of rocky substrate, for example, *Tachysurus ondon* (Shaw 1930), *T. adiposalis* (Oshima 1919), *T. albomarginatus* (Rendahl 1928), *T. trilineatus* (Zheng 1979) and *T. tenuis* (Günther 1873). Unlike its congeners, species of *Tachysurus* always possess elongated bodies and rounded, truncated or slightly emarginated (round-tailed) caudal fins regarded herein as key adaptions for the torrent environments (Gosline 1997; Krishnadas et al. 2018). Moreover, the absence of diagnosable characters and ambiguous descriptions have obscured the species boundaries of these species (Ferraris 2007; Shao et al. 2021). For instance, *T. albomarginatus* has long been synonymised under *T. tenuis* (Zheng & Dai, 1999) until Cheng et al. (2021) resurrected the former species, based on morphometric and osteological analyses.

In addition, rheophilic (fast-water) fishes are always confined to a narrow distribution which limits their dispersal ability and contributes to their habitat fragmentation (Lima et al. 2017). Previous works have highlighted the underestimated diversity of Tachysurus, v.gr., *T. albomarginatus* that may be an assemblage of five species (Cheng et al. 2021; Shao et al. 2021). A similar scenario occurs in *T. adiposalis*, originally described by Oshima (1919) on a single specimen of 170 mm SL (standard length) collected from the Tamusui River in Taiwan. *T. adiposalis* has been treated as widespread species, with a distribution including Taiwan and river basins from the southern region of Chinese mainland, such as the mid-lower Yangtze, Pearl River and Qiantang River (= Qiantang-Jiang in Chinese) (Zheng and Dai 1999). The key characters useful in differentiating *Tachysurus* species are absent or obscured in the original description of *T. adiposalis*, which resulted in the taxonomic confusion. Recent studies have suggested that specimens from the Xi-Jiang (the Pearl River Basin) and the Yuan-Jiang (the middle Yangtze River Basin) belonging to *T. adiposalis* s.l. were determined as *Tachysurus gracilis* (Li, Chen & Chan, 2005) and *Tachysurus brachyrhabdion* (Cheng, Ishihara & Zhang, 2008). However, the taxonomic status of specimens from the Qiantang-Jiang which were also recognised as *Tachysurus adiposalis* has not been mentioned in previous studies and it potentially represents an undescribed species.

A fish field survey conducted by the authors in the Qiantang-Jiang Basin of Zhejiang and Anhui Provinces yielded 14 specimens initially identified as *T. adiposis*. Careful morphological examination revealed that these were, in fact, not conspecific with any other known species of *Tachysurus* and represent a new species. The purpose of the present paper is to provide a formal description of this unnamed species, based on multiple lines of evidence containing morphological and phylogenetic datasets.

Materials and methods

Fourteen specimens of the new species were caught during two field surveys conducted, respectively, in September 2020 and May 2023 into the Qiantang-Jiang flowing into the East China Sea. Amongst them, six specimens were fixed in 10% formalin after removal of right-side pelvic-fin clips. These fin clips were stored in 95% ethyl alcohol and utilised for molecular analysis. The remaining caught specimens were directly preserved in 10% formalin preservative for morphological examination. Their voucher specimens are deposited in the Museum of Aquatic Organisms of the Institute of Hydrobiology (IHB), Chinese Academy of Sciences, Wuhan. Eight species, including *T. gracilis*, *T. truncatus*, *T. pratti*, *T. brachyrhabdion*, *T. crassilabris*, *T. albomarginatus*, *T. adiposalis* and *T. tenuis*, were morphologically examined in this study, which came from the following collections: Museum of Aquatic Organisms of Institute of Hydrobiology, Chinese Academy of Sciences, Wuhan (IHB), the Natural History Museum, London (BMNH) and French Museum of Natural History, Paris (FMNH).

Measurements were taken point to point with digital calipers linked to a data recording computer and data were recorded to the nearest 0.1 mm and made on the left side of each individual whenever possible, following the methods for Cheng et al. (2008). The head length and measurements of other parts of the body are estimated as percentages of the standard length (SL). Subunits of head are provided as percentages of the head length (HL). The number of rays from the dorsal- and anal fins were counted using the method by Watanabe (1995). Other fin rays were counted under a binocular dissecting microscope utilising transmitted light. Vertebral count was taken from X-ray photographs, with the anterior five vertebrae, namely the Weberian complex, not counted.

Morphometric measurements were subject to principal component analysis (PCA) in order to examine external morphological differentiation and determine the relative contributions of specific variables to morphological differences in the target species. PCA was run with SPSS 16 (SPSS, Chicago, IL, USA). Prior to the analysis, all morphometric measurements, except standard length, were normalised following the method of Reist (1985) to eliminate the influence of allometry of body parts and sample size.

Phylogenetic analysis was performed on cyt. *b* and the sequences uploaded to NCBI GenBank (Table 1). The thirty-eight cyt. *b* gene sequences, here amplified from twenty-five species of *Tachysurus*, were used for molecular phylogenetic analysis. *Tachysurus trilineatus* was used as the outgroup which is the basal lineage of *Tachysurus* genus (Ku et al. 2007). The sequences were revised manually and then aligned using ClustalW in MEGA7 (Kumar et al. 2016). Both Maximum Likelihood (ML) and Bayesian Inference (BI) methods were utilised to reconstruct the phylogenetic relationships. The optimal nucleotide substitution model was selected by ModelFinder (Kalyaanamoorthy et al. 2017) according to the Akaike Information Criterion. Maximum Likelihood analysis was run by IQ-tree (Nguyen et al. 2015), with the selected TIM3+F+I+G4 model and 1,000 non-parametric bootstrap replicates. Bayesian Inference was performed in MrBayes (Ronquist et al. 2012) under the selected GTR+F+I+G4 model. Two independent runs were carried out with four Monte Carlo Markov chains (three hot chains and one cold chain) for 20 million generations to calculate posterior probability. Trees were sampled every 1000 generations. The initial 25% of sampled trees were discarded as burn-in. Convergence of the runs was assessed by the average standard deviation of split frequencies (< 0.01).

Table 1. GenBank accession numbers for molecular phylogenetic analysis.

	Taxon	Locality	Distribution	Accession number
	Ingroup			
(1)	*Tachysurus albomarginatus*	Zhejiang, China	Qiantang-Jiang	PP266663
(2)	*Tachysurus analis*	Jiangxi, China	Gan-Jiang of lower Yangtze River	PP266668
(3)	*Tachysurus argentivittatus*	Jiangxi, China	Gan-Jiang of lower Yangtze River	PP266678
(4)	*Tachysurus brachyrhabdion* 1	Guizhou, China	Yuan-Jiang of middle Yangtze River	PP266650
	Tachysurus brachyrhabdion 2	Guizhou, China		PP266651
	Tachysurus brachyrhabdion 3	Hunan, China		PP266652
(5)	*Tachysurus crassilabris*	Hunan, China	Xiang-Jiang of middle Yangtze River	PP266665
(6)	*Tachysurus dumerili*	Jiangsu, China	Lower Yangtze River	PP266661
(7)	*Tachysurus gracilis*1	Guangxi, China	Xiang-Jiang of middle Yangtze River	PP266654
(8)	*Tachysurus gracilis* 2	Hunan, China	Lijiang River of Pearl River	PP266655
(9)	*Tachysurus intermedius*	Hainan, China	Nandu-Jiang	PP266676
(10)	*Tachysurus kyphus*	Guangxi,China	Fangcheng- Jiang	PP266671
(11)	*Tachysurus lani*	Guangxi, China	Gui-Jiang of the Pearl River	PP266662
(12)	*Tachysurus longispinalis*	Vietnam	Red River	PP266672
(13)	*Tachysurus nitidus*	Hunan, China	Xiang-Jiang of middle Yangtze River	PP266660
(14)	*Tachysurus ondon*	Zhejiang, China	Ou-Jiang	PP266677
(15)	*Tachysurus pratti* 1	Sichuan, China	Jinsha-Jiang of upper Yangtze River	PP266656
	Tachysurus pratti 2	Yunan, China		PP266657
(16)	*Tachysurus similis*	Fujian, China	Min-Jiang	PP266664
(17)	*Tachysurus sinensis*	Hubei, China	Middle Yangtze River	PP266674
(18)	*Tachysurus tenuis*	Zhejiang, China		PP266666
(19)	*Tachysurus truncatus* 1	Sichuan, China	Upper Yangtze River	PP266658
	Tachysurus truncatus 2	Shaanxi, China	Han-Jiang of middle Yangtze River	PP266659
(20)	*Tachysurus ussuriensis*	Heilongjiang, China	Heilong-Jiang	PP266669
(21)	*Tachysurus vachelli*	Hubei, China	Middle Yangtze River	PP266670
(22)	*Tachysurus virgatus*	Hainan, China	Jiajihe River	PP266673
(23)	*Tachysurus wuyueensis* (SUIC55690)	Zhejiang, China	Qiantang-Jiang	PP266644
	Tachysurus wuyueensis (SUIC55691)			PP266645
	Tachysurus wuyueensis (SUIC55692)			PP266646
	Tachysurus wuyueensis (XIUN65294)	Anhui, China		PP266647
	Tachysurus wuyueensis (XIUN65295)			PP266648
	Tachysurus wuyueensis (XIUN65296)			PP266649
(24)	*Tachysurus zhangfei*	Hunan, China	Yuan-Jiang of middle Yangtze River	PP266667
	Outgroup			
(25)	*Tachysurus trilineatus*	Guangdong, China	Dong-Jiang of Pearl River	PP266679

The genetic distances, based on cyt. *B*, were computed in MEGA 7 using the Kimura-2-parameter (K2P) model (Kimura 1980).

Results

Phylogenetic analysis

A total of 1092 bps were included in the aligned dataset of the cyt. *b* gene, with 668 conservative sites, 492 variable sites, 375 Parsim-informative sites and 117 singleton sites. The mean frequency of the four nucleotides in the sequences of *Tachysurus wuyueensis* are A = 29.1%, G = 15.6%, C = 27.7% and T = 28.5%. The phylogenetic trees reconstructed by ML and BI methods are identical in topology (Fig. 1). A monophyly formed by samples of *Tachysurus wuyueensis* was recovered with 100% posterior probabilities (pp) and 1.00 bs in ML and BI trees, respectively and belonged to a clade containing *T. gracilis*, *T. brachyrhabdion*, *T. truncatus* and *T. pratti*. *Tachysurus wuyueensis* is sister to a species pair consisting of *T. gracilis* and *T. brachyrhabdion* and the above all are sister to another species pair: *T. truncatus* and *T. pratti*. Herein, these five species are designated as belonging to the *T. truncatus*-*T. pratti* group given their affinities in both morphology and molecular phylogeny.

The estimated K2P genetic distances of the cyt. *b* gene between *T. wuyueensis* and congenerics range from 6.9% to 12.6% (Table 2). The distances between *T. wuyueensis* and members of the *T. pratti*-*T. truncatus* group are in a range of 6.9–8.3%. The paired species, *T. truncatus* and *T. pratti*, endemic to the upper Yangtze River Basin have a 1.4% genetic distance, while another paired species, *T. brachyrhabdion* and *T. gracilis*, displays a 4.1% distance. The range of intraspecific genetic distances within *T. wuyueensis* is 0.1%.

Table 2. K2P distances (%) for species within the *Tachysurus pratti*-*Tachysurus truncatus* group, based on the cyt. *b* gene.

	1	2	3	4
1. T. wuyueensis sp. nov.				
2. T. pratti	7.1			
3. T. truncatus	6.9	1.4		
4. T. gracilis	8.3	9.1	8.6	
5. T. brachydhrbdion	7.5	8.3	8.0	4.1

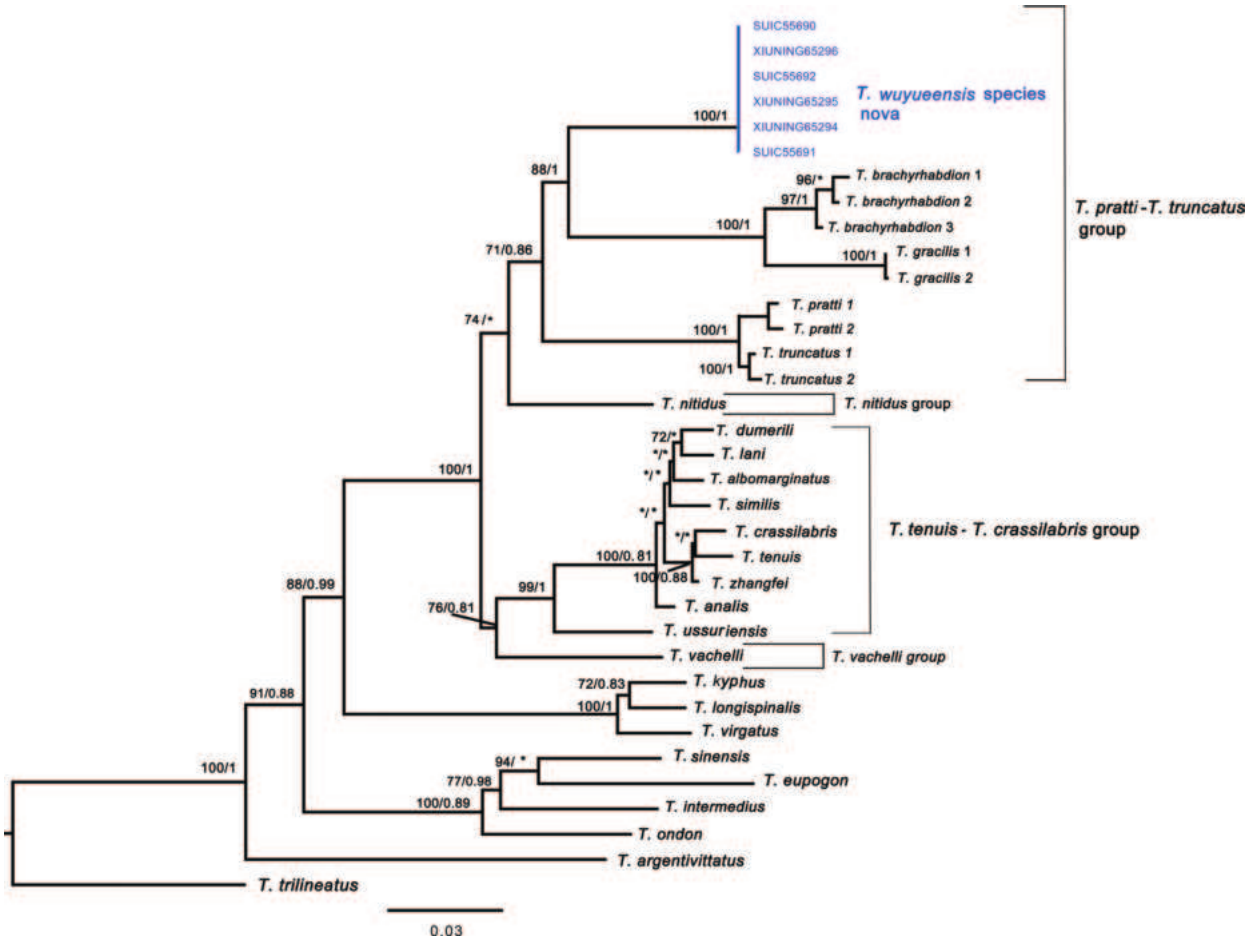

Figure 1. Phylogenetic tree of *Tachysurus* species inferred from cyt. *b* using Bayesian Inference and Maximum Likelihood methods. Bayesian posterior probabilities (> 0.8) and Maximum Likelihood bootstrap values (> 70%) are shown, respectively.

Principal component analysis

The *T. truncatus*-*T. pratti* group can be differentiated from all other *Tachysurus* species by having a smooth anterior margin of the pectoral spine, short dorsal spine not exceeding two-thirds of head length and short maxillary barbels not extending beyond the base of the pectoral spine.

Amongst these five species, excluding *T. pratti* which has a deeply forked caudal fin (Fig. 2), the other four round-tailed species were included in the principal component analysis performed on the variance-covariance matrix of log-transformed measurements (Table 3; Fig. 3). The results show that the combination of PC1 against PC3 and PC2 against PC3 enabled the separation of *T. wuyueensis* from *T. truncatus*, *T. gracilis* and *T. brachyrhabdion*. Characters with main loadings in PC1 were the adipose to caudal distance and body depth at anus; in PC2, they were the outer mandibular barbel length, anal-fin base length, nasal-barbel length and maxillary barbel length; and, in PC3, they were the inner mandibular barbel length, eye diameter and interorbital width (Table 3).

Table 3. Loadings on the first three principal components extracted from morphometric data for *T. wuyueensis*, *T. truncatus*, *T. brachyrhabdion* and *T. gracilis*.

	PC1	PC2	PC3
Standard length	21.2	18.5	7.8
Body depth at anus	21.3	5.6	26.4
Predorsal length	19.4	7.0	6.7
Pre-anal length	21.1	9.6	9.1
Prepelvic length	20.7	9.3	7.5
Prepectoral length	18.0	3.6	14.0
Length of dorsal-fin spine	15.8	14.2	8.5
Length of dorsal-fin base	20.3	2.2	6.8
Length of pectoral-fin spine	16.1	17.2	1.7
Length of anal-fin base	19.6	**41.2**	29.2
Height of adipose fin	16.5	13.7	20.2
Adipose to caudal distance	**23.9**	19.1	13.8
Length of caudal peduncle	**24.7**	21.9	24.2
Depth of caudal peduncle	19.7	4.2	23.5
Head length at latera	19.0	1.2	5.5
Head depth	18.3	0.08	12.2
Head width	19.8	3.0	18.0
Snout length	18.5	0.9	14.7
Interorbital width	20.2	8.8	**30.2**
Eye diameter	12.9	22.6	**36.2**
Mouth width	20.4	7.7	12.2
Length of nasal barbel	21.8	**37.6**	23.4
Length of maxillary barbel	22.6	**36.3**	3.8
Length of inner mandibular barbel	21.4	24.7	**45.9**
Length of outer mandibular barbel	22.7	**46.2**	19.5

Morphological comparisons

Amongst the characters displaying main loading in PCA, some exhibit stable variations between species and can

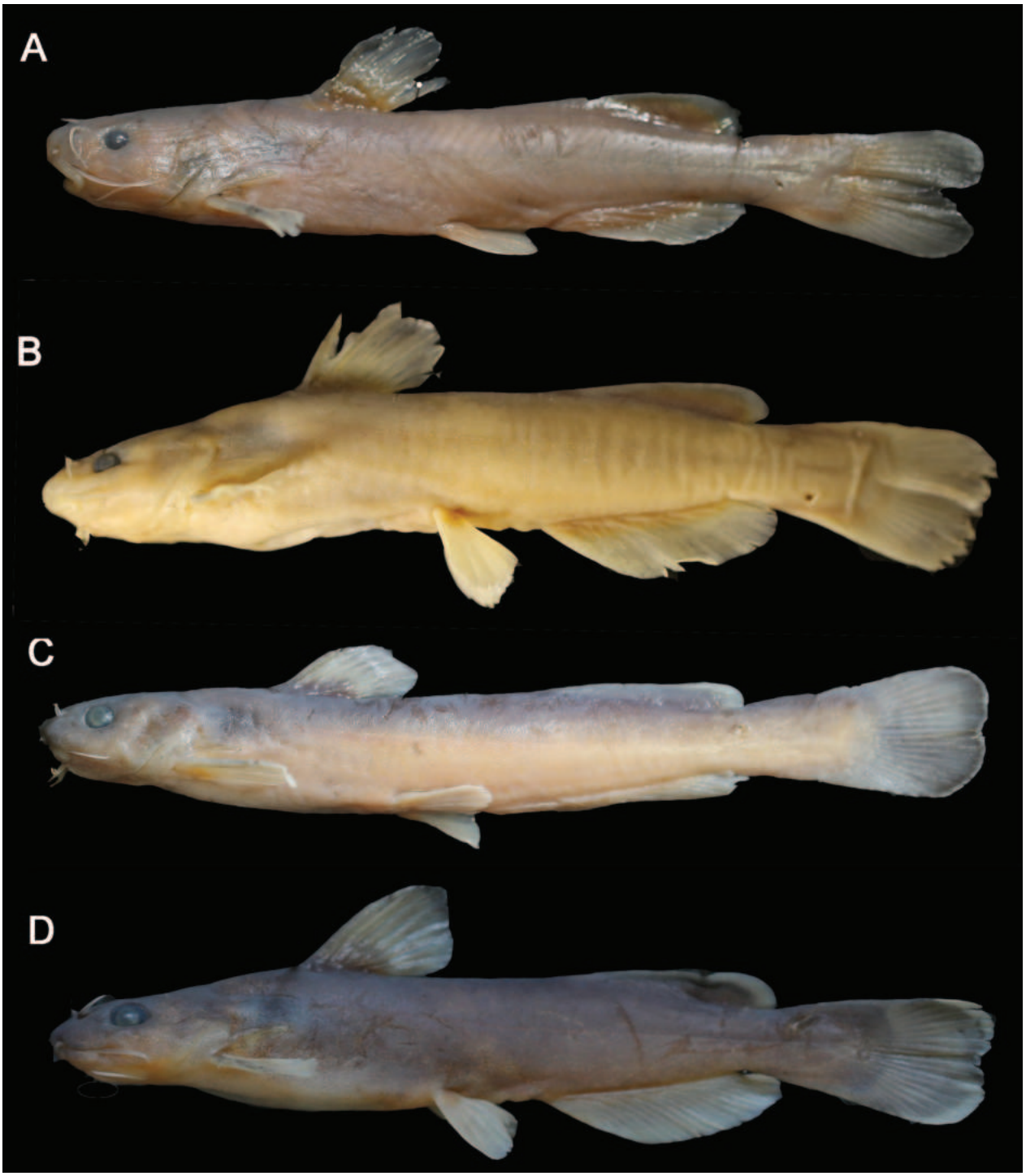

Figure 2. Lateral view of *T. pratti* (**A**) for IHB201909013758, 114.2 mm SL, Huili County, Sichuan Province, *T. truncatus* (**B**) for IHB201812028889, 79.5 mm SL, Qianwei County, Sichuan Province, *T. brachyrhabdion* (**C**) for IHB 2017090539, 120.8 mm SL, Songtao County, Guizhou Province, *T. gracilis* (**D**) for IHB 201803023401, 98.2 mm SL, Guanyang County, Guangxi Zhuang Autonomous Region.

be used to distinguish between them (Fig. 4). *Tachysurus wuyueensis* is distinct from the other three species in having a shorter prepelvic body (length 40.0–46.4% of HL vs. 45.8–54.8%; see Fig. 4A), from *T. truncatus* and *T. gracilis* in having more anal-fin rays (21–25 vs. 17–20) and vertebrae (45–47 vs. 37–43) (Fig. 5), from *T. truncatus* and *T. brachyrhabdion* in having a more slender body (depth 10.1–13.5% of HL vs. 13.1–20.6%; see Figure 4B). It further differs from *T. truncatus* in having a shorter pre-anal length (53.0–60.1% vs. 61.0–67.7%;Fig. 4C), longer anal-fin base (length 25.4–31.1% SL vs. 19.1–25.5%, Fig. 4D), narrower mouth (width 8.1–10.6% SL vs. 10.0–13.7%; Fig. 4E), narrower interorbital space (width 5.0–7.9% SL vs. 8.7–10.5%; Fig. 4F) and from *T. gracilis* in having longer inner mandibular barbels (length 4.9–6.0% of SL vs. 3.2–5.0%; Fig. 4G).

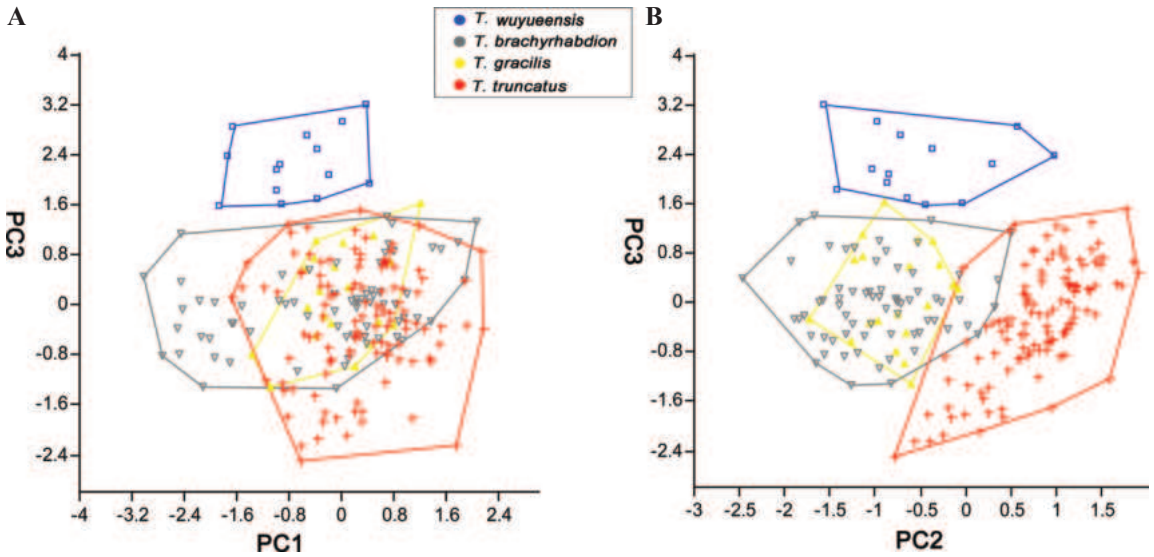

Figure 3. Scatter plot of **A.** PC2 against PC3 and **B.** PC1 against PC2 extracted from morphometric data for *T. wuyueensis*, *T. truncatus*, *T. brachyrhabdion* and *T. gracilis*

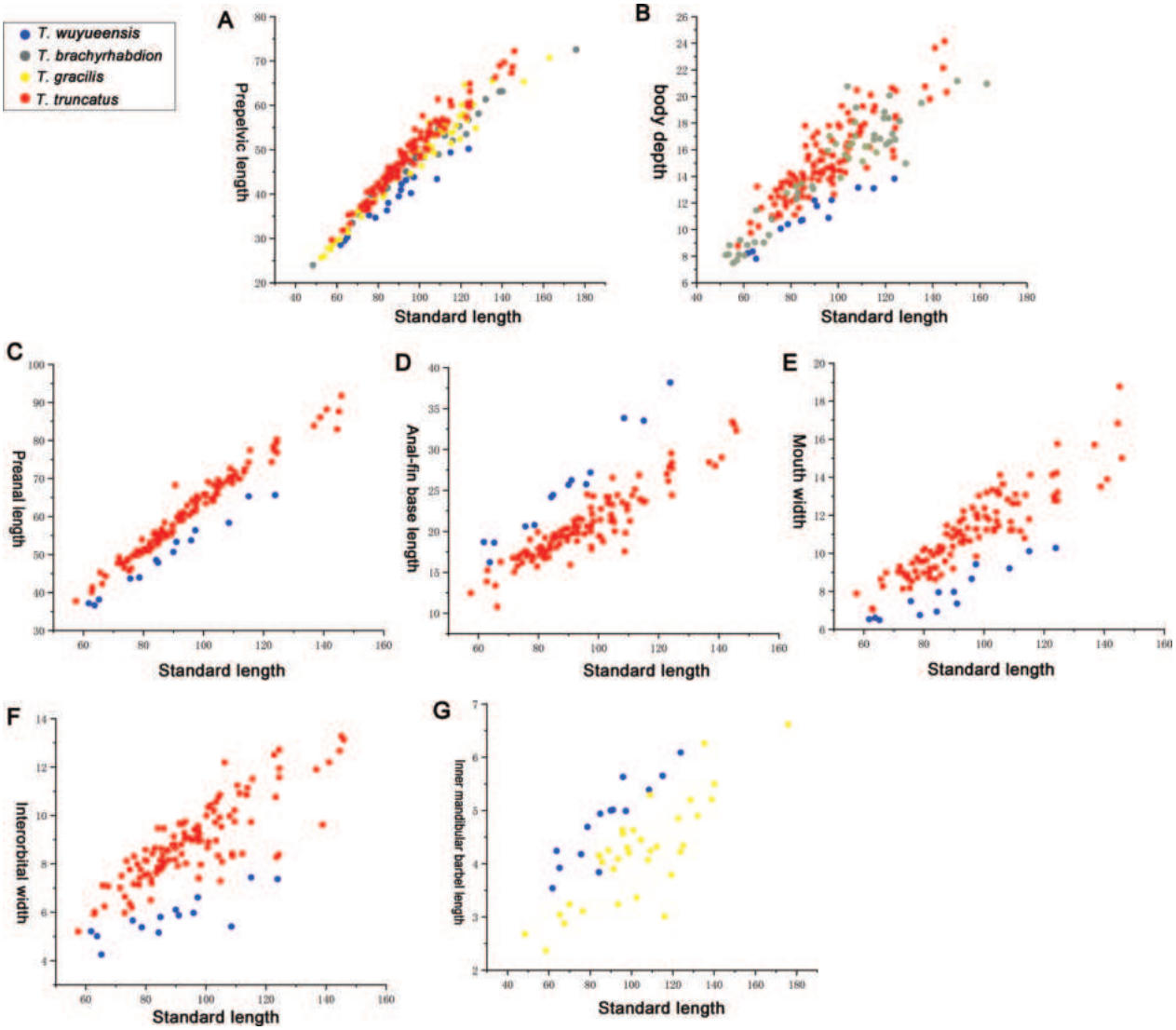

Figure 4. Relationship between **A.** Prepelvic length and SL for *T. wuyueensis*, *T. truncatus*, *T. brachyrhabdion* and *T. gracilis*; relationship between; **B.** Body depth and SL for *T. wuyueensis*, *T. truncatus* and *T. brachyrhabdion*; relationship between; **C.** Pre-anal length and SL; **D.** Anal fin base length and SL; **E.** Mouth width and SL; **F.** Interorbital width and SL for *T. wuyueensis* and *T. truncatus*; relationship between; **G.** Inner mandibular barbel length and SL for *T. wuyueensis* and *T. gracilis*.

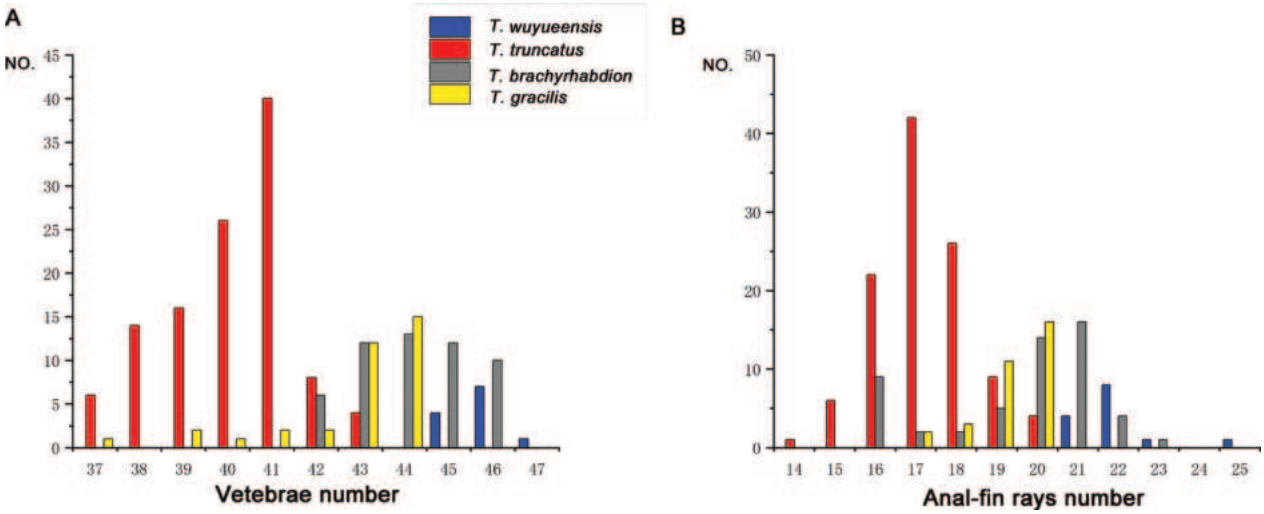

Figure 5. Meristic counts difference amongst *T. wuyueensis*, *T. truncatus*, *T. brachyrhabdion* and *T. gracilis* in vertebrae number (**A**) and anal fin ray number (**B**).

***Tachysurus wuyueensis* Zhou, Yuan & Shao, sp. nov.**

https://zoobank.org/18A16B30-C113-4285-8A76-058999C3D0E1

Fig. 6

Pseudobagrus adiposis: Mao 1991: 169 (coastal rivers in Zhejiang Province).

Type materials. ***Holotype*.** IHB 202009055690, 70.7 mm SL, South China: Zhejiang Prov.: Suichang County: the Qiantang-Jiang at Jiulongshan National Natural Reserve (28°23'38"N, 118°53'41"E) (Fig. 7); collected by Zhi-Gang Xie in Sept 2020.

***Paratypes*.** IHB 202009055691-2, two ex., 63.8–65.2 mm SL; other data same as holotype. IHB202212165294-304, 11 ex., 61.8–123.9 mm SL, south China: Anhui Prov.: Xiuning County: the Qiantang-Jiang at Liukou Township (29°48'57"N, 117°53'11"E) (Fig. 7); collected by Wei-Han Shao in May 2023.

Diagnosis. Distinguished from its congeners by the following combination of characters: a smooth anterior margin of the pectoral-fin spine, short maxillary barbels not extending beyond the base of the pectoral-fin spine, short dorsal spine not exceeding two-thirds of head length, prepelvic length 40.0–46.4% SL, 45–47 vertebrae, 21–25 anal-fin rays, body depth 10.1–13.5% SL, a slightly emarginated caudal fin.

Description. Morphometric measurements taken from the holotype (78.7 mm SL) and 13 paratypes (61.8–123.9 mm SL) summarised in Table 4.

Body elongated, anteriorly cylindrical and slightly compressed posteriorly. Dorsal profile rising gradually from snout tip to dorsal-fin origin, then sloping evenly from there to posterior end of adipose-fin base, and gradually increasing to dorsal origin of procurrent caudal-fin rays. Ventral surface of head flattened; ventral profile of body straight or slightly rounded from head to anal-fin origin, decreasing evenly from posterior end of anal-fin base to origin of ventral procurrent caudal-fin rays. Lateral line complete, straight and mid-lateral in position. Vertebrae 5 + 45 (46, 47).

Table 4. Morphomertric data for *Tachysurus wuyueensis* species nova.

	Holotype	Paratypes (n = 13)	
		Range	Mean ± SD
Standard length	78.7	61.8–115.1	69.7 ± 14.3
%SL			
Body depth at anus	13.2	10.1–13.5	13.1 ± 1.5
Predorsal length	32.6	27.2–35.3	32.5 ± 2.8
Pre-anal length	55.8	53.0–60.1	57.6 ± 1.9
Prepelvic length	44.1	40.0–46.6	44.0 ± 1.4
Prepectoral length	20.9	16.1–23.1	20.8 ± 2.1
Length of dorsal-fin spine	59.2	46.4–63.8	59.2 ± 3.3
Length of dorsal-fin base	11.4	8.6–11.7	11.3 ± 1.3
Length of pectoral-fin spine	14.7	10.7–15.5	14.7 ± 2.2
Length of anal-fin base	26.4	25.4–30.8	27.0 ± 1.6
Height of adipose fin	3.1	2.4–5.1	4.1 ± 0.9
Adipose to caudal distance	13.9	13.2–16.8	15.3 ± 2.1
Length of caudal peduncle	16.4	16.0–18.1	17.3 ± 0.9
Depth of caudal peduncle	7.9	6.5–8.0	7.6 ± 0.3
Head length at latera	22.8	17.9–24.8	23.7 ± 2.5
Head depth	11.7	9.0–13.2	12.3 ± 1.5
Head width	14.2	13.1–15.7	15.2 ± 1.1
Snout length	5.5	4.2–8.7	6.0 ± 1.9
Interorbital width	6.8	5.0–8.4	7.7 ± 1.3
Eye diameter	4.5	4.3–5.6	4.9 ± 0.3
Mouth width	8.6	8.1–10.4	10.1 ± 1.0
Length of nasal barbel	6.5	5.2–7.5	7.1 ± 1.4
Length of maxillary barbel	14.5	8.6–13.7	13.1 ± 3.8
Length of inner mandibular barbel	6.0	4.6–6.6	6.1 ± 0.7
Length of outer mandibular barbel	9.5	5.9–10.7	9.6 ± 2.1

Head depressed, broad, and covered with thin skin. Supra-occipital process slender, with evenly converging sides and pointed tip, separated from nuchal plate by a broad interspace. Snout slightly pointed in dorsal view and obtuse or blunt in lateral view, longer than eye diameter. Interorbital space moderately space wide and slightly flattish. Eyes moderately large, elliptical, covered with thick membrane and anterolateral in head, visible when viewed dorsally, but not ventrally, with slightly convex and comparatively narrow interorbital space.

Figure 6. Lateral (**A**), dorsal (**B**) and ventral (**C**) views of *Tachysurus wuyueensis* species nova, IHB202009055690, holotype, 70.7 mm SL.

Mouth subterminal, transverse. Upper jaw anteriorly protruded, longer than lower jaw in length; interorbital space narrower than mouth opening. Teeth villiform, in irregular rows on all tooth-bearing surfaces. Premaxillary tooth plates broad, of equal width throughout. Dentary tooth plates arched, broadest at symphysis and narrowing laterally, of same width at symphysis as premaxillary tooth plates. Vomerine tooth plate unpaired, continuous across mid-line, slightly curved anteriorly and much narrower than premaxillary plate. Gill opening wide, extending from the post-temporal region to beyond isthmus.

Barbels in four pairs; nasal barbels small, thread-like, not reaching beyond posterior margin of eye; maxillary barbels slender, slightly exceeding posterior margin of eye; mandibular barbels in two pairs, thick, short, inner barbels positioned in transverse row at level of posterior naris, extending beyond mid-point of eye, outer barbels rooted posterolateral to inner mandibular barbel, just extending to posterior margin of eye.

Dorsal fin with a spinelet, one spine and seven soft branched rays. Dorsal-fin origin equidistant to pectoral-fin insertion and ventrally to pelvic-fin insertion, also equidistant to anal-fin origin and snout tip. Spinelet flattened, with long blunt distal tip. Dorsal-fin spine slender, with smooth anterior margin and slightly serrated distal posterior margin, equal to or slightly longer than pectoral-fin spine. First dorsal-fin soft ray longest, surpassing tip of last ray. Distal margin of dorsal-fin rays nearly straight. Nuchal plate triangular, with anterior pointed tip anteriorly.

Adipose fin inserted slightly behind vertical through pectoral-fin origin, with convex distal margin along entire length and deeply incised posterior part to form rounded apex. Adipose fin base moderately long, equal to or slightly longer than anal fin base length.

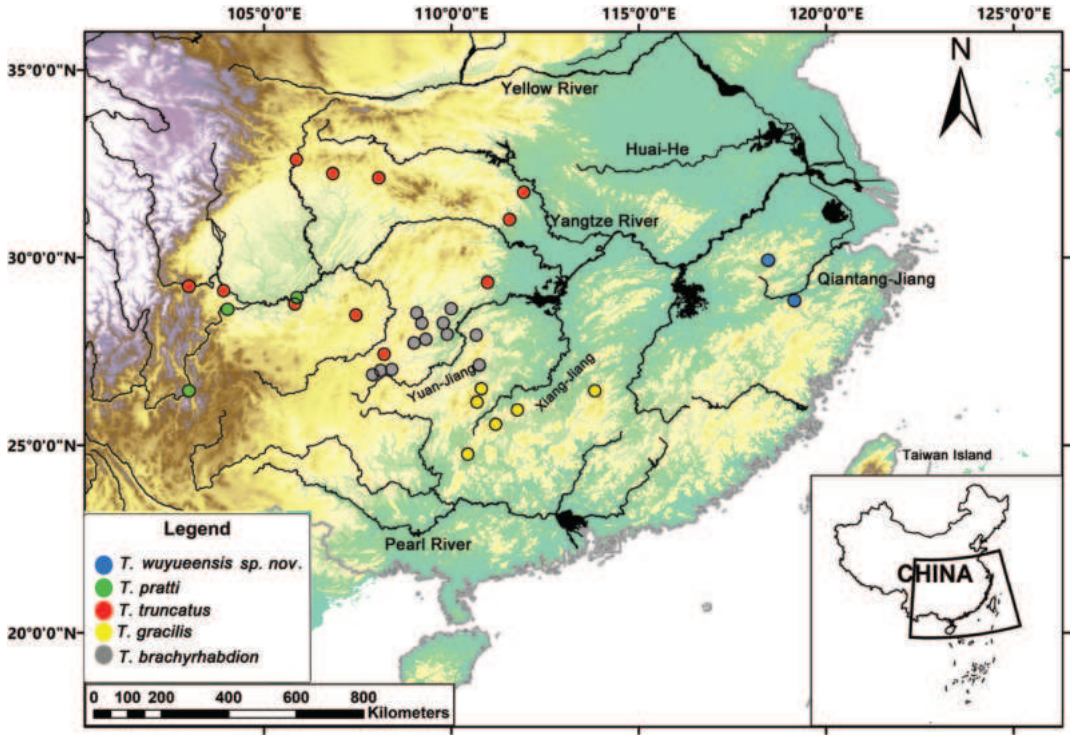

Figure 7. Map showing distributions of five species of *Tachysurus* in China: *T. wuyueensis* species nova, *T. pratti*, *T. truncatus*, *T. brachyrhabdion* and *T. gracilis*.

Pectoral fin with one spine and seven (or eight) soft branched rays, inserted slightly anterior or at level of posteriormost point of opercle, not reaching halfway to pelvic-fin insertion. Pectoral-fin spine very stout, sharply pointed at tip, equidistant to or slightly longer than dorsal-fin spine, with a smooth anterior margin and 8 (9, mean 8.3) strong serrations along posterior margin. Cleithral process triangular with a sharp pointed tip, extending for half of pectoral fin spine length.

Pelvic fin with one unbranched and five branched soft rays, inserted closer to tip of snout than to posterior end of anal fin base, closer to depressed tip of dorsal fin than to anterior end of anal fin base. Tip of depressed pelvic fin reaching or slightly extending beyond anal fin origin. Pelvic fin distal margin convex. Anus and urogenital opening nearer to anal fin origin than to posterior end of pelvic fin base. Males with a conical genital papilla not reaching base of first anal fin soft ray.

Anal fin long, with 21 (22, 23, 25) branched rays; adipose fin posterior margin away from caudal fin. Anal fin origin to caudal fin than to tip of snout. Distal margin of anal fin convex; anterior rays shortest.

Caudal fin with 9+10 principal rays, slightly emarginated, with middle rays longer than two-thirds of longest rays; both lobes rounded, with upper lobe slightly longer than lower lobe; procurrent rays slightly extending from anterior to fin base. Lowest point of caudal peduncle behind posterior end of anal fin base.

Colouration. Body yellowish-grey with three obscured and broad vertical brown blotches in smaller individuals (the first one below the dorsal fin, the second one closely above the anal fin and the third occupying the caudal peduncle) (Fig. 6) and fading to a more uniform yellow or brown in larger individuals (Fig. 8). Adipose fin brownish, with a yellow anterodorsal margin and a slightly transparent posterodorsal margin. Dorsal fin transparent for anterior two-thirds, rest of fin greyish-brown. Caudal fin greyish in posterior third, rest of fin transparent with a slightly white margin in smaller individuals. Pectoral, pelvic and anal fins transparent.

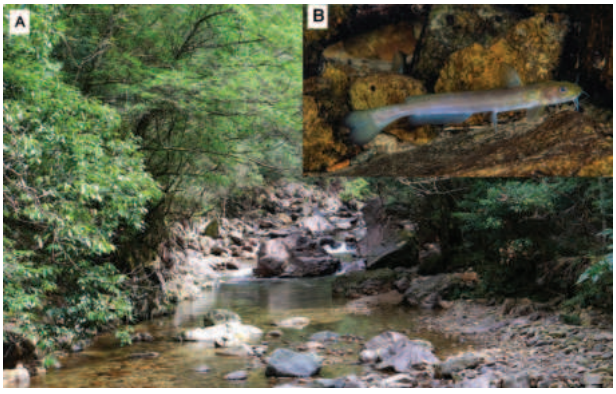

Figure 8. A. Habitat of *Tachysurus wuyueensis*; **B.** *T. wuyueensis* in situ.

Distribution and habitat. Currently only known from the Qiantang-Jiang in Suichang County, Zhejiang Province and Xiuning County, Anhui Province, south China (Fig. 7). *T. wuyueensis* is found in montane streams of this river basin (Fig. 8), co-existing with *Acrossocheilus fasciatus*, *Pseudogastromyzon fasciatus*, *Rhinogobius niger* and *Tachysurus albomarginatus*.

Etymology. The specific epithet is based on the two rival states Wu and Yue which were bordered by the Qiantang-Jiang in southeast China more than 2000 years ago. The onomatopoeic Chinese sound of this species is "Wu Yue Ni Chang".

Discussion

Shao and Zhang (2023) erected the *Tachysurus pratti* group using morphological characters, such as smooth anterior margin of the pectoral spine, short maxillary-barbel not extending to the base of pectoral-fin, fewer than 20 anal-fins and uniform yellow or brown body in adults. Under this taxonomic treatment, the *T. pratti* group is the largest group within the genus, with more than twenty species. However, the monophyly of the *T. pratti* group was not supported under the molecular scrutiny in this study (Fig. 1), indicating these species were wrongly clustered due to retention of conservative morphological features, common in catfishes (Zhou et al. 2016). Members in the *T. pratti* group formed two distinct phylogenetic entities in our analyses: *T. wuyueensis* clustering with *T. truncatus*, *T. pratti*, *T. gracilis* and *T. brachyrhabdion* form a well-supported monophyletic clade, namely the *T. pratti-T. truncatus* group, that is sister to *T. nitidus*. The remaining species of the "*T. pratti* group" form another monophyly here defined as the *T. tenuis-T. crassilabris* group, sister to *T. vachelli*. In addition, the *T. pratti-T. truncatus* group plus *T. nitidus* appears to be sister to a clade with *T. vachelli* and *T. tenuis-T. crassilabris* group.

Although the morphological similarities between these two newly-erected species groups are numerous, there are some distinguishing features that can be used to diagnose them. The *T. pratti-T. truncatus* group differs from the *T. tenuis-T. crassilabris* group in having a shorter dorsal spine (length not longer than vs. longer than two-thirds of HL) (Figs 2, 9, 10). Differences in colour patterns were also found to be apparent between the two clades. The body colour of the *T. pratti-T. truncatus* group is yellowish-brown (Fig. 2), but dark brown in the *T. tenuis-T. crassilabris* group (Fig. 10). The distinction in colouration of the abdomen is conspicuous with numerous dark spots in the *T. tenuis-T. crassilabris* group, but is absent in the *T. pratti-T. truncatus* group (Fig. 11). In addition, the caudal-fin colouration of round-tailed species can be used as another diagnostic character between these two clades. Except for *T. tenuis*, the white or yellowish caudal-fin margin is broad in the *T. tenuis-T. crassilabris* group (Fig. 10), but which is narrow or absent in the *T. pratti-T. truncatus* group (Fig. 2). The *T. pratti-T. truncatus* group can also be distinguished from other species groups of *Tachysurus* in the external morphology. It differs from the *T. aurantiacus* group, the *T. vachelli* group and the *T. trilineatus* group in having short maxillary barbels not extending to (vs. extending beyond or reaching) the base of pectoral fin, from the *T. nitidus* group, the *T. vachelli* group and *T. virgatus* group in having a dorsal fin spine shorter (vs. longer) than two-thirds of HL.

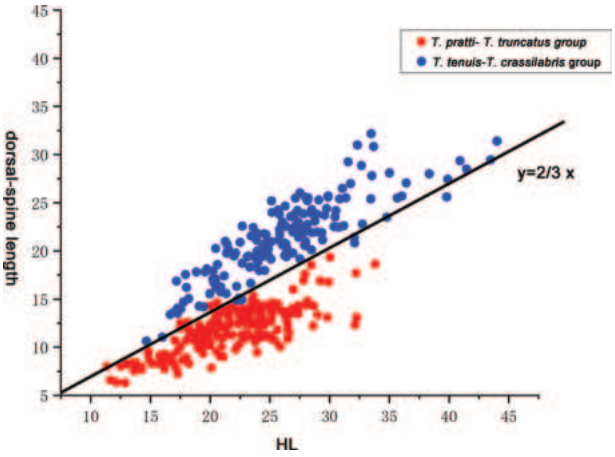

Figure 9. Relationship between dorsal spine length and HL for the *T. pratti-T. truncatus* group (including *T. wuyueensis*, *T. pratti*, *T. truncatus*, *T. brachyrhabdion*, *T. gracilis*) and the *T. tenuis-T. crassilabris* group (including *T. tenuis*, *T. albomarginatus*, *T. analis*, *T. lani*, *T. zhangfei*, *T. ussuriensis*, *T. crassilabris*).

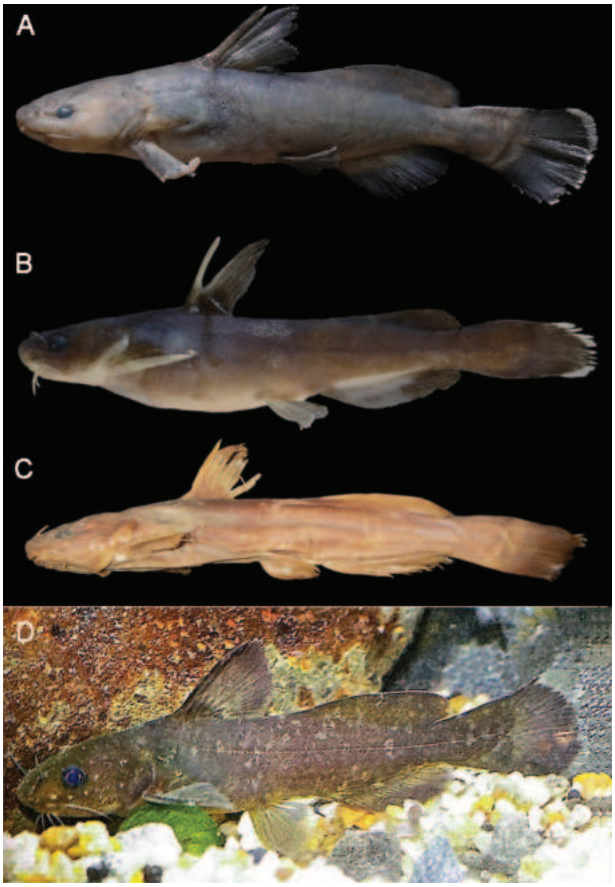

Figure 10. Lateral view of *T. albomarginatus* (**A**) for IHB 202110025885, 133.5 mm SL, Macheng County, Hubei Province; *T. analis* (**B**) for IHB201707014311, 124.2 mm SL, Yudu County, Jiangxi Province, in Gan-Jiang; *T. adiposalis* (**C**) for FMNH 59079, holotype, 172 mm SL, Tamusui River, Taiwan Island; (**D**) Colour in life of adult of *T. adiposalis,* cited from Zhou and Gao (2011).

The topotypes of *T. adiposalis* were not available in this study, but our photographic examination on the type (FMNH59079) confirmed that *T. adiposalis* has a long dor-

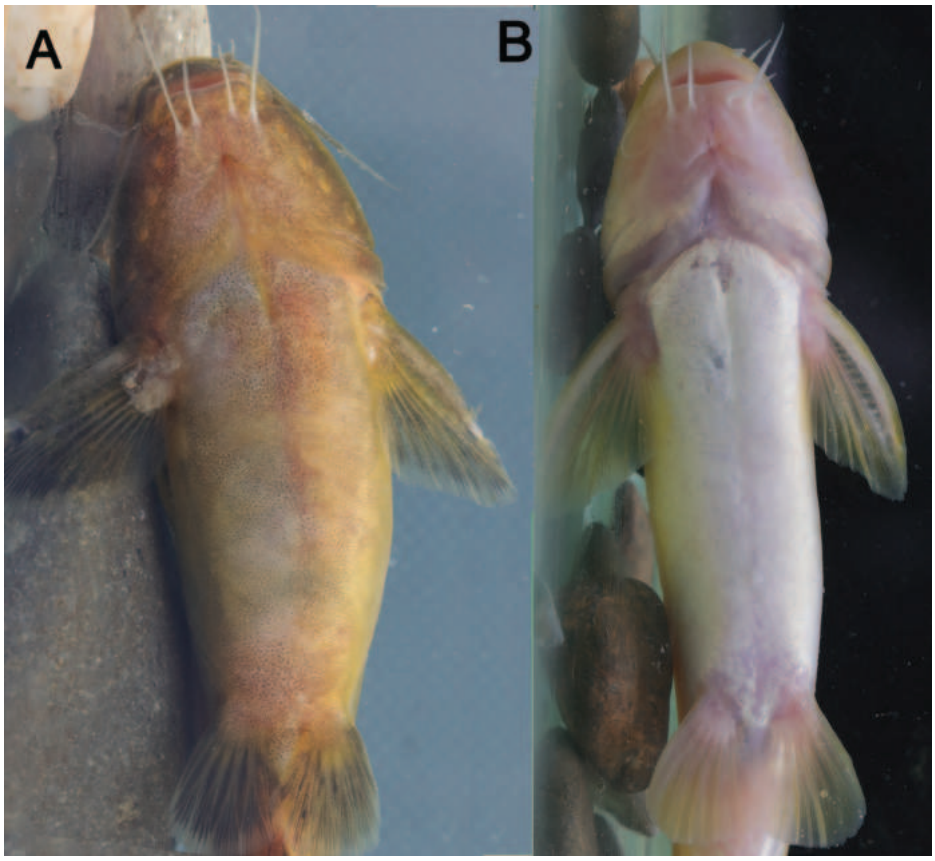

Figure 11. Ventral view of *T. zhangfei* (**A**) and *T. gracilis* (**B**) that belong to the *T. tenuis-T. crassilabris* group and the *T. pratti-T. truncatus* group, respectively.

sal-fin spine (longer than two-thirds of HL) and 19 anal-fin rays (Fig. 10C), which is distinct from *T. wuyueensis*. Based on data from Taiwan, the dark brown body and wide white margin in the caudal fin are present in a living specimen of *T. adiposalis* (Fig. 10D) (Zhou and Gao 2011), suggesting this species may belong to the *T. tenuis-T. crassilabris* group. Moreover, a phylogenetic analysis, based on a short segment of mtDNA, showed the specimens of *T. adiposalis* collected from Taiwan are closely related to *T. ussuriensis* of the *T. tenuis-T. crassilabris* group. These data confirm our conclusion (Watanabe et al. 2007).

High levels of inter-specific variations in the shape of the caudal fin occur in the *T. pratti-T. truncatus* group; for example, *T. pratti* has a deeply forked caudal fin, but the remaining species of the group have round-tailed caudal fins. A similar scenario also occurs in the *T. tenuis-T. crassilabris* group. It suggests the convergent evolution of caudal fin morphology in *Tachysurus*. There is a tight link between the shape of the caudal fin and habitat preference: round-tailed species present habitat affinities to montane streams, while fork-tailed species are restricted to rivers' main stream and lakes. The observation describes the effects of ecological niches by shaping the caudal fin in *Tachysurus*.

Comparative materials examined

1. *T. adiposis*: FMNH59079, 170 mm SL, China: Tamusui River in Taiwan Island.
2. *Tachysurus albomarginatus*: IHB200605264–7, 200605269–86, 220605268 72.1–128.5 mm SL, topotypes, China: Anhui Province: Dangtu County: the lower Yangtze River.
3. *Tachysurus brachyrhabdion*: IHB2017090535–9, 107.6–121.8 mm SL, China: Guizhou Province: Songtao County, the Yuan-Jiang of middle Yangtze River Basin; IHB2017090522–31, China: Chongqing City: Xiushan County, the Yuan-Jiang of the middle Yangtze River Basin; IHB2016106554, 6, 7, China: Hunan Province: Jishou County, the Yuan-Jiang of the middle Yangtze River Basin; IHB2017090548–58, 588, China: Guizhou Province: Tongren City, the Yuan-Jiang of the middle Yangtze River Basin; IHB 201906012028–31, 104.0–127.3 mm SL, China: Hunan Province: Xupu County, the Yuan-Jiang of the middle Yangtze River Basin; IHB2016106295–500, 104.4–124.2 mm SL, China: Hunan Province: Mayang County, the Yuan-Jiang of the middle Yangtze River Basin; IHB2017090495–6, 135.3–150.1 mm SL, China: Guizhou Province: Jiangkou County, the Yuan-Jiang of the middle Yangtze River Basin; IHB2017090427–34, 65.4–89.4 mm SL, China: Guizhou Province: Huangping County, the Yuan-Jiang of the middle Yangtze River Basin.
4. *Tachysurus crassilabris* (Günther 1864): BMNH 1864.7.9.9 (holotype), 155.2 mm SL, China (photograph and X-ray examined); IHB 201909034566–9,

97.1–107.2 mm SL, China: Sichuan Province: Huili County: the Jinsha Jiang of the upper Yangtze River; IHB201909017347–61, 69.1–120.5 mm SL, China: Jiangsu Province: Nanjing City: the lower Yangtze River.

5. *T. gracilis*: IHB201803023394–403, 93.6–140.1 mm SL, China: Guangxi Zhuang Autonomous Region: Guanyang County: the middle Yangtze River Basin; IHB2017122195, 2017090542–6, 84.1–119.3 mm SL, China: Guangxi Zhuang Autonomous Region: Yangshuo County: the Pearl River Basin; IHB201909019374–83, 69.9–112.3 mm SL, China: Hunan Province: Shuangpai County: the Xiang-Jiang of the middle Yangtze River Basin; IHB201906011312, 175.9 mm SL, China: Hunan Province: Xinning County: the Zi-shui of the middle Yangtze River Basin; IHB201906011084, 132.0 mm SL, China: Hunan Province, Dongkou County, the Zi-shui of the middle Yangtze River Basin; IHB201906011497–503, 100.8–125.0 mm SL, China: Guangxi Zhuang Autonomous Region: Ziyuan County: the Zi-shui of the middle Yangtze River Basin; IHB201809019719–22, 201809019850–1, 48.4–138.8 mm SL, China: Yanling County, the Xiang-Jiang of the middle Yangtze River Basin.
6. *Tachysurus tenuis*: IHB201909113617–13629, 124.5–159.6 mm SL, China: Zhejiang Province: Jiaxing City, the Qiantang-Jiang.
7. *Tachysurus truncatus*: IHB201909038001–10, 84.9–109.5 mm SL, China: Sichuan Province: Wanyuan County, the Jialing-Jiang of the upper Yangtze River; IHB2019090112599–613, 76.0–111.2 mm SL, China: Sichuan Province: Nanjiang County, the Jialing-Jiang of the upper Yangtze River; IHB201909037495–506, 20210505666–70, 73.6–123.5 mm SL, China: Hubei Province: Yuan'an County, the Qing-Jiang of the middle Yangtze River; IHB201904028989-96, 71.5–138.8 mm SL, China: Hubei Province: Nanzhang County, the Han-Jiang of the middle Yangtze River Basin; IHB2015030702–7, 70.6–124.2 mm SL, China: Hunan Province: Cili County, the Li-Shui of the middle Yangtze River Basin; IHB2017090517–21, 91.2–101.5 mm SL, China: Sichuan Province: Leshan City, the Tuo-Jiang of the upper Yangtze River Basin; IHB201812028889–94, 65.7–124.4 mm SL, China: Qianwei County, the Tuo-Jiang of the upper Yangtze River Basin; IHB2019090212127–45, 81.90–145.92 mm SL, China: Sichuan Province: Hejiang County, the Chishui-He of the upper Yangtze River.
8. *Tachysurus pratti*: IHB202009013755-64, 81.4–143.8 mm SL, China: Sichuan Province: Huili County, the Jinsha-Jiang of the upper Yangtze River Basin; IHB2019090212149-55, 80.8–138.1 mm SL, China: Sichuan Province: Hejiang County, the Chishui-He of the upper Yangtze River Basin; IHB201909034750, 57.3 mm SL, Shuifu County, the Jinsha-Jiang of the upper Yangtze River Basin; IHB202009016033-6, 48.8–56.0 mm, SL, China: Yunnan Province: Binchuan County, the Jinsha-Jiang of upper Yangtze River Basin.

Conflict of interest

The authors declare that they have no conflict of interest.

Funding

This work was partially funded by a grant from the National Science & Technology Fundamental Resources Investigation Program of Mount Dabie (Grant No. 2019FY101800).

Authors' contributions

Jia-Jun Zhou designed the study and revised the manuscript. Yuan Le-Yang extracted the genomic DNA and performed the molecular analysis. Wei-Han Shao examined the specimens and prepared the manuscript. All authors read and approved the final version of the manuscript.

Acknowledgements

We are grateful to Huan-Shan Wang (Museum of Aquatic Organisms at the Institute of Hydrobiology, IHB) for providing comparative specimens; to Zhan-sheng Tang (Zhejiang Jiulongshan National Natural Reserve) for assistance in field surveys.

References

Cheng JL, Ishihara H, Zhang E (2008) *Pseudobagrus brachyrhabdion*, a new catfish (Teleostei: Bagridae) from the middle Yangtze River drainage, South China. Ichthyological Research 55(2): 112–123. https://doi.org/10.1007/s10228-007-0020-3

Cheng JL, Shao WH, Lopez JA (2021) *Tachysurus lani*, a new catfish species (Teleostei: Bagridae) from the Pearl river basin, south china. Ichthyological Exploration of Freshwaters 2021(4): 30. https://doi.org/10.23788/IEF-1156

Ferraris CJ (2007) Checklist of catfshes, recent and fossil (Osteichthyes: Siluriformes), and catalogue of Siluriform primary types. Zootaxa 1418: 81–107. https://doi.org/10.11646/zootaxa.1418.1.1

Gosline WA (1997) Functional morphology of the caudal skeleton in teleostean fishes. Ichthyological Research 44(2–3): 137–141. https://doi.org/10.1007/BF02678693

Günther A (1864) Catalogue of the Physostomi, containing the families Siluridae, Characinidae, Haplochitonidae, Sternoptychidae, Scopelidae, Stomiatidae in the collection of the British Museum. Catalog of the Fishes in the British Museum 5: [i–xxii +] 1–455.

Günther A (1873) Report on a collection of fishes from China. Annals and Magazine of Natural History 4: 239–250. https://doi.org/10.1080/00222937308680749

Kalyaanamoorthy S, Minh BQ, Wong TKF, von Haeseler A, Jermiin LS (2017) ModelFinder: Fast model selection for accurate phylogenetic estimates. Nature Methods 14(6): 587–589. https://doi.org/10.1038/nmeth.4285

Kimura M (1980) A simple method for estimating evolutionary rate of base substitutions through comparative studies of nucleotide sequences. Journal of Molecular Evolution 16(2): 111–120. https://doi.org/10.1007/BF01731581

Krishnadas A, Ravichandran S, Rajagopal P (2018) Analysis of biomimetic caudal fin shapes for optimal propulsive efficiency. Ocean Engineering 153(APR.1): 132–142. https://doi.org/10.1016/j.oceaneng.2018.01.082

Ku X, Peng Z, Diogo R, He S (2007) MtDNA phylogeny provides evidence of generic polyphyleticism for East Asian Bagrid catfishes. Hydrobiologia 579(1): 147–159. https://doi.org/10.1007/s10750-006-0401-z

Kumar S, Stecher G, Tamura K (2016) MEGA7: Molecular evolutionary genetics analysis version 7.0 for bigger datasets. Molecular Biology and Evolution 33(7): 1870–1874. https://doi.org/10.1093/molbev/msw054

Li J, Chen XL, Chan BPL (2005) A new species of *Pseudobagrus* (Teleostei: Siluriformes: Bagridae) from southern China. Zootaxa 1067(1): 49–57. https://doi.org/10.11646/zootaxa.1067.1.3

Lima SMQ, Berbel-Filho WM, Araújo Thais FP, Henrique L, Andrey T, Avise JC (2017) Headwater capture evidenced by paleo-rivers reconstruction and population genetic structure of the armored catfish (*Pareiorhaphis garbei*) in the serra do mar mountains of southeastern Brazil. Frontiers in Genetics 8: 199. https://doi.org/10.3389/fgene.2017.00199

López-Pujol J, Zhang F-M, Sun H-Q, Ying T-S, Ge S, López-Pujol Jordi (2011) Mountains of southern China as "plant museums" and "plant cradles": Evolutionary and conservation insights. Mountain Research and Development 31(3): 261–269. https://doi.org/10.1659/MRD-JOURNAL-D-11-00058.1

Nguyen LT, Schmidt HA, von Haeseler A, Minh BQ (2015) IQ-TREE: A fast and effective stochastic algorithm for estimating maximum-likelihood phylogenies. Molecular Biology and Evolution 32(1): 268–274. https://doi.org/10.1093/molbev/msu300

Oshima M (1919) Contributions to the study of the fresh water fshes of the Island of Formosa. Annals of Carnegie Museum 12(2–4): 185–204. https://doi.org/10.5962/p.34608

Reist JD (1985) An empirical evaluation of several univariate methods that adjust for size variation in morphometric data. Canadian Journal of Zoology 63(6): 1429–1439. https://doi.org/10.1139/z85-213

Rendahl H (1928) Beiträge zur kenntnis der Chinesischen Süsswasserfsche. I. Systematischer Teil. Arkiv för Zoologi 20 A: 1–194.

Ronquist F, Teslenko M, van der Mark P, Ayres DL, Darling A, Höhna S, Larget B, Liu L, Suchard MA, Huelsenbeck JP (2012) MrBayes 3.2: Efficient Bayesian phylogenetic inference and model choice across a large model space. Systematic Biology 61(3): 539–542. https://doi.org/10.1093/sysbio/sys029

Shao WH, Zhang E (2023) *Tachysurus latifrontalis*, a new bagrid species from the Jiulong-Jiang basin in Fujian Province, South China (Teleostei: Bagridae). Ichthyological Research 70(1): 110–122. https://doi.org/10.1007/s10228-022-00867-0

Shao WH, Cheng JL, Zhang E (2021) Eight in one: Hidden diversity of the bagrid catfish *Tachysurus albomarginatus* s.l. (Rendhal, 1928) widespread in lowlands of south China. Frontiers in Genetics 12: 2195. https://doi.org/10.3389/fgene.2021.713793

Shaw TH (1930) Notes on some fshes from Ka-Shing and ShingTsong, Chekiang Province. Bulletin of the Fan Memoal Institute of Biology 1: 109–121.

Sun X, Luo Y, Gao X, Wu M, Xu H (2021) On the localized extreme rainfall over the Great Bay area in South China with complex topography and strong UHI effects. Monthly Weather Review 149(8): 2777–1881. https://doi.org/10.1175/MWR-D-21-0004.1

Wang G, Guan DS, Xiao L, Peart MR (2018) Forest biomass-carbon variation affected by the climatic and topographic factors in pearl river delta, South china. Journal of Environmental Management 232: 781–788. https://doi.org/10.1016/j.jenvman.2018.11.130

Watanabe K (1995) P*seudobagrus pratti* (Gunther, 1892), a senior synonym of *P. emarginatus* (Regan, 1913) (Siluriformes: Bagridae). Japanese Journal of Ichthyology 42(3–4): 321–324. https://doi.org/10.11369/jji1950.42.321

Watanabe K (2010) Mating behavior and larval development of *Pseudobagrus ichikawai* (Siluriformes: Bagridae). Japanese Journal of Ichthyology 41:243–251. https://doi.org/10.1007/BF00042890

Watanabe K, Jang-Liaw NH, Zhang CG, Jeon S-R, Nishida M (2007) Comparative phylogeography of bagrid catfishes in Taiwan. Ichthyological Research 54(3): 253–261. https://doi.org/10.1007/s10228-007-0398-y

Zheng BS, Dai DY (1999) Bagridae. In: Chu XL, Zheng BS, Dai DY (Eds) Fauna Sinica: Osteichthyes: Siluriforms. Science Press, Beijing, 35–73.

Zheng CY (1979) On a new catfsh of the genus *Leiocassis* from Guangdong Province, China. Acta Zootaxonomica Sinica 4:182–184.

Zhou MT, Gao RQ (2011) The freshwater and estuarine fish of Taiwan. Morning Star Press, Taiwan, 115 pp.

Zhou C, Wang X, Gan X, Zhang Y, Irwin DM, Mayden RL, He S (2016) Diversification of Sisorid catfishes (Teleostei: Siluriformes) in relation to the orogeny of the Himalayan Plateau. Science Bulletin 61(13): 991–1002. https://doi.org/10.1007/s11434-016-1104-0

Zoosyst. Evol. 100 (2) 2024, 597–602 | DOI 10.3897/zse.100.118068

PENSOFT

für Natur MUSEUM FÜR NATURKUNDE BERLIN

Osteology of the skull of the blind snake *Helminthophis flavoterminatus* (Peters, 1857) (Serpentes, Anomalepididae)

Fidélis Júnio Marra Santos[1]

1 *Pontifícia Universidade Católica do Rio Grande do Sul (PUCRS), Laboratory of Vertebrate Systematics. Av. Ipiranga, 6681 Partenon; 90619-900, Porto Alegre, Rio Grande do Sul, Brazil*

https://zoobank.org/EDE9AABA-4D35-426C-B837-056E865E97F2

Corresponding author: Fidélis Júnio Marra Santos (fidelismarra@gmail.com)

Academic editor: Johannes Penner ♦ **Received** 1 January 2024 ♦ **Accepted** 8 April 2024 ♦ **Published** 17 May 2024

Abstract

The blind snake *Helminthophis flavoterminatus* (Peters, 1857) is a species of Anomalepididae with distribution throughout northwestern Venezuela and western Colombia. Its osteology is poorly known, and thus this study presents information on its skull structure based on High-Resolution X-Ray Computed Tomography. The absence of the supraoccipital bone can be used for the determination of *H. flavoterminatus* in relation to its congeners, *Helminthophis frontalis* (Peters, 1860) and *Helminthophis praeocularis* Amaral, 1924.

Key Words

Helminthophis sp., HRXCT, reptiles, snakes, systematics, taxonomy

Introduction

Within the family Anomalepididae Taylor, 1939, the genus *Helminthophis* Peters, 1860, is a group of small blind snakes, distributed in the Neotropics, from lower Central America and northwestern South America: Costa Rica, Panama, Colombia, and Venezuela. *Helminthophis* is currently composed of three species (McDiarmid et al. 1999; Marra Santos and Reis 2018; Boundy 2021): *Helminthophis flavoterminatus* (Peters, 1857); *Helminthophis frontalis* (Peters, 1860); and *Helminthophis praeocularis* Amaral, 1924.

The osteology of the skull of some species of snakes Anomalepididae, for example *Anomalepis aspinosus* Taylor, 1939 and *Liotyphlops albirostris* (Peters, 1857), has already been very well studied and presented by other researchers (Tihen 1945; Haas 1964, 1968; List 1966), and, in recent years, the use of High-Resolution X-Ray Computed Tomography (HRXCT) has increased the knowledge of the osteology of Anomalepididae, for example *Anomalepis colombia* Marx, 1953; *Liotyphlops albirostris* (Peters, 1857); *Liotyphlops anops* (Cope, 1899); *Liotyphlops palauophis* Marra Santos, 2023; *Liotyphlops taylori* Marra Santos & Reis, 2018; *Liotyphlops ternetzii* (Boulenger, 1896); and *Typhlophis squamosus* (Schlegel, 1839) (Rieppel et al. 2009; Marra Santos and Reis 2018; Marra Santos and Reis 2019; Marra Santos 2023; Szyndlar and Georgalis 2023). An interesting and important aspect of HRXCT is that, in important ways, it permits replication of many aspects of the traditional techniques, and the resulting digital models allow for three-dimensional and rotational investigation similar to traditional observations of dry skulls or skeletons in hand (Bell et al. 2021).

In this paper, the osteology of the skull of *Helminthophis flavoterminatus* is presented based on HRXCT data. This study is the first detailed description of the cranial osteology of *Helminthophis*, adding new information to the knowledge of the skull anatomy of Anomalepididae snakes.

Materials and methods

The head of *H. flavoterminatus* (AMNH R 59407) was studied by HRXCT at the CT facility at Pontifícia Universidade Católica do Rio Grande do Sul (PUCRS) using a SkyScan 1173. Additional information will be available on MorphoBank (http://morphobank.org/permalink/?P5113). The skull measures 4.6 mm in length, 2.4 mm in width, and 1.3 mm in height. The dataset is compared with HRXCT datasets for *Helminthophis frontalis* and *Helminthophis praeocularis*. The specimen of *H. praeocularis* (AMNH R 38125) was also scanned at PUCRS. The head of *Helminthophis flavoterminatus* (AMNH R 59407) and the head of *H. praeocularis* (AMNH R 38125) were scanned at 46 kV and 55 μA, and each reconstructed slice represents a thickness and spacing of 7.16 μm. The head of *H. frontalis* (MCZ R-55117) was scanned at the CT facility of the University of Texas at Austin using an Xradia microCT scanner. This specimen was scanned at 80 kV and 10 W, and each reconstructed slice represents a thickness and spacing of 3.58 μm. The datasets were rendered in three dimensions using CTVox v. 3.2 (Bruker MicroCT, Inc., Billerica, MA) for Windows. The terminology used for bones follows Rieppel et al. (2009) and Marra Santos (2023).

Results

Description of skull

High-Resolution X-Ray Computed Tomography of skull bones in Figs 1–5.

Neurocranium

Main body of premaxilla on ventral surface of snout. Maxilla-premaxilla contact widely separated. Lateral maxillary foramina absent. Maxilla alveolar row oriented transversely. Nasal fused. Nasal-frontal boundary convex posteriorly in a shallow W-shaped suture. Prefrontal separated from nasal. Prefrontal moveably articulated to frontal. Postorbital element present. Posterior orbital margin incomplete. Frontals gradually tapering anteriorly. Frontal fused. Frontal-parietal contact (dorsal aspect) anteriorly concave, i.e., frontals extending posteriorly into broad median embayment in parietals. Parietal paired. Posterior border of parietal in contact with otico-occipital. Supraoccipital absent. Supratemporal present. Posteromedial flange of septomaxilla short, not contacting frontal. Septomaxilla with lateral flange contributing to posterior border of external naris. Fenestra for duct of Jacobson's organ (fenestra vomeronasalis) posteroventrally positioned. Palatine not in contact with vomer, maxilla, or pterygoid. Ectopterygoid present.

Mandible and dentition

Splenial not present as discrete element. Coronoid and angular separated by prearticular portion of compound bone. Retroarticular process long, longer than articular facet. Teeth present in maxilla and dentary, but lacking in premaxilla, palatine, and pterygoid.

Discussion

The osteology of the skull of *Helminthophis* reveals to us a character that readily distinguishes this genus from the other three belonging to Anomalepididae, which is the fused frontal (Figs 1B, 4A–C). The frontal paired in *Anomalepis* Jan, 1860; *Liotyphlops* Peters, 1881; and *Typhlophis* Fitzinger, 1843, has already been presented and discussed by other researchers (Haas 1964, 1968; List 1966; Rieppel et al. 2009; Marra Santos and Reis 2018; Marra Santos and Reis 2019; Marra Santos 2023). In addition to the frontal fused, which is a bony character of *Helminthophis* that distinguishes it from the other genera of Anomalepididae, *H. flavoterminatus* is readily differentiated from *H. frontalis* and *H. praeocularis* by the absence of supraoccipital (Figs 1B, 4A, 5A). An important observation is that, if it were not for the presence of the fused frontal, the skull of *Helminthophis* could easily be confused with the skull of some of the species of *Liotyphlops* that also do not have the supraoccipital (for example, *Liotyphlops schubarti*, *Liotyphlops taylori*, *Liotyphlops ternetzii*, and *Liotyphlops wilderi*) or even with the skull of *Typhlophis squamosus*.

With the exception of the fused frontal, *H. flavoterminatus* presents other skull characters shared by other taxa Anomalepididae: (1) the nasal bone fused (Figs 1B, D, 4A); (2) absence of the lateral maxillary foramina (Fig. 1A); (3) absence of a prefrontal-nasal contact (Figs 1B, C, 4A); (4) presence of a discrete ossification (postorbital element) (Figs 1A–D, 2A, B); and (5) by having an ectopterygoid (Figs 1A, C, 2B, C).

One of the most interesting and novel consequences of HRXCT is that it has opened the door to the development and documentation of detailed data on the internal anatomy even of type specimens, which otherwise have historically remained immune to internal anatomical investigations that were, of necessity, invasive and destructive (Bell et al. 2021). In this sense, the information on the osteology of the skull of *H. flavoterminatus* presented here, thanks to the use of HRXCT, can contribute to the knowledge of the anatomy and systematics of snakes, especially extant non-caenophidian snakes. It is important to note that the data presented here on the osteology of the skull of *H. flavoterminatus* will contribute to future publications focused on the taxonomy of *Helminthophis*.

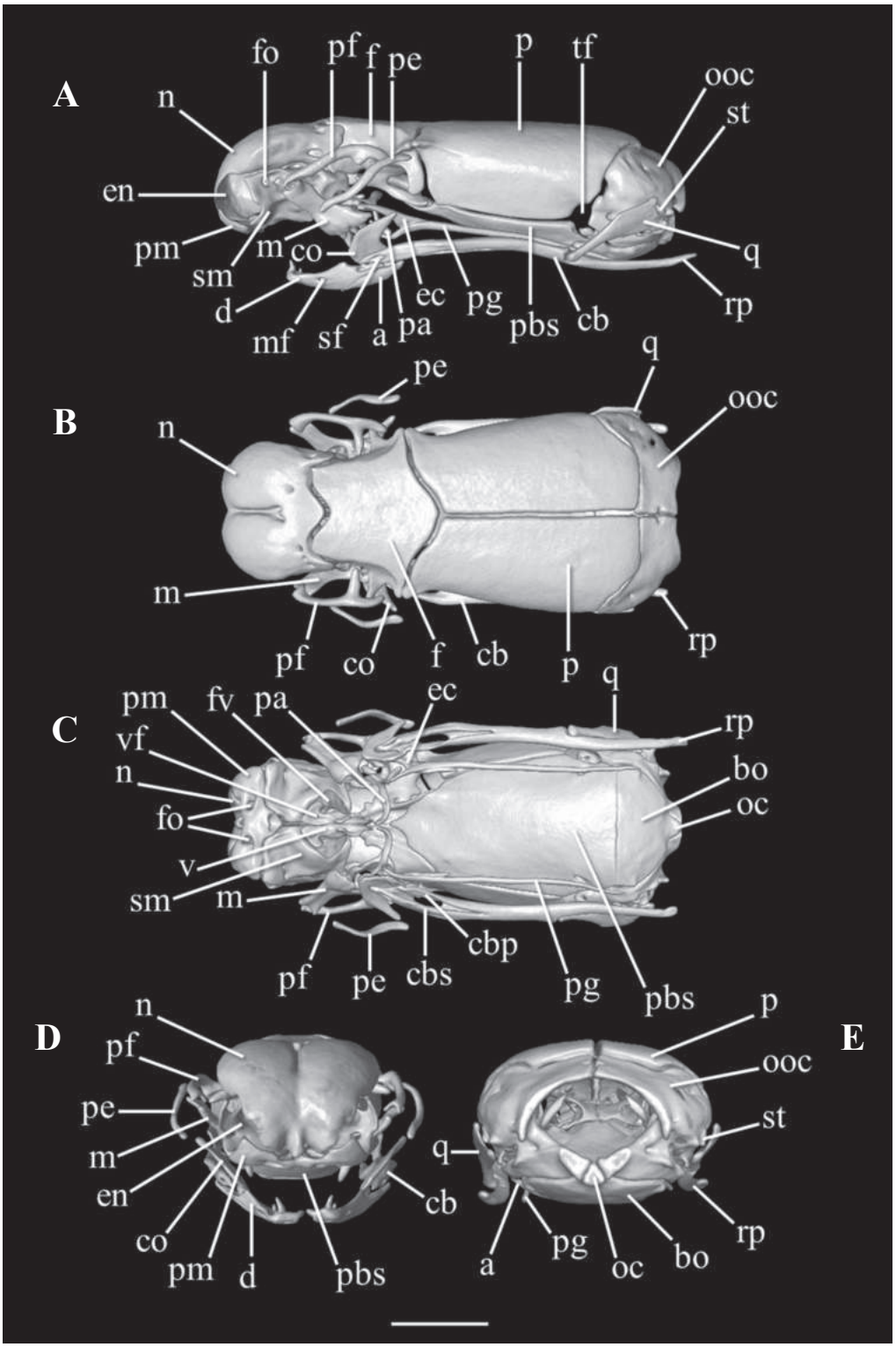

Figure 1. Three-dimensional reconstruction of the skull of *Helminthophis flavoterminatus* (AMNH R 59407), based on HRXCT data. **A.** Lateral view; **B.** Dorsal view; **C.** Ventral view with the lower jaw partially digitally removed; **D.** Anterior view; **E.** Posterior view. Scale bar: 1 mm. Anatomical abbreviations: **a,** angular; **bo,** basioccipital; **cb,** compound bone; **cbp,** compound bone prearticular component; **cbs,** compound bone surangular component; **co,** coronoid; **d,** dentary; **ec,** ectopterygoid; **en,** external naris; **f,** frontal; **fo,** foramen; **fv,** fenestra vomeronasalis; **m,** maxilla; **mf,** mental foramen; **n,** nasal; **oc,** occipital condyle; **ooc,** otico-occipital (fused prootic + opisthotic + exoccipital); **p,** parietal; **pa,** palatine; **pbs,** parabasisphenoid; **pe,** postorbital element; **pf,** prefrontal; **pg,** pterygoid; **pm,** premaxilla; **q,** quadrate; **rp,** retroarticular process; **sf,** surangular foramen; **sm,** septomaxilla; **st,** supratemporal; **tf,** trigeminal foramen; **v,** vomer; **vf,** vomerine foramen.

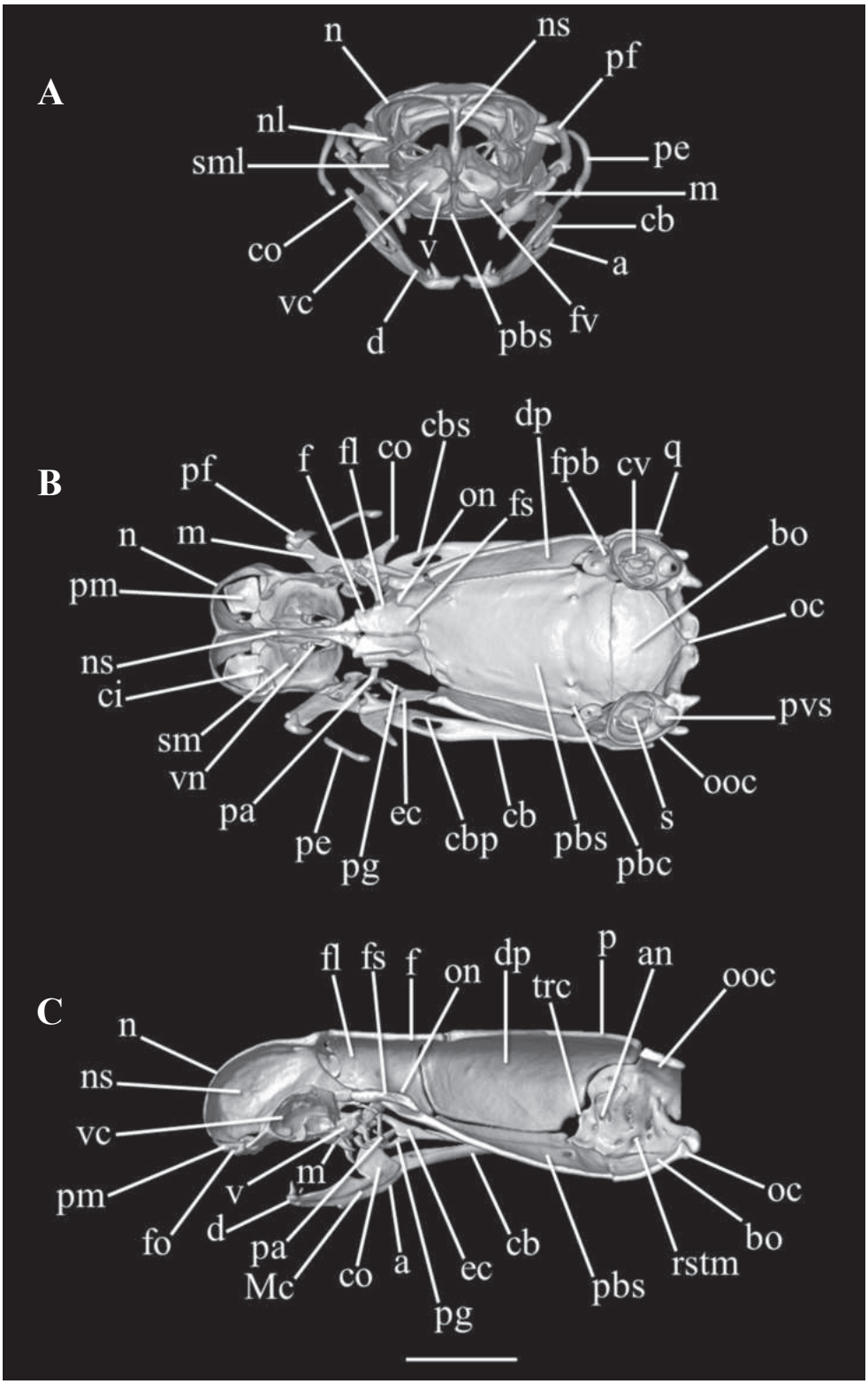

Figure 2. Three-dimensional reconstruction of the skull of *Helminthophis flavoterminatus* (AMNH R 59407), based on HRXCT data. **A.** Transversal view; **B.** Frontal view; **C.** Sagittal view. Scale bar: 1 mm. Anatomical abbreviations: **a,** angular; **an,** acoustic nerve foramen; **bo,** basioccipital; **cb,** compound bone; **cbp,** compound bone prearticular component; **cbs,** compound bone surangular component; **ci,** conchal invagination; **co,** coronoid; **cv,** cavum vestibuli; **d,** dentary; **dp,** descensus parietalis; **ec,** ectopterygoid; **f,** frontal; **fl,** frontal laterally descending flange; **fo,** foramen; **fpb,** facial nerve palatine branch foramen; **fs,** frontal subolfactory process; **fv,** fenestra vomeronasalis; **m,** maxilla; **Mc,** Meckel's canal; **n,** nasal; **nl,** nasal lateral flange; **ns,** medial nasal septum; **oc,** occipital condyle; **on,** optic nerve foramen; **ooc,** otico–occipital (fused prootic + opisthotic + exoccipital); **p,** parietal; **pa,** palatine; **pbc,** parabasal (Vidian) canal; **pbs,** parabasisphenoid; **pe,** postorbital element; **pf,** prefrontal; **pg,** pterygoid; **pm,** premaxilla; **pvs,** posterior vertical semicircular canal; **q,** quadrate; **rstm,** recessus scalae tympani medial aperture; **s,** stapes; **sm,** septomaxilla; **sml,** septomaxilla lateral flange; **trc,** trigeminofacialis chamber; **v,** vomer; **vc,** vomeronasal cupola; **vn,** vomeronasal nerve passage.

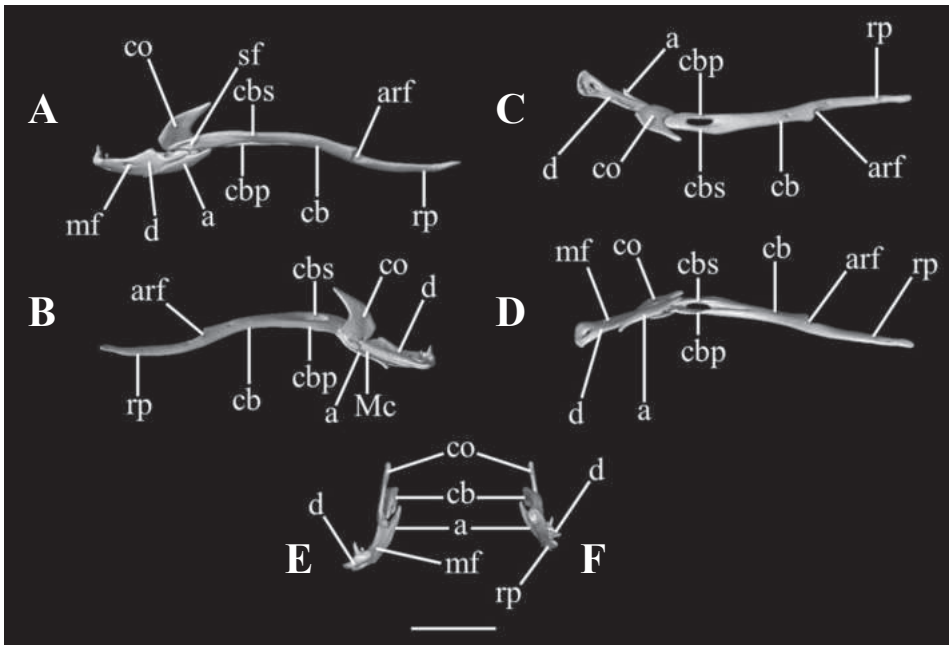

Figure 3. Three-dimensional reconstruction of the lower jaw of *Helminthophis flavoterminatus* (AMNH R 59407), based on HRXCT data. **A.** Lateral view; **B.** Medial view; **C.** Dorsal view; **D.** Ventral view; **E.** Anterior view; **F.** Posterior view. Scale bar: 1 mm. Anatomical abbreviations: **a,** angular; **arf,** articular fossa; **cb,** compound bone; **cbp,** compound bone prearticular component; **cbs,** compound bone surangular component; **co,** coronoid; **d,** dentary; **Mc,** Meckel's canal; **mf,** mental foramen; **rp,** retroarticular process; **sf,** surangular foramen.

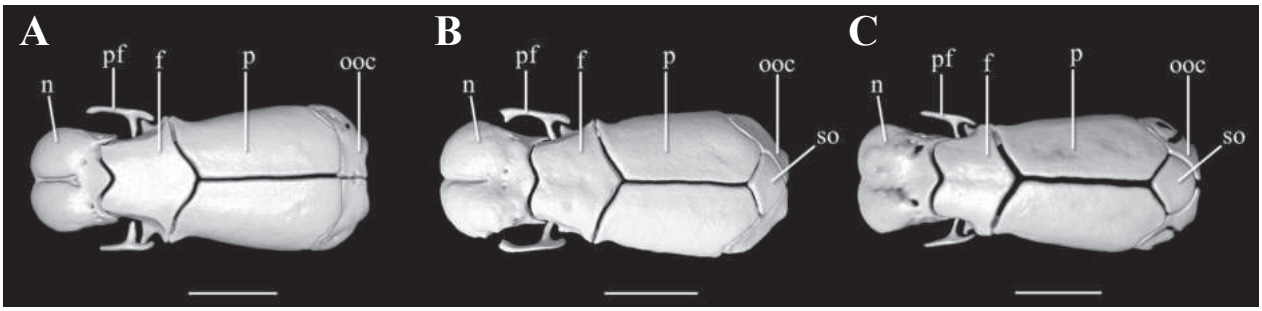

Figure 4. Incomplete dorsal view (some bones are not shown) of the three-dimensional reconstruction of the skulls of **A.** *Helminthophis flavoterminatus* (AMNH R 59407); **B.** *Helminthophis frontalis* (MCZ R-55117); and **C.** *Helminthophis praeocularis* (AMNH R 38125), showing the absence of supraoccipital in *H. flavoterminatus*. Scale bars: 1 mm. Anatomical abbreviations: **f,** frontal; **n,** nasal; **p,** parietal; **pf,** prefrontal; **ooc,** otico-occipital (fused prootic + opisthotic + exoccipital); **so,** supraoccipital.

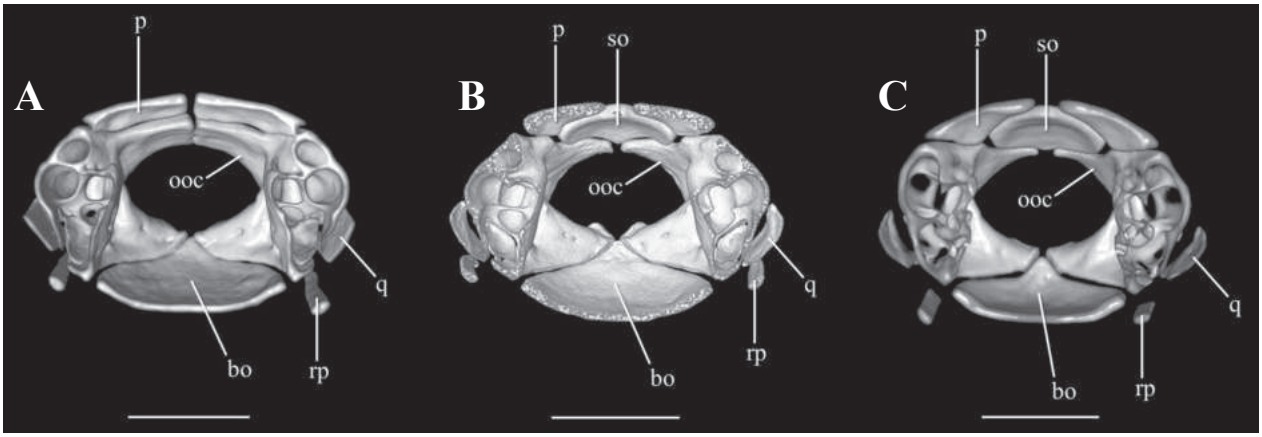

Figure 5. Transversal views of three-dimensional reconstruction of the posterior part of the skulls of **A.** *Helminthophis flavoterminatus* (AMNH R 59407); **B.** *Helminthophis frontalis* (MCZ R-55117); and **C.** *Helminthophis praeocularis* (AMNH R 38125), showing the contribution of the supraoccipital to the internal sidewall of the neurocranium in *H. frontalis* and *H. praeocularis*. Scale bars: 1 mm. Anatomical abbreviations: **bo,** basioccipital; **p,** parietal; **ooc,** otico-occipital (fused prootic + opisthotic + exoccipital); **q,** quadrate; **rp,** retroarticular process; **so,** supraoccipital.

Acknowledgements

I am grateful to all curators, collection managers, and their respective institutions for the loan of specimens and for permission to examine specimens in their care: David A. Kizirian and Lauren Vonnahme (American Museum of Natural History, New York) and José Rosado (Museum of Comparative Zoology, Harvard University). I thank Christopher J. Bell, Jessie Maisano, and Patrick Stafford of the University of Texas at Austin for their support in the acquisition of specimens and CT scanning. I thank Adolpho Augustin of the Pontifícia Universidade Católica do Rio Grande do Sul for help with CT scanning of specimens. I thank the Museum für Naturkunde, Berlin, for their support in the publication of this manuscript. I thank Johannes Penner, Polina Petrakieva, Vassil Peev (Zoosystematics and Evolution editors) and the reviewers, Van Wallach and Claudia Koch, for valuable suggestions during the review process.

References

Amaral A (1924) Helminthophis. Proceedings of the New England Zoological Club 9: 25–30.

Bell CJ, Daza JD, Stanley EL, Laver RJ (2021) Unveiling the elusive: X-rays bring scolecophidian snakes out of the dark. The Anatomical Record 304(10): 2110–2117. https://doi.org/10.1002/ar.24729

Boulenger GA (1896) Catalogue of the snakes in the British Museum (Natural History). Vol. III, containing the Colubridae (Opisthoglyphae and Proteroglyphae), Amblycephalidae, and Viperidae. British Museum (Natural History), London, 727 pp.

Boundy J (2021) Snakes of the World: a Supplement. CRC Press, Boca Raton, 273 pp. https://doi.org/10.1201/9780429461354

Cope ED (1899) Contributions to the herpetology of New Granada and Argentina with descriptions of new forms. The Philadelphia Museums Scientific Bulletin 1: 3–26. https://doi.org/10.5962/bhl.title.54674

Fitzinger L (1843) Systema Reptilium, fasciculus primus, Amblyglossae. Braumüller et Seidel, Wien, 1–106. https://doi.org/10.5962/bhl.title.4694

Haas G (1964) Anatomical observations on the head of *Liotyphlops albirostris* (Typhlopidae, Ophidia). Acta Zoologica (Stockholm, Sweden) 45(1–2): 1–62. https://doi.org/10.1111/j.1463-6395.1964.tb00709.x

Haas G (1968) Anatomical observations on the head of *Anomalepis aspinosus* (Typhlopidae, Ophidia). Acta Zoologica (Stockholm, Sweden) 49(1–2): 63–139. https://doi.org/10.1111/j.1463-6395.1968.tb00147.x

Jan G (1860) Iconographie générale des ophidiens. Première livraison. https://doi.org/10.5962/bhl.title.4885

List JC (1966) Comparative osteology of the snake families Typhlopidae and Leptotyphlopidae. Illinois Biological Monographs (36) [6] + 112. https://doi.org/10.5962/bhl.title.50341

Marra Santos FJ (2023) A new species of the genus *Liotyphlops* Peters, 1881 (Serpentes, Anomalepididae) from Colombia and the synonymization of *Liotyphlops beui* (Amaral, 1924) with *Liotyphlops ternetzii* (Boulenger, 1896). ZooKeys 1146: 87–114. https://doi.org/10.3897/zookeys.1146.94607

Marra Santos FJ, Reis RE (2018) Two new blind snake species of the genus *Liotyphlops* Peters, 1881 (Serpentes: Anomalepididae), from Central and South Brazil. Copeia 106(3): 507–514. https://doi.org/10.1643/CH-18-081

Marra Santos FJ, Reis RE (2019) Redescription of the blind snake *Anomalepis colombia* (Serpentes, Anomalepididae) using High-Resolution X-Ray Computed Tomography. Copeia 107(2): 239–243. https://doi.org/10.1643/CH-19-181

Marx H (1953) A new worm snake from Colombia, genus *Anomalepis*. Fieldiana. Zoology 34: 197–198. https://doi.org/10.5962/bhl.title.2876

McDiarmid RW, Campbell JA, Touré T (1999) Snake Species of the World. A Taxonomic and Geographic Reference. The Herpetologist's League, Washington DC, [xi +] 511 pp.

Peters WCH (1857) Vier neue amerikanische Schlangen aus der Familie der Typhlopinen und darüber einige vorläufige Mittheilungen. Monatsberichte der Königlichen Preussische Akademie des Wissenschaften zu Berlin 1857(8): 402–403.

Peters WCH (1860) Drei neue Schlangen des k. zoologischen Museums aus America und Bemerkungen über die generelle Unterscheidung von anderen bereits bekannten Arten. Monatsberichte der Königlichen Preussischen Akademie der Wissenschaften zu Berlin 1860(10): 517–521.

Peters WCH (1881) Einige herpetologische Mittheilungen, 1. Uebersicht der zu den Familien der Typhlopes und Stenostomi gehörigen Gattungen oder Untergattungen. Sitzungsberichte der Gesellschaft Naturforschender Freunde zu Berlin 1881(4): 69–71.

Rieppel O, Kley NJ, Maisano JA (2009) Morphology of the skull of the White-Nosed Blindsnake, *Liotyphlops albirostris* (Scolecophidia, Anomalepididae). Journal of Morphology 270(5): 536–557. https://doi.org/10.1002/jmor.10703

Schlegel H (1839) Abbildungen neuer oder unvollständig bekannter Amphibien, nach der Natur oder dem Leben entworfen und mit einem erläuternden Texte begleitet. Arne and Co., Düsseldorf, [xiv +] 141 pp.

Szyndlar Z, Georgalis GL (2023) An illustrated atlas of the vertebral morphology of extant non-caenophidian snakes, with special emphasis on the cloacal and caudal portions of the column. Vertebrate Zoology 73: 717–886. https://doi.org/10.3897/vz.73.e101372

Taylor EH (1939) Two new species of the genus *Anomalepis* Jan, with a proposal of a new family of snakes. Proceedings of the New England Zoölogical Club 17: 87–96.

Tihen JA (1945) Notes on the osteology of typhlopid snakes. Copeia 1945(4): 204–210. https://doi.org/10.2307/1438352

Appendix 1

Examined specimens:

Helminthophis flavoterminatus. Venezuela. Distrito Capital: AMNH R 59407.

Helminthophis frontalis. Costa Rica. San José: MCZ R-55117.

Helminthophis praeocularis. Colombia. Tolima, Honda: AMNH R 38125.

Zoosyst. Evol. 100 (2) 2024, 603–623 | DOI 10.3897/zse.100.118912

PENSOFT

für Natur MUSEUM FÜR NATURKUNDE BERLIN

On the occurrence of the deep-sea barnacle *Tetrachaelasma southwardi* Newman & Ross, 1971 (Cirripedia, Balanomorpha, Bathylasmatidae) in the Mar del Plata Submarine Canyon, Argentina: supplementary description and taxonomic remarks on the genus

Ignacio L. Chiesa[1], Emanuel Pereira[2,3], Daniel Roccatagliata[2]

1 *Centro Austral de Investigaciones Científicas (CADIC-CONICET), CP 9410, Ushuaia, Tierra del Fuego, Argentina*

2 *Instituto de Biodiversidad y Biología Experimental y Aplicada (IBBEA), Universidad de Buenos Aires-CONICET, CP 1428, Buenos Aires, Argentina*

3 *Universidad de Buenos Aires, Facultad de Ciencias Exactas y Naturales, Departamento de Biodiversidad y Biología Experimental (DBBE), CP 1428, Buenos Aires, Argentina*

https://zoobank.org/07F55091-6F85-44BB-BBC5-09BE2F0C733A

Corresponding author: Daniel Roccatagliata (daniel.roccatagliata@gmail.com)

Academic editor: Luiz F. Andrade ♦ **Received** 16 January 2024 ♦ **Accepted** 2 April 2024 ♦ **Published** 17 May 2024

Abstract

Tetrachaelasma southwardi Newman & Ross, 1971, a bathylasmatine balanomorph, has been recorded from the Mar del Plata Submarine Canyon (ca. 38°S, off the coast of Argentina), at two stations located at significantly different depths (1950 m and 2934 m). A total of 29 specimens, complete or damaged but with soft parts intact, were collected. This unusually large number of well-preserved specimens allows us to add supplementary descriptions and document intraspecific morphological variations. The differences between *T. southwardi* and *T. tasmanicum* Buckeridge, 1999, the second species of this genus, are re-evaluated. A map and an updated list including all the records of the genus *Tetrachaelasma* Newman & Ross, 1971 are provided. The distribution of the genus *Tetrachaelasma* in the Southern Ocean is discussed. Furthermore, a single specimen of another bathylasmatine balanomorph, which was assigned to the genus *Bathylasma* Newman & Ross, 1971, was also obtained at the 1950 m station herein studied. This is the first record of the genus *Bathylasma* from the South-West Atlantic. This specimen has one *T. southwardi* attached to it, marking the first time that members of these two genera have been found living together.

Key Words

Bathylasma sp., distribution, South-West Atlantic, *Tetrachaelasma southwardi*, *T. tasmanicum*

Introduction

On the genera *Tetrachaelasma* and *Bathylasma*

The genus *Tetrachaelasma* contains only two species, which inhabit much greater depths than any other Balanomorpha, up to 3600 m (Newman and Ross 1971, 1976; Buckeridge 2010; Table 1). Newman and Ross (1971) erected this genus for the reception of *T. southwardi*, a new species that these authors described based on seven complete specimens taken by the RV "Eltanin" at a single station in the Central South Pacific (2304–2328 m depth). Newman and Ross (op. cit.) also listed among the material studied loose plates taken by the RV "Eltanin" at three other localities, i.e., off southern Chile (1190–1263 m depth), off Malvinas/Falkland Is. (1720–1739 m depth), and at the Sars Bank in the Drake Passage (1207–1591 m depth). Furthermore, Newman and Ross (1976) reported extensive accumulations of loose plates of *Tetrachaelasma* sp. on the flanks of a seamount off Madagascar at comparable depths (~1800 m). In addition, the RV "Atlantis II" obtained about 70 disarticulated plates of *T.* cf. *southwardi*

at the Mid-Atlantic Ridge (ca. 41°S) in 1980 (see the SIO-BIC website in the References section). More recently, Buckeridge (1999) described the second species of the genus, *T. tasmanicum*, based on a single incomplete specimen (comprising the carina, left carinolateral, scuta, and terga, plus body parts) and numerous loose plates collected at the South Tasman Rise (2030–3600 m depth) by the RV "Rig Seismic". All these records, and a few others retrieved from the website, are listed in Table 1 and charted in Fig. 9.

An unusually high number of *T. southwardi* specimens, complete or damaged but all with soft parts intact, were recently collected at two stations from considerably different depths (1950 m and 2934 m). This material was taken from the Mar del Plata Submarine Canyon (ca. 38°S, off the coast of Argentina) during the Talud Continental I and III expeditions performed by the RV "Puerto Deseado". Based on this material, supplementary descriptions of *T. southwardi* are presented, and intraspecific morphological variations are documented. In addition, the differences between *T. southwardi* and *T. tasmanicum* are discussed. Furthermore, a second bathylasmatine balanomorph was collected at the 1950 m depth station, which was assigned to the genus *Bathylasma* Newman & Ross, 1971. This genus encompassed four extant and four fossil species (see Araya and Newman 2018). This is the first time that the genus *Bathylasma* has been recorded from the South-West Atlantic.

A brief review of the family Bathylasmatidae Newman & Ross, 1971

Newman and Ross (1971) erected the deep-sea family Bathylasmatidae to include the new genera *Bathylasma*, *Tetrachaelasma*, and *Aaptolasma* (currently a synonym of *Hexelasma*), as well as the previously known genera *Hexelasma* Hoek, 1913 and *Tessarelasma* Withers, 1936. Later, Newman and Ross (1976) grouped Bathylasmatidae, Tetraclitidae Gruvel, 1903, and Coronulidae Leach, 1817, under the superfamily Balanomorphoidea (new status, Coronuloidea Leach, 1817; see Newman and Ross (1977)), and divided the bathylasmatids into the subfamilies Bathylasmatinae and Hexelasmatinae. In addition, Newman and Ross (1976) suggested that Bathylasmatidae gave rise to Tetraclitidae (see fig. 5).

Foster (1978) stated that "the relationship between *Pachylasma* and *Hexelasma* is obvious; they are weakly constructed, deep-sea forms with wide parietal alae and no radial interlocking of the plates." Accordingly, Foster (1978) placed the bathylasmatids in the family Pachylasmatidae Utinomi, 1968, contradicting the proposal by Newman and Ross (1976). Foster's nomenclatural decision was subsequently followed by Jones (2000, 2012), who included the subfamilies Bathylasmatinae and Hexelasmatinae in Pachylasmatidae, under the superfamily Pachylasmatoidea Utinomi, 1968.

Buckeridge and Newman (2010) revised the classification of Balanomorpha and grouped Bathylasmatidae and Tetraclitidae under the superfamily Tetraclitoidea Gruvel, 1903. More recently, Chan et al. (2017), in a molecular phylogenetic study for Balanomorpha, proposed that Bathylasmatidae is more closely associated with Tetraclitoidea than with Pachylasmatoidea. This result is consistent with the proposal by Newman and Ross (1976), Buckeridge and Newman (2010), as well as with a molecular phylogenetic study of Tetraclitoidea presented by Tsang et al. (2015). Finally, Chan et al. (2021), in a thorough revision of the barnacle classification, placed Bathylasmatidae in the superfamily Coronuloidea, together with Tetraclitidae, Austrobalanidae Newman & Ross, 1976, Coronulidae, and Chelonibiidae Pilsbry, 1916.

Bathylasmatidae currently encompasses the subfamilies Hexelasmatinae (genus *Hexelasma*) and Bathylasmatinae (genera *Bathylasma*, *Tetrachaelasma*, *Tessarelasma*, and *Mesolasma* Foster, 1981). The former subfamily has a wall of six plates with longitudinal chitinous laminae and/or strips, whereas the latter subfamily has four or six plates and lacks chitinous material. *Tessarelasma* is only known from a fossil record from India. *Tetrachaelasma* is the only living genus with four wall plates. A key for the identification of extant genera is presented by Araya and Newman (2018). For diagnoses of the subfamilies and genera, see Jones (2000).

Description of the study area

The Mar del Plata Submarine Canyon is located in the southwestern Atlantic Ocean at around 38°S (Fig. 1). This canyon is not connected to the Argentine continental shelf and has a typical "V" shape (Violante et al. 2010; Bozzano et al. 2017). It begins on the upper continental slope at a depth of ~500–1000 m and extends for about 110 km downslope to reach a depth of ~3900 m (Voigt et al. 2013). Oceanographically, this canyon is located in one of the most dynamic and highly variable areas of the world ocean, the Brazil/Malvinas Confluence, which is generated by the encounter of the Brazil and Malvinas/Falklands currents (Piola and Matano 2001; Matano et al. 2010; Preu et al. 2013).

Material and methods

Field work

Twenty-nine specimens (complete or damaged) and a few loose plates of *Tetrachaelasma southwardi* were collected from the Mar del Plata Submarine Canyon during the Talud Continental I and III expeditions, carried out by the RV "Puerto Deseado" in 2012 and 2013, respectively. The specimens were obtained at two stations, one at 1950 m depth using an epibenthic sledge, similar to the one designed by Hessler and Sanders (1967), and the other at 2934 m depth using a bottom otter trawl (Fig. 1). In addition, one specimen identified as *Bathylasma* sp. was also collected at the 1950 m depth station (see Material Examined section).

Table 1. Records of *Tetrachaelasma* species reported in this study and by previous authors. Abbreviations: CSIRO-MIIC — Commonwealth Scientific and Industrial Research Organization – Marine Invertebrate Image Collection; GBIF — Global Biodiversity Information Facility; NMNH — National Museum of Natural History, Smithsonian Institution; SIO-BIC — Scripps Institution of Oceanography – Benthic Invertebrate Collection. Links to these institutions/organizations in the References section. Note: The catalog numbers for *T. southwardi* are those published on the NMNH website, not those mentioned in Newman and Ross (1971) and Jones (2000).

Species	Ships and/ or Cruises (Institutions)	Stations	Geographic coordinates	Depths (m)	Dates	Locations	Catalog numbers	References and/ or websites
T. southwardi	RV "Eltanin" (SOSC)	Sta. 6	52°10'S, 142°10'W	2304–2328	Mar 21, 1965	South Pacific Ocean	USNM 125305 (Holotype) USNM 125306 USNM 125307	Newman and Ross (1971), NMNH
T. southwardi	RV "Eltanin" (USARP)	Sta. 216	52°53'S, 75°36'W	1190–1263	Sep 16, 1962	Off southern Chile	USNM 125309	Newman and Ross (1971), NMNH
T. southwardi	RV "Eltanin" (USARP)	Sta. 376	54°03'S, 56°03'W	1720–1739	Dec 20–21, 1962	Off Malvinas/ Falkland Is.	USNM 125308	Newman and Ross (1971), NMNH
T. southwardi	RV "Eltanin" /Cruise 05	†	59°45'S, 68°50'W to 59°46'S, 68°50'W	1207–1591	Oct 10, 1962	Sars Bank in Drake Passage	-	Weisbord (1965, 1967)
T. southwardi	RV "Puerto Deseado" / Talud Continental I	Sta. 25	37°51.688'S, 54°10.550'W	1950	Aug 15, 2012	Mar del Plata Submarine Canyon	MACN-In 44478	Current study
T. southwardi	RV "Puerto Deseado" / Talud Continental III	Sta. 45	38°1.913'S, 53°39.268'W	2934	Sep 05, 2013	Mar del Plata Submarine Canyon	MACN-In 44479	Current study
T. cf. *southwardi*	RV "Atlantis II" (WHOI)	Dredge 06	41°14.9'S, 16°36.2'W	2175–2600	Jun 20, 1980	Mid-Atlantic Ridge, South Atlantic Ocean	BIC C8156	SIO-BIC
T. tasmanicum	RV "Rig Seismic" / Cruise 147	Sta. D12	45°09.0'S to 45°10.2'S, 145°25.1'E to 145°23.8'E	2100–3000	Feb 05, 1995	South Tasmania	-	Buckeridge (1999)
T. tasmanicum	RV "Rig Seismic" / Cruise 147	Sta. D25	49°04.3'S to 49°04.0'S, 146°16.0'E to 146°17.4'E	2420–3300	Feb 12, 1995	South Tasmania	CPC 34698-34702	Buckeridge (1999)
T. tasmanicum	RV "Rig Seismic" / Cruise 147	Sta. D41	44°14'S, 149°26'E	2850	Feb 18, 1995	South Tasmania	-	Buckeridge (1999)
T. tasmanicum	RV "Rig Seismic" / Cruise 147	Sta. D43	43°54.0'S, 151°19.2'E to 43°54.0'S, 151°17.8'E	2030–3600	Feb 19, 1995	South Tasmania	-	Buckeridge (1999)
T. tasmanicum	RV "Rig Seismic" / Cruise 147	Sta. D44	44°36.3'S to 44°36.0'S, 147°14.7'E to 147°14.8'E	2250–2400	Feb 22, 1995	South Tasmania	-	Buckeridge (1999)
T. tasmanicum	RV "Rig Seismic" / Cruise 147	Sta. D45	44°39.2'S to 44°39.5'S, 147°26.4'E to 147°26.5'E	2600–2800	Feb 22, 1995	South Tasmania	-	Buckeridge (1999)
T. tasmanicum	RV "Rig Seismic" / Cruise 147	Sta. D53	45°21.8'S to 45°21.1'S, 146°43.2'E to 146°43.7'E	2770–3000	Feb 25, 1995	South Tasmania	–	Buckeridge (1999)
T. tasmanicum	RV "Rig Seismic" / Cruise 147	Sta. D57	44°31.7'S to 44°32.8'S, 146°00.4'E to 146°00.6'E	2300–2850	Feb 26, 1995	South Tasmania	CPC 34697 (Holotype)	Buckeridge (1999)
T. tasmanicum	RV "Thomas G. Thompson" / Cruise TT200801	Sta. J2-390-008-002	43°48'25.2"S, 150°20'24.0"E	2082	Jan 05, 2009	South Tasmania	MIIC 02727	CSIRO-MIIC
T. tasmanicum	RV "Thomas G. Thompson" / Cruise TT200801	Sta. J2-392-012-001	45°18'01.4"S, 146°07'15.6"E	2213	Jan 11, 2009	South Tasmania	MIIC 02729	CSIRO-MIIC
T. tasmanicum	RV "Thomas G. Thompson" / Cruise TT200801	Sta. J2-390-015	43°49'42.2"S, 150°30'00.0"E	1061	Jan 08, 2009	South Tasmania	NMV J68079	GBIF
T. tasmanicum	RV "Thomas G. Thompson" / Cruise TT200801	Sta. J2-391-011	45°22'27.2"S, 144°35'34.8"E	3271	Jan 08, 2009	South Tasmania	NMV J68084	GBIF
Tetrachaelasma sp.	RV "Argo" / CIRCE Expedition	Sta. DR124	26°29'S, 46°07'E	1783–1838	Sep 29, 1968	South Madagascar	BIC C8158	Newman and Ross (1976), SIO-BIC

† Weisbord (1965, 1967) did not report the station number. Newman and Ross (1971) ambiguously mentioned "Sta. 225" and "Sta. 255", for the material taken in the Sars Bank.

All the specimens were fixed on board in 10% seawater formalin (buffered with sodium borate) and later transferred to 96% ethanol in the laboratory.

Laboratory work

The shell and opercular plates were disassembled from most of the specimens. When necessary, terga and scuta were cleaned by soaking in dilute bleach (sodium hypochlorite). Parietes, opercular plates, and rostral-carina diameters were measured to the nearest 0.01 mm using a digital calliper.

Some specimens were dissected under a stereomicroscope (Leica MZ8), and appendages were temporarily mounted on slides in glycerin medium. Drawings of the appendages were prepared using a Carl Zeiss (Axioskop) compound microscope equipped with a camera lucida. Line drawings were rendered in digital format using a Wacom tablet and the Adobe Illustrator program after Coleman (2003). All dissected appendages were finally dismounted from the temporary slides and stored in 96%

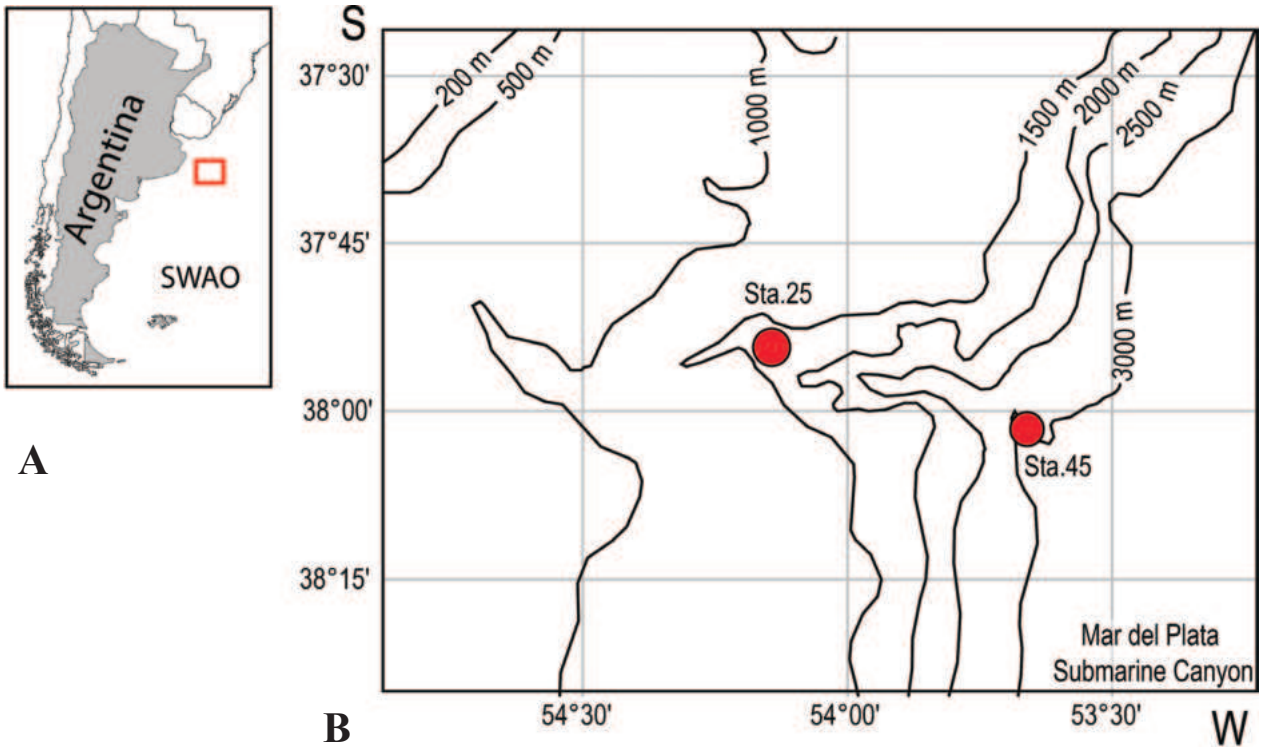

Figure 1. A. Study area location (inset); **B.** Map including the two stations sampled at the Mar del Plata Submarine Canyon. The seabed topography of the study area is represented by roughly calculated isobaths. Abbreviation: **SWAO** — South-West Atlantic Ocean.

ethanol, along with other soft body remains, the wall, and opercular plates.

Light photographs were taken with a Nikon D7500 digital camera equipped with a Sigma 105 mm f2.8 EX macro lens and the Zerene stacking software v.1.04 (Zerene Systems LLC 2023).

For SEM images, the labrum of two specimens was cleaned with 0.5% Triton X-100 nonionic detergent and ultrasonicated. Afterwards, the specimens were dehydrated through a graded ethanol series and later transferred to increasing concentrations of hexamethyldisilazane (HMDS). Specimens in HMDS 100% were allowed to air dry and then mounted on aluminum stubs and coated with gold-palladium. Finally, the material was examined using a Zeiss Gemini SEM 360 microscope.

High-resolution images of the parietes, terga, and scuta of the holotype of *Tetrachaelasma southwardi* Newman & Ross, 1971, deposited in the National Museum of Natural History (USNM 125305), were used for comparison purposes.

Table 1 includes records from regular scientific publications as well as records taken from web databases where the name of a trained taxonomist in Cirripedia is responsible for the identification.

The two stations at the Mar del Plata Submarine Canyon (Fig. 1) and all the records of the *Tetrachaelasma* species around the world (Fig. 9) were charted using the PanMap software v.0.9.6 (Diepenbroek et al. 2002).

All specimens studied were deposited in the Invertebrate Collection of the Museo Argentino de Ciencias Naturales "Bernardino Rivadavia" (MACN-In).

Abbreviations and terminology

The following abbreviations are used in the text: R for rostrum, C for carina, CL for carinolateral, S for scutum, and T for tergum.

Antenniform cirral articles are defined as those articles with only one whorl of distal setae; however, if the antenniform cirral article also has lateral filter setae, then the latter are equal to or shorter than the whorl of distal setae.

The following terminology is used to describe the scuto-tergal articulation:

- Scutal articular ridge (***sar***): prominent outgrowth extending along a-a' that fits into the tergal articular furrow (Fig. 2A, B).
- Upper articular furrow (***uaf***): scutal distal groove that receives the tergal articular ridge (Fig. 2C).
- Lower articular furrow (***laf***): scutal proximal groove that receives the vertical articular ridge of the tergum (Fig. 2C).
- Tergal articular ridge (***tar***): prominent distal outgrowth that fits into the upper articular furrow of the scutum (Fig. 2E).
- Vertical articular ridge (***var***): slanted outgrowth of the tergum extending along b-b'. Its wider basal part fits into the lower articular furrow of the scutum (Fig. 2D, E).
- Tergal articular furrow (***taf***): broad and deep groove extending along c-c' that receives the scutum articular ridge (Fig. 2D, E, F).

Results

Superfamily Coronuloidea Leach, 1817
Family Bathylasmatidae Newman & Ross, 1971
Subfamily Bathylasmatinae Newman & Ross, 1976

Genus *Tetrachaelasma* Newman & Ross, 1971

Diagnosis. Shell conical or columnar, with 4 thick, solid, calcareous wall plates, including compound rostral plate, paired CL, and C (R-CL-C). Parietes covered with numerous fine bristles along horizontal growth lines; chitinous laminae absent. External alar growth lines diverge from the inferior alar margin; superior alar margin with narrow, coarse welting. Carina supports large alae that internally contribute to nearly half the total sheath circumference. Radii absent. Basis membranous. Scutum articular ridge distinctly projected beyond the articular margin. Tergum slightly thinner than scutum; articular margin sinusoidal in internal view but smoothly concave in external view; with few depressor muscle crests, weak to well developed, extending at the most ⅓ along basal margin. Rami of cirri II and III antenniform; intermediate articles of cirrus VI bearing 3 or 4 pairs of major setae. Mandible quadridentoid. Caudal appendages absent. Deep-sea species, Southern Ocean.

Type species. *Tetrachaelasma southwardi* Newman & Ross, 1971.

Current species composition. *T. southwardi* Newman & Ross, 1971 and *T. tasmanicum* Buckeridge, 1999.

Remarks. Newman and Ross (1971) established the genus *Tetrachaelasma* (a name that refers to the wall of four plates) to include *T. southwardi*. In addition, they discussed the affinities with *Bathylasma* and presented a key to separate the five genera of the family Bathylasmatidae. Newman and Ross (1976) placed this genus in the subfamily Bathylasmatinae. Buckeridge (1999) gave a brief diagnosis of this genus and described its second species, *T. tasmanicum*. Jones (2000) re-examined the holotype of *T. southwardi* and provided a more complete diagnosis of the genus. However, this author failed to include *T. tasmanicum*, a species that had been published the previous year. More recently, Araya and Newman (2018) presented an updated key to separate the extant genera currently in the family.

Tetrachaelasma southwardi Newman & Ross, 1971

Figs 2–9, 11

Hexelasma antarcticum Borradaile, 1916. —Weisbord 1965: 1015–1016 (Sars Bank material); 1967: 51–56, pl. I, figs 7–8, pl. II, figs 7–8 (Sars Bank material).

Tetrachaelasma southwardi Newman & Ross, 1971: 152–155, fig. 74, pls. XXVI–XXXI (description). —Buckeridge 1999: 521, 522, 526 (comparison with *T. tasmanicum*). —Jones 2000: 150, 237–239 (remarks on the holotype, tables 24, 25, fig. 50 (distribution map)).

Material examined. ***Talud Continental I*** expedition, RV "Puerto Deseado", Mar del Plata Submarine Canyon, Sta. 25, 37°51.688'S, 54°10.550'W, 1950 m depth, 15 Aug 2012, epibenthic sledge, coll. I. Chiesa; 21 complete or damaged specimens (all with soft body parts intact) and 1 batch of disarticulated plates, namely: 1 damaged specimen (R missing) [wall and opercular plates disarticulated, mouthparts dissected, T and S photos] (MACN-In 44478a); 1 complete specimen [wall and opercular plates disarticulated, mouthparts dissected, T and S photos, labrum SEM] (MACN-In 44478b); 1 complete specimen [not dissected] (MACN-In 44478c); 1 complete specimen [not dissected] (MACN-In 44478d); 1 complete specimen [not dissected, photos of the habitus] (MACN-In 44478e); 1 complete specimen [wall and opercular plates disarticulated; mouthparts dissected; R, C, T, and S photos; cirral counts] (MACN-In 44478f); 1 complete specimen [not dissected, photos of the habitus] (MACN-In 44478g); 4 complete specimens, attached one over the other [not dissected, photos of the habitus] (MACN-In 44478h-k); 1 complete specimen [wall and opercular plates disarticulated; mouthparts and cirri drawn; R, C, T, and S photos; cirral counts] (MACN-In 44478l); 1 damaged specimen (R and both CL missing) [wall and opercular plates disarticulated, mouthparts dissected] (MACN-In 44478m); 1 complete specimen [not dissected] (MACN-In 44478n); 1 damaged specimen, with a large number of developing eggs in the mantle cavity (R and left CL missing) [wall and opercular plates disarticulated, mouthparts dissected] (MACN-In 44478o); 1 complete specimen [wall and opercular plates disarticulated, mouthparts dissected, photo serpulid epibiont] (MACN-In 44478p); 1 complete specimen [not dissected] (MACN-In 44478q); 1 damaged specimen (R missing) [wall plates disarticulated] (MACN-In 44478r); 1 damaged specimen (R missing) [not dissected] (MACN-In 44478s); 1 complete specimen [not dissected] (MACN-In 44478t); 1 complete specimen [not dissected, photo soft octocoral *Alcyonium* sp. epibiont] (MACN-In 44478u); batch of plates: 4 R, 3 C, 3 CL (MACN-In 44478v).

Talud Continental III expedition, RV "Puerto Deseado", Mar del Plata Submarine Canyon, Sta. 45, 38°1.913'S, 53°39.268'W, 2934 m depth, 05 Sep 2013, bottom otter trawl, colls. I. Chiesa and A. Martinez; 8 complete or damaged specimens (all with soft body parts intact) and 1 batch of disarticulated plates, namely: 1 complete specimen [wall plates articulated, opercular plates disarticulated; mouthparts dissected; habitus, T and S photos] (MACN-In 44479a); 1 complete specimen [wall and opercular plates disarticulated] (MACN-In 44479b); 1 complete specimen [not dissected, photos of the habitus] (MACN-In 44479c); 1 damaged specimen (R and left CL missing) [wall and opercular plates disarticulated, mouthparts dissected, T and S photos, cirral counts] (MACN-In 44479d); 1 damaged specimen (R and right CL missing) [wall and opercular plates disarticulated] (MACN-In 44479e); 1 damaged specimen (R and both CL missing) [wall and opercular plates disarticulated, mouthparts dissected] (MACN-In 44479f); 1 damaged specimen (R and 1 CL missing) [wall and opercular plates disarticulated,

mouthparts dissected] (MACN-In 44479g); 1 damaged specimen (R and both CL missing) [wall and opercular plates disarticulated, mouthparts dissected, T and S photos, labrum SEM, cirral counts] (MACN-In 44479h); batch of plates: 3 R (one of them with a *Regioscalpellum* epibiont, photo), 3 C, 4 CL (MACN-In 44479i).

Supplementary description. Newman and Ross (1971) gave a detailed description of *T. southwardi*. Jones (2000) re-examined the holotype and summarized the main features of the species in tables 24–25. All the information presented in these tables had already been mentioned by Newman and Ross (1971). Therefore, we only consider the original description of Newman and Ross (1971) for comparison purposes.

Size (rostro-carinal diameter): 13.0–47.1 mm (n = 13).

Shell conical in young specimens and conical or columnar in older (larger) specimens (Fig. 3).

Shell wall covered with yellow cuticle and numerous fine bristles. Growth lines all along the plates are equidistant from each other (Fig. 3A–E). However, basally growth lines are narrowly spaced in a columnar specimen (Fig. 3G) as well as in some isolated plates (Fig. 11E), all of them collected at 2934 m depth. Bristles are as long as, or longer than, the distance between growth lines.

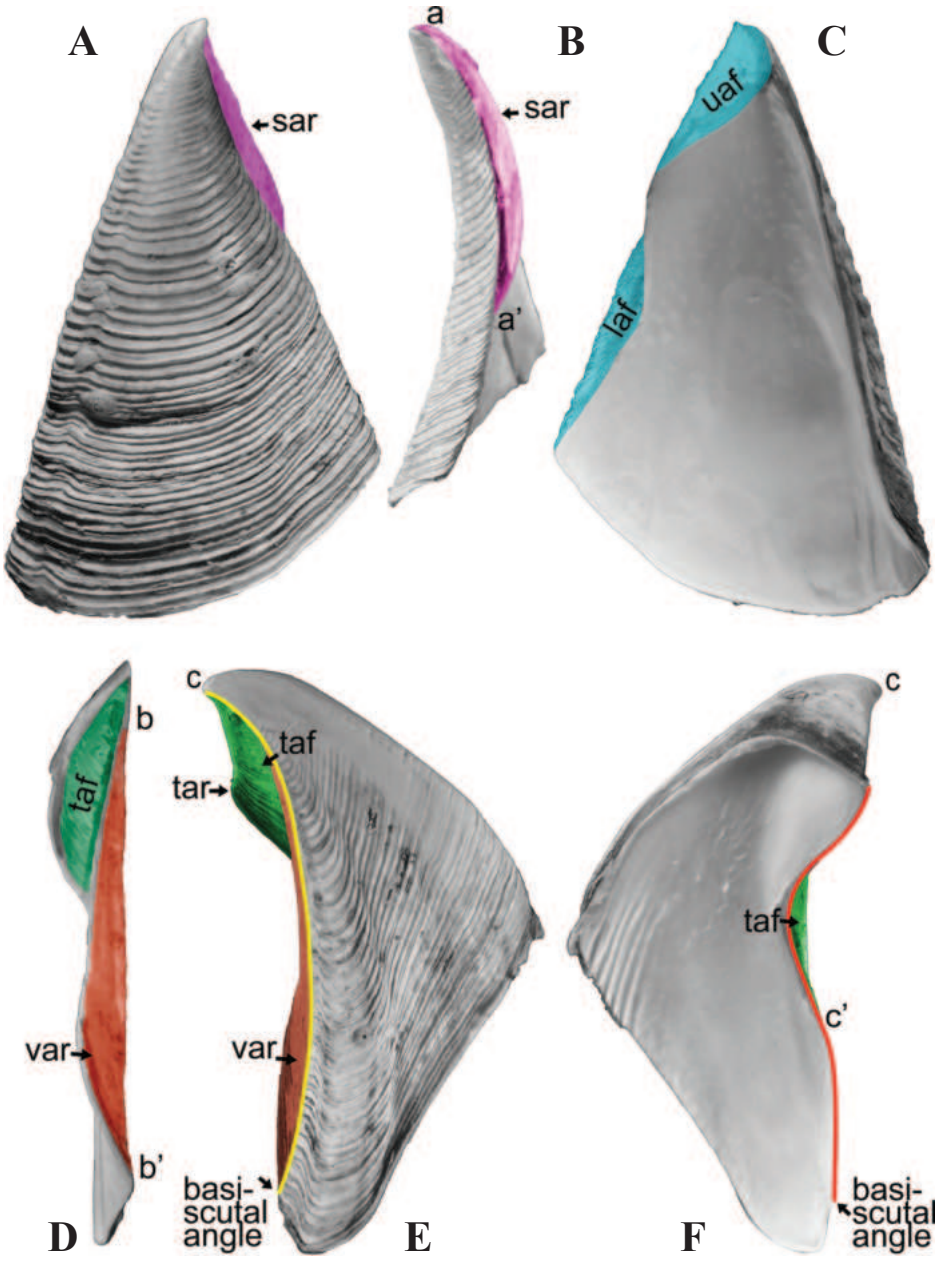

Figure 2. *Tetrachaelasma southwardi* Newman & Ross, 1971. Nomenclature used for the scuto-tergal articulation (the specimen shown in Fig. 4J–L is taken as a model). Scutum: **A.** Exterior view; **B.** Lateral view; **C.** Interior view. Tergum: **D.** Lateral view; **E.** Exterior view, smoothly concave articular margin painted in yellow; **F.** Internal view, sinusoidal articular margin painted in red. Abbreviations: **a-a'** – distal and basal ends of the scutum articular ridge; **b-b'** – distal and basal ends of the vertical articular ridge; **c-c'** – distal and basal ends of the tergal articular furrow; ***laf*** – lower articular furrow; ***sar*** – scutum articular ridge; ***taf*** – tergal articular furrow; ***tar*** – tergal articular ridge; ***uaf*** – upper articular furrow; ***var*** – vertical articular ridge.

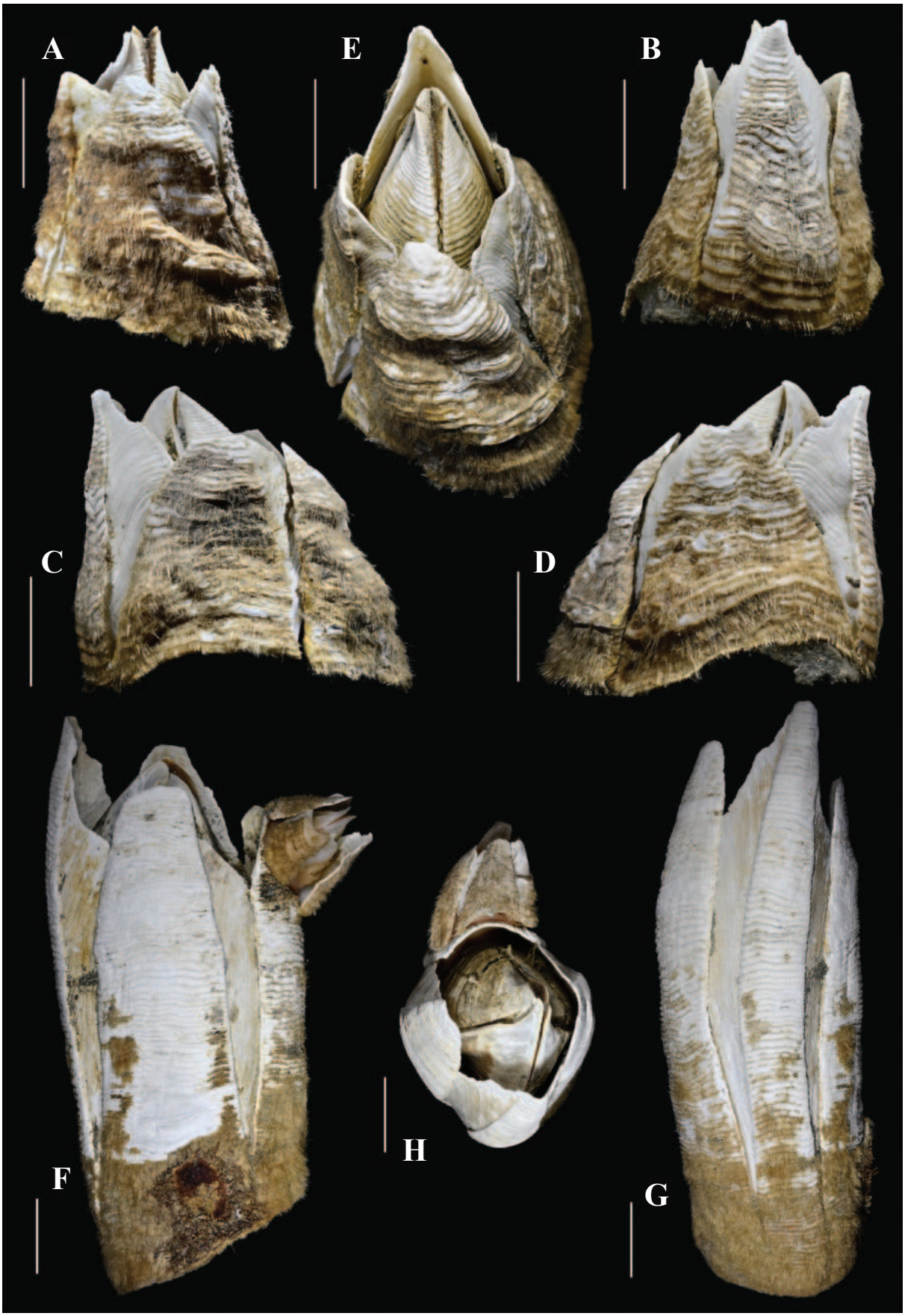

Figure 3. *Tetrachaelasma southwardi* Newman & Ross, 1971. Specimen (MACN-In 44478g): **A.** Rostral view; **B.** Carinal view; **C, D.** Left and right carinolateral views, respectively; **E.** Top view. Specimen (MACN-In 44479a, columnar) with a small specimen (MACN-In 44479b) attached to its rostrum: **F.** Left carinolateral view; **G.** Carinal view; **H.** Top view. Scale bars: 10 mm.

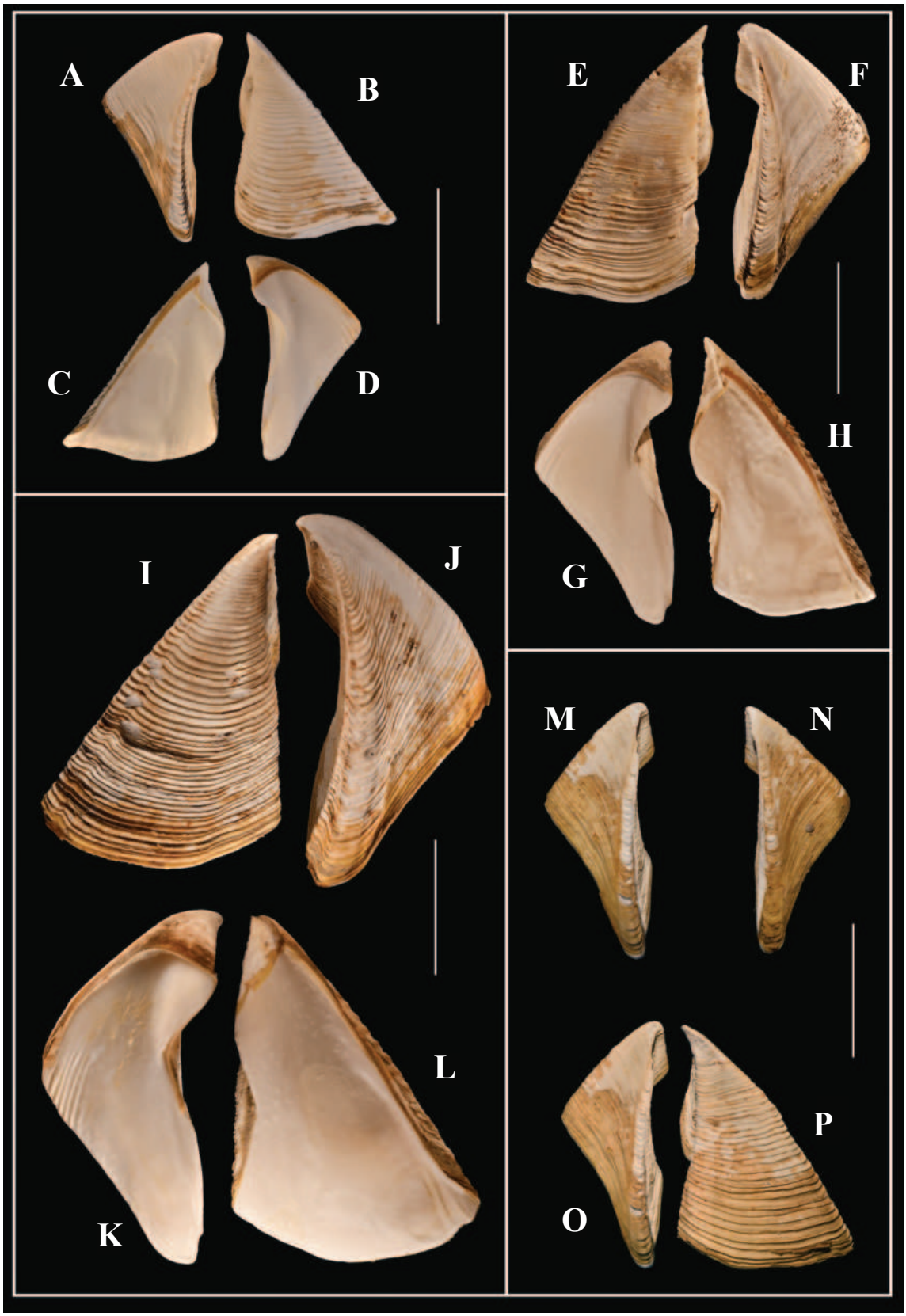

Figure 4. *Tetrachaelasma southwardi* Newman & Ross, 1971. Intraspecific variation of opercular plates among the material collected at 1950 m depth. Specimen (MACN-In 44478f): **A, D.** Left tergum in external and internal views, respectively; **B, C.** Left scutum in external and internal views, respectively. Specimen (MACN-In 44478a): **E, H.** Right scutum in external and internal views, respectively; **F, G.** Right tergum in external and internal views, respectively. Specimen (MACN-In 44478b): **I, L.** Right scutum in external and internal views, respectively; **J, K.** Right tergum in external and internal views, respectively. Specimen (MACN-In 44478l): **M, N.** Left and right terga in external view; **O, P.** Left tergum and scutum in external view. Scale bars: 10 mm.

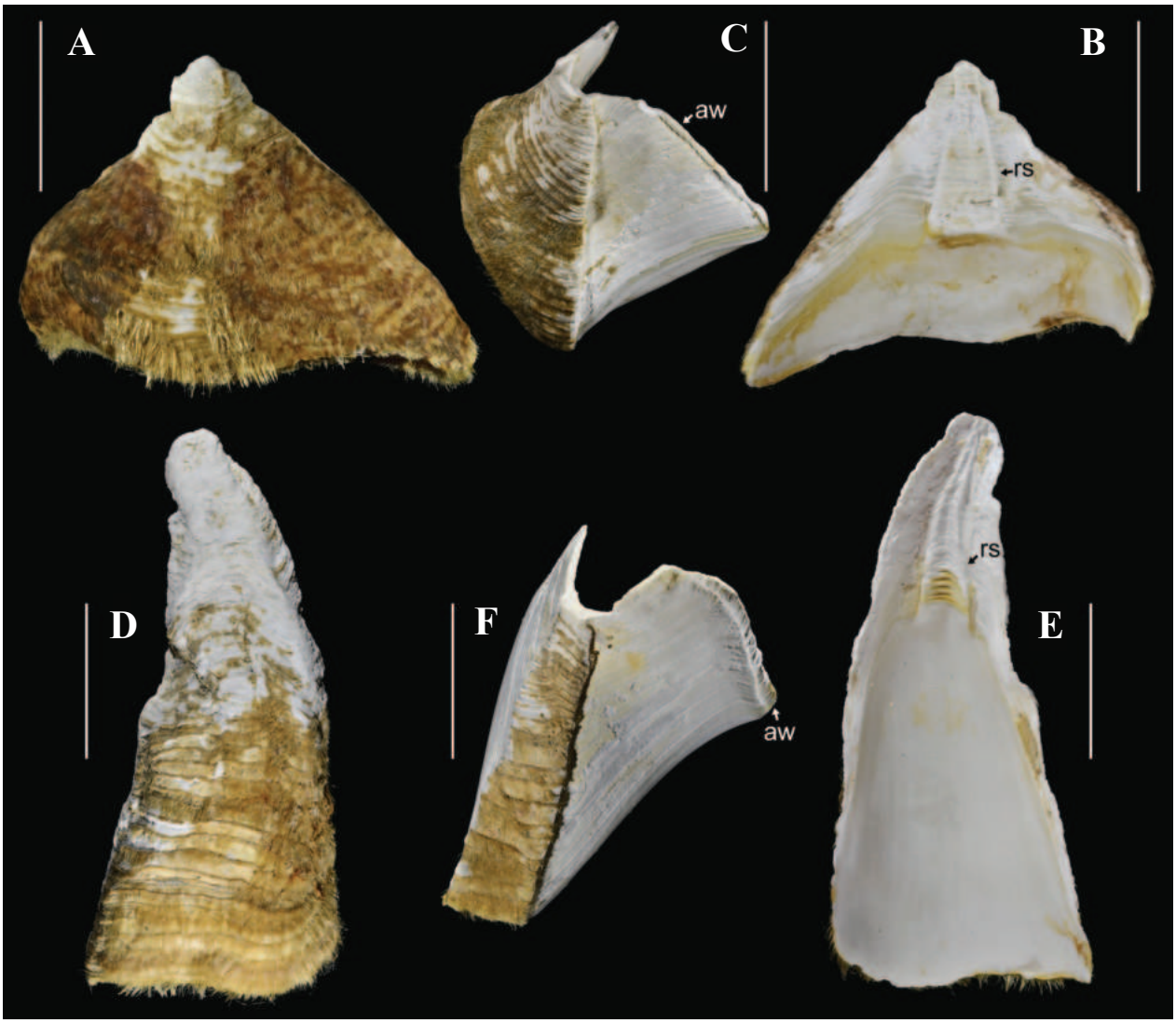

Figure 5. *Tetrachaelasma southwardi* Newman & Ross, 1971. Specimen (MACN-In 44478f): **A, B.** Rostrum in external and internal views, respectively; **C.** Carina in lateral view. Specimen (MACN-In 44478l): **D, E.** Rostrum in external and internal views, respectively; **F.** Carina in lateral view. Abbreviations: **aw** – alar welting; **rs** – rostral sheath. Scale bars: 10 mm.

Rostrum (Figs 3, 5A, B, D, E), 1.4–2.7 times (n = 13) wider than carina, only slightly bowed transversely, shape variable. In eight of the 13 specimens measured, the rostrum is the widest plate. In contrast, in five specimens, one of the CL plates (exceptionally both) is slightly wider than the rostrum. The sheath is flanked by very broad articular areas receiving alae of CL plates and occupies 1/2 to 1/3 of the height of the rostrum in nine out of the 11 specimens dissected (Fig. 5E); in the remaining two specimens, it occupies almost 2/3 of the height of the plate (Fig. 5B).

Carinolaterals (Fig. 3C, E, F), as mentioned by Newman and Ross (1971).

Carina (Figs 3, 5C, F) is the highest and narrowest of the wall plates. Shape variable. As mentioned by Newman and Ross (1971), it supports large alae that internally contribute to nearly half the total circumference of the sheath. Externally, alar growth lines similar to those of CL plates.

Scutum (Figs 4, 6), as mentioned by Newman and Ross (1971), except for the articular ridge (***sar***), which varies from prominent to moderately projected beyond the articular margin (compare Fig. 4B, C, E, H, with Fig. 4I, L). Note: The exposure of the ***sar*** depends on the shape (straight or twisted) of the scutum and on the angle of inclination at which the scutum is positioned. Adductor muscle pit shallow; boundaries weakly defined, i.e., not limited above and laterally by a distinct line (Figs 4C, H, L, 6D, I, M). External surface worn smooth at the apex in large specimens (Figs 4E, 6H, L). Some external growth lines may be slightly inflected close to the occludent margin, occasionally forming a weak apico-basal ridge (see Fig. 6E). Note: This apico-basal ridge is also present in *T. tasmanicum* (see Buckeridge 1999).

Tergum (Figs 4, 6) fully agrees with Newman and Ross's 1971 description, except for: the separation of the tergal spur from the articular margin, measured at base, varies from almost imperceptible to as much as 0.48 of

Figure 6. *Tetrachaelasma southwardi* Newman & Ross, 1971. Intraspecific variation of opercular plates among the material collected at 2934 m depth. Specimen (MACN-In 44479h): **A, D.** Right scutum in external and internal views, respectively; **B, C.** Right tergum in external and internal views, respectively; **E.** Left scutum in external view, slightly slanted to make the apico-basal ridge more visible; **F.** Joined right tergum and scutum in internal view. Specimen (MACN-In 44479d): **G, J.** Left tergum in external and internal views, respectively; **H, I.** Left scutum in external and internal views, respectively. Specimen (MACN-In 44479a): **K, N.** Left tergum in external and internal views, respectively; **L, M.** Left scutum in external and internal views, respectively. Abbreviations: **abr** – apico-basal ridge; **in** – indentation (worn) on articular margin. Scale bars: 10 mm.

spur width (n = 12; compare Fig. 4A, F, J with Fig. 6G, K). Internal surface with 2–7 depressor muscle crests, weak to well developed, extending at the most ⅓ along the basal margin (n = 13; compare Fig. 4G with Fig. 4K).

The following information not reported by Newman and Ross (1971) is added: in six of the specimens obtained at 1950 m depth, the basal margin of the tergum is 1.2 times the length of the occludent margin (Fig. 4A, D, F, G) [exception: basal and occludent margins are equal in length in the largest specimen dissected, Fig. 4J, K]. In contrast, in six of the specimens obtained at 2934 m depth, the basal margin is equal to or slightly shorter

than the occludent margin (Fig. 6B, C, F, G, J, K, N) [exception: basal margin longer than the occludent margin in two very small specimens]. The apex of the tergum is worn smooth only in the largest specimens (Figs 4F, J, 6G, K). In a few specimens, the articular margin of both terga is eroded near distal end, resulting in two rounded indentations (Fig. 6K).

In addition, Newman and Ross (1971) stated, "Terga… with articular margin thrown into sinusoidal curve;" This character is herein described in more detail: Sinusoidal articular margin only fully visible in the internal view of tergum (Fig. 2F, red line); the amplitude of the sinusoidal curve increases as the basal part of the ***var*** develops (compare Fig. 4A, D with Fig. 4F, G). On the other hand, the articular margin is smoothly concave in the external view of tergum, running parallel to the outer edge of the external furrow (Fig. 2E, yellow line; see also Figs 4A, F, J, 6G). In some specimens, the basal part of the ***var*** is more developed in one tergum than in the opposite one (see Fig. 4M, N).

The crest of the labrum (Fig. 7) is slightly concave, with many small serrate setae and a few small teeth just below it; in contrast, Newman and Ross (1971) reported that the crest is smooth. Interior surface of the labrum with a dense bundle of downwardly pointed setae on either side. Palps as described by Newman and Ross (1971).

Mandibles (Fig. 8A, B) agree with the description presented by Newman and Ross (1971) and the photograph of the holotype USNM 125305 (left mandible?) available on the website of the National Museum of Natural History, Smithsonian Institution (link to the NMNH website in the References section).

First maxillae slightly differ from Newman and Ross's (1971) description, i.e., lower lobe rounded (Fig. 8D) or somewhat straighter (Fig. 8C). Lower cutting margin with about 18–22 strong setae and 5–17 short—some of them pectinate—setae, just above the inferior angle (n = 3).

Second maxillae (Fig. 8E) slightly bilobed (not bilobed after Newman and Ross (1971)).

Cirri (Fig. 8F–I), as mentioned by Newman and Ross (1971). The cirral formula is provided in Table 2. Cirrus II: rami subequal in length, anterior ramus with the largest numbers (up to 8) of antenniform articles. Cirrus III: posterior ramus slightly longer than anterior one, carrying the largest number (up to 30) of antenniform articles.

Penis (Fig. 8J), as mentioned by Newman and Ross (1971). A more detailed description is provided: 3 or 4 times longer than the pedicel of cirrus VI, finely annulated along all its length (annuli more evident on proximal two thirds); distal third with small setae lateral and distally. Basidorsal point absent.

Caudal appendages absent.

Settlement and epibionts. Of the 21 specimens of *Tetrachaelasma southwardi* collected at Sta. 25 (1950 m depth), 16 were complete. Most of these specimens were detached from the substrate (Fig. 11C) or attached to single rocks (Fig. 11A). One complete specimen was attached to an isolated CL plate, which has its external surface covered with yellow cuticle and numerous fine bristles and, therefore, most likely belongs to a living specimen of *T. southwardi* that was disarticulated during dredging. In addition, four complete specimens had settled one over the other (Fig. 11D).

Table 2. *Tetrachaelasma southwardi* Newman & Ross, 1971. Cirral formula of four specimens (two collected at 1950 m depth, two at 2934 m depth) from the Mar del Plata Submarine Canyon. Articles not fully separated (partially fused) were counted as single ones. The numbers of antenniform articles of the cirri II and III are given in parentheses. The cirri I-IV of the specimen (MACN-In 44781) are illustrated in Fig. 8.

Specimen (Depth)	Cirral ramus	I	II	III	IV	V	VI
MACN-In 44478l (1950 m)	Left anterior	17	22 (4)	25 (4)	30	32	38
	Left posterior	16	24 (4)	42 (30)	33	36	40
	Right anterior	15	22 (4)	22 (3)	33	36	38
	Right posterior	15	25 (4)	36 (25)	31	36	36
MACN-In 44478f (1950 m)	Left anterior	15	20 (5)	25 (3)	27	30	32
	Left posterior	14	22 (2)	30 (9)	29	30	25
	Right anterior	16	23 (8)	24 (3)	27	29	31
	Right posterior	14	22 (4)	28 (11)	27	32	25
MACN-In 44479d (2934 m)	Left anterior	16	24 (5)	30 (7)	33	34	41
	Left posterior	14	24 (3)	40 (3)	33	39	42
	Right anterior	13	23 (7)	32 (5)	33	39	33
	Right posterior	15	25 (6)	39 (26)	35	38	37
MACN-In 44479h (2934 m)	Left anterior	12	20 (2)	31 (9)	29	33	34
	Left posterior	12	19 (2)	46 (39)	30	32	34
	Right anterior	13	23 (3)	28 (8)	29	34	34
	Right posterior	13	24 (3)	24†	30	33	34

† Broken (terminal articles missing).

Of the eight *T. southwardi* obtained at Sta. 45 (2934 m depth), three were complete. Of these, one small specimen is attached to the R plate of a second one (Fig. 3F, H). The third specimen has a rounded mark on its R and right CL plates, evidence that another specimen had been living on them (Fig. 11F).

Several associations were observed among the materials studied. Two specimens of *T. southwardi* from Sta. 25 (1950 m depth) carried epibionts: one has a soft octocoral *Alcyonium* sp. on its R and left CL plates (Fig. 11C), and the other has tubes of serpulid polychaete worms on its scuta (Fig. 11B). Station 45 (2934 m depth) includes a pilose scalpellid barnacle attached to an isolated R plate (Fig. 11E). As this plate was covered with cuticles and numerous fine bristles, it likely belongs to a living specimen (of *T. southwardi*?) that was disarticulated during dredging. This scalpellid fits well with the diagnosis of the genus *Regioscalpellum* proposed by Gale (2016); however, this author pointed out that the classification of the Scalpellidae is clearly provisional. In addition, one specimen of *T. southwardi*, also from Sta. 25, is attached to a specimen of the genus *Bathylasma* (additional information in the *Bathylasma* sp. section).

Distribution. *Tetrachaelasma southwardi* was previously recorded in the Southern Ocean—from both the

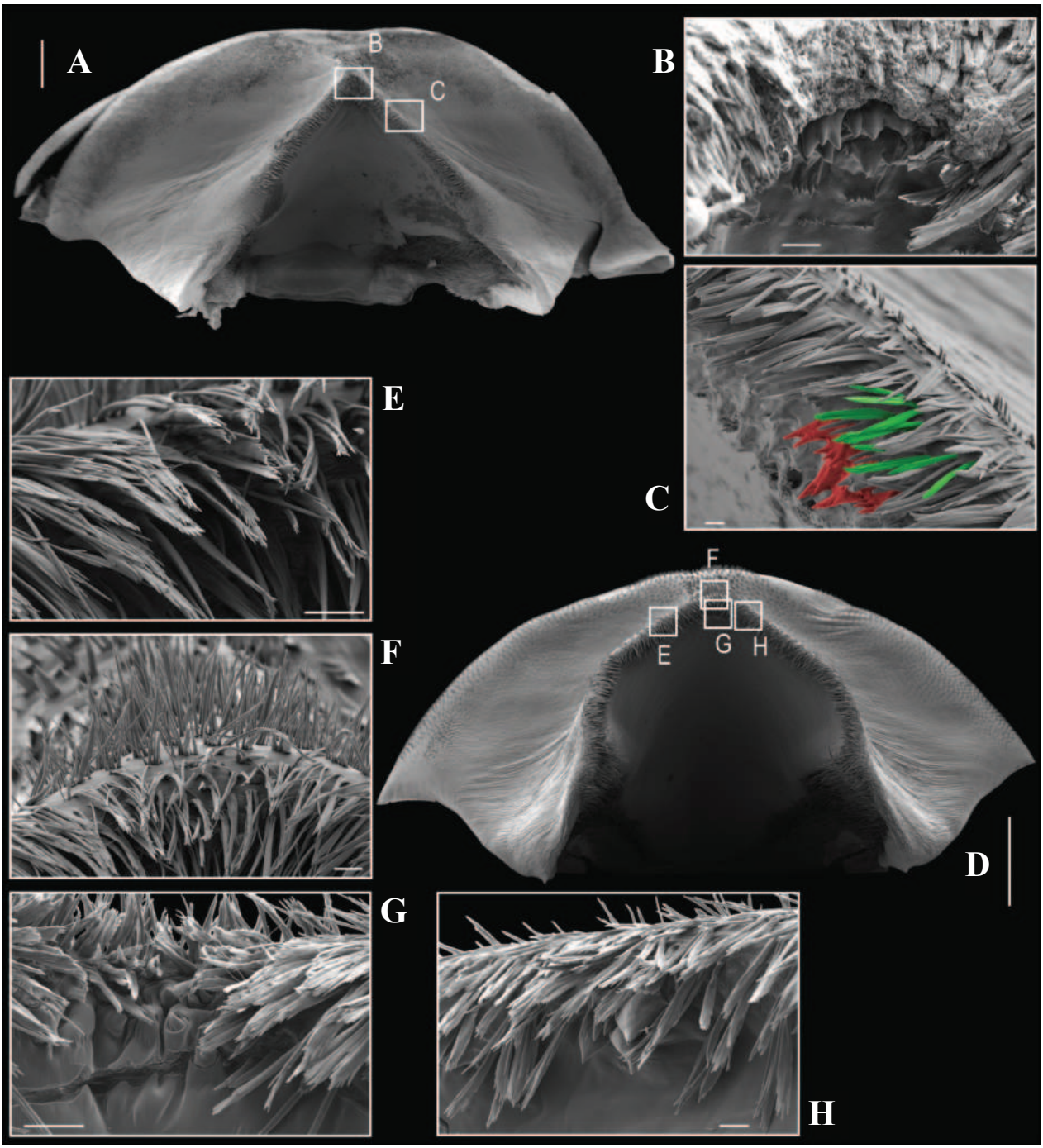

Figure 7. *Tetrachaelasma southwardi* Newman & Ross, 1971. Labrum SEM photographs (palps removed). Specimen (MACN-In 44478b): **A.** General aspect from above; **B, C.** Details of the crest; serrate setae in green, teeth in red. Specimen (MACN-In 44479h): **D.** General aspect from above; **E–H.** Details of the crest. Scale bars: 300 µm (**A, D**); 10 µm (**B, C, E–H**).

Pacific and the Atlantic—and is now reported from the Mar del Plata Submarine Canyon. Depths range: 1190–2934 m. All the records are listed in Table 1 and mapped in Fig. 9.

Remarks. The supplementary description presented above is based on 29 specimens and a few loose plates collected in the Mar del Plata Submarine Canyon at two localities with significantly different depths (1950 m and 2934 m, Fig. 1). All these specimens have been assigned to *Tetrachaelasma southwardi* Newman & Ross, 1971. However, it should be noted that these specimens differ from the original description of *T. southwardi* as follows (characters mentioned in the original description are included in parentheses): (1) the adductor muscle pit of the scutum, which is weakly developed (pit deep, bounded above and lateral by a distinct line); (2) the crest of the labrum with abundant setae (without setae); and (3) the second maxilla, which is slightly bilobed (not bilobed).

(1) In regard to the adductor muscle pit, we had the opportunity to examine images of the scutum of the

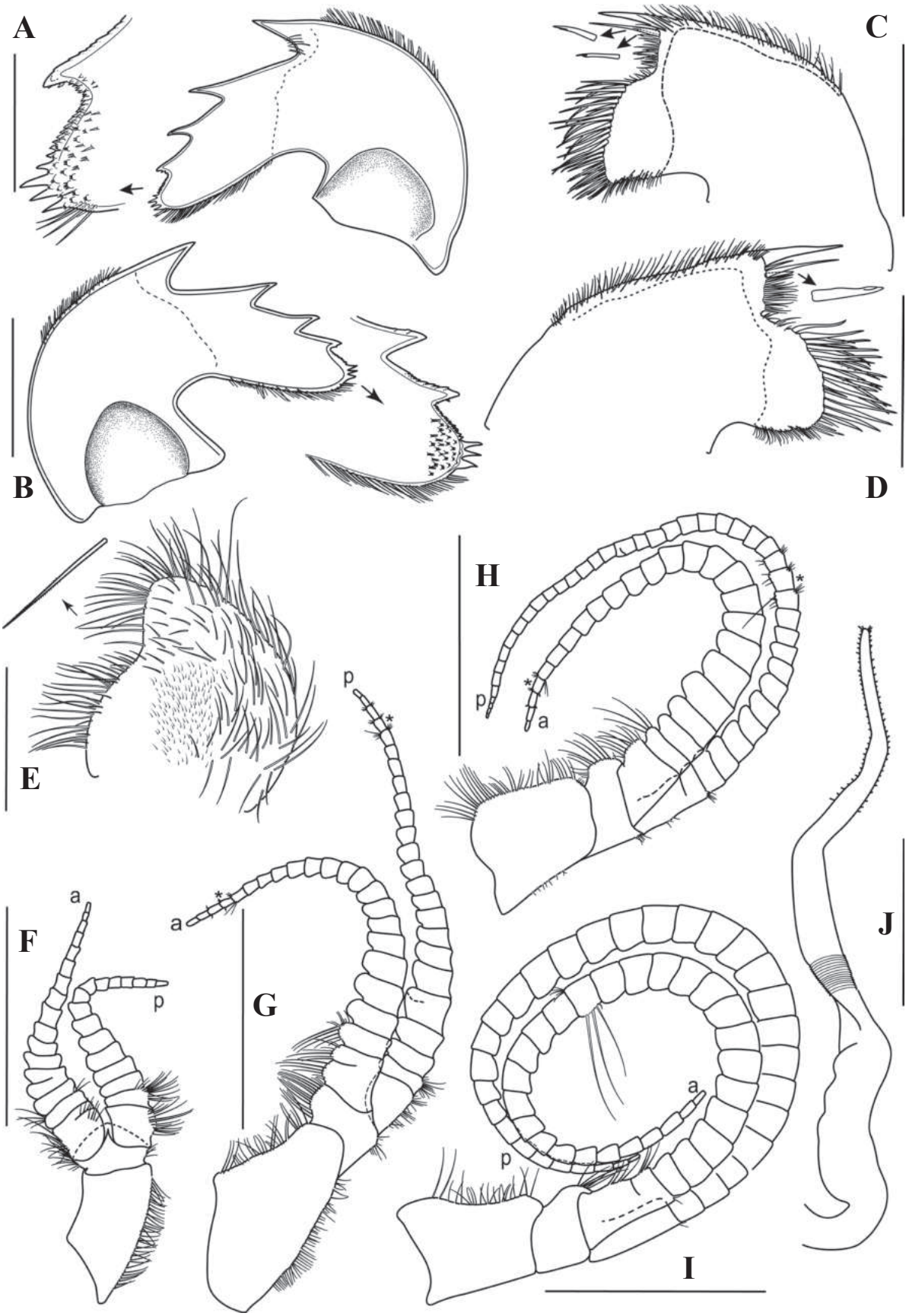

Figure 8. *Tetrachaelasma southwardi* Newman & Ross, 1971. Specimen (MACN-In 44478l): **A, B.** Left and right mandibles, respectively, inferior angles enlarged; **C, D.** Right and left first maxillae, respectively; **E.** Second maxilla, only some setae drawn, all of them serrulate (see detail); **F–I.** Left cirri I-IV, respectively; the first antenniform article is indicated with an asterisk; **J.** penis, only a short section of annuli is drawn. Abbreviations: **a** – anterior ramus; **p** – posterior ramus. Scale bars: 1 mm (**A–E**); 0.5 mm (**F–J**).

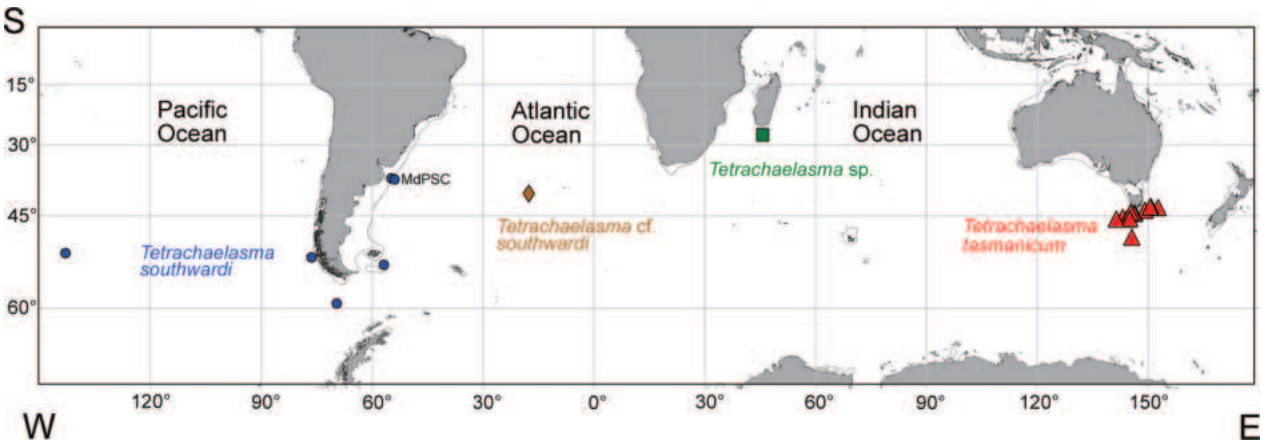

Figure 9. Distribution of the genus *Tetrachaelasma* Newman & Ross, 1971. *T. southwardi* Newman & Ross, 1971 (circles); *T.* cf. *southwardi* (diamond); *T. tasmanicum* Buckeridge, 1999 (triangles); *Tetrachaelasma* sp. (square). See Table 1 for additional information. Abbreviation: **MdPSC** – Mar del Plata Submarine Canyon.

holotype (see Material and Methods). In these images, the adductor muscle pit does not appear to be sharply delimited. However, this character is difficult to quantify and depends on the assessment of the individual taxonomist to some extent.

(2) The crest of the labrum of the material studied herein is covered with many short serrate setae but lacks teeth projecting beyond it. In contrast, Newman and Ross (1971) stated that the crest of the labrum of *T. southwardi* is smooth; however, these authors show in fig. 74G small setae on each side of the crest (see also the Discussion section).

(3) The second maxilla of the material studied herein is slightly bilobed. However, Newman and Ross (1971) wrote, "Second maxillae not bilobed, but setae divided in 2 groups by a median nearly naked area." As the concavity between the two lobes is very shallow in our material (Fig. 8E), this difference with the holotype is subtle.

In addition, the specimens from the Mar del Plata Submarine Canyon show some degree of intraspecific variation in the development of the scutum articular ridge (***sar***) and the tergum vertical articular ridge (***var***), the separation of the tergal spur from the basi-scutal angle, and the tergal basal/occludent proportions. Furthermore, the parietes also show great intraspecific variation, i.e., most of the specimens are roughly conical, but two are columnar (cylindrical). Only one of all these characters, the tergal basal/occludent proportion, seems to be associated with the station, i.e., the terga are usually more elongated in the specimens from 1950 m depth than in those from 2934 m depth. Intraspecific morphological variation has also been reported for other deep-sea barnacles (Chan et al. 2016; Lin et al. 2020). Molecular studies are needed to confirm whether the observed differences in the tergal basal/occludent proportions are phenotypic variations induced by environmental conditions or reflect genetic distance between the specimens from the two sampled stations. However, these studies will only be possible when additional specimens suitable for molecular techniques are available.

Genus *Bathylasma* Newman & Ross, 1971

Bathylasma Newman & Ross, 1971: 142, 143 (diagnosis, list of species, key). —Jones 2000: 231–233 (diagnosis, tables 20, 21, fig. 49 (distribution map)). —Araya and Newman 2018: 4, 5, 10, 11 (diagnosis, table 2, key).

Type species. *Balanus corolliformis* Hoek, 1883.

Bathylasma sp.

Figs 10, 11G

Material examined. ***Talud Continental I*** expedition, RV "Puerto Deseado", Mar del Plata Submarine Canyon, Sta. 25, 37°51.688'S, 54°10.550'W, 1950 m depth, 15 Aug 2012, epibenthic sledge, coll. I. Chiesa. 1 complete specimen assigned to the genus *Bathylasma* (MACN-In 44480), having a specimen of *T. southwardi* (MACN-In 44478l) attached to it.

Remarks. This specimen is assigned to the genus *Bathylasma* Newman & Ross, 1971, by having: six solid wall plates with prominent horizontal growth lines covered with fine bristles; articular margin of tergum straight (not sinusoidal as in *Tetrachaelasma*); and basis membranous. It has the wall plates severely eroded, but the hirsute cuticle remains partially visible on the left CL2.

This genus encompassed four extant and four fossil species (see Araya and Newman 2018). This new finding represents the first record of the genus *Bathylasma* from the South-West Atlantic. In addition, our specimen was collected at 1950 m, a depth comparable to the deepest record for the genus, i.e., 1800–2000 m reported for *Bathylasma chilense* Araya & Newman, 2018 in the South-East Pacific (Araya and Newman 2018).

The *Bathylasma* sp. reported herein has a specimen of *T. southwardi* settled on the C and left CL2 plates. In addition, there is a rounded mark on its R and right CL1 plates, evidence that a second specimen (*T. southwardi*?) had also been affixed to it (Fig. 11G). This is the first time

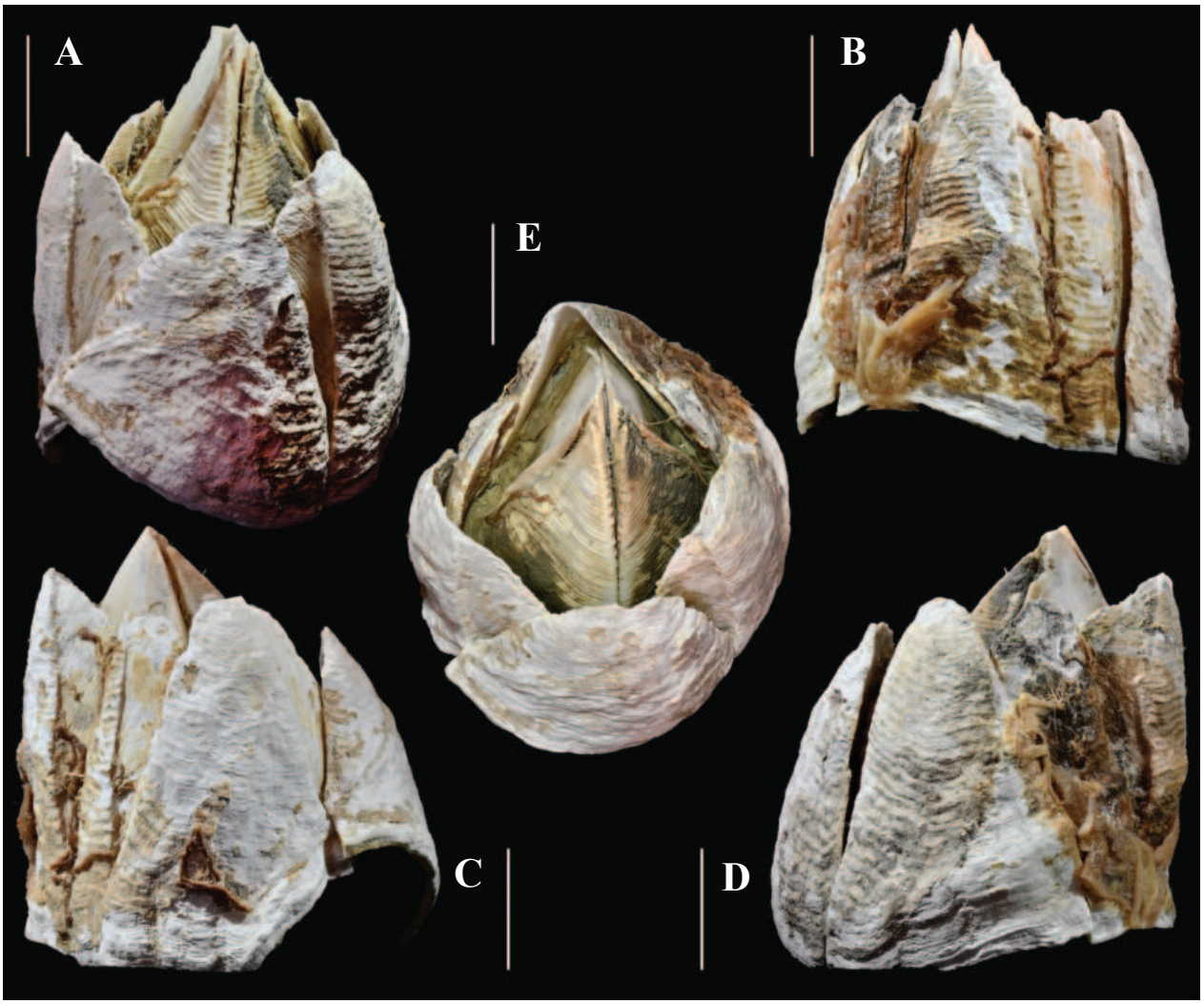

Figure 10. *Bathylasma* Newman & Ross, 1971. Specimen (MACN-In 44480): **A.** Rostral view; **B.** Carinal view; **C, D.** Left and right carinolateral views, respectively; **E.** Top view. Scale bars: 10 mm.

that members of these two genera have been reported living together.

The poor condition of this specimen of *Bathylasma* prevents its identification as a known species or a new species. In order to preserve the only specimen available, it is advisable not to dissect the soft parts of this specimen until additional material is obtained.

Discussion

Taxonomic status of *T. southwardi* and *T. tasmanicum*

Tetrachaelasma encompasses only two species: *T. southwardi* Newman & Ross, 1971, recorded from just a few, widely apart, stations in the Southern Ocean, and *T. tasmanicum* Buckeridge, 1999, restricted to South Tasmania (Table 1, Fig. 9).

Buckeridge (1999) stated that *T. southwardi* and *T. tasmanicum* are two closely related species, distinguished mainly by (1) the tergal articulation (sinusoidal vs. smoothly concave), (2) the ornamentation of the crest of the labrum (smooth vs. with teeth), and (3) the tergal spur (almost contiguous with articular margin vs. removed from articular margin as much as ⅓ its width).

(1) Newman and Ross (1971) stated that the articular margin of the tergum of *T. southwardi* is more or less sinusoidal, a character also used to define the genus. Conversely, Buckeridge (1999) stated that the tergum of *T. tasmanicum* has a smoothly concave articular margin (as opposed to sinusoidal).

The term "sinusoidal" was coined by Newman and Ross (1971) to describe the S-shaped aspect of the tergal articular margin. In our specimens, the sinusoidal margin is only fully visible in the internal view and results from the combination of the concave tergal articular ridge (***tar***) and the convex vertical articular ridge (***var***) (see Fig. 2F, red line). By contrast, in external view, the articular margin is smoothly concave and runs parallel to the outer edge of the external furrow (Fig. 2E, yellow line). Thus, the tergal articular margin is sinusoidal or smoothly concave, depending on the view (internal or external).

Figure 11. *Tetrachaelasma southwardi* Newman & Ross, 1971. **A.** Specimen (MACN-In 44478e) attached to a rock; **B.** Scuta of specimen (MACN-In 44478p) with serpulid tubes (Polychaeta); **C.** Specimen (MACN-In 44478u) with *Alcyonium* sp. (Octocorallia) epibiont; **D.** Group of four specimens (MACN-In 44478h–k); **E.** Isolated rostral plate (MACN-In 44479i) with a *Regioscalpellum* sp. (Scalpellidae) on it; **F.** Specimen (MACN-In 44479c) with a rounded mark left by another specimen attached to it. *Bathylasma* Newman & Ross, 1971. **G.** Specimen (MACN-In 44480) with a *T. southwardi* specimen attached to it and a rounded mark left by a second balanomorph barnacle. Abbreviation: **rm** – rounded mark.

Newman and Ross (1971: pl. XXVI) presented images of the tergum of the holotype of *T. southwardi*. In these images, the articular margin of the tergum looks sinusoidal in both external (fig. E) and internal (fig. G) views. However, in the holotype, the articular margin is eroded in the middle part, and the external furrow is eroded distally. This condition was confirmed after examining high-resolution images of the holotype, which is deposited in the NMNH, Smithsonian Institution (see Material and Methods). In conclusion, the S-shaped aspect of the articular margin of the tergum of the holotype, in external view, is due to it being worn in the middle part.

Based on this new information, it appears that the tergal articular margin of both *T. southwardi* (including the type material and our specimens) and *T. tasmanicum* do not differ from each other, i.e., the articular margin is sinusoidal in the internal view and smoothly concave in the external view for both species. Thus, the S-shaped tergal articular margin is an important character to define the genus, but it seems not to be a reliable character to separate its two current species.

(2) The labrum of the specimens herein examined has short serrate setae on the crest and small teeth contiguous to them on its inner surface, i.e., teeth are neither on the top of the crest nor projecting beyond the crest. Newman and Ross (1971) stated that the crest of the labrum of *T. southwardi* is smooth. Although neither setae nor teeth are shown in the central part of the crest by these authors in fig. 74H, setae are shown on the lateral part of the crest in fig. 74G. It remains to be confirmed whether the central setae are actually absent in the holotype of *T. southwardi*. One possibility is that the holotype´s setae were worn, detached, or covered with biofilm (see embedded top setae in Fig. 7B), thus preventing their observation under a light microscope. In contrast, Buckeridge (1999) stated that *T. tasmanicum* has small teeth on the crest of the labrum. However, fig. 4D presented by this author is not detailed enough, and there is a possibility that the teeth are actually setae. It is worth noting that high magnification is necessary to distinguish small teeth from short serrate setae. Thus, the type material of these two species should be re-examined, preferably under SEM, to clarify this matter.

(3) The distance that separates the tergal spur from the articular margin is quite variable in our material. Thus, this character does not appear to be useful to separate *T. southwardi* from *T. tasmanicum*.

One character not mentioned in previous descriptions is the shape of the basal margin of the scutum. This appears to be gently convex in the holotype of *T. southwardi* (see figs F and H in pl. XXVI, in Newman and Ross (1971)), and also in our material (Figs 4, 6). In contrast, in *T. tasmanicum*, the basal margin of the scutum is strongly flexed, with an obtuse angle of about 120 degrees (see figs 1C, 2C, D in Buckeridge (1999)).

In addition, neither Newman and Ross (1971) nor Buckeridge (1999) reported the ratio between the basal and occludent margins of the tergum. The basal/occludent ratio of the holotype of *T. southwardi* was calculated from high-resolution images provided by the curator of the NMNH (see Material and Methods). These images correspond to figs E and G (pl. XXVI) presented by Newman and Ross (1971). In addition, the basal/occludent ratio of *T. tasmanicum* was calculated based on figs 2C and D (Buckeridge 1999). These measurements result in a basal margin longer than the occludent margin for the holotype of *T. southwardi* and similar basal and occludent lengths for the holotype of *T. tasmanicum*. However, this comparison is based on indirect evidence obtained from the holotypes. The examination of additional specimens from both type localities (Central South Pacific and South Tasmania) is required to confirm whether or not these two species differ in their basal/occludent ratio of the tergum.

The cuticular growth lines are related to the molting cycle, but how these lines depend on parameters such as food availability, temperature, and other environmental factors is unknown for deep-sea barnacles (Yusa et al. 2018). In a large columnar specimen (MACN-In 44479a) collected at 2934 m depth and in a few isolated plates (MACN-In 44479i) from the same station, most basal horizontal growth lines are narrowly spaced (Figs 3F, G, 11E). Newman and Ross (1971) did not have columnar specimens, but the holotype, a medium-sized (carina: ca. 2.9 mm) conical individual, shows a few narrowly spaced horizontal growth lines basally (see figs A–C in pl. XXVI, in Newman and Ross (1971)). It is worth noting that the holotype of *T. tasmanicum*, a large columnar specimen, has narrowly spaced horizontal growth lines. However, these closely spaced lines are not confined to the basal part of the parietes but extend along their entire surface (figs 1A, B, in Buckeridge (1999)). This narrowly spaced pattern was also observed in additional columnar specimens of *T. tasmanicum* collected recently (see the CSIRO-MIIC website in the References section CSIRO-MIIC 2024).

In conclusion, *Tetrachaelasma southwardi* and *T. tasmanicum* are suspected to be cryptic species that require additional morphological and molecular studies to be distinguished from each other.

Distribution and biology of the genus *Tetrachaelasma*

Tetrachaelasma southwardi was not common among the material collected during the Talud Continental I, II, and III expeditions. This species was found in only two out of the 46 stations taken between 1000 m and 3447 m depth during these three surveys. No images were captured or quantitative data recorded at any of the 46 stations sampled, preventing an assessment of the abundance of *T. southwardi*. However, finding 29 specimens in these two samples suggests that this deep-sea barnacle could be relatively abundant in some benthic assemblages in the Mar del Plata Submarine Canyon. In support of this, a deep-sea barnacle tentatively identified as *T. tasmanicum* was reported at high density (32.1 ind/m^2) off southern Tasmania at 2171 m depth (Thresher et al. 2014).

Regarding the presence of *T. southwardi* in southern South America, only loose plates have been reported until now. These plates were collected by the RV "Eltanin" in 1962 and 1965, off the Malvinas/Falkland Is. (1720–1739 m depth), at the Sars Bank in the Drake Passage (1207–1591 m depth), and off southern Chile (1190–1263 m depth) (see Newman and Ross (1971); Table 1, Fig. 9). The current record of *T. southwardi* at ca. 37°50'S is the most septentrional latitude reported for this species in the South-West Atlantic. This finding, however, is not entirely unexpected, as many other benthic invertebrate species that are distributed in Antarctic and/or sub-Antarctic waters have also been recorded from the Mar del Plata Submarine Canyon (Farias et al. 2015; Olguín et al. 2015; Pastorino 2016, 2019; Pastorino and Sánchez 2016; Roccatagliata and Alberico 2016; Lauretta and Penchaszadeh 2017; Rivadeneira et al. 2017; Maggioni et al. 2018; Bernal et al. 2019, 2021; Lauretta and Martinez 2019; Teso et al. 2019; Pereira et al. 2020; Roccatagliata 2020; Flores et al. 2021; Pertossi et al. 2021; Rumbold et al. 2021; Schejter et al. 2021; Pacheco et al. 2022; Pereira 2022; Sánchez et al. 2023). This distribution pattern can be explained by the presence of the Malvinas/Falklands Current, a branch of the Antarctic Circumpolar Current (ACC) that flows northward along the continental slope of Argentina up to around 38°S (Piola and Gordon 1989; Matano et al. 2010).

Tetrachaelasma species inhabit great depths around the Southern Ocean (Fig. 9). Most of its distribution area is under the influence of the Antarctic Circumpolar Current. The ACC is a large and strong ocean current that encircles Antarctica and connects the major ocean basins—the Pacific, Atlantic, and Indian Oceans (Rintoul et al. 2001). This current flows eastward between 40° and 60°S, and its influence extends to the seafloor down to 4000 m depth (Orsi et al. 1995; Barker and Thomas 2004; Barker et al. 2007; Dueñas et al. 2016).

Circumpolar Subantarctic/Antarctic distributions have been documented for *Bathylasma corolliforme* (Hoek, l883) as well as for other living and fossil barnacles (Newman and Ross 1971; Buckeridge 2015). This circumpolar distribution has also been reported for many other invertebrates, including stylasterid corals, molluscs, echinoids, sea stars, isopods, and decapods (Leese et al. 2010; Díaz et al. 2011; Pérez-Barros et al. 2014; Farias et al. 2015; Moles et al. 2015; Dambach et al. 2016; Pastorino 2016; Lauretta and Martinez 2019; Güller et al. 2020; Bernal et al. 2021; Pacheco et al. 2022).

Knowledge about the life cycle of deep-sea balanomophs is very limited, and no information is available on the *Tetrachaelasma* species. A closely related Antarctic deep-sea species, *Bathylasma corolliforme*, has nauplius larvae that are well adapted to planktonic life (Dayton et al. 1982; Foster 1989). Thus, it can be inferred that the members of *Tetrachaelasma* have free nauplii as well.

Seamounts are numerous but poorly sampled in the Southern Ocean and may act as stepping stones for species dispersal (Auscavitch and Waller 2017). Due to the patchy distribution of hard substrata in the deep sea, barnacle larvae must travel long distances on inhospitable soft bottoms to reach a suitable habitat for settlement. Therefore, it is expected that the nauplius larvae of *T. southwardi* have an extended life and are passively transported over long distances by the ACC (and off Argentina by one of its branches, the Malvinas/Falklands Current). A comparable hypothesis was proposed by Buhl-Mortensen and Høeg (2006) for the dispersal of the widespread deep-sea *Arcoscalpellum michelottianum* (Seguenza, 1876).

Bathylasma hirsutum (Hoek, 1883) and *B. corolliforme* feed passively, with the cirri simply extending into the current (Southward and Southward 1958; Dayton et al. 1982). Since *Bathylasma* is a genus closely related to *Tetrachaelasma*, we can assume that its members are also passive feeders. The presence of medium to strong bottom currents around the Mar del Plata Submarine Canyon (see Steinmann et al. 2020; Bozzano et al. 2021) supports this hypothesis.

Acknowledgements

This paper would not have been possible without the fruitful exchange of ideas and views we had with William A. Newman (Scripps, UCSD, USA) during the initial steps of this research five years ago. We thank Diana S. Jones (WA Museum, Australia) for her advice and suggestions. We also express our gratitude to John S. Buckeridge (RMIT University, Australia) for his critical reading of an earlier version of the manuscript. Appreciation is also given to the cruise leader Guido Pastorino (MACN), Alejandro Martinez (INFIP, Argentina), officers, and crew for their help on board during the Talud Continental I and III expeditions. We are very grateful to curator Martha Nizinsky and technician Nina Ramos (NMNH, Smithsonian Institution, USA) for kindly providing us with high-resolution images of the holotype of *T. southwardi*. We are indebted to collection manager Charlotte Seid (Scripps, UCSD, USA) for providing us with data and images of the specimens of *T.* cf. *southwardi* collected in the Mid-Atlantic Ridge. Thanks are also given to Marina Malyutina (NSCMB, Russia) and Cristiana Serejo (UFRJ, Brazil) for their help with the literature, to Fabián Tricárico (MACN) for SEM technical assistance, to Patricia Torres (IBBEA), Sofía Calderón López (IBBEA), and Julián Santiago (DBBE) for their aid with photographs, and to Sofía Calla (MACN) and Lucía Bergagna (CADIC) for their help with the identification of the epibionts. We are also grateful to John S. Buckeridge, Diana S. Jones, Benny K. K. Chan (BRCAS, Taiwan), and the subject editor, Luiz F. Andrade, for their comments and suggestions on the manuscript. This research was partially funded by the National Scientific and Technical Research Council (CONICET, PIP 11220200102070CO) and the University of Buenos Aires (UBACyT 20020220400064BA).

References

Araya JF, Newman WA (2018) A new deep-sea balanomorph barnacle (Cirripedia: Thoracica: Bathylasmatidae) from Chile. PLOS ONE 13(6): e0197821. https://doi.org/10.1371/journal.pone.0197821

Auscavitch SR, Waller RG (2017) Biogeographical patterns among deep sea megabenthic communities across the Drake Passage. Antarctic Science 29(6): 531–543. https://doi.org/10.1017/S0954102017000256

Barker PF, Thomas E (2004) Origin, signature and palaeoclimatic influence of the Antarctic Circumpolar Current. Earth-Science Reviews 66(1–2): 143–162. https://doi.org/10.1016/j.earscirev.2003.10.003

Barker PF, Filippelli GM, Florindo F, Martin EE, Scher HD (2007) Onset and role of the Antarctic Circumpolar Current. Deep-sea Research, Part II, Topical Studies in Oceanography 54(21–22): 2388–2398. https://doi.org/10.1016/j.dsr2.2007.07.028

Bernal MC, Cairns SD, Penchaszadeh PE, Lauretta D (2019) *Errina argentina* sp. nov., a new stylasterid (Hydrozoa: Stylasteridae) from Mar del Plata submarine canyon (Southwest Atlantic). Marine Biodiversity 49(2): 833–839. https://doi.org/10.1007/s12526-018-0861-1

Bernal MC, Cairns SD, Penchaszadeh PE, Lauretta D (2021) Stylasterids (Hydrozoa: Stylasteridae) from Mar del Plata submarine canyon and adjacent area (southwestern Atlantic), with a key to the species off Argentina. Zootaxa 4969(3): 401–452. https://doi.org/10.11646/zootaxa.4969.3.1

Borradaile LA (1916) Crustacea. Part III.—Cirripedia. British Antarctic ("Terra Nova") expedition, 1910. Natural History Report. Zoology: Analysis of Complex Systems, ZACS 3(4): 127–136.

Bozzano G, Martín J, Spoltore DV, Violante RA (2017) Los cañones submarinos del margen continental argentino: Una síntesis sobre su génesis y dinámica sedimentaria. Latin American Journal of Sedimentology and Basin Analysis 24(1): 85–101. [LAJSBA]

Bozzano G, Cerredo ME, Remesal M, Steinmann L, Hanebuth TJJ, Schwenk T, Baqués M, Hebbeln D, Spoltore D, Silvestri O, Acevedo RD, Spiess V, Violante RA, Kasten S (2021) Dropstones in the Mar del Plata Canyon Area (SW Atlantic): Evidence for Provenance, Transport, Distribution, and Oceanographic Implications. Geochemistry, Geophysics, Geosystems 22(1): e2020GC009333. https://doi.org/10.1029/2020GC009333

Buckeridge JS (1999) A new deep sea barnacle, *Tetrachaelasma tasmanicum* sp. nov. (Cirripedia: Balanomorpha) from the South Tasman Rise, South Pacific Ocean. New Zealand Journal of Marine and Freshwater Research 33(4): 521–531. https://doi.org/10.1080/00288330.1999.9516897

Buckeridge JS (2010) Some biological consequences of environmental change: A study using barnacles (Cirripedia: Balanomorpha) and gum trees (Angiospermae: Myrtaceae). Integrative Zoology 5(2): 122–131. https://doi.org/10.1111/j.1749-4877.2010.00195.x

Buckeridge JS (2015) Revision of Southern Hemisphere taxa referred to *Fosterella* (Crustacea: Cirripedia), and their extinction in response to Pleistocene cooling. Integrative Zoology 10(6): 555–571. https://doi.org/10.1111/1749-4877.12161

Buckeridge JS, Newman WA (2010) A review of the subfamily Elminiinae (Cirripedia: Thoracica: Austrobalanidae) including a new genus, *Protelminius* nov., from the Oligocene of New Zealand. Zootaxa 2349(1): 39–54. https://doi.org/10.11646/zootaxa.2349.1.3

Buhl-Mortensen L, Høeg JT (2006) Reproduction and larval development in three scalpellid barnacles, *Scalpellum scalpellum* (Linnaeus 1767), *Ornatoscalpellum stroemii* (M. Sars 1859) and *Arcoscalpellum michelottianum* (Seguenza 1876) (Crustacea: Cirripedia: Thoracica): implications for reproduction and dispersal in the deep sea. Marine Biology 149(4): 829–844. https://doi.org/10.1007/s00227-006-0263-y

Chan BKK, Chen HN, Rodriguez Moreno PA, Corbari L (2016) Diversity and biogeography of the little known deep-sea barnacles of the genus *Waikalasma* Buckeridge, 1983 (Balanomorpha: Chionelasmatoidea) in the Southwest Pacific, with description of a new species. Journal of Natural History 50(47–48): 2961–2984. https://doi.org/10.1080/00222933.2016.1226445

Chan BKK, Corbari L, Rodríguez Moreno PA, Tsang LM (2017) Molecular phylogeny of the lower acorn barnacle families (Bathylasmatidae, Chionelasmatidae, Pachylasmatidae and Waikalasmatidae) (Cirripedia: Balanomorpha) with evidence for revisions in family classification. Zoological Journal of the Linnean Society 180(3): 542–555. https://doi.org/10.1093/zoolinnean/zlw005

Chan BKK, Dreyer N, Gale AS, Glenner H, Ewers-Saucedo C, Pérez-Losada M, Kolbasov GA, Crandall KA, Høeg JT (2021) The evolutionary diversity of barnacles, with an updated classification of fossil and living forms. Zoological Journal of the Linnean Society 193(3): 789–846. https://doi.org/10.1093/zoolinnean/zlaa160

Coleman CO (2003) "Digital Inking": how to make perfect line drawings on computers. Organisms Diversity & Evolution 3, Electronic Supplement 14: 1–14. https://doi.org/10.1078/1439-6092-00081

CSIRO-MIIC (2024) Codes for Australian Aquatic Biota (CAAB) Taxon Report. https://www.cmar.csiro.au/data/caab/taxon_report.cfm?caab_code=27554007 [January 9, 2024]

Dambach J, Raupach MJ, Leese F, Schwarzer J, Engler JO (2016) Ocean currents determine functional connectivity in an Antarctic deep-sea shrimp. Marine Ecology (Berlin) 37(6): 1336–1344. https://doi.org/10.1111/maec.12343

Dayton PK, Newman WA, Oliver J (1982) The vertical zonation of the deep-sea Antarctic acorn barnacle, *Bathylasma corolliforme* (Hoek): Experimental transplants from the shelf into shallow water. Journal of Biogeography 9(2): 95–109. https://doi.org/10.2307/2844695

Díaz A, Féral JP, David B, Saucède T, Poulin E (2011) Evolutionary pathways among shallow and deep-sea echinoids of the genus *Sterechinus* in the Southern Ocean. Deep-sea Research, Part II, Topical Studies in Oceanography 58(1–2): 205–211. https://doi.org/10.1016/j.dsr2.2010.10.012

Diepenbroek M, Grobe H, Reinke M, Schindler U, Schlitzer R, Sieger R, Wefer G (2002) PANGAEA – an information system for environmental sciences. Computers & Geosciences 28(10): 1201–1210. https://doi.org/10.1016/S0098-3004(02)00039-0

Dueñas LF, Tracey DM, Crawford AJ, Wilke T, Alderslade P, Sánchez JA (2016) The Antarctic Circumpolar Current as a diversification trigger for deep-sea octocorals. BMC Evolutionary Biology 16(1): 1–17. https://doi.org/10.1186/s12862-015-0574-z

Farias NE, Ocampo EH, Luppi TA (2015) On the presence of the deep-sea blind lobster *Stereomastis suhmi* (Decapoda: Polychelidae) in Southwestern Atlantic waters and its circum-Antarctic distribution. New Zealand Journal of Zoology 42(2): 119–125. https://doi.org/10.1080/03014223.2015.1013041

Flores JN, Penchaszadeh PE, Brogger MI (2021) Heart urchins from the depths: *Corparva lyrida* gen. et sp. nov. (Palaeotropidae), and new records for the southwestern Atlantic Ocean. Revista de Biología Tropical 69(Suppl.1): 14–33. https://doi.org/10.15517/rbt.v69iSuppl.1.46320

Foster BA (1978) The marine fauna of New Zealand: Barnacles. New Zealand Oceanographic Institute Memoir 69: 1–160.

Foster BA (1989) Balanomorph barnacle larvae in the plankton at McMurdo Sound, Antarctica. Polar Biology 10(3): 175–177. https://doi.org/10.1007/BF00238492

Gale AS (2016) Phylogeny of the deep-sea cirripede family Scalpellidae (Crustacea, Thoracica) based on shell capitular plate morphology. Zoological Journal of the Linnean Society 176(2): 266–304. https://doi.org/10.1111/zoj.12321

GBIF (2024) Global Biodiversity Information Facility, *Tetrachaelasma tasmanicum* Buckeridge, 1999. https://www.gbif.org/species/4335596 [January 9, 2024]

Güller M, Puccinelli E, Zelaya DG (2020) The Antarctic Circumpolar Current as a dispersive agent in the Southern Ocean: Evidence from bivalves. Marine Biology 167(10): 143. https://doi.org/10.1007/s00227-020-03746-2

Hessler RR, Sanders HL (1967) Faunal diversity in the deep-sea. Deep-Sea Research and Oceanographic Abstracts 14: 65–78. https://doi.org/10.1016/0011-7471(67)90029-0

Hoek PPC (1883) Report on the Cirripedia collected by the H.M.S. Challenger during the years 1873–1876. Report on the Scientific Results of the Voyage H.M.S. Challenger during the years 1873–1876. Zoology: Analysis of Complex Systems, ZACS 8(25): 1–169.

Jones DS (2000) Crustacea Cirripedia Thoracica: Chionelasmatoidea and Pachylasmatoidea (Balanomorpha) of New Caledonia, Vanuatu and Wallis and Futuna Islands, with a review of all currently assigned taxa. In: Crosnier A (Ed.) Résultats des Campagnes MUSORSTOM, Vol. 21. Mémoires du Muséum National d'Histoire Naturelle 184: 141–283.

Jones DS (2012) Australian barnacles (Cirripedia: Thoracica), distributions and biogeographical affinities. Integrative and Comparative Biology 52(3): 366–387. https://doi.org/10.1093/icb/ics100

Lauretta D, Martinez MI (2019) Corallimorpharians (Anthozoa: Corallimorpharia) from the Argentinean Sea. Zootaxa 4688(2): 249–263. https://doi.org/10.11646/zootaxa.4688.2.5

Lauretta D, Penchaszadeh PE (2017) Gigantic oocytes in the deep sea black coral *Dendrobathypathes grandis* (Antipatharia) from the Mar del Plata submarine canyon area (southwestern Atlantic). Deep-sea Research, Part I, Oceanographic Research Papers 128: 109–114. https://doi.org/10.1016/j.dsr.2017.08.011

Leese F, Agrawal S, Held C (2010) Long-distance island hopping without dispersal stages: Transportation across major zoogeographic barriers in a Southern Ocean isopod. Naturwissenschaften 97(6): 583–594. https://doi.org/10.1007/s00114-010-0674-y

Lin HC, Cheang CC, Corbari L, Chan BKK (2020) Trans-Pacific genetic differentiation in the deep-water stalked barnacle *Scalpellum stearnsii* (Cirripedia: Thoracica: Scalpellidae). Deep-sea Research, Part I, Oceanographic Research Papers 164: 103359. https://doi.org/10.1016/j.dsr.2020.103359

Maggioni T, Taverna A, Reyna PB, Alurralde G, Rimondino C, Tatián M (2018) Deep-sea ascidians (Chordata, Tunicata) from the SW Atlantic: Species richness with descriptions of two new species. Zootaxa 4526(1): 1–28. https://doi.org/10.11646/zootaxa.4526.1.1

Matano RP, Palma ED, Piola AR (2010) The influence of the Brazil and Malvinas Currents on the Southwestern Atlantic Shelf circulation. Ocean Science 6(4): 983–995. https://doi.org/10.5194/os-6-983-2010

Moles J, Figuerola B, Campanyà-Llovet N, Monleón-Getino T, Taboada S, Avila C (2015) Distribution patterns in Antarctic and Subantarctic echinoderms. Polar Biology 38(6): 799–813. https://doi.org/10.1007/s00300-014-1640-5

Newman WA, Ross A (1971) Antarctic Cirripedia. Antarctic Research Series 14. American Geophysical Union, Washington, 257 pp. https://doi.org/10.1029/AR014

Newman WA, Ross A (1976) Revision of the balanomorph barnacles; including catalog of the species. Memoirs of the San Diego Society of Natural History 9: 1–108.

Newman WA, Ross A (1977) Superfamilies of the Balanomorpha (Cirripedia, Thoracica). Crustaceana 32(1): 102. https://doi.org/10.1163/156854077X00953

NMNH (2024) Invertebrate Zoology Collections, *Tetrachaelasma southwardi* Newman & Ross, 1971. https://collections.nmnh.si.edu/search/iz/?q=qn+Tetrachaelasma+southwardi [January 9, 2024]

Olguín N, Ocampo EH, Farias N (2015) New record of *Paralomis spinosissima* Birstein & Vinogradov (Decapoda: Anomura: Lithodidae) from Mar del Plata, Argentina. Zootaxa 3957(2): 239–242. https://doi.org/10.11646/zootaxa.3957.2.9

Orsi AH, Whitworth III T, Nowlin Jr WD (1995) On the meridional extent and fronts of the Antarctic Circumpolar Current. Deep-sea Research. Part I, Oceanographic Research Papers 42(5): 641–673. https://doi.org/10.1016/0967-0637(95)00021-W

Pacheco LI, Teso V, Pastorino G (2022) Taxonomy and Biogeography of Bivalves of the Genus *Cuspidaria* Nardo, 1840, from the Southern Southwestern Atlantic Deep Sea. Malacologia 65(1–2): 137–175. https://doi.org/10.4002/040.065.0109

Pastorino G (2016) Revision of the genera *Pareuthria* Strebel, 1905, *Glypteuthria* Strebel, 1905 and *Meteuthria* Thiele, 1912 (Gastropoda: Buccinulidae) with the description of three new genera and two new species from Southwestern Atlantic waters. Zootaxa 4179(3): 301–344. https://doi.org/10.11646/zootaxa.4179.3.1

Pastorino G (2019) A new deep water gastropod of the genus *Parabuccinum* (Neogastropoda: Buccinulidae) from southwestern Atlantic waters with new data on the distribution of all species. Marine Biodiversity 49(2): 913–922. https://doi.org/10.1007/s12526-018-0876-7

Pastorino G, Sánchez N (2016) Southwestern Atlantic species of conoidean gastropods of the genus *Aforia* Dall, 1889. Zootaxa 4109(4): 458–470. https://doi.org/10.11646/zootaxa.4109.4.4

Pereira E (2022) Sistemática filogenética y biogeografía de isópodos Valvifera (Crustacea: Peracarida) de la Plataforma Continental y el Talud de Argentina. PhD Thesis, Universidad de Buenos Aires, Buenos Aires, Argentina.

Pereira E, Roccatagliata D, Doti BL (2020) On the antarcturid genus *Fissarcturus* (Isopoda: Valvifera): Description of *Fissarcturus argentinensis* n. sp., first description of the male of *Fissarcturus patagonicus* (Ohlin, 1901), and biogeographic remarks on the genus. Zoologischer Anzeiger 288: 168–189. https://doi.org/10.1016/j.jcz.2020.08.002

Pérez-Barros P, Lovrich GA, Calcagno JA, Confalonieri VA (2014) Is *Munida gregaria* (Crustacea: Decapoda: Munididae) a truly transpacific species? Polar Biology 37(10): 1413–1420. https://doi.org/10.1007/s00300-014-1531-9

Pertossi RM, Penchaszadeh PE, Martinez MI (2021) Brooding comatulids from the southwestern Atlantic, Argentina (Echinodermata: Crinoidea). Marine Biodiversity 51(4): 59. https://doi.org/10.1007/s12526-021-01194-9

Piola AR, Gordon AL (1989) Intermediate waters in the southwest South Atlantic. Deep-Sea Research, Part A, Oceanographic Research Papers 36(1): 1–16. https://doi.org/10.1016/0198-0149(89)90015-0

Piola AR, Matano RP (2001) Brazil/Falklands (Malvinas) Currents. In: Steele JH, Turekian KK, Thorpe SA (Eds) Encyclopedia of Ocean Sciences, Academic Press, 340–349. https://doi.org/10.1006/rwos.2001.0358

Preu B, Hernández-Molina FJ, Violante R, Piola AR, Paterlini CM, Schwenk T, Voigt I, Krastel S, Spiess V (2013) Morphosedimentary and hydrographic features of the northern Argentine margin: The interplay between erosive, depositional and gravitational processes and its conceptual implications. Deep-sea Research, Part I, Oceanographic Research Papers 75: 157–174. https://doi.org/10.1016/j.dsr.2012.12.013

Rintoul SR, Hughes CW, Olbers D (2001) Chapter 4.6 The Antarctic Circumpolar Current System. In: Siedler G, Church J, Gould J (Eds) International Geophysics, Vol. 77, Academic Press, 271–302. https://doi.org/10.1016/S0074-6142(01)80124-8

Rivadeneira PR, Brogger MI, Penchaszadeh PE (2017) Aboral brooding in the deep water sea star *Ctenodiscus australis* Lütken, 1871 (Asteroidea) from the Southwestern Atlantic. Deep-sea Research, Part I, Oceanographic Research Papers 123: 105–109. https://doi.org/10.1016/j.dsr.2017.03.011

Roccatagliata D (2020) On the deep-sea lampropid *Platytyphlops sarahae* n. sp. from Argentina, with remarks on some morphological characters of Cumacea. Zoologischer Anzeiger 286: 135–145. https://doi.org/10.1016/j.jcz.2020.03.009

Roccatagliata D, Alberico NA (2016) Two new cumaceans (Crustacea: Peracarida) from the South-West Atlantic with remarks on the problematic genus *Holostylis* Stebbing, 1912. Marine Biodiversity 46(1): 163–181. https://doi.org/10.1007/s12526-015-0349-1

Rumbold CE, Chiesa IL, Farías NE (2021) New epibiotic association in the deep-sea: The amphipod *Caprella ungulina* and the Patagonian lobsterette *Thymops birsteini* in the South-western Atlantic. Journal of the Marine Biological Association of the United Kingdom 101(8): 1171–1179. https://doi.org/10.1017/S0025315422000170 [JMBA]

Sánchez N, Damborenea C, Pastorino G (2023) Unravelling the conoidean gastropods assigned to the genus *Propebela* (Gastropoda: Mangeliidae) from south-western Atlantic deep waters. Journal of Natural History 57(1–4): 243–256. https://doi.org/10.1080/00222933.2023.2174056

Schejter L, Mauna C, Pérez CD (2021) New record and range extension of the primnoid octocoral *Verticillata castellviae* in the Southwest Atlantic Ocean. Marine and Fishery Sciences 34(2): 275–281. https://doi.org/10.47193/mafis.3422021010608 [MAFIS]

SIO-BIC (2024) Scripps Institution of Oceanography, Benthic Invertebrate Collection. https://sioapps.ucsd.edu/collections/bi/ [January 9, 2024]

Southward AJ, Southward EC (1958) On the occurrence and behaviour of two little known barnacles, *Hexelasma hirsutum* and *Verruca recta* from the continental slope. Journal of the Marine Biological Association of the United Kingdom 37: 633–647. https://doi.org/10.1017/S0025315400005683 [JMBA]

Steinmann L, Baques M, Wenau S, Schwenk T, Spiess V, Piola AR, Bozzano G, Violante R, Kasten S (2020) Discovery of a giant cold-water coral mound province along the northern Argentine margin and its link to the regional Contourite Depositional System and oceanographic setting. Marine Geology 427: 106223. https://doi.org/10.1016/j.margeo.2020.106223

Teso V, Urteaga D, Pastorino G (2019) Assemblages of certain benthic molluscs along the southwestern Atlantic: From subtidal to deep sea. BMC Ecology 19(1): 49. https://doi.org/10.1186/s12898-019-0263-7

Thresher R, Althaus F, Adkins J, Gowlett-Holmes K, Alderslade P, Dowdney J, Cho W, Gagnon A, Staples D, McEnnulty F, Williams A (2014) Strong Depth-Related Zonation of Megabenthos on a Rocky Continental Margin (~700–4000 m) off Southern Tasmania, Australia. PLOS ONE 9(1): e85872. https://doi.org/10.1371/journal.pone.0085872

Tsang LM, Chu KH, Achituv Y, Chan BKK (2015) Molecular phylogeny of the acorn barnacle family Tetraclitidae (Cirripedia: Balanomorpha): validity of shell morphology and arthropodal characters in systematics of Tetraclitid barnacles. Molecular Phylogenetics and Evolution 82: 324–329. https://doi.org/10.1016/j.ympev.2014.09.015

Violante RA, Paterlini CM, Costa IP, Hernández-Molina FJ, Segovia LM, Cavallotto JL, Marcolini S, Bozzano G, Laprida C, García Chapori N, Bickert T, Spieß V (2010) Sismoestratigrafía y evolución geomorfológica del talud continental adyacente al litoral del este bonaerense, Argentina. Latin American Journal of Sedimentology and Basin Analysis 17(1): 33–62. [LAJSBA]

Voigt I, Henrich R, Preu BM, Piola AR, Hanebuth TJJ, Schwenk T, Chiessi CM (2013) A submarine canyon as a climate archive — Interaction of the Antarctic Intermediate Water with the Mar del Plata Canyon (Southwest Atlantic). Marine Geology 341: 46–57. https://doi.org/10.1016/j.margeo.2013.05.002

Weisbord NE (1965) Two new localities for the barnacle *Hexelasma antarcticum* Borradaile. Journal of Paleontology 39(5): 1015–1016.

Weisbord NE (1967) The barnacle *Hexelasma antarcticum* Borradaile — Its description, distribution, and geologic significance. Crustaceana 13(1): 51–60. https://doi.org/10.1163/156854067X00071

Yusa Y, Yasuda N, Yamamoto T, Watanabe HK, Higashiji T, Kaneko A, Nishida K, Høeg JT (2018) Direct growth measurements of two deep-sea scalpellid barnacles, *Scalpellum stearnsii* and *Graviscalpellum pedunculatum*. Zoological Studies (Taipei, Taiwan) 57: 29. https://doi.org/10.6620/ZS.2018.57-29

Zoosyst. Evol. 100 (2) 2024, 625–643 | DOI 10.3897/zse.100.118879

PENSOFT

MUSEUM FÜR NATURKUNDE BERLIN

Underestimated species diversity within the *Rhacophorus rhodopus* and *Rhacophorus bipunctatus* complexes (Anura, Rhacophoridae), with a description of a new species from Hainan, China

Shangjing Tang[1,2], Fanrong Xiao[3], Shuo Liu[4], Lijun Wang[3], Guohua Yu[1,2], Lina Du[1,2]

1 *Key Laboratory of Ecology of Rare and Endangered Species and Environmental Protection (Guangxi Normal University), Ministry of Education, Guilin 541004, China*

2 *Guangxi Key Laboratory of Rare and Endangered Animal Ecology, College of Life Science, Guangxi Normal University, Guilin 541004, China*

3 *Ministry of Education Key Laboratory for Ecology of Tropical Islands & Key Laboratory of Tropical Animal and Plant Ecology of Hainan Province, College of Life Sciences, Hainan Normal University, Haikou 571158, China*

4 *Kunming Natural History Museum of Zoology, Kunming Institute of Zoology, Chinese Academy of Sciences, Kunming 650223, China*

https://zoobank.org/675CD047-159E-4363-A0A6-ECD9549A989B

Corresponding authors: Guohua Yu (yugh2018@126.com); Lina Du (Dulina@mailbox.gxnu.edu.cn)

Academic editor: Umilaela Arifin ♦ **Received** 16 January 2024 ♦ **Accepted** 6 April 2024 ♦ **Published** 21 May 2024

Abstract

Taxonomy and species boundaries within the *Rhacophorus rhodopus* and *Rhacophorus bipunctatus* complexes are very confusing. In this study, we attempt to delimit the species boundaries and test the currently accepted taxonomic assignments within these two complexes based on newly collected samples and previously published data across their distributions. Phylogenetic analyses revealed that the *R. rhodopus* and *R. bipunctatus* complexes consisted of six distinct clades (labeled A–F) that diverged from each other by genetic distances (p-distance) ranging from 5.3% to 9.2% in 16S rRNA sequences, and accordingly analyses of species delimitation placed them into six species, of which three correspond to known species (*R. rhodopus*, *R. bipunctatus*, and *R. napoensis*) and three represent different cryptic species. *Rhacophorus rhodopus* (Clade C) is distributed in southern Yunnan, China, northern Laos, and northern and central Thailand; *R. bipunctatus* (Clade F) is distributed in northeastern India and western and northern Myanmar; and *R. napoensis* (Clade B) is distributed in Guangxi, China and northern Vietnam. Based on both molecular and morphological evidence, we described the clade consisting of samples from Hainan, China and central Vietnam (Clade A) as a new species, *Rhacophorus qiongica* **sp. nov.** There are two cryptic species requiring additional morphological studies: one only contains samples from Motuo, Xizang, China (Clade E), and the other is distributed in western Yunnan, China, central Myanmar, central Thailand, and Malaysia (Clade D). Additionally, our results supported the idea that some old GenBank sequences of *R. reinwardtii* need to be updated with the correct species name.

Key Words

Cryptic species, Hainan, *Rhacophorus qiongica* sp. nov., Species complex, Species delimitation

Introduction

Rhacophorus Kuhl & Van Hassalt, 1822, a genus of the family Rhacophoridae that originated ca. 19.3–33.0 million years ago (O'Connell et al. 2018; Chen et al. 2020; Ellepola and Meegaskumbura 2023), is widely distributed in India, Bhutan, China (Xizang, Yunnan, Guangxi, Hainan), Myanmar, Thailand, Laos, Cambodia, Vietnam, Indonesia (Sumatra, Sulawesi), Philippines, and Kalimantan (Frost 2023). It is characterized by medium or large body size, intercalary cartilage between the end of the finger and penultimate phalanges of digits, Y-shaped distal end of terminal phalanx, tip of digits expanded into rounded disks with circum-marginal grooves, web

between fingers, horizontal pupil, skin not co-ossified to skull, absence of upper eyelid projections and presence of tarsal projections in most species, extensive dermal folding usually on forearm and tarsus, anal folds, and brown or green dorsal color (Li et al. 2012; Pan et al. 2017; Jiang et al. 2019), and currently it contains 43 species excluding *Rhacophorus verrucopus* Huang, 1983, which was considered a synonym of *Rhacophorus tuberculatus* Anderson, 1871 by Che et al. (2020). In China, there are eight *Rhacophorus* species, namely *Rhacophorus bipunctatus* Ahl, 1927; *Rhacophorus kio* Ohler & Delorme, 2006; *Rhacophorus laoshan* Mo, Jiang, Xie & Ohler, 2008; *Rhacophorus napoensis* Li, Liu, Yu & Sun, 2022; *Rhacophorus orlovi* Ziegler & Köhler, 2001; *Rhacophorus rhodopus* Liu & Hu, 1960; *Rhacophorus translineatus* Wu, 1977; and *Rhacophorus tuberculatus* (Anderson, 1871) (AmphibiaChina 2023).

Rhacophorus rhodopus is mainly distributed in northeastern India to Myanmar (Kachin State, Shan State), Thailand, Laos, Vietnam (Lao Cai, Ha Tinh, Bac Giang, Quang Binh, Lai Chau, Quang Tri, Thua Thien Hue, Kon Tum, Gia Lai, Lam Dong, and Dong Nai), southern China (southeast Tibet, southern Yunnan, northeastern Guangxi, Hainan), and Peninsular Malaysia (Frost 2023). This species was originally described by Liu and Hu (1960) based on specimens from Mengyang, Yunnan, China. It is characterized by reddish-brown dorsal color, pointed snout, smooth head skin, black spots at axillary region, and bright scarlet webs, resembling *R. bipunctatus*, a species originally discovered from northeastern India (type locality: Khasi Hills) and later widely recorded from Bangladesh (e.g. Reza and Mukul 2009; Hakim et al. 2020), Cambodia (e.g. Ohler et al. 2002; Stuart and Emmett 2006; Neang and Holden 2008), Thailand (Taylor 1962; Chan-ard 2003; Chan-ard et al. 2011), Malaysia (Leong and Lim 2003; Grismer et al. 2006), Vietnam (Nguyen et al. 2005; Bain et al. 2007), Laos (Stuart 2005), Myanmar (Zug and Mulcahy 2020; Zug 2022), and China (Fei 1999; Fei et al. 2004, 2009, 2010; Che et al. 2020).

The disputes over the taxonomy of *R. rhodopus* and *R. bipunctatus* have been going on for many years. Inger et al. (1999) compared *R. bipunctatus* from northern and central Vietnam with *R. rhodopus* and concluded that the two species are synonymous. However, Bordoloi et al. (2007) considered that this conclusion is not reliable owing to the fact that Inger et al. (1999) did not compare the specimens from Vietnam with topotypes of *R. bipunctatus*, and suggested that records of *R. bipunctatus* from Thailand and Vietnam actually refer to *R. rhodopus*. Nguyen et al. (2008) also suggested that all records of *R. bipunctatus* in Vietnam should be classified as *R. rhodopus*. Fei et al. (2009) considered that *R. rhodopus* from the type locality obviously differs from *R. bipunctatus* from northern India in body size and color pattern, so they suggested maintaining the validity of *R. rhodopus* and considered that *R. bipunctatus* from Vietnam is more similar to *R. rhodopus* from China.

Analysis of molecular data can more accurately test the taxonomic hypothesis based on morphology (Jablonski and Finarelli 2009). Previous molecular phylogenetic analyses have demonstrated that the taxonomy of *R. rhodopus* and *R. bipunctatus* complexes (Chan et al. 2018) is complicated. Yu et al. (2007, 2008) found that *R. rhodopus* is not monophyletic, and *R. rhodopus* from Hainan, China is closer to *R. bipunctatus* collected from Vietnam. Li et al. (2012) found that samples of *R. rhodopus* from Hainan, China and Vietnam form a clade that did not cluster together with the clade containing *R. rhodopus* from the type locality, indicating that *R. rhodopus* from Hainan, China and Vietnam likely represents a cryptic species. Nguyen et al. (2014) also revealed that *R. rhodopus* is not monophyletic since *R. rhodopus* from Vietnam did not cluster together with the clade of samples from Yunnan and Malaysia. Dang et al. (2015) revealed two distinct lineages within *R. rhodopus* from Yunnan and considered that one of them could be a cryptic species. Moreover, Chan et al. (2018) suggested tentatively moving Malaysian *R. bipunctatus* to *R. rhodopus* and revealed that *R. rhodopus* from Vietnam is composed of two distinct clades, one only containing samples from Vietnam and one containing samples from Vietnam and Hainan, China. Over all, these previous molecular phylogenetic analyses revealed that *R. bipunctatus* and *R. rhodopus* represent two complexes (Chan et al. 2018), and at least two cryptic species may exist in the *R. rhodopus* complex: one occurs in Hainan, China and Vietnam, and one is only known from Vietnam. Recently, Li et al. (2022) described a new species resembling *R. rhodopus* from Guangxi, China (*R. napoensis*). This finding raises another question. That is, whether *R. napoensis* is conspecific with one of the two potential cryptic species within the *R. rhodopus* complex mentioned above. Additionally, Li et al. (2012) and Che et al. (2020) found that *R. bipunctatus*, which is likely restricted to northeastern India, Myanmar, and Xizang, China (Fei et al. 2009; Chan et al. 2018; Poyarkov et al. 2021), is not monophyletic since samples from Motuo, Xizang, China formed a clade whereas samples from northern Myanmar formed another clade. Because no samples from India were included in these two studies, it is necessary to investigate which of these two clades represents the true *R. bipunctatus* by employing *R. bipunctatus* samples from northeastern India.

In this study, we attempt to delimit the species boundary and test the currently accepted taxonomic assignments within *R. rhodopus* and *R. bipunctatus* complexes based on newly collected and previously sequenced samples across their distributions. Our results revealed that there are probably three cryptic species, and one of them was described as a new species herein based on morphological and molecular evidence. The samples from northern Vietnam belong to *R. napoensis*, and populations from central Vietnam are conspecific with the new species described here.

Materials and methods

Sampling

This study was carried out in accordance with the ethical guidelines issued by the Ethics Committee of Guangxi Normal University (permit number: GXNU-202308-010). A total of 58 individuals of *R. rhodopus* and *R. bipunctatus* complexes collected from 33 sites across China, Vietnam, Laos, Thailand, Malaysia, Myanmar, and India (Fig. 1) were included in this study. Of the 58 samples, 18 were collected and sequenced by this study, and the homologous sequences of the other 40 individuals were downloaded from GenBank (Table 1). All newly collected specimens in this study were deposited at Guangxi Normal University (**GXNU**). *Rhacophorus norhayatiae* Chan & Grismer, 2010, *Rhacophorus reinwardtii* (Schlegel, 1840), *Rhacophorus borneensis* Matsui, Shimada & Sudin, 2013, *Rhacophorus helenae* Rowley, Tran, Hoang & Le, 2012, *R. kio*, *Rhacophorus lateralis* Boulenger, 1883, and *Rhacophorus nigropalmatus* Boulenger, 1895 were included in this study, and *Leptomantis gauni* (Inger, 1966), *Zhangixalus smaragdinus* (Blyth, 1852), *Buergeria buergeri* (Temminck & Schlegel, 1838), *Kurixalus idiootocus* (Kuramoto & Wang, 1987), *Chiromantis rufescens* (Günther, 1869), *Nyctixalus pictus* (Peters, 1871), and *Theloderma albopunctatum* (Liu & Hu, 1962) were selected as the outgroup according to Yu et al. (2019) and Li et al. (2022).

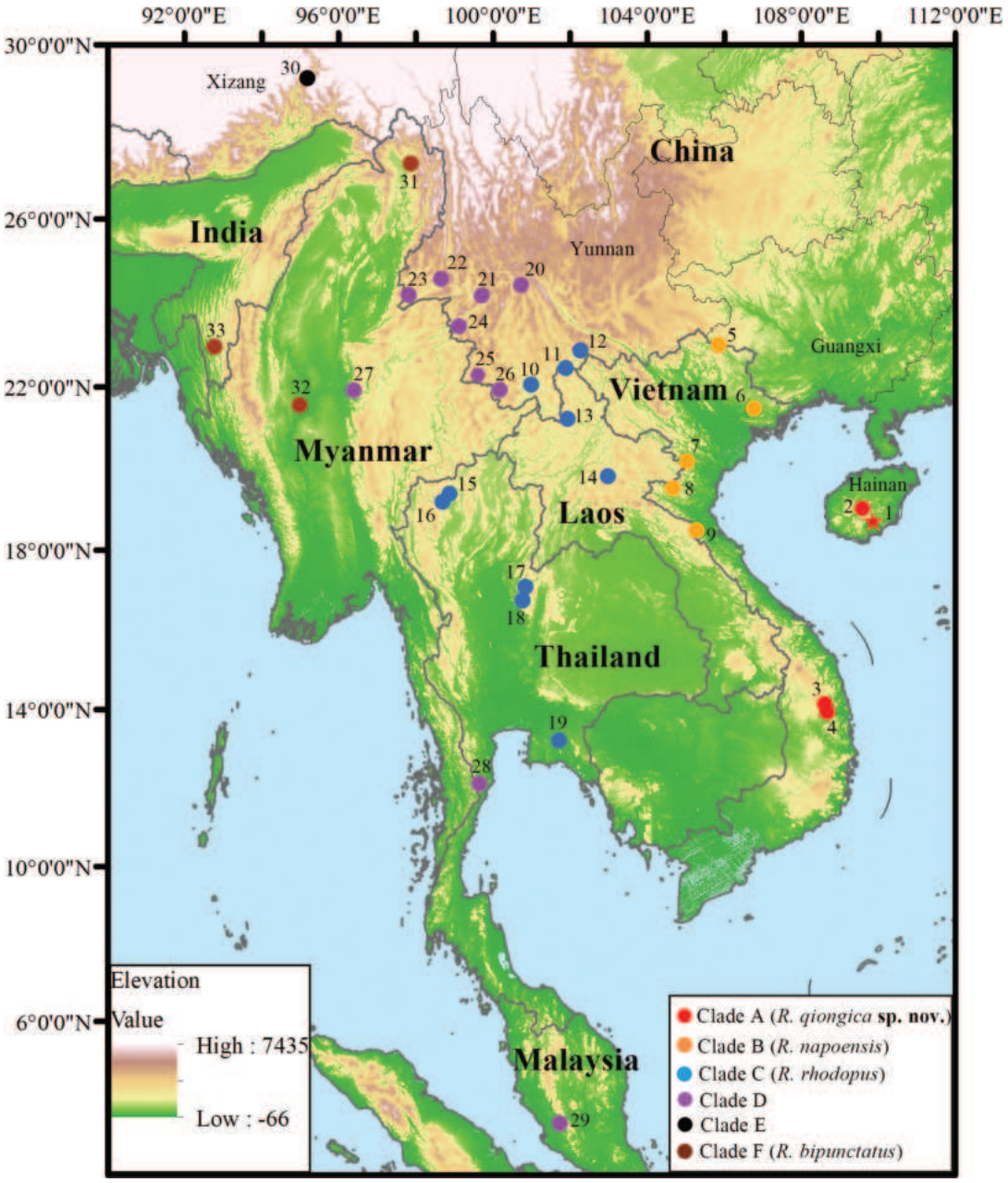

Figure 1. Map showing the collection sites of samples of the *R. rhodopus* and *R. bipunctatus* complexes used in this study. Sites are labeled as in Table 1, and the star represents the type locality of *R. qiongica* sp. nov. in Hainan, China.

Table 1. Species used in phylogenetic analyses of this study.

Species	Voucher	Locality (ID)	Accession No.
Buergeria buergeri	TTU-R-11759	Japan	AF458122
Nyctixalus pictus	FMNH 231094	Lahad Datu, Sabah, Malaysia	AF458135
Theloderma albopunctatum	ROM 30246	Vietnam	AF458148
Chiromantis rufescens	CAS 207601	Bioko Norte Province, Equatorial Guinea	AF458126
Kurixalus idiootocus	CAS 211366	Taipei, Taiwan, China	AF458129
Zhangixalus smaragdinus	HM05292	Xima, Yingjiang, Yunnan, China	MN613221
Leptomantis gauni	FMNH 273928	Bintulu, Sarawak, Malaysia	JX219456
Rhacophorus borneensis	BORN 22411	Sabah, Maliau Basin, Malaysia	AB781694
R. helenae	UNS 00451	Binh Thuan, Vietnam	JQ288090
R. kio	KUHE 55165	Xuan Lien, Than Hoa, Vietnam	AB781695
R. lateralis	-	Mudigere, India	AB530548
R. nigropalmatus	Rao081204	Malaysia	JX219437
R. norhayatiae	NNRn	Johor, Endau Rompin, Malaysia	AB728191
R. reinwardtii	NMBE 1056517	Batang Ai NP, Sarawak, Malaysia	JN377366
R. reinwardtii	Rao081205	Malaysia	JX219443
R. reinwardtii	ENS 16447 (UTA)	Sumatra, Bandung, Indonesia	KY886335
R. reinwardtii	ENS 16179 (UTA)	Java, Patuha, Indonesia:	KY886328
R. qiongica **sp. nov.**	GXNU HN110501	Diaoluo Mountain, Hainan, China (1)	OP740711
R. qiongica **sp. nov.**	GXNU HN110502	Diaoluo Mountain, Hainan, China (1)	OP740712
R. qiongica **sp. nov.**	GXNU HN110503	Diaoluo Mountain, Hainan, China (1)	OP740713
R. qiongica **sp. nov.**	GXNU YU000691	Yinggeling, Hainan, China (2)	PP115440
R. qiongica **sp. nov.**	GXNU YU000693	Yinggeling, Hainan, China (2)	PP115441
R. qiongica **sp. nov.**	GXNU YU000696	Yinggeling, Hainan, China (2)	PP115442
R. qiongica **sp. nov.**	GXNU YU000697	Yinggeling, Hainan, China (2)	PP115443
R. qiongica **sp. nov.**	GXNU YU000698	Yinggeling, Hainan, China (2)	PP115444
R. qiongica **sp. nov.**	VNMN:4117	K' Bang, Gia Lai, Vietnam (3)	LC010604
R. qiongica **sp. nov.**	FMNH253114	Ankhe Dist, Gia Lai, Vietnam (4)	GQ204716
R. napoensis	GXNU YU000171	Napo, Guangxi, China (5)	ON217796
R. napoensis	GXNU YU000173	Napo, Guangxi, China (5)	ON217798
R. rhodopus	VNMN:4118	Yen Tu, Bac Giang, Vietnam (6)	LC010605
R. bipunctatus	AMNH-A 161418	Huon Son Reserve, Ha Tinh, Vietnam (7)	AY843750
R. rhodopus	VNMN:4120	Pu Huong, Nghe An, Vietnam (8)	LC010609
R. rhodopus	VNMN:4121	Thanh Hoa, Vietnam (9)	LC010608
R. rhodopus	clone 5	Mengyang, Yunnan, China (10)	EF646366
R. rhodopus	SCUM 060692L	Mengyang, Yunnan, China (10)	EU215531
R. rhodopus	GXNU HP018	Jiangcheng, Yunnan, China (11)	OP740717
R. rhodopus	KIZ060821229	Lvchun, Yunnan, China (12)	EF564574
R. rhodopus	clone 3	Lvchun, Yunnan, China (12)	EF646364
R. rhodopus	2004.0409	Long Nai Khao, Phongsali, Laos (13)	KR828049
R. rhodopus	2006.2519	Ban Vang Thong, Louangphrabang, Laos (14)	KR828069
R. rhodopus	K3353	Ban Keng Koung, Louangphrabang, Laos (14)	KR828071
R. rhodopus	K3046	Doi Chiang Dao, Chiang Mai, Thailand (15)	KR828066
R. rhodopus	K3085_1	Mae Lao-Mae Sae Wildlife Sanctuary, Chiang Mai, Thailand (16)	KR828067
R. rhodopus	0909Y3	Phu Hin Rong Kla NP, Phitsanulok, Thailand (17)	KR828052
R. rhodopus	0906Y5	Phu Hin Rong Kla NP, Phitsanulok, Thailand (17)	KR828078
R. rhodopus	0954Y	Thung Salaeng Luang NP, Phetchabun, Thailand (18)	KR828061
R. rhodopus	0955Y	Thung Salaeng Luang NP, Phetchabun, Thailand (18)	KR828062
R. rhodopus	1000Y	Khao Ang Rui Ni wildlife sanctuary, Chachoengsao, Thailand (19)	KR828065
R. rhodopus	clone 4	Jingdong, Yunnan, China (20)	EF646365
R. rhodopus	KIZ060821248	Jingdong, Yunnan, China (20)	EF564575
R. rhodopus	KIZ060821175	Yongde, Yunnan, China (21)	EF564573
R. rhodopus	clone 2	Yongde, Yunnan, China (21)	EF646363
R. rhodopus	KIZ587	Longling, Yunnan, China (22)	EF564577
R. rhodopus	KIZ589	Longling, Yunnan, China (22)	EF564578
R. rhodopus	GXNU 039927	Longchuan, Yunnan, China (23)	OP740718
R. rhodopus	GXNU 039928	Longchuan, Yunnan, China (23)	OP740719
R. rhodopus	GXNU YU20160263	Mengding, Yunnan, China (24)	PP106375
R. rhodopus	GXNU YU20160264	Mengding, Yunnan, China (24)	PP106376
R. rhodopus	GXNU YU000492	Menglian, Yunnan, China (25)	OP740720
R. rhodopus	GXNU YU000493	Menglian, Yunnan, China (25)	OP740721

Species	Voucher	Locality (ID)	Accession No.
R. rhodopus	GXNU YU000485	Xiding, Menghai,Yunnan, China (26)	OP740714
R. rhodopus	GXNU YU000486	Xiding, Menghai,Yunnan, China (26)	OP740715
R. rhodopus	GXNU YU000487	Xiding, Menghai,Yunnan, China (26)	OP740716
R. rhodopus	USNM:Herp:587063	Kandawgyi National Gardens, Mandalay, Myanmar (27)	MG935991
R. rhodopus	0937Y1	Kui Buri NP, Prachuap Khiri Khan, Thailand (28)	KR828056
R. rhodopus	0937Y4	Kui Buri NP, Prachuap Khiri Khan, Thailand (28)	KR828058
R. bipunctatus	KUHE:53375	Genting, Pahang, Malaysia (29)	LC010569
R. bipunctatus	KIZ016380	Motuo, Xizang, China (30)	MW111517
R. bipunctatus	YPX40427	Motuo, Xizang, China (30)	MW111518
R. rhodopus	L06245	Motuo, Xizang, China (30)	JX219441
R. rhodopus	L062456	Motuo, Xizang, China (30)	JX219442
R. bipunctatus	CAS229913	Nagmung Township, Putao District, Kachin State, Myanmar (31)	JX219445
R. bipunctatus	CAS235303	Mindat Township, Mindat District, Chin State, Myanmar (32)	JX219444
R. bipunctatus	PUCZM/IX/SL360	Mizoram, Inida (33)	MH087073
R. bipunctatus	PUCZM/IX/SL612	Mizoram, India (33)	MH087076

Molecular analyses and species delimitation

The total genomic DNA of the specimens was extracted from liver tissue preserved in 99% ethanol. Tissue samples were digested with proteinase K and purified using standard phenol/chloroform separation and ethanol precipitation. A fragment encoding partial 12S rRNA, complete $tRNA^{val}$, and partial 16S rRNA (16S) was amplified using the protocol of Yu et al. (2019) and the primer pair L1091 (Kocher et al. 1989)/16H1 (Hedges 1994). Sequencing was conducted using the corresponding PCR primers and the internal primer Rh-int (Yu et al. 2019). All new sequences have been deposited in GenBank under accession Nos. OP740711–OP740721, PP106375–PP106376, and PP115440–PP115442 (Table 1).

Sequences were aligned in MEGA v. 7 (Kumar et al. 2016) using the MUSCLE option with the default parameters. The uncorrected pairwise distances (p-distances) between species were calculated in MEGA v. 7. The best substitution model (GTR + I + G) was selected in jMODELTEST v. 2.1.10 (Darriba et al. 2012) based on the corrected Akaike Information Criterion (AICc). Bayesian phylogenetic inference and maximum likelihood analysis were performed based on the best model. Bayesian phylogenetic inference was performed using MrBayes v. 3.2.6 (Ronquist et al. 2012). Two runs were performed simultaneously with four Markov chains starting from a random tree. The chain was run for 3,000,000 generations and sampled every 100 generations. When the average standard deviation of the split frequency was less than 0.01, the first 25% of the sampled trees were discarded as burn-in, and the remaining trees were used to create a consensus tree and estimate the Bayesian posterior probabilities (BPPs). The maximum likelihood analysis was conducted using raxmlGUI 2.0 (Edler et al. 2020) with 1000 bootstrap replicates.

We used Assemble Species by Automatic Partitioning (ASAP; Puillandre et al. 2021) and multirate PTP (mPTP; Kapli et al. 2017) to delineate the species boundary within the *R. rhodopus* and *R. bipunctatus* complexes based on 16S rRNA sequences. For the ASAP method, the substitution model of p-distances was used to compute the distances under the default values for other parameters. We selected the partition with the lowest ASAP-score as the best partition, according to Puillandre et al. (2021). The mPTP analysis was conducted in mPTP v. 0.2.5 using a maximum likelihood tree generated from 16S sequences by raxmlGUI 2.0. For this analysis, 10 different runs were performed with the following settings: mcmc run of 50 million generations, samples every 1000 generations, and the first 10 million generations were discarded as burn-in.

Morphology

As the molecular phylogenetic and species delimitation analyses revealed that species diversity in the *R. rhodopus* and *R. bipunctatus* complexes was underestimated and Hainan populations represent one of the three putative species (see below), we further conducted morphological analyses to confirm its taxonomic status and to officially describe it. The other two putative species were not included in morphological analyses owing to the fact that not enough morphometric data on them is available for the time being.

Morphometric data were taken using electronic digital calipers to the nearest 0.1 mm. The terminology followed Fei (1999). Measurements included the following: snout-vent length (SVL); head length (HL); head width (HW); snout length (SL); internarial distance (IND); interorbital distance (IOD); upper eyelid width (UEW); diameter of eye (ED); diameter of tympanum (TD); distance from nostril to eye (DNE); length of forearm and hand (FHL); tibia length (TL); length of tarsus and foot (TFL); and foot length (FL). Comparative morphological data of congeneric species were obtained from published literature (Liu and Hu 1960; Ohler and Delorme 2006; Bordoloi et al. 2007; Fei et al. 2009, 2012; Chan and Grismer 2010; Rowley et al. 2012; Matsui et al. 2013; Li et al. 2022).

Measurements were corrected for size (measurements divided by SVL). We used the *t*-test in SPSS v. 17.0 (SPSS Inc., Chicago, IL, USA) to evaluate the differences in quantitative characters of adult males between Hainan populations and its two relatives (*R. rhodopus* and *R. napoensis*) because the Hainan populations were once placed in *R. rhodopus* and both the clade containing Hain-

an populations and the clade of *R. napoensis* occur in Vietnam (see below). Principal component analyses (PCA) were conducted based on a correlation matrix of size-corrected measurements of males using SPSS v. 17.0. Scatter plots of the first two PCA factors were used to examine the morphological differentiation between specimens from Hainan, *R. rhodopus*, and *R. napoensis*. Females were not included as a separate analysis for both the *t*-test and PCA analysis owing to the small sample size (n = 2; one female from Hainan and one female of *R. rhodopus*).

Results

Phylogeny and species delimitation

The BI and ML analyses yielded similar topologies, and both analyses revealed that there are six distinct clades in the *R. rhodopus* and *R. bipunctatus* complexes (Clades A–F; Fig. 2): Clade A contains samples from Hainan, China (sites 1 and 2) and Gia Lai, Vietnam (sites 3 and 4); Clade B contains types of *R. napoensis*

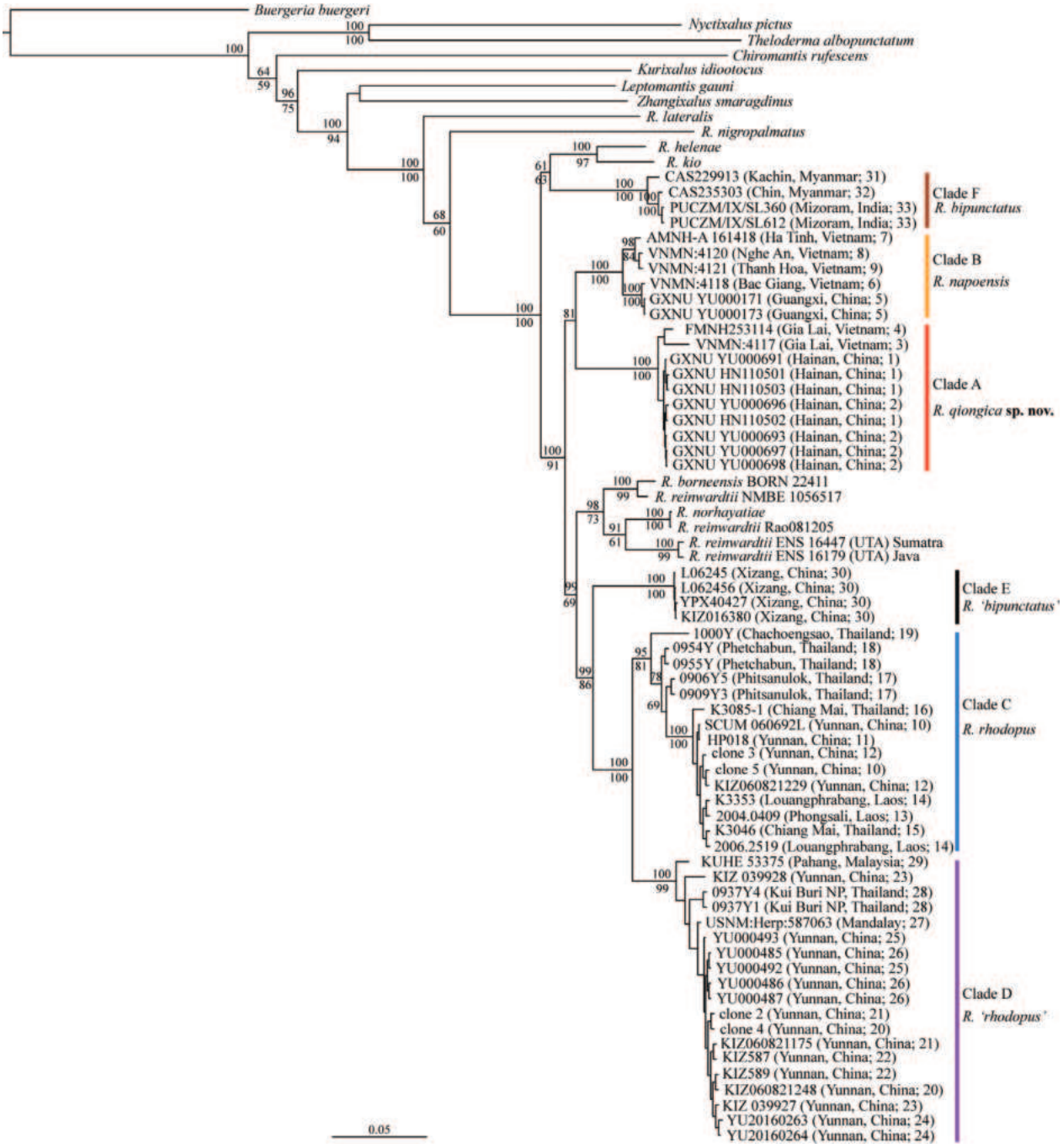

Figure 2. Bayesian phylogenetic tree of *R. rhodopus* and *R. bipunctatus* complexes and related species inferred from 12S rRNA, $tRNA^{Val}$, and 16S rRNA genes. The numbers above and below the branches are Bayesian posterior probabilities (BPP) and maximum likelihood (ML) bootstrap values, respectively (only values greater than 50% are shown).

(site 5) and samples from northern Vietnam (Bac Giang, Ha Tinh, Nghe An, and Thanh Hoa; sites 6–9); Clade C contains *R. rhodopus* from the type locality (Mengyang, Yunnan, China; site 10) and samples from southern Yunnan (Jiangcheng and Lvchun; sites 11 and 12), northern Laos (Phongsali and Louangphrabang; sites 13 and 14), and northern and southeastern Thailand (Chiang Mai, Phitsanulok, Phetchabun, and Chachoengsao; sites 15–19); Clade D contains samples from western and southwestern Yunnan, China (Jingdong, Yongde, Longling, Longchuan, Mengding, Menglian, and Xiding; sites 20–26), Myanmar (Mandalay; site 27), Thailand (Prachuap Khiri Khan; site 28), and Malaysia (Pahang; site 29); Clade E is consisted of Xizang population (site 30) that was previously identified as *R. rhodopus* or *R. bipunctatus*. Clade F is consisted of *R. bipunctatus* from northern (Kachin State; site 31) and western (Chin State; site 32) Myanmar and northeastern India (Mizoram; site 33). All phylogenetic analyses supported that clades C, D, and E form a monophyly, and clade C is sister to clade D. Clade F was recovered as sister to the clade of *R. helenae* and *R. kio* with moderate support, and clade A was recovered as sister to clade B with weak support.

The sequences of specimens under the name *R. reinwardtii* in GenBank did not form monophyly. The two specimens that came from Malaysia (NMBE 1056517 and Rao081205) clustered together with *R. borneensis* and *R. norhayatiae*, respectively, and the two specimens that came from Indonesia (Java and Sumatra) formed a clade.

Genetically, the pairwise distances between the six clades in *R. rhodopus* and *R. bipunctatus* complexes ranged from 5.3% to 9.2%, which is greater than the distance between *R. kio* and *R. helenae* (4.5%), the distance between *R. helenae* and *R. borneensis* (4.9%), and the distances between *R. norhayatiae*, *R. borneensis*, and *R. reinwardtii* (4.0%–4.8%; Table 2).

The best partition (score = 2.50) obtained by the ASAP species delimitation analysis grouped all samples of *R. rhodopus* and *R. bipunctatus* complexes used in this study into six species completely corresponding to the six distinct clades (A–F) mentioned above (Fig. 3a), with a distance threshold of about 4% (Fig. 3b). The clade consisting of *R. borneensis* and the specimen under the name *R. reinwardtii* (NMBE 105617), the clade containing *R. norhayatiae* and the specimen under the name *R. reinwardtii* (Rao081205), and the clade comprising of *R. reinwardtii* from Indonesia were identified as three different species (Fig. 3a). These operational taxonomic units were also supported by the mPTP analysis (Fig. 4).

Morphological study

Morphological data are summarized in Table 3. The *t*-tests revealed that the male specimens from Hainan differ significantly ($p < 0.05$) from male topotypes of *R. rhodopus* in tympanum diameter (TD), upper eyelid width (UEW), and distance between nostril and eye (DNE; Table 4), and differ from *R. napoensis* in body size (SVL), head length (HL), internarial distance (IND), and distance between nostril and eye (Table 5). PCA analysis on Hainan populations and *R. rhodopus* revealed that the first two principal components accounted for 66.13% of the total variance (Table 6), and loadings for PC2 were heavily loaded on TD and UEW, which separated Hainan samples from *R. rhodopus* along the PC2 axis (Fig. 5a). PCA analysis on Hainan populations and *R. napoensis* showed that loadings for PC2 were heavily loaded on HL, which can effectively separate Hainan populations from *R. napoensis* along the PC2 axis (Fig. 5b). Additionally, morphological comparison indicated that specimens from Hainan can be distinguished from known members of *R. rhodopus* and *R. bipunctatus* complexes and other related species of *Rhacophorus* by a series of characters (see below).

Based on the above molecular and morphological evidence, we considered that misidentifications were involved in the *R. rhodopus* and *R. bipunctatus* complexes, and herein, the clade consisting of specimens from Hainan and central Vietnam (Clade A) is described as a new species.

Table 2. Mean uncorrected pairwise distances (%) between clades of *Rhacophorus rhodopus* and *R. bipunctatus* complexes and related species based on 16S rRNA sequences.

ID	Species	1	2	3	4	5	6	7	8	9	10
1	Clade A (*R. qiongica* **sp. nov.**)										
2	Clade B (*R. napoensis*)	6.0									
3	Clade C (*R. rhodopus*)	6.7	7.6								
4	Clade D (*R.* '*rhodopus*')	8.0	7.3	5.3							
5	Clade E (*R.* '*bipunctatus*')	7.4	6.0	7.9	6.7						
6	Clade F (*R. bipunctatus*)	9.2	7.0	8.7	8.3	9.1					
7	*R. helenae*	7.9	7.1	9.6	7.3	6.8	7.4				
8	*R. kio*	8.2	7.7	9.9	8.4	8.2	8.7	4.5			
9	*R. norhayatiae*	7.4	7.0	7.5	6.5	7.7	9.5	7.3	8.3		
10	*R. borneensis*	6.1	5.8	8.0	6.2	6.2	8.6	4.9	6.8	4.8	
11	*R. reinwardtii*	5.7	5.3	7.1	5.9	5.2	6.8	6.3	7.5	4.0	4.5

Table 3. Measurements (mm) of *Rhacophorus qiongica* sp. nov., *R. rhodopus*, and *R. napoensis*.

Species	Voucher	SEX	SVL	HL	HW	SL	IND	IOD	UEW	ED	TD	DNE	FHL	TL	TFL	FL
Rhacophorus qiongica **sp. nov.**	GXNU YU000690	M	35.5	11.4	13.1	5.4	3.7	4.6	3.7	4.7	2.3	2.8	17.3	18.1	25.3	16.5
Rhacophorus qiongica **sp. nov.**	GXNU YU000691	M	37.8	12.0	13.2	5.5	3.8	4.2	3.6	4.7	2.3	2.6	18.2	18.6	25.6	16.7
Rhacophorus qiongica **sp. nov.**	GXNU YU000693	M	37.8	12.3	13.4	5.6	3.9	4.4	3.9	4.7	2.2	2.8	18.5	21.0	27.5	17.6
Rhacophorus qiongica **sp. nov.**	GXNU YU000696	M	36.1	11.1	12.7	5.4	3.9	4.1	3.7	4.8	2.0	2.8	17.8	18.7	25.8	16.6
Rhacophorus qiongica **sp. nov.**	GXNU YU000697	M	35.1	11.1	12.7	5.2	3.8	4.0	3.8	4.7	1.9	2.7	17.2	17.2	24.3	15.6
Rhacophorus qiongica **sp. nov.**	GXNU YU000698	F	49.3	14.6	16.8	7.4	4.8	5.5	4.2	5.4	2.6	3.7	23.6	24.9	34.3	23.1
Rhacophorus qiongica **sp. nov.**	GXNU HN110501	M	38.2	11.5	13.6	5.4	3.6	4.4	3.5	4.8	2.3	2.7	17.3	17.9	24.5	16.2
Rhacophorus qiongica **sp. nov.**	GXNU HN110502	M	38.1	11.0	13.6	5.2	3.7	4.2	3.5	4.7	2.2	2.8	18.1	19.2	25.5	16.8
Rhacophorus qiongica **sp. nov.**	GXNU HN110503	M	37.8	11.7	13.7	5.1	3.6	4.3	3.8	4.7	2.1	2.7	18.0	18.4	25.1	16.8
Rhacophorus rhodopus	GXNU YU090185	M	33.1	10.7	11.5	5.0	3.5	3.8	2.6	4.0	2.1	2.1	16.4	16.5	22.4	14.8
Rhacophorus rhodopus	GXNU YU090186	M	33.6	11.2	12.4	4.8	3.8	4.1	2.8	4.2	2.3	2.3	17.0	17.1	23.2	15.5
Rhacophorus rhodopus	GXNU YU090187	M	33.4	10.6	12.0	4.6	3.6	4.0	3.0	4.3	2.0	2.1	16.4	16.5	22.8	14.8
Rhacophorus rhodopus	GXNU YU090188	M	38.7	11.8	13.8	5.5	3.9	4.3	3.2	4.9	2.5	2.5	18.0	18.3	25.4	16.8
Rhacophorus rhodopus	GXNU YU090189	F	50.2	14.9	17.6	7.5	5.4	5.9	4.1	5.6	3.3	3.3	25.6	24.4	35.4	23.6
Rhacophorus rhodopus	GXNU YU090190	M	37.4	11.7	12.8	5.2	4.0	4.4	2.6	4.0	2.4	2.5	18.2	18.5	26.5	17.2
Rhacophorus rhodopus	GXNU YU090194	M	35.5	10.8	12.5	4.9	3.8	4.1	2.8	4.0	2.5	2.4	17.0	16.4	23.4	15.6
Rhacophorus napoensis	GXNU YU000169	M	39.9	12.8	14.1	5.7	4.3	4.4	4.0	4.9	2.1	2.8	19.9	19.2	28.4	18.7
Rhacophorus napoensis	GXNU YU000170	M	44.2	15.3	16.2	6.9	4.7	4.7	4.5	5.3	2.5	3.0	20.1	20.8	29.2	19.2
Rhacophorus napoensis	GXNU YU000171	M	41.2	14.5	15.3	6.4	4.6	4.6	4.3	5.2	2.5	2.8	20.7	19.9	28.7	19.0
Rhacophorus napoensis	GXNU YU000172	M	39.7	13.1	14.2	5.9	4.3	4.3	4.1	5.2	2.3	2.8	18.9	19.1	26.7	17.4
Rhacophorus napoensis	GXNU YU000173	M	41.4	13.9	15.2	6.3	4.5	4.5	4.0	4.9	2.3	2.9	20.6	20.5	28.3	18.7

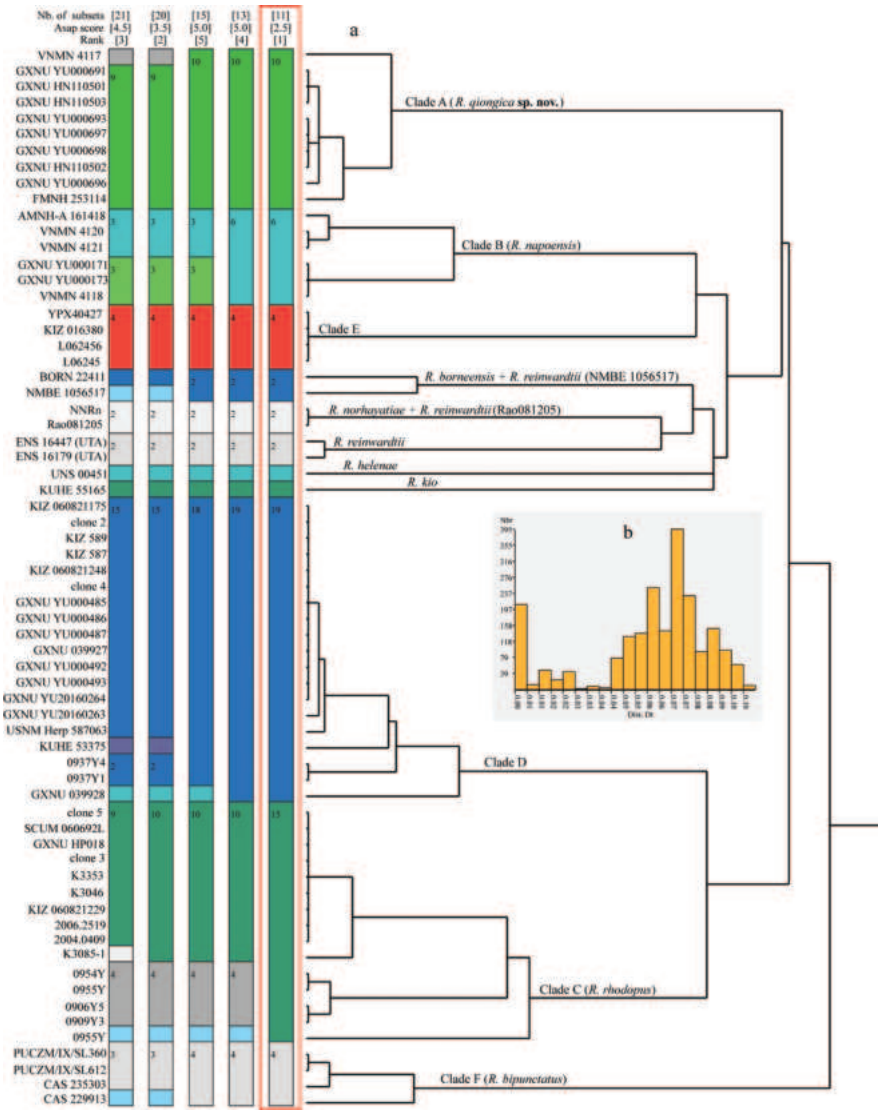

Figure 3. ASAP species delimitation based on 16S rRNA sequences used in this study. The best partition with the lowest score is highlighted with a red frame.

Table 4. Results of the t-test between male specimens of *Rhacophorus qiongica* sp. nov. and *R. rhodopus* based on the size-adjusted data except SVL.

Character	Mean ± SD (n = 8)	Mean ± SD (n = 6)	Levene's test		t-test	
	***R. qiongica* sp. nov.**	***R. rhodopus* (clade C)**	**F**	**p-value**	**t**	**p-value**
SVL	37.1 ± 1.3	35.3 ± 2.3	4.016	0.068	1.825	0.093
HL	0.311 ± 0.012	0.316 ± 0.011	0.022	0.883	−0.816	0.430
HW	0.358 ± 0.006	0.354 ± 0.009	0.871	0.369	0.774	0.454
SL	0.144 ± 0.006	0.142 ± 0.005	1.036	0.329	0.872	0.400
IND	0.101 ± 0.005	0.107 ± 0.004	2.199	0.164	−2.094	0.058
IOD	0.115 ± 0.006	0.117 ± 0.004	0.143	0.712	−0.470	0.647
UEW	0.100 ± 0.006	0.080 ± 0.007	0.019	0.891	5.581	0.000*
ED	0.128 ± 0.005	0.120 ± 0.009	3.321	0.093	2.127	0.055
TD	0.058 ± 0.004	0.065 ± 0.004	0.021	0.887	−3.488	0.004*
DNE	0.074 ± 0.004	0.066 ± 0.002	1.212	0.293	4.948	0.000*
FHL	0.481 ± 0.013	0.487 ± 0.014	0.034	0.857	−0.892	0.390
TL	0.503 ± 0.026	0.488 ± 0.018	0.392	0.543	1.181	0.261
TFL	0.687 ± 0.030	0.679 ± 0.020	1.908	0.192	0.601	0.559
FL	0.448 ± 0.014	0.447 ± 0.011	0.539	0.477	0.106	0.917

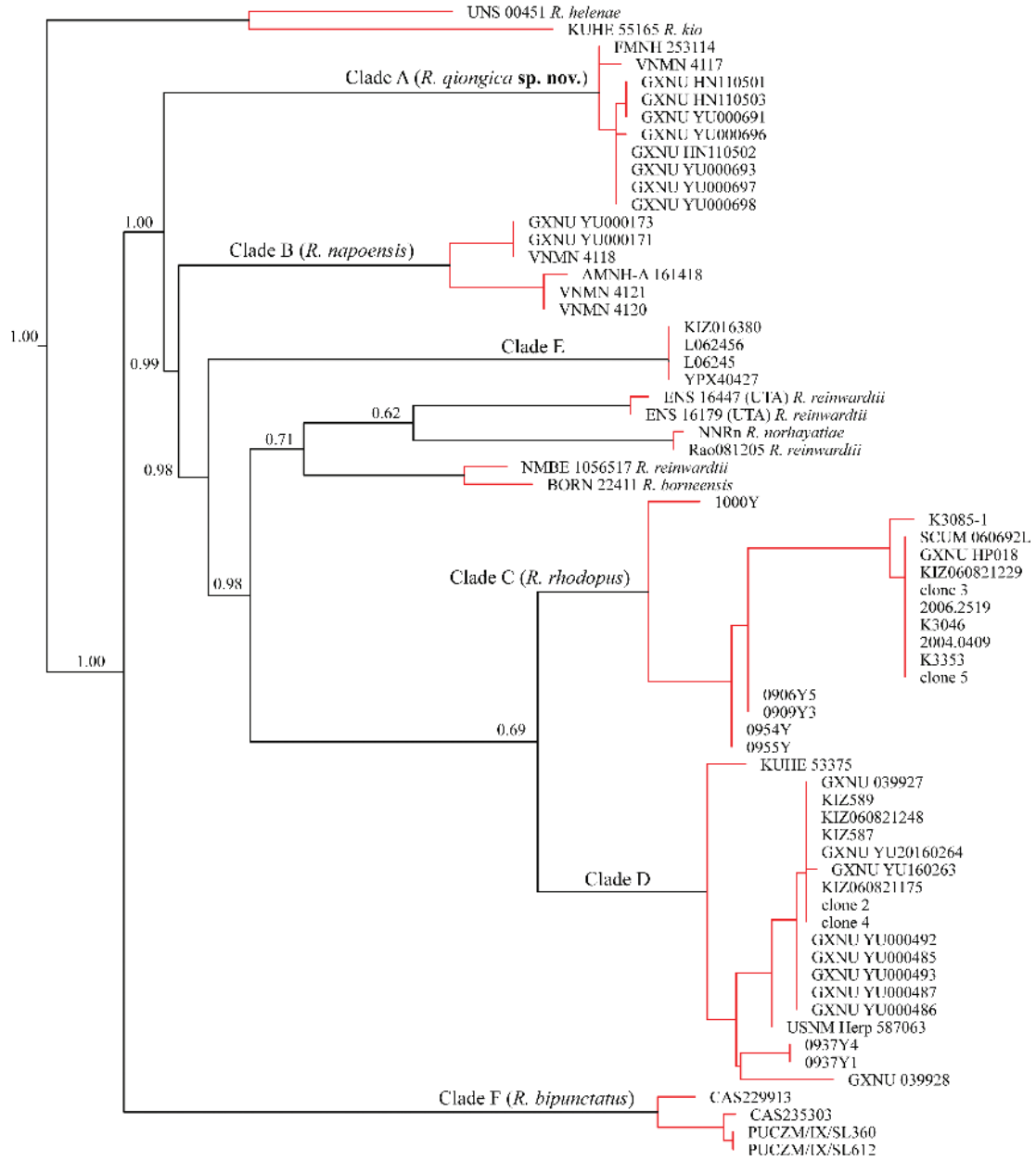

Figure 4. mPTP species delimitation based on ML tree generated from 16S rRNA sequences. The support values above the branches indicate the fraction of sampled delimitations in which a node was part of the speciation process.

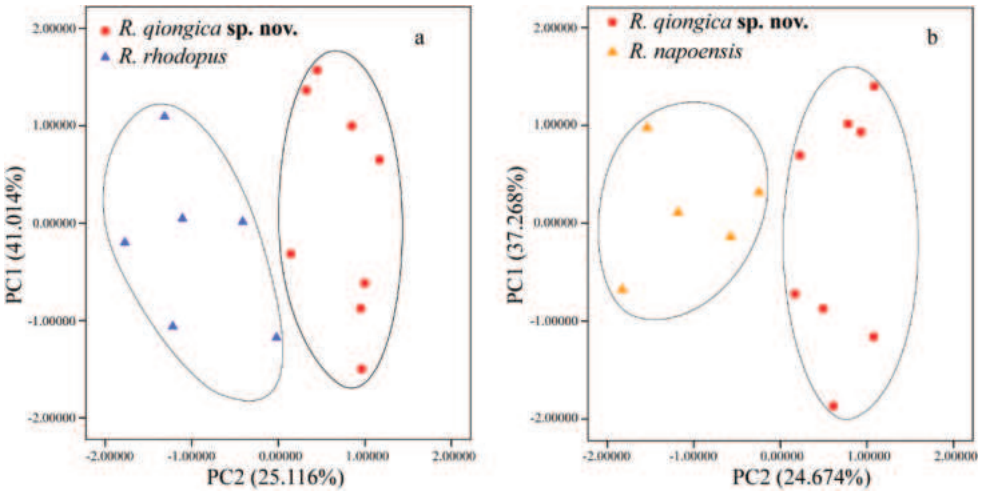

Figure 5. The scatter plot of the principal component analysis based on size-adjusted morphological data from males of the new species plus *R. rhodopus* (**a**) and data from males of the new species plus *R. napoensis* (**b**).

Table 5. Results of the t-test between male specimens of *Rhacophorus qiongica* sp. nov. and *R. napoensis* based on the size-adjusted data except SVL.

Character	Mean ± SD (n = 8)	Mean ± SD (n = 5)	Levene's test		t-test	
	R. qiongica sp. nov.	*R. napoensis* (clade B)	F	p-value	t	p-value
SVL	37.1 ± 1.3	41.3 ± 1.8	0.053	0.823	−5.006	0.000*
HL	0.311 ± 0.012	0.337 ± 0.012	0.019	0.892	−3.778	0.003*
HW	0.358 ± 0.006	0.363 ± 0.007	0.364	0.559	−1.420	0.183
SL	0.144 ± 0.006	0.151 ± 0.005	0.365	0.558	−1.897	0.084
IND	0.101 ± 0.005	0.109 ± 0.002	7.240	0.021	−3.387	0.008*
IOD	0.115 ± 0.006	0.109 ± 0.002	1.146	0.307	2.267	0.045*
UEW	0.100 ± 0.006	0.101 ± 0.003	4.071	0.069	−0.536	0.603
ED	0.128 ± 0.005	0.124 ± 0.005	0.012	0.916	1.480	0.167
TD	0.058 ± 0.004	0.057 ± 0.003	0.282	0.606	0.892	0.391
DNE	0.074 ± 0.004	0.069 ± 0.001	4.361	0.061	2.756	0.019*
FHL	0.481 ± 0.013	0.486 ± 0.020	2.125	0.173	−0.572	0.579
TL	0.503 ± 0.026	0.482 ± 0.009	2.803	0.122	1.705	0.116
TFL	0.687 ± 0.030	0.685 ± 0.020	1.570	0.236	0.156	0.879
FL	0.448 ± 0.014	0.451 ± 0.015	0.003	0.957	−0.317	0.757

Table 6. Factor loadings of first two principal components of 13 size-adjusted morphometric characteristics of male specimens of *Rhacophorus qiongica* sp. nov., *R. rhodopus*, and *R. napoensis*.

Character	*R. qiongica* sp. nov. and *R. rhodopus*		*R. qiongica* sp. nov. and *R. napoensis*	
	PC1	PC2	PC1	PC2
Eigenvalue	5.332	3.265	4.845	3.208
% variation	41.014%	25.116%	37.268%	24.674%
HL	0.724	−0.399	0.425	−0.852
HW	0.354	0.351	0.270	−0.506
SL	0.682	0.113	0.590	−0.597
IND	0.604	−0.577	0.729	−0.573
IOD	0.603	−0.269	0.437	0.615
UEW	0.459	0.853	0.785	−0.185
ED	0.419	0.715	0.458	0.460
TD	−0.111	−0.790	0.063	0.186
DNE	0.507	0.675	0.500	0.738
FHL	0.791	−0.409	0.775	−0.029
TL	0.794	0.112	0.544	0.529
TFL	0.891	−0.079	0.907	0.217
FL	0.885	−0.246	0.849	0.108

Taxonomy

Rhacophorus qiongica sp. nov.

https://zoobank.org/182E48F4-9743-4B7F-A825-FA63499F15F2

Figs 6–9

Rhacophorus rhodopus — Fei 1999; Fei et al. 2004, 2009, 2010, 2012; Shi 2011; Nguyen et al. 2014.

Rhacophorus bipunctatus — Orlov et al. 2002.

Type material. ***Holotype.*** GXNU YU000691, adult male, collected on 14 July 2023 by Lingyun Du from Diaoluo Mt., Lingshui, Hainan, China (18°43'28"N, 109°52'12"E, ca 914 m a.s.l.).

Paratypes. GXNU YU000690, an adult male, collected at the same time as the holotype from the type locality by Lingyun Du and Jiaqi Luo; GXNU HN110501–HN110503, three adult males, collected on 20 July 2021 by Fanrong Xiao from the type locality; and three adult males (GXNU YU000693, GXNU YU000696, GXNU

YU000697) and an adult female (GXNU YU000698) collected on 11 July 2023 by Qiumei Mo and Chunyi Pang from Yinggeling, Hainan, China (19°2'24"N, 109°34'12"E, ca 670 m a.s.l.).

Etymology. The specific name *qiongica* is derived from Qiong (琼), referring to Hainan, China, and meaning good and beautiful in Chinese. The specific name means that this species is very beautiful, and in China, it is distributed in Hainan. We suggest the English common name "Hainan flying frog" and the Chinese common name "琼树蛙 (Qióng Shù Wā)".

Diagnosis. The new species is assigned to *Rhacophorus* by the presence of intercalary cartilage between terminal and penultimate phalanges of digits, terminal phalanges of fingers and toes Y-shaped, the tip of the digits expanded into disks with circummarginal grooves, fingers webbed, tarsal projections present, dermal folds along the forearm and tarsus present, and a horizontal pupil (Jiang et al. 2019). *Rhacophorus qiongica* sp. nov. differs from its congeners by a combination of the following characters: 1) medium body size (adult males SVL 35.1–38.2 mm); 2) dorsal surface red brown; 3) entire web between fingers and toes; 4) webbing between toes purely scarlet; 5) small black blotches on flank; 6) bands on limbs distinct; 7) throat smooth; 8) absence of dermal appendage on snout tip; 9) absence of small black spots on head sides; 10) palm smooth without small tubercles; and 11) tibiotarsal articulation reaching beyond eye.

Description of holotype. Adult male, body size medium (SVL 37.8 mm); head width (HW 13.2 mm) longer than head length (HL 12.0 mm); snout blunt pointed, sloping in profile, protruding beyond the margin of lower jaw in ventral view; snout length (SL 5.5 mm) longer than diameter of eye (ED 4.4 mm); canthus rostralis distinct, curved; loreal region oblique, concave; nostril oval, lateral, slightly protuberant, slightly closer to tip of snout than to eye; internarial space (IND 3.8 mm slightly smaller than interorbital distance (IOD 4.2 mm), nearly equal to the width of the upper eyelid (UEW 3.6 mm); pupil horizontal; pineal ocellus absent; tympanum distinct (TD 2.3 mm), rounded, about half eye diameter (ED 4.4 mm); supratympanic fold narrow, flat; tongue cordiform, attached anteriorly, notably notched posteriorly; choanae oval; vomerine teeth present in two series, touching the inner front edges of the choanae; an internal single subgular vocal sac; a vocal sac opening on the floor of the mouth at each corner.

Forelimbs thin, length of forearm and hand (FHL 18.2 mm) is about half snout-vent length; relative length of fingers I < II < IV < III; tips of all fingers expand into discs with circummarginal and transverse ventral grooves, disc of finger I smaller than discs of other fingers; entire web between fingers, webbing formula: I2–2II1–1.5III1–1IV; subarticular tubercles rounded and prominent, formula 1, 1, 2, 2, proximal one smaller than distal one on the third and fourth fingers; supernumerary tubercles below the base of finger absent; metacarpal tubercle single, inner, oval and prominent (Fig. 7).

Hindlimbs slender and long, heels overlapping when legs at right angle to body, tibiotarsal articulation reaching beyond eye; tibia length (TL 18.6 mm) nearly equal to length of forearm and hand (FHL 18.2 mm), longer than foot length (FL 16.7 mm), and shorter than length of tarsus and foot (TFL 25.6 mm); relative length of toes I < II < III < V < IV; tips of all toes expanded into discs with circummarginal and transverse ventral grooves; entire web between toes, webbing formula I1–1II1–1III1–1IV1–1V; subarticular tubercles rounded and prominent, formula 1, 1, 2, 3, 2; supernumerary tubercles absent; single inner metatarsal tubercle, oval (Fig. 7).

Dorsal skin smooth with very fine granules; throat and ventral surface of forelimbs smooth; chest, belly, and ventral surface of thighs granular (Figs 6, 7); dermal folds on forearm, tarsus, heels, and vent present.

Coloration in life. Iris light brown; dorsal surface red brown, mottled with two discontinued rows of dark patches and scattered with small black spots on dorsum; dark brown bands and small black spots on dorsal surface of limbs; upper part of flank orange red and lower part of flank orange yellow, scattered with a few small black blotches; skin of ventral surface semi-transparent, mottled with orange yellow on throat and belly; ventral, anterior, and posterior surfaces of limbs orange yellow; discs of fingers and dorsal surface of fingers I–III orange yellow; discs of toes and toes I–IV red; web between fingers yellow, mottled with red; web between toes completely red.

Figure 6. Lateral, dorsal, and ventral views of the holotype of *R. qiongica* sp. nov. (GXNU YU000691) in life.

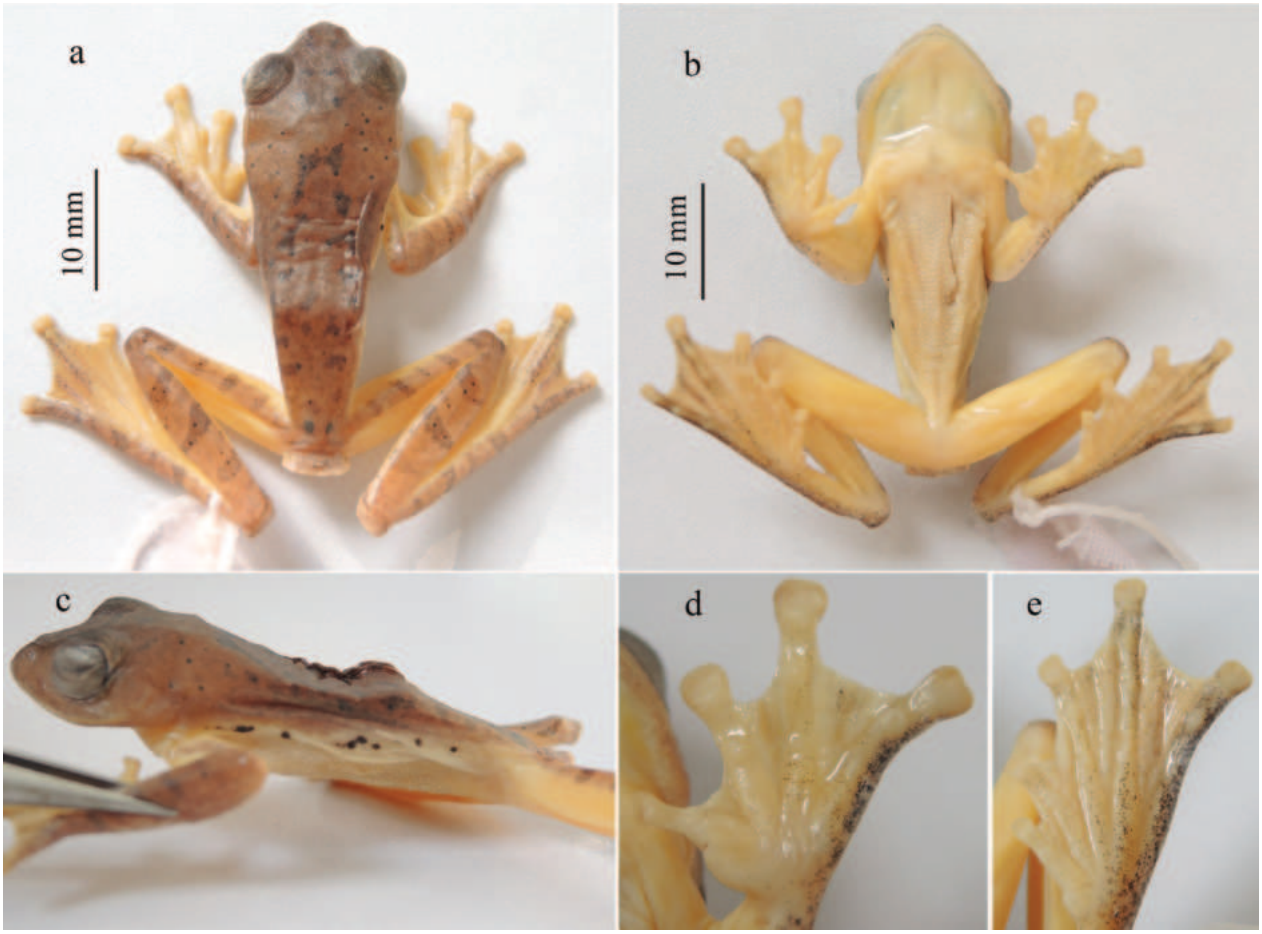

Figure 7. Dorsal, ventral, and lateral views of the holotype of *R. qiongica* sp. nov. (**a–c**) in preservative and ventral views of its hand (**d**) and foot (**e**).

Color of holotype in preservative. The color faded, but the pattern remained the same as in life. Dorsal surface brown, with dark patches and spots; dorsal side of limbs barred with dark brown; throat, chest, belly, webbing, ventral surface of limbs, and anterior and posterior parts of thighs faded to yellowish; a few small black blotches on flank.

Sexual dimorphism. The body size of males is smaller than that of female; adult males have an internal single subgular vocal sac with a pair of slit-like openings on the floor of the mouth at each corner. Additionally, adult males have a milk-white nuptial pad on the inner side of the base of finger I.

Morphological variation. The number of small black spots on the flank varied among specimens. The holotype GXNU YU000691 and two paratypes (GXNU YU000698 and GXNU HN110502) have multiple small black spots on flank; paratypes GXNU YU000690 and GXNU YU000697 have no black spots on flank; and paratypes GXNU YU000693 and GXNU YU000696 have two small black spots on flank (Fig. 8). Additionally, dorsal color pattern also varied among specimens, as the two paratypes GXNU YU000696 and GXNU YU000698 have yellowish-brown blotches on dorsal surfaces of the body and limbs (Fig. 9).

Distribution and ecology. The species is distributed in Hainan, China and Gia Lai, Vietnam. In Hainan, the species was found usually in shrubs and small arbors at elevations ranging from 600 to 850 m (Shi 2011; as *R. rhodopus*) and called from 19:00 to 03:00 every night during the breeding season (from May to July), with a peak at about 22:00 (Sun et al. 2017; as *R. rhodopus*). The types in this study were found in roadside bushes ca. 1–2 m above the ground (Fig. 10). There were temporary puddles under the bushes, and there is a lake (Tianchi) and a stream nearby the road in the type locality. *Chirixalus doriae* Boulenger, 1893, *Kurixalus hainanus* (Zhao, Wang & Shi, 2005), and *Polypedates megacephalus* Hallowell, 1861 were also found in sympatry at the type locality.

Comparisons. Currently, there are three known species in the *R. rhodopus* and *R. bipunctatus* complexes, namely *R. bipunctatus*, *R. napoensis*, and *R. rhodopus*. The new species differs from *R. bipunctatus* by smaller body size (male SVL 35.1–38.2 mm, n = 8 vs. 37.8–50.4 mm, n = 28; Table 7), dorsal surface red brown (vs. green; Fig. 11), spots on flanks small (vs. large; Fig. 11b), bands on limbs distinct (vs. indistinct), and throat smooth (vs. granular; Bordoloi et al. 2007); from *R. napoensis* by smaller body size (male SVL 35.1–38.2 mm [37.1 ± 1.3, n = 8] vs.

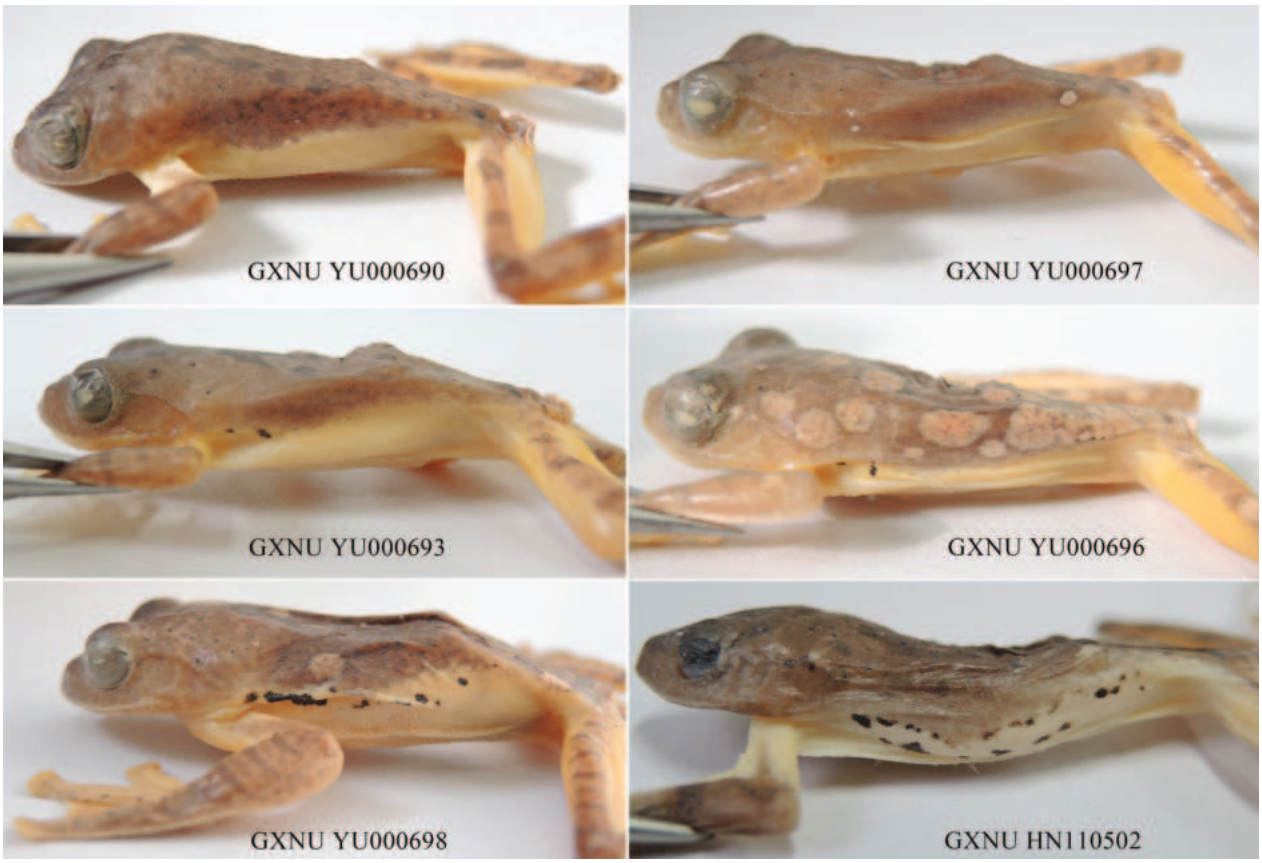

Figure 8. Variation of black spots on flank among paratypes of *R. qiongica* sp. nov. from Hainan, China.

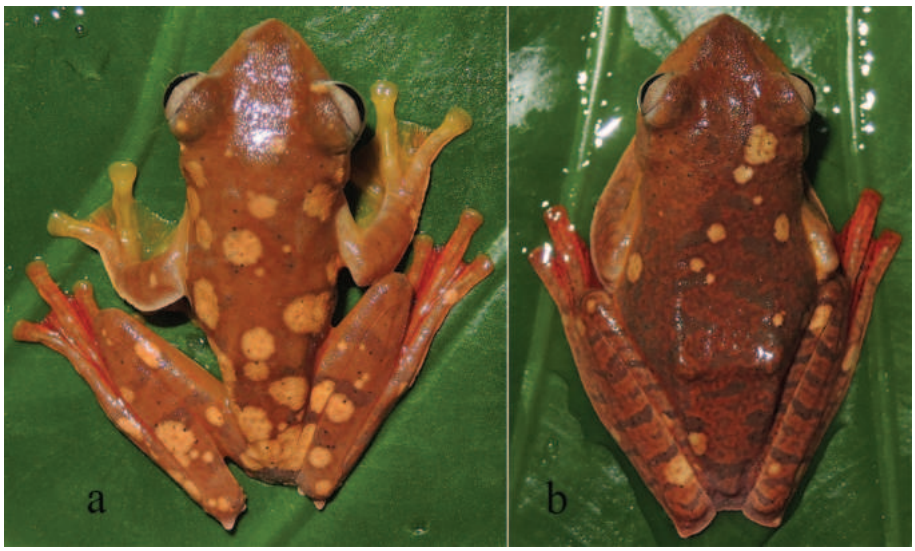

Figure 9. Dorsal view of paratypes GXNU YU000696 (**a**) and GXNU YU000698 (**b**) in life.

39.7–44.2 mm [41.3 ± 1.8, n = 5]), snout pointed without dermal appendage on tip (vs. snout pointed with a dermal appendage on tip; Fig. 11), black spots on flanks small (vs. large; Fig. 11), and throat smooth (vs. granular; Fig. 11); and from *R. rhodopus* (Clade C) by black spots on axillar and flanks small (vs. usually large), absence of small black spots on head sides (vs. present; Fig. 12), palm smooth without small tubercles (vs. palm rough with rows of small tubercles; Fig. 12), smaller tympanum, wider upper eyelid, larger distance between nostril and eye (Table 4), and tibiotarsal articulation reaching beyond eye (vs. tibiotarsal articulation reaching eye).

Both the present and previous phylogenetic analyses revealed that *R. norhayatiae*, *R. reinwardtii*, *R. kio*, *R. borneensis*, and *R. helenae* are imbedded in the *R. rhodopus* and *R. bipunctatus* complexes. The new species can be easily distinguished from these five species by the dorsal surface being red brown (vs. green) and the web between toes being red with no black pigmentation (vs. black pigmentation present).

Table 7. Morphological comparison between the new species and members of *Rhacophorus rhodopus* and *R. bipunctatus* complexes. Characters are: ① dorsal color: 0 = brown, 1 = green; ② black spots on flank: 0 = small, 1 = large; ③ bands on limbs: 0 = distinct, 1 = indistinct; ④ throat: 0 = smooth, 1 = granular; ⑤ snout: 0 = pointed without appendage on tip, 1 = pointed with appendage on tip; ⑥ black spots on head side: 0 = absent, 1 = present; ⑦ palm: 0 = smooth without tubercles, 1 = rough with tubercles; ⑧ tibiotarsal articulation: 0 = reaching beyond eye, 1 = reaching eye. "?" means unknown.

Species	Male SVL	①	②	③	④	⑤	⑥	⑦	⑧
R. qiongica sp. nov.	35.1–38.2 (37.1 ± 1.3, n = 8)	0	0	0	0	0	0	0	0
R. rhodopus	33.1–38.7 (35.3 ± 2.3, n = 6)	0	1	0	0	0	1	1	1
R. bipunctatus	37.8–50.4 (n = 28)	1	1	1	1	0	?	0	0
R. napoensis	39.7–44.2 (41.3 ± 1.8, n = 5)	0	1	0	1	1	1	1	0

Discussion

The taxonomy within the *R. rhodopus* and *R. bipunctatus* complexes is complicated owing to the similar external morphology among members of these two complexes, which has heavily hampered the identification of species and understanding of the species boundary in these two complexes. For example, the Xizang population was once recorded as *R. rhodopus* (e.g., Fei et al. 2010; Li et al. 2012) or *R. bipunctatus* (Che et al. 2020); Nguyen et al. (2008) and Poyarkov et al. (2021) suggested that existing records of these two complexes from Vietnam are actually of *R. rhodopus*, but it has been revealed that Vietnamese *R. rhodopus* may represent a cryptic species (Li et al. 2012), suggesting that a species delimitation within these two complexes based on broad sampling is necessary. In this study, based on newly collected samples and previously published data,

Figure 10. Habitat of *R. qiongica* sp. nov. at the type locality.

our phylogenetic analyses revealed that the *R. rhodopus* and *R. bipunctatus* complexes contain six distinct clades (A–F), and they were assigned to six species by the analysis of species delimitation, indicating the species diversity of these two complexes was underestimated and the distribution range of members of these two complexes needs to be re-defined.

According to previous phylogenetic analyses (Yu et al. 2007; Li et al. 2012), there are two distinct clades (C and D) in Yunnan, China. Clade C contains samples from southern Yunnan, China, northern Laos (Phongsali and Louangphrabang), northern (Phetchabun, Phitsanulok, and Chiang Mai) and central (Chachoengsao) Thailand. Undoubtedly, this clade represents the true *R. rhodopus* because the topotypes of this species were grouped in it. Clade D contains samples from western and southwestern Yunnan, central Myanmar (Mandalay), central Thailand (Prachuap Khiri Khan), and Malaysia. Although it was recovered as the sister taxon to the clade C that represents the true *R. rhodopus*, genetic divergence in 16S sequences between them reaches 5.3%, which is greater than the distance between *R. helenae* and *R. kio* (4.5%), the distance between *R. helenae* and *R. borneensis* (4.9%),

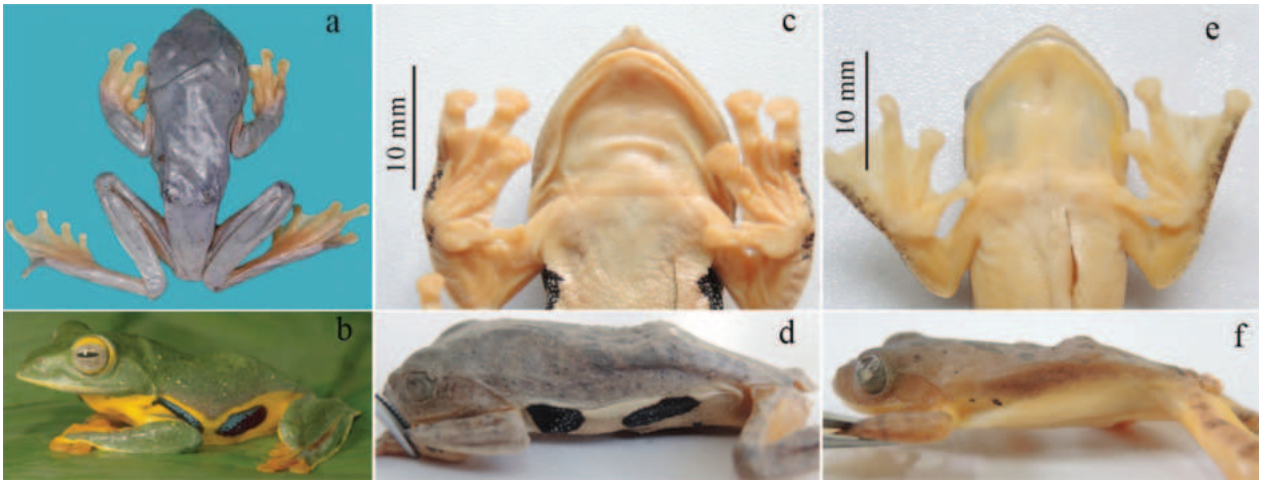

Figure 11. Dorsal (**a.** BMNH 1872.4.17.127, lectophoront from Khasi Hills, India) and lateral (**b.** CAS 229893, collected from Putao, Kachin State, Myanmar) views of *R. bipunctatus*, throat (**c**) and lateral view (**d**) of *R. napoensis* (GXNU YU000170), and throat (**e**) and lateral view (**f**) of *R. qiongica* sp. nov. (GXNU YU000693). The images of **a** and **b** were reproduced from Bordoloi et al. (2007) and Wilkinson et al. (2005), respectively.

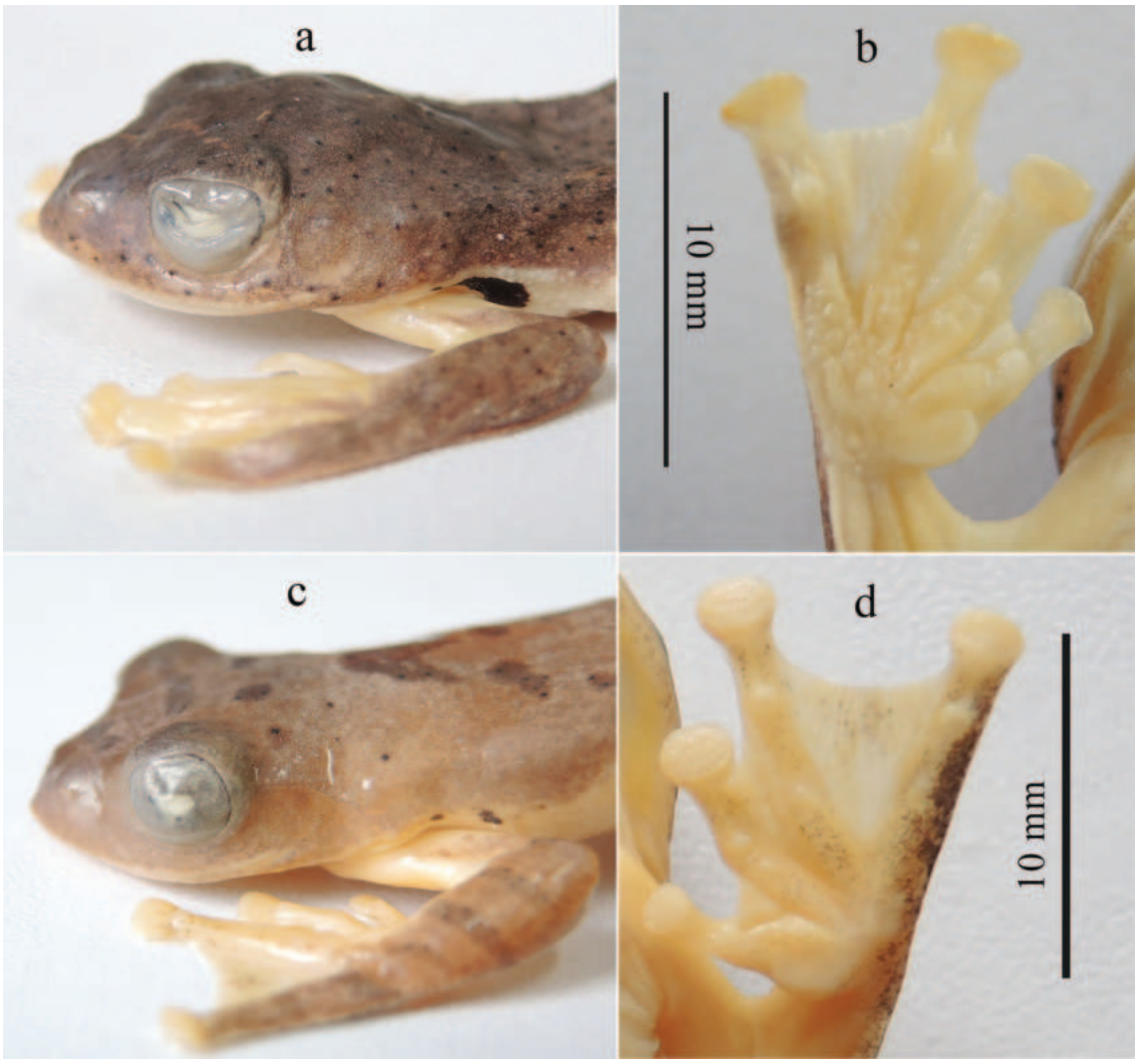

Figure 12. Head side and ventral surface of the hand of *R. rhodopus* (**a, b.** GXNU YU090186) and *R. qiongica* sp. nov. (**c, d.** GXNU YU000693).

and the distance between *R. norhayatiae*, *R. borneensis*, and *R. reinwardtii* (4.0%–4.8%; Table 2), and they were assigned into two different species by the analyses of species delimitation. Therefore, we consider that clade D probably represents a cryptic species pending additional morphological studies.

Rhacophorus bipunctatus was originally described from Khasi Hills, Northeast India. Previous phylogenetic analyses (Li et al. 2012; Che et al. 2020) revealed that samples of *R. bipunctatus* from Myanmar and southern Xizang, China form two distinct clades. Owing to the absence of *R. bipunctatus* samples from Northeast India in these two previous studies, it is confusing which clade represents the true *R. bipunctatus*. In this study, we found that *R. bipunctatus* from Northeast India (Mizoram), north Myanmar (Kachin), and west Myanmar (Chin) form a clade (Clade F), whereas samples from southeastern Xizang form an independent clade (Clade E). Considering that Mizoram is close to Khasi Hills, the type locality of *R. bipunctatus*, and records from there have been confirmed based on morphology (Decemson et al. 2020), we consider that clade F is true *R. bipunctatus* and the Xizang population (Clade E) probably represents a cryptic species. Morphologically, the Xizang population differs from *R. rhodopus* and *R. qiongica* sp. nov. by throat granular (Che et al. 2020) since the latter two are smooth (Liu and Hu 1960; this study), and from *R. napoensis* by smaller body size (male SVL 31.6–38.7 mm, mean = 34.9 mm, n = 10), head slightly longer than wide, and tibiotarsal articulation reaching eyes (Che et al. 2020) (vs. SVL 39.7–44.2 mm [mean = 41.3, n = 5] in males, head wider than long, and tibiotarsal articulation reaching snout; Li et al. 2022). Additionally, bands on limbs in the Xizang population are distinct (Che et al. 2020), but bands on limbs in specimens of *R. bipunctatus* from northeastern India and Myanmar are indistinct (Bordoloi et al. 2007; Fig. 11).

Records in Vietnam were once placed in *R. bipunctatus* or *R. rhodopus*, and recently, Poyarkov et al. (2021) conjectured that all existing records of *R. rhodopus* and *R. bipunctatus* complexes in Vietnam are actually of *R. rhodopus*. In this study, we found that there are two

distinct clades in Vietnam (Clades A and B). The samples from northern Vietnam formed Clade B with *R. napoensis*, indicating that they actually refer to *R. napoensis*, while the samples from central Vietnam (Gia Lai) and Hainan, China formed Clade A, which is morphologically distinguishable from other known species of *R. rhodopus* and *R. bipunctatus* complexes and is described as *R. qiongica* sp. nov. herein. The amphibian and reptile flora of Hainan Island is clearly dominated by Oriental species (Shi 2002; Wang et al. 2004, 2009), and the species composition seems to be closely related to the southern part of the Chinese mainland and Vietnam. Although Hainan is separated from the Asian mainland by the Beibu Gulf and Qiongzhou Strait, they have been joined frequently over the past million years (Ali 2018). *Rhacophorus qiongica* sp. nov. likely colonized Hainan via landbridge dispersal during Pleistocene climatic oscillations, which has been suggested for another tree frog in Hainan, *K. hainanus*, a species widely distributed in Vietnam and southern China (Yu et al. 2020).

Like Li et al. (2012) and Chan et al. (2018), phylogenetic relationships within *R. rhodopus* and *R. bipunctatus* complexes were also not resolved well in the present study. Our results strongly supported that the clade containing topotypes of *R. rhodopus* (Clades C) is sister to the clade containing samples from western Yunnan (Clade D), and the two together are sister to the clade composed of samples from Xizang, China (Clade E), which is consistent with Li et al. (2012). Chan et al. (2018) also recovered the clade containing samples from Laos (labeled as Clade 2 in Fig. 4 of Chan et al. (2018) and corresponds to Clade C of this study) as sister to the clade containing samples from Malaysia (labeled as Clade 3 in Fig. 4 of Chan et al. (2018) and corresponds to Clade D of this study) with strong support, but they recovered these two clades together as sister to the clade containing samples from Hainan, China and Gia Lai, Vietnam (labeled as Clade 1 in Fig. 4 of Chan et al. (2018) and corresponds to Clade A of this study). This difference may be caused by the absence of samples from Xizang, China in Chan et al. (2018). In addition, Chan et al. (2018) did not resolve the phylogenetic placement of the clade of the *R. reinwardtii* group, but both the present study and Li et al. (2012) recovered that the clade consisted of the *R. reinwardtii* species group as sister to the group formed by clades C–E with strong support. Neither this nor the two previous studies (Li et al. 2012; Chan et al. 2018) resolved the phylogenetic placement of the three clades corresponding to *R. bipunctatus*, *R. napoensis*, and *R. qiongica* sp. nov., respectively. Therefore, more studies are needed to resolve the phylogenetic relationship among the *R. rhodopus* and *R. bipunctatus* complexes.

Additionally, it is worth noting that some old GenBank sequences of *R. reinwardtii* need to be updated with the correct species name. *Rhacophorus norhayatiae* and *R. borneensis* were described as distinct species by Chan and Grismer (2010) and Matsui et al. (2013), respectively, and both of them were confused with *R. reinwardtii* prior to their naming (Chan and Grismer 2010; Matsui et al. 2013). The type locality of *R. reinwardtii* is Mount Pangerango, Java, Indonesia. In this study, we found that the two samples under the name of *R. reinwardtii* from Malaysia (Rao081205 and NMBE 1056517) were not grouped together with the lineage of *R. reinwardtii* from Indonesia (Java and Sumatra), but clustered together with *R. norhayatiae* and *R. borneensis*, respectively. The sequence from the specimen Rao081205 (JX219443) was submitted to GenBank in June 2012, posterior to the taxonomic revision of the *R. reinwardtii*/*R. norhayatiae* group (Chan and Grismer 2010), and the sequence from the specimen NMBE 1056517 (JN377366) was submitted to GenBank in July 2011, prior to the taxonomic revision of the *R. reinwardtii*/*R. borneensis* group (Matsui et al. 2013). These evidences suggest that the specimen Rao081205 is a misidentification of *R. norhayatiae*, and the name of the specimen NMBE 1056517 is not yet updated in GenBank. This result is partially consistent with the viewpoint of Chan and Grismer (2010) that records of *R. reinwardtii* from Malaya are referable to *R. norhayatiae*.

In summary, based on newly collected samples and previously published data, we obtained a clearer delineation of species boundaries within the *R. bipunctatus* and *R. rhodopus* complexes. We recovered six distinct clades (A–F) in these two complexes. *Rhacophorus rhodopus* (Clade C) is distributed in southern Yunnan, China, northern Laos, and northern and central Thailand; *R. bipunctatus* (Clade F) is only distributed in northeast India and western and northern Myanmar; *R. napoensis* (Clade B) is distributed in Guangxi, China and northern Vietnam; and *R. qiongica* sp. nov. (Clade A) is distributed in Hainan, China and central Vietnam. There are two cryptic species requiring additional morphological studies: one only contains samples from Motuo, Xizang, China (Clade E), and the other is distributed in western Yunnan, China, central Myanmar, central Thailand, and Malaysia (Clade D). More studies are needed to resolve the phylogenetic relationship among the *R. rhodopus* and *R. bipunctatus* complexes.

Acknowledgements

We thank Lingyun Du, Qiumei Mo, Jiaqi Luo, Chunyi Pang, and Decai Ouyang for their assistance with sample collection. This work was supported by grants from the National Natural Science Foundation of China (32060114), Guangxi Natural Science Foundation Project (2022GXNSFAA035526), Key Laboratory of Ecology of Rare and Endangered Species and Environmental Protection (Guangxi Normal University), Ministry of Education (ERESEP2022Z04), and Guangxi Key Laboratory of Rare and Endangered Animal Ecology, Guangxi Normal University (19-A-01-06).

References

Ahl E (1927) Zur Systematik der asiatischen Arten der Froschgattung *Rhacophorus*. Sitzungsberichte der Gesellschaft Naturforschender Freunde zu Berlin 1927: 35–47.

Ali JR (2018) Islands as biological substrates: Continental. Journal of Biogeography 45(5): 1003–1018. https://doi.org/10.1111/jbi.13186

AmphibiaChina (2023) The database of Chinese amphibians. Kunming Institute of Zoology (CAS), Kunming, Yunnan, China. http://www.amphibiachina.org/

Anderson J (1871) A list of the reptilian accession to the Indian Museum, Calcutta from 1865 to 1870, with a description of some new species. Journal of the Asiatic Society of Bengal 40: 12–39.

Bain RH, Nguyen QT, Doan VK (2007) New herpetofaunal records from Vietnam. Herpetological Review 38: 107–117.

Blyth E (1852) Report of Curator, Zoological Department. Journal of the Asiatic Society of Bengal 21: 341–358.

Bordoloi S, Bortamuli T, Ohler A (2007) Systematics of the genus *Rhacophorus* (Amphibia, Anura): Identity of red-webbed forms and description of a new species from Assam. Zootaxa 1653(1): 1–20. https://doi.org/10.11646/zootaxa.1653.1.1

Boulenger GA (1883) Description of new species of reptiles and batrachians in the British Museum. Annals and Magazine of Natural History (Series 5) 12: 161–167. https://doi.org/10.1080/00222938309459605

Boulenger GA (1893) Concluding report on the reptiles and batrachians obtained in Burma by Signor L. Fea dealing with the collection made in Pegu and the Karin Hills in 1887–88. Annali del Museo Civico di Storia Naturale di Genova (Serie 2) 13: 304–347.

Boulenger GA (1895) Descriptions of four new batrachians discovered by Mr. Charles Hose in Borneo. Annals and Magazine of Natural History (Series 6) 16: 169–171. https://doi.org/10.1080/00222939508680249

Chan KO, Grismer LL (2010) Re-assessment of the Reinwardt's Gliding Frog, *Rhacophorus reinwardtii* (Schlegel 1840) (Anura, Rhacophoridae) in Southern Thailand and Peninsular Malaysia and its re-description as a new species. Zootaxa 2505(1): 40–50. https://doi.org/10.11646/zootaxa.2505.1.2

Chan KO, Grismer LL, Brown RM (2018) Comprehensive multi-locus phylogeny of Old World tree frogs (Anura, Rhacophoridae) reveals taxonomic uncertainties and potential cases of over- and underestimation of species diversity. Molecular Phylogenetics and Evolution 127: 1010–1019. https://doi.org/10.1016/j.ympev.2018.07.005

Chan-ard T (2003) A Photographic Guide to Amphibians in Thailand. Bangkok, Thailand: Darnsutha Press Co., Ltd.

Chan-ard T, Cota M, Makchai S (2011) The Amphibians of the Eastern Region, With a Checklist of Thailand. National Science Museum, Bangkok, Thailand, 1–160.

Che J, Jiang K, Yan F, Zhang YP (2020) Amphibians and Reptiles in Tibet—Diversity and Evolution. Science Press, Beijing, China.

Chen JM, Prendini E, Wu YH, Zhang BL, Suwannapoom C, Chen HM, Chen HM, Jin JQ, Lemmon EM, Lemmon AR, Stuart BL, Raxworthy CJ, Murphy RW, Yuan ZY, Che J (2020) An integrative phylogenomic approach illuminates the evolutionary history of Old World tree frogs (Anura, Rhacophoridae). Molecular Phylogenetics and Evolution 145: 1–9. https://doi.org/10.1016/j.ympev.2019.106724

Dang NX, Sun FH, Lv YY, Zhao BH, Wang JC, Murphy RW, Wang WZ, Li JT (2015) DNA barcoding and the identification of tree frogs (Amphibia: Anura, Rhacophoridae). Mitochondrial DNA, Part A, DNA Mapping, Sequencing, and Analysis 27(4): 1–11. https://doi.org/10.3109/19401736.2015.1041113

Darriba D, Taboada GL, Doallo R, Posada D (2012) jModelTest 2: More models, new heuristics and parallel computing. Nature Methods 9(8): 772. https://doi.org/10.1038/nmeth.2109

Decemson H, Biakzuala L, Solanki GS, Barman BK, Lalremsanga HT (2020) The Twin-spotted Treefrog (*Rhacophorus bipunctatus* Ahl 1927) in Mizoram, India. Reptiles & Amphibians: Conservation and Natural History 27(2): 242–244. https://doi.org/10.17161/randa.v27i2.14193

Edler D, Klein J, Antonelli A, Silvestro D (2020) RaxmlGUI 2.0: A graphical interface and toolkit for phylogenetic analyses using RAxML. Methods in Ecology and Evolution 12(2): 373–377. https://doi.org/10.1111/2041-210X.13512

Ellepola G, Meegaskumbura M (2023) Diversification and biogeography of Rhacophoridae—A model testing approach. Frontiers in Ecology and Evolution 11(1195689): 1–14. https://doi.org/10.3389/fevo.2023.1195689

Fei L (1999) Atlas of Amphibians of China. Henan Science and Technology Press, Zhengzhou, China.

Fei L, Ye CY, Jiang JP, Xie F, Huang YZ (2004) An Illustrated Key to Chinese Amphibians. Sichuan Science and Technology Publishing House, Chengdu, China.

Fei L, Hu SQ, Ye CY, Huang YZ (2009) FAUNA SINICA Amphibia Vol. 2 Anura. Science Press, Beijing, China.

Fei L, Ye CY, Jiang JP (2010) Colored Atlas of Chinese Amphibians. Sichuan Science and Technology Publishing House, Chengdu, China.

Fei L, Ye CY, Jiang JP (2012) Colored Atlas of Chinese Amphibians and Their Distributions. Sichuan Science and Technology Publishing House, Chengdu, China.

Frost DR (2023) Amphibian Species of the World: an Online Reference. Version 6.2. American Museum of Natural History, New York. Electronic Database. https://amphibiansoftheworld.amnh.org/index.php [Accessed at 7 January 2024]

Grismer LL, Youmans TM, Wood PL, Ponce A, Wright SB, Jones BS, Johnson R, Sanders KL, Gower DJ, Yaakob NS, Lim KKP (2006) Checklist of the herpetofauna of Pulau Langkawi, Malaysia, with comments on taxonomy. Hamadryad 30(1&2): 61–74.

Günther ACLG (1869) First account of species of tailless batrachians added to the collection of the British Museum. Proceedings of the Zoological Society of London 1868: 478–490.

Hakim J, Trageser SJ, Ghose A, Das K, Rashid SMA, Rahman SC (2020) Amphibians and reptiles from Lawachara National Park in Bangladesh. Check List 16(5): 1239–1268. https://doi.org/10.15560/16.5.1239

Hallowell E (1861) Report upon the Reptilia of the North Pacific Exploring Expedition, under command of Capt. John Rogers, U.S. N. Proceedings of the Academy of Natural Sciences of Philadelphia 12: 480–510.

Hedges SB (1994) Molecular evidence for the origin of birds. Proceedings of the National Academy of Sciences of the United States of America 91(7): 2621–2624. https://doi.org/10.1073/pnas.91.7.2621

Huang YZ (1983) A new species of flying frog from Xizang—*Rhacophorus verrucopus*. Acta Herpetologica Sinica 2(4): 63–65.

Inger RF (1966) The systematics and zoogeography of the Amphibia of Borneo. Fieldiana. Zoology 52: 1–402. https://doi.org/10.5962/bhl.title.3147

Inger RF, Orlov N, Darevsky I, Bourret A (1999) Frogs of Vietnam: A report on new collections. Fieldiana. Zoology 92: 1–46. https://doi.org/10.5962/bhl.title.3478

Jablonski D, Finarelli JA (2009) Congruence of morphologically-defined genera with molecular phylogenies. Proceedings of the National Academy of Sciences of the United States of America 106(20): 8262–8266. https://doi.org/10.1073/pnas.0902973106

Jiang DC, Jiang K, Ren JL, Wu J, Li JT (2019) Resurrection of the genus *Leptomantis*, with description of a new genus to the family Rhacophoridae (Amphibia: Anura). Asian Herpetological Research 10(1): 1–12. https://doi.org/10.16373/j.cnki.ahr.180058

Kapli T, Lutteropp S, Zhang J, Kobert K, Pavlidis P, Stamatakis A, Flouri T (2017) Multi-rate Poisson tree processes for single-locus species delimitation under maximum likelihood and Markov chain Monte Carlo. Bioinformatics 33(11): 1630–1638. https://doi.org/10.1093/bioinformatics/btx025

Kocher TD, Thomas WK, Meyer A, Edwards SV, Pääbo S, Villablanca FX, Wilson AC (1989) Dynamics of mitochondrial DNA evolution in animals: Amplification and sequencing with conserved primers. Proceedings of the National Academy of Sciences of the United States of America 86(16): 6196–6200. https://doi.org/10.1073/pnas.86.16.6196

Kuhl H, Van Hasselt JC (1822) Uittreksels uit breieven van de Heeren Kuhl en van Hasselt, aan de Heeren C. J. Temminck, Th. van Swinderen en W. de Haan. Algemeene Konst-en Letter-Bode 7: 99–104.

Kumar S, Stecher G, Tamura K (2016) MEGA7: Molecular Evolutionary Genetics Analysis Version 7.0 for Bigger Datasets. Molecular Biology and Evolution 33(7): 1870–1874. https://doi.org/10.1093/molbev/msw054

Kuramoto M, Wang CS (1987) A new rhacophorid treefrog from Taiwan, with comparisons to *Chirixalus eiffingeri* (Anura, Rhacophoridae). Copeia 1987(4): 931–942. https://doi.org/10.2307/1445556

Leong TM, Lim KKP (2003) Herpetofaunal records from Fraser's Hill, peninsular Malaysia, with larval descriptions of *Limnonectes nitidus* and *Theloderma asperum* (Amphibia, Ranidae and Rhacophoridae). The Raffles Bulletin of Zoology 51(1): 123–136.

Li JT, Li Y, Murphy RW, Rao DQ, Zhang YP (2012) Phylogenetic resolution and systematics of the Asian tree frogs, *Rhacophorus* (Rhacophoridae, Amphibia). Zoologica Scripta 41(6): 557–570. https://doi.org/10.1111/j.1463-6409.2012.00557.x

Li J, Liu S, Yu GH, Sun T (2022) A new species of *Rhacophorus* (Anura, Rhacophoridae) from Guangxi, China. ZooKeys 1117: 123–138. https://doi.org/10.3897/zookeys.1117.85787

Liu CC, Hu SQ (1960) Preliminary report of Amphibia from southern Yunnan. Dong Wu Xue Bao 11(4): 509–538.

Liu CC, Hu SQ (1962) A herpetological report of Kwangsi. Dong Wu Xue Bao 14: 73–104. https://doi.org/10.1080/00845566.1962.10396361

Matsui M, Shimada T, Sudin A (2013) A New Gliding Frog of the Genus *Rhacophorus* from Borneo. Current Herpetology 32(2): 112–124. https://doi.org/10.5358/hsj.32.112

Mo YM, Jiang JP, Xie F, Ohler A (2008) A new species of *Rhacophorus* (Anura, Ranidae) from China. Asiatic Herpetological Research 11: 85–92.

Neang T, Holden J (2008) A Field Guide to the Amphibians of Cambodia. Fauna & Flora International, Phnom Penh, Cambodia.

Nguyen VS, Ho TC, Nguyen QT (2005) A checklist of amphibians and reptiles of Vietnam. Nha Xuat Ban Nong Nghiep, Hanoi, Vietnam.

Nguyen TT, Tran TT, Nguyen TQ, Pham CT (2008) Geographic distribution: *Rhacophorus rhodopus*. Herpetological Review 39: 364.

Nguyen TT, Matsui M, Eto K, Orlov NL (2014) A preliminary study of phylogenetic relationships and taxonomic problems of Vietnamese *Rhacophorus* (Anura, Rhacophoridae). Russian Journal of Herpetology 21(4): 274–280.

O'Connell KA, Smart U, Smith EN, Hamidy A, Kurniawan N, Fujita MK (2018) Within-island diversification underlies parachuting frog (*Rhacophorus*) species accumulation on the Sunda Shelf. Journal of Biogeography 45(4): 929–940. https://doi.org/10.1111/jbi.13162

Ohler A, Delorme M (2006) Well known does not mean well studied: Morphological and molecular support for existence of sibling species in the Javanese gliding frog *Rhacophorus reinwardtii* (Amphibia, Anura). Comptes Rendus Biologies 329(2): 86–97. https://doi.org/10.1016/j.crvi.2005.11.001

Ohler A, Swan SR, Daltry JC (2002) A recent survey of the amphibian fauna of the Cardamom Mountains, Southwest Cambodia with descriptions of three new species. The Raffles Bulletin of Zoology 50(2): 465–481.

Orlov NL, Murphy RW, Ananjeva NB, Ryabov SA, Cuc HT (2002) Herpetofauna of Vietnam, a checklist. Part I. Amphibia. Russian Journal of Herpetology 9(2): 81–104.

Pan T, Zhang YN, Wang H, Wu J, Kang X, Qian LF, Li K, Zhang Y, Chen JY, Rao DQ, Jiang JP, Zhang BW (2017) A New Species of the Genus *Rhacophorus* (Anura, Rhacophoridae) from Dabie Mountains in East China. Asian Herpetological Research 8: 1–13. https://doi.org/10.16373/j.cnki.ahr.160064

Peters WCH (1871) Über neue Reptilien aus Ostafrica und Sarawak (Borneo), vorzüglich aus der Sammlung des Hrn. Marquis J. Doria zu Genua. Monatsberichte der Königlichen Preussische Akademie des Wissenschaften zu Berlin 1871: 566–581.

Poyarkov NA, Nguyen TV, Popov ES, Geissler P, Pawangkhanant P, Neang T, Suwannapoom C, Orlov NL (2021) Recent progress in taxonomic studies, biogeographic analysis, and revised checklist of amphibians in Indochina. Russian Journal of Herpetology 28(3A): 1–110. https://doi.org/10.30906/1026-2296-2021-28-3A-1-110

Puillandre N, Brouillet S, Achaz G (2021) ASAP: Assemble species by automatic partitioning. Molecular Ecology Resources 21(2): 609–620. https://doi.org/10.1111/1755-0998.13281

Reza A, Mukul SA (2009) Geographic distribution: *Rhacophorus bipunctatus*. Herpetological Review 40(4): 447.

Ronquist F, Teslenko M, van der Mark P, Ayres DL, Darling A, Höhna S, Larget B, Liu L, Suchard MA, Huelsenbeck JP (2012) MrBayes 3.2: Efficient Bayesian Phylogenetic Inference and Model Choice Across a Large Model Space. Systematic Biology 61(3): 539–542. https://doi.org/10.1093/sysbio/sys029

Rowley JJL, Tran DTA, Hoang HD, Le DTT (2012) A new species of large flying frog (Rhacophoridae, *Rhacophorus*) from Lowland forests in Southern Vietnam. Journal of Herpetology 46(4): 480–487. https://doi.org/10.1670/11-261

Schlegel H (1840) Abbildungen neuer oder unvollständig bekannter Amphibien, nach der Natur oder dem Leben entworfen, herausgegeben und mit einem erläuternden. Atlas. Düsseldorf: Arnz & Co.

Shi HT (2002) The Amphibian Fauna and Geographical Division of Hainan Island. Sichuan. Journal of Zoology 21(3): 174–176.

Shi HT (2011) The Amphibia and Reptillia Fauna of Hainan. Science Press, Beijing, China.

Stuart BL (2005) New frog records from Laos. Herpetological Review 36(4): 473–479.

Stuart BL, Emmett DA (2006) A collection of amphibians and reptiles from the Cardomom Mountains, southwestern Cambodia. Fieldiana. Zoology 109: 1–27. https://doi.org/10.3158/0015-0754(2006)109[1:ACOAAR]2.0.CO;2

Sun ZX, Wang TL, Zhu BC, Wang JC (2017) Calls characteristics and temporal rhythm of calling behavior of *Rhacophorus rhodopus* in the breeding season. Shengtaixue Zazhi 36(6): 1672–1677.

Taylor EH (1962) The Amphibian Fauna of Thailand. The University of Kansas Science Bulletin 8: 487–491. https://doi.org/10.5962/bhl.part.13347

Temminck CJ, Schlegel H (1838) Fauna Japonica sive Descriptio animalium, quae in itinere per Japonianum, jussu et auspiciis superiorum, qui summum in India Batava Imperium tenent, suscepto, annis 1823–1830 colleget, notis observationibus et adumbrationibus illustratis. Volume 3 (Chelonia, Ophidia, Sauria, Batrachia). Leiden: J. G. Lalau.

Wang LJ, Hong ML, Wang JC, Lv SQ, Shi HT (2004) Diversity and Fauna Analysis of Amphibians in Limushan Nature Reserve of Hainan Province. Dongwuxue Zazhi 39(6): 54–57.

Wang W, Cheng LS, Liang YH (2009) Investigation and Conservation Measures on Amphibians in Rice Field of Hainan Island. Sichuan. Journal of Zoology 28(2): 250–253.

Wilkinson JA, Thin T, Lwin KS, Shein AK (2005) A new species of *Rhacophorus* (Anura, Rhacophoridae) from Myanmar (Burma). Proceedings of the California Academy of Sciences 56(4): 42–52.

Wu (1977) In: Sichuan Institute of Biology Herpetology Department. A survey of amphibians in Xizang. Acta Zoologica Sinica 23: 54–63.

Yu GH, Rao DQ, Yang JX, Zhang MW (2007) Non-monophyly of *Rhacophorus rhodopus*, *Theloderma* and *Philautus albopunctatus* Inferred from Mitochondrial 16S rRNA Gene Sequences. Zoological Research 28(4): 437–442.

Yu GH, Rao DQ, Yang JX, Zhang MW (2008) Phylogenetic relationships among Rhacophorinae (Rhacophoridae, Anura, Amphibia), with an emphasis on the Chinese species. Zoological Journal of the Linnean Society 153(4): 733–749. https://doi.org/10.1111/j.1096-3642.2008.00404.x

Yu GH, Hui H, Hou M, Wu ZJ, Rao DQ, Yang JX (2019) A new species of *Zhangixalus* (Anura, Rhacophoridae), previously confused with *Zhangixalus smaragdinus* (Blyth, 1852). Zootaxa 4711(2): 275–292. https://doi.org/10.11646/zootaxa.4711.2.3

Yu GH, Du LN, Wang JS, Rao DQ, Wu ZJ, Yang JX (2020) From mainland to islands: Colonization history in the tree frog *Kurixalus* (Anura, Rhacophoridae). Current Zoology 66(6): 667–675. https://doi.org/10.1093/cz/zoaa023

Zhao EM, Wang LJ, Shi HT, Wu GF, Zhao H (2005) Chinese rhacophorid frogs and description of a new species of *Rhacophorus*. Sichuan Journal of Zoology 24: 297–300.

Ziegler T, Köhler J (2001) *Rhacophorus orlovi* sp. n., ein neuer Ruderfrosch aus Vietnam (Amphibia, Anura, Rhacophoridae). Sauria 23: 37–46.

Zug GR (2022) Amphibians and Reptiles of Myanmar: Checklists and Keys. I. Amphibians, Crocodilians, and Turtles. Smithsonian Scholarly Press, Washington, D.C. https://doi.org/10.5479/si.19098995

Zug GR, Mulcahy DG (2020) The Amphibians and Reptiles of South Tanintharyi. Fauna & Flora International, Cambridge, U.K.

Zoosyst. Evol. 100 (2) 2024, 645–662 | DOI 10.3897/zse.100.114758

PENSOFT

für Natur MUSEUM FÜR NATURKUNDE BERLIN

A new species of *Eusirus* Krøyer, 1845 (Amphipoda, Amphilochidea, Eusiridae) from the seamount of the Caroline Plate, with redescription of *Meteusiroides keyensis* Pirlot, 1934

Yan-Rong Wang[1,2], Zhong-Li Sha[1,2,3,4], Xian-Qiu Ren[1]

1 *Department of Marine Organism Taxonomy and Phylogeny, Institute of Oceanology, Chinese Academy of Sciences, Qingdao 266071, China*
2 *College of Biological Sciences, University of Chinese Academy of Sciences, Beijing 100049, China*
3 *Laoshan Laboratory, Qingdao 266237, China*
4 *Shandong Province Key Laboratory of Experimental Marine Biology, Institute of Oceanology, Chinese Academy of Sciences, Qingdao, China*

https://zoobank.org/938B8E54-3E6F-4281-83CE-E3D32393F8F3

Corresponding author: Zhong-Li Sha (shazl@qdio.ac.cn)

Academic editor: Luiz F. Andrade ♦ **Received** 26 October 2023 ♦ **Accepted** 13 April 2024 ♦ **Published** 23 May 2024

Abstract

A new *Eusirus* Krøyer, 1845 species within the family Eusiridae Stebbing, 1888 is described based on specimens collected from seamounts of the Caroline Plate. *Eusirus carolinus* **sp. nov.** is characterized by having large, well-pigmented eyes, the distomiddorsal mediodorsal pointed process only present on pleonites 1 and 2, epimeral plate 3 with a smooth posterior margin, the elongated telson only cleft 20%, and the rami of uropod 3 being equal in length. A rare eusirid species, *Meteusiroides keyensis* Pirlot, 1934, is redescribed as providing the living coloration based on one female specimen. Sequences of two genes (16S rRNA and COI) were used to analyze their relationships with other species in the family Eusiridae and confirm the taxonomic placement. The result supports the monophyly of *Cleonardo* Stebbing, 1888; *Eusirus* and *Rhachotropis* S.I. Smith, 1883; and is consistent with morphological classification.

Key Words

Deep sea, Eusiridae, morphology, systematics, taxonomy, western Pacific

Introduction

Seamounts are isolated islands that can give rise to unique ecological communities (Richer de Forges et al. 2000; Hobbs et al. 2008). Hence, seamounts harbor vibrant biodiversity (Morato et al. 2010). However, despite wide recognition as important marine habitats, in both tropical and temperate oceans, seamounts remain one of the least explored and studied marine biomes on Earth (Clark et al. 2010; Yesson et al. 2011). The tropical Indo-West Pacific region, which is considered a global center of marine biodiversity, lacks significant research on seamounts (Clark et al. 2010). Most studies on Pacific seamount ecosystems and biodiversity have focused on the middle-eastern and eastern Pacific, as well as the southwestern Pacific (George 2013; Kitahashi et al. 2020).

As one of the largest orders of the Crustacea, Amphipoda encompasses over 10,000 reported species that inhabit all types of aquatic environments (cf. Barnard and Karaman 1991; Lowry and Myers 2017; Arfianti and Costello 2021; Horton et al. 2024). A few numbers of species have been described from seamounts (Bucklin et al. 1987; Lowry and Myers 2003; Kilgallen 2009; Lörz 2012; Hughes 2016; Wang et al. 2020; Espinosa-Leal et al. 2021; Lörz and Horton 2021; Frutos and Sorbe 2022). During the biodiversity of seamounts survey conducted by the Chinese research vessel KEXUE in the Caroline Plate, NW Pacific, between 2017 and 2019, three individuals belonging to the family Eusiridae Stebbing, 1888, were collected.

The status of the superfamily Eusiroidea Stebbing, 1888, is controversial (Verheye et al. 2016; d'Udekem d'Acoz and Verheye 2017; Myers and Lowry 2018).

According to the current classification by Lowry and Myers (2017), the superfamily Eusiroidea contains four independent families, including Bateidae Stebbing, 1906; Eusiridae, Miramarassidae Lowry, 2006; and Thurstonellidae Lowry & Zeidler, 2008 (Horton et al. 2024). The family Eusiridae contains 13 valid genera with 125 species (Corbari et al. 2019; Ariyama and Kohtsuka 2022; Horton et al. 2024), which occur from intertidal to abyss (Bousfield and Hendrycks 1995; Lörz 2010). Among the collected individuals in the present study, two specimens were identified as a new species of the genus *Eusirus* Krøyer, 1845, which is described herein. We also highlight the morphological distinctions between the new species and other species within the genus. Additionally, one female specimen was identified as *Meteusiroides keyensis* Pirlot, 1934, which was first reported outside its type locality. The present study redescribed and illustrated *M. keyensis* and provided the living coloration of the species.

Material and methods

The examined material was collected by ROV FAXIAN during expeditions to seamounts on the Caroline Plate by the Institute of Oceanology, Chinese Academy of Sciences (IOCAS) during August 2017 and June 2019. The specimen is deposited in the Marine Biological Museum, Chinese Academy of Sciences, Qingdao, China. The individual was examined and dissected with a dissecting microscope (ZEISS Discovery V20). Line drawings were completed using the software Adobe Photoshop CS6 on a graphics tablet. The length measurement was made along the outline of the animal, beginning from the rostrum to the posterior margin of the telson.

DNA was obtained from their mitochondrial genome (unpublished works) by homologous alignment: 16S rRNA (16S, approximately 860 bp) and cytochrome oxidase I (COI, 1542 bp). 27 described and undescribed species within Eusiridae and two outgroup taxa of Liljeborgiidae Spence Bate, 1863 were encompassed in the phylogenetic analysis (Suppl. material 1).

The sequences obtained were aligned using MEGA 6 (Tamura et al. 2013) and concatenated using SequenceMatrix 1.8 (Vaidya et al. 2011), resulting in a combined sequence length of 995 bp. Phylogenetic trees were constructed by two methods: maximum likelihood (ML) and Bayesian inference (BI). The ML analyses were conducted online using W-IQ-TREE (http://iqtree.cibiv.univie.ac.at/) (Trifinopoulos et al. 2016), with clade support evaluated via 10,000 ML bootstrap replications. The optimal model of evolution for each dataset was determined using jModelTest 0.1.1 based on the Akaike information criterion (AIC) (Posada 2008). BI analyses were performed with MrBayes 3.2.7 (Huelsenbeck and Ronquist 2001), employing a Markov Chain Monte Carlo (MCMC) algorithm with two runs, each consisting of four chains, for 1,000,000 generations and sampling trees every 500 generations, totaling 2,000 sampled trees. The effective sample size (ESS) values for all sampling parameters were checked with Tracer v1.7 (Rambaut et al. 2018). The initial 500 trees were discarded as burn-in, and posterior probabilities (PP) were calculated from the remaining trees.

Multiple species delimitation methods were utilized to assess the hypothesis that the specimen is a distinct species. The COI data, comprising 58 homologous sequences, were subjected to Automated Barcode Gap Discovery (ABGD) analysis using a web-based interface (https://bioinfo.mnhn.fr/abi/public/abgd/abgdweb.html), as described by Puillandre et al. (2012). The analysis was conducted using the Kimura 2-parameter substitution model (TS/TV = 2.0), with a prior range for maximum intraspecific divergence set between 0.001 and 0.1, encompassing 10 recursive steps, and a relative gap width (X) of 1.0. Additionally, Bayesian implementation of the Poisson Tree Processes (bPTP) species delimitation model was employed as per Zhang et al. (2013), conducted on the web server of the Heidelberg Institute for Theoretical Studies, Germany (http://species.h-its.org/), using BI phylogenetic trees as the input data.

Systematic account

Order Amphipoda Latreille, 1816
Suborder Amphilochidea Boeck, 1871
Superfamily Eusiroidea Stebbing, 1888
Family Eusiridae Stebbing, 1888

Genus *Eusirus* Krøyer, 1845

Diagnosis. See Barnard and Karaman (1991).

***Eusirus carolinus* sp. nov.**

https://zoobank.org/20295258-98BE-489C-9CBA-C5FF0E4F1960

Figs 1–5

Material examined. *Holotype*: Western Pacific • 1 brooding female (with 9 intra-marsupial individuals), 12.9 mm; seamount on Caroline Plate; 10°30'N, 140°9–10'E; depth 520–862 m; 26 Aug. 2017; MBM 286609.

***Paratype*:** Western Pacific • 1 male; 13 mm; seamount on Caroline Plate; 10°30'N, 140°9–10'E; depth 520–862 m; 26 Aug. 2017; MBM 286608.

Description. *Body*. Pleonites 1–3 carinate dorsally; pleonites 1 and 2 with acute distomiddorsal teeth; epimera 1 and 2 postero-distal corner subacute; epimeron 3 postero-distal corner rounded, without serration. ***Head*.** Lateral cephalic lobe with apically-oblique rostrum. Eyes large, reniform. Antenna 1 stout, with peduncular articles 1–3 in length ratio of 1: 0.95: 0.36; distal margin of peduncular article 1 with inner surface bearing two distal processes; article 2 distal margin produced as two triangular distal processes in outer and inner surfaces, respectively; primary flagellum 55-articulate; first article

Figure 1. *Eusirus carolinus* sp. nov. female holotype (MBM 286609). Photographed immediately after collection by Jun-long Zhang.

nearly as long as the third peduncular article; accessory flagellum 1-articulate. Antenna 2 shorter than antenna 1, with peduncular article 4 subequal in length to article 5; flagellum distinctly longer than fifth peduncular article, 29-articulate.

***Mouthparts*.** Upper lip distally rounded, apex convex, and weakly produced, bearing fine submarginal setae. Right mandible with incisor bearing one blunt anterodistal tooth and not dentate lacinia mobilis; accessory setal row composed of 5 stout setae; molar triturative, columnar; palp 3-articulate, much longer than mandible body; article 1 shortest; article 2 slightly shorter than article 3, with row of long simple setae; article 3 with ventral margin heavily setose; and outer margin bearing one long (about 3/5 length of third palp article) simple seta. Left mandible, incisor with one blunt large anterodistal tooth, lacinia mobilis 8-dentate; accessory setal row composed of 6 setae; molar and palp similar to those of right mandible. Lower lip with weak inner lobe; outer lobe subovoid, rounded distally; both inner and outer lobes covered with marginal and submarginal setae. Maxilla 1 outer plate with 11 stout multicuspidate setae on apical margin; inner plate subovoid, apex bearing one seta; palp long far beyond outer lobe, 2-articulate; article 2 with about 15 setae along apex and mediodistal margin. Maxilla 2 with inner plate broader than outer plate, both with fine marginal setae. Maxilliped heavily setose, inner plate short, not reaching to distal margin of first palp article, distally armed with about 10 stout setae; outer plate extending to about 1/2 length of article 2 of palp, laterally armed with short robust setae and distally armed with long plumose setae; palp 4-articulate, slender, article 2 slightly longer and broader than article 3; dactylus shorter than article 3, claw-like, unguis very short, ventral margin bearing 5 long stout setae.

Coxal gills present on pereopods 2–7. Oostegites present on pereopods 2–5.

***Gnathopods and pereopods*.** Gnathopods similar in shape: gnathopod 1 subchelate, eusirid form; coxa 1 broadened distally, slightly expanded anteroventrally; basis steady in width, not distinctly broadened distally; anterior margin flat, bearing several setae; posterior margin with a group of setae distally; ischium short, with rounded lobe anterodistally; carpus lobe linguiform, narrow, covered with long setae anterior margin; outer face with acute pointed process distally and inner face rounded distally; propodus wider than long, subrectangular, shorter than carpus in length of anterior margin, with one group of defining setae; palm lined with numerous crooked setae submarginally; dactylus falcate, fitting palm. Gnathopod 2 similar to gnathopod 1, stout, eusirid form, coxa rectangular, ventral margin convex; basis slightly longer than that of gnathopod 1; ischium, merus, carpus propodus, and dactylus similar in appearance to gnathopod 1. Pereopod 3 slender, coxa rectangular; basis linear; anterior margin with simple setae; merus about twice as long as carpus, distinctly longer than propodus; propodus with posterior margin bearing several small stout setae; dactylus elongate, slightly curved; posterior margin dentate. Pereopod 4 broken, coxa subequal in length to coxa 3, posteriorly emarginated, postero-distal corner subacute, basis linear, anterior margin with simple setae. Pereopod 5 shorter than pereopods 6 and 7; coxa equilobate, both expanded posteroventrally; basis increasing in length from pereopods 5 to 7, with posteroventral lobe, posterior margins lateral border moderately expanded,

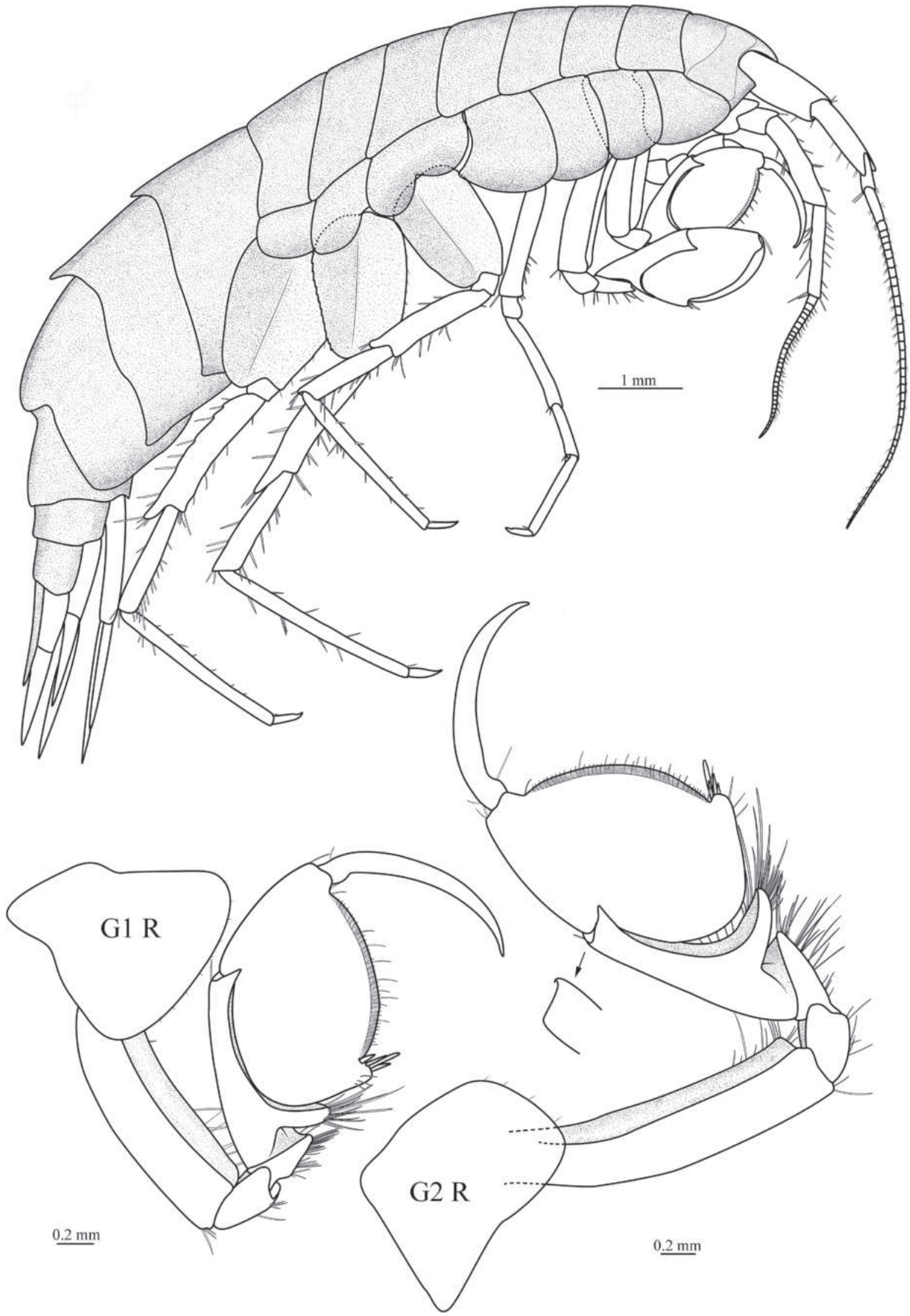

Figure 2. *Eusirus carolinus* sp. nov. female holotype (MBM 286609). **G1 R.** Right gnathopod 1; **G2 R.** Right gnathopod 2 (also showing the medial side of the distal margin of the carpus).

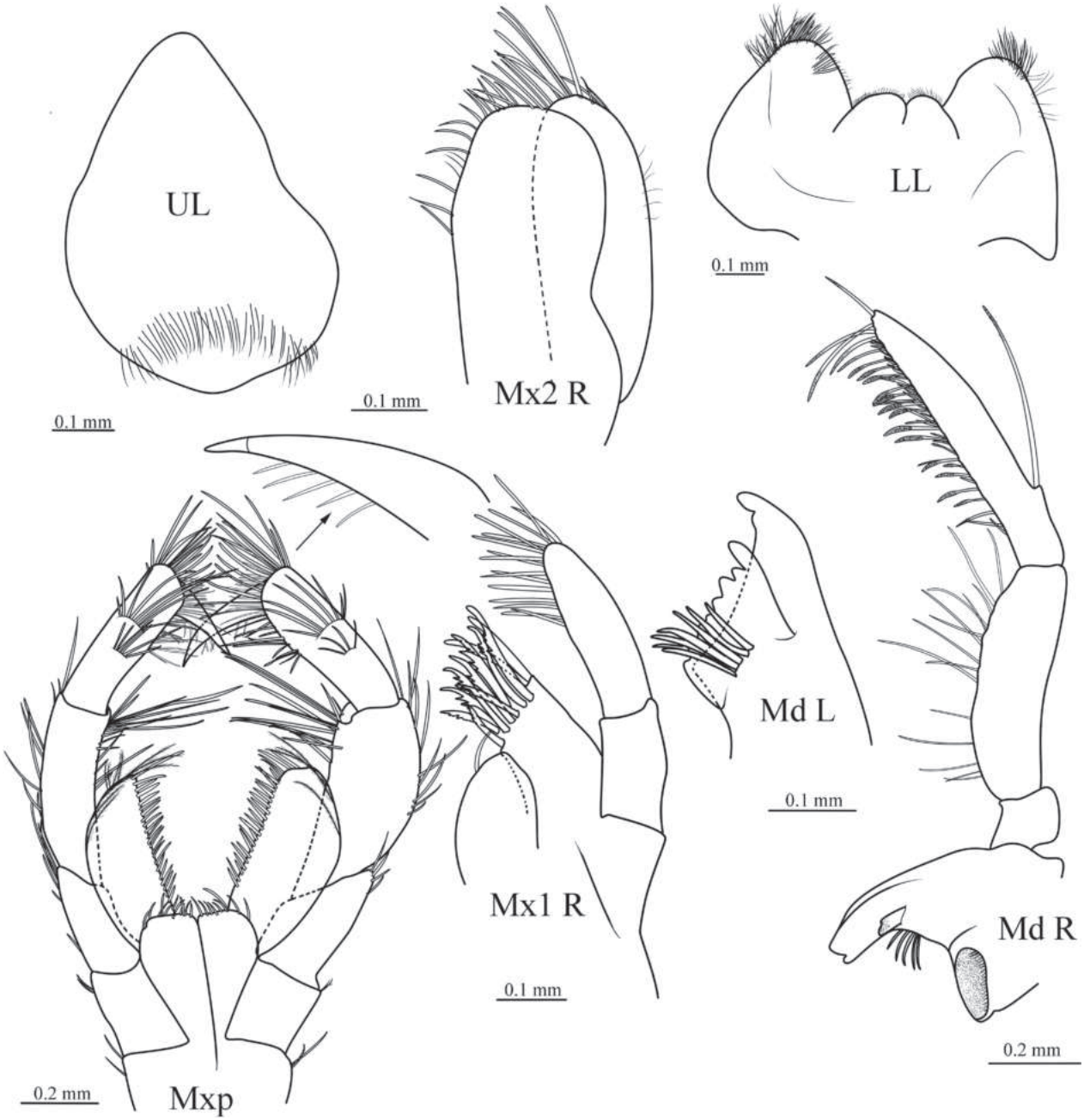

Figure 3. *Eusirus carolinus* sp. nov. female holotype (MBM 286609). **UL.** Upper lip; **LL**. Lower lip; **Md L.** Left mandible (not showing molar and palp); **Md R.** Right mandible; **Mx1 R.** Right maxilla 1; **Mx2 R.** Right maxilla 2; **Mxp.** Maxillipeds.

serrate, anterior margin with short robust setae; merus increasing in length from pereopods 5 to 7, posterodistally strongly produced, margins with stout setae; carpus subequal in length to merus, margins with stout setae; length ratios of merus to propodus 1: 0.77: 1.20; dactylus nearly straight, anterior margin with about distal 1/3 length dentate. Pereopods 6 and 7 subequal in length; coxa 6 bilobate; merus longer than that of pereopod 5; carpus distinct shorter than merus; propodus slender; margins with stout setae; length ratios of merus to propodus 1: 0.77: 1.31. Pereopod 7 with posterior margins of basis lateral border moderately expanded and distinctly concave, posterodistal corner subacute; length ratios of merus to propodus 1: 0.68: 1.25.

***Uropods and telson*.** Uropod 1 with peduncle subequal in length to outer ramus, bearing numerous short laterals and long medial robust setae dorsally, with one enlarged stout seta at mesiodistal corner; inner ramus 1.3 times as long as outer ramus, both rami bearing robust setae and lateral and medial margins. Uropod 2 with rami lanceolate; peduncle slightly shorter than outer ramus; lateral margin with two subdistal robust setae dorsally; medial margin with seven robust setae; inner ramus nearly twice as long as outer ramus; both rami with inner and medial margins bearing dense robust setae; outer ramus narrower than inner ramus. Uropod 3 shortest, rami lanceolate, subequal in length; peduncle 0.5 times as long as rami; lateral margin bearing one long distal robust sate

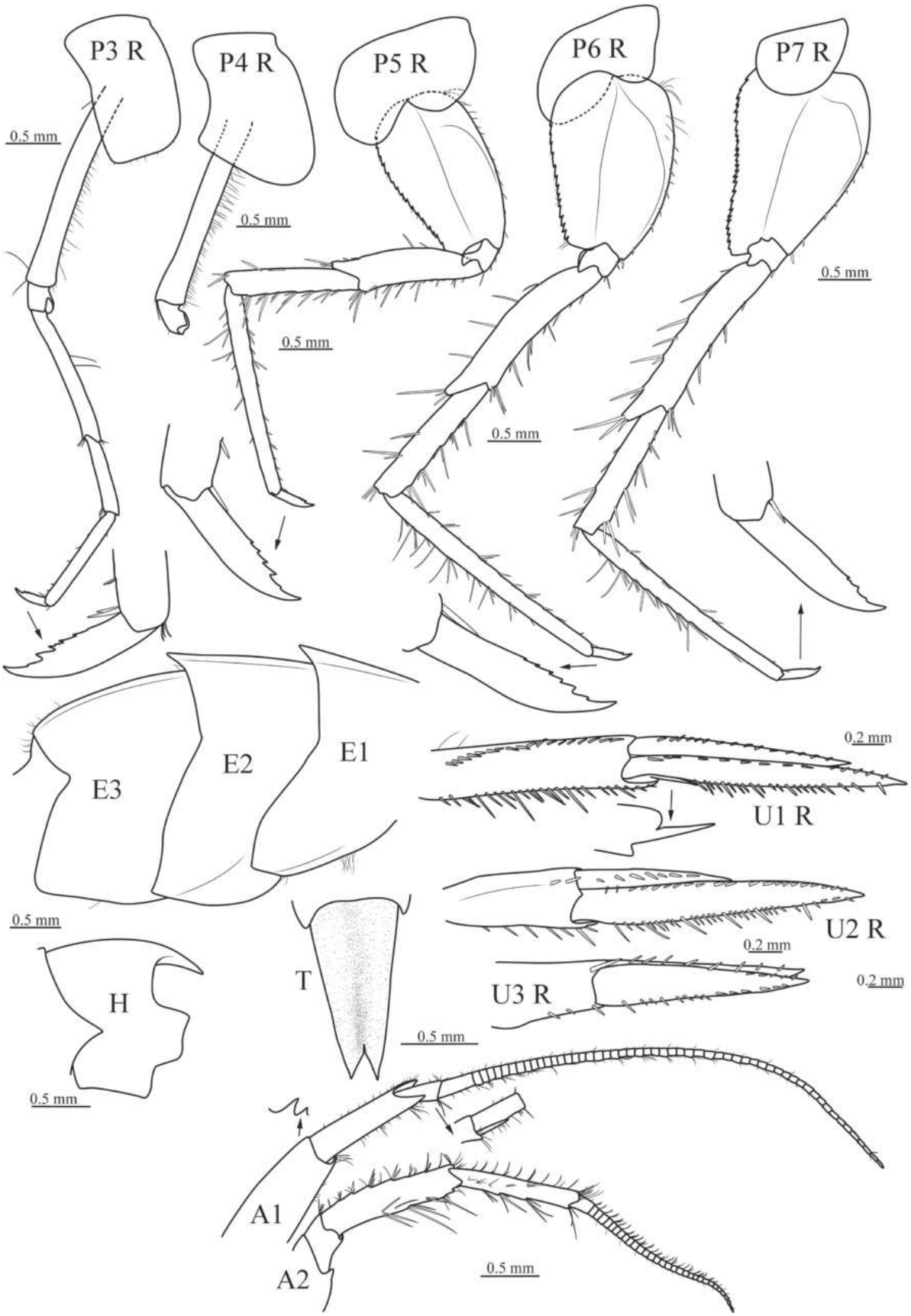

Figure 4. *Eusirus carolinus* sp. nov. female holotype (MBM 286609). **P3 R.** Right pereopod 3; **P4 R.** Right pereopod 4; **P5 R.** Right pereopod 5; **P6 R.** Right pereopod 6; **P7 R.** Right pereopod 7; **E1–3.** Epimeral plates 1–3; **U1 R.** Right uropod 1; **U2 R.** Right uropod 2; **U3 R.** Right uropod 3; **T.** Telson; **H.** Head; **A1.** Antenna 1 (also showing ventral side of distal margin of peduncular article 1 and accessory flagellum); **A2.** Antenna 2.

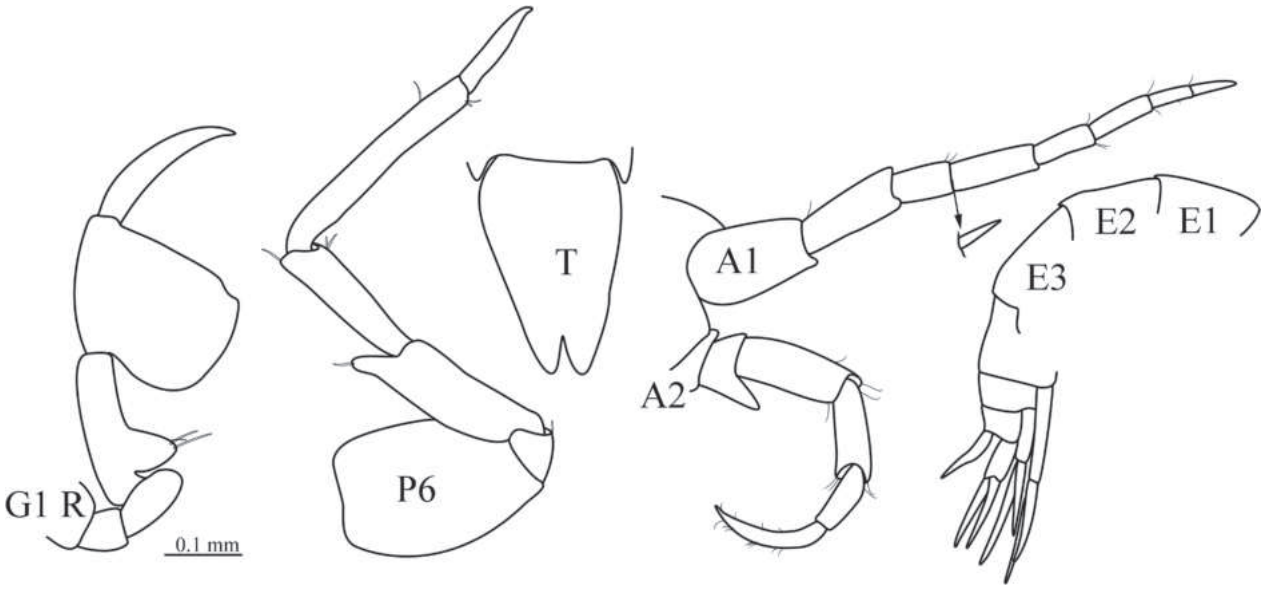

Figure 5. *Eusirus carolinus* sp. nov., one of the intra-marsupial individuals of female holotype (MBM 286609, 2.5 mm). **G1 R.** Right gnathopod 1; **P6 R.** Right pereopod 6; **T.** Telson; **A1.** Antenna 1 (showing accessory flagellum); **A2.** Antenna 2; **E1–3.** Dorsolateral parts of epimeral plates 1–3.

dorsally; medial margin bearing three small robust setae dorsally; both rami with lateral and medial margin setose dorsally. Telson long, slightly tapering distally, reaching about half of the length of uropod 3 rami, length about twice its breadth at base, cleft 15% of length.

Description of intra-marsupial individual. Based on one of the intra-marsupial individuals of the holotype. Rostrum present. Antenna 1 with peduncle articles less setose; primary flagellum only slightly longer than peduncle, 5-articulate; each article slightly longer than the third peduncular article, less setose; accessory flagellum 1-articulate. Antenna 2 much shorter than antenna 1, peduncle less setose; articulations of flagellum inconspicuous and less setose. Gnathopods 1–2 similar in shape and size, subchelate, eusirid form; carpus lobe linguiform broader than that of adult, only covered with several setae mediodistally; propodus similar in form to that of the adult, but without setae; anterior margin subequal in length to carpus; palm not bearing crooked setae submarginally; dactylus stout, slightly curved. Pereopods 3 and 4 subequal in length and similar in form, less setose; dactylus nearly straight, slightly shorter than propodus, with posterior margin not dentate. Pereopod 5 shorter than pereopods 6 and 7. Pereopod 6 basis with posterior margin smooth, not serrate, anterior margin without setae; merus with large posterodistal pointed process bearing one seta; length ratios of merus to propodus 1: 0.83: 1.33; dactylus elongate, about half length of propodus, nearly straight, anterior margin not dentate. Pleonites 1–3 not carinate; pleonites 1–2 with small acute mid-dorsal tooth. Uropods 1–3 similar to those of adults but without robust setae on peduncles and rami. Telson long, length 1.6 times its breadth at base, cleft 15% of length, narrower than that of adult, slightly tapering distally.

Coloration. Anterior part of body is red with yellow eyes; gnathopods 1–2 are deep red; and antennae 1–2 and posterior part of body are pale red.

Etymology. The new species is named after its type locality, the Caroline Plate.

Distribution. Presently known only from a seamount of the Caroline Plate at a depth of 520–862 meters.

Remarks. Table 1 shows the distribution, depth information, and important characters of *Eusirus* species. Nine species have been reported from the Pacific, including *Eusirus antarcticus* Thomson, 1880; *E. bathybius* Schellenberg, 1955; and *E. bulbodigitus* Jung, Kim, Soh & Yoon, 2016; *E. columbianus* Bousfield & Hendrycks, 1995; *E. cuspidatus* Krøyer, 1845; *E. fragilis* Birstein & M. Vinogradov, 1960; *E. hirayamai* Bousfield & Hendrycks, 1995; *E. liui* Wang, Sha & Ren, 2021; and *E. parvus* Pirlot, 1934. *Eusirus carolinus* sp. nov. can be distinguished from *E. bathybius*, *E. fragilis*, and *E. liui* by having large, well-pigmented eyes (Schellenberg 1955; Birstein and Vinogradov 1960; Wang et al. 2021). The new species differs from the remaining six Pacific *Eusirus* species by presenting the posterior margin of epimeron 3 as smooth, while epimeron 3 presents a serrate posterior margin in the mentioned six species (Krøyer 1845; Stebbing 1906; Pirlot 1934; Gurjanova 1951; Bousfield and Hendrycks 1995; Jung et al. 2016; Othaitz and Sorbe 2020). The body of *Eusirus carolinus* sp. nov. only has distomiddorsal teeth on pleonites 1–2, while the pereonite 7 of three species, *E. cuspidatus*, *E. hirayamai*, and *E. parvus*, also has a distomiddorsal tooth other than the teeth on pleonites 1–2 (Krøyer 1845; Pirlot 1934; Hirayama 1985). The new species also differs from *E. hirayamai* by the rami of uropod 3 subequal in length and from *E. parvus* by having a unilobed coxa 7 (Pirlot 1934; Hirayama 1985; Bousfield and Hendrycks 1995).

Table 1. Distribution, depth, and important characters of *Eusirus* species.

Species	Distribution	Important characters	Depth	References
E. abyssi	N Atlantic 60°37'N, 27°52'W	eyes absent, pereonite 7 unknown, pleonites 1–3 with distomiddorsal teeth, epimeron 3 unknown, coxa 7 unilobed, uropod 3 unknown, telson unknown.	1505 m	Stephensen 1944
E. antarcticus	S Pacific (New Zealand), S Indian Ocean, Antarctica	eyes present, pereonite 7 (with distomiddorsal tooth described by Stebbing (1906), while in the key of Andres et al. (2002) without that tooth, pleonites 1–2 with distomiddorsal teeth, epimeron 3 with posterior margin serrate, coxa 7 unknown, uropod 3 unknown, telson cleft 40% of length.	0–1800 m	Stebbing 1906; Andres et al. 2002; Othaitz and Sorbe 2020
E. bathybius	NW Pacific, off Japan	eyes absent, pereonite 7 and pleonites unknown, epimeron 3 smooth, coxa 7 unilobed, uropod 3 with outer ramus shorter than inner one, telson only apex notched.	0–7900 m	Schellenberg 1955; Bousfield and Hendrycks 1995; Othaitz and Sorbe 2020
E. biscayensis	N Atlantic, Bay of Biscay, off Iceland	eyes present, pereonite 7 with distomiddorsal tooth, pleonites 1–3 with distomiddorsal teeth, epimeron 3 with posterolateral margin serrate, coxa 7 unilobed, uropod 3 with outer ramus slightly shorter than inner one, telson only apex notched.	358–4330 m	Bonnier 1896; Stebbing 1906
E. bonnieri	NE Atlantic Ocean	eyes absent, pereonite 7 with small distomiddorsal tooth, pleonites 1–3 with small distomiddorsal teeth, epimeron 3 serrate, coxa 7 unilobed, uropod 3 with outer ramus shorter than inner one, telson cleft 20% of length.	370–1099 m	Othaitz and Sorbe 2020
E. bouvieri	Southern Ocean	eyes present, pereonite 7 without distomiddorsal tooth, pleonites 1–2 with distomiddorsal teeth, Pleonite 3 with dorsal longitudinal carina, epimeron 3 serrate, coxa 7 and uropod 3 unknown, telson cleft less than 20% of length.	0–400 m	Chevreux 1911; Andres et al. 2002
E. bulbodigitus	NW Pacific, off Korea	eyes present, pereonite 7 without distomiddorsal tooth, pleonites 1–2 with distomiddorsal teeth, pleonite 3 without dorsal carina, epimeron 3 serrate, coxa 7 unilobed, uropod 3 with outer ramus slightly shorter than inner one, telson cleft less than 20% of length.	33 m	Jung et al. 2016
E. carolinus sp. nov.	Pacific	eyes present, pereonite 7 without distomiddorsal tooth, pleonites 1–2 with distomiddorsal teeth, epimeron 3 smooth, coxa 7 unilobed, uropod 3 with rami subequal in length, telson cleft about 15% of length.	520–862 m	the present study
E. columbianus	NE Pacific, 52°–55°19'N, 128°30'–130°27'W	eyes present, pereonite 7 without distomiddorsal tooth, pleonites 1–2 with distomiddorsal teeth, epimeron 3 serrate, coxa 7 bilobed, uropod 3 with outer ramus shorter than inner one, telson cleft about 30% of length.	12–150 m	Bousfield and Hendrycks 1995
E. crosnieri	Indian Ocean, NW Madagascar, 12°43'S, 48°15'E	eyes present but not pigmented, pereonite 7 with distomiddorsal tooth, pleonites 1–3 with distomiddorsal teeth, epimeron 3 serrate, coxa 7 unknown, uropod 3 with rami subequal in length, telson cleft about 30% of length.	245–255 m	Ledoyer 1982; Andres 1996; Othaitz and Sorbe 2020
E. cuspidatus	N Pacific; Arctic Basin	eyes present, pereonite 7 with distomiddorsal tooth, pleonites 1–2 with distomiddorsal teeth, epimeron 3 with posterior margin serrate, coxa 7 unilobed, uropod 3 with outer ramus shorter than inner one, and telson cleft 50% of length.	37–400 m	Krøyer 1845; Stebbing 1906; Gurjanova 1951; Bousfield and Hendrycks 1995; Jung et al. 2016; Othaitz and Sorbe 2020
*E. fragilis**	N Pacific	eyes absent, pereonite 7 without distomiddorsal tooth, pleonites 1–2 with distomiddorsal teeth, epimeron 3 smooth, coxa 7 unilobed, uropod 3 unknown, and telson cleft less than 15% of length.	abyssal	Birstein and M. Vinogradov 1960; Bousfield and Hendrycks 1995
E. giganteus	Antarctica, 63°09'S, 59°10'W	eyes present, pereonite 7 with distomiddorsal tooth, pleonites 1–3 with distomiddorsal teeth, epimeron 3 serrate, coxa 7 unilobed, uropod 3 with outer ramus slightly shorter than inner one, telson cleft 18% of length.	221–690 m	Andres et al. 2002
E. hirayamai	NW Pacific, off Japan	eyes present, pereonite 7 with distomiddorsal tooth, pleonites 1–2 with distomiddorsal teeth, epimeron 3 with posterior margin fully serrate, coxa 7 unilobed, uropod 3 with rami subequal in length, telson cleft less than 30% of length.	<50 m	Hirayama 1985; Bousfield and Hendrycks 1995
E. holmii	Arctic Ocean, N Atlantic	eyes present, pereonite 7 with distomiddorsal tooth, pleonites 1–2 with distomiddorsal teeth, epimeron 3 with posterior margin fully serrate, coxa 7 unilobed, uropod 3 with rami subequal in length, telson cleft about 10% of length.	172–1900 m	Stebbing 1906; Stephensen 1912; 1944; Macnaughton et al. 2007
E. laevis	Antarctica	eyes present, pereonite 7 without distomiddorsal tooth, pleonites without distomiddorsal tooth, epimeron 3 smooth, coxa 7 unilobed, uropod 3 and telson unknown.	<48 m, epipelagic	Walker 1903; Andres et al. 2002
E. laticarpus	Antarctica	eyes present, pereonite 7 without distomiddorsal tooth, pleonites 1–2 with distomiddorsal teeth, epimeron 3 only with 3 serrations at distomiddorsal corner, coxa 7 unilobed, uropod 3 with rami subequal in length, telson cleft 40% of length.	0–400 m	Chevreux 1906; Andres et al. 2002; Othaitz and Sorbe 2020
E. latirostris	Indian Ocean	eyes absent, pereonite 7 without distomiddorsal tooth, pleonite 3 with distomiddorsal tooth, epimeron 3 with posterior margin smooth, coxa 7, uropod 3 and telson unknown.	2500 m	Ledoyer 1982
E. leptocarpus	NE Atlantic	eyes present, pereonite 7 without distomiddorsal tooth, pleonites 1–3 with distomiddorsal teeth, epimeron 3 with posterior margin fully serrate, coxa 7 unilobed, uropod 3 with rami subequal in length, telson cleft about 20% of length.	346–1098 m	Krøyer 1845; G.O. Sars 1893; Stebbing 1906; Othaitz and Sorbe 2020

Species	Distribution	Important characters	Depth	References
E. liui	NW Pacific, Okinawa Trough, 27°32'N, 126°58'E	eyes absent, pereonite 7 without distomiddorsal tooth, pleonites 1–2 with distomiddorsal teeth, epimeron 3 with posterior margin and posteroventral corner serrate, coxa 7 unilobed, uropod 3 with outer ramus slightly shorter than inner one, telson unknown.	1243 m	Wang et al. 2021
E. longipes	Arctic Ocean, NE Atlantic	eyes present, pereonite 7 without distomiddorsal tooth, pleonites 1–2 with distomiddorsal teeth, epimeron 3 with posterior margin serrate, coxa 7 unilobed, uropod 3 with rami subequal in length, telson cleft about 20% of length.	6–1098 m	Krøyer 1845; Stebbing 1906; Lincoln 1979; Bousfield and Hendrycks 1995; Othaitz and Sorbe 2020
E. meteorae	NE Atlantic	eyes present, pereonite 7 with distomiddorsal tooth, pleonites 1–3 with distomiddorsal teeth, epimeron 3 with only distal part of posterior margin serrate, coxa 7 unilobed, uropod 3 with rami subequal in length, telson cleft about 30% of length.	50–150 m	Andres 1996
E. microps	Antarctica	eyes present, pereonite 7 with distomiddorsal tooth, pleonites 1–2 with distomiddorsal teeth, epimeron 3 with posterior margin fully serrate, coxa 7 and uropod 3 unknown, telson less than 30% of length.	epi- and mesopelagic	Walker 1906; Andres et al. 2002
E. minutus	Off Norway, off South Africa	eyes present, pereonite 7 with distomiddorsal tooth, pleonites 1–2 with distomiddorsal teeth, epimeron 3 with lower 1/3 length of posterior margin serrate, coxa 7 unilobed, uropod 3 with outer ramus much shorter than inner one, telson cleft about 15% of length.	200 m, 752 m	Krøyer 1845; G.O. Sars 1893; Stebbing 1906
E. nevandis	Indian Ocean, off Kenya, 4°00'S, 41°27'E	eyes present, pereonite 7 with small distomiddorsal tooth, pleonites 1–2 with small distomiddorsal teeth, epimeron 3 with posterior margin smooth, coxa 7and uropod 3 unknown, telson less than 20% of length.	1510–2500 m	Barnard 1961; Ledoyer 1982
E. parvus	Western Pacific, Indonesia	eyes present, pereonite 7 with distomiddorsal tooth, pleonites 1–2 with distomiddorsal teeth, epimeron 3 with half-length of posterior margin serrate, coxa 7 bilobed, uropod 3 and telson unknown.	315 m	Pirlot 1934; Jung et al. 2016
E. perdentatus	Antarctica	eyes present, pereonite 7 carinate, with large distomiddorsal tooth, pleonites 1–3 carinate, with large distomiddorsal teeth, epimeron 3 only posteroventral corner serrate, coxa 7 unilobed, uropod 3 with rami subequal in length, telson cleft less than 20% of length.	0–928 m	Emison 2000; Andres et al. 2002; Verheye and d'Udekem d'Acoz 2020
E. pontomedon	Antarctica	eyes present, pereonite 7 carinate, with large distomiddorsal tooth, pleonites 1–3 carinate, with large distomiddorsal teeth, epimeron 3 only posteroventral corner serrate, coxa 7 unilobed, uropod 3 with rami subequal in length, telson less than 20% of length.	107–668 m	Verheye and d'Udekem d'Acoz 2020
E. propeperdentatus	Antarctica, 61°30'S, 55°00'W	eyes present, pereonite 7 carinate, with large distomiddorsal tooth, pleonites 1–3 carinate, with large distomiddorsal teeth, pleonites, epimeron 3 smooth, only with small spines, coxa 7 unilobed, uropod 3 with outer ramus slightly longer than inner one, telson less than 20% of length.	epi-and mesopelagic	Andres 1979; Othaitz and Sorbe 2020
E. propinquus	N Atlantic	eyes present, pereonite 7 without distomiddorsal tooth, pleonites 1–2 with distomiddorsal teeth, epimeron 3 with posterior margin serrate, coxa 7 unilobed, uropod 3 with rami subequal in length, telson cleft about 47% of length.	183–1141 m	Krøyer 1845; G.O. Sars 1893; Stebbing 1906; Othaitz and Sorbe 2020
E. tjalfiensis	Davis Strait, 70°41'N, 52°07'W	eyes present but not pigmented, pereonite 7 without distomiddorsal tooth, pleonites 1–2 with distomiddorsal teeth, epimeron 3 with posterior margin serrate, coxa 7 unilobed, uropod 3 with outer ramus much shorter than inner one, telson cleft less than 20% of length.	750–800 m	Stephensen 1912; 1944
E. tridentatus	Antarctica	eyes present but not pigmented, pereonite 7 with distomiddorsal tooth, pleonites 1–2 with distomiddorsal teeth, epimeron 3 with posterior margin smooth, distoventral margin lightly serrate, coxa 7, uropod 3 and telson unknown.	unknown	Bellan-Santini and Ledoyer 1974; Andres et al. 2002

*Translation of the original description: eyes absent; pereonites and pleonite 1 with weak longitudinal carina, pleonites 1 and 2 with small distomiddorsal teeth, pleonite 3 and segment 1 of without tooth, posteroventral angle of epimeron 1 produced into small acute tooth; head with anterolateral angle acute, rostrum extending 1/3 length of basal article of antenna 1, antennae 1 broken off at peduncular article 1; antenna 2 article 3 four times shorter than article 4 and three times shorter than article 5; upper lip rounded, mandible with stout cylindrical molar process, serrated incisor process, large lacinia mobilis and spine row, palp article 1 much longer than article 2, maxilla 1 inner lobe with 2 very short distal setae, outer lobe with 11 multi-cusped spine-teeth, palp thin, bearing row of fine setae on its end, palp article 1 two times shorter than article 2, maxilla 2 inner lobe rounded, as long as, but two times broader than outer lobe, both lobes equipped with setae distally; maxilliped similar with those of *E. bathybius*, but outer lobes slightly broader than inner lobes; coxa 1 strongly expanding distally, with rounded anterior margin; coxa 2 smaller than coxa 1; plate 4 small, with convex anterior and concave posterior margins; plates 5–7 oval, gnathopods 1 and 2 typical for *Eusirus*, gnathopod 1 significantly shorter than gnathopod 2, carpus with posterior margin bearing a tuft of setae on acute projection distally, propodus of gnathopods 1 and 2 similar in shape and size, width less than 1.5 times exceeding their length, Pereopods 3, 4, and 6 broken off; Pereopod 5 with basis slightly expanding distally; basis of pereopod 7 strongly expanding distally; width almost equal to the length, epimera 1 and 3 rounded, with smooth posterior margin, epimeron 2 with acute posteroventral angle, uropod 1 rami equal in length, uropod 2 exopod slightly shorter than endopod, uropod 3 broken off, telson triangular, width slightly less than length; distal end with an acute-angled notch. Remarks. The species described herein sharply differs from all other species of the genus by the smooth epimer III posterior margin and short triangular telson (Birstein and M. Vinogradov 1960, translated by Dr. Olga A. Golovan).

Genus *Meteusiroides* Pirlot, 1934

Diagnosis. See Pirlot (1934) and Barnard and Karaman (1991).

***Meteusiroides keyensis* Pirlot, 1934**

Figs 6–9

Meteusiroides keyensis Pirlot, 1934: 52–56, figs. 94–96.

Material examined. Western Pacific • 1 female (ovigerous), 12.2 mm; seamount on Caroline Plate; St. FX-Dive 218; 10°07'N, 140°14'E; depth 813–1242 m; 6 Jun. 2019; M6090; MBM 286612.

Description. ***Body*.** Smooth; epimera 1 and 2 with posteroventral angle produced into small acute tooth; epimeron 3 with posteroventral angle broadly rounded. ***Head*.** Rostrum longer than anterior cephalic lobe, extending to 1/4 length of peduncular article 1 of antenna 1; anterior cephalic lobe rounded; eyes large, reniform. Antenna 1 with peduncular article 1 subequal in length to article 2, ventral margin produced distally; article 2 narrower than article 1, outer margin convex distally; inner margin bilobate distally; article 3 shortest, shorter than 1/2 length of flagellar article 1; primary flagellum 82-articulate; accessory flagellum lacking. Antenna 2 much shorter than antenna 1, peduncular article 4 about twice as long as article 5; flagellum 61-articulate.

***Mouthparts*.** Upper lip margin smooth. Mandible with right incisor bearing 13 teeth, left incisor bearing 11 teeth; right lacinia mobilis with distal margin smooth, without tooth; left lacinia mobilis with 10 teeth; accessory setal row with 8 slender setae; molar strong, columnar; palp article 3 distinctly longer than article 2, with 7 apical long setae; inner margin with row of long simple setae. Lower lip with inner lobes distinctly smaller than outer lobes. Maxilla 1 inner plate subtriangular, with two long distal robust setae and one small setae; outer plate with 11 multicuspidated setae in two rows; palp 2-articulate, with 6 apical robust setae and a row of subapical slender long setae. Maxilla 2 with inner plate shorter and broader than outer plate, bearing about 16 fine simple marginal setae; outer plate bearing row of slender long apical setae. Maxilliped with inner plate subrectangular, short; outer plate bearing about 6 plumose setae on distal margin and more than 10 slender setae on inner margin; palp article 3 expanded distally, bearing a row of setae on distal and inner margins; dactylus very slender, as long as article 3.

Coxae 1–4 subrectangular, gradually increasing posteriorly; coxa 1 anteroventral corner subacute; coxa 4 excavate posteriorly. Coxae 5 and 6 bilobate, posterior lobe deeper and larger than anterior lobe. Coxa 7 smallest, rounded. Coxal gills present on pereopods 2–7.

***Gnathopods and pereopods*.** Gnathopods 1–2 similar in shape, but gnathopod 2 slightly longer. Gnathopod 1 basis with dense long simple setae on distal half of mesial surface; ischium posterior margin bearing group of setae distally; merus much shorter than carpus, posterior margin bearing groups of setae, distal margin with two acute mediodorsal pointed processes; carpus shorter than propodus, posterior margin bearing more than 10 groups of slender setae; propodus sub-ovate, propodus less than twice longer than wide, palmar margin obliquely convex, with a row of large

Figure 6. *Meteusiroides keyensis* Pirlot, 1934. Photographed immediately after collection by Shao-qing Wang.

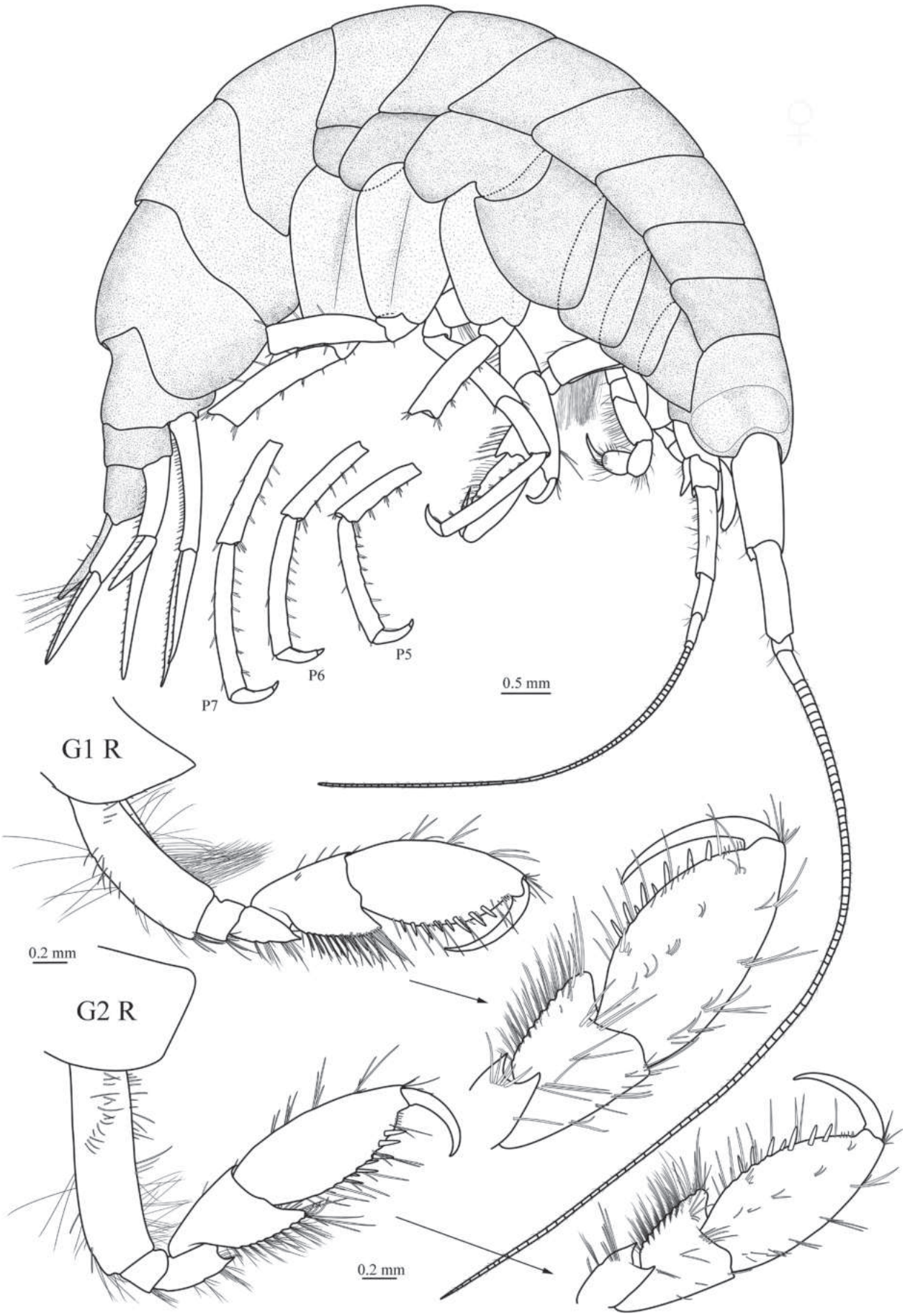

Figure 7. *Meteusiroides keyensis* Pirlot, 1934. **G1 R.** Right gnathopod 1; **G2 R.** Right gnathopod 2.

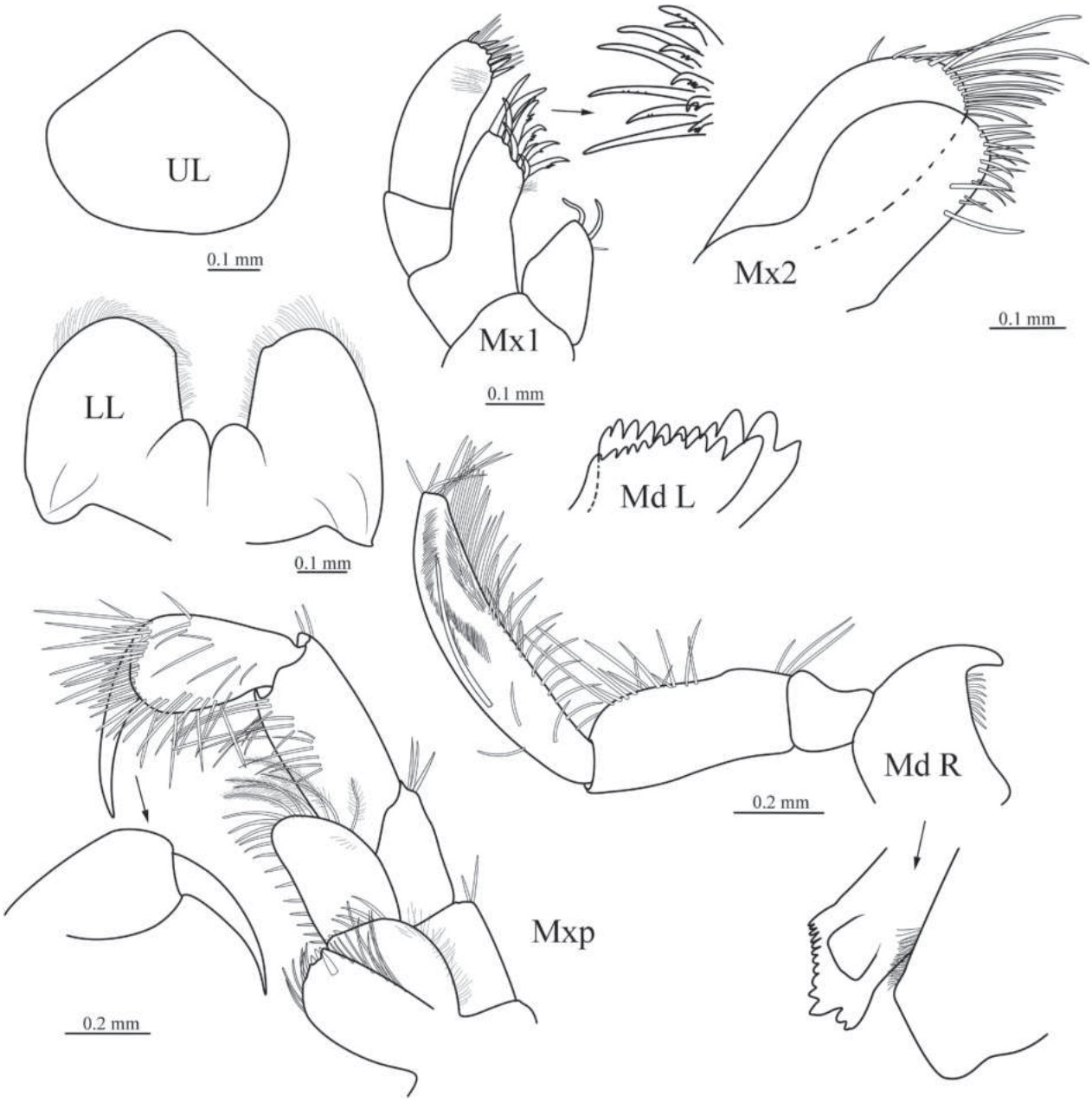

Figure 8. *Meteusiroides keyensis* Pirlot, 1934. **UL.** Upper lip; **LL.** Lower lip; **Md L.** Left mandible (not showing molar and palp); **Md R.** Right mandible; **Mx1.** Maxilla 1; **Mx2.** Maxilla 2; **Mxp.** Maxillipeds.

robust setae and slender setae, posterior margin with 6 groups of slender setae, surfaces with 6 clusters of setae; dactylus 3/5 the length of propodus, curved. Gnathopod 2 basis not bearing dense setae on mesial surface, but margins setose; ischium to carpus similar to gnathopod 1; propodus about twice longer than wide, similar in shape to gnathopod 1; dactylus 1/2 the length of propodus, curved. Pereopods 3 and 4 slender, basis linear, margins setose; merus longer than carpus but shorter than propodus, margins bearing short robust setae; dactylus slender. Pereopods 5–7 slightly increasing in length; basis expanded, narrowing distally; posterodistal lobes shallow; postero-ventral corner rounded; merus to propodus with margins setose; merus longer than carpus but shorter than propodus; dactylus slender.

***Uropods and telson*.** Uropod 1 with peduncle slightly longer than inner ramus, margins setose; rami lanceolate, lacking apical setae, margins setose; outer ramus shorter than inner one. Uropod 2 with peduncle shorter than outer ramus, margins setose, with ventromedial spur; rami lanceolate, lacking apical setae, margins setose; outer ramus much shorter than inner one. Uropod 3 with peduncle shorter than rami, outer margin lacking setae; rami subequal in length; both rami outer and inner margins setose; inner ramus with inner margin bearing long plumose setae. Telson linguiform; cleft about 70% of its length; posterior margin of each lobe concave; bearing three pairs

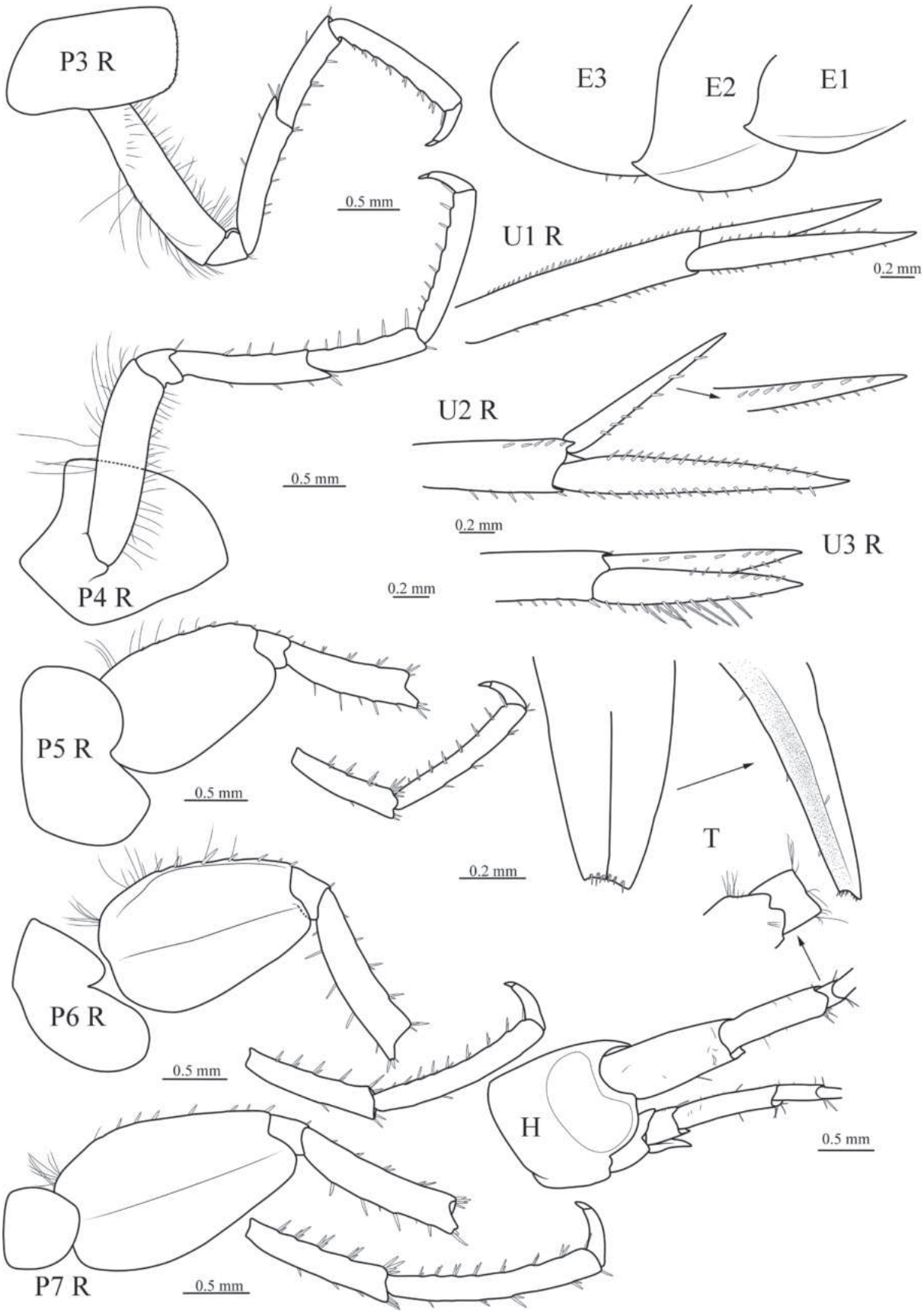

Figure 9. *Meteusiroides keyensis* Pirlot, 1934. **P3 R.** Right pereopod 3; **P4 R.** Right pereopod 4; **P5 R.** Right pereopod 5; **P6 R.** Right pereopod 6; **P7 R.** Right pereopod 7; **E1–3.** Epimeral plates 1–3; **U1 R.** Right uropod 1; **U2 R.** Right uropod 2; **U3 R.** Right uropod 3; **T.** Telson; **H.** Head, with antenna 1 and antenna 2.

of stout setae; keeled ventroproximally; margins bearing several stout setae on each side laterally.

Coloration. The body is transparent, pale red in color, with red gnathopods 1–2, and antennae 1–2, and deep red eyes.

Distribution. A seamount of the Caroline Plate at a depth of 813–1242 meters; Indonesia (5°48'S, 132°13'E) at a depth of 304 meters (Pirlot 1934; Barnard and Karaman 1991).

Remarks. *Meteusiroides keyensis* Pirlot, 1934, was originally described from Indonesia, with the description based on a female holotype found at a depth of 304 meters. The current ovigerous female specimen was collected from a depth of at least 813 meters, significantly deeper than the depth originally recorded. Morphologically, the present specimen only slightly differs from the original description of *M. keyensis* by the rami of Uropod 3 subequal in length, while the outer ramus is somewhat shorter than the inner ramus in the original illustration (Pirlot 1934, fig. 96). Nonetheless, the present specimen should be identified as *M. keyensis*.

Molecular data analysis

The phylogenetic trees produced by BI and ML analyses were congruent and generally well supported (Fig. 10).

The monophyly of the genera *Eusirus* and *Rhachotropis* S.I. Smith, 1883, was recovered in both ML and BI trees (BP = 54% and PP = 0.96). The genus *Meteusiroides* and *Dorotea* Corbari, Frutos & Sorbe, 2019 clustered together and were separated from *Cleonardo* Stebbing, 1888 (BP = 51% and PP = 0.87) The genus *Eusirus* was separated into two relatively moderately supported clades (BP = 50% and PP = 0.94). The new species, *E. carolinus* sp. nov., was separated from *E. hirayamai* with strong support (BP = 97% and PP = 0.83), with *E. pontomedon* Verheye & d'Udekem

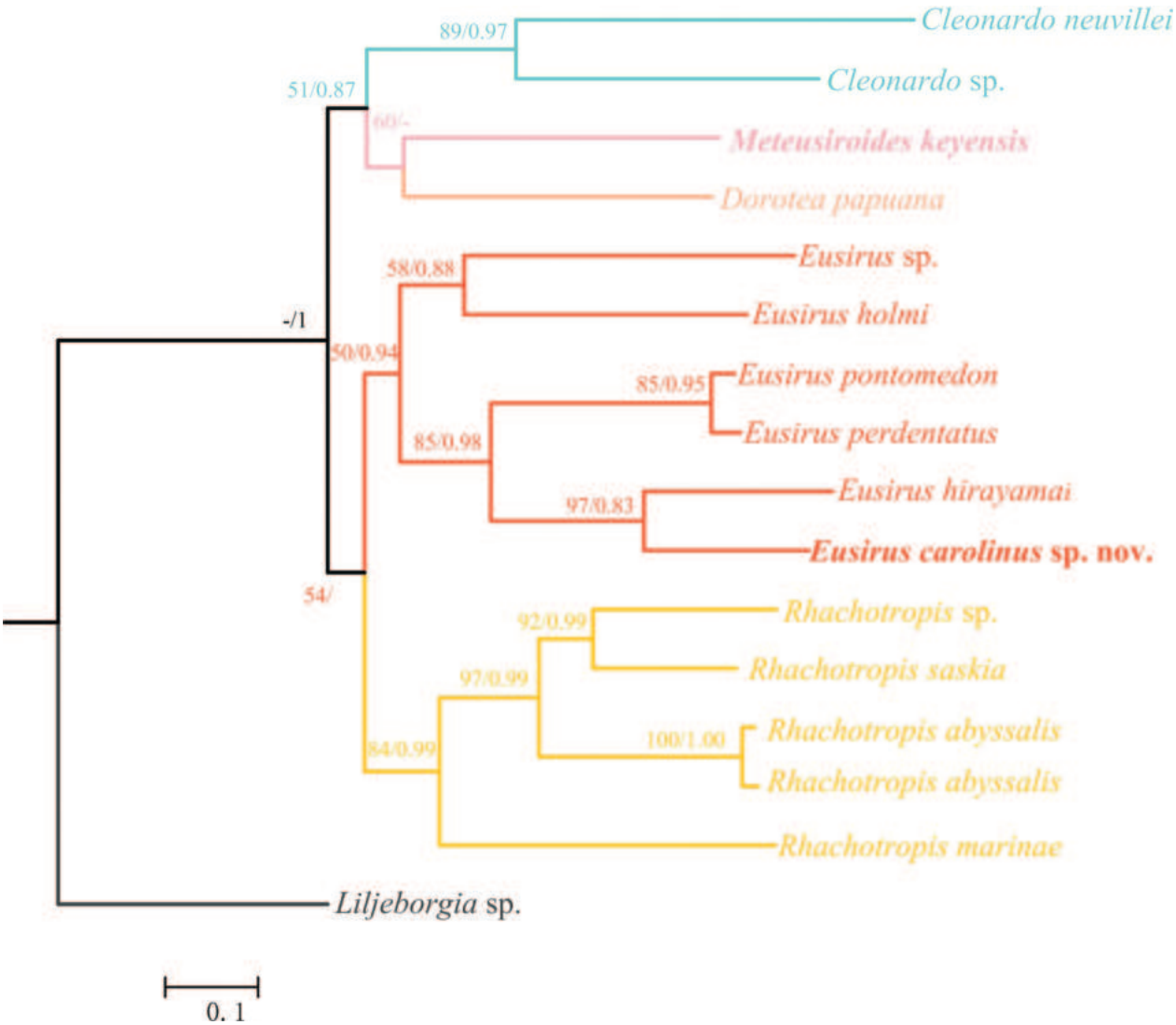

Figure 10. Maximum likelihood (ML) and Bayesian inference (BI) trees of Tropiometroidea using combined sequences of COI and 16S. The numbers at each node represent bootstrap values (BP) (left) and posterior probabilities (PP) (right). *Eusirus carolinus* sp. nov. is highlighted in bold.

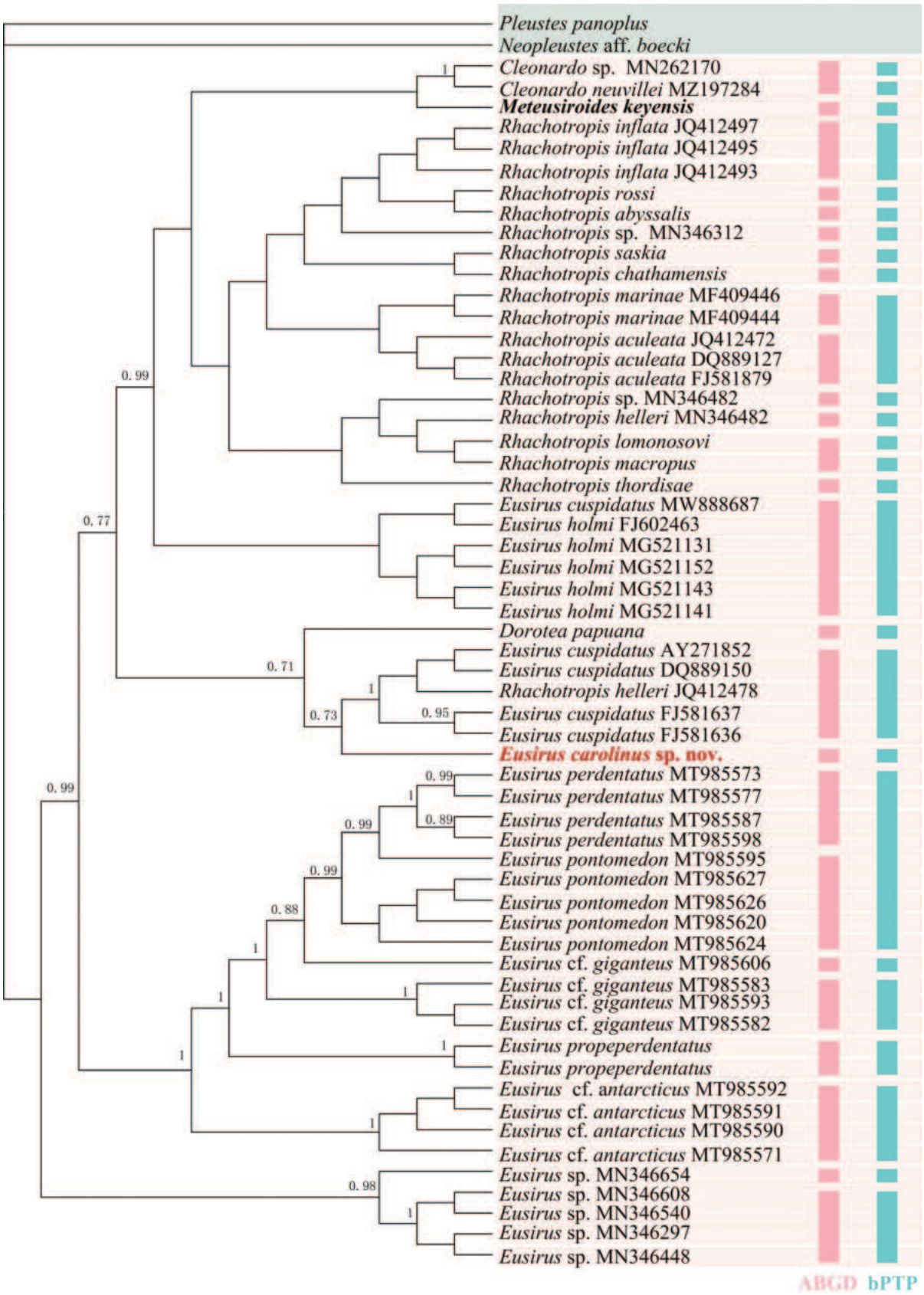

Figure 11. Bayesian Inference (BI) phylogenic tree based on COI showing the phylogenetic relationship between *Eusirus carolinus* sp. nov. and related eusirids, with bootstrap replications (BS) labeled (>50). Putative species identified by DNA-based species delimitation methods [Automated Barcode Gap Discovery (ABGD) and Bayesian implementation of the Poisson Tree Processes (bPTP)] applied to the COI tree/distance matrices are indicated by bars on the concatenated tree. Color codes indicate the support of each putative species.

d'Acoz, 2020, and *E. perdentatus* Chevreux, 1912, as sister groups (BP = 85% and PP = 0.98). The species delimitation based on both ABGD and bPTP methods has validated the new species (Fig. 11).

Discussion

Nine species of the genus, including the present new species and one mentioned by Pirlot (1934) as *Eusirus* sp., were documented in the Pacific (Jung et al. 2016; Wang et al. 2021). Among these, three species, *E. carolinus* sp. nov., *E. parvus*, and *Eusirus* sp., were found in the deep waters of the tropical western Pacific. *Eusirus bathybius* and *E. fragilis* were located at abyssal depths, while only *E. liui* inhabited vent fields. *Eusirus bulbodigitus* and *E. hirayamai* were reported from sublittoral depths. Furthermore, the depth range of *Meteusiroides keyensis* extended to at least 813 meters in the present study.

As one of the controversial families of Amphipoda (Verheye et al. 2016; d'Udekem d'Acoz and Verheye 2017; Myers and Lowry 2018), the higher classification of Eusiridae needed molecular and morphological investigations (Ariyama and Kohtsuka 2022). However, phylogenetic resolution falls outside the scope of this study.

The results of the present integrative taxonomic study reveal the validity of *Eusirus carolinus* sp. nov. Owing to the lack of molecular sequences, the phylogenetic relationships between this new species and the remaining *Eusirus* species are still unexplained. At the genus level, the analysis of molecular evidence is consistent with the morphological studies (Bousfield and Hendrycks 1995; Corbari et al. 2019), indicating a close relationship between *Eusirus* and *Rhachotropis*. Both of the above genera exhibit a strong eusirid form of gnathopods 1 and 2. Similarly, the other three genera, *Cleonardo*, *Dorotea*, and *Meteusiroides*, which have normal gnathopods 1 and 2, also cluster together in the current molecular study. However, a comprehensive understanding of the systematic relationships among genera within the Eusiridae calls for further taxonomic and molecular data sampling.

Acknowledgements

Many thanks to Dr. Charles Oliver Coleman from the Museum für Naturkunde-Leibniz Institute for Evolution and Biodiversity Science for offering papers, which proved crucial during the identification of the new species. Many thanks to Dr. Olga A. Golovan from the Russian Academy of Sciences for helping with the translation of *Eusirus fragilis* Birstein & M. Vinogradov, 1960. This work was supported by the National Science Foundation for Distinguished Young Scholars (42025603), the Science and Technology Innovation Project of Laoshan Laboratory (LSKJ202203102), the Strategic Priority Research Program of the Chinese Academy of Sciences (XDB42000000), and the National Natural Science Foundation of China (42306110).

References

Andres HG (1979) Gammaridea (Amphipoda, Crustacea) der Antarktis-Expedition 1975/76. Auswertung der Dauerstation südlich von Elephant Island. Meeresforschung 27(3): 88–102.

Andres HG (1996) A new pelagic eusirid amphipod, *Eusirus meteorae*, from the tropical NE-Atlantic (Crustacea, Gammaridea). Mitteilungen aus den Hamburgischen Zoologischen Museum und Institut 93: 83–90.

Andres HG, Lörz A-N, Brandt A (2002) A common but undescribed huge species of *Eusirus* Krøyer, 1845 (Crustacea, Amphipoda, Eusiridae) from Antarctica. Mitteilungen aus dem Hamburgischen Zoologischen Museum und Institut 99: 109–126.

Arfianti T, Costello MJ (2021) The distribution of benthic amphipod crustaceans in Indonesian seas. PeerJ 9: e12054. https://doi.org/10.7717/peerj.12054

Ariyama H, Kohtsuka H (2022) *Metarhachotropis parva*, a new genus and species of Eusiridae (Crustacea: Amphipoda) from Sagami Bay, central Japan. Zootaxa 5188(1): 95–100. https://doi.org/10.11646/zootaxa.5188.1.6

Barnard JL (1961) Gammaridean Amphipoda from depths of 400 to 6,000 meters. Galathea Report 5: 23–128.

Barnard JL, Karaman GS (1991) The families and genera of marine gammaridean Amphipoda (except marine gammaroids). Records of the Australian Museum 13(1, Supplement 13): 1–866. https://doi.org/10.3853/j.0812-7387.13.1991.91

Bellan-Santini D, Ledoyer M (1974) Gammariens (Crustacea, Amphipoda) des Iles Kerguelen et Crozet. Tethys (Cornella de Llobregat) 5(4): 635–708.

Birstein W, Vinogradov ME (1960) Pelagicheskie gammaridy tropicheskoi chasti Tixogo Okeana. Akademija Nauk SSSR. Trudy Instituta Okeanologii 34: 165–241.

Boeck A (1871) Crustacea Amphipoda borealia et arctica. Forhandlinger i Videnskabs-Selskabet i Christiania 1870: 81–280 [+ i–viii] [index]. https://doi.org/10.5962/bhl.title.2056

Bonnier J (1896) Édriophthalmes. In: Koehler, R., Résultats scientifiques de la campagne du "Caudan" dans le Golfe de Gascogne. Edriophthalmes. Annales de l'Université de Lyon 26: 527–689[, pls. 28–40].

Bousfield EL, Hendrycks EA (1995) The amphipod superfamily Eusiroidea in the North American Pacific regions. I. family Eusiridae: Systematics and distributional ecology. Amphipacifica 1(4): 3–59.

Bucklin A, Wilson Jr RR, Smith Jr KL (1987) Genetic differentiation of seamount and basin populations of the deep-sea amphipod Eurythenes gryllus. Deep-Sea Research, Part A, Oceanographic Research Papers 34(11): 1795–1810. https://doi.org/10.1016/0198-0149(87)90054-9

Chevreux E (1906) Crustacés amphipodes. In: Joubin L (Ed.) Expédition Antarctique Francaise (1903–1905) commandée par le Dr Jean

Charcot. Sciences Naturelles: Documents Scientifiques. Masson, Paris, 1–100.

Chevreux E (1911) Sur quelques amphipodes des iles Sandwich de sud. Anales de Museo Nacional Buenos Aires 21, 14(3): 403–407[, 3 figs].

Clark MR, Schlacher TA, Rowden AA, Stocks KI, Consalvey M (2010) Science Priorities for Seamounts: Research Links to Conservation and Management. PLOS ONE 7(1): e29232. https://doi.org/10.1371/journal.pone.0029232

Corbari L, Frutos IA, Sorbe JC (2019) *Dorotea* gen. nov., a new bathyal genus (Amphipoda, Eusiridae) from the Solomon Sea (Papua New Guinea). Zootaxa 4568(1): 069–080. https://doi.org/10.11646/zootaxa.4568.1.4

d'Udekem d'Acoz C, Verheye ML (2017) *Epimeria* of the Southern Ocean with notes on their relatives (Crustacea, Amphipoda, Eusiroidea). European Journal of Taxonomy 359(359): 1–553. https://doi.org/10.5852/ejt.2017.359

Emison WB (2000) Revision of *Eusirus perdentatus* Chevreux, 1912 and *E. propeperdentatus* Andres, 1979 (Crustacea: Amphipoda). ANARE Reports 145: 1–80.

Espinosa-Leal L, Medellín-Mora J, Corredor-Acosta A, Escribano R (2021) The community structure of hyperiid amphipods associated with two seamount regions in the South-east Pacific. Journal of the Marine Biological Association of the United Kingdom 101(1): 97–108. https://doi.org/10.1017/S0025315420001344

Frutos I, Sorbe JC (2022) Seamounts, canyons and slope: The preference of a new stilipedid amphipod (Crustacea: Amphipoda) for the Bay of Biscay. Estuarine, Coastal and Shelf Science 275: 107992. https://doi.org/10.1016/j.ecss.2022.107992

George KH (2013) Faunistic research on metazoan meiofauna from seamounts-a review. Meiofauna Marina 20: 1–32.

Gurjanova EF (1951) Bokoplavy morej SSSR i sopredel'nykh vod (Amphipoda-Gammandea). Akademiia Nauk SSSR, Opredeliteli po Faune SSSR 41, 1029 pp. [In Russian]

Hirayama A (1985) Taxonomic studies on the shallow-water gammaridean Amphipoda of West Kyushu, Japan. IV. Dexaminidae (*Guernea*), Eophliantidae (sic), Eusiridae, Haustoriidae, Hyalidae, Ischyroceridae. Publications of the Seto Marine Biological Laboratory 30: 1–53[, figs. 124–161]. https://doi.org/10.5134/176102

Hobbs JPA, Choat JH, Robbins WD, Ayling AM, van Herwerden L, Feary DA (2008) Unique fish assemblages at world's southernmost oceanic coral reefs, Elizabeth and Middleton Reefs, Tasman Sea, Australia. Coral Reefs 27(1): 15. https://doi.org/10.1007/s00338-007-0301-3

Horton T, Lowry J, De Broyer C, Bellan-Santini D, Copila-Ciocianu D, Corbari L, Costello MJ, Daneliya M, Dauvin J-C, Fišer C, Gasca R, Grabowski M, Guerra-García JM, Hendrycks E, Hughes L, Jaume D, Jazdzewski K, Kim Y-H, King R, Krapp-Schickel T, LeCroy S, Lörz A-N, Mamos T, Senna AR, Serejo C, Souza-Filho JF, Tandberg AH, Thomas JD, Thurston M, Vader W, Väinölä R, Valls Domedel G, Vonk R, White K, Zeidler W (2024) World Amphipoda Database. Epimeria A. Costa in Hope, 1851. [Accessed through: World Register of Marine Species at:] https://www.marinespecies.org/aphia.php?p=taxdetails&id=101506 [on 2024-02-01]

Huelsenbeck JP, Ronquist F (2001) MRBAYES: Bayesian Inference of Phylogeny. Bioinformatics 17: 754–755. https://doi.org/10.1093/bioinformatics/17.8.754

Hughes LE (2016) New genera, species and records of Maeridae from Australian Waters: *Austromaera*, *Ceradocus*, *Glossomaera*, *Hamimaera*, *Huonella* gen. nov., *Linguimaera* and *Maeraceterus* gen. nov. (Crustacea: Amphipoda). Zootaxa 4115(1): 1–81. https://doi.org/10.11646/zootaxa.4115.1.1

Jung TW, Kim MS, Soh HY, Yoon SM (2016) A new species of *Eusirus* from Jeju Island, Korea (Crustacea, Amphipoda, Eusiridae). ZooKeys 640: 19–35. https://doi.org/10.3897/zookeys.640.10630

Kilgallen NM (2009) New species of lysianassoid Amphipoda (Crustacea) associated with seamounts, marine canyons and cold seeps of New Zealand. Zootaxa 2298(1): 1–30. https://doi.org/10.11646/zootaxa.2298.1.1

Kitahashi T, Sugime S, Inomata K, Nishijima M, Kato S, Yamamoto H (2020) Meiofaunal diversity at a seamount in the pacific ocean: A comprehensive study using environmental DNA and RNA. Deep-sea Research, Part I, Oceanographic Research Papers 160: 103253. https://doi.org/10.1016/j.dsr.2020.103253

Krøyer H (1845) Karcinologiske Bidrag. Naturhistorik Tidsskrift (NS) 1: 283–345[, 3 pls.]; 493, 453–638[, pls. 6, 7].

Latreille PA (1816) Amphipoda. In: Nouveau Dictionaire d'histoire naturelle, appliquée aux Arts, à l'Agriculture, à l'Économie rurale et domestique, à la Médecine, etc. Par une société de Naturalistes et d'Agriculteurs. Deterville, Paris, 2nd ed., vol. 1, 467–469.

Ledoyer M (1982) Crustacés Amphipodes Gammariens. Familles des Acanthonotozomatidae à Gammaridae. Faune de Madagascar 59(1): 1–598.

Lincoln RJ (1979) British marine Amphipoda: Gammaridea. Bulletin of the British Museum (Natural History) Zoology, London, 658 pp. [280 figs]

Lörz AN (2010) Deep-sea *Rhachotropis* (Crustacea: Amphipoda: Eusiridae) from New Zealand and the Ross Sea with key to the Pacific, Indian Ocean and Antarctic species. Zootaxa 2482(1): 22–48. https://doi.org/10.11646/zootaxa.2482.1.2

Lörz AN (2012) First records of Epimeriidae and Iphimediidae (Crustacea, Amphipoda) from Macquarie Ridge, with description of a new species and its juveniles. Zootaxa 3200(1): 49–60. https://doi.org/10.11646/zootaxa.3200.1.3

Lörz AN, Horton T (2021) Investigation of the Amathillopsidae (Amphipoda, Crustacea), including the description of a new species, reveals a clinging lifestyle in the deep sea worldwide. ZooKeys 1031: 19–39. https://doi.org/10.3897/zookeys.1031.62391

Lowry JK (2006) New families and subfamilies of Amphipod Crustaceans. Zootaxa 1254(1): 1–28. https://doi.org/10.11646/zootaxa.1254.1.1

Lowry JK, Myers AA (2003) New amphipod crustaceans from the Indo-West Pacific (Amathillopsidae: Eusiridae: Iphimediidae). The Raffles Bulletin of Zoology 51(2): 219–256. https://doi.org/10.5281/zenodo.4619401

Lowry JK, Myers AA (2017) A phylogeny and classification of the amphipoda with the establishment of the new order Ingolfiellida (Crustacea: Peracarida). Zootaxa 4265(1): 1–89. https://doi.org/10.11646/zootaxa.4265.1.1

Lowry JK, Zeidler W (2008) *Thurstonella*, replacement name for the Antarctic amphipod genus *Clarencia* K.H. Barnard, 1931 (Crustacea, Amphipoda, Thurstonellidae), preoccupied by *Clarencia* Sloane, 1917 (Insecta, Coleoptera, Carabidae). Zootaxa 1840(1): 67–68. https://doi.org/10.11646/zootaxa.1840.1.3

Macnaughton MO, Thormar J, Berge J (2007) Sympagic amphipods in the Arctic pack ice: Redescriptions of *Eusirus holmii* Hansen, 1887 and *Pleusymtes karstensi* (Barnard, 1959). Polar Biology 30(8): 1013–1025. https://doi.org/10.1007/s00300-007-0260-8

Morato T, Hoyle SD, Allain V, Nicol SJ (2010) Seamounts are hotspots of pelagic biodiversity in the open ocean. Proceedings of the National Academy of Sciences of the United States of America 107(21): 9707–9711. https://doi.org/10.1073/pnas.0910290107

Myers AA, Lowry JK (2018) The Senticaudata, a suborder of the Amphipoda –A commentary on d'Udekem d'Acoz and Verheye (2017). ZooKeys 730: 151–155. https://doi.org/10.3897/zookeys.730.22126

Othaitz JP, Sorbe JC (2020) *Eusirus bonnieri* sp. nov. (Crustacea: Amphipoda: Eusiridae), a new deep species from the southeastern Bay of Biscay (NE Atlantic Ocean). Zootaxa 4751(2): 238–256. https://doi.org/10.11646/zootaxa.4751.2.2

Pirlot JM (1934) Les amphipodes de l'expédition du Siboga. Deuxième partie. Les amphipodes gammarides. II. Les amphipodes de la mer profonde. 2. (Hyperiopsidae, Pardaliscidae, Astyridae nov. fam. Tironidae, Calliopiidae, Paramphithoidae, Amathillopsidae nov. fam., Eusiridae, Gammaridae, Aoridae, Photidae, Ampithoidae, Jassidae). Siboga-Expeditie 33d: 167–235. https://doi.org/10.1016/j.ympev.2008.03.024

Posada D (2008) jModelTest: Phylogenetic Model Averaging. Molecular Biology and Evolution 25(7): 1253–1256. https://doi.org/10.1093/molbev/msn083

Puillandre N, Lambert A, Brouillet S, Achaz G (2012) ABGD, Automatic Barcode Gap Discovery for primary species delimitation. Molecular Ecology 21(8): 1864–1877. https://doi.org/10.1111/j.1365-294X.2011.05239.x

Rambaut A, Drummond AJ, Xie D, Baele G, Suchard MA (2018) Posterior summarization in Bayesian phylogenetics using Tracer 1.7. Systematic Biology 67(5): 901–904. https://doi.org/10.1093/sysbio/syy032

Richer de Forges B, Koslow JA, Poore GCB (2000) Diversity and endemism of the benthic seamount megafauna in the southwest Pacific. Nature 405(6789): 944–947. https://doi.org/10.1038/35016066

Sars GO (1893) Amphipoda. Part XIX. Pardaliscidae (concluded), Eusiridae. An account of the Crustacea of Norway, with short descriptions and figures of all the species. I: 413–432[, pls 145–152].

Schellenberg A (1955) Amphipoda. Reports of the Swedish Deep-Sea Expedition 1947–1948. II Zoology 14: 181–195.

Stebbing TRR (1888) Report on the Amphipoda collected by H. M. S. Challenger during the years 1873–1876. Zoology 29: 1–1737[, 210 pl.].

Stebbing TRR (1906) Amphipoda I. Gammaridea. Das Tierreich. 21: 1–806[, 127 figs].

Stephensen K (1912) Report on the Malacostraca collected by the "Tjalfe"-Expedition, under the direction of cand. mag. Ad. S. Jensen, especially at W. Greenland. Videnskabelige Meddelelser fra Dansk Naturhistorisk Forening 64: 57–134[, 36 figs].

Stephensen K (1944) Crustacea Malacostraca VIII (Amphipoda IV). Danish Ingolf-Expedition 3(13): 1–51.

Tamura K, Stecher G, Peterson D, Filipski A, Kumar S (2013) MEGA6: Molecular Evolutionary Genetics Analysis version 6.0. Molecular Biology and Evolution 30(12): 2725–2729. https://doi.org/10.1093/molbev/mst197

Trifinopoulos J, Nguyen LT, von Haeseler A, Minh BQ (2016) W-IQ-TREE: A fast online phylogenetic tool for maximum likelihood analysis. Nucleic Acids Research 44(W1): W232–W235. https://doi.org/10.1093/nar/gkw256

Vaidya G, Lohman DJ, Meier R (2011) Sequencematrix: Concatenation software for the fast assembly of multi-gene datasets with character set and codon information. Cladistics 27(2): 171–180. https://doi.org/10.1111/j.1096-0031.2010.00329.x

Verheye ML, d'Udekem D'Acoz C (2020) Integrative taxonomy of giant crested *Eusirus* in the Southern Ocean, including the description of a new species (Crustacea: Amphipoda: Eusiridae). Zoological Journal of the Linnean Society 20: 1–47. https://doi.org/10.1093/zoolinnean/zlaa141

Verheye M, Martin P, Backeljau T, d'Udekem d'Acoz C (2016) DNA analyses reveal abundant homoplasy in taxonomically important morphological characters of Eusiroidea (Crustacea, Amphipoda). Zoologica Scripta 45: 300–321[, supplements S1–S3]. https://doi.org/10.1111/zsc.12153

Walker AO (1903) Amphipoda of the "Southern Cross" Antarctic Expedition. Journal of the Linnean Society of London, Zoology 29(187): 38–64. https://doi.org/10.1111/j.1096-3642.1903.tb00425.x

Walker AO (1906) Preliminary descriptions of new species of Amphipoda from the 'Discovery' Antarctic Expedition, 1902–1904. Annals and Magazine of Natural History (Ser. 7) 17: 452–458. https://doi.org/10.1080/00222930608562555

Wang Y, Zhu C, Sha Z, Ren X (2020) *Epimeria liui* sp. nov., a new calcified amphipod (Amphipoda, Amphilochidea, Epimeriidae) from a seamount of the Caroline Plate, NW Pacific. ZooKeys 922: 1–11. https://doi.org/10.3897/zookeys.922.49141

Wang Y, Sha Z, Ren X (2021) A new species of *Eusirus* (Amphipoda, Amphilochidea, Eusiridae) described from a hydrothermal vent in the Okinawa Trough, North-West Pacific. Crustaceana 94(11–12): 1395–1405. https://doi.org/10.1163/15685403-bja10162

Yesson C, Clark MR, Taylor ML, Rogers AD (2011) The global distribution of seamounts based on 30 arc seconds bathymetry data. Deep-sea Research,Part I, Oceanographic Research Papers 58(4): 442–453. https://doi.org/10.1016/j.dsr.2011.02.004

Zhang J, Kapli P, Pavlidis P, Stamatakis A (2013) A general species delimitation method with applications to phylogenetic placements. Bioinformatics (Oxford, England) 29(22): 2869–2876. https://doi.org/10.1093/bioinformatics/btt499

Supplementary material 1

Additional data

Authors: Yan-Rong Wang, Zhong-Li Sha, Xian-Qiu Ren
Data type: xlsx

Link: https://doi.org/10.3897/zse.100.114758.suppl1

Zoosyst. Evol. 100 (2) 2024, 663–673 | DOI 10.3897/zse.100.118061

PENSOFT

MUSEUM FÜR NATURKUNDE BERLIN

Taxonomic revision of the cavefish genus *Karstsinnectes* (Cypriniformes, Nemacheilidae), with a description of a new species from Guangxi Province, China

Jia-Yue Ge[1,2*], Zheng-Quan Nong[3*], Jian Yang[4], Li-Na Du[1,2], Jia-Jun Zhou[5,6]

1 *Key Laboratory of Ecology of Rare and Endangered Species and Environmental Protection (Guangxi Normal University), Ministry of Education, Guilin, Guangxi 541004, China*

2 *Guangxi Key Laboratory of Rare and Endangered Animal Ecology, College of Life Science, Guangxi Normal University, Guilin, Guangxi 541004, China*

3 *Administration Center of Guangxi Nonggang National Nature Reserve, Longzhou Guangxi 532400, China*

4 *Key Laboratory of Environment Change and Resource Use, Beibu Gulf, Nanning Normal University, Nanning, Guangxi, 530001, China*

5 *Zhejiang Forest Resource Monitoring Center, Hangzhou, Zhejiang 310020, China*

6 *Zhejiang Forestry Survey Planning and Design Company Limited, Hangzhou 310020, China*

https://zoobank.org/0440F4DE-BECE-4B8B-9D84-88E17489226C

Corresponding authors: Li-Na Du (dulina@mailbox.gxnu.edu.cn); Jia-Jun Zhou (cnwaters@foxmail.com)

Academic editor: Nicolas Hubert ♦ **Received** 1 January 2024 ♦ **Accepted** 17 April 2024 ♦ **Published** 27 May 2024

Abstract

The blind cavefish genus *Karstsinnectes*, established in 2023, is the subject of taxonomic revision in the present study. Five valid species are recognized, including one new species, *Karstsinnectes longzhouensis* **sp. nov.**, described from Guangxi, China, based on a combination of morphological evidence. *Karstsinnectes longzhouensis* **sp. nov.** can be distinguished from all other congeners based on the presence of a lateral line, 11–12 branched pectoral fin rays, and five branched pelvic fin rays. Additionally, due to the loss of the type specimens, a neotype is designated for *K. parvus*. The lateral line of *K. hyalinus* is revised as lacking in this study. A key to all valid *Karstsinnectes* species is provided. Blind cavefish serve as a valuable natural framework for investigating convergent and adaptive evolutionary processes. The survival of cavefish is under significant threat due to human activities, climate change, water pollution, and invasive species. Thus, to preserve these valuable species, it is crucial to implement various conservation measures, such as habitat protection, artificial breeding, and fundamental research.

Key Words

Blind cavefish, complete mitochondrial genome, morphology, Taxonomy, Xijiang River

Introduction

Karst caves and subterranean streams represent dominant geomorphological features in the Guangxi, Guizhou, Sichuan, and Yunnan provinces and Chongqing City of China. These regions are renowned for harboring many unique cave-dwelling fish species (Zhao and Zhang 2009). Ma et al. (2019) recorded 148 hypogean species in China, including 65 nemacheilids in *Heminoemacheilus*, *Oreonectes*, *Protocobitis*, *Paranemachilus*, *Schistura*, *Troglonectes*, *Triplophysa*, and *Yunnanilus*. Luo et al. (2023) described a new genus, *Karstsinnectes* Zhou, Luo, Wang, Zhou & Xiao, 2023, with *Oreonectes anophthalmus* Zheng, 1981, as the type specimen, based on morpho-

* These authors contributed equally to this work.

logical characters and molecular evidence. The diagnostic characters of *Karstsinnectes* include body scaleless and colorless, anterior and posterior nostrils separated, the base of the anterior nostril tube-shaped, a tip not elongated to barbel-like, adipose crests present on the caudal peduncle, lateral line and cephalic lateral line canals present, and the body capsule of the swim bladder open posteriorly (Luo et al. 2023). Four species within the genus *Karstsinnectes* have been recorded, including *K. acridorsalis* (Lan, 2013), *K. anophthalmus* (Zheng, 1981), *K. hyalinus* (Lan, Yang & Chen, 1996), and *K. parvus* (Zhu & Zhu, 2014).

In December 2022, four *Karstsinnectes* specimens were collected from a cave in Longzhou County, Chongzuo City, Guangxi, China. Morphological characters and molecular analyses indicated that these specimens represented an undescribed species of *Karstsinnectes*. Additionally, a taxonomic revision of *K. acridorsalis* and *K. hyalinus* is provided, and a neotype is designated for *K. parvus* herein.

Materials and methods

All care and use of experimental animals complied with the relevant laws of the Chinese Laboratory of Animal Welfare and Ethics (GB/T 35892-2018). Specimens of *Karstsinnectes longzhouensis* sp. nov. were rapidly euthanized by an overdose of anesthetic clove oil. The right-side pectoral fin and pelvic fin were excised and preserved in 99% ethanol. Specimens for morphological study were initially stored in 10% formalin, then transferred to 75% alcohol for long-term preservation at the Kunming Natural History Museum of Zoology, Kunming Institute of Zoology (KIZ), Chinese Academy of Sciences (CAS).

Counts and measurements followed Du et al. (2021) and Luo et al. (2023). Data were initially processed using Microsoft Excel software for preliminary statistical analysis. The original data were converted to percentages of standard length (SL) or lateral head length (HL), followed by logarithmic conversion (log10) to remove the effects of allometry. Comparative morphometry was examined using principal component analysis (PCA) in IBM SPSS Statistics v20.0. Non-parametric analysis of variables with principal component loadings greater than 60% was used to determine the degree of differences between subjects, and the scores of each principal component were used to generate scatter plots for analysis.

Complete mitochondrial genome sequencing data were submitted to GenBank under Accession No. OR947935. The mitogenome of OR947935 was sequenced on Illumina Novaseq 6000 (Origingene Bio-pharm Technology Co. Ltd., Shanghai, China). The quality of sequencing raw data was evaluated by Fastqc (v.0.11.8) and trimmed using Cutatapt (v.4.8) software (Martin 2011). Obtained Illumina reads were de novo assembled using the NOVOPlasty software (Dierckxsens et al. 2017), and the assembled genome was annotated by Mitos2 (Bernt et al. 2013). Relative synonymous codon usage (RSCU) in protein coding sequences and simple sequence repeats (SSRs) of OR947935 were determined in CodonW (v.1.4.2) and MISA, respectively (Peden 1999; Beier et al. 2017). To test the phylogenetic position of *Karstsinnectes longzhouensis* sp. nov., Bayesian inference (BI) was performed using MrBayes in XSEDE (v3.2.7a) by CIPRES Science Gateway (Miller et al. 2010). The entire sequence of the mitochondrial genomes was used as a single partition. The substitution model GTR + I + G was selected as the best model using jModelTest v.2.1.10 (Darriba et al. 2012). Likelihood Model parameters were set as number of substitution types allow all rates to be different, subject to the constraint of time-reversibility (Nst = 6), nucleotide substitution model. Nucmodel was standard model of DNA substitution in which there are only four states (Nucmodel = 4×4), the rate at a site is drawn from a gamma distribution, and all site patterns had the possibility of being sampled (Coding = all). Forty complete mitochondrial genomes obtained from GenBank were included in the data. *Parabotia fasciata* Dabry de Thiersant, 1872 and *Leptobotia elongata* (Bleeker, 1870), two botiid species, were used as outgroups. Two runs were performed simultaneously with four Markov chains starting from a random tree. The chains were run for five million generations and sampled every 100 generations. The first 25% of sampled trees were discarded as burn-in, and the remaining trees were used to create a consensus tree and estimate Bayesian posterior probabilities (BPPs). Uncorrected pairwise distances between species of Karstsinnectes were calculated in MEGA v11.

Results

Genus *Karstsinnectes* Zhou, Luo, Wang, Zhou & Xiao, 2023

Karstsinnectes Zhou, Luo, Wang, Zhou & Xiao, 2023, 696 original descriptions.

Type species. *Oreonectes anophthalmus* Zheng, 1981.

Diagnosis. Base of anterior nostril tube-like and tip not elongated to barbel-like; anterior and posterior nostrils adjacent; lips with furrows; caudal peduncle with adipose crests; bony capsule of swim bladder opens posteriorly.

Remarks. In the family Nemacheilidae, the genera *Eonemachilus* Berg, 1938; *Karstsinnectes*; *Micronemacheilus* Rendahl, 1944; *Protonemacheilus* Yang & Chu, 1990; *Traccatichthys* Freyhof & Serov, 2001; and *Yunnanilus* Nichols, 1925, are characterized by a tube-like anterior nostril with tip not elongated to barbel-like structure (Du et al. 2021, 2023). However, *Karstsinnectes* can be distinguished from *Eonemachilus*, *Protonemacheilus*, *Traccatichthys*, and *Yunnanilus* by anterior and posterior nostrils adjacent (vs. separated in *Eonemachilus* and *Yunnanilus*, closely set in *Protonemacheilus* and *Traccatichthys*) and from *Micronemacheilus* and *Traccatichthys* by lips with furrows (vs. with papillae).

Species included. *Karstsinnectes acridorsalis* (Lan, 2013), *K. anophthalmus* (Zheng, 1981), *K. hyalinus* (Lan, Yang & Chen, 1996), *K. longzhouensis* sp. nov., and *K. parvus* (Zhu & Zhu, 2014).

Key to species of *Karstsinnectes*

1 Caudal fin truncated ..... *K. anophthalmus*
– Caudal fin forked 2
2 Body covered by scales ..... *K. hyalinus*
– Body scaleless 3
3 Lateral line present 4
– Lateral line absent ..... *K. acridorsalis*
4 Pectoral fin with 10 branched rays, five branched pelvic fin rays ..... *K. parvus*
– Pectoral fin with 11 or 12 branched rays, six branched pelvic fin rays ..... *Karstsinnectes longzhouensis* sp. nov.

Karstsinnectes acridorsalis (Lan, 2013)

Figs 1A, 2; Table 1

Oreonectes acridorsalis Lan, 2013: 68, fig. 50 (Bamu Town, Tian'e County, Hechi City, Guangxi).

Troglonectes acridorsalis Xiao & Lan, 2023: 33 (Bamu Town, Tian'e County, Hechi City, Guangxi).

Karstsinnectes acridorsalis Luo et al., 2023, 696 (Bamu Town, Tian'e County, Guangxi).

Material examined. *Paratypes*. 2 ex. China; Guangxi, Hechi City, Tian'e County, Bamu Town, 22.8754°N, 107.1947°E, 284 m a.s.l. CLJH 1202001, CLJH 04100607, 37.9–38.1 mm SL, deposited in the Fishery and Animal Husbandry Bureau of Du'an, Guangxi, China.

Diagnosis. *Karstsinnectes acridorsalis* differs from *K. anophthalmus* by caudal fin forked (vs. truncated), 14 branched caudal-fin rays (vs. 12), longer and lower head (length 29.9%–32.7% of SL vs. 22.7%–24.6%, height 34.6%–39.6% of head length vs. 41.0%–44.0%), longer pectoral fin (61.6%–67.7% of distance between pectoral-fin origin and pelvic-fin origin vs. 35.9%–48.9%); from *K. hyalinus* by scaleless (vs. scaled), five branched anal-fin rays (vs. four), 14 branched caudal-fin rays (vs. 11 or 12); from *K. parvus* and *K. longzhouensis* sp. nov. by lateral line absent (vs. present), lower body (body depth 13.9%–15.5% of SL vs. 17.1%–18.4% and 16.1%–19.4%, respectively), shorter caudal peduncle (length 15.7%–15.9% of SL vs. 18.4%–22.3% and 17.3%–19.5%, respectively).

Description. Body elongated, head depressed, snout depressed, forehead raised, head height at nostril 46.1%–67.9% of maximum head height. Body trunk compressed, with maximum body depth anterior to dorsal-fin origin, deepest body depth 13.9%–15.5% of SL. Dorsal profile of head and predorsal profile slightly convex, clearly concave from dorsal-fin origin to tip of dorsal fin, and gradually convex from tip of dorsal fin to anterior quarter of caudal fin due to caudal adipose keel on upper edge of caudal peduncle. Ventral profile of head straight, nearly straight from pectoral-fin insertion to anal-fin origin, convex from posterior margin of anal-fin base to anterior quarter of caudal fin due to caudal adipose keel on lower edge of caudal peduncle.

Anterior and posterior nostrils adjacent, distance less than posterior nostril diameter, base of anterior nostril tube-shaped and tip not elongated to barbel-like. Eyes absent. Mouth inferior, snout rounded, upper and lower lips smooth, lower lip with V-shaped median notch. Three pairs of barbels, inner and outer rostral barbels reaching mouth corner, and maxillary barbel reaching anterior margin of interopercle. Inner gill rakers on first gill arch nine (one specimen).

Dorsal fin with three unbranched and eight branched rays, distal margin straight, origin posterior to pelvic-fin origin, predorsal length 54.3%–55.5% of SL. Pectoral fin with one unbranched and 10 branched rays, pectoral-fin length 61.6%–67.7% of distance between pectoral-fin origin and pelvic-fin origin. Pelvic fin with one unbranched and five branched rays, tip of pelvic fin not reaching anus. Anal fin with two unbranched and five branched rays, distal margin straight. Anus abutting anal-fin base. Caudal fin forked. High caudal adipose keels on upper and lower edges of caudal peduncle, height at most of upper adipose keel nearly 1/2 caudal peduncle depth. Caudal peduncle depth 46.1%–51.9% of its length (containing adipose keels). Lateral line and cephalic sensory pores absent. Body scaleless.

Coloration. Whole body translucent, without color pattern. Fin membrane hyaline.

Distribution and habitat. Only known from the type locality. *Karstsinnectes acridorsalis* inhabits a subterranean river, 22.8754°N, 107.1947°E, 284 m a.s.l. Co-inhabitants of the stream include *Triplophysa tianeensis* Chen, Cui & Yang, 2004, *Sinocyclocheilus furcodorsalis* Chen, Yang & Lan, 1997, and *Hongshuia megalophthalmus* (Chen, Yang & Cui, 2006).

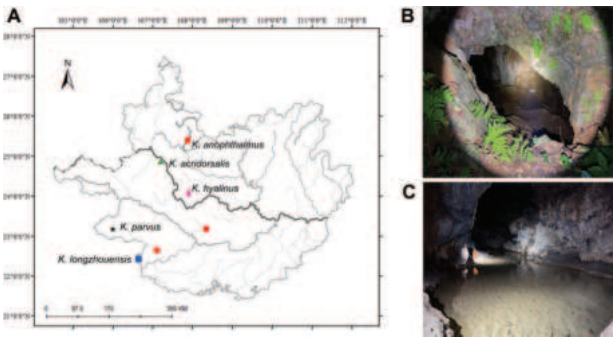

Figure 1. Collection sites (**A**), *K. anophthalmus* (red round), *K. acridorsalis* (green triangle), *K. hyalinus* (purple rhombus), *K. longzhouensis* sp. nov. (blue square), *K. parvus* (black star), and habitat of *Karstsinnectes longzhouensis* sp. nov. (**B**) and *K. parvus* (**C**).

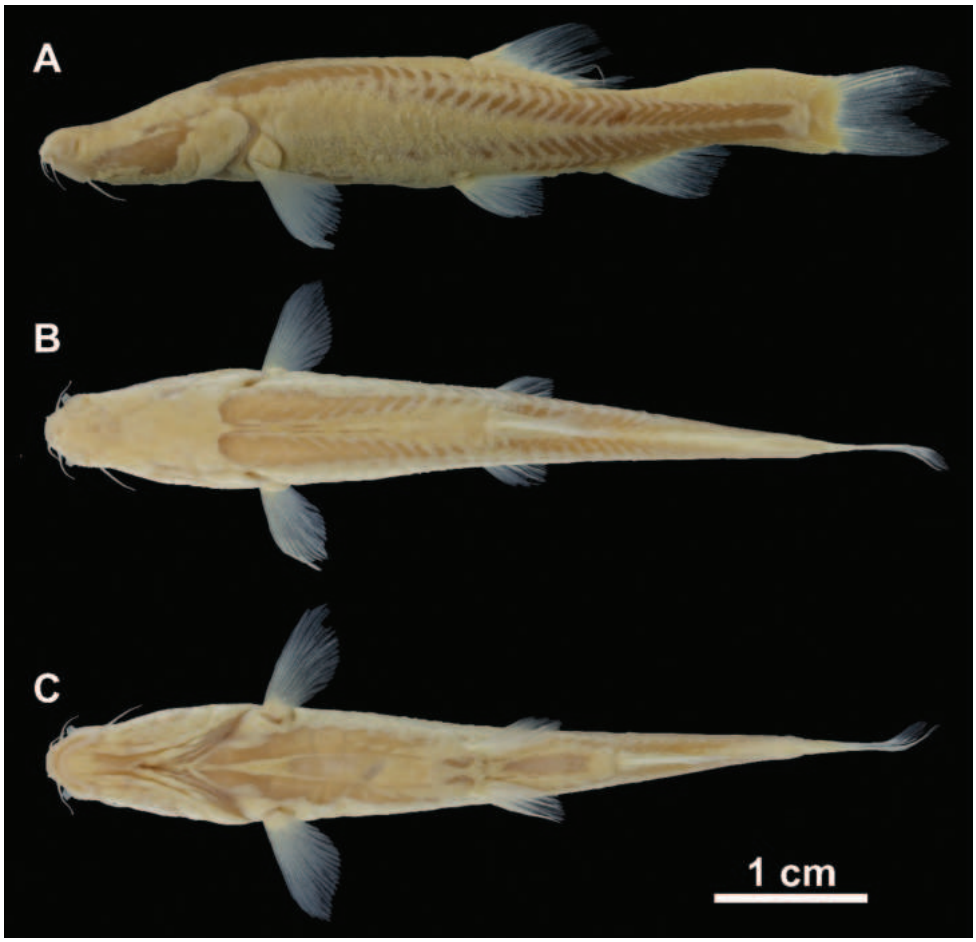

Figure 2. Lateral, dorsal, and ventral views of *Karstsinnectes acridorsalis*, holotype, CLJH04100608 (photograph from J.H. Lan). Scale bar: 1 cm.

Remarks. The population of *K. acridorsalis* is small. Initially described by Lan et al. (2013) based on three specimens, subsequent collections yielded only one specimen, collected in 2019 by J.J. Zhou.

Karstsinnectes hyalinus (Lan, Yang & Chen, 1996)

Figs 1A, 3; Table 1

Heminoemacheilus hyalinus Lan, Yang & Chen, 1996, 109–112 (Bao'an Township, Du'an County, Hechi City, Guangxi).

Karstsinnectes hyalinus Luo et al., 2023: 696 (Bao'an Township, Du'an County, Hechi City, Guangxi).

Material examined. 3 ex. China; Guangxi, Hechi City, Du'an County, Bao'an Township, 24.0709°N, 107.9027°E, 283 m a.s.l. GXNU 94098009–94098011, 38.9–40.2 mm SL.

Diagnosis. *Karstsinnectes hyalinus* can be distinguished from other members of *Karstsinnectes* based on body-scaled (vs. scaleless). It can be further differentiated from *K. anophthalmus* by caudal fin forked (vs. truncated); from *K. acridorsalis*, *Karstsinnectes longzhouensis* sp. nov., and *K. parvus* by seven branched dorsal-fin rays (vs. eight in *K. acridorsalis* and nine in *Karstsinnectes longzhouensis* sp. nov. and *K. parvus*).

Description. Body elongated, head depressed. Body trunk compressed, dorsal profile of head and predorsal profile gradually convex, with maximum body depth in middle of pectoral-fin origin and pelvic-fin origin. After dorsal-fin base, dorsal profile of caudal peduncle convex due to developed caudal adipose keel on upper edge of caudal peduncle. Ventral profile of head straight, slightly convex from pectoral-fin origin to pelvic-fin origin, straight from pelvic-fin origin to caudal-fin base.

Anterior and posterior nostrils adjacent, distance less than posterior nostril diameter, base of anterior nostril tube-shaped and tip not clearly elongated to barbel-like. Eyes absent. Mouth inferior, snout obtuse, upper and lower lips smooth. Three pairs of barbels, inner rostral barbel reaching mouth corner, outer rostral and maxillary barbels reaching anterior margin of interopercle. One specimen with one outer and 12 inner gill rakers on first gill arch.

Dorsal fin with two branched and seven branched rays, distal margin straight, origin slightly anterior to pelvic-fin origin. Pectoral fin with one unbranched and 11 branched rays, pectoral-fin length 66.1%–74.8% of distance between pectoral-fin origin and pelvic-fin origin. Pelvic fin with one unbranched and five branched rays, tip of pelvic fin reaching anus. Anal fin with two unbranched and four branched rays, distal margin straight.

Table 1. Morphometric and meristic data of the genus *Karstsinnectes*. Range, mean, and standard deviation (mean ± standard deviation (SD)).

	***K. acridorsalis* (N = 2)**	***K. anophthalmus* (N = 4)**	***K. hyalinus* (N = 3)**	***Karstsinnectes longzhouensis* sp. nov. (N = 4)**	***K. parvus* (N = 3)**
Total length (mm)	44.8–45.9 (45.3 ± 0.8)	30.5–42.8 (36.4 ± 5.1)	47.4–47.5 (47.4 ± 0.1)	57.8–73.3 (64.6 ± 6.8)	32.3–34.8 (33.4 ± 1.3)
Standard length (mm)	37.9–38.1 (38.0 ± 0.1)	25.3–36.9 (31.4 ± 4.8)	38.9–40.2 (39.5 ± 1.0)	49.4–60.1 (53.6 ± 4.8)	26.5–28.3 (27.1 ± 1.1)
Percentage of standard length (%)					
Deepest body depth	13.9–15.5 (14.7 ± 1.1)	11.0–14.4 (13.2 ± 1.6)	19.9–23.6 (21.6 ± 1.8)	16.1–16.4 (17.8 ± 1.4)	17.1–18.4 (17.9 ± 0.7)
Lateral head length	29.9–32.7 (31.3 ± 2.0)	22.7–24.6 (23.5 ± 0.8)	27.1–29.2 (28.0 ± 1.1)	30.2–34.0 (32.2 ± 1.6)	32.5–33.0 (32.7 ± 0.2)
Prodorsal length	54.4–55.5 (54.9 ± 0.8)	59.5–62.6 (60.5 ± 1.4)	55.9–59.0 (57.7 ± 1.6)	55.1–57.3 (56.2 ± 1.1)	52.9–56.3 (54.8 ± 1.8)
Prepelvic length	52.9–54.6 (53.7 ± 1.2)	57.4–58.3 (57.8 ± 0.5)	52.2–56.8 (55.1 ± 2.6)	55.6–58.3 (57.4 ± 1.3)	53.5–58.1 (56.0 ± 2.3)
Preanal length	74.2–75.1 (74.7 ± 0.6)	68.0–76.3 (73.7 ± 3.9)	74.4–79.8 (77.8 ± 2.9)	74.7–76.0 (75.4 ± 0.6)	71.8–76.1 (74.6 ± 2.4)
Preanus length	67.5–70.8 (69.1 ± 2.3)	-	70.6–74.0 (72.5 ± 1.7)	69.4–71.8 (70.2 ± 1.1)	61.7–74.1 (69.2 ± 6.6)
Caudal peduncle length	15.7–15.9 (15.8 ± 0.1)	13.2–17.0 (15.4 ± 1.7)	15.1–16.2 (15.7 ± 0.5)	17.3–19.5 (18.1 ± 1.0)	18.4–22.3 (19.9 ± 2.1)
Caudal peduncle depth (containing caudal adipose keels)	7.3–8.3 (7.8 ± 0.7)	5.7–8.7 (6.9 ± 1.3)	13.0–14.7 (13.8 ± 0.9)	9.2–11.7 (10.5 ± 1.1)	8.4–9.8 (9.2 ± 0.7)
Head width	11.7–12.3 (12.0 ± 0.4)	14.1–16.8 (15.3 ± 1.2)	16.1–17.6 (16.7 ± 0.8)	17.7–21.5 (19.4 ± 1.6)	14.9–18.0 (16.8 ± 1.7)
Percentage of lateral head length (%)					
Head depth	34.6–39.6 (37.1 ± 3.5)	41.0–44.0 (42.6 ± 1.3)	45.1–48.5 (46.9 ± 1.7)	42.3–49.1 (45.4 ± 3.0)	40.8–44.6 (42.7 ± 1.9)
Head width	37.5–39.2 (38.4 ± 1.2)	60.0–73.4 (65.5 ± 6.0)	59.5–60.3 (59.8 ± 0.4)	52.1–71.1 (60.4 ± 8.2)	45.8–54.5 (51.3 ± 4.8)
Percentage of caudal-peduncle length (%)					
Caudal peduncle depth (containing caudal adipose keels)	46.1–51.9 (49.0 ± 4.1)	33.6–57.2 (45.4 ± 9.9)	81.3–97.4 (87.8 ± 8.5)	47.0–66.1 (58.5 ± 8.1)	37.7–53.1 (46.8 ± 8.1)
Percentage of distance from pectoral-fin origin to pelvic-fin origin					
Pectoral-fin length	61.6–67.7 (64.6 ± 4.3)	35.9–48.9 (40.5 ± 6.1)	66.1–74.8 (70.8 ± 4.4)	72.4–85.9 (77.9 ± 5.8)	67.5–76.8 (73.3 ± 5.0)
Dorsal-fin rays	3, 8–9	3, 7	3, 7	3, 9	3, 9
Pectoral-fin rays	1, 10	1, 10	1, 11	1, 11–12	1, 10
Pelvic-fin rays	1, 5	1, 4	1, 5	1, 5	1, 6
Anal-fin rays	3, 5	3, 5	3, 4	3, 5	3, 5
Caudal-fin branched rays	14	12	11–12	13–14	12–13

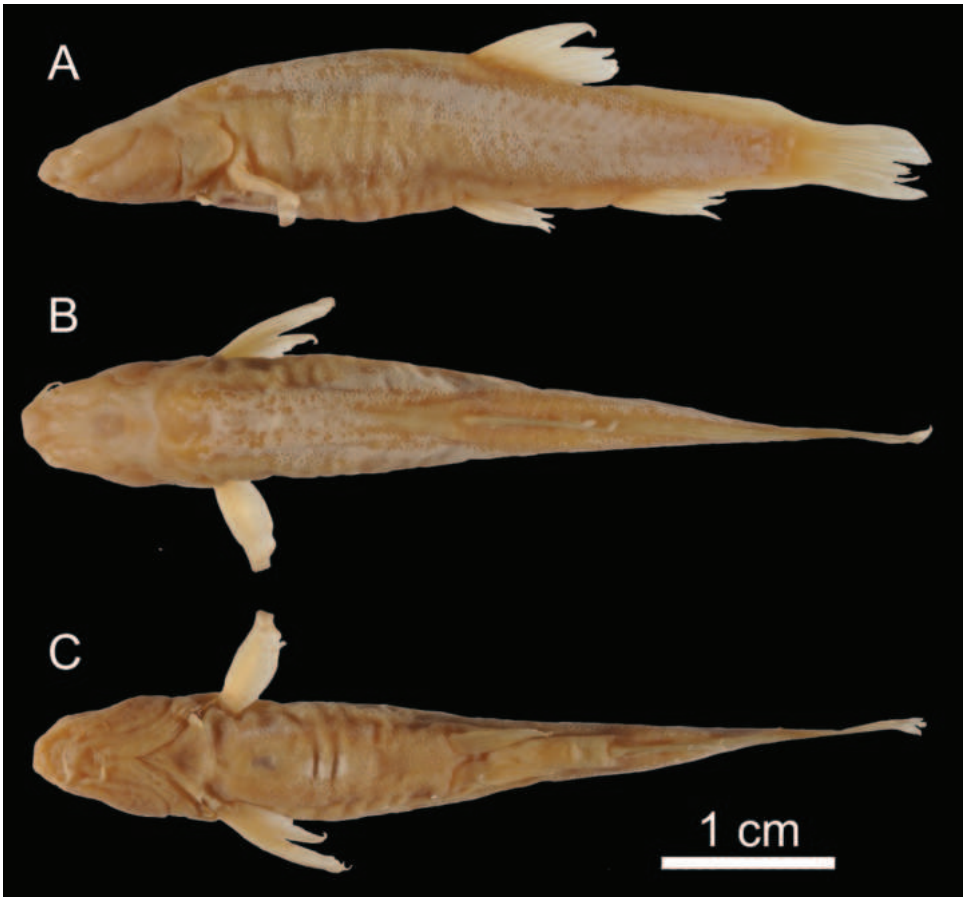

Figure 3. Lateral, dorsal, and ventral views of *K. hyalinus*, holotype KIZ1994000011 (photograph from R. Min). Scale bar: 1 cm.

Anus abutting anal-fin base. Caudal fin forked, with 11 or 12 branched rays. High caudal adipose keels on upper and lower edges of caudal peduncle, height at most of upper adipose keel nearly 1/2 caudal peduncle depth. Caudal peduncle length 102.7%–123.1% of its depth (containing adipose keels). Lateral line and cephalic sensory pores absent. Body covered by scales, except head and thorax.

Coloration. Whole body translucent, without color pattern. Fin membrane hyaline.

Distribution and habitat. Known only from the type locality, China; Guangxi, Hechi City, Du'an County, Bao'an, 24.0709°N, 107.9027°E, 283 m a.s.l. The cave water in which this species resides serves as the only source of drinking water for nearby residents. The decline in its population is primarily attributed to habitat alterations resulting from the extraction of cave water for domestic purposes (Zhang and Cao 2021).

Remarks. The population of *K. hyalinus* is extremely small, with its presence currently known only through type specimens collected in 1994, with no additional specimens gathered since. Although the lateral line of *K. hyalinus* was mentioned in the original description, a re-examination of all type specimens by R. Min, the administrator of the Fish Collection Room, Kunming Natural History Museum of Zoology, Kunming Institute of Zoology, revealed no obvious lateral line pores. Hence, *K. hyalinus* is described as lacking a lateral line in this study.

Karstsinnectes longzhouensis Ge, Du & Zhou, sp. nov.

https://zoobank.org/7D4659FE-C737-4F36-A56F-7DB474246352

Figs 1A, B, 4; Table 1

Type materials. ***Holotype.*** China (permanent whole specimen in 75% alcohol); Guangxi, Chongzuo City, Longzhou County, Xiadong Town; 22.4222°N, 106.6385°E, 170 m a.s.l.; collected by Z.Q. Nong and J.J. Zhou, 29 December 2022. Kunming Natural History Museum of Zoology, KIZ 2023000001, 50.6 mm standard length (SL).

Paratypes. China (permanent whole specimens in 75% alcohol); same collection data as for holotype, collected by Z.Q. Nong and J.J. Zhou, 29 December 2022; KIZ 2023000002–04, 3 ex., 49.4–60.1 mm SL.

Diagnosis. *Karstsinnectes longzhouensis* sp. nov. can be distinguished from all other members of *Karstsinnectes* based on the combination characteristics of the lateral line present, 11 or 12 branched pectoral-fin rays, and five branched pelvic-fin rays. It can be further distinguished from *K. anophthalmus* by caudal fin forked (vs. truncated), five branched pelvic-fin rays (vs. four), nine branched dorsal-fin rays (vs. seven), 13 or 14 branched caudal-fin rays (vs. 12); from *K. acridorsalis* by nine branched dorsal-fin rays (vs. eight), body depth 16.1%–19.4% of SL (vs. 13.9%–15.5%); from *K. hyalinus* by body scaleless (vs. scaled), lateral line present (vs. absent), nine branched dorsal-fin rays (vs. seven), five branched anal-fin rays (vs. four); from *K. parvus* by 11 or 12 branched pectoral-fin rays (vs. 10), five branched pelvic-fin rays (vs. six), and uncorrected *p* distance is 3.9%.

Description. Morphometric data of the type specimens of *Karstsinnectes longzhouensis* sp. nov. are given in Table 1. Body elongated, head depressed, forehead raised, head height at nostril 60.8%–71.0% of maximum head height. Body trunk compressed, with maximum body depth in middle of pectoral-fin origin and pelvic-fin origin, deepest body depth 16.1%–19.4% of SL. Dorsal profile of forehead and predorsal profile convex, concave from dorsal-fin origin to anterior margin of upper caudal adipose keel. Caudal adipose keel on upper edge of caudal of peduncle slightly convex. Ventral profile of head straight, slightly convex from pectoral-fin origin to pelvic-fin origin, straight between pelvic-fin and anal-fin origin, and gradually concave from anal-fin base to anterior quarter of caudal fin due to caudal adipose keel on lower edge of caudal peduncle.

Anterior and posterior nostrils adjacent, distance less than posterior nostril diameter, base of anterior nostril tube-shaped and tip not elongated to barbel-like. Eyes absent. Mouth inferior, snout rounded, upper and lower lips smooth, lower lip with V-shaped median notch. Three pairs of barbels, inner rostral barbel reaching anterior nostril, outer rostral barbel reaching posterior margin of posterior nostril, and maxillary barbel reaching anterior margin of interopercle. Two specimens with 11–12 inner gill rakers on first gill arch.

Dorsal fin with three unbranched and nine branched rays, distal margin of dorsal fin straight, origin anterior to pelvic-fin origin, predorsal length 55.1%–57.3% of SL. Pectoral fin with one unbranched and 10 branched rays, pectoral-fin length 72.4%–85.9% of distance between pectoral-fin origin and pelvic-fin origin. One unbranched and five branched pelvic-fin rays, tip of pelvic fin reaching, but not exceeding anus. Anus abutting anal-fin base. Caudal fin forked, with 13 or 14 branched caudal-fin rays. High caudal adipose keels on upper and lower edges of caudal peduncle, height at most of upper adipose keel less than 1/2 caudal peduncle depth. Caudal peduncle length 151.2%–212.9% of its depth (containing adipose keels). Lateral line and head sensory pores absent. Body scaleless.

Coloration. Dorsal and trunk of body yellowish, abdomen gray and translucent, stomach and intestine visible from outside. Without color pattern. Fin membrane hyaline.

Distribution and habitat. *Karstsinnectes longzhouensis* sp. nov. inhabits karst caves located in the Guangxi Qinglongshan provincial natural reserve, specifically in Xiadong Town, Longzhou County, Chongzuo City, Guangxi, China (22.4222°N, 106.6385°E, 171 m a.s.l.). The species was observed in a subterranean pool accessed through an oval cave entrance and a narrow passage. The pool water depth exceeded 1 m and was characterized by a substratum of mud and cobblestones.

Etymology. The specific name "*longzhouensis*" is derived from the Chinese name of the type locality in Longzhou County. Therefore, the Chinese and English common names for this new species are "龙州中华喀鳅" and "Longzhou Chinese Karst Loach," respectively.

Figure 4. Lateral, dorsal, and ventral views of *Karstsinnectes longzhouensis* sp. nov., holotype KIZ2023000001. Scale bar: 1 cm.

Remarks. On 29 December 2022, Z.Q. Nong collected type specimens within a karst cave. By May 2023, the cave showed significant signs of drying. In another cave located 300 m away, J.J. Zhou collected a deteriorated specimen. Decreased precipitation and the removal of domestic water from the cave appear to have negatively influenced the viability of cavefish during the dry season.

Karstsinnectes parvus (Zhu & Zhu, 2014)

Figs 1A, C, 5; Table 1

Heminoemacheilus parva Zhu & Zhu, 2014: 18–21 (Ande Town, Napo County, Guangxi).

Karstsinnectes parvus Luo et al., 2023, 696 (Ande Town, Napo County, Guangxi).

Neotype designation. Both holotype and paratypes were originally deposited at the Guangxi Fisheries and Animal Husbandry School under registration numbers 2011006–2011009 (Zhu and Zhu 2014) but were broken and lost three years ago (Y. Zhu, pers. comm.). Conforming with Article 75.3 of the Code (ICZN 1999), a neotype from the type locality is herein designated (Fig. 5).

Neotype. China; Guangxi, Baise City, Napo County, Nongma Village, 23.1803°N, 106.0020°E, 934 m a.s.l., collected by J.J. Zhou, J.Q. Luo, X.M. Luo, and Z.X. Qin on 1 May 2023; KIZ 2023000005 (Fig. 5), 26.5 mm SL.

Non-type material. 2 ex. China; same collected with neotype, collected by J.J. Zhou, J.Q. Luo, X.M. Luo, and Z.X. Qin on 1 May 2023; GXNU 20230501001, GXNU 20230501003, 26.5–28.3 mm SL.

Diagnosis. *Karstsinnectes parvus* can be distinguished from *K. acridorsalis* by lateral line present (vs. absent), nine branched dorsal-fin rays (vs. eight), six branched pelvic-fin rays (vs. five), 12 or 13 branched caudal-fin rays (vs. 14); from *K. anophthalmus* by caudal fin forked (vs. truncated), lateral line present (vs. absent), nine branched dorsal-fin rays (vs. seven), six branched pelvic-fin rays (vs. four); from *K. hyalinus* by body scaleless (vs. scaled), lateral line present (vs. absent), nine branched dorsal-fin rays (vs. seven), five branched anal-fin rays (vs. four); from *Karstsinnectes longzhouensis* sp. nov. by 10 branched pectoral-fin rays (vs. 11 or 12), six branched pelvic-fin rays (vs. five).

Description. Body elongated, slightly flattened in front, strongly compressed in back. Maximum body depth anterior to dorsal-fin origin, deepest body depth 17.1%–18.4% of SL. Head depressed and flattened, maximum width greater than maximum depth. Anterior and posterior nostrils adjacent, distance less than posterior nostril diameter, base of anterior nostril tube-shaped and tip not elongated to barbel-like. Eyes absent. Mouth inferior, snout rounded, upper and lower lips smooth, lower lip with V-shaped median notch. Three pairs of barbels, inner rostral barbel reaching anterior nostril, outer rostral barbel reaching posterior margin of posterior nostril, and maxillary barbel reaching anterior margin of interopercle. One specimen with 11 inner gill rakers on first gill arch.

Dorsal fin with three unbranched and nine branched rays, distal margin of dorsal fin straight, origin anterior to pelvic-fin origin, predorsal length 52.9%–56.3% of SL. Pectoral fin with one unbranched and 10 branched

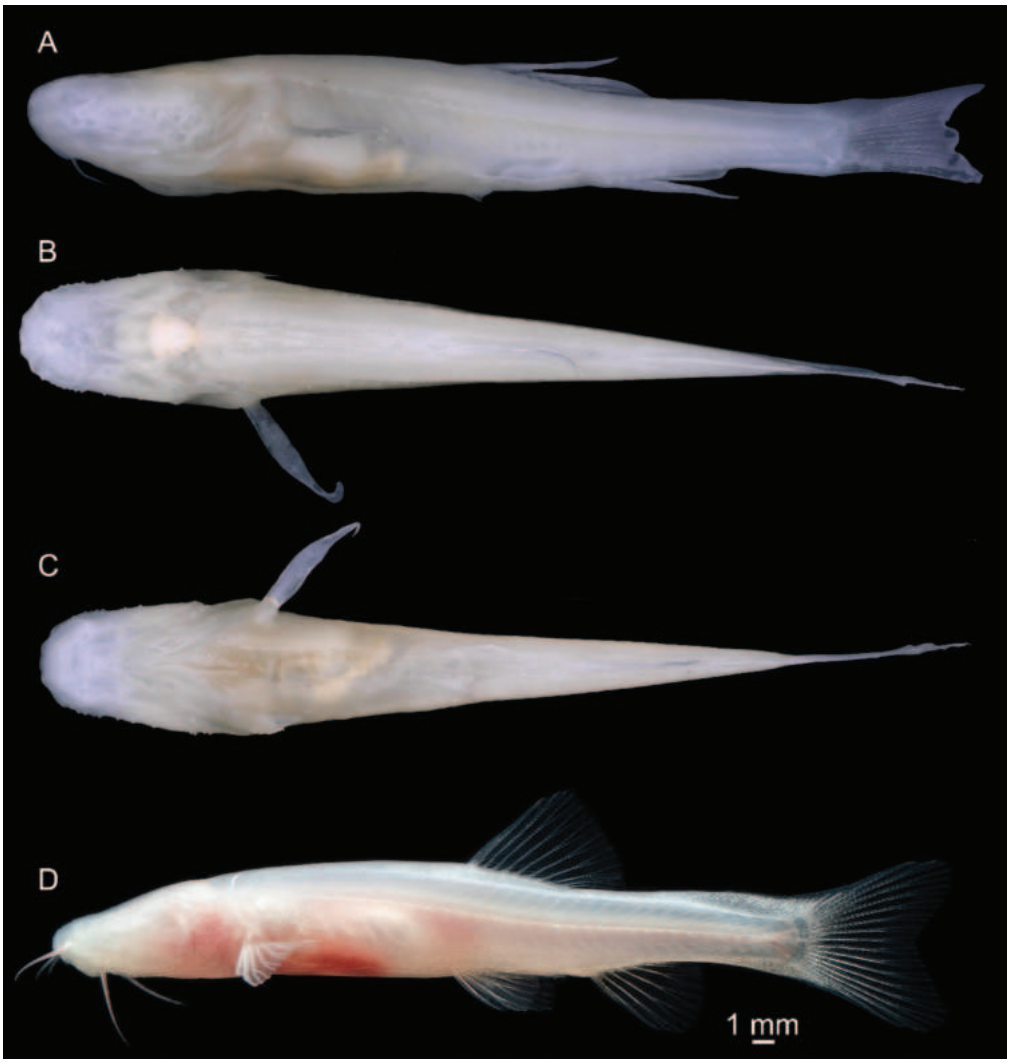

Figure 5. Lateral, dorsal, ventral views, and living photo of *K. parvus*, neotype KIZ2023000005 (photograph from M. Liang). Scale bar: 1 mm.

rays, pectoral-fin length 67.5%–76.8% of distance between pectoral-fin origin and pelvic-fin origin. Pelvic fin with one unbranched and six branched rays, tip of pelvic fin exceeding anus. Anal fin with three unbranched and five branched rays, distal margin straight. Anus abutting anal-fin base. Caudal fin forked, with 12 or 13 branched rays. High caudal adipose keels on upper and lower edges of caudal peduncle, height at most of upper adipose keel less than 1/2 caudal peduncle depth. Caudal peduncle length 188.4%–265.6% of its depth (containing adipose keels). Lateral line present. Body scaleless.

Coloration. Dorsal and trunk of body gray and translucent, stomach and intestine visible from outside. Without color pattern. Fin membrane hyaline.

Distribution and habitat. *Karstsinnectes parvus* inhabits a karst cave in Nongma Village, Napo County, Baise City, Guangxi, China; 23.1803°N, 106.0020°E, 934 m a.s.l., in a small and shallow river (approximately 300 m long, depths of less than 20 cm), characterized by substrata composed of mud and cobblestones. Five to six specimens were caught in each survey in 2021.

Remarks. Given the loss of the type specimens three years ago (Y. Zhu, pers. comm.), three specimens of *K. parvus* were newly collected from the type locality. These specimens conformed to the original description in all aspects except for the caudal fin count. The caudal fin of the holotype was damaged in the original account, preventing verification of the fin ray count from the holotype photograph in the initial description. Lan et al. collected this species from the type locality in 2021 and noted 13 branched rays of the caudal fin (Xiao and Lan 2023). This observation suggests that the unbranched rays of the caudal fin may have been included in the count of branched rays in the original description.

Genetic comparisons

Based on BI analyses, molecular phylogenies demonstrated that species of *Karstsinnectes* constituted a monophyletic group with robust support (100% bootstraps). Furthermore, they were sister to the clade com-

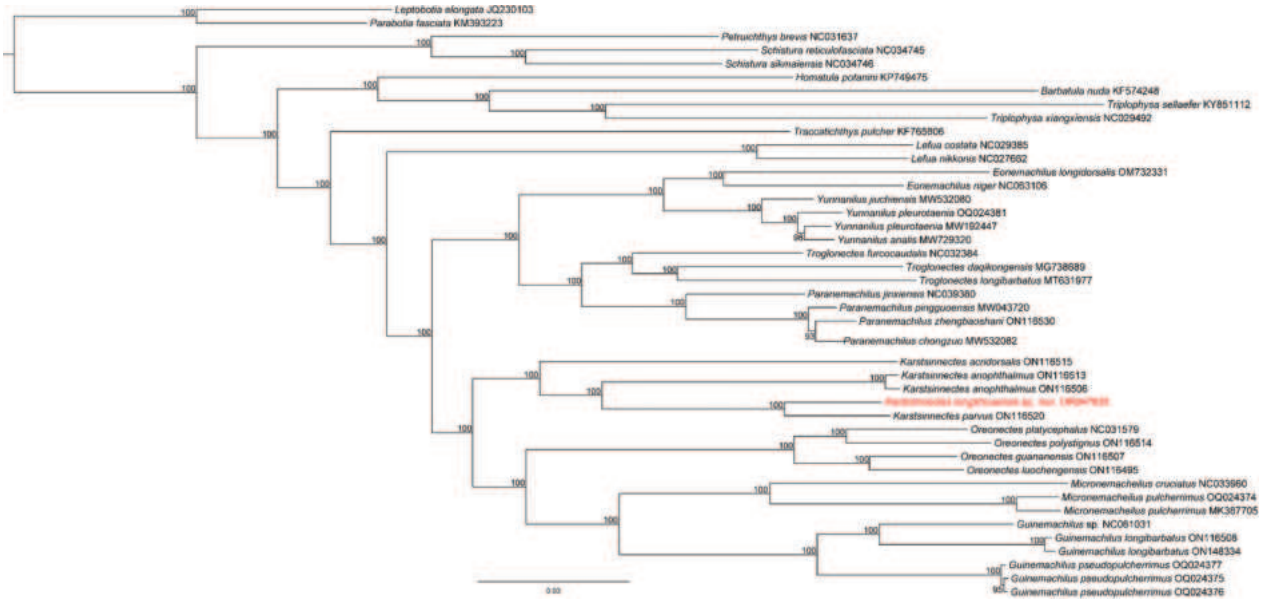

Figure 6. Bayesian phylogram of *Karstsinnectes* based on the mitochondrial genomes of 40 nemacheilid and two botiid species (outgroups). The numbers above the branches are Bayesian posterior probabilities (BPP%).

prised of *Oreonectes*, *Micronemacheilus*, and *Guinemachilus* species. *Karstsinnectes longzhouensis* sp. nov. was determined to be a sister group to *K. parvus* and further sister to *K. anophthalmus* and *K. acridorsalis* (Fig. 6). Additionally, pairwise comparisons of complete mitochondrial genomes revealed that the average uncorrected *p* distance between species of *Karstsinnectes* ranged from 3.96% to 11.38% (average 9.65%). The minimum uncorrected *p* distance is between *K. longzhouensis* sp. nov. and *K. parvus* (3.96%), and the maximum uncorrected *p* distance is both between *K. acridorsalis* and *K. anophthalmus* (11.38%) and between *K. acridorsalis* and *K. parvus* (11.38%) (Table 3). In consideration of both molecular and morphological comparisons, we confidently assign the new species to the genus *Karstsinnectes*.

Principal component analysis (PCA)

The first two principal components (PCs) explained 71.1% of the variance (Table 2). The first principal component (PC1) accounted for 46.7% of the morphological variation and distinguished variables such as body depth/SL, head lateral length/SL, caudal peduncle depth/SL, pectoral-fin length/SL, and pelvic-fin length/SL. Additionally, it separated pectoral-fin length relative to the distance between pectoral- and pelvic-fin origins and pelvic-fin length relative to the distance between pelvic- and anal-fin origins. Predorsal length/SL demonstrated a positive correlation with PC1 scores, while predorsal length/SL exhibited a negative correlation, with factor loadings exceeding 0.60. The second factor (PC2) accounted for 24.4% of the morphological variation, distinguishing variables such as head width to SL, head depth to head lateral length, and head width to head lateral length, which all showed a positive correlation with PC2 scores. Conversely, caudal peduncle length to caudal peduncle depth was negatively correlated with PC2 scores. Scatter plot analysis revealed that species within the genus *Karstsinnectes* could be differentiated based on their morphometric traits (Fig. 7).

Table 2. Loadings of the first three PCs for the morphometric characters of *Karstsinnectes*. * loadings > 60%.

Character	PC1	PC2	PC3
Body depth/SL	0.871*	0.271	-0.126
Head lateral length/SL	0.798*	-0.445	0.221
Prodorsal length/SL	-0.704*	0.592	0.099
Propelvic length/SL	-0.314	0.387	0.577
Preanal/SL	0.392	0.343	-0.310
CPL/SL	0.489	-0.415	0.690*
CPD/SL	0.830*	0.455	-0.242
Head width/SL	0.462	0.662*	0.498
Pectoral-fin length/SL	0.912*	0.157	0.146
Pelvic-fin length/SL	0.883*	-0.195	-0.247
Head depth/head lateral length	0.404	0.779*	0.248
Head width/head lateral length	-0.206	0.896*	0.257
Pectoral-fin length/distance between pectoral-fin and pelvic-fin origin	0.912*	-0.193	0.083
Pelvic-fin length/distance between pelvic-fin and anal-fin origin	0.858*	-0.274	0.075
CPL/CPD	-0.579	-0.607*	0.522
Prp. Tot1	**46.70%**	**24.40%**	**11.90%**

Table 3. Uncorrected pairwise distances between species of Karstsinnectes based on complete mitochondrial genomes.

		1	2	3
1	*K. anophthalmus*			
2	*K. acridorsalis*	0.1138		
3	*K. longzhouensis*	0.1008	0.1071	
4	*K. parvus*	0.1036	0.1138	0.0396

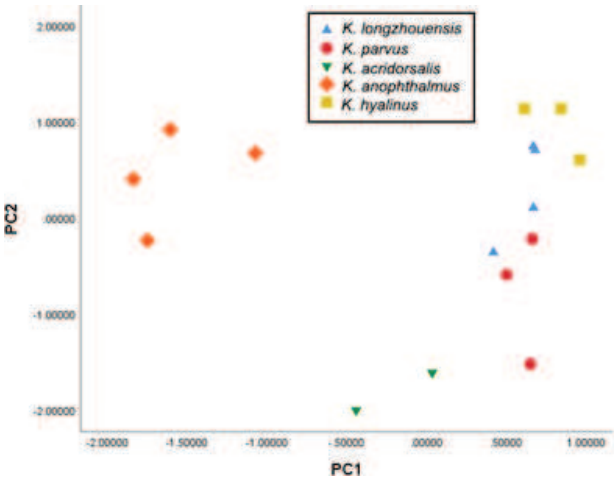

Figure 7. Scatter plots of first and second PCs of pooled morphometric data of *Karstsinnectes*.

Discussion

While Luo et al. (2023) established the genus *Karstsinnectes*, its diagnosis remains unclear. Du et al. (2023) indicated that the location of the anterior and posterior nostrils serves as an important characteristic for the generic diagnosis of Chinese nemacheilids with tube-shaped anterior nostrils and can be categorized into three types based on their location, namely separated, adjacent, and closed-set (Du et al. 2023). The anterior nostrils of *Karstsinnectes* are tube-shaped and located adjacent to the posterior nostrils, with the intervening distance shorter than the diameter of the posterior nostril. Additionally, the tip of the anterior nostril does not extend in a barbel-like manner. Therefore, the primary diagnostic features of *Karstsinnectes* include anterior nostril tube-shaped, adjacent to posterior nostril, anterior nostril tip not elongated to barbel-like, lips with furrows, caudal peduncle with adipose crests, and bony capsule of the swim bladder open posteriorly.

In morphology, *K. anophthalmus* possesses distinct characteristics from other congeneric species, including an obtuse snout, shorter pectoral and pelvic fins, a pectoral-fin length less than half the distance from its origin to the pelvic-fin origin, and a pelvic fin tip that does not reach the anus. Scatter plots of the first and second PCs of pooled morphometric data of *Karstsinnectes* also indicated the morphological difference of *K. anophthalmus*. The morphological difference could indicate that *K. anophthalmus* represents a new genus. However, the molecular analysis is inconsistent with the morphological evidence. In the phylogenetic tree, *K. longzhouensis* sp. nov. was determined to be a sister group to *K. parvus* and further sister to *K. anophthalmus* and *K. acridorsalis*. According to Luo et al. (2023), the specimens collected from Daxin County, Chongzuo City, Guangxi, China, were identified as *K. anophthalmus*. However, J.H. Lan and J. Yang observed that the morphology of the specimens from Daxin differed from those found in the type locality. However, the samples of ON116513 and ON116506 were from Daixin County; the specimens were not sequenced from the type locality. Therefore, further investigations are required to determine the taxonomic status of these specimens.

Blind cavefish represent a powerful natural model for studying adaptations in extreme environments. Cave habitats, characterized by limited food resources, low oxygen levels, and perpetual darkness (Zhao and Zhang 2009), present considerable challenges. To adapt and thrive in such environments, cavefish have undergone a series of evolutionary changes, including eye and pigmentation loss, enhancement of non-visual senses, development of specialized jaws for feeding, increased number of taste buds and barbels, and enhanced ability to store adipose tissue (Yang et al. 2016; Ma et al. 2019, 20233). Blind cavefish within the genus *Karstsinnectes* exhibit a suite of troglomorphic traits, including scaleless and colorless bodies, absence of eyes, elongated snouts (except *K. anophthalmus*), and caudal peduncles with well developed adipose crests. Current studies suggest that surface-dwelling species, upon colonizing cave environments and being granted sufficient time, undergo analogous transformations. Consequently, cave-dwelling organisms serve as a valuable natural framework for investigating convergent and adaptive evolutionary processes.

The survival of cavefish is significantly threatened by human activities, climate change, water pollution, and invasive species. As of 2021, the Red List of Biodiversity in China includes 13 cavefish species from the Nemacheilidae family (Zhang and Cao 2021). Zhang and Cao (2021) stated that the population of *K. anophthalmus* is very small, with only one or two specimens caught in each survey in 1996, 2003, and 2010, respectively. Major threats include road infrastructure construction, tourism activities, and groundwater contamination from agricultural operations in the recharge areas of the cave (Zhang and Cao 2021). Additionally, Shu et al. (2013) highlighted the impact of droughts and human extraction of water from cave pools on cave biodiversity in southwestern China. Thus, to conserve these valuable cavefish species, the implementation of conservation measures, such as habitat protection, artificial breeding, and fundamental research, is crucial.

Conclusions

In this paper, a new blind species is described from Guangxi, China. The phylogenetic tree indicated that the new species belongs to the genus *Karstsinnectes*. Additionally, the genus diagnosis is redefined, a neotype for *K. parvus* is designated due to the type specimens lost, and the morphology character of *K. hyalinus* is revised. The population of these species is quite small and sensitive to human activity. The protection of cave fish is often neglected due to the difficulty of cave exploration. The findings of this study improve our understanding of the species diversity of the genus *Karstsinnectes* and provide the basis for cavefish protection.

Competing interests

The authors declare that they have no competing interests.

Authors' contributions

J.Y.G. and L.N.D. measured the specimens, analyzed the data, and prepared the manuscript. L.N.D. and J.Y. conceived and designed the study, analyzed the molecular data, constructed the phylogenetic tree, and provided funding for complete mitochondrial genomes and field surveys. Z.Q.N. and J.J.Z. conducted the field survey. All authors read and approved the final version of the manuscript.

Acknowledgments

This study was funded by the Guangxi Natural Science Foundation Project (2022GXNSFAA035563), Key Laboratory of Ecology of Rare and Endangered Species and Environmental Protection (Guangxi Normal University), Ministry of Education, China (ERESEP2022Z05), Survey and Assessment of Priority Areas for Terrestrial Biodiversity Conservation in Guangxi (2022–2023), and Guangxi Zhuang Autonomous Region Project of Undergraduate on Innovation and Entrepreneurship (S202310602180). We are grateful to J.H. Lan for providing photographs of *K. acridorsalis*, R. Min for providing photographs of *K. anophthalmus and K. hyalinus*, and M. Liang for taking photographs of *K. parvus*. We thank H. Zhou, B.M. Wang, X.M. Luo, J.Q. Luo, and Z.X. Qin for collecting specimens of *Karstsinnectes*.

References

Beier S, Thiel T, Münch T, Scholz U, Mascher M (2017) MISA-web: A web server for microsatellite prediction. Bioinformatics 33(16): 2583–2585. https://doi.org/10.1093/bioinformatics/btx198

Bernt M, Donath A, Jühling F, Externbrink F, Florentz C, Fritzsch G, Pütz J, Middendorf M, Stadler PF (2013) MITOS: Improved de novo Metazoan Mitochondrial Genome Annotation. Molecular Phylogenetics and Evolution 69(2): 313–319. https://doi.org/10.1016/j.ympev.2012.08.023

Darriba D, Taboada GL, Doallo R, Posada D (2012) jModelTest 2: More models, new heuristics and parallel computing. Nature Methods 9(8): e772. https://doi.org/10.1038/nmeth.2109

Dierckxsens N, Mardulyn P, Smits G (2017) NOVOPlasty: De novo assembly of organelle genomes from whole genome data. Nucleic Acids Research 45(4): e18. https://doi.org/10.1093/nar/gkw955

Du LN, Yang J, Min R, Chen XY, Yang JX (2021) A review of the Cypriniform tribe Yunnanilini Prokofiev, 2010 from China, with an emphasis on five genera based on morphologies and complete mitochondrial genomes of some species. Zoological Research 42(3): 310–334. https://doi.org/10.24272/j.issn.2095-8137.2020.229

Du LN, Li SJ, Xu F, Luo T, Luo FG, Yu GH, Zhou J (2023) Clarification of Phylogenetic Relationships among Chinese Nemacheilids with Tube-Shaped Anterior Nostrils, with a Description of a New Genus and Two New Species. Journal of Zoological Systematics and Evolutionary Research 2023: 3600085. https://doi.org/10.1155/2023/3600085

ICZN [International Commission on Zoological Nomenclature] (1999) International Code of Zoological Nomenclature. Fourth edition. London: International Trust for Zoological Nomenclature, 84–84.

Lan JH, Gan X, Wu TJ, Yang J (2013) Cave Fishes of Guangxi, China. Beijing: Science Press, 104–139. [in Chinese]

Luo T, Yang Q, Wu L, Wang YL, Zhou JJ, Deng HQ, Xiao N, Zhou J (2023) Phylogenetic relationships of Nemacheilidae cavefish (*Heminoemacheilus*, *Oreonectes*, *Yunnanilus*, *Paranemachilus*, and *Troglonectes*) revealed by analysis of mitochondrial genome and seven nuclear genes. Zoological Research 44(4): 693–697. https://doi.org/10.24272/j.issn.2095-8137.2022.266

Ma L, Zhao YH, Yang JX (2019) Chapter 28 - Cavefish of China. In: White WB, Culver DC, Pipan T (Eds) Encyclopedia of Caves. 3rd edn. Waltham: Academic Press, 237–254. https://doi.org/10.1016/B978-0-12-814124-3.00027-3

Ma L, Yang JX, Lei FK, Xu MZ, Zhao YH, Jeffery WR (2023) Protection and exploration of the scientific potential of Chinese cavefish. Zoological Research 44(4): 675–677. https://doi.org/10.24272/j.issn.2095-8137.2022.484

Martin M, MARTIN M (2011) Cutadapt removes adapter sequences from high-throughput sequencing reads. EMBnet.Journal 17(1): 10–12. https://doi.org/10.14806/ej.17.1.200

Miller MA, Pfeiffer W, Schwartz T (2010) Creating the CIPRES Science Gateway for inference of large phylogenetic trees. In 2010 Gateway Computing Environments Workshop (GCE), 8 pp., New Orleans, LA, USA, November 2010. https://doi.org/10.1109/GCE.2010.5676129

Peden JF (1999) Analysis of codon usage. PhD Thesis, University of Nottingham, UK.

Shu SS, Jiang WS, Whitten T, Yang JX, Chen XY (2013) Drought and China's cave species. Science 340(6130): 272. https://doi.org/10.1126/science.340.6130.272-a

Xiao S, Lan JX (2023) Guangxi Danshui Yulei Fenlei Tujian. Henan Science and Technology Press, 20–20. [in Chinese]

Yang JX, Chen XL, Bai J, Fang D, Qiu Y, Jiang W, Yuan H, Bian C, Lu J, He S, Pan X, Zhang Y, Wang X, You X, Wang Y, Sun Y, Mao D, Liu Y, Fan G, Zhang H, Chen X, Zhang X, Zheng L, Wang J, Cheng L, Chen J, Ruan Z, Li J, Yu H, Peng C, Ma X, Xu J, He Y, Xu Z, Xu P, Wang J, Yang H, Wang J, Whitten T, Xu X, Shi Q (2016) The *Sinocyclocheilus* cavefish genome provides insights into cave adaptation. BMC Biology 14(1): 1. https://doi.org/10.1186/s12915-015-0223-4

Zhang E, Cao WX (2021) China's Red List of Biodiversity: Vertebrates, Volume V, Freshwater Fishes. Beijing: Science Press, 870 pp.

Zhao YH, Zhang CG (2009) Endemic Fishes of *Sinocyclocheilus* (Cypriniformes: Cyprinidae) in China Species Diversity, Cave Adaptation, Systematization and Zoogeography. Beijing: Science Press. [in Chinese]

Zhu Y, Zhu DG (2014) Description of a new species of the genus Heminoemachilus (Teleostei: Balitoridae) in Guangxi, China. Journal of Guangdong Ocean University 34(6): 18–21.

Zoosyst. Evol. 100 (2) 2024, 675–689 | DOI 10.3897/zse.100.121499

PENSOFT

für Natur MUSEUM FÜR NATURKUNDE BERLIN

A new species of *Chrysobrycon* Weitzman & Menezes, 1998 (Characiformes, Characidae, Stevardiinae) with remarkable sexually dimorphic pigmentation from the upper Río Vaupés basin, Colombian Amazon, with taxonomic key

James Anyelo Vanegas-Ríos[1*], Alexander Urbano-Bonilla[2*], Gian Carlo Sánchez-Garcés[3]

1 *División Zoología Vertebrados, Facultad de Ciencias Naturales y Museo, Unidades de Investigación Anexo Museo, Gabinete 104, CONICET, UNLP, La Plata, Buenos Aires, Argentina*

2 *Pontificia Universidad Javeriana, Departamento de Biología, Facultad de Ciencias, Laboratorio de Ictiología, Unidad de Ecología y Sistemática (UNESIS), Carrera 7 N° 43-82, Bogotá, D.C., Colombia*

3 *Corporación para la Gestión Ambiental Biodiversa. Calle 13-A Oeste Casa Villa Eugenia, Grupo de Investigación en Peces Neotropicales Fundación FUNINDES, Calle 55 # 99-250 Cali, Colombia*

https://zoobank.org/1821B69C-FFC0-46D9-B8F0-3E8A7CAE4460

Corresponding author: James Anyelo Vanegas-Ríos (anyelovr@gsuite.fcnym.unlp.edu.ar)

Academic editor: Nicolas Hubert ♦ **Received** 24 February 2024 ♦ **Accepted** 17 April 2024 ♦ **Published** 28 May 2024

Abstract

This study describes *Chrysobrycon calamar*, a new stevardiine fish from the upper Río Vaupés basin in Colombia. The new species differs from its congeners by the following combined characters: adult males have a dark vertical blotch on the abdominal flanks that is confined to a small area immediately dorsal to the urogenital region and anterior to the third anal-fin ray; adult males with a well-developed vertically humeral blotch, numerous tiny bony hooks on nearly all the upper lobe caudal-fin rays (except *C. guahibo*, *C. hesperus*, and *C. mojicai*), and bony hooks on nearly all branched anal-fin rays (except *C. hesperus*); the number of vertebrae (43 *vs.* 38–42); an elongated maxillary anterior process, representing 40% or more of the total length of the bone (*vs.* with a shorter maxillary anterior process, representing less than 40% of that length); and the posterior portion of the maxilla not reaching the vertical through the anterior border of the eye when the mouth is closed (except from *C. yoliae*). Additionally, *C. calamar* differs from *C. mojicai* by the number of maxillary teeth (2–4 *vs.* 9–17) and shape of the distal tips of most maxillary teeth (straight along their lengths *vs.* lateroventrally curved). Remarks on the interspecific color variation associated with sexual dimorphism and other characteristics of the genus are provided. A key to the species of *Chrysobrycon* is presented. The discovery of *C. calamar* is a key advance in the understanding of fish biodiversity associated with endemism-rich regions that could be explored after the guerrilla demobilized in Colombia.

Key Words

Chiribiquete National Natural Park, cis-Andean basins, Neotropical freshwater fishes, sexual dimorphism, Stevardiini

* These authors contributed equally to this work.

Introduction

The Neotropical genus *Chrysobrycon* Weitzman & Menezes, 1998, is currently classified phylogenetically within Stevardiinae as a member of the tribe Stevardiini (Thomaz et al. 2017; Vanegas-Ríos 2018; Mirande 2019; Vanegas-Ríos et al. 2020). This genus was traditionally recognized by having hypertrophied scales that form a laterally open pocket on the lower caudal-fin lobe in adult males (Weitzman and Menezes 1998; Vanegas-Ríos et al. 2011, 2014). This pocket consists of a pouch scale (small in comparison with other stevardiines presenting pouch scale) that is characterized by being somewhat elongate, curved, confined to the dorsal region of the pouch opening, and horizontally folded so that its lateral face is laterally concave (Weitzman and Menezes 1998). More recently, Vanegas-Ríos and Urbano-Bonilla (2017) proposed an additional diagnostic character for *Chrysobrycon*: the extensive contact of the frontals along the midline in adults. Based on an extensive phylogenetic dataset including these variations in the frontals and hypertrophied caudal-fin squamation, the monophyly of most species of *Chrysobrycon* was corroborated by Vanegas-Ríos (2018) and Vanegas-Ríos et al. (2020).

Chrysobrycon is composed of six cis-Andean species distributed in the Orinoco and Amazon basins in Colombia, Ecuador, and Peru (Vanegas-Ríos et al. 2011; Vanegas-Ríos et al. 2013b; Vanegas-Ríos et al. 2014; Vanegas-Ríos et al. 2015; Vanegas-Ríos and Urbano-Bonilla 2017). The type species of the genus, *Chrysobrycon hesperus* (Böhlke, 1958), is known from the Río Marañon, Río Napo, and Río Putumayo basins (Böhlke 1958; Vanegas-Ríos et al. 2013b; Valdiviezo-Rivera et al. 2018; Toledo-Piza et al. 2024). *Chrysobrycon myersi* (Weitzman & Thomerson, 1970) occurs in the Río Pachitea and Río Ucayali basins (Weitzman and Thomerson 1970; Vanegas-Ríos et al. 2013b). *Chrysobrycon eliasi* Vanegas-Ríos, Azpelicueta & Ortega, 2011 is distributed in the Río Acre, Río Madre de Dios, and Río Manuripe basins (Vanegas-Ríos et al. 2011; Claro-García et al. 2013). *Chrysobrycon yoliae* Vanegas-Ríos, Azpelicueta & Ortega, 2014 occurs in the Río Yucamia system (Río Ucayali basin) (Vanegas-Ríos et al. 2014). *Chrysobrycon mojicai* Vanegas-Ríos & Urbano-Bonilla, 2017, the last described species of the genus from the Amazon basin, is known from several streams in Leticia, Colombia (Vanegas-Ríos and Urbano-Bonilla 2017). The only *Chrysobrycon* species known from the Orinoco basin is *C. guahibo* Vanegas-Ríos, Urbano-Bonilla & Azpelicueta, 2015, which is distributed along the upper Río Guaviare basin in Colombia (Vanegas-Ríos et al. 2015).

The Colombian Amazon exhibits some basins that remain unexplored (Jézéquel et al. 2020a), such as areas occupied by the Guerrilla (FARC-EP) that, after the signing of the peace agreements, have been studied, which has led to the discovery of new species (Irwin 2023). In fact, within these areas, some fish species have been described from the Río Vaupés basin (Londoño-Burbano and Urbano-Bonilla 2018; Lima et al. 2020; Urbano-Bonilla et al. 2023), a drainage with high values of richness and endemism (Jézéquel et al. 2020b). Furthermore, this basin is characterized by having its origin in the foothills of the Colombian eastern mountain range and running through outcrops of the Guiana Shield and the sandy soils of the Amazonian lowlands (Hernández-Camacho et al. 1992), in a series of numerous rapids that can act as natural ecological barriers limiting fish dispersal (Lima et al. 2005; Torrente-Vilara et al. 2011; Urbano-Bonilla et al. 2024 (in press)).

In expanding the area of the Serranía de Chiribiquete National Natural Park, explorations were carried out in the headwaters of the Vaupés basin, that is, the rapids of the Río Itilla, Río Unilla basin, and some associated streams and lagoons. As part of an ongoing revision of *Chrysobrycon*, we detected numerous specimens from these sampling efforts presenting a striking sexually dimorphic pigmentation in adult males, which diverges from what is known for the genus. Therefore, these specimens are described herein as a new species based on a comprehensive morphological comparison. We found several specimens collected in the upper Río Putumayo basin in Colombia that resemble the specimens from the Río Vaupes basin. These former specimens are analyzed comparatively to understand their taxonomic status with respect to the new species presented here. Additionally, a key to the species of *Chrysobrycon* is provided.

Materials and methods

The specimens are deposited in the following collections (acronyms according to Sabaj 2020): ANSP, CI-FML, FMNH, IAvH-P, ICN-MHN, LACM, MUSM, MLP-Ict (formerly MLP), MPUJ, ROM, and USNM. Counts of the pectoral-, pelvic-, and dorsal-fin rays follow Böhlke (1958). Measurements and other counts were taken according to Fink and Weitzman (1974), adding the following measurements: the dorsal-fin base length, anal-fin base length, and anal-fin lobe length by Menezes and Weitzman (1990), and the dorsal fin to pectoral fin distance, dorsal fin to adipose fin distance, pectoral fin to pelvic fin distance, pelvic fin to anal fin distance, and postorbital head length by Vanegas-Ríos et al. (2013a). Measurements were taken point-to-point with digital calipers under a stereomicroscope and are expressed as percent of standard length (SL) or head length (HL) for units of the head. Specimens that were analyzed from digitized photos using tpsDig 2.26 (Rohlf 2015) are indicated by an asterisk. The frequency of a particular meristic character is reported in parentheses, and the holotype values are indicated by an asterisk. Specimens were cleared and counterstained (c&s), according to Taylor and Van Dyke (1985). The total number of vertebrae was counted in c&s specimens. Those counts included the first preural centrum plus the first ural centrum (PU1+U1), counted as one element, and all four vertebrae of the Weberian apparatus.

To explore the morphometric variation between the specimens examined from the Río Vaupés and Río Putumayo basins, we conducted a morphometric comparison

using a size-corrected principal component analysis (PCA), based on the "allometric *vs.* standard" procedure (Elliott et al. 1995). PCA was computed using the covariance matrix. The number of significant principal components (PCs) was decided by the broken-stick model (Frontier 1976) and the scree plot method (Cattel 1966). Statistical procedures were carried out in PAST 4.16 (Hammer et al. 2001) and GraphPad Prism 9.4.1 (GraphPad Software, San Diego, CA, USA). Coordinates were rounded off to the nearest second. Altitudes were rounded off to the nearest meter (expressed as above sea level = a.s.l.).

Results

***Chrysobrycon calamar* sp. nov.**

https://zoobank.org/52F50C79-0444-4AC2-ADDA-8F43DA1FABF5

Figs 1–6, Table 1, Suppl. material 1: F–G

Type material. ***Holotype*.** MPUJ 18618, male, 39.3 mm SL, COLOMBIA, Guaviare department, San José del Guaviare, upper Río Vaupés, Calamar, Río Unilla, Caño Toño; 2°09'50"N, 72°50'16"W, c. 250 m a.s.l., Maldonado-Ocampo JA, Prada-Pedreros S, Moreno-Arias C, Zamudio JE, Cubides F, & Urbano-Bonilla A leg.; 5 Jan. 2017.

***Paratypes*.** All from COLOMBIA, Guaviare department, San José del Guaviare, upper Río Vaupés: ICN-MHN 24743, 3, 31.4–37.7 mm SL; Calamar, Chiribiquete National Natural Park, Río Unilla, Caño Salado; 1°59'20"N, 72°53'22"W, c. 270 m a.s.l.; Maldonado-Ocampo JA, Prada-Pedreros S, Moreno-Arias C, Zamudio JE, Cubides F, & Urbano-Bonilla A leg.; 7 Jan. 2017. MLP-Ict 11733, 2, 34.6–36.5 mm SL; El Retorno, Río Unilla; 2°11'51"N, 72°44'59"W, c. 250 m a.s.l.; Maldonado-Ocampo JA, Prada-Pedreros S, Moreno-Arias C, Zamudio JE, Cubides F. & Urbano-Bonilla A leg.; 3 Jan. 2017. MPUJ 12850, 3, 32.9–36.9 mm SL, Calamar, Chiribiquete National Natural Park, Raudal del Río Itilla; 1°59'30"N, 72°53'15"W, c. 260 m a.s.l.; Maldonado-Ocampo JA, Prada-Pedreros S, Moreno-Arias C, Zamudio JE, Cubides F, & Urbano-Bonilla A leg.; 7 Jan. 2017. MPUJ 12965, 3, 34.8–41.2 mm SL; Calamar, Chiribiquete National Natural Park, Río Unilla, Caño Salado; 1°59'20"N, 72°53'22"W, c. 270 m a.s.l.; Maldonado-Ocampo JA, Prada-Pedreros S, Moreno-Arias C, Zamudio JE, Cubides F, & Urbano-Bonilla A leg.; 7 Jan. 2017. MPUJ 12966, 8 (2 c&s, 35.7–35.8 mm SL), 33.2–40.9 mm SL; same data as for holotype. MPUJ 12967, 7, 31.1–39.4 mm SL; Calamar, Río Unilla, Caño La Tigra; 2°10'57"N, 72°50'16"W; c. 250 m a.s.l., Maldonado-Ocampo JA, Prada-Pedreros S, Moreno-Arias C, Zamudio JE, Cubides F, & Urbano-Bonilla A leg.; 4 Jun. 2017. MPUJ 12969, 3, 33.2–37.2 mm SL, El Retorno, Río Unilla; 2°11'51"N, 72°44'59"W, c. 250 m a.s.l.; Maldonado-Ocampo JA, Prada-Pedreros S, Moreno-Arias C, Zamudio JE, Cubides F, & Urbano-Bonilla A leg.; 3 Jan 2017.

Diagnosis. *Chrysobrycon calamar* differs from its congeners by the following combined characters: a distinctive dark vertical blotch placed laterally on the abdominal flanks in adult males, just immediately dorsal to the urogenital region (*vs.* this pigmentation weak, diffuse, poorly

Figure 1. *Chrysobrycon calamar*: **A.** MPUJ 18618, male, holotype, 39.3 mm SL, Colombia, Guaviare department, San José del Guaviare, upper Río Vaupés, Calamar, Río Unilla, Caño Toño; **B.** MPUJ 12966, female, paratype, 34.1 mm SL, same data as holotype.

developed, or if well-defined, more developed longitudinally than vertically, never forming a distinctive vertical blotch); a well-developed vertically humeral blotch in adult males (almost rectangular-shaped, see additional details in sexual dimorphism section *vs.* scarcely expanded vertically, somewhat irregular, or circular-shaped mark); the possession of numerous (two to 12) tiny bony hooks on nearly all the upper lobe caudal-fin rays in adult males (*vs.* hooks confined to the lower lobe caudal-fin rays, except in *C. guahibo*, *C. hesperus*, and *C. mojicai*, with hooks arranged in a set of one to three hooks on a single ray), the number of vertebrae (43 *vs.* 38–42); the posterior portion of the maxilla not reaching the vertical through the anterior border of the eye when the mouth is closed, except from *C. yoliae* (*vs.* this portion reaching or surpassing the vertical through the anterior border of eye); an elongated maxillary anterior process, representing proportionally 40% or more of the total length of the bone (*vs.* with a shorter maxillary anterior process, representing less than 40% of its length); and the presence of bony hooks in adult males on nearly all the branched anal-fin rays, except *C. hesperus* (*vs.* bony hooks restricted up to the anterior half of fin or not extending to the posteriormost rays).

The presence of a simple terminal lateral-line tube between the caudal-fin rays 11 and 12 (*v.* tube absent) distinguishes *C. calamar* from *C. hesperus* and *C. myersi*. Additionally, *C. calamar* is also distinguished from *C. myersi* by the number of circumpeduncular scales (13–14 *vs.* 17–19), distance between dorsal- and adipose-fin origins (20.4–24.4% SL *vs.* 28.2–33.5% SL), dorsal-fin to caudal-fin base (33.0–39.6% SL *vs.* 40.1–47.4% SL), eye to dorsal-fin origin (51.9–57.2% SL *vs.* 45.8–49.2% SL), and upper jaw length (38.1–45.5% HL *vs.* 48.9–54.9% HL), and from *C. hesperus* by the maximum number of cusps on the maxillary teeth (tricuspid *vs.* pentacuspid) and number of supraneurals (11 *vs.* 12–14). The number of dentary teeth differentiates *C. calamar* from *C. mojicai* and *C. yoliae* (13–17 *vs.* 20–27). Furthermore, *C. calamar* is also distinguished from *C. mojicai* by the number of radii on the lateral-line scales (5–9 *vs.* 11–18), number of maxillary teeth (2–4 *vs.* 9–17), and shape of the distal tips of most maxillary teeth (straight along their lengths *vs.* lateroventrally curved), and from *C. yoliae* by the body depth at dorsal-fin origin (27.5–33.5% SL *vs.* 34.4–42.2% SL), and distance between dorsal- and adipose-fin origins (20.4–24.4% SL *vs.* 26.8–28.8% SL).

Description. Morphometric data in Table 1. Largest male 41.2 mm SL, largest female 35.8 mm SL. Body laterally compressed, maximum depth at vertical through area immediately anterior to anal-fin origins (Fig. 1).

Table 1. Morphometric data of *Chrysobrycon calamar*. Males were sexed by presence of bony hooks on fins and pouch scale on lower caudal-fin lobe. Range and mean of males include values of holotype. SD: standard deviation. Data of specimens treated as *C.* aff. *calamar* from the Putumayo basin are provided.

	Holotype	Paratypes						Putumayo basin		
		Males			Females			both sexes		
		n	Range	Mean+± SD	n	Range	Mean+± SD	n	Range	Mean+± SD
Standard length (mm)	39.3	15	33.2–41.2	37.5±2.3	15	31.1–35.8	33.5±1.5	7	34.2–44.4	41.4±3.6
Percent of standard length:										
Depth at dorsal-fin origin	31.9	15	27.5–33.5	30.6±1.8	15	27.7–31.4	29.0±1.1	7	29.5–33.8	32.1±1.3
Snout to dorsal-fin origin	66.1	15	61.1–69.8	65.4±2.2	15	64.7–68.7	67.0±1.2	7	65.2–68.3	66.4±1.0
Snout to pectoral-fin origin	28.7	15	26.3–29.6	27.9±0.9	15	26.4–29.3	27.7±0.8	7	26.3–28.9	27.4±0.9
Snout to pelvic-fin origin	44.3	15	42.6–48.6	45.7±1.6	15	44.2–48.2	45.7±1.1	7	45.9–48.4	47.7±0.9
Snout to anal-fin origin	59.2	15	57.2–63.9	59.6±1.5	15	58.4–62.2	60.4±1.1	7	59.1–62.8	61.5±1.3
Distance between dorsal- and pectoral-fin origins	48.6	15	45.8–49.9	48.2±1.1	15	44.8–50.6	47.3±1.5	7	44.4–50.0	48.5±1.8
Distance between dorsal- and adipose-fin origins	22.1	15	20.9–24.4	22.4±1.2	15	20.4–24.2	22.1±1.0	7	22.1–25.2	23.6±1.0
Dorsal fin to caudal-fin base	37.4	15	33.0–39.6	36.5±1.6	15	34.7–38.9	36.0±1.2	7	33.4–38.0	35.9±1.7
Eye to dorsal-fin origin	55.5	15	52.1–57.2	54.2±1.4	15	51.9–56.4	54.5±1.2	7	52.3–57.1	54.7±1.5
Distance between pectoral- and pelvic-fin insertions	17.9	15	17.0–19.7	18.2±0.8	15	17.1–20.4	18.8±1.0	7	18.9–22.8	20.7±1.3
Distance between pelvic- and anal-fin origins	15.8	15	14.3–16.3	15.4±0.6	15	12.1–15.5	14.7±0.8	7	14.6–17.1	15.6±0.9
Dorsal-fin length	17.3	15	14.5–20.7	18.2±1.6	15	15.9–21.2	18.2±1.8	7	17.7–23.2	19.4±1.9
Dorsal-fin base length	8.1	15	8.1–11.4	9.6±0.9	15	8.4–10.5	9.3±0.7	7	8.9–10.8	10.0±0.6
Pectoral-fin length	25.1	15	23.5–30.5	27.1±1.7	15	24.2–28.7	26.8±1.3	7	24.0–28.4	26.7±1.7
Pelvic-fin length	18.0	15	12.7–18.0	16.5±1.3	15	13.6–16.8	15.0±0.9	7	13.7–15.9	14.7±0.8
Anal-fin lobe length	16.1	15	16.1–21.6	18.6±1.6	15	16.0–19.7	18.3±0.9	7	16.3–19.6	17.7±1.1
Anal-fin base length	31.2	15	29.8–34.1	31.5±1.1	15	29.6–32.8	31.4±0.9	7	28.9–32.7	31.3±1.6
Caudal peduncle depth	10.8	15	9.3–11.6	10.8±0.5	15	8.3–10.6	9.6±0.6	7	8.5–11.3	10.0±1.1
Caudal peduncle length	13.9	15	11.5–14.0	12.9±0.8	15	9.3–13.3	11.7±1.0	7	11.1–13.5	12.6±0.9
Head length	23.5	15	23.5–25.5	24.4±0.5	15	22.5–25.2	24.2±0.7	7	22.9–25.9	24.3±1.2
Percent of head length:										
Snout length	32.6	15	24.5–33.7	29.9±2.3	15	26.6–31.4	28.5±1.6	7	30.1–33.8	31.5±1.4
Horizontal eye length	30.7	15	28.5–36.3	32.4±2.2	15	32.2–38.2	34.8±1.6	7	30.3–33.7	32.0±1.5
Postorbital head length	43.2	15	35.6–43.5	40.7±2.2	15	35.6–41.0	38.5±1.7	7	35.5–45.8	40.0±3.1
Least interorbital width	36.7	15	34.4–37.1	35.9±0.8	15	32.3–37.2	36.1±1.2	7	34.7–37.1	36.2±0.8
Upper jaw length	45.5	15	39.8–45.5	42.3±1.6	15	38.1–43.2	40.7±1.6	7	40.8–43.4	42.4±1.0

Dorsal profile of body: straight from tip of premaxilla to posterior region of head; slightly convex from posterior end of supraoccipital area to dorsal-fin origin; straight and slanting ventrally from first dorsal-fin ray to caudal peduncle. Dorsal profile of caudal peduncle straight. Ventral profile of body convex from tip of snout to pelvic-fin origin, slightly convex between pelvic- and anal-fin origins, straight and slanting dorsally from this point to caudal peduncle. Belly with like keel-shaped area between pelvic-fin origin and urogenital pore, consisting of one row of four to six scales forming sharp edge. Ventral profile of caudal peduncle straight. Head with anterior region acute. Frontal fontanel absent. Epiphyseal branch of supraorbital canal absent. Anterior nostril round, separated by skin fold from posterior nostril; posterior nostril opening considerably larger than anterior one. Two well-developed pit organs along grooves in head; anterior groove round, between nasal bone and nostril; posterior groove larger, extended along entire frontal, and covered with rows of neuromasts.

Mouth superior, lower jaw projecting slightly anterior to upper jaw. Premaxillary teeth arranged in two rows (Fig. 2). Outer row with four (5), five (22), or six* (3) tricuspid teeth. Inner row with four (1) or five* (29) teeth; symphyseal tooth tetracuspid; contiguous teeth pentacuspid; and posteriormost tooth conical to pentacuspid. Maxilla not fully toothed, with two (1), three* (23), or four (6) teeth tricuspid, sometimes conical. Maxillary teeth straight along their lengths, not distally curved laterovent rally. Maxilla short, with elongated anterior process, and extending on point at vertical between nostrils and anterior margin of orbit, but never reaching anterior margin of eye when mouth closed and body horizontally straight.

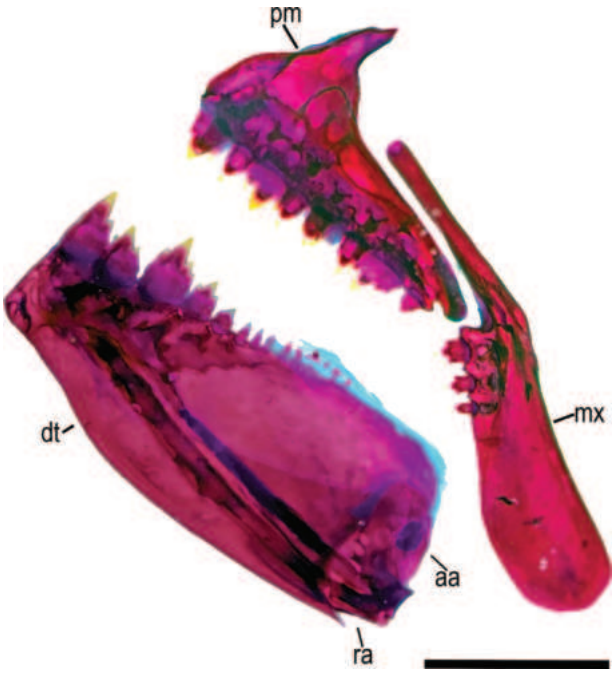

Figure 2. Jaws and dentition of *Chrysobrycon calamar*. MPUJ 12966, paratype, 35.8 mm SL. Premaxilla: pm; maxilla: mx; dentary: dt; anguloarticular: aa; retroarticular: ra. Bones reflecting an upper mouth. Scale bar: 1 mm.

Dentary moderately toothed, with 13 (3), 14 (12), 15* (6), 16 (5), or 17 (4) teeth; three anteriormost teeth large, pentacuspid (rarely tetracuspid); one median-sized tooth tri to pentacuspid, followed by 9 (3), 10 (12), 11* (6), 12 (5), or 13 (4) smaller conical or biscupid posterior teeth (Fig. 2).

Dorsal-fin rays ii (30), 8*(28), or 9 (2). Nine proximal dorsal-fin pterygiophores (2 c&s). Dorsal-fin origin at vertical between anal-fin rays 10 and 13. Adipose-fin origin at vertical crossing the second scale posterior to anal-fin termination. Anal-fin rays iv (6) or v* (24), 24 (1), 25 (1), 26 (8), 27* (6), 28 (8), or 29 (6). Twenty-seven to 29 proximal pterygiophores in anal fin (2 c&s). Anal-fin origin at posterior half of body, always anterior to vertical through dorsal-fin origin. Pectoral-fin rays i,9 (17), or 10* (13), last ray usually simple but counted as branched. Pectoral-fin distal tip reaching or surpassing one-half of pelvic-fin length (Fig. 1). Pelvic-fin rays i,7* in all specimens; last ray simple but counted as branched. Pelvic-fin origin slightly anterior to half of body. Caudal fin forked with 10/9 principal rays in all specimens.

Scales cycloid, with six to nine radii along posterior field, circuli on anterior, dorsal, and ventral fields, surpassing one-half scale length. Lateral line completely pored: 42 (8), 43* (8), 44 (11), 45 (2), or 46 (1). Terminal lateral-line tube present on caudal-fin interradial membrane. Predorsal scales 21 (1), 22* (13), 23 (14), or 24 (2) forming nearly continuous row. Scale rows between dorsal fin and lateral line five (24) or six* (6). Five* (28) or six (2) scale rows between lateral line and anal fin. Four (1) or five* (29) scale rows between lateral line and pelvic fin. Circumpeduncular scales 13 (1) or 14* (29). One row of 13 (1), 14 (1), 15 (4), 16 (5), 17 (9), 18* (7), or 19 (3) scales forming sheath along anal-fin base. Total number of vertebrae 43 (2 c&s), 17 precaudal, and 26 caudal. Six* (27), or seven (3) gill rakers on upper arm of first branchial arch; lower arm with 11 (11), 12*(14), or 13 (5).

Color in alcohol. Ground color pale yellow in preserved males and females, moderately darker dorsally. Dark chromatophores on all body, in minor proportion in ventral region, forming dark brown narrow band along mid-dorsal line, often diffuse. Humeral blotch dark, widely developed vertically, forming a rectangular-shaped pattern in most specimens (Fig. 1); frequently less developed vertically or somewhat rounded in female specimens. Dark black midlateral stripe extending from vertical through pelvic-fin origin to caudal peduncle. Wider lateral band of dark brown chromatophores located dorsal and ventral to this black stripe, less intense but more dorsoventrally developed, especially toward lateral line, and usually forming somewhat oval-shaped blotch from last portion of caudal peduncle, crossing interradialis muscles, to middle caudal-fin rays. Dark chromatophores forming stripes between myomeres ventrally located to midlateral stripe on posterior half of body. Dorsal fin mostly hyaline, with dark chromatophores mainly distributed on interradial membranes. Adipose fin mostly hyaline, with few dark chromatophores. Anal fin somewhat dusky, with dark chromatophores extending over interradial membranes, more concentrated on base and distal portions of fin.

Figure 3. Coloration in life of *Chrysobrycon calamar* from the upper Río Vaupes basin, Amazon basin, Colombia. **A.** MPUJ 12966, 40.9 mm SL (type locality: Caño Toño), paratype; **B.** MPUJ 12967, 39.4 mm SL, paratype.

Caudal fin mostly hyaline, with dark chromatophores extending mainly on interracial membranes and borders of rays; middle caudal-fin rays slightly pigmented with dark chromatophores. Pectoral and pelvic fins mostly hyaline with scarce dark chromatophores, but pectoral fins slightly more pigmented by having chromatophores on borders of rays. Head darker dorsally and light yellow ventrally, except for intense dark pigmentation on anterior region to isthmus. Dark chromatophores concentrated on premaxilla, maxilla, and lower jaw. Opercle dusky, with dark chromatophores intensely concentrated, especially on posterior region. Infraorbitals light yellow with scattered dark chromatophores (first infraorbital usually less pigmented).

Color in life. Based on adult male specimens photographed (Fig. 3). Ground color pale yellow dorsally and white or whitish yellow ventrally, being darker on midflanks. Dark chromatophores on all body, with abdominal region lighter below lateral line. Head yellowish orange dorsally but silvery laterally, with scattered dark chromatophores. Well-defined dark humeral blotch expanded vertically. Dark black midlateral stripe extending from vertical through pelvic-fin origin to caudal peduncle. Red half-moon shaped spot situated dorsally on pupil. Snout slightly bright yellow anteriorly. Wider lateral band of dark chromatophores located dorsal and ventral to this black stripe, usually forming somewhat oval-shaped blotch from last portion of caudal peduncle, crossing interradialis muscles, to middle caudal-fin rays. Dark blotch vertically expanded on abdominal flanks, located dorsally to urogenital region and anterior to first anal-fin rays. Pectoral and pelvic fins somewhat hyaline. Dorsal fin somewhat dusky. Orange adipose fin. Anal fin somewhat dusky, especially on base and distal tips of rays, but with yellowish-orange pigmentation in middle region of first anterior rays. Caudal fin somewhat yellowish orange on outer rays.

Sexual dimorphism. Adult males differ from females by the presence of bony hooks on the caudal-, pelvic-, and anal-fin rays. The caudal fin of males has four to 32 short, slender antrorse hooks that are usually paired (one or two pairs per segment) and placed on the dorsal margin of the lower caudal-fin rays 11 to 17. Additionally, two to 12 unpaired (sometimes paired) tiny antrorse hooks are placed on the ventral margin of the caudal-fin rays 2 to 10. All pelvic-fin rays of males bear slender antrorse hooks positioned lateroventrally along most rays length (on their margins) and are much more numerous and longer on the segmented and branched portions of each one (usually grouped in two pairs per segment). The anal fin of males has four to 30 variable-sized hooks distributed in one or two pairs per segment along the posteriormost simple ray and on all the branched rays; from the fifth to 10th branched anal-fin rays, the bony hooks are discontinuously arranged along the rays' length, clearly forming two separated groups of hooks (one closer to the

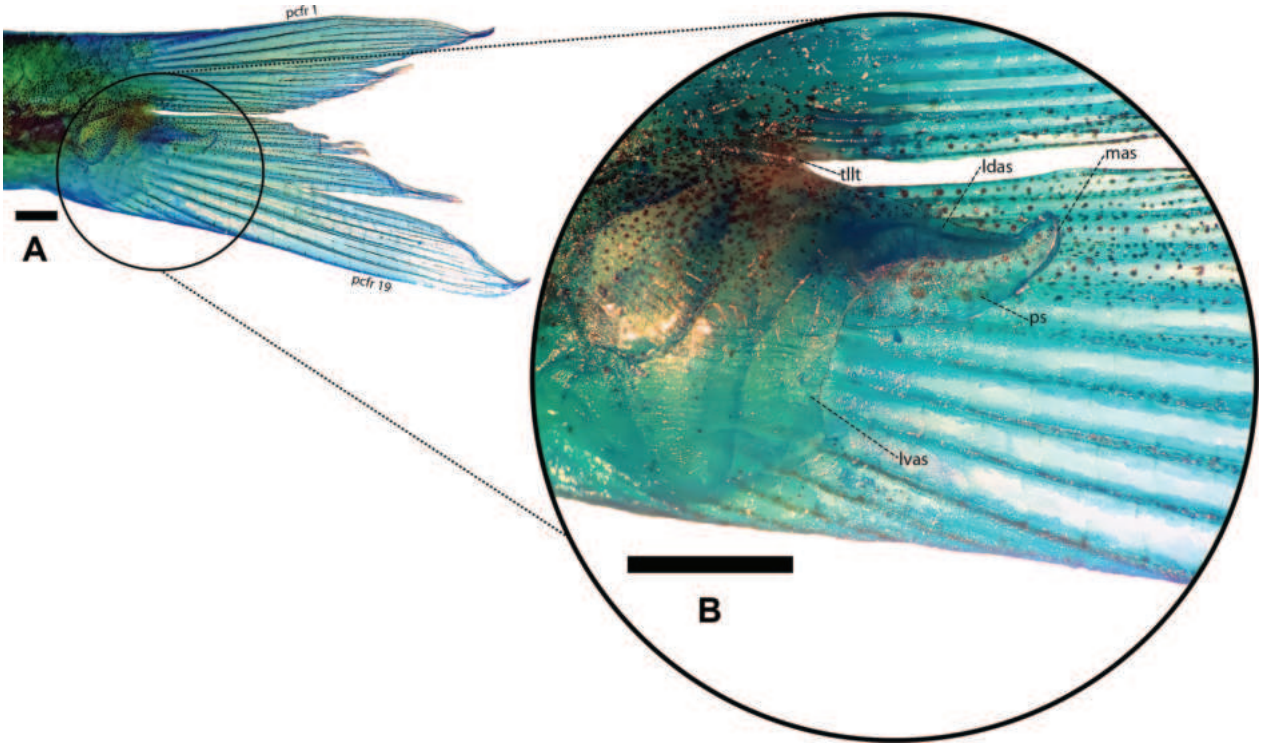

Figure 4. Caudal fin of *Chrysobrycon calamar* (**A**), with details of the hypertrophied caudal-fin squamation on the lower caudal-fin lobe (**B**). MLP-Ict 11733, male, 35.6 mm SL. Laterodorsal accessory scale: ldas; lateroventral accessory scale: lvas; medial accessory scale: mas; pouch scale: ps; principal caudal-fin ray: pcfr; terminal lateral-line tube: tllt. Specimen stained with Alcian Blue solution. Scale bar: 1 mm.

base and another nearer the distal portion). The anal-fin bony hooks placed closer to the base are more lateroventrally oriented in comparison with the hooks distributed on the distal portion. From the eighth or ninth anal-fin ray, the bony hooks are much more restricted to the distal portions, gradually decreasing in size anteroposteriorly.

The lower caudal-fin lobe of adult males has a broadly open pocket consisting of a single pouch scale and at least three accessory scales (Fig. 4). The pouch scale is relatively small, elongate, curved, and slightly folded laterally on its posterior portion; its hypertrophied radii are ventrally arranged at an obtuse angle, almost perpendicular to the caudal-fin rays. Underneath the pouch scale is located a medial accessory scale of similar shape, which is usually indistinguishable in lateral view. Lateral to the pouch scale, there are two accessory scales that largely outline the outermost margin of the pocket opening. One of them is curved and elongated, forming mainly the laterodorsal face of the pocket (its border with radii is almost completely concave). This laterodorsal accessory scale is independent from the pouch scale, but both are strongly attached to each other dorsally through a well-developed medial mass of connective tissue. The other accessory scale is extended between the previous ones but is not displaced posteroventrally, and for this reason, its radii are almost parallel to the horizontal axis of the body. The posterior border of this accessory scale delineates almost the entire lateroventral region of the pocket opening. A small scale laterally placed on the lateroventral accessory scale often closes the ventral margin of the pocket over the caudal-fin ray 19.

The gill gland of males is relatively long, formed by the fusion of the anterior 17 (3), 18 (4), 19* (5), 20 (2), or 22 (2) gill filaments of the ventral arm of the first gill arch. The gill-gland length ranged between 7.8 and 10.4% SL (mean = 9.0% ± 0.7, n = 15). Adult males have the anal-fin distal margin slightly straight or convex, whereas in females it is slightly concave.

The scale rows forming a sharp region between the pelvic-fin origin and urogenital pore are covered by dark chromatophores in both sexes, but the area is more intensely pigmented in adult males. The anal-fin distal margin of adult males is convex, whereas in females it is straight. Additionally, adult males are distinguished from females by possessing an irregular dark blotch vertically extended on the dorsal region between the anus and third anal-fin ray, reaching up to three or four scale rows of height and expanding up to three or four scales longitudinally (Fig. 1; Suppl. material 1: fig. S1F–G). Both types of pigmentations were observed to be dark or black in live or alcohol-preserved specimens (Figs 1, 2). In adult males, the oval-shaped caudal peduncle blotch is incompletely developed horizontally by the presence of a less intense or clearer area on the region associated with the hypertrophied caudal-fin squamation. The humeral mark was observed to be more greatly developed vertically in adult males, but it was less developed vertically in most females, being somewhat rounded.

Distribution. *Chrysobrycon calamar* is known from several streams flowing into the upper portion of the Vaupés basin in Colombia (Fig. 5; Suppl. materials 2, 3).

Etymology. The species is named "*calamar*" in reference to Calamar, a municipality in the department of Guaviare, which is part of its type locality. This is treated as a noun in apposition. Despite the fact that the municipality was the epicenter of slavery for the Carijona and Witoto indigenous people in the rubber era (1879 and 1912) and the Second World War (1942 and 1945), in addition to processes of colonization, extraction of natural resources, introduction of illicit crops, subversion, and paramilitarism (Arcila et al. 1999), it is currently a peaceful territory.

Ecological notes. *Chrysobrycon calamar* inhabits the main tributaries of the upper Vaupés (Río Itilla and Río Unilla basins) and associated drainages (Fig. 5; Suppl. materials 2, 3) between 250 and 270 m of altitude. It is generally found in shallow, clear, black water (< 1 m) with moderate flow over sand, pebbles, and rocks. In the rapids of the Río Itilla, the water has a temperature of 25.7 °C with high concentrations of dissolved oxygen (7.99 mg/l), a slightly acidic pH (6.5), and a low conductivity of 14.0 µS/cm. The gastrointestinal content of two samples examined (MPUJ 12966) mainly evidences a high consumption of aquatic and terrestrial invertebrates (remains of Diptera, Lepidoptera, Formicidae). The new species was collected in syntopy with other characids such as *Aphyocharax pusillus* (Günther, 1869), *Charax tectifer* (Cope, 1870), *Moenkhausia oligolepis* (Günther, 1864), *M. comma* Eigenmann, 1908, *Brachychalcinus copei* (Steindachner, 1882), *Jupiaba abramoides* (Eigenmann, 1909), *Hyphessobrycon agulha* Fowler, 1913, and *Hemigrammus yinyang* Lima & Sousa, 2009, *Tyttocharax* sp. and *Phenacogaster* sp.

Remarks. Comparing the morphometric and meristic data between the specimens from the Río Vaupés and Río Putumayo basins, no discrete differences were observed between the ranges obtained. However, the specimens from the Río Putumayo basin are slightly larger than those from the Río Vaupés basin (34.2–44.4% SL, mean = 41.4% SL vs. 33.2–41.2% SL, mean = 35.5% SL). Across the PCA comparing the specimens of both basins, the first four components (which accounted for 64.4% of the total variance) were chosen as consensus between the scree plot method and broken-stick model (Suppl. materials 4, 5). In the plots obtained (Fig. 6A, B), the individuals of both basins did not separate in shape. In fact, we observed that the females and males from the Vaupés and Putumayo basins also overlapped each other slightly in the plots. The measures that most influenced the first four components were the snout to dorsal-fin origin (PC1: -0.6), dorsal fin to caudal-fin base (PC2: 0.4), dorsal-fin length (PC2: 0.4), pelvic-fin length (PC3: -0.3), and pectoral-fin length (PC4: -0.3) (Suppl. material 6). The specimens from the Río Putumayo basin shared almost completely the diagnostic characteristics of the new species. However, we observed that the dark

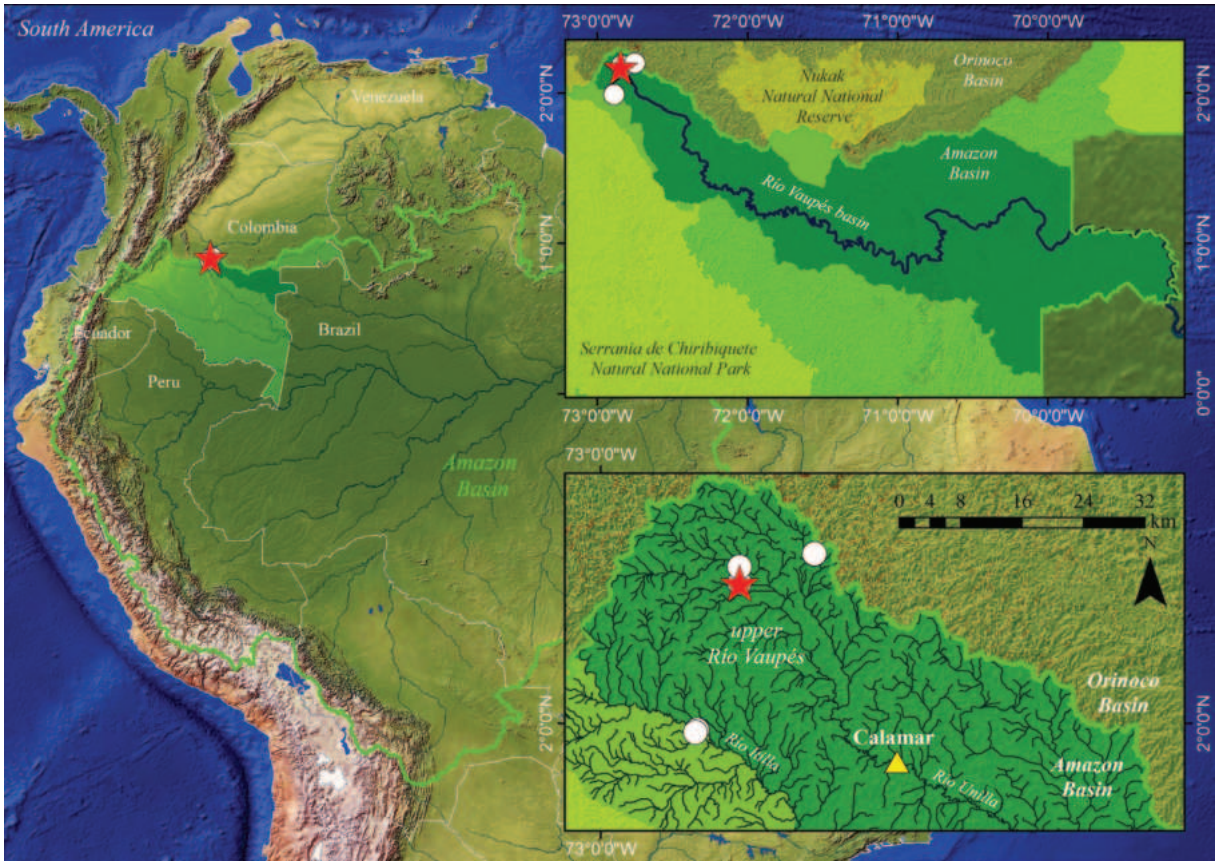

Figure 5. Geographical distribution of *Chrysobrycon calamar* along the upper Río Vaupés basin in Colombia, South America. Red star: type locality; white circle: paratype localities.

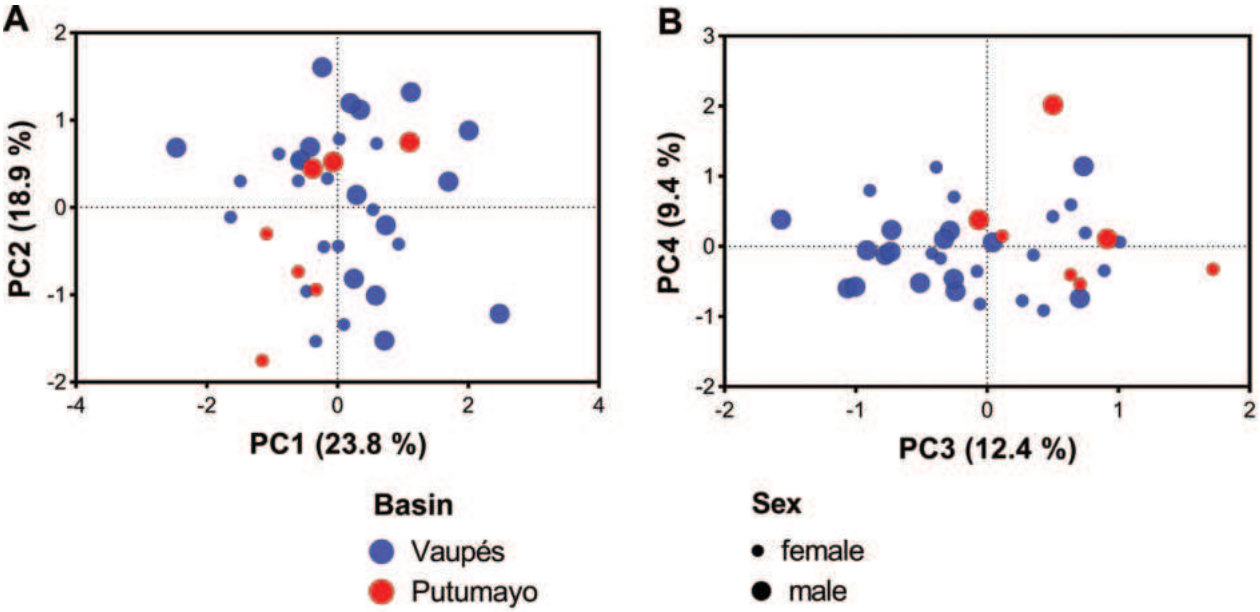

Figure 6. Size-corrected PCA performed comparing the morphometric data of *Chrysobrycon calamar* (blue circle) and the specimens examined from the Río Putumayo basin (red circle). **A.** PC1 *vs.* PC2 plot; **B.** PC3 *vs.* PC4 plot.

blotch on the abdominal flanks is slightly more developed laterally to the urogenital region than dorsally, and the number of maxillary teeth is slightly greater (3–7, mode = 6 *vs.* 2–4, mode = 3). In addition, we did not have enough well-preserved adult males to observe in more detail the variation associated with this pigmentation. For these reasons, we treat this population as *C.* aff. *calamar* and are cautious in this regard, pending further specimens or DNA samples that can become available to conduct additional comparisons. We hope this population can be reanalyzed in the future as part of the ongoing revision of the genus that the first author performs in the Amazon basin.

Key to the species of *Chrysobrycon* (modified from Vanegas-Ríos and Urbano-Bonilla, 2017)

1 Distal tips of maxillary teeth straight along their lengths 2
– Distal tips of most maxillary teeth lateroventrally curved ..... *C. mojicai*
2 Irregular, or circular-shaped humeral mark, always scarcely developed vertically; adult males with subtle or weak dark pigmentation on lateroventral portion of body between the pelvic- and anal-fin origins or slightly developed dorsally on first eight anal-fin rays, but never widely developed dorsally to anus on abdominal flanks; caudal-fin bony hooks of adult males restricted to lower lobe rays or, if present on upper lobe rays, with 1–3 hooks restricted to single ray; posterior portion of maxilla reaching or surpassing vertical through anterior margin of eye when mouth closed (intraspecifically variable in *C. yoliae*, not reaching such vertical in some specimens) 3
– Dark humeral mark intensely developed vertically in adult males (and some females); dark vertical blotch on abdominal flanks in adult males on small area between pelvic- and first two anal-fin rays, being widely expanded dorsally up to 3 or 4 scale rows; caudal-fin bony kooks of adult males present and numerous (4–10) on nearly all rays; posterior portion of maxilla not reaching vertical through anterior margin of eye when mouth closed ..... *C. calamar*
3 24–32 branched anal-fin rays; 14–16 circumpeduncular scales; adult males with shorter and unexpanded anal fin and lacking spinelets on pelvic-, anal-, and caudal-fin rays; pelvic-fin rays i,7 (rarely i,6 or i,8 in *C. eliasi* or *C. guahibo*); outer premaxillary row teeth with 4–6 (mode = 5 in *C. eliasi*; 5 in *C. guahibo*; 5 in *C. hesperus*; and 4 in *C. yoliae*) 4
– 33–39 branched anal-fin rays; 17–19 circumpeduncular scales; adult males with longer and expanded anal fin and with series of spinelets developed on pelvic-, anal-, and caudal-fin rays; pelvic-fin rays i,6 (rarely i,7); outer premaxillary row teeth with 2–4 teeth (mode = 3) ..... *C. myersi*
4 Anal-fin bony hooks distributed on anterior branched anal-fin rays 1–12 in adult males (≤ 60% of total number of rays); larger adult specimens (usually > 30 mm SL in *C. eliasi*; > 28 mm SL in *C. guahibo*; and > 35 mm SL in *C. yoliae*) with anteriormost maxillary tooth usually tricuspid (rarely conical, bicuspid, or tetracuspid); terminal lateral-line tube on middle caudal-fin rays present; irregular or rounded humeral mark usually overlapped by pored lateral line 5
– Anal-fin bony hooks located on nearly all branched anal-fin rays in adult males (> 80% of total number of rays); larger adult specimens (usually > 50 mm SL) with anteriormost maxillary tooth usually pentacuspid (rarely tri- or tetracuspid); terminal lateral-line tube on middle caudal-fin rays absent; circular-shaped humeral mark usually not overlapping with pored lateral line ..... *C. hesperus*

5 Maxillary teeth 6–16; anal-fin bony hooks on third to seventh branched anal-fin rays forming single, continuous series along each ray in adult males 6
– Maxillary teeth 1–3 (occasionally absent in juvenile specimens); anal-fin bony hooks on third to seventh branched rays forming two separate series along each ray in adult males ..... *C. guahibo*
6 Dentary teeth 20–26; body depth at dorsal-fin origin 34.4–42.2% SL (mean = 36.7% SL); dorsal fin to adipose fin distance 26.8–28.8% SL (mean = 27.9% SL); dorsal-fin origin situated at vertical between anal-fin rays 5–7 ..... *C. yoliae*
– Dentary teeth 12–19; body depth at dorsal-fin origin 24.1–34.5% SL (mean = 29.8% SL); dorsal fin to adipose fin distance 23.9–26.8% SL (mean = 25.4% SL); dorsal-fin origin situated at vertical between anal-fin rays 8–10 ..... *C. eliasi*

Comparative material examined

Chrysobrycon eliasi. All from PERU, Madre de Dios department, Tambopata: MUSM 39970, holotype, 34.3 mm SL; Madre de Dios basin, Loboyoc creek; 12°27'07"S, 69°7'43"W, c. 210 m a.s.l. MLP-Ict 10831, 3 paratypes, 33.0–43.5 mm SL (2 c&s specimens 33.0–39.9 mm SL); Río Manuripe basin, creek at km 50; 12°11'21"S, 69°6'57"W, c. 250 m a.s.l.; CI-FML 6153, 2 paratypes, 37.3–37.6 mm SL, Río Manuripe basin, Yarinal creek; 12°3'06"S, 69°4'50"W, c. 250 m a.s.l.; MUSM 39971, 14 paratypes, 26.1–40.8 mm SL; same data as for holotype. MUSM 39972, 8 paratypes, 28.0–43.2 mm SL; Manuripe basin, creek at km 50; 12°11'21"S, 69°6'5"W; c. 250 m a.s.l.; MUSM 39973, 2 paratypes, 36.11–37.63 mm SL; Río Madre de Dios basin, Loboyoc creek; 12°27'21"S, 69°7'42"W, c. 230 m a.s.l.; MUSM 39974, 3 paratypes, 29.3–41.2 mm SL, San Antonio, Río Heath basin, San Antonio creek; 12°41'03"S, 68°43'09"W, c. 190 m a.s.l. ROM 66378, 4, 27.6–31.6 mm SL; Tambopata, La Colpa, lodge, Río Tambopata, stream at left bank at 2.1 km. *Chrysobrycon* aff. *calamar*. All from COLOMBIA, Río Putumayo basin: MLP-Ict 11734, 5, 34.1–44.4 mm SL; Valle del Guamuez municipality, Río Cohembí. MLP-Ict 11735, 2, 42.4–43.9 mm SL; Puerto Asís municipality, Quebrada Tuayá. MPUJ 18619, 1, male. 34.2 mm SL; Putumayo, Puerto Asís municipality, Quebrada NN4. *Chrysobrycon guahibo*. All from COLOMBIA, Meta department, Río Orinoco basin, Río Guaviare basin, Río Ariari basin: MPUJ 7160, holotype, 31.9 mm SL; Fuente de Oro municipality, Caño Abrote; 3°17'39"N, 73°32'02"W, 260 m a.s.l. All are paratypes, Puerto Lleras municipality, Caño Cunimia; 3°11'24"N, 73°39'39"W, c. 270 m: CI-FML 6152, 6, 26.5–33.6 mm SL; MLP-Ict 10829, 2 c&s specimens, 30.4–31.3 mm SL; MPUJ 7162, 11, 26.7–29.0 mm SL; MLP-Ict 10830, 4, 28.9–31.3 mm SL. All are paratypes: MPUJ 7161, 10, 23.0–29.6 mm SL, same data as for holotype. MPUJ 7163, 1, 31.0 mm SL; Puerto Lleras municipality, Caño Cunimia; 3°11'24"N, 73°39'39"W, c. 270 m a.s.l. MPUJ 7164, 3, 31.0–34.8 mm SL; Puerto Lleras municipality, Caño Cunimia; 3°11'24"N, 73°39'39"W, c. 270 m a.s.l. MPUJ 7165, 6, 28.7–35.3 mm SL; San Juan de Arama municipality, Caño Casa Roja; 3°22'25"N, 73°52'13"W, c. 450 m a.s.l. MPUJ 7166, 8, 31.3–36.6 mm SL; Vista Hermosa municipality, Caño Uricacha; 3°16'56"N, 73°36'45"W, c. 270 m a.s.l. MPUJ 7167, 10, 29.0–35.2 mm SL; Fuente de Oro municipality, Caño Abrote; 3°17'39"N, 73°32'02"W, c. 250 m a.s.l. MPUJ 7168, 2, 43.5–44.6 mm SL; Vista Hermosa municipality, Caño Guapaya, 3°2'59"N, 73°49'17"W, c. 290 m a.s.l. *Chrysobrycon hesperus*. All from ECUADOR: All from Napo-Pastaza provinces, upper Río Villano near Villano, Río Napo system: ANSP 75912, 1 paratype, 77.4 mm SL; ANSP 79513, 1 paratype, 67.4 mm SL. All from Napo-Pastaza provinces, Río Pucuno, tributary of Río Suno, Pucuno enters of Suno: USNM 164056, holotype of *Hysteronotus hesperus*, 72.3 mm SL (radiographed); USNM 175124, 1 paratype, 59.1 mm SL (radiographed). ANSP 75914, 1 paratype, 63.2 mm SL; Napo-Pastaza provinces, Río Suno near mouth, tributary upper Río Napo. ANSP 79159, 2 paratypes, 60.3–76.0 mm SL; Río Pucuno, a tributary of Río Suno, upper Río Napo system. USNM 164042, 1 paratype, 70.5 mm SL; Napo-Pastaza provinces, Río Villano, upper Río Curaray, near Villano. FMNH 94557, 2*, 49.3–68.4; Napo, Río Arajuno, Quebrada to Río Gusano [Cusano], joins Río Gusano [Cusano] about 100 m upstream from mouth; [c. 1°05'25"S, 77°32'46"W, 420 m a.s.l.]. All from PERU, Loreto department: MUSM 26607, 2, 59.9–66.1 mm SL; Andoas, upper Amazon basin, Río Corrientes basin, Caballo creek, 2°33'41"S, 76°13'45"W, c. 210 m a.s.l. MUSM 26617, 2, 29.8–33.1 mm SL, upper Amazon basin, Río Corrientes, drainage flowing into Huayuri creek; 2°35'51"S, 76°13'53"W, c. 210 m a.s.l. MUSM 28640, 2, 25.5–27.0 mm SL; Forestal creek, Río Corrientes basin, 2°19'14"S, 76°10'31"W, c. 220 m a.s.l. MUSM 28665, 3, 36.2–54.6 mm SL (1 c&s specimen, 54.6 mm SL); Andoas, upper Amazon basin, Río Corrientes basin, Forestal creek; 2°21'28"S, 76°9'25"W, c. 240 m a.s.l. MUSM 28682, 3, 41.6–46.1 mm SL, Andoas, upper Amazon basin, San Carlos creek, flowing into Río Manchari; 2°24'35"S, 76°6'36"W, c. 200 m a.s.l. MUSM 32124, 1, 27.1 mm SL, Andoas, upper Amazon basin, Río Corrientes basin, Río Platanoyacu; 3°8'27"S, 75°45'09"W; c. 150 m a.s.l. MUSM 33159, 2, 29.3–43.9 mm SL, Andoas, upper Amazon basin, Río Pastaza, Carmen creek; 2°22'44"S, 76°9'44"W, c. 220 m a.s.l. *Chrysobrycon myersi*. All from PERU: Huanuco department, small creek directly tributary to Río Pachitea (itself tributary to Río Ucayali) at the northeastern outskirts of Tournavista; ANSP 112325, 2 paratypes, 30.1–46.1 mm SL; ANSP 112326, 3 paratypes, 28.3–32.0 mm SL; USNM 203697, holotype of *Hysteronotus myersi*, 46.5 mm SL; USNM 203698, 6 paratypes, 24.9–31.3 mm SL (1 radiographed, 31.3 mm SL). LACM 37720.4, 3, 34.3–63.8 mm SL, Pasco department, Iscozacin Valley, Pan de Azúcar, stream about 100 yards

above entrance into Río Iscozacin. MUSM 12040, 1, 29.7 mm SL, Cusco department, La Convención province, Echarate, Urubamba basin, Río Picha, Cocha Kamariampiveni; c. 11°36'00"S, 73°05'00"W, 380 m a.s.l. MUSM 18908, 2, 42.4–48.6 mm SL; Pasco department, Oxapampa province, Puerto Bermudez, Río Pachitea basin, Atas creek; c. 10°17'47"S, 74°56'11"W, 260 m a.s.l. MUSM 36068, 1, 31.6 mm SL, Curso department, La Convencion province, Echarate, Río Urubamba basin, Río Parotori system, Río Poyiriari; 12°10'44"S, 73°5'06"W, c. 540 m a.s.l. MUSM 36084, 3, 37.1–58.7 mm SL, Cusco department, La Convención province, Echarate, Urubamba basin, Río Parotori system, Río Poyriari; 12°10'45"S, 73°5'18"W, c. 590 m a.s.l. MUSM 36109, 2, 32.8–36.3 mm SL, Cusco department, La Convención province, Echarate, Río Urubamba, Río Parotori, Río Poyiriari, Piriabindeni creek; 12°1'13"S, 73°0'24"W, c. 590 m a.s.l. MUSM 36125, 3, 29.2–38.6 mm SL, Cusco department, La Convención province, Echarate, Río Parotori basin, Piriabindeni creek; 12°1'19"S, 73°4'15"W, c. 550 m a.s.l. MUSM 37889, 2, 45.1–51.0 mm SL, Junin department, Satipo province, Mashira, Río Tambo basin, Capirosankari creek; 11°1'25"S, 73°33'36"W, c. 420 m a.s.l. MUSM 37933, 3, 58.0–60.8 mm SL, Cusco department, La Convención province, Echarate, Kinterani, Naca-naca creek; 11°28'09"S, 73°18'02"W, c. 420 m a.s.l. MUSM 38671, 3, 50.9–60.7 mm SL (1 c&s specimen, 58.6 mm SL), Junin department, Satipo province, Río Tambo basin, Pukakunga creek; 73°28'02"W, 11°24'37"S, c. 590 m a.s.l. *Chrysobrycon mojicai*. All from COLOMBIA, Amazonas department, Río Amazon basin, Leticia: IAvH-P 13932, holotype, 50.6 mm SL; Amacayacu National Natural Park, unnamed forest stream tributary of Río Mata-Matá; 3°48'23"S, 70°15'58"W, c. 90 m a.s.l. All are paratypes: IAvH-P 8291, 5, 25.0–50.4 mm SL (one c&s specimen, 50.4 mm SL), same data as for the holotype. IAvH-P 8295, 9, 29.0–47.7 mm SL; Amacayacu National Natural Park, unnamed forest stream, tributary of Río Pureté headwaters, 3°41'54"S, 70°12'24"W, c. 130 m a.s.l. IAvH-P 8300, 2, 33.5–40.8 mm SL; Amacayacu National Natural Park, unnamed forest stream tributary of Río Pureté headwaters; 3°41'38"S, 70°12'27"W. IAvH-P 8917, 14, 17.1–47.5 mm SL; Sufragio stream in front of Zafire Biological Station, 4°0'19"S, 69°53'56"W, c. 120 m a.s.l. IAvH-P 8951, 9, 17.9–50.5 mm SL, Sufragio stream in front of Zafire Biological Station; 4°0'20"S, 69°53'56"W, c. 120 m a.s.l. IAvH-P 9022, 6, 43.8–50.8 mm SL (including 3 c&s specimens fully disarticulated as non-types), Sufragio stream in front of Zafire Biological Station; 4°0'19"S, 69°53'56"W, c. 120 m a.s.l. IAvH-P 9070, 4, 48.6–55.0 mm SL, unnamed forest stream tributary of Río Calderon, 45 min. NE of Zafire Biological Station; 3°58'40"S, 69°53'32"W, c. 130 m a.s.l. IAvH-P 9093, 4, 23.7–47.8 mm SL; unnamed stream, tributary of Río Calderon, 45 min. NE of Zafire Biological Station; 3°58'40.14"S, 69°53'31.8"W, 130 m a.s.l. MPUJ 8058, 1, 49.5 mm SL, same data as for the holotype. MPUJ 8059, 1 c&s, 50.3 mm SL; unnamed forest stream tributary of Río Calderon, 45 min. NE of Zafire Biological Station; 3°58'40"S, 69°53'32"W, c. 130 m a.s.l. *Chrysobrycon yoliae*. All from PERU, Ucayali department, Coronel Portillo province, Abujao, Río Yucamia subsystem, unnamed creek, 8°39'14"S, 73°21'17"W, c. 273 m: MUSM 46140, holotype, 51.6 mm SL; CI-FML 5882, 3 paratypes, 44.8–52.3 mm SL (one c&s specimen, 44.8 mm SL); MLP-Ict 10517, 1 paratype, 48.4 mm SL; MUSM 46141, 8 paratypes, 38.2–51.5 mm SL.

Discussion

Based on morphological data, Vanegas-Ríos et al. (2020) found nine synapomorphies supporting the monophyly of five species of *Chrysobrycon* analyzed as part of a phylogenetic hypothesis of Stevardiinae. The synapomorphies proposed in that study (some not exclusive, with varied degrees of homoplasy in Stevardiinae) are: 1) the absence of the frontal fontanel (Character 26); the absence or reduced parietal fontanel (character 40); the dorsolateral process of the anguloarticular with greatest vertical dimension as large as that of the posterior region of the horizontal process of the anguloarticular (character 128); the posterior margin of the hypural 2 as large as vertical distance between the bases of the caudal-fin rays 11 to 13 (character 341); bony hooks on the base of the pelvic-fin rays in small number compared to the segmented portion of rays (character 456); interradialis muscle fibers not exceeding the posterodorsal border of the pouch scale (character 475); pouch scale horizontally folded, forming a laterally concave pocket (character 494); 35 or fewer pouch-scale radii (character 499); and the presence of a medial accessory pouch scale (character 517). *Chrysobrycon calamar* shares the traditional characteristics used by Weitzman and Menezes (1998) and Vanegas-Ríos and Urbano-Bonilla (2017) to define the genus, as well as the synapomorphies found in Vanegas-Ríos et al. (2020) (character 128 is polymorphic).

In all *Chrysobrycon* species, the accessory lateral membranes located on all the dorsal-fin rays have lamellae that are extended from the ventral surface of rays, covering partially the interradial membranes, being slightly more developed in males than in females. Comparatively, these lamellae are less developed laterally in *C. calamar*, *C. eliasi*, and *C. guahibo*. The distinctive dark blotch on the abdominal flanks along the urogenital region in adult males of *C. calamar* is a remarkable characteristic that seems to be rare in Characidae. However, the presence of dark pigmentation on the belly is also found in related members of Stevardiini, for instance, in *Gephyrocharax caucanus* Eigenmann, 1912 (Vanegas-Ríos 2016), which possesses a urogenital pigmentation in adult males that partially resembles that of *C. calamar* or *C. mojicai*. This pigmentation in Stevardiini seems to be associated with courtship behavior, so that is exclusive to adult males with bony hooks. We observed in adult males of the *Chrysobrycon* species several sexually dimorphic patterns of color variation associated with the region between the pelvic and

anal fins (Suppl. material 1): (1) region poorly pigmented ventrally or laterally, not forming a detectable blotch (*e.g. C. eliasi*); (2) area with scattered dark chromatophores extending dorsally between the anus and anal-fin origin, being weak or diffuse lateroventrally (*e.g. C. guahibo*); (3) region slightly darkened by scattered chromatophores lateroventrally, being a little more developed laterally between the pelvic- and anal-fin origins (*e.g. C. hesperus*); (4) urogenital region without distinguishable blotch or pigmentation, but with dark longitudinal pigmentation extended dorsally on the first anal-fin rays (*e.g. C. myersi*); (5) area moderately darkened ventrally, but forming a dark vertical blotch that reaches dorsally up to three or four scales between the urogenital pore and first two anal-fin rays (*C. calamar*); and 6) area strongly darkened lateroventrally but confined to the region between the scale rows covering the urogenital pore and those rows located immediately dorsal to that area (*e.g. C. mojicai*). This sexually dimorphic pigmentation is present in life and most well-preserved adult male specimens, but in some species where it is found to be less developed, it could be erroneously estimated if the body color is not well preserved. In further contributions, we expect to continue analyzing the morphological variations associated with this pigmentation in a phylogenetic context and using additional male specimens to explore its potential significance within the genus and/or Stevardiini.

In *Chrysobrycon* species (except *C. myersi*), we also observed that the urogenital region in both sexes is modified as follows (but more noticeably developed in adult males): the urogenital pore is completely covered by one row of four to six scales in each flank, which face each other, forming a sharp edge between the anal- and pelvic-fin origins (Suppl. material 7). These scales are also slightly projected ventrally beyond the ventral profile of the belly, like a keel. This characteristic was not extensively described before for the species of the genus, but it was partly observed by Böhlke (1958) as some preventral scales forming a distinctive edge in *C. hesperus*. These scale rows forming a sharp edge ventrally are also observed in other members of Stevardiini (*e.g.*, *G. caucanus* or *Pseudocorynopoma doriae* Perugia, 1891). In *C. myersi*, no sharp keel between the pelvic-fin base and urogenital pore was observed, in agreement with Weitzman and Thomerson (1970); the preanal scales are not projected ventrally beyond the skin. In fact, in some females, a small triangular urogenital papilla was observed to be developed externally.

Currently, Brazilian colleagues (C. Silva-Oliveira, A. L. C. Canto, and F. R. V. Ribeiro) and the first author are studying some specimens from the Amazon basin in Brazil that could represent a new species for the genus. *Chrysobrycon calamar* can be distinguished from that morphotype by the dark pigmentation between the urogenital region and anal fin (vertically developed, reaching up to the first two anal-fin rays *vs.* longitudinally developed, reaching up to the first ten anal rays). It is worth mentioning that, although four species have been described within *Chrysobrycon* in the last 15 years, we still continue to reveal the hidden richness of this outstanding group of Stevardiinae.

It is important to recognize that the demobilization of FARC-EP troops between 2016 and 2018 had a strong impact on Colombia´s biodiversity. Many regions with previously scarce information were now the target of a series of biological expeditions by different universities and institutions throughout the country (Restrepo-Santamaria et al. 2023; Bogotá-Gregory et al. 2024). As a result of these studies in previously unexplored areas, from 2017 to date, 13 new fish species have been described just for the Colombian Amazon (DoNascimiento et al. 2024). Thus, the present description of *C. calamar* constitutes a priceless result of the achievement of having regained access in this type of area to understand their biodiversity and, at the same time, exemplifies the potential associated with such regions to have hidden diversity. In both cases, there are positive impacts not only on scientific progress but also on the increase of the country's biological heritage.

Conclusions

We concluded that the specimens analyzed from the Río Vaupés basin are a new species based on the exhaustive morphological comparison using morphometric, meristic, and osteological data. The specimens examined from the upper Río Putumayo are considered *C.* aff. *calamar* based on the inconsistency observed in the urogenital pigmentation and the few adult males available to better assess this variation. It is important to emphasize that the urogenital pigmentation associated with sexual dimorphism has begun to play a prominent role in resolving the alpha taxonomy within the genus and can be very useful for identifying the species of *Chrysobrycon* in the field. The discovery of *C. calamar* is really significant because this is one of several new species that have been found in endemism-rich regions that could be explored after the guerrilla demobilized in Colombia.

Acknowledgments

We thank the following staff and institutions for their assistance and support: J. Lundberg, M. Sabaj Pérez, M. Arce, and K. Luckenbill (ANSP), C. DoNascimiento (IAvH, UDEA), C. MacMahan, and K. Swagel (FMNH); H. Agudelo-Zamora (ICN-MHN); R. Feeny (LACM); S. Prada and T. P. Carvalho (MPUJ); P. Burchardt, F. Merli, and D. Nadalin (MLP-Ict); D. R. Faustino and H. Ortega (MUSM); A. Ortega-Lara (FUNINDES); and L. Parenti and D. Pitassy (USNM). Financial support was received from FONCyT and CONICET (BID-PICT 2019–02419 and PIBAA 0654 to JAV-R). We sincerely thank our friends, J. Zamudio, C. Moreno, S. Prada, and J. Maldonado-Ocampo (R.I.P.), who participated in the

field collections. To F. Cuvides for the logistical support during the expedition to the upper Vaupés. Tiago P. Carvalho (MPUJ) assisted with the preparation of the c&s specimens. We also thank the families of G. Castañeda and M. Rodríguez for their hospitality during fieldwork. Macarena Frias helped with the edition of Suppl. material 7. Additionally, A. Urbano-Bonilla would like to thank two projects carried out by the Pontifical Javeriana University that promoted field expeditions in the upper Vaupés. "Assessing ichthyofauna diversity and the potential response to climatic change in the Orinoco basin in Colombia, supported by National Geographic (NGS-72883R-20)" and "Riverscape genetics: linking river environments with adaptive potential in Neotropical freshwater fish." We are grateful to the peer reviewers for their suggestions and feedback on this article.

References

Arcila OH, González GI, Salazar CA (1999) Guaviare, población y territorio. Instituto Amazónico de Investigaciones Científicas "SINCHI", Bogotá DC, 196 pp.

Bogotá-Gregory JD, Jenkins DG, Acosta-Castro A, Agudelo Córdoba E (2024) Fish diversity of Colombian Andes-Amazon streams at the end of conflict is a reference for conservation before increased land use. Ecology and Evolution 14(3): e11046. https://doi.org/10.1002/ece3.11046

Böhlke J (1958) Studies on fishes of the family Characidae.: No. 14. A report on several extensive recent collections from Ecuador. Proceedings. Academy of Natural Sciences of Philadelphia 110: 1–121.

Cattel R (1966) The scree test for the number of factors. Multivariate Behavioral Research 1(2): 245–276. https://doi.org/10.1207/s15327906mbr0102_10

Claro-García A, Vieira LJS, Jarduli LR, Abrahão VP, Shibatta OA (2013) Fishes (Osteichthyes: Actinopterygii) from igarapés of the rio Acre basin. Check List 9(6): 1410–1438. https://doi.org/10.15560/9.6.1410

DoNascimiento C, Agudelo-Zamora HD, Bogotá-Gregory JD, Méndez-López A, Ortega-Lara A, Lasso CA, Cortés-Hernández M, Albornoz-Garzón JG, Villa-Navarro FA, Netto-Ferreira AL, Lima FCT, Thomaz A, Arce-Hernández M (2024) Lista de especies de peces de agua dulce de Colombia / Checklist of the freshwater fishes of Colombia. Dataset/Checklist. 2.16. https://ipt.biodiversidad.co/sib/resource?r=ictiofauna_colombiana_dulceacuicola [accessed 1 Feb 2024]

Elliott NG, Haskard K, Koslow JA (1995) Morphometric analysis of orange roughy (*Hoplostethus atlanticus*) off the continental slope of southern Australia. Journal of Fish Biology 46: 202–220. https://doi.org/10.1111/j.1095-8649.1995.tb05962.x

Fink WL, Weitzman SH (1974) The so-called Cheirodontin fishes of Central America with descriptions of two new species (Pisces: Characidae). Smithsonian Contributions to Zoology 172(172): 1–45. https://doi.org/10.5479/si.00810282.172

Frontier S (1976) Etude de la dècroissance des valeurs propres dans une analyse en composantes principales: Comparaison avec le modèle du bâton brisé. Journal of Experimental Marine Biology and Ecology 25(1): 67–75. https://doi.org/10.1016/0022-0981(76)90076-9

Hammer Ø, Harper DAT, Ryan PD (2001) PAST: Paleontological statistics software package for education and data analysis. Palaeontologia Electronica 4: 1–9.

Hernández-Camacho J, Hurtado A, Ortiz R, Walschburger T (1992) Unidades biogeográficas de Colombia. In: Halfter G (Ed.) La diversidad biológica de Iberoamérica. Instituto de Ecología, A. C., México, 105–173.

Irwin A (2023) The race to understand Colombia's exceptional biodiversity. Nature 619: 450–453. https://doi.org/10.1038/d41586-023-02300-6

Jézéquel C, Tedesco PA, Bigorne R, Maldonado-Ocampo JA, Ortega H, Hidalgo M, Martens K, Torrente-Vilara G, Zuanon J, Acosta A, Agudelo E, Barrera Maure S, Bastos DA, Bogotá Gregory J, Cabeceira FG, Canto ALC, Carvajal-Vallejos FM, Carvalho LN, Cella-Ribeiro A, Covain R, Donascimiento C, Dória CRC, Duarte C, Ferreira EJG, Galuch André V, Giarrizzo T, Leitão RP, Lundberg JG, Maldonado M, Mojica JI, Montag LFA, Ohara WM, Pires THS, Pouilly M, Prada-Pedreros S, de Queiroz LJ, Rapp Py-Daniel L, Ribeiro FRV, Ríos Herrera R, Sarmiento J, Sousa LM, Stegmann LF, Valdiviezo-Rivera J, Villa F, Yunoki T, Oberdorff T (2020a) A database of freshwater fish species of the Amazon Basin. Scientific Data 7(1): 96. https://doi.org/10.1038/s41597-020-0436-4

Jézéquel C, Tedesco PA, Darwall W, Dias MS, Frederico RG, Hidalgo M, Hugueny B, Maldonado-Ocampo J, Martens K, Ortega H, Torrente-Vilara G, Zuanon J, Oberdorff T (2020b) Freshwater fish diversity hotspots for conservation priorities in the Amazon Basin. Conservation Biology 34(4): 956–965. https://doi.org/10.1111/cobi.13466

Lima FCT, Ramos L, Barreto T, Cabalzar A, Tenório G, Barbosa A, Tenório F, Resende A, Lopes M (2005) Peixes do alto Tiquié: ictiologia e conhecimentos dos tuyuka e tukano. In: Cabalzar A (Ed.) Peixe e Gente no Alto Rio Tiquié São Paulo, Instituto Socioambiental, 339 pp. São Paulo, 111–282.

Lima FCT, Urbano-Bonilla A, Prada-Pedreros S (2020) A new *Hemigrammus* from the upper Río Vaupés, Colombia (Characiformes: Characidae), with a discussion on the presence of an enlarged urogenital papilla in the family. Journal of Fish Biology 96(4): 868–876. https://doi.org/10.1111/jfb.14267

Londoño-Burbano A, Urbano-Bonilla A (2018) A new species of *Rineloricaria* (Teleostei: Loricariidae) from the upper Vaupés River, Amazon River basin, Colombia. Ichthyological Exploration of Freshwaters 28: 375–384. https://doi.org/10.23788/IEF-1071

Menezes NA, Weitzman SH (1990) Two new species of *Mimagoniates* (Teleostei: Characidae: Glandulocaudinae), their phylogeny and biogeography and a key to the glandulocaudin fishes of Brazil and Paraguay. Proceedings of the Biological Society of Washington 103: 380–426.

Mirande JM (2019) Morphology, molecules and the phylogeny of Characidae (Teleostei, Characiformes). Cladistics 35(3): 282–300. https://doi.org/10.1111/cla.12345

Restrepo-Santamaria D, Valencia-Rodríguez D, Herrera-Pérez J, Muñoz-Duque S, Galeano AF, Jiménez-Segura L (2023) Bio Anorí, the biological expedition that documented fish diversity after the post-conflict in Antioquia, Colombia. Global Ecology and Conservation 43: e02445. https://doi.org/10.1016/j.gecco.2023.e02445

Rohlf FJ (2015) The tps series of software. Hystrix 26: 9–12. https://doi.org/10.4404/hystrix-26.1-11264

Sabaj MH (2020) Codes for natural history collections in ichthyology and herpeteology. Copeia 108(3): 593–669. https://doi.org/10.1643/ASIHCODONS2020

Taylor WR, Van Dyke GC (1985) Revised procedures for staining and clearing small fishes and other vertebrates for bone and cartilage study. Cybium 9: 107–119.

Thomaz AT, Malabarba LR, Knowles LL (2017) Genomic signatures of paleodrainages in a freshwater fish along the southeastern coast of Brazil: Genetic structure reflects past riverine properties. Heredity 119(4): 287–294. https://doi.org/10.1038/hdy.2017.46

Toledo-Piza M, Baena EG, Dagosta FCP, Menezes NA, Ândrade M, Benine RC, Bertaco VA, Birindelli JLO, Boden G, Buckup PA, Camelier P, Carvalho FR, Castro RMC, Chuctaya J, Decru E, Derijst E, Dillman CB, Ferreira KM, Merxem DG, Giovannetti V, Hirschmann A, Jégu M, Jerep FC, Langeani F, Lima FCT, Lucena CAS, ZMS Lucena, Malabarba LR, Malabarba MCSL, Marinho MMF, Mathubara K, Mattox GMT, Melo BF, Moelants T, Moreira CR, Musschoot T, Netto-Ferreira AL, Ota RP, Oyakawa OT, Pavanelli CS, Reis RE, Santos O, Serra JP, Silva GSC, Silva-Oliveira C, Souza-Lima R, Vari RP, Zanata AM (2024) Checklist of the species of the Order Characiformes (Teleostei: Ostariophysi). Neotropical Ichthyology 22: e230086. https://doi.org/10.1590/1982-0224-2023-0086

Torrente-Vilara G, Zuanon J, Leprieur F, Oberdorff T, Tedesco PA (2011) Effects of natural rapids and waterfalls on fish assemblage structure in the Madeira River (Amazon Basin). Ecology of Freshwater Fish 20: 588–597. https://doi.org/10.1111/j.1600-0633.2011.00508.x

Urbano-Bonilla A, García-Melo JE, Peña-Bermudez ME, Melo-Ortiz OE, Ordoñez OE, Correa SB, Carvalho TP, Maldonado-Ocampo JA (2024) [in press] Fishes (Actinopterygii) of the rapids and associated enviroments in the lower Vaupés River basin: an undiscovered Colombian Amazon diversity. ZooKeys.

Urbano-Bonilla A, Londoño-Burbano A, Carvalho TP (2023) A new species of rheophilic armored catfish of *Rineloricaria* (Siluriformes: Loricariidae) from the Vaupés River, Amazonas basin, Colombia. Journal of Fish Biology 103: 1073–1084. https://doi.org/10.1111/jfb.15500

Valdiviezo-Rivera J, Carrillo-Moreno C, Gea-Izquierdo E (2018) Annotated list of freshwater fishes of the Limoncocha Lagoon, Napo river basin, northern Amazon region of Ecuador. Check List 14(1): 55–75. https://doi.org/10.15560/14.1.55

Vanegas-Ríos JA (2016) Taxonomic review of the Neotropical genus *Gephyrocharax* Eigenmann, 1912 (Characiformes, Characidae, Stevardiinae). Zootaxa 4100(1): 1–92. https://doi.org/10.11646/zootaxa.4100.1.1

Vanegas-Ríos JA (2018) Phylogeny of the Neotropical genus *Gephyrocharax* (Characiformes: Characidae: Stevardiinae), with remarks on the tribe Stevardiini. Zoological Journal of the Linnean Society 182(4): 808–829. https://doi.org/10.1093/zoolinnean/zlx045

Vanegas-Ríos JA, Urbano-Bonilla A (2017) A new species of *Chrysobrycon* (Characiformes, Characidae, Stevardiinae) from the Amazon River basin in Colombia, with a new diagnostic characteristic for the genus. Journal of Fish Biology 90(6): 2344–2362. https://doi.org/10.1111/jfb.13317

Vanegas-Ríos JA, Azpelicueta MM, Ortega H (2011) *Chrysobrycon eliasi*, new species of stevardiine fish (Characiformes: Characidae) from the río madre de dios and upper río manuripe basins, Peru. Neotropical Ichthyology 9(4): 731–740. https://doi.org/10.1590/S1679-62252011000400004

Vanegas-Ríos JA, Azpelicueta MM, Mirande JM, Gonzales MDG (2013a) *Gephyrocharax torresi* (Characiformes: Characidae: Stevardiinae), a new species from the Río Cascajales basin, Río Magdalena system, Colombia. Neotropical Ichthyology 11(2): 275–284. https://doi.org/10.1590/S1679-62252013000200005

Vanegas-Ríos JA, Meza-Vargas V, Azpelicueta MM (2013b) Extension of geographic distribution of *Chrysobrycon hesperus* and *C. myersi* (Characiformes, Characidae, Stevardiinae) for several drainages flowing into the Amazon River Basin in Peru and Colombia. Revista Mexicana de Biodiversidad 84(1): 384–387. https://doi.org/10.7550/rmb.29591

Vanegas-Ríos JA, Azpelicueta MM, Ortega H (2014) *Chrysobrycon yoliae*, a new species of stevardiin (Characiformes: Characidae) from the Ucayali basin, Peru. Neotropical Ichthyology 12(2): 291–300. https://doi.org/10.1590/1982-0224-20130123

Vanegas-Ríos JA, Urbano-Bonilla A, Azpelicueta MM (2015) *Chrysobrycon guahibo*, a new species from the Orinoco River basin, with a distribution expansion of the genus (Teleostei: Characidae). Ichthyological Exploration of Freshwaters 26: 171–182.

Vanegas-Ríos JA, Faustino-Fuster DR, Meza-Vargas V, Ortega H (2020) Phylogenetic relationships of a new genus and species of stevardiine fish (Characiformes: Characidae: Stevardiinae) from the Río Amazonas basin, Peru. Journal of Zoological Systematics and Evolutionary Research 58(1): 387–407. https://doi.org/10.1111/jzs.12346

Weitzman SH, Menezes NA (1998) Relationships of the tribes and genera of Glandulocaudinae (Ostariophysi: Characiformes: Characidae) with a description of a new genus, *Chrysobrycon*. In: Malabarba LR, Reis RE, Vari RP, Lucena ZMSd, Lucena CA (Eds) Phylogeny and classification of Neotropical Fishes. EDIPUCRS, Porto Alegre, 171–192.

Weitzman SH, Thomerson JE (1970) A new species of glandulocaudine characid fish, *Hysteronotus myersi*, from Peru. Proceedings of the California Academy of Sciences 38: 139–156.

Supplementary material 1

Interspecific variation of the dark pigmentation on the urogenital region in adult males of *Chrysobrycon* species

Authors: James Anyelo Vanegas-Ríos, Alexander Urbano-Bonilla, Gian Carlo Sánchez-Garcés

Data type: pdf

Link: https://doi.org/10.3897/zse.100.121499.suppl1

Supplementary material 2

Photographs of the typical localities where *Chrysobrycon calamar* was collected in Colombia

Authors: James Anyelo Vanegas-Ríos, Alexander Urbano-Bonilla, Gian Carlo Sánchez-Garcés
Data type: pdf

Link: https://doi.org/10.3897/zse.100.121499.suppl2

Supplementary material 3

Coordinates used

Authors: James Anyelo Vanegas-Ríos, Alexander Urbano-Bonilla, Gian Carlo Sánchez-Garcés
Data type: xlsx

Link: https://doi.org/10.3897/zse.100.121499.suppl3

Supplementary material 4

Total variance accounted for the size-corrected PCA performed for the morphometric data

Authors: James Anyelo Vanegas-Ríos, Alexander Urbano-Bonilla, Gian Carlo Sánchez-Garcés
Data type: pdf

Link: https://doi.org/10.3897/zse.100.121499.suppl4

Supplementary material 5

Scree plot obtained from the morphometric data analyzed

Authors: James Anyelo Vanegas-Ríos, Alexander Urbano-Bonilla, Gian Carlo Sánchez-Garcés
Data type: pdf

Link: https://doi.org/10.3897/zse.100.121499.suppl5

Supplementary material 6

Loadings obtained from the size-corrected PCA comparison using the morphometric data

Authors: James Anyelo Vanegas-Ríos, Alexander Urbano-Bonilla, Gian Carlo Sánchez-Garcés
Data type: pdf

Link: https://doi.org/10.3897/zse.100.121499.suppl6

Supplementary material 7

Ventral view of preanal scales

Authors: James Anyelo Vanegas-Ríos, Alexander Urbano-Bonilla, Gian Carlo Sánchez-Garcés
Data type: pdf

Link: https://doi.org/10.3897/zse.100.121499.suppl7

Zoosyst. Evol. 100 (2) 2024, 691–704 | DOI 10.3897/zse.100.123441

PENSOFT

MUSEUM FÜR NATURKUNDE BERLIN

The missing piece of the puzzle: A new and widespread species of the genus *Rhynchocalamus* Günther, 1864 (Squamata, Colubridae) from the Arabian Peninsula

Fulvio Licata[1,2*], Lukáš Pola[3*], Jiří Šmíd[3,4], Adel A. Ibrahim[5], André Vicente Liz[1,2], Bárbara Santos[1,2], László Patkó[6], Ayman Abdulkareem[6], Duarte V. Gonçalves[1,7], Ahmed Mohajja AlShammari[8], Salem Busais[9], Damien M. Egan[10], Ricardo M. O. Ramalho[11], Josh Smithson[12], José Carlos Brito[1,2]

1 *Centro de Investigação em Biodiversidade e Recursos Genéticos (CIBIO), InBIO Laboratório Associado, Universidade do Porto, Campus de Vairão, 4485–661 Vairão, Portugal*
2 *BIOPOLIS Program in Genomics, Biodiversity and Land Planning, CIBIO, Campus de Vairão, 4485–661 Vairão, Portugal*
3 *Department of Zoology, Faculty of Science, Charles University, Viničná 7, 12844 Prague, Czech Republic*
4 *Department of Zoology, National Museum, Cirkusová 1740, Prague, Czech Republic*
5 *Department of Zoology, Faculty of Science, Suez University, 43527 Suez, Suez, Egypt*
6 *The Royal Commission for AlUla, Oud Dunes - Amr Aldamri, Riyadh 07747, Saudi Arabia*
7 *CIIMAR/CIMAR – Interdisciplinary Centre of Marine and Environmental Research, University of Porto, Terminal de Cruzeiros do Porto de Leixões, Av. General Norton de Matos s/n, 4450–208, Matosinhos, Portugal*
8 *Biology Department, Faculty of Sciences, University of Ha'il, Ha'il, Saudi Arabia*
9 *Biology Department, Faculty of Education, University of Aden, Aden, Yemen*
10 *Natural History Collective Ventures, Jalan Awan Cina, Taman Yarl, 58200 Kuala Lumpur, Wilayah Persekutuan Kuala Lumpur, Malaysia*
11 *KAUST Beacon Development, KAUST Innovation Cluster, Building 24, 4700 King Abdullah University of Science and Technology, Thuwal 23955–6900, Saudi Arabia*
12 *Prince Mohammed bin Salman Royal Reserve Development Authority, Al-Wajh 43929, Abdulla bin Abdul Aziz Street, Tabuk Governorate, Saudi Arabia*

https://zoobank.org/EEC07811-7DAA-4BD1-AAA1-52222AA81434

Corresponding authors: Fulvio Licata (fulvio.licata@cibio.up.pt); Lukáš Pola (polal@natur.cuni.cz)

Academic editor: Justin Bernstein ♦ **Received** 19 March 2024 ♦ **Accepted** 10 April 2024 ♦ **Published** 30 May 2024

Abstract

Discovery rates of new species are uneven across taxonomic groups and regions, with distinctive and widely distributed species being more readily described than species with secretive habits. The genus *Rhynchocalamus* includes five species of secretive snakes distributed from Egypt eastwards to Iran, including the Arabian Peninsula. A wide biogeographic gap exists within the genus, which separates *R. dayanae* found in south Israel from *R. arabicus*, which occurs in the coastal areas of south Yemen and Oman. We describe *Rhynchocalamus hejazicus* **sp. nov.**, a small, secretive snake, with a distinctive colouration and a melanistic morph. The new species occurs in the northwestern Hejaz region of the Kingdom of Saudi Arabia (KSA) and fills a large part of the existing distribution gap of the genus in the Arabian Peninsula. Molecular analyses of mitochondrial (*12S*, *16S*, *cytb*) and nuclear genes (*cmos*, *MC1R*, *NT3*, *RAG1*) indicate that *R. hejazicus* **sp. nov.** is closely related to *R. dayanae* and *R. arabicus*, but uncertainty on the deep relationship within the genus remains. The new species has a large distribution range which potentially includes other regions in Jordan and KSA, and is associated with mountainous areas with cold wet seasons. Furthermore, it inhabits sandy and stony soils with varying vegetation cover and can be found in anthropogenically disturbed habitats, suggesting that the species should not be categorised as threatened according to IUCN criteria. The discovery of such a distinctive species highlights the existing gap in the description of rare and secretive species, and the need to enhance sampling efforts and monitoring strategies to fully capture species diversity in unexplored areas.

* These authors contributed equally to this work.

Key Words

Biogeography, Colubrinae, Middle East, secretive species, Serpentes, species distribution model

Introduction

Closing the gap between extant and described species is a daunting task hampered by the intrinsically slow pace of the taxonomic process and the paucity of resources therein deployed (Engel et al. 2021), and is ultimately determined by the rate at which taxonomists discover species (May 2004). Recent advancements in molecular genetic techniques have boosted new species descriptions, however, discovery rates remain uneven across taxonomic groups and regions, being determined by species' morphology, life–history, and distribution range. For instance, small–bodied, less obvious, and small–ranged species are generally described later than bigger, more brightly coloured or widely distributed ones. Furthermore, geographical remoteness, along with behaviours and life–histories, may play a major role in determining species' discovery, and secretive species or species from remote areas are more unlikely to be discovered (Scheffers et al. 2012).

Snakes are a diverse group of reptiles (Uetz et al. 2024) but are notoriously hard to detect due to their secretive behaviour and rarity (Rodda 1993; Kéry 2002). This is reflected in wide taxonomic and knowledge gaps, especially in small, secretive species (Vilela et al. 2014) and undersampled regions of the world, such as the Middle East, where systematic and biogeographic data for several snake taxa is still lacking.

A remarkable example and one of the most obscure Arabian snakes is a small and rather secretly living colubrid genus *Rhynchocalamus* Günther, 1864. The genus currently comprises five recognized species (Uetz et al. 2024): (i) *R. arabicus* Schmidt, 1933, from Aden, Yemen and Dhofar in south Oman; (ii) *R. dayanae* Tamar, Šmíd, Göçmen, Meiri & Carranza, 2016, from the Negev area, south Israel with potential presence also in the Sinai Peninsula, Egypt; (iii) *R. levitoni* (Torki, 2017), from the Zagros Mountains of western Iran with potential presence also in neighbouring Iraq; (iv) *R. melanocephalus* (Jan, 1862), from the Sinai Peninsula, Egypt, Israel, Jordan, Lebanon, Syria, Turkey, and recently discovered on Cyprus and in Medina Province, Saudi Arabia; and (v) *R. satunini* (Nikolsky, 1899), from Turkey, Armenia, Iraq, and Iran (Avcı et al. 2015; Šmíd et al. 2015; Tamar et al. 2016, 2020; Fathinia et al. 2017; Torki 2017; Aloufi et al. 2021).

The phylogenetic relationships within the *Rhynchocalamus* genus showed a relevant biogeographic gap in the species distribution, with two sister species *R. dayanae* and *R. arabicus* separated by more than 2,500 km (Tamar et al. 2016). The existing gap extends along the Kingdom of Saudi Arabia, where sampling effort is still scarce or non-existent for certain regions (e.g., Alatawi et al. 2020; Šmíd et al. 2021).

In this study, we contribute to filling taxonomic and biogeographic gaps in the reptile diversity of the Arabian Peninsula and, in particular, in the understudied genus *Rhynchocalamus*, by providing (i) a formal description of a new species of *Rhynchocalamus* snake corroborated by morphological and molecular analyses, and (ii) a distribution model of this new species and its environmental requirements, including a proposal of its conservation status. Lastly, (iii) we report the exceptional finding of a melanistic morphotype of the new species.

Materials and methods

Field sampling

Field sampling was conducted in the Kingdom of Saudi Arabia (KSA) in 2017, 2021, 2022, and 2023. Field surveys in Hail Province, KSA were conducted by AAI, AMS, and SB in May 2017 and by AMS in July 2021. Field surveys carried out in the Prince Mohammad bin Salman Royal Reserve (PMBSRR), Tabuk Province, KSA were conducted by DME and LP in March and April 2022. Field surveys in Al-Ula County (Medina Province) were carried out by FL, JCB, AVL, BS, and DGV in May, June, and November 2023. GPS coordinates (datum WGS84) and high–resolution photographs were taken for each individual encountered.

We collected and stored tissue samples in 96% ethanol, whereas all vouchers were first fixed in 96% ethanol and then stored in 70% ethanol. We deposited the vouchers in the herpetology collections of National History Museum Prague, Czech Republic (NMP), Muséum National d'Histoire Naturelle, Paris, France (MNHN), and AlUla Museum (RCU-URN). The complete list of tissue samples and specimens analysed in this study is listed in Suppl. material 1: table S1.

Morphological analysis

We selected the morphological characters based on previous taxonomic studies of the genus *Rhynchocalamus* (Tamar et al. 2016). We measured the following characters on the right side of the specimens using the image processing software ImageJ (vers. 1.53; Schneider et al. 2012) on macroscopic images: snout-vent length, measured from the tip of snout to vent (SVL); tail length measured from vent to tip of tail (TL). In addition, we collected the following

pholidotic variables: number of preoculars (PreO); number of postoculars (PostO); number of temporal scales (TS); number of post-temporal scales (PTS); number of loreal scales (LS); number of ventrals (VS); number of subcaudal scales (SCS); number of upper labial scales (UL); number of lower labial scales (LL); number of lower labials in contact with anterior inframaxillar (InfLC). Lastly, we also report the shape of internasal scales (IntN; whether it was triangular or trapezoidal), and whether they were separated by the rostral scale (IntNsep).

Original photographs of all specimens in high resolution have been uploaded to the Morphobank database (https://morphobank.org/; Project no. 5111) where they are publicly available for download.

Sex determination

We used molecular markers located on the gametologous genes (i.e., homologous genes located in non–recombining regions of sex chromosomes) to determine the sex of the specimens, following the method of Laopichienpong et al. (2017). Colubrids have a female heterogametic ZZ/ZW sex-determination system (Bull 1980), with males being identified by the presence of a single band on gel electrophoresis (i.e., the alleles have the same length on the Z chromosomes), whereas females have two bands (i.e., the allele on the W sex chromosome is shorter than that on the Z chromosome; Laopichienpong et al. 2017). We amplified the gametologous gene CTNNB1 using the primers Eq–CTNNB1–11–F1 and Eq–CTNNB1–13–R (Matsubara et al. 2016; Laopichienpong et al. 2017) and following the PCR conditions reported by Laopichienpong et al. (2017).

Molecular analyses

DNA extraction, PCR, and sequence analysis

Genomic DNA was extracted from the ethanol–preserved tissue samples using the Tissue Genomic DNA Mini Kit (Geneaid, Taiwan) or the DNeasy® Blood & Tissue Kit (Qiagen, Germany). We PCR–amplified up to seven genetic markers, three mitochondrial (mtDNA): ribosomal 12S rRNA (*12S*) and 16S rRNA (*16S*), cytochrome b (*cytb*); and four nuclear (nDNA), the oocyte maturation factor MOS (*cmos*), the melanocortin 1 receptor (*MC1R*), the neurotrophin–3 (*NT3*), and the recombination activation gene 1 (*RAG1*). We used the same primers and PCR conditions as described in detail in Šmíd et al. (2015, 2021), Tamar et al. (2016), and Jablonski et al. (2019). The PCR products were then visualised on electrophoresis in 2% agarose gel, subsequently purified using EXOSAP–IT® PCR Product Cleanup Reagent (Thermo Fisher Scientific, USA) and bidirectionally Sanger–sequenced in Macrogen (the Netherlands) and at the Centre for Molecular Analyses (BIOPOLIS/CIBIO).

Apart from generating sequences for the newly obtained material, we generated an additional 27 new sequences for 11 samples from the studies by Šmíd et al. (2015) and Tamar et al. (2016). We retrieved all available sequences for *Rhynchocalamus* species from GenBank originating from the two above studies and Avcı et al. (2015), Fathinia et al. (2017), and Tamar et al. (2020). *Lytorhynchus diadema* was used as an outgroup. Geneious R11 (Kearse et al. 2012) was used to inspect raw sequence files, assemble contigs, generate consensus sequences, and concatenate alignments. Heterozygous positions in the nuclear markers were identified by the Heterozygous Plugin, checked by eye, and coded according to the IUPAC ambiguity codes.

Sequences of each genetic marker were aligned separately using MAFFT online service (Katoh et al. 2019). The Q–INS–i strategy that considers the secondary structure of the RNA was applied for the *12S* and *16S* gene fragments, while the sequences of the remaining genetic markers were aligned using default settings. Finally, the sequences of protein-coding genes were translated into amino acids using appropriate genetic codes and no stop codons were detected, indicating that no pseudogenes were amplified.

Phylogenetic analyses and nuclear networks reconstruction

We conducted Maximum Likelihood (ML) and Bayesian inference (BI) phylogenetic analyses applying a partition scheme by gene. The ML analysis was carried out in IQ–TREE (Nguyen et al. 2015) using its online web interface W–IQ–TREE (Trifinopoulos et al. 2016). The best substitution model for each gene was selected automatically by ModelFinder (Kalyaanamoorthy et al. 2017) as implemented in IQ–TREE. Branch support was assessed by the Shimodaira–Hasegawa–like approximate likelihood ratio test (SH–aLRT; Guindon et al. 2010) and the Ultrafast bootstrap approximation algorithm (UFBoot; Minh et al. 2013), both with 1000 replicates.

We also carried out a Bayesian inference using MrBayes v.3.2.1 (Ronquist et al. 2012) with the same partitioning strategy as for the ML analysis. The best-fit substitution models were selected using PartitionFinder v.2.1.1 (Lanfear et al. 2017) with the following parameters: branch lengths linked; MrBayes models; AICc model selection; and each gene representing a separate partition specified as a user scheme search. The BI was set to run through the CIPRES Science Gateway (Miller et al. 2010) in three independent runs, each for 10 million generations with parameters and trees sampled every 10,000 generations. All parameters (statefreq, revmat, shape, and pinvar) were unlinked for the partitions. After inspecting that the runs had converged, we discarded as burn-in 25% of posterior trees from each run. A 50% majority-rule consensus tree was then produced from all post-burnin posterior trees. Stationarity was determined by examining the standard deviation of the split frequencies between the three runs (being lower than 0.01), the Potential

Scale Reduction Factor diagnostic (PSRF approaching 1.0), and by confirming that all parameters had reached stationarity and had sufficient effective sample sizes (ESS >200) using Tracer v.1.7.2 (Rambaut et al. 2018).

To inspect genealogical relationships and the level of nuclear allele sharing among the *Rhynchocalamus* species, we reconstructed haplotype networks for the four nuclear loci. To resolve the heterozygous single nucleotide polymorphisms, the alignments of the four nuclear loci were phased separately using the PHASE algorithm (Stephens et al. 2001) as implemented in DnaSP v.6 (Rozas et al. 2017) with the probability threshold set to 0.7. The outgroup was excluded from the alignment for this analysis. Haplotype networks were constructed from the phased alignments using the TCS algorithm (Templeton et al. 1992; Clement et al. 2000) implemented in PopART (Leigh and Bryant 2015). Inter- and intraspecific uncorrected *p*-distances with pairwise deletion were calculated for *12S*, *16S*, and *cytb* in MEGA v11 (Tamura et al. 2021).

Species distribution models

The extent of the study area ranged from the northwesternmost tip of the Sinai Peninsula to the northernmost tip of Israel, Jordan, and Kuwait, including the whole of the Arabian Peninsula. To describe the climatic conditions of the study area, we obtained 19 bioclimatic variables from Worldclim2 (Fick and Hijmans 2017), with a ~1 km^2 resolution. Furthermore, we included the soil type (FAO; http://www.fao.org/), and the following topographic variables: altitude (meters), slope (degrees), Topographic Position Index (TPI; i.e., the difference between the elevation of a cell and the eight neighbouring cells), and degree of exposure to the east and the north (hereafter referred to as eastness and northness), with values ranging from –1 to 1 (i.e, complete exposure). Eastness and northness were obtained by computing cosine and sine transformations of the angular direction of the raster cell to the geographical east and north, respectively. We used the function "get_elev_raster" (package elevatr; Hollister et al. 2023) to extract the Digital Elevation Model (approx. 150 m resolution) of the study area, and the function "terrain" (package raster; Hijmans et al. 2021) to compute the other topographical variables. We assessed multicollinearity among variables by performing a Variance Inflation Factor analysis using the function "vif" (package usdm; Naimi et al. 2014) and retained the variables with vif values < 10 (Curto and Pinto 2011; Dormann et al. 2013). As a result, the bioclimatic variables included in the models were the mean diurnal range of temperatures (BIO2), isothermality (BIO3), mean temperature of the wettest and driest quarter (BIO8 and BIO9, respectively), precipitation of the wettest and driest month (BIO13 and BIO14, respectively), precipitation seasonality (coefficient of variation; BIO15), and precipitation of warmest and coldest quarter (BIO18 and BIO19, respectively). All variables were scaled to ~1 km^2 resolution.

We built and evaluated our Species Distribution Models (SDMs) using the sdm package (Naimi and Araújo 2016) in R environment (R vers. 4.3.2; R Core Team 2024), using three different modelling techniques: Generalized Linear Models (GLMs), Random Forests (RFs), and Maximum Entropy Models (Maxent), as they are considered the best-performing ones (Kaky et al. 2020; Ancillotto and Labadessa 2023). To run the presence–background SDMs, we randomly generated 10,000 background points selected within the study area. For each technique, we performed 10 replicates. We performed an ensemble forecasting approach, weighting models based on their AUC scores, which allows reducing the uncertainty of predictions by single model algorithms (Watling et al. 2015). We used 30% of randomly selected occurrence data for model performance testing and 70% for model training. Model performance was assessed by inspecting the values of the area under the receiver operating characteristic curve (AUC), True Skill Statistics (TSS) (Araújo and New 2007), and the continuous Boyce Index (Boyce et al. 2002; Hirzel et al. 2006), which was computed using the "ecospat.boyce" function of the R package ecospat (Broennimann et al. 2023). We assessed the effect of each environmental predictor on the probability of occurrence of the new *Rhynchocalamus* species by inspecting the response curves and estimated each variable's relative importance by using the "getVarImp" function in the sdm package (Naimi and Araújo 2016). Lastly, we binarised the model predictions by using as thresholds the lowest predicted suitability value among the occurrence points of the species.

Evaluation of conservation status

We used GeoCAT (Bachman et al. 2011; at https://geocat.kew.org) and all the distributional records of the new species (see Suppl. material 1) to compute the Extent of Occurrence (EOO) and the Area of Occupancy (AOO; 2–km grid cell width), two metrics related to the geographic range used in the process of evaluating the threat category of a species by the International Union for Conservation of Nature (IUCN). Lastly, we propose an evaluation of the conservation status of the new taxon following the IUCN Red List guidelines (IUCN SSC Standards and Petitions Committee 2022).

Results

Phylogenetic analyses

The final concatenated alignment of the three mtDNA and four nDNA genetic markers included 48 samples and 172 sequences. The total length was 4,823 base pairs (bp; 625 bp of *12S*, 512 bp of *16S*, 1092 bp of *cytb*, 408 bp of *cmos*, 665 bp of *MC1R*, 486 bp of *NT3*, and 1035 bp of *RAG1*).

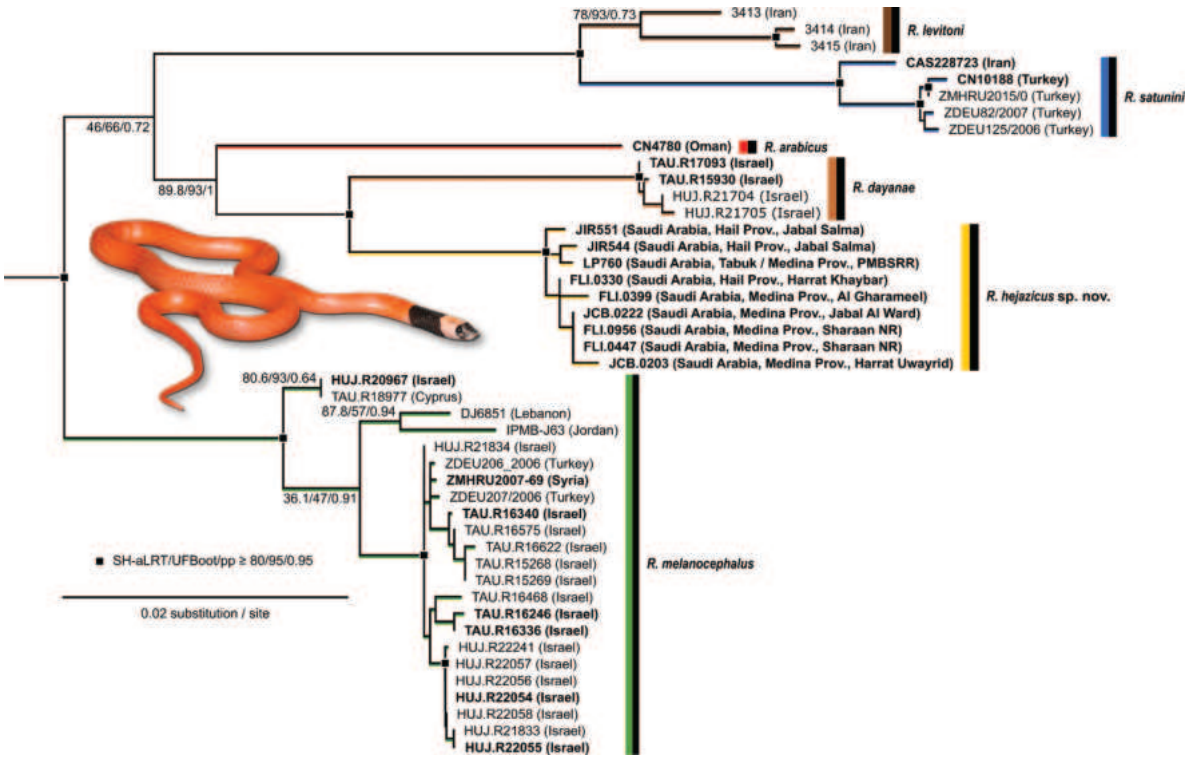

Figure 1. Maximum Likelihood phylogenetic tree reconstructed from the concatenated dataset of *12S*, *16S*, *cytb*, *cmos*, *MC1R*, *NT3*, and *RAG1* genes (4,823 bp). The tree was rooted using *Lytorhynchus diadema* (not shown in the figure). Support values are indicated by the black squares (SH-aLRT/UFBoot/pp ≥ 80/95/0.95) or by exact values near nodes. Samples for which new genetic data were generated are highlighted in bold. Complete trees with original ML and BI support values are provided as Suppl. material 1: figs S1, S2, respectively. The specimen depicted is the individual NMP 76815 (sample code LP760) from the PMBSRR, Tabuk / Medina Province, Saudi Arabia.

Both ML and BI phylogenetic analyses resulted in almost identical topologies (Fig. 1). The clade of all six *Rhynchocalamus* species was strongly supported (SH-aLRT = 100/UFBoot = 100/pp = 1, support values are given in this order hereafter), as well as all the species within the genus. *Rhynchocalamus melanocephalus* was recovered to be sister to the remaining species of the genus but with poor support (46/66/0.72). *Rhynchocalamus levitoni* and *R. satunini* formed a clade (100/100/1). *Rhynchocalamus arabicus* was recovered to be a sister species to *R. dayanae* and the new species described herein (89.8/93/1), which were supported as sister species (99.9/100/1). The deeper relationships of the *Rhynchocalamus* phylogeny, however, remained unresolved (Figs 1, 2).

The reconstructed haplotype networks (Fig. 2) showed a certain degree of allele sharing in three out of four nuclear loci. The new species of *Rhynchocalamus* had private alleles (i.e., not shared with other species) only in *RAG1*, which is also the only gene free of allele sharing among all the *Rhynchocalamus* species. The new species shared alleles with its sister species *R. dayanae* in *MC1R* and *NT3*. Additionally, the new species shared alleles with *R. arabicus*, *R. melanocephalus*, and *R. satunini* in *cmos*, indicating signs of incomplete lineage sorting rather than ongoing gene flow among, to our current knowledge, largely allopatric species.

Inter- and intraspecific uncorrected *p*-distances for all three mtDNA genes are summarised in Table 2.

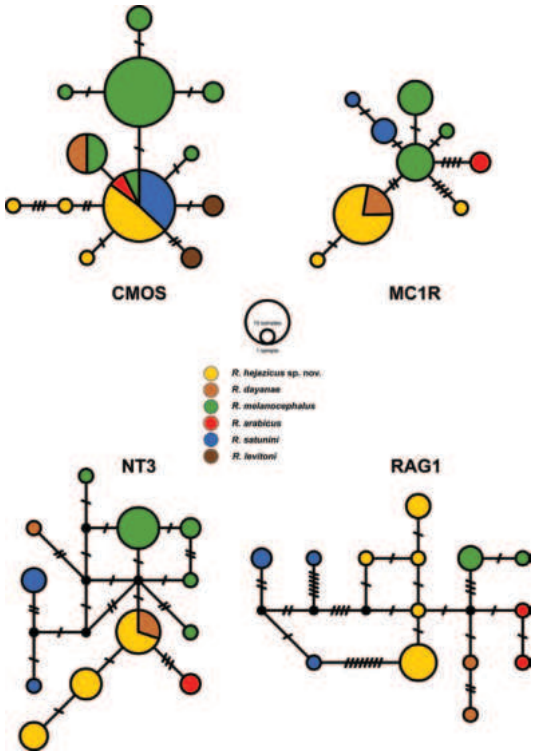

Figure 2. Haplotype networks of the four nDNA genes (*cmos*, *MC1R*, *NT3*, and *RAG1*). Circle sizes are proportional to the number of samples that share that allele. Short transverse bars on the connecting lines indicate the number of mutational steps between alleles.

Taxonomic implications

The results of the phylogenetic analyses, as well as the morphological comparison, indicate that the unknown species of *Rhynchocalamus* from Saudi Arabia represents a new distinct species in need of formal taxonomic recognition provided here:

Rhynchocalamus hejazicus sp. nov.

https://zoobank.org/2742A9E2-DE67-4C02-ABA5-9F284E009747

Type material. ***Holotype.*** RCU-URN-93850 (sample code FLI447; Fig. 3; Table 1). Adult male; Kingdom of Saudi Arabia, Medina Province, Shaaran Nature Reserve (26.85895°N, 38.30387°E), 1035 m asl.; collected by Fulvio Licata on May 24, 2023. MorphoBank accessions: M902248–M902255.

Paratypes. RCU-URN-94064 (sample code FLI330; Fig. 3; Table 1), melanistic adult female collected by Fulvio Licata and Leili Khalatbari on May 11, 2023, KSA, Medina Province, Harrat Khaybar (25.60676°N, 39.96734°E), elevation 1616 m asl, MorphoBank accessions: M902243–M902247; RCU-URN-94065 (sample code JCB222), juvenile male collected by José Carlos Brito on November 2, 2023, KSA, Medina Province, Jabal Al Ward (26.36263°N, 37.38780°E), elevation 1277 m asl, MorphoBank accessions: M902256–M902261; NMP 76815 (sample code LP760; Fig. 4; Table 1), juvenile male collected by Damien M. Egan and Lukáš Pola on April 22, 2022, KSA, Tabuk / Medina Provinces, Prince Mohammed bin Salman Royal Reserve, 26 km east of Al Qurr village (26.6028142°N, 37.1225145°E), elevation 781 m asl, MorphoBank accessions: M902293–M902338; NMP 76816 (sample code JIR551), adult, sex undetermined, collected by Ahmed Mohajja AlShammari and Mubarak Al–Aslami in July 2021, KSA, Hail Province, Jabal Salma, south of An Niayy village (27.165278°N, 42.294444°E), elevation 1052 m asl, MorphoBank accessions: M902290–M902292; MNHN–RA–2023.0013 (sample code JIR544; Fig. 4; Table 1) adult female collected by Adel A. Ibrahim and Ahmed Mohajja AlShammari on May 11, 2017, KSA, Hail Province, Jabal Salma, Wadi Al–Azraq, east of Zekheen village (26.948889°N, 41.973889°E), elevation 1099 m asl, MorphoBank accessions: M902262–M902289.

Other material. Additional unvouchered individuals, assigned to this species based on phenotypical resemblance and unique head pattern, were encountered in May, June, and November 2023 by Vidak Lakušić, Gholam Hosein Yusefi, and Fulvio Licata in Harrat Uwayrid, Al-Gharameel, Wadi Nakhlah, and Sharaan (conservation areas located in the AlUla County, Medina Province). Other individuals were observed in July and August 2023 by Neil

Table 1. Measurements (in mm) of the type series of *Rhynchocalamus hejazicus* sp. nov. For abbreviations see the Methods section.

Voucher code	*RCU-URN-93850*	*MNHN-RA-2023.0013*	*NMP 76815*	*RCU-URN-94065*	*RCU-URN-94064*
Sample Code	FLI447	JIR544	LP760	JCB222	FLI330
Type status	Holotype	Paratype	Paratype	Paratype	Paratype
Sex	Male	Female	Male	Male	Female
SVL	321.11	339.51	214	166.18	226.48
TL	63.60	64.24	45.50	38.32	–
PreO	1/1	1/1	1/1	1/1	1/1
PostO	2/2	1/1	1/1	2/2	1/1
TS	1/1	1/1	1/1	1/1	1/1
PTS	1/0	1/1	2/1	1/1	1/1
LS	1/1	1/1	1/1	1/1	1/1
VS	247	250	228	227	240
SCS	67	70	68	70	–
UL	6/6	6/6	6/6	6/6	6/6
LL	8/8	8/8	8/8	8/8	8/8
InfLC	4	4	4	4	3
IntN	Triangle	Trapezoid	Trapezoid	Trapezoid	Triangle
intNsep	Yes	No	No	No	No

Table 2. Mean genetic distances (uncorrected p-distances) between the *Rhynchocalamus* species based on the *12S* and *16S* (below the diagonal), and *cytb* (above the diagonal). Intraspecific distances are shown on the diagonal in bold for *12S*, *16S*, and *cytb*, respectively.

	R. arabicus	*R. dayanae*	*R. melanocephalus*	*R. satunini*	*R. hejazicus* sp. nov.	*R. levitoni*
R. arabicus	NA	10%	10.5%	12.9%	9.5%	9.9%
R. dayanae	5.9 / 4.2%	0.1 / 0.3 / 0.5%	10.1%	11.9%	9.5%	9.8%
R. melanocephalus	7.3 / 3.9%	6.7 / 4%	0.6 / 0.5 / 1.6%	12.9%	10.3%	11.6%
R. satunini	8.9 / 4.6%	7.4 / 5.3%	9 / 3.7%	1.3 / 0.4 / 1.5%	12.3%	7.6%
***R. hejazicus* sp. nov.**	6.1 / 3.7%	3.8 / 3.1%	5.7 / 3.8%	5.5 / 5.1%	0.2 / 0.2 / 0.7%	11.1%
R. levitoni	NA	NA	NA	NA	NA	NA / NA / 2.7%

Rowntree and Euan Ferguson in NEOM, the northwestern region of Tabuk Province, KSA. One record was found in the public database iNaturalist (https://www.inaturalist.org/observations/20014261). Based on the provided information, the snake was recorded on February 1, 2019 at As Salam, Medina Province (24.464058°N, 39.537669°E). An additional individual was reported to us by Muteb Masad Al–Malki from the vicinity of Adham city (20.4486525°N, 40.8792636°E) from Mecca Province.

Etymology. The species name is a latinized noun in masculine gender derived from the word *"Hejaz–"* = Hejaz Mountains, a mountain range located in the Hejaz re-

Figure 3. Holotype (RCU-URN-93850, sample code FLI447, bottom left) and paratype (RCU-URN-94064, sample code FLI330, bottom right) specimens in life. Lateral and ventral views of their heads (above each life picture). Photo credit: FL.

Figure 4. Colour variation within *R. hejazicus* sp. nov. (or its lack, thereof). Top row: two unvouchered specimens from NEOM, Tabuk Province, KSA (photo credit: Euan Ferguson and Neil Rowntree); bottom left: paratype NMP 76815 (sample code LP760, photo credit: DME); bottom right: paratype MNHN–RA–2023.0013 (sample code JIR544, photo credit: AAI).

gion (an important region located in western Saudi Arabia, where the two holy cities of Islam, Mecca, and Medina are located) where most individuals were observed, and the Latin suffix *"–icus"* = "belonging to". We suggest the common name "Hejaz black–collared snake" in English and أبو حناء [Abu Henna] in Arabic for the new species.

Diagnosis. The new species of *Rhynchocalamus* from the Hejaz Mountain range in western Saudi Arabia is characterised by the following morphological characters: (1) SVL 209.2–339.5 mm in adults; (2) tail length 38.3–64.2 mm in adults; (3) loreal scale present; (4) large 3rd and 4th upper labial scales in contact with the eye; (5) one preocular scale; (6) 1–2 postocular scales; (7) one temporal scale; (8) 0–2 post–temporal scales; (9) six upper labial scales; (10) eight lower labial scales; (11) usually four lower labial scales in contact with the anterior inframaxillars; (12) usually one gular scale in contact with anterior inframaxillars, situated between the posterior inframaxillars; (13) 15 smooth dorsal scales at mid-body; (14) 11–12 dorsal and temporal scales surrounding the margin of parietals; (15) 227–250 ventrals; (16) anal and subcaudal scales divided; (17) 67–70 subcaudal scales; (18) dorsal colouration in life deep reddish with a distinctive black collar extending behind the parietal scales and abruptly stopping or tapering backward in the middle, and a pale reddish band passing behind the eyes, through the middle of the supraoculars and the frontal scale, encompassing the temporal and parietal scales.

Colouration in life (adults). The upper surface of the head is shiny black from the middle of the supraoculars and the frontal scale to the tip of the snout, which is whitish; a wide band, pale reddish dorsally and fading to whitish ventrally, passes behind the eyes, through the middle of the supraoculars and the frontal scale, encompassing the temporal and parietal scales; a black collar around the neck reaches the ventrals, and abruptly stops or tapers dorsally towards the centre; dorsal surface of the body and tail uniformly deep reddish from the end of the collar to the tail tip; ventral surface of the body deep reddish fading to whitish in the upper part of the body, narrowing in correspondence of the black collar; colour pattern paler in alcohol preserved specimen. A melanistic morph, uniformly black, also occurs.

Comparison. *Rhynchocalamus hejazicus* sp. nov. is morphologically similar to the other *Rhynchocalamus* species, and it can be distinguished by slight differences in size, colouration, and head and body scalation.

In comparison with *R. arabicus*, *R. hejazicus* sp. nov. has a lower number of subcaudal scales (67–70 vs. 71–81 in *R. arabicus*). We show that a melanistic morph of *R. hejazicus* sp. nov. also occurs, therefore the new species can be easily misidentified as *R. arabicus*.

Rhynchocalamus hejazicus sp. nov. differs from *R. dayanae* by smaller maximum body size (339.5 vs. 432.1 in *R. dayanae*), a shorter tail (38.3–64.2 vs. 59.2–94.1 in *R. dayanae*), by a higher number of ventrals (227–250 vs. 198–229 in *R. dayanae*) and subcaudals (67–70 vs. 54–62 in *R. dayanae*), Lastly, *R. hejazicus* sp. nov. can be further differentiated from *R. dayanae* by the presence of a pale reddish band passing between the eyes and the neck.

Rhynchocalamus hejazicus sp. nov. differs from *R. melanocephalus* (both Southern population from the Negev region in Israel and Northern population from the Mediterranean ecoregion; *sensu* Tamar et al. 2020) by a smaller maximum body size (339.5 vs. 499.2 in *R. melanocephalus*), a lower number of post-temporal scales (1 vs 2 in *R. melanocephalus*), a higher number of lower labial scales (8 vs. 7 in *R. melanocephalus*), a higher number of ventrals (227–250 vs. 164–235 in *R. melanocephalus*), and subcaudals (67–70 vs. 29–69 in *R. melanocephalus*). Lastly, *R. hejazicus* sp. nov. can be further differentiated from *R. melanocephalus* by a pale reddish band between the eyes and the neck.

Rhynchocalamus hejazicus sp. nov. differs from *R. satunini* in having a longer tail (64.2 vs. 54 mm in *R. satunini*), a higher number of ventrals (227–250 vs. 201–226 in *R. satunini*) and subcaudals (67–70 vs. 53–64 in *R. satunini*), and a lower number of upper labials (6 vs. 7 in *R. satunini*). Lastly, *R. satunini* is characterised by two black patches on a pale reddish/whitish background on the prefrontals and the parietals, and a black band around the neck that does not reach the ventrals.

In comparison with *R. levitoni*, *R. hejazicus* sp. nov. has a lower number of upper labials (6 vs. 7 in *R. levitoni*), and it can be distinguished by the overall different colouration (deep reddish vs. lemon yellow in *R. levitoni*), and the absence of a V-shaped band on the neck, and dark markings on the parietals.

Description of the holotype. Adult male (voucher code RCU-URN-93850) (Fig. 3). Snout-vent length 321.1 mm, tail length 63.6 mm. Body cylindrical and slender. The head is small and relatively narrow, slightly distinct from the neck. Head scales not keeled. Rostral scale elongated, extending backwards and wedged between the internasals, which are separated, and touching the bottom of the suture between the prefrontals. The rostral is bordered by two upper labials, two nasals, two internasals, and two prefrontals. Nostrils are situated on undivided nasal scales internasals of triangular shape, separated by the rostral scale. A trapezoid loreal scale at either side in contact with the 2nd and 3rd upper labials. The eyes are small, with circular pupils. One preocular scale on both sides. Two postocular scales on both sides. Bell-shaped frontal scale, located between the supraoculars and wedged between the parietals. Six squarish upper labials, the 3rd and 4th in contact with the eye. two large parietal scales; one temporal and one post–temporal scale on the left side, while on the right side, only one enlarged temporal is present. Eight lower labials. Four lower labials are in contact with anterior inframaxillars on each side. Two gular scales are positioned between the posterior inframaxillars and in connection with the anterior inframaxillars. Anterior inframaxillars are almost double in size than posterior inframaxillars. Eleven dorsal and temporal scales surround the posterior margin of the parietals. Fifteen dorsal scale rows at mid-body. 247 ventrals and 67 subcaudals, including a conical scale at the tail tip.

Known and potential distribution and habitat. The known extent of occurrence (EOO) of *R. hejazicus* sp. nov. is more than 274,674 km^2 and the area of occurrence (AOO) is 56 km^2. The individual reported from the vicinity of Adham city (20.4486525°N, 40.8792636°E) from Mecca Province represents the southernmost record to our knowledge.

Available material and photographic records suggest that the species is scattered across Tabuk, Medina, Hail and Mecca Provinces, and is likely endemic to KSA. Nevertheless, it should be noted that additional range extensions of many overlooked species are now being reported with each herpetofaunal survey carried out in the unexplored regions of northwestern and western KSA (e.g., Aloufi et al. 2020, 2021, 2022; Pola et al. 2024), suggesting that the range of this rather secretive species could be even wider. Currently, the northwesternmost individual is reported from the area west of Jabal Al Lawz, approx. 70 km south of the Jordanian border. Given the presence of similar habitats harbouring many shared species, we cannot rule out the species occurrence in that area, especially in the mountains of Aqaba.

Rhynchocalamus hejazicus sp. nov. has been observed between 456 and 1610 m a.s.l., in the following habitats: (i) sandy flatland with sparse vegetation (*Acacia* sp., bushes, and tussock grasses; Fig. 5); (ii) large, stony wadis in lava fields (=harrat) with dense patches of woody vegetation (*Acacia* sp.; Fig. 5); (iii) sparsely vegetated rocky creek with temporary pools.

The species distribution models achieved good performance levels (AUC: 0.9–0.94; TSS: 0.78–0.87; Boyce Index: 0.42–0.99), resulting in an overall good predictive accuracy of the final ensemble models (Boyce index: 0.71). The potential distribution of *R. hejazicus* sp. nov. mostly includes the known range of the species, but other extralimital suitable areas are identified to the northwest (i.e., the Sinai Mountains in South Sinai, Aqaba mountains, and Wadi Rum in Jordan), and to the north (i.e., Jabal Tubaiq hills at the border with Jordan and Upper Galilee mountains in North Israel; Fig. 6). The main drivers of environmental suitability in our models were the altitude (26.7% of explained variance) and the mean temperature of the wettest quarter (BIO8; 15.6%), suggesting that *R. hejazicus* sp. nov. is associated with altitudes above 1,000 m a.s.l., in regions characterised by cold wet months (<20 °C). Furthermore, the precipitation of the warmest quarter (BIO18; 13.5%) and the precipitation seasonality (BIO15; 13%) were also related to the probability of occurrence of the species, indicating that the species is likely to occur in areas with relatively dry hot months (precipitations < 50 mm) and stable rainfall regimes.

Natural history. Little is known about the species' natural history and behaviour. Although the current number of observations is limited, it appears that *R. hejazicus* sp. nov. has mainly nocturnal activity as all individuals were encountered active at night. We assume that in many biological aspects, it will be concordant with its

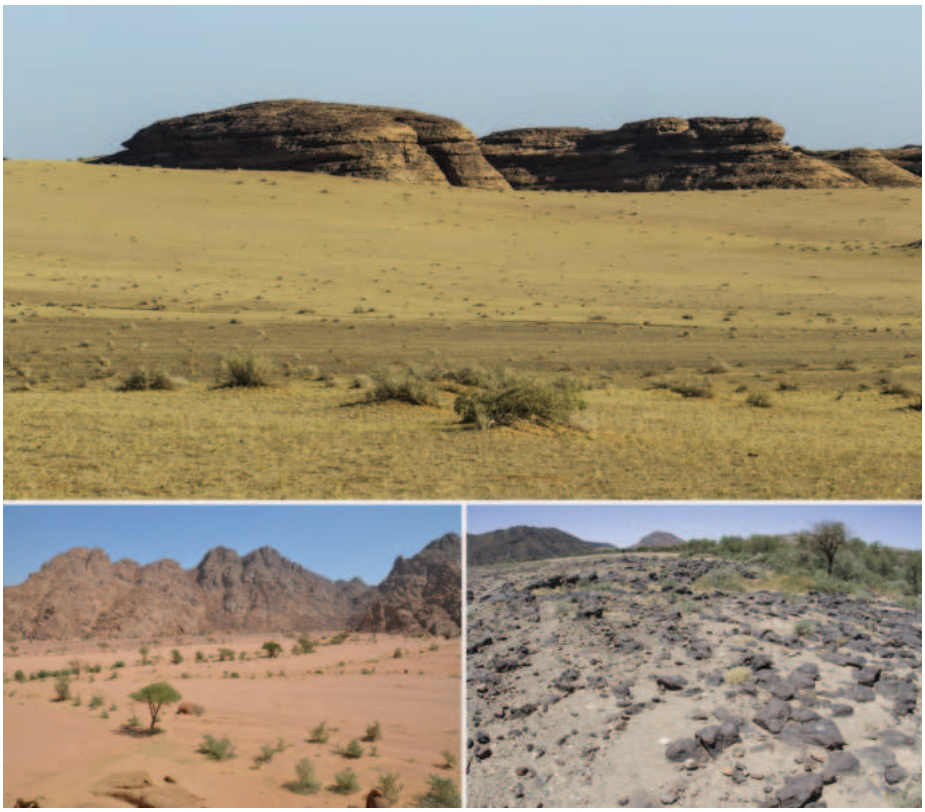

Figure 5. Habitats of the holotype and two paratype specimens of *R. hejazicus* sp. nov. Top: locality of the holotype RCU-URN-93850 at the Shaaran NR, AlUla County, Medina Province, KSA (photo credit: FL); bottom left: habitat of the paratype MNHN–RA–2023.0013 at Wadi Al-Azraq, Jabal Salma, Hail Province, KSA (photo credit: AAI); bottom right: habitat of the paratype RCU-URN-94065 the Harrat Khaybar, Hail Province, KSA (photo credit: FL).

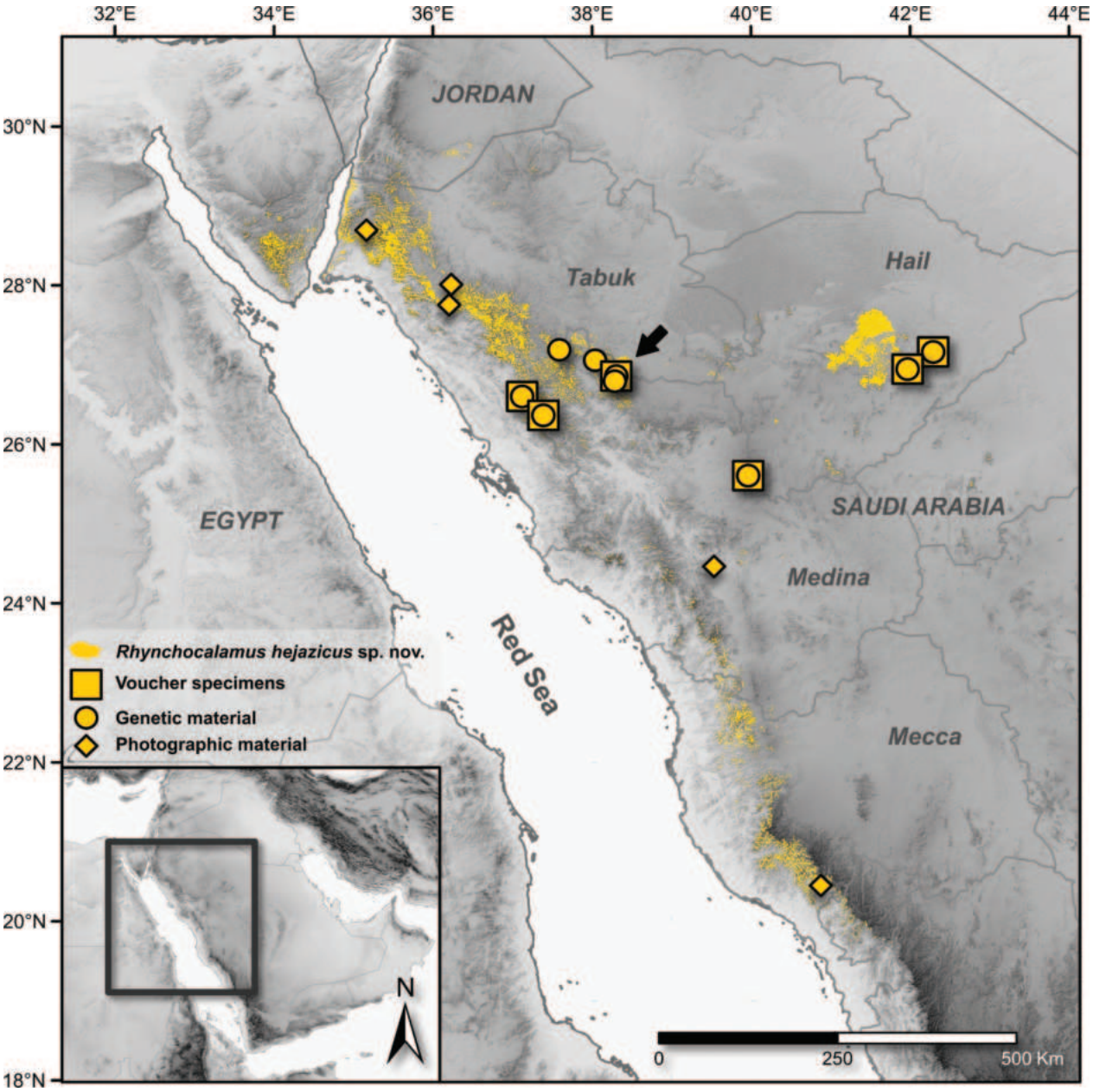

Figure 6. Distribution of *Rhynchocalamus hejazicus* sp. nov. showing the location of the material examined in this study. Circles indicate samples used for the genetic analyses, squares indicate examined voucher specimens, and diamonds indicate photographic records. The black arrow denotes the type locality (Shaaran NR in AlUla County, Medina Province). Geographical sampling is overlaid by the predicted species distribution model categorised into binary predictions of the suitable areas. The threshold used for the categorisation was the lowest predicted suitability value among the occurrence points (= 0.05).

congeners (Amr and Disi 2011; Tamar et al. 2016; Torki 2017; Fathinia et al. 2017).

Other reptile species observed in syntopy of the NMP 76815 (LP760) were *Ptyodactylus* cf. *hasselquistii* (Phyllodactylidae), *Pristurus guweirensis* (Sphaerodactylidae), and *Echis coloratus* (Viperidae). In Hail Province, at Jabal Salma range, *Echis coloratus*, *Cerastes gasperettii* (Viperidae) and *Walterinnesia aegyptia* (Elapidae) were found in sympatry (Alshammari and Ibrahim 2015; Alshammari et al. 2017). In AlUla County, it was found in sympatry with *Ptyodactylus guttatus* (in prep.), *Ptyodactylus* cf. *hasselquistii*, *Bunopus tuberculatus*, *Hemidactylus granosus*, *Stenodactylus doriae*, *Stenodactylus slevini*, *Tropiocolotes yomtovi* (the latter five all Gekkonidae), and *Echis coloratus*.

Conservation status. We propose to classify *R. hejazicus* sp. nov. as Least Concern, based on the wide EOO, and the diverse and continuous habitats where the species is encountered, including habitats with heavy anthropogenic disturbance (e.g., overgrazing) and urban habitats (see https://www.inaturalist.org/observations/20014261). Although *R. hejazicus* sp. nov. is at the moment known from 14 localities and its AOO is only 56 km^2, we consider it premature to classify it as Near

Threatened as the limited number of localities could reflect the generally undersampled distribution and secretive habits of the species. Furthermore, six of the known localities occur within conservation areas located in Al-Ula County (Medina Province), where protection measures have been implemented.

Discussion

We describe a new species of the genus *Rhynchocalamus* based on phylogenetic and morphological analyses. The meristic and morphometric traits of *R. hejazicus* sp. nov. are largely similar to the other species of *Rhynchocalamus*, from which, however, the new species can be distinguished for its unique colouration. The phylogenetic analyses show that the new *Rhynchocalamus* species is sister to *R. dayanae* from south Israel and closely related to *R. arabicus* from Yemen and Oman. The presence of this species in western Saudi Arabia fills a large biogeographic gap between northerly and southerly distributed *Rhynchocalamus* sister taxa, highlighting the potential relevance of mountainous areas as biogeographic corridors for the spread of this genus in the Arabian Peninsula. Previous phylogenetic studies were unable to resolve deep relationships within the genus due to low support of the deepest nodes (Šmíd et al. 2015; Tamar et al. 2016; Fathinia et al. 2017). Despite the additional three nuclear genes included here in the phylogenetic dataset, the deep relationships within the genus remained unresolved in our analyses, preventing clear conclusions on the relationships between the clades within the genus as well as its biogeographic history. This may be caused by a high degree of allele sharing in most of the nuclear markers analysed, and only genome-wide data (e.g., SNPs) will likely be able to fully resolve the phylogeny of *Rhynchocalamus*.

The distribution modelling identified potentially suitable extralimital areas north and northwest of the known distribution range of the new *Rhynchocalamus* species. It is unlikely that the species occurs in the well-sampled Upper Galilee mountains in north Israel, where the congeneric *R. melanocephalus* instead occurs (Tamar et al. 2016; Werner 2016). The distribution models may overpredict species' distributions, especially if there is a lack of *a priori* knowledge of species interactions and dispersal abilities, which are difficult to take into account in the modelling procedure (Briscoe et al. 2019; Velazco et al. 2020). Conversely, our models might also have underpredicted suitable areas for the species, as they did not include fine-scale habitat and soil variables which could represent important determinants of distribution in fossorial snakes (e.g., Wagner et al. 2014).

We report a melanistic morph of the new species (Fig. 3). Melanism may have a significant adaptive role in ectotherms, having, among others, thermoregulatory and antipredatory functions (Trullas et al. 2007). In desert animals, melanism is found to have aposematic effects, except for habitats with dark substrates such as black sands or lava fields, where it has cryptic functions (Cloudsley-Thompson 1979). The melanistic individual of *R. hejazicus* sp. nov. was found in Harrat Khaybar, a lava field located north of Medina (Fig. 5), where melanism might have been positively selected for antipredatory, cryptic functions. This represents an exceptional finding, but it might not be uncommon, taking into account the limited number of observations of this species and the elusiveness of these snakes. Melanism could have a deeper role in the evolution of the genus, as suggested by the southerly distributed, melanistic *R. arabicus*.

Although a recent boost in herpetological surveys is rapidly contributing to filling up knowledge gaps in reptile diversity in KSA (e.g., Aloufi et al. 2020, 2021, 2022), still vast areas remain unexplored and secretive, potentially widespread species can be expected to occur. *Rhynchocalamus hejazicus* sp. nov. is the sixth species of *Rhynchocalamus* snakes and yet is not the lesser-known, having more occurrence records and a larger distribution range than most congeneric species.

The description of *R. hejazicus* sp. nov. benefited from previous taxonomic and biogeographical insights into the genus (Tamar et al. 2016). However, the detection of secretive species in underexplored areas, such as the Hejaz region, primarily stems from rigorous sampling efforts. This emphasises the significance of developing efficient monitoring strategies aimed at comprehensively documenting species diversity in uncharted territories. Such efforts are crucial for advancing our knowledge of ecosystems and community functions and thus bolstering global conservation efforts.

Author contributions

FL, LP, JŠ, JCB, and DGV conceived the ideas and designed the methodology; FL, LP, DME, and JCB collected the data; AMA, SB, AAI, DGV, AVL, BS, PL, and JCB contributed to the field sampling; FL, LP, AVL, and BS analysed the data; FL and LP led the writing of the manuscript. JŠ, JCB, PL, and AA contributed critically to the draft. All authors have read critically the draft and gave final approval for publication.

Funding

LP was supported by Charles University grant no. SVV260685/2023. JŠ was supported by the Czech Science Foundation (GACR, project number 22-12757S) and by the Ministry of Culture of the Czech Republic (DKRVO 2024–2028/6.I.a, 00023272). JCB and DVG were supported by FCT (CEECINST/00014/2018/CP1512/CT0001; 2020.03848.CEECIND). JCB, DVG, FL, BS, AVL were supported by the project Inventory of AlUla Fauna (PR6869) from RCU – The Royal Commission for AlUla.

Acknowledgements

We would like to thank Nicolas Vidal (MNHN, Paris, France) for providing the photos of the specimen under his care. LP and DME would like to thank Talal Assaf Al–Atawi for his company, and technical support during the fieldwork. The fieldwork of LP and DME was part of a project focused on biological inventory of the PMBSRR developed and funded by Prince Mohammed bin Salman Royal Reserve Development Authority. AMA would like to thank Mubark Alshammari for the company and technical support during the fieldwork. We would like to express our thanks to Neil Rowntree and Euan Ferguson (United Kingdom) for sharing their records from NEOM, the new region in northwestern Saudi Arabia, with us along with the photographs and the accompanying information, as well as to Muteb Masad Al–Malki (Saudi Arabia) for sharing the record from Mecca Province. We would like to thank Leili Khalatbari, Gholam Hosein Yusefi, and Vidak Lakušić for contributing to the finding of the animals and for sharing their records from the AlUla region, and Nina Séren for contributing to the genetic analyses. Acknowledgements extended to Alaaeldin I Soultan, Ingrid Stirnemann, and the Royal Commission for AlUla for their support in developing fieldwork in the AlUla region.

References

Alatawi AS, Gilbert F, Reader T (2020) Modelling terrestrial reptile species richness, distributions and habitat suitability in Saudi Arabia. Journal of Arid Environments 178: 104153. https://doi.org/10.1016/j.jaridenv.2020.104153

Aloufi A, Baker MAA, Amr ZS (2020) First record of the Variable Racer, *Platyceps variabilis* (Boulenger, 1905), for Saudi Arabia. Herpetology Notes 13: 973–975.

Aloufi AA, Amr ZS, Baker MA (2021) Reptiles and Amphibians of Al Madinah Al Munawwarah Province, Saudi Arabia. Russian Journal of Herpetology 28(3): 123–137. https://doi.org/10.30906/1026-2296-2021-28-3-123-137

Aloufi A, Amr Z, Baker MA (2022) Reptiles from 'Uruq Bani Ma'arid and Harat al Harrah protected areas in Saudi Arabia: Reptiles from two protected areas in Saudi Arabia. Herpetology Notes 15: 483–491.

Alshammari AM, Ibrahim AA (2015) Lizards and snakes in the historical Faid protected area (Faid Hema), Ha'il region, Saudi Arabia. Herpetological Conservation and Biology 10: 1021–1029.

Alshammari AM, Busais SM, Ibrahim AA (2017) Snakes in the Province of Ha'il, Kingdom of Saudi Arabia, including two new records. Herpetozoa (Wien) 30: 59–63.

Amr Z, Disi AM (2011) Systematics, distribution and ecology of the snakes of Jordan. Vertebrate Zoology 61(2): 179–266. https://doi.org/10.3897/vz.61.e31150

Ancillotto L, Labadessa R (2023) Can protected areas and habitats preserve the vulnerable predatory bush cricket Saga pedo? Journal of Insect Conservation 27(4): 615–624. https://doi.org/10.1007/s10841-023-00484-w

Araújo MB, New M (2007) Ensemble forecasting of species distributions. Trends in Ecology & Evolution 22(1): 42–47. https://doi.org/10.1016/j.tree.2006.09.010

Avcı A, Ilgaz Ç, Mahdi Rajabizadeh, Yılmaz C, Üzüm N, Adriaens D, Kumlutaş Y, Olgun K (2015) Molecular phylogeny and micro ct-scanning revealed extreme cryptic biodiversity in Kukri snake, *Muhtarophis* gen. nov., a new genus for *Rhynchocalamus barani* (Serpentes: Colubridae). Russian Journal of Herpetology 22: 159–174.

Bachman S, Moat J, Hill AW, de la Torre J, Scott B (2011) Supporting Red List threat assessments with GeoCAT: Geospatial conservation assessment tool. ZooKeys 150: 117–126. https://doi.org/10.3897/zookeys.150.2109

Boyce MS, Vernier PR, Nielsen SE, Schmiegelow FKA (2002) Evaluating resource selection functions. Ecological Modelling 157(2–3): 281–300. https://doi.org/10.1016/S0304-3800(02)00200-4

Briscoe NJ, Elith J, Salguero-Gómez R, Lahoz-Monfort JJ, Camac JS, Giljohann KM, Holden MH, Hradsky BA, Kearney MR, McMahon SM, Phillips BL, Regan TJ, Rhodes JR, Vesk PA, Wintle BA, Yen JDL, Guillera-Arroita G (2019) Forecasting species range dynamics with process-explicit models: Matching methods to applications. Ecology Letters 22(11): 1940–1956. https://doi.org/10.1111/ele.13348

Broennimann O, Cola VD, Petitpierre B, Breiner F, Scherrer D, D'Amen M, Randin C, Engler R, Hordijk W, Mod H, Pottier J, Febbraro MD, Pellissier L, Pio D, Mateo RG, Dubuis A, Maiorano L, Psomas A, Ndiribe C, Salamin N, Zimmermann N, Collart F, Smith T, Guisan A (2023) ecospat: Spatial Ecology Miscellaneous Methods. https://cran.r-project.org/web/packages/ecospat/index.html [April 2, 2024]

Bull JJ (1980) Sex Determination in Reptiles. The Quarterly Review of Biology 55(1): 3–21. https://doi.org/10.1086/411613

Clement M, Posada D, Crandall K (2000) Clement MD, Posada D, Crandall KA. TCS: a computer program to estimate gene genealogies. Molecular Ecology 9(10): 1657–1659. https://doi.org/10.1046/j.1365-294x.2000.01020.x

Cloudsley-Thompson JL (1979) Adaptive functions of the colours of desert animals. Journal of Arid Environments 2(2): 95–104. https://doi.org/10.1016/S0140-1963(18)31785-3

Curto JD, Pinto JC (2011) The corrected VIF (CVIF). Journal of Applied Statistics 38(7): 1499–1507. https://doi.org/10.1080/02664763.2010.505956

Dormann CF, Elith J, Bacher S, Buchmann C, Carl G, Carré G, Marquéz JRG, Gruber B, Lafourcade B, Leitão PJ, Münkemüller T, McClean C, Osborne PE, Reineking B, Schröder B, Skidmore AK, Zurell D, Lautenbach S (2013) Collinearity: A review of methods to deal with it and a simulation study evaluating their performance. Ecography 36(1): 27–46. https://doi.org/10.1111/j.1600-0587.2012.07348.x

Engel MS, Ceríaco LMP, Daniel GM, Dellapé PM, Löbl I, Marinov M, Reis RE, Young MT, Dubois A, Agarwal I, Lehmann AP, Alvarado M, Alvarez N, Andreone F, Araujo-Vieira K, Ascher JS, Baêta D, Baldo D, Bandeira SA, Barden P, Barrasso DA, Bendifallah L, Bockmann FA, Böhme W, Borkent A, Brandão CRF, Busack SD, Bybee SM, Channing A, Chatzimanolis S, Christenhusz MJM, Crisci JV, D'elía G, Da Costa LM, Davis SR, De Lucena CAS, Deuve T, Fernandes Elizalde S, Faivovich J, Farooq H, Ferguson AW, Gippoliti S, Gonçalves FMP, Gonzalez VH, Greenbaum E, Hinojosa-Díaz IA, Ineich I, Jiang J, Kahono S, Kury AB, Lucinda PHF, Lynch JD, Malécot V, Marques MP, Marris JWM, Mckellar RC, Mendes LF, Nihei SS, Nishikawa K, Ohler A, Orrico VGD, Ota H, Paiva J, Parrinha D, Pauwels OSG, Pereyra MO, Pestana LB, Pinheiro PDP,

Prendini L, Prokop J, Rasmussen C, Rödel M-O, Rodrigues MT, Rodríguez SM, Salatnaya H, Sampaio Í, Sánchez-García A, Shebl MA, Santos BS, Solórzano-Kraemer MM, Sousa ACA, Stoev P, Teta P, Trape J-F, Dos Santos CV-D, Vasudevan K, Vink CJ, Vogel G, Wagner P, Wappler T, Ware JL, Wedmann S, Zacharie CK (2021) The taxonomic impediment: A shortage of taxonomists, not the lack of technical approaches. Zoological Journal of the Linnean Society 193(2): 381–387. https://doi.org/10.1093/zoolinnean/zlab072

Fathinia B, Rastegar-Pouyani E, Rastegar-Pouyani N, Darvishnia H (2017) A new species of the genus *Rhynchocalamus* Günther, 1864 (Reptilia: Squamata: Colubridae) from Ilam province in western Iran. Zootaxa 4282(3): 473–486. https://doi.org/10.11646/zootaxa.4282.3.3

Fick SE, Hijmans RJ (2017) WorldClim 2: New 1-km spatial resolution climate surfaces for global land areas. International Journal of Climatology 37(12): 4302–4315. https://doi.org/10.1002/joc.5086

Guindon S, Dufayard J-F, Lefort V, Anisimova M, Hordijk W, Gascuel O (2010) New Algorithms and Methods to Estimate Maximum-Likelihood Phylogenies: Assessing the Performance of PhyML 3.0. Systematic Biology 59(3): 307–321. https://doi.org/10.1093/sysbio/syq010

Hijmans RJ, van Etten J, Sumner M, Cheng J, Baston D, Bevan A, Bivand R, Busetto L, Canty M, Fasoli B, Forrest D, Ghosh A, Golicher D, Gray J, Greenberg JA, Hiemstra P, Hingee K, Ilich A Geosciences I for MA, Karney C, Mattiuzzi M, Mosher S, Naimi B, Nowosad J, Pebesma E, Lamigueiro OP, Racine EB, Rowlingson B, Shortridge A, Venables B, Wueest R (2021) raster: Geographic data analysis and modeling. https://CRAN.R-project.org/package=raster [January 12, 2022]

Hirzel AH, Le Lay G, Helfer V, Randin C, Guisan A (2006) Evaluating the ability of habitat suitability models to predict species presences. Ecological Modelling 199(2): 142–152. https://doi.org/10.1016/j.ecolmodel.2006.05.017

Hollister J, Shah T, Robitaille AL, Beck MW, Johnson M (2023) elevatr: Access Elevation Data from Various APIs. https://cran.r-project.org/web/packages/elevatr/index.html [August 10, 2023]

IUCN SSC Standards and Petitions Committee (2022) Guidelines for Using the IUCN Red List Categories and Criteria. Version 15.1. https://www.iucn.org/our-union/commissions/group/iucn-ssc-standards-and-petitions-committee [January 24, 2024]

Jablonski D, Kukushkin OV, Avcı A, Bunyatova S, Kumlutaş Y, Ilgaz Ç, Polyakova E, Shiryaev K, Tuniyev B, Jandzik D (2019) The biogeography of *Elaphe sauromates* (Pallas, 1814), with a description of a new rat snake species. PeerJ 7: e6944. https://doi.org/10.7717/peerj.6944

Kaky E, Nolan V, Alatawi A, Gilbert F (2020) A comparison between Ensemble and MaxEnt species distribution modelling approaches for conservation: A case study with Egyptian medicinal plants. Ecological Informatics 60: 101150. https://doi.org/10.1016/j.ecoinf.2020.101150

Kalyaanamoorthy S, Minh BQ, Wong TKF, von Haeseler A, Jermiin LS (2017) ModelFinder: Fast model selection for accurate phylogenetic estimates. Nature Methods 14(6): 587–589. https://doi.org/10.1038/nmeth.4285

Katoh K, Rozewicki J, Yamada KD (2019) MAFFT online service: Multiple sequence alignment, interactive sequence choice and visualization. Briefings in Bioinformatics 20(4): 1160–1166. https://doi.org/10.1093/bib/bbx108

Kearse M, Moir R, Wilson A, Stones-Havas S, Cheung M, Sturrock S, Buxton S, Cooper A, Markowitz S, Duran C, Thierer T, Ashton B, Meintjes P, Drummond A (2012) Geneious Basic: An integrated and extendable desktop software platform for the organization and analysis of sequence data. Bioinformatics (Oxford, England) 28(12): 1647–1649. https://doi.org/10.1093/bioinformatics/bts199

Kéry M (2002) Inferring the absence of a species: A case study of snakes. The Journal of Wildlife Management 66(2): 330–338. https://doi.org/10.2307/3803165

Lanfear R, Frandsen PB, Wright AM, Senfeld T, Calcott B (2017) PartitionFinder 2: New methods for selecting partitioned models of evolution for molecular and morphological phylogenetic analyses. Molecular Biology and Evolution 34: 772–773. https://doi.org/10.1093/molbev/msw260

Laopichienpong N, Tawichasri P, Chanhome L, Phatcharakullawarawat R, Singchat W, Kantachumpoo A, Muangmai N, Suntrarachun S, Matsubara K, Peyachoknagul S, Srikulnath K (2017) A novel method of caenophidian snake sex identification using molecular markers based on two gametologous genes. Ecology and Evolution 7(13): 4661–4669. https://doi.org/10.1002/ece3.3057

Leigh JW, Bryant D (2015) popart: full-feature software for haplotype network construction. Nakagawa S (Ed.). Methods in Ecology and Evolution 6: 1110–1116. https://doi.org/10.1111/2041-210X.12410

Matsubara K, Nishida C, Matsuda Y, Kumazawa Y (2016) Sex chromosome evolution in snakes inferred from divergence patterns of two gametologous genes and chromosome distribution of sex chromosome-linked repetitive sequences. Zoological Letters 2(1): 19. https://doi.org/10.1186/s40851-016-0056-1

May RM (2004) Tomorrow's taxonomy: Collecting new species in the field will remain the rate–limiting step. Philosophical Transactions of the Royal Society of London, Series B, Biological Sciences 359(1444): 733–734. https://doi.org/10.1098/rstb.2003.1455

Miller MA, Pfeiffer W, Schwartz T (2010) Creating the CIPRES Science Gateway for inference of large phylogenetic trees. In: 2010 Gateway Computing Environments Workshop (GCE), 1–8. https://doi.org/10.1109/GCE.2010.5676129

Minh BQ, Nguyen MAT, von Haeseler A (2013) Ultrafast Approximation for Phylogenetic Bootstrap. Molecular Biology and Evolution 30(5): 1188–1195. https://doi.org/10.1093/molbev/mst024

Naimi B, Araújo MB (2016) sdm: A reproducible and extensible R platform for species distribution modelling. Ecography 39(4): 368–375. https://doi.org/10.1111/ecog.01881

Naimi B, Hamm NAS, Groen TA, Skidmore AK, Toxopeus AG (2014) Where is positional uncertainty a problem for species distribution modelling? Ecography 37(2): 191–203. https://doi.org/10.1111/j.1600-0587.2013.00205.x

Nguyen L-T, Schmidt HA, von Haeseler A, Minh BQ (2015) IQ-TREE: A fast and effective stochastic algorithm for estimating maximum-likelihood phylogenies. Molecular Biology and Evolution 32(1): 268–274. https://doi.org/10.1093/molbev/msu300

Pola L, Crochet PA, Geniez P, Shobrak M, Busais S, Jablonski D, Masroor R, Abduraupov T, Carranza S, Šmíd J (2024) Some like it hot: Past and present phylogeography of a desert dwelling gecko across the Arabian Peninsula. Journal of Biogeography 00: 1–15. https://doi.org/10.1111/jbi.14823

R Core Team (2024) R: A language and environment for statistical computing. https://www.R-project.org/

Rambaut A, Drummond AJ, Xie D, Baele G, Suchard MA (2018) Posterior Summarization in Bayesian Phylogenetics Using Tracer 1.7. Systematic Biology 67(5): 901–904. https://doi.org/10.1093/sysbio/syy032

Rodda GH (1993) Where's Waldo (and the snakes)? Herpetological Review 24: 44–45.

Ronquist F, Teslenko M, van der Mark P, Ayres DL, Darling A, Höhna S, Larget B, Liu L, Suchard MA, Huelsenbeck JP (2012) MrBayes 3.2: Efficient Bayesian phylogenetic inference and model choice across a large model space. Systematic Biology 61(3): 539–542. https://doi.org/10.1093/sysbio/sys029

Rozas J, Ferrer-Mata A, Sánchez-DelBarrio JC, Guirao-Rico S, Librado P, Ramos-Onsins SE, Sánchez-Gracia A (2017) DnaSP 6: DNA sequence polymorphism analysis of large data sets. Molecular Biology and Evolution 34(12): 3299–3302. https://doi.org/10.1093/molbev/msx248

Scheffers BR, Joppa LN, Pimm SL, Laurance WF (2012) What we know and don't know about Earth's missing biodiversity. Trends in Ecology & Evolution 27(9): 501–510. https://doi.org/10.1016/j.tree.2012.05.008

Schneider CA, Rasband WS, Eliceiri KW (2012) NIH Image to ImageJ: 25 years of image analysis. Nature Methods 9(7): 671–675. https://doi.org/10.1038/nmeth.2089

Šmíd J, Martínez G, Gebhart J, Aznar J, Gallego J, Göçmen B, de Pous P, Tamar K, Carranza S (2015) Phylogeny of the genus *Rhynchocalamus* (Reptilia; Colubridae) with a first record from the Sultanate of Oman. Zootaxa 4033(3): 380–392. https://doi.org/10.11646/zootaxa.4033.3.4

Šmíd J, Sindaco R, Shobrak M, Busais S, Tamar K, Aghová T, Simó-Riudalbas M, Tarroso P, Geniez P, Crochet P-A, Els J, Burriel-Carranza B, Tejero-Cicuéndez H, Carranza S (2021) Diversity patterns and evolutionary history of Arabian squamates. Journal of Biogeography 48(5): 1183–1199. https://doi.org/10.1111/jbi.14070

Stephens M, Smith NJ, Donnelly P (2001) A new statistical method for haplotype reconstruction from population data. American Journal of Human Genetics 68(4): 978–989. https://doi.org/10.1086/319501

Tamar K, Šmíd J, Göçmen B, Meiri S, Carranza S (2016) An integrative systematic revision and biogeography of *Rhynchocalamus* snakes (Reptilia, Colubridae) with a description of a new species from Israel. PeerJ 4: e2769. https://doi.org/10.7717/peerj.2769

Tamar K, Wiedl HJ, Maza E, Jablonski D, Meiri S (2020) Discovery of the Black-headed Ground Snake *Rhynchocalamus melanocephalus* (Jan, 1862) in Cyprus (Reptilia: Colubridae). Zoology in the Middle East 66(2): 118–123. https://doi.org/10.1080/09397140.2020.1757914

Tamura K, Stecher G, Kumar S (2021) MEGA11: Molecular Evolutionary Genetics Analysis Version 11. Molecular Biology and Evolution 38(7): 3022–3027. https://doi.org/10.1093/molbev/msab120

Templeton AR, Crandall KA, Sing CF (1992) A cladistic analysis of phenotypic associations with haplotypes inferred from restriction endonuclease mapping and DNA sequence data. III. Cladogram estimation. Genetics 132(2): 619–633. https://doi.org/10.1093/genetics/132.2.619

Torki F (2017) Description of a new species of *Lytorhynchus* (Squamata: Colubridae) from Iran. Zoology in the Middle East 63(2): 109–116. https://doi.org/10.1080/09397140.2017.1299319

Trifinopoulos J, Nguyen L-T, von Haeseler A, Minh BQ (2016) W-IQ-TREE: A fast online phylogenetic tool for maximum likelihood analysis. Nucleic Acids Research 44(W1): W232–W235. https://doi.org/10.1093/nar/gkw256

Trullas CS, van Wyk JH, Spotila JR (2007) Thermal melanism in ectotherms. Journal of Thermal Biology 32(5): 235–245. https://doi.org/10.1016/j.jtherbio.2007.01.013

Uetz P, Freed P, Aguilar R, Reyes F, Kudera J, Hošek J (2024) The Reptile Database. http://reptile-database.org/ [January 24, 2024]

Velazco SJE, Ribeiro BR, Laureto LMO, De Marco Júnior P (2020) Overprediction of species distribution models in conservation planning: A still neglected issue with strong effects. Biological Conservation 252: 108822. https://doi.org/10.1016/j.biocon.2020.108822

Vilela B, Villalobos F, Rodríguez MÁ, Terribile LC (2014) Body size, extinction risk and knowledge bias in New World snakes. PLOS ONE 9(11): e113429. https://doi.org/10.1371/journal.pone.0113429

Wagner RO, Pierce JB, Rudolph DC, Schaefer RR, Hightower DA (2014) Modeling Louisiana pine snake (*Pituophis ruthveni*) habitat use in relation to soils. Southeastern Naturalist (Steuben, ME) 13(sp5): 146–158. https://doi.org/10.1656/058.013.s514

Watling JI, Brandt LA, Bucklin DN, Fujisaki I, Mazzotti FJ, Romañach SS, Speroterra C (2015) Performance metrics and variance partitioning reveal sources of uncertainty in species distribution models. Ecological Modelling 309–310: 48–59. https://doi.org/10.1016/j.ecolmodel.2015.03.017

Werner YI (2016) Reptile Life in the Land of Israel with Comments on Adjacent Regions. Frankfurt am Main.

Supplementary material 1

Supporting information

Authors: Fulvio Licata, Lukáš Pola, Jiří Šmíd, Adel A. Ibrahim, André Vicente Liz, Bárbara Santos, László Patkó, Ayman Abdulkareem, Duarte V. Gonçalves, Ahmed Mohajja AlShammari, Salem Busais, Damien M. Egan, Ricardo M. O. Ramalho, Josh Smithson, José Carlos Brito

Data type: docx

Explanation note: **table S1.** List of material analysed in this study including information on voucher and tissue codes, country, province and locality of origin, GPS coordinates (datum WGS84), and GenBank accession numbers. Accession numbers of sequences generated for this study are highlighted in bold. Rows with neither voucher nor tissue codes are observations used only for the species distribution modelling. **figure S1.** Phylogenetic tree resulting from the Maximum likelihood analysis of three mitochondrial and four nuclear markers concatenated. Values by branches indicate SH-aLRT/UFBoot (see Materials and methods for abbreviations). **figure S2.** Phylogenetic tree resulting from the Bayesian analysis of three mitochondrial and four nuclear markers concatenated. Values by branches indicate posterior probabilities.

Link: https://doi.org/10.3897/zse.100.123441.suppl1

Zoosyst. Evol. 100 (2) 2024, 705–720 | DOI 10.3897/zse.100.124160

PENSOFT

MUSEUM FÜR NATURKUNDE BERLIN

Five new species of the spider genus *Bifurcia* Saaristo, Tu & Li, 2006 (Araneae, Linyphiidae) from Sichuan, China

Lan Yang[1], Shuqiang Li[2], Zhiyuan Yao[1]

1 *College of Life Science, Shenyang Normal University, Shenyang 110034, Liaoning, China*

2 *Institute of Zoology, Chinese Academy of Sciences, Beijing 100101, China*

https://zoobank.org/0E190BDE-BF4D-4F7E-A8C0-9AB5383D8BC8

Corresponding authors: Zhiyuan Yao (yaozy@synu.edu.cn); Shuqiang Li (lisq@ioz.ac.cn)

Academic editor: Danilo Harms ♦ **Received** 1 April 2024 ♦ **Accepted** 11 May 2024 ♦ **Published** 4 June 2024

Abstract

Five new species of the genus *Bifurcia* are described: *B. kangding* **sp. nov.** (♂♀), *B. labahe* **sp. nov.** (♂), *B. luding* **sp. nov.** (♂♀), *B. shuangqiao* **sp. nov.** (♂♀), and *B. xiaojin* **sp. nov.** (♂♀) from western Sichuan, China. A distribution map of the species and illustrations of genital characters are provided in this paper.

Key Words

Biodiversity, micronetine, morphology, sheet-web spiders, taxonomy

Introduction

The spider family Linyphiidae Blackwall, 1859, is the second-largest family in the world, consisting of 4,847 species in 634 genera (WSC 2024). It has a worldwide distribution, but members of the family are found mostly in temperate regions and mountainous regions in the tropics (Murphy and Murphy 2000; Irfan et al. 2022a). Their habitats can range from foliage in the forest canopy to vegetation at eye level, among leaf litter, and under rocks at ground level (Murphy and Murphy 2000; Platnick 2020). Linyphiidae is composed of seven subfamilies: Dubiaraneinae Millidge, 1993; Erigoninae Emerton, 1882; Ipainae Saaristo, 2007; Linyphiinae Blackwall, 1859; Micronetinae Hull, 1920; Mynogleninae Lehtinen, 1967; and Stemonyphantinae Wunderlich, 1986 (Saaristo 2007; Tanasevitch 2024), but such a classification has not been supported by any phylogenetic analyses and seems to be controversial. In Arnedo et al. (2009), the phylogenetic analyses agreed on the monophyly of 'linyphioids', Pimoidae Wunderlich, 1986, Linyphiidae, Erigoninae, Mynogleninae, as well as *Stemonyphantes* Menge, 1866, as a basal lineage within Linyphiidae. Wang et al.'s (2015) analyses resulted in seven robustly supported clades within Linyphiidae, but the placements of four deep and long branches are sensitive to variations in both outgroup and ingroup sampling. Hormiga et al. (2021) confirmed that *Weintrauboa* Hormiga, 2003; *Putaoa* Hormiga & Tu, 2008; *Pecado* Hormiga & Scharff, 2005; and *Stemonyphantes* form a clade (Stemonyphantinae) sister to all remaining linyphiids, and they re-circumscribed Stemonyphantinae. *Bifurcia* Saaristo, Tu & Li, 2006 is classified as Micronetinae (Tanasevitch 2024), but no phylogenetic analysis has ever found Micronetinae to be a monophyletic group. *Bifurcia* comprised ten known species, including four from Russia (south of the Far East) and six from China, stretching from Hebei Province to Sichuan Province (Saaristo et al. 2006; Irfan et al. 2022b; WSC 2024).

Sichuan Province, in the southwest of China, is a biodiversity hotspot with 22 genera and 46 species of linyphiids recorded so far (Tanasevitch 2006; Tu and Li 2006; Song and Li 2010; WSC 2024). Nevertheless, only one species of *Bifurcia*, namely *B. curvata* (Sha & Zhu, 1987), has been recorded from Sichuan Province (Li et al. 1987). In the present study, we describe five new species belonging to *Bifurcia* from western Sichuan (Fig. 1). This region of Sichuan may be characterized as a highland (2,000 to 7,500 meters above sea level), although one of the type localities (Tianquan County) has an elevation of only 600 to 800 meters.

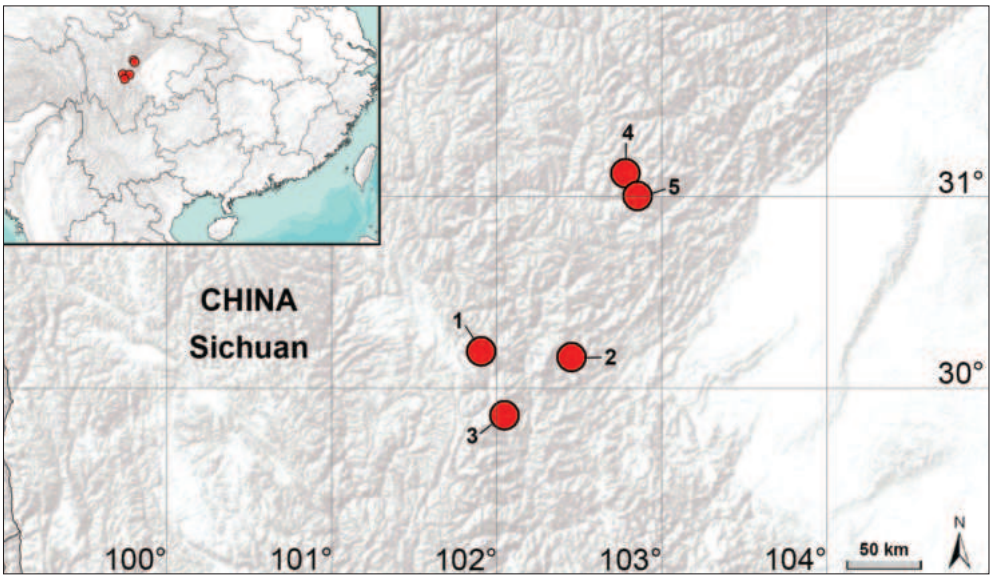

Figure 1. Distribution of the new *Bifurcia* species from Sichuan, China: **1.** *B. kangding* sp. nov.; **2.** *B. labahe* sp. nov.; **3.** *B. luding* sp. nov.; **4.** *B. shuangqiao* sp. nov.; **5.** *B. xiaojin* sp. nov.

Materials and methods

Specimens were examined and measured with a Leica M205 C stereomicroscope. Left palps were photographed. Epigynes in ventral view were photographed before dissection. Epigynes in dorsal view were photographed after being treated with lactic acid to dissolve soft tissues. Images were captured with an Olympus C7070 wide-zoom digital camera (7.1 megapixels) mounted on the stereomicroscope mentioned above and assembled using Helicon Focus v. 6.7.1 image stacking software (Khmelik et al. 2005). All measurements are given in millimeters (mm). Leg measurements are shown as total length (femur, patella, tibia, metatarsus, and tarsus). Leg segments were measured on their dorsal side. The distribution map was generated with ArcGIS v. 10.8 (ESRI Inc.). The specimens studied were preserved in 75% ethanol and deposited in the Institute of Zoology, Chinese Academy of Sciences in Beijing (IZCAS).

Terminology and taxonomic descriptions follow Saaristo et al. (2006). Metatarsal trichobothrium (Tm) is given as the ratio of the distance between the proximal margin of the metatarsus and the root of the trichobothrium divided by the total length of the metatarsus (Denis 1949; Locket and Millidge 1953). The following abbreviations are used:

Somatic morphology: **ALE** = anterior lateral eye; **AME** = anterior median eye; **AME-AME** = distance between AMEs; **AME-ALE** = distance between AME and ALE; **PLE** = posterior lateral eye; **PME** = posterior median eye; **PME-PME** = distance between PME; **PME-PLE** = distance between PME and PLE.

Male palp: **APR** = anterior part of radix; **ATA** = anterior terminal apophysis; **AX** = apex of embolus; **CPM** = chitinized part of median membrane; **E** = embolus; **EP** = embolus proper; **FG** = Fickert's gland; **LE** = lamellar extension of pseudolamella; **MM** = median membrane; **MTA** = median terminal apophysis; **P** = paracymbium; **PCA** = proximal cymbial apophysis; **PH** = pit hook on suprategulum; **PL** = pseudolamella; **PTA** = posterior terminal apophysis; **R** = radix; **SPT** = suprategulum; **ST** = subtegulum; **T** = tegulum; **TH** = thumb of embolus.

Epigyne: **BS** = basal part of scape; **DPS** = distal part of scape; **LL** = lateral lobe; **PMP** = posterior median plate; **S** = spermatheca.

Taxonomy

Family Linyphiidae Blackwall, 1859

Genus *Bifurcia* Saaristo, Tu & Li, 2006

Type species. *Arcuphantes ramosus* Li & Zhu, 1987.

The five new species described below are assigned to the genus *Bifurcia* by the following characters: proximal cymbial apophysis (PCA) pointing retrolaterally; bifurcated paracymbium (P); distal part of suprategulum (SPT) large, blunt, and strongly sclerotized in retrolateral view; suprategular pit hook (PH) reduced to small; median membrane (MM) with chitinized basal part (CPM); relatively thick and stout tipped pseudolamella (PL); basal part of scape (BS) nearly T-shaped (Saaristo et al. 2006).

Bifurcia kangding sp. nov.

https://zoobank.org/BFCA8CFF-92DE-4C0F-97B3-5A27552EA929

Figs 2–4, 16A, D

Type material. ***Holotype*** ♂ (IZCAS-Ar44925) and ***paratypes*** 1♂2♀ (IZCAS-Ar44926–28), Mugecuo Scenic Area (30°11.72'N, 101°54.43'E, 3760 m elev.), Wangmu Village, Yala Town, Kangding, Garze Tibetan Autonomous Prefecture, **Sichuan**, **China**, 14/07/2004, Lihong Tu leg.

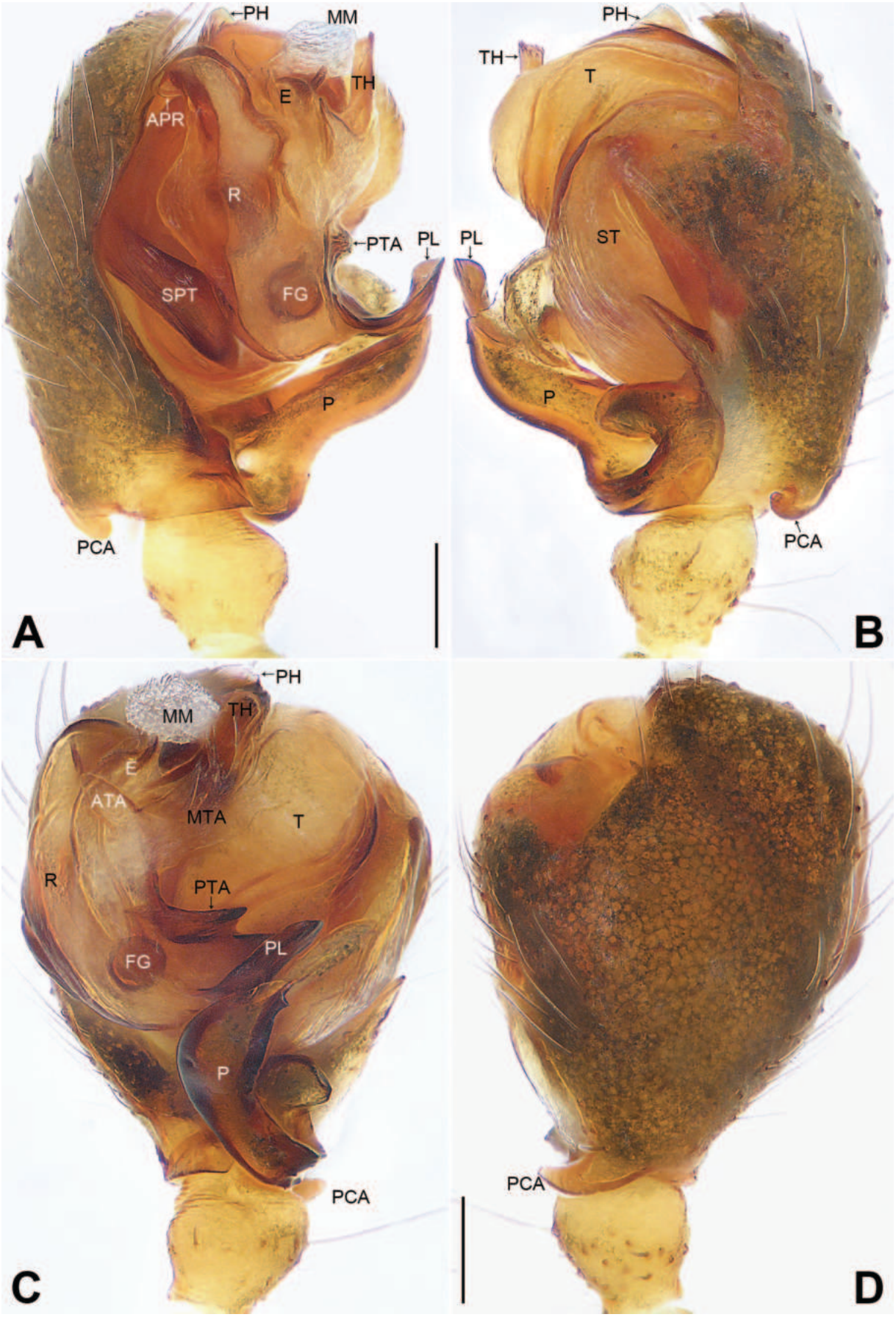

Figure 2. *Bifurcia kangding* sp. nov., holotype male palp: **A.** Prolateral view; **B.** Retrolateral view; **C.** Ventral view; **D.** Dorsal view. Scale bars: 0.10 mm (**A–D**).

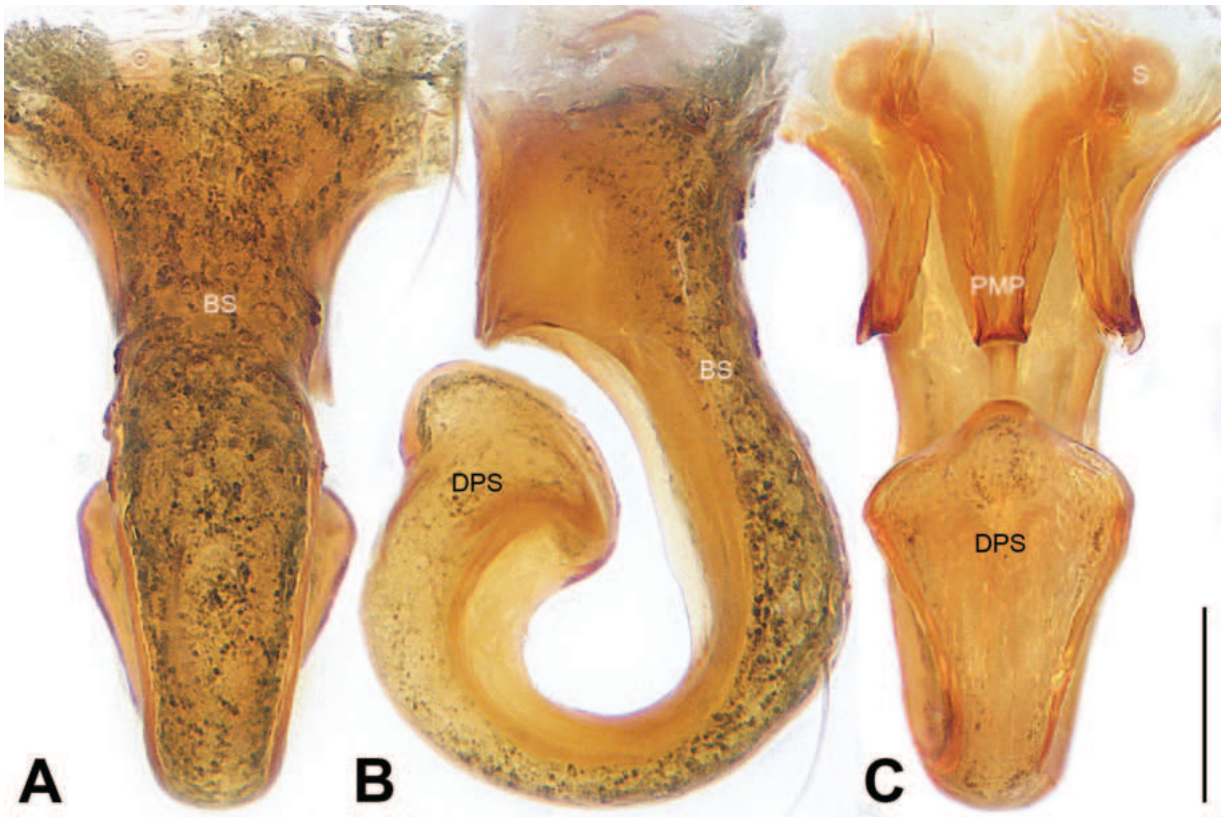

Figure 3. *Bifurcia kangding* sp. nov., paratype female epigyne: **A.** Ventral view; **B.** Lateral view; **C.** Dorsal view. Scale bar: 0.10 mm (**A–C**).

Figure 4. *Bifurcia kangding* sp. nov., holotype male (**A, B**) and paratype female (**C, D**) habitus: **A, C.** Dorsal view; **B, D.** Ventral view. Scale bars: 0.50 mm (**A–D**).

Etymology. The specific name refers to the type locality; noun in apposition.

Diagnosis. The new species resembles *B. xiaojin* sp. nov. with similar paracymbium (P) and epigyne (Figs 2B, 3A), but can be easily distinguished by embolus thumb (TH) with dentate end (Figs 2B, 16D vs. spinous, Figs 13B, 16J), by chitinized basal part of median membrane (CPM) small with tip end (Fig. 16A vs. finger-shaped, Fig. 16H), and by spermathecae (S) separated by diameter less than their inter-distance (Fig. 3C vs. inter-distance less than their diameter, Fig. 14C).

Description. Male (*holotype*). Total length: 2.12, carapace 0.92 long, 0.74 wide, abdomen 1.30 long, 0.80 wide. Eye inter-distances and diameters: AME 0.06, AME-AME 0.03, ALE 0.08, AME-ALE 0.06, PME 0.08, PME-PME 0.05, PLE 0.07, and PME-PLE 0.06. Sternum 0.54 long, 0.52 wide. Clypeus 0.12 high. Chelicerae promargin with 3 teeth, retromargin with 4 teeth. Length of legs: I 5.50 (1.54, 0.28, 1.44, 1.34, 0.90), II 4.90 (1.26, 0.26, 1.44, 1.14, 0.80), III 3.10 (0.78, 0.22, 0.76, 0.76, 0.58), IV 4.44 (1.24, 0.24, 1.12, 1.10, 0.74). Leg formula: I-II-IV-III. TmI 0.16, TmIV absent. Tibial spine formula: 2-2-2-2. Carapace brown. Sternum dark brown. Abdomen with greenish gray dorsal spots (Fig. 4A, B).

Palp (Fig. 2). Patella with long dorsal bristle. Tibia unmodified. Cymbium with hook-shaped proximal apophysis (PCA) pointing retrolaterally. Paracymbium (P) bifurcate with three branches: distally triangular branch, sharp-pointed branch and lower sclerotized branch. Pit hook (PH) on stout distal part of suprategulum (SPT) extremely reduced to small outgrowth. Embolic division (Fig. 16A, D): anterior part of radix (APR) hook-shaped; sperm duct inside the radix (R) inconspicuous with Fickert's gland (FG); pseudolamella (PL) strongly sclerotized and lamellar extension (LE) absent. Anterior terminal apophysis (ATA) short-pointing anterodorsally; median terminal apophysis (MTA) membranous with many slender branches; posterior terminal apophysis (PTA) with serrated margin. Embolus (E) with short basal part, apical part with conical embolus proper (EP), L-shaped thumb (TH), and sharp apex (AX). Median membrane (MM) leaf-shaped with numerous papillae, and basal part of median membrane chitinized (CPM).

Female (*paratype*). Total length: 2.42, carapace 0.94 long, 0.72 wide, abdomen 1.48 long, 1.10 wide. Eye inter-distances and diameters: AME 0.05, AME-AME 0.02, ALE 0.07, AME-ALE 0.05, PME 0.07, PME-PME 0.05, PLE 0.08, and PME-PLE 0.04. Sternum 0.56 long, 0.52 wide. Clypeus 0.12 high. Chelicerae promargin with 3 teeth, retromargin with 5 teeth. Length of legs: I 5.28 (1.44, 0.32, 1.34, 1.30, 0.88), II 4.74 (1.32, 0.30, 1.18, 1.14, 0.80), III 3.38 (1.02, 0.30, 0.80, 0.72, 0.54), IV 4.36 (1.26, 0.30, 1.06, 1.06, 0.68). Leg formula: I-II-IV-III. TmI 0.15, TmIV absent. Tibial spine formula: 2-2-2-2. Coloration generally as in male (Fig. 4C, D).

Epigyne (Fig. 3). Basal part of scape (BS) nearly T-shaped. Posterior part of posterior median plate (PMP) M-shaped. Distal part of scape (DPS) forming a circle with basal part of scape. Spermathecae (S) round.

Distribution. China (Sichuan, type locality; Fig. 1).

Bifurcia labahe sp. nov.

https://zoobank.org/0C7C6235-50F6-4DAE-B2AB-C1B996ACE792

Figs 5, 6, 16B, E

Type material. ***Holotype*** ♂ (IZCAS-Ar44929), Labahe Nature Reserve (30°9.89'N, 102°27.24'E), Tianquan County, Ya'an, **Sichuan**, **China**, 10/07/2004, Lihong Tu leg.

Etymology. The specific name refers to the type locality; noun in apposition.

Diagnosis. The species resembles *B. kangding* sp. nov. with similar pseudolamella (PL) and median membrane (MM) (Fig. 16B, E), but can be easily distinguished by thumb of embolus (TH) 0.6 times radix (R) length (Figs 5A, 16B vs. 0.3, Figs 2A, 16A), by anterior part of radix (APR) round (Fig. 16E vs. hooked, Fig. 16D), by median terminal apophysis (MTA) with jagged edge (Fig. 16B vs. branched, Fig. 16A), and by posterior terminal apophysis (PTA) thick and 0.7 times pseudolamella (PL) length (Fig. 16B vs. thin and 0.2, Fig. 16A).

Description. Male (*holotype*). Total length: 2.24, carapace 1.06 long, 0.96 wide, abdomen 1.18 long, 0.78 wide. Eye inter-distances and diameters: AME 0.05, AME-AME 0.02, ALE 0.09, AME-ALE 0.06, PME 0.06, PME-PME 0.07, PLE 0.09, and PME-PLE 0.05. Sternum 0.61 long, 0.45 wide. Clypeus 0.08 high. Chelicerae promargin with 2 teeth, retromargin with 1 tooth. Length of legs: I 7.00 (1.84, 0.34, 1.92, 1.80, 1.10), II 5.80 (1.64, 0.28, 1.62, 1.44, 0.82), III 4.34 (1.27, 0.27, 1.08, 1.09, 0.63), IV 5.70 (1.68, 0.28, 1.54, 1.48, 0.72). Leg formula: I-II-IV-III. TmI 0.17, TmIV absent. Tibial spine formula: 2-2-2-2. Carapace brown. Sternum dark brown. Abdomen with greenish gray dorsal spots (Fig. 6).

Palp (Fig. 5). Patella with long dorsal bristle. Tibia unmodified. Cymbium with hook-shaped proximal apophysis (PCA) pointing retrolaterally. Paracymbium (P) bifurcate with three branches: mushroom-shaped branch and two short branches proximally. Pit hook (PH) on stout distal part of suprategulum (SPT) extremely reduced to small outgrowth. Embolic division (Fig. 16B, E): anterior part of radix (APR) round; sperm duct inside the radix (R) inconspicuous with Fickert's gland (FG); pseudolamella (PL) smooth and pointed; lamellar extension (LE) absent. Anterior terminal apophysis (ATA) short; median terminal apophysis (MTA) board; posterior terminal apophysis (PTA) thick with dentate anterior margin. Embolus (E) with conical embolus proper (EP), large thumb (TH), and apex (AX). Median membrane (MM) round with numerous papillae, and basal part of median membrane chitinized (CPM).

Female. Unknown.

Distribution. China (Sichuan, type locality; Fig. 1).

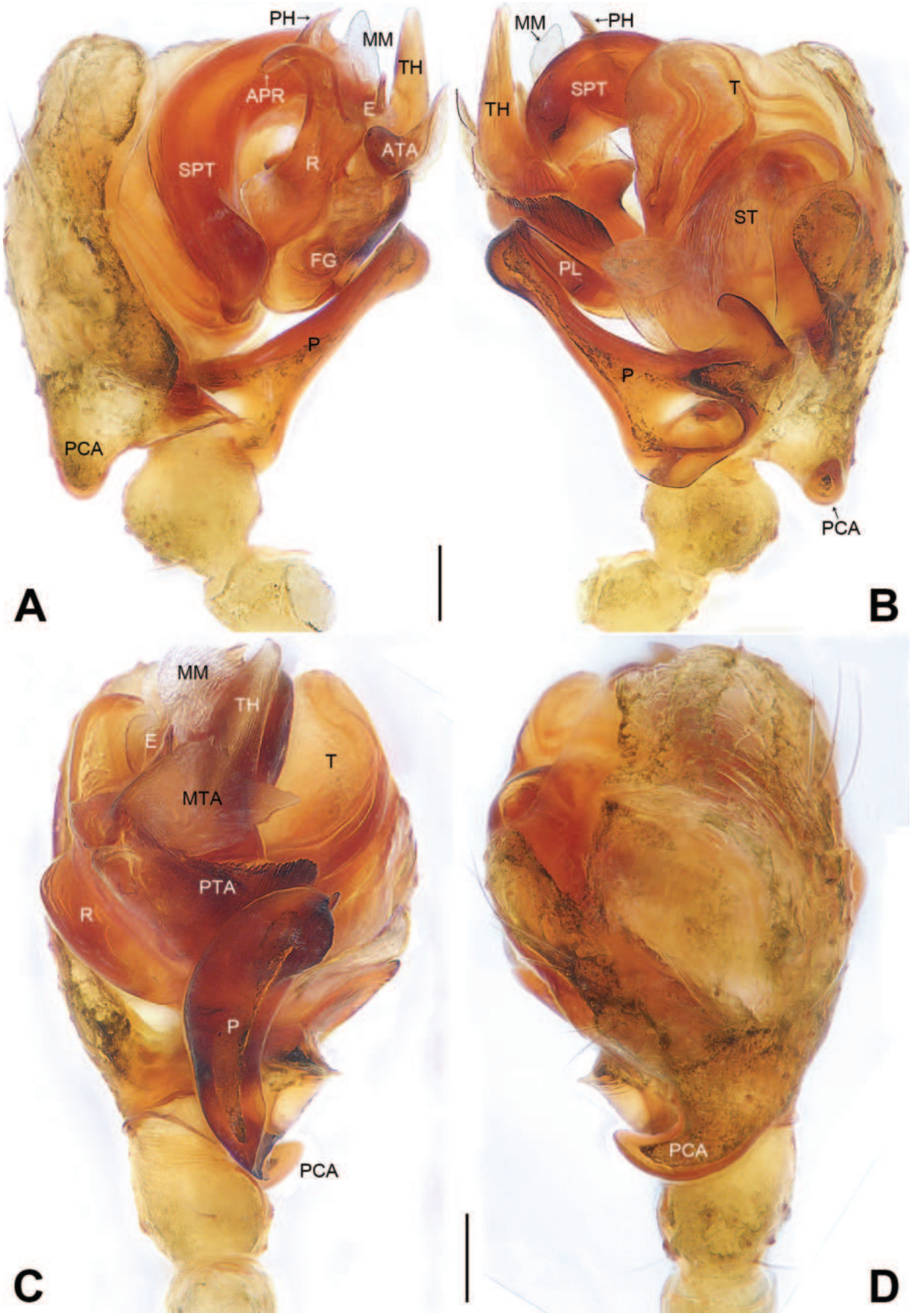

Figure 5. *Bifurcia labahe* sp. nov., holotype male palp: **A.** Prolateral view; **B.** Retrolateral view; **C.** Ventral view; **D.** Dorsal view. Scale bars: 0.10 mm (**A–D**).

Figure 6. *Bifurcia labahe* sp. nov., holotype male habitus: **A.** Dorsal view; **B.** Ventral view. Scale bar: 0.50 mm (**A, B**).

***Bifurcia luding* sp. nov.**

https://zoobank.org/3031952B-E440-40FB-8DB8-A68AC1D35336

Figs 7–9, 16C, F

Type material. ***Holotype*** ♂ (IZCAS-Ar44930) and ***paratype*** 1♀ (IZCAS-Ar44931), Luding County (29°51.60'N, 102°2.83'E, 2936 m elev.), Garze Tibetan Autonomous Prefecture, **Sichuan**, **China**, 20/07/2004, Lihong Tu leg.

Etymology. The specific name refers to the type locality; noun in apposition.

Diagnosis. The new species can be easily distinguished from other congeners by having embolus apex (AX) that is curved and distally pointed (Fig. 16C vs. angular, column-shaped, distally blunt, Fig. 16A, B, G, H, Saaristo et al. 2006: figs 4, 12), by embolus thumb (TH) membranous (Figs 7C, 16C vs. sclerotized, Figs 2C, 5C, 13C, 16A, B, G, H), by lamellar extension of pseudolamella (LE) with flower-shaped distal end (Figs 7C, 16C vs. lacking LE or LE ribbon-shaped, Figs 2C, 5C, 10C, 13C, 16A, B, G, H, Saaristo et al. 2006: figs 4, 12), and by basal part of scape (BS) shield-shaped (Fig. 8A vs. T-shaped, Figs 3A, 11A, 14A, Saaristo et al. 2006: figs 6, 14).

Description. Male (*holotype*). Total length: 2.23, carapace 1.10 long, 0.90 wide, abdomen 1.12 long, 0.74 wide. Eye inter-distances and diameters: AME 0.06, AME-AME 0.02, ALE 0.07, AME-ALE 0.06, PME 0.08, PME-PME 0.05, PLE 0.07, and PME-PLE 0.06. Sternum 0.50 long, 0.48 wide. Clypeus 0.11 high. Chelicerae promargin with 4 teeth, retromargin with 4 teeth. Length of legs: I 7.57 (1.98, 0.33, 1.96, 2.00, 1.30), II 6.78 (1.90, 0.32, 1.70, 1.74, 1.12), III 4.78 (1.38, 0.30, 1.10, 1.24, 0.76), IV 6.28 (1.84, 0.32, 1.58, 1.62, 0.92). Leg formula: I-II-IV-III. TmI 0.16, TmIV absent. Tibial spine formula: 2-2-2-2. Carapace yellowish. Sternum dark brown. Abdomen with greenish gray dorsal spots (Fig. 9A, B).

Palp (Fig. 7). Patella with long dorsal bristle. Tibia unmodified. Cymbium with hook-shaped proximal apophysis (PCA) pointing retrolaterally. Paracymbium (P) bifurcate with three branches: S-shaped branch, finger-shaped branch and lower branch. Pit hook (PH) on stout distal part of suprategulum (SPT) extremely reduced to small outgrowth. Embolic division (Fig. 16C, F): anterior part of radix (APR) hook-shaped; sperm duct inside the radix (R) inconspicuous with Fickert's gland (FG); pseudolamella (PL) strongly sclerotized; and lamellar extension (LE) slightly sclerotized with flower-shaped distal end. Anterior terminal apophysis (ATA) longer than wide; median terminal apophysis (MTA) membranous with serrated margin; posterior terminal apophysis (PTA) small and semicircle. Embolus (E) with conical embolus proper (EP), indistinct thumb (TH), and hooked apex (AX). Median membrane (MM) fan-shaped and small chitinized basal part of median membrane (CPM).

Female (*paratype*). Total length: 2.53, carapace 0.96 long, 0.84 wide, abdomen 1.66 long, 1.16 wide.

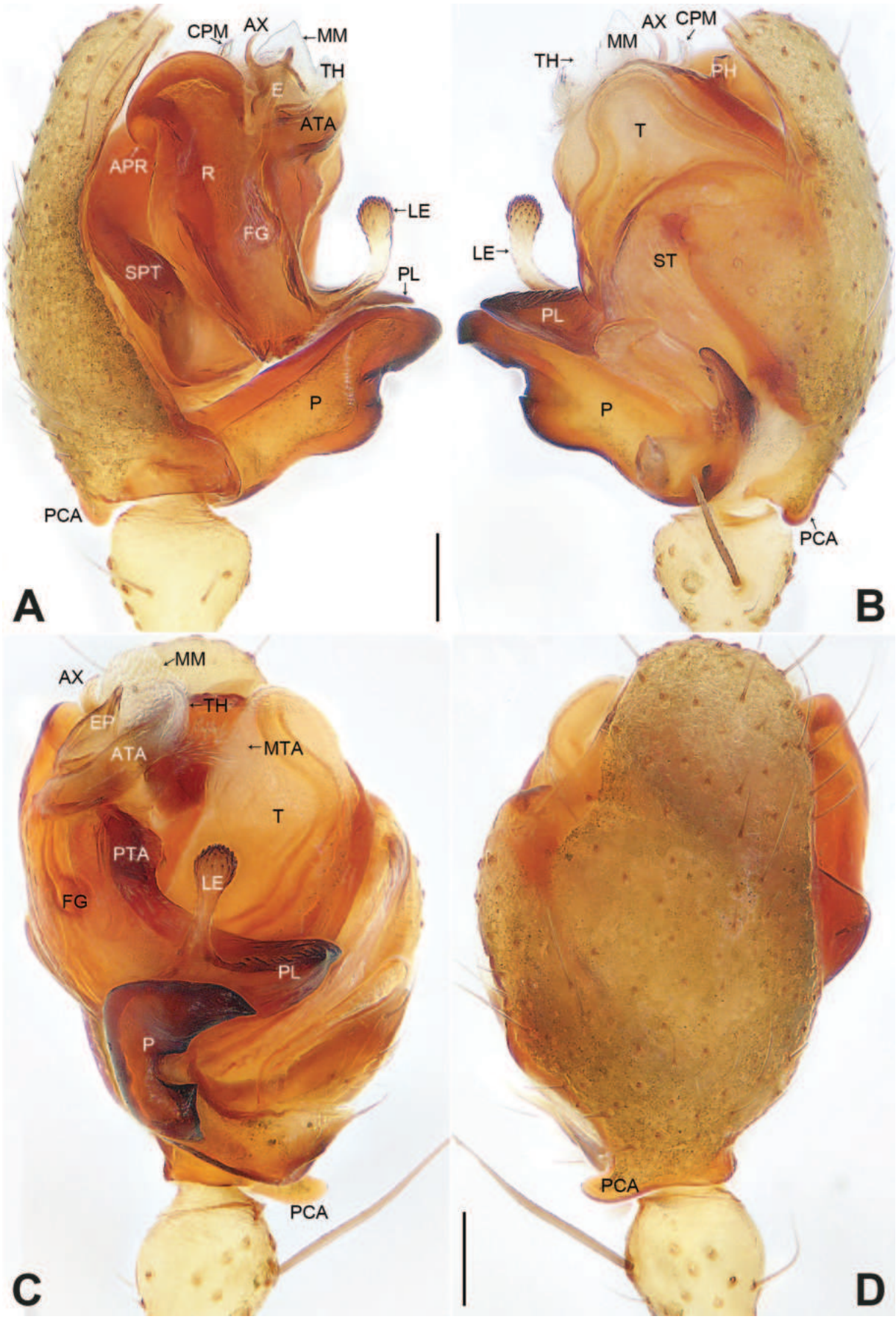

Figure 7. *Bifurcia luding* sp. nov., holotype male palp: **A.** Prolateral view; **B.** Retrolateral view; **C.** Ventral view; **D.** Dorsal view. Scale bars: 0.10 mm (**A–D**).

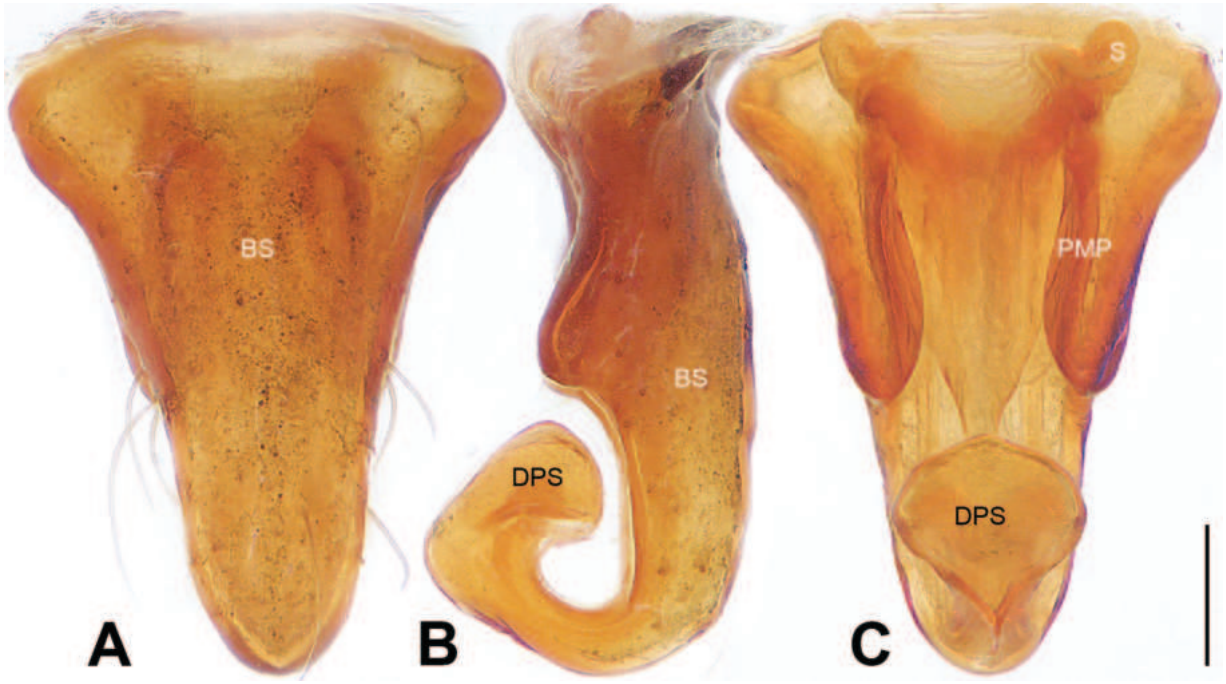

Figure 8. *Bifurcia luding* sp. nov., paratype female epigyne: **A.** Ventral view; **B.** Lateral view; **C.** Dorsal view. Scale bar: 0.10 mm (**A–C**).

Figure 9. *Bifurcia luding* sp. nov., holotype male (**A, B**) and paratype female (**C, D**) habitus: **A, C.** Dorsal view; **B, D.** Ventral view. Scale bars: 0.50 mm (**A–D**).

Eye inter-distances and diameters: AME 0.06, AME-AME 0.02, ALE 0.09, AME-ALE 0.06, PME 0.09, PME-PME 0.06, PLE 0.07, and PME-PLE 0.06. Sternum 0.66 long, 0.56 wide. Clypeus 0.09 high. Chelicerae promargin with 3 teeth, retromargin with 5 teeth. Length of legs: I 7.01 (1.82, 0.36, 1.92, 1.80, 1.11), II 6.27 (1.74, 0.32, 1.63, 1.56, 1.02), III 4.62 (1.42, 0.28, 1.14, 1.10, 0.68), IV 5.90 (1.78, 0.30, 1.50, 1.46, 0.86). Leg formula: I-II-IV-III. TmI 0.16, TmIV absent. Tibial spine formula: 2-2-2-2. Coloration generally as in male (Fig. 9C, D).

Epigyne (Fig. 8). Basal part of scape (BS) shield-shaped. Both sides of posterior median plate (PMP) developed well. Distal part of scape (DPS) forming an incomplete circle with basal part of scape. Spermathecae (S) nearly elliptic.

Distribution. China (Sichuan, type locality; Fig. 1).

Bifurcia shuangqiao sp. nov.

https://zoobank.org/8B4565AA-8C81-4F24-B83D-9067D2795EB4

Figs 10–12, 16G, I

Type material. ***Holotype*** ♂ (IZCAS-Ar44932) and ***paratype*** 1♀ (IZCAS-Ar44933), Shuangqiaogou (31°7.34'N, 102°46.71'E), Siguniangshan National Scenic Area, Siguniangshan Town, Xiaojin County, Aba Tibetan and Qiang Autonomous Prefecture, **Sichuan**, **China**, 02/08/2004, Lihong Tu leg.

Etymology. The specific name refers to the type locality; noun in apposition.

Diagnosis. The new species resembles *B. curvata* (Sha & Zhu, 1987) (Saaristo et al. 2006: figs 9–17) with similar large chitinized basal part of median membrane (CPM) and epigyne (Figs 10B, 11A, 16G, I), but can be distinguished by embolus with hooked apex (AX) (Fig. 16G vs. sharp, Saaristo et al. 2006: fig. 12), by anterior terminal apophysis (ATA) finger-shaped (Figs 10A, 16G vs. handle-shaped, Saaristo et al. 2006: figs 11, 12), by lamellar extension of pseudolamella (LE) absent (Figs 10C, 16G vs. present and ribbon-shaped, Saaristo et al. 2006: figs 10, 12), and by posterior part of posterior median plate (PMP) straight (Fig. 11C vs. curved, Saaristo et al. 2006: fig. 17).

Description. Male (*holotype*). Total length: 1.78, carapace 0.88 long, 0.78 wide, abdomen 0.89 long, 0.62 wide. Eye inter-distances and diameters: AME 0.05, AME-AME 0.02, ALE 0.08, AME-ALE 0.06, PME 0.08, PME-PME 0.04, PLE 0.08, and PME-PLE 0.04. Sternum 0.53 long, 0.51 wide. Clypeus 0.12 high. Chelicerae promargin with 3 teeth, retromargin with 4 teeth. Length of legs: I 5.43 (1.41, 0.28, 1.48, 1.34, 0.92), II 4.63 (1.24, 0.26, 1.21, 1.14, 0.78), III 3.42 (0.97, 0.22, 0.80, 0.83, 0.60), IV 4.47 (1.33, 0.25, 1.13, 1.06, 0.70). Leg formula: I-II-IV-III. TmI 0.15, TmIV absent. Tibial spine formula: 2-2-2-2. Carapace yellowish-brown. Sternum dark brown. Abdomen with greenish gray dorsal spots (Fig. 12A, B).

Palp (Fig. 10). Patella with long dorsal bristle. Tibia unmodified. Cymbium with hook-shaped proximal apophysis (PCA) pointing retrolaterally. Paracymbium (P) bifurcate with three branches: proximally short branch, medianly robust branch with round lateral branch and distal branch. Pit hook (PH) on stout distal part of suprategulum (SPT) extremely reduced to small outgrowth. Embolic division (Fig. 16G, I): anterior part of radix (APR) hook-shaped; sperm duct inside the radix (R) inconspicuous with Fickert's gland (FG); pseudolamella (PL) strongly sclerotized and lamellar extension (LE) absent. Anterior terminal apophysis (ATA) extending out handle-shaped tip pointing anterodorsally; median terminal apophysis (MTA) membranous with serrated margin; posterior terminal apophysis (PTA) rectangular and strongly sclerotized. Embolus (E) with conical embolus proper (EP), sclerotized thumb (TH), and hooked apex (AX). Median membrane (MM) with large chitinized basal part (CPM).

Female (*paratype*). Total length: 1.86, carapace 0.95 long, 0.80 wide, abdomen 0.94 long, 1.33 wide. Eye inter-distances and diameters: AME 0.04, AME-AME 0.02, ALE 0.09, AME-ALE 0.05, PME 0.08, PME-PME 0.05, PLE 0.08, and PME-PLE 0.04. Sternum 0.60 long, 0.56 wide. Clypeus 0.10 high. Chelicerae promargin with 3 teeth, retromargin with 5 teeth. Length of legs: I 5.37 (1.48, 0.33, 1.44, 1.28, 0.84), II 4.79 (1.33, 0.31, 1.22, 1.13, 0.80), III 3.70 (1.10, 0.26, 0.88, 0.86, 0.60), IV 4.69 (1.42, 0.27, 1.19, 1.11, 0.70). Leg formula: I-II-IV-III. TmI 0.17, TmIV absent. Tibial spine formula: 2-2-2-2. Coloration generally as in male (Fig. 12C, D).

Epigyne (Fig. 11). Basal part of scape (BS) sparsely clothed with long curved hairs, turned under basal part forming large circle. Posterior part of posterior median plate (PMP) curved. Distal part of scape (DPS) T-shaped, laterally directed lateral lobes (LL) extending out of either side in ventral view. Spermathecae (S) S-shaped.

Distribution. China (Sichuan, type locality; Fig. 1).

Bifurcia xiaojin sp. nov.

https://zoobank.org/7136AE47-587C-47F6-9951-588B3337E324

Figs 13–15, 16H, J

Type material. ***Holotype*** ♂ (IZCAS-Ar44934) and ***paratypes*** 2♂3♀ (IZCAS-Ar44935–39), Changpinggou (31°0.29'N, 102°51.16'E), Siguniangshan National Scenic Area, Siguniangshan Town, Xiaojin County, Aba Tibetan and Qiang Autonomous Prefecture, **Sichuan**, **China**, 01/08/2004, Lihong Tu leg.

Etymology. The specific name refers to the type locality; noun in apposition.

Diagnosis. The new species resembles *B. kangding* sp. nov. with similar paracymbium (P) and epigyne (Figs 13B, 14A), but can be distinguished by embolus thumb (TH) with spinous end (Figs 13C, 16H vs. dentate, Figs 2C, 16A), by chitinized basal part of median membrane (CPM) finger-shaped (Fig. 16H vs. pointed, Fig. 16A), and by spermathecae (S) close to each other (Fig. 14C vs. widely separated, Fig. 3C).

Description. Male (*holotype*). Total length: 2.12, carapace 1.01 long, 0.99 wide, abdomen 1.11 long, 0.81 wide. Eye inter-distances and diameters: AME 0.05, AME-AME 0.02, ALE 0.06, AME-ALE 0.08, PME 0.06, PME-PME 0.06, PLE 0.07, and PME-PLE 0.08. Sternum 0.55 long, 0.53 wide. Clypeus 0.15 high. Chelicerae promargin with 2 teeth, retromargin with 1 tooth. Length of legs: I 5.49 (1.45, 0.31, 1.46, 1.38, 0.89), II 4.51 (1.22, 0.28, 1.17, 1.10, 0.74), III 3.29 (0.94, 0.25, 0.75, 0.77, 0.58), IV 4.34 (1.27, 0.27, 1.06, 1.02, 0.72). Leg formula: I-II-IV-III. TmI 0.17, TmIV absent. Tibial spine formula: 2-2-2-2. Carapace brown. Sternum dark brown. Abdomen with greenish gray dorsal spots (Fig. 15A, B).

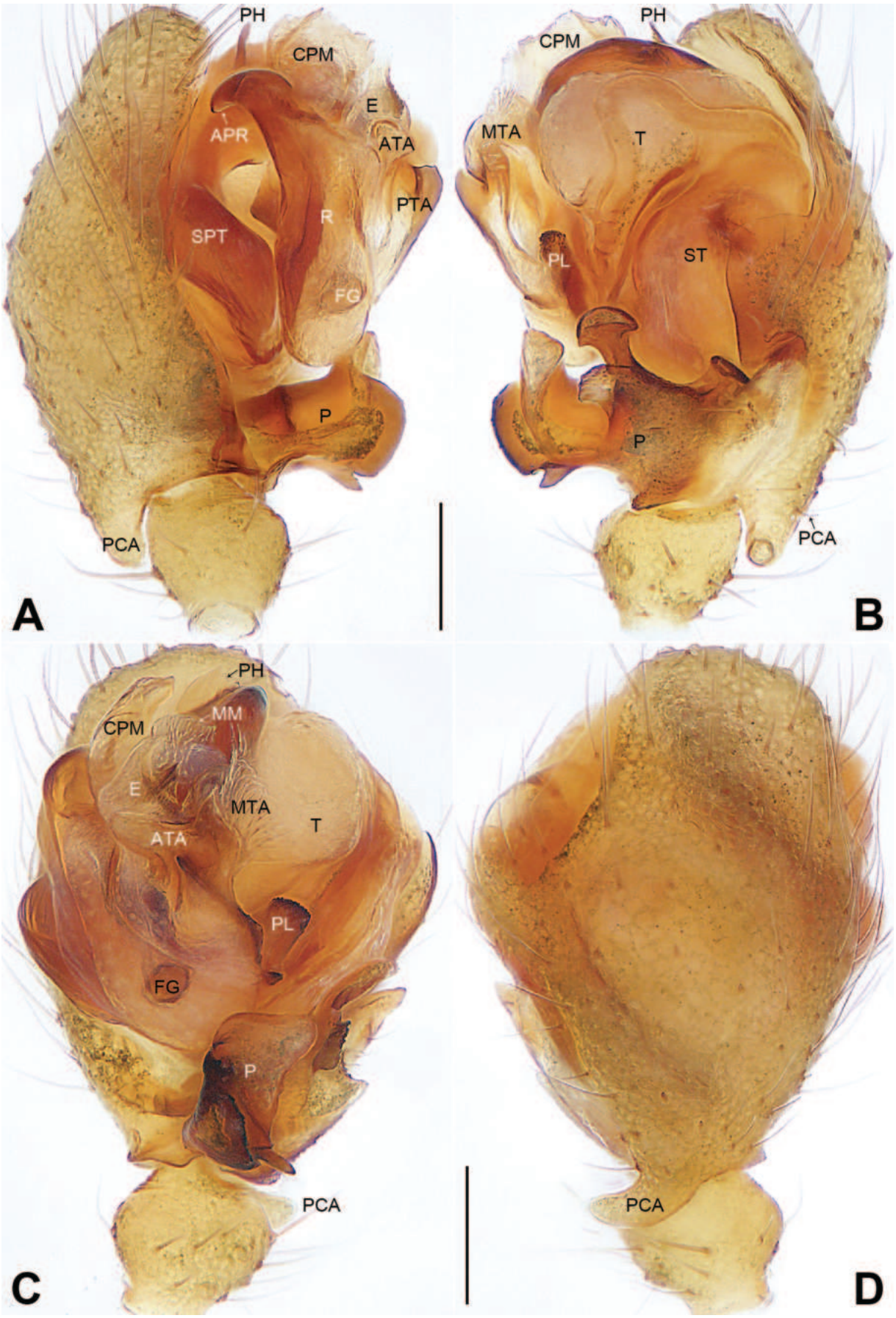

Figure 10. *Bifurcia shuangqiao* sp. nov., holotype male palp: **A.** Prolateral view; **B.** Retrolateral view; **C.** Ventral view; **D.** Dorsal view. Scale bars: 0.10 mm (**A–D**).

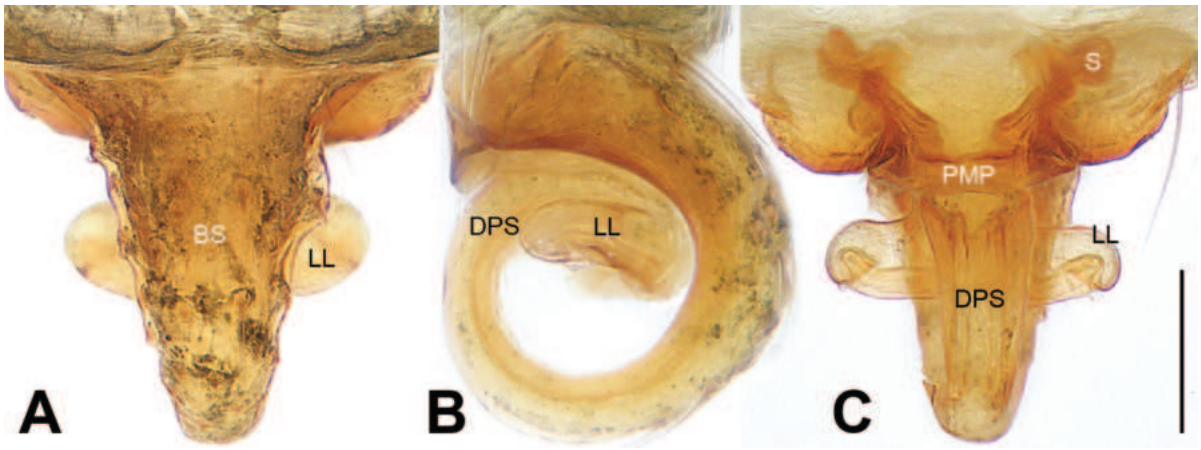

Figure 11. *Bifurcia shuangqiao* sp. nov., paratype female epigyne: **A.** Ventral view; **B.** Lateral view; **C.** Dorsal view. Scale bar: 0.10 mm (**A–C**).

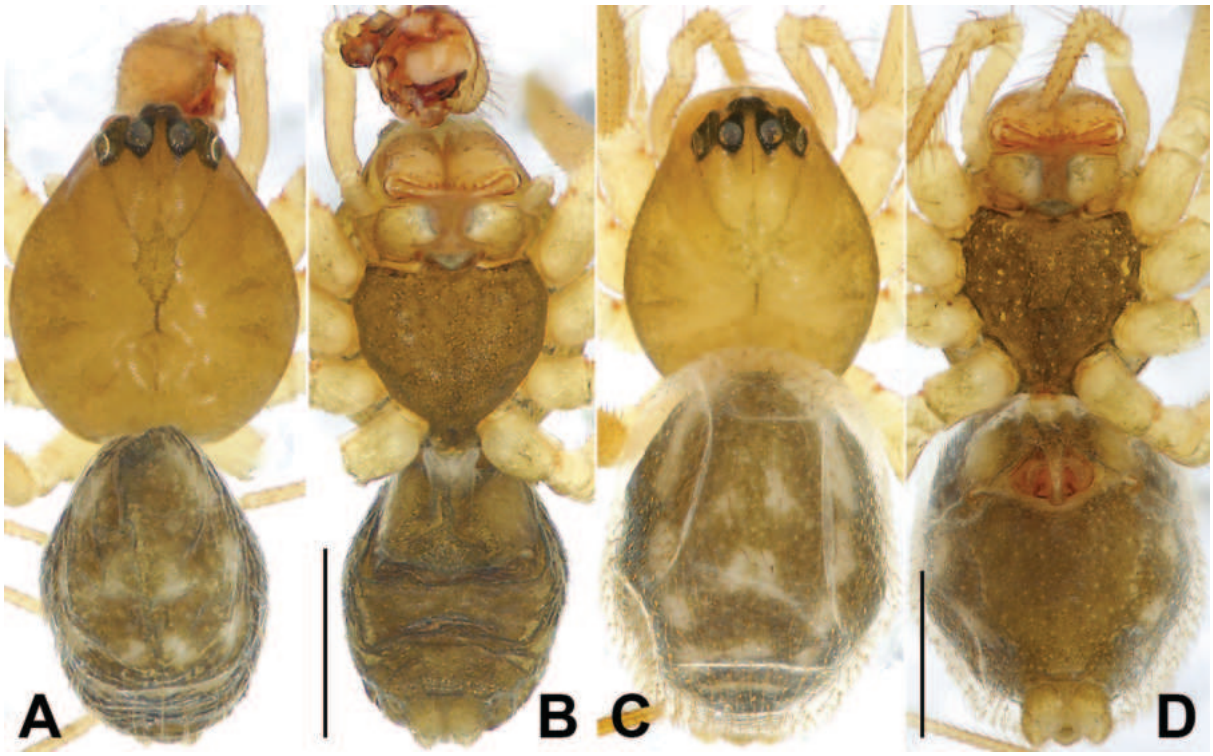

Figure 12. *Bifurcia shuangqiao* sp. nov., holotype male (**A, B**) and paratype female (**C, D**) habitus: **A, C.** Dorsal view; **B, D.** Ventral view. Scale bars: 0.50 mm (**A–D**).

Palp (Fig. 13). Patella with long dorsal bristle. Tibia unmodified. Cymbium with hook-shaped proximal apophysis (PCA) pointing retrolaterally. Paracymbium (P) bifurcate with three curved branches. Pit hook (PH) on stout distal part of suprategulum (SPT) extremely reduced to small outgrowth. Embolic division (Fig. 16H, J): anterior part of radix (APR) hook-shaped; sperm duct inside the radix (R) inconspicuous with Fickert's gland (FG); pseudolamella (PL) strongly sclerotized, with distally angular end and lamellar extension (LE) absent. Anterior terminal apophysis (ATA) pointing anterodorsally; median terminal apophysis (MTA) membranous with four branches; posterior terminal apophysis (PTA) serrated. Embolus (E) with conical embolus proper (EP), short apex (AX), and thumb (TH) with a long thorn. Median membrane (MM) leaf-shaped with finger-shaped chitinized basal part (CPM).

Female (*paratype*). Total length: 2.22, carapace 1.04 long, 0.86 wide, abdomen 1.20 long, 0.92 wide. Eye inter-distances and diameters: AME 0.06, AME-AME 0.03, ALE 0.09, AME-ALE 0.06, PME 0.07, PME-PME 0.07, PLE 0.09, and PME-PLE 0.06. Sternum 0.58 long, 0.55 wide. Clypeus 0.15 high. Chelicerae promargin with 3 teeth, retromargin with 5 teeth. Length of legs: I 5.95 (1.60, 0.39, 1.58, 1.42, 0.96), II 4.93 (1.36, 0.33, 1.29, 1.17, 0.78), III 3.67 (1.09, 0.28, 0.84, 0.87, 0.59), IV 4.68 (1.45, 0.28, 1.11, 1.14, 0.70). Leg formula: I-II-IV-III. TmI 0.21, TmIV absent. Tibial spine formula: 2-2-2-2. Carapace yellowish-brown. Coloration generally as in male (Fig. 15C, D).

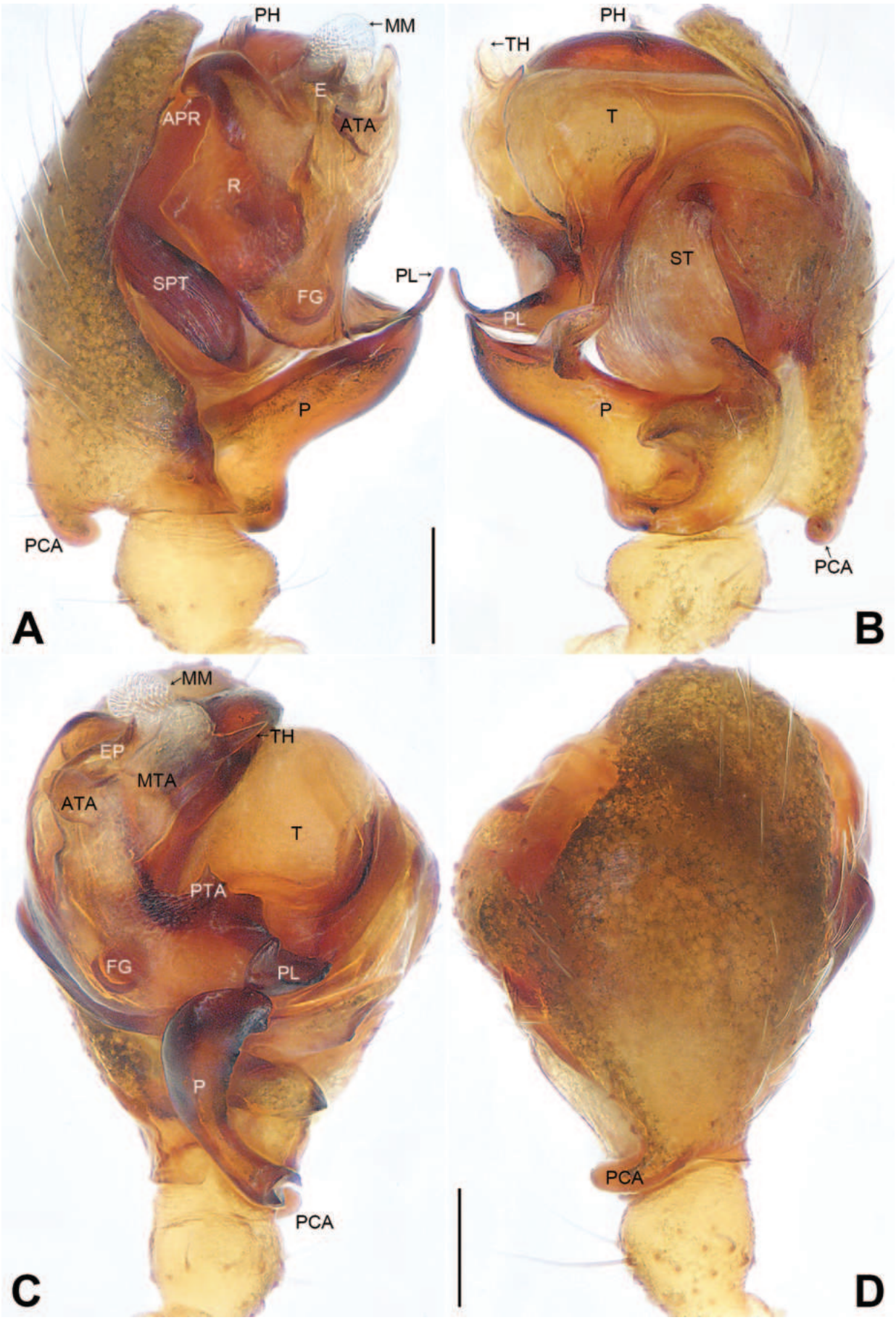

Figure 13. *Bifurcia xiaojin* sp. nov., holotype male palp: **A.** Prolateral view; **B.** Retrolateral view; **C.** Ventral view; **D.** Dorsal view. Scale bars: 0.10 mm (**A–D**).

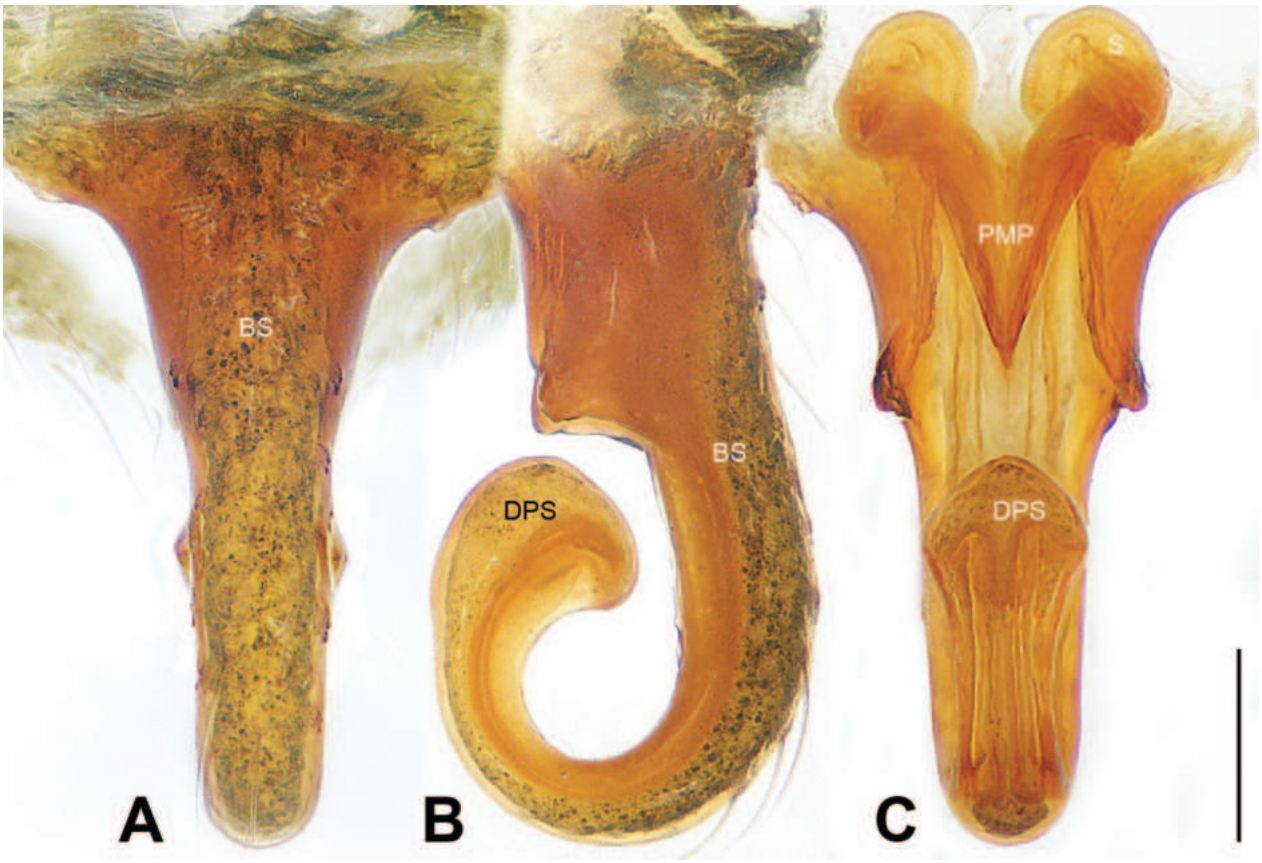

Figure 14. *Bifurcia xiaojin* sp. nov., paratype female epigyne: **A.** Ventral view; **B.** Lateral view; **C.** Dorsal view. Scale bar: 0.10 mm (**A–C**).

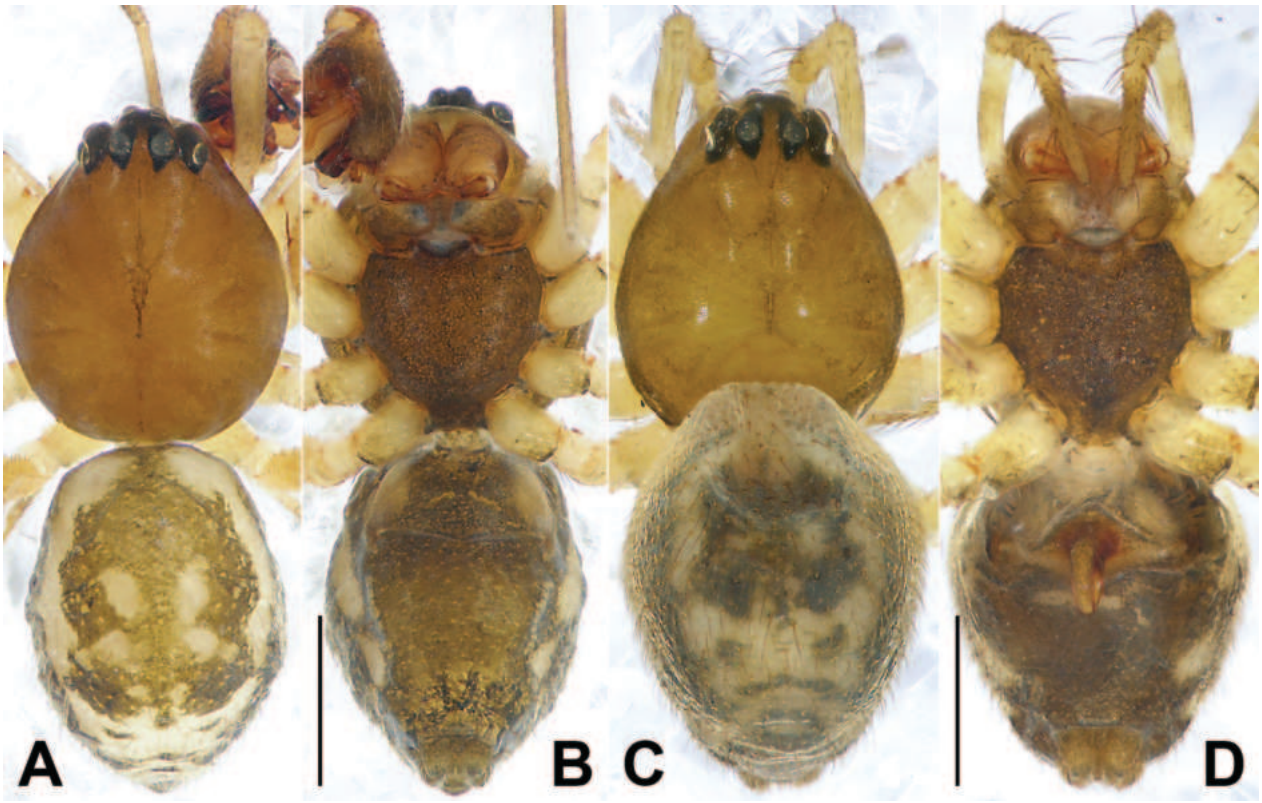

Figure 15. *Bifurcia xiaojin* sp. nov., holotype male (**A, B**) and paratype female (**C, D**) habitus: **A, C.** Dorsal view; **B, D.** Ventral view. Scale bars: 0.50 mm (**A–D**).

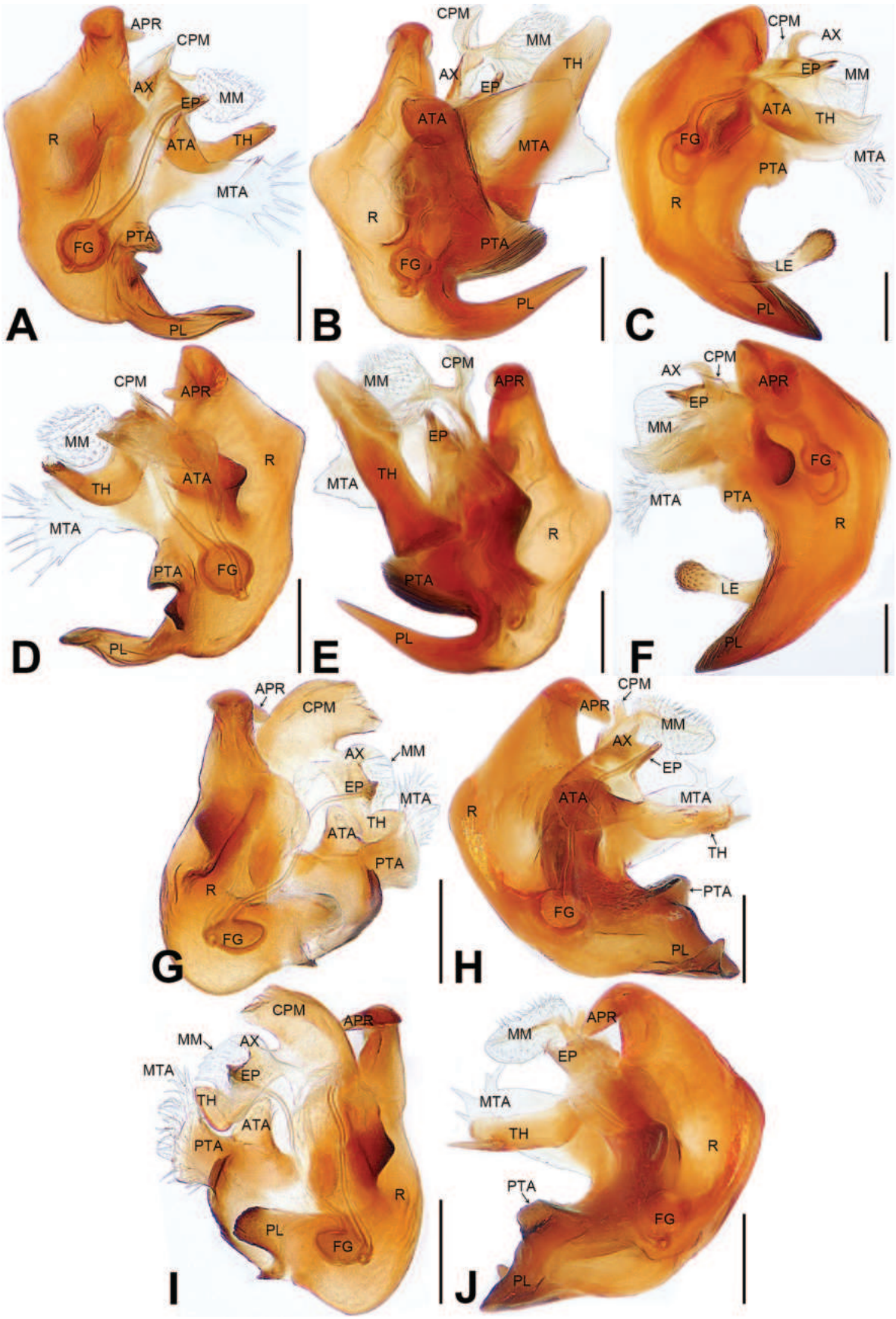

Figure 16. *Bifurcia* spp., embolic division: **A, D.** *B. kangding* sp. nov.; **B, E.** *B. labahe* sp. nov.; **C, F.** *B. luding* sp. nov.; **G, I.** *B. shuangqiao* sp. nov.; **H, J.** *B. xiaojin* sp. nov.; **A–C, G, H.** Prolateral view; **D–F, I, J.** Retrolateral view. Scale bars: 0.10 mm (**A–J**).

Epigyne (Fig. 14). Basal part of scape (BS) long and sparsely clothed with long, curved hairs. Posterior part of posterior median plate (PMP) M-shaped. Distal part of scape (DPS) forming a circle with basal part of scape together. Spermathecae (S) round.

Distribution. China (Sichuan, type locality; Fig. 1).

Acknowledgements

The manuscript has greatly benefited from the comments provided by Danilo Harms, Mikhail M. Omelko, and an anonymous reviewer. We thank Joseph KH Koh for language editing and Lihong Tu for her contribution to the collection of specimens. This study is supported by the Science and Technology Fundamental Resources Investigation Program of China (2023FY100200) and the National Natural Science Foundation of China (NSFC-32170461, 31872193).

References

Arnedo MA, Hormiga G, Scharff N (2009) Higher-level phylogenetics of linyphiid spiders (Araneae, Linyphiidae) based on morphological and molecular evidence. Cladistics 25(3): 1–32. https://doi.org/10.1111/j.1096-0031.2009.00249.x

Denis J (1949) Notes sur les érigonides. XVI. Essai sur la determination des femelles d'érigonides. Bulletin de la Société d'Histoire Naturelle de Toulouse 83: 129–158.

Hormiga G, Kulkarni S, Moreira TDS, Dimitrov D (2021) Molecular phylogeny of pimoid spiders and the limits of Linyphiidae, with a reassessment of male palpal homologies (Araneae, Pimoidae). Zootaxa 5026(1): 71–101. https://doi.org/10.11646/zootaxa.5026.1.3

Irfan M, Zhang Z, Peng X (2022a) Survey of Linyphiidae (Arachnida: Araneae) spiders from Yunnan, China. Megataxa 8(1): 1–292. https://doi.org/10.11646/megataxa.8.1.1

Irfan M, Wang L, Zhang Z (2022b) Two new species of Micronetinae Hull, 1920 spiders (Araneae: Linyphiidae) from Yintiaoling Nature Reserve, Chongqing, China. Acta Arachnologica Sinica 31(1): 17–26. https://doi.org/10.3969/j.issn.1005-9628.2022.01.003

Khmelik VV, Kozub D, Glazunov A (2005) Helicon Focus 6.7.1. https://www.heliconsoft.com/heliconsoft-products/helicon-focus/ [Accessed 10 January 2024]

Li S, Sha Y, Zhu C (1987) Notes on spiders of genera *Floronia* and *Arcuphantes* from China (Araneae, Linyphiidae). Journal of Hebei University 7: 42–48.

Locket GH, Millidge AF (1953) British Spiders. Vol. 2. Ray Society, London, 449 pp.

Murphy F, Murphy J (2000) An introduction to the spiders of South East Asia with notes on all the genera. Malaysian Nature Society, Kuala Lumpur, 388 pp.

Platnick N (2020) Spiders of the World: A Natural History. Ivy Press, London, 256 pp. https://doi.org/10.1525/9780691204987

Saaristo MI (2007) A new subfamily of linyphiid spiders based on a new genus created for the *keyserlingi*-group of the genus *Lepthyphantes* (Aranei: Linyphiidae). Arthropoda Selecta 16(1): 33–42.

Saaristo MI, Tu L, Li S (2006) A review of Chinese micronetine species (Araneae: Linyphiidae). Part I: species of ex-*Arcuphantes* and ex-*Centromerus*. Animal Biology (Leiden, Netherlands) 56(3): 383–401. https://doi.org/10.1163/157075606778441886

Song Y, Li S (2010) The spider genera *Araeoncus* Simon, 1884 and *Diplocephalus* Bertkau (1883) (Arachnida, Araneae, Linyphiidae) of China. Zoosystema 32(1): 117–137. https://doi.org/10.5252/z2010n1a6

Tanasevitch AV (2006) On some Linyphiidae of China, mainly from Taibai Shan, Qinling Mountains, Shaanxi Province (Arachnida: Araneae). Zootaxa 1325(1): 277–311. https://doi.org/10.11646/zootaxa.1325.1.18

Tanasevitch AV (2024) Linyphiid spiders of the world. Russian Academy of Science. http://old.cepl.rssi.ru/bio/tan/linyphiidae/ [accessed: 14 February 2024]

Tu L, Li S (2006) A review of *Gongylidioides* spiders (Araneae: Linyphiidae: Erigoninae) from China. Revue Suisse de Zoologie 113(1): 51–65. https://doi.org/10.5962/bhl.part.80339

Wang F, Ballesteros JA, Hormiga G, Chesters D, Zhan Y, Sun N, Zhu C, Chen W, Tu L (2015) Resolving the phylogeny of a speciose spider group, the family Linyphiidae (Araneae). Molecular Phylogenetics and Evolution 91: 135–149. https://doi.org/10.1016/j.ympev.2015.05.005

WSC (2024) World Spider Catalog, Version 25.0. Natural History Museum Bern. http://wsc.nmbe.ch [Accessed 10 March 2024]

Zoosyst. Evol. 100 (2) 2024, 721–738 | DOI 10.3897/zse.100.118051

PENSOFT

für Natur MUSEUM FÜR NATURKUNDE BERLIN

Two new species of groundwater-inhabiting amphipods belonging to the genus *Niphargus* (Arthropoda, Crustacea), from Iran

Seyyed Ahmad Mirghaffari[1], Somayeh Esmaeili-Rineh[1]

1 *Department of Biology, Faculty of Science, Razi University, Baghabrisham 6714967346, Kermanshah, Iran*

https://zoobank.org/7982E5C8-B398-4249-97D8-C9DBB82752A1

Corresponding author: Somayeh Esmaeili-Rineh (sesmaeili@razi.ac.ir)

Academic editor: Luiz F. Andrade ♦ **Received** 31 December 2023 ♦ **Accepted** 22 March 2024 ♦ **Published** 5 June 2024

Abstract

In Iran, the Elburz and Zagros Mountain ranges include substantial karst regions housing numerous aquifers and groundwater resources. *Niphargus* Schiødte, 1849, a diverse subterranean amphipod genus, inhabits Western Palearctic groundwater environments, with Iran marking the eastern limit of its distribution. This study examined specimens collected from springs along the Elburz and Zagros Mountains, revealing two distinct taxonomic units through a combination of morphological observations and molecular analyses, utilizing COI and 28S rDNA genes. *N. elburzensis* **sp. nov.** is characterized by produced epimeral plates I to III; a telson lobe with five distal, two lateral, and one mesial spine each, a rectangular shape of gnathopod II propodi with two L-setae on palmar corner and maxilla I outer plate spines with 2-2-1-1-3-0-1 denticles. *N. zagrosensis* **sp. nov.** is distinguished by a triangular shape gnathopod II propodi, pereopod VI longer than pereopod VII, maxilliped outer plate less than half of palp article 2, and uropod III distal article exceeding 80% of the proximal article. Pairwise genetic distances between *N. elburzensis* **sp. nov.** and other species ranged from 10.70% (*N. fiseri*) to 23.48% (*N. daniali*) for COI gene and 1.56% (*N. urmiensis*) to 10.98% (*N. daniali*) for 28S gene. Also, *N. zagrosensis* **sp. nov.** exhibited COI gene distances from 5.73% (*N. alisadri*) to 20.66% (*N. daniali*) and from 0.13% (*N. alisadri*) to 11.36% (*N. daniali*) for 28S gene distances. Bayesian analysis suggests that the two newly discovered species are part of the expansive local Iranian clade. These species are supported phylogenetically by separate and independent lineages, as indicated by high bootstrapping values.

Key Words

Molecular analyses, morphological characters, novel species, subterranean amphipods

Introduction

Amphipod genus *Niphargus* encompasses around 500 known species, making it one of the most diverse taxa in subterranean freshwater ecosystems. These organisms inhabit caves, springs, and subterranean streams, with only a limited number of species observed in surface waters (Fišer et al. 2009; Copilaş-Ciocianu and Boros 2016; Morhun et al. 2022; Marin and Palatov 2023). The diversity of *Niphargus* species in subterranean freshwater ecosystems exhibits a declining trend as one moves from southern to northern parts of Europe (Väinölä et al. 2008).

The classification of the genus *Niphargus* is complex due to limited distribution, habitat inaccessibility, homoplasy, and complex morphological diversity within species (Ozkahya and Camur-Elipek 2015; Fišer et al. 2018; Stoch et al. 2020). The application of molecular techniques has significantly facilitated the identification of species boundaries, particularly in cases where morphological characteristics may be unclear (Mamaghani-Shishvan and Esmaeili-Rineh 2019; Weber and Weigand 2023). Sometimes, molecular analysis reveals the presence of multi-species while morphologically classified as a single species. Consequently, it is recommended to use a combination of morphological and molecular characteristics for species identification and delimitation within this genus (Balázs et al. 2023; Weber and Weigand 2023).

Iran represents the eastern boundary of *Niphargus* range. Within this region, most of the species belong to a distinct clade that diverged from their European counterparts 11–9 million years ago (Esmaeili-Rineh et al. 2015; Borko et al. 2021). To date, more than 20 species of amphipods belonging to the genus *Niphargus* have been identified in Iran, and the greatest diversity is observed in subterranean aquifers within the Zagros Mountains region (Esmaeili-Rineh et al. 2015). Approximately 10% of Iran's land area is composed of karst formations, predominantly found within the Alborz and Zagros mountain ranges; it is likely that these regions contain numerous additional species, with only a limited number discovered so far.

The present study, conducted from 2021 to 2023, encompassed sampling in various karst regions in Iran, leading to the discovery of two new species of subterranean freshwater amphipods from the Alborz and Zagros mountain ranges.

Materials and methods

Sampling area

The materials examined in this study were collected using a handnet and subsequently preserved in 70% and 96% ethanol for morphological and molecular studies, respectively. The geographic distribution of these materials is illustrated in Fig. 1. First, six samples (three for each species) were examined for morphological studies and then, one appendage was removed from each specimen for DNA analyses and the rest of the individuals were mounted on slides in Euparal® medium.

The slides were studied using a Zeiss Primostar microscope and a LABOMED Lx500 stereomicroscope. Details were photographed using an Olympus LABOMED iVu7000 camera mounted on the stereomicroscope. Measurements and counts of morphological characters were conducted using the digitized photos and the computer program PROGRES CAPTURE PRO 2.7, referring to characters and landmarks defined by Fišer et al. (2009). Illustrations were prepared in ADOBE ILLUSTRATOR CS5, using photos as background images. All specimens were deposited in the Zoological Collection of Razi University (ZCRU).

Molecular and phylogenetic analyses

The total genomic DNA was extracted from a part of an animal using Tissue Kits (GenNet Bio™, Seoul, Korea) following the manufacturer's instructions. The modified primer pair LCO1490-JJ and HCO2198-JJ (Astrin and Stüben 2008) were used to amplify a fragment of the mitochondrial COI gene. A fragment of 28S ribosomal DNA (rDNA) was amplified and sequenced following Verovnik et al. (2005) and Zakšek et al. (2007), for the forward and reverse primer, respectively.

Each 25 µl PCR mix comprised of water, 12.5 µl of Master Mix kit (Sinaclon, Iran), 0.2 µl of each primer (10 µM), and 50–100 ng of genomic DNA template. An initial denaturation step at 94 °C for 3 minutes was followed by 36 cycles of 40 seconds at 94 °C, 40 seconds at 52.5 °C and 2 min at 65 °C with a final extension step of 8 minutes at 72 °C to amplify the COI gene. Cycling parameters for the 28S rDNA gene were as follows: initial denaturation of 94 °C for 7 minutes, 35 subsequent cycles

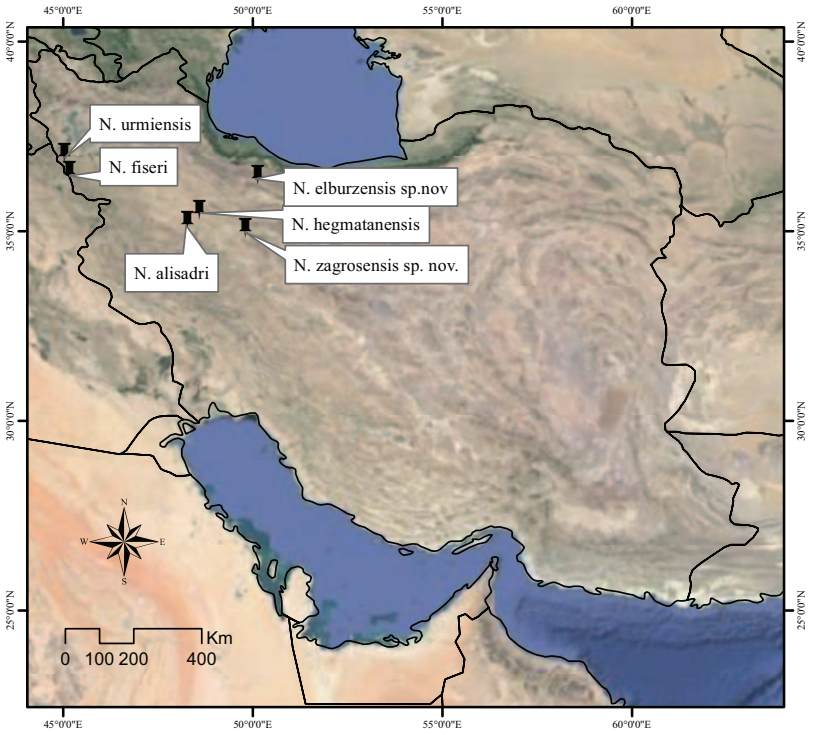

Figure 1. Map showing the type locality of *N. elburzensis* sp. nov. and *N. zagrosensis* sp. nov. along the Elburz and Zagros Mountains of Iran.

of 94 °C for 45 seconds, 55 °C for 30 seconds, 72 °C for 1 minute, and a final extension of 72 °C for 7 minutes. PCR products were purified and sequenced by Macrogen Inc. (Korea), using the primer pairs mentioned above.

The chromatograms were edited in BIOEDIT, version 7.0.5.3. The acquired sequences (with GenBank accession numbers PP496406 to PP496411 for COI and PP495485 to PP495490 for 28S) were analysed within the data set of Esmaeili-Rineh et al. (2015, 2017a) and Bargrizaneh et al. (2021), to identify the phylogenetic position of the newly collected specimens. The out-groups were selected based on previous phylogenetic analyses. The NCBI available sequences for *Niphargus krameri* Schellenberg, 1935, *Niphargus aquilex* Schiödte, 1855 and *Niphargus schellenbergi* S. Karaman, 1932 were used as outgroup (accession numbers: EF617274 and KF719253, EF617264 and JF420841, JF420854 and EU693321). All sequences were edited and aligned using CLUSTALW (Thompson et al. 1994), as implemented in the BIOEDIT, version 7.0.5.3, program sequence alignment editor (Hall 1999), using the default settings.

We conducted phylogenetic reconstruction using Bayesian inference in MRBAYES, version 3.1.2 (Ronquist and Huelsenbeck 2003). The Bayesian analyses were run for 15 million generations, employing the TIM3+G and TIM3+I+G models (selected using JMODELTEST, version 0.1.1, Posada 2008) for the 28S and COI genes, respectively. We ran four chains, with trees sampled every 1000 generations. The initial 3750 sampled trees were discarded as burn-in. We assessed tree likelihood convergence using Tracer 1.5.0 (Drummond and Rambaut 2009). A consensus tree representing the majority rule at fifty percent was computed using the remaining trees and visualized using FIGTREE v1.4.0 software. For detailed information about the analyzed species, please refer to the Electronic Supplement provided in Esmaeili-Rineh et al. (2015) and Bargrizaneh et al. (2021). To assess the genetic divergence from previously described Iranian species of *Niphargus*, we calculated genetic distances using the Kimura two-parameter (K2P) model (Kimura 1980), implemented in MEGA ver. 5 (Tamura et al. 2011).

Results

Phylogenetic position of the new species and their genetic distinctness

The results of genetic distance analysis strongly supported the species status of the *Niphargus* specimens collected in this study. Six individuals, three from Alamout and three from Kahak springs were sequenced and analyzed. The specimens from the Kahak population shared a single haplotype for a 902 base-pair segment of the 28S ribosomal DNA gene but had two haplotypes for a 513 base-pair segment of the COI gene. The specimens from the Alamout population displayed a unique haplotype for both of these genes. Herein studied specimens were nested within the Middle East clade as illustrated in Fig. 2.

For the 28S gene fragment, the pairwise K2P genetic distance among *N. zagrosensis* sp. nov. from Kahak spring and the other species ranged from a minimum of 0.13% (*N. alisadri*) to a maximum of 11.36% (*N. daniali*). The pairwise K2P genetic distance among *N. zagrosensis* sp. nov. and the other species ranged from a minimum of 5.73% (*N. alisadri*) to a maximum of 20.66% (*N. daniali*), based on COI gene fragment.

The pairwise K2P genetic distance among *N. elburzensis* sp. nov. and the other species ranged from a minimum of 1.56% (*N. urmiensis*) to a maximum of 10.98% (*N. daniali*), for the 28S gene fragment. The pairwise K2P genetic distance among *N. elburzensis* sp. nov. from Alamout spring and the other species ranged from a minimum of 10.70% (*N. fiseri*) to a maximum of 23.48% (*N. daniali*), based on COI gene fragment. The pairwise K2P genetic distance between two new species is 2.21% and 17.63% based on 28S and COI gene fragments, respectively. This indicates that the new species are well differentiated genetically. A comprehensive overview of the pairwise Kimura two-parameter genetic distances among the Iranian taxa is presented in Table 1.

Taxonomic part

Order Amphipoda Latreille, 1816
Family Niphargidae Bousfield, 1977
Genus *Niphargus* Schiödte, 1849

***Niphargus elburzensis* sp. nov.**
https://zoobank.org/DDB40AED-D8D2-42B2-A957-09F517DF2E30
Figs 3–6

Diagnosis (based on male only). Each telson lobe with five distal spines, two lateral spines and one mesial spine. The propodi of gnathopod II rectangular shape with two L-setae on palmar corner. Ventro-posterior corner of epimeral plates I to III produced. Outer plate of maxilla I with seven long spines with 2-2-1-1-3-0-1 denticles.

Etymology. The name "elburzensis" refers to Elburz Mountains in the north of Iran, where the species was found.

Material examined. *Holotype*. Iran • male; Qazvin Province, Northeastern Qazvin City, Alamout Spring; coordinates: 36°28.56'N, 50°8.52'E. Specimens collected by S.A. Mirghaffari; 25 July 2022. Holotype with two paratypes are stored under catalogue number ZCRU Amph. 1503.

Description of holotype. Total length of specimen 9 mm. Body strong. Head length 9% of body length. Lateral cephalic lobes sub-rounded (Fig. 3A).

***Antennae I–II*.** Antenna I is 0.4 times body length. Peduncular articles 1–3 progressively shorter; length of peduncular article 3 exceeds half of peduncular article 2 (ratio 1.00: 1.80). Main flagellum with 20 articles (most with short setae). Accessory flagellum bi-articulated and reaching half of article 4 of main flagellum; articles with one and two setae, respectively (Fig. 3B).

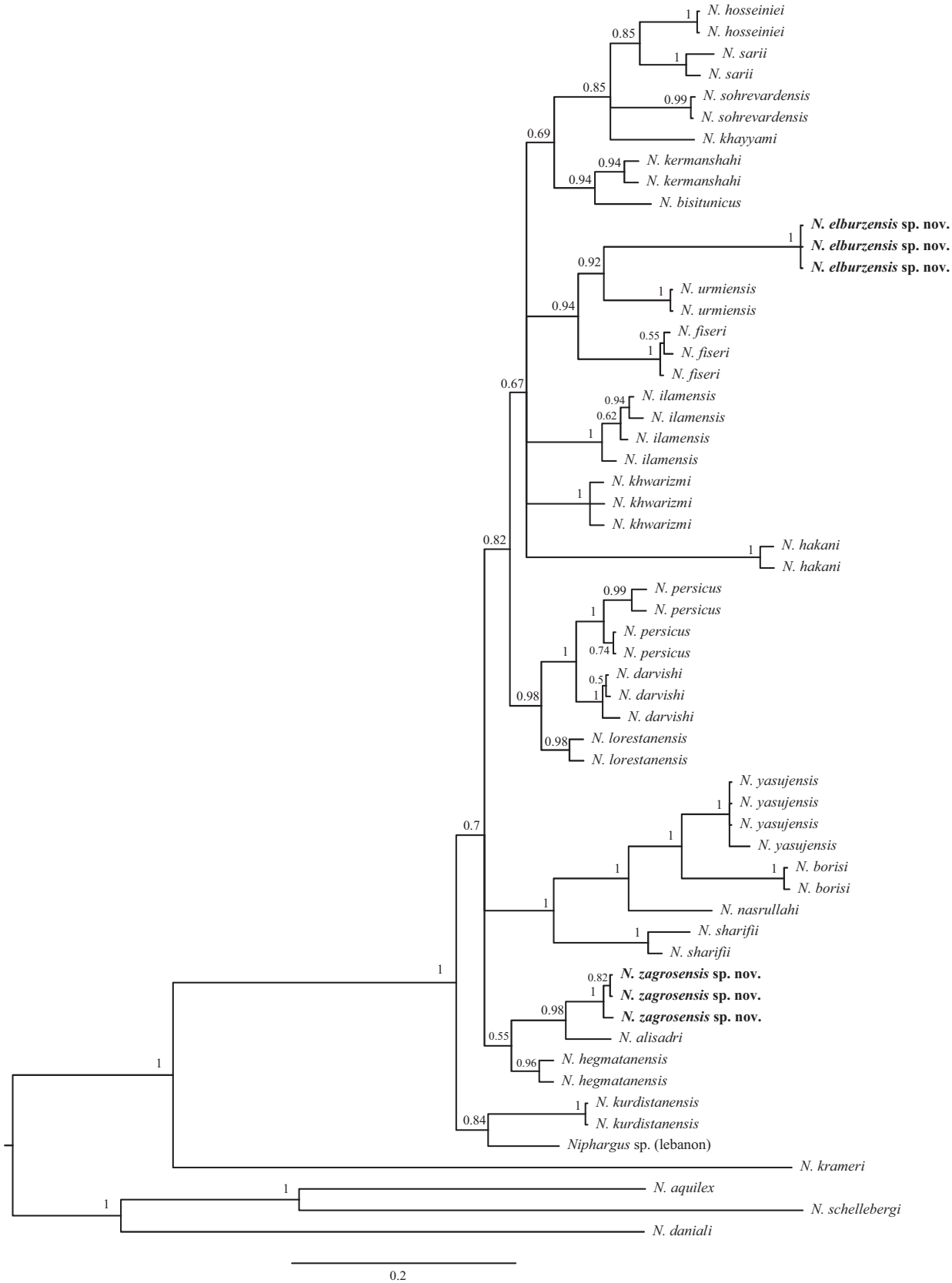

Figure 2. Bayesian consensus tree of 58 *Niphargus* Schiödte, 1849 specimens based on the 28S ribosomal DNA and COI gene sequences. Species are identified and named according to available taxonomic descriptions. Posterior probabilities are indicated on branches.

Table 1. Kimura 2-Parameter distances (K2P) comparing Iranian species with newly collected populations of the genus *Niphargus* Schiödte, 1849, based on 28S ribosomal DNA gene (below Diagonal) and mtDNA (COI) gene (above Diagonal).

	1	2	3	4	5	6	7	8	9	10	11	12	13	14	15	16	17	18	19	20	21	22	23	24
1: *N. zagrosensis* sp.nov.		0.98	17.63	5.94	9.65	17.35	20.39	11.65	11.97	11.40	11.90	12.15	11.39	11.19	14.66	11.45	14.74	12.18	11.24	14.67	N/A	N/A	N/A	N/A
2: *N. zagrosensis* sp.nov.	0.00		17.89	5.73	10.34	17.60	20.66	11.89	12.45	12.34	12.61	12.87	11.62	11.66	15.15	11.69	14.99	12.66	11.72	14.92	N/A	N/A	N/A	N/A
3: *N. elburzensis* sp.nov.	2.21	2.21		15.60	13.72	16.06	23.48	13.21	10.70	16.81	14.61	13.91	15.80	14.61	17.28	13.44	15.59	18.67	10.91	17.59	N/A	N/A	N/A	N/A
4: *N. alisadri*	0.13	0.13	2.35		11.03	16.88	20.91	12.35	12.16	11.9	13.08	12.38	12.1	12.36	15.41	12.36	15.76	14.15	12.15	15.93	N/A	N/A	N/A	N/A
5: *N. bisitunicus*	1.03	1.03	2.21	1.15		14.7	21.67	10.49	10.72	10.51	11.16	11.16	12.07	12.8	14.9	8.7	14.71	13.6	9.8	13.5	N/A	N/A	N/A	N/A
6: *N. borisi*	2.33	2.33	3.41	2.17	2.7		23.23	13.19	14.12	17.07	15.34	15.82	14.88	14.37	10.04	13.9	12.76	17.86	13.91	7.38	N/A	N/A	N/A	N/A
7: *N. daniali*	11.36	11.36	10.98	11.2	11.67	11.49		17.12	19.62	22.18	21.96	19.89	19.87	17.06	23.05	17.82	22.18	21.7	18.59	21.93	N/A	N/A	N/A	N/A
8: *N. darvishi*	0.90	0.90	2.61	0.76	1.4	2.69	11.51		9.58	12.08	10.27	9.82	12.27	10.01	13.65	3.82	14.86	13.33	8.69	11.8	N/A	N/A	N/A	N/A
9: *N. fiseri*	1.42	1.42	1.96	2.57	2.96	4.29	11.47	3.09		12.52	12.98	11.37	11.59	11.37	12.98	10.02	13.95	13.78	7.62	15.14	N/A	N/A	N/A	N/A
10: *N. hosseiniei*	1.29	1.29	2.08	1.4	1.27	2.82	12.28	1.4	2.83		13.99	12.1	13.22	14.18	13.44	12.09	15.65	9.65	13.7	14.16	N/A	N/A	N/A	N/A
11: *N. ilamensis*	1.16	1.16	2.35	1.27	1.15	2.83	11.84	1.27	2.83	0.89		8.98	12.52	11.87	15.61	10.07	14.67	13.31	10.02	14.42	N/A	N/A	N/A	N/A
12: *N. khwarizmi*	0.90	0.90	2.21	1.02	1.15	2.56	11.99	1.27	2.83	1.14	1.02		11.61	10.52	13.43	8.95	15.85	15.53	9.13	16.09	N/A	N/A	N/A	N/A
13: *N. kurdistanensis*	0.77	0.77	2.48	0.63	1.27	2.04	11.05	1.14	2.96	1.66	1.66	1.4		9.78	13.7	11.58	14.7	15.44	12.05	14.42	N/A	N/A	N/A	N/A
14: *Niphargus* sp. (Lebanon)	0.77	0.77	2.48	0.63	1.53	2.04	11.37	1.14	2.97	1.66	1.66	1.4	0.25		15.82	9.57	15.61	16.16	9.82	14.62	N/A	N/A	N/A	N/A
15: *N. nasrullahi*	1.03	1.03	2.75	0.89	1.53	1.78	11.36	1.4	3.23	1.79	1.66	1.4	1.27	1.28		13.9	14.99	16.94	13.22	8.98	N/A	N/A	N/A	N/A
16: *N. persicus*	1.03	1.03	2.75	0.89	1.53	2.82	11.67	0.25	3.23	1.53	1.4	1.4	1.27	1.27	1.53		14.87	14.33	8.9	12.98	N/A	N/A	N/A	N/A
17: *N. sharifii*	0.77	0.77	2.48	0.63	1.02	1.78	11.05	1.14	2.96	1.53	1.4	1.15	0.76	0.76	0.76	1.27		15.71	13.7	14.48	N/A	N/A	N/A	N/A
18: *N. sohrevardensis*	0.90	0.90	2.08	1.02	0.89	2.56	12.1	1.01	2.56	0.38	0.51	0.76	1.4	1.4	1.4	1.14	1.15		14.72	16.42	N/A	N/A	N/A	N/A
19: *N. urmiensis*	2.20	2.20	1.56	2.33	2.2	3.79	11.61	2.59	2.06	2.59	2.6	2.46	2.46	2.47	2.73	2.73	2.2	2.46		13.47	N/A	N/A	N/A	N/A
20: *N. yasujensis*	1.81	1.81	3.29	1.66	2.31	1.14	11.21	2.18	4.03	2.57	2.44	2.18	1.79	1.79	1.27	2.31	1.27	2.18	3.26		N/A	N/A	N/A	N/A
21: *N. hakani*	1.68	1.68	2.22	2.43	2.56	3.88	11.76	2.95	2.83	2.56	2.43	2.3	2.83	2.83	2.83	3.09	2.56	2.17	2.2	3.35		N/A	N/A	N/A
22: *N. hegmatanensis*	0.38	0.38	2.21	0.25	1.15	1.91	11.51	0.76	2.83	1.4	1.27	1.02	0.63	0.63	0.89	0.89	0.63	1.02	2.33	1.4	2.43		N/A	N/A
23: *N. kermanshahi*	0.77	0.77	2.21	0.89	0.51	2.43	11.67	1.14	2.96	1.01	0.89	0.63	1.02	1.28	1.27	1.27	1.02	0.63	2.46	2.05	2.3	0.89	N/A	N/A
24: *N. lorestanensis*	0.51	0.51	2.48	0.38	1.27	2.56	11.36	0.38	2.7	1.27	1.15	1.15	1.02	1.02	1.27	0.5	1.02	0.89	2.46	2.05	2.83	0.63	1.02	
25: *N. sarii*	1.29	1.29	2.21	1.4	1.27	2.96	12.28	1.4	3.23	0.76	1.14	1.14	1.79	1.79	1.79	1.53	1.53	0.63	2.73	2.57	2.82	1.4	1.01	1.27

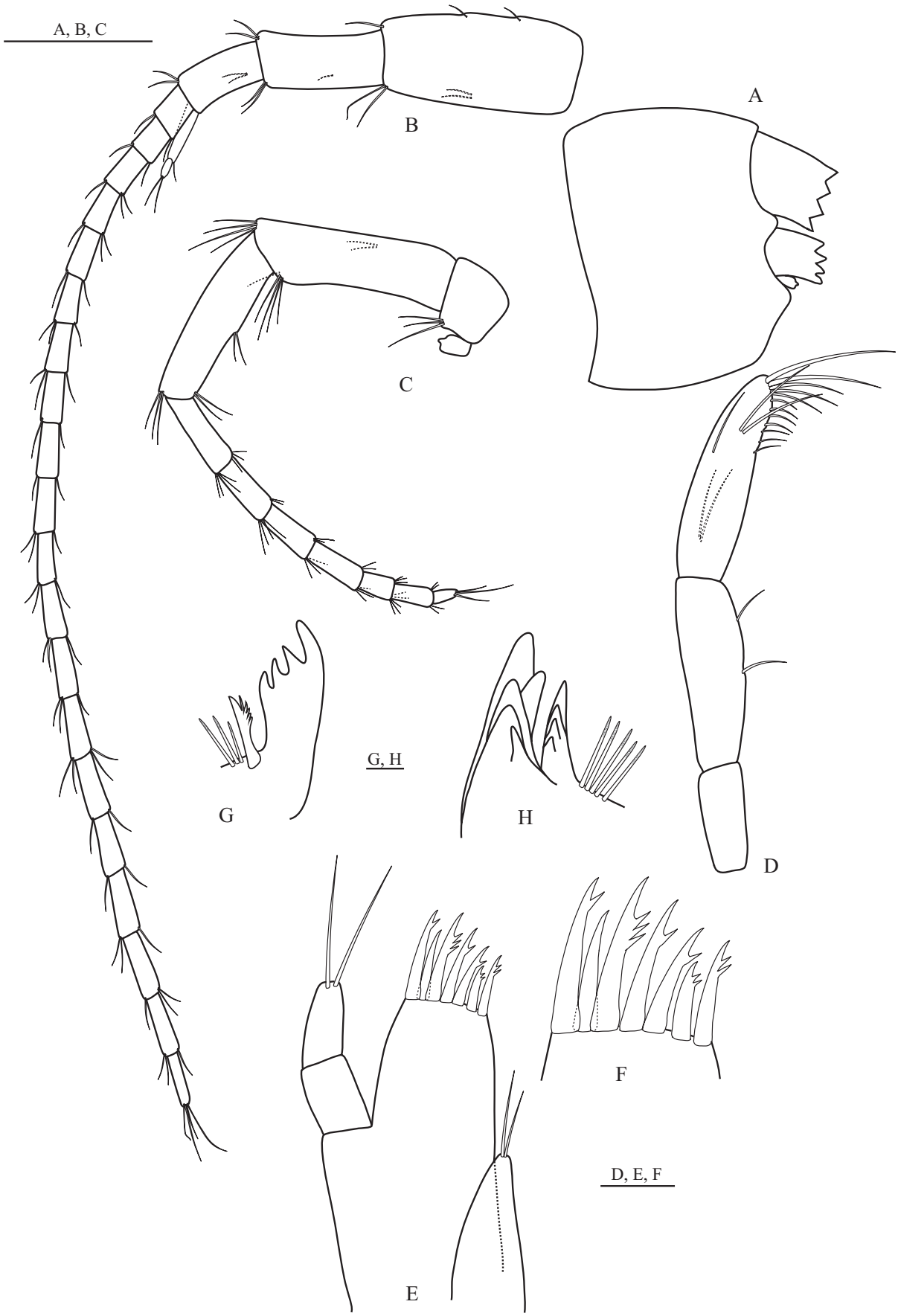

Figure 3. *Niphargus elburzensis* sp. nov., holotype, male, 9 mm (ZCRU Amph.1503). **A.** Head; **B.** Antenna I; **C.** Antenna II; **D.** Mandibular palp; **E, F.** Maxilla I; **G.** Right mandible; **H.** Left mandible. Scale bars: 0.25 mm (**G–H**); 0.5 mm (**A, D–F**); 1 mm (**B, C**).

Antenna II with flagellum formed of seven articles. Length ratio antenna I: II as 1: 0.49. Flagellum length is 0.9 times length of peduncle articles 4 + 5. Peduncular article 4 of antenna II is longer than article 5 (1.3: 1.00), peduncle articles 4 and 5, with three groups of simple setae each (Fig. 3C).

***Mouthparts*.** Labium bi-lobate; both lobes with numerous fine distal and lateral setae (Fig. 4D). Mandible: right mandible with four teeth on incisor process, lacinia mobilis pluritoothed, between pars incisiva and pars molaris a row of three setae with lateral projections (Fig. 3G). Left mandible with five teeth on incisor process, lacinia mobilis with four teeth, between pars incisiva and pars molaris a row of five setae with lateral projections (Fig. 3H). Mandibular palp articles 1:2:3 represent 20%, 37% and 43% of total palp length, respectively. Proximal article without setae; second article with two setae along ventral margin and third article with one group of two A-setae, two groups of B-setae, no C-setae, eight D-setae and four E-setae (Fig. 3D). Inner plate of maxilla I with two long apical setae, outer plate with seven long spines with 2-2-1-1-3-0-1 denticles; palp bi-articulated, slightly longer than outer lobe, with two apical setae (Fig. 3 E, F). Both plates of maxilla II with numerous long distal setae (Fig. 4C). Maxilliped with short inner plate bearing three distal spines intermixed with four distal setae and two lateral setae sub-distally; outer plate exceeding half of palp article 2, with nine spines along inner margin and three setae distally; Maxilliped palp article 3 with one group of simple setae at outer and inner margins; palp terminal article with one simple seta at outer margin, nail shorter than pedestal (Fig. 4E).

***Gnathopods*.** Coxal plate of gnathopod I shorter than gnathopod II. Coxa of gnathopod I rectangular, broader than long, anterior and ventral margins with five setae. Basis with several single setae on anterior and posterior margins; ischium and merus with one posterior group of setae. Carpus with one group of five setae anterio-distally, bulge with setae; carpus 0.58 times basis length and 0.89 times propodus length. Propodus of gnathopod I trapezoid shape and broader than long; anterior margin with five setae in one group in addition to antero-distal group of four setae. Palm slightly convex, defined by one strong long corner S-seta accompanied laterally by three L-setae with lateral projections, on inner surface of palmar corner one short sub-corner R-seta. Dactylus reaching the posterior margin of propodus, outer and inner margins of dactylus with one and two simple setae, respectively. Nail length 0.33 times total dactylus length (Fig. 4A). Coxal plate of gnathopod II of rectangular shape, longer than broad, anterio-ventral margin with five setae. Basis with single setae on anterior and posterior margins; ischium and merus with one posterior group of setae. Carpus with one group of three setae antero-distally, bulge with long setae; carpus 0.7 times basis length and 0.90 times propodus length. Propodus of gnathopod II of rectangular shape, longer than broad; anterior margin with three setae in two groups in addition to antero-distal group of four setae. Palm slightly convex, defined by one strong long corner S-seta accompanied laterally by two L-setae with lateral projections, on inner surface of palmar corner one short sub-corner R-seta. Dactylus reaching the posterior margin of propodus, outer and inner margins of dactylus with one and two setae, respectively; nail short, 0.3 times total dactylus length (Fig. 4B).

***Pereonites I–VII*.** Without setae.

***Pereopods*.** Coxal plate III rectangular, length to width ratio is 1.07: 1; antero-ventral margin with four simple setae. Coxal plate IV rectangular, antero-ventral margin with five setae, posterior concavity shallow and approximately 0.1 times coxa width. Coxal plate V–VI with large anterior lobe; Coxal plate V with three setae on anterior and posterior lobes each. Coxal plate VI with two setae on anterior lobe. Coxal plate VII with one seta on posterior margin (Fig. 5A–E).

***Pereopod III*:** IV length ratio is 1: 1.03. Dactylus III length 0.39 times propodus length, nail shorter than pedestal. Dactylus IV length 0.32 times propodus length, nail shorter than pedestal (Fig. 5A, B). Pereopods length V: VI: VII ratios as 1: 1.2: 1.36, respectively (Fig. 5C–E). Pereopod VII 0.48 times total body length. Pereopod bases V–VII with five, six and five groups of spines along anterior margins and with six, 10 and nine setae along posterior margins, respectively. Antero-ventral lobe of ischium in pereopods V–VII slightly developed. Merus and carpus in pereopods V–VII with several groups of spines and setae along anterior and posterior margins; propodus of pereopod VII longer than these in V–VI, dactyli in pereopods V–VII with one seta on outer margin, nail length of pereopod VII 0.34 times total dactylus length (Fig. 5C–E).

***Pleonites I–III*.** Each with one seta along the dorsal margin.

***Pleopods*.** Peduncle of pleopods I–III with two-hooked retinacles distally; Peduncle of pleopod III with two setae along of inner margin. Rami of pleopods I–III with five to eight articles (Fig. 6A–C).

***Urosomites I–III*.** At the base of uropod I with one strong spine; Urosomites I-II postero-dorso-laterally with one and two spines, respectively. Urosomite II with two simple setae on postero-dorso-laterally. Urosomite III without setae.

***Uropods*.** Peduncle of uropod I with six and five large spines along dorso–lateral and dorso–medial margins, respectively. Inner ramus of uropod I longer than outer ramus (ratio 1: 1.05); inner ramus with five groups of spines laterally and five spines distally; outer ramus with three groups of five spines laterally and five spines distally (Fig. 6D). Inner ramus in uropod II longer than outer, both rami with lateral and distal long spines (Fig. 6E). Uropod III normal, almost 0.2 of body length. Peduncle of uropod III with five spines on distal margin. Outer ramus bi-articulated, distal article 0.11 times proximal article. The proximal article of outer ramus bearing five and four groups of spines along inner and outer margins, respectively; distal article with setae laterally and four setae distally. Inner ramus normal, with three distal spines (Fig. 6F).

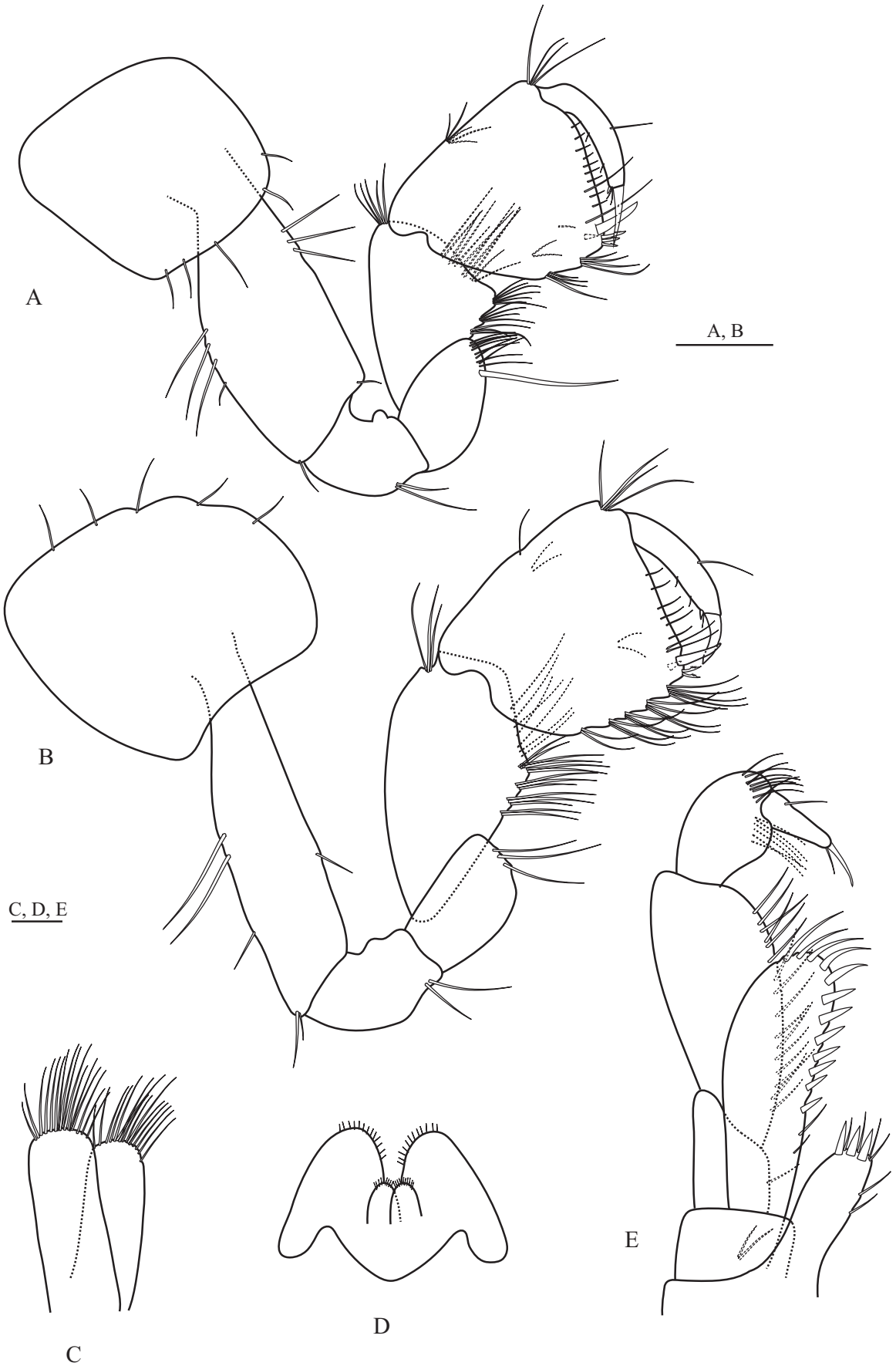

Figure 4. *Niphargus elburzensis* sp. nov., holotype, male, 9 mm (ZCRU Amph.1503). **A.** Gnathopod I; **B.** Gnathopod II; **C.** Maxilla II; **D.** Labium; **E.** Maxilliped. Scale bars: 0.5 mm (**C–E**); 1 mm (**A, B**).

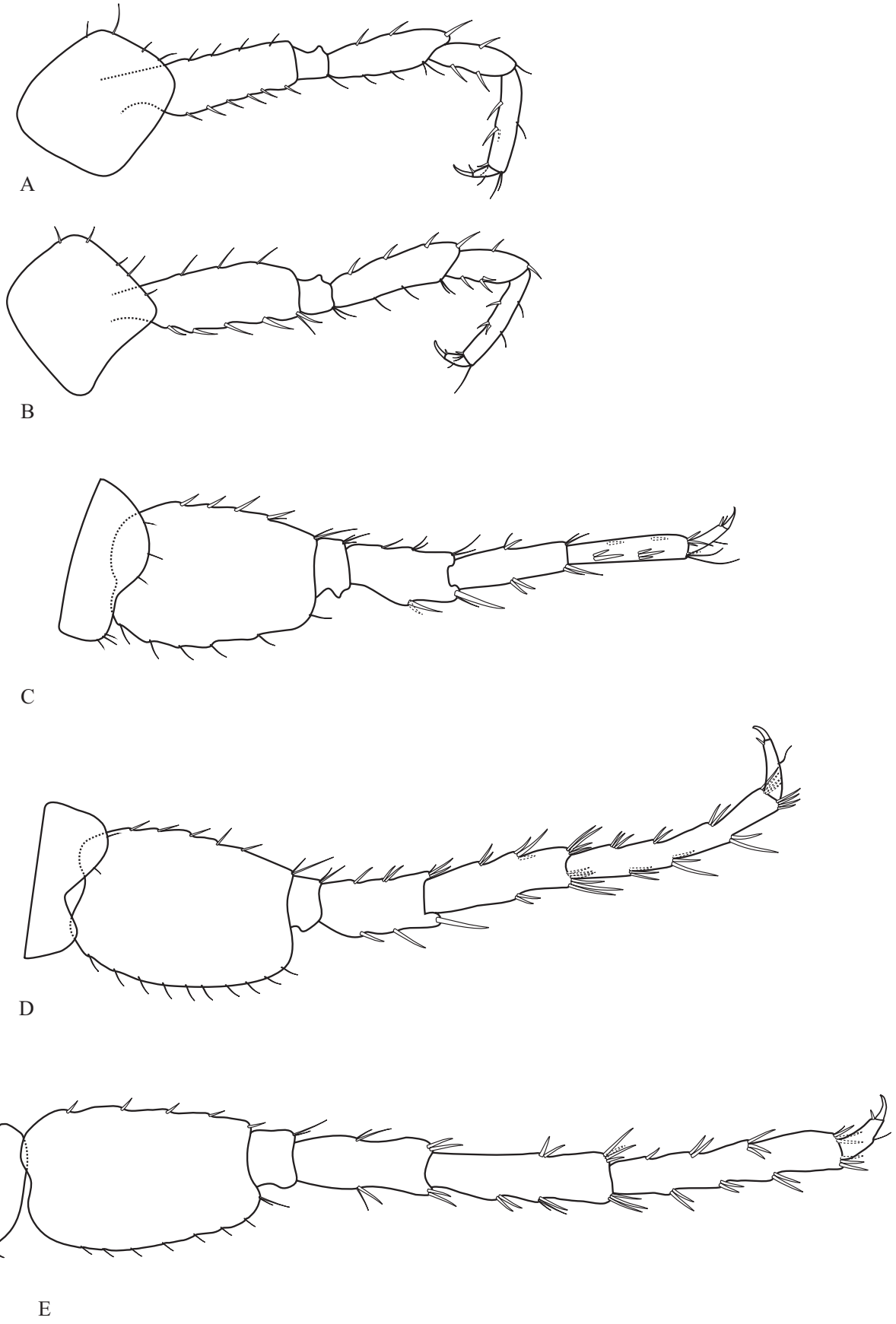

Figure 5. *Niphargus elburzensis* sp. nov., holotype, male, 9 mm (ZCRU Amph.1503). **A.** Pereopod III; **B.** Pereopod IV; **C.** Pereopod V; **D.** Pereopod VI; **E.** Pereopod VII. Scale bar: 1 mm.

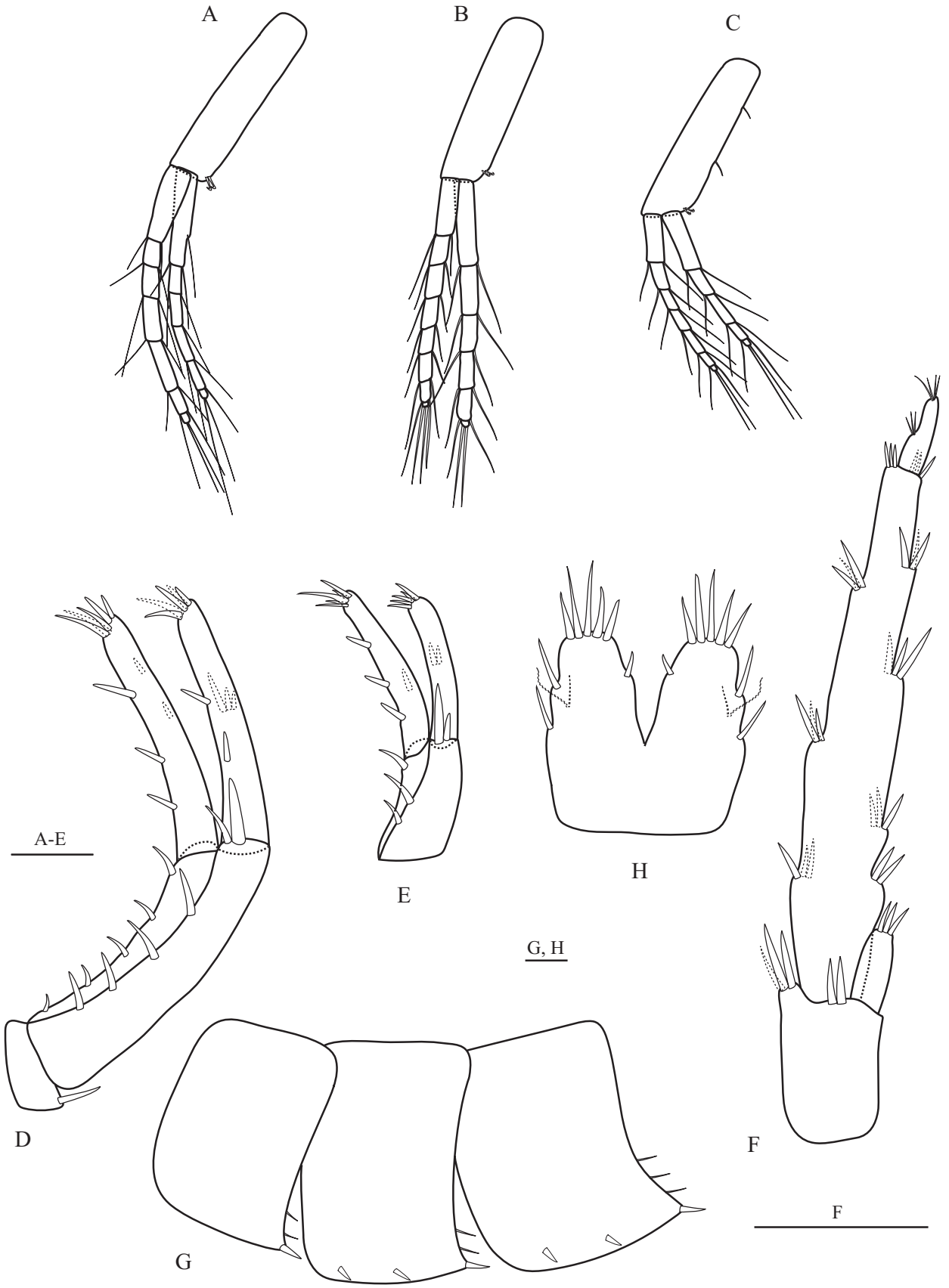

Figure 6. *Niphargus elburzensis* sp. nov., holotype, male, 9 mm (ZCRU Amph.1503). **A.** Pleopod I; **B.** Pleopod II; **C.** Pleopod III; **D.** Uropod I; **E.** Uropod II; **F.** Uropod III; **G.** Epimeral plates I–III; H. Telson. Scale bars: 0.5 mm (**G, H**); 1 mm (**A–E**); 2 mm (**F**).

***Epimeral plates I–III*.** With angular postero-ventral corners, plates I–III posteriorly with three, three and four setae and spines, respectively. Epimeral plates II–III each with two spines along of ventral margin (Fig. 6G).

***Telson*.** Telson length as long as broad; each lobe with five spines distally, with two long spines and two setae laterally, with one spine mesially (Fig. 6H).

Female. Unknown.

Genus *Niphargus* Schiödte, 1849

Niphargus zagrosensis sp.nov.

https://zoobank.org/27331B3E-2F2A-4DE4-ACA9-7EFA51D7B453

Figs 7–10

Diagnosis (based on male only). The propodi of gnathopod II triangular shape. Gnathopod II dactylus does not reach posterior margin of palm. Pereopod VI longer than pereopod VII. Maxilliped outer plate does not reach half of the posterior margin of palp article 2. Uropod III distal article exceeds more than 80% times proximal article. Outer plate of maxilla I with seven long spines with 4-2-1-2-1-1-0 denticles.

Etymology. The name "zagrosensis" refers to Zagros Mountains in the west of Iran, where the species was found.

Material examined. ***Holotype*.** Iran • male; Markazi Province, 54 km to Saveh City, Kahak Spring; coordinates 35°5.28'N, 49°49.02'E. Specimens collected by S.A. Mirghaffari; 20 July 2022. Holotype with two paratypes are stored under catalogue number ZCRU Amph. 1501.

Description of holotype. The total length of specimen 10.5 mm. Body strong and stout. Head length 10.5% of body length. Lateral cephalic lobes sub-rounded (Fig. 7A).

***Antennae I–II*.** Antennae I 0.45 times body length. Peduncular articles 1–3 progressively shorter; length of peduncular article 3 not exceeds half of peduncular article 2 (ratio 1: 0.4). Main flagellum with 23 articles (most of which with short setae); accessory flagellum biarticulated and reaching 1/3 of article 4 of main flagellum, articles with two simple setae each (Fig. 7B). Antennae II flagellum with 11 articles, approximately 0.54 as long as antenna I. Peduncular article 4 longer than article 5, with 11 and 10 groups of simple setae, respectively. Flagellum length is 0.71 peduncle article 4 + 5 (Fig. 7C).

***Mouthparts*.** Labium bi-lobate; with fine setae on tip of both lobes (Fig. 8D). Right mandible with four teeth on incisor process, lacinia mobilis pluritoothed; between pars incisiva and pars molaris a row of six setae with lateral projections (Fig. 7G). Left mandible with five teeth, lacinia mobilis with four teeth; between pars incisiva and pars molaris a row of six setae with lateral projections (Fig. 7H). Mandibular palp articles 1:2:3 represent 19%, 40% and 41% of total palp length, respectively. The proximal article has no setae, the second article with seven setae along ventral margin and the third article with one group of two A-setae, three groups of B-setae, no C-setae, 14 D-setae and five E-setae (Fig. 7D). Inner plate of maxilla I with two long distal simple setae; outer plate with seven long spines with 4-2-1-2-1-1-0 denticles; palp bi-articulated, slightly longer than the tip of outer lobe, with three long distal simple setae (Fig. 7E, F). Maxilla II bi-lobate (Fig. 8C). Both plates of maxilla II with numerous distal simple setae. Inner lobe with lateral simple setae (Fig. 7C). Maxilliped with short inner plate bearing four distal spines intermixed with six distal simple setae; outer plate less than half of the posterior margin of palp article 2, with 10 spines along inner margin and seven setae distally. Maxilliped palp article 3 with one proximal and one distal group of long simple setae at outer margin; palp terminal article with one seta at outer margin and two small setae at base of nail, nail shorter than pedestal (Fig. 8E).

***Gnathopods*.** Coxa of gnathopod I shorter than gnathopod II. Coxal plate of gnathopod I trapezoid shape, ventro-posterior margins with 12 simple setae. Basis with several setae on anterior and posterior margins; ischium and merus with one posterior group of setae each. Carpus with one group of four setae antero-distally, a bulge with long simple setae; carpus 0.7 times basis length and 0.75 times propodus length. Propodus of gnathopod I rectangular shape; anterior margin with one group of five setae in addition to antero-distal group of five simple setae. Palm slightly convex, defined by one strong long corner S-seta accompanied laterally by three L-setae with lateral projections, on inner surface of palmar corner one short sub-corner R-seta. Dactylus reaching the posterior margin of propodus, outer and inner margins of dactylus with a row of two and three simple setae, respectively; nail short, 0.33 of total dactylus length (Fig. 8A).

Coxal plate of gnathopod II rectangular shape, with 13 setae along antero-ventro-posterior margins. Basis with single setae along anterior margin and with setae in group along posterior margin; ischium and merus with one posterior group of setae each. Carpus 0.4 times basis length and 0.59 times propodus length. Carpus with one group of four setae antero-distally. Propodus of gnathopod II larger than gnathopod I, triangle shape and broader than long; anterior margin with three setae in one group in addition to antero-distal group of three simple setae. Palm slightly convex, defined by one strong long corner S-seta accompanied laterally by two L-setae with lateral projections, on inner surface of palmar corner one short sub-corner R-seta. Dactylus does not reach the posterior margin of propodus, outer and inner margins of dactylus with two and three simple setae, respectively. Nail length 0.29 times total dactylus length (Fig. 8B).

***Pereonites I–VII*.** Pereonites II and IV with one seta each; others pereonites without setae.

***Pereopods*.** Coxal plate III rectangular shape, length to width ratio as 1.2: 1; antero-ventral margin with nine simple setae. Coxal plate IV rectangular shape, length to width ratio as 1: 1.02, antero-ventro-posterior margins with 12 simple setae, posterior concavity shallow and approximately 0.1 of coxa width. Coxal plate V with large anterior lobe, with five and three simple setae on anterior and posterior lobes, respectively. Coxal plate VI with anterior lobe, with four and three simple setae on anterior and posterior lobes, respectively. Coxal plate VII with one simple seta on posterior margin (Fig. 9A–E).

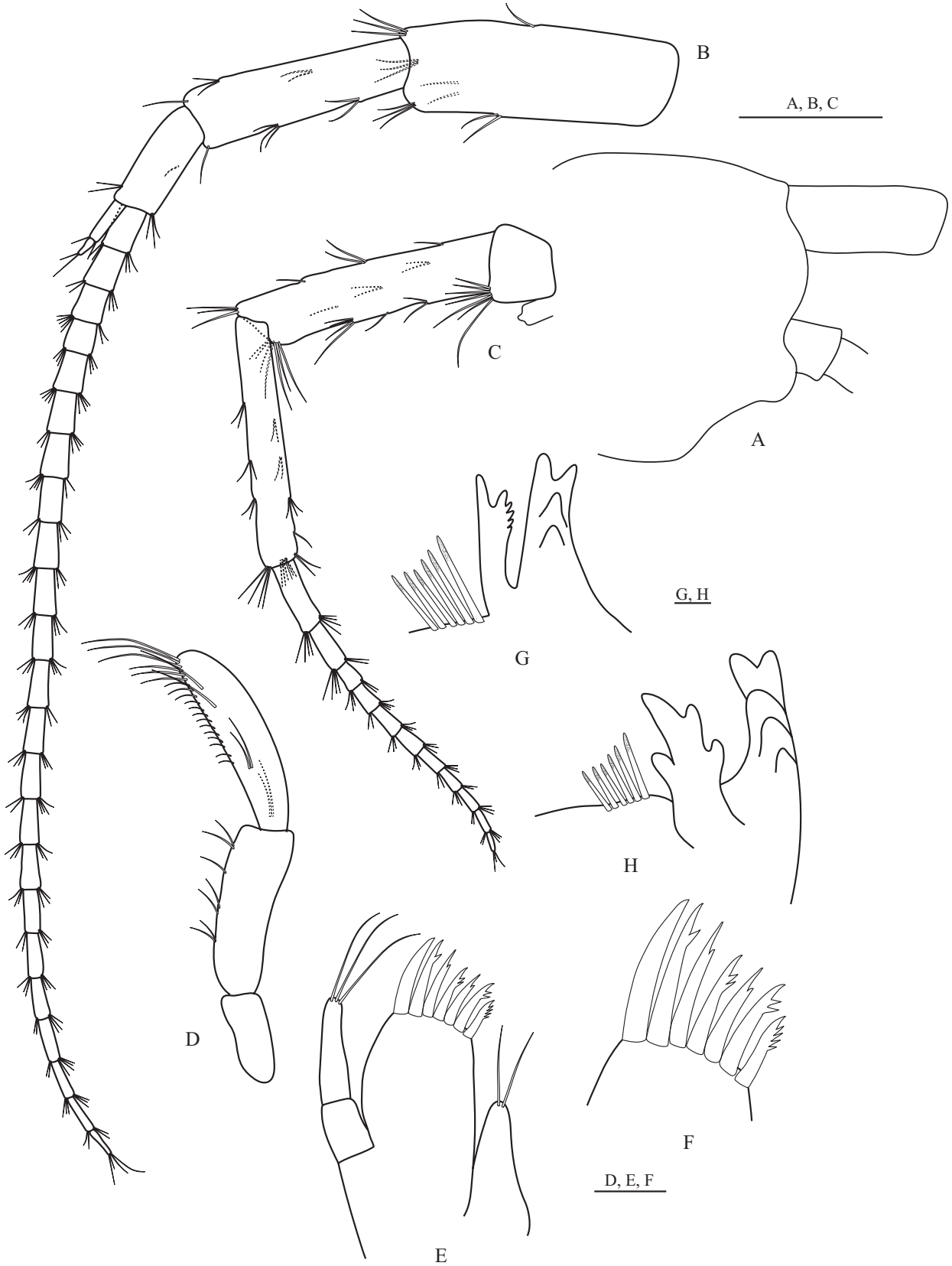

Figure 7. *Niphargus zagrosensis* sp. nov., holotype, male, 10.5 mm (ZCRU Amph.1501). **A.** Head; **B.** Antenna I; **C.** Antenna II; **D.** Mandibular palp; **E, F.** Maxilla I. **G.** Right mandible. **H.** Left mandible. Scale bars: 0.25 mm (**G–H**); 0.5 mm (**A, D–F**); 1 mm (**B, C**).

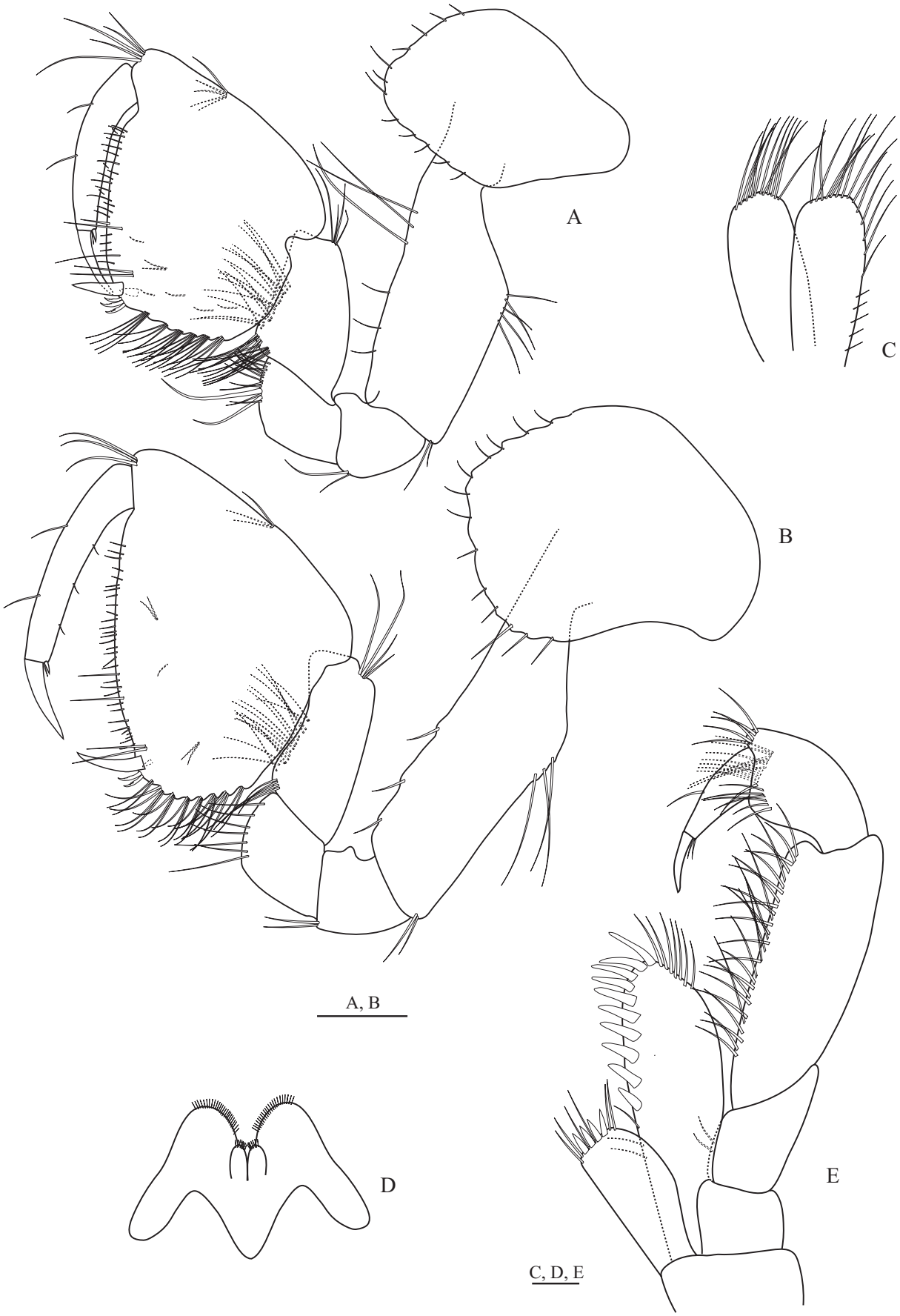

Figure 8. *Niphargus zagrosensis* sp. nov., holotype, male, 10.5 mm (ZCRU Amph.1501). **A.** Gnathopod I; **B.** Gnathopod II; **C.** Maxilla II; **D.** Labium; **E.** Maxilliped. Scale bars: 0.5 mm (**C–E**); 1 mm (**A, B**).

Pereopods length III: IV ratio is 1: 0.94. Dactylus III length 0.40 times propodus length, nail shorter than pedestal (Fig. 9A). Dactylus IV length 0.43 times propodus length, nail shorter than pedestal (Fig. 9B). Dactyli of pereopods III–IV with one seta on inner margin (Fig. 9A, B).

Pereopods length V: VI: VII ratios is 1: 1.28: 1.25, respectively. Pereopod VII 0.48 times total body length. Pereopod bases V–VII each with seven, seven and six groups of spines along anterior margins and 13, 13 and 14 simple setae along posterior margin, respectively. Ischium, merus and carpus in pereopods V–VII with several groups of spines and simple setae along anterior and posterior margins; propodus of pereopod VI longer than these in V and VII, dactyli of pereopods V–VII with one spine at the base of nail on inner margin, nail length of pereopod VII 0.33 times total dactylus length (Fig. 9A–E).

Epimeral plates I–III. With angular postero-ventral corner, anterior and ventral margins convex; postero-ventral corners of plates I-III with three, four and five spines and setae, respectively. Epimeral plates II–III with three and four spines along of ventral margin, respectively (Fig. 10G).

Pleonites I–III. With one simple seta along the dorsal margin each.

Pleopods I–III. Peduncle of pleopods I–III with two-hooked retinacles distally; peduncle of pleopod III with three simple setae along of inner margin. Rami of pleopods I–III with nine to 14 articles (Fig. 10A–C).

Urosomites I–III. At the base of uropod I with one strong spine. Urosomites I and II with one and three spines on postero-distally, respectively. Urosomite III without setae.

Uropods I–III. Peduncle of uropod I with seven and four large spines along dorso-lateral and dorso-medial margins, respectively. Inner ramus of uropod I longer than outer ramus (ratio 1: 1.06). Inner ramus with five groups of spines laterally and five spines distally; outer ramus with four groups of six spines laterally and five spines distally (Fig. 10D). Inner ramus in uropod II longer than outer, both rami with lateral and distal long spines (Fig. 10E). Uropod III long, almost 0.44 times body length. Peduncle of uropod III with four spines on distal margin. Outer ramus bi-articulated, distal article 87% times proximal article. The proximal article of outer ramus bearing five and four groups of spines along of outer and inner margins, respectively; distal article with several groups of simple setae laterally and four simple setae distally. Inner ramus short, with two distal spines (Fig. 10F).

Telson. Telson longer than broad; lobes slightly narrowing; each lobe with four spines apically, with two spines and two simple setae laterally (Fig. 10H).

Female. Unknown.

Intraspecific variation

Intraspecific variabilities of each species were investigated by three individuals. In *N. elburzensis*, only a difference in the number of L-setae in gnathopod I (ranging between 2–3) was found among individuals. In *N. zagrosensis* was observed a greater number of intraspecific differences. These differences included the number of apical spines in each telson lobe (between 3–4), the ratio of antennal length II to I, and the ratio of segments 4 + 5 to the flagellum length in antenna II. It's important to note that the diagnostic characteristics of each species are based on the fixed characters, which exhibit a consistent state for all individuals of a species.

Discussion

In this research, two populations of the genus *Niphargus* were collected from Iran and examined based on morphological and molecular characteristics. DNA sequences support the species status of two new species, *N. elburzensis* sp. nov. and *N. zagrosensis* sp. nov. The Bayesian analysis revealed that the two newly identified species are phylogenetically separate and independent lineages, as indicated by high bootstrap values.

Niphargus elburzensis sp. nov. is characterized by two clearly visible characters. The first one is the presence of five distal, two lateral and one mesial spines on each telson lobe. Although the presence of a mesial spine on the telson lobe is common among European species (for example *N. podogoricensis* Karaman, 1950; *N. vinodolensis* Fišer, Sket & Stoch, 2006), this trait was observed only in *N. arasbaranensis* (in press) and *N. elburzensis* between Iranian species. However, *N. elburzensis* is distinguished from *N. arasbaranensis* by the presence of five distal spines on each telson lobe (compared to four distal spines in *N. arasbaranensis*) and the greater length of the palpus to the tip of the outer lobe in maxilla I (compared to equal length of the palpus and outer plate in *N. arasbaranensis*). The second distinguishing characteristic involves the presence of two setae along the inner margin of pleopod III. We found this trait in three species in Iran. However, neither *N. kurdistanensis*, *N. urmiensis* nor *N. fiseri* share produced epimeral plates (Mamaghani-Shishvan et al. 2017; Mamaghani-Shishvan and Esmaeili-Rineh 2019).

Although *N. elburzensis* is genetically close to *N. fiseri* and *N. urmiensis*, it differs from these two species by several characteristics. These differences include a long palpus in maxilla I, which passes from the tip of the outer lobe, in contrast to *N. urmiensis* and *N. fiseri* exhibit equal lengths of the palpus and outer plate. Moreover, *N. elburzensis* exhibit two and three L-setae on palmar corner of both gnathopods, whereas *N. urmiensis* and *N. fiseri* each bear only one L-seta on palmar corner of their gnathopods. Additionally, *N. elburzensis* is distinguished by the presence of five distal spines on each telson lobe, while *N. urmiensis* and *N. fiseri* each have three distal spines on each telson lobe. *N. elburzensis* and its sister taxa *N. urmiensis* and *N. fiseri* inhabit the shallow subterranean habitats. Geographic distances between the new species and its sister taxa are 462–448 km, respectively.

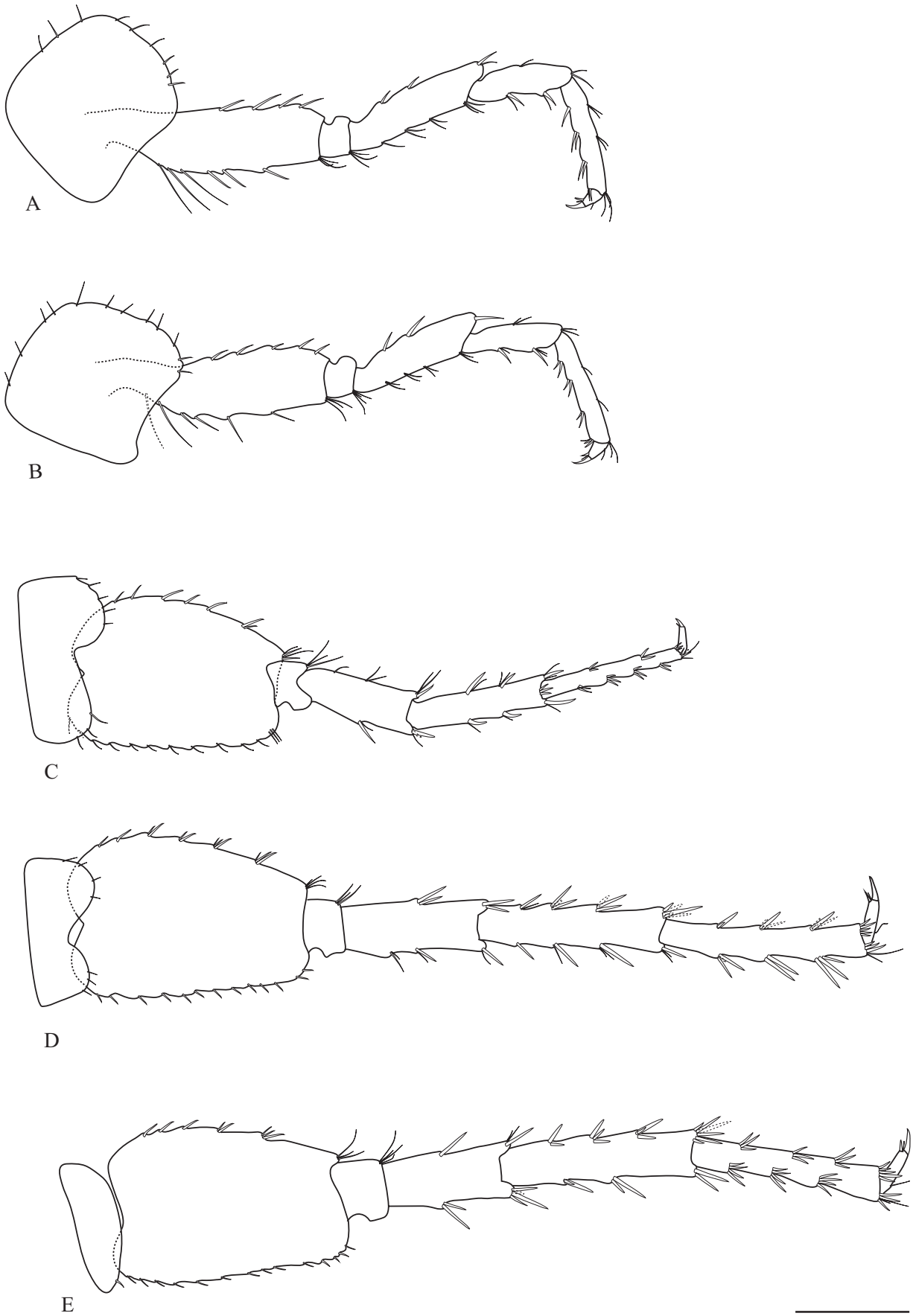

Figure 9. *Niphargus zagrosensis* sp. nov., holotype, male, 10.5 mm (ZCRU Amph.1501). **A.** Pereopod III; **B.** Pereopod IV; **C.** Pereopod V; **D.** Pereopod VI; **E.** Pereopod VII. Scale bar: 1 mm.

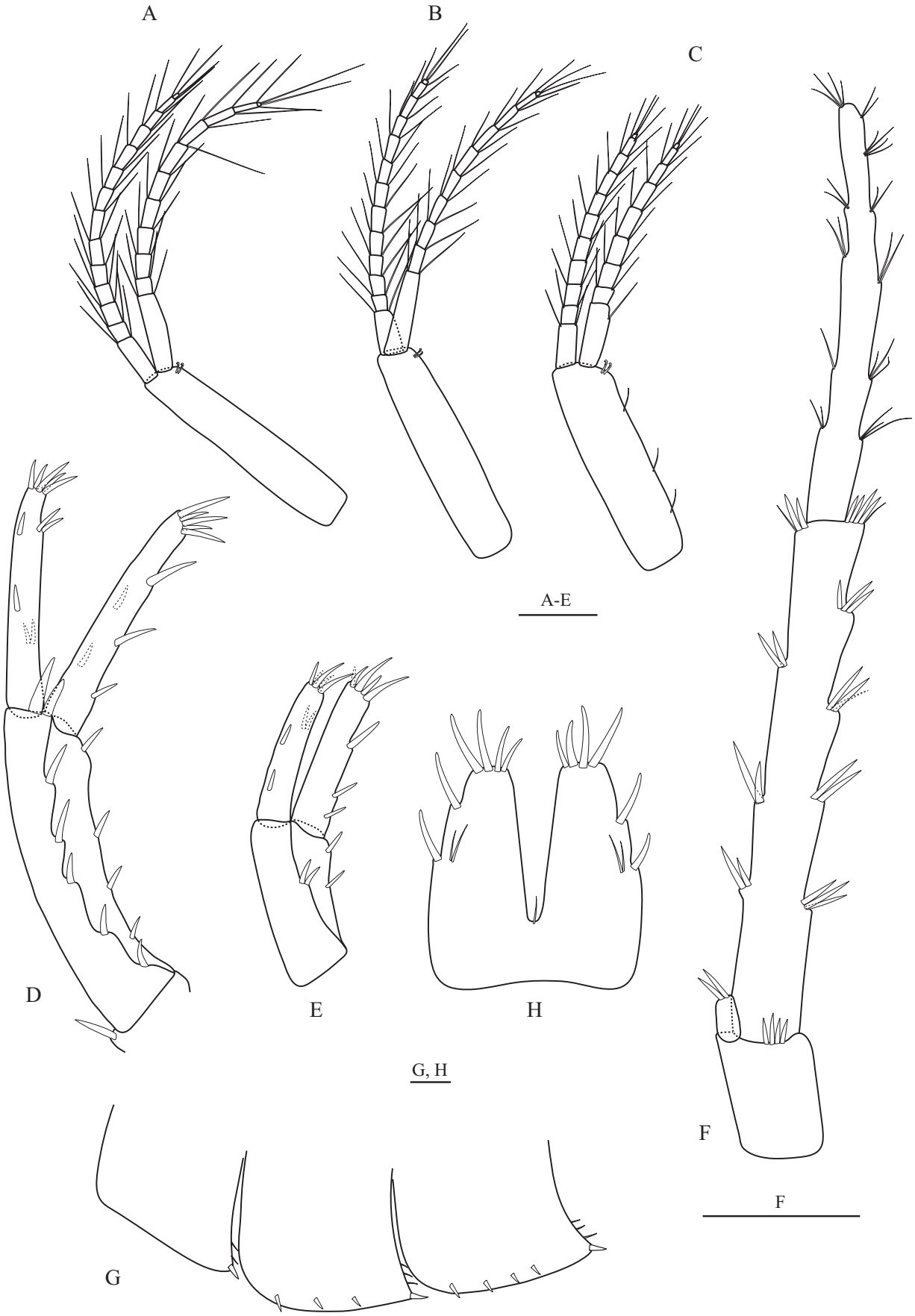

Figure 10. *Niphargus zagrosensis* sp. nov., holotype, male, 10.5 mm (ZCRU Amph.1501). **A.** Pleopod I; **B.** Pleopod II; **C.** Pleopod III; **D.** Uropod I; **E.** Uropod II; **F.** Uropod III; **G.** Epimeral plates I–III; **H.** Telson. Scale bars: 0.5 mm (**G, H**); 1 mm (**A–E**); 2 mm (**F**).

Niphargus zagrosensis is characterized by a distinctive combination of features, including a longer size of pereopod VI to pereopod VII and the maxilliped outer plate length less than half of posterior margin of palp article 2.

Although *N. zagrosensis* is genetically close to *N. alisadri*, it differs from *N. alisadri* in several morphological features: 1) Gnathopod II propodus shape: *N. zagrosensis* has a triangular shape, whereas *N. alisadri* has a rectangular shape. 2) Ratio of palpus to outer plate lobe length in maxilla I: *N. zagrosensis* has a long palpus in maxilla I, which passes from the tip of the outer lobe, while *N. alisadri* has a short palpus, which does not reach to maxilla I outer lobe. 3) L-setae in gnathopods I–II propodi: *N. zagrosensis* possesses three and two L-setae on gnathopods I–II propodi, respectively, while *N. alisadri* has two and zero L-setae (Esmaeili-Rineh and Sari 2013).

The sister taxa of *N. zagrosensis* are *N. alisadri* and *N. hegmatanensis*. While the new species and *N. hegmatanensis* inhabit shallow subterranean habitats, *N. alisadri* dwells in a cave lake habitat. The geographic distance between *N. zagrosensis* and *N. hegmatanensis* is 124 km, and between *N. zagrosensis* and *N. alisadri* is 141 km. Additionally, there is a geographic distance of 163 km between the two new species.

Recent studies suggest that the northern and western regions of Iran harbor considerable richness in groundwater amphipods (Mamaghani-Shishvan and Esmaeili-Rineh 2019; Bargrizaneh et al. 2021), highlighting the complexity of the ecosystem and its biodiversity. The presence of these organisms is crucial for nutrient cycling, energy flow, and overall ecosystem stability. Moreover, the abundance of amphipod species can serve as indicators of groundwater systems' health, providing valuable insights for environmental monitoring and conservation efforts.

Acknowledgments

This project was financially supported by Razi University as a part of the PhD thesis of the first author. We express our gratitude to editor Dr. Andrade and reviewers Dr. Cene Fišer and Dr. Denis Copilaş-Ciocianu for their valuable comments on the manuscript.

References

Astrin JJ, Stüben PE (2008) Phylogeny in cryptic weevils: molecules, morphology and new genera of western Palaearctic Cryptorhynchinae (Coleoptera: Curculionidae). Invertebrate Systematics 22(5): 503–522. https://doi.org/10.1071/IS07057

Balázs G, Borko Š, Angyal D, Zakšek V, Biró A, Fišer C, Herczeg G (2023) Not the Last Piece of the Puzzle: *Niphargus* Phylogeny in Hungary. Diversity 15(2): 223. https://doi.org/10.3390/d15020223

Bargrizaneh Z, Fišer C, Esmaeili-Rineh S (2021) Groundwater amphipods of the genus *Niphargus* Schiødte, 1834 in Boyer-Ahmad region (Iran) with description of two new species. Zoosystema 43(7): 127–144. https://doi.org/10.5252/zoosystema2021v43a7

Borko Š, Trontelj P, Seehausen O, Moškrič A, Fišer C (2021) A subterranean adaptive radiation of amphipods in Europe. Nature Communications 12(1): 1–12. https://doi.org/10.1038/s41467-021-24023-w

Copilaş-Ciocianu D, Boroş BV (2016) Contrasting life history strategies in a phylogenetically diverse community of freshwater amphipods (Crustacea: Malacostraca). Zoology : Analysis of Complex Systems, ZACS 119(1): 21–29. https://doi.org/10.1016/j.zool.2015.11.001

Drummond AJ, Rambaut A (2009) Bayesian evolutionary analysis by sampling trees. The phylogenetic handbook: a practical approach to phylogenetic analysis and hypothesis testing, 564–574. https://doi.org/10.1017/CBO9780511819049.020

Esmaeili-Rineh S, Sari A (2013) Two new species of *Niphargus* Schiödte, 1849 (Crustacea: Amphipoda: Niphargidae) from two caves in Iran. Journal of Natural History 47(41–42): 2649–2669. https://doi.org/10.1080/00222933.2013.802041

Esmaeili-Rineh S, Sari A, Delić T, Moškrič A, Fišer C (2015) Molecular phylogeny of the subterranean genus *Niphargus* (Crustacea: Amphipoda) in the Middle East: A comparison with European Niphargids. Zoological Journal of the Linnean Society 175(4): 812–826. https://doi.org/10.1111/zoj.12296

Esmaeili-Rineh S, Mirghaffari SA, Sharifi M (2017a) The description of a new species of *Niphargus* from Iran based on morphological and molecular data. Subterranean Biology 22: 43–58. https://doi.org/10.3897/subtbiol.22.11286

Fišer C, Trontelj P, Luštrik R, Sket B (2009) Toward a unified taxonomy of *Niphargus* (Crustacea: Amphipoda): a review of morphological variability. Zootaxa 2061(1): 1–22. https://doi.org/10.11646/zootaxa.2061.1.1

Fišer C, Alther R, Zaksek V, Borko S, Fuchs A, Altermatt F (2018) Translating *Niphargus* barcodes from Switzerland into taxonomy with a description of two new species (Amphipoda, Niphargidae). ZooKeys 760: 113–141. https://doi.org/10.3897/zookeys.760.24978

Hall TA (1999) BioEdit: a user-friendly biological sequence alignment editor and analysis program for Windows 95/98/NT. In: Nucleic acids symposium series. Oxford, 95–98.

Kimura M (1980) A simple method for estimating evolutionary rates of base substitutions through comparative studies of nucleotide sequences. Journal of Molecular Evolution 16(2): 111–120. https://doi.org/10.1007/BF01731581

Mamaghani-Shishvan M, Esmaeili-Rineh S (2019) Two new species of groundwater amphipods of the genus *Niphargus* Schiödte, 1849 from northwestern Iran. European Journal of Taxonomy 546: 1–23. https://doi.org/10.5852/ejt.2019.546

Mamaghani-Shishvan M, Esmaeili-Rineh S, Fišer C (2017) An integrated morphological and molecular approach to a new species description of Amphipods in the Niphargidae from two caves in West of Iran. Zoological Studies (Taipei, Taiwan) 56: 33. https://doi.org/10.6620/ZS.2017.56-33

Marin IN, Palatov DM (2023) Insights on the existence of ancient glacial refugee in the Northern Black/Azov Sea lowland, with the description of the first stygobiotic microcrustacean species of the genus *Niphargus* Schiödte, 1849 from the Mouth of the Don River. Diversity 15(5): 682. https://doi.org/10.3390/d15050682

Morhun H, Son MO, Rewicz T, Kazanavičiūtė E, Copilas-Ciocianu D (2022) The first records of *Niphargus hrabei* and *N. potamophilus* in Ukraine and Bulgaria significantly enlarge the ranges of these species. The European Zoological Journal 89(1): 1191–1200. https://doi.org/10.1080/24750263.2022.2126534

Ozkahya P, Camur-Elipek B (2015) A study on determining of macroinvertebrate biodiversity in water wells with stygobiont species findings. Biologija (Vilnius, Lithuania) 61(3–4): 167–172. https://doi.org/10.6001/biologija.v61i3-4.3209

Posada D (2008) jModelTest: Phylogenetic model averaging. Molecular Biology and Evolution 25: 1253–1256. https://doi.org/10.1093/molbev/msn083

Ronquist F, Huelsenbeck JP (2003) MrBayes 3: Bayesian phylogenetic inference under mixed models. Bioinformatics (Oxford, England) 19(12): 1572–1574. https://doi.org/10.1093/bioinformatics/btg180

Stoch F, Christian E, Flot J-F (2020) Molecular taxonomy, phylogeny and biogeography of the *Niphargus tatrensis* species complex (Amphipoda, Niphargidae) in Austria. Organisms, Diversity & Evolution 20(4): 701–722. https://doi.org/10.1007/s13127-020-00462-z

Tamura K, Peterson D, Peterson N, Stecher G, Nei M, Kumar S (2011) MEGA5: Molecular evolutionary genetics analysis using maximum l2015ikelihood, evolutionary distance, and maximum parsimony methods. Molecular Biology and Evolution 28(10): 2731–2739. https://doi.org/10.1093/molbev/msr121

Thompson JD, Higgins DG, Gibson TJ (1994) CLUSTAL W: improving the sensitivity of progressive multiple sequence alignment through sequence weighting, position-specific gap penalties and weight matrix choice 22: 4673–4680. https://doi.org/10.1093/nar/22.22.4673

Väinölä R, Witt J, Grabowski M, Bradbury JH, Jazdzewski K, Sket B (2008) Global diversity of amphipods (Amphipoda; Crustacea) in freshwater. Freshwater Animal Diversity Assessment, 241–255. https://doi.org/10.1007/978-1-4020-8259-7_27

Verovnik R, Sket B, Trontelj P (2005) The colonization of Europe by the freshwater crustacean *Asellus aquaticus* (Crustacea: Isopoda) proceeded from ancient refugia and was directed by habitat connectivity. Molecular Ecology 14(14): 4355–4369. https://doi.org/10.1111/j.1365-294X.2005.02745.x

Weber D, Weigand AM (2023) Groundwater amphipods of the hyporheic interstitial: A case study from Luxembourg and The Greater Region. Diversity 15(3): 411. https://doi.org/10.3390/d15030411

Zakšek V, Sket B, Trontelj P (2007) Phylogeny of the cave shrimp Troglocaris: Evidence of a young connection between Balkans and Caucasus. Molecular Phylogenetics and Evolution 42(1): 223–235. https://doi.org/10.1016/j.ympev.2006.07.009

Zoosyst. Evol. 100 (2) 2024, 739–746 | DOI 10.3897/zse.100.122293

PENSOFT

für Natur MUSEUM FÜR NATURKUNDE BERLIN

DNA barcoding suggests hidden diversity within the genus *Zenopsis* (Zeiformes, Zeidae)

Florencia Matusevich[1], Valeria Gabbanelli[1], Gonzalo Vulcano[2], Natalia Plá[3], Victoria M. Lenain[1], Diego M. Vazquez[4], Juan M. Díaz de Astarloa[1], Ezequiel Mabragaña[1]

1 *Laboratorio de Biotaxonomía Morfológica y Molecular de Peces, Instituto de Investigaciones Marinas y Costeras (IIMyC), Facultad de Ciencias Exactas y Naturales, Universidad Nacional de Mar del Plata–CONICET, CC1260, Funes 3350, 7600 Mar del Plata, Argentina*

2 *Facultad de Ciencias Exactas y Naturales, Universidad Nacional de Mar del Plata, Funes 3350, 7600 Mar del Plata, Argentina*

3 *Laboratorio de Virología, Área de Producción Animal, Facultad de Ciencias Agrarias, Universidad Nacional de Mar del Plata, Ruta 226 km 73,5, Balcarce, Buenos Aires B7620, Argentina*

4 *Instituto Nacional de Limnología (INALI), Universidad Nacional del Litoral (UNL), CONICET, Ruta Nacional 168 km 0, Ciudad de Santa Fe, Santa Fe S3001XAI, Argentina*

https://zoobank.org/66BE7D3A-255C-47E5-8FB7-2AE4C4EFCFD1

Corresponding author: Valeria Gabbanelli (vgabbanelli@mdp.edu.ar)

Academic editor: Nalani Schnell ♦ **Received** 4 March 2024 ♦ **Accepted** 15 May 2024 ♦ **Published** 7 June 2024

Abstract

Currently, the genus *Zenopsis*, also known as silver John Dory, comprises at least five valid species with a wide range of distribution. However, recent studies have proposed the existence of a new *Zenopsis* species inhabiting the Indian Ocean, and a preliminary search in the Barcode of Life Database reveals the presence of different barcode index numbers (BIN) for the nominal species *Zenopsis conchifer*. In the Southwest Atlantic Ocean (SWA), *Z. conchifer* is the only species reported so far. Therefore, the aim of this work was to evaluate, at the molecular level, the potential taxonomic diversity within the genus *Zenopsis* and to assess if the species occurring in the SWA corresponds with *Z. conchifer*. Using data available in worldwide genetic databases, a maximum likelihood tree, a BIN, and an automatic barcode gap discovery analysis were carried out. Additionally, specimens sampled from the SWA were morphologically compared with specimens from different parts of its distribution using available data. The specific identity at the molecular level of specimens occurring in the SWA was confirmed as *Z. conchifer*. The results of the molecular analysis highlight the existence of hidden specific diversity within the genus.

Key Words

Barcode index number, distribution area, silver John Dory, Southwest Atlantic Ocean

Introduction

Fishes of the genus *Zenopsis* Gill, 1862, also known as "silver John Dory," are a group of marine species characterized by a similar body plan with laterally flattened bodies (Swaby and Potts 1999), scales present only along the lateral line, and large bucklers along the bases of dorsal and anal fins, ventrally anterior to the pelvic fin, and between pelvic and anal fins (Tyler et al. 2003; Nakabo et al. 2006). Currently, the genus comprises five valid species: *Zenopsis conchifer* (Lowe, 1852), *Z. nebulosa* (Temminck & Schlegel, 1845), *Z. oblonga* Parin et al., 1997, *Z. stabilispinosa* Nakabo et al., 2006, and *Z. filamentosa* Kai & Tashiro, 2019. Additionally, a recent genetic study suggests the occurrence of a new *Zenopsis* species in the Eastern Indian Ocean (Kai and Tashiro 2019). These species are ecologically successful due to their ability to withstand episodic recruitment (Zidowitz et al. 2002) and are widely distributed around the world. *Zenopsis filamentosa*, *Z. stabilispinosa*, and *Z. nebulosa* are found in the Pacific Ocean around Asia and Oceania; *Z. nebulosa* is also present along the coast of America in the Pacific

Ocean. *Zenopsis oblonga* is present in the Eastern Pacific Ocean (Froese and Pauly 2021). *Zenopsis conchifer* is distributed in the Atlantic Ocean along the coasts of America, Europe, and Africa; in the Pacific Ocean off the coasts of Chile; and in the Indian Ocean (Maurin and Quéro 1982; Sáez and Lamilla 2017; Froese and Pauly 2021). *Zenopsis conchifer* has recently been reported along the coast of north-eastern Brazil (Malafaia et al. 2015) and for the first time in the Mediterranean Sea (Ragonese and Giusto 2007; Fernández et al. 2012; Pinto et al. 2023). Ragonese and Giusto (2007) suggested that this range expansion of *Z. conchifer* distribution could be explained by the tropicalization phenomenon, which states that the increase in sea temperature could be responsible for the increasing range of thermophilic species (Bombace 2001). However, there is no evidence of a self-sustaining population found in the Mediterranean Sea (Fernández et al. 2012).

In the last few decades, molecular taxonomy, specifically DNA barcoding, has emerged as a way to complement morphological taxonomy (Teletchea 2010). Barcoding is a methodology that includes the sequencing and analysis of the mitochondrial cytochrome c oxidase subunit I (COI) gene and is used for species identification (Hebert et al. 2003). It has been widely used to study fish biodiversity (Ward et al. 2005, 2008; Hubert et al. 2008; Mabragaña et al. 2011) and to assess the species composition of the fishery industry catches (e.g., Bineesh et al. 2016 Delpiani et al. 2020). The Barcode of Life Database System (BOLD) aims to be a worldwide reference library for species identification through the storage of COI sequences (BOLD; https://www.boldsystems.org) (Hebert et al. 2003). To do so, BOLD performs a barcode index number (BIN) analysis, which clusters the sequences as taxonomic operational units that generally agree with nominal species. A preliminary search in the BOLD database reveals the presence of more than one BIN for the nominal species *Z. conchifer*, suggesting that further analysis into the diversity of the genus is needed. In this sense, the aim of this work is to evaluate the potential taxonomic diversity within the genus *Zenopsis* based on the analysis of DNA barcoding and to assess, at the molecular level, if the species occurring in the Southwest Atlantic Ocean (SWA) corresponds with *Z. conchifer*.

Materials and methods

Forty-five COI sequences available in BOLD (https://www.boldsystems.org) for *Z. stabilispinosa* (n=1), *Z. conchifer* (n=17; one submitted previously by the authors), *Z. nebulosa* (n=15), and samples identified exclusively at the genus level, named *Zenopsis* (n=11), *Zeus faber* (n=1), and seventeen sequences obtained in Kai and Tashiro (2019) from the International Nucleotide Sequence Database Collaboration (INSDC; https://www.insdc.org) of specimens of *Z. stabilispinosa* (n=1), *Z. conchifer* (n=3), *Z. nebulosa* (n=5), *Zenopsis* sp. (n=4), and *Z. filamentosa* (n=4) were downloaded. Sequence data are shown in Suppl. material 1. Additionally, two specimens of *Z. conchifer* from the Argentine Sea were sequenced; however, one of these sequences had low quality and was excluded from the analysis (the sequence was uploaded to NCBI at https://www.ncbi.nlm.nih.gov). Sequences of *Z. oblonga* were not available in either database.

The DNA extraction was carried out in the Argentine International Barcode of Life Reference Laboratory (IIMyC, CONICET, Mar del Plata, Argentina) from muscle tissue preserved in 70% ethanol. DNA extraction, polymerase chain reaction (PCR), and sequencing of the 5′ region of the COI gene were performed following standard DNA barcoding protocols (Ivanova et al. 2006) coupled with primers and primer cocktails specifically designed for fishes (Ward et al. 2005; Ivanova et al. 2006) for base positions 6474–7126 of the *Danio rerio* mitochondrial genome. PCR reaction mixtures and the reaction profile were carried out following Díaz de Astarloa et al. (2008). The PCR products were purified and sequenced at the Canadian Centre for DNA Barcoding in Ontario. The full set of sequences was aligned using MEGA 11 (Tamura et al. 2021; Stecher et al. 2020). A maximum likelihood (ML) tree was reconstructed with a bootstrap of 1000 replications. The HKY model was chosen for cluster analysis as it was determined to be the best-fit model under the Akaike information criterion.

Sequences were also analyzed using the BIN analysis provided by the BOLD platform, and species limits were explored using the automatic barcode gap discovery method (ABGD) (Puillandre et al. 2012). The ABGD sorts sequences into putative species based on the barcode gap distance. This analysis was run with the default settings (P min=0.001, P max= 0.1, steps=10, X relative gap width=1.5, Nb bins=20) and K2P distance on the ABGD web server (https://bioinfo.mnhn.fr/abi/public/abgd/). Additionally, within-group and between-group mean distance analyses were carried out using MEGA 11 (Stecher et al. 2020; Tamura et al. 2021) with the K2P model (Kimura 1980) and the default parameters. Two sets of groups were defined and analyzed. (1) Grouped by species name: *Z. nebulosa*, *Z. filamentosa*, *Z. stabilispinosa*, *Z. conchifer*, *Zenopsis*, and *Zenopsis* sp. (Kai and Tashiro 2019), and (2) grouped by ABGD groups (as shown in Fig. 2).

Ten specimens of *Zenopsis* cf. *conchifer*, collected in the Argentinean Sea (Fig. 1A), were used for the morphometric analysis. Two specimens are housed in the collection of the Instituto de Investigaciones Marinas y Costeras, Facultad de Ciencias Exactas y Naturales, Universidad Nacional de Mar del Plata-CONICET (IIMyC) (n=2, UNMDP 4500, UNMDP 4881), and five in the Instituto Nacional de Investigación y Desarrollo Pesquero (INIDEP) (n=5; catalogue number 76), both found in Mar del Plata, Argentina. Three fresh specimens were obtained from fish markets and included in the analysis; afterwards, they were accessed in the IIMYC collection (UNMDP 5159, UNMDP 5160, and UNMDP 5161). Counts, measurements, and terminology were used following Kai and Tashiro (2019) and are summarized in Fig. 1B. Measurements were standardized to the standard length and compared with available data on *Z. conchifer* from different areas of its distribution: North Western Africa (NW Africa) (Kai and Tashiro 2019), the Mediterranean Sea (Ragonese and Giusto 2007), and North Eastern Brazil (NE Brasil)

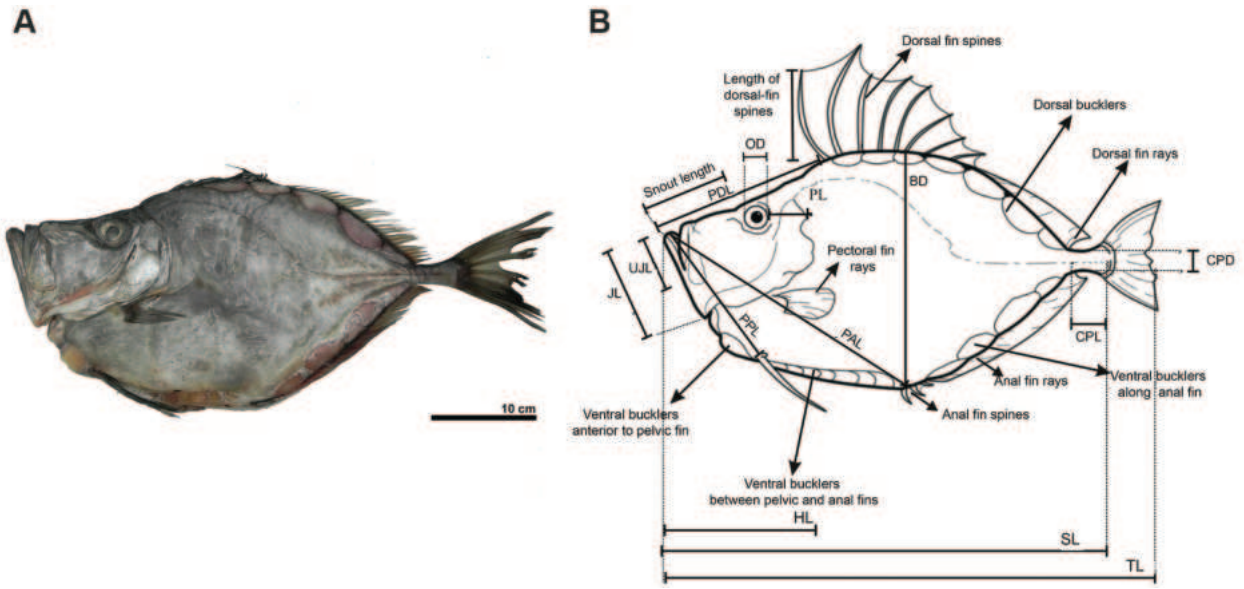

Figure 1. A. *Zenopsis* cf. *conchifer* specimen from the Argentine Sea; **B.** Measurements taken on specimens of *Zenopsis* cf. *conchifer*. **TL**—total length. **SL**—standard length. **BD**—body depth. **CPD**—caudal peduncle depth. **CPL**—caudal peduncle length. **HL**—head length. **JL**—jaw length. **OD**—orbit diameter. **PAL**—preanal length. **PDL**—predorsal length. **PL**—postorbital length. **PPL**—prepelvic length. **UJL**—upper jaw length. (Illustration carried out by the co-author, Vulcano, G.).

(Malafaia et al. 2015). Due to the small number of specimens studied, the analysis was exclusively descriptive.

Results

The ML tree (Fig. 2) showed that the COI sequences of the different *Zenopsis* species were grouped into six different clusters; these clusters corresponded to: *Z. nebulosa*, *Z. stabilispinosa*, a cluster with sequences of *Z. filamentosa* and specimens identified exclusively at the genus level, named *Zenopsis*; two clusters with sequences identified as *Z. conchifer*; and one cluster with sequences of *Z. conchifer* and *Zenopsis* sp. (Kai & Tashiro, 2019). The three clusters that included sequences identified as *Z. conchifer* did not form a single clade in the ML tree.

In the BOLD database, six different BINs for the *Zenopsis* genus were found. However, these sequences were recorded as four nominal species: *Z. conchifer*, *Z. nebulosa*, *Z. filamentosa*, and *Z. stabilispinosa*.

Sequences identified as *Z. conchifer* were grouped in three different clusters in the ML tree (Fig. 2) that corresponded to the three different BINs (BOLD:AAC3708; BOLD:ADK0258; BOLD:AAZ3127). Although the three BINs are assigned to *Z. conchifer* in BOLD, the specimens are from different sample locations (Fig. 2; Suppl. material 1). Sequences identified as *Zenopsis* sp. by Kai and Tashiro (2019) were grouped with sequences from BIN BOLD:ADK0258. Sequences for *Z. nebulosa* and *Z. stabilispinosa* were included in a singular BIN for each species (BOLD:AAB79893, BOLD:ACH5427, respectively), in accordance with the clusters found in the ML (Fig. 2). All four sequences of *Z. filamentosa* from Kai and Tashiro (2019) clustered with sequences of BIN BOLD:AEB2424. Within this BIN, a single sequence was registered as *Z. filamentosa*, and the remaining sequences were identified exclusively at the genus level and named *Zenopsis*. Thus, BIN BOLD:AEB2424 was determined to correspond with *Z. filamentosa*.

The analysis of ABGD resulted in eight initial partitions. In six partitions (P= 1.00 e-3, 1.67 e-3, 2.78 e-3, 4.64 e-3, 7.74 e-3, and 1.29 e-2), seven candidate species were found, which grouped consistently with the clusters found in the ML tree (Fig. 2). The other two partitions (P= 2.15 e-2, 3.5 e-2) presented two candidate species, which corresponded with one group with sequences of all *Zenopsis* species together, separated from a group with the sequence of the outgroup, *Zeus faber*.

In the first distance analysis, which grouped sequences by species, *Z. conchifer* presented 3% (SE=0) mean within-group distance and *Z. nebulosa* 1% (SE=0), while the other species showed a distance value close to 0%. The between-group distance analysis (Table 1) ranged from 0.08% to 20.33%. The lower distance of 0.08% was found between *Z. filamentosa* and sequences exclusively identified at genus level in BOLD (named as *Zenopsis*), and the highest distances (ranging between 18.23 and 20.33%) were found between each *Zenopsis* species and the outgroup *Zeus faber*. Within the genus *Zenopsis*, the highest distance value was found between *Z. stabilispinosa* and *Zenopsis* sp. (6.9%). However, when analyzed by ABGD groups, group 4 (containing sequences of BIN BOLD:AAB7893) presented a 1% (SE=0) mean within-group distance, while the mean distance for the rest of the groups was close to 0. The between-group distance ranged from 2.66% to 20.33% (Table 2). The highest values corresponded with the comparisons between each *Zenopsis* group and the outgroup. Within the genus, the lowest value was found between group 4 and group 5 (BINs BOLD:AAB7893 and BOLD:AAZ3127,

Figure 2. Maximum likelihood tree for the *Zenopsis* species analyzed. The tree was based on the Cytochrome Oxidase Subunit I gene and reconstructed with MEGA 11. Sequences from Kai and Tashiro (2019) are indicated with a grey triangle. Sequences obtained by the authors are indicated with a blue pentagon. All remaining sequences were obtained from BOLD. Color bars represent different clusters resulting from ML analysis with 1000 bootstraps. Black bars represent groups resulting from ABGD analysis. Country abbreviations were made following ISO 3166 Alpha-2 and Alpha-3. AR—Argentina. AU—Autralia. IN—India. JP—Japan. NA—Namibia. NZ—New Zeland. PT—Portugal. ES-Spain. TW—Taiwan. US—United States. At. Oc.—Atlantic Ocean. Pac. Oc.—Pacific Ocean. S. CN Sea—South China Sea. † Sequence GCA4525-13, originally identified as *Z. nebulosa* in BOLD, is actually a misidentification and corresponds to *Z. stabilispinosa*, as previously determined by Kai and Tashiro (2019).

respectively), and the highest one between group 3 and group 6 (BINs BOLD:ADK0258 and BOLD:ACH5427).

Regarding species distribution, BINs identified in BOLD as *Z. conchifer* contained specimens collected in different locations. BIN BOLD:AAC3708 contained specimens from the Atlantic Ocean, including the United States, Argentina, and Portugal (near the type locality) (Fig. 2; Suppl. material 1). BIN BOLD:ADK0258 contained specimens from the Indian Ocean (Fig. 2; Suppl. material 1). Samples included in BIN BOLD:AAZ3127 came from Namibia (Fig. 2; Suppl. material 1); also, private sequences within this BIN (therefore not included in this study) were sampled in Cape Verde, Guinea-Bissau, and Morocco. Sequences of *Z. nebulosa* were collected from Australia, New Zealand, Taiwan, Japan, the South China Sea, and the Pacific Ocean (Fig. 2; Suppl. material 1). All the sequences of *Z. filamentosa* were collected from Japan (Fig. 2; Suppl. material 1). *Zenopsis stabilispinosa* was collected in Taiwan and the South China Sea (Fig. 2; Suppl. material 1).

A summary of the morphological measurements found in a bibliographic revision (Ragonese and Giusto 2007; Malafaia et al. 2015; Kai and Tashiro 2019) is shown in Table 3, and the full set of measurements is available in Suppl. material 2. To avoid errors based on differences associated with size or stage (i.e., juveniles, immature adults, mature adults), the *Z. conchifer* specimens revised for this study were compared exclusively with those analyzed by Kai and Tashiro (2019), considering that the standard length (SL) range was similar in both studies (141–339 mm for specimens from the Argentine Sea and 140–173.4 mm for specimens from Kai and Tashiro 2019). Slight differences between them were found in some measurements (Table 3). Specimens of *Z. conchifer* captured in NW Africa (Kai and Tashiro 2019) presented a longer orbital diameter (9.5–10.6 times SL) than those found in the Argentine Sea (5.84–9.87 times SL). Specimens from NW Africa (Kai and Tashiro 2019) showed a shorter snout (15.2–16.1 times SL vs. 18.6–21.5 times SL) and a longer postorbital length (12.9–14.1 times SL vs. 7.7–11.9 times SL) than those from the Argentine Sea. The specimens collected from the Argentine Sea had a smaller number of bucklers at the base of the anal fin than the specimens from other parts of the world (4 vs. 5–6).

Table 1. Between-groups mean distance (and standard error). Sequences were grouped by species names: *Z. nebulosa*, *Z. filamentosa*, *Z. stabilispinosa*, *Z. conchifer*, *Zenopsis*, and *Zenopsis* sp. (Kai and Tashiro 2019).

	Z. conchifer	***Z. nebulosa***	***Z. stabilispinosa***	***Z. filamentosa***	***Zenopsis* sp.**	***Zenopsis***	***Zeus faber***
Z. conchifer		0.04 (0.006)	0.06 (0.009)	0.04 (0.007)	0.03 (0.005)	0.04 (0.007)	0.2 (0.024)
Z. nebulosa			0.05 (0.009)	0.05 (0.009)	0.04 (0.008)	0.05 (0.009)	0.18 (0.024)
Z. stabilispinosa				0.06 (0.01)	0.07 (0.011)	0.06 (0–01)	0.19 (0.024)
Z. filamentosa					0.05 (0.01)	0.0008 (0.0009)	0.19 (0.024)
Zenopsis sp.						0.05 (0.01)	0.2 (0.256)
Zenopsis							0.19 (0.024)

Table 2. Between-groups mean distance (and standard error). Sequences were grouped by ABGD analysis (as shown in Fig. 2).

	G1	**G2**	**G3**	**G4**	**G5**	**G6**	***Zeus faber***
G1		0.04 (0.008)	0.05 (0.01)	0.05 (0.009)	0.04 (0.009)	0.06 (0.01)	0.19 (0.024)
G2			0.04 (0.009)	0.04 (0.008)	0.04 (0.008)	0.06 (0.01)	0.2 (0.025)
G3				0.04 (0.007)	0.03 (0.007)	0.07 (0.011)	0.2 (0.025)
G4					0.03 (0.006)	0.05 (0.009)	0.18 (0.024)
G5						0.05 (0.009)	0.19 (0.024)
G6							0.19 (0.024)

Table 3. Comparison of morphological and meristic data for *Zenopsis conchifer* analyzed in this study and information taken from available bibliography (Ragonese and Giusto 2007; Malafaia et al. 2015; Kai and Tashiro 2019), including different areas of its distribution. NW: North Western; NE: North Eastern. Standard length is in mm. All remaining measurements are standardized with regard to the standard length. The range and mean between parenthesis are given for each measurement as a percentage of the standard length.

	Argentine Sea (Present Study) (N=10)	**NW Africa (Kai and Tashiro 2019) (n=5)**	**Mediterranean Sea (Ragonese and Giusto 2007) (n=1)**	**NE Brasil (Malafaia et al. 2015) (n=1)**
Standard Length (SL; mm)	141–395	140.0–173.4	550	525
Snout length	18.6–21.5 (19.9)	15.2–16.1 (15.7)		16.2
Orbit diameter	5.84–9.87 (8.57)	9.5–10.6 (10.1)	6.4	6.3
Postorbital length	7.7–11.9 (10.3)	12.9–14.1 (13.5)	16.5	11.42
Body depth	49.1–62.2 (56.0)	26.3–62.2 (59.5)	50.9	48.6
Upper jaw length	13.9–17.8 (16.0)	16.3–17.8 (17.4)	14.9	15.4
Dorsal bucklers	5–7	1–2 + 5	8	7
Ventral bucklers anterior to pelvic fin	2		2	2
Ventral bucklers between pelvic and anal fins	6–8	5	7	7–8
Ventral bucklers along anal fin	4	5–6	5	5

Discussion

The molecular analysis, based on COI, suggests that the genus *Zenopsis* is more specious than previously assumed. Furthermore, information about the known distribution range (Maurin and Quéro 1982; Froese and Pauly 2021; Fricke et al. 2023) was added based on the location of the specimens analyzed here. This information aids in the determination of possible distribution areas for each potential species found in the ML tree.

In the ML tree, for each cluster, a BIN number from the BOLD database could be associated. These clusters also corresponded with the seven groups found in the ABGD analysis (Fig. 2). For *Z. nebulosa*, *Z. filamentosa*, and *Z. stabilispinosa*, a single cluster and BIN were found. For *Z. conchifer*, three clusters corresponding to three different BINs were found, and these three clusters did not form a single clade in the ML tree. BINs usually correspond with a nominal species, and sequences of one species tend to cluster together in a ML tree. Additionally, the within-group mean distance analysis showed that if all three *Z. conchifer* BINs are grouped together, the mean distance is 3%, the highest found for any species analyzed in this study. However, if these sequences are separated into the three groups determined by ML, BIN, and ABGD analysis, the mean within-group distance of each group decreases by close to 0%. Thus, these results suggest the existence of hidden diversity within this species.

BIN BOLD:AAC3708 contained *Z. conchifer* from the Atlantic Ocean, including those of waters off Portugal, close to the type locality of *Z. conchifer* (Lowe, 1852) (Fig. 2; Suppl. material 1). The sequence of the samples from the Argentine Sea is grouped within this cluster. This leads us to the assumption that the molecular identity of the species inhabiting these waters corresponds to *Z. conchifer*.

On the other hand, the sequences of BIN BOLD:ADK0258 corresponded with specimens from the Indian Ocean and clustered together with *Zenopsis* sp., which was proposed as a possible new species by Kai and Tashiro (2019). Our results showed that sequences from this area did not cluster with specimens collected in the type locality; therefore, we hypothesize that *Z. conchifer* does not occur in the Indian Ocean and that the captures recorded in this area correspond to the new species, *Zenopsis* sp., proposed by Kai and Tashiro (2019).

Finally, our results suggest the existence of another new species from Namibia, Cape Verde, Guinea-Bissau, and Morocco, corresponding to BIN BOLD:AAZ3127, from now on named *Zenopsis* sp. 1. These sequences were previously identified as *Z. conchifer* but clustered independently from this species, and they were closely related to the sequences from *Z. nebulosa*. *Zenopsis conchifer* is also found in other regions of the west coast of Africa; thus, it is possible that in Namibia, Cape Verde, Guinea-Bissau, and Marocco, there are two sympatric *Zenopsis* species.

The current distribution of *Z. conchifer* includes the Atlantic Ocean along the coasts of America, Europe, and Africa, the Pacific Ocean off the coasts of Chile, and the Indian Ocean (Maurin and Quéro 1982; Sáez and Lamilla 2017; Froese and Pauly 2021). However, the specimens available from the eastern coast of Africa were identified solely based on morphological and meristic analysis, and no genetic data is available. Therefore, the occurrence of this species in this area should be confirmed through genetic and morphological studies. Additionally, all the specimens analyzed here that were collected in India clustered together with the sequences of the new species proposed by Kai and Tashiro (2019) (Fig. 2). In this sense, it is probable that *Z. conchifer* is not found in the Indian Ocean.

We observed some morphological differences between specimens of *Z. conchifer* from different localities. These differences could be the result of population variability, allometric growth, or a small sample size. Further morphological studies based on a larger number of specimens from each locality are needed to establish potential causes for these differences.

This work highlights the importance of the existence of worldwide reference libraries (e.g., the BOLD system and INSDC) to carry out large-scale studies, especially for wide-range distribution species like *Zenopsis conchifer*. Using the information available in these databases, the species identity at the molecular level of *Zenopsis* specimens found in the Southwest Atlantic Ocean was confirmed. Additionally, the results shown here suggest that the genus *Zenopsis* has a higher specific diversity than previously stated and could be used as a starting point for future taxonomic and genetic studies.

Author contributions

Funding acquisition: JMDA and EM. Conceptualization and methodology: EM, VG, and FM. Investigation: FM, NP, GV, and VG. Formal analysis: FM, NP, GV, VG, and DMV. Illustration: GV. Writing–original draft: FM. Writing–review and editing: VML and FM. All authors read and contributed critically to the drafts and gave final approval for publication.

Data availability

All sequence data generated during this study have been deposited at the National Center for Biotechnology Information (NCBI; https://www.ncbi.nlm.nih.gov) together with associated metadata under BioProject OR750557.

Acknowledgements

We would like to thank the Instituto Nacional de Investigaciones y Desarrollo Pesquero (INIDEP) and the people responsible for their collection for allowing us to see the specimens of *Zenopsis conchifer* stored there. We would also like to thank Dr. Mariana Deli Antoni for providing three specimens of *Z. conchifer* analyzed in this work.

We want to thank the Consejo Interuniversitario Nacional, as this study was carried out as part of an Estímulo a las Vocaciones Científicas grant.

This research was partly supported by funding from the Agencia Nacional de Promoción Científica y Tecnológica (Grant Nos. PICT 2018-2974 and PICT 2018-0790), the Universidad Nacional de Mar del Plata (Grant Nos. EXA 970/20 and EXA 1069/22), and the Consejo Nacional de Investigaciones Científicas y Técnicas CONICET (Grant No. PIP 11220200101475CO).

References

Bineesh KK, Gopalakrishnan A, Akhilesh KV, Sajeela KA, Abdussamad EM, Pillai NGK, Basheer VS, Jena JK, Ward RD (2016) DNA barcoding reveals species composition of sharks and rays in the Indian commercial fishery. Mitochondrial DNA. Part A, DNA Mapping, Sequencing, and Analysis 28(4): 458–472. https://doi.org/10.3109/19401736.2015.1137900

Bombace G (2001) Influence of climatic changes on stocks, fish species and marine ecosystems in the Mediterranean Sea. Archivio di Oceanografia e Limnologia 22: 67–72.

Delpiani G, Delpiani SM, Deli Antoni MY, Covatti Ale M, Fisher L, Lucifora LO, Díaz de Astarloa JM (2020) Are we sure we eat what we buy? Fish mislabelling in Buenos Aires province, the largest sea food market in Argentina. Fisheries Research 221: 105373. https://doi.org/10.1016/j.fishres.2019.105373

Díaz de Astarloa JM, Mabragaña E, Hanner R, Figueroa DE (2008) Morphological and molecular evidence for a new species of longnose skate (Rajiformes: Rajidae: *Dipturus*) from Argentinean waters based on DNA barcoding. Zootaxa 1921(1): 35–46. https://doi.org/10.11646/zootaxa.1921.1.3

Fernández AM, Gil JP, Esteban A (2012) On the occurrence of *Zenopsis conchifer* (Lowe, 1852)(Osteichthyes, Zeidae) in the Mediterranean Sea. Arxius de Miscel.Lania Zoologica 10: 50–54. https://doi.org/10.32800/amz.2012.10.0050

Fricke R, Eschmeyer WN, van der Laan R (Eds.) (2023) Catalog of fishes: genera, species, references. Online Version, Updated 6 June 2023 http://researcharchive.calacademy.org/research/ichthyology/catalog/fishcatmain.asp [Accessed 04 July 2023]

Froese R, Pauly D (Eds.) (2021) FishBase. World Wide Web electronic publication. www.fishbase.org [February 2021]

Gill T (1862) On the Limits and Arrangement of the Family of Scombroids. Proceedings. Academy of Natural Sciences of Philadelphia 14: 124–127. http://www.jstor.org/stable/4059436

Hebert PDN, Cywinska A, Ball SL, Ward JR (2003) Biological identifications through DNA barcodes. Proceedings Biological Sciences 270(1512): 313–322. https://doi.org/10.1098/rspb.2002.2218

Hubert N, Hanner R, Holm E, Mandrak NE, Taylor E, Burridge M, Watkinson D, Dumont P, Curry A, Bentzen P, Zhang J, April J, Bernatchez L (2008) Identifying Canadian freshwater fishes through DNA barcodes. PLoS ONE 3(6): e2490. https://doi.org/10.1371/journal.pone.0002490

Ivanova NV, Dewaard JR, Hebert PDN (2006) An inexpensive, automation-friendly protocol for recovering high-quality DNA. Molecular Ecology Notes 6(4): 998–1002. https://doi.org/10.1111/j.1471-8286.2006.01428.x

Kai Y, Tashiro F (2019) *Zenopsis filamentosa* (Zeidae), a new mirror dory from the western Pacific Ocean, with redescription of *Zenopsis nebulosa.* Ichthyological Research 66(3): 340–352. https://doi.org/10.1007/s10228-018-00679-1 [dataset]

Kimura M (1980) A simple method for estimating evolutionary rate of base substitutions through comparative studies of nucleotide sequences. Journal of Molecular Evolution 16: 111–120. https://doi.org/10.1007/BF01731581

Lowe RT (1852) An account of fishes discovered or observed in Madeira since the year 1842. Proceedings of the Zoological Society of London 1850(18): 247–253.

Mabragaña E, Díaz de Astarloa JM, Hanner R, Zhang J, Gonzalez Castro M (2011) DNA barcoding identifies Argentine fishes from marine and brackish waters. PLoS ONE 6(12): e28655. https://doi.org/10.1371/journal.pone.0028655

Malafaia PN, Lopes PRD, Sampaio CLS, Silva JTDO (2015) Primeiros registros de *Zenopsis conchifer* (Lowe, 1852) e *Evoxymetopon taeniatus* Gill, 1863 (Actinopterygii: Zeidae: Trichiuridae) para o Estado da Bahia, Brasil. Arquivos de Ciências do Mar, Fortaleza 48(1): 96–99. http://www.repositorio.ufc.br/handle/riufc/28633 [dataset]

Maurin C, Quéro J-C (1982) Poissons des côtes nord–ouest africaines (campagne de la «Thalasa» 1962, 1968, 1970 et 1973). Revue des Travaux de L'Institute des Pêches Maritimes 45: 5–69.

Nakabo T, Bray DJ, Yamada U (2006) A new species of *Zenopsis* (Zeiformes: Zeidae) from the South China Sea, East China Sea and off western Australia. Memoirs of the Museum of Victoria 63(1): 91–96. https://doi.org/10.24199/j.mmv.2006.63.11

Parin NV, Mironov AN, Nesis KN (1997) Biology of the Nazca and Sala y Gómez Submarine Ridges, an Outpost of the Indo-West Pacific Fauna in the Eastern Pacific Ocean: Composition and Distribution of the Fauna, its Communities and History. Advances in Marine Biology 32: 145–225. https://doi.org/10.1016/S0065-2881(08)60017-6

Pinto C, Valente GR, Rasore N, Olmi E, Lanteri L, Garibaldi F, et al. (2023) Range expansion of the Atlantic fish *Zenopsis conchifer* (Lowe, 1852), family Zeidae, in the western Mediterranean Sea. Mediterranean Marine Science 24(1): 90–95. https://doi.org/10.12681/mms.31409

Puillandre N, Lambert A, Brouillet S, Achaz G (2012) ABGD, Automatic Barcode Gap Discovery for primary species delimitation. Molecular Ecology 21(8): 1864–1877. https://doi.org/10.1111/j.1365-294X.2011.05239.x

Ragonese S, Giusto GB (2007) *Zenopsis conchifer* (Lowe, 1852) (Pisces, Actinopterygii, Zeidae): A new alien fish in the Mediterranean Sea. Journal of Fish Biology 71(6): 1853–1857. https://doi.org/10.1111/j.1095-8649.2007.01636.x [dataset]

Sáez S, Lamilla J (2017) Taxonomic update and illustrated key of Zeiformes from Chile (Pisces: Actinopterigii). Latin American Journal of Aquatic Research 45(1): 94–103. https://doi.org/10.3856/vol45-issue1-fulltext-9

Stecher G, Tamura K, Kumar S (2020) Molecular Evolutionary Genetics Analysis (MEGA) for macOS. Molecular Biology and Evolution 37(4): 1237–1239. https://doi.org/10.1093/molbev/msz312

Swaby SE, Potts GW (1999) The sailfin dory, a first British record. Journal of Fish Biology 54(6): 1338–1340. https://doi.org/10.1111/j.1095-8649.1999.tb02061.x

Tamura K, Stecher G, Kumar S (2021) MEGA11: Molecular Evolutionary Genetics Analysis version 11. Molecular Biology and Evolution 38(7): 3022–3027. https://doi.org/10.1093/molbev/msab120

Teletchea F (2010) After 7 years and 1000 citations: Comparative assessment of the DNA barcoding and the DNA taxonomy proposals for taxonomists and non- taxonomists. Mitochondrial DNA 21(6): 206–226. https://doi.org/10.3109/19401736.2010.532212

Temminck CJ, Schlegel H (1845) Pisces. Pts 7–9. In: Siebold, PF von (ed) P.F. de Siebold's Fauna Japonica. Müller, Amsterdam, 113–172. [pls. 1–143]

Tyler JC, O'Toole B, Winterbottom R (2003) Phylogeny of the genera and families of zeiform fishes, with comments on their relationships with tetraodontiforms and caproids. Smithsonian Contributions to Zoology 618(618): 1–110. https://doi.org/10.5479/si.00810282.618

Ward RD, Zemlak TS, Innes BH, Last PR, Hebert PDN (2005) DNA barcoding Australia's fish species. Philosophical Transactions of the Royal Society of London. Series B, Biological Sciences 360(1462): 1847–1857. https://doi.org/10.1098/rstb.2005.1716

Ward RD, Holmes BH, White WT, Last PR (2008) DNA barcoding Australasian chondrichthyans: Results and potential uses in conservation. Marine and Freshwater Research 59(1): 57–71. https://doi.org/10.1071/MF07148

Zidowitz H, Fock HO, Westernhagen HV (2002) The role of *Zenopsis* spp. as a predator in seamount and shelf habitats. ICES CM 1000: 28.

Supplementary material 1

Sequences data of the cytochrome oxidase subunit I mitochondrial gene

Authors: Florencia Matusevich, Valeria Gabbanelli, Gonzalo Vulcano, Natalia Plá, Victoria M. Lenain, Diego M. Vazquez, Juan M. Díaz de Astarloa, Ezequiel Mabragaña

Data type: xls

Explanation note: Sequences data of the cytochrome oxidase subunit I mitochondrial gene, used in the present paper, correspond to *Zenopsis* species and *Zeus faber* (used as an outgroup). INSDC: International Nucleotide Sequence Database Collaboration; BOLD: barcode of life datasystem. Footnotes: † Sequence GCA4525-13, originally identified as *Z. nebulosa* in BOLD, is actually a misidentification and corresponds to *Z. stabilispinosa*, as previously determined by Kai and Tashiro (2019). ‡ Near the type locality (Lowe 1852). § Sequenced for this study. | Sequences originally named *Z. conchifer*, identified in the present study as a potential new species, *Zenopsis* sp. 1.

Link: https://doi.org/10.3897/zse.100.122293.suppl1

Supplementary material 2

Comparison of all morphological and meristic data of specimens of *Zenopsis conchifer*

Authors: Florencia Matusevich, Valeria Gabbanelli, Gonzalo Vulcano, Natalia Plá, Victoria M. Lenain, Diego M. Vazquez, Juan M. Díaz de Astarloa, Ezequiel Mabragaña

Data type: xls

Explanation note: Comparison of all morphological and meristic data of specimens of *Zenopsis conchifer* analyzed in this study and information taken from available bibliography (Ragonese and Giusto 2007; Malafaia et al. 2015; Kai and Tashiro 2019), including different areas of its distribution. NW: North Western; NE: North East. Standard length is presented as mm. All remaining measurements are standardized with regard to the standard length. The range and mean between parenthesis are given for each measurement as a percentage of the standard length.

Link: https://doi.org/10.3897/zse.100.122293.suppl2

Zoosyst. Evol. 100 (2) 2024, 747–754 | DOI 10.3897/zse.100.122962

PENSOFT

MUSEUM FÜR NATURKUNDE BERLIN

A new species of *Yunnanilus* (Cypriniformes, Nemacheilidae) from Yunnan, southwest China

Zhi-Xian Qin[1,2*], Wei-han Shao[3*], Li-Na Du[1,2], Zhen-Xing Wang[4]

1 *Key Laboratory of Ecology of Rare and Endangered Species and Environmental Protection (Guangxi Normal University), Ministry of Education, Guilin, Guangxi 541004, China*

2 *Guangxi Key Laboratory of Rare and Endangered Animal Ecology, College of Life Science, Guangxi Normal University, Guilin, Guangxi 541004, China*

3 *Institute of Hydrobiology, Chinese Academy of Sciences, Wuhan, Hubei 430072, China*

4 *Guangxi Lujin Ecological Technology Company, Nanning, Guangxi, 530001, China*

https://zoobank.org/9ACE21C4-8D00-4C34-B7F5-EA8F5FE07243

Corresponding authors: Li-Na Du (dulina@mailbox.gxnu.edu.cn); Zhen-Xing Wang (shangzhuxing@163.com)

Academic editor: Nicolas Hubert ♦ **Received** 13 March 2024 ♦ **Accepted** 3 May 2024 ♦ **Published** 11 June 2024

Abstract

A new species of *Yunnanilus* is described from the Nanpanjiang River, Yunnan, China. The new species, *Yunnanilus polylepis*, can be distinguished from other species of *Yunnanilus* by the following combination of characteristics: Processus dentiformis absent; eye diameter smaller than interorbital width; outer gill raker absent and 10 inner gill rakers on first gill arch; whole trunk covered by scales; nine branched dorsal-fin rays; 10 or 11 branched pectoral-fin rays; six branched pelvic-fin rays. Despite our phylogenetic analysis, which sheds light on the complex relationships among *Yunnanilus* species, the majority of *Yunnanilus* species are restricted to more localized environments and habitats. It is urgent to address the environmental threats that jeopardize their survival, especially given their generally restricted distribution.

Key Words

Loach, mitochondrial gene, morphology, Nanpanjiang River, taxonomy

Introduction

Species belonging to the genus *Yunnanilus* Nichols, 1925 are primarily found in lakes, marshes, and slow-flowing waters, exhibiting an affinity for karstic regions, particularly in the Yunnan and Sichuan provinces of China (Du et al. 2021). Kottelat and Chu (1988), who identified eight valid species and six previously undescribed species from the Yunnan Plateau. Subsequently, Yang and Chen (1995) divided the species of *Yunnanilus* into the *Y. nigromaculatus* and *Y. pleurotaenia* species groups based on the absence or presence of lateral line and cephalic lateral line canals, respectively. Prokofiev (2010) classified the family Nemacheilidae into five tribes, i.e., Lefuini, Nemacheilini, Triplophysini, Vaillantellini, and Yunnanilini. However, the monophyly of the Yunnanilini tribe was not supported in subsequent studies, with Du et al. (2021) and Luo et al. (2023) revising the classification of Yunnanilini using both morphological characteristics and molecular evidence, resulting in the placement of the *Y. nigromaculatus* group into *Eonemachilus* Berg, 1938, *Y. pulcherrimus* Yang, Chen & Lan, 2004 into *Micronemacheilus* Rendahl, 1944, *Y. retrodorsalis* (Lan, Yang & Chen, 1995) into *Troglonectes* Zhang & Zhao, 2016, and *Y. jinxiensis* Zhu, Du & Chen, 2009 into *Paranemachilus* Zhu, 1983. In addition, Du et al.

* These authors contributed equally to this work.

(2023) delineated the phylogenetic relationships among Chinese nemacheilids possessing tube-shaped anterior nostrils, categorizing the spatial relationship between the anterior and posterior nostrils into three distinct types, i.e., separated, adjacent, and closely set. Within this framework, Du et al. (2023) described a new genus, *Guinemachilus* Du et al., 2023, into which *Y. bailianensis* Yang, 2013 and *Y. longibarbatus* Gan, Chen & Yang, 2007 were placed. Subsequently, He et al. (2024) described a new species, *Yunnanilus Yangi* He et al., 2024, from Nanpan Jiang based on morphological and molecular data. Currently, 19 species of *Yunnanilus* have been recognized, with diagnostic characters including inferior mouth, anterior and posterior nostrils separated, anterior nostril base tube-shaped and tip without elongated barbel-like structure, and lateral line and cephalic lateral-line canals present (Kottelat and Chu 1988; Du et al. 2021, 2023).

In November 2023, 13 *Yunnanilus* specimens were collected from a tributary of the Nanpanjiang River in Huaning County, Yuxi City, Yunnan Province, China. Based on morphological characteristics and molecular evidence, these specimens represent a previously undescribed species of *Yunnanilus*. Herein, we provide a description of the new species and its comparison to congeners.

Materials and methods

All care and use of experimental animals complied with the relevant laws of the Chinese Laboratory of Animal Welfare and Ethics (GB/T 35892-2018). Specimens were rapidly euthanized by an overdose of anesthetic clove oil soon after being collected. Five specimens were preserved in 99% ethanol for molecular analyses, and eight specimens were stored in 10% formalin for morphological study. Specimens were deposited in the Kunming Natural History Museum of Zoology, Kunming Institute of Zoology (KIZ), Chinese Academy of Sciences (CAS).

All counts and measurements followed Kottelat (1990). The data were initially processed using Excel software for preliminary statistical analysis. Genomic DNA was extracted from fins fixed in ethanol. Partial sequences of the mitochondrial cytochrome c oxidase subunit I (COI) and cytochrome *b* (cyt *b*) were sequenced by Tsingke Biotechnology Co., Ltd. (China). All sequences were assembled by Seqman in the DNAstar software package and aligned in MEGA v11.0 (Tamura et al. 2021). Sequences have been submitted to GenBank (Accession Nos. PP254216–254236 for COI, PP262976–62996 for cyt *b*). The phylogenetic position of *Yunnanilus polylepis* sp. nov. was determined by maximum likelihood (ML) and Bayesian inference (BI) methods, which were implemented in the CIPRES Science Gateway (Miller et al. 2010). The ML was constructed in RAxML-HPC v8 (Stamatakis 2014). Selected was the rapid bootstrapping configuration, and the bootstrapping iterations were 1000. The BI tree was conducted by MrBayes in XSEDE v3.2.7a (Ronquist et al. 2012). Two runs were performed simultaneously with four Markov chains starting from a random tree. The chains were run for five million generations and sampled every 100 generations. The first 25% of sampled trees were discarded as burn-in, and the remaining trees were used to create a consensus tree and estimate Bayesian posterior probabilities (BPPs). The constructed phylogenetic trees were viewed and edited by FigTree v1.4.4 (Rambaut 2009).

Results

***Yunnanilus polylepis* sp. nov.**

https://zoobank.org/B34187E3-BE59-4EC6-90AE-72F3266CFD89

Type materials. *Holotype*. KIZ2023000009 (Kunming Natural History Museum of Zoology, KIZ, CAS), female, 43.7 mm standard length (SL), Qixitan Park, Panxi Town, Huaning County, Yuxi City, Yunnan, P. R China; Nanpanjiang River; 24.2434°N, 103.1221°E, C.S. Yang collected in November 2023.

***Paratypes*.** Seven specimens. KIZ2023000010–14, female, 31.9–37.1 mm SL, KIZ2023000039–40, male, 30.3–31.8 mm SL; same as holotype.

Other materials. DLN20230180–184, preserved in 99% ethanol for molecular study, same as type specimens.

Etymology. The specific name *polylepis* is derived from the characteristic of being entirely covered by scales Gender: Masculine. We suggest the Chinese and English common names as "多鳞云南鳅" and "densely scaled Yunnan loach," respectively.

Diagnosis. The new species is distinguished from all other members of the genus based on the following characters: whole trunk covered by scales; processus dentiformis absent; eye diameter smaller than interorbital width; nine branched dorsal-fin rays; 10 or 11 branched pectoral-fin rays; six branched pelvic-fin rays; outer gill raker absent and 10 inner gill rakers on first gill arch.

Description. Morphometric and meristic data are given in Table 1. Whole trunk covered with small and dense tubercles. Greatest body depth anterior to dorsal-fin origin, posterior portion gradually compressed from dorsal-fin to caudal-fin base. Head length longer than depth and deeper than width. Snout slightly blunt, shorter than postorbital length of head. Eye diameter smaller than interorbital width, posterior nostril closer to anterior margin of eye than to tip of snout; anterior and posterior nostrils separated, distance greater than diameter of posterior nostril, base of anterior nostril tube-shaped, not elongated to barbel-like (Fig. 1I).

Body densely scaled except for head and thorax; pectoral-fin origin to pelvic-fin origin covered by smaller and sparse scales. Upper jaw processus dentiformis absent. Three pairs of barbels, two rostral pairs and one maxillary pair; inner rostral barbel reaching posterior nostril; outer rostral barbel reaching anterior margin of eye; maxillary barbel reaching posterior margin of eye.

Table 1. Morphometric and meristic data of *Yunnanilus polylepis* sp. nov.

Characters	Holotype	Paratypes (Mean±*SD*)
Total length (mm)	53.8	38.1–45.6 (42.2±2.8)
Standard length (mm)	43.7	30.3–37.1 (33.9±2.6)
Percent of standard length (%)		
Deepest body depth	15.7	16.3–19.6 (17.6±1.1)
Head width	13.4	12.6–15.7 (13.9±1.1)
Lateral head length	25.2	25.2–28.2 (26.5±1.0)
Prepelvic length	54.3	52.5–55.9 (54.3±1.4)
Preanal length	75.4	72.9–78.4 (76.0±2.1)
Preanus length	71.9	70.1–77.3 (73.7±2.3)
Caudal-peduncle length	12.5	11.6–13.7 (13.0±0.8)
Caudal-peduncle depth	10.1	10.0–11.5 (10.6±0.6)
Percent of lateral head length (%)		
Head width	53.0	49.9–57.7 (52.4±2.9)
Head depth	57.4	51.5–62.4 (57.9±4.1)
Eye diameter	19.6	16.7–27.0 (21.8±3.3)
Interorbital width	27.0	23.9–32.9 (29.4±3.0)
Snout length	39.4	31.1–41.7 (37.7±4.2)
Percent of caudal-peduncle length (%)		
Caudal-peduncle depth	80.8	73.2–88.7 (81.8±5.6)
Dorsal-fin rays	iv, 9	iv, 9
Pectoral-fin rays	i, 11	i, 10–11
Pelvic-fin rays	i, 6	i, 6
Anal-fin rays	iii, 5	iii, 5
Branched caudal-fin rays	16	15

Dorsal fin with four unbranched and nine branched rays; origin nearer to snout tip than to base of caudal fin; pectoral fin with one unbranched and 10 or 11 branched rays (mostly 10), inserted immediately anterior to vertical through posteriormost point of operculum; pelvic fin with one unbranded and six branched rays, tips of pelvic fin not reaching anus; anal fin with three unbranched and five branched rays, origin closer to anus; caudal fin emarginate, with 15 or 16 branched rays (mostly 15). Ten inner gill rakers, without outer gill rakers on the first gill arch; lateral line incomplete, with 15–20 lateral line pores, reaching between tip of pectoral-fin and dorsal-fin origin; cephalic lateral system with 13–14+3 infraorbital canal pores, 7–9 supraorbital canal pores, 6–8 supratemporal canal pores, and 9–10 preoperculomandibular canal pores.

Stomach U-shaped, intestine long and straight (Fig. 2B). Swim bladder divided into two chambers, anterior chamber covered by dumbbell-shaped bony capsule, posterior chamber developed, connected with anterior chamber by slender tube, tube length about half of posterior chamber length (Fig. 2A).

Coloration. In life, both sexes, head and trunk with grayish background color. Lower margin of eye to dorsal head surface dark brown, dorsal head with heart-shaped dark brown pattern, ventral head surface without color pattern.

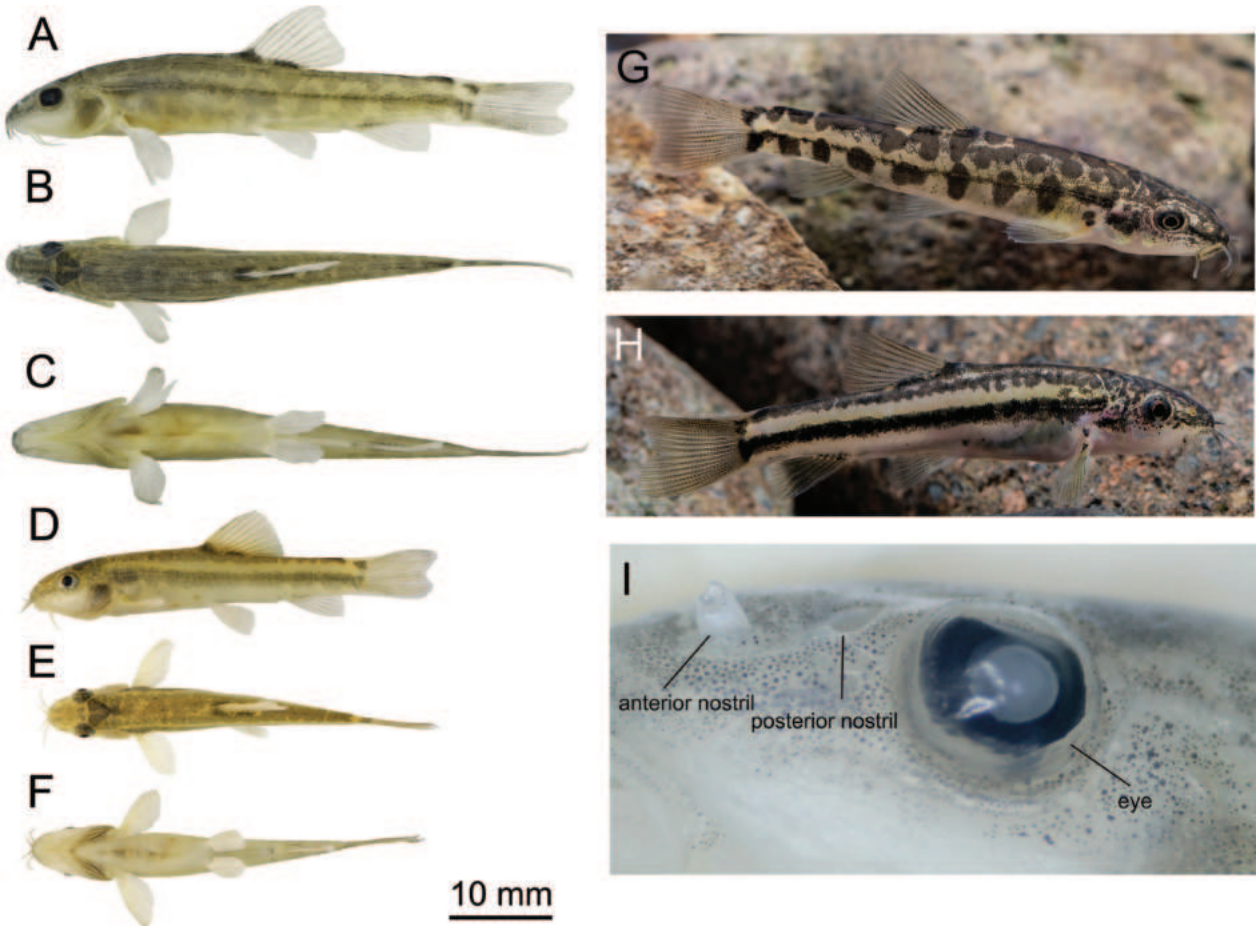

Figure 1. Morphometric characters of *Yunnanilus polylepis* sp. nov. **A–C.** Lateral, dorsal, and ventral views of female, holotype KIZ2023000009; **D–F.** Lateral, dorsal, and ventral views of male, paratype KIZ2023000041; **G–H.** Living photo of female and male; **I.** Location of anterior and posterior nostrils.

Predorsal trunk with five or six dark brown blotches, larger width than interspace. Four or five dark brown blotches after dorsal fin. Two elliptical, dark brown spots at base of dorsal fin, two dark brown spots at base of caudal fin. Fin rays with dark pigments, fin membrane hyaline. In females, upper line of flank with 12–14 dark brown large spots (Fig. 1G). In males, body with black longitudinal stripe on both sides (Fig. 1H). In formalin-fixed specimens, lateral stripe and blotches somewhat faded, body generally light yellow.

Distribution and habitat. *Yunnanilus polylepis* sp. nov. is currently only known from Qixitan Park, Panxi Town, Huaning County, Yuxi City, Yunnan, China; Nanpanjiang River (24.2434°N, 103.1221°E). This species inhabits a deep pool with water depths ranging from 3 to 8 m, characterized by a rich presence of macrophytes (Fig. 3). Other fish species present in the pool include *Discogobio brachyphysallidos* and *Sinocyclocheilus* sp. Despite its confined distribution, the population of *Yunnanilus polylepis* sp. nov. remains stable, largely due to the enforcement of a fishing ban within the park.

Genetic comparisons. Of the 1737 bp in combined alignment, *Y. polylepis* sp. nov. and *Y. pleurotaenia* were amplified in this study. These sequences were used for molecular phylogenetic analysis together with 34 complete mitochondrial genomes and six cyt *b* sequences from GenBank. *Parabotia fasciata* Dabry de Thiersant, 1872 and *Leptobotia elongata* (Bleeker, 1870), two botiid species, were used as outgroups. Given that BI and ML analyses produced overall identical topologies, only the BI tree with Bayesian posterior probabilities (BPP) and bootstrap support (BS) values are presented here (Fig. 4). The phylogenetic tree strongly supports samples of *Yunnanilus polylepis* sp. nov. to group into *Yunnanilus*. Furthermore, *Yunnanilus polylepis* sp. nov. was identified as a sister to the clade containing *Y. analis*, *Y. chuanheensis*, *Y. jiuchiensis*, and *Y. pleurotaenia* (BPP = 1; BS = 100). However, the molecular phylogenies do not support the monophyly of *Yunnanilus*. *Yunnanilus yangi* was weakly supported to be a sister group to *Eonemachilus* (BPP = 59; BS = 61), and then cladded together with those specimens of *Yunnanilus* (Fig. 4).

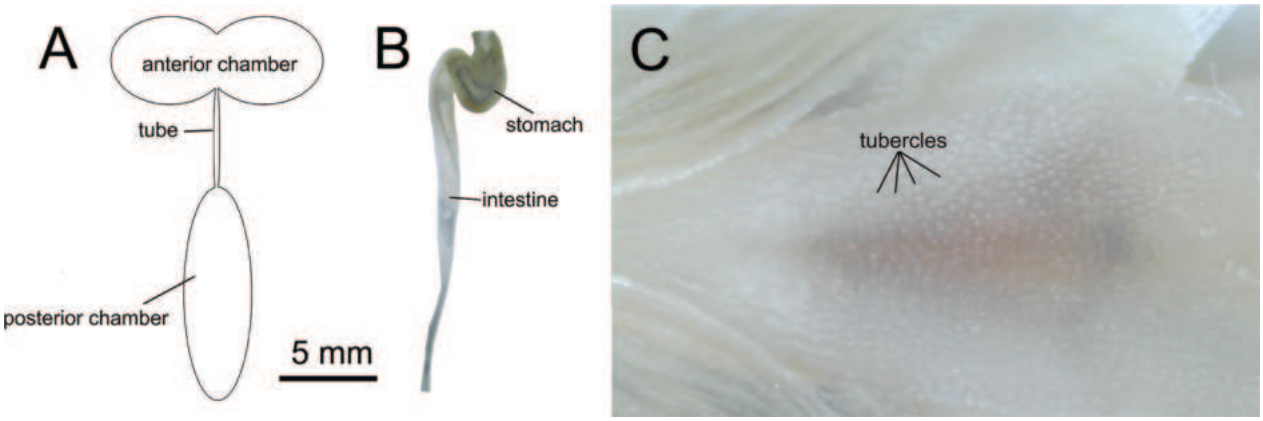

Figure 2. The air baldde (**A**), stomach and intestine (**B**), KIZ 2023000010, and tubercles on the trunk (**C**), KIZ2023000011 of *Yunnanilus polylepis* sp. nov.

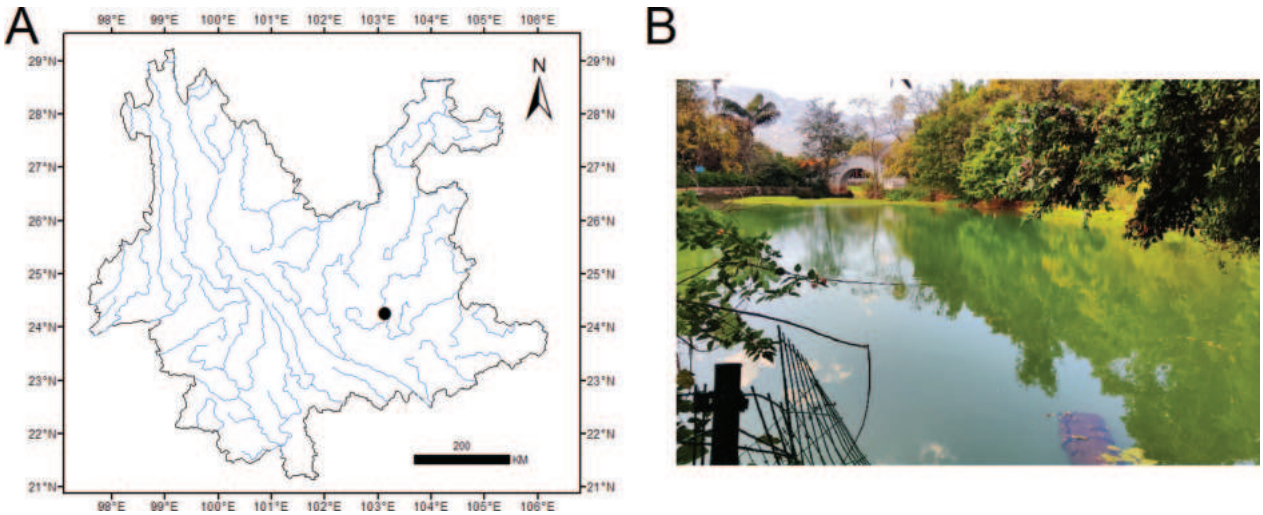

Figure 3. Type locality of *Yunnanilus polylepis* sp. nov. **A.** Distribution map; **B.** Habitat photo of the type locality at the time of collection.

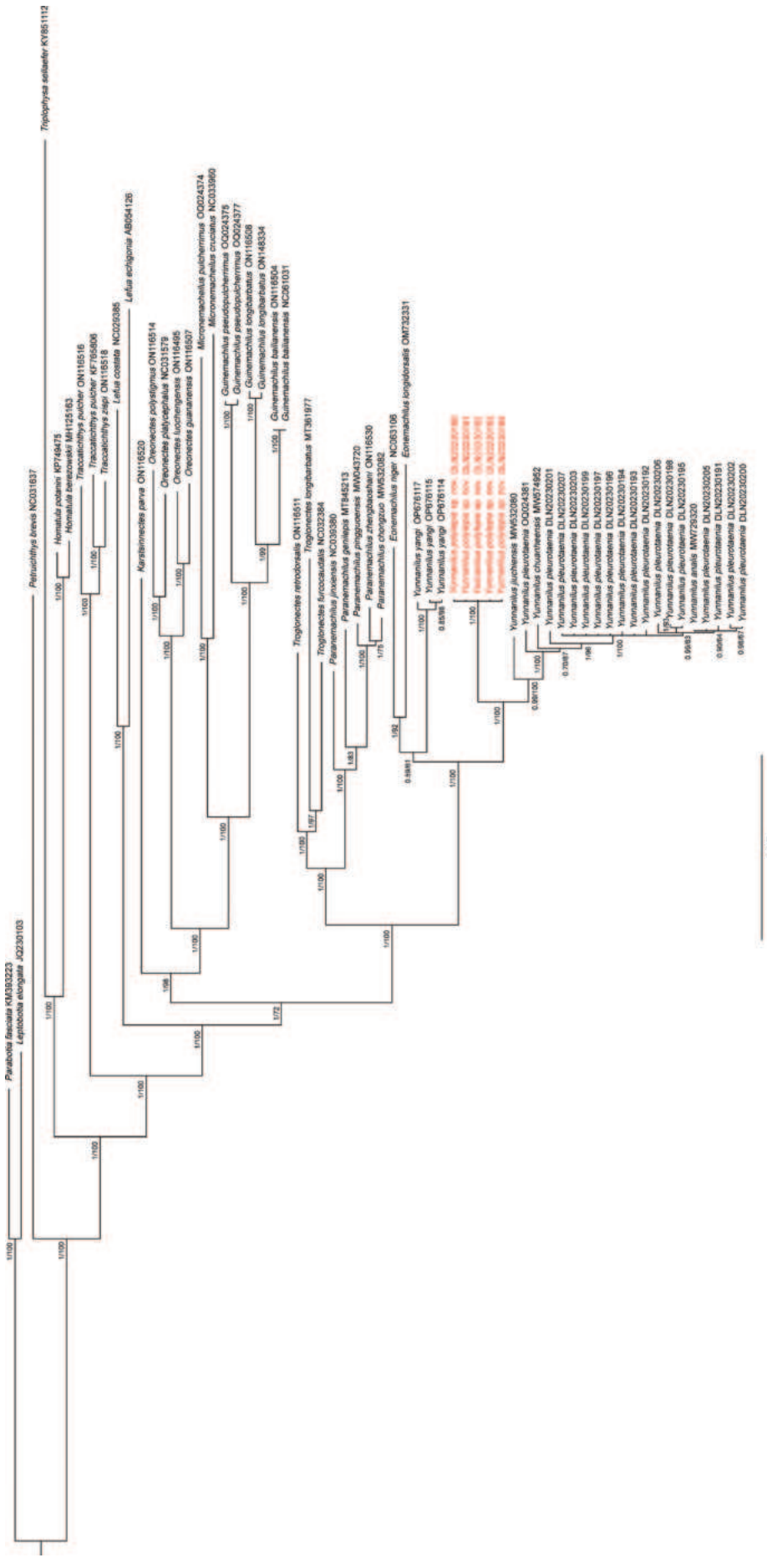

Figure 4. Bayesian phylogram of *Yunnanilus* based on a concatenated dataset of mitochondrial cytochrome c oxidase subunit I (COI) and cytochrome *b* (cyt *b*) sequences. The numbers on the branches represent BPPs from BI and bootstrap supports from ML.

Key to species of the genus Yunnanilus

1 Body scaleless 2
– Body covered by scales 7
2 Caudal fin forked 3
– Caudal fin emarginated 4
3 Outer gill raker present on first gill arch ..... *Y. forkicaudalis*
– Outer gill raker absent on first gill arch ..... *Y. discoloris*
4 Eye diameter smaller than interorbital width 5
– Eye diameter larger than interorbital width 6
5 Processus dentiformis present on upper jaw ..... *Y. paludosus*
– Processus dentiformis absent on upper jaw ..... *Y. yangi*
6 Eight inner gill rakers on first gill arch ..... *Y. analis*
– Ten inner gill rakers on first gill arch ..... *Y. beipanjiangensis*
7 Posterior trunk covered by scales 8
– Whole body covered by scales except head 11
8 Caudal fin forked, outer gill raker present on first gill arch ..... *Y. macrositanus*
– Caudal fin emarginated, outer gill raker absent on first gill arch 9
9 Processus dentiformis absent on upper jaw ..... *Y. sichuanensis*
– Processus dentiformis present on upper jaw 10
10 Interorbital width less than 25% of lateral head length, caudal peduncle length larger than 130% of its depth ..... *Y. nanpanjiangensis*
– Interorbital width larger than 26% of lateral head length, caudal peduncle length smaller than its depth ..... *Y. elakatis*
11 Eye diameter larger than interorbital width 12
– Eye diameter smaller than interorbital 13
12 Processus dentiformis absent on upper jaw; eight inner gill rakers on first gill arch ..... *Y. jiuchiensis*
– Processus dentiformis present on upper jaw, 10–12 inner gill rakers on first gill arch ..... *Y. longiballa*
13 Outer gill raker present on first gill arch 14
– Outer gill raker absent on first gill arch 15
14 Predorsal length 55%–58% of SL; 14–15 inner gill rakers on first gill arch ..... *Y. macrolepis*
– Predorsal length 51%–55% of SL; 11–12 inner gill rakers on first gill arch ..... *Y. spanisbripes*
15 Processus dentiformis absent on upper jaw 16
– Processus dentiformis present on upper jaw 17
16 Ventral area between pectoral and pelvic fins scaleless ..... *Y. chuanheensis*
– Ventral area between pectoral and pelvic fins covered by scales ..... *Y. polylepis* sp. nov.
17 12–13 branched pectoral fin rays; eye diameter less than 12% of lateral head length ..... *Y. macrogaster*
– Ten or eleven branched pectoral fin rays; eye diameter larger than 17% of lateral head length 18
18 10–13 inner gill rakers on first gill arch; six branched pelvic fin rays ..... *Y. pleurotaenia*
– Eight or nine inner gill rakers on first gill arch; seven branched pelvic fin rays ..... *Y. parvus*

Discussion

Yunnanilus polylepis sp. nov. possesses typical characteristics of the genus *Yunnanilus*, including an inferior mouth, anterior and posterior nostrils separated, a tube-shaped base of anterior nostrils that is not elongated into a barbel-like structure, and lateral line and cephalic lateral-line canals present (Du et al. 2021, 2023).

To date, 20 species of *Yunnanilus*, including the newly described species, have been recorded from the Yunnan and Sichuan provinces. Among these species, 12 occur in the Nanpanjiang River (*Y. analis* Yang, 1990, *Y. chui* Yang, 1991, *Y. elakatis* Cao & Zhu, 1989, *Y. forkicaudalis* Li, 1999, *Y. macrogaster* Kottelat & Chu, 1988, *Y. macrolepis* Li, Tao & Mao, 2000, *Y. macrositanus* Li, 1999, *Y. nanpanjiangensis* Li, Tao & Lu, 1994, *Y. paludosus* Kottelat & Chu, 1988, *Y. parvus* Kottelat & Chu, 1988, *Y. yangi* He et al., 2024, and *Yunnanilus polylepis* sp. nov.), six occur in the Yangtze River (*Y. discoloris* Zhou & He, 1989, *Y. jiuchiensis* Du, Hou, Chen & Yang, 2018, *Y. longibulla* Yang, 1990, *Y. pleurotaenia* (Regan, 1904), *Y. sichuanensis* Ding, 1995, and *Y. spanisbripes* An, Liu & Li, 2009), and one species each occurs in the Beipanjiang (*Y. beipanjiangensis* Li, Mao & Sun, 1994) and Honghe rivers (*Y. chuanheensis* Jiang, Zhao, Du & Wang, 2021). Within the genus, *Y. analis*, *Y. beipanjiangensis*, *Y. chui*, *Y. discoloris*, *Y. forkicaudalis*, *Y. paludosus*, and *Y. yangi* are characterized by the absence of scales, while *Y. elakatis*, *Y. macrositanus*, and *Y. nanpanjiangensis* are characterized by scales exclusively present on the caudal peduncle. Although *Yunnanilus polylepis* sp. nov., *Y. chuanheensis*, *Y. jiuchiensis*, *Y. longibulla*, *Y. macrogaster*, *Y. macrolepis*, *Y. parvus*, *Y. pleurotaenia*, and *Y. spanisbripes* share the

character of bodies covered by scales, *Y. chuanheensis* and *Y. jiuchiensis* are scaleless between the pectoral-fin and pelvic-fin bases. *Yunnanilus polylepis* sp. nov. can be further distinguished from *Y. chuanheensis* by six branched pelvic fin rays (vs. seven) and from *Y. jiuchiensis* by 10 inner gill rakers on the first gill arch (vs. eight) and an eye diameter smaller than the interorbital width (vs. larger). *Yunnanilus polylepis* sp. nov. can be distinguished from *Y. longibulla*, *Y. macrogaster*, *Y. macrolepis*, *Y. parvus*, *Y. pleurotaenia*, and *Y. spanisbripes* by processus dentiformis absent (vs. present). It can be further distinguished from *Y. longibulla* by eye diameter smaller than interorbital width (vs. larger), six branched pelvic fin rays (vs. seven or eight), caudal peduncle depth 12%–14% of SL (vs. 8%–10%), from *Y. macrolepis* and *Y. spanisbripes* by outer gill raker absent on first gill arch (vs. present), predorsal length 51%–55% of SL (vs. 56%–58% in *Y. macrolepis*), preanal length 73%–78% of SL (vs. 80%–82% in *Y. macrolepis*, 79%–82% in *Y. spanisbripes*), from *Y. macrogaster* by 10–11 branched pectoral fin rays (vs. 12 or 13), six branched pelvic fin rays (vs. seven), 10 inner gill rakers on first gill arch (vs. 13), body height 16%–20% of SL (vs. 22%–23%), eye diameter 17%–27% of lateral head length (vs. 12%), and from *Y. parvus* by nine branched dorsal fin rays (vs. eight), six branched pelvic fin rays (vs. seven), body height 15%–20% of SL (vs. 20%–23%).

Based on phylogenetic analysis, *Y. analis* was clustered with *Y. pleurotaenia*. However, due to the ambiguous geographical origin of *Y. analis* in GenBank (MW729320), its validity is not discussed in this study. Although molecular evidence from He et al. (2024) supported that *Y. yangi* belongs to *Yunnanilus*, the wrong sequence of *niger* was used in this publication (Du et al. 2023). Additionally, the phylogenetic tree weakly supported *Y. yangi* as a sister group to *Eonemachilus*; hence, the phylogenetic relationship between *Eonemachilus* and *Yunnanilus* will be discussed in the future. Despite the widespread distribution of *Y. pleurotaenia*, the majority of *Yunnanilus* species are restricted to more localized environments and habitats, including small ponds, streams, and lakes. While our phylogenetic analysis sheds light on the complex relationships among *Yunnanilus* species, it also underscores the urgency of addressing the environmental threats that jeopardize their survival, especially given their generally restricted distribution. Overfishing, agricultural runoff and siltation, organic pollution, habitat degradation, and increasing droughts have profoundly affected these endemic species. Notably, Jin et al. (2018) highlighted that the frequency, intensity, and impact of regional droughts have increased in Yunnan in recent years, with a particularly severe drought occurring in the spring and early summer of 2019 due to an abnormally delayed rainy season (Ding and Gao 2020). However, the specific effects of such droughts on the *Yunnanilus* population remain uncertain. Future studies focusing on taxonomic classification, biodiversity surveillance, and conservation assessments are deemed essential.

Nomenclatural acts registration

The electronic version of this article in portable document format represents a published work according to the International Commission on Zoological Nomenclature (ICZN), and hence the new name contained in the electronic version is effectively published under the Code in the electronic edition alone (see Articles 8.5–8.6 of the Code). This published work and the nomenclatural acts it contains have been registered in ZooBank LSIDs (Life Science Identifiers) and can be resolved, and the associated information can be viewed through any standard web browser by appending the LSID to the prefix http://zoobank.org/.

Competing interests

The authors declare that they have no competing interests.

Authors' contributions

Z.-X. Q. and L.-N.D. measured the specimens, analyzed the data, conceived and designed the study, and prepared the manuscript. W.-H. S. analyzed the molecular data and constructed the phylogenetic tree. Z.-X. W. provided funding for the field survey. All authors read and approved the final version of the manuscript.

Acknowledgments

This study was funded by the Guangxi Natural Science Foundation Project (2022GXNSFAA035563) and the Key Laboratory of Ecology of Rare and Endangered Species and Environmental Protection (Guangxi Normal University), Ministry of Education, China (ERESEP2022Z05). We are grateful to C. S. Yang for collecting specimens. We thank H. J. Chen for providing the living photographs of this species.

References

Ding T, Gao H (2020) The record-breaking extreme drought in Yunnan Province, Southwest China during spring-early summer of 2019 and possible causes. Journal of Meteorological Research 34(5): 997–1012. https://doi.org/10.1007/s13351-020-0032-8

Du LN, Yang J, Min R, Chen XY, Yang JX (2021) A review of the Cypriniform tribe Yunnanilini Prokofiev, 2010 from China, with an emphasis on five genera based on morphologies and complete mitochondrial genomes of some species. Zoological Research 42(3): 310–334. https://doi.org/10.24272/j.issn.2095-8137.2020.229

Du LN, Li SJ, Xu F, Luo T, Luo FG, Yu GH, Zhou J (2023) Clarification of Phylogenetic Relationships among Chinese Nemacheilids with Tube-Shaped Anterior Nostrils, with a Description of a New Genus and Two New Species. Journal of Zoological Sys-

tematics and Evolutionary Research 2023: 3600085. https://doi.org/10.1155/2023/3600085

He YR, Li XR, Che XJ, Yang XJ, Wang JS, Wang M (2024) A new species of *Yunnanilus* (Cypriniformes: Nemacheilidae) from upper Pearl River, Yunnan, China. Zootaxa 5428(2): 194–206. https://doi.org/10.11646/zootaxa.5428.2.2

Jin Y, Kuang XY, Yan HM, Wan YX, Wang P (2018) Studies on distribution characteristics and variation trend of the regional drought events over Yunnan in recent 55 years. Qixiang 44: 1169–1178. https://doi.org/10.7519/j.issn.1000-0526.2018.09.005

Kottelat M (1990) Indochinese nemacheilines: A revision of nemacheiline loaches (Pisces: Cypriniformes) of Thailand, Burma, Laos, Cambodia and southern Viet Nam. Druckerei braunstein, München. Indochinese Nemacheilines, 262 pp.

Kottelat M, Chu XL (1988) Revision of *Yunnanilus* with descriptions of a miniature species flock and six new species from China (Cypriniformes: Homalopteridae). Environmental Biology of Fishes 23(1–2): 65–93. https://doi.org/10.1007/BF00000739

Luo T, Yang Q, Wu L, Wang YL, Zhou JJ, Deng HQ, Xiao N, Zhou J (2023) Phylogenetic relationships of Nemacheilidae cavefish (*Heminoemacheilus*, *Oreonectes*, *Yunnanilus*, *Paranemachilus*, and *Troglonectes*) revealed by analysis of mitochondrial genome and seven nuclear genes. Zoological Research 44(4): 693–697. https://doi.org/10.24272/j.issn.2095-8137.2022.266

Miller MA, Pfeiffer W, Schwartz T (2010) Creating the CIPRES Science Gateway for inference of large phylogenetic trees. Gateway Computing Environments Workshop (GCE) 2010: 1–8. https://doi.org/10.1109/GCE.2010.5676129

Prokofiev AM (2010) Morphological classification of loaches (Nemacheilinae). Journal of Ichthyology 50(10): 827–913. https://doi.org/10.1134/S0032945210100012

Rambaut A (2009) FigTree. Version 1.4.4. http://tree.bio.ed.ac.uk/software/figtree

Ronquist F, Teslenko M, van der Mark P, Ayres DL, Darling A, Höhna S, Larget B, Liu L, Suchard MA, Huelsenbeck JP (2012) MrBayes 3.2: Efficient Bayesian phylogenetic inference and model choice across a large model space. Systematic Biology 61(3): 539–542. https://doi.org/10.1093/sysbio/sys029

Stamatakis A (2014) RAxML Version 8: A tool for phylogenetic analysis and post-analysis of large phylogenies. Bioinformatics 30(9): 1312–1313. https://doi.org/10.1093/bioinformatics/btu033

Tamura K, Stecher G, Kumar S (2021) Mega11: Molecular evolutionary genetics analysis version 11. Molecular Biology and Evolution 38(7): 3022–3027. https://doi.org/10.1093/molbev/msab120

Yang JX, Chen YR (1995) The biology and resource utilization of the fishes of Fuxian Lake, Yunnan. Yunnan Science and Technology Press, Kunming, China, 224 pp.

Zoosyst. Evol. 100 (2) 2024, 755–767 | DOI 10.3897/zse.100.118000

PENSOFT

MUSEUM FÜR NATURKUNDE BERLIN

A new rare catfish species from southeastern Brazil provides insights into the origins of similar colour patterns in syntopic, distantly related mountain trichomycterines (Siluriformes, Trichomycteridae)

Wilson J. E. M. Costa[1], Caio R. M. Feltrin[1], José Leonardo O. Mattos[1], Axel M. Katz[1]

1 *Laboratory of Systematics and Evolution of Teleost Fishes, Institute of Biology, Federal University of Rio de Janeiro, Caixa Postal 68049, CEP 21941-971, Rio de Janeiro, Brazil*

https://zoobank.org/C3BED28C-2D3A-416F-BEBA-73DF1BECA132

Corresponding author: Wilson J. E. M. Costa (wcosta@acd.ufrj.br)

Academic editor: Nicolas Hubert ♦ **Received** 30 December 2023 ♦ **Accepted** 2 April 2024 ♦ **Published** 11 June 2024

Abstract

Colour patterns are diverse in trichomycterine catfishes and are often used to diagnose species. Here, we analyse the first case of adults of two syntopic species of *Trichomycterus* sharing nearly identical colour patterns: a rare new species of the subgenus *Paracambeva* and *Trichomycterus maculosus*, a distantly related species of the subgenus *Trichomycterus*. Both species are endemic to the upper Rio Paraíba do Sul basin (RPSB), which had a different course until the Tertiary period and is situated within the Southeastern Brazilian Continental Rift, mostly active in the Eocene-Oligocene. A time-calibrated multigene analysis, 3144 bp, supported the new species as sister to *Trichomycterus itatiayae*, both comprising a lineage with Middle Miocene age, when that colour pattern would have first arisen. The new species is diagnosed by characters from the latero-sensory system and bone morphology. Our results, combined with available biogeographical data, indicated the colour pattern of *T. maculosus* arising in the Late Pliocene, following the dispersal of its group to the upper RPSB after river course changing. Two hypotheses for the independent origin of the same colour pattern are discussed. First, a case of evolutionary convergence for adaptation to live on a similarly coloured gravel substrate, giving some cryptic advantage against predators. Second, mimetic association through anti-predation features. In the latter case, although trichomycterids lack fin spines to inoculate venom as in other catfishes, the species here studied have a supposed axillary gland above the pectoral fin, just posterior to the opercular odontodes, but with properties and functions still unknown.

Key Words

Atlantic forest, molecular systematics, mountain biodiversity, Rio Paraíba do Sul basin, Serra da Mantiqueira

Introduction

Colouration has an important role in the biology of teleost fish species, involving attributes related to their behaviour and ecology (e.g., Price et al. 2008). Colour patterns are particularly diverse among the Trichomycterinae (Eigenmann 1918), one of the most diverse groups of Neotropical catfishes, and as a consequence, they have been frequently used to diagnose species and groups since the 19th century (Valenciennes 1832). During field studies, colour patterns are often the primary tool to distinguish sympatric trichomycterine species, although chromatic polymorphism within species is not uncommon (Arratia et al. 1978; Sarmento-Soares et al. 2005; da Silva et al. 2010; Costa et al. 2023a; Vilardo et al. 2023). On the other hand, the occurrence of sympatric, non-closely related trichomycterine species exhibiting identical colour patterns is a rarely reported event (Costa et al. 2020a; Reis et al. 2020). The only report of two distantly related trichomycterines with the same colour pattern and found sharing the same habitat was made by Barbosa and Costa (2008) for *Trichomycterus itatiayae* Miranda Ribeiro, 1906, a species of the subgenus *Paracambeva* Costa, 2021, and *Trichomycterus nigroauratus* Barbosa & Costa, 2008 of the subgenus *Trichomycterus* (Costa 2021).

Herein we first report a rare new trichomycterine catfish species, with only four specimens found in the last two collections of six collecting trips between 1991 and 2023 to the upper Rio do Peixe drainage, Rio Paraíba do Sul basin (hereafter RPSB), southeastern Brazil. This species is morphologically similar to the syntopic *Trichomycterus maculosus* Barbosa & Costa, 2010, which is sister to *T. nigroauratus*. Specimens of this new species had a colour pattern approximately identical to that exhibited by larger adult specimens above 70 mm SL of *T. maculosus* (small spots on the dorsal part of the flank and a narrow dark grey longitudinal stripe along the flank midline; see description and included illustrations below), found in the same habitat (i.e., over gravel stream bottom). The two species are externally distinguishable by a few characters, comprising the relative position of the dorsal and anal fins, with the anal-fin origin positioned at a vertical line through the posterior-most portion of the dorsal-fin base in *T. maculosus*, vs. at a vertical line just posterior to the middle of the dorsal-fin base in the new species; number of pectoral-fin rays, eight in *T. maculosus* vs. seven in the new species; and body depth, with *T. maculosus* being more slender than the new species, reaching 12.8–13.8% of the standard length (SL) in *T. maculosus*, vs. 16.6–20.0% SL in the new species. Preliminary analysis in the laboratory revealed that the new species is sister to *T. itatiayae*, a member of *Paracambeva*, thus contrasting with the syntopic *T. maculosus*, a common species endemic to the upper Rio do Peixe drainage, belonging to the *Trichomycterus nigroauratus* group of the subgenus *Trichomycterus* (Barbosa and Costa 2010; Costa 2021). *Paracambeva* is diagnosed by an anterior infraorbital canal not attached to the lacrimal, a relatively short interopercle, and a relatively slender parapophysis of the second free vertebra (Costa 2021).

The new species and *T. maculosus* are only known from streams belonging to the upper Rio do Peixe drainage, Rio Paraiba do Sul basin (hereafter RPSB), in the southern plateau of the Serra da Mantiqueira, a mountain range that is an important centre of biodiversity in the Atlantic Forest, with a great concentration of endemic trichomycterines of the genus *Trichomycterus* Valenciennes, 1832 (e.g., Costa and Katz 2021). The origin of the southern plateau of the Serra da Mantiqueira is related to an uplift during the Neo-Cretaceous as a result of the process of separation of the South American and African plates (Riccomini et al. 2004, 2010). The southern plateau of the Serra da Mantiqueira is presently a divisor between the Rio Paraná basin and the RPSB. Geological evidence indicates that the upper portion of the present RPSB, including all the area today inhabited by the new species *T. itatiayae*, *T. maculosus*, and *T. nigroauratus* between the Neo-Cretaceous and the Tertiary, had a different course, directed to the northwest and being connected to the Rio Tietê drainage, the Rio Paraná basin, instead of the middle and lower sections of the RPSB (King 1956; Riccomini et al. 2010). In addition, the Rio do Peixe drainage is situated in a core area of the region known as the South-eastern Brazilian Continental Rift, which had its greatest development in the Eocene-Oligocene, including the paleo-lake Tremembé formed during the Oligocene (e.g., Riccomini et al. 2004, 2010). The objectives of the present study are to describe the new species, perform a time-calibrated analysis to test the positioning of the new species, and infer the timing of the origin of derived colour patterns in both lineages using a biogeographical temporal context.

Materials and methods

Specimens

Field procedures were approved by CEUA-UFRJ (Ethics Committee for Animal Use of the Federal University of Rio de Janeiro; permit numbers: 065/18 and 084/23) and collecting permits were given by ICMBio (Instituto Chico Mendes de Conservação da Biodiversidade; permit number: 38553-11). For details about specimen euthanasia, fixation, and conservation, see Costa et al. (2023b). Specimens were deposited in the ichthyological collection of the Instituto de Biologia, Universidade Federal do Rio de Janeiro (UFRJ). Comparative material is listed in Barbosa and Costa (2008), Costa and Katz (2021), and Costa et al. (2023b). A complete list of specimens used in morphological comparisons, with their respective catalogue numbers and locality coordinates, appears in Suppl. material 1.

Morphological data

Methods for taking and describing morphological characters were according to recent studies on *Paracambeva*, including morphometric and meristic data following Costa (1992) and Costa et al. (2020b), osteological preparations following Taylor and Van Dyke's (1985), latero-sensory system nomenclature following Arratia and Huaquin (1995) and Bockmann and Sazima (2004), bone terminology following Costa (2021) and Kubicek (2022), and fin ray formulae following Bockmann and Sazima (2004).

DNA extraction, amplification, and sequencing

Methods for DNA extraction, amplification, and sequencing followed the most recent phylogenetic analysis of *Paracambeva* (Costa et al. 2023b), with PCR reactions performed in 45 µl with the following reagent concentrations: 5× GreenGoTaq Reaction Buffer (Promega), 1.0 mM $MgCl_2$, 1 µM of each primer, 0.2 mM of each dNTP, 1 u of Promega GoTaq Hot Start polymerase, and 50 ng of total genomic DNA; thermal profile: 95 °C for 5 min; 35 cycles of 94 °C for 1 min; 50–60 °C for 1–1.5 min;

and 73 °C for 7 min; sequencing reactions performed in 20 µL reaction volumes containing 4 µL BigDye, 2 µL sequencing buffer 5× (Applied Biosystems), 2 µL of the PCR products (30–40 ng), 2 µL primer, and 10 µL ultrapure water; and the thermal profile was 35 cycles of 30 s at 95 °C, 30 s at 55 °C, and 1.5 min at 73 °C. Primers used for mitochondrially encoded genes were: Cytb Siluri F and Cytb Siluri R (Villa-Verde et al. 2012) for *cytochrome b* (CYTB); FISHF1 and FISHR1 (Ward et al. 2005) for *cytochrome c oxidase I* (COX1). Primers for the nuclear encoded genes were: MYH6 TRICHO F and MYH6 TRICHO R (Costa et al. 2020c) for *myosin heavy chain 6* (MYH6), and RAG2 TRICHO F and RAG2 TRICHO R (Costa et al. 2020c) for *recombination activating 2* (RAG2). MEGA 11 (Tamura et al. 2021) was used to read and interpret sequencing chromatograms, to perform the sequence annotation, and to translate DNA sequences into amino acid residues to verify the absence of premature stop codons or indels. GenBank accession numbers are in Table 1.

Phylogenetic analyses

The terminal taxa for the phylogenetic analyses include all species of *Paracambeva*, including the new species herein described, and all species of the subgenus *Trichomycterus.* The remaining species of *Trichomycterus* and outgroups included in the analysis are the same as those used in Costa et al. (2023b). See Costa et al. (2023b) for justification for outgroup selection. Each gene dataset was aligned using the Clustal W algorithm (Chenna et al. 2003) implemented in MEGA 11 and analysed for determination of the optimal partitioning and evolutionary models (Table 2) using the Corrected Akaike Information (AICc) in PartitionFinder 2.1.1 (Lanfear et al. 2016). Phylogenetic analyses followed the methods described in Costa et al. 2023b), comprising Bayesian Inference performed with Beast 1.10.4 (Suchard et al. 2018), using the Yule process as the tree prior (Gernhard, 2008), two independent Markov chain Monte Carlo (MCMC) runs with 9×10^7 generations with a

Table 1. Terminal taxa and GenBank accession numbers by gene used in molecular analyses.

	COI	CYTB	RAG2	MYH6
Diplomystes nahuelbutaensis	AP012011.1	MN640590	DQ492317	–
Callichthys callichthys	MZ051783.1	KP960058	DQ492324	–
Corydoras panda	NC049097.1	NC049097.1	KP960362.1	–
Nematogenys inermis	EU359428	–	KY858182.1	KY858107.1
Trichogenes longipinnis	OQ810037	MK123704	MF431117	MF431104.1
Microcambeva ribeirae	MN385807.1	OK334290	MN385832	MN385819.1
'Trichomycterus' areolatus	AP012026.1	FJ772214	KY858188	–
Ituglanis boitata	OQ810038	MK123706	MK123758	MK123734.1
Cambeva barbosae	MK123689	MK123713	MN385820	MK123740.1
Scleronema minutum	MK123685	MK123707	MK123759.1	KY858109.1
Trichomycterus nigricans	MN813005.1	MT470415.1	MK123765.1	MK123750.1
Trichomycterus albinotatus	MN813007.1	MT459172.1	MN812990.1	MK123743.1
Trichomycterus brasiliensis	MT470418.1	MT470418.1	MK123763.1	MK123744.1
Trichomycterus itatiayae	MW671552	MW679291	OR995282	OL779229
Trichomycterus reinhardti	MK123698.1	MK123727.1	MK123698.1	MF431106.1
Trichomycterus funebris	MT941786.1	MT941823.1	KY858194	KY858121
Trichomycterus pauciradiatus	MT941796	MT941833	MW196782	MW196769.1
Trichomycterus ingaiensis	MT941790	MT941829	OR995283	–
Trichomycterus piratymbara	KY857970	KY858040	KY858121	KY858194
Trichomycterus sainthilairei	MT941814	MT941851	OR995284	–
Trichomycterus septemradiatus	MK123700	MK123729	MW196781	MK123755.1
Trichomycterus humboldti	MT941787	MT941824	OR995285	–
Trichomycterus luetkeni	MT941793	MT941831	KY858214	KY858148
Trichomycterus anaisae	MT941782	MT941820	OR995286	–
Trichomycterus coelhorum	OR981611	OQ660192	OQ660183	–
Trichomycterus adautoleitei	OR981612	OQ660193	–	–
Trichomycterus antiquus	OR981613	OR995280	OR995287	–
Trichomycterus giganteus	MK123693.1	MK123720	MT446426	MK123746.1
Trichomycterus maculosus	MN813010.1	OR995281	MN812994.1	MN812998.1
Trichomycterus nigroauratus	MK123696	OK247569	MK123766	MK123751.1
Trichomycterus quintus	MT299917.1	MN812999	–	MT305242.1
Trichomycterus mutabilicolor	OR981614	OK247576	–	–
Trichomycterus santaeritae	MN813009	MN813001	MN812993	MN812997
Trichomycterus immaculatus	MK123694	MK144348	MF431120	MK123747
Trichomycterus santaeritae	MN813009	MN813001	MN812993	MN812997

Table 2. Best-fitting partition schemes with the respective number of base pairs and the best-suited evolutionary models.

Partition	Base pairs	Evolutive Model
COX1 3rd	251	TRN+I+G
COX1 1st	251	TRN+I+G
COX1 2nd, CYTB 2nd	594	GTR+I+G
CYTB 3rd	343	GTR+G
CYTB 1st	343	GTR+I+G
RAG2 2nd, RAG2 1st	546	SYM+G
RAG2 3rd	273	GTR+G
MYH6 1st	181	GTR+G
MYH6 2nd	181	TRN
MYH6 3rd	181	K80+G

sampling frequency of 1000; determination of the convergence of the MCMC chains and the proper burn-in values through the stationary phase of the runs using the effective sample size analysed with Tracer 1.7.1 (Rambaut et al. 2018), combination of generated trees using LogCombiner v.1.10.4 (Suchard et al. 2018) following a 25% burn-in at the outset of each run, and calculation of the consensus tree and Bayesian posterior probabilities using Tree Annotator version 1.10.4 (Suchard at al., 2018); and Maximum Likelihood analysis performed with IQTREE 2.2.2.6 (Minh et al. 2020), with support node expressed by ultrafast bootstrap (Hoang et al. 2018) and the Shimodaira-Hasegawa-like approximate likelihood ratio test (SH-aLRT; Guindon et al. 2010), both using 1000 replicates. In order to evaluate the contribution of each genetic locus dataset analysed, we generated individual trees for each of the nuclear genes and one for the mitochondrial genes, using ML as above described.

Divergence-time estimation

The divergence time analysis was conducted in Beast 1.10.4 using the same dataset, partitions, evolution models, and parameters as described above. Additionally, the analysis incorporated a lognormal uncorrelated relaxed clock model and a Yule speciation process as the tree prior (Gernhard 2008). Calibration points were established as follows: the origin of the Trichomycteridae with a normal prior distribution (mean = 106 MA, SD = 5.0), following the estimative of Betancur-R et al. (2015), which is often used as an indirect calibration strategy in other studies on trichomycterids (e.g., Ochoa et al. 2017; Vilardo et al. 2023); and the origin of the genus *Corydoras* with a lognormal prior distribution (mean = 55 MA, SD = 1), based on the dating of *Corydoras revelatus* Cockerell, 1925, the oldest known fossil of callichthyid catfishes. MCMC chains were assessed to verify convergence by evaluating the effective sample size of the runs in Tracer 1.7.1. The time-scaled tree was obtained using Tree Annotator version 1.10.4 to generate the consensus tree.

Results

Taxonomic accounts

Trichomycterus (*Paracambeva*) *antiquus* sp. nov.

https://zoobank.org/

Figs 1–3, Table 3

Type material. ***Holotype.*** Brazil • 1 ex., 72.2 mm SL; Estado de São Paulo: Município de São José dos Campos: small stream tributary of the Rio Santa Bárbara, Rio do Peixe drainage, Rio Paraíba do Sul basin, São Francisco Xavier, Serra dos Poncianos, part of the Serra da Mantiqueira; 22°51'47"S, 45°54'60"W; about 980 m asl; 21 April 2023; C.R.M. Feltrin, leg.; UFRJ 13674.

Paratypes. (all from Estado de São Paulo: Município de São José do Campos: Rio do Peixe drainage, Rio Paraíba do Sul basin, São Francisco Xavier, Serra dos Poncianos, part of the Serra da Mantiqueira): BRAZIL • 1 ex., 75.6 mm SL (stained with alizarin and partially dissected); collected with holotype; UFRJ 13673; 1 ex., 79.1 mm SL; stream tributary of Rio Santa Bárbara; 22°53'45"S, 45°56'34"W; about 765 m asl; same collector and date as holotype; UFRJ 13681; 1 ex., 44.5 mm SL (cleared and stained for osteological analysis); same locality and collector as holotype; 29 October 2023; UFRJ 14201.

Diagnosis. *Trichomycterus antiquus* is distinguished from all other species of *Paracambeva*, except *T. itatiayae*, by having a relatively large head, its length 20.4–22.8% SL (vs. 11.4–18.1% SL), the presence of a deep concavity on the postero-ventral margin of the metapterygoid, accommodating a pronounced expansion of the postero-dorsal quadrate outgrown (Fig. 3B, see also Costa 2021: fig. 3B for similar condition in *T. itatiayae*; vs. metapterygoid concavity, when present, never deep and quadrate expansion, when present, never pronounced in other species of *Paracambeva*, e.g. Costa et al. 2023b: figs. 6G, H) and the presence of a a deep U-shaped concavity on the dorsal margin of the anterior hyomandibular anterior outgrown (Fig. 3B, see also Costa 2021: fig. 3B for similar condition in *T. itatiayae*; vs. concavity, when present, never U-shaped, e.g. Costa et al. 2023b: figs. 6G, H). *Trichomycterus antiquus* differs from *T. itatiayae* by the presence of the anterior infraorbital canal (vs. absence), jaw teeth sharply pointed (vs. incisiform), a wider body and head (body width 11.9–15.0 vs. 6.2–8.8% SL; head width 51.8–58.4 vs. 68.7–75.7% SL), a longer pre-dorsal length (66.0–65.2 vs. 59.2 – 64.0% SL), a longer pre-pelvic length (60.7– 65.2 vs. 54.9–56.9% SL), a deeper head (head depth 51.5–58.4 vs. 39.0–50.8% SL), a large eye (eye diameter 8.8–11.3 vs. 7.4–8.2% of the head length), a short sesamoid supraorbital, about twice longer than the lacrimal (Fig. 3A; vs. long, about four times longer, Costa 2021: fig. 2B); a well-developed postero-lateral process of the autopalatine (Fig. 3A; vs. rudimentary, Costa 2021: fig. 2B); and a slender and long maxilla, longer than premaxilla (Fig. 3A; vs. relatively deep, shorter than premaxilla, Costa 2021: fig. 2B).

Figure 1. *Trichomycterus* (*Paracambeva*) *antiquus* sp. nov., UFRJ 13674, holotype, 72.2 mm SL. **A.** Left lateral view; **B.** Dorsal view; **C.** Ventral view.

Description. ***General morphology.*** Morphometric data appear in Table 3. Body relatively deep (Fig. 1A), greatest body depth at vertical through midway between pectoral and pelvic-fin bases. Trunk subcylindrical to compressed on caudal peduncle, dorsal and ventral lateral profiles weakly convex to almost straight. Whole body, except venter, covered with minute papillae. Small putative axillary gland above pectoral fin, below lateral line, with small orifice just posterior to opercular patch of odontodes (Fig. 2A). Lateral line of trunk consisting of anterior minute canal with two pores obliquely arranged, posterior followed by almost imperceptible line between humeral region and caudal-fin base with minute superficial neuromasts. Anterior-most pore of lateral line more ventrally positioned than posterior one. Urogenital opening consisting of transverse aperture situated in shallow depression. Anus positioned immediately in front of urogenital opening, at vertical just posterior to dorsal-fin origin.

Head sub-trapezoidal in dorsal view, dorsal surface flat (Fig. 1B). Eye small, positioned on dorsal head surface, nearer snout tip than posterior margin of opercle. Distance between anterior and posterior nostrils approximately

Table 3. Morphometric data of *Trichomycterus antiquus* sp. nov.

	Holotype	Paratypes (n=3)
Standard length (SL)	72.2	44.5–79.1
Percentage of standard length		
Body depth	20.0	16.1–18.1
Caudal peduncle depth	14.7	12.1–14.9
Body width	17.3	11.9–15.0
Caudal peduncle width	6.0	4.0–8.1
Pre-dorsal length	68.1	66.0–68.5
Pre-pelvic length	62.4	60.7–65.2
Dorsal-fin base length	10.5	10.1–12.0
Anal-fin base length	10.1	9.2–10.3
Caudal-fin length	15.3	13.1–17.6
Pectoral-fin length	10.5	12.1–13.9
Pelvic-fin length	8.2	8.2–9.2
Head length	22.8	20.4–22.1
Percentage of head length		
Head depth	52.2	51.5–58.4
Head width	90.8	85.7–90.2
Snout length	52.3	40.4–49.5
Interorbital width	26.9	24.5–28.1
Preorbital length	13.8	15.5–16.1
Eye diameter	9.8	8.8–11.3

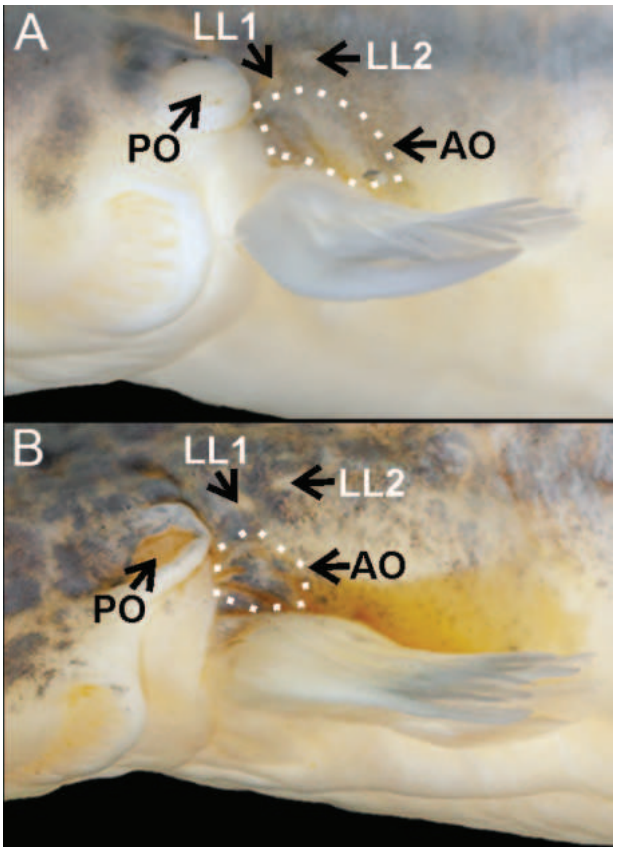

Figure 2. Lateral view of the head, left side, of **A.** *Trichomycterus* (*Paracambeva*) *antiquus* sp. nov., UFRJ 13674, holotype, 72.2 mm SL; **B.** *Trichomycterus* (*Trichomycterus*) *maculosus*, UFRJ 13676, 97.6 mm SL. AO, supposed axillary organ; LL 1–2, lateral line pores 1–2; PO, preopercular patch of odontodes.

half distance between posterior nostril and orbit. Tip of nasal barbel posteriorly reaching area between orbit and opercular patch of odontodes, tip of maxillary and rictal barbels reaching middle of interopercular patch of odontodes. Mouth subterminal. Jaw teeth pointed, irregularly arranged. Cleared and stained specimen with 48 teeth on premaxilla, 38 on dentary. Odontodes narrow, pointed to sub-incisiform in larger odontodes of larger specimens, about straight, irregularly arranged, 14 or15 on opercle and 44 or 45 on interopercle. Cephalic latero-sensory system comprising long canal interconnecting supraorbital, posterior section of infraorbital, and postorbital canals, and isolated anterior infraorbital canal. Supraorbital sensory canal with three pores, s1, s3, and s6; anterior section of infraorbital canal with two pores, i1 and i3; posterior section of infraorbital canal with two pores, i10 and i11; and postorbital canal with two pores, po1 and po2. All pores paired. Pore s6 about equidistant from orbit than its homologous pore.

Fins thin with thick bases and convex free margins (Fig. 1A). Anal-fin origin at vertical, immediately posterior to middle of dorsal-fin base, at vertical through base of 4th bifid dorsal-fin ray. First pectoral-fin ray terminating in short filament, its length about 20% of pectoral-fin length. Pelvic posteriorly overlapping anus and urogenital papilla. Posterior extremity of pelvic fin at vertical through area just anterior to middle of dorsal-fin base. Pelvic-fin bases medially separated by minute interspace. Caudal fin subtruncate. Total dorsal-fin rays 11 (ii + II + 7), total anal-fin rays 9 (ii + II + 5), total pectoral-fin rays 7 (I + 6), total pelvic-fin rays 5 (I + 4), total principal caudal-fin rays 13 (I + 11 + I), total caudal dorsal procurrent rays 15 (xiv + I), total caudal ventral procurrent rays 13 (xii + I).

***Osteology* (Fig. 3).** Mesethmoid slender, T-shaped, anterior margin about straight, cornu narrow, longitudinal main axis gently laterally widening close anterior margin of lateral ethmoid. Lateral ethmoid without lateral projections. Lacrimal thin, not associated to infraorbital canal, separated from sesamoid supraorbital by long interspace. Sesamoid supraorbital short and slender, its length about twice lacrimal length, its width about equal lacrimal width. Premaxilla sub-trapezoidal in dorsal view, slightly tapering laterally. Maxilla slender, boomerang-shaped, slightly longer than premaxilla.

Autopalatine robust, sub-rectangular in dorsal view when excluding postero-lateral process, its largest width about half autopalatine length including anterior cartilage. Lateral margin of autopalatine nearly straight, medial margin concave. Autopalatine posterolateral process well-developed, triangular, its length about equal autopalatine length, excluding anterior cartilage. Metapterygoid subtrapezoidal, deeper than long. Postero-ventral margin of metapterygoid deeply concave, accommodating pronounced dorsal expansion of quadrate. Dorsal extremity of metapterygoid truncate, anterior margin convex, posterior margin about straight. Quadrate L-shaped, with pronounced postero-dorsal outgrowth, anterior margin concave. Hyomandibula moderately long. Anterior hyomandibular outgrowth deep, antero-dorsal margin about horizontal, posteriorly followed by deep U-shaped concavity.

Opercle elongate, slightly longer than interopercle. Dorsal opercular process short and blunt. Opercular articular facet for hyomandibula laterally protected by laminar shield articular facet for preopercle inconspicuous. Opercular odontode patch moderately slender, its width about half length of dorsal hyomandibula articular facet. Interopercle moderate in length, about equal hyomandibular anterior outgrowth length. Anterior margin of interopercle with pronounced anterior projection. Preopercle slender, without distinctive ventral projections.

Parurohyal lateral process relatively short, with blunt extremity, slightly curved posteriorly. Parurohyal head well-developed, with pronounced anterolateral paired process. Middle parurohyal foramen large, longitudinally elongate. Posterior process of parurohyal long, its length about four fifths distance between anterior margin of parurohyal and anterior insertion of posterior process. Branchiostegal rays 8.

Vertebrae 38. Ribs 15. Dorsal-fin origin at vertical through centrum of 21st vertebra, anal-fin origin at vertical through centrum of 24th vertebra. Two dorsal hypural plates

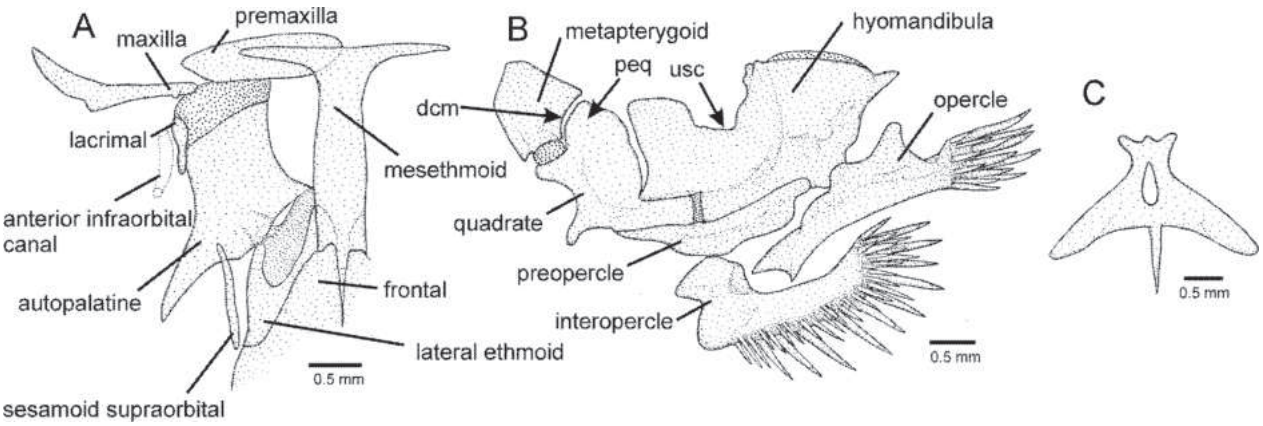

Figure 3. Osteological structures of *Trichomycterus* (*Paracambeva*) *antiquus* sp. nov. **A.** Mesethmoidal region and adjacent structures, left and middle portions, dorsal view; **B.** Left jaw suspensorium and opercular series, lateral view; **C.** Parurohyal, ventral view. Larger stippling represents cartilaginous areas. Abbreviations: dcm, deep concavity on the postero-ventral margin of the metapterygoid; peq, pronounced expansion of the postero-dorsal quadrate outgrown; usc, deep U-shaped concavity on the dorsal margin of the anterior hyomandibular anterior outgrown.

corresponding to hypurals 3 + 4 + 5; single ventral hypural plate corresponding to hypurals 1 + 2 + parhypural.

Colouration in alcohol. Flank pale yellow to yellowish white ventrally, with diffuse dark grey stripe along longitudinal midline, widening and breaking into small spots posteriorly. Great concentration of small dark grey spots on dorsal portion of flank, no or few similar spots on ventral portion. Dorsal surface of trunk and head pale brown, with small, faint grey spots, ventral surface white. Nasal and maxillary barbels pale brown, rictal barbel white. Fins hyaline, with whitish bases. In specimen UFRJ 13681, longitudinal stripe broader and darker, brown spots on dorsum, dorsal, and ventral portions of flank.

Etymology. From the Latin *antiquus* (old), referring to the relatively old estimated age of the species lineage in the Miocene (see below), when compared with the major species diversification of *Paracambeva* in the Pliocene.

Distribution. *Trichomycterus antiquus* is only known from the upper Rio do Peixe drainage, Rio Paraíba do Sul basin, south-eastern Brazil, at altitudes between about 765 and 980 m asl (Fig. 4).

Positioning of *Trichomycterus antiquus* and time-calibrated analysis

All phylogenetic analyses resulted in identical tree topologies (Fig. 5), in which *T. antiquus* is supported as sister to *T. itatiayae*, a species endemic to another region of the RPSB, with broad occurrence in streams draining the Maciço de Itatiaia, a massif forming a distinct nucleus of the Serra da Mantiqueira, and the adjacent Serra da Bocaina (Fig. 4). The clade comprising *T. antiquus* and *T. itatiayae*, hereafter the *Trichomycterus itatiayae* group, is supported as sister to a clade comprising all other species of *Paracambeva* known as the *T. reinhardti* species group (Costa 2021; Costa and Katz 2021). The independent analysis of individual gene trees indicated that all loci collaborated for this topology, since all gene trees corroborated monophyly of *Paracambeva* and both the RAG2 tree and the mitochondrial locus tree corroborated monophyly of the clade comprising *T. antiquus* and *T. itatiayae*, which is supported in both trees as sister to a clade comprising the remaining species of *Paracambeva* (Suppl. material 2). The age of the *Paracambeva* lineage was estimated at about 24.5 Ma, Late Oligoceno (95% HPD age interval 15.68–36.01), whereas according to the analysis, the divergence between the *T. itatiayae* group and the *T. reinhardti* group occurred at about 14.9 Ma, Middle Miocene (95% HPD age interval 7.16–24.84), and between *T. antiquus* and *T. itatiayae* at about 9.8 Ma, Late Miocene (95% HPD age interval 4.74–16.87).

Temporal origin of similar colour patterns

The presence of a broad black longitudinal stripe along the midline of the flank in juveniles, which often gradually becomes diffuse and fragmented into small spots in adults, combined with dark spots on the dorsum, occurs in most species of *Paracambeva* (Costa 2021; Costa and Katz 2021; Costa et al. 2023b), as well as in most species of the *T. nigroauratus* group of the subgenus *Trichomycterus* (e.g., Barbosa and Costa 2008; Costa et al. 2022). However, the specific colour pattern described here for *T. antiquus* and *T. maculosus* above about 70 mm SL, including a narrow stripe that posteriorly breaks into small spots, combined with the scarcity or absence of dark spots on the ventral part of the flank, occurs only in these two species and in *T. itatiayae* (Barbosa and Costa 2008: fig. 5). According to our analysis, this specific pattern would have first appeared in the ancestor of the clade comprising *T. antiquus* and *T. itatiayae*, around 14.9 Ma (95% HPD age interval 8.87–23.64), and a second time in the exclusive ancestor of *T. maculosus*, around 2.3 Ma (95% HPD age interval 0.85–4.56) (Fig. 5; Suppl. material 3).

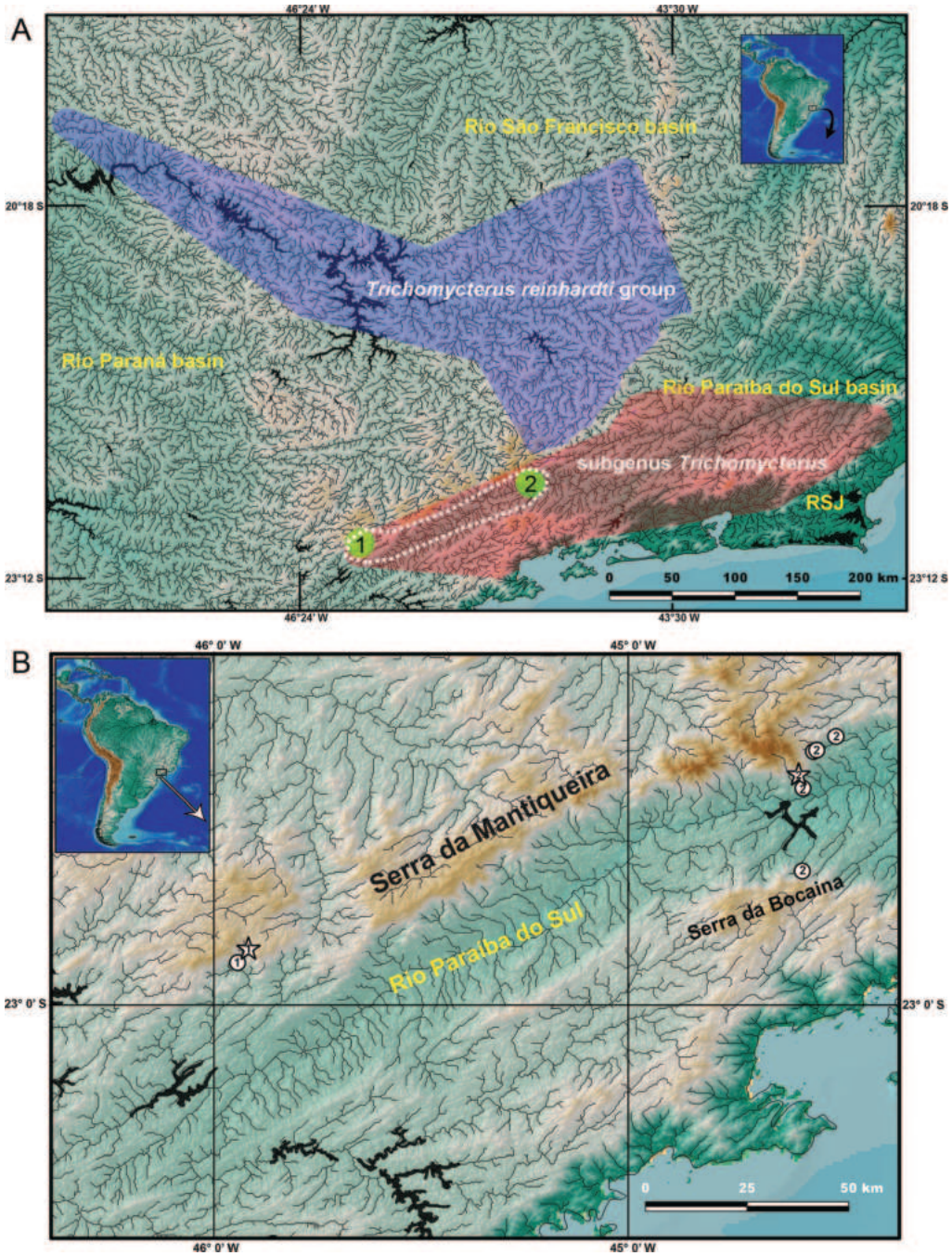

Figure 4. Map of south-eastern Brazil, showing: **A.** Geographical distribution of the *Trichomycterus* (*Paracambeva*) *itatiayae* group (delimited by a white dotted line), the *Trichomycterus* (*Paracambeva*) *reinhardti* group, and the subgenus *Trichomycterus*; **B.** collecting sites of 1, *Trichomycterus* (*Paracambeva*) *antiquus* sp. nov., and 2, *Trichomycterus* (*Paracambeva*) *itatiayae*. RSJ means Rio São João; stars indicate type localities.

Discussion

Temporal diversification and biogeographical context

According to a recent biogeographical analysis, the most recent common ancestor of *Paracambeva* lived in an area presently occupied by the upper Rio Paraná, upper Rio São Francisco, and Rio Paraíba do Sul basins (Vilardo et al. 2023). Presently, *Paracambeva* occupies a large region encompassing these three basins, with the *T. itatiayae* group occurring in a portion of the RPSB between the Rio do Peixe and the area close to the Serra da Bocaina and the *T. reinhardti* group occurring in a broad area of the upper Rio Paraná and upper Rio São Francisco basins (Fig. 4). Timing estimates support a Late Oligocene origin for the *Paracambeva* lineage and a Middle Miocene age for the split between the *T. itatiayae* and *T. reinhardti* groups (Fig. 5). Despite conclusive hypotheses about the time of origin of the present configuration of these basins that are not yet available, geological data point to a past connection between the upper section of the Rio Paraíba

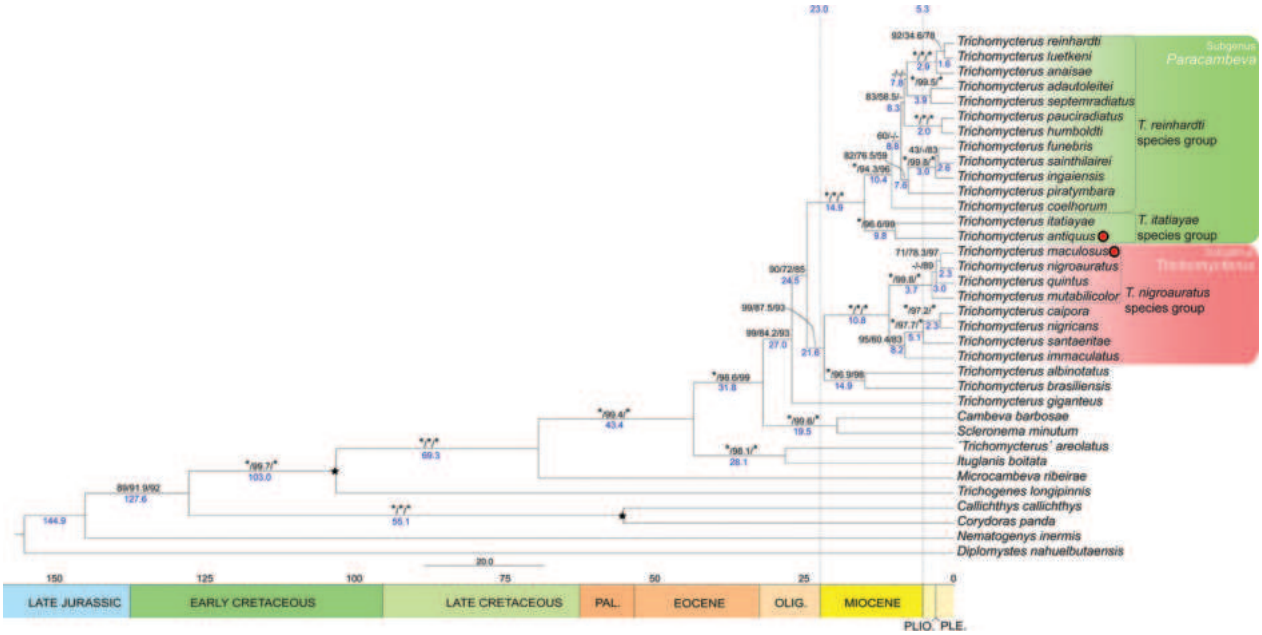

Figure 5. Time-scaled tree obtained from the Bayesian analysis in Beast for 28 species of Trichomycteridae and 4 species as outgroups, using a multigene data set (COX1, CYTB, RAG2, and MYH6 with a total of 3144 bp). Asterisks (*) indicate maximum support values, and dashes (-) indicate support values below 50. Black stars indicate the calibration points, and the coloured bars below the tree represent the geological epochs. Numbers above branches indicate posterior probabilities of the Bayesian Inference, followed by SH-aLRT support (%) and ultrafast bootstrap support (%) of the Maximum Likelihood (ML) analysis; blue numbers below nodes indicate its median age; Red dots after species names indicate the syntopic species discussed in this paper.

do Sul, above the area close to the Serra da Bocaina, and the Rio Paraná basin (King 1956; Riccomini et al. 2010), and between the upper section of the latter basin and the upper section of the Rio São Francisco basin (Rezende et al. 2018). Therefore, the present distribution of *Paracambeva* and our estimates for the time of origin of this subgenus fit into this model of river basin evolution, with the rupture between the upper Paraíba do Sul and the Paraná-São Francisco basin that would have occurred in the Paleogene (Riccomini et al. 2010) corresponding to the divergence between the *T. itatiayae* and *T. reinhardti* groups, which preceded the rupture of the connection between the upper Rio Paraná and upper Rio São Francisco basins during the Middle Miocene (Rezende et al. 2018), corresponding to the wide distribution of the *T. reinhardti* group in these basins (Fig. 4; Costa and Katz 2021).

On the other hand, temporal estimates indicated the origin of the subgenus *Trichomycterus* lineage in the early Miocene. The biogeographical analysis performed by Vilardo et al. (2023) indicated that the MRCA of the subgenus *Trichomycterus* inhabited an ancestral area comprising only the Rio Paraíba do Sul, contrasting with its present distribution that includes both this basin and smaller coastal basins (Fig. 4; Costa 2021). However, geological data support a Cenozoic configuration of the RPSB different from the present one, in which its lower course corresponded to the present lower course of the Rio São João (Riccomini et al. 2010), which is now an isolated coastal basin. Thus, geological data are congruent with the hypothesised ancestral area of the subgenus in the Rio Paraíba do Sul alone, which in the past did not include the present upper course but included a present coastal basin in its lower course. The upper course of the RPSB probably was blocked for dispersion of trichomycterine catfishes that live in fast flowing streams by the great depression in its main channel responsible for the formation of the paleolake Tremembé during the Oligocene (Riccomini et al. 2004). Thus, it is possible that these two subgenera lineages, *Paracambeva* and *Trichomycterus*, were not in contact in the upper Rio Paraíba do Sul before the Middle Miocene. The origin of the specific colour pattern shared by the syntopic *T. antiquus* and *T. maculosus* is estimated to have occurred first in the *T. itatiayae* group during the Middle Miocene and much later in *T. maculosus* during the Late Pliocene in *T. maculosus*, which is compatible with the hypothesis of a more recent occupation of the upper RPSB by the subgenus *Trichomycterus.*

Interestingly, the other case involving similarly coloured syntopic species of trichomycterines from eastern South America involves *T. itatiayae*, the sister group of *T. antiquus*, and *T. nigroauratus*, the sister group of *T. maculosus* (Fig. 5). These two species are endemic to streams of the RPSB draining the Serra da Mantiqueira and the adjacent Serra da Bocaina (Barbosa and Costa 2008) and are commonly found associated with bottom leaf litter (Costa 2021). Juvenile specimens of these species share a colour pattern consisting of a broad black longitudinal stripe along the flank midline, whereas larger specimens assume a different colour pattern (Barbosa and Costa 2008). A broad black longitudinal stripe is present in all other species of *Paracambeva* (Costa and Katz 2021; Costa et al. 2023b), therefore already present in the

MRCA of this subgenus, whereas this colour pattern is present in part of the species of the *T. nigroauratus* group among species of the subgenus *Trichomycterus* (Costa et al. 2022), thus arising after the initial diversification of this group. Considering the estimated age of *Paracambeva* in the Late Oligocene and the initial diversification of the *T. nigroauratus* group in the Late Pliocene, over 20 million years later, the most plausible hypothesis is that the colour pattern in the *T. nigroauratus* group had arisen after this group was in contact with species of *Paracambeva* in RPSB.

Possible explanations for the occurrence of syntopic trichomycterines with similar colour patterns

The sympatric occurrence of distantly related species of Neotropical catfishes exhibiting similar derived colour patterns has been often aprioristically considered as primary evidence of mimetic association (Axenrot and Kullander 2003; Alexandrou et al. 2011; Slobodian and Bockmann 2013), but may also be a result of evolutionary convergence for adaptation to live in special habitats like those occurring among sympatric psammophilic species (Zuanon et al. 2006; Costa et al. 2020c). Therefore, the occurrence of two species of *Trichomycterus* in the same habitat sharing the same colour pattern (Figs 1A, 6) but belonging to two distantly related subgenera could suggest a case of mimetic association or convergence for adaptation to live in a gravel bottom where both species were found, since their colour pattern is cryptic in this habitat. However, direct evidence to explain syntopic trichomycterines with similar colour patterns is not available for any of these hypotheses.

In the case of evolutionary convergence for adaptation to live in special habitats, a possible explanation is that the colour pattern gives these two species some cryptic advantage in their habitat against predators since the colours are similar to the gravel substrate where they live. In the case of mimetic associations, including both Batesian and Müllerian mimicry, the model species (Batesian) or both species (Müllerian) have effective anti-predation features, which among catfishes usually comprise venom glands associated with fin spines (Wright 2009; Harris and Jenner 2019). For example, in mimetic associations involving siluroids with a well-developed pectoral-fin spine, the main anti-predation morpho-physiological attribute is the presence of an axillary venom gland associated with a pungent pectoral-fin spine (e.g., Greven et al. 2006; Wright 2011; Carvalho et al. 2021). The defence mechanism involves not only glands and the pectoral-fin spine but also special muscles and connective tissue (Wright 2015; Harris and Jenner 2019). However, mechanisms for anti-predation in trichomycterines are still unknown, and potential trichomycterine predators living in the Rio do Peixe drainage have not been presently recorded, although the Neotropical otter *Lontra longicaudis* (Olfers, 1818) and the catfish *Steindachneridion parahybae* (Steindachner, 1877) today rare or absent in the region, were until recently potential predators.

Although anti-predation features consisting of venom glands associated with fin spines occur in most catfish lineages (Wright 2009, 2015), they are unknown among trichomycterids. Unlike other catfishes, trichomycterids do not have pectoral and dorsal spines. In a survey on the presence of venom axillary glands in catfish lineages, Wright (2009) did not detect them in *'Trichomycterus' areolatus* Valenciennes, 1846, concluding that these glands are not present in trichomycterids. However, a supposed axillary gland (e.g., Eigenmann 1918) or suprapectoral adipose organ according to Myers and Weitzman (1966) and axillary organ according to de Pinna (1989), situated at the same place as the venom axillary glands of other catfishes and having a similar orifice, have been superficially described for candirus and other trichomycterids (e.g., Eigenmann 1918). This supposed axillary gland, comprising a sack-like protuberance above the pectoral fin and just below the anterior pores of the lateral line of the flank, is also present in trichomycterines (Fig. 2), which is proportionally smaller than in other trichomycterids (e.g., sarcoglanidines, Myers and Weitzman 1966), with an orifice that is more conspicuous in juvenile specimens below about 40 mm SL, often having a great concentration of melanophores around its margin. Both *T. antiquus* and *T. maculosus* have a small axillary gland-like protuberance below the short lateral line canal and above the pectoral fin (Fig. 2). The absence of a pectoral spine in trichomycterids also imposes a limitation on the possibility of the axillary organ acting as a venom gland. Nonetheless, the stinging action of the opercular odontodes, which are located close to the ax-

Figure 6. *Trichomycterus* (*Trichomycterus*) *maculosus*, UFRJ 13676, 97.6 mm SL, left lateral view.

illary gland-like protuberance (Fig. 2) and may become bristly when the fish is molested, could be performed as the pectoral spine of other catfishes. However, a more detailed morphological study at the histological and biochemical level is necessary to investigate the presence of glandular tissue and toxic substances in *T. antiquus* and close relatives, which is not presently possible with the small sample of specimens currently available. Future studies are necessary to check what hypothesis best explains the unexpected syntopic occurrence of similarly coloured *T. antiquus* and *T. maculosus*.

Acknowledgements

Thanks are due to Léia C. Medeiros, Gustavo L. Canella, and Ronaldo dos Santos-Junior for field assistance. We are also grateful for the comments and criticisms provided by F. Langeani, H.H. Ng, F. Ottoni, and an anonymous reviewer, who contributed to improving the present version of the manuscript. The Instituto Chico Mendes de Conservação da Biodiversidade provided collecting permits. This work was partially supported by the Conselho Nacional de Desenvolvimento Científico e Tecnológico (CNPq; grant 304755/2020-6 to WJEMC) and Fundação Carlos Chagas Filho de Amparo à Pesquisa do Estado do Rio de Janeiro (FAPERJ; grant E-26/201.213/2021 to WJEMC, E-26/202.005/2020 to AMK, and E-26/203.524/2023 to JLM). This study was also supported by CAPES (Finance Code 001) through the Programa de Pós-Graduação em Biodiversidade e Biologia Evolutiva/UFRJ and the Programa de Pós-Graduação em Genética/UFRJ.

References

Alexandrou MA, Oliveira C, Maillard M, McGill RAR, Newton J, Creer S, Taylor MI (2011) Competition and phylogeny determine community structure in Müllerian co-mimics. Nature 469(7328): 249–272. https://doi.org/10.1038/nature09660

Arratia G, Huaquin L (1995) Morphology of the lateral line system and of the skin of diplomystid and certain primitive loricarioid catfishes and systematic and ecological considerations. Bonner Zoologische Monographien 36: 1–110.

Arratia G, Chang A, Menu-Marque S, Rojas G (1978) About *Bullockia* gen. nov., *Trichomycterus mendozensis* n. sp. and revision of the family Trichomycteridae (Pisces, Siluriformes). Studies on Neotropical Fauna and Environment 13(3–4): 157–194. https://doi.org/10.1080/01650527809360539

Axenrot TE, Kullander SO (2003) *Corydoras diphyies* (Siluriformes: Callichthyidae) and *Otocinclus mimulus* (Siluriformes: Loricariidae), two new species of catfishes from Paraguay, a case of mimetic association. Ichthyological Exploration of Freshwaters 14: 249–272.

Barbosa MA, Costa WJEM (2008) Description of a new species of catfish from the upper Rio Paraíba do Sul basin, south-eastern Brazil (Teleostei: Siluriformes: Trichomycteridae) and re-description of *Trichomycterus itatiayae*. Aqua International Journal of Ichthyology 14: 175–186.

Barbosa MA, Costa WJEM (2010) Description of a new species of the catfish genus *Trichomycterus* (Teleostei: Siluriformes: Trichomycteridae) from the RPSB, southeastern Brazil. Vertebrate Zoology 60(3): 193–197. https://doi.org/10.3897/vz.60.e31010

Betancur-R R, Órti G, Pyron RA (2015) Fossil-based comparative analyses reveal ancient marine ancestry erased by extinction in ray-finned fishes. Ecology Letters 18(5): 441–450. https://doi.org/10.1111/ele.12423

Bockmann FA, Sazima I (2004) *Trichomycterus maracaya*, a new catfish from the upper rio Paraná, southeastern Brazil (Siluriformes: Trichomycteridae), with notes on the *T. brasiliensis* species-complex. Neotropical Ichthyology 2(2): 61–74. https://doi.org/10.1590/S1679-62252004000200003

Carvalho TI, Klaczko J, Slobodian V (2021) Pectoral-fin glands and delivery apparatus in the catfish genus *Brachyrhamdia* Myers, 1927 (Siluriformes: Heptapteridae). Papéis Avulsos de Zoologia 61: e20216174. https://doi.org/10.11606/1807-0205/2021.61.74

Chenna R, Sugawara H, Koike T, Lopez R, Gibson TJ, Higgins DG, Thompson JD (2003) Multiple sequence alignmentwith the Clustal series of programs. Nucleic Acids Research 31(13): 3497–3500. https://doi.org/10.1093/nar/gkg500

Costa WJEM (1992) Description de huit nouvelles espèces du genre *Trichomycterus* (Siluriformes: Trichomycteridae), du Brésil oriental. Revue Française d'Aquariologie et Herpetologie 18: 101–110.

Costa WJEM (2021) Comparative osteology, phylogeny and classification of the eastern South American catfish genus *Trichomycterus* (Siluriformes: Trichomycteridae). Taxonomy 1(2): 160–191. https://doi.org/10.3390/taxonomy1020013

Costa WJEM, Katz AM (2021) Integrative taxonomy supports high species diversity of south-eastern Brazilian mountain catfishes of the *T. reinhardti* group (Siluriformes: Trichomycteridae). Systematics and Biodiversity 19(6): 601–621. https://doi.org/10.1080/14772000.2021.1900947

Costa WJEM, Mattos JLO, Amorim PF, Vilardo PJ, Katz AM (2020a) Relationships of a new species support multiple origin of melanism in *Trichomycterus* from the Atlantic Forest of south-eastern Brazil (Siluriformes: Trichomycteridae). Zoologischer Anzeiger 288: 74–83. https://doi.org/10.1016/j.jcz.2020.07.004

Costa WJEM, Katz AM, Mattos JLO, Amorim PF, Mesquita BO, Vilardo PJ, Barbosa MA (2020b) Historical review and redescription of three poorly known species of the catfish genus *Trichomycterus* from south-eastern Brazil (Siluriformes: Trichomycteridae). Journal of Natural History 53(47–48): 2905–2928. https://doi.org/10.1080/00222933.2020.1752406

Costa WJEM, Henschel E, Katz AM (2020c) Multigene phylogeny reveals convergent evolution in small interstitial catfishes from the Amazon and Atlantic forests (Siluriformes: Trichomycteridae). Zoologica Scripta 49(2): 159–173. https://doi.org/10.1111/zsc.12403

Costa WJEM, Mattos JLO, Lopes S, Amorim PF, Katz AM (2022) Integrative taxonomy, distribution and ontogenetic colouration change in Neotropical mountain catfishes of the *Trichomycterus nigroauratus* Group (Siluriformes, Trichomycteridae). Zoological Studies (Taipei, Taiwan) 61: 11. https://doi.org/10.6620/ZS.2022.61-11

Costa WJEM, Mattos JLO, Amorim PF, Mesquita BO, Katz AM (2023a) Chromatic polymorphism in *Trichomycterus albinotatus* (Siluriformes, Trichomycteridae), a mountain catfish from south-eastern Brazil and the role of colouration characters in trichomycterine taxonomy. Zoosystematics and Evolution 99(1): 161–171. https://doi.org/10.3897/zse.99.98341

Costa WJEM, Azevedo-Santos VM, Mattos JLO, Katz AM (2023b) Molecular phylogeny, taxonomy and distribution patterns of trichomycterine catfishes in the middle Rio Grande drainage, south-eastern Brazil (Siluriformes: Trichomycteridae). Fishes 8(4): 206. https://doi.org/10.3390/fishes8040206

da Silva CCF, da Matta SLSF, Hilsdorf AWS, Langeani F, Marceniuk AP (2010) Color pattern variation in *Trichomycterus iheringi* (Eigenmann, 1917) (Siluriformes: Trichomycteridae) from rio Itatinga and rio Claro, São Paulo, Brazil. Neotropical Ichthyology 8(1): 49–56. https://doi.org/10.1590/S1679-62252010000100007

de Pinna MCC (1989) A new sarcoglandine catfish, phylogeny of its subfamily, and an appraisal of the phyletic status of the Trichomycterinae (Teleostei, Trichomycteridae). American Museum Novitates 2950: 1–39.

Eigenmann CH (1918) The Pygidiidae, a family of South American catfishes. Memoirs of the Carnegie Museum 7(5): 259–398. https://doi.org/10.5962/p.34486

Gernhard T (2008) The conditioned reconstruction process. Journal of Theoretical Biology 253(4): 769–778. https://doi.org/10.1016/j.jtbi.2008.04.005

Greven H, Flasbeck T, Passia D (2006) Axillary glands in the armoured catfish *Corydoras aeneus* (Callichthyidae, Siluriformes). Verhandlungen der Gesellschaft für Ichthyologie 5: 65–69.

Guindon S, Dufayard JF, Lefor V, Anisimova M, Hordijk W, Gascuel O (2010) New algorithms and methods to estimate maximum-likelihood phylogenies: Assessing the performance of PhyML 3.0. Systematic Biology 59(3): 307–321. https://doi.org/10.1093/sysbio/syq010

Harris RJ, Jenner RA (2019) Evolutionary ecology of fish venom: Adaptations and consequences of evolving a venom system. Toxins 11(2): 60. https://doi.org/10.3390/toxins11020060

Hoang DT, Chernomor O, von Haeseler A, Minh BQ, Vinh LS (2018) UFBoot2: Improving the ultrafast bootstrap approximation. Molecular Biology and Evolution 35(2): 518–522. https://doi.org/10.1093/molbev/msx281

King LC (1956) A Geomorfologia do Brasil Oriental. Revista Brasileira de Geografia 18: 147–265.

Kubicek KM (2022) Developmental osteology of *Ictalurus punctatus* and *Noturus gyrinus* (Siluriformes: Ictaluridae) with a discussion of siluriform bone homologies. Vertebrate Zoology 72: 661–727. https://doi.org/10.3897/vz.72.e85144

Lanfear R, Frandsen PB, Wright AM, Senfeld T, Calcott B (2016) PartitionFinder 2: New methods for selecting partitioned models of evolution for molecular and morphological phylogenetic analyses. Molecular Biology and Evolution 34: 772–773. https://doi.org/10.1093/molbev/msw260

Minh BQ, Schmidt HA, Chernomor O, Schrempf D, Woodhams MD, von Haeseler A, Lanfear R (2020) IQ-TREE 2: New models and efficient methods for phylogenetic inference in the genomic era. Molecular Biology and Evolution 37(5): 1530–1534. https://doi.org/10.1093/molbev/msaa015

Myers GS, Weitzman SH (1966) Two remarkable new trichomycterid catfishes from the Amazon basin in Brazil and Colombia. Journal of Zoology (London, England) 149(3): 277–287. https://doi.org/10.1111/j.1469-7998.1966.tb04049.x

Ochoa LE, Roxo FF, DoNascimiento C, Sabaj MH, Datovo A, Alfaro M, Oliveira C (2017) Multilocus analysis of the catfish family Trichomycteridae (Teleostei: Ostariophysi, Siluriformes) supporting a monophyletic Trichomycterinae. Molecular Phylogenetics and Evolution 115: 71–81. https://doi.org/10.1016/j.ympev.2017.07.007

Price AC, Weadick CJ, Shim J, Rodd FH (2008) Pigments, Patterns, and Fish Behavior. Zebrafish 5(4): 297–307. https://doi.org/10.1089/zeb.2008.0551

Rambaut A, Drummond AJ, Xie D, Baele G, Suchard MA, Rambaut A, Drummond AJ, Xie D, Baele G, Suchard MA (2018) Posterior summarisation in Bayesian phylogenetics using Tracer 1.7. Systematic Biology 67(5): 901–904. https://doi.org/10.1093/sysbio/syy032

Reis VJC, dos Santos SA, Britto MR, Volpi TA, de Pinna MCC (2020) Iterative taxonomy reveals a new species of *Trichomycterus* Valenciennes 1832 (Siluriformes, Trichomycteridae) widespread in Rio Doce Basin: A pseudocryptic of *T. immaculatus.* Journal of Fish Biology 97(6): 1607–1623. https://doi.org/10.1111/jfb.14490

Rezende EA, Salgado AAR, Castro PTA (2018) Evolução da rede de drenagem e evidências de antigas conexões entre as bacias dos rios Grande e São Francisco no sudeste brasileiro. Revista Brasileira de Geomorfologia 19(3): 483–501. https://doi.org/10.20502/rbg.v19i3.1304

Riccomini C, Sant'Anna LG, Ferrari AL (2004) Evolução geológica do Rift Continental do Sudeste do Brasil. In: Mantesso-Neto V, Bartorelli A, Carneiro CDR, Brito-Neves BB (Eds) Geologia do continente Sul-Americano: evolução da obra de Fernando Flávio Marques de Almeida. Beca, São Paulo, 383–405.

Riccomini C, Grohmann CH, Sant'Anna LG, Hiruma ST (2010) A captura das cabeceiras do Rio Tietê pelo Rio Paraíba do Sul. In: Modenesi-Gauttieri MC, Bartorelli A, Mantesso-Neto V, Carneiro CDR, Lisboa MBAL (Eds) A obra de Aziz Nacib Ab'Sáber. Beca, São Paulo, 157–169.

Sarmento-Soares LM, Martins-Pinheiro RF, Aranda AT, Chamon CC (2005) *Trichomycterus pradensis*, a new catfish from southern Bahia coastal rivers, northeastern Brazil (Siluriformes: Trichomycteridae). Ichthyological Exploration of Freshwaters 16: 289–302.

Slobodian V, Bockmann FA (2013) A new *Brachyrhamdia* (Siluriformes: Heptapteridae) from Rio Japurá basin, Brazil, with comments on its phylogenetic affinities, biogeography and mimicry in the genus. Zootaxa 3717(1): 1–22. https://doi.org/10.11646/zootaxa.3717.1.1

Suchard MA, Lemey P, Baele G, Ayres DL, Drummond AJ, Rambaut A (2018) Bayesian phylogenetic and phylodynamic data integration using BEAST 1.10. Virus Evolution 4(1): vey016. https://doi.org/10.1093/ve/vey016

Tamura K, Stecher G, Kumar S (2021) MEGA11: Molecular Evolutionary Genetics Analysis Version 11. Molecular Biology and Evolution 38(7): 3022–3027. https://doi.org/10.1093/molbev/msab120

Taylor WR, Van Dyke GC (1985) Revised procedures for staining and clearing small fishes and other vertebrates for bone and cartilage study. Cybium 9: 107–119.

Valenciennes A (1832) Nouvelles observations sur le Capitan de Bogota, *Eremophilus mutisii.* In: Humboldt A, Bonpland A (Eds) Recueil d'observations de Zoologie et d'Anatomie Comparée, faites dans l'Ocean Atlantique, dans l'interieur du Nouveau Continent et dans la Mer du Sud pendant les annés 1799, 1800, 1801, 1802 et 1803, deuxième volume. Observations de Zoologie et d'Anatomie comparée, 341–348.

Vilardo PJ, Katz AM, Costa WJEM (2023) Chromatic polymorphism in *Trichomycterus jacupiranga* from eastern Brazilian coastal basins (Siluriformes: Trichomycteridae). Zootaxa 5285(2): 360–372. https://doi.org/10.11646/zootaxa.5285.2.8

Villa-Verde L, Lazzarotto H, Lima SQM (2012) A new glanapterygine catfish of the genus *Listrura* (Siluriformes: Trichomycteridae) from southeastern Brazil, corroborated by morphological and molecular data. Neotropical Ichthyology 10(3): 527–538. https://doi.org/10.1590/S1679-62252012000300005

Ward RD, Zemlak TS, Innes BH, Last PR, Hebert PD (2005) DNA barcoding Australia's fish species. Philosophical Transactions of the Royal Society of London. Series B, Biological Sciences 360(1462): 1847–1857. https://doi.org/10.1098/rstb.2005.1716

Wright JJ (2009) Diversity, phylogenetic distribution, and origins of venomous catfishes. BMC Evolutionary Biology 9(1): 282. https://doi.org/10.1186/1471-2148-9-282

Wright JJ (2011) Conservative coevolution of Mullerian mimicry in a group of rift lake catfish. Evolution; International Journal of Organic Evolution 65(2): 395–407. https://doi.org/10.1111/j.1558-5646.2010.01149.x

Wright JJ (2015) Evolutionary History of Venom Glands in the Siluriformes. In: Gopalakrishnakone P. & Malhotra, A. (Eds.). Evolution of Venomous Animals and Their Toxins. Dordrecht, Springer, 1–19. https://doi.org/10.1007/978-94-007-6727-0_9-1

Zuanon J, Bockmann FA, Sazima I (2006) A remarkable sand-dwelling fish assemblage from central Amazonia, with comments on the evolution of psammophily in South American freshwater fishes. Neotropical Ichthyology 4(1): 107–118. https://doi.org/10.1590/S1679-62252006000100012

Supplementary material 1

List of comparative material of the subgenus *Paracambeva*

Authors: Wilson J. E. M. Costa, Caio R. M. Feltrin, José Leonardo O. Mattos, Axel M. Katz

Data type: pdf

Link: https://doi.org/10.3897/zse.100.118000.suppl1

Supplementary material 2

The independent analysis of individual gene trees

Authors: Wilson J. E. M. Costa, Caio R. M. Feltrin, José Leonardo O. Mattos, Axel M. Katz

Data type: pdf

Link: https://doi.org/10.3897/zse.100.118000.suppl2

Supplementary material 3

Beast divergence-time estimation

Authors: Wilson J. E. M. Costa, Caio R. M. Feltrin, José Leonardo O. Mattos, Axel M. Katz

Data type: pdf

Link: https://doi.org/10.3897/zse.100.118000.suppl3